CONTENTS

No 1 JULY 1967

No 2 SEPTEMBER 1967

No 3 NOVEMBER 1967

The Distribution of Cholinergic and Adrenergic Nerves in the Mammalian Epididymis

A COMPARATIVE HISTOCHEMICAL STUDY [1]

AHMAD EL-BADAWI [2] AND ERIC A. SCHENK

Division of Urology and Department of Pathology University of Rochester School of Medicine and Dentistry Rochester New York

ABSTRACT The distribution of cholinergic and adrenergic nerves in the epididymis was studied in the dog, cat, rat and rabbit using specific histochemical techniques for acetylcholinesterase and norepinephrine. Both cholinergic and adrenergic nerves are associated with tunical, septal and interstitial blood vessels, run independently in the intertubular connective tissue, and surround the epididymal tubules.

Throughout the epididymis there are rich adrenergic and cholinergic perivascular plexuses. The distribution and pattern of interstitial and peritubular cholinergic and adrenergic nerves vary in the three anatomical regions of the epididymis in different animals. In the dog and cat the nerves form plexuses in relation to the ductuli efferentes in the caput, and run as isolated fibers in the corpus epididymidis. In the rat and rabbit there are no interstitial or peritubular nerves in the caput and proximal part of the corpus and few nerves in the distal part of the corpus. The cauda epididymidis is the most richly innervated part of the epididymis. Both interstitial and peritubular cholinergic and adrenergic nerves form plexuses of nerve fibers and bundles, which progressively become more prominent and more intricate as the cauda is traced distally towards its junction with the vas deferens. These changes in innervation pattern follow the distalward increase in thickness of the muscular wall of the ductus epididymidis and are noted in all animals studied.

Ganglia are encountered only in the caput epididymidis in the cat. Cholinergic and adrenergic epithelial fibers are present in the caput and cauda but not in the corpus epididymidis. In the cauda they penetrate through most of the thickness of the epithelium; the cholinergic fibers in this region form a loose intra-epithelial plexus.

The source and gross anatomy of the autonomic nerves supplying the epididymis are well documented in the literature. However there are relatively meager data on the relative abundance and distribution of sympathetic and parasympathetic nerves within the organ.

In a histologic study of the normally innervated and denervated epididymis in the cat and rat by a silver impregnation technique Kuntz and Morris (46) found that there is an abundant nerve plexus around the ductus epididymidis and in association with the vascular bed. They concluded that the vascular bed is innervated solely through sympathetic nerves that the parasympathetic nerves are distributed solely to the musculature of the ductus epididymidis, and that this muscle is also probably innervated through sympathetic nerves.

More recently Risley and Skrepetos ('64) described the distribution of acetylcholinesterase-containing cholinergic nerve fibers in the rat epididymis. They found that (1) in the caput epididymidis the nerve fibers are exclusively associated with the larger intertubular blood vessels (2) the nerves become more numerous and become distributed to the duct wall as one proceeds distally from the junction of the caput and corpus, (3) the nerve plexus is most complex in the cauda epididymidis especially in its distal part, and (4) the fibers of the nerve plexus in the cauda are *not only* associated with the smooth muscle cells in the tubular wall, but also pass "very near to the basement membrane of the epithelial cells."

The present investigation has been undertaken to outline the distribution of both

[1] This investigation was supported in part by USPHS Institutional grant [illegible] and by [illegible] grant from the American Cancer Society.

[2] Lecturer in Urology, Faculty of Medicine, University of Alexandria, Alexandria, U. A. R. Presently on leave as [illegible] Fellow in Urologic Research, The University of Rochester School of Medicine and Dentistry, Rochester, New York 14620.

cholinergic and adrenergic nerve fibers in the epididymis of some mammalian species Particular attention has been paid to regional variations in the innervation pattern of the organ

MATERIAL AND METHODS

The epididymis was excised bilaterally under light nembutal anesthesia (intra peritoneal or intravenous) from five dogs six cats ten rats and five rabbits. The specimens were quick frozen with dry ice-acetone and stored at − 80 C Serial cryostat sections 10–20 μ thick, were obtained from the whole epididymis in its long axis and from the caput, corpus and cauda epididiymidis cut transversely at three to six successive levels.

The modified histochemical procedures for acetylcholinesterase (AChE) and nor epinephrine (NE) described by El Badawi and Schenk ('66) were used for the demon stration of cholinergic and adrenergic nerves In the former procedure the incu bation period ranged between three and eight hours

RESULTS

General innervation pattern

In the dog the intrinsic nerves of the epididymis are derived from nerve trunks and bundles composed of cholinergic and/or adrenergic fibers which run alongside and send fibers to the main-stem epididymal vessels and their branches. Piercing the tunica of the epididymis the nerve trunks divide into smaller nerve bundles which run for variable distances in and beneath the tunica. The branch bundles follow the fibrous septa through which the epididymis is partitioned into lobar and lobular units repeatedly subdivide to thinner bundles and ultimately break up into indi vidual nerve fibers. The nerve bundles and fibers run alongside the tunical, septal and interstitial blood vessels (vascular nerves) in the intertubular connective tissue (inter stitial nerves) and in relation to the ductus epididymidis (peritubular nerves) The adrenergic nerves are far more numerous ramify more extensively and more frequently have a plexiform arrangement than the corresponding cholinergic nerves.

The vascular nerves accompany the ar teries ateriole some veins and a few venules. Throughout the epididymis they form cholinergic and more prominent adrenergic perivascular plexuses from which fine fibers extend into the vascular tunica media (figs. 9 16 17)

The cholinergic and adrenergic interstitial and peritubular nerves run as isolated fibers or form a plexus The ramifica tions of the peritubular nerves surround individual or groups of smooth muscle cells in the tubular wall and extend in variable numbers into the tubular epithelium The relative abundance and arrangement of the interstitial and peritubular nerves and their parent tunical and septal bundles vary in the three anatomical regions of the epididymis namely the caput, corpus and cauda epididymidis

Caput epididymidis There are a few cholinergic and several adrenergic tunical septal and interstitial nerve bundles. The peritubular nerves run as isolated fibers in relation to the proximal (fig. 1) and form wide meshed tridimensional plexuses around the distal segments of the ductuli efferentes. Few epithelial fibers extend through the basal part of the epithelium

Corpus epididymidis (figs. 2 7) There are a few tunical and septal bundles. In the proximal part of the corpus there is a moderate number of cholinergic and adrenergic interstitial and very few peritubular nerves which include scattered thin bundles In some areas the adrenergic nerves form a very wide meshed interstitial or peritubular plexus. The nerves rapidly become less abundant and more dispersed further distally No epithelial fibers are found.

Cauda epididymidis There are numer ous tunical and septal nerve bundles. Compared to the rest of the epididymis the interstitial and peritubular nerves — par ticularly the adrenergic nerves — in the cauda are generally more numerous ramify and inosculate more extensively include more nerve bundles and more often communicate with one another as well as with the perivascular plexus These features become more manifest as the cauda is fol lowed distally from its junction with the corpus to that with the vas deferens. The zonal variations in innervation pattern cor respond to the distalward change in the morphology of the ductus epididymidis

notably to the increasing thickness of the tubular musculature.

In the proximal third of the cauda (figs. 3 8) the interstitial nerves usually run separately. Both the interstitial and peritubular nerves include a few bundles which undergo limited branching. The peritubular plexuses have a bidimensional arrangement and supply fibers to the tenuous musculature and the epithelium. Isolated epithelial fibers enter the epithelium perpendicularly and penetrate through most of its thickness.

In the middle third of the cauda (figs. 4 9) there is an open meshed adrenergic interstitial plexus of nerve fibers and bundles. In contrast, the cholinergic interstitial nerves rarely form a plexus. The peritubular plexuses have a tridimensional arrangement and are composed partially or entirely of interlacing nerve bundles. The plexuses supply cholinergic and adrenergic fibers to the moderately thick tubular musculature and to the epithelium. The epithelial fibers are similar to those seen in the proximal third of the cauda except that they are relatively more abundant. They run for variable distances in contact with the basement membrane and often intercommunicate before penetrating the epithelium almost perpendicularly

The distal third of the cauda (figs. 5, 10) is the most richly innervated part of the epididymis. There are extremely intricate peritubular and interstitial plexuses of cholinergic and adrenergic nerve fibers and bundles (fig. 11) The cholinergic fibers are arranged as a nucleated neuroterminal plexus, and the adrenergic fibers as closed interconnected networks. Both the cholinergic and adrenergic peritubular plexuses are differentiated into tridimensional muscular and subepithelial plexuses, especially near the epididymovasal junction. The most intricate parts of the subepithelial plexuses occupy the deepest part of the lamina propria adjacent to the muscularis. The epithelial fibers (figs. 14 15) are far more abundant than in the rest of the epididymis. Near the junction with the vas deferens some epithelial fibers — chiefly cholinergic — arborize as a loose intra-epithelial network, and end freely close to the luminal surface of the epithelium.

Species variations

In the rat both the cholinergic and adrenergic nerves in the caput epididymidis are exclusively associated with blood vessels (fig 6) In the rabbit the cholinergic nerves are exclusively vascular but the adrenergic nerves include a few discrete interstitial and peritubular fibers as well. In both species the extra-epididymal ductuli efferentes have a very poor innervation. The innervation of the caput in the cat is much more prominent than in the dog. The peritubular cholinergic and adrenergic nerves form moderately rich bidimensional plexuses around the proximal and tridimensional plexuses around the distal segments of the ductuli efferentes (figs. 12, 13) There are numerous epithelial fibers. Moderate sized ganglia composed of both AChE- and NE-containing cells are constantly encountered in the proximal part of the caput epididymidis in the cat.

DISCUSSION

As elsewhere in the body the adrenergic nerve fibers in the epididymis are functionally postganglionic sympathetic fibers. In a study of the innervation of the urinary bladder it was pointed out (El-Badawi and Schenk, '66) that the cholinergic nerves may represent preganglionic sympathetic or parasympathetic fibers, postganglionic parasympathetic fibers, or — according to the Burn-Rand hypothesis — postganglionic sympathetic fibers.

Since relatively few ganglia were *found* only in the caput epididymidis in the cat, it must be concluded that very few of the cholinergic fibers are preganglionic parasympathetic. At this time it is not possible to state definitively whether any of the cholinergic fibers are preganglionic sympathetic. Short adrenergic *neurons* that have cell bodies lying close to the effector tissues have been described recently in the mammalian urinary bladder and accessory male genitalia (Hamberger and Norberg, '65; Sjöstrand, '65 El-Badawi and Schenk, '66) and were occasionally encountered in the epididymis in the present study (vide infra) The existence of cholinergic sympathetic postganglionic fibers — as proposed by Burn and Rand — in the epididymis is doubtful because of (1) the presence

of adrenergic nerve bundles which ramify repeatedly to smaller and smaller bundles and ultimately to anastomosing nerve fibers and (2) the fact that adrenergic nerve trunks bundles and fibers far out number the corresponding cholinergic nerves throughout the epididymis in all species studied.

In view of the foregoing discussion it may be assumed that the cholinergic nerves in the epididymis represent for the most part postganglionic parasympathetic fibers.

The terminal cholinergic ramifications are arranged as a nucleated neuroterminal plexus similar to that described in the uri nary bladder (El Badawi and Schenk 66) The plexus is most clearly seen in the inter stitial and peritubular plexuses in the cauda epididymidis The adrenergic fibers form apparently closed interconnected net works in the intertubular tissues and around the blood vessels and tubules This network arrangement is especially distinct and intricate in the cauda epididymidis near the origin of the vas deferens Intensely fluorescent cell bodies are occasion ally interspersed in the adrenergic network. Their nature is not quite clear from the material examined though in the light of pertinent studies they presumably repre sent the NE-containing cell bodies of short adrenergic neurons

Although the innervation pattern in the corpus and cauda epididymidis is essen tially similar in the four species studied that of the caput varies from animal to animal This may be correlated with the variable construction of the caput in differ ent mammalian species According to Benoit ('26) the caput is composed entirely of the ductuli efferentes in the dog and cat, and of the proximal part of the ductus epi didymidis in the rat and rabbit The ductuli efferentes in the latter two species are totally extra-epididymal and unlike those forming the caput in the cat and dog have a very poor innervation. The innervation pattern of the caput in both rat and rabbit is comparable to that seen in the proximal part of the corpus epididymidis in the dog and cat, both regions being composed of the proximal segment of the ductus epididymidis.

Neurophysiologic considerations

Little is known about the nervous control of epididymal function The morphological data included in this report suggest that the nerves perform at least two functions in the epididymis namely a vasomotor function and the regulation of contractility of the periductal smooth musculature.

Vascular innervation

In all species studied the epididymal blood vessels chiefly the arteries and arterioles have a dual cholinergic and adrenergic innervation The adrenergic fibers represent postganglionic sympathetic vasoconstrictor nerves The cholinergic fibers probably have an antagonistic active vasodilator function and may be postganglionic sympathetic or parasympathetic in nature.

The neuromuscular mechanism

It has been postulated that a neuromuscular mechanism is involved in the for ward movement of spermatozoa in the epididymis (Moore and Quick, '24 Young and Simeone '30 Toothill and Young '31 Simeone '33) The close correlation between the innervation pattern and the thickness of periductal musculature, as well as the intimate relationship between terminal neural ramifications and smooth muscle cells observed in this study lend support to the existence of such a mechanism.

Studies on the effects of various autonomic drugs and of denervation on the epididymis (Simeone '33 Muratori, '56 Cross and Glover '58) suggest that the contractility of the epididymal musculature is augmented by sympathetic and inhibited by parasympathetic neural stimuli. In the light of our morphologic data these stimuli would be transmitted through the adrenergic network and the cholinergic neuroterminal plexus respectively

The regional differences in the richness and pattern of the epididymal muscular innervation may be explained on a func tional basis The ductuli efferentes transmit spermatozoa rapidly from the testicle to the ductus epididymidis This is achieved by the ciliary activity of their epithelial lining cells supplemented by the contrac tions of their meager musculature In the

poorly innervated and relatively short duc tuli efferentes in the rat and rabbit, these contractions are apparently independent of neural factors (Risley '63) In the cat and dog the prominent innervation of the duc tuli probably exerts an important influence on their contractions, and this may be related to the fact that in these two species the ductuli pursue a long sinuous course in the caput epididymidis. The proximal part of the ductus epididymidis transports spermatozoa to the cauda usually over a period of days (Risley '63) This is effected solely through the spontaneous rhythmic activity of its poorly developed musculature as there are no vibratile cilia in the epithelial lining of the ductus in mammals. Since it is known that the rhythmic activity of the proximal ductus is principally peristaltic in nature (Muratori and Contro '51; Muratori, 53 '56 Risley '58 Risley and Turbyfill, '57) and is still noticeable in excised specimens (Battaglia, '58 Risley and Van de Velde, '59) it seems that the nerves related to this segment of ductus — like those related to the ductuli efferentes — perform only a subsidiary regulatory function. For such a function the poorly developed innervation of the proximal ductus i.e. in the caput and/or corpus epididymidis, appears to be adequate. The ductus epididymidis in the cauda performs two functions, namely storage of transported spermatozoa, and delivery of the sperm stores into the vas deferens at emission. In this region the ductal musculature is many times thicker than in the rest of the ductus, and yet it hardly shows any spontaneous rhythmic activity (Risley '63) A mere regulatory function would not be sufficient, as a mechanism is needed for initiation of muscular relaxation to allow for storage, and for excitation of powerful muscular contraction at the time of emission. The rich and intricate innervation and the apparent continuity of the inter stitial and peritubular plexuses throughout the cauda provide for such a mechanism, and make possible a muscular response that is selectively segmental or well coordinated in the entire caudal ductus. The differences in the relative importance of the role played by nerves in the proximal and caudal parts of the ductus are further substantiated by some observations on the histogenesis of muscular and neural elements in the rat epididymis (Van de Velde and Risley '63 Risley and Skrepetos 64)

Epithelial innervation

Intra-epithelial nerve fibers in the epididymis have not been depicted in the literature. Sclavunos (1893) vaguely stated that branches of the muscular plexus in the epididymis penetrate the epithelium. Kuntz and Morris (46) using silver stains described nerve fibers that are "related" to the epithelium. Risley and Skrepetos (64) found that fibers of the cholinergic nerve plexus "pass very near to the basement membrane of the epithelial cells." Our findings indicate that both cholinergic and adrenergic nerve fibers penetrate the epithelium in variable numbers and to different depths in the caput and cauda but not in the corpus epididymidis. The nerves either have free unbranched terminations or form a loose intra-epithelial network.

It is not possible to differentiate afferent sensory nerve fibers by the techniques used in the present study However the freely ending intra-epithelial (and interstitial) nerve fibers in the epididymis are morphologically similar to afferent fibers described in other mammalian tissues (Seto '63 El Badawi and Schenk, '66) and therefore may subserve a sensory function.

The role of epithelial nerves in epididymal secretory activity is not clear Benoit ('26) has shown that secretion in the ductuli efferentes still continues after the gonadal neurovascular pedicle has been sectioned in the guinea pig. He postulated an indirect neurosecretory mechanism whereby the nerves influence epithelial secretion through regulation of blood flow to the epithelial cells. There is a great discrepancy between the degree of secretory activity and the distribution of epithelial nerves in the different segments of the ductus epididymidis. Benoit ('26) stated that the "initial segment" of the ductus is its most actively secreting portion. But hardly any epithelial fibers are seen in this segment in any of the species studied. The secretory cycle is much slower in the cauda than in the caput epididymidis (Maneely '59) yet the epithelial fibers are much more numerous, more deeply penetrating, and more complicated in arrangement in the

former region. Although these observations seem to indicate that epididymal secretion is independent of neural stimuli the presence of a neurosecretory mechanism cannot be entirely ruled out.

LITERATURE CITED

Battaglia, G. 1956 Prime osservazioni sui movimenti dell'epididimo del ratto in culture or ganotipiche rotanti. Boll. Soc. Ital. Biol. Sper., 32 265–267

Benoit, M. J 1926 Recherches anatomiques, cytologiques et histophysiologiques sur les voies excrétrices du testicule chez les mammiferes. Arch. d'Anat. d'Hist. d'Embryol., 5: 173–412.

Cross, B A., and T D Glover 1958 The hypothalamus and seminal emission. J Endocr., 16 385–395

El Badawi, A., and E. A. Schenk 1968 Dual innervation of the mammalian urinary bladder. A histochemical study of the distribution of cholinergic and adrenergic nerves. Am. J Anat., 119: 405–428.

Hamberger B and K.-A. Norberg 1965 Adrenergic synaptic terminals and nerve cells in bladder ganglia of the cat. Int. J Neuropharm., 4: 41–45.

Kuntz, A., and R. E. Morris Jr 1946 Components and distribution of the spermatic nerves and the nerves of the vas deferens. J Comp. Neur., 85: 33–44

Maneely R. B 1959 Epididymal structure and function: a historical and critical review Acta Zool., 40 1–21

Moore, C. R. and W J Quick 1924 Properties of the gonads as controllers of somatic and psychical characteristics. VII. Vasectomy in the rabbit. Am. J Anat., 34: 317–336.

Muratori, G. 1953 Sulla motilita spontanea del canale dell'epididimo del ratto. Anatomia Umana, 1: 29–36.

——— 1953 Ulteriori osservazioni sulla motilita spontanea del canale dell epididimo. Boll. Soc. Ital. Biol. Sper., 29: 1026–1028

——— 1956 Osservazioni perliminari sull' azione dell'adrenalina e dell'acetilcolina sui movimenti del canale dell epididimo del ratto. Boll. Soc. Ital. Biol. Sper., 32 248–249

Muratori, G., and S. Contro 1951 Osservazioni sui movimenti del canale dell'epididimo. Boll. Soc. Ital. Biol. Sper., 27: 538–539.

Risley P L. 1958 The contractile behavior in vivo of the ductus epididymidis and vasa efferentia of the rat. Anat. Rec., 130: 471 (Abst.)

——— 1963 Physiology of the male accessory genital organs. In: Mechanisms Concerned with Conception. C. G. Hartman. McMillan, New York pp. 73–133.

Risley P L., and N Skrepetos 1964 Histochemical distribution of cholinesterases in the testis, epididymis and vas deferens of the rat. Anat. Rec., 148: 231–241

Risley P L., and C. Turbyfill 1957 Studies in vivo of the contractile behavior of the epididymis. Anat. Rec., 128: 607–608 (Abst.)

Risley P L., and R. L. Van de Velde 1959 Contractility of the ductus epididymidis in newborn male rats, and histogenesis of smooth muscles of the Wolffian duct. Anat. Rec., 134: 629 (Abst.)

Sclavunos, G. 1893 Ueber die feineren Nerven und ihre Endigungen in den männlichen Genitalien. Anat. Anz., 9: 42–51.

Seto H 1963 Sensibility of the urogenital organs. In: Studies on the sensory innervation. Thomas, Springfield, Illinois, p. 277

Simeone F A. 1933 A neuromuscular mechanism in the ductus epididymidis and its impairment by sympathetic denervation. Am. J Physiol., 103: 582–591

Sjöstrand, N O 1965 The adrenergic innervation of the vas deferens and the accessory male genital glands. Acta Physiol. Scand., 65 suppl. 257 pp 1–82.

Toothill, M. C., and W C. Young 1931 The time consumed by spermatozoa in passing through the ductus epididymidis of the guinea pig as determined by means of India ink injections. Anat. Rec. 50: 95–107

Van de Velde, R. L., and P L. Risley 1963 The origin and development of smooth muscle and contractility in the ductus epididymidis of the rat. J Embry Exp. Morph., 11 369–382.

Young W C., and F A. Simeone 1930 Development and fate of spermatozoa in the epididymis and vas deferens in the guinea pig. Proc. Soc. Exp. Biol. Med., 27 838–841.

PLATES

PLATE 1

EXPLANATION OF FIGURES

Cholinergic innervation of caput, corpus and cauda epididymidis (dog)

1 Caput epididymidis: proximal parts of ductuli efferentes. There are few interstitial and peritubular nerve fibers. AChE. × 10.

2 Corpus epididymidis: proximal end. A moderate number of interstitial, few peritubular and some tunical nerves (T) are seen. AChE. × 10

3 Cauda epididymidis: proximal third. Both interstitial and peritubular nerve fibers and bundles are more abundant than in either caput or corpus epididymidis. The peritubular nerves form a loose bidimensional plexus. AChE. × 10.

4 Cauda epididymidis: middle third The peritubular plexus is more prominent, more intricate (tangentially cut tubules TT) and has more nerve bundles (NB) than in the proximal third. AChE. × 10.

5 Cauda epididymidis: distal third. The tubule is surrounded by a very rich peritubular plexus which is differentiated into a subepithelial (SE) and muscular (M) plexus. The muscular plexus has the appearance of a neuroterminal plexus with interspersed AChE-containing "interstitial cells" The ramifications of the plexus are related to individual or more frequently to groups of smooth muscle cells. AChE. × 10.

DUAL INNERVATION OF MAMMALIAN EPIDIDYMIS

Ahmed El-Badawi and Eric A. Schenk

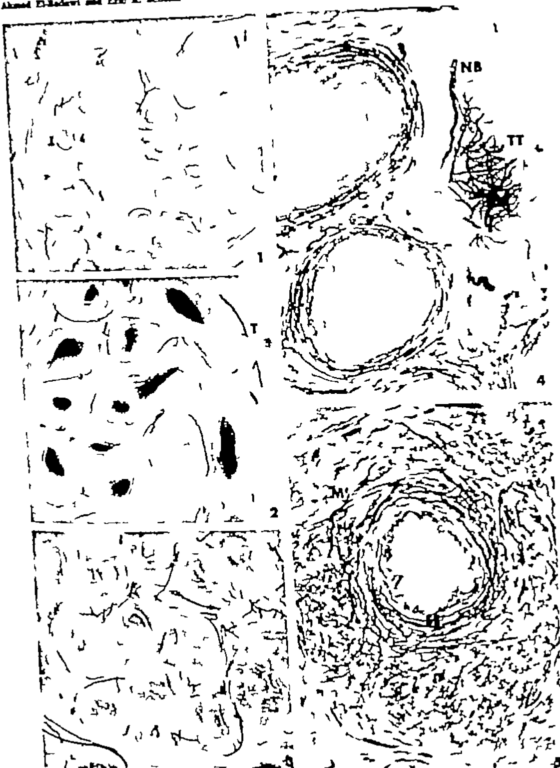


PLATE 2

EXPLANATION OF FIGURES

Adrenergic innervation of caput corpus and cauda epididymidis.

6 Caput epididymidis rat. Nerves are confined to interstitial blood vessels. NE. × 200

7 Corpus epididymidis; distal end rat. There are some interstitial fibers, and a few peritubular and tunical perivascular (T) fibers Autofluorescent pigment granules are present in the epithelial cells of the ductus epididymidis. NE. × 80

8 Cauda epididymidis; proximal third rabbit There are a moderately prominent bidimensional peritubular plexus and numerous branching and intercommunicating interstitial nerve bundles NE. × 80

9 Cauda epididymidis middle third rabbit There are a tridimensional peritubular and a rich perivascular plexus (V) An interstitial nerve bundle (NB) branches into the peritubular plexus Few epithelial fibers (E) are seen. NE. × 80

10 Cauda epididymidis distal third rabbit. There are very rich and highly intricate subepithelial (SE) and muscular (M) peritubular plexuses The latter communicate freely with a narrow meshed interstitial plexus (I) The arrangement of the fibers of the muscular plexus suggests a closed network pattern NE. × 80

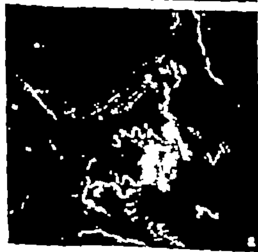
11 Cauda epididymidis distal third dog Interstitial nerve bundles form a plexus. NE. × 200


6


E
NB
V
9


T
7


M
SE
10


8

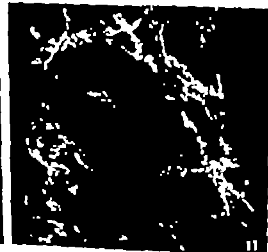

11

PLATE 2

EXPLANATION OF FIGURES

Adrenergic innervation of caput, corpus and cauda epididymidis.

6 Caput epididymidis, rat. Nerves are confined to interstitial blood vessels. NE. × 200

7 Corpus epididymidis: distal end rat. There are some interstitial fibers and a few peritubular and tunical perivascular (T) fibers. Autofluorescent pigment granules are present in the epithelial cells of the ductus epididymidis NE. × 80

8 Cauda epididymidis proximal third rabbit. There are a moderately prominent bidimensional peritubular plexus and numerous branching and intercommunicating interstitial nerve bundles. NE. × 80

9 Cauda epididymidis middle third rabbit There are a tridimensional peritubular and a rich perivascular plexus (V) An interstitial nerve bundle (NB) branches into the peritubular plexus Few epithelial fibers (E) are seen. NE. × 80.

10 Cauda epididymidis distal third rabbit. There are very rich and highly intricate subepithelial (SE) and muscular (M) peritubular plexuses The latter communicate freely with a narrow-meshed interstitial plexus (I) The arrangement of the fibers of the muscular plexus suggests a closed network pattern NE. × 80

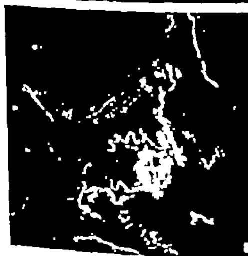
11 Cauda epididymidis distal third dog. Interstitial nerve bundles form a plexus NE. × 200


V
6


E
NB
V
9


T
7


M
SE
10


8

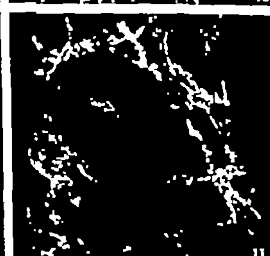

11

PLATE 2

EXPLANATION OF FIGURES

Adrenergic innervation of caput, corpus and cauda epididymidis

6 Caput epididymidis, rat. Nerves are confined to interstitial blood vessels. NE. × 200

7 Corpus epididymidis distal end rat. There are some interstitial fibers and a few peritubular and tunical perivascular (T) fibers Autofluorescent pigment granules are present in the epithelial cells of the ductus epididymidis. NE. × 80

8 Cauda epididymidis proximal third rabbit There are a moderately prominent bidimensional peritubular plexus and numerous branching and intercommunicating interstitial nerve bundles. NE. × 80

9 Cauda epididymidis; middle third rabbit. There are a tridimensional peritubular and a rich perivascular plexus (V) An interstitial nerve bundle (NB) branches into the peritubular plexus. Few epithelial fibers (E) are seen. NE × 80

10 Cauda epididymidis distal third rabbit. There are very rich and highly intricate subepithelial (SE) and muscular (M) peritubular plexuses. The latter communicate freely with a narrow meshed interstitial plexus (I) The arrangement of the fibers of the muscular plexus suggests a closed network pattern NE. × 80

11 Cauda epididymidis; distal third dog. Interstitial nerve bundles form a plexus. NE. × 200

DUAL INNERVATION OF MAMMALIAN EPIDIDYMIS
Ahmed El-Badawi and Eric A. Schenk

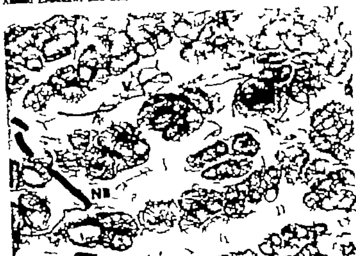












PLATE 3

EXPLANATION OF FIGURES

Cholinergic and adrenergic innervation of caput and cauda epididymidis.

12 Caput epididymidis: distal segments of ductuli efferentes cat. There are numerous isolated cholinergic interstitial nerve fibers a large interstitial nerve bundle (NB) which gives rise to interstitial and peritubular fibers a moderately well developed perivascular plexus (V) and a prominent bidimensional cholinergic peritubular plexus. AChE. × 10

13 Caput epididymidis: distal segments of ductuli efferentes, cat. There is a tridimensional adrenergic peritubular plexus NE. × 80.

14 Epithelial nerves: distal third of cauda epididymidis rabbit. An epithelial fiber (E) derived from the adrenergic subepithelial peritubular plexus (SE) penetrates through most of the thickness of the epithelium NE. × 200

15 Epithelial nerves: distal third of cauda epididymidis rabbit. Numerous epithelial fibers arise from the cholinergic subepithelial peritubular plexus penetrate through most of the thickness of the epithelium (E) and branch and intercommunicate as a loose *intra-epithelial network* AChE. × 100

16 Vascular nerves cauda epididymidis dog Large tunical arteries are surrounded by a rich cholinergic perivascular plexus from which fibers extend into the tunica media. Tunical nerve bundles (NB) lie next to the arteries AChE. × 40

17 *Vascular nerves: cauda epididymidis dog Nerve fibers extend from the adrenergic* perivascular plexus into the tunica media of a moderate sized interlobar artery (A) A large septal nerve bundle (NB) lies next to the artery NE. × 80

Skeletal Changes in Murine Runt Disease [1]

DAVID J. SIMMONS AND RICHARD L. SIMMONS[2]

Radiological Physics Division, Argonne National Laboratory, Argonne, Illinois and Department of Surgery, Columbia University College of Physicians and Surgeons, New York, New York

ABSTRACT Runt disease was produced in neonatal F_1 hybrid mice by the injection of spleen cells from a mature donor of the parental strain. Clinically apparent running appeared after the tenth day. Mice were serially sacrificed when 11–19 days old, and their long bones were examined histologically and histochemically. In runt disease, development of the epiphyseal secondary centers of ossification was retarded. The cells and protein polysaccharides did not mature normally, and the tissue contained acellular cartilage. Accumulations of hypertrophic chondrocytes signified impaired endochondral ossification. While the osteogenic cells in the medullary spaces had been replaced largely by mononuclear lymphoid cell infiltrates, bone collagen was present on unremodeled metaphyseal trabeculae which possessed wide cartilage cores. The intertrabecular spaces were moderately fibrotic. Large remnants of unossified unresorbed cellular cartilage were frequently observed in the metaphysis. It appeared that the generalized graft-versus-host reaction induced by the spleen cell "grafts" was extended to the skeleton, but that the changes in the cartilage and bone tissue had occurred largely before the onset of clinical runting.

It is well known that newborn F_1 hybrid mice injected with competent spleen cells from a mature parental strain donor become sickly, fail to grow normally, and die shortly thereafter from runt disease. Runt disease — a term originally coined by Billingham, Brent and Medawar ('56) appears to be the result of the immunologic attack of the grafted cell population against the immunologically incompetent host. Such graft-versus-host reactions (GVH reactions) have been the subject of several recent reviews (Billingham, '59; Nisbet and Heslop, '62; Simonsen, '62). The runt disease in mice may involve involution of the thymus and lymph nodes, splenomegaly, hepatomegaly and hepatic and skin lesions (Billingham and Brent, '59; Nisbet and Heslop, '62; Russell, '60; Simonsen et al., '58; Simonsen, '60). No previous studies of the effect of this syndrome on skeletal development have been reported.

Many studies, however, have been concerned with the immunologic reactions to transplanted bone and cartilage. Isogenic bone grafts survive better than allogenic grafts which behave as do most other tissue allografts in activating a host immune response (Marchand, '01; Ham and Harris, '56; Heiple et al., '63; Heslop et al., '60; Nisbet et al., '60; Williams, '62; Zeiss et al., '60). Few cells survive the allograft response to fresh bone transplants although long-term osteocyte survival has been observed in a small number of experiments (Heslop et al., '60). The inability of immunologically competent cells to pass through the small diameter canaliculi of bone to gain access to the cells is deemed responsible for this occasional survival (Heslop et al., '60). Cartilage allografts appear to be exempted from rejection even in recipients rendered immune by donor skin grafts (Gibson et al., '57; Peer, '58; Craigmyle, '60). This privileged nature of the cartilage graft is probably the result of the peculiar physiochemical nature of the mucoprotein cartilage matrix which acts to interfere with the release of transplantation antigens and prevents host lymphocytes from gaining contact with the chondrocytes (Akamine et al., '54; Peer, '54).

Grafts of embryonic (Chalmers and Ray, '61; Ray et al., '52) and early postnatal intact bones (Bert, 1863; Barnicot, '41; Felts, '57, '59; Gill, '15; Gillett et al., '37; Huggins and Blocksom, '36; Koski et al., '62; Peer, '55; Ray and Sabet, '63; Sabet et al., '61; Willis, '36) also elicit allograft reactions which cause abnormal cartilagin-

[1] This work was performed under the auspices of the U. S. Atomic Energy Commission and was supported in part by grant CA-07[illegible] awarded by the National Institutes of Health.

[2] Recipient Mead-Johnson Award, American College of Surgeons.

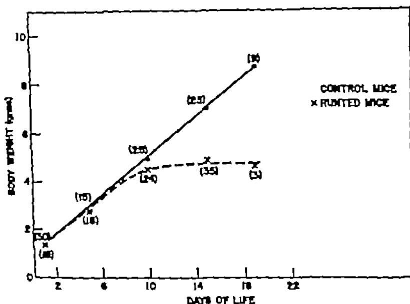


Fig. 1 A plot of weight gained vs. time (days) which shows that F hybrid mice affected by runt disease fail to sustain normal increments 10–19 days after injection of parental spleen cells.

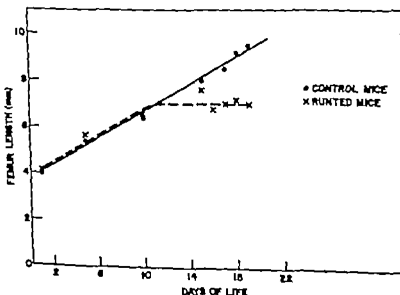


Fig. 2 A plot of femur length vs. time (days) which shows that the longitudinal growth of the femur of newborn F hybrid mice is abolished ten days after the injection of parental spleen cells.

ous and osseous growth While the transplanted bones may grow longitudinally for some days or weeks they are ultimately rejected (Felts 57 '59)

All such studies suffer the disadvantages of transplants of tissues which are removed from their normal vascular supply The present studies were undertaken to investigate the effects of immunologically com petent allogenic spleen cells upon the development of the normally vascularized growing limb bones in host mice during the lethal progress of runt disease.

METHOD

Highly inbred strains of mice obtained from the Jackson Memorial Laboratory Bar Harbor Maine were used throughout these experiments C_3H/HeJ females were mated with C57BL/6J males and on the day of delivery the ($C_3H \times C57$)F hybrid offspring were injected intraperitoneally with $15 \times 10_6$ spleen cells from C57BL/6J donors suspended in saline The spleen cells were prepared by the technique de scribed by Billingham et al ('56)

Littermate controls were injected with *an equal volume of saline (0 1 ml) These* were appropriately marked by tail clipping and kept in cages with their mothers until sacrifice or death The litter members were weighed on the day of birth and three times a week thereafter as well as on day of sacrifice Randomly selected litter pairs were sacrificed on days 1 5 10 15 16 17 18 and 19 At autopsy the spleens were dissected out and weighed on a Mettler Balance A spleen index — the standard index of runting (Simonsen 62) — was computed for certain groups (days 1 5 *10 15 18*) by dividing the average spleen weight/body weight ratio of the runted mice by the ratio of the normal littermate *controls The femurs of these groups of* mice were measured from radiographs by calipers and both femurs and tibias (10–19 day old mice) were fixed in 10% neu tral formalin decalcified in 10% EDTA (pH 7 4) embedded in paraffin and cut longitudinally at 5 μ on a rotary microtome The sections were stained with hematoxylin eosin and azure II toluidine blue for metachromasia the Periodic Acid Schiff reaction and the Masson's Tri chrome stain to demonstrate connective tissue

RESULTS

Weight gain femur length and spleen index

The results comparing the weight gain of the control and runted mice have been plotted in figure 1 Few runted animals *survived after 17 days* The graph shows that the mice in both groups gained equivalent amounts of weight during the first *ten days but, thereafter the recipients* of parental spleen cells failed to grow and the survivors were only half as heavy as the controls by 19 days Identical results were obtained when femur lengths were compared (fig 2) The spleen indices suggested that the size of the spleen of the injected mice increased three fold after ten days and the peak value occurred at the point when the curves for femur length and weight gain diverged (fig 3)

Bones from control mice 10–19 days after spleen cell "grafts

The epiphyseal secondary center of ossification was well-developed 11 days post *natally in control littermates* The chondrocytes had hypertrophied and were being eroded by capillaries accompanied by osteogenic cells Replacement of the epiphyseal center by thick actively remodelling bony trabeculae occurred by 15 days when the transverse epiphyseal bone separating the epiphyseal medullary cavity from the growth cartilage was established

The epiphyseal growth cartilages of the long bones had already differentiated *into* proliferative and hypertrophic zones by 11 days of age and the chondrocytes were arranged *in regular columns* Narrowing of the cartilage prior to 15 days proceeded by capillary invasion into the hypertrophied chondrocytes on both epiphyseal and metaphyseal surfaces Numerous chondroclasts were seen on the epiphyseal profile The thickness of the zone of hyper trophied cells in the growth cartilage was rapidly diminished during the eleventh (7–8 cells deep) to the fifteenth (3–6 cells deep) postnatal day and *capillary invasion* progressed evenly across the metaphyseal ossification front (fig 4) Cartilage resorp*tion* and endochondral ossification by

low) It was not apparent why most of the abnormalities were limited to the central portions of the cartilages. The result ing histologic picture was of thick irregularly branched cores of cartilage deposited in the metaphyses subsequent to capillary invasion and further removal of the growth cartilage. In several instances the invading vessels isolated segments of cartilage tissue with viable chondrocytes which were preserved intact in the metaphysis during the period when the bones were growing in length (figs. 8 9) Inasmuch as the intertrabecular spaces contained few osteoblasts or precursor cells ten days after injection, the amount of new bone deposited on the cartilage rests was always extremely limited. Similarly the metaphyseal bone was not remodelled to any great degree by osteoclastic action; in fact, the number of osteoclasts counted in a 200 μ deep band immediately below the growth cartilages were markedly reduced (7–8 mice/group: controls = 3.8 ± 0.8 osteoclasts/$4 \times 10^4 \mu^2$; runt disease = 1.9 ± 0.7 osteoclasts/$4 \times 10^4 \mu^2$)

There was no consistent distinction between normal and runt diseased mice with respect to the lengths of the metaphyseal trabeculae. Failure of resorption, observed in some mice which had survived 19 days after injection, did result, however in abnormally long trabeculae. The cortical bone of the runted mice was also thinner than normal suggesting deficient periosteal osteogenesis.

Toluidine blue staining

Metachromasia was not developed in any of the tissues examined owing perhaps to partial extraction of acid mucopolysaccharides by EDTA decalcification and alcohol dehydration subsequent to staining (Yaeger '59) In the control cartilages, only the perilacunar walls of the chondrocytes were stained blue while the hyaline cartilage matrix and thin cores of cartilage in the metaphyseal trabeculae were pale. The matrix of the cartilages from runt diseased mice, however stained very intensely The stain was taken up by granules" arranged in irregular patches and reactive material was also detected within the lacunae of the hypertrophic cells. Figure 9 shows that the depth of staining in a cellular unossified cartilaginous rest deep within the metaphysis was quite variable.

Metachromatic toluidine blue (a basic analine dye) staining a cartilage mucopolysaccharides appears to be related to the presence of free electronegative charges (Pearse, '60) in areas of active matrix formation. Its acidic groups are thought to bind calcium, and normally metachromasia disappears as the matrix calcifies (Cabrini, '61) The quality of staining, then, indicates both the presence of acid mucopolysaccharides and the degree to which they are polymerized. The observed changes in this experiment suggest that the acid mucopolysaccharides of the cartilages of mice affected by runt disease are less well-developed compared to the controls.

Periodic Acid-Schiff reaction

The intensity of the PAS-reaction depends upon the number of reactive aldehyde groups formed by periodic acid oxidation, and is inversely related to the content of mucopolysaccharides and to their state of polymerization (McLean and Urist, '61)

In the control cartilages PAS-positive material (neutral mucopolysaccharides of mucoproteins) was seen only in the lacunae of the hypertrophic cells of cartilage. The cartilage matrix stained faintly pink, while the layers of new bone deposited on the metaphyseal trabeculae stained somewhat more intensely In the tissues from runted mice, a strong PAS reaction was located not only in the hypertrophic cells of cartilage, but also in the lacunae situated in the zones of proliferation and cell enlargement. These changes suggest that the ground substance of the cartilage contained mucopolysaccharides which were poorly developed. However the bony trabeculae stained normally

Masson's trichrome stain

The slides showed that the amount of collagen deposited in the epiphyseal medullary cavities of the injected mice was slight compared to the controls. However, while collagen was present in normal amounts on the irregular cartilage cores in the metaphysis none could be detected on the rests of cellular cartilage (fig. 8) Cortical bone stained strongly in regions of periosteal

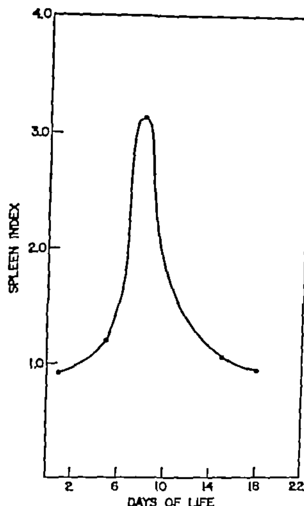


Fig. 3 A plot of spleen indices vs. time (days) which shows that the spleens of F_1 hybrid mice become 3 × normal size ten days after injection of parental spleen cells.

osteoblasts upon the residual calcified cartilage cores produced straight trabeculae projecting toward the diaphysis. The intertrabecular spaces were occupied largely by osteogenic cells. Osteoclasts were generously distributed over the diaphyseal tips of the trabeculae and along the ossification front.

Bones from runt diseased mice 10–19 days after spleen cell "grafts"

The secondary epiphyseal ossification centers were smaller and more irregularly fashioned than in the control bones, and they frequently extended into regions which would normally differentiate into articular cartilage. The degree of ossification in the affected tissues at 15 days after injection resembled that present in the controls at 11 days Complete development of the transverse epiphyseal bone was also delayed until the ninteenth day (controls = 15 days) The failure of the tissue to undergo ossification and remodelling was clearly related to the nearly complete absence of osteogenic cells (precursor cells osteoblasts) and osteoclasts on the surfaces of the cartilage bars. The cells in the developing medullary cavities were largely mononuclear lymphoid elements (fig 9)

The epiphyseal cartilages were always somewhat thicker in the mice suffering from runt disease due to impaired resorption of the tissue on both epiphyseal and metaphyseal surfaces In one mouse at 11 days fibrous tissue had completely replaced the cartilage in the center of the plate and had extended laterally between the cells of the proliferative and hypertrophic zones (fig. 10) Large patches of hyaline cartilage with a few nests of cells were commonly encountered in these tissues as well (fig 5) Preliminary cell counts (unpublished observations) suggested that there were fewer cells than normal in the proliferative zones At 12 days unresorbed hyaline cartilage could be seen projecting into the immature epiphyseal medullary cavity (fig 6) The failure of chondrocyte maturation was quite apparent. By 15 days the columns of cells in the proliferative zones were discontinuous with the columns in the hypertrophic zone and discoidal cells typical of the proliferating zones were found admixed with hypertrophic cells (fig 7)

Endochondral ossification was impaired in the bones of mice affected by runt disease a finding entirely consistent with the abnormal pattern of cellular development in the growth cartilages There was a generalized failure of capillary invasion into the columns of hypertrophic cells In some tissues the hypertrophic columns in the center of the cartilage became very long roughly V-shaped and conical aggregations of cells projected towards the diaphysis (fig 7) In other tissues capillaries had invaded some columns of cells but had avoided contact with others The selection was perhaps dictated by the presence of variable degrees of cellular hypertrophy and attendent matrix calcification (see be-

low). It was not apparent why most of the abnormalities were limited to the central portions of the cartilages. The resulting histologic picture was of thick irregularly branched cores of cartilage deposited in the metaphyses subsequent to capillary invasion and further removal of the growth cartilage. In several instances the invading vessels isolated segments of cartilage tissue with viable chondrocytes which were preserved intact in the metaphysis during the period when the bones were growing in length (figs. 8, 9). Inasmuch as the intertrabecular spaces contained few osteoblasts or precursor cells ten days after injection, the amount of new bone deposited on the cartilage rests was always extremely limited. Similarly the metaphyseal bone was not remodelled to any great degree by osteoclastic action; in fact, the number of osteoclasts counted in a 200 μ deep band immediately below the growth cartilages were markedly reduced (7–8 mice/group; controls = 3.8 ± 0.8 osteoclasts/4 × $10^4\mu^2$; runt disease = 1.9 ± 0.7 osteoclasts/4 × $10^4\mu^2$).

There was no consistent distinction between normal and runt diseased mice with respect to the lengths of the metaphyseal trabeculae. Failure of resorption, observed in some mice which had survived 19 days after injection, did result, however, in abnormally long trabeculae. The cortical bone of the runted mice was also thinner than normal suggesting deficient periosteal osteogenesis.

Toluidine blue staining

Metachromasia was not developed in any of the tissues examined owing perhaps to partial extraction of acid mucopolysaccharides by EDTA decalcification and alcohol dehydration *subsequent to staining* (Yaeger '59). In the control cartilages only the perilacunar walls of the chondrocytes were stained blue while the hyaline cartilage matrix and thin cores of cartilage in the metaphyseal trabeculae were pale. The matrix of the cartilages from runt diseased mice however stained very intensely. The stain was taken up by "granules" arranged in irregular patches and reactive material was also detected within the lacunae of the hypertrophic cells. Figure 9 shows that the depth of staining in a cellular unossified cartilaginous rest deep within the metaphysis was quite variable.

Metachromatic toluidine blue (a basic analine dye) staining a cartilage mucopolysaccharides appears to be related to the presence of free electronegative charges (Pearse, '60) in areas of active matrix formation. Its acidic groups are thought to bind calcium, and normally metachromasia disappears as the matrix calcifies (Cabrini, '61). The quality of staining, then, indicates both the presence of acid mucopolysaccharides and the degree to which they are polymerized. The observed changes in this experiment suggest that the acid mucopolysaccharides of the cartilages of mice affected by runt disease are less well-developed compared to the controls.

Periodic Acid-Schiff reaction

The intensity of the PAS-reaction depends upon the number of reactive aldehyde groups formed by periodic acid oxidation, and is inversely related to the content of mucopolysaccharides and to their state of polymerization (McLean and Urist, '61).

In the control cartilages PAS-positive material (neutral mucopolysaccharides of mucoproteins) was seen only in the lacunae of the hypertrophic cells of cartilage. The cartilage matrix stained faintly pink, while the layers of new bone deposited on the metaphyseal trabeculae stained somewhat more intensely. In the tissues from runted mice, a strong PAS reaction was located not only in the hypertrophic cells of cartilage, but also in the lacunae situated in the zones of proliferation and cell enlargement. These changes suggest that the ground substance of the cartilage contained mucopolysaccharides which were poorly developed. However the bony trabeculae stained normally.

Masson's trichrome stain

The slides showed that the amount of collagen deposited in the epiphyseal medullary cavities of the injected mice was slight compared to the controls. However while collagen was present in normal amounts on the irregular cartilage cores in the metaphysis none could be detected on the rests of cellular cartilage (fig. 8). Cortical bone stained strongly in regions of periosteal

and endosteal growth doubtless due to the preferred orientation of the collagen fibers normal to the long axis of the bone but these "growth lines" were always thinner in the tissue from runt disease mice

DISCUSSION

Body weight and spleen index

The changes in body weight and spleen index detailed in this study are consistent with the description of experimental runt disease in the literature. Our data confirm the findings by Russell (60) that F_1 hybrid mice injected with spleen cells from a mature animal of a parental strain grow normally during the first ten days and that a growth plateau supervenes thereafter as a prelude to death. That few of our runted mice survived after 17 days and that these gained only 50% of the final control weight was also reported by Billingham and Brent ('59) In mice Russell ('60 '62) and others have remarked that the weight gain plateau is accompanied by atrophy of the lymph nodes splenic enlargement and in certain cases by liquifaction necrosis of liver tissue at the free edges of the lobules

Splenomegaly a reliable criterion of runting in mice 8–10 days after grafting (Simonsen and Jensen, '59 Simonsen '62) was also present. The histologic changes in the spleen owing to the GVH reaction were not investigated in this study but Billingham and his co-workers (59 '60) and others (Russell '60) have described hyperplasia of the germinal centers of Malpighian corpuscles and/or disappearance of original lymphoid structure with lymphatic cell infiltration Grossly the organ may pale proportionately to the dose of spleen cells and to the severity of the GVH reaction It is considered that splenomegaly is a direct consequence of the GVH reaction for it fails to occur when isogeneic spleen cells are administered (Siskind et al '60) and it occurs at approximately the same time at which skin allografts of similar genetic disparity are rejected

Femur length and the epiphyseal growth cartilage

In these studies the rate of longitudinal bone growth paralleled the changes in body weight and splenomegaly It seemed probable that the cessation of growth in the runts after ten days was also a manifestation of the GVH-reaction The cause of death and weight retardation in runt diseased mice has variously been ascribed to decreased resistance to bacterial endotoxins continuously absorbed from the gut and more generally to a widespread inhibition of mitosis in all tissues. We have observed fewer chondrocytes than normal in the growth cartilages of the long bones and it is recognized that cellular proliferation in this specialized tissue is required for longitudinal growth While normally the chondrocytes mature (hypertrophy) and mineral salts are deposited in the intervening cartilage matrix, these events do not progress in an orderly fashion in runt disease. Wide areas of essentially acellular matrix described in humerus homotransplants as necrosis by Felts (57) were found in the zones of cartilage occupied by proliferating and maturing cells The irregular patterns of toluidine blue staining suggested further that the mucopolysaccharides of cartilage were abnormally developed and that the tissue would not be properly mineralized (Bernick and Ershoff 63)

Endochondral ossification

In this study replacement of cartilage by bone proceeded discontinuously across the ossification front. The points at which capillaries invaded the cartilage were without doubt selected by the mineral content of the tissue Consequently the vessels bypassed and isolated large units of deficiently mineralized matrix which appeared as cellular cartilaginous rests deep within the metaphysis as the bone grew in length The data on femur length make it apparent that these changes must have occurred within the first ten days after spleen cell injection for the bones were not elongating during the period under study Persistance of irregular cartilaginous cores deep within the metaphysis is quite common in rats when resorption has been diminished by estrogen (Urist et al 48) or cortisone (Follis 51) treatment. However the adrenals of mice suffering from runt disease are apparently unaffected by the GVH reaction (Gorer and

Boyse, '59) Cellular cartilaginous rests were also described recently by Thomson ('66) in calf bone where resorption had failed. The extent to which abnormally large accumulations of hypertrophic cells in the growth cartilages *per se* may have resulted from continued chondrocyte proliferation after the onset of severe runting (10–19 days) cannot be determined by this study However since the bones were not growing in length during the period of histologic observation, it may be presumed that the residual mitotic activity of the cells was at best, minimal. A somewhat similar picture has been produced in experimental animals by ligating (Trueta and Amato, '60) or otherwise destroying the blood vessels supplying the metaphyseal side of the epiphyseal plate by periosteal stripping (Yabsley and Harris '65) or epiphyseal fracture (Hiller '27 in man — Brashear '59) Rickets is also characterized by abnormally long columns of hypertrophic cells in the growth cartilage proper owing to failure of calcification.

Cellular disorganization in the growth cartilage and failure of endochondral ossification are common anomalies attending homotransplantation of entire limb bones (Felts '57; Sabet et al., 61) Our results (toluidine blue staining) suggest that one of the primary skeletal involvements in runt disease is some change in the protein-polysaccharides in cartilage which prevents its normal calcification and removal. As in other tissues the skeletal effects probably first occur some time prior to the clinical appearance of the runting syndrome. Although chondrocytes seem to possess transplantation antigens (Craigmyle, '60) the survival of cartilage cells was perhaps due to tissue avascularity and the protective influence of the mucopolysaccharides which surround them. In constrast, the lymphoid tissues and medullary marrow is quickly destroyed by the GVH-reaction. These cells in cartilage allografts may demonstrate evidence of sustained metabolic activity such as intracellular glycogen (Akamine et al., '54) and mucopolysaccharide synthesis (Bacsich and Wyburn, '55a b)

Bone formation and bone resorption

These studies have not revealed any specific abnormalities of bone formation. The metaphyseal trabeculae and growth "lines" marking osteogenesis on the periosteum and endosteum were normally invested with collagen (Masson's trichrome stain) but few osteoblasts could be demonstrated. Nevertheless, the reaction of the bone of runted mice to PAS-staining was normal suggesting that its ground substance contained only highly polymerized mucopolysaccharides. The evidence of decreased resorption was based on low osteoclast counts and the presence of unresorbed metaphyseal tissue. Although the systemically debilitating effects of the graft-versus-host reaction are only beginning by the tenth day following the parental cellular infusion, it appears certain that the metabolically active cells of the growing bone had been inactive for some time. In fact osteoblasts and osteoclasts are diminished, and it is likely that the death of most of the osteogenic cells and their precursors was the direct result of the immunologic reaction The extensive involvement of the marrow by the mononuclear cell infiltrate is also evidence in favor of an immunologic death for these cells Masson's trichrome staining revealed more fibers in the intertrabecular spaces than normal, suggesting that some of the surviving bone precursor cells were induced to form fibroblasts rather than osteoblasts and osteoclasts. Osteocyte death (and extensive replacement of marrow by fibrous tissue) reported in studies of whole limb transplantation did not occur in these experiments It is assumed that the bone cells were protected from direct lethal contact with the immunologically competent cells of donor origin by their favored location deep in the matrix of bone.

From the observations reported in this paper it appears that the changes in the bones from mice affected with runt disease primarily involve alterations in the ground substance of cartilage which prevents its normal calcification, leading to impaired endochondral ossification and resorption of the tissue and concomitant cytolysis of osteogenic cells.

LITERATURE CITED

Akamine, R. N., M. B. Engel and B. G. Sarnat 1954 Cartilage. Transpl. Bull. *1:* 199

Bacsich, P and G. M. Wyburn 1955a Subcutaneous Homografts of the Xiphoid Cartilage in the Guinea Pig. Transpl. Bull., *2:* 4–6.

——— 1955b The Uptake of S^{35} in Cartilage Homografts. Transpl. Bull., *2:* 97

Barnicot, N A. 1941 Studies on the factors involved in bone absorption. I. The effect of subcutaneous transplantation of the grey-lethal house mouse into normal hosts and of normal bones into grey-lethal hosts. Am. J Anat., *68:* 497–531.

Bernick, S., and B H. Ershoff 1963 Histochemical study of bone in cortisone-treated rats. Endocrinol. *72:* 231–237

Bert, P 1863 De la Greffe Animale Paris, J B Balliere et Fils. (cited by Huggins and Blocksom, '36)

Billingham, R. E. 1959 Reactions of grafts against their hosts. Science, *130:* 947–953

Billingham, R. E., and L. Brent 1959 Quantitative studies on tissue transplantation immunity IV Induction of tolerance in newborn mice and studies on the phenomenon of runt disease. Phil. Trans. Roy Soc., London, Ser. B *242:* 439–477

Billingham, R. E., L. Brent and P B Medawar 1956 Quantitative studies on tissue transplantation immunity III. Actively acquired tolerance. Phil. Trans. Roy Soc., B., *239:* 357–414

Billingham, R. E., J B Brown, V Defendi, W K. Silvers and D Steinmuller 1960 Quantitative studies on the induction tolerance of homologous tissues and on runt disease in the rat. Ann. N Y Acad. Sci., *87:* 457–467

Cabrini, R. L. 1961 Histochemistry of ossification. International Review of Cytology (eds. G H Bourne and J F Danielli) Academic Press, *11:* 283–306.

Chalmers, J and R. D Ray 1961 The Growth of Transplanted Foetal Bones in Different Immunological Environments (unpublished report cited by Sabet et al., '61)

Craigmyle, M. B. L. 1960 A study of cartilage homografts in rabbits sensitized by a skin homograft from the cartilage donor Transpl. Bull., *26:* 150.

Felts, W J L. 1957 A comparison of subcutaneous implants of isologous and homologous immature whole mouse bones. Transpl. Bull., *4:* 131–135

——— 1959 Transplantation studies of factors in skeletal organogenesis of the rat and mouse. I The subcutaneously implanted immature long-bone of the rat mouse. Am. J Phys. Anthrop *17:* 201–216.

Follis, R. H., Jr 1951 Effect of cortisone on growing bones of the rat. Proc. Soc. Exptl. Biol. Med., *76:* 722–724.

Gibson, T., R. C. Curran and W B Davis 1957 The survival of living homograft cartilage in man. Transpl. Bull., *4:* 105–106.

Gill, A. B 1915 Transplantation of entire bones with their joint surfaces. Ann. Surg., *61:* 658–671

Gillette R., D Mardfin and L Schour 1957 Osteogenesis in subcutaneous rib transplants between normal and ia rats. Am. J Anat., *99:* 447–472.

Gorer P A., and E. A. Boyse 1959 Pathological changes in F_1 hybrid mice following transplantation of spleen cells from donors of the parental strains. Immunol., *2:* 182–193.

Ham, A. W., and W R. Harris 1956 Repair and Transplantation of Bone. In: Biochemistry and Physiology of Bone (ed. G H. Bourne), Academic Press pp. 475–505.

Heiple, I. G., S W Chase and C. H. Herndon 1963 A comparative study of the healing process following different types of bone transplantations. J Bone Joint Surg., *45-A:* 1593–1616.

Heslop, B. F L M. Zeiss and N W Nisbet 1960 Studies on transference of bone. I. A comparison of autologous and homologous bone implants with reference to osteocyte survival, osteogenesis and host reaction. Brit. J Exp. Path., *41:* 269–297

Huggins, C., and B. H. Blocksom, Jr. 1936 Changes in outlying bone marrow accompanying a local increase of temperature within physiological limits. J Exp. Med., *64:* 253–276.

Koski, K., A. L. Laadsonen and E. Luostarinen 1962 Heterologous human foetal bone transplants. Am. Med. Exp. Biol. Fenn., *40:* 319–325.

Marchand, F 1901 Der Process der Wundheilung mit Einschluss der Transplantation. Deutsche Chir Stuttgart, F Enke., *16:* 487 (cited by Huggins and Blocksom '36)

McLean, F C. and M. R. Urist 1961 Bone University of Chicago Press Chicago, Ill.

Nisbet, N W., B F Heslop and I. M. Zeiss 1960 Studies on transference of bone. III. Manifestations of immunological tolerance to implants of homologous cortical bone in rats. Brit. J Exp Path., *41:* 443–451.

Nisbet, N W., and B F Heslop 1962 Runt Disease. Brit. Med. J., Jan. 20–27 pp 129–135 206–213.

Pearse A. G E. 1960 Histochemistry Little, Brown and Co., Boston, Massachusetts.

Peer L. A. 1954 Bibliography of cartilage transplantation. Transpl. Bull., *1:* 104–107

——— 1955 The fate of complete human finger and toe bones transplanted into abdominal fat. Transpl. Bull., 2 90–91

——— 1956 Bibliography of cartilage transplantation. Addenum no. 2 Transpl. Bull., *3:* 108–109.

Ray R. D., J Degge, P Gloyd and G. Mooney 1952 Bone regeneration. An experimental study of bone-grafting materials. J Bone and Joint Surg., 34-A 635–647

Ray R. D., and T Y Sabet 1963 Bone grafts cellular survival versus induction: An experimental study J. Bone and Joint Surg. *45-A:* 337–344.

Russell, P S 1960 The weight-gain assay for runt disease in mice. Ann. N Y Acad. Sci., 87 445–451

——— 1962 Modification of Runt Disease in Mice by Various Means. In: Ciba Foundation Symposium on Transplantation (eds., G E. W

Wolstenholme and M. P Cameron) Little, Brown and Co., Boston, pp. 350–378.

Sabet, T E. B. H. Hidvegi and R. D Ray 1961 Bone immunology II. Comparison of embryonic mouse isografts and homografts. J Bone and Joint Surg., 43-A: 1007–1021.

Simonsen, M., J. Engelbreth-Holm, E. Jensen and H. Poulsen 1958 A study of the graft-versus-host reaction in transplantation to embryos, F_1 hybrids and irradiated animals. Ann. N Y Acad. Sci., 73 834–839.

Simonsen, M., and E. Jensen 1959 Graft versus Host Assay in Transplantation Chimaeras. In Biological Problems of Grafting (eds., Albert F and P B. Medawar) Blackwell Sci. Publ., Oxford, pp. 214–236.

Simonsen, M. 1960 On the acquisition of tolerance by adult cells. Ann. N Y Acad. Sci., 87: 382–387

——— 1962 Graft versus host reactions. Their natural history and applicability as tools of research. Progr. Allergy 6 349–467

Siskind, G., L. Leonard and L. Thomas 1960 The runting syndrome. Ann. N. Y Acad. Sci., 87 452–455.

Thomson, R. G. 1966 Failure of bone resorption in a calf. Path. Vet., 3: 234–246.

Trueta, J., and V P Amato 1960 The vascular contribution to osteogenesis. III. Changes in the growth cartilage caused by experimentally induced ischaemia. J Bone and Joint Surg., 42-B 571–587

Urist, M. R., A. M. Budy and F C. McLean 1948 Species difference in the reaction of the mammalian skeleton to estrogens. Proc. Soc. Exp. Biol. Med., 68 324–326.

Williams, R. G. 1962 Comparison of living autogenous and homogenous grafts of cancellous bone heterotopically placed in rabbits. Anat. Rec., 143: 93–106.

Willis, R. A. 1936 The growth of embryo bones transplanted whole in the rat's brain. Proc. Roy Soc. London, Ser B., 120: 496–498.

Yaeger, J A. 1959 Histochemistry of bone matrix during rest and resorption. J Dent. Res., 38: 1083–1095.

Zeiss, I. M., N W Nisbet and B F Heslop 1960 Studies on transference of bone. II. Vascularization of autologous and homologous implants of cortical bone in rats. Brit. J Exp. Path., 41 345–363.

PLATE 1

EXPLANATION OF FIGURES

4 A photomicrograph of the distal end of a femur from a normal F_1 hybrid mouse 15 days old showing the fully matured epiphyseal medullary cavity (EM) and cartilage growth plate (C). Note the regularity of the columns of chondrocytes Hematoxylin and eosin. 63 ×

5 A photomicrograph of the proximal end of a tibia from a 16 day old F_1 hybrid mouse injected with parental spleen cells within the first day of life. The central region of the epiphyseal plate is abnormally thick and largely acellular (compare with fig. 4) Toluidine blue stain. 63 ×

6 A photomicrograph of the distal end of a femur from a 12 day old F_1 hybrid mouse injected with parental spleen cells within the first day of life The central region of the epiphyseal plate is abnormally thick in part acellular (arrow) and contains fewer than normal numbers of dividing cells. The hypertrophic zone of cells is very thick. Compare with figure 4 Toluidine blue stain. 63 ×

7 A photomicrograph of the proximal end of a tibia from a 15 day old F_1 hybrid mouse injected with parental spleen cells within the first day of life. The central region of the epiphyseal cartilage is in part acellular and there is little continuity between the columns of cells in the proliferating and hypertrophic zones (compare with fig. 4) The columns of hypertrophic cells are abnormally long and project into the metaphysis. Note the lack of development of the epiphyseal transverse bony plate (compare with fig 4) Hematoxylin and eosin. 63 ×

PLATE 1









PLATE 2

EXPLANATION OF FIGURES

8 A photomicrograph of the distal end of a femur from a 15 day old F_1 hybrid mouse injected with parental spleen cells within the first day of life Note the enlarged zone of hypertrophic cartilage in the epiphyseal growth plate and the unresorbed unossified cellular cartilaginous rest (arrow) in the metaphysis. Masson s trichrome stain. 63 ×

9 A photomicrograph of the metaphyseal region in the distal femur of a 15 day old F_1 hybrid mouse injected with parental spleen cells within the first day of life Note the unresorbed unossified cellular cartilaginous rest the matrix of which is stained irregularly by toluidine blue and the absence of osteogenic cells on its profile The intertrabecular spaces are filled by mononuclear lymphoid cell infiltrates. Alcian blue stain 400 X

10 A photomicrograph of the proximal end of the a tibia from an 11 day old F_1 hybrid mouse which had been injected with parental spleen cells within the first day of life Fibrous tissue (F) has invaded and replaced much of the cartilage in the zone of proliferating cells. Toluidine blue stain 63 ×







Physical Histological and Roentgenographic Characteristics of the Grey Lethal Mouse

JOHN D. DOYKOS, III,[1] M. MICHAEL COHEN AND GERALD SHKLAR

Departments of Oral Pediatrics and Oral Pathology Tufts University School of Dental Medicine Boston, Massachusetts

ABSTRACT A project was undertaken to investigate the development of dental and osseous abnormalities in the grey lethal mouse. In this study particular attention was focused on the nature of these anomalies and the exact time of onset.

Twenty-five grey lethal mice, with siblings serving as controls, were sacrificed at two day intervals from the eighth to the twentieth day Color photographs and lateral full body radiographs were taken at each developmental stage studied. Microscopic sections of the jaws and femurs of each animal were prepared and stained with hematoxylin and eosin.

Abnormalities in the incisor region of the grey lethal mouse were demonstrated radiographically at the eighth day Interference with Hertwig's sheath of the developing first molar tooth was observed histologically at the eighth day Establishment of molar root bifurcation was not observed in the grey lethal mice. Bone resorption was retarded in both jaws and femurs. Differences between experimental and control animals became more apparent with increasing age.

It was thought that apical root development and osseous apposition in the area of bifurcation of developing molars, as well as resorption of bone occlusal to the crowns of the teeth are constituents in axial movement of developing teeth. Evidence tending to support this concept is presented, since all three functions were shown to be altered in the noneruption dentition of the grey lethal mouse.

The grey lethal mouse presents a challenge to investigators in the field of growth and development since the animal is characterized by the inability to resorb bone retardation of growth, abnormalities of hair pigmentation, failure of tooth eruption, cessation of weight gain after the fourteenth day of post natal life and following weaning a rapid cachectic course with an invariably fatal outcome between 21 and 30 days.

The difficulty in maintaining an adequate population of grey lethal mice is possibly the reason for the paucity of information available about this animal. Since the first report of the mutation in 1935 by Gruneberg, not more than a dozen papers have discussed various aspects of this complex creature. There is no adequate analysis of the development of the dentition of the grey lethal mouse in the literature. Since our concepts of tooth eruption are in the formative stage it was thought that a study of the nonerupting grey lethal dentition might advance some information applicable to our present day knowledge of the subject. No previous investigation of the grey lethal mouse has evaluated the tooth follicle-bone response at the base of the developing crypt which is considered by Sicher (42) and O'Brien ('58) to be of importance in the mechanism of eruption. It was felt that a radiographic and microanatomic description of the grey lethal mouse dentition could establish baselines for future attempts to modify this bizarre developmental anomaly by systemic therapy

The grey lethal mouse (symbol gl) a mutation of the house mouse (Mus musculus L.) was originally described by Gruneberg in 1935 The gene was found in an extreme dilute stock (symbol c^e) and was the homozygous product of a gl/+ c^e/+ gl/+ c^e/+ mating. Grey lethal was the simple recessive condition and the strain was perpetuated by breeding from gl/+ heterozygotes which are phenotypically indistinguishable from the normal.

For the first week of life the gl could not be differentiated from its littermates. On the eighth day post partum alterations from the typical brownish-gray fur color and the normal craniofacial profile were apparent (Gruneberg, '36) The gl lacked phaeomelanotic pigment and was therefore ren-

[1] Present address The Childrens' Hospital Medical Center Boston, Massachusetts.

dered a pure slate grey A shortened and more blunt snout was the other distinguishing characteristic. After a comparatively normal growth period of two weeks gl weight gain reached a plateau at the fifteenth day Following weaning the gl normally expired between the twenty first and the thirtieth day The precise cause of death has never been established and artificial liquid supplements have been found to afford only a temporary reprieve (Gruneberg '37)

The thymus was the only internal organ found to be abnormal. Gruneberg ('38) reported that the cortex of the thymus of the gl underwent a rapid and complete degeneration during the third week of life. Since subcutaneous injections of Thymocreain did not alter this degeneration Gruneberg hypothesized that thymus degeneration was a consequence and not the cause of the poor condition of these animals.

Retardation of bone resorption in the entire skeleton was characteristic of the gl (Bateman '54) Growing and developing bones showed a generalized osteosclerosis, and lack of remodeling at areas of normal osteoclastic activity resulted in disfigurement of the typical osseous architecture. Radiographs of the gl revealed a generalized retarded and more opaque skeletal development (Gruneberg '35) The failure of bone resorption was confirmed in histological sections of long bones which demonstrated persistence of spongiosa the product of endochondral ossification and poorly developed periosteal bone. The amount of hemopoetic tissue was reduced greatly by persisting osseous spicules.

In the jaws a lack of physiological resorption caused distortion and ankylosis of developing molars (Gruneberg, '37) Microanatomical illustrations on the tenth and eighteenth day were used to document this finding Also the continuously forming incisors did not penetrate the oral mucosa and at their apices bizarre odontomas were found. The normal arc-like configuration of the incisor was absent "eagle s beak" incisors were noted in the gl (Gruneberg 50)

Three experiments by Barnicot presented some evidence that the bone in the gl was absorbable. If transplanted into an unaffected littermate, a rib of the gl became structurally similar to that of the host (Barnicot, 41) Large doses of parathyroid hormone which killed a normal house mouse were tolerated by the gl and produced resorption of rib radius and tibia (Barnicot 45) When gl parathyroid gland and a section of gl parietal bone were transplanted into the meninges or the brain of another mouse the parietal bone adjacent to the gland showed signs of resorption (Barnicot 48)

Barnicot (47) found that, although the number of osteoclasts in the parietal bone was reduced several giant forms were present which were probably derived from the fusion of smaller ones. Therefore it was felt that the reduction in volume of available osteoclastic tissue was not significant. Watchorn in 1938 found no alteration in the chemical composition of gl bone as compared to the normal

Although thyroid and parathyroid endocrinopathies have not definitely been ruled out as the primary manifestation of the genetic mutation in the gl Gruneberg (63) thought that the gl produced normal amounts of parathyroid hormone, and its bones were capable of responding to the hormone in the normal way However the gl inactivated or destroyed parathormone at an increased rate In the same discussion Gruneberg further states "Whereas it is clear that all the bone effects are coordinated and that the dental anomalies are secondary in nature the connection of these anomalies with the absence of phaeomelanina remains obscure "

GROSS FINDINGS

Once the gl can be differentiated from its littermates at eight days of age several manifestations of the mutation are apparent on gross appraisal Generalized retarded development is responsible for the somewhat smaller than normal stature throughout its life span Absence of yellow hair pigment results in pure slate grey color rather than the typical brownish-grey pigmentation

The short dumpy grey lethal snout and more rounded configuration of the occipital region produce a craniofacial profile less tapered than that observed in the control animals Normal agile and well coordi

nated movements are not observed in the gl. Mobility is restricted and the gait of the animal is similar to that of an individual with wooden legs.

The incisors of the house mouse usually erupt on the tenth day post partum followed by the first, second and third molars on the fifteenth, twentieth, and twenty-eighth day respectively In its abbreviated life span the teeth of the gl do not appear in the oral cavity The incisors, however can be palpated through the overlying mucosa after the sixteenth day

Following weaning, the gl becomes lethargic and fails rapidly until it expires after three weeks of life. Siblings continue to grow in size and become quite obese after the fifth month.

RADIOGRAPHIC FINDINGS

Serial radiographic assessment of the gl offers an added dimension to the study The occipital region appears more obtuse in shape than that of the control animal. The osseous outline of the gl craniofacial complex is less tapered and the anteroposterior dimension is reduced in size. The differences are more apparent with increasing age.

Development of the gl incisor teeth presents an abnormal pattern on serial radiographs. In control animals at the eighth day the arc-shaped outline of the maxillary incisor is seen. This increases in size as the incisors continuously erupt. However in the eight day gl, only a radiopaque mass is seen in the maxillary incisor region which does not change significantly during subsequent periods studied. Alterations in mandibular incisor development are apparent after the tenth day As in the maxilla, control mandibular incisors on subsequent radiographs show an increase in size which is not seen in the mandibular incisors of the gl.

The long bones of the control animals present distinct cortical and central medullary areas. This differentiation cannot be made in long bones of the gl which also appear to be somewhat reduced in length at the later stages.

MICROSCOPIC FINDINGS

Teeth. As the development of maxillary and mandibular molars are almost identical in time sequence, reference will be made to these teeth only in terms of their relative position in the arch. Normally after completion of the first molar crown proliferation of Hertwig's epithelial root sheath across the coronal pulp cavity precedes the establishment, at the twelfth day of the bifurcation. The roots become calcified and grow in length through the remainder of the period studied. The first molar pierces the oral epithelium on the sixteenth day

The development of the gl first molar parallels the normal until the eighth day Infringement upon the dental follicle by surrounding unresorbed bone causes an interruption in the epithelial root sheath. No radicular calcification is seen. However an attempt at the establishment of an area of bifurcation is noted in some gl's at the twentieth day (fig. 5) The morphological outline of the tooth is interrupted on its periphery by persisting alveolus (fig. 5) Indentations are seen on both the mesial and distal surfaces, and the cusps of the first molars appear compressed. In the twenty day gl, the developing root sheath has been so compressed that it can be seen curled back upon itself (fig. 5)

Dentinogenesis in the gl is irregular and areas of interglobular dentin are seen commencing on the twelfth day (fig. 3) It will be recalled that differences in root morphology between the control and the gl also become apparent on day twelve

The development of second molars parallels the normal until the formation of the bifurcation at the twelfth day (tables 1 2) As in the first molar no growth of roots in length was observed. Calcification of radicular dentin was observed however in the gl third molars (tables 1 2)

Jaws. The jaws of the normal house mouse consist of cancellous bone enclosed within a cortical plate. Marrow spaces and well defined Haversian systems are seen. Normally axial movement of the molars is accompanied by the apposition of bone in newly formed interradicular areas starting at the twelfth day Resorption of the overlying osseous shelf (fig. 2) allows interaction of the rapidly growing root ends and the formation of bone in the bifurcation to lift the tooth occlusally (fig. 6)

TABLE 1

Summary of microscopic changes in developing grey lethal mouse and control animal molar teeth (8–20 days)

8 Day control	8 Day grey lethal
First molar — Enamel formation complete in cervical area. Epithelial diaphragm (the horizontal extension of Hertwig's epithelial root sheath) does not completely bridge apical area. Tooth surrounded by bone. Connective tissue between bone and tooth.	*First molar* — Ameloblastic layer and connective tissue on mesial aspect interrupted by bone. Continuity of Hertwig's root sheath irregular in cervical area. Tooth surrounded by bone. Epithelial diaphragm does not completely bridge apical portion of crown.
Second molar — Crown complete.	*Second molar* — Crown complete
Third molar — In proliferation stage (cap)	*Third molar* — In proliferation stage (cap)
10 Day control	10 Day grey lethal
First molar — Tooth still enshrouded by bone. Hertwig's root sheath proliferating apically *Dentinogenesis seen in crown area.*	*First molar* — Greater distance between oral epithelium and tooth than in control. Inter*ruption on mesial aspect of Hertwig's* root sheath. Bone seen encroaching on distal periodontal membrane.
Second molar — Hertwig's epithelial root sheath and epithelial diaphragm across *coronal pulp cavity*	*Second molar* — Hertwig's epithelial root sheath and epithelial diaphragm across *coronal pulp cavity*
Third molar — Morphodifferentiation stage Stratum intermedium seen.	*Third molar* — Morphodifferentiation.
12 Day control	12 Day grey lethal
First molar — Bifurcation established. Bone in area of bifurcation seen. Bone above molars no longer seen. Three layers in periodontal membrane seen. Radicular *dentin seen.*	*First molar* — More encroachment on periodontal area on mesial by bone spicules. Interglobular dentin seen On mesial no connective tissue seen in apical area has *been replaced by bone* Dense bone seen overlying tooth. Plexus intermedius partially obliterated. Dense bone also seen at fundus.
Second molar — Crown complete. Epithelial *diaphragm seen bridging apical area of* pulp tissue. No evidence of bifurcation.	*Second molar* — Enamel complete. Bone occlusal *to teeth seen.* No evidence of bifurcation
Third molar — Appositional growth of enamel and dentin.	*Third molar* — Appositional growth of enamel and dentin.
14 Day control	14 Day grey lethal
First molar — Two distinct lengthened roots visible Bony apposition in bifurcation. Plexus intermedius seen in periodontal membrane Epithelial diaphragm seen on mesial and distal of roots. Interglobular dentin.	*First molar* — Bone on mesial has interrupted enamel formation. Afunctional osteoclasts seen in bone occlusal to tooth.
Second molar — Bifurcation established. Well defined connective tissue surrounds developing tooth.	*Second molar* — Roots starting to form. Hertwig's epithelial root sheath seen with epithelial diaphragm.
Third molar — Apposition continues.	*Third molar* — Calcification of molar continues.

TABLE 1 (Continued)

Summary of microscopic changes in developing grey lethal mouse and control animal molar teeth (8–20 days)

16 Day control	16 Day grey lethal
First molar — Tooth has perforated oral mucosa. Root length has increased. More bony apposition in interradicular area. In periodontal membrane triple layered structure visible.	*First molar* — Bone still covers occlusal. Periodontal membrane invaded by bone in apical, medial and distal regions. No evidence of bifurcation. Dense bone at apical area of crown.
Second molar — Root formation continues with bifurcation apposition. Outer enamel epithelium fusing with oral epithelium.	*Second molar* — Bone overlying tooth. Root formation beginning.
Third molar — Enamel complete. Root sheath visible.	*Third molar* — Most of crown complete.
18 Day control	**18 Day grey lethal**
First molar — Continuation of development seen in 16 day animal.	*First molar* — In apical area predentin is seen curled back upon itself
Second molar — Growth of roots and apposition of bone continues.	*Second molar* — No appreciable radicular development.
Third molar — Crown complete.	*Third molar* — No adequate section available
20 Day control	**20 Day grey lethal**
First molar — Further occlusal movement apices still open.	*First molar* — Bone still enshrouded by bone. No bifurcation seen. Preradicular structures wrinkled back upon itself.
Second molar — Continuation of bony apposition in bifurcation and increase in root lengths. Tooth has pierced oral mucosa.	*Second molar* — Bifurcation established.
Third molar — Root formation initiated.	*Third molar* — Radicular lengthening seen.

TABLE 2

Life cycle of grey lethal mouse and control animal molars (8–20 days)

	First molar		Second molar		Third molar	
	Control	Grey lethal	Control	Grey lethal	Control	Grey lethal
Initiation						
Proliferation						
Histodifferentiation					8	8
Morphodifferentiation					10	10
Dentin formation begins					12	
Enamel formation begins					14	12
Crown complete	8	8	8	8	14	14
Origin of Hertwig's epithelial root sheath with epithelial diaphragm across floor of coronal pulp cavity	10	Not observed	10	14	18	18
Bifurcation established	12				20	20
Growth of root in length	12–20		14	20		
Eruption into oral cavity	16		14–20			
			20			

Connective tissue surrounding the tooth apparently disperses the forces of the proliferating odontogenic tissue in a manner which protects the bone at the bifurcation of the crypt from being resorbed The peri odontal membrane of the normally devel oping molar has three distinct zones. A central zone is flanked by two layers ad jacent to bone and tooth respectively Dur ing active eruption the fibers of this intermediate layer are constantly undergoing rearrangement Two types of connective tissue fibers adjacent to the bone can be distinguished from a network of more dense fibers approximating the bifurcation

In the gl aberrations in the alveolar tooth complex are seen even at the eighth day Spicules of bone are evident penetrating the periodontal membrane on the mesial aspect of the first molar Encroachment upon the connective tissue at the distal surface of the first molar is appar ent two days later On the eighteenth day this surrounding connective tissue is al most totally obliterated by nonresorbing spicules of bone. The bone occlusal to the molars is greatly retarded in resorption and osteocast like cells can be seen (fig 1) The vast majority of these osteoclasts are not associated with areas of resorption

At all stages studied the jaws of the gl present an irregular mosaic of calcified tissue consisting of immature trabeculated bone. Fibrous connective tissue predomi nates in the marrow spaces which nor mally would contain hematopoietic cells The jaws of gl s show atypical appositional lines

Roots of the molars never attain any appreciable length (fig 5) and sclerosed bone can be seen surrounding the tooth and from the interdental septa to inferior and superior borders of the maxilla and mandible respectively (fig 6) The distinct connective tissue membrane normally seen in the area of bifurcation is replaced by a heterogeneous layer of bone and connec tive tissue cells.

One of the purposes of this study has been to determine the characteristic den tal development in the gl Previous work has indicated that the grey lethat muta tion is first discernible at the eighth day (Lane '64) and therefore this period was used as the initial stage in our investiga tion In this study lateral full body radiographs have revealed that abnormalities in developing incisors are already visible at eight days. The possibility of detecting the presence of the grey lethal mutation at an earlier age by exposing radiographs of entire litters starting at birth and daily thereafter is being investigated.

The appearance of interglobular dentin in the gl molar concomitant with radicular and osseous abnormalities at day twelve is suggestive of a generalized metabolic alteration The persistence of spongiosa and obliteration of marrow spaces in the gl femur as seen in this study confirms previous investigations This study has shown that the jaws are composed also of immature bone with reduced numbers of osteoclasts and fibrous connective tissue filling areas normally occupied by hemopoietic cells The osteoclasts seen were not located in typical lacunae of resorption.

The microscopic sections of the gl revealed partial obliteration of the periodontal membrane by alveolar bone. Fibers of the intermediate plexus seen in control animals were not observed in the gl.

Previous reports indicate that the axial movement of the developing molars is a function of root elongation interradicular bone formation and resorption of bone occlusal to the developing tooth (Sicher 42 O'Brien, '63 Massler 41) It has also been shown that connective tissue sur rounding developing molars transmits the force of eruption such that proper func tional alterations of bones are achieved (Sicher 42) Gruneberg ('37) attributed the failure of eruption of the gl molar to the nonresorption of the bone overlying the teeth This study has demonstrated that the continuity of Hertwig's epithelial root sheath at the eighth day has already been interrupted by spicules of bone. At successive stages this preradicular structure is altered in its course by nonresorbing bone apical to the completed crown. Consequently since a bifurcation is never established the opportunity for normal apposition of bone in the interradicular area does not evolve. Obliteration of periodontal connective tissue was also considered to be responsible for the markedly reduced oc clusal movement of gl molars (Sicher 42)

The 25 gl in this investigation represent the largest number of this mutation ever examined for abnormalities of tooth and jaw development.

LITERATURE CITED

Barnicot, N A. 1941 Studies on the factors involved in bone absorption. I. The effect of subcutaneous transplantation of bones of the grey lethal house mouse into normal hosts and of normal bones into lethal hosts. Am. J Anat. 68 497–531.

——— 1945 Some data on the effect of parathormone on the grey lethal mouse. J Anat., 79 83–93.

——— 1947 The supravital staining of osteoclasts with neutral red; their distribution on the parietal bone of normal growing mice and a comparison with the mutants grey lethal and hydrocephalus-3. Proc. Roy Soc. B., 134 467–485.

——— 1948 The local action of the parathyroid and other tissues on bone in intracerebral grafts. J Anat., 82, 233–248.

Bateman, N 1954 Bone growth: a study of the grey lethal and microphthalmic mutants of the mouse. J Anat., 88 212–262.

Grüneberg, H. 1935 A new sub-lethal color mutation in the house mouse. Proc. Roy Soc. B 118 321–342.

——— 1936 Grey lethal, a new mutation in the house mouse. J Hered., 27 105–109

——— 1937 The relationships of endogenous and exogenous factors in bone and tooth development. The teeth of the grey lethal mouse J Anat., 71: 236–244.

——— 1938 Some new data on the grey lethal mouse. J Genetics, 36 153–170.

——— 1950 Animal genetics and orthodontics. The Dental Record, 70 159–160

Lane, P W 1964 Personal communication.

Massler M., I. Schour 1941 Studies in tooth eruption: theories of eruption. Amer. J Orthodont., 27 552.

O'Brien, C., S N Bhaskar and A. G. Brodie 1958 Eruptive mechanism and movement in the first molar of the rat. J D. Res., 37 467–484.

Sicher, H. 1942 Tooth eruption: the axial movement of teeth with limited growth. J D. Res., 21 395.

Warchorn, E. 1938 Some biochemical data on the grey lethal mouse. J. Genet., 36 171–178.

PLATE 1

EXPLANATION OF FIGURES

1 Fourteen day old grey lethal mouse. Nonresorbing bone noted between oral epithelium and reduced enamel epithelium. 200 ×

2 Fourteen day old control animal. Bone occlusal to cusps has been restored as tooth actively erupts. 200 ×

3 Fourteen day old grey lethal mouse. Wide area of predentin and with irregular interglobular dentin. 200 ×

4 Fourteen day old control animal. Regular dentin with narrow predentin layer 200 ×

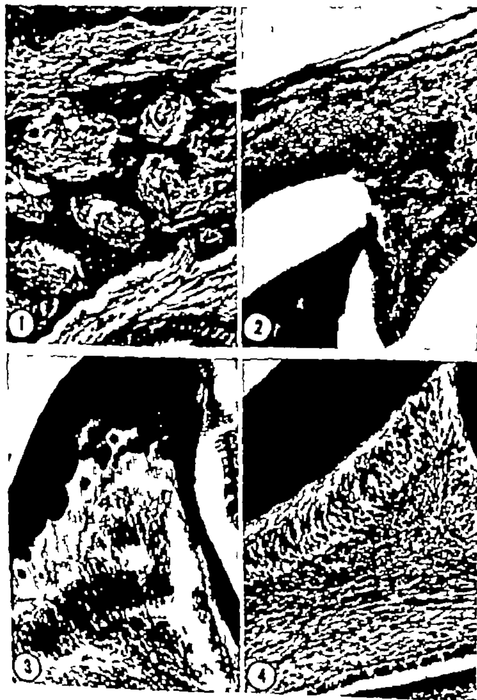

1
2
3
4

PLATE 1

EXPLANATION OF FIGURES

1 Fourteen day old grey lethal mouse. Nonresorbing bone noted between oral epithelium and reduced enamel epithelium. 200 ×

2 Fourteen day old control animal. Bone occlusal to cusps has been restored as tooth actively erupts 200 ×

3 Fourteen day old grey lethal mouse. Wide area of predentin and with irregular interglobular dentin. 200 ×

4 Fourteen day old control animal. Regular dentin with narrow predentin layer 200 ×

John D. Doykos, III, M. Michael Cohen and Gerald Shklar



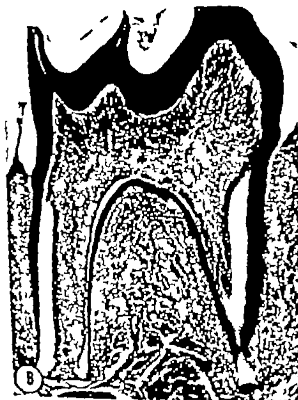


PLATE 2

EXPLANATION OF FIGURES

5 Twenty day old grey lethal mouse. Unerupted tooth. No root elongation seen. Failure of resorption of occlusal bone noted. Attempt to establish bifurcation altered by nonresorbing bone apical to crown. 90 ×

6 Twenty day old control animal. Well defined connective tissue separates bone from roots of erupted tooth. 90 ×

Efferent Fibers of the Subthalamic Nucleus in the Monkey [1]

A COMPARISON OF THE EFFERENT PROJECTIONS OF THE SUBTHALAMIC NUCLEUS SUBSTANTIA NIGRA AND GLOBUS PALLIDUS

MALCOLM B. CARPENTER AND NORMAN L. STROMINGER [2]
Department of Anatomy College of Physicians and Surgeons Columbia University, New York

ABSTRACT A study was made to determine the efferent projections of the subthalamic nucleus in the monkey Because of the impossibility of producing lesions in this nucleus, not involving adjacent structures, lesions were produced by different stereotaxic approaches. Comparisons were made with degeneration resulting from localized lesions in substantia nigra and globus pallidus. Degeneration resulting from these lesions was studied in transverse and sagittal sections stained by the Nauta-Gygax method.

Efferent fibers from the subthalamic nucleus pass through the internal capsule into the medial pallidal segment; a few fibers are distributed to the lateral pallidum. Some subthalamic efferent fibers pass to the contralateral globus pallidus via the dorsal supraoptic decussation, but none projection to the thalamus.

Nigral efferent fibers project to parts of the ventral anterior (VAmc) and ventral lateral (VLm) thalamic nuclei. The medial pallidal segment gives fibers to: (1) ventral anterior (VA) ventral lateral (VLo) and centromedian (CM) thalamic nuclei, and (2) the pedunculopontine nucleus. The lateral pallidal segment projects exclusively to the subthalamic nucleus. Thalamic projections of the substantia nigra and globus pallidus are distinctive. Subthalamic projections to the globus pallidus are more profuse than those of the substantia nigra.

The following hypothesis is presented: Subthalamic dyskinesia, due to lesions in the subthalamic nucleus, is consequence of removal of inhibitory influences acting upon the medial segment of the globus pallidus.

Clinicopathological reports (Martin, '27; Whittier '47; Jubb, '65) and experimental studies (Whittier and Mettler 49b Carpenter Whittier and Mettler, '50; Carpenter '61) indicate that discrete lesions in the subthalamic nucleus, which fulfill certain criteria almost invariably results in severe dyskinesia in the contralateral extremities. This dyskinesia, the most forceful and violent variety known, has been referred to as hemiballism or hemichorea. Experimental studies in the monkey (Carpenter Whittier and Mettler '50 Carpenter '61) suggest that this dyskinesia is the physiolog ical expression of removal of inhibitory influences that normally act upon the neurons of the globus pallidus. This thesis is supported by the fact that lesions in the medial segment of the globus pallidus abolish or ameliorate the dyskinesia. Lesions in the ventral lateral nucleus of the thalamus also can reduce or abolish this form of dyskinesia (Martin and McCaul, '59 Andy and Brown, '60) presumably by interruption of pallidothalamic fiber systems and thalamocortical projections

Although a number of studies (Carpenter and Brittin, '58; Carpenter, Correll and Hinman, '60; Strominger and Carpenter '65 Carpenter Strominger and Weiss, '65; Stein and Carpenter 65) have been done to establish structures involved in the neural mechanism of this dyskinesia in the monkey many questions remain unanswered. A full understanding of the basic neural mechanisms involved would appear to require additional evidence concerning the anatomical connections of the sub-

[1] This investigation was supported by a research grant (NB-04083-04) from the Institute of Neurological Diseases and Blindness of the National Institutes of Health, Bethesda, Maryland 20014.

[2] Predoctoral trainee in neuroanatomy supported by a grant (5T1 NB-5373-06) from the Institute of Neurological Diseases and Blindness. Dr. Strominger currently is in the Department of Anatomy at Albany Medical College of Union University

Efferent Fibers of the Subthalamic Nucleus in the Monkey [1]

A COMPARISON OF THE EFFERENT PROJECTIONS OF THE SUBTHALAMIC NUCLEUS SUBSTANTIA NIGRA AND GLOBUS PALLIDUS

MALCOLM B. CARPENTER AND NORMAN L. STROMINGER
Department of Anatomy College of Physicians and Surgeons, Columbia University New York

ABSTRACT A study was made to determine the efferent projections of the subthalamic nucleus in the monkey. Because of the impossibility of producing lesions in this nucleus, not involving adjacent structures, lesions were produced by different stereotaxic approaches. Comparisons were made with degeneration resulting from localized lesions in substantia nigra and globus pallidus. Degeneration resulting from these lesions was studied in transverse and sagittal sections stained by the Nauta-Gygax method.

Efferent fibers from the subthalamic nucleus pass through the internal capsule into the medial pallidal segment; a few fibers are distributed to the lateral pallidum. Some subthalamic efferent fibers pass to the contralateral globus pallidus via the dorsal supraoptic decussation, but none projection to the thalamus.

Nigral efferent fibers project to parts of the ventral anterior (VAmc) and ventral lateral (VLm) thalamic nuclei. The medial pallidal segment gives fibers to: (1) ventral anterior (VA) ventral lateral (VLo) and centromedian (CM) thalamic nuclei, and (2) the pedunculopontine nucleus. The lateral pallidal segment projects exclusively to the subthalamic nucleus. Thalamic projections of the substantia nigra and globus pallidus are distinctive. Subthalamic projections to the globus pallidus are more profuse than those of the substantia nigra.

The following hypothesis is presented: Subthalamic dyskinesia, due to lesions in the subthalamic nucleus, is a consequence of removal of inhibitory influences acting upon the medial segment of the globus pallidus.

Clinicopathological reports (Martin, '27; Whittier '47 Jubb, '65) and experimental studies (Whittier and Mettler 49b; Carpenter Whittier and Mettler, '50; Carpenter '61) indicate that discrete lesions in the subthalamic nucleus which fulfill certain criteria, almost invariably results in severe dyskinesia in the contralateral extremities. This dyskinesia, the most forceful and violent variety known, has been referred to as hemiballism or hemichorea. Experimental studies in the monkey (Carpenter Whittier and Mettler '50; Carpenter '61) suggest that this dyskinesia is the physiological expression of removal of inhibitory influences that normally act upon the neurons of the globus pallidus. This thesis is supported by the fact that lesions in the medial segment of the globus pallidus abolish or ameliorate the dyskinesia. Lesions in the ventral lateral nucleus of the thalamus also can reduce or abolish this form of dyskinesia (Martin and McCaul, '59 Andy and Brown, '60) presumably by interruption of pallidothalamic fiber systems and thalamocortical projections

Although a number of studies (Carpenter and Brittin, '58; Carpenter Correll and Hinman, '60 Strominger and Carpenter '65 Carpenter Strominger and Weiss, '65 Stein and Carpenter 65) have been done to establish structures involved in the neural mechanism of this dyskinesia in the monkey many questions remain unanswered. A full understanding of the basic neural mechanisms involved would appear to require additional evidence concerning the anatomical connections of the sub-

[1] This investigation was supported by research grant (NB-04083-04) from the Institute of Neurological Diseases and Blindness of the National Institutes of Health, Bethesda, Maryland 20014.

Postdoctoral trainee in neuroanatomy supported by a grant (5T1 NB-5343-05) from the Institute of Neurological Diseases and Blindness. Dr. Strominger currently is in the Department of Anatomy at Albany Medical College of Union University

thalamic nucleus Few experimental studies (Morgan '27 Glees and Wall, 46 Whittier and Mettler 49a Knook, '65) have been made of these anatomical connections presumably because of the technical difficulties involved in producing localized lesions in this small nucleus

The object of the current study was to determine the efferent fiber connections of the subthalamic nucleus in the rhesus monkey The virtual impossibility of producing stereotaxic lesions in the subthalamic nucleus without destroying adjacent structures necessitated the study of fiber degeneration resulting from other structures known to project fibers into this region As a consequence comparisons were made of the fiber degeneration resulting from localized lesions in: (1) the subthalamic nucleus (2) the substantia nigra and (3) the globus pallidus

MATERIAL AND METHODS

This study was based upon anatomical observations in 23 monkeys taken from a larger series in which attempts were made in different animals to produce discrete lesions in the subthalamic nucleus the substantia nigra (SN) and the globus pallidus

Lesions in the subthalamic nucleus were produced by three different stereotaxic approaches (1) frontal (2) posterior infratentorial and (3) lateral In the *frontal approach*, electrodes were introduced into the frontal cortex at an angle and advanced ventrocaudally into subthalamic nucleus (Carpenter Whittier and Mettler '50; Carpenter Correll and Hinman '60) When this approach was used electrodes traversed the caudate nucleus internal capsule and sometimes portions of the thalamus and/or globus pallidus In the *posterior infratentorial approach* electrodes introduced into the posterior aspect of the cerebellum traversed parts of cerebellum pons and mesencephalon and entered the caudal pole of the subthalamic nucleus While this stereotaxic approach invariably resulted in degeneration of some fibers of the superior cerebellar peduncle these fibers cross completely in the mesencephalon Thus unilateral lesions of the subthalamic nucleus made by this approach would not concomitantly interrupt cerebellar efferent fibers passing to the ipsilateral thalamus Involvement of the lateral lemniscus at isthmus levels could be detected and no degeneration from this source was followed beyond the inferior colliculus and the medial geniculate body Occasional damage to fibers of the medial lemniscus and the spinothalamic tract resulted in ascending degeneration which could be identified The advantage of this stereotaxic approach was that lesions in the subthalamic nucleus could be produced without passing electrodes through the thalamus or basal ganglia. In the *lateral approach* to the subthalamic nucleus electrodes traversed the posterior insular region the dorsal part of the putamen the dorsal part of the globus pallidus and the internal capsule The limitations of this method are obvious

Lesions in the substantia nigra (SN) were produced by a posterior infratentorial stereotaxic approach similar to that described for the subthalamic nucleus Electrodes were inserted in planes 1 or 2 mm more ventrally but were not protruded as far

Lesions in the globus pallidus were produced in different regions by electrodes introduced into the lateral surface of the brain that traversed the insular region and the putamen

Lesions in the subthalamic nucleus were produced in most instances by a single electrode placement. A direct current of 400 volts and 3 ma was applied for 10 or 15 seconds. Lesions of the SN and globus pallidus usually were made by multiple electrode placements but the current and time used to produce the lesions were the same as for the subthalamic lesions

Postoperatively daily observations were made of animals in their home cages Cinematographic records of animals with dyskinesia were made on at least one occasion At the conclusion of observation periods ranging from 14 to 26 days animals were examined in a restraining chair anesthetized and sacrificed by perfusion with a liter of normal saline followed by an equal volume of 10% neutral formalin The brains and spinal cords were removed *in toto* and further fixed in 10% neutral formalin. Brains were sectioned either perpendicular to the axis of the brain stem or

in sagittal planes. Blocks of brain were sectioned serially on a freezing microtome at 20 μ and every section was preserved in neutral formalin in plastic containers with multiple small compartments. Multiple sections through the lesion were mounted and stained by the Weil technic as well as with cresyl violet, in order to evaluate the location and extent of the lesions. In animals with lesions appropriate for study multiple representative sections from all levels of the brain were stained by the Laidlaw modification of the Nauta-Gygax ('54) technic.

OBSERVATIONS

Lesions of the subthalamic nucleus

Posterior infratentorial approach. Unilateral lesions in the left subthalamic nucleus suitable for detailed study were produced in seven monkeys (C-828 C-850 C-851 C-852, C-854 C-855 and C-857) Sections of the brains of these animals were cut perpendicular to the axis of the brain stem.

The lesion in one animal (C-855) of this group was confined within the borders of the subthalamic nucleus. Although some unavoidable degeneration resulted from concomitant interruption of fibers by the electrode *en route to* the corpus Luysi, the lesion did not involve the internal capsule, the zona incerta, the lenticular fasciculus, or the ansa lenticularis The electrode used to produce this lesion passed through the dorsolateral part of the SN and entered the caudal pole of the subthalamic nucleus, where medial parts of the nucleus were destroyed. As the subthalamic nucleus enlarged at rostral levels, the lesion destroyed the more central portions of the nucleus. Through maximal dimensions of the subthalamic nucleus, a circular lesion occupied a region of the nucleus a little lateral from the center without touching either the superior or inferior borders (fig. 4) Rostrally the lesion diminished in size and was confined to the lateral half of the nucleus The lesion terminated within the nucleus without involving its rostral pole.

Degeneration resulting from this lesion was particularly profuse in the lateral parts of the subthalamic nucleus, while medial portions of the nucleus contained smaller amounts of degeneration except ventrally Moderately large fascicles of degenerated fibers from lateral parts of the nucleus traversed the peduncular part of the internal capsule and entered the medial segment of the globus pallidus Some fascicles of degenerated fibers passed dorsally into the zona incerta and ventral parts of the thalamic reticular nucleus before crossing through the capsule to the pallidum In sections through the caudal part of the globus pallidus degeneration was concentrated in the region close to the internal capsule. At rostral levels where the lesion in the subthalamic nucleus was small, a larger number of degenerated fibers crossed through the internal capsule Most of these fiber bundles traversed the internal capsule at an acute angle and crossed through the medial pallidal segment in an oblique ventrolateral direction. Although abundant degeneration was present in the apex of the medial pallidal segment caudally a large number of the fiber bundles described above passed laterally along the ventral border of the globus pallidus to enter the internal medullary lamina. In the internal medullary lamina, these fibers passed dorsally and entered portions of both medial and lateral pallidal segments

Fibers entering the external medullary lamina were less numerous and did not project as far dorsally Pallidal degeneration was *maximal* in the medial segment in sections near and immediately rostral to the subthalamic nucleus. At more rostral levels, a progressive reduction in the amount of degeneration was seen in the pallidum. Degeneration first disappeared from the apical region but continued to be present in lateral and dorsal parts of the medial pallidal segment. The most rostral portions of the globus pallidus were free of degenerated fibers. Degenerated fibers in the globus pallidus were dispersed in the neuropil and did not arborize about large neurons. No degenerated fibers could be traced into the caudate nucleus or the putamen

Subthalamic efferent fibers coursing along the ventral surface of the globus pallidus in some instances passed between cells of the substantia innominata (basal

ganglia of Meynert) but none of the degenerated fibers appeared to establish close relationships with these cells None of these fibers entered central portions of this nucleus

A small number of degenerated fibers passing through the apical region of the globus pallidus entered the dorsal supraoptic decussation (Meynert) and could be followed across the dorsal border of the optic tract and optic chiasma into the apical region of the contralateral globus pallidus Some fibers traversing the medial pallidal segment seemed to course rostrally for a slight distance before entering the dorsal supraoptic decussation More medial subthalamic efferent fibers entered this bundle directly by crossing through the ventral parts of the internal capsule in a slightly rostral direction Crossed fibers of the dorsal supraoptic decussation entered the medial segment of the contralateral globus pallidus where most fibers projected caudally for a slight distance. Some of these seemed to pass dorsomedially between capsular fibers toward the subthalamic nucleus In this animal no unquestioned degeneration was seen in the contralateral subthalamic nucleus

A considerable number of degenerated fibers were seen medial to the subthalamic nucleus in Forel's field H A few individual fibers from this region passed rostrally and dorsally through the ventral posterior medial nucleus of the thalamus to reach the centromedian nucleus (CM) Most of the degenerated fibers in the prerubral area passed rostrally and dorsally to form a concentrated group of degenerated fibers in the medial part of the ventral lateral nucleus (VLm) lateral to the mammillothalamic tract. From this thalamic nucleus small amounts of degeneration passed dorsolaterally into the magnocellular part of the ventral anterior nucleus (VAmc) (fig. 14) These fibers seemed to terminate about large cells in this nucleus. No preterminal degeneration was seen in any other part of the ventral anterior nucleus

One or two degenerated fibers emanating from the region medial to the subthalamic nucleus crossed in the supramammillary decussation These fibers entered the contralateral prerubral area and were lost among degenerated ascending cerebellar efferent fibers. None of these fibers could be followed into the opposite subthalamic nucleus

In sections through the caudal pole of the subthalamic nucleus degenerated fibers passed ventrally toward the SN and medially toward the red nucleus. Degenerated fibers in the dorsolateral part of the pars compacta of the substantia nigra were so intimately related to the electrode track that their significance could not be determined Caudal to the subthalamic nucleus degeneration in lateral parts of the SN persisted close to the electrode track, this degeneration diminished at lower levels but did not disappear

Part of the degenerated fibers seen in the prerubral area entered rostral portions of the red nucleus where fibers closely surrounded individual neurons Arborizations about cells of the red nucleus were most numerous rostrally and diminished at successively caudal levels. No degenerated fibers descended on the ventral or lateral borders of the red nucleus.

Passage of the electrode through the cerebellum produced moderate degeneration in the ipsilateral superior cerebellar peduncle which could be followed into the right red nucleus thalamic fasciculus the ventral part of the ventral lateral nucleus including parts of its medial subdivision and portions of the more rostral intralaminar nuclei.

At midbrain levels degenerated fibers dorsal to the electrode track projected into the superior colliculus. These appeared to be mainly corticotectal fibers. Injury to the lateral lemniscus at isthmus levels produced ascending degeneration in the ipsilateral inferior colliculus and a small part of the medial geniculate body Although distinct degeneration was present in the ipsilateral pedunculopontine nucleus (Olszewski and Baxter '54) its significance could not be determined in the presence of other tegmental degeneration No descending degeneration was seen in the corticospinal tract or in the principal portions of the pontine or medullary reticular formation.

Lesions in six other animals of this group were not as discrete or perfectly localized as in rhesus C-855. These lesions

involved structures adjacent to the subthalamic nucleus, usually the internal capsule the lenticular fasciculus or the zona incerta.

In three of these animals (C-850 C-852, and C-854) (fig 3) the lesions destroyed relatively few fibers of the internal capsule, but some fibers of the lenticular fasciculus were concomitantly interrupted. Degeneration projecting to the globus pallidus in these animals was similar to that described in rhesus C-855 (figs. 7 8) A few of the degenerated fibers coursing laterally along the ventral surface of the pallidum traversed dorsal parts of the substantia innominata, but few of these fibers seemed to end among cells in this nucleus. No degeneration was seen among more ventrally located cells of this nucleus. No degenerated fibers entered any part of the neostriatum.

A number of small bundles of degenerated fibers originating from the lesions in the subthalamic nucleus, and in some instances, from the region of the electrode track caudal to the lesion, crossed through the peduncular part of the internal capsule. Caudally these fibers entered the area between the cerebral peduncle and either the lateral geniculate body or the optic tract. Rostrally similar fibers crossed through the internal capsule traversed parts of the medial globus pallidus, and formed a bundle of degenerated fibers on the dorsal surface of the optic tract. These degenerated fibers, located dorsal to the optic tract, could be followed across the optic chiasma to the opposite side In two animals (C-852 and C-854) degeneration appeared to be present in both the dorsal (Meynert) and ventral (Gudden) supra optic decussation. Contralateral fibers of the dorsal supraoptic decussation entered the apex of the globus pallidus. A few fibers projected dorsally between capsular fibers, but these could not be followed through the internal capsule. Fibers entering the opposite globus pallidus appeared to pass somewhat caudally; some of these fibers also passed dorsomedially into the internal capsule. In rhesus C-854 a few degenerated fibers were seen in caudal parts of the right subthalamic nucleus. Caudal to the globus pallidus and the subthalamic nucleus degenerated fibers, thought to be associated with the ventral supraoptic decussation, were seen between the cerebral peduncle and the lateral geniculate body These fibers mainly entered the capsule of the medial geniculate body Similar degeneration in the dorsal supraoptic decussation was seen in rhesus C-850 (figs. 9 10) The distribution of these fibers contralaterally was virtually the same as described above One or two degenerated fibers seemed to enter the caudal part of the opposite subthalamic nucleus.

Ipsilateral thalamic degeneration in these animals was more profuse and more widely distributed than in rhesus C-855 Degeneration passing medially from the lesions entered VLm and projected from this location into VAmc as previously described. In addition, considerable degeneration of pallidothalamic fibers was present due to concomitant involvement of the lenticular fasciculus. These degenerated fibers could be followed laterally into the thalamic fasciculus and into ventral portions of the ventral lateral (VLo) and the ventral anterior (VA) nuclei. Degeneration in VA was scattered and less profuse than that present in VAmc. Pallidofugal fibers were traced also into the ipsilateral CM in all of these animals. These fibers passed rostrally and dorsally through the ventral posterior medial nucleus to enter the centromedian nucleus.

In two (C-850 and C-854) of these animals, some degeneration was present in the ventral posterior lateral and medial thalamic nuclei as a consequence of passage of the electrode through parts of the medial lemniscus. No similar degeneration was present in these nuclei in rhesus C-852 in which the medial lemniscus was not involved by the electrode.

Descending degeneration seen in these three animals was essentially the same as described in rhesus C-855. Considerable degeneration was present in lateral portions of the substantia nigra in the vicinity of the electrode track. Most of these fibers were in the pars compacta, but degeneration was not confined to this subdivision.

Rostral portions of the ipsilateral red nucleus contained large numbers of degenerated fibers that closely surrounded in-

dividual cells. In addition, a distinct bundle of degenerated fibers was present along the lateral and ventral borders of the red nucleus. A few of these latter fibers seemed to enter mediodorsal regions of the substantia nigra. In successively caudal sections the degeneration seen in the red nucleus disappeared. Fibers descending ventrolateral to the red nucleus coursed dorsolaterally into the tegmentum where they were lost in degeneration associated with passage of the electrode through the brain stem. Degeneration was seen in the ipsilateral pedunculopontine nucleus and in a small number of corticopontine fibers. No degeneration was present in the medullary pyramids.

In the remaining three animals of this group, lesions in the subthalamic nucleus concomitantly involved fibers of the internal capsule. Lesions in two animals (C-826 and C-851) destroyed capsular fibers ventral to the subthalamic nucleus. Neither of these lesions directly involved the lenticular fasciculus, ansa lenticularis, zona incerta or thalamic fasciculus. The circular subthalamic lesion in rhesus C-857 destroyed the most medial part of the nucleus but extended rostrally to involve fibers of the internal capsule as well as part of the lenticular fasciculus.

Pallidal degeneration resulting from these lesions was essentially the same as previously described. Involvement of capsular fibers did not seem to modify the distribution or the amount of degeneration in the globus pallidus.

In both of these animals, degenerated fibers from the lesion coursed through the cerebral peduncle and entered the dorsal supraoptic decussation. Fibers in more rostral regions crossed the internal capsule and passed through medial parts of the globus pallidus. These fibers crossed to the opposite side and appeared to enter the medial part of the globus pallidus. Contralateral degenerated fibers passed caudally and seemed to project dorsomedially between fibers of the cerebral peduncle. A few questionably degenerated fibers were seen in caudal parts of the subthalamic nucleus in rhesus C-851. No degeneration was seen in the ventral supraoptic decussation in either animal.

In addition, a few individual degenerated fibers crossed to the opposite side in the supramammillary decussation but could not be traced beyond the prerubral region.

The lesion in rhesus C-857 in the medial part of the subthalamic nucleus appeared to be associated with more degeneration passing among the cells of the substantia innominata than in other animals. Fibers entered this nucleus from the ventral surface of the ipsilateral globus pallidus but did not arborize about individual cells.

Thalamic degeneration in rhesus C-826 and C-851 was selectively distributed to VLm from which region it projected into the ventral and caudal parts of VAmc. Preterminal fibers closely surrounded these large cells in a manner suggesting a terminal arborization. Caudal portions of CM contained a relatively scant degeneration as did the VLo and VA.

Ipsilateral thalamic degeneration in rhesus C-857 was extensive. It was distributed to all parts of the ventral anterior nucleus (VA and VAmc) to parts of the ventral lateral nucleus (VLo and VLm) and to CM.

Degeneration in the ipsilateral substantia nigra in these animals was profuse in lateral parts of the nucleus and scattered in other areas. This degeneration was associated with injury caused by the electrode and interruption of fibers descending in and traversing the internal capsule. Rostral portions of the ipsilateral red nucleus contained considerable degeneration closely surrounding cells in rhesus C-826 and C-851. At successively caudal levels degeneration in the nucleus became spotty and disappeared.

In rhesus C-857 the red nucleus contained very little degeneration but profuse degeneration was seen ventrolateral to the nucleus. Similar but less marked, degeneration was seen in rhesus C-826. Some of these fibers passed among large cells in the most medial and dorsal parts of the substantia nigra. This bundle of degenerated fibers passed dorsolaterally into the lower midbrain tegmentum. Although degenerated fibers were seen about cells of the ipsilateral pedunculopontine nucleus as in other animals of this group the source of the fibers could not be de-

terminated. Degenerated fibers of the superior cerebellar peduncle coursed through this nucleus and some degeneration was present in the lateral lemniscus. Other degeneration in the brain stem appeared related to passage of the electrode and concomitant injury to descending fibers in the internal capsule.

Frontal approach. Relatively discrete unilateral lesions in the left subthalamic nucleus were produced in two animals (C-842 and C-859) by electrodes inserted into the frontal cortex and advanced ventrocaudally (fig 5). Electrodes passed through the head of the caudate nucleus, entered the anterior limb of the internal capsule between the caudate nucleus and putamen and, at more caudal levels, traversed the posterior limb of the internal capsule between the globus pallidus and the thalamus. Electrodes enter the oral part of the subthalamic nucleus damaging some, but not all, of the fibers of the lenticular fasciculus. Lesions developed in rostrolateral parts of the subthalamic nucleus, but, as the nucleus enlarged, were situated more centrally. A small number of capsular fibers were destroyed ventral to the subthalamic nucleus but the lesions terminated without destroying any part of the SN.

Degeneration in the globus pallidus resulting from these lesions was essentially the same as described for lesions produced by the posterior infratentorial approach. In the vicinity of the lesion numerous fascicles of degenerated fibers traversing the internal capsule formed a group of degenerated fibers medioventral to the pallidum and dorsal to the optic tract. These degenerated fibers crossed to the opposite side in the dorsal supraoptic decussation (Meynert). Contralaterally they entered the globus pallidus, but convincing evidence of termination upon pallidal neurons was not seen. At various locations, a few fibers passed dorsomedially between capsular fibers, but none of these fibers could be traced in the contralateral subthalamic nucleus. No degenerated fibers were present in the supramammillary commissure.

Thalamic degeneration in these animals appeared to be almost exclusively pallidothalamic as a consequence of passage of the electrode through the internal capsule and interruption of fibers in the lenticular fasciculus. These fibers entered the principal part of the ventral anterior (VA) and the ventral (VLo) nuclei via the thalamic fasciculus. VAmc was free of degeneration and only minimal degeneration was seen in the most lateral parts of VLm. Considerable degeneration from the thalamic fasciculus entered CM. No degeneration was seen in any part of the hypothalamus or in the contralateral thalamus.

Degeneration in Forel's field H was profuse but oral parts of the red nucleus contained degeneration mainly in medial regions. A concentrated bundle of descending degenerated fibers formed along the ventral border of the red nucleus; some of these fibers entered dorsomedial parts of the substantia nigra. In successively caudal sections degeneration within the red nucleus gradually disappeared, but fibers ventral to this nucleus continued. Near the caudal pole of the red nucleus and the decussation of the superior cerebellar peduncle, these degenerated fibers migrated dorsolaterally into the tegmentum. At levels through the inferior colliculus, these fibers closely surrounded cells of the pedunculopontine nucleus. Areas of the tegmentum caudal to this nucleus contained few degenerated fibers. While rostral midbrain sections contained numerous degenerated fibers passing dorsally to the superior colliculus, no similar fibers entered the inferior colliculus.

Although the lesion did not involve the substantia nigra, it was difficult to evaluate degeneration in that nucleus because of concomitant injury to the internal capsule. Both the pars compacta and pars reticularis contained degenerated fibers. Portions of the substantia nigra ventromedial to the subthalamic nucleus contained profuse degeneration. In more caudal regions, degeneration in the SN was scattered except in medial portions of the pars compacta.

Degenerated fibers in the pons and medulla could be traced into the left pontine nuclei, the reticulotegmental nucleus, the pontine and medullary reticular formation and the medullary pyramid. All

of these degenerated fibers appeared to represent interrupted corticofugal fibers

Bilateral lesions of the subthalamic nucleus attempted by a frontal approach were successful in three animals (C-766, C-777 and C-787) but, in a fourth animal (C 792) a lesion in this nucleus was produced only on the right side. Bilateral symmetrical lesions in the subthalamic nuclei in rhesus C-766 and C-777 were remarkably similar these lesions destroyed dorsal and central parts of the subthalamic nucleus as well as some fibers of the lenticular fasciculus Although fibers in the internal capsule were injured by passage of the electrode no part of the substantia nigra was destroyed by the lesion or the electrode The degeneration on each side resulting from these lesions was the same as described above for unilateral lesions produced in this fashion. The only degenerated fibers observed to cross the midline were those in the dorsal supra optic decussation No degenerated fibers were seen in the supramammillary decussation

The lesion in the right subthalamic nucleus in rhesus C-792 was the same as the bilateral lesions described above except that the lesion extended caudally in rostral parts of the substantia nigra. Degeneration resulting from this lesion was the same as in all other animals with lesions produced by this stereotaxic approach, except in the thalamus In addition to degenerated fibers passing to the ipsilateral VA VLo and CM degenerated fibers were present in VLm and from this nucleus they could be followed into ventral portions of VAmc

Bilateral symmetrical lesions of the subthalamic nuclei in rhesus C-787 appeared unique among the animals of this group in that they destroyed very few fibers of the lenticular fasciculus on either side Caudally these lesions extended into the SN Pallidal degeneration resulting from these lesions was profuse in the apical part of the medial segment caudally and about the internal and external medullary laminae Degeneration crossing in the dorsal supraoptic decussation was especially prominent, apparently because the lesions were bilateral These fibers could not be traced beyond their entrance into the apical part of the globus pallidus on each side nor due to other degeneration could unusually prominent degeneration present in the supramammillary commissure be traced laterally

Bilateral thalamic degeneration resulting from these symmetrical lesions resembled that seen ipsilateral to subthalamic lesions produced by the posterior infratentorial approach This degeneration was profuse and largely limited to VLm and the VAmc Only sparse degeneration was seen in the VA VLo and CM

In the substantia nigra degenerated fibers were most numerous in the vicinity of the lesions and were present in both the pars compacta and pars reticularis. In caudal parts of the nigra, degenerated fibers were sparse

Although oral parts of the red nuclei and the areas ventromedial to the nuclei contained degenerated fibers they were not numerous Degeneration in these locations rapidly disappeared at more caudal levels Sections through the level of the inferior colliculus revealed only sparse degeneration in the right pedunculopontine nucleus Other relatively modest descending degeneration in the lower brain stem appeared related to the interruption of corticofugal fibers in the internal capsule

Lateral approach. In one animal (C-975) a lesion was produced in the left subthalamic nucleus by an electrode inserted at an angle into the lateral surface of the brain The electrode traversed the insular cortex, the dorsal part of the putamen the dorsal part of the lateral segment of the globus pallidus, and passed obliquely through the internal capsule to enter the dorsolateral part of the subthalamic nucleus (fig 6) The lesion began in the internal capsule ventral to the lenticular fasciculus and destroyed the entire lateral half of the subthalamic nucleus rostrally Futher caudally the lesion involved more medial parts of the subthalamic nucleus The caudal third of the nucleus was not destroyed, and no part of the SN was injured Passage of the electrode through the internal capsule dorsal to the medial segment of the globus pallidus interrupted fibers of the lenticular fasciculus but the extent of the degeneration in this bundle

was much less than might have been expected.

Evaluation of pallidal degeneration in this animal was extremely difficult because of the presence of the electrode track. Considerably more degeneration was present in the lateral pallidal segment than in other animals. However sections through caudal parts of the pallidum contained many degenerated fascicles that entered the medial segment by traversing the internal capsule. A large number of these fibers continued laterally along the ventral surface of the pallidum to enter the internal medullary lamina. Although a few fibers on the ventral surface of the pallidus passed between cells of the substantia innominata, none entered the main part of the nucleus and no arborizations were seen about individual cells. Degenerated fibers entering the dorsal supraoptic decussation could be followed into the contralateral globus pallidus; these fibers were more widely dispersed in the medial pallidal segment than in most animals (figs. 11 12)

Thalamic degeneration in this animal was entirely ipsilateral and reached the lateral nuclear group via the thalamic fasciculus. This degeneration was distributed to parts of VA and VLo At more caudal levels fibers passed into the centromedian (CM) nucleus where degeneration seemed greatest in more medial regions. No other degeneration was seen in the thalamic nuclei.

Descending degeneration in this animal passed medially towards the prerubral area. Some of these fibers entered oral parts of the red nucleus while others passed ventrally between the red nucleus and the substantia nigra. A few of these fibers seemed to enter among the large cells of the most medial part of the pars compacta of the SN A larger number of these fibers coursed dorsolaterally into the tegmentum to enter the pedunculopontine nucleus. The presence of other tegmental degeneration suggested that not all of these fibers were derived from the same source.

Degenerated fibers entered the substantia nigra laterally as well as from dorsal regions. These fibers were distributed to both the pars compacta and the pars reticularis. Because both corticonigral and strionigral fibers were interrupted in this animal, it was not possible to determine if any fibers from the subthalamic nucleus projected to the substantia nigra. A considerable central part of the cerebral peduncle contained degenerated fibers. Descending degeneration in the pons and medulla appear to represent only corticofugal fibers interrupted in the internal capsule.

Lesions in the substantia nigra

In two animals unilateral lesions in the substantia nigra were produced by a posterior infratentorial approach, slightly modified from that used for producing lesions in the subthalamic nucleus The lesions in rhesus C-896 began in the lateral part of the SN caudal to root fibers of the oculomotor nerve and extended rostrally to levels of the fasciculus retroflexus Two coalescing lesions sharply delineated from the underlying peduncle destroyed central portions of the SN ventrally Although this lesion mainly occupied the pars reticularis of the SN numerous groups of large cells also were destroyed (fig. 15) No part of the subthalamic nucleus was destroyed by the lesion. The lesion in rhesus C-906 destroyed only a small dorsal part of the rostral substantia nigra (fig. 19) The electrode passed over the dorsal surface of the SN and the lesion was situated in the dorsal part of the SN immediately caudal to the subthalamic nucleus. The lesion destroyed a moderate number of cells in the pars compacta of the nigra and the tip of electrode penetrated the caudal border of the subthalamic nucleus. Observations in this animal were significant because the lesion interrupted ascending fibers from a relatively large part of the SN No fibers in the cerebral peduncle were destroyed in either animal.

Degeneration resulting from these lesions was studied in transverse (C-896) and sagittal sections (C-906) and only the most pertinent observations will be reported. Ascending fibers from these lesions passed lateral to the red nucleus and entered Forel's field H. From this location, the largest number of fibers passed dorsally and rostrally into VLm where many fibers closely surrounded individual cells.

A considerable number of these fibers projected rostrally and laterally into VAmc (*fig 20*) *None of these fibers* were distributed to the more lateral principle part of VA (fig 1)

A relatively small number of SN efferent fibers passed laterally from Forel's field H across the dorsal surface of the subthalamic nucleus, penetrated the peduncular part of the internal capsule and entered the medial segment of the globus pallidus Most of these fibers remained relatively close to the internal capsule but *small numbers of individual fibers* were seen in other parts of the globus pallidus None of these SN *efferent fibers appeared* to enter the putamen Rostral portions of both the medial and lateral pallidal segment were free of degeneration

No degeneration was seen in the subthalamic nucleus in rehesus C-896 a relatively small number of degenerated fibers *in this nucleus in rhesus C-906* appeared due to minimal direct injury It *was of interest in rhesus C-906 that the* lesion located mainly dorsal to the rostral part of the SN interrupted many descending fibers distributed to dorsal parts of the SN These appear to be corticonigral fibers No degenerated fibers entered the ipsilateral red nucleus

Because the electrodes *traversed* the brain stem degeneration observed at various lower levels was only questionably related to the lesion. Degeneration was consistently present in the superior and inferior colliculi lateral parts of the midbrain tegmentum and portions of the pontine nuclei Degenerated fibers passing *to the inferior colliculus were due to* injury to the lateral lemniscus. Although degeneration was present in the ipsilateral pedunculopontine nucleus the continuity of descending fibers passing to this nucleus could not be followed.

SN lesions and the resulting degeneration were restudied in three other animals (C-688 C-723 and C-724) previously reported (*Carpenter and McMasters '64*) These unilateral lesions were produced by electrodes introduced in a coronal plane at an angle which nearly corresponded to that of the lateromedial axis of the SN The lesions in two animals (C-723 and C-724) destroyed nearly the entire medial half of the SN while the lesion in rhesus C-688 primarily involved the pars compacta in *the lateral half of the nucleus* (fig. 17) The electrodes used to produce these lesions destroyed portions of the medial geniculate body and some fibers of the medial lemniscus. Damage to the cerebral peduncle was minimal and no part *of the* putamen globus pallidus or subthalamic *nucleus was damaged by the electrode or* the lesion

---

Abbreviations

AC, anterior commissure
AV anterior ventral thalamic nucleus
BC, brachium conjunctivum
CG central grey
CI, inferior colliculus
CL, central lateral thalamic nucleus
CM centromedian thalamic nucleus
CS superior colliculus
DM, dorsomedial thalamic nucleus
FX, fornix
GPl, lateral segment globus pallidus
GPm medial segment globus pallidus
H_1 thalamic fasciculus
H_2, lenticular fasciculus
Hb habenular nucleus
IC, internal capsule
LD lateral dorsal thalamic nucleus
LL, lateral lemniscus
ML, medial lemniscus
MM mammillary nucleus
MTT mammillothalamic tract
OC, optic chiasma
OT optic tract
PCN paracentral thalamic nucleus
Pf parafasciculus nucleus
Pul, pulvinar
Put, putamen
PY medullary pyramid
RN red nucleus
SN substantia nigra
STN subthalamic nucleus
VA ventral anterior thalamic nucleus
VLc ventral lateral thalamic nucleus (pars caudalis)
VLm, ventral lateral thalamic nucleus (pars medialis)
VLo, ventral lateral thalamic nucleus (pars oralis)
VPM ventral posterior medial thalamic nucleus
x, cell group x, Olszewski
ZI, zona incerta
III N oculomotor nerve
IV N trochlear nerve
VI N abducens nerve

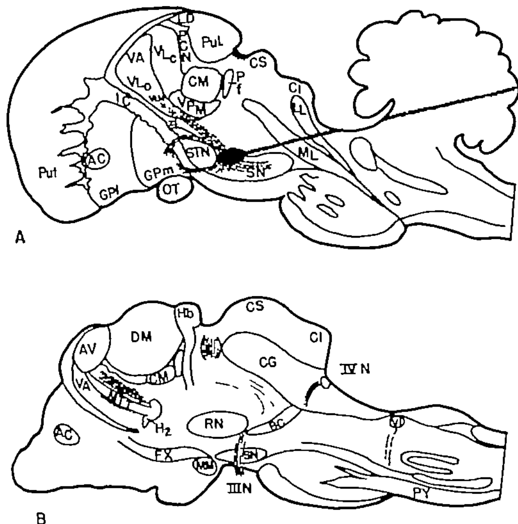


Fig. 1 Drawings of sagittal sections of the brain based upon observations made in rhesus C-906. In A, the electrode track and lesion are shown. Ascending degeneration is shown coursing dorsal to the subthalamic nucleus, to the ventral lateral nucleus (VLm) of the thalamus, and through the internal capsule to the globus pallidus. A small number of fibers to the globus pallidus pass ventral to the subthalamic nucleus. In B a more medial section, ascending degeneration is seen in the magnocellular part of the ventral anterior nucleus (VAmc) and in parts of VLm. The latter nuclei are not labeled but both lie dorsal to the mammillothalamic tract (MTT) with VAmc occupying most of this region.

Ascending degeneration resulting from these lesions was virtually identical with that described above. Quantitatively the largest number of ascending fibers projected to VLm and to VAmc (fig. 16) In these animals, the lesion in the lateral part of the SN produced the most abundant thalamic degeneration. Pallidal degeneration, passing laterally from Forel's field H over the dorsal surface of the subthalamic nucleus and traversing the peduncular part of the internal capsule, was more modest in amount and distributed largely to caudal and medial portions of the medial segment. Only a few degenerated fibers were seen in the lateral pallidal segment. No

degeneration was seen in the contralateral thalamus or globus pallidus In all of these animals degeneration was seen in the ventral supraoptic decussation (Gudden) These degenerated fibers were followed from the damaged area near the right medial geniculate body along the optic tract optic chiasma, and opposite optic tract into ventrolateral parts of the contralateral medial geniculate body

In only one (C-723) of these animals were degenerated fibers seen in the subthalamic nucleus these fibers located in the ventromedial part of the nucleus were relatively sparse. Degenerated fibers in the red nucleus were relatively modest in number although considerable numbers of degenerated fibers were present along the lateral and ventral borders of this nucleus.

Degeneration observed in the superior and inferior colliculi, lateral parts of the midbrain tegmentum and portions of the pontine nucleus appeared related to interruption of corticotectal fibers or the passage of the electrode Cells of the ipsilateral pedunculopontine nucleus were surrounded by degenerated fibers but degeneration of multiple descending fiber systems from higher levels precluded precise evaluation of the source of these fibers Relatively few corticospinal fibers were degenerated at medullary levels.

Lesions of the globus pallidus

Lesions in different portions of the globus pallidus were produced by electrodes introduced from the lateral surface of the brain in five monkeys Because observations concerning pallidofugal fibers from lesions of this type have been reported in detail recently (Nauta and Mehler 66) only the most pertinent findings will be described here

Lateral pallidal segment. In three animals (C-894 C-898 and C-961) lesions were largely limited to the lateral segment of the globus pallidus Sections of the brain were cut transversely perpendicular to the axis of the brain stem. Although lesions in these animals were not identical in size or position the resulting degeneration was similar and findings can be presented in a composite fashion Lesions in the lateral pallidal segment were present at levels through the optic chiasma where both segments of the pallidum were well developed. The lesions in rhesus C-894 and C-898 destroyed dorsal parts of the lateral pallidal segment (fig 25) while the lesion in rhesus C-961 destroyed ventral portions of this pallidal segment. In all animals lesions involved the entire width of the lateral pallidal segment and extended slightly beyond the internal medullary lamina. Electrodes traversed parts of the insular cortex and the putamen, but no fibers of the internal capsule were damaged by the electrode or the lesion

Degeneration resulting from these pallidal lesions passed medially and caudally into the medial segment of the globus pallidus. This degeneration was in more dorsal parts of the medial pallidal segment in rhesus C-894 and C-898 and in more ventral regions in C-961 At levels near the oral pole of the subthalamic nucleus bundles of degenerated fibers turned dorsally passed through the internal capsule at a steep angle and entered the dorsolateral part of the subthalamic nucleus Profuse preterminal degeneration within rostral portions of the subthalamic nucleus was confined to roughly the lateral half of the nucleus (fig 26) but at successively caudal levels the most concentrated region of degeneration shifted to central portions of the nucleus. Caudal portions of the subthalamic nucleus contained less degeneration limited to dorsocentral regions. The pattern of degeneration described above was virtually the same in rhesus C-894 and C898 In rhesus C-961 degeneration from the lesion in the ventral part of the lateral pallidal segment entered the subthalamic nucleus at more caudal levels, and was more profuse in portions of the nucleus nearest the internal capsule This pattern of disposition persisted at more caudal levels. In none of these animals, was degeneration present in the most medial third of the subthalamic nucleus

Moderate degeneration was seen in the external and internal medullary laminae of the globus pallidus but few of these fibers could be followed for any distance In two animals (C-894 and C-961) small amounts of scattered degeneration were seen in lateral portions of the ventral anterior nucleus This modest degeneration

appeared to result from minimal injury to the medial pallidal segment and consequent degeneration in the lenticular fasciculus (C-894) and ansa lenticularis (C-961). Sparse degeneration was seen in CM in rhesus C-894. In this animal, a few pallidotegmental fibers were traced to the ipsilateral pedunculopontine nucleus similar degeneration was not seen in other animals. All animals of the group showed degenerated fibers passing into the lateral part of the SN which seemed to be limited to the pars reticularis. SN degeneration appeared to be related to passage of the electrode through the putamen.

Medial pallidal segment. Lesions in two animals destroyed selectively portions of the medial pallidal segment. The lesion in rhesus C-980 was confined to the central part of the medial pallidal segment and was maximal at levels through the optic chiasma (fig. 21) In rhesus C-960 a smaller slightly more rostral lesion destroyed portions of the medial pallidal segment but infringed upon the lateral pallidum (fig. 23) No fibers of the internal capsule were destroyed by these lesions. Degeneration resulting from these lesions was studied in transverse (C-980) and sagittal (C-960) sections.

Lesions in these animals produced similar degeneration in pallidofugal projections with one notable exception. In rhesus C-960 no fibers of the lenticular fasciculus were degenerated. In rhesus C-980 degeneration was seen in both pallidal segments rostral to the lesion. Degenerated fibers were more profuse in the lateral part of the medial pallidal segment. As the lesion developed in more caudal sections distinct fascicles of degenerated fibers passed: (1) medially and dorsally towards the internal capsule to form the lenticular fasciculus, and (2) directly medially to form the ansa lenticularis. Degenerated fibers of the lenticular fasciculus penetrated the internal capsule at a steep angle and coursed along the internal border of the internal capsule. Fibers of the ansa lenticularis swept around the medial border of the internal capsule to join the lenticular fasciculus in Forel's field H. The bulk of these pallidofugal fibers curved laterally in the thalamic fasciculus. Degenerated fibers in the thalamic fasciculus coursed dorsolaterally into VLo and VLm where degeneration was profuse. At more rostral levels these fibers were distributed to the lateral part of VA (fig. 22) No degenerated fibers were seen in VAmc or in Olszewski's ('52) cell group x. Degenerated fibers passing to CM separated from the thalamic fasciculus at nearly right angles coursed through the ventral posterior medial nucleus, and entered the ventral surface of CM over a rather broad area. Degenerated fibers were seen in nearly all parts of CM, but degeneration in this nucleus was not as profuse as that seen in VLo and VLm and VA.

A small distinct bundle of degenerated fibers from Forel's field H projected medially over and through the fibers of the fornix. These fibers coursed ventromedially toward the hypothalamus, diminishing rapidly in number Relatively few fibers appeared to reach the medial nuclei of the hypothalamus. Close scrutiny of these fiber bundles did not reveal that these fibers "looped" backward to join other pallidofugal fibers, as described by Nauta and Mehler ('66)

Profuse degeneration was seen in rostral and lateral parts of the subthalamic nucleus. Degenerated fibers entering this nucleus passed through the internal capsule at levels caudal to the lenticular fasciculus. At successively caudal levels diminished degeneration was seen in the subthalamic nucleus. The medial third of the subthalamic nucleus was free of degeneration at all levels.

A small number of degenerated fibers coursing along the dorsal border of the subthalamic nucleus passed medial to the nucleus. This bundle of degenerated fibers also received some fibers that coursed ventral to the subthalamic nucleus. At more caudal levels, these descending fibers were loosely scattered along the ventrolateral border of the red nucleus. As these fibers descended they shifted laterally and dorsally to become partially intermingled with the fibers of the medial lemniscus. At isthmus levels, these fibers were seen arborizing about large cells of the pedunculopontine nucleus above and below the fibers of the superior cerebellar peduncle (fig. 24) Levels of the brain stem caudal

to the isthmus did not contain degenerated fibers

Sections through the SN revealed a moderate number of degenerated fibers in lateral portions of the nucleus These fibers passed through the peduncular part of the internal capsule at subthalamic levels Most of the degenerated fibers were seen in the pars reticularis A few degenerated fibers descending ventral to the red nucleus appeared to enter the pars compacta of the SN but these were not numerous

Observations made from the sagittal sections in rhesus C-060 were qualitatively similar to those described above even though no fibers of the lenticular fasciculus were degenerated Degenerated fibers in the ansa lenticularis could be traced into Forel s field H and into the thalamic fasciculus Thalamic degeneration was present in VLo and VLm VA and CM Pallidofugal fibers passing to the subthalamic nucleus traversed the internal capsule and were distributed mainly to oral and lateral parts of the nucleus Fibers passing to the substantia nigra (presumably from the putamen) crossed the internal capsule ventral to the subthalamic nucleus and entered the oral pole of the SN These fibers descended for a considerable distance within the SN mostly within the pars reticularis

In sections through medial parts of the subthalamic region descending pallidotegmental fibers could be followed dorsal to the substantia nigra directly to the pedunculopontine nucleus Although only part of these fibers were present in single sections their entire descending course was beautifully displayed

DISCUSSION

Comparisons of the degeneration resulting from lesions in the subthalamic nucleus produced by different stereotaxic approaches emphasizes the virtual impossibility of producing localized lesions in this nucleus that do not involve adjacent structures or fiber systems With the Nauta technic passage of the electrode through the brain stem or subcortical regions alone can produce significant degeneration that complicates interpretation of observations. For these reasons it was considered essential to produce lesions in the subthalamic nucleus by multiple stereotaxic approaches. As a control it was considered necessary to study the degeneration resulting from localized lesions in the SN and globus pallidus since fibers arising from these nuclei commonly were involved in producing lesions in the subthalamic nucleus.

The pattern of degeneration within the thalamus following lesions in the subthalamic nucleus produced by different stereotaxic approaches was not the same which suggested that different thalamic afferent fibers were interrupted concomitantly in producing these lesions When lesions in the subthalamic nucleus were produced by the frontal approach, some fibers of the lenticular fasciculus were almost invariably interrupted and thalamic degeneration was seen ipsilaterally in VA, VLo and CM Degeneration seen in these nuclei was never as profuse or as widely distributed as the resulting from lesions in the medial pallidal segment, but the pattern of distribution was the same Thalamic degeneration seen following subthalamic lesions produced in this manner and following lesions in the medial pallidal segment was entirely ipsilateral Bilateral lesions of the subthalamic nucleus in rhesus C-787 presented an instructive difference Lesions in this animal spared most but not all, of the lenticular fasciculus and only sparse degeneration was seen in thalamic nuclei that receive pallidofugal fibers. The lesions in this animal however directly involved the substantia nigra As a consequence profuse degeneration was seen in VLm and VAmc

In all animals in which lesions of the subthalamic nucleus were produced by the posterior infratentorial stereotaxic approach thalamic degeneration was seen in VLm and VAmc Degeneration in these thalamic nuclei appeared to result from injury to the SN or interruption of ascending nigral efferent fibers The distribution of these fibers within the thalamus was identical with that resulting from localized lesions of the SN that did not involve the subthalamic nucleus Additional thalamic degeneration in VA VLo and in CM in some of these animals resulted when pallidofugal fibers were interrupted

The above observations strongly suggest that the subthalamic nucleus does not pro-

ject fibers to any part of VA, VAmc VLo VLm or CM. The observations of Nauta and Mehler ('66) are confirmed concerning the distribution of pallidothalamic fibers. Data with respect to nigrothalamic fibers are consistent with the observations of Cole, Nauta and Mehler ('64) and Afifi and Kaelber ('65)

There are certain important anatomical questions which cannot be answered definitely from this study One of these concerns a possible projection from the subthalamic nucleus to the SN Since lesions of the subthalamic nucleus made by a frontal stereotaxic approach almost invariably involved striofugal, pallidofugal, and corticofugal fibers no definite statement concerning subthalamonigral fibers can be made. It appears well established that strionigral fibers pass to the pars reticularis (Voneida, '60; Szábo '62) and that putaminonigral fibers traverse the globus pallidus (Nauta and Mehler '66) Whether pallidal fibers project to the SN or not is unresolved in spite of acceptance of this pathway by some authors (Wilson, '14; Kodama, '28a Johnson and Clemente, '59). The suggestion of Nauta and Mehler ('66) that collaterals of pallidotegmental fibers may terminate in a small medial part of the pars compacta of the SN seems likely Corticonigral fibers have been regarded as one of the largest groups of afferent fibers passing to the SN (Dejerine '01 von Monakow '14 Levin, '36 44; Mettler 47) but a recent study (Rinvik, '66) in the cat indicates that this fiber system (1) arises almost exclusively from motor and sensory areas, (2) is less substantial than indicated in the literature, and (3) terminates mainly in the neuropil of the substantia nigra.

Although authors of prior experimental studies of the subthalamic nucleus (Morgan, '27; Glees and Wall, 46; Whittier and Mettler 49a) have described subthalmonigral fibers in Marchi-stained material, it is obvious that the above criticisms also apply to their studies. However there is good evidence (Carpenter and McMasters, '64 Cole, Nauta and Mehler '64) that the subthalamic nucleus does not receive fibers from the substantia nigra.

Another anatomical point not entirely resolved in the current study concerns the origins of descending tegmental fibers that arborize about cells of the pedunculopontine nucleus. Ipsilateral degeneration passing to the pedunculopontine nucleus unquestionably arises from the medial segment of the globus pallidus as described by Nauta and Mehler ('66) These fibers become identifiable as a distinct bundle dorsomedial to the subthalamic nucleus and further caudally are dispersed about the ventral and lateral borders of the red nucleus. Some pallidotegmental fibers appear to pass from the main bundle into a wedge-shaped group of large cells in the most dorsomedial part of the SN but the main bundle passes dorsolaterally into the midbrain tegmentum. These fibers arborize about the relatively large cells in the compact part of the pedunculopontine nucleus which lies dorsal to the fibers of the superior cerebellar peduncle. Cells of this nucleus actually are traversed by fibers of the superior cerebellar peduncle as they shift ventromedially towards their decussation.

Fibers passing to the pedunculopontine nucleus were seen frequently in association with lesions in the subthalamic nucleus and SN Concomitant involvement of pallidofugal fibers would seem to account for this descending degeneration in animals where lesions were made by a frontal approach. Because electrodes passed through parts of the midbrain in the infratentorial approach, no conclusions concerning this tract can be based upon this material, but it seems likely that these lesions interrupted pallidotegmental fibers There is also the possibility that these lesions interrupted corticotegmental fibers. Knook ('65) considered the subthalamic nucleus to be surrounded by corticotegmental fibers, thus making it virtually impossible to determine if this nucleus gives rise to fibers descending into the midbrain tegmentum.

Similar descending tegmental degeneration also was seen in association with lesions of the SN produced by a lateral approach in this study and in that of Cole Nauta and Mehler ('64). The latter authors were reluctant to consider these descending fibers as nigral efferent fibers because hemidecortication also produced descend-

ing degeneration in the pedunculopontine nucleus

Subthalamotegmental fibers have been described by several authors (Marburg 17 Környey, '26 Gurdjian, '27 Papez, '38 41 Papez and Stotler 40 Woodburne 46 Woodburne Crosby and McCotter 46) The descriptions of this tract and is termination in the midbrain tegmentum appear virtually identical with the pallidotegmental tract (Nauta and Mehler '66) except for variations in the terminology used to designate the pedunculopontine nucleus In at least three cases of human ballism (Martin '27, von Santha, '28; Moersch and Kernohan '39) fibers of the subthalamotegmental tract were said to be degenerated In each of these cases the lesions in the subthalamic nucleus destroyed some fibers of the lenticular fasciculus According to Papez (41), the pedunculopontine nucleus (referred to as the nucleus profondus mesencephali) receives both subthalamotegmental and nigrotegmental fibers In experimental studies (Morgan '27; Whittier and Mettler 49a) using the Marchi method no degeneration was traced from lesions in the subthalamic nucleus to the pedunculopontine nucleus but these authors mention fibers descending ventral to the red nucleus Whittier and Mettler (49a) reported that descending degeneration in this location was consistently associated with lesions involving the lenticular fasciculus

Available evidence suggests that most of the descending tegmental fibers appearing to arise from the medial subthalamic region and referred to by some authors as the subthalamopeduncular tract, probably are pallidotegmental fibers The possibility that some corticotegmental fibers may be intermingled with these seems likely

Although subthalamorubral projections have been described (Mirto 1896; Morgan '27; Winkler '28 Glees and Wall, 46) this connection remains in doubt. According to Glees and Wall (46) the subthalamic nucleus projects fibers bilaterally to the red nuclei; fibers were described as reaching the contralateral red nucleus via the supramammillary commissure and the ventral tegmental decussation.

In the present study proterminal degeneration was seen frequently in oral portions of the ipsilateral red nucleus but the amount of degeneration and its disposition were not consistent Available evidence suggests that most, if not all of the degeneration seen in the red nucleus was a consequence of the interruption of corticorubral fibers (Rinvik and Walberg, '63) which are said to be given off from the cerebral peduncle rostrolateral to the red nucleus Comparisons indicate that the globus pallidus gives rise to few if any pallidorubral fibers (Nauta and Mehler 66) Lesions in the SN (Carpenter and McMasters '64) likewise produced minimal degeneration in the red nucleus.

The current study indicates that the principal efferent projections of the subthalamic nucleus in the monkey are specific and not widespread (fig 2) The largest number of efferent fibers pass to the medial segment of the globus pallidus by traversing the internal capsule. A small number of subthalamic efferent fibers pass to the contralateral globus pallidus and possibility to the subthalamic nucleus, via the dorsal supraoptic decussation (Meynert) Since these efferent fibers involve primarily the globus pallidus, it seems best to turn to the discussion of pallidofugal fibers.

Pallidofugal fibers Nauta and Mehler (66) recently have reviewed this subject in detail and include important fresh observations from their own studies Briefly these authors provide superb evidence that the lenticular fasciculus (dorsal division of the ansa lenticularis von Monakow 1895) and the ansa lenticularis (ventral division of the ansa lenticularis von Monakow 1895) arise exclusively from the medial segment of the globus pallidus These pallidofugal fibers project to VA VLo and VLm and CM In addition the medial pallidal segment projects fibers to (1) the lateral habenular nucleus via the stria medullaris (2) the pedunculopontine nucleus via the pallidotegmental tract and (3) the tegmental nuclei of Forel s field H Lesions of the medial pallidal segment also produced degeneration in the subthalamic nucleus but it was not possible to determine what part of these fibers if any arose from this pallidal segment. No pallidofugal fibers were found to project to the hypothalmus or the zona incerta Most of

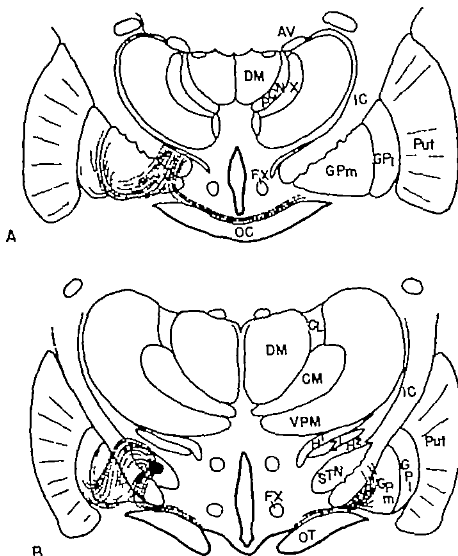


Fig. 2 Drawings of transverse sections of the brain to show the distribution of degeneration considered to arise from a lesion in the subthalamic nucleus (B) The principal degeneration traverses the internal capsule to be distributed to the medial pallidal segment (A, B). Some of these fibers enter both the internal and external medullary laminae of the pallidum. A small number of subthalamic afferent fibers enter the dorsal supraoptic decussation, cross to the opposite side, and enter the contralateral globus pallidus (A, B)

these observations were confirmed in the current study

The literature concerning pallidosubthalamic projections is extensive [Wernicke, 1881; Flechsig, 1881; von Monakow 1895 Kodama, '28a; Papez, '38 Verhaart, '50 Johnson and Clemente, '59; Knook, '65 (see review and list of references)] Excellent experimental studies (Wilson '14 Ranson, Ranson and Ranson, 41 Nauta and Mehler '66) have verified this connection in the monkey While virtually all lesions of the globus pallidus produce degeneration which passes to the subthalamic nucleus available evidence indicates that the projections of the lateral pallidal segment pass exclusively to the subthalamic nucleus and appear to ter

minate mainly in rostral and lateral parts of the nucleus. These fibers reach the subthalamic nucleus by traversing the internal capsule in the subthalamic fasciculus (middle division of the anse lenticularis von Monakow, 1895)

In pathological material Vogt and Vogt ('20) reported cell loss in the subthalamic nucleus associated with a lesion confined to the lateral pallidal segment. This observation which indicates a definite relationship between the lateral pallidal segment and the subthalamic nucleus might be interpreted as indicating that: (1) cell changes in the subthalamic nucleus represent a form of transsynaptic degeneration or (2) subthalamic efferent fibers pass in significant numbers to the lateral pallidal segment. Similar cell loss in the subthalamic nucleus following large lesions in the putamen and globus pallidus has been reported by other authors (van Monakow 1895 Dejerine '01; Riese '24; Kodama '28a)

Subthalamopallidal fibers The literature concerning subthalamopallidal fibers seems less conclusive than that establishing pallidosubthalamic projections koelliker (1896) carefully described efferent fibers from the subthalamic nucleus which traversed the internal capsule to enter the medial pallidal segment and the internal medullary lamina of the pallidum Similar descriptions of these fibers were given by Mirto (1896) Bechterew (1899) and Sano (10)

In a review of the connections of the subthalamic nucleus Whittier and Mettler (49a) interpreted reports (von Monakow 1895 Vogt and Vogt '20 Riese '24 Sougues and Bertrand '26 Balthasar '39) of loss of cells in the subthalamic nucleus following lesions in the pallidum as strong evidence that the subthalamic nucleus projects fibers to the pallidum.

In experimental studies subthalamopallidal projections have been described by several authors According to Glees and Wall (46) efferent fibers from the subthalamic nucleus project to both medial and lateral segments of the globus pallidus as well as to many other structures. These observations are open to criticism mainly because large lesions in the subthalamic region in the five monkeys studied in volved multiple structures. The most extensive study in the monkey is that of Whittier and and Mettler ('49a) based upon the study of Marchi degeneration resulting from relatively discrete lesions in the subthalamic nucleus Lesions in 18 of 75 monkeys were sufficiently well localized in this nucleus to produce contralateral subthalamic dyskinesia. Anatomical observations were interpreted carefully with cognizance of encroachment upon neighboring structures. These authors concluded that subthalamic efferent fibers projected only to the medial segment of the globus pallidus and the SN Subthalamopallidal fibers from the lateral aspect of the nucleus were described as perforating the internal capsule and scattering diffusely within the medial pallidal segment. Only rarely were such fibers said to continue into the medullary laminae or any part of the lateral pallidal segment. Knook ('65) the only author to use silver-staining technics reported that in the rat the only certain efferent fibers from the corpus Luysi were those that projected to the globus pallidus and the nucleus entopeduncularis The nucleus entopeduncularis is considered to correspond to the medial pallidal segment in the the primate (Knook, '65 Nauta and Mehler '66) This author regarded the pallidal projection as so massive that all other efferent projections must be considered minor Efferent fibers to the globus pallidus crossed through the internal capsule and reached the ventral border of the globus pallidus from which location they curved dorsally Degenerated fibers within the globus pallidus were distributed especially to the posterior half of the nucleus in anterior regions degeneration was seen only in ventrolateral parts. Fibers terminating in the nucleus entopeduncularis were considered to be mostly *collaterals* of subthalamopallidal fibers coursing between the internal capsule and the optic tract In the experimental study of Morgan ('27) no mention was made of fibers projecting to the globus pallidus.

The current study indicates that the principal efferent fibers of the subthalamic nucleus in the monkey are to the medial segment of the globus pallidus These fibers appear to become especially concentrated in the lateral part of the nucleus and

many pass dorsolaterally for a short distance before traversing the fibers of the internal capsule at an acute angle. Other fibers cross the internal capsule to the pallidum directly A considerable number of fibers traverse the pallidum in an oblique ventrolateral direction and pass laterally along the ventral border of the globus pallidus. These fascicles of degenerated fibers enter the internal and external medullary laminae of the globus pallidus a large number of such fibers pass dorsally in the internal medullary lamina. Fibers passing dorsally in the medullary lamina project to parts of both medial and lateral pallidal segments. Subthalamic efferent fibers in the globus pallidus are most numerous in regions of the medial pallidal segment near and immediately rostral to the subthalamic nucleus. While degenerated fibers are present in the lateral pallidal segment, they are not numerous. Within the globus pallidus, subthalamic efferent fibers do not arborize about individual neurons; most of these fibers appear to terminate in the neuropil. Rostral portions of both the medial and lateral pallidal segments do not receive subthalamic efferent fibers. No fibers from the subthalamic nucleus project to the putamen or caudate nucleus.

Substantia innominata (basal ganglia of Meynert) While the anatomical connections of the substantia innominata are not fully known, Nauta and Mehler ('66) indicate that this nucleus is closely related to fibers of the ansa peduncularis. There is some evidence that this nucleus may supply fibers to the most medial part of the subthalamic nucleus. Conversely there are suggestions (Shaner '36 Knook, '65) that fibers from the subthalamic nucleus may project to the basal nuclei. Although Knook ('65) stated that a small projection from the corpus Luysi to the basal nuclei seems likely his statement was cautious. In the current study subthalamic efferent fibers coursing along the ventral surface of the pallidum passed dorsal to the main part of the substantia innominata, but none of these fibers entered central parts of the nucleus. While it is possible that lesions in more medial parts of the subthalamic nucleus (rhesus C-657) may produce more degeneration in this location, no evidence of preterminal arborizations was seen about cells of the substantia innominata.

Dorsal supraoptic commissure (Meynert) According to Darkschewitsch and Pribytkow (1891) Bechterew (1899) and Flechsig ('21) fibers of the dorsal supraoptic commissure arise from the globus pallidus, cross to the opposite side and enter the contralateral subthalamic nucleus Marburg's ('17) descriptions were similar except that he considered these fibers to arise from the corpus striatum. In human embryos, Koelliker (1896) found fibers of the dorsal supraoptic commissure to arise and terminate in the subthalamic nuclei, after crossing dorsal to the optic tract and chiasma, these fibers perforated the peduncular part of the internal capsule and entered lateral parts of the opposite subthalamic nucleus. Denny-Brown ('62) considered fibers of this commissure to interconnect the subthalamic nuclei, while Dejerine ('01) considered the fibers of this commissure to interconnect the globus pallidus. Tsai ('25) found it virtually impossible to separate fibers of the tractus opticus accessorius anterior (Bochenek) from those of the commissure of Meynert and reported that both these bundles terminate in the subthalamic nucleus. Thus, fibers of the anterior accessory optic tract were considered to represent a retinosubthalamic pathway A similar retinosubthalamic bundle has been described by Roussy and Mosinger ('35) and Marburg ('41)

In experimental studies of the subthalamic nucleus Meynert's commissure is mentioned only by Knook ('65) This author found no degenerated fibers in the dorsal supraoptic decussation following lesions in the corpus Luysi, the globus pallidus, or the medial lemniscus and direct lesions of the commissure produced no degeneration that could be followed into the contralateral subthalamic nucleus. Wilson ('14) frequently observed degeneration in Meynert's commissure but careful study convinced him that these fibers did not arise from the globus pallidus. In other experimental studies of the globus pallidus (Ranson, Ranson and Ranson, '41 Nauta and Mehler '66) no mention is made of degeneration in this commissure even in

those cases with lesions involving the substantia innominata.

In the current study degenerated fibers in the dorsal supraoptic decussation were consistently seen in association with subthalamic lesions produced by different stereotaxic approaches These degenerated fibers could be followed into the apical region of the contralateral globus pallidus Some of these fibers appeared to project dorsomedially through the internal capsule but, in only a few instances could any of them be followed into the opposite subthalamic nucleus On the other hand fibers entering the globus pallidus did not appear to establish intimate contact with pallidal neurons No degeneration in the dorsal supraoptic commissure or the contralateral pallidum was seen following lesions of the globus pallidus reported here However lesions in the medial pallidal segment close to the internal capsule may interrupt subthalamic efferent fibers as they pass through the pallidum towards the dorsal supraoptic commissure

In some animals degenerated fibers were seen also in the ventral supraoptic decussation (Gudden) when electrodes traversed parts of the medial geniculate body or regions close to it. None of the fibers of the ventral supraoptic decussation were observed to enter the contralateral globus pallidus or subthalamic nucleus. Fibers of this commissure were traced contralateral to the opposite medial geniculate body and the capsule surrounding it.

Supramammillary commissure A number of authors (Dejerine '01; Jakob 11 Jakob '23 Foix and Nicolesco '25 Kodama '26 '28b von Santha '28 Rioch '29; Glees and Wall 46) have described fibers from the medial part of the subthalamic nucleus which cross in the supramammillary commissure and pass to this same nucleus on the opposite side This commissure has been designated variously as the commissure of Forel the posterior hypothalamic commissure and the posterior subthalamic decussation Papez Bennett and Cash (42) postulated that fibers crossing in this commissure by passed the subthalamic nucleus and descented as crossed subthalamotegmental fibers According to Glees and Wall (46) fibers crossing in the supramammillary commissure of the monkey passed to both the subthalamic and red nuclei Studies of Golgi stained sections in the rat (Gurdjian, '27) indicated that fibers of the supramammillary commissure pass from the zona incerta to the opposite subthalamic nucleus Whitter and Mettler (49a) found little or no degeneration in the supramammillary commissure following destruction of the medial part of the subthalamic nucleus in the monkey It was their impression that most of these commissural fibers came from nuclei of the tegmental field

In the present study a small number of degenerated fibers crossing in the supramammillary commissure were seen consistently in association with subthalamic lesions produced by the posterior infratentorial approach These fine parallel fibers could not be followed beyond the contralateral prerubral area due primarily to degenerated crossed ascending cerebellar efferent fibers The contralateral subthalamic nuclei were free of degenerated fibers except in two animals (C-850 and C-854) Degenerated fibers in the supramammillary commissure were seen in only one animal (C-787) when lesions were made by the frontal stereotaxic approach While the above observations cannot be regarded as conclusive they suggest that fibers of the supramammillary commissure probably do not interconnect portions of the subthalamic nuclei in the monkey

Comparisons of efferent projections of subthalamic nucleus substantia nigra (SN) and globus pallidus Comparisons of the efferent projections of these three nuclei offer interesting contrasts. Efferent fibers from each of these nuclei are distinctive even through their complex pathways are partially intermingled

The subthalamic nucleus appears unique among these nuclei in that it does not appear to have any projections to the thalamus Pallidothalamic fibers arise exclusively from the medial pallidal segment and are widely distributed in the thalamus These fibers project to VA VLo and VLm and CM Nigrothalamic fibers pass to VAmc and VLm There is virtually no overlap of pallidothalamic and nigrothalamic fibers although some pallidal fibers pass to the small-celled part of VLm

These thalamic projections are entirely ipsilateral.

Both the subthalamic nucleus and substantia nigra project fibers to the globus pallidus. Subthalamopallidal projections mainly to the medial pallidal segment, are more profuse than those arising from the SN. Quantitatively nigropallidal fibers are far less impressive than nigrothalamic projections. Based on silver degeneration technics, no fibers from the subthalamic nucleus or the substantia nigra pass to the neostriatum. The subthalamic nucleus gives rise to a small number of fibers that cross to the opposite globus pallidus in the dorsal supraoptic decussation. Whether some of these crossed fibers enter the contralateral subthalamic nucleus, or not, remains unresolved.

The lateral pallidal segment gives rise to large numbers of fibers that pass to the rostrolateral part of the subthalamic nucleus. These pallidosubthalamic fibers appear to represent the largest subcortical source of afferent fibers to the subthalamic nucleus. Available data are not conclusive concerning pallidonigral fibers, mainly because of technical difficulties in producing pallidal lesions that do not injure portions of the putamen.

The globus pallidus is the only nucleus of this group which definitely gives rise to descending fibers. These fibers pass to the pedunculopontine nucleus; none of these fibers appear to project to more caudal brain stem structures. While it is possible that the subthalamic nucleus and SN may give rise to some descending fibers passing to midbrain levels, such pathways remain doubtful because lesions in these nuclei almost invariably involve pallidotegmental or corticotegmental fibers.

Subthalamic dyskinesia. All of the monkeys with discrete lesions in the subthalamic nucleus exhibited contralateral subthalamic dyskinesia of the type described in prior publications (Whittier and Mettler '49b Carpenter Whittier and Mettler '50 Carpenter and Brittin '58 Carpenter Correll and Hinman, '60 Strominger and Carpenter '65; Carpenter Strominger and Weiss, '65 Stein and Carpenter '65) It is apparent from these studies that most experimental lesions in the subthalamic nucleus provoking dyskinesia involve some pallidofugal fibers, especially those of the lenticular fasciculus. The fact that lesions of the medial segment can abolish or greatly reduce subthalamic dyskinesia (Carpenter Whittier and Mettler '50) suggests that a considerable part of the pallidothalamic fiber system must be destroyed to ameliorate the dyskinesia. The current study provides anatomical evidence to support the thesis that subthalamic dyskinesia resulting from lesions in the subthalamic nucleus probably is a consequence of removal of inhibitory influences acting upon the medial pallidal segment. This conclusion seems inescapable since the bulk of subthalamic efferent fibers passes to the medial pallidal segment. These findings imply that subthalamic dyskinesia differs from cerebellar dyskinesia in that the "release phenomenon" in subthalamic dyskinesia involves portions of the globus pallidus while that in cerebellar dyskinesia probably directly affects thalamic neurons.

The fact that subthalamic dyskinesia is not modified by lesions in the SN (Strominger and Carpenter '65) and persists in spite of interruption of nigrothalamic fibers would seem to indicate that neither the substantia nigra nor nigrothalamic fibers passing to VAmc or VLm are implicated in the basic neural mechanism. Other evidence (Carpenter Strominger and Weiss '65) suggests that pallidofugal fibers to the centromedian nucleus, and the efferent projections of this nucleus, do not play an essential role in subthalamic dyskinesia. Collectively these data imply that impulses concerned with subthalamic dyskinesia must arise from pallidal neurons which project upon the ipsilateral VA and VLo thalamic nuclei.

SUMMARY AND CONCLUSIONS

A study was made to determine the efferent projections of the subthalamic nucleus in the rhesus monkey Because of the virtual impossibility of producing lesions in the subthalamic nucleus which do not involve adjacent structures lesions in this nucleus were produced by three different stereotaxic approaches. Since lesions in the subthalamic nucleus usually involve efferent fibers of the substantia nigra and glo-

bus pallidus degeneration resulting from localized lesions in these structures also was studied Comparisons of degeneration resulting from these lesions were made in representative sections stained by the Nauta-Gygax method

The following conclusions were drawn from this study

1 Efferent fibers from the subthalamic nucleus traverse the internal capsule and are distributed primarily to caudal parts of the ipsilateral medial segment of the globus pallidus; a small number of fibers enter the internal and external medullary lami nae to be distributed to parts of both medial and lateral pallidal segments.

2 A small number of fibers from the subthalamic nucleus traverse the internal capsule enter the dorsal supraoptic decussation and pass into the contralateral globus pallidus

3 No efferent fibers from the subtha lamic nucleus project to any part of the thalamus or hypothalamus

4 Evidence from this study suggests that efferent fibers from the subthalamic nucleus probably do not project to the red nucleus or nuclei in the midbrain teg mentum

5 The substantia nigra projects fibers ipsilaterally to (a) the magnocellular part of the ventral anterior (VAmc) and the medial part of the ventral lateral (VLm) tha lamic nuclei and (b) the medial pallidal segment.

6 The lateral pallidal segment projects fibers exclusively to rostrolateral regions of the ipsilateral subthalamic nucleus.

7 The medial pallidal segment gives rise to fibers passing ipsilaterally to: (a) the ventral anterior (VA) the ventral lateral (VLo and VLm) and the centromedian (CM) thalamic nuclei and (b) the pedunculopontine nucleus

8 Thalamic projections of the substantia nigra and globus pallidus are distinctive without overlap

9 The projections of the subthalamic nucleus to the globus pallidus are more profuse than those of the substantia nigra

The following hypothesis is presented Subthalamic dyskinesia due to lesions in the subthalamic nucleus is a consequence of removal of inhibitory afferent influences acting upon the medial segment of the globus pallidus This hypothesis is supported by the fact that the principal subthalamic efferent fibers pass to the medial pallidal segment.

LITERATURE CITED

Afifi, A., and W W Kaelber 1965 Efferent connections of the substantia nigra in the cat. Exper Neur., 11: 474–482.

Andy O J and J S. Brown 1960 Diencephalic coagulation in the treatment of hemiballismus. Surg. Forum, 10: 795–799.

Balthasar K 1939 Über die Beteiligung des Globus pallidus bei Athetose und Paraballismus Deutsche Ztschr f Nervenh., 143: 243–261

Bechterew W von 1899 Die Leitungsbahnen im Gehirn und Rückenmark. A. Georgi, Leipzig

Carpenter M. B 1961 Brain stem and infratentorial neuraxis in experimental dyskinesia. Arch. Neur., 5: 504–524.

Carpenter M. B., and G. M. Brittin 1958 Subthalamic hyperkinesia in rhesus monkey Effects of secondary lesions in red nucleus and brachium conjunctivum. J Neurophysiol., 21: 400–413.

Carpenter M B., J W Correll and A. Hinman 1960 Spinal tracts mediating subthalamic hyperkinesia. Physiological effects of selective partial cordotomies upon dyskinesia in rhesus monkey J Neurophysiol., 23: 288–304

Carpenter M. B., and R. E. McMasters 1964 Lesions of the substantia nigra in the rhesus monkey Efferent fiber degeneration and behavioral observations. Am. J Anat., 114: 293–320.

Carpenter M B. N L. Strominger and A. H. Weiss 1965 Effects of lesions in the intralaminar thalamic nuclei upon subthalamic dyskinesia. A study in the rhesus monkey Arch. Neur 13 113–125.

Carpenter M. B., J R. Whittier and F A. Mettler 1950 Analysis of choreoid hyper kinesia in the rhesus monkey Surgical and pharmacological analysis of hyperkinesia resulting from lesions in the subthalamic nucleus of Luys. J Comp. Neur 92 293–332.

Cole M., W J H. Nauta and W R. Mehler 1964 The ascending efferent projections of the substantia nigra Trans. Am. Neur Assoc. 89 74–78

Darkschewitsch L., and G. Pribytkow 1891 Über die Fasersysteme am Boden des dritten Hirnventrikels. Neur Centralbl., 10: 417–429.

Déjerine, J 1901 Anatomie des centres nerveux 2: 397–404. J Rueff Paris

Denny-Brown D 1962 The Basal Ganglia and Their Relation to Disorders of Movement. Oxford Univ Press, London p 11

Flechsig, P 1881 Zur Anatomie und Entwicklungsgeschichte der Leitungsbahnen im Grosshirn des Menschen. Arch. f Anat. Physiol., Anat. Abth., 12–75

——— 1921 Die myelogenetische Gliederung der Leitungsbahnen des Linsenkerns beim Menschen. Berichte über die Verhand-

hungen der Sächsischen Akademie der Wissenschaften zu Leipzig. Math.-Physische Klasse, 73: 295–302.

Foix, C., and J Nicolesco 1925 Les noyaux gris centraux et la région mésencéphalo-sous-optique. Corps de Luys. Masson et Cie, Paris.

Glees, P and P D Wall 1946 Fiber connections of the subthalamic region and the centro-median nucleus of the thalamus. Brain, 69 195–209.

Gurdjian, E. S. 1927 The diencephalon of the albino rat. Studies on the brain of the rat. J Comp. Neur., 43 1 114.

Jakob, A. 1923 Die extrapyramidalen Erkrankungen. Monographien aus dem Gesamtgebiete der Neurologie und Psychiatrie. Berlin.

Jakob, C. 1911 Das Menschenhirn. Eine Studie über den Aufbau und die Bedeutung seiner grauen Kerne und Rinde. J F Lehmann, Munich. Part I.

Johnson, T N and C. D. Clemente 1959 An experimental study of the fiber connections between the putamen, globus pallidus, ventral thalamus and midbrain tegmentum in cat. J. Comp. Neur., 113 83–101.

Juba, A. 1955 Pathologie des Ballismus. Akadémiai Kiado, Budapest, 136 pp.

Kodama, S. 1926 Über die sogenannten Basalganglien. Schweizer Arch. f Neur., u. Psychiat., 18 179–241; 19 153–177

——— 1928a Über die sogenannten Basalganglien. II. Pathologischanatomische Untersuchungen mit Bezug auf die sogenannten Basalganglien und ihre Adnexe. Schweizer Arch. f. Neur u. Psychiat., 23, 38–100.

——— 1928b Über die sogenannten Basalganglien. II. Pathologischanatomische Unter suchungen mit Bezug auf die sogenannten Basalganglien und ihre Adnexe. Schweizer Arch. f. Neur., u. Psychiat., 23. 179–265.

Kölliker A. von 1896 Handbuch der Gewebelehre des Menschen. Corpus Luyd. W Engelmann, Leipzig. 6th Ed., 2: 458–470.

Khrayzy S. 1926 Zur Faseranatomie des Striatum, des Zwischen-und Mittelhirns auf Grund der Markreifung in den ersten drei Lebensmonaten. Ztschr f Anat. u. Entwicklungsgesch., 81 620–632.

Kuypers, H. L. 1953 The Fibre-Connections of the Forebrain. Van Gorcum and Co., N. V Leiden.

Levin, P M. 1936 The efferent fibers of the frontal lobe of the monkey (Macaca mulatta) J Comp. Neur., 63, 369–419.

——— 1944 Efferent fibers. In The Precentral Motor Cortex. Ed., P C. Bucy Univ Ill., Urbana, pp. 134–148.

Marburg, O. 1917 Vergleichend-anatomische Studien über den Nucleus hypotalamicus. Jahrb. f Psychiat. u. Neur 38 184–196.

——— 1942 Primary endings of the optic nerve in man and in animals. Arch. Ophthal., 28 61 78.

Martin, J P 1927 Hemichorea resulting from local lesion of the brain (Syndrome of the body of Luys) Brain, 50: 637–651

Martin, J P and L R. McCaul 1959 Acute hemiballismus treated by ventrolateral thalamolysis. Brain, 82, 104–108.

Mettler F A. 1947 Extracortical connections of the primate frontal cerebral cortex. I. Thalamocortical connections. J Comp. Neur., 86: 95–118.

Mirto, D 1896 Sulla fina anatomia delle regioni peduncolare e subthalamica nell'uomo. Riv di pat. nerv e ment., 1 57–60.

Moersch, F P., and J W Kernohan 1939 Hemiballismus, a clinicopathologic study Arch. Neur Psychiat., 41 365–372.

Monakow C. von 1895 Experimentelle und pathologisch-anatomische Untersuchungen über die Haubenregion, den Sehhügel und die Regio subthalamica, nebst Beiträgen zur Kenntnis früh erworbener Gross-und Kleinhirndefecte. Arch. f. Psychiat., 27 1–128; 386–478.

——— 1914 Die Lokalisation im Grosshirn und der Abbau der Funktion durch kortikale Herde. J F Bergmann, Wiesbaden, p. 1033.

Morgan, L. O 1927 Symptoms and fiber degeneration following experimental lesions in the subthalamic nucleus of Luys in the dog. J Comp Neur., 44 379–397

Nauta, W J H., and Gygax, P 1954 Silver impregnation axons in the central nervous system A modified technique. Stain Tech., 29 91–93

Nauta, W J H., and W R. Mehler 1966 Projection of the lentiform nucleus in the monkey Brain Research, 1 3–42.

Olszewski, J and D Baxter 1954 Cytoarchitecture of the Human Brain Stem. J. B. Lippincott Co., Philadelphia.

Papez, J W 1938 Reciprocal connections of the striatum and pallidum in the brain of Pithecus (Macacus) rhesus. J Comp. Neur 69 329–349

——— 1941 A summary of fiber connections of the basal ganglia with each other and with other portions of the brain. Res. Publ. Assoc. nerv ment. Dis., 21 21–68.

Papez, J W A. E. Bennett and P T Cash 1942 Hemichorea (Hemiballismus); association with a pallidal lesion involving afferent and efferent connections of the subthalamic nucleus; curare therapy Arch. Neur Psychiat., 47 667–676.

Papez, J W and W A. Stotler 1940 Connections of the red nucleus. Arch. Neur. Psychiat., 44 776–791

Ranson, S. W S. W Ranson, Jr., and M. Ranson 1941 Fiber connections of corpus striatum as seen in Marchi preparations. Arch. Neur. Psychiat., 46 230–249.

Riese, W 1924 Beiträge zur Faseranatomie der Stammganglien. J f. Psychol. u. Neur., 31 81–122.

Rinvik, E. 1966 The cortico-nigral projection in the cat. An experimental study with silver impregnation methods. J Comp. Neur., 126 241–254.

Rinvik, E., and F Walberg 1963 Demonstration of a somatotopically arranged corticorubral projection in the cat. An experimental study with silver methods. J Comp. Neur 120 393–407

Rioch, D. McK. 1929 Studies on the diencephalon of carnivora. II. Certain nuclear configu-

rations and fiber connections of the subthalamus and midbrain of the dog and cat. J Comp Neur., *49:* 121–154

Roussy G. and G Mosinger 1935 Le subthalamus et les formations subthalamo-mésencéphaliques. Rev Neur., *64:* 637–661

Sano T 1910 Beitrag zur vergleichenden Anatomie der Substantia nigra, des Corpus Luysii und der Zona incerta. Monatschr f Psychiat. u Neur., *27:* 110–274

Sántha, K. von 1928 Zur Klinik und Anatomie des Hemiballismus. Arch. f Psychiat. *84:* 664–678.

Shaner R. F 1936 Development of the finer structure and fiber connections of the globus pallidus, corpus of Luys and substantia nigra in the pig J Comp. Neur., *64:* 213–325

Souques, A., and I. Bertrand 1926 Sur la fonction motrice du *corps strié à propos d'un cas* d'hémichorée suivi d'autopsi. Rev Neur *45:* 988–1002.

Stein, B. M. and M B Carpenter 1965 Effects of dorsal rhizotomy upon subthalamic dyskinesia in the monkey Arch Neur., *13:* 567–583.

Strominger N L., and M. B Carpenter 1965 Effects of lesions in the substantia nigra upon subthalamic dyskinesia in the monkey Neur 15 587–594

Szabo, J 1962 Topical distribution of striatal efferents in the monkey Exper Neur., *5:* 21–36.

Tsai, C. 1925 The optic tracts and centers of the opossum, Didelphis virginiana J Comp Neur., *39:* 173–216.

Verhaart, W J C 1950 Fiber analysis of the basal ganglia. J Comp. Neur., 93 425–440.

Vogt, C., and O Vogt 1920 Zur Lehre der Erkrankungen des striären Systems. J Psychol. u Neur *25:* 627–846.

Voneida, T J 1960 An experimental of the course and destination of fibers arising in the head of the caudate nucleus in the cat and monkey J Comp. Neur., *115* 75–87

Wernicke, C. 1881 Lehrbuch der Gehirnkheiten für Arzte und Studierende. T Fischer Kassel and Berlin. Part II (quoted by Nauta and Mehler 1966)

Whittier J R. 1947 Ballism and the subthalamic nucleus (nucleus hypothalamicus; corpus Luysi) Arch. Neur. Psychiat., *58:* 672–692.

Whittier J R., and F A. Mettler 1949a Studies on the subthalamus of the rhesus monkey I. Anatomy and fiber connections of the subthalamic nucleus of Luys. J Comp Neur 90. 281–318.

——— *1949b Studies on the subthalamus of* the rhesus monkey II. Hyperkinesia and other physiologic effects of subthalamic lesions, with special reference to the subthalamic nucleus *of Luys. J Comp. Neur., 90:* 319–372.

Wilson, S A. K. 1914 An experimental research into the anatomy and physiology of the corpus striatum. Brain, *36:* 427–492.

Winkler C. 1928 Ein abnormes, aberrierendes Bündel im Nucleus subthalamicus und in der Substantia *nigra. Monatschr f. Psychiat. u.* Neur., *68:* 701–705.

Woodburne, R. T 1946 The major efferent connections of the basal ganglia. Anat. Rec., 94 507

Woodburne R. T E. C. Crosby and R. E. McCotter 1946 The mammalian midbrain and isthmus regions. II. The fiber connections. A. The relations of the tegmentum of the midbrain with the basal ganglion in Macaca mulatta J Comp Neur 85 67–92.

PLATE 1

EXPLANATION OF FIGURES

3–4 Rhesus C-654 and C-655. Photomicrographs of lesions in the left subthalamic nucleus produced stereotaxically by the posterior infratentorial approach. Nissl, × 10; Weil, × 10

5 Rhesus C-659 Photomicrograph of lesion in the left subthalamic nucleus produced by an *electrode* introduced into the *frontal* lobe. Nissl, × 8

6 Rhesus C-675 Photomicrograph of a large lesion in the left subthalamic nucleus produced by an electrode introduced into the lateral surface of the brain. The electrode traversed the putamen, dorsal parts of the globus pallidus and the internal capsule. Weil × 8.

7 Rhesus C-650. Photomicrograph of degeneration in the left globus pallidus resulting from a lesion in the ipsilateral subthalamic nucleus. Degenerated *fibers can be seen sweeping dorsally into the* internal medullary lamina of the pallidum. Nauta-Gygax, × 90

8 Rhesus C-654 Photomicrograph of degeneration in the left globus pallidus resulting from the lesion seen in figure 3 All of this degeneration *is* within the medial pallidal segment. Nauta-Gygax, × 250.

PLATE 1

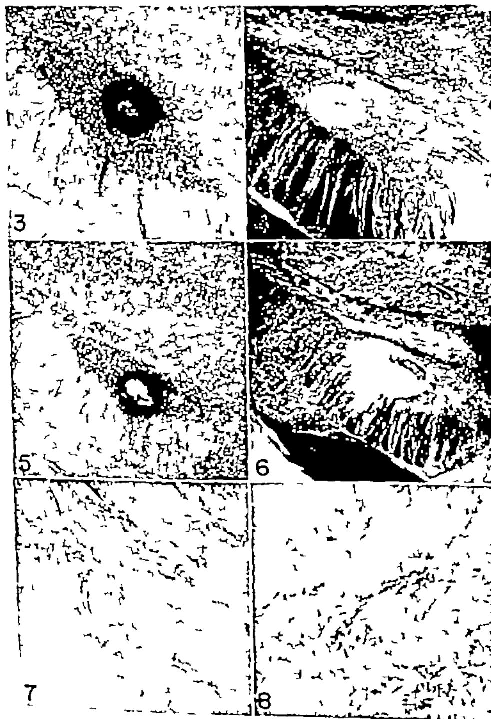


PLATE 2

EXPLANATION OF FIGURES

9–10 Rhesus C-850 Photomicrographs of degenerated fibers from a lesion in the subthalamic nucleus passing through the medial part of the globus pallidus to enter the dorsal supraoptic decussation (fig 9) Figure 10 shows fibers of the dorsal supraoptic decussation entering the contralateral globus pallidus. Some of these fibers can be seen passing dorsally towards the internal capsule Nauta-Gygax × 80 × 100

11–12 Rhesus C-875 Degeneration in the dorsal supraoptic decussation on the right side over the optic tract (fig. 11) and entering the right globus pallidus (fig 12) Nauta-Gygax, × 80 × 100

13 Rhesus C-852. Degeneration ipsilateral to the subthalamic lesion is seen in both the dorsal and ventral supraoptic decussations. Nauta-Gygax × 80

14 Rhesus C-855 Degeneration seen in the magnocellular part of the ventral anterior nucleus (VAmc) of the thalamus. This degeneration resulted from concomitant interruption of ascending nigral efferent fibers Nauta-Gygax, × 250

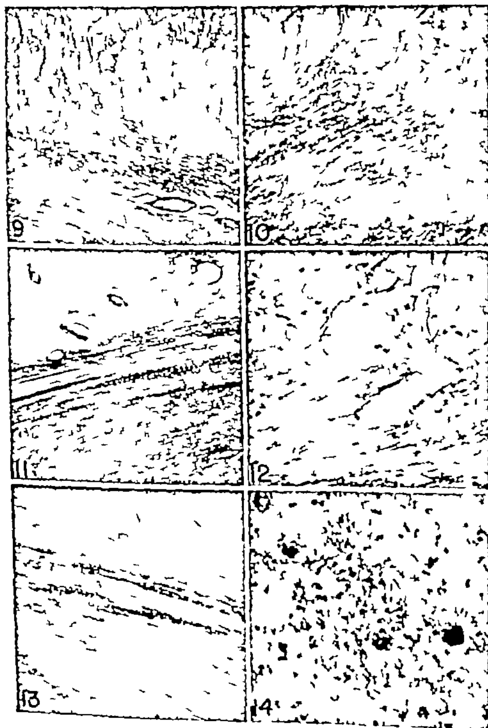

9
10
11
12
13
14

PLATE 3

EXPLANATION OF FIGURES

15 and 17 Rhesus C-896 and C-688. Photomicrographs of lesions in the substantia nigra produced by the posterior infratentorial approach (fig. 15) and by a lateral approach (fig. 17) The lesion in rhesus C-896 was mainly in the pars reticularis. Nissl, × 8; Weil, × 6.

16 and 18 Rhesus C-688 Photomicrographs of degeneration from the nigral lesion shown in figure 17 passing to the medial part of the ventral lateral nucleus (VLm) of the thalamus. Nauta-Gygax × 40 × 80.

19 Rhesus C-906 Photomicrograph of a sagittal section showing a lesion and electrode track caudal to the subthalamic nucleus. This lesion destroyed nigral efferent fibers passing to the thalamus. Nauta-Gygax, × 8.

20 Rhesus C-906. Photomicrograph of ascending nigral efferent fibers passing into the magnocellular part of the ventral anterior nucleus of the thalamus. Nauta-Gygax × 250.

SUBTHALAMIC EFFERENT FIBERS
Malcolm B. Carpenter and Norman L. Strominger











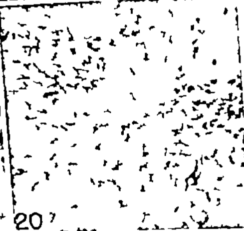


PLATE 4

EXPLANATION OF FIGURES

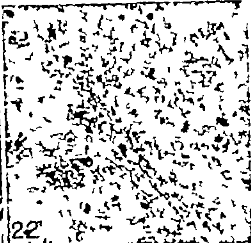
21 and 23 Rhesus C-980 and C-960. Photomicrographs of lesions in the medial pallidal segment produced by a lateral stereotaxic approach. Sections in rhesus C-980 (fig. 21) were cut transversely while sections in rhesus C-960 (fig. 23) were cut sagittally Weil, × 6, × 5

22 Rhesus C-980 Photomicrograph of degeneration resulting from the lesion shown in figure 21 passing into the ventral anterior nucleus of the thalamus (VA) Nauta-Gygax, × 200.

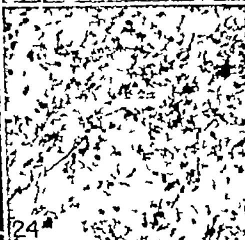
24 Rhesus C-960. Photomicrograph of descending pallidotegmental fibers in the pedunculopontine nucleus. Nauta-Gygax, × 220.

25–26 Rhesus C-896. Photomicrographs of a lesion largely limited to the lateral segment of the globus pallidus (fig. 25) and degeneration seen in the rostrolateral part of the subthalamic nucleus (fig. 26) Degeneration resulting from this pallidal lesion projected exclusively to the ipsilateral subthalamic nucleus. Weil, × 7; Nauta-Gygax, × 200


21


22


23


24


25


26

PLATE 4

EXPLANATION OF FIGURES

21 and 23 Rhesus C-980 and C-960. Photomicrographs of lesions in the medial pallidal segment produced by a lateral stereotaxic approach. Sections in rhesus C-980 (fig. 21) were cut transversely while sections in rhesus C-960 (fig 23) were cut sagittally Weil, × 6, × 5.

22 Rhesus C-980. Photomicrograph of degeneration resulting from the lesion shown in figure 21 passing into the ventral anterior nucleus of the thalamus (VA) Nauta-Gygax, × 200

24 Rhesus C-980 Photomicrograph of descending pallidotegmental fibers in the pedunculopontine nucleus. Nauta-Gygax × 220.

25-26 Rhesus C-898. Photomicrographs of a lesion largely limited to the lateral segment of the globus pallidus (fig. 25) and degeneration seen in the rostrolateral part of the subthalamic nucleus (fig. 26) Degeneration resulting from this pallidal lesion projected exclusively to the ipsilateral subthalamic nucleus. Weil, × 7; Nauta-Gygax, × 200.

Observations on the Development of Mouse Blastocysts Transferred to the Testis and Kidney [1]

DAVID G. PORTER
Department of Anatomy Washington University School of Medicine St. Louis Missouri

ABSTRACT The development of mouse blastocysts transferred to the kidney and testis was studied by light and electron microscopy Approximately 50% of the blastocysts transferred to both sites survived for more than five days. Although trophoblast proliferation was characteristic of all 31 successful transplants which were serially sectioned, inner cell masses differentiated in only nine. Transplants were invasive in kidney but were encapsulated in testis. In both organs, however, transplants produced considerable hemorrhage. That trophoblast invades by phagocytosis was not substantiated in this study nor was there evidence that trophoblast elaborates a cytolytic factor Although transplants caused gross lesions in the host organs, the cytology of cells in close proximity to invading trophoblast was almost normal. The only abnormal features observed were the presence of fine fibrillar material in the basal cytoplasm of renal tubule cells and a thickening of their basement membranes. No correlation could be demonstrated between the antigenic dissimilarity of host and transplant and extent of host tissue response.

Although the mammalian blastocyst requires a variety of specific conditions before it will implant in utero it will readily grow in non-uterine tissues. Successful transplants of blastocysts have been made to the anterior chamber of the eye (Runner 47 Fawcett, Wislocki and Waldo 47; Grobstein, '50 Jones, '51 Shapiro and Harvey '57) the kidney (Nicholas, 42; Fawcett, '50 Jones '51 Kirby '60 '62a) the peritoneum (Loeb '14; Fawcett et al., 47; Jollie, '61 McClaren and Tarkowski, '63) the spleen (Kirby '63a) and the testis (Kirby '63b) Transplants to ectopic sites have been carried out successfully in immature, adult virgin, pregnant and nonpregnant females as well as in normal, cryptorchid and castrated males. Most transplants have been made in mice but successful transfers have been made also in the rat (Nicholas, 42; Kirby '62b) rabbit (Shapiro and Harvey '57) and guinea pig (Loeb '14)

Characteristically the blastocyst developing in a non-uterine site establishes a nexus of trophoblast cells. These cells invade the surrounding host tissue and form a meshwork resembling that which invests the developing embryo in normal implantation sites. In ectopic sites the trophoblastic proliferation occurs irrespective of the development of an embryo. The mechanism by which trophoblast cells invade tissue is not fully understood. Orsini ('54) claimed that primary and secondary trophoblastic giant cells in the placenta of the hamster were phagocytic. In the mouse Wislocki Deane and Dempsey (46) were unable to demonstrate that giant cells phagocytose trypan blue unless very high doses of the dye were administered to the pregnant animals. Although Bridgman (48) found that rat trophoblast was not phagocytic until after the eighth day of pregnancy Jollie ('65) in an electron microscopic study concluded that rat giant cells are actively phagocytic at least until the fourteenth day of pregnancy The trophoblastic invasion of non-uterine tissue is also poorly understood. Kirby ('62c) has suggested that the mechanism may vary depending upon the tissue which is invaded. Thus histological examination of blastocysts growing in the testis (Kirby '63b) suggested that trophobalst may secrete a "cytolytic" substance which causes necrosis of the seminiferous tubules peripheral to the transplant whereas in the spleen invasion is apparently accomplished by active phagocytosis (Kirby '63a) Phagocytosis has also been said to

[1] This work was supported by United States Public Health Grants HD-01660 from the Institute of Child Health and Development and 2-T1-GM-440 from the Institutes of General Medical Sciences.

cytoplasm. The plasma membrane of the giant cells in electron micrographs was irregular due to the presence of microvilli and pseudopodia-like processes. Various inclusions were seen in the cytoplasm including many smooth-walled vesicles. Ergastoplasm was scant and mitochondria were not numerous. Myelin figures were frequently present and occasionally reached large dimensions. Glycogen, although present in a few giant cells (fig. 3) was not commonly observed. This is consistent with the observations made on normal trophoblast by other workers (Wislocki et al., 46 Bulmer and Dickson, '60; Deane, Rubin, Driks Lobel and Leipsner '62; Larson, '63)

Nuclei

The nuclei of giant cells were usually very large. The nuclear membrane was irregular and often deeply indented. Occasionally fragments of nuclear membrane appeared to be located within the nucleoplasm (fig. 4) Only one nucleus was observed within each trophoblast cell which is consistent with the view expressed by Kirby and Malhotra ('64) and Kirby ('65) that the invasive cells of the mouse placenta have a cellular rather than a syncytial organization.

Blood supply

After six or seven days growth, transplants macroscopically resembled small hematomas in the substance of the host organ. The blood in the transplants contained only non-nucleated erythrocytes, presumably derived from the host. Because no signs of coagulation were observed histologically prior to the eleventh day after transplantation it would seem that blood circulated through the trophoblast meshwork and was confluent with the blood stream of the host. This conclusion was supported by the following findings.

Animals bearing transplants were given two injections of 0.05 ml of a 1% aqueous solution of trypan blue 24 hours apart. The animals were killed 24 hours after the latter injection and their transplants examined histologically for evidence of phagocytosis of dye particles (see below) In the transplant of one of the animals thus injected an embryo was present. In the visceral yolk sac cells of this embryo trypan blue particles were concentrated. Since trypan blue was not present in the giant cells, the dye probably reached the yolk sac via the blood sinuses of the transplant.

Eleven or more days after transplantation, erythrocytes were seldom lying free within the interstitial spaces and areas of coagulation were present. As these areas increased in size trophoblast cells became reduced in number and showed signs of degeneration. Eventually trophoblast cells were found only at the periphery of the hematoma in the form of a tenuous layer of weakly staining degenerating cells apposed to the host tissue.

Host response

As reported above the development of blastocysts in both the testis and the kidney was characterized by the formation of a trophoblastic nexus. However the response of the host tissue was not the same in the two organs. In the testis a distinct capsule composed of several layers of fibroblasts formed between the trophoblast cells and the surrounding seminiferous tubules (figs. 1 7) The thickness of the capsule varied among the transplants but no correlation between thickness and the age of the transplant could be found.

It may be questioned whether the fibroblasts were of host origin but the rapidity with which the capsule is formed prior to the formation of the trophoblastic meshwork, and the failure of such a capsule to form around transplants in the kidney suggests that they are derived from the host. Furthermore it would seem unlikely that metaplasia of giant cells into fibroblasts could occur without any obvious transition stages being observed.

The reaction of the kidney differed in that no fibrous capsule was formed between the trophoblast and renal tissue (fig. 2) Indeed, trophoblastic giant cells actively invaded the surrounding parenchyma and were frequently insinuated between renal tubules at some distance from the main focus of the transplant (fig. 3) In some cases, a varying degree of leucocytic infiltration a feature not observed to occur in the testis, occurred around the developing transplant.

occur in the anterior chamber of the eye (Fawcett et al. 47) although Grobstein (50) in reporting that trophoblast in the anterior chamber elicits massive haemorrhage made no mention of the phenomenon.

With one exception (Jollie '65) the above studies were exclusively light microscopic studies and it was thought that an electron microscopic investigation of blastocysts growing in non-uterine sites might provide information concerning the nature of trophoblastic invasion and tissue response

MATERIALS AND METHODS

Mice of several strains (Swiss albino C3H leaden and C57) were used as a source of blastocysts and as recipients.

Females were killed on the fourth day of pregnancy (day of plug-day one) the uterine horns were removed and flushed with saline containing 10% fetal calf serum (v/v) Blastocysts thus obtained were transplanted either to the testis or the kidney using a micropipette similar to that described by Kirby ('62a)

Animals were killed from 5 to 19 days after transplantation and transplant sites were removed for light and electron microscopic study Tissue for light microscopy was fixed in Bouin s fixative or in 10% buffered formalin. Serial sections were cut at 8 μ and apart from special staining procedures mentioned below were stained with haematoxylin and eosin Tissue for electron microscopy was fixed in cold buffered 1% osmium tetroxide (Caulfield 57) and embedded in Durcopan or in Dow epoxy resin (Lockwood, '64) Sections were mounted on uncoated copper grids and stained with lead citrate according to the method of Reynolds ('63)

RESULTS

Number of successful transplantations

It was found that blastocysts could be successfully transplanted to the testis and kidney Indeed almost half of the number of blastocysts (and morulae) transferred survived for more than five days after transplantation (table 1)

TABLE 1

Total number of blastocysts and morulae transplanted (both organ sites)	156
Number of surviving five days or more	75

The majority of transplants were of blastocysts but some morulae were also transferred and their survival frequency was comparable to that of blastocysts (table 2)

TABLE 2

Number of blastocysts transferred (both sites)	144
Survived five days or more	70
Number of morulae transferred (both sites)	12
Survived five days or more	5

The survival rate of transplants in the two host organs differed (table 3)

TABLE 3
Number of blastocysts surviving in testis and kidney

Host organ	No. transplanted	No. survived (5 days or more)
Testis	90	49
Kidney	66	26

Trophoblast proliferation was a feature of all successful transplants but embryos formed in only nine cases. Of these seven developed in kidneys and two in testes. Six embryos developed from blastocysts obtained from different donors and three from sibling blastocysts.

Trophoblast

In early transplants (5 to 6 days) trophoblast was present only as a nexus of a few closely packed cells but, in later transplants, giant cells were usually numerous. They were stellate in shape and in contact with neighboring cells only at the ends of their cytoplasmic processes thus producing extensive intercellular space This space was filled with blood with the result that a meshwork closely resembling that which invests an early intra-uterine implant site was formed (fig. 1)

The giant cells were of the order of 200 μ in diameter Histologically they were slightly basophilic and possessed foamy

was almost normal in appearance except in one instance. Where embryos had not developed, an abnormal Reichert's membrane was present occasionally. This has been described more fully elsewhere (Porter, '66).

DISCUSSION

Figures quoted by other workers (Fawcett, '50; Kirby '60, '62a) for the proportion of successful transplants are higher than those of this study. However the latter include data obtained while the technique was being learned and this may account for the discrepancy.

The question of the mechanism of trophoblast invasion has not been resolved by this study although it would appear that, at least in non-uterine tissue, phagocytosis is not a major factor. Eosinophilic droplets similar to those observed in this study were described by Fawcett et al. ('47) in trophoblast growing in the anterior chamber of the eye and assumed to be ingested host erythrocytes. Phagocytosis of erythrocytes has also been described in the normal placenta of the rat (Jollie, '65). In the electron micrographs of the present series erythrocytes were seen in intimate association with the cytoplasmic processes of the giant cells and structures similar to those reported by Jollie ('65) which resembled erythrocytes in size and electron density were observed within the cytoplasm. These observations are very suggestive that phagocytosis of host red blood cells takes place. However the refractile bodies seen histologically were found to be P.A.S. positive thus confirming the earlier reports of Bulmer and Dickson ('60) and Dickson and Bulmer ('60). It would seem unlikely therefore that these structures were erythrocytes or their breakdown products. Furthermore giant cells have a negative staining reaction with Turnbull's method and also failed to accumulate trypan blue even though the dye was stored by visceral yolk sac cells. Thus although phagocytosis cannot be completely excluded it would seem unlikely that this process plays an important role in trophoblast invasion of the testis or kidney.

In the testis Kirby ('63b), Billington ('65) and Bland and Donovan ('65) have suggested that trophoblast secretes a "cytolytic" agent which diffuses from the periphery of the transplant. However the appearance of the transplants of this series is not consistent with this view. The distribution of necrotic tubules about the periphery of the transplants was not uniform and could be explained more readily on the basis of surgical trauma plus interference with the vascular supply to the tubules by the growing transplant than on the elaboration of a cytolytic substance. Furthermore in the kidney little tissue necrosis was observed and tubule cells with nearly normal cytology were frequently seen in contact with invading trophoblast cells. This suggests that cytotoxic substances are probably not elaborated by the trophoblast.

There was evidence that the transplants might have produced substances which caused hemorrhage since blood-filled sinuses were a feature of all transplants. This is consistent with the observations of Fawcett et al. ('47) and Grobstein ('50) that considerable hemorrhage occurs from vessels at some distance from the transplant when blastocysts develop in the anterior chamber of the eye.

Billington ('64) and James ('65) claimed that the proliferation of trophoblast was greater in an environment from which it was markedly dissimilar antigenically than in one with which it was homologous. Quantitative estimates of trophoblast volume were not made in the present study but an attempt to determine whether the extent of host reaction to trophoblast was influenced by host-transplant incompatibility failed to reveal any correlation.

The development of embryos was random with respect to donors and recipients but the occurrence of more embryos among transfers performed late in the study suggests that improvement in technique was a factor. Embryos were obtained from transplants of 8 to 12 days of age. Development of embryos appeared to be retarded approximately four days by transplantation (see Porter '66).

ACKNOWLEDGMENTS

The author wishes to thank Dr. A. Duncan Chiquoine for his interest and criticism and Mrs. H. Goessling for valuable technical assistance.

In view of the varying degrees of antigenic dissimilarity between host and transplant which might have occurred as a result of the various strains of mice used in these experiments an appraisal was made to determine whether a correlation existed between the estimated degree of antigenic dissimilarity of the tissues involved and the extent of encapsulation or leucocytic infiltration Estimates were made on the basis that a blastocyst produced by mating for example a C3H strain with a Swiss albino mouse would have maximum dissimilarity from its host when transplanted to a C57 recipient whereas blastocysts from a C3H × C3H mating transplanted to a C3H recipient would have minimum dissimilarity No correlation between host response and antigenic dissimilarity could be demonstrated

Nature of invasion

In the testis transplants increased in volume with age despite the presence of a capsule This enlargement could not be attributed to direct trophoblastic invasion to any great extent, because trophoblastic elements were rarely observed outside the transplant capsule. Necrotic tubules were frequently observed but their distribution appeared to be random and normal tubules were seen contiguous to the transplant capsule as frequently as necrotic ones (fig 1)

In the kidney active trophoblastic invasion of the renal parenchyma occurred. Giant cells were observed among the renal tubules and their cell surfaces were directly contiguous to the basement membrane of renal tubule cells Little necrosis occurred in the kidney and tubule cells with nearly normal cytoplasm were frequently in contact with invading trophoblast cells (fig 6) However two minor abnormalities were noted in these cells. The basement membrane of the tubule cells in contact with trophoblast was thickened (figs 5 6 8) The increase in thickness was estimated care being taken to avoid bias due to obliqueness of section and was found to be of the order of 50% In addition tubule cells close to trophoblast possessed a fine fibrillar material in their basal cytoplasm (fig 8) These fibrils were orientated with their long axes parallel to the basement membrane.

Phagocytosis

Despite considerable disruption of renal tissue produced by the transplants and the close proximity of giant cell processes to host red blood cells (fig. 3), unequivocal evidence of phagocytosis was not obtained. In electron micrographs osmiophilic inclusions which closely resembled erythrocytes in texture and density, were present within trophoblast cells. Refractile eosinophilic bodies similar to erythrocytes were also observed histologically However staining with Turnbull's method failed to reveal the presence of ferrous iron in trophoblast cells while the eosinophilic bodies were stained positively with the periodic acid Schiff method. Thus although the micrographic and histologic appearance of the trophoblast cells was suggestive histochemical evidence failed to confirm extensive phagocytosis of erythrocytes. To further investigate the question animals bearing transplants were injected with trypan blue as described above. Although the dye was concentrated by visceral yolk sac cells within the transplant, none was observed within the trophoblastic giant cells

Embryo formation

Whenever transplanted blastocysts grew in testis or in kidney trophoblast was present. However in addition, (fig 1) embryos occasionally developed although in only 9 cases out of 31 examined histologically (Only 31 transplant sites were sectioned out of 75 successful transfers as some were rejected as unsuitable for sectioning owing to blood coagulation others were used for different experiments and still others were examined only macroscopically) All nine embryos had developed from transplanted blastocysts, none having developed from a transplanted morula Although the figures were small this is consistent with the findings of Kirby (62a) that embryos develop ectopically only from blastocysts.

The embryos developing in transplant sites had many normal features Yolk sacs were well developed in all embryos and were differentiated into parietal and visceral layers In some cases blood islands developed in association with the yolk sac Reichert's membrane (fig 7)

LITERATURE CITED

Billington W D 1964 Uterine development of mouse trophoblast. J Reprod. Fertil. 8: 274–275

Bland, K P., and B T Donovan 1965 Experimental ectopic implantation of eggs and early embryos in guinea pigs. J Reprod. Fertil., 10: 189–196.

Bridgman, J 1948 A morphological study of the development of the placenta of the rat. I. An outline of the development of the placenta of the white rat. J Morph. 83: 61–86.

Bulmer D., and A. Dickson 1960 Observations on carbohydrate materials in the rat placenta. J Anat., 94: 46–58

Caulfield, J B 1957 Effects of varying the vehicle for OsO_4 in tissue fixation. J Biophys. Biochem. Cytol., 3 827–829

Deane H. W., B L. Rubin E. C. Driks, B L. Lobel and G. Leipsner 1962 Trophoblastic giant cells in the placentas of rats and mice and their probable role in steroid-hormone production. Endocrinology 70 407–419

Dickson A., and D Bulmer 1960 Observations on the placental giant cells of the rat. J Anat., 94 418–426.

Fawcett, D W 1950 Development of mouse ova under the capsule of the kidney Anat. Rec., 108: 71–92.

Fawcett, D W., G Wislocki and C. M Waldo 1947 The development of mouse ova in the anterior chamber of the eye and in the abdominal cavity Am. J Anat. 81: 413

Grobstein C. 1950 Production of intra-ocular haemorrhage by mouse trophoblast. J Exp. Zool., 114: 359–374

James, D A. 1965 Effects of antigenic dissimilarity between mother and foetus on placental size in mice. Nature, 205: 613–614

Jollie, W P 1961 The incidence of experimentally produced abdominal implantations in the rat. Anat. Rec. 141: 159–167

——— 1965 Fine structural changes in the functional zone of the rat placenta with increasing gestational age J Ultrastruct. Res., 12: 420–438

Jones C. L. 1951 Endocrine effects in the virgin female host of fertilized mouse ova developing in extra-uterine sites. J Endocrinology 7: IX 111

Kirby D R. S 1960 Development of mouse eggs under the kidney capsule. Nature (Lond.) 187: 707–708.

——— 1962a Influence of the uterine environment on the development of mouse eggs. J Embryol. Exp Morphol. 10: 496–506.

——— 1962b Reciprocal transplantation of blastocysts between rats and mice. Nature, 194: 785.

——— 1962c Ability of trophoblast to destroy cancer tissue. Nature, 194: 696–697

——— 1963a Development of the mouse blastocyst transplanted to the spleen. J Reprod. Fertil. 5: 1–12.

——— 1963b The development of mouse blastocysts transplanted to the scrotal and cryptorchid testis. J Anat., 97: 119–130.

——— 1964 Cellular nature of the invasive mouse trophoblast. Nature (Lond.) 201: 520–521.

——— 1965 The role of the uterus in the early stages of mouse development. In: "Preimplantation stages of pregnancy" Ciba Foundation Symposium ed. by G. Wolstenholme and M. O'Connor 325–339

Larson, J F 1963 Histology and fine structure of the avascular and vascular yolk sac placentae and the obplacental giant cells in the rabbit. Am. J Anat., 112 269–283.

Lockwood W R. 1964 A reliable and easily sectioned epoxy embedding medium. Anat. Rec., 150: 129–139

Loeb, L. 1914 The experimental production of an early stage of extra-uterine pregnancy Proc. Soc. Exp Biol. Med., 11: 103–106.

McLaren, A., and A. K. Tarkowski 1963 Implantation of mouse eggs in the peritoneal cavity J Reprod. Fertil., 6: 385–392.

Nicholas, J S 1942 Experiments on developing rats. IV The growth and differentiation of eggs and egg cylinders when transplanted under the kidney capsule. J Exp. Zool., 90: 41–64

Orsini, M. W 1954 The trophoblastic giant cells and endovascular cells associated with pregnancy in the hamster Cricetus auratus. Am. J Anat., 94 273–331

Porter D G. 1966 Observations on the yolk sac and Reichert's membrane of ectopic mouse embryos. Anat. Rec., 154 847–860.

Reynolds, E. S. 1963 The use of lead citrate at high pH in an electron opaque stain in electron microscopy J Cell Biol 17: 208–213.

Runner M. N 1947 Development of mouse eggs in the anterior chamber of the eye. Anat. Rec., 98 1–13.

Shapiro H., and T S. Harvey 1957 Ocular implantation of the mammalian ovum. Proc. Am. Philos. Soc., 101: 164–176.

Wislocki, G. B., H. W Deane and E. W Dempsey 1946 The histochemistry of the rodent's placenta. Am J Anat. 78 281–346.


N
E
1
T
2
K
B
G
3

PLATE 1

EXPLANATION OF FIGURES

1 Section of an embryo and trophoblast which developed from a blastocyst transplanted to the testis of a mouse. Tissue was fixed ten days after transplantation. The major part of the transplant is made up of a meshwork of giant trophoblast cells (T) and blood sinuses. An embryo with many normal features (E) is located to one side. The transplant is clearly demarcated from the surrounding seminiferous tubules by a fibrous capsule (C) Both necrotic (N) and normal seminiferous tubules are randomly distributed about the periphery of the transplant. Bouin s fixative. Tetrachrome stain. × 60

2 Section of trophoblast cells invading renal parenchyma from a ten-day-old transplant to the kidney Only trophoblast cells developed in this case Note the absence of a fibroblastic capsule and the direct contiguity of trophoblast giant cells (T) with kidney tubules (K) Bouin s fixative. Haematoxylin and eosin. × 100.

3 Electron micrograph of trophoblastic giant cells invading renal inter tubular space Tissue obtained seven days after transplantation of a blastocyst. In this micrograph giant cell processes (T) can be seen in contact with host erythrocytes (R) kidney tubule cell (K) ?Glycogen (G) is present in one giant cell process. Stained with lead hydroxide. × 9 700


4
5
T
6
T
T
K
K

PLATE 2

EXPLANATION OF FIGURES

4 Electron micrograph of part of a giant trophoblast cell seven days after transplantation of a blastocyst to the kidney The irregular contour of the very large nucleus can be seen and a fragment of nuclear membrane (arrowed) is located within the nucleoplasm. Stained with lead hydroxide. × 23,600.

5 Electron micrograph of trophoblast cell processes (T) between two almost normal renal tubule cells (K) Note that the basement membrane (arrowed) of the tubule cells is thicker than normal. Seven day transplant to the kidney Stained with lead hydroxide. × 10,500

6 Electron micrograph showing the almost unaltered cytology of renal tubule cells (K) despite the close proximity of cell processes of giant trophoblast cells (T) One abnormality is the thickened basement membrane (arrowed) Stained with lead hydroxide × 8 000

C
M
Y
K
B

PLATE 3

EXPLANATION OF FIGURES

7 Electron micrograph of the fibrous capsule which invariably forms around transplants to the testis The capsule (C) is composed of several layers of fibroblasts (F) and in this specimen is apposed to the abembryonic surface of Reichert's membrane (M) Parietal (P) and visceral (V) yolk sac cells can be seen separated by the yolk sac cavity (Y) From an eight day transplant. Stained with lead hydroxide × 11,000.

8 Electron micrograph of part of a kidney tubule cell (K) and part of a giant trophoblast cell (T) in close proximity Note the presence of fine fibrillar material (arrowed) in the basal region of the tubule cells and the thickened basement membrane (B) From a seven day transplant. Stained with lead hydroxide × 41 000

Ultrastructure of Mouse Olfactory Mucosa[1]

DONALD FRISCH
New York University School of Medicine
Department of Anatomy New York, N Y

ABSTRACT The fine structure of the olfactory mucosa has been investigated with particular reference to those aspects of the morphology which may be significant in chemoreception. Morphology of the supporting cells of the epithelium indicate that they function in mucus production or regulation. Bowman's glands were found to consist of two cell types, both of which also seem to contribute to mucus production. Olfactory receptor cells were found to be completely covered by the mucus including the atypical olfactory cell cilia that project above the surface of the epithelium. The potential role of these cilia in initial reception is discussed. Lack of intervening cytoplasm between adjacent olfactory cell cytoplasm has been noted with the consequent possibility that electrical interaction between cells may occur. This may be significant in subsequent evaluations of electrical potentials recorded from the mucosa.

Investigations into the physiology of the sense of smell have been reported with increasing frequency for at least, the last three decades. The information that accumulated over only the ten year period between 1954 and 1964 was sufficient to stimulate publication of a number of the Annals of the New York Academy of Sciences devoted exclusively to recent progress (Kuehner '64) This intense effort has not been accompanied by similar efforts to visualize the morphology of the olfactory mucosa although Gasser ('56 '58) in studies which combined both physiologic and ultrastructural observations, stressed the importance which the peculiar morphology may have in terms of the function of the receptor tissue Some early electron microscope studies were reported (Bloom and Engstrom '52 Bloom, '54) but few investigations have appeared since All of the reports, except the most recent (Andres '66) have concentrated on one or a few aspects of the morphology and none have included the associated Bowman's glands. The present study was undertaken to provide a relatively complete description of the fine structure of the olfactory mucosa utilizing recently developed preparatory techniques.

METHODS

The nasal cavities of adult Swiss Webster mice or C-57 Black mice were flooded with fixative introduced through the external nares after ether anesthesia The principle fixative was cold 3 0% glutaraldehyde buffered to pH 7 4 with 0 1 M phosphate buffer containing 0 1% calcium chloride. After 20 minutes exposure to this fixative *in situ*, the tissue was excised and immersed in 2.0% osmium tetroxide for 90 minutes. Other specimens were similarly fixed except that either 2.0% or 4.0% glutaraldehyde was used. Tissue fixed *in situ* with osmium tetroxide was also studied. After fixation, tissue was dehydrated in graded alcohols and embedded in Epon 812 (Luft, '61) Sections, stained with lead citrate (Reynolds '63) were examined with an RCA EMU 2E or a Siemens Elmiskop I.

RESULTS

The olfactory mucosa includes both the sensory epithelium and the subjacent connective tissue in which the olfactory glands of Bowman occur Olfactory cells, supporting cells and basal cells constitute the pseudostratified epithelium. Each cell type will be described separately in the body of the results, but it is appropriate to distinguish between them with a sentence or two here Olfactory cells are usually described as bipolar ganglion cells with the superficial process considered distal, and the process which terminates in the olfactory bulb designated proximal. The distal proc

[1] This investigation was supported in part by an institutional grant [illegible] from the National Institutes of Health, United States Public Health Service

[2] Present address Northwestern University Medical School, Department of Anatomy Chicago, Illinois.

occur in the region of the Golgi apparatus (fig. 6) These bodies are each bounded by a trilaminar membrane that dimensionally is identical to Golgi cisternal membranes (60 Å) (inset, fig 6) The contained lamellar structures show a periodic cross-striation in which the repeat distance is approximately 30 Å.

Granular endoplasmic reticulum is found in the perikaryon, but no areas rich enough in ribosomes to be termed Nissl bodies are seen. Some of the smooth-surfaced membranes of the perikaryon form cisternae which are separated by thin layers of cytoplasm. Round glycogen granules fill these cytoplasmic spaces (fig. 6)

Olfactory cell proximal processes. The *proximal processes of the olfactory cells* arise at the basal end of the perikaryon. The most prominent cytoplasmic constituents of the proximal processes are neurotubules and occasional mitochondria. As with other axons ribosomes and granular endoplasmic reticulum have not been observed in proximal processes. These narrow diameter processes (0.2 μ) come together and form small bundles while still within the epithelium. The bundles are invested by processes of basal cell cytoplasm that all but surround the group (fig 7) Cytoplasmic processes that are less electron dense than the basal cell cytoplasm have also been observed on the epithelial side of the basement membrane in association with the proximal processes (fig. 8) This cytoplasm displays a cytology identical to the Schwann cells which invest the bundles of proximal processes in the subjacent connective tissues. After passing through the thin basement membrane which demarcates the epithelium, bundles merge forming larger groups (fig. 9) Individual fibers in any one bundle occupy the same intercellular space without separation by intervening Schwann cell or basal cell processes

Supporting cells

Free surface and apical cytoplasm The supporting cells of the olfactory epithelium are not ciliated, although the free surface carries both microvilli (figs. 1 2) and complex branching processes that may fuse or at least possess multiple origins from the surface of the cell (fig 10) An organelle-free terminal web area of cytoplasm directly underlies the free surface of the supporting cells. The rod-shaped mitochondria, usually oriented with their long axis parallel to the long axis of the cell bend or are oriented parallel to the free surface at or near the border of this organelle-free zone (fig. 1) These organelles are large and rod-shaped and have an electron dense matrix. Regardless of the plane of section, each mitochondrion is almost completely surrounded by smooth-surfaced membranes. This association of membranes and mitochondria is a constant finding throughout the cell, being absent or incomplete only in the most basal part of the foot process.

Randomly oriented membranous profiles and stacked lamellae of smooth-surfaced membranes are also present in the apical area of the cell (fig. 11) In those cells where stacked membranes have been observed, secretory granules also have been noted.

The cytoplasm basal to the supporting cell nuclei contains another arrangement of smooth-surfaced membranes. This consists of loose whorl systems in close association with glycogen granules (fig. 12) This area of the cell is the only one in which glycogen granules seem to occur as a regular finding.

The cytoplasm of the supporting cells contains very few electron dense bodies that display the morphology associated with pigment granules, lysosomes or microbodies. Such structures seem to be present only in that part of the foot process which is closest to the basement membrane (fig. 13) Even in this region of the supporting cells these electron dense bodies are not consistently observed.

Attachment points have been observed between adjacent supporting cells including terminal bars at the free surface and small infrequent desmosomes along the lateral borders.

Basal cells

Basal cells are confined to the region of the olfactory epithelium that is adjacent to the basement lamina. The most prominent feature of these cells is the attenuation of cytoplasm into long thin processes. Many of these processes invest bundles of olfac

ess ends in a ciliated apical expansion usually termed olfactory rod or olfactory vesicle. Supporting cells are nonciliated columnar epithelial cells The olfactory glands of Bowman are thought to be branched and of the tubulo-alveolar type with the secretory cells often considered serous

Olfactory cells

Olfactory vesicle and distal process Ciliated olfactory vesicles extend above the free surface of the olfactory epithelium where they are surrounded by projections from adjacent supporting cells (fig 1) The cilia of these olfactory vesicles are specialized structures They contain the usual nine plus two pairs of ciliary tubules for only the proximal 1 μ At that point they taper to a narrow cylinder containing as few as two tubules (fig 2) Occasional ovoid dilations occur along the length of these cylindrical ciliary extensions (figs 2, 3) These dilations affect only the matrix of the extension and not the diameter of the contained tubules Further from the surface of the epithelium the dilations increase both in size and number resulting in numerous balloon like profiles In some areas along the length of these ciliary extensions an extraneous coat of fuzzy material is present (fig 3)

The cytoplasm of the olfactory vesicles contains the ciliary basal bodies neurotubules a few vesicles and some mitochondria No consistent relationship between these structures has been observed Ordinarily the basal bodies show no basal feet rootlets or any other cytoplasmic filamentous apparatus although basal feet have been observed in one specimen Even in that specimen the basal feet are not as prominent as in the neighboring ciliated cells of the respiratory epithelium

The ciliated olfactory vesicles are apical expansions of olfactory cell distal processes The electron density and granularity of the cytoplasmic matrix are essentially the same in the olfactory vesicle and in the distal process (fig 1) There is no apparent barrier between the two areas but there is a difference in mitochondrial morphology All mitochondria of the olfactory vesicles have cristae which are perpendicular to the long axis of the organelle (fig 1) Mitochondria of the distal process usually contain cristae that are arranged in a longitudinal orientation In addition to the characteristic mitochondria, the distal process shows large numbers of neurotubules that are quite regularly aligned in parallel with the long axis of the process (fig 1) In cross-sectioned processes, the neurotubule diameter approximates 280 Å. An electron dense dot of approximately 90 Å is present in the center of many of these round profiles (fig 4) In appropriate longitudinal section the central structure is seen as a filament although it has not been possible to follow each filament over long distances (fig 4 inset)

The proximal area of the olfactory vesicles is closely apposed to the adjacent supporting cells with the apposed membranes displaying a modification similar to a terminal-bar (fig 1) The distal process is also closely associated with the surrounding supporting cells but an irregular intercellular space not less than 200 Å wide intervenes between the cells Attachment points or other membrane specializations have not been observed between supporting cells and olfactory cell distal processes other than the terminal-bar (fig 1)

Only one olfactory cell distal process usually occupied the space between the apical cytoplasm of two supporting cells but on some occasions two distal processes have bene observed in the same intercellular space (fig 4) That the two processes illustrated in figure 4 are actually two separate processes is indicated by the appearance of the two plasma membranes as sharp lines and also by the slight difference in electron opacity of the two cytoplasms

Olfactory cell nuclear region As is the case with the distal processes the perikarya of the olfactory cells can be in direct contact with each other They may also be in contact with distal processes of other olfactory cells (fig 5) No specialized organization of the cell membrane such as desmosomes or synaptic thickenings has been observed in the areas of contact

In the perikaryon of the olfactory cells an extensive Golgi apparatus is situated on the apical side of the nucleus One or more lamellated electron dense bodies

amount of osmiophilic smooth-surfaced membranes that occupy the bulk of the cytoplasm (fig. 17). Often, these smooth surfaced membranes will be organized into tightly packed whorl systems that seem to be centered about mitochondria or remnants of mitochondria (fig. 18). These whorl systems are extensive enough to be observable with phase microscopy as round dark structures if the tissue has been first fixed with osmium tetroxide. At the periphery of a whorl, the smooth-surfaced membranes may be continuous with rough-surfaced membranes (fig. 18). Outer elements of the whorl may also diverge and approach mitochondria on the periphery. Mitochondria throughout the rest of the cytoplasm are associated with smooth-surfaced membranes in an organization similar to that described above in the supporting cells of the epithelium.

A small Golgi apparatus has been observed in the dark cell cytoplasm (fig. 17) usually close to the nucleus. There is usually a proximity to secretory granules which allows the possibility that the Golgi apparatus plays some role in elaboration of the product. Granules close to the Golgi apparatus may appear less electron dense than those occurring at the cell apex (fig. 17) but the size range of sectioned granules is similar.

Dark cells containing secretory granules have also been observed within the limits of the epithelium where they form the initial cells of the ducts of Bowman's glands (fig. 19). Cells more superficially placed in the ducts resemble the dark cells in that they possess large quantities of smooth surfaced membranous elements. These flattened duct cells are provided with branching microvilli on the luminal surface (fig. 20).

One negative finding in the investigation of the cytology of Bowman's glands merits mention here. A basement membrane has not been observed in association with either the dark cells or the light cells. Under the conditions of preparation used, basement membranes have been demonstrated underlying both the olfactory epithelium and respiratory epithelium, surrounding nerve bundles and smooth muscle cells underlying capillary endothelium and surrounding alveoli of the serous glands of the respiratory mucosa.

DISCUSSION

The diagram (fig. 21) summarizes the fine structure of the olfactory mucosa as observed in this study. The drawing is principally a modification of micrographs, although some attempt has been made to indicate three-dimensionality particularly with respect to the olfactory cilia.

The fact that the receptor cell of the olfactory epithelium is a ciliated nerve cell has been established and described in virtually every vertebrate class (Alcock, '10; Dogiel, 1886; Hopkins, '26; Jagodowski, '01; Le Gros Clark, '57; Read, '08). In general, the cilia have been described as extremely long, sometimes exceeding twice the length of the rest of the cell. Bloom ('54) in one of the first electron microscope studies of the olfactory epithelium reported that the cilia were at least 40 μ long in the frog. Reese ('65) has reported frog olfactory cilia up to 200 μ in length. De Lorenzo ('60) reported short cilia in the rabbit. Although no individual cilium was followed for more than 4 μ in this study, there is no doubt that they are considerably longer. Perhaps, of even greater significance, is the observation that the cilia do not conform to the ciliary morphology observed in the neighboring respiratory epithelium or, for that matter, in numerous other tissues from numerous other organisms. The observations reported here and in earlier reports (Frisch, '64a,b, '83; Reese, '65) seem to be the first descriptions of cilia which taper down to long narrow cylinders containing reduced numbers of ciliary tubules. Nor have the dilations that occur along the length of the extensions previously been reported, although Reese ('65) observed large vesicles within the ciliary extensions. At those points, the extension diameter is enlarged to accommodate the vesicle. The similarity between these two sets of observations lends credence to the occurrence but does not eliminate the possibility of preparation artifact.

The morphology of the olfactory cell cilia should be considered in terms of their possible functions. The cilia must be considered candidates for sites of initial re-

tory cell processes (fig 7) while others loosely interdigitate with processes from neighboring basal cells and the foot processes of the supporting cells Large compartments of extracellular space occur in this region of the epithelium since the basal cell processes are usually finger-like rather than plate-like The cytology of the basal cells has few distinguishing features The usual cytoplasmic organelles are present and occasional prominent bundles of fine filaments have been observed The nucleus is invariably indented

Olfactory-respiratory epithelium junction

The supporting cells of the olfactory epithelium are quite different from the columnar cells of the respiratory epithelium of the nasal mucosa. The latter may or may not be ciliated They have small mitochondria isolated profiles of rough surfaced endoplasmic reticulum and a quite small Golgi apparatus A direct comparison may be made between these supporting cell types by examination of junctions between the two tissues (fig. 14) Cells of the two tissues are joined at the surface by terminal bars, but no desmosomes have been observed in the lateral borders. Junctions between the two tissues are always abrupt and show no intermixing of cell types.

Bowman's glands

Figure 15 is an electron micrograph showing a section through the connective tissue immediately adjacent to the sensory epithelium A number of different kinds of cytoplasm are contained within the section but the most prominent elements are two separate groupings of what appears to be three cells each The first grouping has electron lucent vesicular appearing cytoplasm and the second has quite electron dense cytoplasm containing a considerable number of almost clear secretory granules Other profiles of similar electron dense cytoplasm are present throughout the field Both the vesicular appearing cells and the electron-dense cells "light" and "dark" cells respectively form part of Bowman's glands The gland system is diffuse with no regular alveolar structure discernible particularly with regard to the highly ramified dark cells (fig 15)

That both cell types contribute to the formation of a secretory unit derives from the observation that both cell types may share one lumen (fig 16) This may be an acinar lumen or the lumen of an intercellular secretory canaliculus. The latter is more likely since the central cell of the group shown in figure 16 contributes to the border of at least two such lumens. The discrimination between lumenal space and non-secretory but widened intercellular space is difficult at these low magnifications. The luminal surfaces of both cell types are provided with microvilli that at low magnification appear similar to the long slender processes arising from the cell surfaces that face connective tissue spaces or intercellular spaces. The necessary criterion for identification of a lumen is the presence of tight junctions at the cell apices (fig 17) Terminal bars occur between adjacent dark cells, adjacent light cells and between light and dark cells but all occur only at the border of the lumen. Desmosomes occur close to the terminal bars but are not constantly observed in all sections

The vesicular appearing light cells possess extensive granular endoplasmic reticulum (fig 17) and this is their most prominent characteristic. There is a large Golgi apparatus with a number of vesicles filled or partly filled with material that approximates the electron density and granularity of the substance contained within the dilated cisternae of the granular endoplasmic reticulum. Similar vesicles appear occasionally near the apex of the cell (fig 17) but this is an infrequent finding. No other granule or vesicle type is constantly found at the apex and thus either these small vesicles represent secretory granules or the cells produce none. The latter seems more likely

Secretory granules are prominent constituents of the dark cell cytoplasm (figs. 15 16 17) Each granule consists of a single membrane bound space that is filled with a finely granular substance Small areas of what appears to be denser aggregations of the same material are often present.

Much of the electron density of the dark cells as seen in low magnification electron micrographs is a result of the vast

amount of osmiophilic smooth-surfaced membranes that occupy the bulk of the cytoplasm (fig 17) Often, these smooth surfaced membranes will be organized into tightly packed whorl systems that seem to be centered about mitochondria or remnants of mitochondria (fig 18) These whorl systems are extensive enough to be observable with phase microscopy as round dark structures if the tissue has been first fixed with osmium tetroxide. At the periphery of a whorl, the smooth-surfaced membranes may be continuous with rough-surfaced membranes (fig. 18) Outer elements of the whorl may also diverge and approach mitochondria on the periphery Mitochondria throughout the rest of the cytoplasm are associated with smooth-surfaced membranes in an organization similar to that described above in the supporting cells of the epithelium.

A small Golgi apparatus has been observed in the dark cell cytoplasm (fig. 17) usually close to the nucleus There is usually a proximity to secretory granules which allows the possibility that the Golgi apparatus plays some role in elaboration of the product. Granules close to the Golgi apparatus may appear less electron dense than those occurring at the cell apex (fig 17) but the size range of sectioned granules is similar

Dark cells containing secretory granules have also been observed within the limits of the epithelium where they form the initial cells of the ducts of Bowman's glands (fig. 19) Cells more superficially placed in the ducts resemble the dark cells in that they possess large quantities of smooth surfaced membranous elements. These flattened duct cells are provided with branching microvilli on the luminal surface (fig. 20)

One negative finding in the investigation of the cytology of Bowman's glands merits mention here. A basement membrane has not been observed in association with either the dark cells or the light cells. Under the conditions of preparation used, basement membranes have been demonstrated underlying both the olfactory epithelium and respiratory epithelium, surrounding nerve bundles and smooth muscle cells underlying capillary endothelium and surrounding alveoli of the serous glands of the respiratory mucosa.

DISCUSSION

The diagram (fig 21) summarizes the fine structure of the olfactory mucosa as observed in this study The drawing is principally a modification of micrographs although some attempt has been made to indicate three-dimensionality particularly with respect to the olfactory cilia.

The fact that the receptor cell of the olfactory epithelium is a ciliated nerve cell has been established and described in virtually every vertebrate class (Alcock, '10; Dogiel, 1886 Hopkins '26; Jagodowski, '01 Le Gros Clark, '57; Read, '08) In general, the cilia have been described as extremely long sometimes exceeding twice the length of the rest of the cell. Bloom ('54) in one of the first electron microscope studies of the olfactory epithelium reported that the cilia were at least 40 μ long in the frog. Reese ('65) has reported frog olfactory cilia up to 200 μ in length. De Lorenzo ('60) reported short cilia in the rabbit. Although no individual cilium was followed for more than 4 μ in this study there is no doubt that they are considerably longer Perhaps of even greater significance is the observation that the cilia do not conform to the ciliary morphology observed in the neighboring respiratory epithelium or for that matter in numerous other tissues from numerous other organisms. The observations reported here and in earlier reports (Frisch, '64a,b 65 Reese, '65) seem to be the first descriptions of cilia which taper down to long narrow cylinders containing reduced numbers of ciliary tubules. Nor have the dilations that occur along the length of the extensions previously been reported, although Reese ('65) observed large vesicles within the ciliary extensions. At those points the extension diameter is enlarged to accommodate the vesicle. The similarity between these two sets of observations lends credence to the occurrence but does not eliminate the possibility of preparation artifact.

The morphology of the olfactory cell cilia should be considered in terms of their possible functions The cilia must be considered candidates for sites of initial re-

actions in the process of olfaction if only because of their position extending above the epithelium into the mucus In support of this Parker ('22) recognized that con ditions which affected the integrity of the cilia disturbed normal olfactory response Ottoson ('58) succeeded in recording potentials from the olfactory epithelium which were quite similar to generator potentials recorded from the retina where the receptor elements are known to be modified cilia. Moreover these potentials were recorded above the surface of the epithelium where cilia are known to occur (Ottoson '54) Other investigators have noted at least three separate slow poten tials, all clearly a result of olfactory cell activity (Takagi and Yojima '65)

The dilations that occur in the ciliary extensions may also support the possibility that olfactory cilia can serve as initial receptor sites for olfactory stimuli. Swelling would seem to indicate that at least some change in state has occurred It is not un reasonable to assume that this change is a reflection of a localized chemical reaction between the cell and possible stimulating molecules Again the possibility that the dilations as observed in this study represent only artifacts of preparation has not been eliminated They do not appear to be fixation artifacts since they occur in tissue fixed with three concentrations of glutaraldehyde and in tissue fixed directly with osmium tetroxide

The question remains as to the kinds of responses cilia may make to olfactory stimulation. One obvious first response is move ment. This possibility is weakened by the observations of Hopkins ('26) who reported that the olfactory cilia were non motile, probably because movement is hindered by the tight network the cilia seem to form Reese ('65) observed that the long cilia were non-motile but shorter ones may have some motility He attributed non-motility to impediment by the mucus Bloom ('54) described the cilia as typical kinetocilia, indicating that they have at least the potential for movement. In the current study the observations made seem to indicate that the network is hardly as restrictive of movement as Hopkins believed and the cilia do appear to be typical kinetocilia, if only for the proximal 1 μ portion. Lack of observable movement may be explained in a number of ways The most evident explanation is that movement does not occur or that excursions are too small to be visualized under the conditions of observation Asynchronous movement of cilia would be difficult to observe since currents established by such movements would be limited. Reese ('65) did observe a slow current which he attributed to constant production of new mucus

The morphology as observed in this study does not yield a great amount of information concerning ciliary motility or lack of it. The basal bodies of the cilia do not display the same morphology as the basal bodies of the motile cilia of the respiratory epithelium (Frisch and Reith '66). Cytoplasmic filamentous structures in association with basal bodies and ciliary rootlets are rare or absent unlike the condition in the frog (Reese '65) There is no consistent relationship of mitochondria or neurotubules to basal bodies although in sectioned olfactory vesicles both kinds of organelles are almost invariably observed. None of these characteristics or combinations of characteristics provides a convincing basis for the apparent lack of motility It is still possible that the cilia are motile under appropriate conditions including perhaps stimulation by olfactants.

The unique morphology of the olfactory cilia is perhaps one of the most interesting observations in a study of the olfactory epithelium If they do function in olfac tion as appears likely this function must be regulated by the specific environment in which they exist. That this environment is liquid rather than air is indicated by the extraneous coat of fuzzy material observed on the ciliary extensions similar to that described by Brandt ('62) and Ito ('64) as a product of fluid media. The observations of Reese ('65) are thus supported in full by observations in this study Before stimulation of the epithelium may occur it is thus necessary for an olfactant molecule to dissolve or become suspended in the mucus.

This chemically undefined mucus or fluid medium overlying the olfactory epi thelium is in large measure a product of the glands of Bowman The mucus pro-

duced by these glands seems to be quite specific as is indicated by the difference between these glands and those of the nasal respiratory mucosa. In the latter the cells are for the most part typical serous cells characterized by extensive rough surfaced endoplasmic reticulum (Frisch '64b) The principal cell type of Bowman's glands seems to be one with large quantities of smooth-surfaced endoplasmic reticulum. Although the secretion of these unique cells has not been characterized chemically smooth-surfaced endoplasmic reticulum has been associated both with the production of lipid products such as steroids, and with carbohydrate metabolism. If the secretion were in part, lipid the stimulatory ability of such organic olfactants as the relatively non-polar esters would be partially explicable in terms of solvation. However it is felt that the unique structure of these cells does not justify an assumption that they secrete lipid. Cells with this extensive development of smooth surfaced endoplasmic reticulum have not been examined with respect to the product formed, although some histochemistry has been done on Bowman's glands (Mira, '63).

It is clear that the mucus produced by cells of Bowman's glands may be modified by the action of the supporting cells of the epithelium. The presence of secretory granules not prominent in the mouse but quite prominent in the toad (Porter and Bonneville '64) indicates that the supporting cells contribute some material to the mucus. Smooth-surfaced membranes are prominent constituents of the cells and are likely to function in the elaboration of the secretory product. The smooth-surfaced membranes in these cells are in association with both mitochondria and glycogen granules. Such an association possibly provides an energetic basis for an active synthetic role for these membrane systems.

The presence of the complex branching processes and microvilli on the free surface of the supporting cells also indicates that absorption of elements of the mucus by the supporting cells may occur The formation of a syncytium through intercellular fusion of the complex branching processes, as reported in oviduct epithelium (Aitken and Johnston, '63) has not been observed in this study

Underlying the free surface the terminal web area, the cytoplasm of the supporting cells seems to be strongly gelated. This is based on the observation that cell organelles do not enter this region and, in fact, mitochondria seem to bend on contact with the terminal web area. No confirmation for De Lorenzo's hypothesis ('63) that this organelle-free zone is sloughed off to form a contribution to the mucus has been obtained in this study

The fine structure of the supporting cell of the olfactory epithelium as observed in this study and the supporting cell of the respiratory epithelium are quite different. Before the application of electron microscopy little difference was noted (Allison, '53) With the light microscope the clearest distinction made between the two tissues was the presence of yellow pigment in the olfactory epithelium. No definitive study of this yellow pigment exists, although there is evidence which indicates it is restricted to the supporting cells and Bowman's glands and it is not present in receptor cells (Takagi and Yajima '65)

In studies of pigmented mice we have yet to identify any difference between these and an albino strain either by visual inspection of the mucosal surface or by microscopic examination It would seem then that the yellow pigment reported in the literature at least in the specific instance of the mouse is not affected by albinism and most certainly is not a close relative of melanin as suggested by Moncrieff ('48) However the extensive membranous systems and secretory products of both the supporting cells and the cells of Bowman's glands indicate a high lipid content that may well be expected to give a yellowish tint to these cells and thus to the entire mucosa. If these membrane systems and secretory products constitute the "yellow pigment," then loss of such systems would result in loss of whatever function these organelle systems have. As has already been discussed, this would affect the quality of the overlying mucus and consequently interfere with normal reception. Moncrieff ('48) has presented an analysis of the behavior of albino animals which does indicate a possible role for the pigment in initial olfactory reception.

The olfactory epithelium is also of interest because it is a specialized constituent of the nervous system which may yield information *not only relating to the sense of* smell but also to all sensory reception and to nerve characteristics in general In the latter terms Gasser ('56) and De Lorenzo ('57) have already reported the lack of insulating cytoplasm between proximal processes of olfactory cells. In the present study this lack of insulating cytoplasm between olfactory cells has been observed in the region of the perikarya and even between neighboring distal processes Recent reports suggest that side-by-side interaction may occur between fibers in the olfactory nerve bundles (Moulton and Tucker 64) What effect a similar lack of insulation may have on mucosal potentials has not been evaluated

ACKNOWLEDGMENTS

The *author wishes to express his* gratitude for the advice and encouragement so kindly tendered by Professors Edward J Reith and Johannes A. G Rhodin during this study

LITERATURE CITED

Aitken, R. N C., and H S. Johnston 1963 Observations on the fine structure of the infundibulum of the avian oviduct. J Anat., *97:* 87–100.

Alcock, N 1910 The histology of the nasal mucous membrane of the pig. Anat. Rec., *4* 123–129

Allison, A. C. 1953 The morphology of the olfactory system in the vertebrates. Biol. Rev., *28:* 195–244

Andres K. H 1966 Der Feinbau der Regio Olfactoria von Makrosmatikern. Zeit. für Zellforschung, *69:* 140–154

Bloom G 1954 Studies on the olfactory epithelium of the frog and the toad with the aid of light and electron microscopy Zeit. für Zellforschung, *41:* 89–100.

Bloom, G., and H. Engström 1952 The structure of the epithelial surface in the olfactory region. Exptl. Cell Research, *3:* 699–701

Brandt, P W 1962 A consideration of the extraneous coats on the plasma membrane Circulation, *26:* 1075–1091.

De Lorenzo, A. J 1957 Electron microscope observations of the olfactory mucosa and olfactory nerve. J Biophys. Biochem. Cytol., *3:* 839–850.

——— *1960 Electron microscopy of the ol*factory and gustatory pathways. Ann. Otol. Rhenol. Laryngol., *69:* 410–420.

——— 1963 Studies on the ultrastructure and histophysiology of cell membranes, nerve fibers and synaptic junctions in chemoreceptors. The Olfaction and Taste. Proceedings of the First *International Symposium* held at the Wenner Gren Center Stockholm. Sept. 1962. Ed. by Y Zotterman, Macmillan Co., New York, N Y *Vol. 1:* 5–18

Dogiel A. S. 1886 Über die Drüsen der Regio olfactoria. Arch. *Mikr* Anat., *26* 50–60.

Frisch, D 1964a Ultrastructural observations of the mouse nasal and olfactory mucosa. Anat. Rec., *148:* 283 (Abst.)

——— 1964b An electron microscope study of the nasal mucosa of the mouse. Doctoral Dissertation. *New* York University Graduate School of Arts and Sciences.

——— 1965 Ultrastructure of mouse olfactory mucosa. Anat. Rec., *151:* 351 (Abst.)

Frisch D., and E. J Reith 1966 An inter-basal body apparatus in mammalian cells. J Ultrastructure. In press.

Gasser H. S. 1956 Olfactory nerve fibers. J. Gen. Physiol., *39:* 473–496.

——— 1958 Comparison of the structure as revealed with the electron microscope and the physiology of the unmyelinated fibers in the skin nerves and in the olfactory nerves. Exptl. Cell Research, *Suppl., 5:* 3–17

Hopkins, A. E. 1926 The olfactory receptors in vertebrates. J Comp Neur., *41:* 253–261

Ito S. 1964 The surface coating of enteric microvilli. Anat. Rec., *148:* 294

Jagodowski, K. P 1901 Zur Frage nach der Endigung der Geruchsnerven bei den Knochenfischen. Anat. Anz., *19:* 257–267

Kuehner R. C. (Editor) 1964 Recent advances in odor: Theory measurement and control. *Ann. N Y Acad. Sci. 116* (2): 357–746.

Le Gros Clark, W E. 1951 The projection of the olfactory epithelium on the *olfactory bulb* of the rabbit. J Neurol. Psychiat., *14* 1–10.

Luft, J H. 1961 Improvements in epoxy resin embedding methods. J Biophys. Biochem. *Cytol., 9: 409–414*

Mira, E. 1963 Oxidative and hydrolytic enzymes in Bowman's glands. Acta Otolaryng., 56 706–714

Moncrieff R. W 1946 The Chemical Senses. Leonard Hill, Ltd., London

Moulton, D G., and D Tucker 1964 Electrophysiology *of* the olfactory system. Ann. N Y Acad. Sci., 116 (2): 380–428.

Ottoson, D 1954 *Sustained* potentials evoked by olfactory stimulation. Acta Physiol. Scand., *32* 384–386.

——— 1958 The slow electrical response of the olfactory end organs. Exptl. Cell Research, *Suppl. 5:* 451–459

Parker G. H. 1922 Smell, Taste and Allied Senses in the Vertebrates. J B. Lippincott, Philadelphia, Pa.

Porter K. R., and M. A. Bonneville *1964* An Introduction to the Fine Structure of Cells and

Tissues, Second Edition. Lea and Febinger Philadelphia, Pa.
Read, E. A. 1908 A contribution to the knowledge of the olfactory apparatus in dog, cat and man. Am. J. Anat., 8 17–47
Reese, T. S. 1965 Olfactory cilia in the frog. J Cell Biol., 25 209–230.
Reynolds E. S. 1963 The use of lead citrate at high pH as an electron-opaque stain in electron microscopy J Cell Biol., 17: 208–212.
Takagi, S. F., and T Yajima 1965 Electrical activity and histological change in the degenerating olfactory epithelium. J Gen. Physiol., 48 559–569

PLATE 1

EXPLANATION OF FIGURE

1 This electron micrograph shows a section through the free surface of the olfactory epithelium. In the center of the figure is an olfactory cell distal process (DP) terminating in an apical expansion the olfactory vesicle (OV) The olfactory vesicle is ciliated (c) and a number of basal bodies (bb) are sectioned in all planes. A number of ciliary extensions (ce) identifiable by the presence of internal microtubules are distinguishable from the microvilli (mv) that arise from the adjacent supporting cells (SU) Neurotubules (nt) and mitochondria (m) are prominent constituents of the cytoplasm of the distal process. The background matrix of the supporting cells is considerably more electron dense than the olfactory cell cytoplasm. In the cytoplasm of the supporting cells are large amounts of agranular endoplasmic reticulum (er) both in a tubular form and a cisternal form associated with each of the plentiful mitochondria. Arrowheads indicate terminal bars between olfactory cells and supporting cells as well as between neighboring supporting cells. × 20,000.


mv
c
bb
OV
DP
Su
DP
nt

PLATE 1

EXPLANATION OF FIGURE

1 This electron micrograph shows a section through the free surface of the olfactory epithelium. In the center of the figure is an olfactory cell distal process (DP) terminating in an apical expansion, the olfactory vesicle (OV) The olfactory vesicle is ciliated (c) and a number of basal bodies (bb) are sectioned in all planes. A number of ciliary extensions (ce) identifiable by the presence of internal microtubules are distinguishable from the microvilli (mv) that arise from the adjacent supporting cells (SU) Neurotubules (nt) and mitochondria (m) are prominent constituents of the cytoplasm of the distal process. The background matrix of the supporting cells is considerably more electron dense than the olfactory cell cytoplasm. In the cytoplasm of the supporting cells are large amounts of agranular endoplasmic reticulum (er) both in a tubular form and a cisternal form associated with each of the plentiful mitochondria. Arrowheads indicate terminal bars between olfactory cells and supporting cells as well as between neighboring supporting cells × 20,000.


c
mv
bb
OV
DP
nt

PLATE 1

EXPLANATION OF FIGURE

1 This electron micrograph shows a section through the free surface of the olfactory epithelium. In the center of the figure is an olfactory cell distal process (DP) terminating in an apical expansion, the olfactory vesicle (OV) The olfactory vesicle is ciliated (c) and a number of basal bodies (bb) are sectioned in all planes. A number of ciliary extensions (ce) identifiable by the presence of internal microtubules are distinguishable from the microvilli (mv) that arise from the adjacent supporting cells (SU) Neurotubules (nt) and mitochondria (m) are prominent constituents of the cytoplasm of the distal process. The background matrix of the supporting cells is considerably more electron dense than the olfactory cell cytoplasm. In the cytoplasm of the supporting cells are large amounts of agranular endoplasmic reticulum (er) both in a tubular form and a cisternal form associated with each of the plentiful mitochondria. Arrowheads indicate terminal bars between olfactory cells and supporting cells as well as between neighboring supporting cells. × 20,000

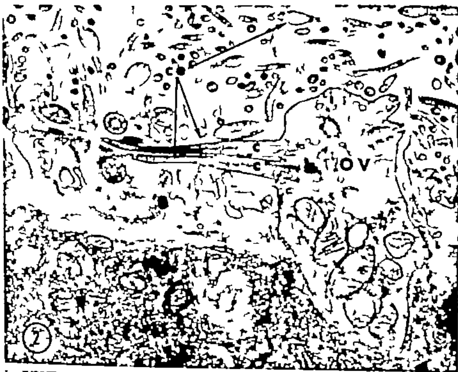

C
C
OV
2

PLATE 2

EXPLANATION OF FIGURES

2 The olfactory cell cilia (c) taper into long cylindrical extensions (ce) approximately one micron distal to the point of origin on the olfactory vesicle (OV). These ciliary extensions contain as few as two microtubules and, close to the free surface of the epithelium, show occasional ovoid dilations. × 20,000.

3 Further from the free surface of the epithelium, the dilations of the ciliary extensions increase in size and number. Microtubules (mt) in the extension maintain the same diameter in dilated regions as they have in the non-dilated regions. The unlabeled arrows indicate areas where an extraneous coat of fuzzy material is present. × 49,000.

SU

DP

DP

SU

C3

DP

C1

C2

PLATE 3

EXPLANATION OF FIGURES

4 Two olfactory cell distal processes (DP_1 and DP) occupy the intercellular space between two supporting cells which have been sectioned at the level of the supporting cell nuclei. One of these dendritic processes (DP_1) is in almost perfect cross-section and the regularly aligned neurotubules appear as round profiles. In many of these round profiles a central dot is present (arrows) In longitudinal section through another distal process (inset) the neurotubules contain a central filamentous structure (arrows) × 60 000 Inset: × 71,000.

5 This section shows a small portion of the olfactory cell zone of the epithelium Olfactory cell perikarya at any point on their surface may be directly adjacent In this section C and C_2 are contiguous and both C_1 and C_2 occupy part of the border of C_3. A number of distal processes (DP) from other olfactory cells also border on the perikarya of both C and C_2 An extensive Golgi apparatus (g) is the most prominent cytologic characteristic of the olfactory cell perikaryon, always occurring on the dendritic or distal process side of the nucleus. × 7 700


m
n
db
n
B
P
B
PP
7
M

PLATE 4

EXPLANATION OF FIGURES

6 The distal process end of the olfactory cell perikaryon has a number of distinguishing cytological features. Frequently there is a series of smooth surfaced cisternae associated with round glycogen granules (gly) Few cisternae of granular endoplasmic reticulum occur and although large numbers of free ribosomes are distributed throughout the region no areas comparable to Nissl bodies are seen. Mitochondria (m) in this region often contain ring-shaped cristae in addition to the usual transverse cristae Under the conditions of preparation used in this study the mitochondrial matrix varies in electron density from the electron lucent character in this figure to the electron dense state shown in the distal processes in figure 1 The nucleus (n) is large, vesicular and sections usually show few nuclear pores. A portion of the extensive Golgi apparatus (g) is present in this section as is a large lamellated electron dense body (db) One or more of these lamellated bodies occur in sections through the Golgi area with up to five observed in a single section. At higher magnification (inset) the contained lamella display a cross striation which often is in close register (arrowhead) The trilaminar structure of the thin (60 Å) limiting membrane of the dense body is shown at the arrow × 19 000 Inset: × 170 000

7 A number of olfactory cell proximal processes (PP) have formed a small bundle all but completely surrounded by cytoplasmic processes of a basal cell (BC) This bundle is completely within the epithelium as demarcated by the thin basement membrane (BM) × 36,000.

8

PP

BM

Sch

9

BM

Sch

PLATE 5

EXPLANATION OF FIGURES

8 This figure and the next are part of a montage that shows the exit of a bundle of olfactory cell proximal processes from the epithelium. In figure 8 the bundle is wholly contained within the continuous basement membrane (BM) that limits the epithelium. Cytoplasmic processes of basal cells (BC) are close to the bundle but not in intimate contact with it. Another kind of cytoplasm less electron dense and containing small vesicles (Sch) is also present on the epithelial side of the basement membrane and is associated with the bundle. × 12,000

9 The basement membrane (BM) is interrupted by both the Schwann cell-like cytoplasm (Sch) and a number of proximal processes. Other proximal processes already outside the limits of the epithelial basement membrane, merge with those processes exiting and form a larger bundle. × 12,000


10


m
11


12


m

PLATE 6

EXPLANATION OF FIGURES

10 This section contains a complex branching process from the surface of a supporting cell. The arrows indicate two points of connection of the process with the surface. × 26 000

11 Stacked lamellae of agranular endoplasmic reticulum (er) frequently occur in the apical cytoplasm of the supporting cells. Secretory granules (sg) bound by a single limiting membrane, are also present in this section × 20 000

12 A loose whorl system of smooth surfaced membranes is present in the supporting cell cytoplasm below the level of the supporting cell nuclei. Glycogen granules (gly) invariably occur in this region. × 29 000

13 The foot process (FP) of a supporting cell usually contains microtubules (mt) and bundles of fine filaments. It may also contain a variety of electron dense bodies (db) × 19,000.

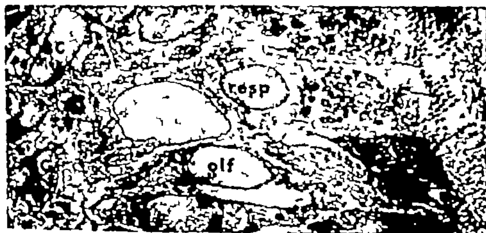

C
resp
olf

PLATE 7

EXPLANATION OF FIGURES

14 The respiratory epithelium (resp) occupies the upper portion of this figure and the olfactory epithelium (olf) the lower portion. The junction between the two tissues is always sharp with no intermixing of cell types The ciliated (c) respiratory epithelial cells are less electron dense than the neighboring olfactory supporting cells, primarily because of the difference in membrane content. Basal cells (BC) of the two epithelia are quite similar Note the olfactory vesicles (OV) close to the border of the two tissues × 3,000

15 Two groups of cells occupy the center and left of this figure with connective tissue and smooth muscle cells prominent on the right of the figure. The upper group of what seems to be three cells (LC) has electron lucent vesicular-appearing cytoplasm. The lower group of cells (DC) has dense cytoplasm containing electron lucent secretory granules (sg) Isolated profiles of similar dense cytoplasm occur throughout the field. An occasional area of greater density (w) within the dark" cytoplasm represents the whorl systems of smooth membranes found in these cells The arrowheads indicate a long, bending extension originating from one "dark cell" that, if it had been cut in another plane would have resulted in an isolated profile of dense cytoplasm similar to others in the field. Direct fixation with 2% OsO_4. × 2,700


G2
sg
ger
16

PLATE 8

EXPLANATION OF FIGURE

16 Both cell types comprising the olfactory glands of Bowman form a cluster in this section. Whorl systems (w) secretory granules (sg) and a prominent Golgi apparatus (g) are indicated in the "dark cells." Granular endoplasmic reticulum (ger) fills the bulk of the cytoplasm of the "light cells." The round nuclei (n) of the "light cells" is indicated Both cell types have long, finger-like projections extending from surfaces that face the connective tissue space (unlabeled arrows) Similar projections occur on the intercellular surfaces. Both cell types may share a secretory lumen (L_1) and any one cell may contribute to the border of more than one lumen (L_1, L_4) × 9,500


16

PLATE 9

EXPLANATION OF FIGURE

17 At higher magnification one of the lumens shown in figure 16 (L_1) can be better characterized. The cells contributing to the border of the lumen are provided with microvilli (mv) and form tight junctions at the surface (arrowheads). Desmosomes (d) may also be present near the lumen. In the "dark cell" at the left of the figure a portion of a whorl system (w) is present, there is a prominent Golgi apparatus (g) and many mitochondria (m). Much of the cytoplasm is occupied by a tubular form of agranular endoplasmic reticulum with smooth surfaced cisternal membranes associated with most of the mitochondria. The "light cell" at the bottom of the figure also has a prominent Golgi apparatus with a number of electron lucent and partially filled vesicles (v) in the region. Similar vesicles occur in this cell near the luminal surface. Some of the dilated cisternae of the granular endoplasmic reticulum (ger) that characterize the "light cells" is at the left of the figure. × 23,000.


g
L
mv
gc
17

PLATE 10

EXPLANATION OF FIGURE

18 This is a section through a portion of a large whorl system in a "dark cell" of a Bowman's gland. The whorl seems to be composed of tightly packed cisternae of the agranular endoplasmic reticulum (er). At the periphery of the whorl these membranes may be continuous with membranes of the granular endoplasmic reticulum (ger). Also at the periphery membranes may diverge and associate with nearby mitochondria. × 26,000. Inset: × 28,000.

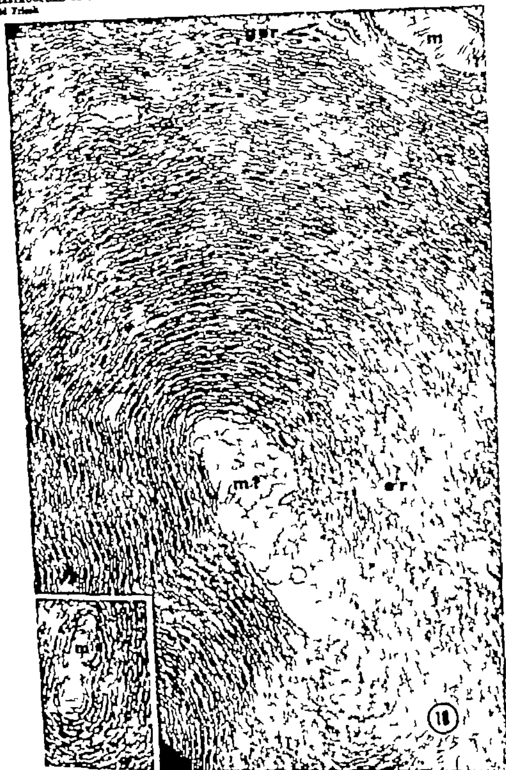

m
m
er
m
11

PLATE 10

EXPLANATION OF FIGURE

18 This is a section through a portion of a large whorl system in a "dark cell" of a Bowman's gland. The whorl seems to be composed of tightly packed cisternae of the agranular endoplasmic reticulum (er) At the periphery of the whorl these membranes may be continuous with membranes of the granular endoplasmic reticulum (ger) Also at the periphery membranes may diverge and associate with nearby mitochondria × 26,000 Inset: × 26 000.

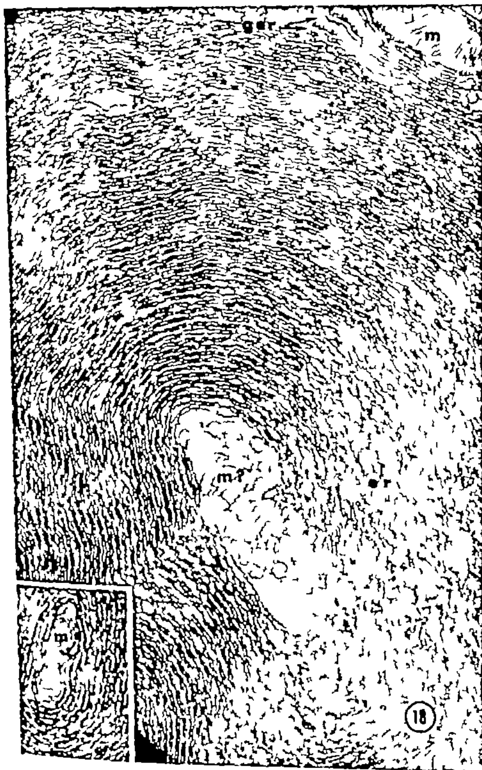

ger
m
m?
er
m
18

PLATE 10

EXPLANATION OF FIGURE

18 This is a section through a portion of a large whorl system in a "dark cell" of a Bowman's gland. The whorl seems to be composed of tightly packed cisternae of the agranular endoplasmic reticulum (er) At the periphery of the whorl these membranes may be continuous with membranes of the granular endoplasmic reticulum (ger) Also at the periphery membranes may diverge and associate with nearby mitochondria. × 26,000. Inset: × 26,000.

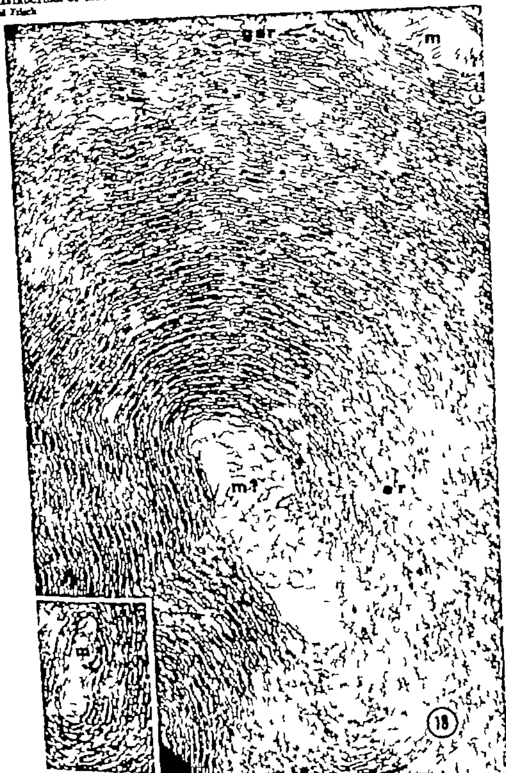

m
m?
r
18

PLATE 11

EXPLANATION OF FIGURES

19 "Dark Cells" (DC) containing secretory granules (sg) are present within the epithelium where they form the initial portion of the intraepithelial duct (L) A basal cell (B C.) marks the boundary of the epithelium and an olfactory nerve bundle (ON) is present in the subsequent connective tissue. × 6,000

20 Higher in the epithelium the duct is formed by flattened cells provided with microvilli (mv) The nucleus (n) of one duct cell is at the lower left. × 10,500.


DC
BC
SB
ON
mv
19
20

PLATE 12

EXPLANATION OF FIGURE

21 The left side of the figure represents a block containing the entire thickness of the epithelium. The upper right shows a portion of the free surface and the lower right a detail of the basal portion of the epithelium and some of the elements in the subjacent connective tissue The diagram is constructed and labeled on a regional basis rather than on a cellular basis. Numbers 1–4 refer to olfactory cilia and the ciliar extensions Cilia have been "sectioned" through the proximal 1 μ (1) where they show the normal nine and two pattern of ciliary tubules through the beginning portion of the extension (2) where the number of tubules is reduced, through a dilation (3) and through an area of the extension near its termination (4) where only two ciliary tubules are present. A complex branching process (BP) is shown at (5) The secretory granules (SG) of the supporting cells occur near the free surface (6) and associated with stacked cisternae of smooth-surfaced endoplasmic reticulum (SmER) at (7) Cisternae of agranular endoplasmic reticulum are also closely associated with mitochondria (8)

Numbers 9–11 indicate areas where olfactory receptor cells are in direct contact At (12) some proximal processes penetrate the basement membrane in association with Schwann cell cytoplasm The foot processes of supporting cells are distinguished by the presence of dense bodies (13) and whorl systems of smooth membranes associated with glycogen (14) Another whorl system (15) is shown in a dark cell of Bowman's glands (BGC) and a secretory granule (SG) is nearby (16) A light cell of Bowman's glands is shown with prominent dilated cisternae of granular endoplasmic reticulum (17)


4
3
2
Cilia
5
supporting
sup. cell
10
olf. cell nuc.
14
foot proc.
12
21
17
14
basal cell
15
17
cell nuc.

The Development of Vagal Innervation of the Bovine Stomach

T. A. McCRADY AND W. O. SACK
Department of Anatomy, New York State Veterinary College, Cornell University, Ithaca, N. Y.

ABSTRACT The development of the vagal innervation of the bovine stomach was examined in serial section from 13 embryos ranging from 10 to 20 mm crown-rump length. Models of the gastric epithelium and nerves were made of an 11, 14 and 20 mm embryo. The vagal innervation of the stomach was also examined in six bovine fetuses ranging from 15 to 62 cm in length. The bovine stomach developed from a spindle-shaped primordium at 10 mm to a four-chambered organ at 20 mm. At 11 mm, the right and left vagus extended to a point dorsal to the heart where they divided into dorsal and ventral branches. The ventral branches fused to form the ventral vagal trunk and the dorsal branches fused to form the dorsal vagal trunk. At the 13 to 14 mm stage, both vagal trunks ran along the lesser curvature of the gastric primordium to the level of the developing abomasum. By 20 mm, the principal branches of the vagal trunks found in the adult were established and it became clear that the dorsal and ventral vagal trunks innervated areas of the ruminant stomach roughly comparable to the visceral and parietal (posterior and anterior (NA)) surfaces, respectively of the simple stomach. The distribution of the vagal trunks in the fetuses was similar to that in the adult. Similarities in the development of the gastric nerves in man and ox were discussed.

The bovine stomach is a four-chambered organ which consists of a proventriculus and a glandular stomach (Sisson and Grossman, '53; Nickel and Schummer, '60). The proventriculus is made up of the rumen, reticulum, and omasum, and the glandular stomach of the abomasum. Contrary to earlier accounts of an esophageal origin of the proventriculus, the four compartments of the bovine stomach develop from a spindle-shaped gastric primordium similar to that from which the simple stomach develops (Pernkopf, '31; Martin and Schauder, '38; Lambert, 48; Warner '58). The rumen and reticulum correspond to the fundus and body of the simple stomach, the abomasum to the pyloric part, and the omasum to an outgrowth of the lesser curvature of the primordium. In the adult ox, the rumen is the largest of the four compartments and lies to the left in relation to the other compartments. The right and left surface of the rumen is marked with longitudinal grooves which are connected cranially and caudally by two deep transverse grooves, the cranial and caudal grooves of the rumen. These longitudinal and transverse grooves divide the rumen into dorsal and ventral sacs. The most cranial part of the rumen, the cranial sac, lies between the ruminoreticular fold and cranial pillar of the rumen. The reticulum is the smallest and most cranially placed of the gastric compartments. It is somewhat piriform and compressed craniocaudally. The omasum, which is almost spherical in shape, lies to the right and is clearly demarcated from the other compartments. The abomasum, or glandular stomach, is in the form of an elongated sac which consists of a body and pyloric part. The body of the sac extends caudally between the ventral sac of the rumen and the omasum, and turns to the right behind the latter. The terminal pyloric part inclines dorsally and joins the duodenum.

The vagal innervation of the adult bovine stomach has been thoroughly studied (Foust, '29; Christ, '30; Habel, '56; Moritz, '57). While there was general agreement among the authors as to the origin, course and distribution of the nerves to the various compartments, controversy existed regarding the nomenclature used by the various authors. This controversy has recently been resolved by the International Committee on Veterinary Anatomical No-

Present address: Department of Veterinary Anatomy, University College Dublin, Dublin 4, Ireland.

TABLE 1

Nomenclature of gastric vagal trunks[1]

Ruminant		Man
Truncus vagalis ventralis	Ventral vagal trunk[2]	Plexus esophageus
Ramus communicans cum trunco dorsali	Branch communicating with dorsal trunk	Truncus vagalis anterior
Rami atriales ruminis	Branches to atrium ruminis	Truncus vagalis posterior
Rami reticuli craniales	Cranial reticular branches	Rami gastrici anteriores
Ramus pyloricus	Pyloric branch	Rami gastrici posteriores
Rami hepatici	Hepatic branches	Rami hepatici
Rami ad sulcum ventriculi	Branches to gastric groove	Rami celiaci
Rami omasiales	Omasal branches	
Rami abomasiales parietales	Parietal abomasal branches	
Truncus vagalis dorsalis	Dorsal vagal trunk	
Rami atriales ruminis	Branches to atrium ruminis	
Rami celiaci	Celiac branches	
Rami ruminis dorsales	Dorsal ruminal branches	
Ramus ruminis dexter	Right ruminal branch	
Ramus ad sulcum cranialem	Branch to cranial groove	
Rami ad sulcum ventriculi	Branches to gastric groove	
Rami reticuli caudales	Caudal reticular branches	
Ramus ad curvaturem majorem abomasi	Branch to the greater curvature of the abomasum	
Rami omasiales	Omasal branches	
Rami abomasiales viscerales	Visceral abomasal branches	

[1] Taken from an unpublished but approved, list prepared by R. C. McClure Missouri R. Kitchell Kansas and J. Schreiber Vienna chairman of the subcommittee on *Systema nervosum periphericum* (Section VI b) of *Nomina Anatomica Veterinaria*.

[2] English equivalents from Habel ('65)

menclature (Habel '65) This Committee which was established to standardize the terminology of the gross anatomy of domestic animals has approved the nomenclature of the cranial nerves and their branches As constant use will be made in this paper of both the approved ruminant nomenclature and of the human nomenclature (Mitchell '66) of the gastric nerves the relevant section of each nomenclature is given in table 1

The following account of the vagal innervation of the adult bovine stomach is based on the accounts of Habel ('56 '64) and Moritz ('57) The left vagus divides caudal to the aortic arch between the esophagus and left principal bronchus into dorsal and ventral branches The right vagus divides into dorsal and ventral branches a little cranial to the right principal bronchus The larger right and left dorsal vagal branches run to the dorsal surface of the esophagus and fuse at about the level of the eighth rib to form the dorsal vagal trunk. The dorsal branches and trunk supply twigs to the esophagus The smaller ventral branches of the right and left vagus give off pulmonary branches and fuse just caudal to the bifurcation of the trachea to form the ventral vagal trunk which runs caudad in the mediastinum to the esophageal hiatus A communicating branch is usually present between the dorsal and ventral trunks across the left side of the esophagus near the diaphragm

The ventral vagal trunk on entering the abdominal cavity gives off branches to the cranial sac of the rumen and to the cranial surface of the reticulum. On the right, the ventral trunk gives off a pyloric branch which runs toward the porta of the liver where it gives off a hepatic branch and runs ventrad to the pylorus The ventral trunk runs ventrad from the esophagus to the parietal surface of the neck of the omasum and supplies branches to the reticular groove[3] It continues caudad in the lesser omentum close to the parietal surface of the base of the omasum and along the lesser curvature of the abomasum to the pylorus Along its course the ven-

[3] The reticular groove represents the proximal segment of the embryonic gastric groove and runs from the cardia to the reticulo-omasal opening The groove is flanked by two lips, the musculature of which correspond to the cardiac loop of other mammals and is derived from the inner muscular layer of the rumen and reticulum, which is homologous to the inner oblique fibers in the simple stomach.

tral trunk gives off branches to the parietal surfaces of both the omasum and abomasum.

The dorsal trunk on passing through the esophageal hiatus gives off branches to the celiac plexus and to the rumen. Some of the smaller ruminal branches run dorsocaudad to the dorsal surface of the rumen. The largest ruminal branch, the right ruminal branch, passes caudad to the right longitudinal groove of the rumen, along which it runs to the caudal ruminal groove The right ruminal branch gives off twigs to the dorsal and ventral sacs. A branch from the dorsal vagal trunk also runs to the cranial ruminal groove. The dorsal vagal trunk passes on to the visceral side of the omasum and runs on the visceral side of the lesser curvature of the abomasum to the pylorus. Along its course it gives off branches to the reticular groove to the caudal surface of the reticulum, to both parietal and visceral surfaces of the omasum, and to the visceral surface of the abomasum.

Despite our knowledge of the innervation of the adult bovine stomach and of the embryology of this organ, nothing is known about the development of its innervation. Froriep (1885) in his study on the sense organs of mammals, made passing reference to the development of the vagus in the ox. He stated that, in a bovine embryo of 8.7 mm (27 days) the vagus surpassed the other cranial nerves in size and that, in a 12 mm (33 days) embryo, the jugular ganglion was well differentiated from the nodose ganglion from which the main trunk extended about 0 4 mm. Shaner ('30) in his study of the fetal innervation of the bovine heart, stated that the vagus nerves were present in the cardiac region in a 12 mm (33 days) embryo. He also described, in a 14 mm (34 days) embryo and in later stages, a communicating branch connecting the right and left vagus across the ventral surface of the esophagus just caudal to the heart. He stated that a median ventral trunk arose from this communicating branch and ran caudad. Christ ('30) described the innervation of the stomach in a six to eight month bovine fetus and found that the stomach at this period of development, was a miniature of the adult in shape and in the distribution of the gastric nerves.

Duncan and Phillipson ('51) while studying motor responses in the stomach of fetal sheep failed to observe nerves in sections from the stomach of a 26 day embryo (At the twenty-sixth day of gestation a sheep embryo is about 12 mm crown-rump length (Green and Winters, 45) Its external features resemble a 33 day (12 mm) bovine embryo (Winters et al., 42) and according to Zietzschmann and Krölling ('55) the ruminoreticular and abomasal primordia are distinguishable at this time.) However in sections from a 41 day(53 mm)-old ovine stomach, the main nerve trunks were present and ganglia were seen external to the inner circular muscle layer

Streeter ('04) studied the origin of the vagus in man but gave no account of the development of its branches to the thoracic or abdominal organs. Blechschmidt ('61) illustrated the course of the developing vagus in models of a 6.3 mm (29 days) 10 mm (31 days) and 17 5 mm (37 days) human embryo. Indir ('55) studied the development of the nerves to the stomach in man from serial sections of embryos ranging from 4 mm to 150 mm. A short account of the development of vagal innervation of the stomach has also been described in the pig (Kuntz, '09) and chick (van Campenhout, '33)

MATERIALS AND METHODS

Twelve serially sectioned bovine embryos selected from the Kingsbury-Adelmann Embryological Collection of the Division of Biological Sciences, Cornell University were used in this study The plane of section of these embryos was either transverse or sagittal and different techniques had been used in staining them (table 2) Three embryos collected by the authors were also examined. These embryos were sectioned transversely at 10 µ and stained with Holmes Silver Stain (Holmes, 43) The ages of the embryos were estimated from their known crown-rump length which was compared with similar measurements from bovine em-

[1] Age of bovine embryos estimated from data of Winters et al. ('42); Foley and Reece ('53); and Warner ('58).

TABLE 1
Nomenclature of gastric vagal trunks[1]

Ruminant		Man
Truncus vagalis ventralis	Ventral vagal trunk[2]	Plexus esophageus
Ramus communicans cum trunco dorsali	Branch communicating with dorsal trunk	Truncus vagalis anterior
Rami atriales ruminis	Branches to atrium ruminis	Truncus vagalis posterior
Rami reticuli craniales	Cranial reticular branches	Rami gastrici anteriores
Ramus pyloricus	Pyloric branch	Rami gastrici posteriores
Rami hepatici	*Hepatic branches*	Rami hepatici
Rami ad sulcum ventriculi	Branches to gastric groove	Rami celiaci
Rami omasiales	Omasal branches	
Rami abomasiales parietales	Parietal abomasal branches	
Truncus vagalis dorsalis	Dorsal vagal trunk	
Rami atriales ruminis	Branches to atrium ruminis	
Rami celiaci	Celiac branches	
Rami ruminis dorsales	Dorsal ruminal branches	
Ramus ruminis dexter	Right ruminal branch	
Ramus ad sulcum cranialem	Branch to cranial groove	
Rami ad sulcum ventriculi	Branches to gastric groove	
Rami reticuli caudales	Caudal reticular branches	
Ramus ad curvaturem majorem abomasi	Branch to the greater curvature of the abomasum	
Rami omasiales	Omasal branches	
Rami abomasiales viscerales	Visceral abomasal branches	

[1] Taken from an unpublished, but approved list prepared by R. C. McClure Missouri R. Kitchell, Kansas and J. Schreiber Vienna, chairman of the subcommittee on *Systema nervosum periphericum* (Section VI b) of *Nomina Anatomica Veterinaria*
[2] English equivalents from Habel ('65)

menclature (Habel '65) This Committee which was established to standardize the terminology of the gross anatomy of domestic animals has approved the nomenclature of the cranial nerves and their branches As constant use will be made in this paper of both the approved ruminant nomenclature and of the human nomenclature (Mitchell 66) of the gastric nerves the relevant section of each nomenclature is given in table 1

The following account of the vagal innervation of the adult bovine stomach is based on the accounts of Habel ('56 '64) and Moritz ('57) The left vagus divides caudal to the aortic arch between the esophagus and left principal bronchus into dorsal and ventral branches The right vagus divides into dorsal and ventral branches a little cranial to the right principal bronchus The larger right and left dorsal vagal branches run to the dorsal surface of the esophagus and fuse at about the level of the eighth rib to form the dorsal vagal trunk. The dorsal branches and trunk supply twigs to the esophagus. The smaller ventral branches of the right and left vagus give off pulmonary branches and fuse just caudal to the bifurcation of the trachea to form the ventral vagal trunk which runs caudad in the mediastinum to the esophageal hiatus. A communicating branch is usually present between the dorsal and ventral trunks across the left side of the esophagus near the diaphragm

The ventral vagal trunk on entering the abdominal cavity gives off branches to the *cranial sac of the rumen and to the cranial* surface of the reticulum. On the right, the ventral trunk gives off a pyloric branch which runs toward the porta of the liver where it gives off a hepatic branch and runs ventrad to the pylorus. The ventral trunk runs ventrad from the esophagus to the parietal surface of the neck of the omasum and supplies branches to the reticular groove It continues caudad in the lesser omentum close to the parietal surface of the base of the omasum and along the lesser curvature of the abomasum to the pylorus Along its course the ven-

[3] The reticular groove represents the proximal segment of the embryonic gastric groove and runs from the cardia to the reticulo-omasal opening. The groove is flanked by two lips, the musculature of which corresponds to the cardiac loop of other mammals and is derived from the inner muscular layer of the rumen and reticulum, which is homologous to the inner oblique fibers in the simple stomach.

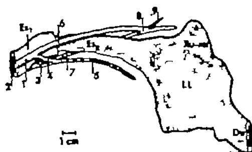


Fig. 1 Left lateral view of the gastric and esophageal epithelium of an 11 mm (30 days) bovine embryo (E21,13C) showing the formation and relationships of the dorsal and ventral vagal trunks. Es, Esophagus; Es, Epithelial lining of esophagus; Ru-ret, Ruminoreticular primordium; Du, Duodenum; LL, Depression caused by primordium of left lip of gastric groove; 1 Left vagus; 2, Right vagus; 3 Ventral branch of right vagus; 4, Ventral branch of left vagus; 5, Ventral vagal trunk; 6, Dorsal branch of left vagus; 7 Dorsal branch of right vagus; 8, Dorsal vagal trunk; 9, Branch of dorsal vagal trunk to ruminoreticular primordium (future right ruminal branch)

trum to a point cranial to the cardia. The larger dorsal branches of the vagi ran caudad, at first lateral and then dorsal to the esophagus, for about 1.2 mm and fused dorsal to the cardia to form the dorsal vagal trunk (fig. 1(8)) The dorsal trunk continued caudad for a short distance beyond this point. Just distal to its formation the dorsal trunk gave off to the left a branch (future right ruminal branch) which ran laterally and slightly caudally to the ruminoreticular primordium (fig. 1(9)) In one of the embryos of this group the dorsal branch of the left vagus gave off communicating fibers to the ventral vagal trunk.

12–14 mm stage (four embryos). At this stage the ruminoreticular primordium was prominent and expanded to the left (figs. 2, 3) An evagination of the gastric epithelium on the lesser curvature of the gastric primordium represented the developing omasum. Just caudal to the embryonic omasum, the gastric primordium was bent to the right and marked the future abomasum. The lips of the gastric groove were more pronounced and caused further constriction of the gastric epithelium between the ruminoreticular primordium and the gastric groove (figs. 2, 3) As a result of the growth and rotation of the gastric primordium to the left, the original right lip of the gastric groove was now dorsal in position and the left lip ventral.

At this stage of development, the ventral vagal branches and trunk gave off branches to the bronchi. At the level of the cardia on the right side, the ventral vagal trunk gave off a branch that ran in the ventral mesogastrium toward the liver (fig. 2(3)) Just caudal to this branch, the ventral trunk gave off on the left a branch

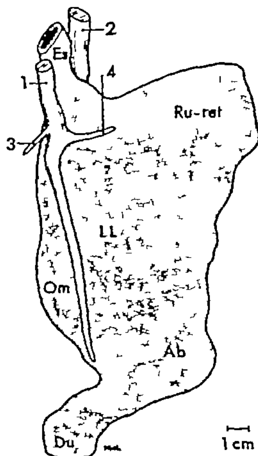


Fig. 2 Ventral view of gastric epithelium of a 14 mm (34 days) bovine embryo (E18,14C) showing course and distribution of the ventral vagal trunk. Es, Esophagus; Ru-ret, Ruminoreticular primordium; Om, Omasal primordium; Ab, Abomasal primordium; Du, Duodenum; LL, Depression caused by left (ventral) lip of reticular groove; 1 Ventral vagal trunk; 2, Dorsal vagal trunk; 3 Branch of ventral trunk toward liver; 4 Branch of ventral trunk to ruminoreticular primordium (future reticular branches)

TABLE 2
List of bovine embryos examined

Series	C–R length	Estimated age	Plane of section	Thickness of section	Stain
	mm	days		μ	
1A	10	29	t	10	H.–E.
S21 13C	11	30	t	10	H.–E.
E25	11	30	t	10	H.–S.
S38	11	30	s	10	H.–E.
S14 12C	11	30	t	10	H.–E.
E38	12	33	t	10	H.–S.
S17	14	34	t	10	H.–O.
S7	14	34	s	10	H.–E.
S18 14C	14	34	t	10	H.–O.
E45	15	35	t	10	H.–S.
1B	16	37	t	15	H.–E.
S50	17	37	s	15	Carm.
S22, 9C	20	39	t	20	H.–O.
S21 23C	20	39	t	10	H.–O.
S1 41C	20	39	s	20	H.–E.

t, transverse; s, sagittal; H.–E., Hematoxylin and Eosin; H.–S., Holmes Silver Stain; H.–O., Hematoxylin and Orange G; Carm., Carmine.

bryos of known age (Winters et al. '42; Foley and Reece '53; Warner '58).

Wax plate models were made of the gastric epithelium and developing nerves of an 11 mm (S21 13C), 14 mm (S18 14C) and a 20 mm (S21,23C) embryo. These models were made to a magnification of 100 using Sack's ('66) modification of the Born/Strasser method.

The origin, course and distribution of the gastric vagal trunks were dissected, under a stereoscopic microscope, in six bovine fetuses ranging from 15 cm (85 days) to 52 cm (180 days) crown-rump length.

OBSERVATIONS

In the following account the embryos have been divided into five groups based on the stages of development of the gastric primordium and of the gastric nerves. The description of the gastric nerves at each stage is preceded by a short account of the gastric primordium in order to relate the development of the nerves to the differentiation of the gastric compartments.

10 mm stage (one embryo). In the 10 mm embryo the gastric primordium was a fusiform dilation of the foregut attached by a dorsal and ventral mesogastrium. The gastric epithelium was laterally compressed, having a dorsal and ventral curvature of which the dorsal was the more pronounced. Along the cranial third of the dorsal curvature the gastric epithelium was slightly expanded and represented the first stage in the development of the rumen and reticulum. The plane of the flattened gastric epithelium inclined to the left forming an angle of about 30° with the median plane of the embryo.

At this stage of development, the right and left vagus lay lateral to the esophagus and trachea and extended caudally to a level in front of the heart.

11 mm stage (four embryos). The ruminoreticular primordium was more pronounced and expanded to the left (fig. 1). The gastric lumen along the lesser curvature was slightly expanded, and indicated the primordium of the gastric groove. Mesodermal thickenings of the right and left lateral walls of the embryonic stomach caused the gastric epithelium to become constricted between the ruminoreticular primordium and the developing gastric groove (fig. 1). These mesodermal thickenings were the primordia of the right and left lips of the gastric groove (fig. 1(LL)).

At this stage of development the right and left vagus lay dorsal to the heart, and at the level of the tracheal bronchus,[4] the right and left vagus divided into dorsal and ventral branches. The smaller ventral branches ran ventromedially for about 300 μ and fused to form the ventral vagal trunk (fig. 1(5)). The ventral vagal trunk thus formed ran caudad in the mediasti-

[4] The right apical bronchus in ruminants and swine which is given off directly from the trachea cranial to the tracheal bifurcation.

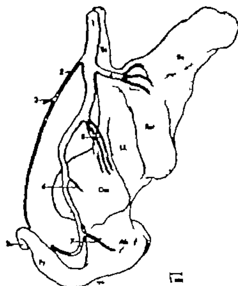


Fig. 4 Ventral view of gastric epithelium of a 20 mm (39 days) bovine embryo (521,23C) showing course and distribution of the ventral vagal trunk. Es, Esophagus; Ru Rumen; Ret, Reticulum; Om, Omasum; Ab, Abomasum; Py, Pylorus; Du, Duodenum; LL, Depression caused by left (ventral) lip of reticular groove; 1, Ventral vagal trunk; 2, Pyloric branch; 3, Hepatic branch; 4, Cranial reticular branches; 5, Branches to left (ventral) lip of reticular groove; 6 Omasal branch; 7 Abomasal branch.

thrown up into small folds. The gastric groove, which in earlier stages was a simple channel running from the cardia along the lesser curvature of the primordium was now divided by the reticulo-omasal and the omasoabomasal openings into three segments the reticular omasal, and abomasal grooves.

The branch of the ventral vagal trunk, which in the previous stage ran caudad in the ventral mesogastrium after giving off a branch to the liver now ran to the pylorus (fig. 4(2)) These are the hepatic and pyloric branches of the adult. The ruminoreticular branch of the ventral trunk now broke up into a number of branches which were distributed to the cranial surface of the reticulum (fig. 4(4)) Caudal to the reticular branches, the ventral trunk supplied branches which ran caudad parallel to the left (ventral) lip of the reticular groove (fig. 4(5)) The ventral trunk also gave off a branch to the parietal surface of the omasum as it passed this surface to reach the lesser curvature of the abomasum, and a branch to the body of the abomasum (fig. 4(6 7))

After the differentiation of the ruminoreticular primordium into ruminal and reticular compartments, the ruminoreticular branch of the dorsal vagal trunk of the previous stages became distributed to the rumen. This large branch the right ruminal branch in the adult ox, ran craniolaterally to the future caudal ruminal groove (fig. 5(2)) In addition to its earlier described branch which ran to the cranial border of the primordium and which is now recognizable as a branch to the future dorsal sac of the rumen (fig. 5(3)) the right ruminal branch gave off a branch to the future cranial groove of the rumen (fig 5(4)) and twigs to the dorsal surface

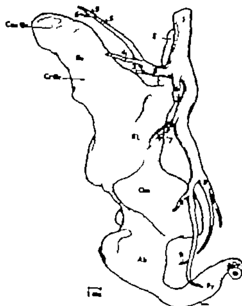


Fig. 5 Dorsal view of gastric epithelium of 20 mm (39 days) bovine embryo (521,23C) showing course and distribution of the dorsal vagal trunk. Es Esophagus; Ru, Rumen; Om, Omasum; Ab, Abomasum; Py Pylorus; Du, Duodenum; CauGr, Depression caused by future caudal groove of the rumen; CrGr, Depression caused by future cranial groove of the rumen; RL, Depression caused by the right (dorsal) lip of reticular groove; 1, Dorsal vagal trunk; 2, Right ruminal branch; 3, Branch to future dorsal sac of rumen; 4, Branch to cranial groove; 5, Ruminal branches; 6, Origin of branch to celiac plexus; 7 Branches to right (dorsal) lip of reticular groove; 8, Branches to omasum; 9 Branch to abomasum.

(the future reticular branches) to the ventral surface of the ruminoreticular primordium (fig 2(4)) The ventral vagal trunk then ran caudad ventral to the gastric groove to reach the lesser curvature of the embryonic omasum (fig 2(1))

The dorsal branches of the right and left vagus and the dorsal vagal trunk supplied branches to the mesoderm of the esophagus The dorsal trunk itself ran caudad *dorsal to the gastric groove and developing* omasum to the lesser curvature of the abomasum It gave off a branch to the omasum (fig 3(4)) The ruminoreticular branch of the dorsal trunk was now prominent and ran dorsal to the dorsocranial border of the primordium It gave off a branch to the cranial border of the primordium (fig 3(3)) this represents the branches to the dorsal sac of the rumen in the adult.

15–17 mm stage (three embryos). The ruminoreticular primordium now extended cranially and to the left between the liver and the mesonephros A slight groove on its ventral surface indicated the beginning division into ruminal and reticular compartments. The omasum and abomasum were further demarcated from one another and the lips of the gastric groove more prominent.

The course of the vagal trunks was similar to that described in the previous stage The ventral vagal trunk, however extended farther caudad along the lesser curvature of the abomasum and its branch which in the previous stage ran to the liver now gave off a hepatic branch and continued caudad in the ventral mesogastrium The dorsal trunk also passed farther caudad along the lesser curvature of the abomasum and gave off further branches to the omasum as it passed over its dorsal surface. In the 16 mm embryo of this group a communicating branch was present between the dorsal and ventral trunk. This branch passed to the left of the esophagus just cranial to the cardia

20 mm stage (three embryos) The ruminoreticular primordium was divided into a craniodorsal ruminal and a caudoventral reticular compartment by the appearance of the ruminoreticular groove. The elongated ruminal compartment was marked by two dorsal transverse grooves the smaller of which, the future caudal ruminal groove lay cranial to the larger future cranial ruminal groove (fig. 5) The later caudal migration of the rumen to its definitive position causes the present relationship of the grooves to one another to become reversed The omasum was well differentiated as a spherical enlargement on the lesser curvature (figs. 4 5) The abomasum was also well demarcated, and *the epithelium of the body of the* organ

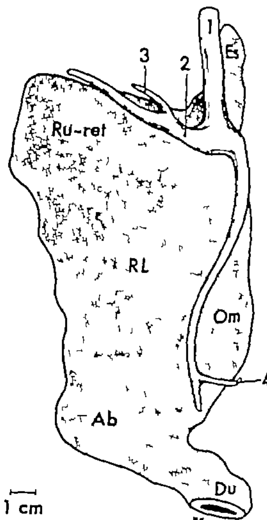


Fig 3 Dorsal view of gastric epithelium o a 14 mm (34 days) bovine embryo (#18,14C showing course and distribution of the dors vagal trunk. Es Esophagus; Ru-ret, Ruminore ticular primordium; Om Omasal primordium Ab Abomasal primordium; Du Duodenum; Rl Depression caused by right (dorsal) lip of gastr groove; 1 Dorsal vagal trunk; 2, Dorsal rumino reticular branch (right ruminal branch); 3 Branch to cranial border of ruminoreticular pr mordium (branch to future dorsal ruminal sac) 4 Omasal branch.

Thus, between the thirtieth and the thirty-seventh day of gestation the gastric nerves in man and ox parallel one another in development. The resemblance between the gastric primordia in both species at this period has previously been noted.

After the 14 mm (34 days) stage in the ox, the similarity of the two species in the distribution of the gastric nerves becomes obscured by the development of the gastric compartments. It should be kept in mind that the rumen, which developed from the dorsal region of the ruminoreticular primordium, became innervated for the most part by branches from the dorsal trunk. The reticulum, which developed from the ventral surface of the ruminoreticular primordium, became innervated mainly by branches from the ventral trunk. The development of the omasum from the lesser curvature of the gastric primordium resulted in the dorsal and ventral vagal trunks passing on the visceral and parietal surfaces, respectively of this organ. The abomasum, which developed from the caudal region of the gastric primordium, became innervated by the continuation of the dorsal and ventral vagal trunks, which passed along the visceral and parietal surfaces, respectively of the lesser curvature of the organ to the pylorus.

Having noted the similarities in the arrangement of the gastric nerves in man and ox, the following differences are mentioned. In man there exists an elaborate esophageal plexus made up of branches of the right and left vagus. Indir ('55) gave no account of this plexus, yet depicted it in his plates nor did he give an account of the origin of the vagal trunks from it. In the adult it has been shown that most of the fibers of the anterior vagal trunk are derived from the left vagus and those of the posterior vagal trunk mainly from the right vagus (Mitchell, '53) An esophageal plexus does not exist in the ox, both vagal trunks receive equal contributions from the right and left vagus though the dorsal branches forming the dorsal vagal trunk are larger than the ventral branches forming the ventral trunk. In the ox a communicating branch, which passes to the left of the esophagus normally exists between the dorsal and ventral vagal trunks. This branch was observed in only two of the 15 embryos examined, an incidence much lower than that observed in the adult.

The parallels in development noted in the early stages of gastric development and its innervation in man and ox are in keeping with previous reports of the similarity in the rate of organ development in the two species. Greenstein and Foley ('58) noted the similarity in external features between human and bovine embryos on the twentieth day of gestation and in the stage of development of the gut and its derivatives on the twenty-sixth day of gestation. Sexual differentiation occurs in both species at approximately the same time: in man at the 17 mm (37 days) stage (Gruenwald, 42) and in the ox on the thirty-ninth day of gestation (Krehbiel, '63) Hager ('65) observed that the primordia of the adrenal glands also appear at nearly the same time in the two species between the twenty-eighth and thirty-third day of development.

The similarity in the distribution of the gastric nerves between species with simple and those with ruminant stomachs reported by Phillipson (46) and Habel ('56) is further substantiated by the findings of this study It also adds support to the nomenclature approved by the International Committee on Veterinary Anatomical Nomenclature for the gastric nerves in ruminants, as this nomenclature is based on a homology existing between the distribution of the gastric nerves in ruminants and animals with simple stomachs.

An interesting feature of this study was the early stage at which the differentiating compartments of the bovine stomach became innervated. At the 11 mm stage with the first appearance of the ruminoreticular primordium, a branch of the dorsal vagal trunk was found to this organ and as each subsequent compartment developed it received branches from the vagal trunks. Thus by 20 mm, when the four compartments of the bovine stomach were clearly outlined, the primordia of the adult gastric nerves were distinguishable. The precocious development of nerve fibers to the differentiating compartments may be related to Detwiler's ('36) experimental findings that developing nerve fibers take directive course toward growing organs.

of the rumen (fig 5(5)) At the level of origin of the right ruminal branch a branch of the dorsal trunk was given off which ran dorsocaudad to the developing celiac plexus (fig. 5(8)) Just caudal to this branch the dorsal vagal trunk supplied branches which ran parallel to the right (dorsal) lip of the reticular groove (fig 5(7)) In its course over the omasum the dorsal trunk gave off branches to both its visceral and parietal surfaces and then passed to the lesser curvature of the abomasum giving a branch to the visceral surface of that organ (fig 5(8 9))

Fetal dissections In the fetuses examined the gastric compartments had already assumed their adult relationships. Also the size of the compartments in relation to each other was similar to that in the adult The origin and course of the vagal trunks at this period was also found to be similar to that described above for the adult ox.

DISCUSSION

The development observed in this study of the transformation of a gastric primordium at 10 mm into a four-chambered stomach at 20 mm was in agreement with earlier accounts given by Pernkopf ('31) Martin and Schauder ('38) Lambert ('48) and Warner ('58) The 10 mm bovine embryo showed a spindle-shaped stomach primordium similar to that described by Lewis ('15) at a comparable stage in mammals with simple stomachs Accelerated growth of the cranial end of the greater curvature of the primordium commencing at 11 mm resulted in the formation of the ruminoreticular primordium from which the rumen and reticulum differentiate by the 20 mm stage At the 12–14 mm stage the omasal primordium developed as an evagination of the lesser curvature and the embryonic abomasum from the caudal area of the gastric primordium Thus in the 20 mm embryo the primordia of the four compartments of the ruminant stomach were clearly demarcated

Even up to the 14 mm stage the bovine gastric primordium despite the fact that the outlines of the four stomach compartments were distinguishable bore a resemblance to the human gastric primordium of up to the 16 mm stage This resemblance may be observed on comparing figures 2 or 3 of this study with figure 212 of Broman's ('04) and figure 6 of Lewis ('12) publications

This study while agreeing with Shaner ('30) that the right and left vagus lay dorsal to the heart in the 12 mm stage, is not in accord with his account that, in the 14 mm embryo and later stages, the two vagi were connected across the ventral surface of the esophagus. It would appear that Shaner failed to observe that the right and left vagus divided into dorsal and ventral branches, which later fused to form the dorsal and ventral vagal trunks. He interpreted the fusion of the right and left ventral vagal branches as a communicating branch between the right and left vagus and described a median trunk arising from this communication. In this study the division of the vagi into dorsal and ventral branches was first observed at the 11 mm stage (fig 1)

Similarities were noted both in the time of development and in the distribution of the gastric nerves in man and ox. In both species the vagal trunks reached the gastric primordium at approximately the same stage of gestation: at 7 mm or 31 days[1] in man (Indir '55) and at 11 mm or 30 days in the ox. By the 17 mm (37 days) stage in man and the 14 mm (34 days) stage in the ox, both vagal trunks ran along the lesser curvature of their respective primordia The posterior vagal trunk in man supplied branches to the posterior surface of the stomach and gave off branches which passed around the lesser curvature of the stomach to its anterior surface The comparable dorsal vagal trunk in the ox innervated the dorsal surface of the ruminoreticular primordium and the developing omasum It did not give off branches to the ventral surface of the developing stomach but in later development, the omasal branches pass to both surfaces of that organ The anterior vagal trunk in man supplied the anterior surface of the stomach and gave off a branch which passed to the liver and pylorus The comparable ventral trunk in the ox supplied the ventral surface of the developing stomach and also gave off a branch to the liver and pylorus.

[1] Age of human embryos estimated from Blechschmidt ('61)

Electron Microscopy of the Early Postnatal Development of Fibrous Astrocytes

JAMES E. VAUGHN AND ALAN PETERS
Department of Anatomy University of Edinburgh

ABSTRACT The early postnatal development of fibrous astrocytes in rat optic nerves, has been studied with the electron and light microscopes. At birth, immature astrocytes form approximately 85% of the total cell population, and they have many features in common with the fibrous astrocytes of adult optic nerve. They are stellate cells whose processes form both the glia limitans and the glial sheets which group the axons into fascicles. However, in respect to their cytoplasmic characteristics, immature and mature astrocytes differ considerably. Early postnatal astrocytes have a more electron-dense cytoplasmic matrix containing an extensive array of organelles. Many microtubules occur in the processes of immature astrocytes, but the characteristic filaments of adult fibrous astrocytes are very sparse. During development, the number of microtubules decreases while the filaments increase until all cytoplasmic areas not occupied by organelles are filled by filaments. This suggests that filaments may be derived from the breakdown of microtubules. This and other possible functions of microtubules in developing astrocytes are discussed.

According to Fujita ('63) the neuroblasts, glioblasts and ependymal cells of the mature chicken central nervous system all arise from a homogeneous population of precursor cells. He calls these precursors the matrix cells" and states they are the only cell type located in the primitive ependymal or matrix" layer of the neural tube. Wechsler ('66) describes intermitotic matrix cells as bipolar cells whose primary processes contain numerous microtubules, and it would appear that, when these cells prepare to divide they round up by a retraction of the processes and move into close proximity to the central canal of the neural tube. Matrix cells have attracted the attention of several electron microscopists (Fujita and Fujita, '63 '64 Glees and LeVay '64) but their studies like those of Wechsler ('63 '66) do not describe the sequence of changes occurring during the differentiation of matrix cells into mature neuroglia and neurons; furthermore these investigations deal only with the chick central nervous system.

Beyond a few accounts limited to neuronal differentiation (e.g. Voeller Pappas and Purpura, '63; Tennyson, '65) and one superficial report on glioblasts and neuroblasts in developing mouse cerebral cortex (Meller Breipohl and Glees, '68) there appear to be no published descriptions of the development of mammalian central nervous system at the electron microscopic level.

In order to rectify this situation the differentiation of neuroglial cells has been studied in rat optic nerve a relatively simple system where developing neuroglia cannot be confused with neuroblasts These initial studies have been confined to adult and early postnatal rat optic nerves, and in effect, neuroglial development has been examined in a retrograde series, using the later stages of development to identify the characteristics of those cells which are less differentiated and therefore more difficult to define, in the earlier developmental stages.

The present account deals only with the early postnatal differentiation of the fibrous astrocytes of the rat optic nerve and no description is given either of the prenatal differentiation of astrocytes or of the maturation of oligodendrocytes and axons, both of which will form the subjects of later reports.

MATERIAL AND METHODS

Since neither perfusion with osmic acid, nor fixation by immersion in this reagent produced good results with early postnatal rat central nervous tissue an attempt was

---

Authors' present address Department of Anatomy, Boston University School of Medicine, 80 East Concord Street, Boston, Massachusetts 02118.

ACKNOWLEDGMENTS

The authors wish to thank Prof W A Wimsatt, Division of Biological Sciences Cornell University for the opportunity to study the Embryological Collection of his department They appreciate the care given by Miss Marion Newson Medical Artist to making the drawings Thanks are due to Prof R E Habel for reviewing the thesis on which this publication is based. The support the principal author received from the W K. Kellogg Foundation is gratefully acknowledged

LITERATURE CITED

Blechschmidt, E. 1961 The stages of human development before birth. W B Saunders Co., Philadelphia.

Broman, I. 1904 Die Entwickelungsgeschichte der Bursa omentalis. Bergmann, Wiesbaden.

van Campenhout, E. 1933 The innervation of the digestive tract in the six day chick embryo. Anat. Rec. 56: 111–118.

Christ H 1930 Der Nervus vagus und die Nervengeflechte der Vormägen der Wiederkäuer speziell der Haube. Z. Zellforsch. 11: 342–374

Detwiler S R. 1936 Neuroembryology: An experimental study The McMillan Co. New York.

Duncan, D L., and A T Phillipson 1951 The development of motor responses in the stomach of fetal sheep. J exp. Biol. 28 32–40.

Foley R. C., and R. P Reece 1953 Histological studies of the bovine uterus placenta, and corpus luteum Bull. Agr Exp Sta. Univ Mass. p. 468.

Foust, H. L. 1929 A dissection of the nerve supply to the gastric compartments in ruminants (bovine) J Am. Vet. med. Assoc 27: 1052–1059

Froriep A. 1885 Über Anlagen von Sinnesorganen am Facialis Glossopharygeus und Vagus über die genetische Stellung des Vagus zum Hypoglossus, und über die Herkunft der Zungenmuskulatur Arch. für Anatomie und Physiologie, 21: 1–55

Green, W W., and L M Winters 1945 Prenatal development of the sheep Minn. Agr Expt. Sta., Tech. Bull. 1: 169

Greenstein, J S., and R. C. Foley 1958 The early embryology of the cow with notes on comparable human development. Int. J Fert., 3: 67–79

Gruenwald, P 1942 The development of the sex cords in the gonads of man and mammals. Am J Anat., 70 359–398.

Habel, R. E. 1956 A study of the innervation of the ruminant stomach. Cornell Vet. 46 555–633.

——— 1964 Guide to the dissection of domestic ruminants. Edwards, Ann Arbor

——— 1965 Anatomical and histological nomenclature of the ruminant stomach. In: Physiology of digestion in the ruminant. Butterworth Inc., Washington D C.

Hager G 1965 Zur Histo- und Morphogenese der Nebennieren des Rinderfetus. Zentbl. Vet. Med 12A: 57–114

Holmes W 1943 Silver staining of nerve axons in paraffin sections. Anat. Rec., 86: 157–187

Indir J 1955 The development of the nerve supply of the human esophagus and stomach. J Anat. India 4: 55–68

Krehbiel E. B 1963 Differentiation of gonads in the bovine embryo. Kansas State University

Kuntz, A. 1909 The role of the vagus in the development of the sympathetic nervous system. Anat. Anz., 95: 381–390.

Lambert, P S. 1948 The development of the stomach in the ruminant. Br vet. J 102 303–310

Lewis F T 1912 The form of the human stomach Am. J Anat. 13: 477–503.

——— 1915 The comparative embryology of the mammalian stomach. Anat. Rec., 9 102–103

Martin, P., and W Schauder 1938 Lehrbuch der Anatomie der Haustiere. Vol. III, Anatomie der Hauswiederkäuer 3rd ed. Schickhardt and Ebner Stuttgart.

Mitchell G A. G 1953 Anatomy of the autonomic nervous system. Livingstone Edinburgh.

——— 1966 Nomina Anatomica. 3rd ed. Ed. by G A. G. Mitchell. Excerpta Medica, Amsterdam.

Moritz, A E. 1957 Verlauf und Verbreitung der Nervi vagi am Rindermagen. Diss. Tierärztl. Hochschule Wien.

Nickel, R. and A Schummer 1960 Lehrbuch der Anatomie der Haustiere. Vol. II, Eingeweide. Parey Berlin.

Pernkopf E. 1931 Die Entwicklung des Vorderdarmes insbesondere des Magens der Wiederkäuer Z. Anat. Entwgesch., 94: 490–622.

Phillipson A T 1946 The mechanical aspects of digestion in the ruminant. In: Some recent advances in veterinary science Nat. Vet. Med. Assoc : London.

Sack, W O 1966 Rapid wax plate modeling Anat. Rec., 154 233–242.

Shaner R. F 1930 On the development of the nerves to the mammalian heart. Anat. Rec. 46 23–39

Sisson S., and J D Grossman 1953 Anatomy of the domestic animals. 4th ed. W B. Saunders Co., Philadelphia.

Streeter G L. 1904 The development of the cranial and spinal nerves in the occipital region of the human embryo. Am. J Anat., 4: 83–118.

Warner E. D 1958 The organogenesis and early histogenesis of the bovine stomach. Am. J Anat., 102 33–64

Winters, L. M. W W Green and R. Comstock 1942 Prenatal development of the bovine. Minn. Agr exp Sta. Tech. Bull. 151

Zietzschmann O. and O Krölling 1955 Lehrbuch der Entwicklungsgeschichte der Haustiere. 2nd ed Parey Berlin.

of the large concentration of filaments. Microtubules are seldom observed within astrocytes, but these cells contain dense inclusion bodies (fig. 1 arrow) and droplets that are probably of a fatty nature (fig. 1 D)

Immature astrocytes

In the following description, it must be borne in mind that while astrocytes exhibit identical features in mature nerves, this is not true of developing nerves. Presumably this is because all of the cells do not begin their differentiation at the same time. Consequently in any given postnatal stage, and most particularly during the first two weeks after birth, immature astrocytes in different stages of differentiation exist side by side.

One day after birth, the components of the rat optic nerve are closely packed together and the spacing between them appears to be essentially the same as in the adult. At this time, immature astrocytes are the predominant cell type and constitute approximately 85% of the total cell population. When examined in transverse sections of the optic nerve, immature astrocytes have an irregular configuration with spindle-shaped perikarya (fig. 3 A) from which two or three primary processes arise. For clarity of presentation, astrocytic processes have been grouped into three categories: primary or broad processes slender processes, and finger-like projections. These terms will be used to designate specific forms of processes. The primary or broad processes (figs. 4 6 B) contain most of the organelles of the cells for the cytoplasm around the nuclei forms only a thin rim. Slender processes may arise: (a) from the perikarya (fig. 6 S) (b) from the sides of the broad processes where they generally arise at right angles (fig. 4 S) and (c) by the terminal branching of the broad processes (fig. 6 S_1) The third category of processes are small finger like projections that arise, usually at right angles, from all parts of the cell surface (fig. 4 6, arrows)

At birth the grouping of axons into fascicles is incomplete. The existing fasciculation is produced by glial sheets formed by the processes of immature astrocytes, and the most elementary consist merely of a pair of slender processes, derived from different cells that extend towards each other and overlap for a short distance (shown at 5 days postnatal in fig. 9) Other glial sheets are composed of three or four processes lying side by side and these thicker sheets are generally made up of wider processes (fig 8) As development proceeds the number of glial sheets extending between the axons increases so that the fascicles contain increasingly smaller numbers of axons (compare figs. 6, 9) Until about two weeks after birth, glial sheets composed of only two overlapping processes still occur although the thicker sheets have become more common. This indicates that the pairs of overlapping processes are the primordia, and that the mature glial sheets result both from the addition of more processes to these primordia, and from an increase in the diameters of the constituent processes.

The fact that both the number of glial sheets and the number of processes contributing to these sheets increases with time indicates a continual formation of slender astrocytic process during the first few weeks of postnatal development. The majority of these slender processes are probably formed by sprouting from astrocytes already contributing to the sheets, but since mitotic figures are frequently seen in the early postnatal stages other slender processes may be derived from newly formed astrocytic precursors.

Occasionally the finger-like projections of early postnatal astrocytes are seen in sections to isolate individual axons either by partially surrounding them or by completely enclosing them within a wrapping consisting of one to one and one-half turns of cytoplasm. Serial sections revealed that such wrappings extend only for short distances along the length of the enclosed axon, in a somewhat similar fashion to the astrocytic wrappings described by Wolff ('65) in grey matter. In some cases the projections continue on their course after having wrapped an axon. There is no suggestion that these wrappings represent an early stage of myelination since a typical mesaxon (Peters, '60 '62a, b) is never formed and cytoplasm is always present in the wrapping processes.

made to fix the tissue by perfusion with aldehydes After a series of emptrical ex periments the following solution was found to produce good fixation when it was perfused though the heart (Vaughn and Peters '66): 0 5% glutaraldehyde and 4% formaldehyde (prepared from paraformaldehyde Pease 64) contained in a phosphate buffer (Millonig '61) at pH 7 2 to 7 4 Trace amounts of calcium chloride were added to the final fixing solution Although it was developed independently the composition of this solution is somewhat similar to that used by Kar novsky (65)

Rats ranging in age from one day post natal to adult, were anesthetised by an in traperitoneal injection of 3 5% chloral hydrate The thorax was then opened and the aldehyde fixing solution perfused through the left ventricle at a constant pressure which was maintained by a mechanical pump acting through a reservoir flask. Following perfusion the optic nerves were removed from the rats and post fixed for two hours in a 1% solution of osmic acid in a phosphate buffer at pH 7.2 to 7 4 (Millonig 61) The nerves were then dehydrated in the usual manner and embedded in Araldite.

Sections prepared for electron microscopy were double stained on the grid with lead citrate and uranyl acetate prior to ex amination in an A.E.I. E.M. 6 electron mi croscope. Thicker sections (0.5–1 0 μ) from the same blocks were stained on glass slides with an alkaline solution containing toluidine blue and Pyronin B Phase con trast photographs of these sections were made for comparison with the electron micrographs.

OBSERVATIONS

Mature astrocytes

The fibrous astrocytes of the adult rat optic nerve are stellate cells which have many processes radiating from the peri karya. These processes extend between the myelinated axons and those arising from different cell bodies come together to form glial sheets in which the processes run parallel to each other but generally at right angles to the path of the axons. These glial sheets do not appear to be complete partitions which extend for the entire length of the optic nerve, but rather a series of short partitions that interlace with the axons in an irregular fashion.

Some of the astrocytic processes extend to the periphery of the nerve while others reach the surface of the capillaries located within the nerve In such situations, the processes form expansions that appear to completely separate the axons both from the walls of the capillaries and from the pia mater surrounding the nerve. These expansions constitute the glia limitans which is covered externally by the associated basal lamina. Between the plasma membranes of adjacent processes of the glia limitans it is common to find junc tions in which the apposed plasma mem branes come together in such a way as t eliminate any intervening extracellula space (Peters '62) Such junctions ar referred to as either quintuple layer junc tions (Muir and Peters, '62) or zonula occludentes (Farquhar and Palade, '63).

Figure 1 illustrates the cell body of typical fibrous astrocyte of the adult r optic nerve. It shows that the nucleus irregularly spindle-shaped and that exc for a very thin condensed rim of chr matin adjacent to the nuclear membra the distribution of chromatin particles homogeneous.

The most distinctive feature of a matu astrocyte is the mass of filaments, or brils that pack the cytoplasm (fig. 1 F Within the processes the filaments arranged parallel to the long axis but, the perikaryon their orientation appears be more random although essentially th have the form of a series of bundles th extend between the bases of the process The external diameter of each filament between 80 A and 90 A and in cross s tion they appear as electron-dense circl with clear centers (fig 2, arrows) Th it appears that the astrocytic filaments cylindrical or tubular structures simi both in form and size to neurofilamer (Sandborn et al. '65 Peters and Vaugh '67)

In comparison with most other types cells the mitochondria, endoplasmic ticulum and Golgi apparatus are spa within the cytoplasm of mature fibro astrocytes Thus only a few profiles of the structures are interspersed between the

casionally a central electron-opaque dot is visible within tubules examined in transverse section (fig. 5) similar to that sometimes observed in the microtubules of axons (Peters Vaughn, '67)

For the first few days after birth, microtubules occur most commonly within the slender astrocytic processes, usually some distance from the perikarya (fig. 7 8 M) In one-day postnatal astrocytes microtubules are less frequently observed within the perikarya and broad processes, but the number of microtubules in these regions of the cell, as well as within the slender processes increases markedly during the next seven to nine days Figure 9 illustrates microtubules in the perikaryon of an immature astrocyte five days after birth. At any time during postnatal development, microtubules only rarely occur within the small finger-like projections.

The presence of microtubules is one of the most distinctive features of the immature fibrous astrocyte. On the other hand, the cytoplasm of mature cells is characterized by the presence of numerous filaments which occupy almost the entire volume of the cell (fig. 1 F) At birth, some of the immature astrocytes also contain filaments but they are not common and are primarily confined to the slender processes (fig. 8 F) With time though, the number of processes and perikarya containing filaments increases. Initially there may only be a small bundle of filaments embedded in cytoplasm containing microtubules, but eventually the cytoplasm of the cells becomes filled with filaments and at the twenty first postnatal day they occupy all of the space not filled by mitochondria, granular endoplasmic reticulum and the Golgi apparatus (figs. 11 12) while only a few microtubles remain (fig. 12 M)

As the number of filaments increases within the cytoplasm of the developing astrocytes the number of microtubules diminishes (figs. 11 12) so that they are extremely uncommon in the fibrous astrocytes of the adult optic nerve (fig. 1)

Concurrent with the increase in filaments there is a gradual reduction in the number of mitochondria, of free ribosomal particles and of the cisternae of both the granular endoplasmic reticulum and the Golgi apparatus, until in adult fibrous astrocytes the number of profiles of these organelles is very small (fig. 1)

The transition from the cytoplasmic characteristics of early postnatal astrocytes to those of fully differentiated astrocytes is gradual. By 21 days after birth, there are many astrocytes which are almost identical in every respect with mature fibrous astrocytes, but alongside are other astrocytes whose cytoplasmic features are intermediate between those of mature and early postnatal astrocytes (figs 11 12) While the perikarya and processes of the intermediate forms contain large numbers of filaments they also have many more microtubules and other organelles than the fully differentiated fibrous astrocytes.

DISCUSSION

Although finger-like projections arising from the cell surfaces are common during the early postnatal development of astrocytes they become fewer in number as development proceeds, and are rarely found in the mature optic nerve This suggests that many of the finger-like projections may be involved in the formation of the additional glial sheets which develop between axons. A projection probably extends between the axons until it meets a similar projection from another cell. When this happens the observations indicate that the two become thicker and are joined by other projections extending from both the same and adjacent cells until a fully developed glial sheet is formed. In effect then, the finger-like projections may be regarded as pilot processes, but it is unlikely that their disappearance during maturation is indicative of the fact that they all become incorporated within glial sheets On the basis of the number of projections apparent at different stages of development, it seems that many of the finger-like projections are ultimately retracted and so play no part in the final formation of glial sheets

The organelles contained within early postnatal astrocytes diminish considerably during maturation, until in fully developed fibrous astrocytes they are very sparse. Most of the cell volume is occu-

Some of the immature astrocytic processes that extend between the unmyelinated axons of the early postnatal optic nerve terminate as expansions either immediately subjacent to the pia mater (figs 3 7) or on capillary surfaces (fig 8) Such expansions form the glia limitans The glia limitans with its associated basal lamina is already present at birth and appears to form a complete sheet entirely separating the axons from the surrounding tissues (figs 7 8)

At birth zonulae occludentes are present between the plasma membranes of adjacent astrocytic processes but in addition, there is another type of adhesion or junction The latter occurs between the plasma membranes of both mature and immature astrocytic processes and the adjacent plasma membranes are separated by a gap of about 150 A At such adhesions (figs 9 10 J) the plasma membranes are arranged strictly parallel to each other There is a slight accumulation of electron-dense material in the intervening gap and a considerable accumulation of electron-dense material on the cytoplasmic aspect of each of the apposed plasma membranes of the adhesion (fig 10 J) It is the latter feature that enables these adhesions to be identified at relatively low magnifications (fig 9) The length of these adhesions seems to be somewhat variable for although they most commonly appear as short punctate structures like those in figure 10 longer ones may occasionally occur (fig 7 J) It is not clear whether the lengths of the adhesions are in fact variable or whether the shorter more common type represents a transverse section of a more extensive adhesion somewhat akin to the zonulae adherentes of Farquhar and Palade ('63)

The adhesions between astrocytic processes differ from the fasciae or zonulae adherentes in that the apposed plasma membranes are closer together and there is never a centrally placed electron-dense line in the gap between the two mem branes Adhesions similar to those described here have been observed by Hamlyn ('62) between synaptic bags and dendrites within the hippocampus and by Peters and Palay ('66) between the plasma membranes of adjacent dendrites in the cat lateral geniculate body

Although immature and mature astrocytes have basically similar shapes, the morphology of their cytoplasm is quite different. The background cytoplasmic matrix of early postnatal astrocytes is more electron-dense than that in the mature forms (fig 1) and contains a much more extensive array of organelles (figs. 4, 6) particularly within and at the bases of th broad processes directly emanating fro the perikaryon In such regions there a numerous mitochondria, while the Golg apparatus is well developed and appea as stacks of flattened cisternae with man associated vesicles (fig 6 G) The gra ular endoplasmic reticulum of immatu astrocytes has the form of long and rel tively wide cisternae which contain el tron-dense material Some areas of t outer surface of the membranes are stu ded with regularly arranged, distinct bosomes while other areas are bare (fi 6 ER) This type of endoplasmic retic lum does not occur within the cytoplas of any other type of cell within the dev oping optic nerve so that it can readily used to identify those astrocytic profi not easily characterised on the basis other criteria. Clusters of ribosomes associated with the granular endopl mic reticulum lie free throughout the toplasm (fig 4 6) Centrioles and bases of cilia have also been seen

Although microtubules are seldom served within the cytoplasm of adult brous astrocytes they are relatively nu erous within the cytoplasm of develop astrocytes Viewed from the side, the crotubules are straight with no obvi dilatations and in processes they run p allel to the long axis (figs 7 8) The crotubules have an external diameter 230–260 A similar to the microtubules scribed in other tissues (e g Silveira Porter 64 de Thé '64 Sanborn et 65 Anderson et al '66) and in tra verse section have the appearance of lectron-dense circles (fig 5 arrow) T 60 A thick electron-dense walls appear be composed of globules and while th outlines are rather indistinct, 10 to such globules can sometimes be dis guished (Peters and Vaughn '67)

simple connecting system between organelles themselves and between organelles and growing cell processes. However it does not discount the possibility of microtubules directly or in some way funneling substances from the areas containing organelles towards the tips of growing processes. Indeed, they may play a dual role during development, providing metabolic and structural support to the extending astrocytic processes that have grown beyond the size of finger-like projections.

In addition to the possible functions discussed above, there is some evidence to suggest that ultimately microtubles may give rise to the astrocytic filaments that appear during maturation. This concept is based primarily on the observation of the balance between microtubules and filaments. As shown, microtubules occur in relatively large numbers in early postnatal astrocytes while filaments are scarce but during maturation this balance is gradually reversed until in the adult, filaments almost completely fill the cytoplasm and microtubules are very seldom seen. Support for the concept of filaments being derived from microtubules also comes from observations of the immature axons of developing optic nerve (Peters and Vaughn, '67). There microtubules occur within the axoplasm in relatively large numbers during the early postnatal stages while at the same time there are very few neurofilaments. When neurofilaments first appear they occur in compact groups each containing four to ten a number not inconsistent with that of the subunit filaments forming the walls of microtubules. In this connection, it must be mentioned that Pease ('63) presents evidence from mechanically disrupted and negatively stained sperm tails that the walls of microtubules are composed of approximately ten filaments which run parallel to the long axis of the tubules. A similar observation has been made by Barnicot ('66) who examined the structure of microtubules from mitotic spindles. Such subunit filaments have not been observed in the walls of microtubules viewed laterally in sectioned material, but globular elements thought to represent such subunit filaments are apparent in cross-sections of walls of microtubules. Our observations agree with those of Ledbetter and Porter ('63) and Silveira and Porter ('64) in that the number of globules is 10 to 13 It is suggested that these subunit filaments may be the precursors of the astrocytic filaments which appear during maturation.

Although microtubules have not been observed to disassociate into component units, oval profiles whose walls are composed of globules with diameters of approximately 100 A are occasionally seen within transverse sections of axons (Peters and Vaughn, '67) These profiles are distinct from those of microtubules and agranular endoplasmic reticulum, both of which have thinner walls. It is thought that the oval profiles may represent an intermediate stage in the formation of filaments from microtubules the 100 Å globular subunits giving rise to groups of neurofilaments as a result of the disruption of the walls of these oval profiles.

Finally Auber's work ('62) on developing insect flight muscles also indicates the possibility of a microtubular origin of filaments. He describes groups of microtubules closely surrounding newly formed myofilaments and states that this relationship suggests that the primary myofilaments are derived from the surrounding microtubules.

This discussion has of necessity been highly speculative. However it is felt that both the above questions and others, such as the function of astrocytic filaments are of sufficient interest and importance to warrant this type of consideration Hopefully it will not be too long before a more factual discussion of these problems can take place.

ACKNOWLEDGMENT

This study has been aided, in part, by a Postdoctoral Fellowship in Brain Research from the United Cerebral Palsy Research and Educational Foundation

LITERATURE CITED

Anderson, W. A., A. Weissman and R. A. Ellis 1966 A comparative study of microtubules in some vertebrate and invertebrate cells. Zeitschr. f. Zellforsch., 71 1–13.

pied by bundles of astrocytic filaments which are composed according to Bairati (58) of a protein of the K.E.M.F group (pseudo-keratin in the α configuration) The dramatic reduction of organelles and accumulation of filaments in astrocytes of the adult rat optic nerve may indicate that these cells have attained a steady and lower state of metabolism when large numbers of organelles are no longer necessary for their maintenance

Can the changes occurring in maturation suggest what the functions of fibrous astrocytes may be in adult optic nerve? Two possible suggestions are: (a) that astrocytes play some role in regulating the transfer of substances in and out of the optic nerve and (b) that they provide a structural support to the nerve by forming an interlacing framework with the axons For the present, any discussion of this problem must be purely speculative but if the sparcity of organelles within the cytoplasm of mature astrocytes is indicative of a low metabolism then it is unlikely that they are playing an active role in the transport of metabolites in and out of the nerve This of course does not preclude the possibility that they are playing a more passive role in transference nor that they take part in the formation of the blood brain-barrier but the work of Kuffler Nicholls and Orkand ('66) strongly suggests that at least in the optic nerves of Amphibians glial cytoplasm is not a pathway for the rapid diffusion of ions and small molecules such as sucrose

In many ways the idea that the fibrous astrocytes have a structural role in binding the axons together is an attractive one. It is consistent with the observation that their processes interlace generally at right angles with the axons but at present there is no direct evidence to favor this hypothesis over any other

The function of the numerous microtubules present within early postnatal astrocytes can also only be a matter of speculation Other investigators have proposed functions which can be grouped into the following general categories: (a) intracellular transport of ions (Slautterback, '63 Philpott, '62) and metabolites (Sandborn et al 64 Sandborn, '66); (b) contraction (Ledbetter and Porter 63; Grimstone and Cleveland, '65 Kane, '62), and (c) intracellular support for maintaining the shape of elongating cytoplasmic processes (Byers and Porter, '64, Silveira and Porter '64 Silveira and Porter '64 Tilney and Porter '65)

Perhaps the present observations on microtubules can be most readily interpreted in favor of the hypothesis that they are responsible for maintaining the shape of an elongating cellular extension. Immature astrocytes have many processes which are very small (0 1 to 0.3 μ in diameter) and grow for relatively long distances with no external support except that provided by the surrounding axons. In respect to this it is germane to mention the work of Tilney and Porter (65) who point out that oriented microtubules may be necessary for the development of the linear extensions of the Heliozoan Actinosphaerium, and also that of Byers and Porter ('64) who have postulated a similar functional relationship between oriented microtubules and the elongation lens cells of chick embryos.

In developing astrocytes one factor which argues against this interpretation is that microtubules are only rarely found in the small finger like projections. This could be due to a lack of fixation of microtubules in a delicate cytoplasmic process offering little in the way of "buffering" properties against the wave of fixation (Tilney and Porter '65) or perhaps, it indicates that an elongating process does not require microtubular support until it reaches a certain size In any case, the observation presents some difficulty in interpreting microtubules as being entirely a shape-maintaining device.

Whether microtubules function as a transport system for ions and metabolites is difficult to discuss from a purely morphological study No direct continuity between microtubules and other organelles has been observed in developing astrocytes in the manner that Sandborn ('66) suggests Futher microtubules do not first appear in cytoplasmic areas of high organelle density Instead they are first observed within the slender processes that are some distance away from the perikaryon These observations would indicate that microtubules do not form a

simple connecting system between organelles themselves and between organelles and growing cell processes. However it does not discount the possibility of microtubules directly or in some way funneling substances from the areas containing organelles towards the tips of growing processes. Indeed, they may play a dual role during development, providing metabolic and structural support to the extending astrocytic processes that have grown beyond the size of finger-like projections.

In addition to the possible functions discussed above there is some evidence to suggest that ultimately microtubles may give rise to the astrocytic filaments that appear during maturation. This concept is based primarily on the observation of the balance between microtubules and filaments. As shown, microtubules occur in relatively large numbers in early post natal astrocytes while filaments are scarce, but during maturation this balance is gradually reversed until, in the adult, filaments almost completely fill the the cytoplasm and microtubules are very seldom seen. Support for the concept of filaments being derived from microtubules also comes from observations of the immature axons of developing optic nerve (Peters and Vaughn, '67). There microtubules occur within the axoplasm in relatively large numbers during the early postnatal stages, while at the same time there are very few neurofilaments. When neurofilaments first appear they occur in compact groups each containing four to ten, a number not inconsistent with that of the subunit filaments forming the walls of microtubules. In this connection, it must be mentioned that Pease ('63) presents evidence from mechanically disrupted and negatively stained sperm tails that the walls of microtubules are composed of approximately ten filaments which run parallel to the long axis of the tubules. A similar observation has been made by Barnicot ('66) who examined the structure of microtubules from mitotic spindles. Such subunit filaments have not been observed in the walls of microtubules viewed laterally in sectioned material, but globular elements thought to represent such subunit filaments are apparent in cross-sections of walls of microtubules. Our observations agree with those of Ledbetter and Porter ('63) and Silveira and Porter ('64) in that the number of globules is 10 to 13. It is suggested that these subunit filaments may be the precursors of the astrocytic filaments which appear during maturation.

Although microtubules have not been observed to disassociate into component units oval profiles whose walls are composed of globules with diameters of approximately 100 A are occasionally seen within transverse sections of axons (Peters and Vaughn, '67). These profiles are distinct from those of microtubules and agranular endoplasmic reticulum both of which have thinner walls. It is thought that the oval profiles may represent an intermediate stage in the formation of filaments from microtubules the 100 A globular subunits giving rise to groups of neurofilaments as a result of the disruption of the walls of these oval profiles.

Finally Auber's work ('62) on developing insect flight muscles also indicates the possibility of a microtubular origin of filaments. He describes groups of microtubules closely surrounding newly formed myofilaments and states that this relationship suggests that the primary myofilaments are derived from the surrounding microtubules.

This discussion has of necessity been highly speculative. However it is felt that both the above questions and others, such as the function of astrocytic filaments are of sufficient interest and importance to warrant this type of consideration. Hopefully it will not be too long before a more factual discussion of these problems can take place.

ACKNOWLEDGMENT

This study has been aided, in part, by a Postdoctoral Fellowship in Brain Research from the United Cerebral Palsy Research and Educational Foundation.

LITERATURE CITED

Anderson, W. A., A. Weissman and R. A. Ellis 1966 A comparative study of microtubules in some vertebrate and invertebrate cells. Zeitschr. f. Zellforsch., 71: 1–13.

Auber J 1962 Mode d'accroissement des myofibrilles au cours de la nymphose de Calliphora erythrocephala Compt. Rend. de l'academie des Sci., 254 4070–4075 Pt. III

Bairati, A 1958 Propriétés biophysiques des fibres névrogliques. C. R. Ass. Anat. 44/98: 113–119

Barnicot N A 1966 A note on the structure of spindle fibres. J Cell Sci. 1 217–222.

Byers B and K R. Porter 1964 Oriented microtubules in elongating cells of the developing lens rudiment after induction. Proc. Nat. Acad Sci., 52 1091–1099

Farquhar M G., and G E. Palade 1963 Junctional complexes in various epithelia. J Cell Biol., 17 375–412.

Fujita S 1963 The matrix cell and cytogenesis in the developing central nervous system. J Comp Neur 120 37–42.

Fujita, H. and S Fujita 1963 Electron microscopic studies on the histogenesis of nerve cells and neuroglia in the domestic fowl II. On neuroglia Acta Anat. Nippon. 38 95–106

——— 1964 Electron microscopic studies of the differentiation of the ependymal cells and the glioblast in the spinal cord of domestic fowl. Zeitschr F Zellforsch. 64 262–272.

Glees P and S Le Vay 1964 Some electron microscopical observations on the ependymal cells of the chick embryo spinal cord. J f Hirnforsch. 6 355–360

Grimstone A V., and L. R. Cleveland 1965 The fine structure and function of the contractile axostyles of certain flagellates. J Cell Biol 24 387–400

Hamlyn L. H. 1962 The fine structure of the mossy fibre endings in the hippocampus of the rabbit. J Anat. 96 112–120

Kane R. E. 1962 The mitotic apparatus. Fine structure of the isolated unit J Cell Biol. 15 279–287

Karnovsky M J 1965 A formaldehyde-glutaraldehyde fixative of high osmolarity for use in electron microscopy J Cell Biol 27 137A–138A Proc. 5th Ann Meet. Am. Soc Cell Biol

Kuffler S W J G Nicholls and R. K Orkand 1966 Physiological properties of glial cells in the central nervous system of Amphibia. J Neurophysiol., 29 768–787

Ledbetter M. C and K. R. Porter 1963 A microtubule in plant cell fine structure J Cell Biol., 19 234–250

Meller K. W Breipohl and P Glees 1966 Early cytological differentiation in the cerebral hemisphere of mice. Zeitschr f Zellforsch., 72 525–533

Millonig G 1961 Advantages of a phosphate buffer for OsO_4 solutions in fixation. J Appl. Phys. 32 1637

Muir A. R. and A. Peters 1962 Quintuple-layered junctions at terminal bars between endothelial cells. J biophy biochem cytol. 12 443–448.

Pease D C 1963 The ultrastructure of flagellar fibrils. J Cell Biol., 18 313–326

——— 1964 Histological Techniques for Electron Microscopy Academic press New York pp 52–63

Peters A. 1960 The formation and structure of myelin sheaths in the central nervous system. J biophys. biochem. Cytol., 8 431–446.

——— 1962a Plasma membrane contacts in the central nervous system. J Anat, 96 237–248

——— 1962b Myelination in the central nervous system In: Proceedings of IV International Congress of Neuropathology Munich, 1961 Ed H. Jacob, George Thieme Stuttgart, 2 50–54

Peters, A. and S L. Palay 1966 The morphology of laminae A and A_1 of the dorsal nucleus of the lateral geniculate body of the cat. J Anat., 100 451–486.

Peters A., and J E. Vaughn 1967 Microtubules and filaments in the axons and astrocytes of early post-natal rat optic nerves. J Cell Biol 32 113–119

Philpott, C. W 1962 The comparative morphology of the chloride secreting cells of three species of Fundulus as revealed by the electron microscope Anat. Rec 142. 267–281

Sandborn E. F Koen, J D McNabb and G Moore 1964 Cytoplasmic microtubules in mammalian cells. J Ultrastruct. Res., 11 123–138.

Sandborn E. 1966 Electron microscopy of the neuron membrane system and filaments Canad J Physiol. Pharmacol. 44 329–338.

Sandborn E., A. Szeberenyi P E. Messier and P Bois 1965 A new membrane model derived from a study of filaments, microtubules and membranes. Rev Canad Biol., 24 243–276

Silveira M. and K. R. Porter 1964 The spermatozoids of flatworms and their microtubular systems. Protoplasma, 59 240–265

Slautterback D B 1963 Cytoplasmic microtubules. I. Hydra. J Cell Biol., 18 367–388.

Tennyson V M. 1965 Electron microscopic study of the developing neuroblast of the dorsal root ganglion of the rabbit embryo. J Comp Neurol 124 267–317

de Thé G 1964 Cytoplasmic microtubules in different animals cells. J Cell Biol., 23 265.

Tilney L G and K. R. Porter 1965 Studies on microtubules in Heliozoa I. Protoplasma, 60 317–344

Vaughn J E. and A Peters 1966 Aldehyde fixation of nerve fibres. J Anat 100 687

Voeller K G D Pappas and D P Purpura 1963 Electron microscope study of development of cat superficial neocortex. Exp. Neurol., 7 107–130.

Wechsler W 1963 Electron microscopic contribution to the development and differentiation of cells as demonstrated in the nervous system. Verh. Deutsch Ges. Path 47 316–322.

——— 1966 Die Feinstruktur des Neuralrohres und der neuroektodermalen Matrixzellen am zentral Nervensystem von Huhnerembryonen. Zeitschr f Zellforsch., 70 240–268

Wolff J 1965 Elektronenmikroskopische Untersuchungen uber Struktur und Gestalt von Astrozytenfortsatzen Zeitschr f Zellforsch., 66 811–828

Abbreviations

A, Astrocytic perikaryon
Ax Axons
B Broad process
BL, Basal lamina
C *Meningeal covering*
D Fat droplet
E, Endothelial cell
ER, Granular endoplasmic reticulum
F Astrocytic filaments
FS, Fascicle
G Golgi apparatus
GS, Elementary glial sheet
J Adhesion or junction
L, *Leptomeningeal cell*
M Microtubules
P Astrocytic process
S Slender process
V Blood vessel

PLATE 1

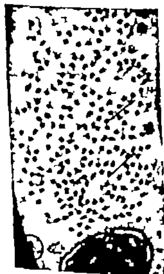
EXPLANATION OF FIGURES

All figures are of transversely sectioned rat optic nerves.

1 Fibrous astrocyte from adult optic nerve. Filaments (F) fill the cytoplasm of the perikaryon and processes and organelles are sparse. Dense inclusions (arrow) and a fat droplet (D) are contained within the cell. All of the axons (AX) are myelinated. × 19,000

2 Part of a transversely sectioned mature fibrous astrocytic process (P) illustrating the tubular appearance of astrocytic filaments (arrows) The myelin sheath in the lower left belongs to an adjacent axon. × 127 000.

3 Phase micrograph of the periphery of a one day postnatal optic nerve. The meningeal covering (C) of the nerve is at the top of the photograph and contains blood vessels (V) The perikarya of two immature astrocytes (A) are included in the field. Notice that some of the astrocytic processes form the glial limitans (arrows) while others (P) segregate the axons into fascicles (FS) × 2,100.




V

PLATE 2

EXPLANATION OF FIGURES

4 Immature astrocyte from a one day postnatal optic nerve The organelles are mainly located in the broad process (B) which is an extension of the cell body A slender process (S) arises at right angles to the broad process and finger-like projections (arrows) emerge from several areas of the cell's surface All axons (AX) are unmyelinated at this stage of development. × 30 400

5 Seven days postnatal. Immature astrocytic process (P) extending between three unmyelinated axons. The process contains many transversely sectioned microtubules. These appear as dark circles and most show an electron-opaque central dot (arrow) × 102,000.



PLATE 3

EXPLANATION OF FIGURE

6 Immature astrocyte (A) at three days after birth. From the cell body a broad process (B) extends. It contains distinctive granular endoplasmic reticulum (ER, see text) numerous mitochondria, and a well developed Golgi apparatus (G) In addition to the broad process, the astrocyte has processes which fit into the other two categories: slender processes (S and S_1) and finger-like projections (arrows) × 16,200

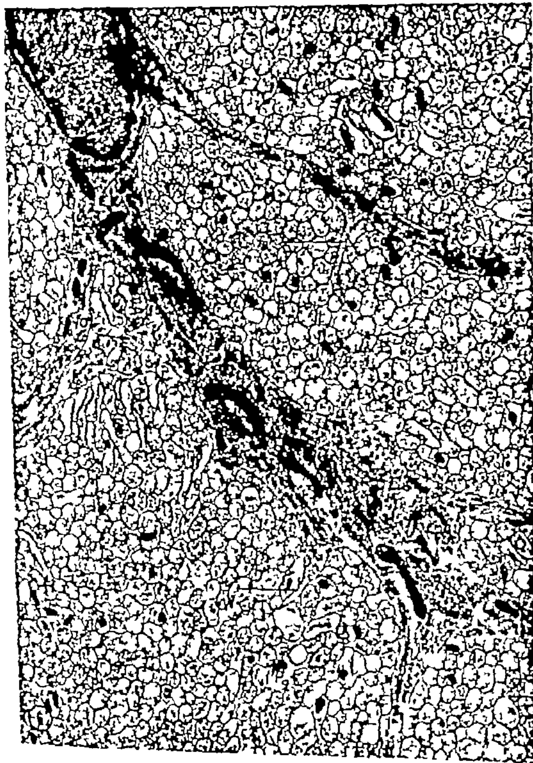


PLATE 4

EXPLANATION OF FIGURES

7 Three days postnatal Expansions of immature astrocytic processes (P) forming part of the glia limitans at periphery of the optic nerve. The dense cell at the top of the photograph is a leptomeningeal cell (L) and interposed between it and the glia limitans is a basal lamina (BL) The astrocytic process (P) extending from the lower right to the glia limitans contains microtubules (M) but no obvious filaments. An adhesion is present between two astrocytic expansions (J) × 27,500

8 One day postnatal. Astrocytic process (P_1) terminating on an endothelial cell (E) of a capillary with a basal lamina (BL) between the two Other astrocytic processes join P to form a glial sheet and they contain both microtubules (M) and filaments (F) while P_1 has only filaments (F) × 22,800

PLATE 5

EXPLANATION OF FIGURES

9 At the top of the photograph is the cell body of an immature astrocyte (A) containing microtubules (M) at five days postnatal. The broad process (B) at the bottom right contains many profiles of granular endoplasmic reticulum (ER) and numerous free ribosomes. Elementary glial sheets (GS) consisting of two parallel astrocytic processes, group the axons into bundles and finger-like projections (arrow) are apparently subdividing some of the existing fascicles. An adhesion (J) between astrocytic processes can be seen in this relatively low magnification micrograph because of the accumualtion of associated electron-dense material. × 21 000.

10 Seven days postnatal. Two adhesions (J) between adjacent astrocytic processes. × 47 000



PLATE 6

EXPLANATION OF FIGURES

11–12 Twenty-one days postnatal. Fibrous astrocytes which have a morphology intermediate to early postnatal and fully mature fibrous astrocytes. Comparison with figure 1 shows that these cells contain more mitochondria granular endoplasmic reticulum (ER) Golgi apparatus (fig 11 G) and microtubules (fig. 12, M) than adult fibrous astrocytes, but that the concentration of filaments (F) is similar to mature cells. × 16,500 × 19,950

11

12

The Fine Structure of Vascular Sympathetic Neuromuscular Contacts in the Rat

C. E. DEVINE[1] AND F. O. SIMPSON
Wellcome Medical Research Institute, University of Otago Medical School, Dunedin, New Zealand

ABSTRACT The fine structure of the neuromuscular contacts of arterioles and small arteries from the jejunum and mesentery of the rat has been studied. There is a rich innervation of these vessels, consisting of bundles of axons in the adventitia around the vessels.

In the typical sympathetic neuromuscular contact on a small blood vessel, the axon bundle is loose, the Schwann cell cover is deficient, the neuromuscular distance is less than 1,500 Å, the basement membranes of axon and smooth muscle cell are fused together, and the axon tends to follow the contour of the smooth muscle cell. However it is not possible to be certain that these criteria are essential for a true functional neuromuscular contact. In particular it appears from the structural findings that a neuromuscular distance of 2,000–3,000 Å or more could well be compatible with effective neuromuscular transmission.

Smooth muscle cells in arterioles often have multiple innervation, and an axon probably innervates more than one smooth muscle cell.

Occasional axons contain mainly or solely vesicles of the "large granular" type.

Electron microscope studies have shown that in smooth muscle tissues such as the vas deferens (Richardson, '62; Merrillees et al. '63) iris (Richardson, '64) and gastrointestinal tract and bladder (Thaemert, '63, '66) the autonomic axons make very close contact with the smooth muscle cells the neuromuscular distance being as little as 200 Å. In vascular smooth muscle (Barajas, '64; Lever et al., '65b Simpson and Devine, '64 '66; Devine '66) the neuromuscular distance is greater being seldom less than 900–1,000 Å, and the problem has arisen of how far distant from a smooth muscle cell a nerve axon can be while yet having some meaningful relationship to it.

In order to investigate further the fine structural relationship between autonomic nerves and vascular smooth muscle a study has been made of arterioles in the submucosal layer of the upper jejunum in the rat (fig. 4) and of small arteries and veins in the most peripheral part of the adjoining mesentery (fig. 3)

METHODS

Albino Wistar rats from the Otago stock colony were anaesthetized with ether. Portions of the wall of the jejunum with associated mesenteric blood vessels were removed from each animal, stripped of fat, and fixed with a large excess of veronal acetate-buffered 1% osmium tetroxide (pH 7.4) for 2–18 (optimum six hours) hours or in phosphate-buffered glutaraldehyde (pH 7.2) for at least four hours. The glutaraldehyde-fixed material was washed in buffer and post-fixed for six hours in osmium tetroxide with the same buffer. In order to obtain good fixation of the axons, and in order to show up the granulations in the vesicles two hours fixation in osmium tetroxide proved to be insufficient and this was the reason for the prolonged fixation times. It was also found to be important to have a considerable excess of osmium tetroxide present, probably because of the amount of fat which was present in this tissue (particularly in the mesentery) and which could not be completely removed.

The tissues were taken through an alcohol series and embedded in Epon 812. Thick sections (approx. 1 µ) were cut with a Porter Blum ultramicrotome, placed with a drop of water on a glass slide with a brush, dried and warmed with 1% aqueous ethyl violet or basic fuchsin solution and observed in a light microscope in

[1] The authors are working under   grant from the New Zealand Medical Research Council.

order to facilitate orientation and trimming of the block. Thin sections were cut, stained with uranyl acetate or Reynolds lead citrate and viewed in a Philips 100B electron microscope or a Hitachi HU 11A electron microscope.

The differentiation between small arteries and arterioles was not always entirely easy although typical examples of either vessel could be readily differentiated The arterioles were vessels 5–75 μ in diameter the smaller ones did not have a complete smooth muscle layer or an internal elastic lamina whereas the larger arterioles had a complete smooth muscle layer and an internal elastic lamina. The small arteries were vessels ranging from 75–200 μ in diameter with a well developed internal elastic lamina, several layers of smooth muscle cells in the media and an external elastic lamina. Both these types of vessel but particularly the small arteries were obviously in a state of contraction, the internal elastic lamina being thrown into folds and the endothelial cells bulging into the lumen Small veins were also seen they had a thin wall in relation to their diameter only one layer of smooth muscle cells in their media and the internal elastic lamina was thin

OBSERVATIONS

Distribution of axons around blood vessels

(a) *Small arteries* Large numbers of axon bundles were present in the tissue around these vessels The axon bundles were 2–10 μ in diameter and contained three to eight axons embedded in a Schwann cell sheath (fig 5) The number of bundles round a small artery varied to some extent depending on the size of the vessel so that the smaller vessels of this class might have eight or ten bundles of axons around them while a small artery about 150 μ in diameter might have up to 20 bundles of axons around it. These bundles appeared to be running approximately in the same direction as the vessel or obliquely round the vessel and presumably were forming part of the autonomic ground plexus (Hillarp '59) Some of these axon bundles could be found lying quite close to the smooth muscle cells of the arterial wall and often a process of smooth muscle cell could be seen penetrating the external elastic lamina towards an axon bundle (fig. 5) The axons were usually partly naked of Schwann cell sheath on the side closest to the smooth muscle cell (fig 6)

(b) *Arterioles* Bundles of axons were similarly found in the tissue around the arterioles (figs. 8 9) The bundles ranged from 2–5 μ in diameter and contained three to five axons partly embedded in a Schwann cell sheath. Occasional large bundles of unmyelinated axons were seen close to the arterioles (fig 7) but may well not have had any functional connection with them.

The number of axon bundles per vessel was smaller than in the case of the small arteries in the mesentery but the number of axon bundles was not reduced when considered in relation to the size of the vessel An arteriole of 50 μ in diameter might have eight bundles of axons around it while a smaller arteriole 5–10 μ in diameter might have two axon bundles beside it. The axon bundles appeared to approach rather closer to the arterioles than was the case with the small arteries (fig. 1) Also, the Schwann cell sheath tended to be a little less complete the bundles of axons less tight and the axons tended to contain rather more granular vesicles. Occasional naked single axons were seen (figs. 11, 12, 14) in close proximity to smooth muscle cells or even lying in a groove between two superficial smooth muscle cells (fig. 16). It was clear that a smooth muscle cell might have a multiple innervation, while equally an axon might innervate more than one smooth muscle cell.

Distances between axons and smooth muscle cells at presumed neuromuscular contacts

A survey was made of the neuromuscular distance in a large number of possible neuromuscular contacts i.e places where an axon was naked of Schwann cell sheath at the side opposite the smooth muscle cell and where the axon was within 10 000 Å of the smooth muscle cell. As the situation appeared to be slightly different in the arterioles on the one hand and the small arteries on the other the survey was made

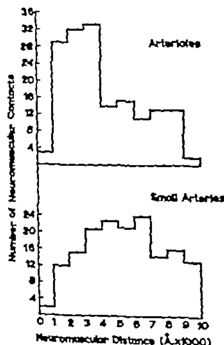


Fig. 1 Histogram of neuromuscular close contacts of arterioles (165 contacts) and small arterioles (181 contacts) Axons considered contained granular vesicles, were partly naked of Schwann cell adjacent to the muscle surface and were less than 10,000 Å away from the smooth muscle.

or each of these types of vessel separately In all, 165 such contacts were examined for arterioles and 181 for small arteries. The neuromuscular distances for these contacts are shown in the histogram in figure 1 and it will be seen that close contacts of the order of 4,000 Å or less were more commonly found in the arterioles than in the small arteries.

At the points of closest contact between axons and smooth muscle cells the neuromuscular distance was about 800–1,100 Å. At such places, the basement membrane of the axons and the smooth muscle cells had fused into one layer and the axons appeared *to follow* the outline of the smooth muscle cell to some extent so that the relationship between them was obviously very close (figs. 8 9 11 12, 13 14, 15, 16)

Axonal contents

The axons contained mitochondria, thick neurotubules approximately 250 Å in diameter and agranular and granular vesicles (figs. 6 10) The neurotubules were most commonly seen in axons well-embedded in the Schwann cell sheath (fig. 7) and appeared to be less common in the axons where there were large numbers of vesicles (figs. 6 10) The number of vesicles, both agranular and granular was usually greatest in the axons which seemed to be making typical neuromuscular contacts (figs. 8 9 10 11 12, 13 14 15 16)

The agranular vesicles were 250–600 Å in diameter and contained no electron-dense material. The granular vesicles were of two types. The smaller ones were 250–750 Å in diameter and had an electron-dense core which either could be very small or could fill the vesicle. The larger granular vesicles were 750–1 500 Å in diameter and their contents were moderately and diffusely electron-dense. A survey of the number of the different types and sizes (overall diameter) of vesicles present in 85 axon profiles from four animals (minimum number of axons from any one animal was 5) is shown in figure 2. The clear vesicles were the most common followed closely by the small granular vesicles, while the larger granular vesicles were less common. It appears that, in fact, there may be two distinct populations of granular vesicles. The relative numbers of the different types of vesicle did not seem to be dependent upon the distance of the axon from the smooth muscle cell. Occasional axons were seen where the granular vesicles were almost entirely of the large type (figs. 17 18 19) even at sites of close neuromuscular contact (fig. 18)

Smooth muscle cells

The smooth muscle cells of these vessels did not show any special characteristics other than those reviewed by other authors, e.g. Rhodin ('62). Pinocytotic vesicles were common particularly on the external surface of the muscle cells as also found by Lever et al. ('65a) in coronary arterioles. A number of instances were seen of protrusions of the surface of a smooth muscle cell towards an axon or bundle of axons (figs 5 11 12) Sacs of endoplasmic reticulum were occasionally present in the smooth muscle cells at points of probable

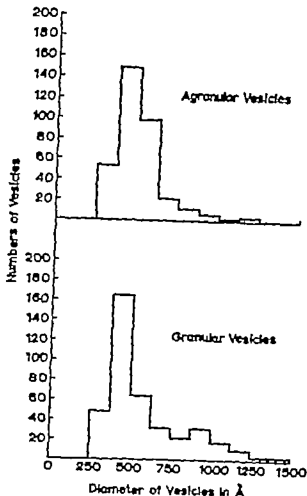


Fig. 2 Histogram showing the size distribution of agranular (top) and granular vesicles (bottom) from axons around arterioles. A total of 85 axons from 4 animals in which all sharply defined vesicles were measured was considered. Large granular vesicles are represented by the small peak (750–1500 Å) and small granulated vesicles are represented by the larger peak (250–750 Å) Agranular vesicles are mainly from 250–750 Å.

neuromuscular contact (figs. 10 18) but such sacs were less common than in the sheep renal arterioles studied previously (Simpson and Devine '66)

Neuromuscular contacts in small veins

In the course of the study small veins and venules were also encountered these could be differentiated from small vessels on the arterial side of the circulation because of their larger lumen and much thinner wall. The outer surface of the smooth muscle cells tended to be crenated (fig. 20) Examples of neuromuscular contacts were seen also in these vessels (fig 20) and these contacts did not appear to differ radically in type from the neuromuscular contacts seen in the arterioles and small arteries.

DISCUSSION

Although it has been demonstrated by fluorescence methods (Falck, '62 Norberg and Hamberger '64) that the most peripheral part of the sympathetic outflow to vessels consists of an adrenergic ground plexus and although a number of examples of more or less definite sympathetic neuromuscular contacts have been demonstrated in different vessels by electron microscopy (Lever et al '61 '65b Zelander et al '62 Thaemert, '63 Appenzeller, '64; Barajas '64 Simpson and Devine, '64 '66; Devine, '66; Uchizono '64; Verity et al., '66) nevertheless the structural details of this innervation have not been finally established For instance, it is not known whether branches come off the plexus to innervate nearby areas of smooth muscle or whether the neurotransmitter is simply released from parts of the plexus direct. The little nodes which have been noted on the plexus in fluorescent microscopical studies (Malmfors, '65) may be identified with areas of widening of the axons in electron microscope studies (Barajas, '64 Simpson and Devine '66) Most of the contacts which an axon makes with smooth muscle cells are probably of an "en passage" type (Richardson '62) but presumably each axon must end somewhere. Our present study in the rat and our previous studies in the sheep renal arterioles (Simpson and Devine '66) have demonstrated that small single axons are sometimes seen close to smooth muscle cells or between the smooth muscle cells of the most superficial layer of the media and such single axons may well be about to terminate completely

The problem of what to accept as a neuromuscular contact is indeed a difficult one In the typical example the axon bundle is loose the Schwann cell cover is deficient the axons are packed with granular and agranular vesicles, the neuromuscular distance is less than 1 500 Å, the basement membranes of axon and smooth muscle cell are fused together and the axon tends to follow the contour of the smooth muscle cell. However there seems no reason to

clude the possibility that an axon 1,500–000 A away from a smooth muscle cell id packed with granulated and clear vesles is not also making meaningful conct with a smooth muscle cell. If it is cepted that this can occur then there ems no reason to deny the possibility at an axon 5,000 or even 10,000 A away om a smooth muscle cell may not also e able to exert some effect on it by dif ision of noradrenaline. It is also possible find instances of axons lying as close as A to a smooth muscle cell and not at hat point containing any vesicles again t does not seem possible to be certain that t such a contact some form of neuromusular transmission is not taking place. At resent, it seems to be best to allow of the ossibility that sympathetic neuromuscuar transmission may be taking place in a elatively diffuse manner and over quite considerable neuromuscular gaps. If this is then the neuromuscular relationship in blood vessels clearly differs quite radically from that in tissues such as the vas deferens and iris (Richardson '62, '64 Merrillees et al., '63) in which the neuromuscular distance is so much less. This is, perhaps not surprising because in these latter two tissues the smooth muscle cells have a different function and are required to produce single concerted contractions to a greater extent than is the case with the smooth muscle of small blood vessels whose function is mainly to maintain a steady tone.

The differences in the innervation of arterioles and arteries observed in this study presumably reflect differences in function of these two types of vessel. Some factor in the selection of the neuromuscular junctions examined could have affected the results of the survey of neuromuscular distances, although every effort was made to avoid any bias. Such bias could perhaps have resulted in a relative deficiency of larger neuromuscular distances round arterioles, but could hardly explain the deficiency of close contacts in the case of the arteries. The arterioles then, appear quite definitely to have more frequent neuromuscular close contacts and this is in keeping with their important role in the regulation of peripheral resistance. The external elastic lamina of the small arteries may act as a partial barrier to diffusion of neurotransmitter to the smooth muscle cells. In this size of vessel, the lamina appears seldom to be complete, however- it rather forms a network of elastic tissue around the vessel, and the close approach of an axon bundle often seems to coincide with a gap in the lamina. No instances of penetration of axons through the external elastic lamina were seen nor were axons found between the layers of smooth muscle cells in the medial coat of the arteries.

The granular vesicles within the axons represent, in all probability stores of catecholamines (Wolfe et al. '62 De Robertis, '66 Grillo '66; Whittaker '66) The examples of axons containing mainly or solely large granular vesicles (figs. 17 18 19) are of considerable interest. Although small granular vesices become "agranular" after reserpine, some at least of the large granular vesicles are unaffected (Hökfelt, '68) suggesting that while the small granular vesicles are concerned with noradrenaline storage the large granular vesicles may have a different function (Hökfelt, '66)

ACKNOWLEDGMENT

The authors wish to thank Miss Janet Ledingham for technical assistance, Dr. D G Rayns for helpful advice the New Zealand Medical Research Council for the use of the Philips 100B electron microscope and Professor A. Wynn Williams of the Pathology Department, University of Otago Medical School for the use of the Hitachi HU 11A electron microscope.

LITERATURE CITED

Appenzeller, O 1964 Electron microscopic study of the innervation of the auricular artery in the rat. J Anat., 98 87–91.

Barajas, L. 1964 The innervation of the juxtaglomerular apparatus. An electron microscopic study of the innervation of the glomerular arterioles. Lab. Invest., 13 916–929.

De Robertis, E. 1966 Adrenergic endings and vesicles isolated from the brain. Pharmacol. Rev 18 413–424.

Devine, C. E. 1968 Neuromuscular relationships in rat intestinal and mesenteric blood vessels. Proc. Univ Otago Med. Sch., 44; 9–11.

Falck, B 1962 Observations on the possibilities of the cellular localization of monoamines by a fluorescence method. Acta Physiol. Scand., 56 suppl. no. 197 1–25.

Grillo, M. A. 1966 Electron microscopy of sympathetic tissues. Pharmacol. Rev., 18 387–399

Hillarp N A. 1959 The construction and functional organisation of the autonomic innervation apparatus Acta Physiol. Scand., *46:* suppl. no. 157 1–38.

Hökfelt, T 1966 The effect of reserpine on the intraneuronal vesicles of the rat vas deferens. Experientia, 22 56.

Lever J D M. Ahmed and G Irvine 1965a Neuromuscular and intercellular relationships in the coronary arterioles. A morphological and quantitative study by light and electron microscopy J Anat., *99:* 829–840

Lever J D., and A. C. Esterhuizen 1961 Fine structure of the arteriolar nerves in the guinea pig pancreas. Nature (Lond.) *192:* 566–567

Lever J D., J D P Graham, G. Irvine and W H. Chick 1965b The vesiculated axons in relation to arteriolar smooth muscle in the pancreas. A fine structural and quantitative study J Anat., *99:* 299–313

Malmfors, T 1965 Studies on adrenergic nerves. The use of rat and mouse iris for direct observations on their physiology and pharmacology at cellular and subcellular levels. Acta Physiol. Scand. *64:* suppl. no. 248 1–93

Merrillees N C. R., G Burnstock and M. E. Holman 1963 Correlation of fine structure and physiology of smooth muscle in the guinea pig vas deferens. J Cell Biol. *19:* 529–540

Norberg, K. A. and B. Hamberger 1964 The sympathetic adrenergic neuron. Some characteristics revealed by histochemical studies on the intraneuronal distribution of the transmitter Acta Physiol. Scand. *63:* suppl. no 238 1–42.

Rhodin, J A. G 1962 Fine structure of vascular walls in mammals with special reference to smooth muscle component. Physiol. Rev., *42:* suppl. no. 5, 48–81

Richardson, K. C. 1962 The fine structure of autonomic nerve endings in smooth muscle of the rat vas deferens. J Anat., *96:* 427–442.

——— 1964 The fine structure of the albino rabbit iris with special reference to the identification of adrenergic and cholinergic nerves and nerve endings in its intrinsic muscles. Am. J Anat. *114:* 173–206.

Simpson, F O., and C. E. Devine 1964 Adrenergic nerve terminals in arterioles of sheep kidney Proc. Univ Otago Med. Sch., 42 26–27

——— 1966 The fine structure of autonomic neuromuscular contacts in arterioles of the sheep renal cortex. J Anat., *100:* 127–137

Thaemert, J C. 1963 The ultrastructure and disposition of vesiculated nerve processes in smooth muscle. J Cell Biol., *16:* 361–377

——— 1966 Ultrastructural interrelationships of nerve processes and smooth muscle cells in three dimension. J Cell Biol., *28:* 37–49.

Uchizono, K. 1964 Innervation of the blood capillary in the heart of dog and rabbit. Jap. J. Physiol., *14:* 587–598.

Verity M. A. J A. Bevan and R. J Ostrom 1966 Plurivesicular nerve endings in the pulmonary artery Nature (Lond.) *211:* 537–538.

Whittaker V P 1966 Catecholamine storage particles in the central nervous system. Pharmacol. Rev *18:* 401–412.

Wolfe D E., L. T Potter K. C. Richardson and J Axelrod 1962 Localizing tritiated norepinephrine in sympathetic axons by electron microscopic autoradiography Science, *138:* 440–442.

Zelander T., R. Ekholm and Y Edlund 1962 The ultrastructural organisation of the rat exocrine pancreas. III. Intralobular vessels and nerves. J Ultrastruct. Res. *7:* 84–101.

Abbreviations

A, Axon
ADV Adventitia
AGV Agranular vessels
BM Basement membrane
COL, Collagen
EEL, External elastic lamina
EL, Elastic material
END Endothelial cell
ER, Endoplasmic reticulum
F Fat cell
FB Fibroblast
IEL, Internal elastic lamina
ISM, Intestinal smooth muscle
LGV Large granular vesicle
M Mitochondrion
NB Nerve bundle
NT Neurotubules
PV Pinocytotic vesicles
SCH, Schwann cell
SGV Small granular vesicles
SM, Smooth muscle cell

PLATE 1

EXPLANATION OF FIGURES

Figures 3 and 4 tissue fixed in osmium tetroxide, embedded in Epon; 0.5–1 μ sections, stained with ethyl violet and basic fuchsin. Light microscope photographs.

3 Transverse section through a small mesenteric artery (*150 μ* in diameter) There is a well developed convoluted internal elastic lamina (IEL) the media contains about four layers of smooth muscle cells and on the outer aspect of the smooth muscle cells there is an external elastic lamina (EEL) Outside the adventitia (ADV) there are fat cells (F) and bundles of nerves (NB) × 533.

4 An oblique section through a large arteriole and several smaller arterioles in the submucosa of the intestine close to intestinal smooth muscle cells (ISM) There is some collagen surrounding the largest vessel, but less than round the small mesenteric artery above. The *convoluted internal elastic lamina (IEL) is well developed* but there is no external elastic lamina. × 533

SYMPATHETIC NEUROMUSCULAR CONTACTS
C. E. Devine and F. O. Simpson

PLATE 2

EXPLANATION OF FIGURES

Figures 5 and 6 tissue fixed in osmium tetroxide and stained with Reynolds lead citrate.

5 Axon bundle lying beside a smooth muscle cell (SM) from a small mesenteric artery The bundle consists of Schwann cell (SCH) and axons (A) and there is a large amount of collagen (COL) surrounding the bundle. On the outer aspect of the smooth muscle cells (SM) an external elastic lamina (EEL) is present, deficient opposite the axon bundle The neuromuscular distance is 3 750 Å and the axons contain relatively few granular vesicles. × 16,500.

6 High power view of an axon beside a smooth muscle cell (SM) of a small mesenteric artery The axon is naked of Schwann cell (SCH) at the surface facing the smooth muscle cell and contains numerous small granular vesicles (SGV) Although the neuromuscular distance is quite large (7,500 Å) there could be a functional relationship between axons and smooth muscle. Note absence of external elastic lamina. × 40,000

SCH
SM
5

SCH
A
SGV
A
A
COL
6
SM

PLATE 2

EXPLANATION OF FIGURES

Figures 5 and 6 tissue fixed in osmium tetroxide and stained with Reynolds lead citrate

5 Axon bundle lying beside a smooth muscle cell (SM) from a small mesenteric artery The bundle consists of Schwann cell (SCH) and axons (A) and there is a large amount of collagen (COL) surrounding the bundle On the outer aspect of the smooth muscle cells (SM) an external elastic lamina (EEL) is present, deficient opposite the axon bundle The neuromuscular distance is 3 750 Å and the axons contain relatively few granular vesicles. × 16,500.

6 High power view of an axon beside a smooth muscle cell (SM) of a small mesenteric artery The axon is naked of Schwann cell (SCH) at the surface facing the smooth muscle cell and contains numerous small granular vesicles (SGV) Although the neuromuscular distance is quite large (7,500 Å) there could be a functional relationship between axons and smooth muscle Note absence of external elastic lamina. × 40,000

5
SCH
A
SM

6
SCH
A
SGV
COL
SM

PLATE 3

EXPLANATION OF FIGURES

Figure 7 tissue fixed in glutaraldehyde/osmium tetroxide stained with aqueous saturated uranyl acetate

Figure 8 tissue fixed in osmium tetroxide and stained with Reynolds lead citrate

7 Large axon bundle lying close to an arteriolar smooth muscle cell. Although the neuromuscular distance at one place is only 2 400 Å there are very few vesicles in the axons and there is a good deal of collagen in the neuromuscular space A functional relationship between axons and smooth muscle here seems unlikely but cannot be excluded × 7,000

8 Oblique section through an intestinal arteriole The bundle of axons, supported by a Schwann cell lies spread against the surface of several muscle cells The axons contain numerous vesicles, some of them granular and follow the contour of the smooth muscle cells The basement membranes of the axons and smooth muscle cells are fused. Thus although the neuromuscular distance (1 400–1,800 Å) is not of the very closest, this is an otherwise typical true functional neuromuscular contact. There does not seem to be any modification of the muscle surface beneath the axons, but some pinocytotic vesicles (PV) are present. × 16,500

LGV
SCH
SM
NT
7

P
V
SCH
SM
BM
END
8

PLATE 4

EXPLANATION OF FIGURES

Figures 9–20 tissue fixed in osmium tetroxide and stained with Reynolds lead citrate

9 Higher power view of an area similar to that in figure 8. The axons contain many granular and agranular vesicles their contour follows that of the smooth muscle cells and there is fusion of the intervening basement membranes. The neuromuscular distance here is 1,300–1,800 Å. × 30,000

10 An axon lying beside an arteriolar smooth muscle cell and packed with large (LGV) and small (SGV) granular vesicles and agranular vesicles (AGV). The neuromuscular distance is quite large (2,800 Å) and the intervening basement membranes are not fused. Nevertheless a functional relationship between axons and smooth muscle seems likely in view of the numerous vesicles in the axon at this point. A sac of endoplasmic reticulum (ER) is present in the smooth muscle cell, apparently formed by an infolding of the plasma membrane × 45,500

PLATE 5

EXPLANATION OF FIGURES

11 A semitangential section of the wall of an arteriole The surface of a smooth muscle cell (SM) has been skiffed so that protuberances of the cell appear as islands. There is clearly an intimate relationship between these protuberances and the axons. × 15,500

12 A high power view of a portion of figure 11 showing one protuberance (SM) of a smooth muscle cell almost enveloped by one — or possibly two — axons The smallest neuromuscular distance is 800 Å Pinocytotic vesicles (PV) are numerous at the smooth muscle cell surface. × 40 000

SM1
SM2
11
800 Å
A
SMa
PV
BM
12

PLATE 6

EXPLANATION OF FIGURES

13 An example of neuromuscular close contacts of two axons (A) and two arteriolar smooth muscle cells (SM) Each axon is about 1 100 Å from a smooth muscle cell. × 22,000.

14 Two naked axons each at the junction of two arteriolar smooth muscle cells; basement membranes of nerve and muscle are fused when the neuromuscular distance is small (in these cases 1 100 Å) × 10,500

15 Two naked axons one of which extends for some distance (3.5 μ) along the surface of two arteriolar smooth muscle cells (SM) The basement membrane of the axon can be seen to fuse with that of the smooth muscle cells. × 15 000.

16 Small naked axon (A) lying in a groove between two arteriolar smooth muscle cells (SM) and separated from each by a gap of about 1 700 Å. × 30 400


SM
SCH
SM
13


END
A
SM
A
14


SM
SM
15

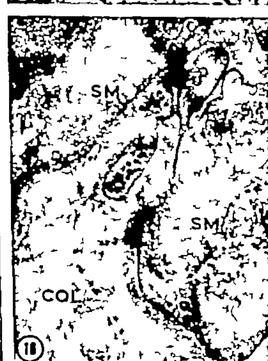

SM
SM
COL
16

PLATE 7

EXPLANATION OF FIGURES

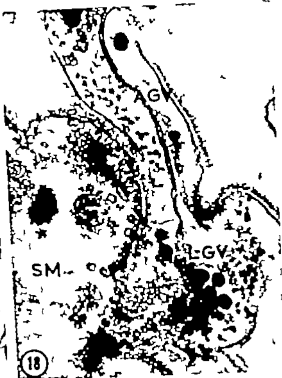
17 Axon (*A*) containing large granular vesicles (LGV) and lying about 7,500 Å away from two arteriolar smooth muscle cells. × 18,000.

18 Close approach of an axon containing large granular vesicles (LGV) and agranular vesicles (AGV) to an arteriolar smooth muscle cell. × 48,000.

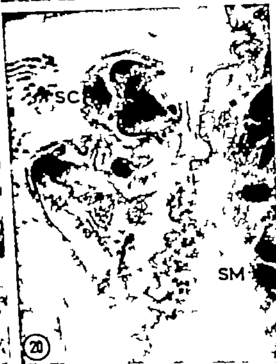
19 Several axons lying beside an arteriolar smooth muscle cell (SM) and containing different types of granular vesicles. One axon contains exclusively large granular vesicles (LGV) while others contain small granular vesicles (SGV) × 31 000

20 Close approach of an axon bundle to a small vein in the mesentery The axon (*A*) is 1,650 Å away from the convoluted surface of the smooth muscle cell (SM) × 24,000


SM
LGV
SM
17


AG
LGV
SM
18


SGV
LGV
SCH
SM
19


SC
SM
20

In Electron Microscopic Study of Esophageal pithelium in the Newborn and Adult Mouse [1]

PAUL F PARAKKAL

Department of Dermatology Boston University School of Medicine Boston University Medical Center Boston, Massachusetts

ABSTRACT The stratified squamous epithelium of the esophagus in the newborn and adult mouse was studied by histological, histochemical and electron microscopic methods. In the newborn, the cells located above the basal layer elaborate mucus. The relative abundance of Golgi zones and rough-surfaced endoplasmic reticulum suggests the involvement of these organelles in the production of mucous granules. The membrane of mature mucous granules ruptures and their contents become dispersed in the cytoplasm. Mature mucous granules are not seen in the outermost cells which are about to be exfoliated. The process of exfoliation begins in the upper layer of the epithelium when the contiguous cell membranes separate and wide intercellular spaces are formed. While the cells reach the surface, the intercellular spaces widen, the cells lose contact and are shed. The distal surfaces of the cells in the upper layer are lined by a surface coat which consists of finely branched filaments.

The esophageal epithelium of the adult mouse is similar to the epidermis and undergoes complete keratinization. The sequential development of differentiation products namely the cytoplasmic filaments, membrane-coating granules (MCG) and keratohyalin granules is seen as the cells migrate toward the surface. After their formation, MCG migrate toward the cell surface where they become confluent with the plasma membrane and are secreted into the intercellular space. Keratohyalin granules are also elaborated in large numbers and become dispersed as the cells become cornified. As the horny cells are formed the cell constituents such as the rough-surfaced endoplasmic reticulum, Golgi complex, ribosomes, mitochondria and the nucleus disintegrate. The fully keratinized cell has a thickened envelope and is filled with filaments embedded in an amorphous matrix.

In mammals, the stratified squamous epithelium of the body surfaces is continuous with the lining of the oral cavity and the esophagus. Embryologically however the epithelium which covers the external surfaces and the oral cavity is different from the lining of the esophagus. While the stratified squamous epithelium of the epidermis and oral mucosa is ectodermal in origin, that of the esophagus is derived from the endoderm (Balinsky '60; Hamilton et al., '62) During ontogeny the esophageal lining undergoes developmental changes which are peculiar to this tissue and not shared by other stratified squamous epithelia (Johns, '52 Bloom and Fawcett, '62) The epithelium is first composed of a layer of columnar cells which becomes thicker and multilayered. During this period of thickening and rapid growth, the superficial cells become ciliated. Subsequently the ciliated cells are shed and a stratified squamous epithelium is formed which persists in the adult.

Even though the adult mammalian esophagus is lined by a stratified squamous epithelium, the extreme variability in the degree of cornification shown by this epithelium is correlated with the dietary habits of the animal (Goetsch '10 Bloom and Fawcett, 62) In animals which consume coarse food (rodents and ruminants), the epithelium undergoes complete cornification, similar to the mammalian epidermis, with a well-developed granular and horny layer On the other hand, mammals living on soft food (carnivores and man) lack a horny layer Instead, the superficial cells of the epithelium retain their nuclei and occasionally contain a few keratohyalin granules.

Stratified squamous epithelia, of the body surfaces and the oral mucosa have been studied rather extensively by means of electron microscopic techniques (Al-

[1] This investigation was supported by research grant AM 06770 from the National Institute of Arthritis and Metabolic Diseases, United States Public Health Service.

bright, 60 Zelickson 63 Brody '64; Odland '64 Listgarten, 64 Matoltsy and Parakkal, '65) Except for Rhodin and Reith s (62) general survey of keratinizing tissues which includes the adult mouse esophagus the fine structure of esophagus has been relatively neglected. The present investigation deals with the normal fine structure of esophageal epithelium in the newborn and adult mouse It was found that in the newborn the esophagus is lined by a noncornified, stratified squamous epithelium which is actively involved in the synthesis of mucus In the adult however the epithelium undergoes complete keratinization with well developed granular and horny layers

MATERIALS AND METHODS

Fragments of esophagus were removed from newborn (1–2 days old) and adult (30–60 days old) mice and fixed in Bouin s and Helly s fixatives. After the usual histological procedures the tissues were embedded in paraffin Sections 7 µ thick were stained with either hematoxylin and eosin or toluidine blue Some sections were stained by periodic acid Schiff technique for the identification of glycogen and mucopolysaccharides Nuclear material was demonstrated by means of the Feulgen method for DNA.

For electron microscopy small pieces of esophagus obtained from newborn and adult mice under light anesthesia, were fixed for two hours in ice-cold 1% osmium tetroxide buffered with veronal acetate or phosphate to pH 7 4–7 6 (Palade 52) Some specimens were fixed in 3% glutaraldehyde in phosphate buffer for three hours and postfixed in 1% osmium tetroxide in phosphate buffer for a period of two hours (Sabatini et al. '63) Subsequently the tissues were dehydrated in ethanol solutions of increasing concentrations then embedded in epoxy resin according to the method of Luft ('61) Thin sections were cut with a Porter Blum microtome and after being doubly stained with aqueous uranyl acetate followed by lead citrate (Reynolds '63) or with lead citrate alone examined in an RCA EMU 3F electron microscope. Thick sections were stained with Azure blue B for orientation purposes.

RESULTS

Light microscopy

The stratified squamous epithelium o the esophagus in the newborn mouse co sists of 6–8 layers of cells. The whole ep thelium appears PAS – positive even aft diastase digestion The PAS reaction is e tremely intense in all the cells above th basal layer The PAS – positive material identified as mucus. The cells in all th layers including the most superficial lay contain Feulgen – positive nuclear mat rial. Even the desquamated cells found the lumen contain Feulgen – positive n clei.

The esophageal epithelium of the adul mouse is thicker than the newborn, bein composed of about 20 layers of cells. Al though the individual cells do not contain any PAS – positive material, the intercel lular spaces between the cells in the super ficial layers are intensely positive for PAS positive material. Due to this intense reaction the limits of the cells are clearly delineated. The superficial cells are cornt fied and do not contain any Feulgen – posi tive material.

Electron microscopy

The entire thickness of the esophageal epithelium in the newborn mouse is illus trated in the low power electron micro graph of figure 1 Several significant fea tures of this epithelium are obvious eve at such a low magnification. The orientat tion of the cells changes from the base t the surface of the epithelium The colum nar basal cells undergo progressive flatten ing and become squamous as they mov upward and reach the surface. Concomi tant with the changes in orientation ther is a gradual increase in the size of the cells The basal cells are relatively small and large part of their volume is occupied b the nucleus On the other hand, the cel of the middle and superficial layers a large with their nuclei occupying only small portion of the cell (fig 1) The supe ficial cells are in the process of exfoli tion and are separated from the underlyin cells by larger spaces.

At higher magnification, the basal cel are seen to be demarcated from the unde lying connective tissue by a well define

basement membrane. The sparse cytoplasm of these cells is rich in ribosomes, many of which are in clusters. Mitochondria are numerous but the elements of endoplasmic reticulum are scant. The Golgi complex is situated in a supranuclear position and is composed of many smooth surfaced membranes and vesicles. Multivesicular bodies and small vesicles are also occasionally found. The rest of the cytoplasm is filled with *filaments measuring* about 70A in thickness. The cell membranes between adjacent cells lie close together and some desmosomes occur along the membranes.

In the cells immediately above the basal layer the Golgi complex and endoplasmic reticulum appear to have undergone some striking changes prior to the synthesis of mucus. Golgi zones are developed in several localized areas in the cytoplasm, and each Golgi complex consists of a collection of smooth walled tubules and vesicles (fig. 2) The latter range in size from a few hundred to 1000 A in diameter Simultaneously with the increase in the complexity of the Golgi complex, there is a moderate proliferation of the elements of rough-surfaced endoplasmic reticulum (fig. 2)

Cells which have undergone further differentiation, can be recognized by the large number of mature mucous granules scattered throughout the cytoplasm (fig. 3) These cells appear to be actively involved in the synthesis of mucus. These cells appear to be actively involved in the synthesis of mucus. The cisternae of the rough-surfaced endoplasmic reticulum are dilated with a flocculent material. The vesicles which are associated with the Golgi complex begin to accumulate material and depending upon the amount of accumulation, show varying densities (fig. 2) The contents of some of the vesicles resemble mature mucous granules. The mature granules are round or oval and measure between 800–1500 A in diameter (figs. 2, 3) The *fully* developed granules are filled with a finely granular material and are always enclosed in a smooth-surfaced membrane (fig. 3)

As the cells move toward the surface of the epithelium many of the mucous granules migrate toward the cell periphery Near the cell membrane, the smooth membrane of the mucous droplets ruptures and the contents are released within the cytoplasm (fig. 3) Mucous granules rarely occur in the most superficial cells which are about to be exfoliated (fig. 1)

The superficial cells are shed from the surface either singly or in groups of two or more cells. The visible changes of exfoliation are seen in the upper layers of the epithelium (fig. 1) The cell membranes which are usually contiguous begin to separate between the adjacent desmosomes to form wide intercellular spaces. The cell membranes however remain adherent to each other in the area of desmosomes. As the cells migrate upward, the intercellular spaces widen and cell membranes begin to diverge even at the desmosomal contact points (figs. 1 4) As this widening process continues the most superficial cells lose contact with the cells underneath and are shed.

Before exfoliation, the plasma membranes of cells tend to become polarized by the deposition of a coating on selective regions on the surface of the cell membranes. For convenience of description, the following terminology will be used. Distal and proximal refer to plasma membranes which face the lumen and the dermis of the esophagus respectively The plasma membrane of the upper two or three layers of cells is polarized with respect to the possession of a surface coat (fig. 1 4) At higher magnification, the surface coat consists of a finely filamentous material, which is intimately associated with the outer leaflet of the unit membrane (fig. 4) The surface coat is present only on the distal and not on the proximal plasma membrane of each cell. This polarization is most evident when the proximal "uncoated" cell surfaces of the exfoliating cells are compared to the distal coated cell surfaces of the underlying adjacent cells (fig. 4) The surface coat begins to form as soon as the cells separate prior to the process of exfoliation. The newly formed intercellular spaces are usually filled with a material similar to the surface coat (fig. 1) At this stage, it is difficult to determine whether the filamentous material of the coat is in close apposition to any cell surfaces.

Desquamated cells are frequently seen in the lumen of the esophagus either singly or in groups The cells usually contain a nucleus and several mitochondria both in varying degrees of disintegration The rest of the cytoplasm is filled with a fine filamentous material. The distal plasma membrane of the desquamated cells can still be distinguished from the proximal plasma membrane of the presence of a surface coat on the former

The esophageal epithelium of the adult mouse is an example of a keratinizing stratified squamous epithelium Figure 5 represents a low power electron micrograph of its entire thickness The changes in orientation as well as volume of the cells as they move from the basal layers to the surface are very similar to the esophageal epithelium of the newborn However significant differences between the newborn and adult are found in the morphology of cells at various levels of the epithelium

The basal cells are relatively small with a large nucleus and little cytoplasm In the scanty cytoplasm the usual cytoplasmic organelles like the ribosomes and mitochondria are abundant. The elements of the Golgi complex and endoplasmic reticulum are scarce The matrix of the cell contains many cytoplasmic filaments which course through in all directions. The cell membranes which are highly convoluted lie close together and possess numerous desmosomes

As the cells migrate upward and begin to differentiate the cytoplasm increases in volume and the elements of the Golgi complex and rough-surfaced endoplasmic reticulum become more evident (fig. 6) The cytoplasmic filaments have increased considerably and permeate the cell.

At this stage of differentiation small cytoplasmic bodies called membrane-coating granules (MCG) are formed (fig 6) The mature membrane-coating granules are ovoid in shape and vary in size from 1000–2000A. The granule is enclosed in a smooth-surfaced membrane and its internal structure which consists of several parallel lamellae is not always apparent When first formed, MCG are seen in the vicinity of the Golgi complex. As these granules increase in number they are seen without any particular orientation throughout the cytoplasm Subsequently they migrate toward the distal cell surfaces which face the lumen of the esophagus (fig. 6). MCG become attached to the plasma membrane and are discharged into the intercellular spaces After discharge, MCG lose their integrity and break down, and their lamellar contents spread over the cell surfaces (fig 7)

Keratohyalin granules another differentiation product of this epithelium, are found in cells of the middle layer which are also active in the synthesis of MCG. Early in the formation, keratohyalin appears as small round dense granules and as the cells migrate upward they increase in size as well as in number (fig. 5). While some granules are surrounded by particles which resemble ribosomes, others may be associated with cytoplasmic filaments. Variability in the morphology of keratohyalin granules is found in the upper layers of the epithelium just below the horny cells (fig 5) The most conspicuous type appears to be composed of an extremely dense rim surrounding material which forms configurations of different density

Another interesting finding is the presence of small dense granules which are morphologically identical to keratohyalin granules in the nucleus of cells in the upper strata of the epithelium (fig. 8) In many instances these dense granules are surrounded by particles which are in the size range of 150–200A in diameter

As differentiation proceeds further and just before the formation of the horny cells, the nucleus and cytoplasmic organelles such as the mitochondria endoplasmic reticulum Golgi complex ribosomes and keratohyalin granules begin to disintegrate. As the cells are transformed into the horny cells they are filled with filaments which are embedded in an amorphous matrix (fig. 8) The horney cells have a thickened membrane which is covered by a superficial coat separated from the plasma membrane by a space of 60–70A (fig 9) This coat appears amorphous and does not show any finer structure (fig. 9).

The desquamated elements consist of long flattened cells The most conspicuous component of the cell is the thickened and coated cell membrane. The cell is filled

ith a fibrous material and does not contain either nuclear material or cytoplasmic organelles.

DISCUSSION

The epithelium of the esophagus in newborn and adult mice is built on a common architectural pattern. In both, the esophageal lining is composed of a continuously renewing stratified squamous epithelium. The basal cells appear similar and undergo mitosis. The daughter cells differentiate as they move up and are finally shed at the surface. However, basic differences become obvious when the morphology of the differentiating and the terminal cells of the two types of epithelia is closely examined. In the newborn, the most characteristic product is mucus, which is actively synthesized in the differentiating cells located above the basal layer. In the adult, however the presence of membrane-coating and keratohyalin granules in the differentiating cells serves as the best distinguishing characteristic of the epithelium. The terminal cells are distinctive in the newborn and adult epithelia. In the newborn they consist of nucleated squamous cells which contain a few cytoplasmic organelles such as mitochondria and ribosomes. On the other hand, in the adult the terminal cells are flattened and filled with a fibrous material embedded in an amorphous matrix.

One of the most interesting features of the epithelium in the newborn is the synthesis of mucus. In this respect, the similarity of this tissue to the stratified squamous epithelium of the frog epidermis is striking (Voute, '63; Parakkal and Matoltsy '64; Farquhar and Palade '65) In both tissues, prior to the synthesis of mucus, the cells located above the basal layer develop synthetic organelles such as the rough-surfaced endoplasmic reticulum and Golgi complex. There is evidence that the synthesis of mucus in the frog epidermis follows the now accepted pathway of initial synthesis and accumulation in the cisternae of rough endoplasmic reticulum and final concentration and packaging in the Golgi complex (Parakkal and Matoltsy '64) Recently by employing combined techniques of autoradiography and electronmicroscopy it was demonstrated that the mechanism of synthesis of mucopolysaccharides is similar in other cell types such as the goblet cells (Neutra and Leblond, '66; Freeman, '66) The increase in the synthetic organelles in the differentiating cells of the esophageal epithelium suggests a similar process for the elaboration of mucous granules in this tissue. However the fate of the mucus in the esophageal epithelium of the newborn is slightly different from that of the frog epidermis. In the cells below the superficial layers of the esophageal epithelium, the membranes of the mucous granules rupture and their contents are dispersed in the cytoplasm however intact mucous granules are seldom seen in the most superficial cells. Since these cells are intensely PAS – positive, it appears that mucus is retained in a finely dispersed form. In the frog epidermis however the majority of the mucous granules are discharged into the intercellular spaces in the upper strata of the epithelium (Parakkal and Matoltsy '64) Some of the epidermal mucous granules may however be dispersed within the cells, as evidenced by the intense staining of the cells of the stratum corneum with Schiff reagent.

Morphologically the surface coat of the superficial cells in the esophageal epithelium in the newborn is similar to the coating found on the free surface of a wide variety of cells, (Bennett, '63) especially those of the gastric and intestinal mucosa (Ito '65) As in the enteric surface coat, the esophageal coat consists of a filamentous material which appears to be intimately associated with the outer leaflet of the plasma membrane. The surface coat of the intestinal microvilli is very stable and is not removed by potent mucolytic or proteolytic agents (Ito, '65) Whether this stability and resistance is shared by the surface coat of the esophageal epithelium is not yet established. However based on their morphological similarity it is reasonable to assume that the surface coat of the esophageal epithelium is also highly resistant. In this connection, it is pertinent to point out that the surface coat remains intact without undergoing any visible changes in the desquamated cells which are free in the esophageal lumen.

The mode of formation of the surface coat of cells is not well understood (Ito,

Desquamated cells are frequently seen in *the lumen of the* esophagus either singly or in *groups* The cells usually contain a nucleus and several mitochondria both in varying degrees of disintegration The rest *of the cytoplasm is filled* with a fine fila *mentous material* The *distal* plasma membrane of the desquamated cells can still be *distinguished* from the proximal plasma *membrane of the* presence *of a* surface coat on the former

The esophageal epithelium *of* the adult mouse is an example of a keratinizing *stratified* squamous epithelium Figure 5 represents a low power electron micrograph of its entire thickness The changes *in* orientation as well as volume of the cells as they move from the basal layers to the surface are very similar to the esophageal epithelium of the newborn However *significant differences* between the newborn and adult are found in the morphology of cells at various levels of the *epithelium.*

The basal cells are relatively small with a large nucleus and little cytoplasm. In the scanty cytoplasm the usual cytoplasmic organelles like the ribosomes and mitochondria are abundant. The elements of the Golgi complex and endoplasmic reticulum are scarce The matrix of the cell contains many cytoplasmic filaments which course through in all directions The cell membranes which are highly convoluted lie close together and possess numerous desmosomes.

As the cells migrate upward and begin to differentiate the cytoplasm increases in volume and the elements of the Golgi complex and rough-surfaced endoplasmic reticulum become more evident (fig. 6) The cytoplasmic filaments have increased considerably and permeate the cell.

At this stage of differentiation small cytoplasmic bodies called membrane-coating granules (MCG) are formed (fig. 6) The mature membrane-coating granules are ovoid in shape and vary in size from 1000–2000A The granule is enclosed in a smooth-surfaced membrane and its internal structure which consists of several parallel lamellae is not always apparent. When first formed, MCG are seen in the vicinity of the Golgi complex. As these granules increase in number they are seen without any particular orientation throughout the cytoplasm. Subsequently they migrate toward the distal cell surfaces which face the lumen of the esophagus (fig. 6). MCG become attached to the plasma membrane and are discharged into the intercellular spaces After discharge MCG lose their integrity and break down, and their lamellar contents spread over the cell surfaces (fig 7)

Keratohyalin granules another differentiation product of this epithelium, are found in cells of the middle layer, which are also active in the synthesis of MCG. Early in the *formation,* keratohyalin appears as small round dense granules and as the cells migrate upward they increase in size as well as in number (fig. 5). While some granules are surrounded by particles which resemble ribosomes, others may be associated with cytoplasmic filaments. Variability in the morphology of keratohyalin granules is found in the upper layers of the epithelium just below the horny cells (fig 5) The most conspicuous type appears to be composed of an extremely dense rim, surrounding material which forms configurations of different density.

Another interesting finding is the presence of small dense granules which are morphologically identical to keratohyalin granules in the nucleus of cells in the upper strata of the epithelium (fig. 6) In many instances these dense granules are surrounded by particles which are in the size range of 150–200A in diameter

As differentiation proceeds further and *just before the formation of the* horny cells, the nucleus and cytoplasmic organelles such as the mitochondria, endoplasmic reticulum, Golgi complex, ribosomes and keratohyalin granules begin to disintegrate. As the cells are transformed into the horny cells they are filled with filaments which are embedded in an amorphous matrix (fig. 8) The horney cells have a thickened membrane which is covered by a superficial coat separated from the plasma membrane by a space of 50–70A (fig 9) This coat appears amorphous and does not show any *finer* structure (fig. 9)

The desquamated elements consist of *long flattened* cells The most conspicuous component of the cell is the thickened and coated cell membrane. The cell is filled

Palade G. E. 1952 A study of fixation for electron microscopy J Exp. Med., 95: 285–298.
Parakkal, P F and A. G. Matoltsy 1964 A study of the fine structure of the epidermis of Rana pipiens. J Cell Biol., 20: 85–94
Reynolds, E. S. 1963 The use of lead citrate at high pH as an electron opaque stain in electron microscopy J Cell Biol., 17 208–212.
Rhodin, J A. G. and E. J Reith 1962 Ultrastructure of keratin in oral mucosa, skin, esophagus, claw and hair. Fundamentals of keratinization. E. O Butcher and R. F Sognnaes eds. Washington, D C. American Ass. for the Adv of Sci., pp. 61–94
Sabatini, D D., K. Bensch and R. J Barrnett 1963 Cytochemistry and electron microscopy The preservation of cellular ultrastructure and enzymatic activity by aldehyde fixation. J Cell Biol., 17 19–58.
Voute, C. L. 1963 An electron microscopic study of the skin of the frog (Rana pipiens) J Ultrastruct. Res., 9 497–510.
Zelickson, A. S. 1963 Electron microscopy of skin and mucous membrane, Charles C Thomas, Springfield Illinois.

'65) To study the geneals of the surface coat, the esophageal epithelium would be an ideal tissue because the development of the surface coat proceeds gradually as the cells move upward from the middle of the epithelium to the surface The cells in basal and middle layers do not have a surface coat but above the middle layer as soon as the cells begin to separate from each other a filamentous material resembling surface coat accumulates in the inter cellular spaces At this early stage in the formation of the coat it is difficult to ascertain whether the filamentous material is attached to the plasma membrane of the cells But as the separation of the cells proceeds further it is evident that surface coat is intimately attached to the distal plasma membrane

The coating around the horny cells in the adult esophageal epithelium is mor phologically different from the surface coat of the superficial cells of the newborn epithelium The coating of the horny cells is composed of an amorphous material which does not show any filamentous structure Moreover it is always separated from the underlying plasma membrane by a space of 50–70A The coating of the horny cells unlike the filamentous surface coat, is not localised to any particular region of the plasma membrane but closely follows the contours of the cell. It is interesting to note that this type of coating which is clearly extracellular in nature is found surround ing the horny cells of a large number of keratinizing epithelia (Matoltsy and Parak kal)

The developmental changes from a mucus-producing, stratified squamous epithelium in the newborn into a keratinizing stratified squamous epithelium in the adult are reminiscent of metaplastic changes that are commonly associated with lack of vitamin A. Lasnitzki ('63) has shown that esophageal epithelium of 20-day rat embryos becomes thickened and keratinizes rapidly when cultured in normal medium. However when cultured in the presence of excess vitamin A the esophageal lining is transformed into a mucus-secreting epithelium Because of its developmental peculiarities as well as its plasticity in changing into either keratiniring or mucus-secreting epithelium the esophageal epithelium may prove to be one of the most suitable tissues to study factors which initiate changes in differentiative pathways.

ACKNOWLEDGMENTS

I wish to thank Drs A. G. Matoltsy, L. Luckenbill and R. Hendrikson for critically reading the manuscript and making helpful suggestions.

I am grateful to Mr. Alan Evans for technical assistance.

LITERATURE CITED

Albright, J T 1960 Electron microscope studies of keratinization as observed in gingiva and cheek mucosa. Ann. N Y Acad. Sci., 85: 351–361

Balinsky B L 1960 An introduction to embryology W B Saunders, Philadelphia, p. 337.

Bennett, H. S 1963 Morphological aspects of extra cellular polysaccharides. J Hist. Cytochem., 11: 14–23.

Bloom, W., and Don W Fawcett 1962 A textbook of histology W B Saunders, Philadelphia, p. 431

Brody I. 1964 Different staining methods for the electron microscopic elucidation of the tonofibrillar differentiation in normal epidermis. In: The Epidermis. W Montagna and W C. Lobitz, eds. Academic Press, New York. p. 251

Farquhar M. G., and G. E. Palade 1965 Cell junctions in amphibian skin. J Cell Biol., 26: 263–291

Freeman J A. 1966 Goblet cell fine structure. Anat. Rec., 154: 121–148.

Goetsch, E. 1910 The structure of the mammalian esophagus. Am. J Anat., 10: 1–40.

Hamilton, W J., J D Boyd and H. W Mossman 1962 Human Embryology William and Wilkins, Baltimore p. 237

Ito S. 1965 The enteric surface coat on cat intestinal microvilli. J Cell Biol., 27: 475–491.

Johns B. A. E. 1952 Developmental changes in the esophageal epithelium in man. J Anat., 86 431–442.

Lasnitzki, Ilse 1963 The effect of excess vitamin A on the embryonic rat esophagus in culture. J Exp Med. 118: 1–6.

Listgarten, M. A. 1964 The ultrastructure of human gingival epithelium. Am. J Anat., 114: 49–69

Matoltsy A. G., and P F Parakkal 1965 Membrane-coating granules of keratinizing epithelia. J Cell Biol., 24: 297–307

——— Keratinization (in press)

Neutra, M.A., and C. P Leblond 1966 Synthesis of the carbohydrate of mucus in the Golgi complex as shown by electron microscopy radioautography of goblet cells from rats injected with glucose-H³ J Cell Biol., 30: 119–137

Odland G. F 1964 Tonofilaments and Keratohyalin The epidermis. W Montagna and W C. Lobitz, eds. Academic Press, New York, p. 237


IS
ML
BL
1

PLATE 1

EXPLANATION OF FIGURE

1 Low power electron micrograph of the entire thickness of the esophageal epithelium in the newborn mouse The epithelium can be divided into basal (BL) middle (ML) and superficial (SL) layers. The basal cells which are separated from the dermis (D) by a basement membrane have prominent nuclei which fill nearly the entire cell. The cells of the middle layer are actively engaged in the formation of mucus (⟵⟶) The superficial cells possess a nucleus and the cytoplasmic organelles such as mitochondria and ribosomes are present in reduced numbers. The plasma membranes of the cells located in the basal and middle layers are closely apposed to each other while those of the superficial cells are separated by small intercellular spaces Intercellular spaces (IS) become extremely wide prior to exfoliation. Note that the distal plasma membrane of the superficial cells possesses a surface coat (→) × 6000

MOUSE ESOPHAGEAL EPITHELIUM
Paul F. Parakkal



PLATE 2

EXPLANATION OF FIGURE

2 Electron micrograph showing portions of cells from the middle layer of the newborn epithelium. Aggregates of Golgi vesicles (GO) appear in several areas in the cytoplasm. Developing mucous granules are seen in the vicinity of the Golgi complex (between arrows) while fully formed granules (MG) occur throughout the cytoplasm. Many profiles of rough-surfaced endoplasmic reticulum (RER) are also present. × 28 000



PLATE 3

EXPLANATION OF FIGURE

3 Portions of the cells from the upper layers of the newborn epithelium. Several *mucous* granules, (MG) near the periphery of the cells, are filled with a finely granular material. Some granules appear ruptured and their contents are confluent with the cytoplasm (arrows). Note abundant fine filaments in the cytoplasm. × 34 400.


CF
V
4

PLATE 4

EXPLANATION OF FIGURE

4 Portions of the most superficial and adjacent underlying cells showing the polarization of the cell membranes. The outer leaflet of the unit membrane of the distal surfaces possesses a finely filamentous surface coat (arrows). Note that it is absent from the proximal membrance. The cytoplasm is filled with many filaments (CF) × 80,000.

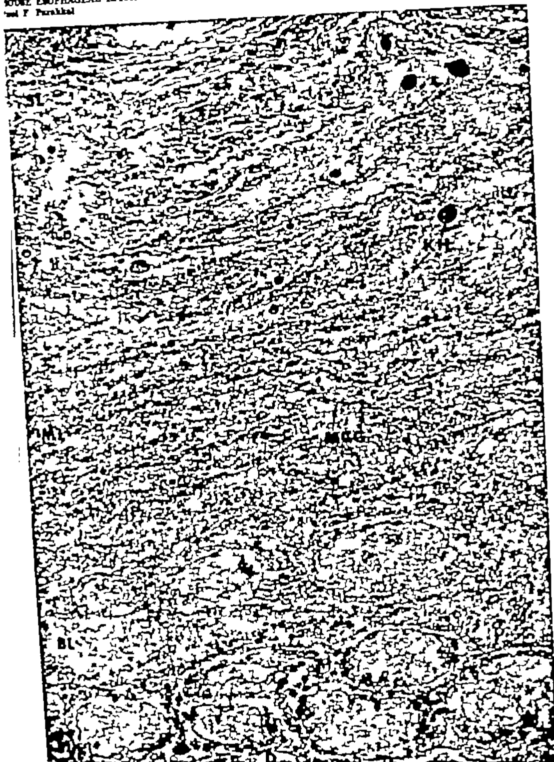

SL
KH
MCG
BL

PLATE 5

EXPLANATION OF FIGURE

5 Low power electronmicrograph showing the full thickness of the epithelium in the esophagus of the adult mouse. The epithelium can be divided into basal (BL) middle (ML) and superficial (SL) layers. The basal cells are demarcated from the underlying dermis (D) by a basement membrane. The nucleus fills a large part of the cytoplasm, as in the basal cells of the epithelium of the newborn. The cells of the middle layers contain differentiation products such as the membrane-coating granules (MCG) and keratohyalin granules (KH). The superficial layers are composed of flattened horny cells having a thickened plasma membrane. Note that throughout the epithelium the plasma membranes of adjacent cells are close together. × 5500.

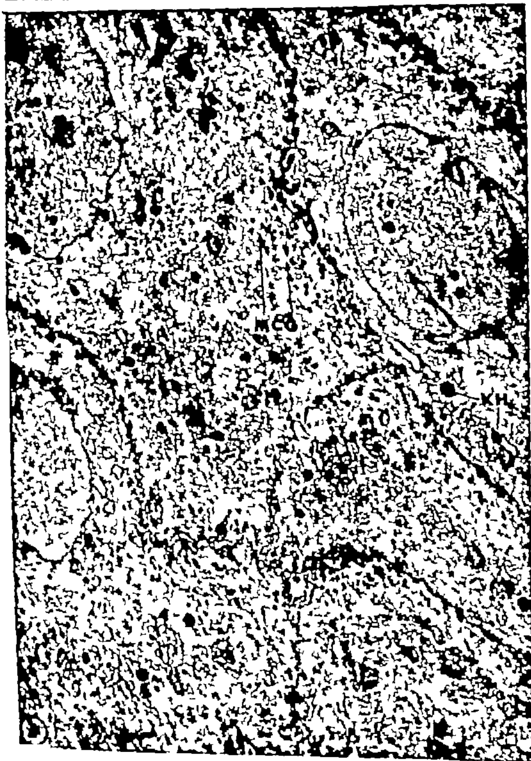

MCG
KH

PLATE 6

EXPLANATION OF FIGURE

6 Enlarged view of portions of granular cells from the esophageal epithelium of the adult. The membrane-coating granules (MCG) are aligned in multiple rows near the periphery of the distal plasma membrane. Keratohyalin granules (KH) are seen in various stages of development in all the cells. The nuclei in the upper part of the figure exhibit dense granules which are morphologically similar to keratohyalin granules. Filaments occupy most of the cytoplasm while the cytoplasmic organelles such as mitochondria, ribosomes, Golgi complex and rough-surfaced endoplasmic reticulum are segregated into small areas. × 39 000

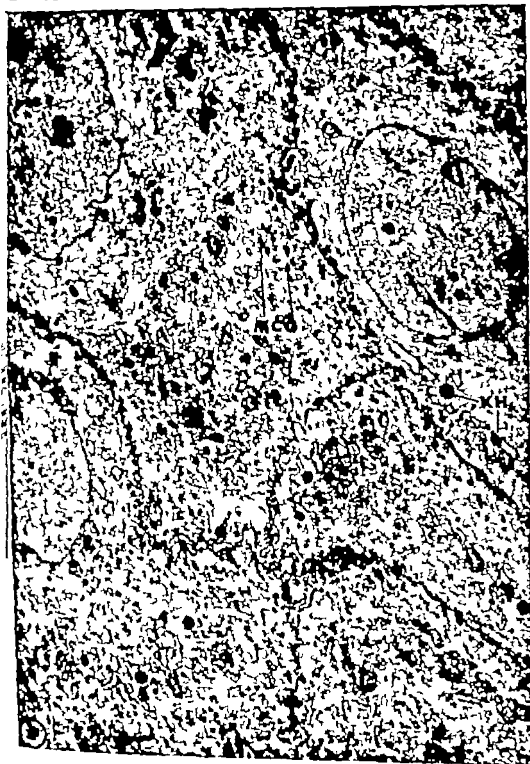


PLATE 7

EXPLANATION OF FIGURES

7 Electron micrograph showing the differential thickness of plasma membranes of adjacent granular cells. Membrane-coating granules appear close to the cell periphery and lamellar remnants of discharged membrane-coating granules occur in the intercellular space (arrow) × 43 000.

8 Electron micrograph of the superficial horny layer of the adult epithelium. The horny cells are filled with filaments embedded in an amorphous matrix. Note the closely apposed thickened plasma membranes (arrows) The amorphous coat is not well defined at this magnification and appears as an indistinct mass in the intercellular spaces. The plasma membrane of the granular cell (GC) has not undergone any thickening. × 50 000

9 Enlarged view of the thick plasma membranes (PM) and the amorphous coat (AC) of a superficial horny cell form the adult epithelium. × 120,000.


AC
g
BM
GC

Morphogenetic Studies of the Rabbit

XXVII. GENOME, GRADIENT GROWTH PATTERN AND MALFORMATION

P. B. SAWIN, MARYANN GOW AND MARJORIE MUEHLKE
The Jackson Laboratory Bar Harbor Maine

ABSTRACT The metameric organization of the skeleton provides a cartograph of reference points and a unique opportunity for analysis of the polygenic background of the genome and its potentialities for maintaining normality or inducing spontaneous malformation. The position of the vertebral borders indicates the relative size of the thoracic and lumbar regions or gradients. Analysis of homeotic variations in progeny from matings of specific parental vertebral formulae has provided a critical evaluation of the relative effects of gene *Da* with that of the residual genomes of races DA and III_{VO}. Significant differences in shift of the vertebral borders have revealed the segregation of several modifying influences interacting at each border in each strain and with *Da* when it is present. The segregation patterns demonstrate the polygenic background of these variations and the interaction effects of DA and III_{VO} genomes which respectively enhance or suppress the retardation effects of *Da* upon thoracic and lumbar gradients. Discussion of these observations with reference to convergence of broadly related concepts in the literature leads to the conclusion that many species or strain differences in experimental response, spontaneous malformations and polymorphisms may arise by similar interactions from residual heterozygosity of minor modifying genes within the genome. The importance of a more intensive scrutiny of the genome with reference to spontaneous and experimentally induced malformations is indicated.

Previous studies of the pleiotropic effects of the dachs (*Da*) gene have shown (1) that both heterozygous and homozygous genotypes are distinguishable from the normal and from each other as early as the 13th day post coitus (Crary '64) (2) that the pleiotropic effects, including deficiency of skeletal units compensatory induction of accessory units and overgrowth of adjacent units leading to homeotic shifts or displacement in position crowding, and fusion arise as either direct or indirect manifestations of retardation and (3) that by their interaction these effects either illustrate the genetic concept of overdominance or modify the species or strain gradient pattern of growth through processes already revealed experimentally by other investigators of growth mechanisms (Sawin and Trask, '65) By transfer of the *Da* gene to a different genetic background Sawin and Gow ('67) showed that the tendency to shift the thoracolumbar (ThL) and lumbosacral (LS) vertebral borders forward (effected by the *Da* gene) can be modified (enhanced or inhibited) according to the genome with which it is associated. These statistically significant effects are associated with the relative position and magnitude of the thoracic and lumbar growth gradients 3 and 4 (Sawin and Crary '64) Since the homozygous and heterozygous effects of the *Da* gene on these borders can be distinguished from the effects of the genome, similar methods might aid in differentiating other individual components. The genome however is not a single entity (Landauer '58) and morphology as a growth phenomenon likewise is polygenic. Such inheritance can involve the contributions of many modifying genes each of which makes its small contribution to a particular trait such as body size. With such traits the identification of any one specific gene is difficult and rarely achieved. Analysis, however is aided by the segmental organization of the skeleton which provides almost unlimited reference points such as the vertebral borders (Sawin and Trask, '65) not found in most other polygenic variations such as body size and growth. If a group of such points can be used as a grid or cartograph to define the limits of gradient activity a basis might be provided for isolation of specific entities of the genome and perhaps also for under

standing their potentialities for maintaining normality or inducing spontaneous variation.

This communication is concerned with a test of this possibility by means of a further classification of the progeny data of our previous study Here the basis is on matings according to vertebral formula (VF) of the parents as well as on the *Da* genotype which reveals the effects of other elements in the genome.

MATERIALS AND METHODS

The data for this study include most of that of Sawin and Gow ('67) which showed the relative effects of the *Da* gene and the genome [1] as a whole upon homeotic variations or shifts at the ThL and LS borders. In that study the progeny of heterozygous (*Da*/+) parents were separated into three genotypes (*Da*/*Da* *Da*/+ and +/+) and comparisons were made between the three New Zealand White strains DA (the strain of *Da* origin); III (partially inbred and selected for VF) and III$_{Da}$, a transfer strain into which *Da* had been introduced by a cross between DA and III followed by subsequent backcrossing to III for 4 to 7 generations. The three *Da* genotype populations in III$_{Da}$ were derived from the respective backcross generations and by intercross matings of the *Da*/+ parents.

In this study by separation of the genome data according to the VF phenotype matings of the parents we hoped to distinguish one or more of the separate elements involved in each of the genomes. Due to the greater number of mating categories and consequent reduction in numbers in any one category the experiment is not as neat as one would wish Some of the possible matings were not secured at all, and in others the numbers were too small to adequately test for significant differences This loss amounted to 260 animals distributed among the three races and their respective genotypes It involved primarily matings of the rarer phenotypes of the respective strains To replace this loss and increase numbers as much as possible matings of the same parents were continued and later generations of the same type have increased the total number to 1910 animals. However they have not provided a complete survey of all possible mating types. To secure all would necessitate continued selective mating for both gene and genotype

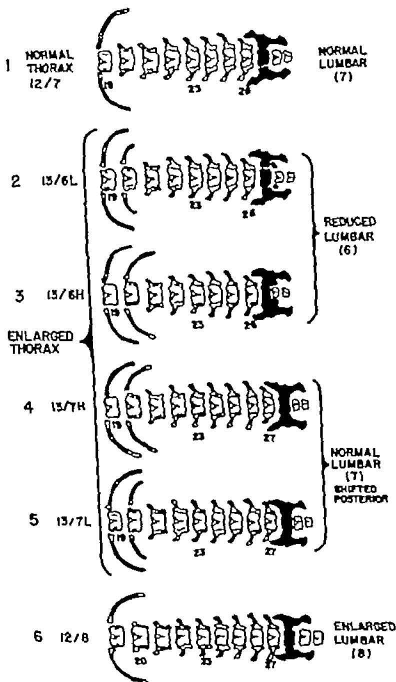
The data of each of two sublines of III (III$_{Da}$ and III$_{+}$) DA and III$_{Da}$ backcross and III$_{Da}$ intercross populations were separated first according to the VF phenotype matings of the parents and then according to the number of ribs and presacral vertebrae so as to consider the homeotic shifts in the two borders. Although a tendency to greater variability could be noted in the intercross data comparisons of the backcross with intercross data showed no statistically significant differences in any *Da* genotypes. Consequently to secure larger numbers the like *Da* genotypes within III$_{Da}$ were pooled The χ^2 test for statistical significance of recognizable phenotype and genotype differences was applied to all population differences in VF and ThL and LS borders. The correction for continuity was used in tests of all separate border differences with one degree of freedom.

All potential breeders (females and males) necessary to succeeding generations were typed roentgenographically for VF χ^2 tests of variation in VF between the age groups (30–34 days) and between generations revealed no significant differences hence the data could be pooled irrespective of age and generation

The method of classification of VF is essentially that described by Sawin ('4 and is diagrammed in figure 1 by six typ The VFs of both alizarin preparations a roentgenograms were read on a scale 0–4 with reference to the 13th rib expr sivity on each side of vertebra 20 and with reference to sacral attachment vertebra 27 or 28 The rib scale was e mated in fourths of the length of adjacent 12th rib on each side and analysis mean values of 2 and less w considered as low expressivity (13L) those above as high (13H) Similarly expressivity of sacropelvic attachment, 1 involved only the 27th vertebra typ

---

[1] In this study, the term genotype will be conf to the three possible segregating types with refer to the gene *Da*. *Genome* refers to the total ge milieu of each of the several strains DA, III$_{Da}$, and III$_{Da}$. It should be noted however that as in Section II under Observations, each mating of a strain may involve small differences in ge wherever minor modifiers are heterozygous.



(from P. B. Sawin and Maryann Gow fig. 1, Anat. Rec., 157 [illegible])

Fig. 1 Shows the six vertebral formulae (VF) with reference to the number of thoracic and lumbar vertebrae and expression portrayed as described in the text. Note the increase in rib expression from types 1–4 and decline from 4–6, whereas the sacral attachment shows gradual shift from 1–6; also the change in transverse processes on vertebrae 26 and 27. These types portray the stepwise change in size and position of the lumbar region. It is the basis for the alphabetical arrangement of the matings shown in bar graphs of figures 3–4 and the statistical comparisons of tables 1 and 7

only the 28th type 3 both 27th and 28th equally and 2 4 and 5 were intermediate classes (note size of transverse processes on v 27) In final anlysis of the sacrum 2 3 and 4 proved to be minority groups and consequently 1 2, and 3 were pooled as 26 presacral vertebrae (PSV) and 4 5 and 6 as 27 Two exceptional individuals (type 6) were noted one with sacral attachment involving vertebra 29 slightly and one 29 completely

OBSERVATIONS

A Homeotic strain or genome differences in normal (nondaclu) +/+ rabbits

1 *Strain III* The vertebral formula in this race is distinguished by its extremely high proportion of individuals with a presacral VF of 7C/13Th/7L (Sawin 45 Sawin and Gow '67) By inbreeding and selection over successive generations this type predominates in both matings of the III subline (top bar graphs, fig 2) The two matings differ from each other only in a nonsignificant proportion of individuals of the other five vertebral types (P = 0.2–0 1) which continue to appear spontaneously (see bottom line, table 1)

In the unselected subline III (bar graphs C–K, fig 2) the 13/7 type also predominates but the proportion of the other types is greater than in III, particularly in the matings (C and D) at the top and (H J and K) at bottom of figure. The matings involving parents both of which were 13/7 (bar graphs F and G) with varied parental expressivity of ribs are the ones in which 13/7 (both H and L) is most frequent among the progeny

The statistical significances of the differences between matings are shown in table 1 The differences between mating F (13/7H × 13/7H) and each of C, H, J and K are highly significant when cons

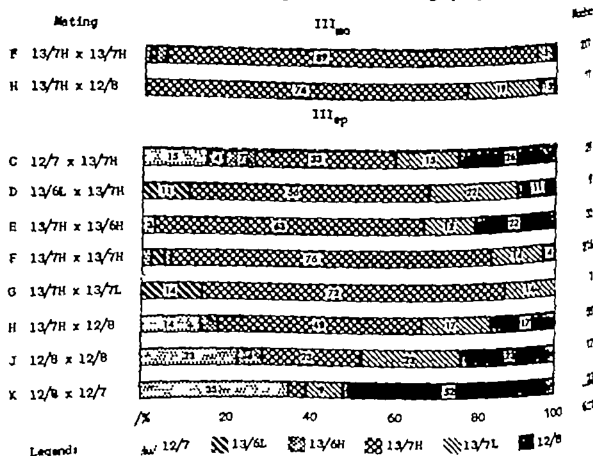


Fig 2 Strain III. The bar graphs show the proportion of vertebral types obtained in progeny of parental matings as listed in order at the left. Total progeny per mating is indicated at right and the proportion of each type by inserted figures. See table 1 for statistical significance

for VF and with reference to either er difference alone In the matings of d G with F the numbers are too small dequately test for significant differ- a. Between E and F the significant rence in VF is primarily at the ThL er. E with C however shows a sig ant difference at LS ($P < 0.05$) and with J in which the VF difference is wise significant. The K mating shows ificant differences in VF when com- d with all matings except J Whereas E and F both border differences are ily significant, with C, D, G H and J the ThL, and with J the significant ct in the ThL ($P < 0.05$) is not suf nt to show also a significant difference reen the two VFs.

These matings within the III genome re- l the effects of inbreeding and selection the consistently high proportion of 7H progeny from parents of this pheno- e in the III$_m$ line whereas the signifi- nt differences between matings of varied der types in III$_m$ is evidence of the segre- tion of modifying genes within the III$_m$ – When in combination (as in the F ing) they tend to perpetuate the 13/7 e, but when segregated they produce re 12/7s and 12/8s (as in C and K)

2. *Strain DA.* In the +/+ matings of e DA race (bar graphs of fig. 3) there is relative paucity of the 13/7 type and edominance of 12/7s. The matings re- ct the non-inbred and unselected back- ound by a generally greater variability in stribution of phenotypes in all matings. the four matings, as arranged in order ere tends to be a progressive decline from maximum of 12/7s in mating A (12/7 × 2/7) to a minimum in mating G (13/7L 13/7H) which is similar to the decline en in the III$_m$ matings. It differs in that he 13th rib is manifest more often without he increase in PSV

Comparisons of the VFs show four sig ificant differences between matings in the +/+ genotypes (table 2 upper half) Those of matings A with C and C with G are highly significant ($P < 0.005$) and in both the greatest effect is at the LS border Matings A and B with G are only signifi- cant at the 0.05 level. Neither border dif ference considered separately is significant in B, but with G the significant difference is concentrated at ThL ($P < 0.005$) Mat ings B with C and G show no significant differences. Although the numbers are small, it is obvious that the proportions of vertebral types are quite different from those of race III. The segregating influ- ences at both borders tend to act inde- pendently and involve primarily the ThL border

3. *The III$_m$ transferred strain.* The first five bar graphs of figure 4 concern the same +/+ phenotype matings (C E F G H) as appear among those of the III$_m$ sub- line populations (fig. 1) Here the D mat ing, which in III$_m$ is small, does not occur and mating I (13/7 × 12/8) appears for the first time Considered mating for mat ing there is the same general tendency as in race III for the 13/7H to predominate and to decline in numbers in the bar graphs toward the top and bottom of the figure. This predominance is accompanied by marked deficiency in the other types ex- cept for the 13/7L.

The significances of the differences be- tween matings are shown in the middle section of table 3. Differences in VF are not significant between adjacent vertebral type matings C to E and H to I (bar graphs of table 4) nor are they significant be- tween adjacent matings E, F and G Mat ings C to H and I, which are not adjacent, are also not significant but have in com- mon one 12-ribbed and one 13-ribbed parent. Between matings F and G to C and E, F and G to H and I, the differences are highly significant ($P < 0.005$) ex- cept C to G ($P < 0.05$) and E to H and I ($P < 0.05$ and 0.01 respectively Only the ThL border shows significant differences when examined separately In no case does it show significance in the compari- sons with I. Thus it is apparent that the significant differences in VF tend to in- volve primarily the anterior border and not the posterior and those differences not significant in VF are not significant at either border considered separately These observations indicate that the III$_m$ genome is relatively homogeneous with reference to factors affecting the posterior border more so than is III$_m$, but with respect to the anterior border segregation of one or more modifying genes is apparent as in III$_m$.

TABLE 1

Significant differences in distribution of vertebral types in progeny matings within the III$_{\mathrm{v}}$ subline are shown. For convenience each mating is designated by a letter (C D E etc.) in the first column to the left and diagonally at the top of columns with the number of progeny below it. The phenotypes of the two parents represented by the letter are shown in the second column. The information within each block includes χ^2 degrees of freedom (df) and significance (P) for three variables as shown at top of first column (< 0.05 ** < 0.01 and *** < 0.005). The top line refers to the distribution of vertebral types (VF) as in the bar graphs of figure 2, the second and third to the thoracolumbar border (ThL) and lumbosacral border (LS) as shown at top of column D*

	Phenotype	C	D	E	F	G	H	J
C (27)	12/7 x 13/7L	χ^2 df P	VF ThL LS					
D (9)	13/6L x 13/7L	— — —						
E (32)	13/6L x 13/7L	— — 4 5 1 *	— — —					
F (216)	13/7L x 13/7L	42 0 5 ** 31 9 1 *** 12 8 1 ***	— — —	17 7 5 ** 13 0 1 *** —				
G (7)	13/7L x 13/7L	— — —	— — —	— — —	— — —			
H (58)	13/7L x 12/8	— — —	— — —	— — 3 8 1	34 2 5 *** 28 2 1 *** 7 4 1 **	12 1 5 * — —		
J (17)	12/8 x 12/8	— — —	— — —	11 3 4 * — 4 8 1	39 1 5 *** 33.3 1 ** 12 3 1 ***	— — —	— — —	
K (23)	12/7 x 12/8	12 7 5 11.1 1 *** —	18 3 4 *** 13 3 1 *** —	23 7 3 *** 20 6 1 *** 7 4 1 **	114 5 5 *** 113 4 1 *** 1 8 1 ***	22 3 4 *** 14 0 1 *** —	21 8 4 *** 20 6 1 *** —	— 5 4 1 * —

TABLE 2

Significant differences shown in distribution of progeny between matings (bar graphs) of the DA race (fig 3). Normal +/+ is in upper portion, heterozygotes in lower. No significant differences were found in those of the Da/Da. Organization of the table is the same as that of table 1

+/+

		A 12/7 × 12/7			B 12/7 × 13/6L			C 12/7 × 13/7H			D 13/7H × 13/7L		
		χ^2	df	P	χ^2	df	P	χ^2	df	P	χ^2	df	P
A	VT				8.2	3	*	13.0	5	***	13.1	4	
	TML					—			—		9.7	1	***
	LS					—		12.2	1	***		—	
B	VT		—						—			—	
	TML	4.4	1						—			—	
	LS		—						—			—	
C	VT		—			—					18.6	5	***
	TML		—			—						—	
	LS		—			—					4.6	1	*
D	VT	14.0	3	*	16.5	5	***	13.7	3	*			
	TML	6.1	1			—		4.6	1				
	LS		—			—			—				

Da/+

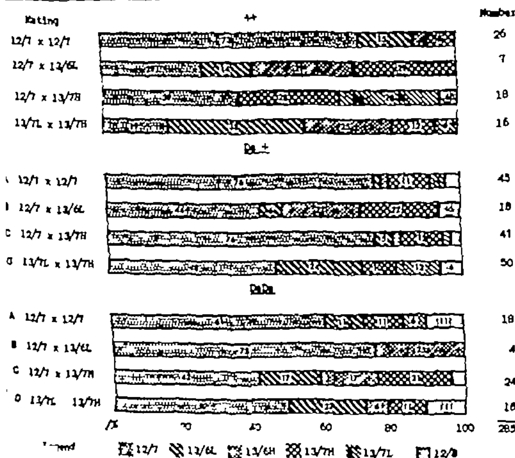


Fig. 3 Shows information for strain DA comparable to that of III (see table 2)

TABLE 3

Significant differences shown in distribution of progeny between matings (bar graphs) of the transfer strain III_{Da} (fig 4). The organization is the same as in table 1 For VF df = 5 for ThL and LS = 1

Mating		+/+ C	E	F	G	H	I	Da/Da C	E	F	G	H
C 12/7 x 13/7E	VF ThL LS	\\	— — —	21 5 *** 13 0 *** —	11 4 * 6 9 ** —	— — —	— — —	\\				
E 13/7E x 13/6E		17 4 *** 4 2 * —	\\	— — —	— — —	14 5 5 3 *	16 1 ** — —	— — —	\\			
F 13/7E x 13/7E		60 2 *** 13 7 *** 19 0 ***	— — —	\\	— — —	33 0 *** 26 7 *** —	44 8 *** — —	10 6 4 * — —	— — —	\\		
G 13/7E x 13/7L		21 5 *** — 11.3 ***	— — —	— — —	\\	24 6 * 13 2 ***	17 4 *** — —	— — —	— — —	— — —	\\	
H 13/7E x 12/8		— — —	25 9 *** 4 9 * —	85 8 *** 19 1 *** 10 3 **	23 5 *** 3 8 * —	\\	— — —	— — —	— — —	18 7 *** 4 6 —	— — —	\\
I 13/7L x 12/8		— — —	17 5 *** 5 6 * —	44 2 *** 13 0 *** 6 7 **	15 5 ** — 3 9 *	— — —	\\	— — —	— 4 4 * —	19 7 ** 4 8 —	— — 4 3	— — —

Da/+ (lower triangle of the left block); +/+ (upper triangle); Da/Da (right block)

Normal (+/+) between strain differ ... in like vertebral phenotype matings. ... significances of differences in comparable vertebral phenotype matings observed in normal genomes are shown in table 4. Matings C and G occur in strains ..., III_{ss}, and III_{vo}. In C there are no significant strain differences, indicating that at least in these samples the genetic factors affecting both borders were similar.

Mating G shows significant differences in VF between DA and III_{vo} ($P < 0.05$) and between DA and III_{ss} ($P < 0.005$) and in both cases only the LS borders are also significant ($P < 0.01$ and < 0.005 respectively).

The other between-strain matings involve only the sublines of *III*. Mating F shows significant differences in VF between III_{ss} and III_{vo} and between III_{ss} and III_{vo}, but not at the separate borders. This indicates some differences in both borders but none sufficient to stand out independently. Matings E and H show significant differences only at ThL ($P < 0.05$ in both cases) and these are not sufficient to show the effects on the VF.

B. Effects of the Da gene upon the homeotic variations

1. *Within the DA strain* the effects of the *Da* gene (as previously observed) were concentrated at the anterior border, significantly reducing expression and penetrance of the 13th pair of ribs (compared with +/+) but with minor effects also at the posterior border (Sawin and Gow '67). These effects are also clearly apparent in the separate matings by vertebral phenotype (table 5 and bar graphs of *Da*/+ and *Da*/*Da* fig. 3).

(a) *Between genotypes.* With respect to VF and border shifts, there are no significant differences between genotypes in matings A or B. In mating C, with one 13/7 parent, the *Da* gene has a significant effect on VF in both one and two doses ($P < 0.02$ and < 0.05 respectively). Significant shifts occur at ThL and LS in heterozygotes ($P < 0.02$ and < 0.005) but in homozygotes only at the posterior border ($P < 0.05$). The difference in vertebral formula between *Da*/+ and *Da*/*Da* is not significant, but that at the anterior border is high ($P < 0.01$).

In mating G the significant effect of *Da* on VF ($P < 0.01$) is essentially derived from the anterior border in heterozygotes ($P < 0.05$). The homozygotes, though not significantly different from +/+ in VF also show significant reduction at the anterior border ($P < 0.05$). No significant differences occur between *Da*/+ and *Da*/*Da*.

(b) *Between matings.* Comparison of the differences between like matings of *Da*/+ and of +/+ (many of which were

TABLE 4

Comparison of like matings between normal (+/+) genomes. Df = 1 for the borders considered separately; χ^2's for those in which the deviations were too small for significance are not shown

Mating	Race or subrace comparison	No. rabbits each race respectively		VF χ^2	VF df	VF P	ThL χ^2	ThL P	LS χ^2	LS P
C 13/7 × 13/7H	DA vs III_{vo}	18	27	8.1	5	ns	—	ns	0.8	ns
	DA vs III_{ss}	18	26	6.2	5	ns	3.3	ns	3.0	ns
	III_{ss} vs III_{vo}	26	27	7.9	5	ns	1.9	ns	1.0	ns
E 13/6H × 13+7H	III_{ss} vs III_{vo}	30	32	9.4	5	ns	4.4		0.47	ns
F 13/7H × 13/7H	III_{ss} vs III_{vo}	211	216	22.6	5		3.7	ns	0.25	ns
	III_{ss} vs III_{ss}	211	151	0.2	5	ns	—	ns	0.28	ns
	III_{ss} vs III_{vo}	151	216	14.6	5		3.3	ns	2.1	ns
G 13/7H × 13/7L	DA vs III_{vo}	16	7	8.9	4		0.04	ns	6.7	
	DA vs III_{ss}	16	64	22.0	5		—	ns	48	*
	III_{ss} vs III_{vo}	64	7	1.0	4	ns	—	ns	—	ns
H 13/7H × 12/8	III_{ss} vs III_{vo}	31	58	7.4	4	ns	4.5		2.8	ns
	III_{ss} vs III_{ss}	31	60	7.4	4	ns	2.9	ns	3.3	ns
	III_{ss} vs III_{vo}	60	58	4.4		ns	0.25	ns	—	ns
F vs H	III	211	21	8.5	5	ns	0.73	ns	1.1	ns

TABLE 5

Significance of differences in distribution of progeny between genotype matings of the DA race (see bar graphs in figure 3). No significant differences were noted in matings A and B

Mating	++/Da+							++/DaDa							Da+/DaDa						
	VF			ThL		LS		VF			ThL		LS		VF			ThL		LS	
	χ^2	df	P	χ^2	P	χ^2	P	χ^2	df	P	χ^2	P	χ^2	P	χ^2	df	P	χ^2	P	χ^2	P
A 12/7 × 12/7	6.8	5	ns	0 4	ns	1.9	ns	5 7	5	ns	0.004	ns	3.1	ns	3.8	5	ns	0.4	ns	0 4	ns
B 12/7 × 13/6L	1.3	4	ns	4.0	ns	0 002	ns	3.0	3	ns	2.3	ns	0.1	ns	2.0	4	ns	0.8	ns	0 4	ns
C 12/7 × 13/7H	14.1	5	*	6.5	*	9 4	***	13.1	5	*	0 003	ns	4 1	*	10.8	5	ns	7 1	**	0.2	ns
G 13/7H × 13/7L	16.6	5	**	4.8	*	0.2	ns	7.5	5	ns	4.7	*	0.06	ns	5.1	5	ns	0.05	ns	0 03	ns

siblings, bar graphs of fig. 3 and table 5) shows that the $Da/+$ genotype reduces the significance of the differences in VF between A and B and between C and G, whereas between B and G the difference is increased. When the borders are considered separately the differences between A and B are significantly greater at ThL. B compared with G shows differences so generally distributed over all VF types that significance is confined to the VF. The significant differences between C and G at $P < 0.05$ are at LS in $+/+$ and at ThL in $Da/+$. Between matings A and C there are no significant differences whereas in the $+/+$ genotype the VF and LS are highly significant. These last two comparisons are evidence that some segregating factor is being transmitted in the C mating to the $+/+$ progeny which in that genotype is responsible for the posterior shift of the border. This effect in the $Da/+$ and $Da/$ genotypes is not apparent due to the effect which shifts both borders anterio particularly ThL.

In $+/+$ significant differences betw mating types are found at both borders, in no comparison do they occur simu neously. In heterozygotes they do not cur at the LS border. Furthermore the gene when homozygous shows no sig cant differences hence that section table 2 has been omitted. Thus the dency is for *Da* in one dose to eliminat LS significant differences and in two d to eliminate all.

This examination of the separate ings according to phenotype supports previous conclusion with respect to relative anterior homeotic shift effect o upon the vertebral borders of DA. complementary effect of gene *Da* an nome DA in combination is also app in the further forward shift of ThL, ing for mating in the *Da* genotypes. greater variability within DA as comp with race III is also indicated, the loc tion of which (for example in matin suggests the existence and segregatio some factor or factors within the DA nome which tends to suppress the *Da* e at the posterior border.

2. *Within the* III_{m} *strain.* As previ found (Sawin and Gow '67) the effe the *Da* gene (shifting of the borders

;) tended to be suppressed by the III$_{ss}$ me as a whole, but when expressed it at the posterior border.

a) *Between genotypes* In this study separate matings based on parental VF w no significant differences between Da otypes in VF or at either ThL or LS. the basis of these observations alone is led to conclude that the effects of Da are completely suppressed by the III$_{ss}$ genome. However of the total 24 non significant differences in the two borders of the 6 matings, 19 reflect the general tendency of *Da* to shift both borders anteriorly

(b) *Between matings* The heterozygous and homozygous *Da* progeny (table 3) manifest the same high expressivity of

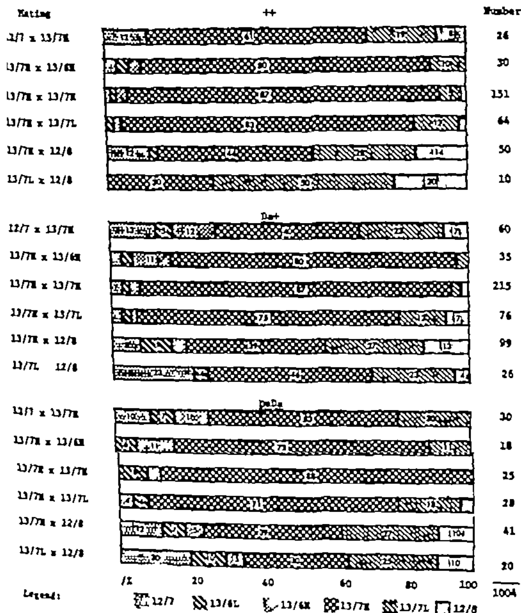


Fig. 4 Shows information for strain III$_{ss}$ comparable to that of III (see table 3).

posterior shift of the borders and significant differences in VF as in +/+ (fig 4 see also Sawin and Gow '67) However these differences in heterozygotes are not confined to the ThL border as in +/+ but appear also at the LS border in 5 of the 9 cases. In three of these comparisons (C to F and F to H and I) both separate borders are significant (P < 0 01) In two of them (C to G and G to I) only LS is significantly different (P < 0 005 and < 0 05 respectively) and in four (C to E E to H and I and G to H) only the ThL (P < 0 05) Hence an effect of the *Da* gene at both ThL and LS is indicated Similar comparisons among the *Da/Da* also show significant differences at both borders which was not the case in DA In the two most significant VF differences (matings F to H and I P < 0 005) the differences are primarily at ThL (P < 0 05)

Comparison of E to I and G to I shows significant differences at ThL and LS respectively but the difference between all vertebral types is not sufficient to show a significant difference in VF In contrast the differences between C and F are such that the difference in VF is significant (P < 0 05) but that at either border is not.

To summarize although the III_{Da} genome effect tends to completely suppress the anterior homeotic shift effect of *Da* as indicated by the separate nonsignificant *Da* genotype differences the trend of *Da* effect still is apparent, and when the matings are considered collectively (as in Sawin and Gow '67) the difference is significant Furthermore the significant differences between the separate matings reveal the existence of segregating components of the genome responsible for the between-strain differences and suppression of the *Da* gene effect

These differences in the effect of the *Da* gene within the two strains, plus the evidence of segregation taking place in the absence of *Da* in all three strains, indicate that homeotic shifts at the vertebral borders are products of genome complexity in which some genes such as *Da* may play a greater or lesser role depending on the remainder of the associated genome.

3 *Between strains* For study of the differences between DA and III_{Da} the only matings with sufficient data for adequate comparisons were C and G Tests of these differences for each *Da* genotype are shown in table 6. In C there are no significant differences between +/+ genotypes of the two races for VF ThL, or LS, but differences in the two *Da* genotypes are highly significant (*P* < 0 005) for all three variations. In the progeny of the G matings significant differences in the VF of the +/+ genotype are apparent at the LS border and in the *Da* genotypes, VF at both borders are highly significant.

These differences again indicate diff... ent interactions of gene and genome determining the position of the two borders.

TABLE 6

Significance of the differences between strains in the same phenotype matings resulting from interaction with 0 1 and 2 doses of Da. Df = 5 for VF 1 for ThL and LS in all cases

Genotype	Mating	Race	N	VF		ThL		LS	
				χ^2	P	χ^2	P	χ^2	P
+/+	C	DA III_{Da}	18 26	6.3	ns	—	ns	3.0	ns
+/+	G	DA III_{Da}	18 64	52.0	***	—	ns	46.3	**
Da/+	C	DA III_{Da}	41 60	41 7	***	33.3	***	27 4	***
Da/+	G	DA III_{Da}	50 76	68.9	*	28 4	***	55 7	**
Da/Da	C	DA III_{Da}	24 30	17 1	*	9 0	***	10.8	**
Da/Da	G	DA III_{Da}	18 25	28.3	**	13.1	***	20.8	*

:1 reveal the strong influence of the III$_{m}$:ome for posterior shifting of these two :ders. They also show that in spite of :s influence the retardation effect of the : gene can persist, altered in each mating :ording to the modifying genes which :gregate.

Relationship between thoracolumbar and lumbosacral borders

The differences in relative significance :tween matings with respect to VF and :e two border shifts when considered :parately suggest that the relative effects : gene and genome may not always be the :me on both borders, as was previously :und when the genomes were considered : *toto* (Sawin and Gow '67) To test this relationship between rib number and PSV the same tests for independence of the borders and for interaction of the three attributes (border strain, and genotype) were made as in the previous paper (Snedecor 46) Although the numbers of individuals are smaller and all possible matings are not represented, those which have been compared are sufficiently critical to indicate the nature of the genetic processes involved. In this study 16 of the 28 tests made of the border relationships involving both strains are not significant (table 7) Of the 12 that are significant, 6 are among *Da* heterozygotes and the others among both +/+ and *Da*/*Da*, thus indicating that dependence or independence of the borders is neither a manifestation or heterozygosity

TABLE 7

Shows the populations (portrayed by bar graphs of figures 2, 3, and 4) arranged to show relationship (independence) of anterior (ThL) to posterior (LS) borders. Calculations were made using the correction for continuity and df = 1 in all cases

Significant interactions		χ^2	P
	1–4	5.2	< 0.02
	5–7	4.8	< 0.05
	6–7	4.0	< 0.05

Mating	Genotype	Strain: DA		III$_{ms}$		III$_{m}$		III$_{ms}$
A	+/+		ns					
	Da/+	(1)18.2						
	Da/Da		ns					
B	+/+							
	Da/+	2.5	ns					
	Da/Da							
C	+/+	(2)10.9		(5) 8.3		1.0	ns	
	Da/+	(3)14.2		(6) 7.5				
	Da/Da		ns	(7) 4.4				
E	+/+				ns	2.4	ns	
	Da/+				ns			
	Da/Da				n			
F	+/+			(8) 4.4		(13)18.4		9.1
	Da/+			(9)27.0	*			
	Da/Da				ns			
G	+/+		ns		ns			
	Da/+	(4) 6.7			ns		ns	
	Da/Da		ns		ns			
H	+/+			(10)11.9	*	(14)10.9	*	ns
	Da/+			3.2	ns			
	Da/Da			(11) 4.1				
I	+/+				ns			
	Da/+			(12)13.6				
	Da/Da				ns			
J	+/+					2.8	ns	
K	+/+					1 7	ns	

nor of gene or genome alone but a matter of interaction of modifying genes within a nonisogenic genome

With respect to the three-way interactions (genotypes borders and strain) only 3 of the 16 tests made show significant differ ences. One of these comparisons (1 with 4 numbers in ( ) in table 7) involves heterozygotes of A and G matings within the DA race. The other two involve all three genotypes of mating C within the $III_{c_{\bullet}}$ strain (5 compared with 7 and 6 with 7) Although these are significant, the small expected cell size involved in this calculation necessitates caution in inter pretation without further study Whereas in the whole population (Sawin and Gow '67) the significant between-order differ ence was confined between strains of the heterozygous *Da*/+ genotype here there is evidence that both genome and gene (or mating and genotype) interaction is in volved This is further evidence that the relative vulnerability to border shift is the overall result of the total genetic back ground of which the effects of a major gene such as *Da* can be enhanced suppressed, or completely hidden by the relative effects of localized minor modifying genes

DISCUSSION

Analysis of these data dealing with homeotic variation based on matings ac cording to vertebral phenotypes of the parents has provided a more critical evalu ation of the genome than was to be had from matings based upon *Da* genotype and VF genome as a whole (Sawin and Gow '67) The evidence of segregation (indi cated by both the interstrain and intra strain differences) which reflect the rela tive effects of inbreeding and selection upon the strain background confirms the validity of the polygenic concept as ex pressed by both Goldschmidt '35 and Landauer '58 (For contrasting interpreta tions see Landauer 58) Their views differ primarily in the nature of the genetic action and were not particularly concerned with the biological mechanism of gene action. Landauer however stressed the fact that each gene within its limits will fulfill its physiological function at a given rate and intensity beyond which gene activities will be modified and eventually cease or be-

come ineffective. He also emphasized t
relative difference in number and kinds c
genes in different stocks the definite limi
tions in activity of each gene, and the fa
that emergence of every trait depends o
the activity of many genes, if not the ent
genome and external agents. Althou
evidence has been obtained of the existen
of component elements of the genome a
ing separately and additively on the V
specific identification must await furth
breeding tests. In $III_{c_{\bullet}}$ their additive effe
tend to suppress the retardation and b
ward shift of the borders by Da, and t
expression tends to be greater at the p
terior border Since it is more significant
some matings than in others, it is c
sidered evidence of localization of spec
modifying genes Of particular sign
cance for the etiology of spontaneous m
formation are the potentialities for va
tion expressed within and between t
several phenotype matings, strains (
nomes) as compared with that of the
genotypes. The study of these in relat
to similar variations in the literature l
revealed the convergence of pathways
inquiry in several fields of clinical and
perimental biology with our studies thro
the gradient growth processes. Landa
(58) was the first to note such con
gence of fields upon the "phenocopy as
common denominator in malformation

In this study the results show con
gence of paths with other concepts
cluding polygenes biological continu
biological interaction, homeostasis, a
polymorphism (spontaneous malformati
upon another common denominator kno
as the growth gradient concept. This c
cept was derived from Huxley's origi
treatment of the allometry equation.
stated by Zuckerman ('50) it concerns
growth potential of an organ or reg
which "seems to be distributed in the fo
of a growth gradient with usually a sin
high point or growth centre from wh
growth intensity grades downwards in b
directions (or in one if the growth cen
be terminal) "

Recognition of this convergence of pa
ways is particularly significant in view
the mysteries which still surround the v
number of gross congenital malformatio
The problems in this field are comp

fehs, '39; Willier '54; Zwilling, '58; .lson and Warkany '64; and Wilson, '64 .) Although many approaches have .n and are being made using laboratory .imals, the wide range of individual strain .d species difference in vulnerability is .h that results of tests of toxic and .atogenic effects made upon one species .nnot be reliably applied to another .raser '63; Wilner '65 Yerushalmy and .ilkovich, '65) Whether there are still .discovered basic principles with refer .nce to mechanisms (Runner '65) or .thways leading to malformation, which .e common to all species is still an open .d grave question.

.Biological continuum of change (in size .ope, and inductive events) This concept .s long been prominent in the thinking of .e morphologist and geneticist. Usually it .s been first observed empirically by .rouping of characteristics without con- .deration of etiology (Ingalls and Kling- .erg, '63) Subsequently the arrangement .ecomes ordered and quantified with refer .nce to processes or mechanisms involved, .heir interactions in time (or better stages .f development) and their response to .nvironment. Quantitative variations such .s growth and *body size are now recognized* .o be due to a number of genes (polygenes) .which operate primarily through a differ- .ntial rate of cell division (Castle and .regory '29; Castle, '31 41) They may .r may not be of equal value but usually .nteract additively resulting in a nor .mal frequency distribution. However the .effects of any one gene in a polygenic sys- .tem are not easily identified or defined.

The morphologist and embryologist by both micro- and macroscopic techniques have developed the concept of continuum of modeling changes, which bring about the specific plan of development and form of vertebrates in general. Some of these changes lead to differences in form, which determine the very special characteristics of classes species and genotypes. More recently the cytologist has been probing the continuity of differential growth cell migration, interaction and degeneration processes at the cellular or tissue levels (Hohlreter '51; Willier '54; Grobstein and Holtzer, '55; Zwilling, '56; Lash '64) Of most importance to the etiology of malformation are the concepts of (1) directional growth, which determines proportion, symmetry and spatial position of parts, and (2) the progressive restrictions in the histo-genetic capabilities. The latter are highly localized and pass through a series of steps such as budding, folding, and differential growth to provide the framework of organization of a number of organ-forming fields.

Not only can body size (weight, length, width etc.) be arranged in a continuous series of variations but morphological entities such as vertebrae show a high degree of continuity in size and form (Sawin and Crary '58) interrupted at various points (such as the vertebral borders) with continuous gradient changes in size occurring between them. As arranged, by matings involving 12/7 parents at the top and 12/8s at the bottom our bar graphs and tables show continuity of change from top to bottom. Each mating tends to *show* all six phenotypes, with a corresponding continuous increase of 13/7s among the progeny toward the center matings and increase of 12/7s and 12/8s at the top and bottom of the scale for each strain. Adjacent matings show least or no significant differ *ences, whereas the more remote tend to* be highly significant. This stepwise shift of the vertebral borders which alters the relative size of the thoracic and lumbar regions and is associated with the sequential changes in size and shape of specific vertebral units is initially related with the metameric organization of the skeleton.

Gradient concept. Sequential changes in size compare favorably with the metabolic gradients demonstrated at the molecular level in invertebrates and with the gradient concept as described by Child, '25 Huxley '30- and with greatest clarity by Zuckerman, '50 Subsequently in vertebrates however the relatively simple anteroposterior growth gradient of the fetus becomes separated into secondary gradients by association with differentiating *vital organs of the thorax* and abdomen and the muscles and nerves of the body wall and limbs. These secondary gradients may occur in the anteroposterior direction, dorsal to ventral or project laterally (Thompson '17; Child, '25; Scammon and Calkins, '29 Huxley '32; *Needham, 42;*

Sawin and Hull 46 Sawin Ranlett and Crary '62) They become varied in pattern according to their size rate of growth associations and functions Thus for example the gradient pattern of the vertebral neural arches in close proximity with the spinal cord differs in time size and localization from that of the centra of the vertebra (Sawin and Crary '56) In at least one case (thoracic Hull 47) the gradient difference has been shown to be associated with ossification rate specific to the ribs and not to humerus or femur

Many models of growth patterns expressed by mathematical equations and growth curves have been used in attempts to associate the various measurements obtained from growing organisms without arriving at conclusive specificity as to underlying biological processes which control body proportions One of the more recent hypotheses is that of *proximity* (Guttman and Guttman '65) Although by their technique the authors have recognized gradients among correlations, they like many others before seem not to have recognized the biological growth gradients which though present in the limbs are more obvious in the vertebrae. These gradients were first recognized by Danforth ('30) and subsequently outlined in connection with studies of histogenetic potency by Willier ('54) Together with the concepts of biological continuum and tissue interaction the gradient concept converges with the gradient fields concept of the histologist and embryologist (Needham 42 Balinsky '65 Sawin and Crary 64) Application of the Guttman technique to the vertebrae the easily recognizable gradient of which consists of more numerous units than are present in the limb would further reveal the basic processes involved.

Interaction (gene and genome) Genetic interaction such as demonstrated here by comparison of the segregated differences in progeny distribution between phenotype matings is well known, involving genes in many species Studies of such genetic interaction concerning morphology include such as those of Dunn and Gluecksohn-Schoenheimer (44) McNutt (54) Green ('57) Forsthoefel ('58) Berry (60) and Kalter (65) in mice. The study of homeotic variations of mice in which the luxoid gene was transferred from C3H to the genome of C57 reveals the same sort of interaction between two specific genes affecting the thoracic and lumbar regions, luxate *lx* and luxoid *lu* (Forsthoefel, '58). The C57 genome and *lx* tend to shift the borders anteriorly the C3H and *lu* posteriorly and by interaction *lu* and *lx* in heterozygotes and homozygotes tend to cancel each other s effects particularly at the posterior border With *Da* in the rabbit the relationship is between one major gene and minor modifiers which differ in the two genomes concerned. With either genome (DA or III) it is noteworthy that the total genome effect is much greater than that of the *Da* gene and that the *Da* effects are enhanced suppressed, or shifted in position according to the genome with which *Da* is associated and interacts. Another concept which looms on the teratological horizon is that of physiological and genetic homeostasis.

Homeostasis This concept refers to the degree to which the morphological pattern of a species or strain of animals has become canalized and buffered against fluctuating internal (genomes) or external environments and is therefore able to resist such influences as may prove adverse (Lerner 54) Derived from population genetics, homeostasis is associated with problems arising from or through the population genome and therefore is of particular importance in evaluating the genetic control on which an experiment is based. In selecting variations at these two vertebral borders as pleiotropic effects of the *Da* gene we are concerned with malformations (homeotic shifts) which prove not to be exclusively *Da* effects. Such shifts are widely known in man and mammals generally are highly canalized in most species and known to be hereditary in at least five although specificity of gene action has proven difficult to demonstrate The last pair of ribs and the sacral attachment mark the limits of the lumbar region and growth gradient (Sawin and Crary '64) and genetic morphological and physiological continuity have been previously demonstrated from generation to generation in both thoracic (Hull, 47) and lumbar (Sawin and Hull, 46) regions. The genetic effects of segregation and alteration of the pheno

and genotype by inbreeding, selection, specific mating all indicate continuity interaction of a group of modifying es acting within the thoracic and lumgradients. In most cases there is nor matching leading predominantly to 7s as in DA, or 13/7s as in III and III_{in} h minimal numbers of the other types. other cases, abnormal matching leads increased border shifting all within the ygenically determined gradient growth tem. Because of the polygenic nature of wth processes action by way of the wth rate of the gradients may be reective, either increasing or decreasing ways in which a given morphological it may be varied depending upon the ative amount of heterozygosity and inter tion of minor modifying genes.

Since experience indicates that most of e smaller sized strains of rabbits (2–3 kg) nsistently have the reduced number of s and vertebrae it may be assumed that a domestic rabbit is canalized around e 12/7 VF The New Zealand White (of rger size 3–4 kg) however has accumuted some modifying genes which by selec on and inbreeding in strain III have beme canalized around 13/7 whereas the A is relatively intermediate and much ore variable. The relative ease of recovery f the 13/7 type by Sawin (45) in 1–3 ackcrosses after outcrossing at that time ed to the assumption of a minimum ("probbly a single) gene difference involving oth borders. The above results do not ompletely rule out the *possible existence* f one such gene within the F mating, but he variation in other matings shows the xistence of additional factors, particularly hose matings in which the progeny distribution differs significantly at only one border or the other indicating *a specificity* of localized action within the gradient. Matings J and K, whose progeny distributions show high proportions of 12/7s and 12/8s to the relative exclusion of 13/7s (fig. 2) or the segregation of a major dif ference only at the LS border particularly show this. A similar tendency can be seen at the ThL border in the +/+ matings of the DA race (fig. 3) Such differences alone do not indicate the nature of the effect between the two borders, but the last pair of ribs and the sacral attachment as limits of the two body regions determine their relative size as of the time of ossification. Since an inherited difference in the ossification rate of the ribs was noted by Hull (47) in race III, and similar "unspecific threshold differences for polydactylism were noted by Truslove ('56) which Landauer viewed as "growth competitions," then such differences as those which occur at the borders between thoracic and lumbar growth gradients (Sawin and Crary '64) are indicators of a highly important mechanism for malformation. Balinsky ('65 p. 68) has concluded *that such gra* dient differences in initial stages of development are never the result of sole stimulation of one of the gradients or of the metabolic system responsible for it, but are brought about by the alternative morpho*genetic response, expansion when* the adjacent gradient is reduced, thus demonstrating the competitive *and compensatory* relationship between the two Such competitive and compensatory relationship is shown in the skulls of *Da/Da* (figs. 29 and 30 Sawin and Trask, 65) Continuity interaction (or overlapping) competition for space and compensatory adjustment to retardation are all processes which are broadly distributed in gradient fashion. As indicated by Jacobson ('66) they also are implicated in the inductive processes which determine position of organs and hence of *malformation.*

One further converging concept, derived from population genetics is that of poly *morphisms i.e. genetic traits determined* by a single gene which occur with a frequency which cannot be accounted *for by* mutation alone.

Polymorphism. This concept has been discussed by Motulsky ('65) in terms of (polygenic) *inheritance with respect to the* physiological response to various drugs and their assessment by the methods of quantitative genetics. He notes that harmful mutations tend to be lost from the population, that single mutations are rare, and that the biochemical *alteration* predisposing the individual to harmful drug effect may be quite silent" physiologically until the drug is administered. Our study has shown the relative physiological silence of *Da* with respect to border shifts when on *the III background. Thus it is* clear that

gene action in morphology and malformation is not necessarily upon a precise skeletal unit or organ but may be by contributions of each one of an unknown number of major and minor genes whose effects overlap to determine the relative size and rate of growth of one gradient to another a process to which external influences can also contribute As has been indicated by Weiss ('39) the gradient is not a cause but a manifestation of underlying metabolic processes and the same is true of these particular homeotic shifts of vertebral borders The borders are but a few of many possible reference points which could be used in recording the nature and relationship of adjacent gradient growth processes

In illustrating the convergence of paths in the various fields of investigation our study does not provide the final solution to all spontaneous abnormality It merely delineates the morphological mechanism through which malformation initiated at the molecular level achieves penetrance and expression If as generally recognized body size is polygenic and influenced also by exogenous factors affecting the rate of body growth it seems equally clear that the skeleton and other organ systems are of like nature We have presented evidence that variation or malformation at the vertebral borders can be influenced by one major gene and by several segregating modifying genes

With the skeleton there is one distinct advantage in that morphology of the separate units (bones) provides reference points which aid in defining limits of localized gradient growth The interaction of these gradients as the result of endogenous genic action usually results in a certain degree of normality as the result of canalization of the species or strain over long periods of time As mutant genes produce dislocation in the integrated functions of the thus stabilized normal genome so also may exogenous physical, chemical or biological agents intervene to prevent them at one time or another from accomplishing their normal interactions and thus lead to abnormality (Lerner 54) Even in the most isogenic lines of mice in which the highest degree of homeostasis might be expected some seem to be more susceptible to environmentally induced polymorphisms than others. Many of the points of interference (in time or in the developmental stage, or by influence of specific agents) are not well known but it is the ontogenetic integration of influences of a polygenic and gradient nature acting as described here which we believe are also in a substantial degree behind spontaneous malformation and polymorphism. The genotype is generally recognized to be basically the source of all endogenous variation and is ranked with the developmental stage in importance for control of tests for teratogenicity (Wilson, '64) The importance of strain differences determining the response to thalidomide was indicated by Sawin, Crary Fox and Wuest ('65)

Although the phenocopy is one denominator with reference to paths of cell formation induction the gradient growth pattern now appears as still another common denominator upon which well established paths of continuity interaction homeostasis and polymorphism concepts Since the gradient concept itself is not new is well grounded in invertebrate biology, it would seem that more extensive exploration with respect to vertebrate malformation could be extremely fruitful.

ACKNOWLEDGMENTS

1 This study was supported in part by Public Health Service Research Grant CA-00281 from the National Cancer Institute and in part by Research Grant E-40 from the American Cancer Society

2. Our thanks are due to Dr R. R. Fox Dorcas Crary Adelaide Cousens, Esther Clark Eugene Farrin and Bruce Plummer who assisted in various ways in analysis and collection and preparation of specimens or roentgenograms.

LITERATURE CITED

Balinsky B I 1965 An Introduction to Embryology Saunders, Philadelphia and London.
Berry R. J 1960 Genetical studies on the skeleton of the mouse. XXVI. Pintail. Genet. Res. Camb. 1: 439–451
Castle, W E. 1931 Size inheritance in rabbits the backcross to the large parent race. J Exp Zool. 60: 325–338
——— 1941 Size inheritance. Amer Nat 75: 488–498.
Castle W E. and P W Gregory 1929 The embryological basis of size inheritance in the rabbit. J Morphol. Physiol., 48: 81–103.

C. M. 1935 The physiological significance of the cephalocaudal differential in vertebrate development. Anat. Rec., 31: 369–383.
Dorcas D. 1964 Development of the ... ear in the dachs rabbit. Anat. Rec., 150: 148.
h, C. H. 1930 Numerical variation and ... logies in vertebrae. Am. J Phys. Anthrop., 63–481.
L. C., and S. Gluecksohn-Schoenheimer ... A specific abnormality associated with a ... ty of genotypes. Proc. Nat. Acad. Sci., 30 176.
... P F 1958 The skeletal effects of ... luxoid gene in the mouse, including its ... actions with the luxate gene. J Morph., 347–383.
F C. 1963 Experimental teratogenesis ... lation to congenital malformations in man. ... Internat. Conf. Congenital Abnormalities, ... York.
... hmidt, R. R. 1935 Gen und Aussenmerkmal ... schaft (Untersuchungen an Drosophila. I. ... Zeits. indukt. Abst. u Vererb., 69 38–131.
..., Margaret 1957 Modifiers of the pleiotropic effects of the short ear gene in the mouse. ... ered., 48: 205–212.
..., C., and H. Holtzer 1953 In vitro ... lies of cartilage induction in mouse somite ... oderm. J Exp Zool., 123 333–358.
... berg, H. 1963 Pathology of Development. ... Wiley New York.
..., Ruth, and L. Guttman 1965 A new ... roach to the analysis of growth patterns ... simplex structure of intercorrelations of ... surements. Growth, 29 219.
... eter, J 1951 Some aspects of embryonic ... duction. Growth XV Suppl. X Symposium on ... and Growth 117–162.
... Inez 1947 Morphogenetic studies of the ... bbit. IV The inheritance of developmental ... terns of rib ossification. J. Exp. Zool., 105.
... y J. S. 1932 Problems of Relative Growth. ... Dial Press, New York.
... lls, T H., and M. A. Klingberg 1965 Congenital malformations, clinical and community ... considerations. Am. J. Med. Sci., 249 316–344.
... heim, A. G. 1966 Inductive processes in embryonic development. Science, 152: 25–34.
..., Harold 1965 Experimental investigation ... teratogenic action. Ann. N Y Acad. Sci., 123: 227
... dauer Walter 1937 Phenocopies and genocopies with special reference to sporadically-occurring developmental variants. Amer. Nat., ... 70–80.
—— 1938 On phenocopies, their developmental physiology and genetic meaning. Am. ... Nat., 72 201 213.
..., J. W 1964 Normal embryology and teratogenesis. Am. J. Obstet. Gynecol., 90: 1193.
... ner I. M. 1954 Genetic Homeostasis. John Wiley New York.
... Nott, Wallace 1954 Gene expression as influenced by genetic background. J Hered., 45 233–240.
Motulsky A. G. 1965 Part III. Genetic factors in drug toxicity The genetics of abnormal drug responses. Ann. N Y Acad. Sci., 123: 167–177
Needham, Joseph 1943 Biochemistry and morphogenesis. Science, 98 155–156.
Runner M. N. 1965 Chapter 4 In: Teratology — Principles and Techniques. J G. Wilson and J Warkany Eds. Univ of Chicago Press, Chicago.
Sawin, P B. 1945 Morphogenetic studies of the rabbit. I. Regional specificity of hereditary factors affecting homeotic variations in the axial skeleton. J Exp. Zool., 100: 301–329.
Sawin, P B., and Dorcas D Crary 1956 Morphogenetic studies of the rabbit. XVI. Quantitative racial differences in ossification patterns of the vertebrae of embryos as an approach to basic principles of mammalian growth. Am. J Phys. Anthrop., 14 625–648.
——— 1964 Genetics of skeletal deformities in the domestic rabbit (Oryctolagus cuniculus L.) Clin. Orthopaedics, 33 71–90.
Sawin, P B., Dorcas Crary R. R. Fox and H. M. Wuest 1965 Thalidomide malformations and genetic background in the rabbit. Experientia, 21 672–677
Sawin, P B., and Maryann Gow 1967 Morphogenetic studies of the rabbit. XXXVI. Effect of gene and genome interaction on homeotic variations. Anat. Rec., 157 425–436.
Sawin, P B., and Inez Hull 1946 Morphogenetic studies of the rabbit. II. Evidence of regionally specific hereditary factors influencing the extent of the lumbar region. J Morph., 78 1–26.
Sawin, P B., Mary Ranlett and Dorcas Crary 1962 Morphogenetic studies of the rabbit. XXIX. Accessory ossification centers at the occipitovertebral articulation of the dachs (Chondrodystrophy) rabbit. Am. J. Anat., 111 239–257
Sawin, P B., and Muriel Trask 1965 Morphogenetic studies of the rabbit. XXXV Pleiotropic effects of the dachs gene and the gradient growth pattern. J Morph., 117 87–114.
Scammon, R. E., and L. A. Calkins 1929 The Development and Growth of the External Dimensions of the Human Body in the Fetal Period. Univ of Minn. Press.
Snedecor G. W 1946 Statistical Methods, 4th ed. Iowa State College Press, Ames, Iowa.
Thompson, D'A. W 1917 On Growth and Form. University Press, Cambridge, England.
Truslove, G. M. 1956 The anatomy and development of the fidget mouse. J. Genet., 54 64–86
Weiss, Paul 1939 Principles of Development. Henry Holt & Co., New York.
Willier B. H. 1954 Phases in embryonic development. J Cell. Comp. Physiol., 43: 307–317
Willner, M. M. 1965 Maturational deficiencies of the fetus and newborn. Relationship to drug effects. Clin. Ped., 4 3–12.
Wilson, J. G. 1964 Experimental teratology Am. J. Obstet. Gynecol., 90: 1181.
——— 1965 Embryological considerations in teratology Ann. N. Y Acad. Sci., 123 219

gene action in morphology and malformation is not necessarily upon a precise skeletal unit or organ but may be by contributions of each one of an unknown number of major and minor genes whose effects overlap to determine the relative size and rate of growth of one gradient to another a process to which external influences can also contribute. As has been indicated by Weiss ('39) the gradient is not a cause but a manifestation of underlying metabolic processes and the same is true of these particular homeotic shifts of vertebral borders The borders are but a few of many possible reference points which could be used in recording the nature and relationship of adjacent gradient growth processes.

In illustrating the convergence of paths in the various fields of investigation our study does not provide the final solution to all spontaneous abnormality It merely delineates the morphological mechanism through which malformation initiated at the molecular level achieves penetrance and expression If as generally recognized body size is polygenic and influenced also by exogenous factors affecting the rate of body growth it seems equally clear that the skeleton and other organ systems are of like nature We have presented evidence that variation or malformation at the vertebral borders can be influenced by one major gene and by several segregating modifying genes

With the skeleton there is one distinct advantage in that morphology of the separate units (bones) provides reference points which aid in defining limits of localized gradient growth The interaction of these gradients as the result of endogenous genic action usually results in a certain degree of normality as the result of canalization of the species or strain over long periods of time As mutant genes produce dislocation in the integrated functions of the thus stabilized normal genome so also may exogenous physical chemical or biological agents intervene to prevent them at one time or another from accomplishing their normal interactions and thus lead to abnormality (Lerner '54) Even in the most isogenic lines of mice in which the highest degree of homeostasis might be expected some seem to be more susceptible to environmentally induced polymorphisms than others. Many of the points of interference (in time or in the developmental stage, or by influence of specific agents) are [illegible] well known but it is the ontogenetic integration of influences of a polygenic [illegible] gradient nature, acting as described here which we believe are also in a substantial degree behind spontaneous malformation and polymorphism. The genotype now is generally recognized to be basically the source of all endogenous variation and is ranked with the developmental stage in importance for control of tests for teratogenicity (Wilson '64) The importance of strain differences determining the response to thalidomide was indicated by Crary Fox and Wuest ('65)

Although the phenocopy is one denominator with reference to paths of malformation induction the gradient growth pattern now appears as still another common denominator upon which well established paths of continuity interaction homeostasis and polymorphism converge Since the gradient concept itself [illegible] is well grounded in invertebrate biology it would seem that more extensive exploration with respect to vertebrate malformation could be extremely fruitful.

ACKNOWLEDGMENTS

1 This study was supported in part by Public Health Service Research Grant CA-00281 from the National Cancer Institute and in part by Research Grant E40 from the American Cancer Society

2 Our thanks are due to Dr R. R. Fox, Dorcas Crary Adelaide Cousens, Esther Clark, Eugene Farrin and Bruce Plummer who assisted in various ways in analysis and collection and preparation of specimens or roentgenograms.

LITERATURE CITED

Balinsky B I 1965 An Introduction to Embryology Saunders, Philadelphia and London.

Berry R. J 1960 Genetical studies on the skeleton of the mouse. XXVI. Pintail. Genet. Res. Camb., 1: 439–451

Castle W E. 1931 Size inheritance in rabbits the backcross to the large parent race. J Exp Zool., 60: 325–338

——— 1941 Size inheritance. Amer. Nat [illegible] 488–498

Castle W E., and P W Gregory 1929 The embryological basis of size inheritance in the rabbit. J Morphol. Physiol., 48: 81 103

C. M. 1935 The physiological signifi- of the cephalocaudal differential in verte- development. Anat. Rec., 21: 380–383.

Dorcas D. 1964 Development of the ex l ear in the dachs rabbit. Anat. Rec., 150: 448.

h, C. H. 1930 Numerical variation and logies in vertebrae. Am. J Phys. Anthrop., 63–481.

L. C., and S. Glueckshn-Schoenheimer A specific abnormality associated with a ty of genotypes. Proc. Nat. Acad. Sci., 30: 178.

oefel, P. F. 1958 The skeletal effects of hroid gene in the mouse including its ractions with the luxate gene. J. Morph., 247–282.

, F. C. 1963 Experimental teratogenesis lation to congenital malformations in man. Internat. Conf. Congenital Abnormalities, r York.

hmidt, R. R. 1935 Gen und Aussermal- schaft (Untersuchungen an Drosophila. I. Zeits. indukt. Abst. u Vererb., 69 38–131.

, Margaret 1957 Modifiers of the pleio- ic effects of the short ear gene in the mouse. lered., 48 205–212.

tein, C., and H. Holtzer 1953 In vitro dies of cartilage induction in mouse somite soderm. J. Exp. Zool., 124 333–356.

berg, H. 1963 Pathology of Development. n Wiley New York.

man, Ruth, and L. Guttman 1965 A new proach to the analysis of growth patterns simplex structure of intercorrelations of easurements. Growth, 29: 219

reter J. 1951 Some aspects of embryonic luction. Growth XV Suppl. X Symposium on y and Growth 117–122.

, Inez 1947 Morphogenetic studies of the bbit. IV The inheritance of developmental tterns of rib ossification. J. Exp. Zool., 105 1.

ley J. S. 1932 Problems of Relative Growth. ncoln MacVeagh, London; Dial Press, New ork.

lle, T. H., and M. A. Klingberg 1965 Con- nital malformations, clinical and community nsiderations. Am. J Med. Sci., 249 316–344.

hson, A. G. 1966 Inductive processes in mbryonic development. Science, 153: 25–34.

er Harold 1965 Experimental investigation f teratogenic action. Ann. N. Y. Acad. Sci., 23: 287

ldman Walter 1957 Phenocopies and geno- ypes, with special reference to sporadically- ccurring developmental variants. Amer. Nat., 91 79–90.

—— 1958 On phenocopies, their develop- mental physiology and genetic meaning. Am. Nat., 92: 201 212.

h, J. W. 1964 Normal embryology and teratogenesis. Am. J. Obstet. Gynecol., 90: 1193.

mer I. M. 1964 Genetic Homeostasis. John Wiley New York.

cNutt, Wallace 1954 Gene expression as in- fluenced by genetic background. J Hered., 45 235–240.

Motulsky A. G. 1965 Part III. Genetic factors in drug toxicity The genetics of abnormal drug responses. Ann. N Y Acad. Sci., 123 167–177

Needham, Joseph 1942 Biochemistry and mor phogenesis. Science 96: 155–158.

Runner M. N. 1965 Chapter 4. In Teratology — Principles and Techniques. J G. Wilson and J Warkany Eds. Univ of Chicago Press Chi- cago.

Sawin, P B. 1945 Morphogenetic studies of the rabbit. I. Regional specificity of hereditary factors affecting homeotic variations in the axial skeleton. J Exp. Zool., 100: 301–329.

Sawin, P B and Dorcas D Crary 1956 Mor- phogenetic studies of the rabbit. XVI. Quantita- tive racial differences in ossification patterns of the vertebrae of embryos as an approach to basic principles of mammalian growth. Am. J Phys. Anthrop., 14: 625–648.

——— 1964 Genetics of skeletal deformities in the domestic rabbit (Oryctolagus cuniculus L.) Clin. Orthopaedics, 33 71–90.

Sawin, P B., Dorcas Crary, R. R. Fox and H. M. Wuest 1965 Thalidomide malformations and genetic background in the rabbit. Experentia, 21 672–677

Sawin, P B., and Maryann Gow 1967 Morpho- genetic studies of the rabbit. XXXVI. Effect of gene and genome interaction on homeotic varia- tions. Anat. Rec., 157 425–436.

Sawin, P B., and Inez Hull 1946 Morphogen- etic studies of the rabbit. II. Evidence of re- gionally specific hereditary factors influencing the extent of the lumbar region. J Morph., 78: 1–26.

Sawin, P B., Mary Ranlett and Dorcas Crary 1962 Morphogenetic studies of the rabbit. XXIX. Accessory ossification centers at the oc- cipitovertebral articulation of the dachs (Chon- drodystrophy) rabbit. Am. J Anat., 111: 239–257

Sawin, P B., and Muriel Trask 1965 Morpho- genetic studies of the rabbit. XXXV Pleiotropic effects of the dachs gene and the gradient growth pattern. J. Morph., 117 87–114

Scammon, R. E., and L. A. Calkins 1929 The Development and Growth of the External Di- mensions of the Human Body in the Fetal Period. Univ of Minn. Press.

Snedecor G. W 1946 Statistical Methods, 4th ed. Iowa State College Press, Ames, Iowa.

Thompson, D'A. W 1917 On Growth and Form. University Press, Cambridge, England.

Truslove, G. M. 1956 The anatomy and devel- opment of the fidget mouse. J Genet., 54 64–86.

Weiss, Paul 1939 Principles of Development. Henry Holt & Co., New York.

Willier B. H. 1954 Phases in embryonic devel- opment. J Cell. Comp. Physiol., 43: 307–317

Willson, M. M. 1965 Maturational deficiencies of the fetus and newborn Relationship to drug effects. Clin. Ped., 4 3–12.

Wilson, J G. 1964 Experimental teratology Am. J Obstet. Gynecol., 90: 1181.

——— 1965 Embryological considerations in teratology Ann. N. Y Acad. Sci., 123: 219

Wilson, J G and J Warkany Eds. 1965 Teratology: Principles and Techniques. Univ Chicago Press Chicago.

Yerushalmy, J., and L. Milkovich 1965 Evaluation of the teratogenic effect of meclizine in man. Am J Obstet. Gynecol., 93: 553

Zuckerman, S. 1950 A discussion on the measurements of growth and form. Proc. Roy. Soc. London Series B 137: 433–443.

Zwilling Edgar 1956 Genetic mechanism in limb development. Cold Spring Harbor Symposia Quant. Biol., 21: 319–334.

Fine Structure of Compensatory Growth in the Rat ney after Unilateral Nephrectomy

WINSTON A. ANDERSON
Division of Biological and Medical Sciences, Brown University Providence Rhode Island

ABSTRACT The structural changes in the nephrons of the rat kidney during compensatory growth were observed for 96 hours following unilateral nephrectomy. Hypertrophy of tubular epithelial cells involves dilation of the cisternae of rough endoplasmic reticulum, proliferation of Golgi membranes and agranular reticulum, and increase in number of cytoplasmic ribosomes. The appearance of absorption droplets and microtubules, that are polarized along the cell axis, coincides with maximal hypertrophy of proximal tubule cells. Premitotic dedifferentiation of these cells involves flattening of the basal infoldings of the plasmalemma, decrease in number and disorientation of mitochondria, loss of apical compartments, and the reduction in number of microvilli. Cilia appear on the apical borders of some cells. Bundles of 30–50 Å filaments occupy the cytoplasm at the base of proximal tubule cells.

In distal tubule cells that are undergoing mitosis, numerous mitochondria remain intimately associated with infoldings of the basal plasmalemma. This persistence of the differentiated basal region prevents complete cell division, and binucleate and multinucleate cells arise as a result of failure of cytoplasmic cleavage after normal karyokinesis. During mitosis, the chromosomes and apical vesicles are restricted to organelle-free masses of cytoplasm that project into the lumen.

In collecting tubules, both intercalated and lining cells undergo mitosis during compensatory growth. By 72 hours, a less differentiated cell type, that is active mitotically appears in the cortical portion of collecting tubules. The number of binucleate epithelial cells increases in the compensating kidney tubules. Unilateral nephrectomy also induces distinct alterations in the fine structure of the glomerulus and the papilla of the contralateral organ.

The epithelium of the nephron possesses istinctive structural specializations that re related to the specific functional activities of the tubular segments. The large umbers of microvilli at the free surfaces f cells in proximal convoluted tubules are elatively stable structures concerned with he absorption of fluids and macromolecules from the lumen, and physiological lata indicate that approximately 80% of he fluid in the glomerular filtrate is reabsorbed by the epithelium of the proximal tubules (Smith, '51). Numerous mitochondria are aligned along the basal invaginations of the plasma membrane in both proximal and distal tubule cells suggesting that this border of the cell is involved in the active transport of material (Fawcett, '62). Thus, in the normal rat kidney the cells of the nephron possess a relatively stable substructure which is intimately related to the physiological activity of the organ.

When half of the renal tissue is removed by unilateral nephrectomy the remaining nephrons excrete the entire volume of urine and the functional workload of the contralateral organ is thus increased greatly. The resulting physiological alterations induce cellular growth and proliferation in a tissue in which cell enlargement and division are normally rare (Goss and Rankin, '60; Williams, '61 Reiter and McCreight, '65). Expansion of the surface area of the kidney cells, caused partly by the increased diameter of the tubules and partly by the elongation of certain segments of the nephron results in the greater physiological efficiency of these cells. Such morphogenetic changes occurring primarily in the segments of the nephron that are physiologically most active restore the kidney tissue to a level of compliance consistent with the increased functional demands placed upon the organ.

Several aspects of the interrelationships of differentiation, cellular growth and cell division in the hypertrophying kidney are not yet clear. Therefore, the present investigation deals primarily with the following

questions. (1) Do fully differentiated kidney cells remain mitotically active and if so do they dedifferentiate before division? (2) Do structural differentiations inhibit hypertrophy or mitosis in these cells? (3) Do the cells redifferentiate to an alter native form? (4) What are the cytological characteristics of pre and postmitotic hypertrophy in the tubular and glomerular cells of the compensating rat kidney? With appropriate experimental methods it is possible to answer some of these questions concerning the morphogenetic events occurring in compensatory renal growth

MATERIAL AND METHODS

General plan of experiments

Female albino rats weighing from 100–200 gms were used in all experiments The animals were maintained in a temperature-controlled room at 76–78°F and exposed to a diurnal light cycle of 14 hours (7 00 AM–9 00 PM) for at least two weeks before the start of each experiment To avoid diurnal variations animals were sacrificed between 12 00 noon and 2 00 PM Operations were performed on animals under ether anesthesia. This procedure involved exteriorization of the left kidney through a dorsolateral incision on the body wall. The kidney was separated from the adrenal gland and associated connective tissue the renal blood vessels were ligated and the organ excised The extirpated kidneys were immediately placed in Susa s fixative for light microscopy and in glutaraldehyde-osmium tetroxide fixatives for electron microscopy Two unilaterally nephrectomized and one sham-operated animal were sacrificed at 6 12 24 30 36 40 48 72 and 96 hours after the operation.

Preparative techniques for light and electron microscopy of plastic embedded tissue

A midventral incision was made in rats under light ether anesthesia, and chilled fixative was dropped on the kidneys following decapsulation. After excision of the organ, slices of tissue taken from the cortex, outer and inner medulla, were placed in glutaraldehyde fixative and cut into small pieces (less than 3 mm)

Consistently good results were obtained when pieces of tissue were fixed in the following buffered glutaraldehyde solu tion

Biological grade glutaraldehyde (30.4%)	[illegible]
Sodium cacodylate (0.1M)	[illegible]
Sucrose (1.5 g)	[illegible]
Distilled water	

pH of mixture is 7.3

Tissue blocks were fixed in glutaraldehyd at room temperature for 30 minut chilled in an ice bath for 30–45 minut and rinsed for three minutes in the follo ing mixture:

Sodium cacodylate (0.1M)	[illegible]
Sucrose (5.0 g)	[illegible]

The tissue was post fixed with constan agitation in 2% osmic acid for 60–90 min utes Following fixation, the samples we rapidly dehydrated through 30% 50 70% and 95% acetone-water solutions (minutes each) and in two changes minutes each) and in two changes 100% acetone (30 minutes each) Follo ing dehydration the samples were plac in a mixture of one part embedding m dium plus activator and one part acet (1:1 v/v) and agitated overnight. Afte one hour of agitation in pure embeddin medium plus activator the samples we embedded in an epon-araldite mixtu (Voelz and Dworkin '62) Final polymer zation was carried out in 100% resin a activator in Beem capsules overnight a 60 C Thin sections (silver and gold) we cut with glass knives on a Porter Blu ultramicrotome and mounted on uncoat copper grids. The sections were stain with a satured solution of uranyl acet in 40% ethyl alcohol for ten minut rinsed immediately in three changes distilled water and placed in undiluted le citrate for 10–15 minutes (Reynolds, '63 The sections were then rinsed in 0.0 sodium hydroxide washed in three chang of distilled water and observed with RCA-3D electron microscope.

Thick, plastic embedded sections w prepared for light microscopy Toluid blue was used as a general stain to dis guish cytoplasmic components and to d onstrate the juxtaglomerular granules. tions of 0 25–2 μ thickness were staine 0 1% toluidine blue dissolved in a 2 solution of Na_2CO_3 (Chandra and Skel 64) or in a 1% toluidine blue solutio 1% aqueous sodium borate. A polychr

in developed by Schantz and Schecter (4) as well as Goodpasture's crystal violet solution (Lee and Hopper '65) gave satisfactory cytological details for light microscopy

OBSERVATIONS

Normal proximal convoluted tubules

Ultrastructural features of the proximal tubules from normal and sham-operated kidneys were consistent with those reported in the literature (Rhodin, '58; Ericsson, '64; Trump and Ericsson, 65) The proximal tubules consist of a single layer of columnar epithelial cells surrounding a lumen which may appear open or closed. The apical surfaces are distinguished by closely packed microvilli that extend into the lumen (fig. 1) Below this brush border small vesicles and apical vacuoles containing electron-lucent material are common cell components. In the basal two-thirds of the proximal tubule cells, numerous mitochondria are aligned parallel to each other and to the longitudinal axis of the cell (fig. 2) Invaginations of the basal plasmalemma, some of which contain elongate mitochondria, form interdigitating cytoplasmic compartments. A round or ovoid nucleus, surrounded by clusters of ribosomes and with Golgi cisternae at its apical or lateral aspect, is located at the base or center of these cells. Few microtubules are present in the proximal tubule cells of the normal rat kidney

The proximal convoluted tubule cells are, therefore, well specialized to perform the absorptive and excretory functions of this segment of the nephron. The microvilli at the free surface of these cells are relatively stable differentiations that greatly increase the area of membrane exposed to substances which are to be absorbed. Similarly cytoplasmic compartments which contain elongate mitochondria are specialized for excretion of reabsorbed fluid from the cell into the basal labyrinth.

Ultrastructural aspects of compensatory growth in the proximal tubule cells of the contralateral kidney

Immediately following unilateral nephrectomy a progression of changes lead to hypertrophy of the proximal tubule cells. The earliest and most conspicuous modification involves dilation of the cisternae of the endoplasmic reticulum and Golgi apparatus. Increased numbers of free ribosomes and small vesicles containing dense material are evident at this stage. An increase in cytoplasmic basophilia after six hours reflects a rise in the ribonucleic acid (RNA) content of the kidney cells (Kurnick, '55 Halliburton and Thomson '65) Maximal hypertrophy of the proximal tubule cells is achieved by 24 hours after unilateral nephrectomy (figs. 3–5) Proximal tubule cells in hypertrophic kidneys lack the precisely oriented mitochondria seen in these cells in the kidneys of normal and sham-operated animals. Instead the enlarged cells contain small and extremely dense mitochondria. A decrease in the number of mitochondria is correlated with lower succinic dehydrogenase (SDH) activity in the cortex of the contralateral kidney (Anderson '66) The base of the hypertrophied cell is markedly altered, since the invaginations of the plasmalemma are no longer present (fig. 5) Hypertrophic cells contain accumulations of smooth endoplasmic reticulum and dilated Golgi cisternae. By *24 hours* cytoplasmic processes containing clusters of ribosomes in their clear groundplasm extend into the lumen. The free surfaces of the apical cytoplasmic processes bear few microvilli. Interdigitating apical compartments are no longer present in the proximal tubules. Nuclei, primarily located at the base of the normal proximal tubule cells, move apically toward the clear cytoplasmic extensions where numerous mitotic figures appear between *40* and *48 hours*

Cilia, which are absent from cells of the proximal tubules in normal rats, appear in rapidly growing renal tumor cells (Mannweiler and Bernhard, '57) and in tubule cells from neonatal rats (Anderson, unpublished) After unilateral nephrectomy cilia are observed at the apices of the proximal tubule cells. Ciliary rootlets with a periodic banding of 600–700 A lie close to the basal bodies. Microtubules which are few in the proximal tubule cells of control kidneys, increase in number by *24 hours* (fig 6) Large numbers of micro-

tubules persist at 72 *hours* (fig. 7) and diminish in number after *96 hours*

Renal absorption droplets are common in the proximal tubule cells in normal and sham-operated kidneys Absorption droplets increase following administration of various proteins suggesting that they contain exogenous proteins absorbed from the glomerular filtrate (Oliver et al. 55; Ericsson 64) At *24 hours* absorption droplets increase in the hypertrophic cells and reach a maximum level when mitotic activity is greatest. Absorption droplets surround the nucleus and lie close to the mitotic apparatus By *72 hours* absorption droplets decrease to normal levels

Binucleate cells occur rarely in normal and sham-operated kidneys but, after nephrectomy multinucleate cells are common at *48* and *72 hours* During the first 72 *hours* extensive cellular growth and hyperplasia in the proximal segment of the nephron frequently causes bending of these tubules. Physical changes of this type may force the basement lamina next to the apical surface of the epithelial cells (figs 8 9) Pronounced invaginations of the intertubular capillaries project into the base of the tubular epithelium

Small patches of filaments occur at the base of proximal tubule cells in normal rats (Ericsson '64 Trump and Ericsson '65) These investigators relate them to structural specializations that bind the cells to the underlying basement lamina Thirty to 50 A filaments run parallel or perpendicular to the longitudinal axis of the enlarged cells. Small "pits" similar to the pinocytotic vesicles in endothelial cells adjoin the filaments

At *96 hours* the cells of the proximal tubules become more cuboidal The population of microvilli at the cell apex is sparse and small mitochondria are randomly distributed in the cytoplasm. The basal plasma membrane remains flattened

Thus shortly after unilateral nephrectomy significant structural differences are observed between normal and compensating rat kidney cells. Hypertrophy of these cells occurs concurrently with loss of basal specializations and apical compartments though the microvilli persist throughout the premitotic stages of compensatory growth Fewer mitochondria and lower levels of a Krebs cycle enz (SDH) indicate that there are functio and structural changes. Reversion of typical proximal tubule cell to a less spe cialized state suggests that, in these cel partial dedifferentiation precedes cell divi sion.

Distal convoluted tubule cells

Normal distal tubule cells do not hav a brush border (Smith '51) Elonga mitochondria at the base of the cells ar smaller and less dense than those in the cells of the proximal tubules. Basal in foldings of the cell membrane form prom inent cytoplasmic compartments and the close relationship between the mitochon dria and plasmalemma indicates that the epithelium is engaged in active transpor of ions (Fawcett, '62) The nucleus whic lies in the base of the cell is surround by a few Golgi membranes and modera numbers of ribosomes (fig 10)

In some respects the pattern of com pensatory growth in the distal tubule cel resembles that in the proximal tubule Increase in ribosomes dilation of the Golg cisternae (fig 11) and migration of th nucleus into the enlarged apical cytopla mic processes characterize the stages premitotic hypertrophy of these cells. U like the proximal tubule cells howeve dedifferentiation does not occur at the ce base Consequently by *24 hours* mito figures appear in the fully differentiat distal tubule cells The presence of ve cles in the apical cytoplasm of cells mitosis presumably represents structu evidence of secretory or transport acti (fig 12) Proliferating distal tubule ce preserve structural specializations and tain their function However because the persistence of the complex basal foldings cytokinesis does not norm follow karoyokinesis producing increa numbers of binucleate cells in this s ment of the nephron (fig 13)

By *48 hours* cellular hypertrophy mitosis cause infoldings in the apical surfaces of the distal tubule cells. Seco ary channels between the epithelium basement lamina and intracellular ca iculi connect with the lumen (Anders '66) Similar structures were noted rapidly dividing renal tumor cells by Ma weller and Bo[illegible] ('57) At *96 hou*

distal tubule cells are still enlarged [...] apical cell processes that contain [...]dei project into the duct. The mitochon[...] of the distal tubule cells remain polar [...] within the basal cytoplasmic infold[...] throughout all stages of compensatory [gro]wth, but, between *72* and *96 hours* [ma]ny mitochondria also surround the nu[...]. At this time the substructure of some [of] the mitochondria is altered and parallel [ba]nds of filamentous material condense to [for]m crystalline structures in the matrix [(fi]gs. 14–18) Helical membranes are also [pr]esent within these elongate atypical mito[cho]ndria (fig. 16)

Collecting tubules

Structural features of the epithelial cells [li]ning the collecting tubules in the normal [ra]t kidney were described by Rhodin ('58) [an]d Young and Wissig ('64) Usually [th]e cortical portion of the collecting tubule [co]ntains two cell types: dark cuboidal or [in]tercalated cells with numerous mito[c]hondria, and light columnar cells with [fe]w mitochondria. In the light microscope [t]he columnar epithelial cells surround a [di]lated lumen.

Following unilateral nephrectomy pro[n]ounced modifications occur in the cells [o]f the cortical and outer medullary por[t]ions of the collecting tubules. Dilation of [t]he Golgi cisternae and increase in the [v]olume of cytoplasm in both cell types [o]ccurs by *36 hours*. An external fuzzy [c]oat on the apical surfaces and the pres[e]nce of numerous apical vesicles indicate that structural specializations of these cells persist during compensatory growth (fig 19) Basal infoldings of the cell membrane are also prominent (fig. 21) Both dark and light cells undergo mitosis by 24 hours (fig. 20) Increased numbers of binucleate dark and light cells suggest that cytokinesis does not keep pace with nuclear division. By *72 hours* a third cell type that has an enlarged nucleus and ribosome-rich cytoplasm, but lacks apical vesicles and infoldings of the plasma lemma, appears in the cortical segments of the collecting tubules. This cell, in the collecting tubules, is frequently seen in division. As a result of cell growth and cell division, the lumen of the collecting tubule that is normally open is instead partially occluded by apical cell processes.

Alterations in the glomerulus of the hypertrophic kidney

Twelve hours following unilateral nephrectomy there is an obvious increase in the rough endoplasmic reticulum and in the numbers of free ribosomes in the capsular epithelial cells. Patches of 30–50 Å filaments run parallel or perpendicular to the underlying basement lamina (figs. 22–25) The filamentous processes are best developed between 36 and 40 *hours*.

Dilation of the cisternae of the rough endoplasmic reticulum and the Golgi apparatus as well as the appearance of dense material within the cisternae of the endoplasmic reticulum accompany an increase in cytoplasmic volume of the glomerular epithelial and mesangial cells. Simultaneously numerous microtubules also appear in these cells, but mitosis is rare. Most mitotic figures are observed in the mesangial cells. Fusion of the foot processes of the epithelial cells is a prominent feature in the glomerulus of the hypertrophic kidney and the dense layer of the glomerular basement lamina is thicker than normal.

The renal papilla

Structural features of the collecting ducts in the papilla, Henle's loops, the vasa recta and interstitial cells have been noted by Young and Wissig ('64) and Bulger et al. ('66) Cytoplasmic processes of the interstitial cells abut the basement lamina of the renal tubules and blood vessels Granules are absent from interstitial cells in the normal renal papilla, but *30 hours* following unilateral nephrectomy numerous granules appear (Anderson, '68). The granules may lie next to cells of the collecting tubule and Henle's loop but are most prominent beneath the fenestrated borders of the vasa recta. The granules do not stain positively with PAS or Sudan black. The closeness of the rough endoplasmic reticulum suggests that the granules may be proteinaceous in nature. Similar granules are observed in the interstitial cells of the papilla in potassium-deficient rats (Spargo et al. '60)

DISCUSSION

Structural features of hypertrophy of the proximal tubule cells

Extensive alterations of the fine structure of proximal tubule cells coincide with changes in the normal pattern of nucleic acid and protein synthesis in the contralateral kidney (Halliburton and Thomson 65) Such alterations convert the mitotically inactive cell to an actively dividing cell

The degree of development of the basal infoldings varies in different epithelia that function in active transport (Fawcett, 62) Basal infoldings in the cells of the ciliary body of the eye (Pappas and Smelser 58) are relatively undeveloped. However cells of the proximal and distal tubules of the vertebrate nephron (Pease '55; Rhodin 58) and the principal secretory cells of the salt gland in marine birds (Doyle 60) possess elaborate infoldings The degree of development of the basal infoldings and their intimate relationship with large numbers of oriented mitochondria reflect the capacity of these cells to transport ions and fluids Flattening of the basal infoldings loss of apical compartments and a decline in the number as well as a disorientation of the mitochondria in the hypertrophied proximal convoluted tubule cells suggest a decreased capacity of cells to transport ions and fluids In addition fewer mitochondria in the dedifferentiated cells and lower SDH activity of the renal cortex indicate that the energy yielding mechanism of the tricarboxylic acid cycle is less significant in the metabolism of these cells

During the early stages of compensatory growth RNA and protein increase (Halliburton and Thomas 65) The increase in RNA coincides with the appearance of numerous clusters of ribosomes in the cytoplasm Since cytoplasmic ribosomes are associated with the production of proteins for intracellular consumption (Fawcett '66) unilateral nephrectomy presumably stimulates this synthetic system Increase in the DNA content of the kidney during compensatory growth parallels the enlargement of the nuclei and their migration towards the apices of the cells In the dividing cells the chromosomes are restricted to cytoplasmic projections that extend into the tubular lumen The increase in binucleate and multinucleate cells at 72 hours after unilateral nephrectomy is evidence for nuclear division without cytoplasmic division.

The Golgi apparatus and smooth endoplasmic reticulum in hypertrophic cells

Cellular hypertrophy is accompanied by the production of intracellular deposits of Golgi membranes and smooth endoplasmic reticulum Marked proliferation of these membranes demonstrates the dynamic turnover of phospholipid components in the enlarging cells. The pleomorphism of the membranous elements suggests functional and structural continuity and flow among the membranes themselves A similar view was proposed by Novikoff et al ('62) and Mercer ('62). Membranes in hypertrophic cells probably represent an intracellular phospholipid pool that is related to: (1) the store of membranous components available to daughter cells in mitosis (2) the transport of enzymes or other substances within the cell (3) the provision of a framework for the accumulation sequestering and transport of absorbed substances and (4) the maintenance of plasma membrane with optimal surface area for the exchange of extracellular material.

Significance of renal absorption droplets in the hypertrophic kidney cells

After the intravenous administration of foreign protein to mammals there is an increase in the number of absorption droplets in the proximal tubule cells (Oliver et al. '55 Straus 57 Farquhar and Palade 60; Ericsson '64) Exogenous proteins filter through the glomerulus and are selectively reabsorbed by the cells lining the proximal tubules (Straus, '64). Absorption droplets increase when the nephron is challenged to absorb proteins in amounts greater than normal (Oliver et al '55)

Unilateral nephrectomy augments the blood flow and the filtration rate in the contralateral kidney of dogs and men (Levy and Blalock, '38; Friedmann et al. 42) and the accumulation of absorption

lets in the proximal tubule cells in e and rats (Leak, '65 Anderson, '63) droplets contain an abundance of spholipids, NH_2-groups, glycoproteins, no acids and a greater concentration protein than in any other cellular comment (Oliver et al., '55) Polypeptides, ino acids and other substrates derived m the droplets may thus serve as nponents in the synthesis of new prolasm. The location of droplets in the ranuclear cytoplasm and their closes to chromosomes suggest a perferential ersion of substrates to the mitotic paratus. Furthermore, the droplets are st abundant just before the peak of totic activity when total protein con t is rising in the compensating organ Halliburton and Thomson, '65)

The presence of droplets around the cleus and mitotic chromosomes in reerating hepatocytes (Kent et al., '65; cker and Lane, '65) may represent a m of dedifferentiation of these cells. e acid phosphatase activity of these oplets places them in the class of lysomes that may lyse organelles in cells eparing for division (Becker and Lane 5) Lysis of cytoplasmic organelles may so account for simplification of kidney ll fine structure during premitotic hyertrophy

Microtubules: relation to cytomorphogenesis

Histological studies of compensatory rowth have consistently failed to reveal he mechanism of cellular hypertrophy which precedes hyperplasia in the kidney Recent electron microscopic studies have reported changes in cell organelles related o modifications in renal cell shape (Anderson, '64; Anderson et al. '66) The development of a system of microtubules coincides with the state of maximal hyper trophy in the proximal tubule cells. Such microtubules persist throughout periods of hypertrophy but diminish in cells that have undergone mitosis. Their precise orientation and organization in the apical regions of the enlarging cells indicate that they constitute a framework about which new cytoplasmic components are laid.

A similar cytoskeleton of microtubules was demonstrated in the palisading cells of the presumptive lens ectoderm (Byers and Porter 64) in undifferentiated ver tebrate cells (Behnke '64) and in the manchette of differentiating spermatocy tes (Burgos and Fawcett, '55 Anderson et al., '66) In these undifferentiated cells, the microtubules seem to participate in shape changes and in determination of form. After differentiation, the number of microtubules in these cells diminishes. The transient appearance of oriented microtubules in hypertrophying proximal tubule cells attests to their involvement in mor phogenetic changes during compensatory growth.

Other cytoplasmic features

Small patches of randomly distributed filaments in the base of proximal tubule cells were described by Trump and Ericsson ('65) Bundles of filaments may represent sites where the basal surfaces of cells are tightly bound to the basement lamina. The base of the hypertrophied proximal tubule cells contains extensive accumulations of filaments. The filaments are similar in appearance and dimension to the thin elements that are basic to all contractile systems. The functional significance of the filamentous aggregates in these cells is not known but their simi larity to elements in myoepithelial and smooth muscle cells suggests that they may be contractile.

Cilia are not found in the differentiated proximal convoluted tubule cell of the rat. Cilia are, however common in rapidly proliferating renal tumors of hamsters (Mannweiler and Bernhard, '57) in dif ferentiating proximal tubule cells of neonatal rat kidneys and in hypertrophic cells of growing rat kidneys The cilia are probably induced to form by an erratic centriole and their presence suggests a return to the embryonic state.

Mitosis in structurally differentiated distal tubule cells

Acidification of urine and the active transport of ions and fluids occur in the distal segment of the nephron (Smith, '51) Mitochondria, closely apposed to the basal infoldings of the cell membrane, probably furnish energy for active transport (Rhodin, '58) In this portion of the

nephron physiological activity depends on an extensive surface area intimately related to the mitochondria

Some highly differentiated cells such as mature neurones apparently never divide This has led to the concept that mitosis is antagonistic to the differentiated state or vice versa. This tenet does not hold true for the distal tubule cells, since these cells retain their structural differentiation during cell division Unlike the proximal tubule cells the distal tubule cells neither lose their basal infoldings nor is there a decrease in the number or the disorientation of the mitochondria. The apical cytoplasm of distal tubule cells in mitosis is pervaded with small vesicles that are considered as structural evidence for secretion or fluid transport Persistence of the differentiated basal regions prevents complete cell division Binucleate and multinucleate distal tubule cells in the compensating kidney arise as a result of failure of cytoplasmic cleavage after normal karyokinesis The fact that skeletal muscle cells which contain myofibrils and that melanin laden melanocytes are able to divide (Wilde '59 61) supports the view that cells which have amassed specialized structures are capable of division The fact that distal tubule cells undergo mitosis in their differentiated state clearly supports this concept.

Alterations in the substructure of mitochondria

Crystalline paracrystalline and helical mitochondrial inclusions have been described in a variety of pathological and normal tissues (Behnke '65 Tandler and Shipkey '64 Wills '65) Even without statistical support, it is evident that the number of atypical mitochondria increase in the cells of the distal convoluted tubules The dense population of mitochondria in the epithelial cells suggests high metabolic activity but histochemical tests indicate that the SDH activity is actually lower than normal in these cells Modified mitochondria are reported to be deficient in oxidative enzymes (Karnovsky '63) and this could account for the decrease in SDH activity in these cells. Novikoff and Potter ('48) have suggested that mitochondrial changes may represent structural equivalents to the depressed oxidative enzymes observed chemically during hepatic regeneration.

The structural pleomorphism of the mitochondria is undoubtedly related to the different functional states of these organelles The alteration in substructure is apparently due to changes in the physicochemical state of the mitochondrial proteins leading to reorganization into crystalline structures (Mercer '62)

The collecting tubules in compensatory growth

The collecting tubules are important in the concentration of urine (Ginetzinski, 58 Gottschalk and Mylle, '59) The collecting tubules may also secrete ammonia by deamination of amino acids, and recover sodium ions in exchange for hydrogen ions (Young and Wissig, '64) Cation exchange is thought to occur in the cortical portions of the tubules while cells participating in urine concentration are restricted to the papilla. At 24–36 hours cellular hypertrophy and hyperplasia occur in mitochondria rich intercalated cells and in lining cells of the cortical segments of the collecting tubules. The basal infoldings do not flatten and the number of mitochondria does not decrease perceptively in dividing cells. Binucleate cells are already abundant at 48 *hours*. By 72 *hours* a third cell type appears in the cortical portion of the collecting tubules. These cells are not highly differentiated and are especially active in mitosis. These rapidly proliferating cells probably arise from transformed intercalated or lining cells or from a reserve population of stem cells that are mitotically active. The cortical portion of the nephron is a primary growth zone in the regenerating kidney

Altered structures in the glomerulus

Data on renal physiology demonstrate that the rate of glomerular filtration depends upon both the blood pressure and the rate of blood flow through the capillaries (Koch '60) Abnormal physiological and experimental conditions that raise the blood pressure and increase the blood flow in the glomerulus also augment the filtration rate Unilateral nephrectomy induces a 70% increase in renal blood

(Levy and Blalock, '38) and in filtration rate (Friedman et al., 42) in the contralateral kidneys of dogs and men. Investigations on the movement of small molecules through the glomerular basement lamina (Farquhar and Palade, '60; '61) indicate that this structure is the primary filtration site in the glomerulus. The glomerular epithelial cells are monitors that compensate for imperfections in the filter (Farquhar and Palade '61). Rhodin ('62) further postulates that diaphragm-dilations in the fenestrae of the endothelium regulates the size of the molecules passing through it. Modifications in the ultrastructure of the glomerular components which follow unilateral nephrectomy are considered as specializations that compensate for the increased workload. Increased protein synthesis and the accumulation of storage or secretory droplets within the cisternae of the endoplasmic reticulum in epithelial and mesangial cells may be related to the synthesis of basement lamina components. Thickening of the basement lamina and fusion of the foot-processes in the compensating kidneys may also be structural modifications that reduce the filtration rate and the protein loss following unilateral nephrectomy (Anderson, '66).

The renal papilla

The structure and arrangement of the interstitial cells of the renal papilla suggest that they perform some function other than provision of support for the urinary tubules and papillary capillaries. Their prominence in desert rodents, that depend on water derived from metabolic *oxidation* of hydrogen for their excretory needs (Sternberg et al., '56), suggests that these cells may function in the conservation of water since desert rodents excrete urine that is twice as concentrated as that from laboratory rats. Furthermore, fresh water mammals (beaver) which need not conserve water have few interstitial cells (Schmidt-Nielsen and O'dell, '61). The chemical specificity of the interstitial cells for diphosphopyridine nucleotide (NAD) diaphorase (Sternberg et al., '56) their elaborate protein synthetic apparatus (Bulger et al., '66) and their specific anatomical organization reflect their possible functional activity and importance.

Dense droplets accumulate in the papilla of potassium-deficient rats (Spargo et al. '60). Potassium repletion causes rapid disappearance of the droplets. The accumulation of droplets in the papilla following potassium deficiency parallels elevated levels of sodium in the papilla, and the loss of the ability to concentrate urine. The dense droplets that appear in the interstitial cells following unilateral nephrectomy may be associated with the ionic imbalance that ensues (Anderson, '66).

The interstitial cells surround the capillaries in the papilla. Their cytoplasmic processes, containing dense droplets, abut the basement lamina of the vasa recta. The anatomical relationship with the vasa recta suggests that droplets may be secreted directly into the blood stream. Thus the micro-anatomy of the distal half of the papilla resembles that of an endocrine gland.

ACKNOWLEDGMENTS

The author is grateful to Drs. Richard A. Ellis, Richard J Goss, and Elizabeth H Leduc for their advice and encouragement during the course of this study and to Dr Richard A. Ellis for reviewing the manuscript. This investigation was supported by a Public Health Service research grant (GM-08380-05) awarded to Dr. R. A. Ellis.

LITERATURE CITED

Anderson, W A. 1964 Ultrastructural changes in the kidney tubule cells following unilateral nephrectomy Anat. Rec., 151 440.

——— 1965 Cellular changes in the glomerulus and epithelial cells in the kidney after unilateral nephrectomy J Cell Biol., 27 124A.

——— 1966 The fine structure of compensatory growth in the rat kidney after unilateral nephrectomy Thesis, Brown University Providence, Rhode Island.

Anderson, W A., A. Weissman and R. A. Ellis 1966 A comparative study of microtubules in some vertebrate and invertebrate cells. Z. Zellforch., 71 1–13.

Becker, F F and B. P Lane 1965 Regeneration of the mammalian liver. I. Auto-phagocytosis during dedifferentiation of the liver cell in preparation for cell division. Am. J Path., 47 783–801.

Behnke, O. 1964 A preliminary report on "microtubules in differentiated and undifferenti-

ated vertebrate cells. J Ultrastruc. Res., *11:* 139–146.

——— 1965 Helical filaments in rat liver mitochondria Exp Cell Res., *37:* 687–689

Bulger R., L. D Griffith and B F Trump 1966 Endoplasmic reticulum in rat renal interstitial cells: molecular rearrangement after water deprivation. Science *151:* 83–86.

Burgos M. H., and D Fawcett 1955 Studies on the fine structure of the mammalian testis. I Differentiation of the spermatid in the cat, Felis domestica J Biophys. Biochem. Cytol., *1:* 287–299

Byers B., and K. R. Porter 1964 Oriented microtubules in elongating cells of the developing lens rudiment after induction. Proc. Nat. Acad. Sci. (Wash.) *52:* 1091–1099

Chandra S., and F R. Skelton 1964 Staining juxtaglomerular cell granules with Toluidine blue or with Basic Fuchsin for light microscopy after Epon embedding. Stain Technol., *39:* 107–110

Doyle, W L. 1960 The principal cells of the salt gland of marine birds. Exp. Cell Res., *21:* 286–293

Ericsson, J L. E. 1964 Absorption and decomposition of homologous hemoglobin in renal proximal tubular cells. An experimental light and electron microscope study Acta Path. Microbiol. Scandinavica. Suppl., 168

Farquhar M. G and G E. Palade 1960 Segregation of ferritin in glomerular protein absorption droplets. J Biophys. Biochem. Cytol., *7:* 297–303

——— 1961 Glomerular permeability II. Ferritin transfer across the glomerular capillary wall in nephrotic rats. J Exp. Med., *114* 699–716.

Fawcett, D W 1962 Physiologically significant specializations of the cell surface. Circulation, *26:* 1105–1125

——— 1966 The cell: its organelles and inclusions. In: An Atlas of Fine Structure. W B. Saunders, Philadelphia.

Friedman, M., A. Selzer H. Kreutzmann and J J Sampson 1942 The changes in the blood pressure and in the renal blood flow and glomerular filtration rate of hypertension patients following unilateral nephrectomy J Clin. Invest., *21:* 19–24

Ginetsynsky A. G 1958 Role of hyaluronidase in the reabsorption of water in renal tubules: the mechanism of action of antidiuretic hormone. Nature *182:* 1218–1219

Goss, R. J., and M. Rankin 1960 Physiological factors affecting compensatory renal hyperplasia in the rat. J Exp Zool., *145:* 209–216.

Gottschalk, C W., and M. Mylle 1959 Micropuncture study of the mammalian urinary concentrating mechanism. Am. J Physiol., *196:* 927–936.

Halliburton, I. W., and R. Y Thomson 1965 Chemical aspects of compensatory renal hypertrophy Cancer Res., *25:* 1882–1887

Karnovsky J J 1963 The fine structure of mitochondria in the frog nephron correlated with cytochrome oxidase activity Exp. Molec. Path., *2:* 347–366.

Kent G., O T Minick, E. Orfei, F I. Volini a[...] F Madera-Orsini 1965 The movement [...] iron-laden lysomes in rat liver cells [...] mitosis. Am. J Path., 46. 803–827

Kurnick, N 1955 Cytochemical changes [...] ing normal growth and compensatory hyp[...] trophy of the rat kidney J. Histochem. Cy[...] chem., 290–294

Koch, A 1960 The kidney In: Medical Phy[...] siology and Biophysics. T C. Ruch and J. [...] Fulton, eds. W B Saunders, Philadelphia.

Leak, L. V 1965 Whorled membranous str[...] tures in renal proximal tubular cells after u[...] lateral nephrectomy J Cell Biol., 27 [...]

Lee J C., and J Hopper 1965 Basic fuchsin[...] crystal violet: a rapid staining sequence [...] juxtaglomerular granular cells embedded [...] epoxy resin. Stain Technol., 40: 37–38.

Levy S. E., and A. Blalock 1938 The effe[...] of unilateral nephrectomy on the renal blo[...] flow and oxygen consumption of unanesthet[...] dogs. Am. J Physiol., 122. 609–614.

Mannweiler K., and W Bernhard 1957 [...] cherches ultrastructurales sur une tumeur [...] nale experimentale du hamster. J. Ultrast[...] Res., *1:* 158–169

Mercer E. H 1962 The evolution of [...] cellular phospholipid membrane system. [...] The Interpretation of Ultrastructure [...] R. J C. Harris, ed. Academic Press, New Y[...]

Novikoff A. B., E. Essner S. Goldfischer [...] M. Heus 1962 Nucleosidephosphatase a[...] ities of cytomembranes. In: The Interpreta[...] tion of Ultrastructure Research, R. J. C. Harr[...] ed. Academic Press, New York.

Novikoff A. B., and V Potter 1948 Biochem[...] ical studies on regenerating liver. J. Bi[...] Chem., *173:* 223–232.

Oliver J., W Strauss, N Kretschmer Y C. L[...] H Dickerman and F Cherot 1955 The his[...] chemical characteristics of absorption drop[...] in the nephron. J Histochem. Cytochem., [...] 277–283

Pappas G., and G K. Smelser 1958 Studies [...] the ciliary epithelium of the zonule. I. E[...] tron microscope observations on the chang[...] induced by alteration of normal aqueous h[...] mor formation in the rabbit. Am. J. Ophthal[...] 46 299–318.

Pease, D C. 1955 Electron microscopy of [...] tubular cells of the kidney cortex. Anat. Re[...] *121:* 733–744

Reiter R. J and C. E. McCreight 1965 A st[...] of induced renal hyperplasia using au[...] radiography J Urology 93: 27–29.

Reynolds, E. S. 1963 The use of lead cit[...] as an electron dense stain in electron micr[...] copy J Cell Biol., *17:* 208–212.

Rhodin, J A. G 1958 Anatomy of kidney tub[...] les. Intern. Rev Cytol., 7: 485–534

——— 1962 The diaphragm of capillary en[...] thelial fenestrations. J Ultrastructure Res., [...] 171–175

Schantz, A., and A. J Schecter 1964 A rap[...] polychrome stain of epon embedded tissue [...] light microscopy Paper distributed at [...] Fourth Annual Meeting American Society [...] Cell Biology Cleveland (mimeographed).

...dt-Nielsen, B., and R. O'dell 1961 Structure and concentrating mechanism in the mammalian kidney Am. J Physiol., 200: 1119–1124.

...h, H. W 1951 The Kidney Structure and Function in Health and Disease. Oxford University Press, New York.

...pe, B., R. Straus and F Fitch 1960 Zonal renal papillary droplets change with potassium depletion. Archiv Path., 70 599–613.

...nberg, W K., E. Farber and C. E. Dunlap 1956 Histochemical localization of specific oxidative enzymes. II. Localization of diphosphopyridine nucleotide and triphosphopyridine nucleotide diaphorases in the succindehydrogenase system in the kidney J Histochem. Cytochem., 4: 267–283.

...s, W 1957 Segregation of an intravenously injected protein by "droplets of cells of rat kidneys. J Biophys. Biochem. Cytol., 3 ...937–1940.

——— 1964 Cytochemical observations on the relationship between lysosomes and phagosomes in kidney and liver by combined staining for acid phosphatase and intravenously injected horseradish peroxidase. J Cell Biol., 20: 497–507

Tandler B., and F H. Shipkey 1964 Ultrastructure of Warthin's Tumor I. Mitochondria. J Ultrastruc. Res., 11 292–305.

Trump B. F., and J L. E. Ericsson 1965 The effect of the fixative solution on the ultrastructure of cells and tissues. A comparative analysis with particular attention to the proximal convoluted tubules of the rat kidney Lab. Invest., 14 507–585.

Voelz, H. G., and M. Dworkin 1962 Fine structure of *Myxococcus xanthus* during morphogenesis. J Bact., 84 943–952.

Wilde, C. E. 1959 Differentiation in response to the biochemical environment. Proc. Soc. Study Develop. Growth, 17 3–43.

——— 1961 The differentiation of vertebrate pigment cells. Advan. Morphogenesis, 1 267–300.

Williams, G. E. G. 1961 Some aspects of compensatory hyperplasia of the kidney Brit. J Exp. Path., 42: 386–396.

Wills, E. J 1965 Crystalline structures in the mitochondria of normal human liver parenchymal cells. J Cell Biol., 24 511–514.

Young, D., and S. L. Wissig 1964 A histologic description of certain epithelial and vascular structures in the kidney of the normal rat. Am. J Anat., 115 43–70.

PLATE 1

EXPLANATION OF FIGURES

1 The apical regions of several proximal tubule cells of the normal rat kidney are illustrated in this micrograph. Microvilli extend into the lumen and the cytoplasm contains elongate mitochondria, small vesicles containing dense material (v) and clear apical vacuoles (V). × 14,000

2 Basal infoldings of the plasmalemma and interdigitations of cell processes containing elongate mitochondria and clusters of ribosomes abut the basement lamina of proximal tubule cells from the normal rat kidney. A portion of an endothelial cell underlies the basement lamina. × 18 000.

3 At 24 hours after unilateral nephrectomy (*24 hours*) the cells of the proximal tubules (PT) have increased greatly in size and mitochondria are randomly distributed in the clear cytoplasm of the enlarged cells. One micron thick Epon-Araldite section. × 450.

on A. Anderson



PLATE 2

EXPLANATION OF FIGURES

4 Light micrograph of a 0.5 μ-thick Epon-Araldite section of the outer cortex of the rat kidney at 36 *hours*. An extensively hypertrophied proximal tubule cell is illustrated. × 600

5 In a hypertrophied proximal tubules cell from the outer cortex, at 24 *hours* the basal surface is flattened and few mitochondria are randomly distributed in the ribosome-rich cytoplasm of the cell. Dilated cisternae of the Golgi apparatus (G) and the endoplasmic reticulum and a few apical vacuoles (V) lie beneath the microvilli. × 13,200.

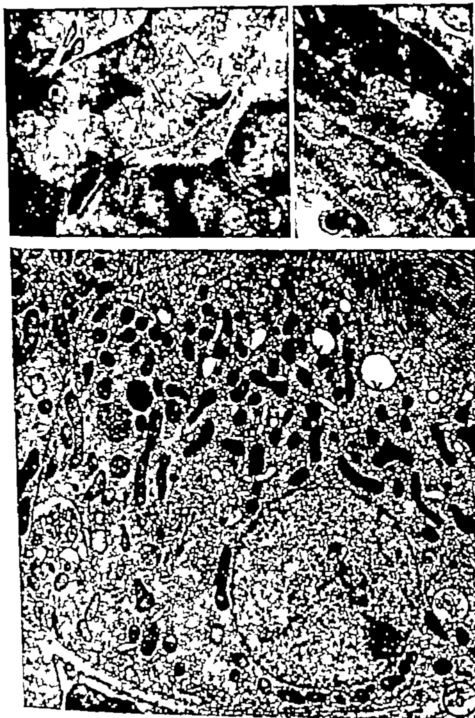


PLATE 3

EXPLANATION OF FIGURES

6 In transverse section a proximal tubule cell shows numerous microtubules (arrows) running parallel to the baso-apical axis of the cell. × 24 000.

7 Microtubules (arrows) are surrounded by clear cytoplasm at the apex of a proximal tubule cell at 72 *hours*. Numerous Golgi membranes occupy the cytoplasm of this hypertrophic cell. × 30 000.

PLATE 3

EXPLANATION OF FIGURES

6 In transverse section a proximal tubule cell shows numerous microtubules (arrows) running parallel to the baso-apical axis of the cell. × 24 000

7 Microtubules (arrows) are surrounded by clear cytoplasm at the apex of a proximal tubule cell at 72 hours. Numerous Golgi membranes occupy the cytoplasm of this hypertrophic cell. × 30,000.



PLATE 4

EXPLANATION OF FIGURES

8 The basement lamina (arrow) transects a proximal tubule cell and makes contact with the apical surface of the tubule. Numerous microvilli occupy the surface of the proximal tubule cell. The cell surface next to the involuted basement lamina is flattened. × 7,250.

9 A portion of the basement lamina involutes the cytoplasm at the base of a proximal tubule cell. Membranes arising from the plasmalemma next to the basement lamina extend into the ribosome-rich basal cytoplasm. × 18 000



PLATE 5

EXPLANATION OF FIGURES

10 This micrograph illustrates some of the typical organization of a distal tubule cell from the normal rat kidney. Some rough endoplasmic reticulum and dilated Golgi cisternae occupy the perinuclear cytoplasm and the extensive infoldings of the plasmalemma contain elongate mitochondria. × 16,200

11 In an electron micrograph of a distal tubule cell from a hypertrophic rat kidney at *24 hours* dilated cisternae of the Golgi apparatus are present in the clear cytoplasm at the cell apex. Small membrane-limited vesicles line the plasmalemma at the apex of this enlarged cell. Elongate mitochondria still occupy the basal infoldings of the plasma membrane. × 14,200.

10

11

PLATE 6

EXPLANATION OF FIGURES

12 In this electron micrograph of a distal tubule cell undergoing mitosis at 48 hours after unilateral nephrectomy (*48 hours*) the chromosomes (Cb) are restricted to the clear ribosome-rich cytoplasm at the cell apex. Membrane-limited vesicles (arrows) pervade the cytoplasm next to the *apical* surface. The basal infoldings of the plasmalemma, which encase large elongate mitochondria, persist in the dividing cell. × 12,500

13 At *40 hours* numerous binucleate cells appear in the distal tubules of the hypertrophic kidney. The extensions of the plasmalemma contain elongate mitochondria, however small rounded mitochondria also occupy the ribosome-rich cytoplasm around the nuclei. ×13,300.

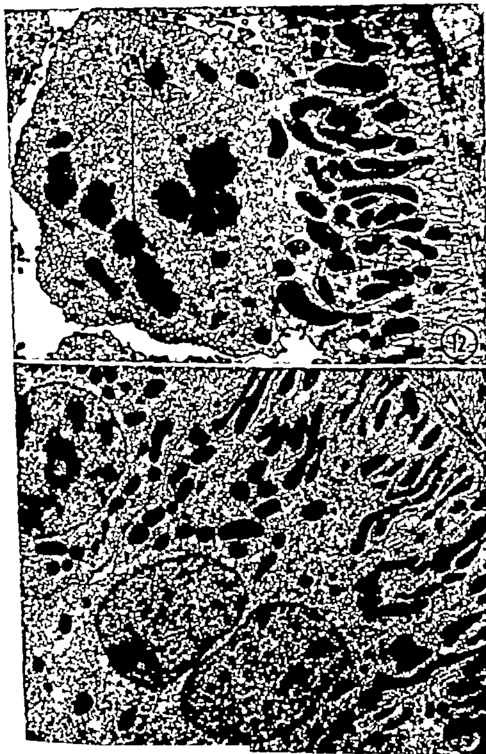

12

PLATE 7

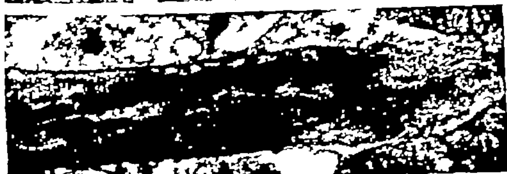
EXPLANATION OF FIGURES

14–18 These electron micrographs of mitochondria are from enlarged distal tubule cells. The atypical mitochondria are larger than normal and contain few cristae. During the early stages of crystallization of the mitochondria, patches of filamentous elements occupy the dense matrix (fig. 14) but at later stages the mitochondria are completely filled with crystalline elements (figs. 15 17 18). Helical membranes are also present in some atypical mitochondria. Figs. 14–17 × 18 000; fig. 18 × 25,000.


14


15


16




18

PLATE 8

EXPLANATION OF FIGURES

19 In this electron micrograph of a hypertrophic intercalated cell from the cortex of the enlarged rat kidney numerous mitochondria are distributed randomly in the ribosome-rich cytoplasm that surrounds the nucleus. The apical cytoplasm is filled with vesicles and the basal plasma membrane is markedly invaginated. × 13,000

20 At *24 hours* a mitochondria-rich intercalated cell from the cortex of the hypertrophic kidney is undergoing cell division. The chromosomes are restricted to the poles of the cell at anaphase and the mitochondria are chiefly located in the peripheral cytoplasm of this dividing cell The dividing cell is attached to adjacent intercalated cells by small attachment plaques. × 11 000.



20

PLATE 8

EXPLANATION OF FIGURES

19 In this electron micrograph of a hypertrophic intercalated cell from the cortex of the enlarged rat kidney numerous mitochondria are distributed randomly in the ribosome-rich cytoplasm that surrounds the nucleus. The apical cytoplasm is filled with vesicles and the basal plasma membrane is markedly invaginated. × 13,000.

20 At *24 hours* a mitochondria-rich intercalated cell from the cortex of the hypertrophic kidney is undergoing cell division. The chromosomes are restricted to the poles of the cell at anaphase and the mitochondria are chiefly located in the peripheral cytoplasm of this dividing cell The dividing cell is attached to adjacent intercalated cells by small attachment plaques. × 11 000


21

PLATE 8

EXPLANATION OF FIGURE

21 The extensive infoldings of the plasmalemma at the base of an enlarged collecting tubule cell from the cortex of the hypertrophic kidney is illustrated in this micrograph. Numerous small mitochondria occupy some of the cytoplasmic processes and a thick basement lamina separates the base of the cell from the fenestrated endothelium of the intertubular capillaries. × 9 000.


22


24


25



PLATE 10

EXPLANATION OF FIGURES

22 In this electron micrograph of a capsular epithelial cell, the basal foot processes (FP) contain dense filamentous material. The amorphous basement lamina material does not completely fill the incursions of the plasma membrane × 18,000.

23 Basal foot processes (arrows) that arise from a capsular epithelial cell appear in this light micrograph of a portion of the rat glomerulus at *40 hours*. The basal extensions are most prominent beneath the nucleus, but are also present in regions of the cell away from the nucleus. *Half* micron-thick Epon-Araldite section stained with toluidine blue × 2,000.

24 Thin filaments appear in the base of a capsular epithelial cell at *48 hours*. A prominent Golgi apparatus is present in the cytoplasm beside an enlarged nucleus. × 18,000.

25 In a highly magnified portion of the previous micrograph, the thin filaments at the base of the capsular epithelial cell are cut transversely. In transverse section the filaments range from 30–50 Å in diameter and they occupy the ribosome-rich cytoplasm at the base of this cell. Few microtubules lie close to the filaments. × 38,000.


22


25


24



PLATE 10

EXPLANATION OF FIGURES

22 In this electron micrograph of a capsular epithelial cell, the basal *foot processes* (FP) contain dense filamentous material. The amorphous basement lamina material does not completely fill the incursions of the plasma membrane. × 18 000.

23 Basal foot processes (arrows) that arise from a capsular epithelial cell appear in this light micrograph of a portion of the rat glomerulus at *40 hours*. The basal extensions are most prominent beneath the nucleus, but are also present in regions of the cell away from the nucleus. *Half* micron-thick Epon-Araldite section stained with toluidine blue. × 2,000

24 Thin filaments appear in the base of a capsular epithelial cell at *48 hours*. A prominent Golgi apparatus is present in the cytoplasm beside an enlarged nucleus. × 18 000

25 In a highly magnified portion of the previous micrograph, the thin filaments at the base of the capsular epithelial cell are cut transversely. In transverse section the filaments range from 30–50 Å in diameter and they occupy the ribosome-rich cytoplasm at the base of this cell. Few microtubules lie close to the filaments. × 35,000.

nduction of Ovulation in the Pregnant Hamster

GILBERT S. GREENWALD
Departments of Obstetrics and Gynecology and Anatomy
University of Kansas School of Medicine Kansas City Kansas

ABSTRACT Pregnant hamsters consistently ovulated when injected with 20 IU of human chorionic gonadotropin (HCG) The induced ovulation rate from days 4–8 of pregnancy was comparable to that observed during the estrous cycle; however starting at day 10, a marked increase occurred, culminating in a peak of 35 ova at day 12. Animals injected with HCG on day 16, the day before delivery ovulated an average of 14.5 ova, although spontaneous postpartum ovulation does not occur in the hamster. The number of ovulations induced by HCG correlated with the varying number of antral follicles present during different stages of pregnancy

Unilaterally ovariectomized pregnant hamsters did not show a compensatory increase in induced ovulation rate in the remaining ovary

The induction of ovulation on days 4 or 10 of pregnancy did not interfere with embryonic development nor influence the time of parturition. Following parturition, the primary and induced corpora lutea regressed synchronously

A recent quantitative study of the ovary of the pregnant hamster revealed that follicular development is divided into two phases (Greenwald, '64) During the first eight days of pregnancy the number of antral follicles is comparable to the number maturing during the estrous cycle However by day 12 of gestation the number of antral follicles is doubled. These morphologic differences are reflected in the ovulatability of large follicles Injection of human chorionic gonadotropin (HCG) at day 4 results in the ovulation of ten ova whereas similar treatment at day 12 induces the ovulation of 35 eggs

The present study is an extension of the previous findings and has two major objectives 1) To correlate throughout pregnancy the number of ova ovulated following HCG administration, with the known size distribution of follicles (Greenwald, '64) 2) To determine the effects of induced ovulation on the histologic development of the corpora lutea vera and on the course of pregnancy and the onset of parturition.

MATERIALS AND METHODS

A total of 120 pregnant hamsters was used in the experiments. In this paper day 1 of pregnancy designates the morning that sperm were present in the vaginal smear and day 1 of lactation corresponds to the morning of parturition. The animals were injected subcutaneously with 20 IU HCG (in 0 1 ml normal saline) between 9 and 10 AM at various intervals during pregnancy (table 1) The hamsters were killed with an overdose of ether the morning after the injection of HCG and the oviducts were flushed with saline via the ostium tubae abdominale The recovered ova were counted with a dissecting microscope at a magnification of 15× Hyaluronidase was added to the medium if granulosa cells were still adherent to the ova

Additional groups of hamsters were injected with HCG on either day 4 or 10 of pregnancy Subsequently two animals were sacrificed at two day intervals for each group and the viability of embryos assessed by the size of embryonic swellings and at later stages by fetal heart beat. Four animals were allowed to go to term in each series and the duration of pregnancy was compared with that of untreated hamsters.

Representative ovaries for all experiments were serially sectioned at 10 µ and stained with hematoxylin and eosin.

RESULTS

Induction of ovulation during pregnancy Injection of HCG at day 2 resulted in ovulation in four of six hamsters but at a reduced level (table 1) Fertilized ova of the preceding ovulation were still present in the oviduct on the morning of *day 3* the ova ovulated by HCG were

—
ANAT., 121 249–258.



Fig. 2 HCG injected on day 6 of pregnancy; hamster ovary on day 9. An increased number of small antral follicles (AF) is present. × 27.5.

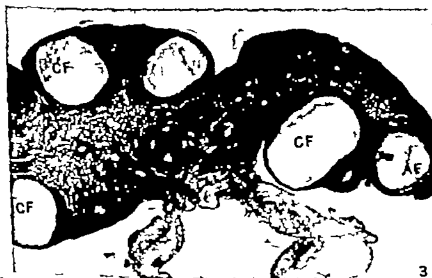


Fig. 3 HCG injected on day 9 of pregnancy; hamster ovary on day 10. An increased number of cystic follicles (CF) is present. The normal antral follicles (AF) have increased in size but are still too small to respond to HCG. × 27.5.

from hamsters injected with HCG on day of lactation (table 1).

Previous studies from this laboratory have dealt with compensatory ovulation in the hamster during the normal estrous cycle (Greenwald, '61) and following the administration of pregnant mares' serum (PMS) in a dose which leads to superovulation (Greenwald, '62). It was therefore of interest to determine whether unilaterally ovariectomized hamsters could also increase the ovulation rate of the remaining ovary in the presence of functional corpora lutea. Accordingly ham-

TABLE 1
Induction of ovulation in the pregnant hamster by 20 IU HCG

Day of pregnancy HCG injected	No. of animals	No. of animals ovulating	Mean no. of ovulations ($\pm$ SE$_m$)
2	6	4	5.3 ± 0.75
4	6	6	10.3 ± 0 67
6	4	4	11.3 ± 0.95
8	4	4	13.8 ± 1.31
9	9	9	8.0 ± 1 01
10	8	8	23 0 ± 2.3
12	6	6	35.5 ± 3 74
13	8	8	27.0 ± 4.5
14	8	6	18.2 ± 4.52
15	6	6	18.2 ± 3.52
16	9	8	14 5 ± 2.93
Parturition (Day 1 L)	4	1	1 0

readily distinguishable inasmuch as they were unfertilized and were usually still surrounded by granulosa cells

The average number of ovulations induced from days 4 through 8 of pregnancy was within the range ovulated at estrus However distinctive histologic changes were apparent between the HCG-stimulated ovaries on days 6 and 8 of gestation The morning after HCG administration on day 6 the ovaries contained a few large unovulated follicles (fig 1) In contrast, on day 8 ovaries following HCG contained a greater number of cystic unovulated follicles plus numerous small antral follicles (fig 2) which were rare on day 6

When HCG was injected at day 9, the ovulation rate was significantly reduced from the previous days (table 1). Histologic examination of the ovaries revealed an increased number of cystic follicles and normal antral follicles which were too small to respond to HCG (fig 3).

A dramatic increase in induced ovulation occurred between days 9 and 10, of pregnancy The increase culminated in a peak on day 12, with a gradual subsidence thereafter Beginning on day 13, there was considerable individual variation in the ovulatory response to HCG as attested by the large standard errors

Administration of the standard dose of HCG at day 16 (the day before delivery) induced ovulation in eight of nine hamsters with a range of 1–18 ova. Of the nine animals injected on day 16, seven delivered by 2 PM the next day The remaining two animals had dead embryos in *utero* when killed at 2 PM and ovulated only one and four eggs, respectively the lowest numbers encountered in the group. Only one newly ovulated egg was recovered



Fig 1 HCG injected on day 6 of pregnancy hamster ovary on day 7 Note initial corpora lutea (CL I) induced corpora lutea (CL II) cystic follicle (CF) and small antral follicle (AF) × 27.5.

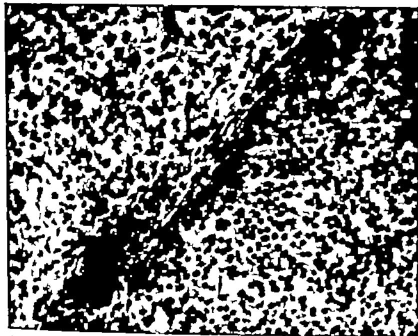


Fig. 5. HCG injected on day 10; hamster ovary on day 12. Compare the two sets of corpora lutea.

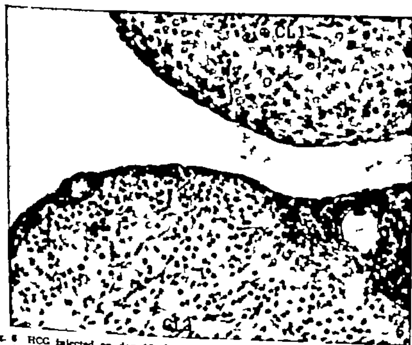


Fig. 6. HCG injected on day 10; hamster ovary on the day of parturition. There are distinctive histologic differences between the two generations of corpora lutea.

TABLE 2

Induction of ovulation following unilateral ovariectomy at day 1 of pregnancy

Day 20 IU HCG injected	Ovulation from remaining ovary (Mean ± SE)	Ovulation when both ovaries present[1] (Mean ± SE)
4	11 0 ± 0 24 (6)[2]	10.3 ± 0 67 (6)
8	9.3 ± 1 0 (6)	13.8 ± 1.3 (4)
12	9.8 ± 1.3 (5)	35.5 ± 3 7 (6)

[1] Data from table 1

[2] Number of animals in parentheses.

sters were unilaterally ovariectomized on day 1 of pregnancy and then injected with 20 IU HCG on either days 4 8 or 12 The results indicate that the semispayed ani mals ovulated the same number of ova at days 4 8 or 12 of pregnancy and that the latter group failed to approach the ovula tion rate of 35 ova which occurred when both ovaries were present (table 2)

Collectively the above experiments sug gested that several waves of follicles arose during pregnancy and that the follicles ovulated by HCG at day 12 might represent a different proliferation from those present at day 4 To test this possibility hamsters were given HCG on day 4 followed by a second injection at day 12. If the above theory was correct, it appeared likely that these animals should still ovulate 35 eggs. In reality seven hamsters ovulated only 10 0 ± 1 3 eggs after such treatment.

Injection of HCG at day 4 or 10 and subsequent reproductive activity These experiments were designed to determine the long range effects of induced ovulation on pregnancy When HCG was administered on day 4 by day 6 two generations of corpora lutea could be distinguished the initial natural corpora lutea (CL I) and those originating from the induced ovulation (CL II) The CL I were more eosinophilic and contained sparse scattered leucocytes which are usually an early sign of degeneration of hamster corpora lutea. The CL II were more vascular with the luteal cells arranged in discrete lobules surrounded by sinusoids The nuclei of CL I were larger than those of CL II (fig 4) By day 8 the corpora lutea were indistinguishable The regressive changes in CL I



Fig 4 HCG injected on day 4 of pregnancy (day 4); hamster ovary on day 6. The initial corpus luteum (CL I) is lighter and contains larger nuclei than the induced corpus luteum (CL II)

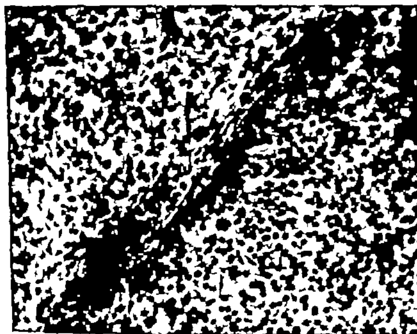


Fig. 5 HCG injected on day 10; hamster ovary on day 12. Compare the two sets of corpora lutea.



Fig. 6 HCG injected on day 10; hamster ovary on the day of parturition. There are distinctive histologic differences between the two generations of corpora lutea.

TABLE 2

Induction of ovulation following unilateral ovariectomy at day 1 of pregnancy

Day 20 IU HCG injected	Ovulation from remaining ovary (Mean ± SE)	Ovulation when both ovaries present[1] (Mean ± SE)
4	11 0±0.24(6)[2]	10.3±0 67(6)
8	9.3±1 0 (6)	13.8±1.3 (4)
12	9.8±1.3 (5)	35.5±3 7 (6)

[1] Data from table 1
[2] Number of animals in parentheses.

sters were unilaterally ovariectomized on day 1 of pregnancy and then injected with 20 IU HCG on either days 4 8 or 12. The results indicate that the semispayed ani mals ovulated the same number of ova at days 4 8 or 12 of pregnancy and that the latter group failed to approach the ovula tion rate of 35 ova which occurred when both ovaries were present (table 2)

Collectively the above experiments sug gested that several waves of follicles arose during pregnancy and that the follicles ovulated by HCG at day 12 might represent a different proliferation from those present at day 4 To test this possibility ham were given HCG on day 4 followed b second injection at day 12. If the t theory was correct, it appeared likely these animals should still ovulate 35 e In reality seven hamsters ovulated 10 0 ± 1 3 eggs after such treatment.

Injection of HCG at day 4 or 10 and sequent reproductive activity The perlments were designed to determin long range effects of induced ovulatio pregnancy When HCG was administer on day 4 by day 6 two generations corpora lutea could be distinguished. t initial, natural corpora lutea (CL I) those originating from the induced ov tion (CL II) The CL I were more eo philic and contained sparse, scattered l cocytes which are usually an early sig degeneration of hamster corpora lutea. CL II were more vascular with the lu cells arranged in discrete lobules s rounded by sinusoids The nuclei of C were larger than those of CL II (fig. By day 8 the corpora lutea were indi guishable The regressive changes in C



Fig. 4 HCG injected on day 4 of pregnancy (day 4) hamster ovary on day 6. The initi corpus luteum (CL I) is lighter and contains larger nuclei than the induced corpus luteu (CL II)

n the present study pregnant hamsters laterally ovariectomized at day 1 and sequently injected with HCG at days 8 or 12 ovulated 9 – 12 ova from the maining ovary (table 2). The failure of ispayed hamsters injected at day 12 ovulate 35 ova was at first unexpected ce cyclic hamsters injected with PMS t ovulate this number of eggs (Green ld, '62)

However several factors differ between PMS-treated hamsters and the present ervations; for one thing the much ter time elapsing between semi-spaying d ovulation and more importantly the sence of the functional corpora lutea as posed to the relatively inactive corpora ea of the estrous cycle. Similarly com- satory hypertrophy of the remaining ry is absent after unilateral ovlectomy the pseudopregnant rat but the phenom- on is exhibited by the cyclic animal Rothchild and Dickey '60) Moreover mpensatory hypertrophy is not observed hemicastrated cyclic rats injected with trogens or progesterone (Peterson, Ed- ton and Jones '64)

The variation in the number of ova ulated after HCG treatment and the anges in ovarian histology between days and 8 indicate that several waves of fol les arise during pregnancy in the ham- er. Thus, the follicles ovulated at day 16 gestation by HCG were most likely not esent as antral follicles during the first alf of pregnancy A life span of approxi ately eight days for antral follicles is nsistent with the data.

It was thought that the presence of veral waves of follicular proliferation uring pregnancy could be demonstrated giving more than one injection of HCG. or example administration of HCG at oth days 4 and 12 of gestation. However ter such treatment, hamsters ovulated nly ten ova compared to 35 eggs when the le injection of HCG was given at day 12. he reasons for the significant drop in vulation are unknown. Inasmuch as HCG a foreign protein, it is possible that the varies may have become partially refrac- ory due to the development of an antibody esponse. Following the injection of HCG t day 4 the ovaries on day 12 of preg nancy contained considerably more antral follicles than the number which actually ovulated. Hence the initial injection of HCG at day 4 did not prevent the antici- pated growth of small antral follicles be- tween days 6 and 8.

A previous quantitative study of the pregnant hamster plotted the size distri bution of follicles per ovary (Greenwald, '64) In the present study pregnant ham- sters given HCG on day 2 ovulated an aver age of 5 3 ova (table 1) The largest fol- licles present at this stage which could account for such an ovulatory rate are 415 μ and larger in diameter It was there- fore of interest to recalculate the previous data (Greenwald, '64) to determine the number of follicles in both ovaries larger than 415 μ throughout pregnancy com- pared to the number of ovulations induced by HCG. The results summarized in fig- ure 7 indicate excellent agreement be tween actual ovulations and follicular num- bers with two notable exceptions. On day 14 the ovaries contain an average of 34 *histologically* normal follicles but the aver age number of induced ovulations is only 18 The HCG-stimulated ovaries contain a number of very large unovulated follicles. The discrepancy between ovulation and follicle numbers may therefore represent failure of ovulation of the larger and pre- sumably older stages. Thus the normalcy of follicles as judged by histological cri- teria may not necessarily reflect their abil ity to ovulate. It is of interest that the ovaries on day 14 have an average of 12 follicles larger than 550 μ, which are atre- tic by day 16 (Greenwald, '64)

A disparity between the number of an- tral follicles and ovulatability also exists

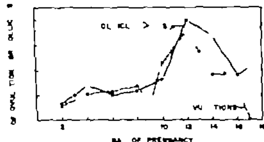


Fig. 7 Correlation between the number of ovulations induced by HCG and the number of follicles larger than 415 μ in diameter in the pregnant hamster

had been checked and there was no dichotomy in size which would facilitate differentiation of the two sets of corpora lutea If histologic differences existed between the corpora lutea they were too subtle to be detected with hematoxylin and eosin staining By day 10 — and until delivery — excellent follicular development was noted comparable to that observed in normal pregnancy

The corpora lutea of pregnancy begin a second growth phase at day 12 to reach their maximal size on day 16 (Greenwald Keever and Grady '67) When ovulation was induced at day 4 an increase in size of corpora lutea was also observed at day 12 but there appeared to be no difference in the sizes attained by CL I and CL II

The induction of ovulation at day 4 did not affect embryonic development nor delay the time of parturition Of four hamsters with induced corpora lutea at day 4 one delivered on the afternoon of day 16 the remaining animals gave birth by the next morning This is within the normal range of parturition Litter size was similarly unaffected by induced ovulation

By the morning of parturition (i e day 1 of lactation) the first regressive changes were observed in all corpora lutea loss of gross vascularity beginning of leucocytic infiltration and shrinkage of individual luteal cells Thus the induced corpora lutea which were 12 days old degenerated at the same time as the corpora lutea vera

Induction of ovulation on day 10 occurred at a stage when CL I were well differentiated By day 12, two definite sizes of corpora lutea were present Histologically CL I were larger and more eosinophilic whereas CL II consisted of lobulated masses of luteal cells which were basophilic (fig 5) These differences existed throughout the duration of pregnancy The CL II lagged considerably behind the growth rate of CL I The luteal cells of CL II were characterized by less cytoplasm and retained the histologic features of early immature corpora lutea throughout pregnancy Large antral follicles were unaffected by the second ovulation and proliferated throughout gestation

Ovulation induced at day 10 also failed to interrupt pregnancy Two animals delivered on day 16 and two others delivered by the next morning. The ovaries on day 1 of lactation contained CL II which had regressed more rapidly than CL I. The CL II had a vacuolated cytoplasm and showed incipient pycnotic changes (fig. 6) The CL I although invaded by a few leucocytes, were still much better preserved than the induced corpora lutea.

It is of interest that the ova ovulated on days 4 and 10 were retained in the oviducts throughout gestation. The eggs were lysed within a few days after the induced ovulation but the much more resistant zonae pellucidae persisted until parturition The extreme example was provided by the presence of tube-locked zonae pellucidae on the morning of parturition in animals which received HCG on day 4 of pregnancy

DISCUSSION

The pregnant hamster is capable of ovulating as early as 48 hours after the establishment of pregnancy (table 1). In contrast the mouse ovary is refractory to HCG during the first three days of gestation (Burdick and Ciampa, 44) the rabbit is also refractory during the first three or four days after ovulation (Snyder and Wislocki '31 Spies, Coon and Gier '65)

During the first eight days of pregnancy the hamster can be induced to ovulate approximately ten ova but a significant decline occurs on administration of HCG on day 9 The drop in ovulation is correlated with an increasing number of large cystic follicles which undergo some of the histological changes associated with ovulation (e g dispersal of the cumulus oophorus) but fail to rupture. It appears likely that these follicles on day 9 represent a senescent group which originally proliferated during the first few days of pregnancy It is of interest that a single injection of 5 mg progesterone to cyclic hamsters prolongs the life span of antral follicles to eight days (Greenwald '65a)

The sudden increase in induced ovulation on day 10 represents the development of a new crop of antral follicles which develop between days 6–8 (figs. 1 and 2) The optimal time for induced ovulation is on day 12 of gestation and this is followed by a steady decline in ovulatability of follicles throughout the remainder of pregnancy

-the present study pregnant hamsters -erally ovariectomized at day 1 and -quently injected with HCG at days -or 12 ovulated 9 – 12 ova from the -ining ovary (table 2) The failure of -payed hamsters injected at day 12 -ulate 35 ova was at first unexpected cyclic hamsters injected with PMS -ovulate this number of eggs (Green-, '62)

-owever several factors differ between PMS-treated hamsters and the present -rvations for one thing, the much -er time elapsing between semi-spaying ovulation and more importantly the ence of the functional corpora lutea as -sed to the relatively inactive corpora a of the estrous cycle. Similarly com-satory hypertrophy of the remaining -y is absent after unilateral oviectomy he pseudopregnant rat but the phenom-n is exhibited by the cyclic animal -thchild and Dickey '60) Moreover -pensatory hypertrophy is not observed -semicastrated cyclic rats injected with -ogens or progesterone (Peterson, Ed-n and Jones, '64)

The variation in the number of ova -lated after HCG treatment and the -nges in ovarian histology between days and 8 indicate that several waves of fol-les arise during pregnancy in the ham-r Thus, the follicles ovulated at day 16 gestation by HCG were most likely not -sent as antral follicles during the first lf of pregnancy A life span of approxi-ately eight days for antral follicles is -nsistent with the data.

It was thought that the presence of -eral waves of follicular proliferation -ring pregnancy could be demonstrated giving more than one injection of HCG. -r example, administration of HCG at -th days 4 and 12 of gestation. However -ter such treatment, hamsters ovulated -ly ten ova compared to 35 eggs when the -le injection of HCG was given at day 12 -e reasons for the significant drop in -ulation are unknown. Inasmuch as HCG a foreign protein, it is possible that the -aries may have become partially refrac-ry due to the development of an antibody -sponse Following the injection of HCG day 4 the ovaries on day 12 of preg-ancy contained considerably more antral follicles than the number which actually ovulated. Hence the initial injection of HCG at day 4 did not prevent the antici pated growth of small antral follicles between days 6 and 8

A previous quantitative study of the pregnant hamster plotted the size distri bution of follicles per ovary (Greenwald '64) In the present study pregnant hamsters given HCG on day 2 ovulated an aver age of 5 3 ova (table 1) The largest fol licles present at this stage which could account for such an ovulatory rate are 415 μ and larger in diameter It was therefore of interest to recalculate the previous data (Greenwald, '64) to determine the number of follicles in both ovaries larger than 415 μ throughout pregnancy compared to the number of ovulations induced by HCG The results summarized in fig ure 7 indicate excellent agreement between actual ovulations and follicular numbers with two notable exceptions On day 14 the ovaries contain an average of 34 *histologically* normal follicles but the average number of induced ovulations is only 18 The HCG-stimulated ovaries contain a number of very large unovulated follicles. The discrepancy between ovulation and follicle numbers may therefore represent failure of ovulation of the larger and presumably older stages. Thus the normalcy of follicles as judged by histological cri teria may not necessarily reflect their abil ity to ovulate. It is of interest that the ovaries on day 14 have an average of 12 follicles larger than 550 μ, which are atretic by day 16 (Greenwald '64)

A disparity between the number of antral follicles and ovulatability also exists

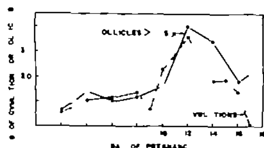


Fig. 7 Correlation between the number of ovulations induced by HCG and the number of follicles larger than 415 μ in diameter in the pregnant hamster

on the morning of parturition (day 1 of lactation) (fig 7) It also appears likely that these follicles are undergoing incipient atresia which cannot be discerned with hematoxylin and eosin Presumptive evidence for this conclusion is provided by the fact that on day 1 of lactation atresia destroyed all follicles in one of three ovaries examined (Greenwald 64) by the following morning degenerating antral follicles were present in all ovaries (Greenwald 65b)

An intriguing point is raised by the last paragraph Ovulation is induced in almost all hamsters treated with HCG on day 16 and yet spontaneous ovulation does not occur in the post parturient hamster This contrasts with the characteristic postpartum ovulation observed in other species of laboratory rodents (Asdell 64) which has been most thoroughly evaluated in the rat (for references see Hoffman and Schwartz 65) It appears likely that differences in the pattern of follicular development and pituitary gonadotropins in the hamster and rat account for the absence of postpartum ovulation in the former species

The rat does not have a significant increase in the number of vesicular follicles during the latter half of gestation in contrast to the hamster (Greenwald '66) In the rat a significant shift does not occur in the size of follicles until day 22 of pregnancy the renewed growth at this time is undoubtedly related to preparation for post partum ovulation Moreover the rat ovary is refractory to HCG until day 21 of pregnancy which correlates with the growth spurt of follicles at day 22

During the last week of gestation the pituitary of the rat contains considerably more FSH than LH (Greenwald 66) The FSH is discharged between day 22 of pregnancy and parturition the LH is presumably released at a later time for postpartum ovulation

The gonadotropic pattern of the pregnant hamster (Greenwald Keever Grady 67) is diametrically opposed to that found in the rat. The hamster pituitary has its highest values of LH shortly before delivery when FSH is comparatively low At parturition pituitary FSH rises and LH drops but plasma values of LH increase The assumed peripheral withdrawal of FSH and increase in LH probably is re- sponsible for the absence of postpartum ovulation in the hamster A similar ex- planation apparently accounts for the ab- sence of postpartum ovulation in the se- (Lauderdale et al. '65)

In the present study induced corpo- lutea did not prolong the duration of pregnancy The onset of parturition is al- unaffected by induced ovulation in la- pregnancy in the guinea pig (Rowland 56) and mouse (Burdick and Crump '51 On the other hand parturition is delay- until day 40 in the rabbit when ovulation is induced at day 25 of pregnancy (Snyder '34) The difference in the time of delivery is related to the *simultaneous* regression of both sets of corpora lutea in the fir- group of species whereas in the rabb- the induced corpora lutea have a norm- life span and regress asynchronously Asynchronous regression of corpora lu- also occurs in the pig (Neill and Day '64

It is possible that the induced corpo- lutea in the hamster guinea pig and mo- are non-functional which could acco- for their concurrent degeneration with the corpora lutea of pregnancy The functio- status of induced corpora lutea might be assessed by determining whether pre- nancy is maintained after experimental ex- tirpation of the primary corpora lutea

The previous discussion has conside- follicular development during pregnancy laboratory animals. When one considers the status of ovarian activity during pregna- in mammals in general a bewildering di- versity of follicular patterns is appare- At one extreme are species in which spo- *taneous* ovulation occurs during gestat- (*mare* Cole Howell and Hart '31 (*phant* Perry '53 *European hare:* Stie- 52 as cited by Asdell 64) In the ma- the first set of corpora lutea appare- have a limited life span and presumab- the new corpora lutea are functional u- a placental source of progestins is est- lished Some doubt on the existence multiple ovulations during pregnancy the elephant has been cast by a recent b- chemical and histological study wh- could not detect progesterone in corp- lutea removed at midpregnancy (Short a- Buss '65) The European hare repres- an even more unusual variant inasmu-

ulation is provoked by coitus. Hence are is one of the few species in which rfetation is feasible.

n other species, the corpus luteum m may be supplemented by luteiniza- of atretic follicles which are trans- ned into accessory corpora lutea. Per s the extreme situation is shown by the er shrew (Price '53) in which the pus luteum merges with luteinized in- stitial cells so that the entire ovary is nsformed into an almost solid luteal ly

Another category of follicular develop- nt is represented by the elephant shrew phantulus (van der Horst and Gillman,) in which cystic follicles accumulate roughout most of pregnancy The large stic follicles eventually disappear and, ward the end of pregnancy normal afian follicles are formed which are stined to ovulate after delivery

Finally there are species in which large ficles are present in early stages of preg- ncy thereafter the number of follicles mains constant but follicle size decreases gnificantly This is exemplified by the regnant ewe (Williams et al., '56)

At first glance, the variations in follicu- r activity in pregnant wild and domesti- ated mammals seem far removed from e patterns characteristic of laboratory ecies. However they merely accentuate atures which are shared in common with e laboratory rodents. Thus, the pregnant amster readily mates, especially during e last half of gestation (Krehbiel, '52) ut does not ovulate Ovulation can be duced during pregnancy with HCG in e guinea pig, hamster mouse and rab- it, but not in the rat. Pregnancy can be rolonged in the rabbit by an induced ovu- ation. Accessory corpora lutea develop in he ovaries of rats. All of these phenomena re paralleled by events which normally ccur in wild mammals.

A salient question raised by the present nvestigation is the role of follicular de- velopment during gestation. Growth of antral follicles towards term is understand- able in species in which postpartum ovula- tion is the rule but what is the function of follicular maturation at earlier stages of pregnancy? There appear to be three pos- sible explanations (1) Follicular develop- ment represents an inherent cycle which, although modified by the presence of func- tional corpora lutea, still persists during pregnancy (2) The development of an- tral follicles is ancillary to the primary effects of gonadotropins during gestation which are mainly directed towards the maintenance of corpora lutea. Hence, fol- licular development is extraneous and of no functional significance. (3) Follicular development during pregnancy is, in some unknown way essential for the continua- tion of pregnancy At present, there is lit tle evidence to substantiate any of these alternatives, but it is a question deserving more attention than it has received in the past.

ACKNOWLEDGMENTS

This is a contribution from the Research Professorship In Human Reproduction. The research was supported by grants from NIH(HD-00596-05) and the Ford Founda- tion. The HCG was generously provided by Ayerst Laboratories.

LITERATURE CITED

Asdell, S. A. 1964 Patterns of Mammalian Re- production. Cornell University Press, Ithaca, N Y

Burdick, H. O., and V Ciampa 1944 Further observations on induced ovulation in mice: a refractory period in early pregnancy Endo- crinology 35 473–476.

Burdick, H. O., and M. Crump 1951 The effect of induced ovulation on pregnancy Endocrino- logy 48 273–276.

Cole, H. E., C. E. Howell and G. H. Hart 1931 The changes occurring in the ovary of the mare during pregnancy Anat. Rec., 49 199–209.

Greenwald, G. S. 1961 Quantitative study of follicular development in the ovary of the in- tact or unilaterally ovariectomized hamster. J Reprod. Fert., 2: 351–361

——— 1962 Analysis of superovulation in the adult hamster. Endocrinology 71 378–389

——— 1964 Ovarian follicular development in the pregnant hamster Anat. Rec., 148 605–610.

——— 1965a The effect of a single injection of diethylstilbestrol or progesterone on the ham- ster ovary J. Endo., 33: 13–23.

——— 1965b Histologic transformation of the ovary of the lactating hamster Endocrinology 77 641–650.

——— 1966 Ovarian follicular development and pituitary FSH and LH content in the preg nant rat. Endocrinology 79 572–578.

Greenwald, G. S., J E. Keever and K. L. Grady 1967 Ovarian morphology and pituitary FSH and LH concentration in the pregnant and lactating hamster. Endocrinology 80 851–856.

Hoffman J C., and N B Schwartz 1965 Timing of post-partum ovulation in the rat. Endocrinology *76*: 620–625

van der Horst, C J., and J Gillman 1945 The behaviour of the Graafian follicle of *Elephantulus* during pregnancy with special reference to the hormonal regulation of ovarian activity S Afr J Med. Sci. Vol. *10* Bio. Suppl. 1–14

Krehbiel, R H 1952 Mating of the golden hamster during pregnancy Anat. Rec., *113*: 117–121

Louderdale J W., R. L. Kirkpatrick N L. First E. R. Hauser and L. E. Casida 1965 Ovarian and pituitary gland changes in periparturient sows J Animal Science. *24*: 1100–1103

Neill, J D., and B. N Day 1964 Relationship of developmental stage to regression of the corpus luteum in swine. Endocrinology *74* 355–360.

Perry J S 1953 The reproduction of the African elephant *Loxodonta africana*. Phil. Trans. Roy Soc. London Series B., *237*: 93–149

Peterson, D L., R. A. Edgren and R. C. Jones 1964 Steroid induced block of ovarian compensatory hypertrophy in hemicastrated female rats. J Endocrinology *29*: 255–262.

Price M 1953 The reproductive cycle of the water shrew *Neomys fodiens* bicolor Shaw Proc. Zool. Soc. London, *123*: 599–621

Rothchild, L., and R. Dickey 1960 The corpus luteum-pituitary relationship: a study of the compensatory hypertrophy of the ovary during pseudopregnancy and lactation in the rat. Endocrinology *67*: 42–47

Rowlands, I. W 1956 The corpus luteum of the guinea pig. In: Ageing in Transient Tissues, Vol. 2, C. Wolstenholme, ed. Ciba Foundation Colloquia on Ageing. pp. 69–85.

Short, R. V., and I O Buss 1965 Biochemical and histological observations on the corpora lutea of the African elephant *Loxodonta africana*. J Reprod. Fert., *9*: 61–67.

Snyder F F 1934 The prolongation of pregnancy and complications of parturition in the rabbit following induction of ovulation near term. Bull. Johns Hopkins Hosp., *54*: 1–23.

Snyder F F., and G. B. Wislocki 1931 Further observations upon the experimental production of ovulation in the rabbit. Bull. Johns Hopkins Hosp., *49*: 106–120.

Spies H G. L. L. Coon and H. T Gier 1966 Luteolytic effect of LH and HCG on the corpora lutea of pseudopregnant rabbits. Endocrinology *78*: 67–74

Williams, S M., U S. Garrigus, H. W Norton and A. V Nalbandov 1956 The occurrence of estrus in pregnant ewes. Journal Animal Science *15*: 978–983.

e Effects of Multiple Pregnancies and Age on the stic Tissue of Uterine Arteries in the Guinea Pig [1]

ERNEST N ALBERT AND B. R. BHUSSRY
Department of Anatomy Schools of Medicine and Dentistry
Georgetown University Washington, D C.

ABSTRACT Mesometrial arteries and representative areas of the uterus were obtained from young and old postpartum guinea pigs. The tissues were fixed in Bouin's solution and then stained with Taenzer's Orcein and Verhoeff's elastic stains. Picro-indigo-carmine and Van Gieson were used as counterstains.

It was found that the distribution of elastic tissue and the number of elastic and muscle layers in the arterial walls in general reflected the number of pregnancies the animal had had. This was found to be reliable only up to three pregnancies, after which the animals could be referred to only as being multiparous. There appeared to be a continuous increase in the amount of elastin in the blood vessels with each successive pregnancy. Further aged animals showed more elastin in their vessels than younger ones of comparable parity. The formation of the new internal elastic membrane appeared to be delayed in older females.

Our observations suggest that there might be a decrease in the postpartum resorption of elastin as a result of successive pregnancies and aging. They also suggest that the delay in the formation of the new internal elastic membrane in older postpartum females is probably due to aging.

The connective tissue of the uterus and associated blood vessels offer one of the ost favorable systems for studying mor hology and the anabolism and catabolism f proteins (Albert, '66). During preg ancy there is an increase of muscle and onnective tissue and during involution, apid breakdown. An increase of up to 300% has been reported by Woessner and Brewer ('63). Thus collagen and elastin proteins which are normally considered relatively inert from the viewpoint of metabolic turnover may behave in an ex tremely dynamic fashion in the uterus.

Gardner and Goodall ('06) recognized two types of changes in arteries during pregnancy. They outlined the differences between alterations in arterial walls due to parturition and to arteriosclerotic lesions.

Pankow ('06) showed that definite alterations were constantly found in the distribution of elastic tissue in the human uterus as a whole and more particularly in the blood vessels during pregnancy and postpartum involution. He also reported that the altered elastic patterns were never observed in nulliparous specimens. Goodall ('10) described the alterations in elastic tissue during involution of the human uterus. Shaw ('14) confirmed most of Goodall's observations. Schwarz ('19) reported similar changes only less marked, in endometrial blood vessels of two women with histories of early abortions. Albert ('66) showed that the internal elastic membrane of guinea pig uterine arteries was disrupted during pregnancy and re-established postpartum. Our previous observations also have shown that these alterations in the elastic tissue are seen only in the pregnant horns of unilaterally pregnant guinea pigs, thus establishing that the changes in the elastica are due to preg nancy and further that they are most prominent in the vessels supplying the placenta.

According to Pankow ('06) and Szasz-Schwarz ('03) the changes in elastic tissue are so characteristic that, by these changes alone, one may decide whether the uterus is parous or nulliparous. Maher ('59) has reported similar findings. In young humans, delicate elastic fibers have been reported which increase in thickness and amount with age as well as with parity (Valle, '35). These observations, though

[1] This study was supported in part by U. S. Public Health Service Grant [illegible] from the National Institute of Child Health and Human Development, National Institutes of Health, Bethesda, Maryland.

[2] Present address: The Jefferson Medical College Daniel Baugh Institute of Anatomy, 307 South Eleventh Street, Philadelphia, Pa. 19107

scant are significant The breakdown of the internal elastic membranes of uterine arteries during pregnancy and its reconstruction postpartum provides a good model for investigating elastogenesis The localized effects on blood vessels in unilaterally pregnant guinea pigs suggests a need for further exploration of the possible interactions between sex hormones and elastic tissue This is of particular interest now that endocrine contraceptive programs are being used widely and for long periods

This investigation was undertaken with the hope of studying the following two points

1 What morphological alteration occurs in the elastic tissue of the uterus and its blood vessels as a result of multiple pregnancies?

2. Whether the changes in the elastic tissue patterns due to pregnancy could be grouped in a more meaningful manner to help establish the parous nature of the female.

Some of the effects of the steroids used as contraceptives on the blood vessels in general and in particular on their elastic tissue will be reported later

MATERIALS AND METHODS

Three groups of guinea pigs were used for this investigation

1 Three- to four month-old virgins

2. Three- to five year-old virgins.

3 Full-term pregnant, multiparous animals.

Each of the young and old virgins were bred up to three times in our laboratory These animals along with the full-term multiparous females were sacrificed at prescribed intervals after parturition.

The mesometrial arteries supplying the placenta and corresponding areas of the uterus were dissected out and fixed in Bouin's solution. For the sake of consistency only short segments of mesometrial arteries near the uterine wall were used. The tissues were washed in running water dehydrated cleared and embedded in paraffin. Sections were cut at 6 µ thickness and stained with Taenzer's Orcein (1891) and Verhoeff's ('08) and Weigert's ('98) elastic stains. Picro-indigo-carmine and Van Gieson were used as counterstains.

OBSERVATIONS

It has been shown (Albert, '66) that the internal elastic membrane of mesometrial arteries is fragmented and removed partially or in its entirety from the arterial walls of primiparous animals during pregnancy About 15–20 days after parturition a new elastic membrane is formed. Thi simple process is somewhat complica with ensuing pregnancies. The modific tions in the elastic tissue of uterine arteri as a result of multiple pregnancies a aging are described below

A. Mesometrial arteries

1 *Arteries of nulliparous female guin pigs* The histological description of the arteries is similar to that of typical mu cular arteries (fig 1) They posses internal elastic membrane (E) and a re tively well defined circular smooth-mus media (M) and adventitia (A)

2. *Arteries of female guinea pigs wi history of one pregnancy* Arteries tained during various stages of pregna from primiparous female guinea pigs hibit a partially fragmented internal ela membrane. The extent of fragmentat will depend on the state of pregnancy nearly complete absence of elastic fib would indicate either a full-term or early postpartum primiparous animal detailed histological sequence of eve pertaining to the time and extent of fragmentation of the internal elastic m branes already have been reported (bert 66)

3 *Arteries of female guinea pigs wi history of two pregnancies* A represe tive section from the mesometrial ar supplying the placenta is shown in figu It demonstrates an internal elastic m brane (E) a media (M) and then ano thick layer of elastic tissue (T) surrou ing the media. Peripheral to the sec elastic layer another smooth muscle l (MM) is present. The entire vessel is rounded by an adventia rich in elastic sue This section was taken from the u ine artery of an animal that had delive her second set of litters 20 days prio sacrifice and one can speculate that layers of elastic tissue and two layers smooth muscle is characteristic for pregnancies

nother variation of arterial morphology a 16 day postpartum animal with a ry of two pregnancies is illustrated in e 3. There is no distinct internal elas membrane or second layer of elastic e as described previously Only fine nds of elastic fiber (E) are seen in the r portion of the vessel wall and ker fragments of elastic tissue (T) ap- t to separate the inner (M) and outer 1) circular muscle layers. One might bute the incomplete appearance of the tic tissue between the two muscle lay to the plane of the section, but serial ions support the view of an incomplete r The adventitia contains the usual unt of elastic fibers

n other cases of animals with two preg cies, the elastic layers which reformed r the first pregnancy persisted through second one, but the reformed internal tic membrane was incomplete. Com- e figures 2 and 4. In figure 4 the two scular layers are separated by an elastic r (T) The beginning of internal elas membrane (E) formation can also be rmed.

t may be concluded from the above e examples that the elastic distribution ariable but still quite meaningful in tion to parity The number of media y also aid in the diagnosis of parity in mals whose pregnancy histories are un- wn.

. *Arteries of female guinea pigs with e or more pregnancies.* Animals with re than three pregnancies were consid- d multiparous. Figure 5 presents a cross- tion of a uterine artery from a 9-day tpartum female. It shows outer (MM) l inner (M) smooth muscle layers sepa- ed by a thick elastic layer (T) Another elastic layer (E) is also evident, which arates the intima (I) from the inner cular smooth muscle layer. The two scular mediae (M) and (MM) and two stic layers (T) and (E) would suggest robable history of two pregnancies. The sence of another layer (I) suggests the sibility of still a third pregnancy Since intimal layer (I) at nine days after turition does not exhibit any elastic fi- s, it differs significantly in rate of re- ery from the primiparous animal.

The correlation between the number of pregnancies and the histological description of mesometrial arteries becomes very confusing after the third pregnancy One usually can estimate a history of two preg nancies accurately and sometimes even three; but beyond this stage, the animals can only be classified as multiparous. Figure 6 illustrates the difficulty in estimat ing the number of pregnancies. This was taken from a multiparous female, and does not give any evidence of elastic layers separating the mediae The elastic tissue is abundant and it appears as if several lay ers (L) have fused. The elastic tissue around arteries of multiparous females does not have the same crisp fibrous appearance as seen in the arteries of nulli- and biparous animals. Instead, it appears rather coarse and globular Whether this indicates a change in structure or not is unknown to us

B. *Medium-sized and small uterine arterioles*

Information regarding the parous nature of the guinea pig can also be obtained to some extent by studying the elastic tissue distribution of the medium-sized and small uterine arterioles in pregnant and nonpreg nant animals. As the arterioles of the nul liparous female travel from the zona vasculosa to the mucous membrane they become smaller in diameter and the muscular media becomes thinner until it is only one or two cells thick. At this level these vessels may be called small arterioles. The internal elastic membrane is absent in the small arterioles of nulliparous females although a few fine strands of elastica may be present in their walls (upper fig. 7) The distribution of elastic tissue in the medium-sized arterioles is also shown (lower fig. 7) They usually contain an internal elastic membrane (E) and some elastic tissue in the adventitia. In contrast to figure 7 figures 8–11 represent the distribution of elastic tissue in the vessels of guinea pigs with one or more pregnancies. It is apparent that the amount of elastic tissue in the walls of these arterioles increases with each successive pregnancy Further the elastic tissue appears globular rather than fibrous in the arteriolar walls of bi and multiparous females (figs. 9–10).

A similar type of globular elastic tissue was seen in mesometrial arteries of multiparous females The distribution of elastic tissue in these vessels does not give any precise information regarding the parous nature of the female However from the amount of it in these vessels, one may estimate whether the female is multiparous or has had only one or two pregnancies

C *The effect of age on the arterial elastic tissue*

There were no significant changes observed in the distribution of elastic tissue in the uterine musculature and arteries of young versus old virgin guinea pigs However larger quantities of elastic tissue were observed in the walls of uterine arteries of older parous animals than seen in comparable younger ones More elastic tissue was present in the media and adventitia of the mesometrial arteries in a 5-year-old uniparous animal than in comparable young animals. Even though this animal was sacrificed 34 days after parturition the internal elastic membrane had not yet formed. This membrane forms about 20 days after parturition in young uniparous females Thus one might suspect that the formation of the internal elastic membrane was delayed or perhaps prevented completely by the old age of the animal.

Similar observations were made on a four and one-half year old female guinea pig with a history of two pregnancies This animal was sacrificed 33 days after parturition. Cross-sections of mesometrial arteries of this animal showed substantial amounts of elastic tissue in the adventitia and between the inner and outer muscle layers. The two muscular mediae are separated by a layer of elastic tissue (T) as expected in a female with a history of two pregnancies (fig 11) The second internal elastic membrane has not formed in this case either even though the animal was sacrificed well past the time required to form the new membrane in young primiparous females. There is more elastic tissue separating the two mediae in this animal than was present in younger animals with similar histories. The elastic tissue appears more globular (compare with figs. 2–5)

These two cases of aged animals suggest that age may have some effects on the amount and distribution of the elastic tissue in mesometrial arteries.

DISCUSSION

It is evident from previous (Albert, '6) and current work that the parous histor of the guinea pig can be correlated wi the morphologic distribution of elastic t the uterine arteries. The first two or thre pregnancies leave well defined traces, bu the morphologic appearance of uterine ar teries in subsequent pregnancies is se only as a diffuse increase in elastin.

It has been shown previously that, i young primiparous guinea pigs, new elas tissue is formed in mesometrial arter after parturition (Albert, '66) and pr ently we have shown an increased accum lation of elastin in large and small uteri vessels after each successive pregnan Older parous females accumulated l amounts of elastin than comparable you ones. These findings essentially agree w the histologic studies on human uter Goodall ('09) and Maher ('59) and che ical studies of Woessner ('63) and Wo ner and Brewer ('63) Goodall and Mah demonstrated a comparable increase i elastic tissue in such vessels with succ sive pregnancies. Woessner and Woessn and Brewer reported increases in elast tissue after chemically extracting it fro the uterine homogenates. However the did not report any comparisons betwe old and young parous females. Good ('09) and Vallo ('35) reported an increas in the elastic tissue surrounding the mu cle fibers of the human myometrium. Th increase in elastic tissue surrounding th muscle fibers resulting from pregnancy continued to increase with repeated pre nancies. Present observations are in co trast to these We did not observe an significant changes in elastic tissue su rounding the muscle cells of the guine pig myometrium This may be simply species difference however it is unlikel since other changes reported in this inve tigation on the guinea pig are similar t those described in humans

Resorption phenomenon must be i volved in the remodeling which takes pla in guinea pig uterine arteries during a after single and multiple pregnancies. Th is particularly evident in the changes o

;rable in the internal elastic membrane. e chemical studies of Woessner ('63) d Woessner and Brewer ('63) clearly monstrated the resorption of elastin in man uteri following each pregnancy

Our observations on guinea pigs with stories of two pregnancies showed conscated morphologic variation. In one se, two complete elastic layers were und in the arterial wall, one of which as the new internal elastic membrane. another case the elastic layers were inmplete and in the third case only the yer between the two mediae was present. hese differences can probably be edlained as being due to individual variaons in the interplay of rates of post artum resorption and reconstruction of lastin in these arteries.

The chronological age of the parous female also plays a role in determining the quantity of elastic tissue seen in uterine vessels. In the arteries of older parous animals, larger quantities are seen than in comparable young ones. The increase in elastic tissue after multiple pregnancies could be due either to the inability of the animal to resorb the same amount of elastic tissue as after the first pregnancy or perhaps the amount of postpartum resorption does not change with repeated pregnancies but excessive amounts of elastic tissue are formed and tend to accumulate. From our observations, we are inclined to think that the postpartum resorption of elastic tissue diminishes with age and parity; and, further that the formation of new tissue is retarded, as has been shown by a delay in the formation of the new internal elastic membrane in the old females. We have not been able to ascertain whether the formation of the new internal elastic membrane would or would not be delayed in young parous guinea pigs with successive pregnancies. One is tempted to speculate that repeated pregnancies tend to cause the vessels of young females to behave like those of older animals. To paraphrase the above conclusions suggest that pregnancy might predispose to precocious aging of certain tissues of the body

LITERATURE CITED

Albert, E. N 1967 The effect of pregnancy on the elastic membranes of mesometrial arteries in the primiparous guinea pig. Accepted for publication in the Am. J Anat., 120: 611

Goodall, J R. 1909 The involution of puerperal uterus, with special reference to the involution of its circulatory system. Am. Jour. Obstet. and Diseases of Women and Children, LX: 921.

Maher J E. 1959 Morphologic and histochemical changes in post-partum uterine blood vessels. Arch. Path., 67 175.

Pankow R. 1906 Graviditats-Menstruations und Ovulationssklerose der uterus und Ovarialgefässe. Arch. f. Gynec., Bd. LXXX.

Schwarz, O H. 1919 The pathology of chronic metritis and chronic subinvolutions. Am. Jour Obstet. and Gynecol., 79 63.

Shaw W F 1914 The subdivisions of chronic metritis. J Obst. and Gynaecol. Brit. Emp., 26 173.

Szasz-Schwarz 1903 Recherches sur les alterations seniles des vaisseaux sanguins. Rev de Gynecol. T VII.

Tlenner P 1961 Elastic tissue. In: Histochemistry Theoretical and Applied. A. G. E. Pearse ed. J A. Churchill, London, p. 168.

Valle, G. 1935 Sull'alleggiamento funzionale del miometrio. Comportamento delle cellule connettivali e delle fibre elastiche nell'utero vuoto e gestante. Ginecologia, 1 873.

Verhoeff F 1908 Some new staining methods of wide applicability including a rapid differential stain for elastic tissue. J Am. Med. Assn., 50: 876.

Weigert, C. 1961 Resorcin-fuchsin methods of elastic tissue stains. In Histochemistry Theoretical and Applied. A. G. E. Pearse, ed. J A. Churchill, London, p. 816.

Woessner J 1963 Age-related changes of the human uterus and its connective tissue framework. J Geront. 18 220.

Woessner J and T Brewer 1963 Formation and breakdown of collagen and elastin in the human uterus during pregnancy and postpartum involution. Biochem. J 89: 75.

PLATE 1

EXPLANATION OF FIGURES

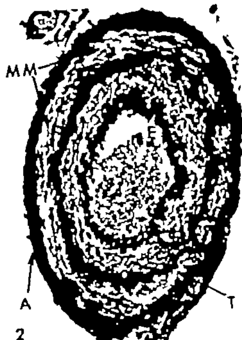
1 Cross-section of a mesometrial artery from an adult nulliparous female. Notice the internal elastic membrane (E) circular smooth-muscle media (media) (M) and adventitia (A) × 250.

2 Cross-section of a mesometrial artery from a 20-day-postpartum female with a history of two pregnancies Internal elastic membrane (E) inner media (M) outer media (MM)

3 Cross-section of a mesometrial artery from a 16-day-postpartum female with a history of two pregnancies. Thick fragments of elastic tissue (T) between inner (M) and outer (MM) media. (E) is elastic fibers attempting to form the new internal elastic membrane. × 250.

4 Cross-section of a mesometrial artery from a 16-day-postpartum female with a history of two pregnancies. The mediae are separated by a complete elastic layer (T) The beginning of the new internal elastic membrane (E) can also be seen here. × 250









1

PLATE 2

EXPLANATION OF FIGURES

5 Cross-section of a mesometrial artery from a 9-day-postpartum female with a history of three pregnancies. The outer (M) and inner (IM) mediae are separated by an elastic layer (T). Another elastic layer (E) separates the intima (I) from the inner muscular layer (M) × 250.

6 Cross-section of a mesometrial artery from a multiparous female. Notice the elastic tissue forming several closely packed layers (L) around the media.

7 Cross-sections of small and large arterioles from zona vasculosa of the uterus. The larger arterioles exhibit an internal elastic membrane (E) and black elastic fibers in the adventitia (A) but the smaller vessels are virtually devoid of elastic tissue. × 250

8 Section from the zona vasculosa of a uniparous female guinea pig. Notice that the elastic fibrils (E) around the vessels are more numerous than in those of nulliparous female. × 250

9 Section from a biparous female guinea pig. Notice the increase in elastic tissue (E) surrounding the arterioles over that seen in vessels of nulli and uniparous females × 250.


E
T
5


L
6

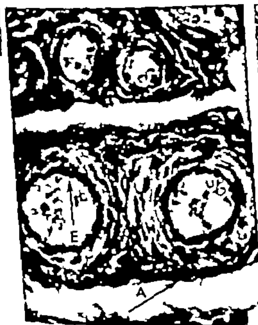

E
A



PLATE 2

EXPLANATION OF FIGURES

5 Cross-section of a mesometrial artery from a 9-day-postpartum female with a history of three pregnancies The outer (M) and inner (MM) mediae are separated by an elastic layer (T) Another elastic layer (E) separates the intima (I) from the inner muscular layer (M) × 250.

6 Cross-section of a mesometrial artery from a multiparous female Notice the elastic tissue forming several closely packed layers (L) *around the media*

7 Cross-sections of small and large arterioles from zona vasculosa of the uterus. The larger arterioles exhibit an internal elastic membrane (E) and black elastic fibers in the adventitia (A) but the smaller vessels are virtually devoid of elastic tissue × 250

8 Section from the zona vasculosa of a uniparous female guinea pig. Notice that the elastic fibrils (E) around the vessels are more numerous than in those of nulliparous female. × 250

9 Section from a biparous female guinea pig Notice the increase in elastic tissue (E) surrounding the arterioles over that seen in vessels of nulli and uniparous females. × 250.


E
T
5


L
6


E
A



PLATE 3

EXPLANATION OF FIGURE

10 Sections of blood vessels taken from a multiparous female The arterioles exhibit a further increase in the amount of elastic tissue over that seen in figures 8 and 9 × 120

11 Cross-section of a mesometrial artery taken from an old (four and one-half year-old) guinea pig. The animal had delivered her third litter 33 days before sacrifice The internal elastic membrane has not yet formed The amount of elastic tissue (T) is more than that seen in mesometrial arteries of younger animals with two pregnancies.


9


10


11

he Adrenergic Nerve Supply to the Female eproductive Tract of the Cat [1]

E. ROSENGREN AND N.-O. SJOBERG
Department of Pharmacology, Institute of Anatomy and Histology and Department of Obstetrics and Gynecology at Malmö University of Lund, Lund, Sweden

ABSTRACT Pilot studies on the fluorescence histochemistry of the adrenergic innervation to the female reproductive tract in different mammals revealed a conspicuously well developed innervation in the cat. Moreover, the female genital tract of the cat is studied extensively with regard to the pharmacology of adrenergic mechanisms. An exact knowledge of the adrenergic innervation apparently would make the cat particularly suitable model for functional studies on the involvement of neuronal adrenergic mechanisms in the reproductive tract.

Fluorimetrically noradrenaline was the only catecholamine occurring in measurable amounts in nonpregnant cats. The amine seemed to have an exclusively neuronal distribution, although a comparatively small fraction may be also located in chromaffin cells present in relation to ganglion formations.

A considerable number of adrenergic nerve terminals were found in all organs of the reproductive tract. Consistent numbers of these terminals were directed to various structures forming the ovarian parenchyma and to the smooth muscle coats of the oviduct, uterus, and vagina. The rest of the innervation seemed to be of vasomotor nature. The histochemical results agree well with the high level of noradrenaline, 1.83–4.83 µg/gm, found in the different organs.

Denervation experiments revealed that the postganglionic sympathetic innervation reaches the oviduct, uterus, and vagina partly by way of the hypogastric nerves, and partly by way of short adrenergic neurons originating from adrenergic ganglia that could be directly visualized in the region of the uterovaginal junction. The ovarian adrenergic innervation seemed to arise more proximally probably directly from the sympathetic chain.

The origin and distribution of the adrenergic innervation of the female reproductive organs in rabbit and man have recently been elucidated by fluorescence histochemistry (Owman et al. '66 '67 Owman and Sjöberg, '66) The entire genital tract was found to receive a varying number of adrenergic nerves. Apart from these adrenergic nerves, no other catecholamine-containing cells occurred in the genital tract, which is in conformance with the fact that only noradrenaline could be measured chemically in the different organs.

The smooth muscle tissue as well as the blood vessels, of the oviduct uterus and vagina in the rabbit are supplied with adrenergic nerves running in characteristic ground plexuses of which the densest are those of the vagina. Nonvascular adrenergic fibers were also demonstrated in the ovary where frequently they were seen to run contiguous to follicles in denervation experiments (Owman et al '66) these fibers were found to arise from the lumbosacral sympathetic chain. About 50% of the postganglionic sympathetic fibers to the oviduct originated in the inferior mesenteric ganglion formations from which they course down the hypogastric nerve(s) But, the rest of the adrenergic fibers to the oviduct, and also those to the uterus and vagina, had a more peripheral origin. Such fibers emanated from large clusters of adrenergic ganglion cells that could be directly demonstrated within, or in the vicinity of the upper portion of the vaginal wall. This shows that the hypogastric nerves carry mainly preganglionic fibers to the genital tract which is thus innervated predominantly by *short* adrenergic neurons. It appears that this sympathetic neuron type which has so far been found to occur only in the urogenital tract (Falck et al., '65; Hamberger and Norberg, '65

[1] This work has been supported by grants from the Swedish Medical Research Council (project B67-14X-712-02A), and the Medical Faculty at the University of Lund.

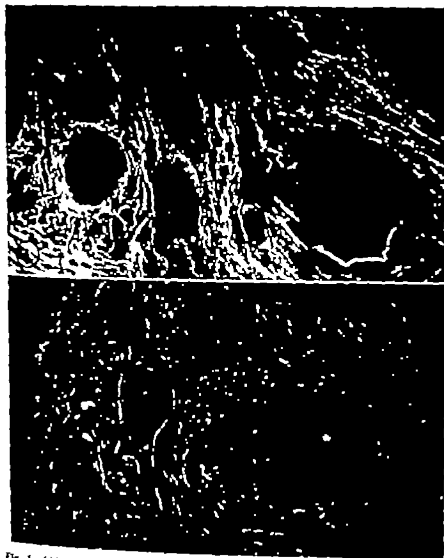


FIG. 1 (A) Ovary normal animal. Perfused with India ink to demonstrate vascular system. Very rich distribution of intensely fluorescent nerve terminals, only few in relation to vessels. Follicles appear as rounded dark areas. × 125
(B) Ovary division of nerve accompanying the ovarian artery. Marked decrease in total amount of fluorescent nerves. × 125.

vessels in the hilar region. Within the ovarian stroma, the bundles split up into a rich terminal network. After injection of India ink into the circulation it appeared evident that the majority of nerves had no relation to the vascular system (fig. 1A).

A conspicuous number of varicose nerve terminals ran in all directions in the stromal tissue that separates the layer of primordial follicles from the germinal epithelium. Some fibers were seen to course immediately underneath this epithelium. The terminals which ran among the primordial follicles sometimes passed contiguously to their epithelial layer. Some of the vessels, down to capillary caliber were accompanied by fluorescent fibers in this region, although a large number of fibers

Owman and Sjöstrand '65 Sjöstrand 65) *constitutes* a specific entity (Owman and Sjöstrand 66) with unique functional properties (Euler and Lishajko 66 Stjärne and Lishajko '66)

The sensitivity and the reproducibility of the histochemical fluorescence method used (Falck 62 Falck et al '62 Corrodi and Hillarp 63 64) allows direct demonstration at a neuronal level of functional changes in the adrenergic transmitter content as has been repeatedly documented (Falck and Owman 66 Hillarp et al '66 Eränkö '67 Norberg '67) In a comprehensive comparative investigation of the adrenergic nervous system of the female genital tract in various laboratory animals preliminary findings indicated that the innervation in the cat was strikingly well developed Detailed knowledge of the adrenergic nerve supply to the female reproductive tract of the cat would therefore seem to lend itself well to functional histochemical and chemical studies on short and long adrenergic neurons Further knowledge might also help to clarify certain contradictory data on adrenergic mechanisms obtained in pharmacological studies utilizing the female reproductive tract of the cat and rabbit as model systems (Langley and Anderson 1896 Cushny 06 Labate and Sheehan 43 Schofield 52 Varagić 56 Miller and Marshall 65)

MATERIAL AND METHODS

A total of 29 adult nonpregnant female cats weighing between 2.0 and 3 3 kg were used

The normal distribution of the monoamine-containing cell system in the genital tract was studied in seven animals killed by an over-dose of nembutal The ovary oviducts (divided into 4–6 pieces, including the tubo-uterine junction) uterine cornua (divided into 6 pieces) and cervices (3 pieces) and vagina (5–7 pieces) were dissected out and frozen to the temperature of liquid nitrogen. After being freeze-dried treated in formaldehyde-gas (+80 C for 1 hour) embedded in paraffin *in vacuo* and sectioned (7 μ thickness) the preparations were mounted and analysed in the fluorescence microscope all according to Falck and Owman ('65) Under the conditions used the catecholamines emitted an intense green light, whereas the fluorescence of 5-hydroxytryptamine is yellow

In order to clarify any relationship between the adrenergic nerves and blood vessels in the various tissues, two of the animals were perfused for 3–4 minutes with India ink (equal volumes of commercial India ink and 0 9% saline containing a few drops of amyl nitrite) through the abdominal aorta at a pressure of 400 mm Hg under nembutal anesthesia.

The content of dopamine noradrenaline and adrenaline was determined fluorimetrically in the various organs from the animals according to Bertler et al. ('58) as modified by Häggendal ('63)

Denervation experiments were performed on 18 of the animals according to the following procedures:

(a) removal of the inferior mesenteric ganglion formation together with the hypogastric nerves to the level of the aortic bifurcation (b) removal of all macroscopically visible ganglia located in the vicinity of the uterovaginal junction. To ascertain the presence of adrenergic ganglion cells in the material excised, this was subsequently freeze-dried and treated with formaldehyde for fluorescence microscopic analysis (c) division of both uteri near the cervical region keeping the vascular supply intact (d) combinations of two of the above procedures in one and the same animal (e) sectioning of the ovarian nerve about 50 mm proximal to the ovary

The animals were killed by nembutal one to two weeks postoperatively and pieces from representative regions were dissected out for fluorescence microscopy or for fluorimetric assay of the monoamines

RESULTS

Normal unoperated animals

The feline *ovary* showed a very rich distribution of intensely green-fluorescent adrenergic nerve fibres (fig 1A) This correlates well with a considerable level of noradrenaline in the organ (table 1) neither adrenaline nor dopamine occurred in measurable quantities.

Thick bundles of characteristically smooth moderately fluorescent preterminal fibers entered the ovary along the blood

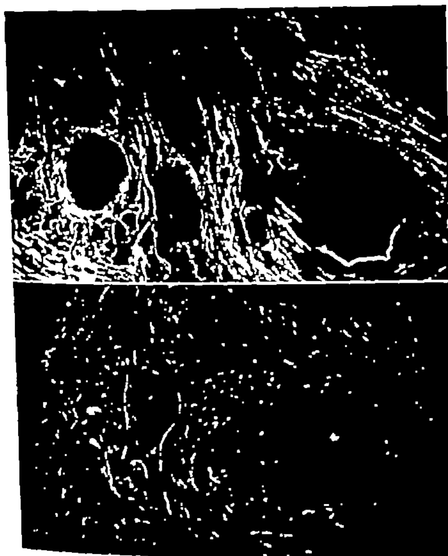


Fig. 1 (A) Ovary normal animal. Perfused with India ink to demonstrate vascular system. Very rich distribution of intensely fluorescent nerve terminals, only a few in relation to vessels. Follicles appear as rounded dark areas. × 125.
(B) Ovary division of nerve accompanying the ovarian rtery Ma ked decrease in total amount of fluorescent nerves. × 125.

vessels in the hilar region. Within the ovarian stroma, the bundles split up into a rich terminal network. After injection of India ink into the circulation it appeared evident that the majority of nerves had no relation to the vascular system (fig. 1A).

A conspicuous number of varicose nerve terminals ran in all directions in the stromal tissue that separates the layer of primordial follicles from the germinal epithelium Some fibers were seen to course immediately underneath this epithelium The terminals which ran among the primordial follicles sometimes passed contiguously to their epithelial layer Some of the vessels down to capillary caliber were accompanied by fluorescent fibers in this region although a large number of fibers

were apparently nonvascular Also the conspicuous stromal layer beneath the primordial follicles contained many of both vascular and nonvascular nerve terminals

Maturing follicles with a well developed theca interna were supplied only by scattered fibers in this layer Part of this innervation was received by some of the vessels constituting the vascular plexus at the innermost region In the lobes of the interstitial gland green fluorescent nerve terminals occurred in varying amounts however mainly in relation to vessels During the course of the study the ovaries from a cat in late pregnancy were investigated incidentally and also found to have a vasomotor innervation of vessels running within the corpus luteum

The ampulla represents by far the longest portion of the *oviduct* (*Fallopian tube*) in the cat The circular muscle portion dominates the fairly thin muscular layer In the ampulla the adrenergic nerves were found to be almost exclusively vascular whereas only a few terminals occurred in the smooth muscles (fig 2) The muscular coat of the isthmus showed an increasing thickness towards the uterus At the junction between the ampulla and isthmus there was an abrupt increase in the amount of innervation of the circular muscle layer which also is itself best developed in the isthmus The general arrangement of the adrenergic fibers in the isthmus is similar to that in the rabbit although in the cat the muscular nerves were more numerous (fig 3A) with little or no variation along their course towards the uterus In the tubo-uterine junction it was sometimes possible to recognize a distinct enhancement in muscular innervation.

Usually a few bundles of preterminal nerve fibers were found in the periphery along the entire oviduct. Also the mucosal layer contained fluorescent fibers, but they appeared to be exclusively vascular

The overall adrenergic innervation of the feline *uterus* was more extensive than that in the rabbit (Owman et al. '66, Owman and Sjöberg '66) which is in accordance with the finding that the uterine noradrenaline content is about four times higher in the cat (table 1) Both the inner circular and the outer longitudinal smooth muscle layers received a large number of intensely green fluorescent varicose terminals (fig 4A) The nerves usually ran parallel to and in intimate contact with the muscle fibers. However some fibers in the circular coat had a more radial direction and accompanied the vessels (fig 4A) that originate from the well developed vascular

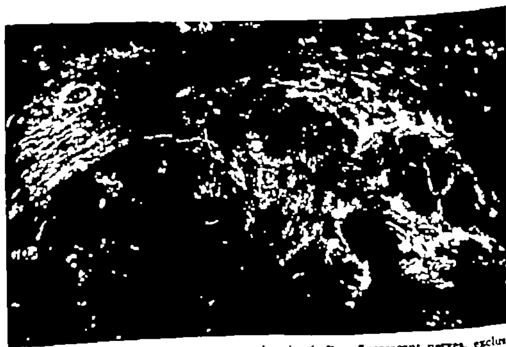


Fig 2 Ampulla transverse section; normal animal. Few fluorescent nerves, exclusively vascular Mucosal layer occupies lower half of figure × 125

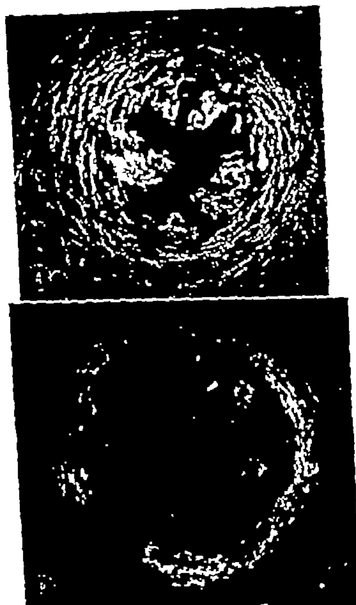


Fig. 3 (A) Isthmus transverse section; normal animal. India ink perfusion of vascular system. Abundance of mainly nonvascular adrenergic nerves with characteristic varicose appearance. Innervation richest in circular smooth muscle layer. × 125.
(B) Isthmus, as above; excision of uterovaginal ganglia. Complete denervation except for one fiber near upper right corner of figure. All other fluorescence is autofluorescence. × 125.

plexus between the two muscle layers. These nerves which formed characteristic meshes superimposed upon the vessel wall were often seen to enter the endometrium. Apart from vascular nerves no fluorescent fibers occurred in any region of the endometrium.

As in the oviduct thick bundles of moderately fluorescent preterminal fibers ran longitudinally in the organ. They were

were apparently nonvascular Also the conspicuous stromal layer beneath the primordial follicles contained many of both vascular and nonvascular nerve terminals

Maturing follicles with a well developed theca interna were supplied only by scattered fibers in this layer Part of this innervation was received by some of the vessels constituting the vascular plexus at the innermost region In the lobes of the interstitial gland green fluorescent nerve terminals occurred in varying amounts however mainly in relation to vessels During the course of the study the ovaries from a cat in late pregnancy were investigated incidentally and also found to have a vasomotor innervation of vessels running within the corpus luteum

The ampulla represents by far the longest portion of the *oviduct* (*Fallopian tube*) in the cat The circular muscle portion dominates the fairly thin muscular layer In the ampulla the adrenergic nerves were found to be almost exclusively vascular whereas only a few terminals occurred in the smooth muscles (fig 2) The muscular coat of the isthmus showed an increasing thickness towards the uterus At the junction between the ampulla and isthmus there was an abrupt increase in the amount of innervation of the circular muscle layer which also is itself best developed in the isthmus. The general arrangement of the adrenergic fibers in the isthmus is similar to that in the rabbit, although in the cat the muscular nerves were more numerous (fig 3A) with little or no variation along their course towards the uterus. In the tubo-uterine junction it was sometimes possible to recognize a distinct enhancement in muscular innervation.

Usually a few bundles of preterminal nerve fibers were found in the periphery along the entire oviduct. Also the mucosal layer contained fluorescent fibers, but these appeared to be exclusively vascular.

The overall adrenergic innervation of the feline *uterus* was more extensive than that in the rabbit (Owman et al., '66; Owman and Sjöberg '66) which is in accordance with the finding that the uterine noradrenaline content is about four times higher in the cat (table 1) Both the inner circular and the outer longitudinal smooth muscle layers received a large number of intensely green fluorescent varicose terminals (fig 4A) The nerves usually ran parallel to and in intimate contact with, the muscle fibers. However some fibers in the circular coat had a more radial direction and accompanied the vessels (fig. 4A) that originate from the well developed vascular

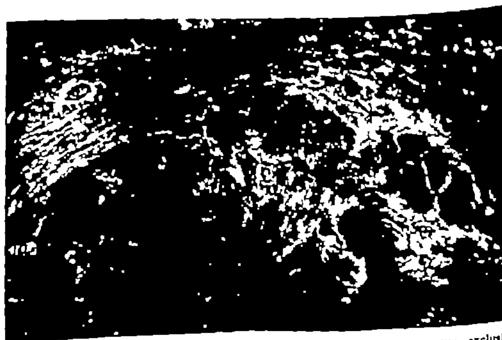


Fig 2 Ampulla transverse section; normal animal Few fluorescent nerves exclusively vascular Mucosal layer occupies lower half of figure × 125

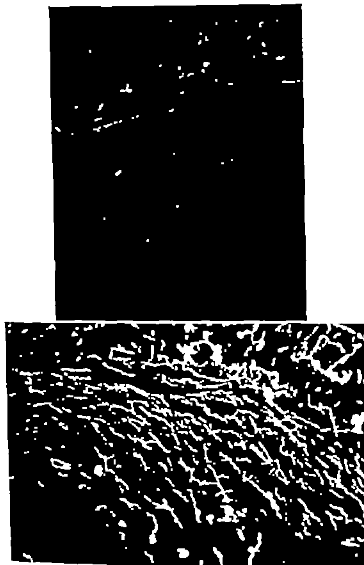


Figure 4(D–E)

Fig. 4 (A) Uterus, transverse section; normal animal. Vascular system perfused with India ink. Large number of fluorescent, varicose nerve terminals mainly nonvascular following direction of smooth muscle cells of circular (below) and outer longitudinal (above) layer. Between the two layers, thick bundle of axons in relation to large vessels. × 100

(B) Uterus, as above; excision of hypogastric nerves together with inferior mesenteric ganglia. Marked reduction of fluorescent nerves in both muscle layers. Note vessel in radial direction in circular layer × 100.

(C) Uterus, as above; removal of uterovaginal ganglia. Fluorescent nerves remain only around vessel. Granular autofluorescent pigment material now stands out as clearly visible dots. × 100.

(D) Uterus, as above; transection of uterus above cervix. Figure illustrates the part above the plane of lesion in which only few fluorescent nerves remain. × 100.

(E) Uterus, as above; same operation as (D). Below the plane of transection a marked accumulation of fluorescence in all nerves as compared with unoperated animal (A) × 100.

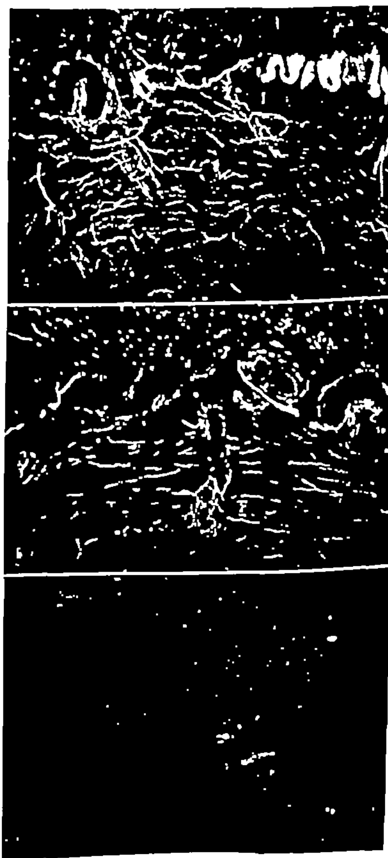


Figure 4(A–C)

cell bodies. Some of the cells of both ...ories were enclosed by varicose termi...bers (fig. 7) suggestive of a synaptic ...ngement. The bulk of the ganglia were ...ted in the vicinity of the uterovaginal ...tion (fig. 8) some clusters however occurred intramurally inside the surface of the lower cervix or the cranial portion of the vagina. In favourable sections, preterminal fiber bundles could be seen to leave the ganglion formations in various directions (fig. 8)



Fig. 6 Vaginal vestibulum, transverse section; normal animal. In epithelium, appearing as dark strand, a number of small, flask-shaped cells, which emit a yellow fluorescence. × [illegible]

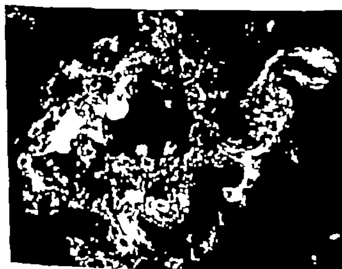


Fig. 7 Uterovaginal junction, animal in which attempts were made to remove all ganglia outside the muscular wall. The figure illustrates intramural clusters of adrenergic ganglion cells with a moderate fluorescence in their cytoplasm. Many cells are enclosed by intensely fluorescent nerve terminals. Area with conspicuous fluorescence intensity (upper left) represent small groups of chromaffin cells (see text) × 200

present both in the perimetrium and between the two muscle layers (fig 4A) where they followed the main vessels

Also the *vagina* had a quite conspicuous adrenergic nerve supply both to the smooth muscles and to the vascular system (fig 5A) In the mucosa the terminals appeared to innervate vessels only whereas the innervation of the muscle coat was predominantly directed to the smooth muscle fibers The vaginal innervation seemed to arise from several preterminal nerve bundles in the adventitial layer

The system of yellow-fluorescent enterochromaffin cells described earlier as occurring in the vestibular epithelium of the rabbit vagina (Forsberg et al., '64) was recognized in the corresponding region of the cat (fig 6)

Large ganglion formations (Owman et al 66 '67) arranged in principally the same way as in other species studied, including man were also found in the uterovaginal region of the cat (figs. 7 8) They contained both fluorescent and nonfluores-

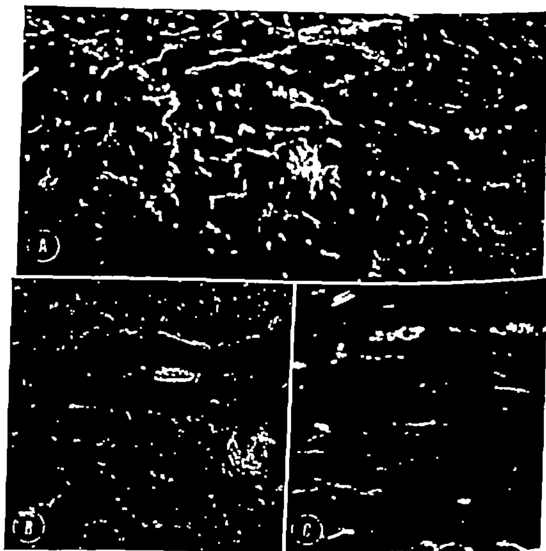


Fig 5 (A) Vagina, transverse section; normal animal. Rich adrenergic innervation of smooth muscle wall. × 125

(B) Vagina, as above; excision of hypogastric nerves together with inferior mesenteric ganglia. Distinct reduction in total amount of fluorescent nerves × 125

(C) Vagina as above; removal of uterovaginal ganglia. Marked reduction in adrenergic innervation The remaining nerves may — at least partly — emanate from ganglia within the vaginal wall and are therefore not accessible to removal × 125.

nt cell bodies. Some of the cells of both tegories were enclosed by varicose terminal fibers (fig. 7) suggestive of a synaptic rangement. The bulk of the ganglia were ated in the vicinity of the uterovaginal nction (fig. 8) some clusters, however occurred intramurally inside the surface of the lower cervix or the cranial portion of the vagina. In favourable sections, preterminal fiber bundles could be seen to leave the ganglion formations in various directions (fig. 8)



Fig. 6 Vaginal vestibulum, transverse section; normal animal. In epithelium, appearing as dark strand, number of small, flask-shaped cells, which emit a yellow fluorescence × 125.



Fig. 7 Uterovaginal junction, animal in which attempts were made to remove all ganglia outside the muscular wall. The figure illustrates intramural clusters of adrenergic ganglion cells with a moderate fluorescence in their cytoplasm. Many cells are enclosed by intensely fluorescent nerve terminals. Area with conspicuous fluorescence intensity (upper left) represent small groups of chromaffin cells (see text) × 200.

present both in the perimetrium and between the two muscle layers (fig 4A) where they followed the main vessels

Also the *vagina* had a quite conspicuous adrenergic nerve supply both to the smooth muscles and to the vascular system (fig 5A) In the mucosa, the terminals appeared to innervate vessels only whereas the innervation of the muscle coat was predominantly directed to the smooth muscle fibers The vaginal innervation seemed to arise from several preterminal nerve bundles in the adventitial layer

The system of yellow-fluorescent enterochromaffin cells described earlier as occurring in the vestibular epithelium of the rabbit vagina (Forsberg et al, '64) was recognized in the corresponding region of the cat (fig 6)

Large ganglion formations (Owman et al 66 67) arranged in principally the same way as in other species studied, including man were also found in the uterovaginal region of the cat (figs. 7 8) They contained both fluorescent and nonfluores-

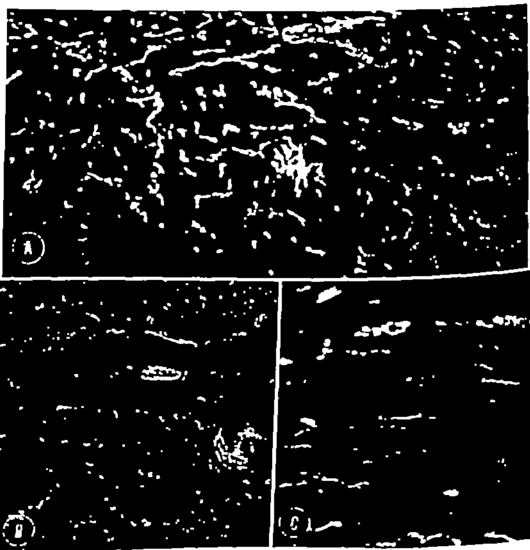


Fig. 5 (A) Vagina, transverse section normal animal Rich adrenergic innervation of smooth muscle wall. × 125
(B) Vagina as above; excision of hypogastric nerves together with inferior mesenteric ganglia. Distinct reduction in total amount of fluorescent nerves. × 125
(C) Vagina as above; removal of uterovaginal ganglia. Marked reduction in adrenergic innervation The remaining nerves may — at least partly — emanate from ganglia within the vaginal wall and are therefore not accessible to removal. × 125

rable number of nerves remained in three organs, which were especially evi- t in the oviduct and uterus on the left e. Additional removal of the inferior senteric ganglia and hypogastric nerves not influence the completeness of ad- ergic denervation.

In those cases where the uteri were nsected in the cervical region only a all number of fluorescent terminals per ted in the oviducts and in the uteri (fig.) above the level of transection. In the rine portions below the transection, the mber of nerves was unaltered; the ax s even showed an increased intensity of orescence (fig 4E) No overt change uld be seen in the vaginal adrenergic nervation after this operation.

Combined transection operation and re- oval of the inferior mesenteric ganglia gether with the hypogastric nerves gave e same result in the organs as when e local uterovaginal ganglion formations re excised in combination with the ferior mesenteric ganglia hypogastric rves.

DISCUSSION

The distribution of monoamines in the male reproductive organs of the non- egnant cat was investigated with a com- nation of the histochemical fluorescence ethod of Falck and Hillarp and fluori- etric determinations. The ovary ovi- ucts, uteri and vagina showed a rich nervation by adrenergic nerves, the num- r and fluorescence intensity of which re well correlated with the levels of nor drenaline in the respective organs Hence ost — if not all — of the noradrenaline these organs is of neuronal origin. leither dopamine nor adrenaline occurred measurable amounts. 5-Hydroxytryp- amine was located exclusively in a spe- ial enterochromaffin cell system in the estibular epithelium of vagina.

The terminal arrangement of the adren- rgic nerves in the ovary strongly suggests hat changes in ovarian activity after in- erference of adrenergic mechanisms with mine-depleting agents or monoamine oxi- ase inhibitors (Spector '61 Hopkins and Pincus, '63 Poulson and Robson '63 Brown, '66; Coppola et al. '66 Deanesly 66) may be due to a peripheral effect me- diated directly by the ovarian adrenergic innervation Further the present results indicate that peripheral adrenergic mech- anisms are of physiological significance for the regulation of the smooth muscles in the oviduct uterus and vagina For example part of the adrenergic innerva tion to the oviduct seems to function as a sphincter mechanism probably of impor tance in the transport of the ova towards the uterus (Brundin '65) Recent findings have demonstrated marked changes in the neuronal noradrenaline in the genital tract during pregnancy as well as after treat ment with female sex hormones (Sjöberg, '67) This may indicate that the adrenergic muscular innervation may be directly in- volved in the motility changes known to occur under these specific conditions (see Holtz and Palm '66)

The results of the denervation experi- ments show that the hypogastric nerves carry a part of the postganglionic adren- ergic fibers directed to the vagina, uterus and probably to some extent also to the oviduct However the remaining part of the sympathetic innervation of these struc tures arises from a more peripheral source as suggested already by Langley and An- derson (1895) although their suggestion has largely been disregarded In the pres- ent study this peripheral relay could be identified directly as the adrenergic gan- glion formations located within or im- mediately outside the uterovaginal junc tion. It seems that those adrenergic fibers within the hypogastric nerves directed to the internal genital organs converge to- wards this area. From here all postgangli- onic fibers then diverge into the different organs The fibers running to the uterus and oviduct are collected in thick bundles extending along the muscular walls of the organs. Some bundles probably also run at some distance away from and parallel to the uterus and the oviduct since transec tion in the cervical region did not abolish the fluorescence in all nerves to the organs above the level of transection.

The adrenergic nerves supplying the ovary have quite a different origin, prob- ably in the paravertebral ganglia of the lower sympathetic chain (Owman et al. '66)

Thus a significant portion of the sym- pathetic innervation reaches the reproduc

Small groups of "chromaffin" cells exhibiting an extremely intense fluorescence that gave them an almost yellowish green colour were sometimes found within or close to the ganglia (fig 7) These tiny cells usually had a coarse process which even could be seen to run for a short distance inside the preterminal bundle

Operated animals

Division of the nerve accompanying the ovarian artery resulted in a marked over all decrease in the number of fluorescent fibers in the ovary (fig 1B) As could be expected with regard to this result neither of the other operative procedures employed influenced the ovarian adrenergic innervation or noradrenaline content (table 1)

Excision of the hypogastric nerves, including the inferior mesenteric ganglia, caused — if anything — a slight reduction in the number of fluorescent nerves to the oviduct the noradrenaline content remained unchanged (table 1) A more marked reduction was observed in the number of the uterine (fig 4B) and vaginal (fig 5B) adrenergic nerves. This agrees with a significant fall in the noradrenaline concentrations in the organs (table 1)

By removing the uterovaginal ganglion formations (fig 8) the fluorescent nerves to the oviduct (fig 3B) uterus (fig 4C) and vagina (fig 5C) could be made to disappear completely — or almost completely However in some instances a con-



Fig. 8 Ganglion formations removed at denervation operation (see text) turned out to contain clusters of adrenergic ganglion cells from which bundles of smooth, moderately fluorescent preterminal axons are seen to arise × 200.

TABLE 1

Noradrenaline content in the different parts of the reproductive tract in normal animals and after removal of the hypogastric nerves together with the inferior mesenteric ganglion formations

Animals	Ovary Mean ± S.E. (n)	Oviduct Mean ± S.E. (n)	Uterus Mean ± S.E. (n)	Vagina Mean ± S.E. (n)
	μg/gm	μg/gm	μg/gm	μg/gm
Controls	4.93 ± 1.3 (4)	1.22 ± 0 19(4)	2.60 ± 0.34(4)	2.02 ± 0.36(4)
Denervated	3.60 ± 0 4 (4)	0.95 ± 0.20(5)	1 15 ± 0.23(5) [d]	0 73 ± 0.16(5)
	μg/pair	μg/pair	μg/pair	μg/organ
Controls	0.94 ± 0.17(4)	0.18 ± 0.02(4)	2.65 ± 0 49(4)	0.37 ± 0 06(4)
Denervated	0.87 ± 0.15(4)	0 14 ± 0 02(5)	0 87 ± 0 12(5)	0 14 ± 0.06(5)

Student's t-test P > 0.05; [b] 0.02 < P < 0.05; 0.01 < P < 0.02; [d] 0.001 < P < 0.01.

—— 1896 The innervation of the pelvic and adjoining viscera. J. Physiol. (Lond.) 20: 372–406.

ller M. D., and J. M. Marshall 1965 Uterine response to nerve stimulation; relation to hormonal status and catecholamines. Am. J. Physiol., 209: 859–865.

mberg, K.-A. 1967 Transmitter histochemistry of the sympathetic adrenergic nervous system. Brain Res., 5: 125–170.

erberg, K.-A., and F. Sjöqvist 1966 New possibilities for adrenergic modulation of ganglionic transmission. Pharm. Rev., 18: 743–751

wman, Ch., E. Rosengren and N.-O. Sjöberg 1966 Origin of the adrenergic innervation to the female genital tract of the rabbit. Life Sci., 5: 1189–1196.

—— 1967 Histochemical and chemical investigation of the adrenergic innervation of the human female reproductive organs. Obst. and Gynec. In press.

wman, Ch., and N.-O. Sjöberg 1966 Adrenergic nerves in the female genital tract of the rabbit. With remarks on cholinesterase-containing structures. Z. Zellforsch., 74: 182–197

—— 1967 Unpublished observations.

wman, Ch., and N. O. Sjöstrand 1965 Short adrenergic neurons and catecholamine-containing cells in vas deferens and accessory male genital glands of different mammals. Z. Zellforsch., 66: 300–320.

—— 1966 On short adrenergic neurons in the accessory male genital organs of the bull. Experientia, 22: 759–761

Poulson, E., and J. M. Robson 1963 The effect of amine oxidase inhibitors on pregnancy. J. Endocr. 27: 147–155.

Schofield, B. M. 1952 The innervation of the cervix and cornu uteri in the rabbit. J. Physiol., 117: 317–328.

Spector, W. G. 1961 Suppression of fertility in rats by an inhibitor of monoamine oxidase. J. Reprod. Fertil., 2: 362–368

Sjöberg, N.-O. Unpublished observations.

Sjöstrand, N. O. 1965 The adrenergic innervation of the vas deferens and the accessory male genital glands. Acta physiol. scand., 65: suppl. 257: 1–82.

Stjärne, L., and F. Lishajko 1966 Comparison of spontaneous loss of catecholamines and ATP in vitro from isolated bovine adrenomedullary vesicular gland, vas deferens and splenic nerve granules. J. Neurochem., 13: 1213–1216.

Varagić, V. 1956 An isolated rabbit hypogastric-nerve-uterus preparation, with observations on the hypogastric transmitter. J. Physiol. (Lond.) 132: 92–99.

tive tract with the exception of the ovary by way of *short* adrenergic neurons In this respect the sympathetic innervation pattern is basically similar to that in the rabbit (Owman and Sjöberg '66 Owman et al 66) the dissimilarities are limited essentially to quantitative differences in the proportions of short and "long" adren ergic neurons to the various organs The special type of short adrenergic neurons has so far been found to occur only in the urogenital tract including the accessory male genital organs (see Falck and Ow man 66) urinary bladder (Hamberger and Norberg 65) and urethra (Owman and Sjöberg 67) Functionally they seem to constitute a unique entity differing from the ordinary "long" adrenergic neu rons (Euler and Lishajko 66 Stjärne and Lishajko '66)

In the uterovaginal ganglion complex a certain number of both fluorescent and nonfluorescent (probably cholinergic) gan glion cells were enclosed by adrenergic varicose terminals in a synaptic manner These terminals were not affected by re moval of the hypogastric nerves and may therefore represent a purely intraganglionic system Such an arrangement may have a modulatory action on the post synaptic nerve cell (Norberg and Sjöquist 66)

LITERATURE CITED

Bertler A., A Carlsson E. Rosengren and B. Waldeck 1958 A method for the fluorimet ric determination of adrenaline noradrenaline and dopamine in tissues. Kungl. Fysiogr Sällsk. Lund Förh., 28 121–123

Brundin, J 1965 Distribution and function of adrenergic nerves in the rabbit Fallopian tube Acta physiol scand., 66 suppl. 259 1–57

Coppola J A. R. G Leonardi and W Lippman 1966 Ovulatory failure in rats after treatment with brain norepinephrine depletors. Endocrinology 78 225–228.

Corrodi, H., and N-A. Hillarp 1963 Fluoreszenzmethoden zur histochemischen Sichtbarmachung von Monoaminen. 1 Identifizierung der fluoreszierenden Produkte aus Modellversuchen mit 6,7-Dimethoxyisochinolinderivaten und Formaldehyd. Helv chim. Acta 46 2425–2430

——— 1964 Fluoreszenzmethoden zur histochemischen Sichtbarmachung von Monoaminen. 2. Identifizierung des fluoreszierenden Produktes aus Dopamin und Formaldehyd Helv chim. Acta, 47 911–912.

Cushny A. R. 1906 On the movements of the uterus. J Physiol. (Lond.) 35 1–19

Deanesly R. 1966 The effects of reserpine [illegible] ovulation and on the corpus luteum of th[e] guinea-pig. J Reprod. Fert., 11 429–431.

Eränkö, O. 1967 Histochemistry of nervo[us] tissues: Catecholamines and cholinesteras[es] Ann. Rev Pharm., 7: 203–222.

Euler U S von, and F Lishajko 1966 A sp[e]cific kind of noradrenaline granules in th[e] vesicular gland and the vas deferens of th[e] bull. Life Sci., 5: 687–691

Falck B 1962 Observations on the possibili[]ties of the cellular localization of monoamine[s] by a fluorescence method. Acta physiol. scand 56 suppl. 197 1–25.

Falck, B., N A. Hillarp, G. Thieme and A. To[rp] 1962 Fluorescence of catechol amines a[nd] related compounds condensed with formald[e]hyde. J Histochem. Cytochem., 10: 348–3[]

Falck B., and Ch. Owman 1965 A detai[led] methodological description of the fluoresce[nce] method for the cellular demonstration of bi[o]genic monoamines. Acta Univ Lund II, 1–23.

——— 1968 Histochemistry of monoamine[] mechanisms in peripheral neurons. In: Me[ch]anisms of Release of Biogenic Amines. U. [S.] von Euler S Rosell and B. Uvnäs, eds. Per[ga]mon Press, Oxford, pp. 59–72.

Falck, B., Ch Owman and N O. Sjöberg [] Peripherally located adrenergic neurons in[ner]vating the vas deferens and the seminal v[esi]cles of the guinea-pig. Experientia (Basel), [] 98–100.

Forsberg J-G. E. Rosengren and N-O. Sjö[berg] 1964 On the occurrence of 5-hydroxytry[pta]mine containing cells in the vaginal and v[es]tibular epithelium of the rabbit. Z. Zellfors[ch] 63: 302–308

Häggendal, J 1963 An improved method [for] fluorimetric determination of small amount[s of] adrenaline and noradrenaline in plasma [and] tissue. Acta physiol. scand 59 242–254.

Hamberger B., and K.-A. Norberg 1965 Stud[ies] on some systems of adrenergic synaptic ter[mi]nals in the abdominal ganglia of the cat. A[cta] physiol scand., 65 235–242.

Hillarp N A., A. Dahlström and K. Fuxe 1[966] Central monoamine neurons. In Mechani[sms] of Release of Biogenic Amines. U S. von Eu[ler] S Rosell and B Uvnäs, eds. Pergamon Pr[ess] Oxford pp 31–57

Holtz, P and D Palm 1966 Brenzkatech[ola]mine und andere Sympathicomimetische a[] Biosynthese und Inaktivierung Freisetzung [] Wirkung. Springer Verlag, Berlin, pp. 321–[]

Hopkins T F and G Pincus 1963 Effect [of] reserpine on gonadotropin-induced ovulation [in] immature rats. Endocrinology 73. 775–78[]

Labate J S., and D Sheehan 1943 Effect [of] atropine on uterine responses to hypogas[tric] nerve stimulation. Action at the ganglion[ic] synapse Am J Physiol., 139 178–182.

Langley J N and H. K. Anderson 1895 The innervation of the pelvic and adjoining viscera Part V Position of the nerve cells on the course of the efferent nerve fibres J Physiol. (Lond.) 19 131–139.

ine Structural Differences in Fast and 'Slow Iuscle Fibers of the Crab [1]

MELVIN J COHEN AND ARTHUR HESS

Department of Biology University of Oregon, Eugene and Department of Physiology University of Utah, College of Medicine Salt Lake City

ABSTRACT The muscle fibers in the accessory flexor muscle of the crab were examined with the electron microscope. The limiting membrane of the muscle fiber invaginates at many points to form an internal extrafibrillar membranous system between the muscle fibrils. Two types of muscle fiber were found. In one the fibrils are well separated from each other by an extensive membranous system, the sarcomere lengths are short, and the filaments in the A band are thick. This muscle fiber is the same as the *fast* fiber previously found physiologically The other type of muscle fiber has large fibrils poorly separated by a relatively scant system of internal membranes. It has relatively long sarcomeres and comparatively thin filaments in the A band. This type of fiber is the same as the *slow* fibers described physiologically Fibers intermediate in type are also found. Nerve terminals with typical synaptic vesicles occur and appear similar on both types of muscle fiber under the electron microscope. Membrane thickenings of nerve ending and muscle fiber also occur at the terminals on both types of muscle fiber The nerve terminals on the fast fiber are much more easily found and hence more numerous than on the slow fiber. A comparison is made between the invertebrate and vertebrate *fast* and *slow* fibers, and some physiological implications of these findings are discussed.

A definite relationship between struc re and function has been demonstrated the muscle fibers of vertebrates. *Twitch* uscle fibers have fibrils of regular size hich are separated evenly from each ther. They are also characterized by bundant amounts of sarcoplasmic reti ulum, a regular transverse tubular T ystem, a straight Z line, and a single ro ust nerve ending, usually with post unctional sarcolemmal infoldings. *Slow* muscle fibers, which exhibit a contracture r graded response after a nerve stimulus ave fibrils of irregular size which are nevenly separated from each other They ave relatively small amounts of reticu um, no regular T system (only aberrant elements occur) a zig-zag Z line, and deli cate multiple nerve terminals without postjunctional sarcolemmal infoldings (Kuffler and Vaughan Williams, '53; Hess '60 '61 '65; Hess and Pilar '63 Page, '65; Pilar and Hess, '66)

Cohen ('63b) found similar morphological differences, using the light microscope, in fibers of the accessory flexor muscle in the walking legs of crabs. He suggested that these structural differences might be related to the functional division of crustacean muscle into *fast* and *slow* types (Hoyle and Wiersma, '58 Wiersma, '61) Combined histological and physiological studies on the crab accessory flexor muscle generally confirmed this suggestion (Doral Raj '64 Doral Raj and Cohen, '64) Muscle fibers which show in cross-section an orderly punctate arrangement of relatively small fibrils have *fast* functional properties; muscle fibers whose fibrils are large and irregularly shaped have *slow* functional properties

The purpose of the present study is to define further the structural differences of the two major fiber types in the crab accessory flexor muscle by examination with the electron microscope. Such an investigation may provide insight into the factors responsible for the differentiation of contractile properties in crustacean muscle

MATERIALS AND METHODS

The accessory flexor muscle is a part of the myochordotonal organ proprioceptive

[1] This investigation was supported by U S. Public Health Research Grants NB-04785 to A. H. and NB-01884 to M. J. C. A. H. is in receipt of Research Career Development Award NB-22,404 from the Institute of Neurological Diseases and Blindness. Many thanks are due to Miss H. Ferguson and Mr. L. Bradshaw for their expert technical assistance.

Present address Department of Anatomy Rutgers Medical School, New Brunswick, New Jersey

) The limiting membrane invaginates separating itself from this fibrillar ath and dipping into the muscle as a ule (figs. 4–6) Sometimes, a thin por n of the connective tissue sheath ac mpanies the invaginating limiting mbrane for a considerable distance so t one portion of the limiting membrane separated by fibrillar material from the er (fig. 4) In this instance the in ginating limiting membrane enclosing fibrillar material appears like a septum trabeculum pushing into the muscle er (fig. 9) This septum becomes more rrow as it penetrates into the muscle er and finally the connective-tissue fi llar material disappears the limiting embranes approach each other and a bole continues into the muscle fiber e limiting membrane on one side can parate from its fibrillar material and nck into the muscle fiber as two closely proximated membranes or tubules (figs 9) The muscle fiber involved, although contains many septa, still appears as a ngle muscle fiber in that it is surrounded a common connective tissue sheath om which the septa arise. However in ctions passing through certain levels of e muscle fiber and its septa, it may ap ar as if there were two separate but djacent fibers separated by fibrillar ma rial (fig. 4)

Differences in internal structure of muscle fibers

Muscle fibers can be seen clearly to ffer in the distribution of the internal ctrafibrillar material and hence in the isposition, degree of separation and size f the fibrils. In general, the muscle fibers re of two major types. However there re some fibers which appear to be inter nediate between these two extremes and re difficult to classify

One type has relatively small fibrils of nore or less regular size which are uni ormly separated from each other by the xtrafibrillar membranous material (figs. 3) This can be seen in cross or longi udinal section. This disposition of fibrils causes the punctate appearance of this ype of fiber seen in cross-section with he light microscope (Cohen '63b) The other major structural type of fiber has much less extrafibrillar material. As a result the fibrils are much larger than those seen in the first fiber type of less uniform diameter and are irregularly separated from each other (figs. 2, 4) This distribution of fibrils is the basis of the appearance of the irregularly clumped second muscle fiber type described in the light microscopic study (Cohen '63b)

The first type of fiber described—with orderly fibrils—is similar to the *twitch* type of vertebrate muscle fiber while the second type corresponds to vertebrate *slow* muscle fibers It has been shown previously that fibers in the crab accessory flexor muscle showing a uniform punc tate appearance in cross-section in the light microscope have *fast* functional properties, while those with an irregular disposition of fibrils have *slow* properties (Doral Raj '64 Doral Raj and Cohen 64)

Another striking difference in these two types of muscle fiber is the length of the sarcomere. The distance between Z lines is ca. 2 μ in *fast* fibers (fig. 1) while the sarcomere of the *slow* fibers usually ap pears about three to five times as long or ca. 6–10 μ in length (fig. 2) This differ ence may be due to varying states of contraction of the fibers during fixation. However the difference in sarcomere length has been seen with phase contrast microscopy in adjacent unfixed fibers (Cohen, '63b) and therefore appears to be a valid structural difference between these two fiber types. Similar relationships between functional properties and sarco mere length in crustacean muscles have been postulated by other workers (Jasper and Pezard, '34 Kuffler '54 Atwood, '63)

A third difference seen constantly be tween these two types of muscle fiber is in the diameter of the thick filaments in the A band. The filaments are ca. 30–40A thick in the *fast* muscle fiber (fig. 1) but are usually only ca. 20A in the *slow* fiber (fig. 2) Both types of muscle fiber have an M line or a thickening of the thick filaments in the middle of the A band.

The invaginations of the limiting mem brane to form the internal extrafibrillar membrane system are of frequent occur rence in both types of muscle fiber (figs 3–6) However since the amount of extra fibrillar membranous material is greater

system in Crustacea The gross and microscopic anatomy of this muscle has been described in conjunction with investigations of this system in the crab *Cancer magister* Dana (Cohen 63a 63b) Adult male crabs of this species ranging in weight from 900–1700 gms were used. The accessory flexor muscle was exposed in the meropodite of walking legs 2–4 and left *in situ* The joint between the mero- and carpopodite was held in the normal resting position of approximately 90° In this position both the proximal and distal heads of the accessory flexor muscle are under tension (Cohen '63a) Two per cent osmium tetroxide buffered to pH 7 4 with sodium barbital was poured onto the exposed intact muscle The muscle remained immersed in the pool of fixative within the meropodite for 30 minutes It was then removed and transferred to a vial of fixative for an additional 60 minutes The specimens were then dehydrated with increasing concentrations of ethyl alcohol and stored in tertiary butyl alcohol. They were subsequently treated with propylene oxide and embedded in Maraglas Sections were cut with a glass or diamond knife on a Porter Blum MT 1 or LKB microtome collected on formvar-coated copper grids and stained with lead They were examined with an RCA EMU 3F electron microscope

RESULTS

Features common to both types of muscle fiber

The majority of the results are from the proximal head of the muscle but fibers from the distal head appear to have the same characteristics The muscle fibers vary greatly in diameter ranging from 10–25 μ Their fibrils exhibit A and I bands and Z lines as in striated muscle elsewhere (figs. 1,2) A few mitochondria, of typical structure with internal folds are located between the fibrils There are areas of sarcoplasm — located, especially near the periphery of the muscle fibers — which are devoid of fibrils and have rather dense accumulations of mitochondria

Two outstanding structures are seen between the fibrils. One consists of granular material dispersed in an amorphous background. This material is the ground cytoplasm of the muscle fiber (sarco plasm) (fig 1)

The second structure consists of thi tubules surrounded by dense membranes, sometimes with irregular borders, or a series of vesicles lined up with each other (figs. 1–6) In longitudinal sections, the tubules are predominantly longitudinally oriented in the muscle fiber and run paral lel to the muscle fibrils (figs. 1 2) a in cross-section many fibrils are se completely surrounded by this extra brillar material (figs. 3, 5) This inter extra fibrillar membrane system is simil to the sarcoplasmic reticulum of verte brate muscle fibers

In longitudinal sections, there are man places where the limiting membrane o the muscle fiber invaginates, runs in the muscle fiber for a short distance, an then turns to run longitudinally an parallel to the muscle fibrils (fig 6). It i often possible to follow the invaginatin limiting membrane for a rather long dis tance and to trace it from its origin at the periphery of the muscle fiber to its inter nal location between and parallel to the muscle fibrils (fig. 6) Frequently the longitudinal course of the invaginated limiting membrane is in areas of sarco plasm near the periphery which are devoid of fibrils Sometimes it appears as a rather well defined tubule and at other times, as a series of vesicles. This invagination of the limiting membrane of the muscle fiber which gains access to the interior of the muscle fiber is similar to that of the T system of vertebrate muscle fibers.

In cross-section the internal extrafibril lar membrane system can be seen to arise from invaginating limiting membrane and to be continuous with it (figs. 4 5) Since the muscle fibrils in cross or longitudinal section appear surrounded by an extra fibrillar membrane system it would appear that the extrafibrillar membranes form a highly branched reticular system enclosing the muscle fibrils Many if not all, of these membranes appear to be continuous with invaginations of the limiting membrane of the muscle fiber

The muscle fiber is surrounded by a connective tissue sheath of about 0.5 μ to 0 75 μ in thickness (figs. 4 6 10 11 13

parate from the axon to spread along a muscle fiber for a short distance be-re terminating. Mitochondria similar to ose in the more proximal portion of the on begin to accumulate. They are attered throughout the axon in this re-on, with no tendency to be disposed ong the periphery of the nerve fiber as scribed above for more proximal por-ons of the axon. The connective-tissue rillar material surrounding the nerve nd that around the muscle fiber fuse g. 10) The nerve then pushes into the uscle fiber for a short distance (figs. 10 1) As the nerve fiber passes into the uscle fiber it is accompanied by the ense innermost layer of the Schwann cell hich was described above (figs. 10 11)

Synaptic vesicles, entirely similar in ize and appearance to those seen in ertebrate synapses and neuromuscular unctions, appear in irregular groups or lumps scattered throughout the terminal axon (figs. 10 11 12) Then the dense ayer of Schwann cell around the axon terminates and the nerve fiber is separated rom sarcoplasm only by the limiting membrane of the axon and that of the muscle fiber (figs. 11 12) Dense thicken-ings of the membranes of axon and mus-cle fiber occur irregularly (figs. 11 12) Accumulations of synaptic vesicles are always seen in the axon adjacent to these membrane thickenings (figs. 11 12)

The sarcoplasm in the neighborhood of the nerve terminal appears different from that elsewhere in the muscle fiber (figs 11, 12) Many mitochondria are gathered and the sarcoplasm is very granular Double membranes are seen coursing in the sarcoplasm near and under the nerve terminal (figs. 11 12) Some of these, at least, are limiting membrane of the mus-cle fiber invaginating to form the internal extrafibrillar material as described above. Some of these *infoldings* then, appear similar to the subjunctional folds or the secondary synaptic clefts seen in the sarcolemma of vertebrate neuromuscular junctions. However they are probably better considered as invaginating limiting membrane than as junctional folds. Under some terminals, these points of invagin-ation of the muscle fiber limiting mem-brane seem more frequent than along the portion of muscle devoid of terminals.

The distribution of nerve terminals All the muscle fibers of both major types appear to have several nerve terminations along their length. As seen with the elec-tron microscope the structures of indi-vidual nerve terminals appear similar in both kinds of fiber (figs. 10 11 13) How-ever a great difference is seen in the number of terminals occurring on indi-vidual muscle fibers of the two types. The *fast* fiber is much more densely innervated than the *slow* fiber (fig 14) i.e. termi-nals are found very frequently on *fast* fibers and are relatively sparse on the *slow*

DISCUSSION

The infolding of the limiting membrane in crab muscle fibers to form part of the internal extrafibrillar material is similar to that described in the muscles of crayfish (Peterson '62 Brandt, Reuben Girardier and Grundfest, '65) Cyclops (Bouligand, '63) horseshoe crabs (Dumont, Anderson and Chomyn, '65) and some insects (Smith, '61) The continuation of the invaginating limiting membrane often turns at right angles and runs parallel to the muscle fibrils The transverse tubular T system in vertebrates is an invagination of the cell membrane which runs transversely across the fiber (Fran-zini-Armstrong and Porter '64) In frog *slow* muscle fibers aberrant T system elements may be found running parallel to the fibrils (Page, '65) Because of the extensive ramifications of the invaginating cell membrane in the interior of the crab muscle fiber it is difficult to determine if all the membranes seen internally are connected to this cell membrane.

Several of the differences seen in the internal structure of the crab *fast* and *slow* muscle fibers are similar to those described for vertebrate *twitch* and *slow* muscle fibers. The vertebrate fibers with small regularly arranged fibrils are called *Fibrillenstruktur* muscle fibers by Krüger (49) and have *fast* functional properties (Peachy and Huxley '62 Hess and Pilar '63) The same correlation between regu-lar fibrillar arrangement and *fast* func-tional properties is also seen in the crab muscle fibers. The vertebrate muscle fibers

in the *fast* than in the *slow* muscle fiber there are probably more points along the *fast* muscle fiber where the limiting membrane invaginates and the internal mem brane system may branch more extensively in the *fast* fiber than in the *slow*

Observations on nerves and nerve endings

Nerve fibers A thick and a thin efferent axon innervate both heads of the accessory flexor muscle The two axons branch profusely as they approach the muscle and each muscle fiber has several nerve terminals along its length (Cohen 63b) All observations on the nerves were in the region close to the muscle after much branching had occurred The thick axon has been shown to be excitatory and the thin axon inhibitory (Doral Raj and Cohen 64) Due to the branching of these axons it is not possible to determine in this study whether a given nerve fiber or terminal is from the excitatory or inhibitory axon

The axons are relatively clear structures containing scattered small mitochondria some granular material and a few vesicles (fig 7) The mitochondria tend to be located around the periphery of the fiber The axon is surrounded by a membrane which appears very dark under the electron microscope (fig 7) Larger nerve fibers are ensheathed by layers of Schwann cell cytoplasm which wrap around the axon (fig 7) Immediately outside the axonal membrane the Schwann cell cytoplasm appears more dense than in other layers (fig 7) More than one nerve fiber can be enveloped in the same Schwann cell lamellar apparatus However larger fibers are usually seen alone and are only occasionally accompanied by one or more small fibers Two or three medium-sized fibers can also appear enclosed in the same Schwann cell apparatus Around the whole nerve fiber and its Schwann cell apparatus is fibrillar connective tissue like that surrounding the muscle fiber (fig 7) This material is included between the lamellae of Schwann cell cytoplasm ensheathing the axon (fig 7) The lamellae of Schwann cell cytoplasm are irregular in disposition and thickness Around axons of ca. 10 μ in diameter a sheath about 5μ thick contains from 7–10 Schwann cell lamellae of unequal thickness. Several lamellae can end abruptly as they wind around the nerve fiber (fig. 7) so that the axon is covered by a variable number of lamellae along its border Between the lamellae fibrillar material is seen. In a few places along the lamellae, the connective tissue material is eliminated for a short distance and the two limiting membranes of adjacent Schwann cell lamellae appose each other (fig. 7) More than one nucleus can be found in the Schwann cell cytoplasm indicating that more than one Schwann cell contributes to the lamellar apparatus on the nerve fiber The cytoplasm of the Schwann cell contains many granules Its mitochondria are few in number small in size and the intramitochondrial matrix is not dense, so that these organelles appear only lightly stained in the electron microscope. The more dense layer of Schwann cell cytoplasm adjacent to the limiting membrane of the axon has in it more granules and some vesicles.

Internal mesaxons can be seen following a winding course from the inner lamella of the Schwann cell toward the surface of the axon (fig 7) Since more than one Schwann cell enters into the formation of the lamellae on the axon more than one mesaxon can also be found on the same nerve fiber

Smaller nerve fibers are usually surrounded by a thinner sheath than that found around the larger fibers. Each lamella of the sheath is thinner and there are fewer lamellae present. Very small fibers (about 0 5 μ in diameter) are not ensheathed by Schwann cell lamellae but are almost completely enclosed in Schwann cell cytoplasm and suspended in the Schwann cell cytoplasm by a mesaxon extending from the limiting membrane of the Schwann cell and enclosing the nerve fiber (fig 8) In these very small crab nerve fibers the relations of Schwann cell nerve fiber and mesaxon appear entirely similar to those seen in vertebrate nonmyelinated nerve fibers

Nerve terminals As the nerve fiber approaches the muscle the Schwann cell lamellae become reduced in number because some of the lamellae terminate. As the nerve fiber further approaches the muscle some of the remaining lamellae

structure histologique. Compt. Rend. Acad. Sci., 198: 498–501.

tger, P 1949 Die Innervation der tetanischen und tonischen Fasern der quergestreiften Skelettmuskulatur der Wirbeltiere. Anat. Anz., 97 169–191.

ffler, S. W 1954 Mechanisms of activation and motor control of stretch receptors in lobster and crayfish. J Neurophysiol., 17 558–574.

ffler S. W and E. M. Vaughan Williams 1953 Small-nerve junctional potentials. The distribution of small motor nerves to frog skeletal muscle, and the membrane characteristics of the fibres they innervate. J Physiol., 121 289–317

ge, S. G. 1965 A comparison of the fine structures of frog slow and twitch muscle fibers. J. Cell Biol., 26 477–497

schy L. D and A. F Huxley 1962 Structural identification of twitch and slow striated muscle fibers of the frog. J Cell. Biol. 13: 177–180.

Peterson, R. P 1962 Continuities between the plasma membrane and the sarcoplasmic reticulum in crayfish stretch receptor muscle as revealed by reconstructions from serial sections. Am. J Anat., 111 89–110.

Pilar G., and A. Hess 1966 Differences in internal structure and nerve terminals of the slow and twitch muscle fibers in the cat superior oblique. Anat. Rec., 159 243–252.

Smith, D S. 1961 The structure of insect fibrillar flight muscle A study made with special reference to the membrane systems of the fiber J Biophysic. Biochem. Cytol., 10 No 4 suppl., 123–158.

Wiersma, C. A. G. 1961 The neuromuscular system. In The Physiology of Crustacea, Vol. II, T H. Waterman, ed. Academic Press, New York, pp. 191–240.

with large irregular fibrils designated as *Felderstruktur* fibers by Krüger have the functional characteristics of *slow* muscle fibers A similar relationship between structure and function is true of the *slow* crab muscle fibers The difference in fila ment thickness and the marked differ ences in sarcomere length of crab *fast* and *slow* fibers have not been reported for the vertebrates

The crab accessory flexor muscle is innervated by an excitatory and an inhibitory axon Since only one structural type of nerve terminal was observed it may be that morphological differences are not exhibited by these two types of axon Furthermore since only a single excita tory axon innervates both the *fast* and *slow* muscle fibers it is clear that in this instance the factors responsible for *fast* and *slow* mechanical responses are not related to specific characteristics of the innervating motor axon but rather to the properties of the muscle fibers

The primary difference in the inner vation of the two major muscle fiber types is in the number of nerve terminals per muscle fiber In vertebrates the *slow* muscle fibers are multiply innervated while the *twitch* fibers have a single end plate (Hess 60 '61 Hess and Pilar '63) In the crab all muscle fibers are multiply innervated as seems generally true for the *Crustacea* (Wiersma '61) However the *fast* fibers have many more nerve terminals per fiber than the *slow* fibers This factor alone might possibly account for some of the functional differences between *fast* and *slow* fibers on the basis that summation of local activity at a lar ger number of points along the *fast* fiber membrane could lead to a rapid depolari zation of a larger area of membrane and thus result in a more rapid activation of the contractile apparatus However the density of nerve terminal innervation may be only one factor contributing to the differences in mechanical response The internal structural differences intrinsic to the muscle fiber itself could be responsible for the observed differences in cable properties responsiveness to indirect stimulation and sensitivity to ions and drugs seen in the two major fiber types (Atwood 64 Dorai Raj '64 Dorai Raj and Cohen 64) It is particularly tempting to speculate for the *fast* fiber that the greater number of points where the limiting membrane invaginates and the resultant greater contact between the contractile and the excitatory elements may contribute substantially to the more rapid mechanical action of the *fast* fibers

LITERATURE CITED

Atwood H. L. 1963 Differences in muscle fibre properties as a factor in "fast" and "slow" contraction in *Carcinus*. Comp. Biochem. Physiol., *10* 17–32.

——— 1964 Gamma-aminobutyric acid and crab muscle fibres. Experientia, 20: 161–162.

Bouligand, Y 1963 Les ultrastructures musculaires des copépodes. II. Membrane sarcoplasmique, reticulum sarcoplasmique et jonction neuromusculaire chez les Cyclops. J. de Microscopie 2. 197–212.

Brandt P W J P Reuben, L. Girardier and H Grundfest 1965 Correlated morphological and physiological studies on isolated single muscle fibers. J Cell Biol., 25 233–260.

Cohen, M. J 1963a The crustacean myochordotonal organ as a proprioceptive system. Comp. Biochem. Physiol., *8*: 223–243.

——— 1963b Muscle fibers and efferent nerves in a crustacean receptor muscle. Quart. J Micr Sci. *104* 551–559.

Dorai Raj B S 1964 Diversity of crab muscle fibers innervated by a single motor axon. J Cell. and Comp. Physiol., 64: 41–51.

Dorai Raj B S., and M. J Cohen 1964 Structural and functional correlations in crab muscle fibers. Naturwissen., 9: 224–225.

Dumont, J N., E. Anderson and E. Chomyn 1965 The anatomy of the peripheral nerve and its ensheathing artery in the horseshoe crab, *Xiphosura (Limulus) polyphemus*. J. Ultrastruc. Res., *13* 38–64

Franzini-Armstrong, C., and K. R. Porter 1964 Sarcolemmal invaginations constituting the T system in fish muscle fibers. J Cell Biol., 22 675–696.

Hess, A. 1960 The structure of extrafusal muscle fibers in the frog and their innervation studied by the cholinesterase technique. Am. J Anat. *107* 129–152.

——— 1961 Structural differences of fast and slow extrafusal muscle fibres and their nerve endings in chickens. J Physiol., *157*: 221–231.

——— 1965 The sarcoplasmic reticulum, the T system and the motor terminals of slow and twitch muscle fibers in the garter snake. J Cell Biol. 26 467–476.

Hess, A., and G. Pilar 1963 Slow fibres in the extraocular muscles of the cat. J Physiol. *169* 780–798

Hoyle G and C. A. G Wiersma 1958 Excitation at neuromuscular junctions in Crustacea. J Physiol. *143* 403–425.

Jasper H. H., and A. Pezard 1934 Relation entre la rapidite d'un muscle strie et sa

cture histologique. Compt. Rend. Acad. L, 198: 499–501.
...er P 1949 Die Innervation der tetanischen und tonischen Fasern der quergestreiften Skelettmuskulatur der Wirbeltiere. Anat. Anz., 169–191.
...ler, S. W 1954 Mechanisms of activation and motor control of stretch receptors in lobster and crayfish. J. Neurophysiol., 17 ...–374.
...ler, S. W and E. M. Vaughan Williams ...51 Small-nerve junctional potentials. The distribution of small motor nerves to frog skeletal muscle, and the membrane characteristics of the fibres they innervate. J Physiol., ...: 289–317
..., S. G. 1965 A comparison of the fine structures of frog slow and twitch muscle fibers. J. Cell Biol., 26: 477–497
...ey L. D and A. F Huxley 1962 Structural identification of twitch and slow striated muscle fibers of the frog. J Cell. Biol. 13 177–180.
Peterson, R. P 1963 Continuities between the plasma membrane and the sarcoplasmic reticulum in crayfish stretch receptor muscle as revealed by reconstructions from serial sections. Am. J Anat., 111 89–110.
Pilar G and A. Hess 1966 Differences in internal structure and nerve terminals of the slow and twitch muscle fibers in the cat superior oblique. Anat. Rec., 159 243–252.
Smith, D S. 1961 The structure of insect fibrillar flight muscle. A study made with special reference to the membrane systems of the fiber J Biophysic. Biochem. Cytol., 10 No. 4 suppl., 123–158.
Wiersma, C. A. G. 1961 The neuromuscular system. In: The Physiology of Crustacea, Vol. II T H. W terman, ed. Academic Press New York, pp. 191 240.

PLATE 1

EXPLANATION OF FIGURES

All illustrations are electron micrographs of crab muscle and nerve fibers. The lines on the photographs indicate 1 μ.

1 Fast muscle fiber longitudinal section. The muscle fibrils are fairly well separated from each other by sarcoplasm, rows of vesicles (arrows) and some double membranes (arrows). The sarcomere length is relatively short, and the filaments in the A band are relatively thick. Compare with figure 2. × 16,000.

2 *Slow* muscle fiber longitudinal section. The muscle fibrils are barely separated from each other by double membranes or rows of vesicles (arrows). The sarcomere length is relatively long (a complete sarcomere is not included in the photograph because of its length), and the filaments in the A band are relatively thin. Compare with figure 1. × 16,000.

PLATE 1

EXPLANATION OF FIGURES

All illustrations are electron micrographs of crab muscle and nerve fibers. The lines on the photographs indicate 1 μ.

1 *Fast* muscle fiber longitudinal section. The muscle fibrils are fairly well separated from each other by sarcoplasm, rows of vesicles (arrows) and some double membranes (arrows) The sarcomere length is relatively short, and the filaments in the A band are relatively thick. Compare with figure 2. × 16,000.

2 *Slow* muscle fiber longitudinal section. The muscle fibrils are barely separated from each other by double membranes or rows of vesicles (arrows) The sarcomere length is relatively long (a complete sarcomere is not included in the photograph because of its length) and the filaments in the A band are relatively thin. Compare with figure 1 × 16,000

PLATE 2

EXPLANATION OF FIGURES

All illustrations are electron micrographs of crab muscle and nerve fibers. The lines on the photographs indicate 1 μ.

3 *Fast* muscle fiber cross-section The muscle fibrils are relatively thin and fairly well separated from each other by rows of vesicles and double membrane (arrows) Compare with figure 4 × 16 000.

4 *Slow* muscle fiber cross-section The muscle fibrils are very poorly separated from each other by double membranes and rows of vesicles (arrows) Compare with figure 3 Septa, which consist of invaginating limiting membrane one portion separated from the other by fibrillar material pass into the muscle fiber at S From the septa invaginating limiting membrane branches off and passes into the muscle fiber between the fibrils as part of the internal extrafibrillar membranous system × 16,000

PLATE 3

EXPLANATION OF FIGURES

All illustrations are electron micrographs of crab muscle and nerve fibers. The lines on the photographs indicate 1 μ.

5 The muscle fibril is surrounded by a series of vesicles which are almost continuous with the limiting membrane of the muscle fiber. *Fast* fiber cross-section × 80 000.

6 The limiting membrane invaginates (at the arrow) changes direction and continues in a direction parallel to the direction of the muscle fibrils, as part of the internal membranous extrafibrillar system Accumulations of mitochondria are seen in peripheral portions of sarcoplasm which are devoid of fibrils *Fast* fiber longitudinal section × 12 500

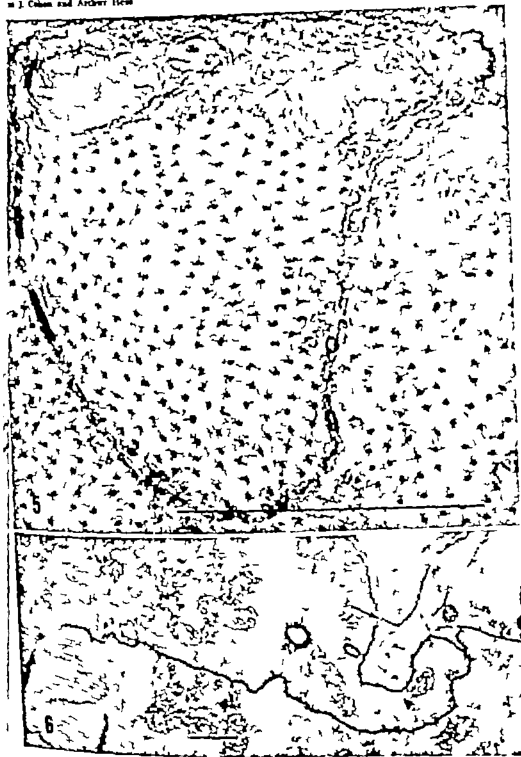

5
6

PLATE 4

EXPLANATION OF FIGURES

All illustrations are electron micrographs of crab muscle and nerve fibers. The lines on the photographs indicate 1 μ.

7 The relatively clear axon (Ax) with mitochondria which tend to be located at the periphery is surrounded by a dense axolemma. The whole nerve fiber is surrounded by connective-tissue fibrillar material (F) The axon is surrounded by Schwann cell lamellae (S); adjacent lamellae are separated by fibrillar material (F) The Schwann cell lamella nearest the axolemma is dense; the devious course followed by the mesaxon (M) is seen in this layer Some Schwann cell lamellae end abruptly (at the arrow) At some places, fibrillar material is absent and Schwann cell lamellae appose each other (A) $\times$ 12,500.

8 Small nerve fibers (A) almost completely enclosed by Schwann cell cytoplasm (S) and suspended by a mesaxon (M) $\times$ 16,000.

9 A septum of a muscle fiber which consists of limiting membrane separated by fibrillar material. From the septum, the limiting membrane invaginates to run between the fibrils as part of the internal extrafibrillar membranous system. *Fast* fiber cross-section $\times$ 32,000.

F
F
S
S
F
A





PLATE 5

EXPLANATION OF FIGURES

All illustrations are electron micrographs of crab muscle and nerve fibers. The lines on the photographs indicate 1 μ.

10 Nerve terminal on a *fast* muscle fiber cross-section. The terminal axon containing vesicles and mitochondria is not yet apposed to the muscle fiber and is still surrounded by the dense inner layer of Schwann cell cytoplasm (S) Fusion of the connective-tissue fibrillar sheath of the nerve fiber to that of the muscle fiber is apparently occuring at the arrow × 10 000

11 Nerve terminal on a *fast* muscle fiber cross-section. The terminal axon, containing vesicles and mitochondria, is apposed to the muscle fiber A membrane density (arrow) with accumulations of vesicles in the axon is seen The sarcoplasm of the muscle fiber (M) near the terminal is granular and devoid of fibrils and has membranes coursing through it Some dense Schwann cell cytoplasm (S) still accompanies the nerve fiber × 10 000.

S

10

O S O

M

O

S

11

PLATE 6

EXPLANATION OF FIGURES

All illustrations are electron micrographs of crab muscle and nerve fibers. The lines on the photographs indicate 1 μ

12 A nerve terminal, containing mitochondria and vesicles is embedded in granular sarcoplasm (M) A membrane density is seen at the arrow × 32 000.

13 Nerve terminal containing mitochondria and vesicles on a slow muscle fiber longitudinal section The structure of the terminal and its relations to the muscle fiber with membrane densities occurring (arrow) are entirely similar to those seen in the nerve terminals on *fast* muscle fibers in figures 10 11 12. × 12,500

14 Nerve terminals on a *fast* muscle fiber longitudinal section. The two nerve terminals are very close together In general, nerve terminals can be found much more frequently on *fast* muscle fibers than on *slow* ones. × 16 000

T" AND "SLOW" CRAB MUSCLE FIBERS
n J. Cohen and Arthur Hess





Morphological and Histochemical Study of the imary and Secondary Immune Responses the Rat Spleen [1]

JAMES C. PETTERSEN, DANIEL F BORGEN AND
KENNETH C. GRAUPNER
Department of Anatomy University of Wisconsin, Madison, Wisconsin

ABSTRACT Macrophages and cells of the plasmocyte series were studied in the rat's spleen during the primary and secondary immune responses to particulate antigen. Evidence is presented to suggest that the plasma cell precursors are located in the marginal zones surrounding the lymphoid nodules and that less than one day following injection of antigen, these cells migrate into the nodules, where mitosis and subsequent differentiation into hemocytoblasts occurs in the presence of nodular macrophages. The hemocytoblasts then migrate across the marginal zone into the red pulp where differentiation into mature plasma cells occurs in the presence of red pulp macrophages. It is suggested that the initiation of the antibody-forming process occurs in the lymphoid nodules where marginal zone cells come into close contact with the marginal metalophils or with germinal center macrophages. The process initiating the migration of cells from the marginal zone to the nodules is unknown.

Studies suggest that the induction of antibody formation occurs following the transfer of an RNA-antigen complex from the macrophage to a potential antibody-producing cell (Fishman, '61 and Fishman and Adler '63) The present investigation is an attempt to determine the location within the rat spleen of the precursors of antibody-forming plasma cells, their topographic relationship to probable inductive macrophages, and their subsequent cycle of differentiation toward mature antibody-forming plasma cells. To do this, we have studied the rat spleen during both primary and secondary responses to particulate antigens

MATERIALS AND METHODS

One hundred and nine male, Holtzman rats weighing between 200–300 g were used. Fifteen animals served as untreated controls and five served as controls injected intravenously with 1.0 cm³ of physiological saline. The remaining animals received 1.0 cm³ injections of broth cultures of heat-killed 0111 B_4 E. coli organisms (about 900 million organisms/cm³) or of 1.0 cm³ of typhoid-paratyphoid vaccine (Eli Lilly and Co) via the lateral tail vein without anesthesia. Spleens from 40 of these animals were studied during the primary response (primary spleens) and spleens from 36 were studied following secondary injections (secondary spleens) given 16–20 days after the primary injections. A series of both primary and secondary spleens was thus obtained for studying the response to both types of antigen suspension Thirteen animals were given two 1 0 cm injections of antigen 24 hours apart. This group represented a pilot attempt to produce a generalized Shwartzman reaction in the rat and is included in the present study as an additional control on the cellular response

All experimental animals were killed with ether at times ranging from 15 minutes to 16 days following the injections. Pilot studies indicated significant changes within the first 24 hours so that during some stages within the first 24 hours, animals were killed at one half-hour intervals. Sixteen primary animals and seventeen secondary animals were killed during this period. The remaining animals were killed at one-day intervals up to ten days, and then at 13 and 16 days.

At autopsy spleens were rapidly removed and pieces fixed in Carnoy's fluid,

[1] This project received support from General Research Support Grant to the University of Wisconsin Medical School from the National Institutes of Health, Division of Research Facilities and Resources.
[2] Summer Research Trainee, Anatomical Sciences Training grant 5 T1 GM 723-02.
[3] Summer Research Fellow, National Institutes of Health Medical Student Training Grant.

15% cold neutral formalin and Helly's solution

The Carnoy fixed tissue was sectioned at 7 μ in paraffin for pyronin Y methyl green staining Control slides were digested for one-half hour in a 10 mgm% solution of ribonuclease at room temperature and further controls were incubated for one-half hour in distilled water These sections were used to identify cells synthesizing RNA.

Pieces fixed in formalin were sectioned with the freezing microtome at 25 μ and stained for acid phosphatase activity according to Burstone (58) Naphthol AS-BI phosphate was used as substrate and Garnet GBC as the diazonium salt Sections were free-floated in the medium buffered to pH 5.2 with acetate buffer and incubated for one-fourth—one-half hour at 37 C The sections were then transferred to distilled water floated onto slides and mounted with glycerin jelly Other formalin fixed frozen sections were stained for nonspecific esterase activity and for metalophilia as described previously (Pettersen 64) These procedures identified the macrophages. Sections from several spleens were stained for 5 nucleotidase activity according to Wachstein and Meisel (57)

Helly-fixed pieces were sectioned in paraffin at 4–5 μ and stained with hematoxylin-eosin-azure II. These were studied for cell detail.

Spleen imprints were made with some of the spleens by touching the cut ends lightly to glass slides They were wet fixed in Carnoy's fluid for PMG staining or in Helly's solution for Giemsa staining They were used for studying individual cells

RESULTS

Macrophages Four criteria were used in examining the acid phosphatase nonspecific esterase 5 nucleotidase and silver stained sections (1) the presence within the lymphoid nodules of increased numbers of macrophages showing hydrolytic enzyme activity (2) the presence of enlarged rounded macrophages within the nodules; (3) narrowing of the marginal zone as measured by the distance from the marginal metalophils to the reactive red pulp cords; (4) the presence of increased numbers of macrophages within the marginal zone

Spleens from untreated and saline-injected animals contained a few scattered macrophoges within the nodules, a distinct rim of macrophages surrounding the nodules and a marginal zone averaging 80–100 μ in width with a scant macrophage population (figs. 1,2) The red pulp cords contained abundant macrophages. Techniques for acid phosphatase, nonspecific esterase 5-nucleotidase and metalophilia gave similar results.

The sequences of events following primary injections of *E coli* and typhoid-paratyphoid vaccine were comparable. The marginal zone narrowed to about one-fourth its normal width several hours following either primary or secondary injections and the nodules enlarged proportionately (fig 3) This narrowing began at two hours in the paratyphoid-typhoid injected (typhoid) animals and somewhat later in the *E. coli*-injected (*E. coli*) animals. During the narrowing stage there were often significant numbers of macrophages within the zone. The zone remained narrow at days two and three, but returned to a normal width of 80 μ four days following either primary or secondary injections (four days)

The increase in number of nodular macrophages began early with accumulation of cells showing acid phosphatase activity in small germinal centers. The germinal centers stood out as lighter staining areas on acid phosphatase-stained sections Up to about three days, these cells retained a stellate configuration but, by four days most of them had enlarged to assume the rounded form characteristic of the cells containing tingible bodies (fig 5) The typhoid animals possessed greater numbers of these rounded forms than the *E coli* animals In some the macrophages retained this configuration up to ten days, but the return to the resting stellate morphology began at about seven days and was virtually complete by 13 days. The 13 and 16-day spleen sections stained for acid phosphatase resembled those of the control groups.

The spleens from animals which received secondary injections (secondary animals) presented the same cycle of

crophage activity except that narrowing the marginal zone was accelerated and re marked. In the typhoid animals the e was almost obliterated at eight hours t approached normal width by 24 hours. e zone narrowed somewhat later in the coli animals and was essentially obliter d at one day. Animals given two in- tions of E. coli 24 hours apart showed s obliteration at its extreme when ex ined 24 hours after the second injection g. 4) Upon enlargement of the zone two and three days, increased numbers macrophages were found in this loca- n in all spleens.

Pyroninophilic cells The most consis- nt pyroninophilia in the spleens of treated and saline-injected animals was und in the cells of the marginal zone e majority of the cells here showed a ine granular type of pyroninophilia in eir cytoplasm. One small nucleolus was ually present in the nuclei of these cells at the nucleolar material was only faintly ained with pyronin. The cells in question sembled medium-sized lymphocytes (fig s) and will be referred to as marginal ne lymphocytes.

At one-half hour following either prim- ry or secondary antigenic stimulation, arginal zone lymphocytes were found at he periphery of the lymphoid nodules ainder the mantle layer of small lympho- ytes. Several hours following stimulation, he marginal zone was almost completely epleted of these cells. The adjacent red ulp contained a sparse cell population at his time with few lymphocytes but the antle layer of small lymphocytes was ow masked by the presence of marginal one lymphocytes (figs 7 8)

The timing of this phenomenon varied with the stimulation used. It was more apid with the typhoid antigen than with he E. coli and also more rapid in second- ary than in primary animals. The margin- al zone was exhausted by eight hours in the secondary typhoid animals and by 24 hours in the secondary E. coli group The primaries lagged by about four hours in each case.

From 1/2–24 hours following stimu- lation, marginal zone lymphocytes could be seen in the marginal sinus and passing through its inner membrane (fig. 9 10)

Very few mitoses were present among the marginal zone lymphocytes at the periphery of the nodules at this time. Many of the lymphocytes could be seen in close apposition to the marginal metalophils (fig. 10)

Germinal centers containing nests of pyroninophilic cells were prominent at two and one-half days in both primary and secondary spleens. These centers were frequently confluent with the marginal zone lymphocytes at the periphery of the nodules. Tingible body macrophages were in the early stages of formation at this time although their occurrence was somewhat unpredictable early in the response. Pyroninophilic cells were in close relation to these macrophages (fig. 11) and were in the process of differentiation. Their cytoplasm now stained more intensely with pyronin and the nucleoli, usually one large one per cell, showed strong affinity for pyronin. Some of these cells were hemocytoblasts but the majority were intermediate stages between marginal zone lymphocytes and hemocytoblasts (fig 11)

The mantle layer of small lymphocytes was again present at two and one-half days and, scattered within it, could be found individual hemocytoblasts (fig. 6c)

The marginal zone had begun to replenish its cell population the predominating type being that seen in the unstimulated spleens. Scattered admidst these were hemocytoblasts (fig 12) Mitotic figures were always present in the marginal zone but were generally few in number There were never suggestions of germinal center type activity in this region. In the spleens of those animals receiving two injections of antigen 24 hours apart, marginal zone lymphocytes and hemocytoblasts could be seen intermingled in the mantle layer (fig. 13)

The red pulp cords contained hemocytoblasts and immature plasma cells from two to five days. This also occured earlier in the secondary spleens. Most of the pyroninophilic cells in the red pulp at two and three days in a secondary spleen were intermediate between hemocytoblasts and plasma cells. The nucleoli showed fragmentation and loss of pyroninophilia, the nucleus assumed an eccentric position and

a perinuclear zone could be observed in many of them By five days in both primary and secondary spleens mature plasma cells were the predominating cell type in the red pulp (fig 6d)

A thorough examination of spleen imprints from all stages of stimulation failed to provide evidence that small lymphocytes converted directly to plasma cells Many plasma cells resembled small lymphocytes on sections but the imprints revealed them to be plasma cells Their nuclei were similar but the pyroninophilic cytoplasm and perinuclear clear zone of the plasma cell were apparent on the imprints This distinction was difficult to make on sectioned material Imprints prepared from spleens obtained five or six days following stimulation showed unequivocally that the major pyroninophilic cell type was the classically described plasma cell. At times earlier than this intermediate types between hemocytoblasts and plasma cells were seen It was our judgment that these latter cells were plasma cell precursors. "Hemocytoblast" is the term adopted by the Committee Concerning Nomenclature of Cells Responsible for Immune Reactions (Holub '64) for describing the large "blast" cells generally regarded to be plasma cell precursors Its characteristic features are its large pyroninophilic nucleolar mass and its pyroninophilic cytoplasm (fig 6c)

By six days the splenic response began to subside Germinal centers were less active and the red pulp cords contained fewer plasma cells than at five days Between 10 and 16 days the stimulated spleens returned gradually to a condition morphologically similar to the unstimulated spleens (fig 14)

DISCUSSION

The results indicate that cells of the marginal zone surrounding the lymphoid nodules and periarteriolar lymphoid sheaths are the precursors of antibody forming cells in the rat spleen They are seen to migrate into the mantle layer of the lymphoid nodules shortly after antigenic stimulation and to incorporate into the germinal centers within the nodules about two days following this migration The possibility was considered that these cells had migrated into the red pulp and

then into the peripheral blood by way o
the splenic venous system. This interpre
tation was incompatible with the followin
observations (1) at all stages during
process of depletion of the margin
zone the red pulp contained few pyro
nophilic cells (2) the periphery of th
nodules contained large numbers of ma
ginal zone cells soon after stimulation, (3
in the early stages, marginal zone cel
(marginal zone lymphocytes) could alwa
be found in the marginal sinus with o
casional cells seen to be passing throu
the walls of this sinus.

The sequence of differentiation in
plasma cells was much like that describe
by Marshall and White ('50) for the ra
bit. Our marginal zone lymphocytes wou
be represented by the primitive reticul
cells illustrated in Marshall and White
figure 3 although the pyronin staining
our cells is more similar to his activat
reticulum cell." We prefer not to call t
marginal zone lymphocytes activated sin
they are a constant feature of the untrea
spleen. The factors causing these cells
migrate into the nodules following an
genic stimulation could not be determin
with the methods used It is especial
interesting that they should migrate in
the lymphoid nodules against the us
outward flow of materials. Snook ('6
has suggested a slow oozing-type fl
through the marginal zone which wou
make such movement less subject to t
effects of a pressure gradient toward t
red pulp In his series of injection expe
ments he showed that particulate mat
accumulates in the interstices of the ma
ginal zone within 10–15 minutes followi
injection. His figure 20 suggests that t
particles are intercellular in positio
Within 4–8 hours most of the particul
material is localized within the red pu
macrophages

In our series of spleens differentiatio
of antibody-forming cells occurs in tho
regions where they are in close appositi
to macrophages. The first opportunity
such a relationship comes when th
must pass the marginal metalophils
enter the periphery of the nodules (s
Snook, '64) The distinct change to t
hemocytoblast form however occurs
the midst of tingible body macrophages

-e germinal centers. These macrophages ve been shown by Hunter ('66) to lack tigen soon after injection but to contain e most significant amounts in the spleen 24 hours. The fact that hemocytoblasts evelop almost exclusively in the vicinity f macrophages containing antigen and at the time sequence of this differenti tion corresponds to the time of presence f antigen in these cells, suggests a relaionship.

Fishman ('61) and Fishman and Adler '63) provide the most definitive evidence for the inductive role of the macrophage n antibody production. Their *in vitro* mmunochemical studies demonstrated the inability of lymphoid cells to produce antibodies in the presence of antigen unless they were incubated in the presence of macrophages or exposed to a ribonuclease-sensitive product from macrophages which had been previously treated with the antigen. A definitive morphological relationship between macrophage and antibody-forming cell has not been clearly demonstrated. Schoenberg et al. ('64) have observed direct cytoplasmic connections between these cell types on electron micrographs but their evidence is not convincing.

La Via, Barker and Wissler ('56) reported that macrophages in the marginal zone of the rat spleen phagocytized par ticulate antigen early in the immune response. These antigen-laden cells were then thought to migrate to the red pulp cords where they induced the proliferation and differentiation of antibody-forming cells. Snook's ('64) study on the flow of particulate material through the rat spleen suggests that this observation was due to the sluggish flow of material through the marginal zone. Histochemical techniques used by Pettersen ('64) demonstrated a dearth of cells in the marginal zone which possess hydrolytic enzyme activity normally associated with the phagocytic process.

The evidence presented in this study to implicate the macrophage as the initiator of the antibody forming process is only supportive. It seems clear from a thorough study of the microscopic material, how ever that the site of initial differentiation of antibody-forming cells occurs in the lymphoid nodules. The close topographical relationship between these differentiating antibody-forming cells and the enlarged phagocytic macrophages within the nodules is consistent with an inductive function for these macrophages. The migration of marginal zone lymphocytes into the nodules prior to their differentiation is strong evidence that the nodular environment is the site where induction occurs. After careful observation there seems little doubt that the marginal zone lymphocytes are the early precursors of the definitive plasma cells found in large numbers at five days in the red pulp cords. If the macrophage is essential to the induction process the likely candidate is the tingible body macrophage which is unique to the nodular regions. At four and five days this type comprises the vast majority of macrophages within the nodules as illustrated by the enlarged rounded forms exhibiting acid phosphatase activity in figure 5.

It is evident that the very early events which occur in the spleen in response to antigen provide the significant clues to the origin of the antibody forming cells and their relationship to the macrophage system of cells. Sections from spleens removed more than 24 hours following antigenic stimulation could easily lead to the interpretation that cells in the red pulp cords are the plasma cell precursors. There may be factors in the red pulp conductive to mature plasma cell formation that are lacking in the nodular regions, but the sequence suggests that hemocytoblasts are already committed to plasma cell formation following their sojourn in the germinal centers. Mature plasma cells can be found in the nodules and also scattered in the marginal zone 2–4 days following the stimulation

Another point of interest is that beginning about day one and extending through five days the marginal zone becomes repopulated with cells morphologically identical to those found in untreated animals This region seems to be replenished constantly with blood-borne cells and this process occurs even at the height of a full-blown immune response to a given set of antigens. It may be that the marginal zone environment is a necessary

prelude to immune competence and in the rat, cells from the thymus bone marrow or other sources may lodge here prior to events necessitating their participation in an immune response. It is also possible that some of these may represent committed cells that will respond to a challenge injection of the same set of antigens The only differences observed between the primary and secondary responses in our animals were the more rapid migration of marginal zone lymphocytes into the nodules the more rapid differentiation into plasma cells and a lesser prominence of tingible body macrophages during the secondary response

Little or no evidence could be observed under the light microscope to suggest that two pyroninophilic cell lines were involved in the immune response in either primary or secondary animals This was supported by a thorough examination of spleen imprints from all stages Additional efforts, such as those by Moore Mumaw and Schoenberg ('65) using the electron microscope with immunochemical techniques would be desirable in an effort to determine whether different cell types are associated with the production of 7S and 19S antibodies in the rat spleen Work such as Fliedner et al. ('64) have done on the kinetics of cells in the germinal centers of the rat spleen might be extended to include those cells found in the marginal zone Their results indicate that the mantle zone lymphocytes do not arise from the germinal centers in pulse-labeled but antigenically unstimulated spleens It would be of interest to determine in which location in the spleen DNA precursors become incorporated into the nuclei of marginal zone lymphocytes. A careful analysis of this might provide evidence implicating the marginal metalophils germinal center macrophages or even the environment of the marginal zone itself as the site of initiation of the antibody forming process in the rat spleen

LITERATURE CITED

Burstone M. S. 1958 Histochemical demonstration of acid phosphatase with naphthol AS-phosphates. J Nat. Cancer Inst, 21: 523-540.

Fishman, M 1961 Antibody formation in vitro. J Exp. Med., 114 837-856.

Fishman M., and F L. Adler 1963 Antibody formation initiated in vitro. II. Antibody synthesis in X-irradiated recipients of diffusion chambers containing nucleic acid derived from macrophages incubated with antigen. J. Exp. Med., 117: 595-602.

Fliedner T M., M. Kesse, E. P Cronkite and J S. Robertson 1964 Cell proliferation in germinal centers of the rat spleen. Ann N. Y. Acad. Sci., 113: 578-594.

Holub, M. 1960 Report of symposium committee concerning nomenclature of cells responsible for immune reactions. In: Mechanisms of Antibody Formation. M. Holub, Acad. Press, New York, pp. 23-24.

Hunter R. L. 1966 Two patterns of splenic phagocytosis. New Physician, 15: 111-118

Le Via, M F., P A. Barker and R. W Wissler 1956 A study of the correlation of splenic phagocytosis and the splenic histologic reaction with antibody formation in protein-depleted rats. J Lab. & Clin. Med., 48. 237-254.

Marshall, A. H. E., and R. G. White Reactions of the reticular tissue to antigens Brit. J Exp. Path., 31: 157-174.

Moore, R. D., V R. Mumaw and M. D. Schoenberg 1965 Changes in antibody producing cells in the spleen during the primary response Exp & Mol. Path., 4: 370-390.

Pettersen, J C. 1964 A comparison of metalophilic reticuloendothelial cells to cells containing acid phosphatase and non-specific esterase in the lymphoid nodules of normal and stimulated rat spleens. Anat. Rec., 269-278.

Schoenberg, M. D., V R. Mumaw R. D. Moore and A. S. Weisberger 1964 Cytoplasmic interaction between macrophages and lymphocytic cells in antibody synthesis. Science, 964-965.

Snook, T 1964 Studies on the perifollicular region of the rat's spleen. Anat. Rec., 148: 149-159.

Wachstein, M., and E. Meisel 1957 A comparative study of enzymatic staining reactions in the rat kidney with necrobiosis induced by ischemia and nephrotoxic agents (mercuhydrin and DL-serine) J Histochem. Cytochem., 5: 204-220.

The following abbreviations apply to all figures: LN lymphoid nodule; MZ, marginal zone; RP red pulp; MS marginal sinus; ML, mantle layer.

PLATE 1

EXPLANATION OF FIGURES

1 Section through a nodule of an unstimulated spleen showing the distribution of macrophages stained for acid phosphatase activity Arrow identifies marginal metalophils of Snook. × 120.

2 Section through a nodule of an unstimulated spleen stained for 5′ nucleotidase activity Arrow identifies marginal metalophils. × 150.

3 Acid phosphatase activity in macrophages of a spleen section from an animal killed four hours following a secondary injection of typhoid-paratyphoid vaccine. The marginal zone is narrowed and the nodule enlarged. Arrow identifies marginal metalophils. × 150.

4 Ammoniacal silver-stained spleen section showing collapse of the marginal zone surrounding a nodule from an animal killed one day following the second of two injections of killed *E. coli* organisms administered 24 hours apart. × 120.

5 Acid phosphatase activity in enlarged rounded, tingible-body macrophages within nodules of a spleen section from an animal killed five days following a primary injection of typhoid-paratyphoid vaccine. × 120


RP
LN
MZ
RP
1
RP
LN
MZ
2
LN
MZ
3
LN
4
LN
MZ
5

PLATE 2

EXPLANATION OF FIGURES

6 Cells photographed from Giemsa-stained imprints of bisected spleens. a, marginal zone lymphocytes intermingled with small lymphocytes of the mantle layer b, tingible body macrophage surrounded by lymphocytes of marginal zone origin. Nucleus of macrophage is seen toward the lower end just to the left of center; c hemocytoblast with its large nucleolus and basophilic cytoplasm; d, plasma cells typical of those found in the red pulp five days following stimulation. a c and d × 1 000; b × 800

7 Nodule in a spleen section from an untreated animal showing marginal zone lymphocytes above and mantle layer lymphocytes below MS marginal sinus which separates marginal zone from mantle layer of nodule; MZ, marginal zone; ML, mantle layer Hematoxylin and azure II. × 300.

8 Nodule in a spleen section from an animal killed three hours following a primary injection of typhoid-paratyphoid vaccine Marginal zone lymphocytes can be seen at the periphery of the nodule and the marginal zone is narrowed. RP red pulp Hematoxylin and azure II × 250

9 Marginal zone lymphocyte in the marginal sinus of a spleen section from an animal killed eight hours following a primary injection of killed *E coli* organisms. Lower arrow identifies the lymphocyte; upper arrow identifies a sinus-lining cell on nodular side of sinus. Lymphocyte is identifiable by its pyroninophilic nucleolus and cytoplasm. Pyronin methyl green × 800

10 Marginal zone lymphocyte passing through membrane on nodular side of marginal sinus. Star overlies a marginal metalophil that is out of focus. Arrow identifies a sinus-lining cell to the right of the migrating lymphocyte The lymphocyte shows a cytoplasmic constriction. Spleen from an animal killed 16 hours following a secondary injection of typhoid-paratyphoid vaccine. Pyronin-methyl green. × 800

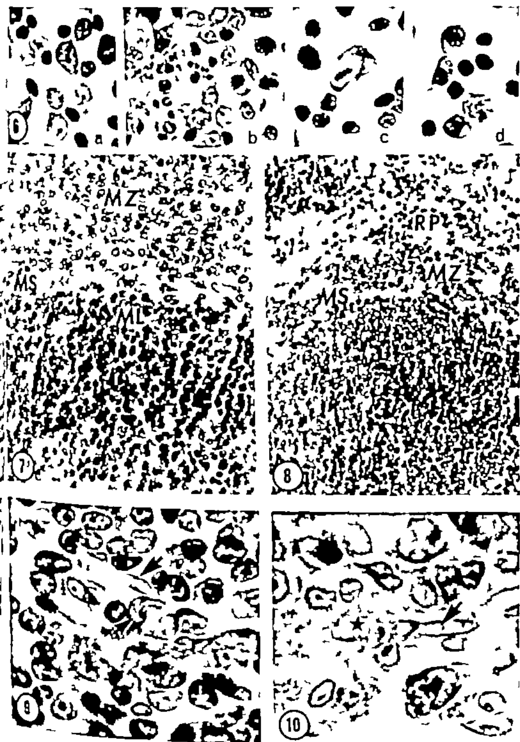

6
a
b
c
d
MZ
MS
ML
7
RP
MZ
MS
8
9
10

PLATE 3

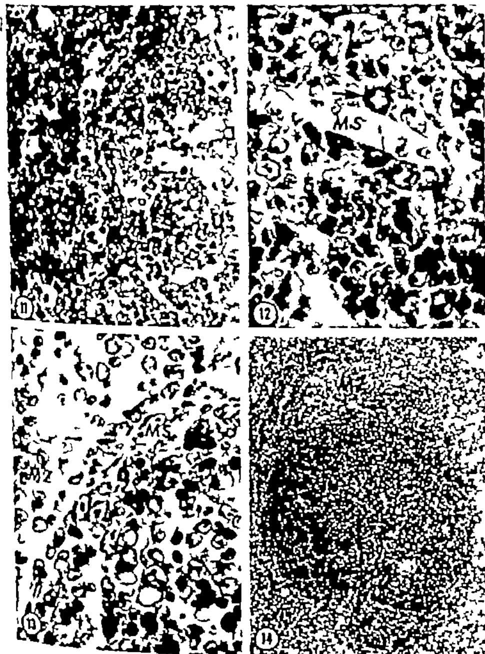
EXPLANATION OF FIGURES

11 Tingible body macrophages in a nodule of a spleen section from an animal killed four days following a primary injection of typhoid-paratyphoid vaccine Arrows identify hemocytoblasts in close proximity to tingible body macrophages. Pyronin-methyl green. × 400.

12 Hemocytoblasts migrating into and across the marginal zone toward the red pulp in a spleen section from an animal killed one day following a secondary injection of typhoid-paratyphoid vaccine. Arrows identify hemocytoblasts in the marginal zone Pyronin-methyl green × 800

13 Hemocytoblasts and marginal zone lymphocytes intermingled at the periphery of a nodule in a spleen section from an animal killed one day following the second of two injections of typhoid-paratyphoid vaccine administered 24 hours apart. Pyronin-methyl green. × 800

14 Nodule in a spleen section from an animal killed ten days following a primary injection of typhoid-paratyphoid vaccine. The mantle layer and the marginal zone MZ, are identical in appearance to those found in untreated animals. Hematoxylin-azure II. × 150.


11
12
MS
13
MS
14

ell Number as a Measure of Distribution and Renewal l Epithelial Cells in the Small Intestine of rowing and Adult Rats

G. G. ALTMANN AND M. ENESCO
Department of Anatomy McGill University Montreal, Canada

ABSTRACT By the use of DNA determinations and cell counts with and without previous colchicine treatment, the absolute numbers of villus epithelial cells, and of dividing and nondividing crypt epithelial cells were determined in ten successive segments of the small intestine of 17-day (weanling) 37-day (young) and 87-day old (adult) male rats.

In adults, the number of villus epithelial cells per segment decreased gradually in the duodenoileal direction, while the number of dividing and nondividing crypt epithelial cells remained fairly constant. It was deduced that the turnover time of the villus epithelium gradually decreases, but that of the crypt epithelium remains constant along the small intestine.

When the entire small intestine was considered, from weanling to adult age, the relative and absolute numbers of dividing and nondividing crypt epithelial cells increased; the calculated number of epithelial cells produced daily rose from 112 million to 1796 million. Meanwhile, the rate of growth of the intestinal epithelium diminished allowing more and more of the produced cells to participate in renewal: about 25, 845 and 1796 million cells daily in weanling, young and adult rats, respectively. The mean turnover time of the intestinal epithelium decreased from about 22 days in weanling rats to about 2.1 days in adult rats, indicating a tenfold increase in renewal rate

Cells are known to contain a fixed amount of deoxyribonucleic acid (DNA) which is constant for any given species (Boivin, Vendrely and Vendrely 48) It follows, then that DNA content can be used to determine the total number of cells present in an organ (Davidson and Leslie, '50) Furthermore the relative frequency of the various cell types within an organ can be measured in histological sections by cell counts or by other histometric methods (Eränkö '55) The method of combining determinations of DNA content with histometric measurements has been initiated and developed in this laboratory (Enesco et al., '56–'64) If for example, the total number of cells in an organ is determined by DNA estimation, and if simultaneously the relative frequency (e g. percentage) of the cell types within the organ is determined by differential cell counts on histological sections of the organ, the total number of cells of various types present in the organ can be calculated using simple arithmetic (Enesco and Puddy 64) In the present work, this dual method with additional use of the colchicine technique (Stevens Hooper '61) has been applied to ten successive regions of the small intestine of rats of various ages in order to determine the number of villus epithelial cells and the number of dividing and nondividing crypt epithelial cells present in unit lengths of the small intestine.

It is known that the epithelial cells in the deeper portions of the intestinal crypts proliferate and thus yield cells which migrate to the villus epithelium; there, cells move in a continuous sheet along the sides of the villi to reach the villus tips where they are exfoliated into the intestinal lumen (Leblond and Stevens 48) This process allows for the continuous renewal of the intestinal epithelium, the newly formed cells replacing the old ones. The present measurements provided a quantitative estimate of the size of the crypt and villus portions of the intestinal epithelium in terms of cell number per unit intestine length and of the size of the mitotic pool within the crypt epithelium The

This work was performed partial fulfillment of the work for the Master of Science degree (Altmann, thesis, '64). The first results appeared in the form of an abstract (Enesco and Altmann, '63)

results of these measurements in themselves revealed important regional and age changes in the renewal process of the intestinal epithelium An approximate quantitative estimate of these changes could be given by combining the results. Thus the size of the mitotic pool indicated the rate of cell production and comparisons between the numbers of epithelial cells present at the various ages furnished some data regarding the growth rate of the intestinal epithelium From combinations of these estimated rates of cell production and growth the rate of renewal of the intestinal epithelium could be calculated in terms of the number of epithelial cells replaced and subsequently exfoliated daily in the small intestine of weanling young and adult rats respectively

MATERIALS AND METHODS

Male Sherman rats of three age groups were used 16–18-day old "weanling rats" 36–39-day-old "young rats" and 85–90-day old "adult rats" whose body weights approximated 30 100 and 300 gm, respectively The animals were exsanguinated under chloroform anesthesia the small intestine was immediately removed and its length from pylorus to cecum measured It was then divided into ten equal parts (segments) The segments were opened along their long axis and their content was washed out with slowly running cold water

DNA content determination

Using 4–5 animals from each age group the DNA content of the segments was determined by the methods of Schneider (45) and Dische ('30) as modified by Enesco (57) The intestinal segments were homogenized in absolute ethanol and the homogenates were centrifuged. The residue was washed successively with cold 10% trichloracetic acid solution water absolute ethanol and a 3 1 mixture of hot ethanol and ether Finally the DNA content of the residue was extracted in hot (90 C) 5% trichloracetic acid solution The concentration of DNA in the extracts was determined colorimetrically with diphenylamine using a Beckmann spectrophotometer (table 1) The DNA content data were converted to cell number data (as discussed later) and the total number of cells present in the segments was thus given (table 4)

Relative number of epithelial cells in the intestinal tissue

The percentage of epithelial cells in the intestinal tissue was determined histometrically using representative histological sections of the segments. From each age group 5–6 animals were sacrificed for this purpose. Pieces of intestine measuring about 1–2 cm were taken from regions corresponding to the segments, cut open, flattened on cardboard and fixed in Carnoy's fluid.

The longitudinally cut, 4-μ thick histological sections were stained with hematoxylin and eosin Cell counts were then performed in areas where the crypts and the villi were sectioned along their length. In microscopic field-wide lengths of intestine (taken randomly) all cells, epithelial and non-epithelial, from the villus tips to the serosa, were counted differentially Altogether 3000–4000 cells were counted per section. Paneth and goblet cells were counted as epithelial cells. From these counts the percentage of intestinal cells present in the epithelium was calculated and averaged for each section (table 2).

Later it became necessary to count the epithelial cells of villi and crypts separately The results of these counts were expressed as the ratio of villus epithelial cell number to crypt epithelial cell number (table 2)

Colchicine technique

Using five animals per age group, colchicine in a dose of 0 1 mg per 100 gm body weight was injected subcutaneously at 8 00 A.M and the animals were sacrificed four hours later The weanling group was treated differently half of the group was injected at 8 00 A.M and the remainder at 10 00 A.M these animals were sacrificed two hours after injection. Histological samples of the small intestine were taken and processed as above except that Susa fluid was used as fixative Choosing areas with longitudinally sectioned crypts, dividing and non-dividing crypt epithelial cells to a total of 3000 cells per section, were enumerated The mitotic figures seen

e colchicine-arrested metaphases with a prophases, while anaphases and telo-ses were not present. The results were pressed as the percentage of crypt cells in mitosis. This percentage was called colchicine index (table 3)

Mitotic index determinations

From each age group five animals were rificed, one at each 50 minutes between 00 A.M. and 12 00 noon, for the esti-ation of the mitotic index (mean per nt of crypt cells in mitosis table 3) he basic purpose of these determinations as to check the reliability of the results of e colchicine technique. Samples now om only a few of the segments were fixed t Bouin fluid and processed as above. Di-iding and non-dividing crypt epithelial ells, to a total of 3000 cells per section, ere counted differentially Cells seen in id- and late prophase metaphase ana-hase and early telophase were considered dividing." Dividing cells were distin-uishable from non-dividing ones mainly y their readily visible chromatin or chro-osome aggregations which are usually oser to the crypt lumen than the nondi-ing nuclei.

Villus height and crypt height determinations

On histological sections from regions corresponding to the segments of five animals per age group the heights of at least five villi and crypts (those that were sectioned along their length) were measured by an ocular micrometer calibrated by means of a stage micrometer The readings were averaged for each section and then for each segment (fig. 2) These measurements were performed for control purposes.

Calculations [4]

The *total number of cells per segment* (table 4) was calculated by dividing the DNA content of the segments by the DNA content of a diploid cell, which was estimated at 6.2 µµg in the rat (Enesco '57)

The *total number of intestinal epithelial cells* (N) per segment (table 4) was calculated in the following manner:

$$N = \frac{\%\ \text{epithelial cells in segment (table 2)} \times \text{total no. of cells in segment (table 4)}}{100}$$

[4] In some cases, experimental data were not obtained for segment 6 (tables 2, 3) In these instances, the average between the results on segments 5 and 7 was used in the calculation of the derived data for segment 6.

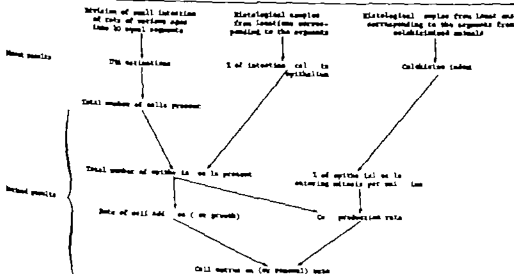


Fig. 1 Scheme of the methods used. The main steps of the experimental procedure and calculations are summarized.

The value of N is the sum of the *number of villus epithelial cells* (V) and the *number of crypt epithelial cells* (C) in other words

$$N = V + C$$

which may be written as

$$N = \frac{V(V+C)}{V} = V\left(1+\frac{C}{V}\right) = V\left(1+\frac{1}{V/C}\right)$$

Since the ratio V / C was determined experimentally (table 2) V (table 4) could be calculated as

$$V = \frac{N}{1+C/V}$$

Similarly C (table 4) could be calculated as

$$C = \frac{N}{1+V/C}$$

The *total number of cells produced* per unit time in the crypt epithelium of the segments (table 3) (which is equivalent to the number of crypt cells undergoing mitosis) was calculated from the number of crypt epithelial cells (C) and from the percentage of crypt cells entering mitosis per unit time (i e colchicine index): number of cells produced per four hours = colchicine index (table 3) $\times \frac{C}{100}$ (in the weanling group the 2 hour colchicine indices were multiplied by 2)

An additional series of calculations was performed with the purpose to assess the rate of nenewal of the intestinal epithelium in the various age groups In these calculations the entire small intestinal epithelium was considered by totaling or averaging the results for the ten segments

First the *daily cell addition rate* to the intestinal epithelium (i e number of cells added daily for growth) was calculated according to the formula of Brody (45)

daily cell addition rate (at age 1) =

$$\frac{N_2 - N_1}{\text{age 2} - \text{age 1 (in days)}}$$

(N is the total number of intestinal epithelial cells and numbers 1 and 2 refer to weanling and young or young and adult ages respectively) Next the *daily rate of cell production* in the intestinal epithelium (i.e number of cells produced daily by the mitotic activity) was estimated by multiplying the number of cells produced per 4 hours by 6 thereby obtaining the number of cells produced per 24 hours. The produced cells can be divided into two categories from the statistical viewpoint those that participate in cell addition to the intestinal epithelium (i.e. in growth) and those that participate in the cell renewal process. The number of produced cells is, therefore the sum of the numbers of cells used for renewal and for growth respectively and it follows that

cell production rate = rate of cell addition + rate of cell renewal,

if all the parameters are measured as the change in cell number per unit time. Using this equation and the known rates of cell production and cell addition, the rate of renewal could be calculated in terms of the *number of cells renewed daily*. This term is equivalent to the *number of cells exfoliated daily* because cell renewal in the intestinal epithelium results in cell exfoliation

As a relative measure of renewal rate, the *turnover time* of the crypt epithelium and of the villus epithelium respectively was also calculated. Turnover time is defined as "the time for the replacement of a number of cells equal to that in the whole population" (Leblond and Walker '56) The following formula was used:

$$\text{turnover time (in days)} = \frac{\text{number of cells present in cell population}}{\text{number of cells renewed (i.e., exfoliated) daily}}$$

In adult rats steady state conditions are present and therefore the number of cells produced must equal the number of cells renewed (Leblond and Stevens 48) As shown above the number of cells produced was obtained by multiplying the colchicine index by one hundredth of the number of crypt epithelial cells. This product can, therefore replace the denominator in the above formula, thereby allowing one to calculate turnover time directly from the colchicine index in the case of adult rats.

DIRECT RESULTS

The *DNA content of the segments* (table 1) was highest in the upper intestinal segments (maximal in segment 1), the values were gradually lower in the more distal segments and reached a minimum in segment 10 The total DNA content of the small intestine calculated from

TABLE 1

DNA content (in mg ± standard error) of the ten segments of the small intestine in rats of various ages

	Segments (numbered from pylorus)										Total
	1	2	3	4	5	6	7	8	9	10	
Weanling rats	0.89 ±0.10	0.59 ±0.05	0.61 ±0.07	0.65 ±0.03	0.64 ±0.03	0.60 ±0.03	0.53 ±0.04	0.53 ±0.04	0.53 ±0.05	0.46 ±0.03	6.03
Young rats	3.37 ±0.25	2.62 ±0.14	3.03 ±0.14	2.83 ±0.22	2.68 ±0.13	2.50 ±0.11	2.48 ±0.14	2.46 ±0.12	2.39 ±0.11	2.37 ±0.16	26.73
Adult rats	6.20 ±0.40	4.99 ±0.35	5.11 ±0.42	4.96 ±0.34	4.64 ±0.32	4 46 ±0.31	4 47 ±0.36	4 45 ±0.43	4.34 ±0.32	4.16 ±0.35	47 70

The sum of the DNA contents of the ten segments, was 6.03 mg, 28 73 mg and 47 70 mg in weanling, young and adult rats, respectively

The *percentage of intestinal cells in the epithelium* of the small intestine (table 2) was estimated in histological sections taken from regions corresponding to the segments. On the average, 53 6% 52.4% and 48.4% of all intestinal cells was found to belong to the intestinal epithelium in the three respective age groups. Significant regional variation was not observed.

The *ratio of villus epithelial cell number to crypt epithelial cell number* averaged 2.10, 1.19 and 1.05 in weanling young and adult rats, respectively (table 2) There was a gradual decrease from segment 1 to 10 (In weanling rats the ratio remained high in the upper half of the small intestine.)

The *colchicine index* was not readily obtained in weanling rats because severe toxic effects of colchicine appeared in the third hour after administration. The animals were, therefore, sacrificed 2 hours after injection. The 2-hour colchicine index (table 3) averaged 5.6% and showed no significant regional variation. In the young and adult groups, the *4-hour colchicine* indices were measured (table 3) and an average of 14.8% and 16.5% respectively was obtained. Again, significant regional variation was not observed in these results, except for segment 1 where the index was slightly below average

The *mitotic index* was estimated only in a few regions (table 3) and averaged 2.7% 5.3% and 6 4% in weanling, young and adult rats, respectively No significant regional variation was observed.

The *average height of the villi* (fig 2) decreased gradually from segment 1 toward segment 10 The range of this decrease was from 0 42 mm to 0.22 mm in weanling rats from 0.54 mm to 0 18 mm in young rats and from 0.58 mm to 0 17 mm in adult rats the average being 0.35 mm, 0.34 mm and 0.33 mm in the three respective age groups. The *average height of the crypts* (fig 2) was 0 16 mm 0 18 mm and 0.20 mm in weanling, young and adult rats respectively with no significant regional variation.

DERIVED RESULTS

Like the DNA content data from which they were derived, the *total number of cells per segment* (table 4) was relatively high in the upper intestinal segments (maximal in segment 1) and gradually lower in the more distal segments (minimal in segment 10) The total number of cells present in the whole small intestine calculated from the sum of the cell numbers present in the ten segments was 973 4312 and 7695 million in weanling, young and adult rats, respectively

The *number of villus epithelial cells per segment* in weanling, young and adult rats respectively (table 4) decreased gradually from 52, 175 and 270 million in segment 1 to 21 94 and 127 million in segment 10 (In weanling rats, the values remained high throughout the proximal half of the small intestine.) The cell content of the villus epithelial compartment showed then an overall diminution of at least 50% from

TABLE 2

Relative number (± standard error) of epithelial cells in the segments of the small intestine in rats of various ages

	Segments (numbered from pylorus)										Average
	1	2	3	4	5	6	7	8	9	10	
Weanling rats											
% Epithelial cells in segment	53.5 ±2.5	56.8 ±1 4	52.3 ±3.0	50.5 ±1 4	55.4 ±2.2	56.9 ±3.5	54.3 ±2.9	53.8 ±2.9	51 4 ±2.4	51.2 ±2.4	53 6
Ratio: villus epith. cell no. over crypt eph. cell no.	2.08 ±0 16	2.44 ±0.22	2.26 ±0 13	2.40 ±0 14	2.44 ±0.21	—	2.12 ±0.25	1.98 ±0.14	1.82 ±0.17	1.28 ±0 16	2.10
Young rats											
% Epithelial cells in segment	53.5 ±1.2	56.6 ±1 4	53.3 ±2.4	54.2 ±1 4	50 1 ±1.5	53 1 ±1 4	49.6 ±0.9	47.5 ±1.8	48.9 ±2.6	52.9 ±1.8	52.4
Ratio: villus epith. cell no. over crypt eph cell no.	1.37 ±0.10	1 43 ±0.02	1 45 ±0.06	1.20 ±0.08	1 14 ±0.06	—	1 14 ±0 07	1 13 ±0 12	1 00 ±0.04	0.87 ±0 13	1 19
Adult rats											
% Epithelial cells in segment	46.7 ±2.0	49 0 ±1 7	52.6 ±2.5	48.6 ±1.2	47.8 ±1.9	49 1 ±2.0	46.8 ±1.9	47.2 ±1.2	46.2 ±2.9	47 7 ±2.1	48 4
Ratio villus epith cell no. over crypt eph. call no.	1.37 ±0 07	1.31 ±0 13	1.21 ±0.06	1 16 ±0 04	1 19 ±0 08	1.07 ±0.06	0.94 ±0.06	0.85 ±0.06	0 78 ±0.06	0 66 ±0.08	1 05

TABLE 8

Colchicine index, mitotic index (± standard error) and calculated number of cells produced in the crypt epithelium of the small intestinal segments of rats of various ages

	Segments (numbered from pylorus)										Average
	1	2	3	4	5	6	7	8	9	10	
Weanling rats											
Colchicine index (%) (for 2 hour period)	5.2 ±0.8	6.0 ±0.6	6.7 ±0.4	5.4 ±0.9	5.8 ±1.0	—	5.4 ±2.1	5.6 ±2.1	6.0 ±2.1	5.5 ±0.7	5.6
Mitotic index (%)	3.4 ±0.3	4.0 ±0.4	—	4.1 ±0.3	4.3 ±0.5	—	3.8 ±0.3	—	3.3 ±0.4	3.2 ±0.4	3.7
Calculated number of epithelial cells produced per 4 hours (× 10⁶)	2.0	1.8	1.6	1.7	1.9	1.9	1.6	1.7	1.9	1.7	Total 18.7
Young rats											
Colchicine index (%) (for 4 hour period)	12.8 ±0.1	15.2 ±1.0	16.9 ±1.5	14.4 ±0.8	14.7 ±1.4	—	13.9 ±0.4	14.8 ±0.3	14.4 ±0.7	16.1 ±0.5	14.8
Mitotic index (%)	—	—	5.2 ±0.6	—	—	—	—	5.3 ±0.5	—	—	5.3
Calculated number of epithelial cells produced per 4 hours (× 10⁶)	16.3	15.5	18.1	16.1	14.9	14.3	12.9	13.2	13.7	17.4	Total 152.4
Adult rats											
Colchicine index (%) (for 4 hour period)	13.5 ±1.0	18.3 ±1.3	16.4 ±1.5	17.8 ±0.7	15.5 ±0.8	—	17.4 ±1.4	16.3 ±0.9	16.0 ±0.8	17.2 ±1.4	16.5
Mitotic index (%)	5.6 ±0.2	6.5 ±0.7	—	6.6 ±0.5	—	—	6.6 ±0.4	—	6.6 ±0.4	6.0 ±0.3	6.4
Calculated number of epithelial cells produced per 4 hours (× 10⁶)	26.6	31.3	32.3	31.3	25.4	28.3	31.5	29.2	28.6	33.2	Total 298.3

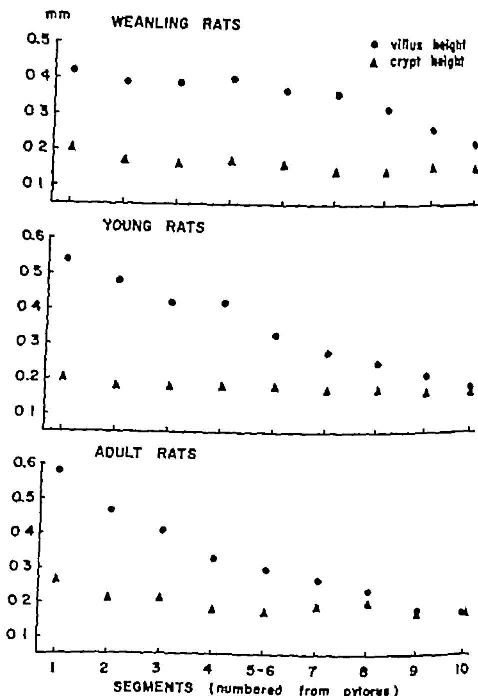


Fig. 2 Average heights of the villi and crypts in the various intestinal segments are illustrated. A gradient in villus height is displayed from segment 1 to 10. In weanling rats, this gradient is present only in the distal segments. The height of the crypts show no significant regional variation with the exception of segment 1 where it is slightly above average

duodenum to terminal ileum. This diminution is also reflected in the height of the villi (figs 2 3 4)

In contrast to the regional variations observed in the villus epithelial cell content, *the number of cells in the crypt epithelial compartment* (table 4) displayed no significant regional variation averaging 17 103 and 182 million in every segment of the three age groups respectively. An exception was segment 1 of weanling and young rats where the number of crypt epithelial cells was significantly above average (table 4)

TABLE 4

Calculated number of cells (× 10⁶) present in the segments and in the villus and crypt epithelia of the segments in rats of various ages

	Segments (numbered from pylorus)										Total
	1	2	3	4	5	6	7	8	9	10	
Weanling rats											
Total number of cells in segment	144	95.2	96.4	105	103	96.8	85.5	83.5	85.5	74.2	973
Number of villus epithelial cells in segment	52.0	38.4	35.7	37.4	40.5	38.3	31.5	30.6	28.3	21.2	354.0
Number of crypt epithelial cells in segment	25.0	15.7	16.8	15.6	16.6	16.8	14.9	15.4	15.6	16.7	168.1
Young rats											
Total number of cells in segment	544	423	469	456	432	403	400	397	386	382	4312
Number of villus epithelial cells in segment	175	146	164	135	115	114	105	100	94	94	1232
Number of crypt epithelial cells in segment	127	102	107	112	101	100	93	89	95	108	1034
Adult rats											
Total number of cells in segment	1000	806	834	784	749	723	721	718	700	671	7695
Number of villus epithelial cells in segment	270	223	238	205	194	183	171	166	138	127	1905
Number of crypt epithelial cells in segment	197	171	197	176	164	172	161	163	185	183	1819

The *number of cells produced per four hours* in the intestinal epithelium of weanling rats (table 3) averaged about 1.87 million for every segment except segment 1 where this number rose significantly above average. In young and adult rats (table 3) it averaged 15.2 and 29.9 million per segment, respectively with no significant regional variation.

Further derivations of the direct results were made for the entire intestinal epithelium. They should be regarded as approximations because their calculation involved multiple combinations of the direct and derived results. The results for the ten segments were totalled or averaged and the data thus obtained were used for these calculations.

The *total number of epithelial cells produced daily* in the small intestine was calculated by simple extrapolation to 24 hours of the total number of epithelial cells produced per four hours (totals in table 3). In this extrapolation, it was assumed that no significant diurnal variation occurs in the mitotic activity of the intestinal epithelium of the rat (Bertalanffy '60). It was thus calculated that approximately 112, 914 and 1795 million cells are produced daily in the crypts of Lieberkühn of the small intestine of weanling, young and adult rats respectively.

By comparing the total number of epithelial (i.e. villus plus crypt epithelial) cells present in the entire small intestine (totals table 4) at the various ages (using the formula of Brody '45) it was possible

[9] As indicated in the section on "Calculations," the 2 hour colchicine indices multiplied by two were used in the calculation of these values.





Figs. 3 and 4 The mucosal layer of the duodenum (fig 3) is compared to the mucosal layer of the ileum (fig. 4) The arrows indicate the villus-crypt junctional area. A substantial difference in villus heights can be seen while the height of the crypts is about the same in both photomicrographs. Adult rat; Carnoy fixative; PA-Schiff hematoxylin. × 90.

to get an approximate estimate of the average *number of cells added daily to the epithelium* for growth It was thus found that about 87 and 29 million cells are added daily to the intestinal epithelium of weanling and young rats respectively whereas in adult rats zero cell addition rate was assumed for reasons explained later

The number of epithelial cells produced daily exceeded the number of epithelial cells added daily for growth by 25 885 and 1796 million in weanling young and adult rats respectively Assuming that these excess numbers of cells are involved in the process of renewal and lost into the lumen subsequently (Leblond and Walker '56) they indicate the approximate number of *epithelial cells replaced and exfoliated daily* that is the turnover rate of the intestinal epithelium (Leblond and Walker '56)

Using these turnover rates to calculate the *turnover time* of the epithelium of the small intestine it was found that the turnover times averaged 21 9 2 6 and 2.1 days in weanling young and adult rats respectively for the whole epithelium 14.2, 1 4 and 1 1 days for the villus part and 6.7 1.2 and 1 1 days for the crypt portion. In adult rats where steady state conditions are expected to be present turnover time values were also calculated for the in-

...idual segments (fig. 7) directly from ...o colchicine index.

DISCUSSION

Validity of the methods

...As previous experience in this laboratory has ...own, the current method for DNA estimation ...n be successfully applied to various tissues of ...e rat including the intestinal tissue (Enesco ...d Leblond, '62). This technique has been dis...ssed in detail previously (Enesco et al., '57–...4). The lowest detectable amount of DNA by ...e presently used colorimetric procedure is 50 μg ...hen a spectrophotometer is used (Dische, '55) ...is amount represents about 1–10% of the ...mounts of DNA measured in our samples, and ...hus indicates the possible error of the determina...tion. Moreover, some loss in DNA (not more than ...%) must have occurred during the chemical pro...cedure. The probable error of the determinations ...as expressed in the form of standard errors (table 1). Besides the data on the DNA content ...f the tissue, the knowledge of the amount of DNA per diploid cell in the rat was also neces...sary. This figure (i.e., 6.2 μμg DNA) was deter...mined earlier in this laboratory (Enesco, '57) ...sing the same method of DNA determination on ...tissue suspensions of known numbers of nuclei.

In the calculation of the total number of cells present in the segments (table 4) from the DNA data, it was assumed that every cell of the small intestine contains 6.2 μμg of DNA since only mononucleated and diploid cells are known to be present in the small intestine of the rat. The only exceptions are those cells that synthesize DNA in preparation for mitosis. In adult rats, most of these cells are located in the crypt epithelium constituting about 70% (Loran and Crocker '63) of this cell population. These cells are in various stages of their DNA synthesis phase and, thus, contain amounts of DNA vary...ing between the normal and the double amounts. Statistically then, half of the DNA synthesizing cells, i.e. 35% of the crypt cells, can be con...sidered as of double DNA content and causing an overestimation of cell number, while the other half can be considered as of normal DNA content. Since according to our present results, the 35% of the crypt cells having double DNA content represents about 9% of all intestinal cells, the extent of the overestimation of the total cell number in the segments would be about 9%.

In growing animals, DNA synthesizing cells contribute largely to tissue growth by their sub...sequent mitoses. The higher DNA content of these cells, therefore, indicates a cell number which will ensue after a short period of time that is, after the completion of mitosis. It follows that DNA synthesizing cells subserving growth are not considered to cause error in cell number estima...tions from DNA data (Enesco and Leblond, '62). The error caused by those DNA synthesizing crypt cells that subserve the renewal process in grow...ing animals was estimated to be less than 9%.

Some intestinal cells other than crypt cells may also synthesize DNA in preparation for mitosis. Most of these cells subserve growth, their higher DNA content, therefore, is not considered to cause error in the cell number estimations. Some of the lamina propria cells, however are known to participate in a renewal-like process which is manifested by a number of lamina propria cells passing through the epithelial layer to be degen...erated or to be exfoliated into the intestinal lu...men (Andrew and Sosa, 47) The mitotic ac...tivity associated with this process could be judged from the histological samples from the colchi...cinized adult rats and appeared to be negligible in comparison with the epithelial mitotic activity It is believed, therefore, that the DNA synthesis in the lamina propria did not interfere signifi...cantly with the cell number results. This prob...lem, however may need some further investiga...tion.

Since the results of the cell counts were ex...pressed as relative number of cells (i.e., percent...ages and ratios; table 2) the varying thickness of the histological sections and the tissue shrink...age during the histological procedure did not affect these results. In the cell counts the error caused by the various nuclear sizes in the tissue was minimized by the Abercrombie correction (Abercrombie, 46)

The reliability of the colchicine technique with the intestinal tissue of the rat has been estab...lished by the work of Stevens Hooper ('61). It is now generally accepted that 0.1 mg per 100 gm body weight dose of colchicine is optimal and that a 3–4 hour period for the action of the drug is the optimal time interval to measure mitotic rate accurately Results from this technique are, however, usually regarded as minimum values pri...marily because of the short lag period between the injection of colchicine and the onset of ac...tion (Leblond and Walker '56).

In the groups of weanling rats, difficulties were encountered in the application of the conventional colchicine method because severe toxic effects of colchicine appeared during the third hour after administration. In this group, then, it became necessary to measure the 2-hour colchicine in...dices. From the few animals that survived four hours it was possible to obtain 4-hour colchicine indices as well. In the duodenal and jejunal re...gions, the 4-hour indices were nearly double the 2-hour ones (11% versus 5.6%) while in the ileal region, the 4-hour indices were unexpectedly almost as low as the 2-hour indices (5.9% versus 5.6%). It is probable that the ileal mitotic ac...tivity has been interfered with by the toxic ef...fects of colchicine. This increased sensitivity of the ileal region to colchicine is possibly also re...flected in the high standard errors of the 2-hour colchicine indices of this region (table 3) In the weanling group then, it became necessary to per...form careful examination of the mitotic index (in untreated animals) in order to ascertain the reliability of the 2-hour colchicine indices. The two methods together presumably gave reliable information about the mitotic activity of the crypt epithelium because both types of results, the 2-hour colchicine indices and the mitotic indices, showed similar patterns of regional and age variation (table 3; fig. 6)

An additional problem in the weanling group was whether the 0.1 mg (per 100 gm body weight) dose of colchicine was adequate Therefore, doses of 0 05 and 0.2 mg colchicine, respectively (per 100 gm body weight) were administered to weanling rats. In the surviving animals (3 per experiment) the 4-hour colchicine indices were measured and compared to the 4-hour indices from the 0 1 mg dose Both 0 1 mg and 0.2 mg doses gave identical results while the 0 05 mg dose yielded relatively low indices. Since the 0.1 mg dose was the lowest dose giving maximum values, the use of this dose in weanling rats was justified.

In young and adult rats, no difficulties were encountered with the use of the conventional colchicine method. However the parallel control experiment on the determination of mitotic indices was performed in order to verify the observed regional and age variations in the cholchicine indices. The mitotic index results confirmed the findings by the colchicine method by showing a similar pattern of regional and age variations (table 3; fig. 8) Furthermore the mitotic duration of the crypt cells calculated from the combination of colchicine and mitotic indices (Leblond and Walker '56) fell within the expected range of 1–2 hours (1.3, 1 4 and 1.5 hours, on the average, in weanling, young and adult rats, respectively) and showed no significant regional variation along the small intestine.

The mitotic index results can be considered reliable for the present comparative purposes. Their absolute value however may hold some error because of the difficulties in recognition of early prophases and late telophases.

The villus height and the crypt height values (fig 2) must be lower than the actual values because of the tissue shrinkage during the histological procedure. For the present work, however only their regional variation was important and in this respect they gave reliable information

With respect to the validity of the derived results an important fact to consider is that the colchicine indices are regarded as minimum values. It is, therefore probable that the calculated numbers of cells produced per unit time were slightly underestimated. The most significant error however must be in the data on growth because the formula used for their calculation allowed only a crude estimate of the number of cells added daily to the epithelium for growth. These cell addition rates given for weanling and young rats, respectively are actually the average daily rates of cell addition for the whole periods between weanling and young age and between young and adult age, respectively according to the formula used for calculation The given rates of cell addition are therefore to be regarded as approximations and lower than the actual values. The error caused by these approximate values is, however likely to be of importance in only weanling animals where growth is active; in the young group, the rate of growth was found to be already negligible in relation to the rate of renewal and in the adult group it was assumed to be even more so.

In calculating the number of cells renewed and exfoliated daily (i.e. turnover rate), the approximate rates of cell production and growth were combined. The resulting figures are, therefore, to be regarded as approximations.

Regional changes in the distribution, production and renewal of epithelial cells

The epithelium of the small intestine is a continuously renewing cell population having its progenitor cells in the crypts and its functional cells in the villi (Leblond and Stevens 48) The regional distribution of the number of villus epithelial cells and of the dividing and non-dividing crypt epithelial cells is expected therefore to reflect certain regional changes in the renewal of the intestinal epithelium.

The rate of cell production in the intestinal epithelium depends on the number of crypt epithelial cells available and on the extent of the mitotic activity of these cells. Since the number of crypt cells per segment was relatively constant regionally (table 4) and since the percentage of mitotic crypt cells (table 3) as well as their mitotic duration[4] was also similar throughout the small intestine, it could be concluded that the rate at which cells are produced in the intestinal epithelium must be the same in every region. Accordingly, the calculated number of epithelial cells produced per segment per unit time (table 3) showed no significant regional variation The duodenal epithelium (segment 1) differed slightly from the rest of the intestinal epithelium by having more than the average number of crypt cells (in weanling and young rats table 4) and a mitotic index below average (table 3) A relatively low mitotic percentage was then associated with a relatively high cell number but the two compensated for each other so that the calculated number of epithelial cells produced in segment 1 (table 3) reached, or in the case of weanling rats even exceeded the number produced in the other segments. The rate of cell production per unit intestine length is, then believed to be fairly uniform along the whole small intestine but in the very young it may be above average in the duodenal region.

---

[4] Mitotic duration can be deduced from the combination of the colchicine index data with the mitotic index data.

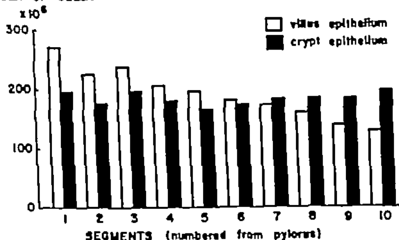


Fig. 5 Number of cells in the villus epithelium and crypt epithelium of the various intestinal segments of adult rats is illustrated. The cell content of the villus epithelium displays a gradient along the small intestine while the cell content of the crypt epithelium shows no significant regional variation.

WEIGHT OF VILLUS EPITHELIUM AND CRYPT EPITHELIUM (ADULT RATS)

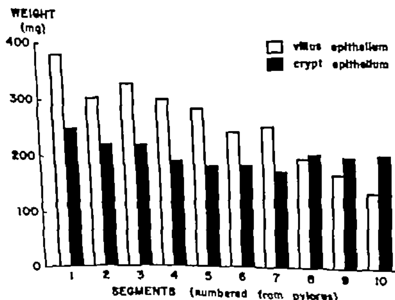


Fig. 6 Besides the results on villus and crypt heights (fig. 2) these results represent
additional evidence in support of the findings illustrated in figure 5. The method used
in obtaining these results is given elsewhere (Altmann, Thesis, '64). The weight of the
villus epithelium displays a duodeno-ileal gradient. The weight of the crypt epithelium
per segment is relatively constant regionally; the slight variation seen is probably due to some
variation in cell size.

In the growing age groups the epithelial cells produced in equal numbers in the various segments must be used partly for growth depending on the extent of growth in the various regions and partly for renewal It follows that to investigate the regional variations of renewal in growing rats a knowledge of regional variations in growth would be required However the present method for measuring growth (i e cell addition for growth) was not applied to the various regions but to the entire intestinal epithelium instead The regional variations in renewal were therefore investigated in detail in adult rats where growth is insignificant.

In the adult animals a clear-cut difference could be seen in the regional distribution patterns of the villus epithelial cells and of the crypt epithelial cells (fig 5) While the number of villus epithelial cells per segment decreased gradually from duodenum to terminal ileum, the number of crypt epithelial cells per segment remained fairly constant in every region. The results on the villus and crypt heights (fig 2) and also results on the weight of the villus and crypt epithelia of the segments (fig 6) supported these observations by showing similar trends in regional distribution As cells are produced at approximately equal rates at all locations of the crypt epithelium, cells must enter the villus epithelium, replace the cells there and exfoliate at the same rate in order to maintain the steady state of the intestinal epithelium (Leblond and Stevens, 48). The average time spent by the cells in the villus compartment between entry and extrusion (i.e the turnover time of the villus epithelium) then depends on the number of villus epithelial cells present. Since this number decreased gradually from duodenum to terminal ileum gradually decreasing turnover time values were found for the villus epithelium along the small intestine (fig

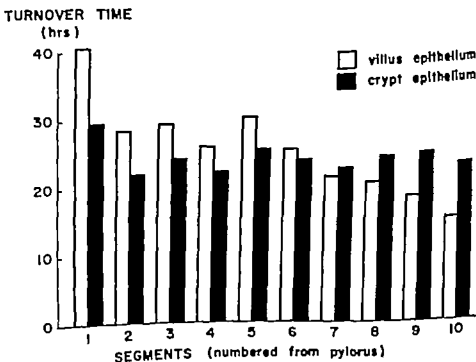


Fig. 7 Turnover times of the villus and crypt portions of the intestinal epithelium of the various intestinal segments of adult rats are illustrated. The turnover time of the villus epithelium displays a trend of gradual decrease along the small intestine while the turnover time of the crypt epithelium shows no significant regional variation with the possible exception of the duodenal region (segment 1) where it is slightly above average.

7). The turnover time of the crypt epithelium, on the other hand, appeared to be the same throughout (slightly higher in duodenum) (fig. 7). It has already been shown by a number of authors that the turnover time of the ileal epithelium is shorter than the turnover time of the epithelium of the upper small intestine (Leblond and Stevens, '48; Creamer, Shorter and Bamforth, '61; Lesher, Fry and Kohn, '61; Fry et al., '61–63). The present results suggested that these regional differences are confined to the villus epithelium and are attained in a gradual manner.

Age changes in the renewal of the intestinal epithelium

With increasing age a marked increase in the size of the progenitor crypt epithelium was observed while the villus epithelium increased to a lesser degree. The total number of crypt cells in the small intestine rose from 168 million to 1819 million between weanling and adult age, that is, about 11 times while the total number of villus epithelial cells increased from 354 million to 1905 million, that is, about 5.5 times (table 4). Furthermore, the percentage of mitotic cells within the crypt epithelium also increased with age (fig. 8).

The marked expansion in the number of crypt epithelial cells and in their mitotic activity suggested a substantial increase in the rate of cell production. At the beginning this cell production must be used largely for growth but as growth subsides with increasing age more and more of the produced cells must be used for the renewal process. It follows that the rate of renewal of the intestinal epithelium must increase substantially between weanling and adult age. It has already been shown by a number of authors that some renewal of the intestinal epithelium is present in suckling and weanling animals (Greulich and Leblond, '53; Bélanger, '54; Walker, '57; Walker and Leblond, '58; Creamer, Shorter and Bamforth, '61). The present data revealed that the rate of this renewal must be relatively low at these ages and it

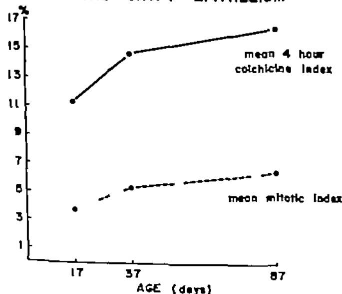


Fig. 8 The mean colchicine index and the mean mitotic index of the crypt epithelium are plotted against age. (The 2-hour colchicine index of the weanling rats was doubled in order to make it comparable to the 4-hour index of young and adult rats.) An increase of mitotic activity with age is indicated by both types of results.

In the growing age groups the epithelial cells produced in equal numbers in the various segments must be used partly for growth depending on the extent of growth in the various regions and partly for renewal. It follows that to investigate the regional variations of renewal in growing rats a knowledge of regional variations in growth would be required However the present method for measuring growth (i.e. cell addition for growth) was not applied to the various regions but to the entire intestinal epithelium instead. The regional variations in renewal were therefore investigated in detail in adult rats where growth is insignificant.

In the adult animals a clear-cut difference could be seen in the regional distribution patterns of the villus epithelial cells and of the crypt epithelial cells (fig 5) While the number of villus epithelial cells per segment decreased gradually from duodenum to terminal ileum the number of crypt epithelial cells per segment remained fairly constant in every region. The results on the villus and crypt heights (fig. 2) and also results on the weight of the villus and crypt epithelia of the segments (fig. 6) supported these observations by showing similar trends in regional distribution As cells are produced at approximately equal rates at all locations of the crypt epithelium, cells must enter the villus epithelium, replace the cells there and exfoliate at the same rate in order to maintain the steady state of the intestinal epithelium (Leblond and Stevens, 48). The average time spent by the cells in the villus compartment between entry and extrusion (i.e. the turnover time of the villus epithelium) then depends on the number of villus epithelial cells present. Since this number decreased gradually from duodenum to terminal ileum, gradually decreasing turnover time values were found for the villus epithelium along the small intestine (fig.

REGIONAL VARIATION IN THE TURNOVER TIME OF THE INTESTINAL EPITHELIUM OF ADULT RATS

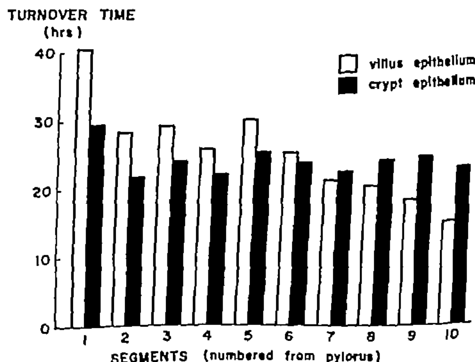


Fig. 7 Turnover times of the villus and crypt portions of the intestinal epithelium of the various intestinal segments of adult rats are illustrated. The turnover time of the villus epithelium displays a trend of gradual decrease along the small intestine while the turnover time of the crypt epithelium shows no significant regional variation with the possible exception of the duodenal region (segment 1) where it is slightly above average.

growth and renewal. These observations are summarized in figure 9. The total number of epithelial cells produced daily in the small intestine increased from 112 million, at weanling age to 914 million at young age, and to 1796 million at adult age. In other words of the total number of epithelial cells present in the small intestine of weanling, young and adult rats 21, 40 and 48% respectively was found to enter mitosis daily to produce new cells. In weanling rats, most of the produced cells, about 78% would be incorporated into the epithelium as a result of growth whereas the remaining 22% that is about 25 million cells, would be involved in the process of renewal and become exfoliated. In young rats, only about 3% of the produced cells was found to be needed for growth; thus the majority of the produced cells, about 97% that is about 885 million cells must enter the renewal process daily and exfoliate subsequently. Since the number of produced cells used for growth was negligible in young rats it was assumed that all or nearly all the produced cells, that is, about 1796 million cells daily are involved in the process of renewal in adult rats. Briefly then an intensive acceleration of renewal was observed between weanling and adult age in association with the rapid expansion of cell production and the concomitant subsidence of growth. The extent of this acceleration of renewal is further illustrated by the turnover time data the mean turnover time of the intestinal epithelium decreased from about 22 days in weanling rats, to 2.6 days in young rats and 2.1 days in adult rats, thereby indicating that between weanling and adult age, at least a tenfold increase must take place in the rate of renewal.

ACKNOWLEDGMENTS

The authors wish to express their appreciation to Drs. C P Leblond and Claire Huckins for their assistance in the preparation of the manuscript.

This work was made possible through a grant of the Medical Research Council of Canada to Dr C. P Leblond and it was partially aided by a Fellowship of the Connaught Fund of the Banting Research Foundation to the senior author

LITERATURE CITED

Abercrombie, M. 1946 Estimation of nuclear populations from microtome sections. Anat. Rec., 94: 239–247

Altmann, G. G. 1964 Cell number as a measure of growth and exfoliation of the epithelium of the small intestine of rats. M.Sc. Thesis, McGill University Montreal, Canada.

Andrew W., and J. M. Sass 1947 Mitotic division and degeneration of lymphocytes within cells of intestinal epithelium in young and adult white mice. Anat. Rec., 97 63–98.

Bélanger L. F 1954 Autoradiographic visualization of S³⁵ incorporation and turnover by the mucous glands of the gasto-intestinal tract and other soft tissues of rat and hamster Anat. Rec., 118 755–772.

Bertalanffy F D. 1960 Mitotic rates and renewal times of the digestive tract epithelia in the rat. Acta Anat., 40: 130–148.

Boivin, A. R. Vendrely and C. Vendrely 1948 L acide desoxyribonucléique du noyau cellulaire dépositaire des caractères héréditaires; arguments d'ordre analytique. C. R. Acad. Sci. (Paris) 226 1061–1063.

Brody S. 1945 Bioenergetics and Growth. Reinhold Publ. Corp., New York, pp. 502–534.

Carleton, H. M. 1939 Histological Technique. Oxford University Press, Oxford.

Creamer B., R. G. Shorter and J. Bamforth 1961 The turnover and shedding of epithelial cells. I. The turnover of the gastro-intestinal tract. II. The shedding in the small intestine. Gut, 2 110–118.

Davidson, J N and I. Leslie 1950 Nucleic acids in relation to tissue growth. Exp. Cell Res., 1 127–134.

——— 1950 Nucleic acids in relation to tissue growth. Cancer Res., 10 587–594.

——— 1950 A new approach in the biochemistry of growth and development. Nature, 165: 49–53.

Dische, Z. 1930 Über einige neue charakteristische Farbreactionen der Thymonukleinsäure und eine Micromethode zur Bestimmung derselben in tierischen Organen mit Hilfe dieser Reactionen. Microchemie, 8 4–32.

——— 1955 Color reactions of nucleic acid components. In: The Nucleic Acids, Chargaff and Davidson, eds. Academic Press, New York, I pp 285–305.

Enesco, M. 1956 Biochemical determination of the growth rate of several organs in male Sherman rats. Anat Rec., 124: 285–286 (Proc.).

——— 1957 Increase in cell number and size and in Extracellular Space during Postnatal Growth of Several Organs in the Albino Rat. Ph.D. Thesis, McGill University Montreal.

——— 1959 Increase in the number of nuclei and the mean cell size during postnatal growth of the heart of male Sherman rats. Anat. Rec., 133: 273 (Proc.)

——— 1960 Change in the nuclei number in the whole body as compared with that of carcass, viscera, and skin during postnatal growth of the male Sherman rat. Anat. Rec., 136 183 (Proc.)

becomes progressively higher as adulthood is approached.[8]

The derived data on the rates of cell production cell addition (for growth) and cell renewal are intended to give an approximate quantitative estimate of the increase of cell production with age and of the associated changes in the rates of

[8] On the basis of estimations of the proportion of villi with extrusion zones, O'Connor ('66) has reported recently that a threefold increase in renewal rate takes place in the intestinal epithelium of the mouse between the fifteenth and twenty-first postnatal days.

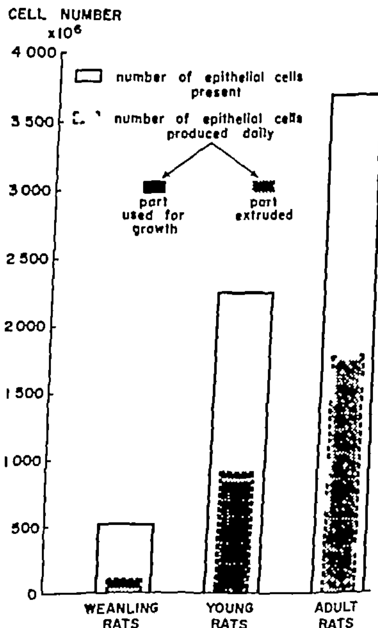


Fig. 9 The total number of epithelial cells present in the small intestine and the total number of epithelial cells produced daily are illustrated. The number of epithelial cells produced can be divided into two fractions statistically: fraction used for growth and fraction used for renewal. It can be seen that with increasing age the rate of cell production becomes accelerated and the relative as well as absolute numbers of epithelial cells participating in renewal increase.

Fine Structure of Steroidogenic Cells of a Primate Cutaneous Organ [1]

JEAN KNEELAND KISSON AND WOLF H. FAHRENBACH
Department of Electron Microscopy, Oregon Regional Primate Research Center, Beaverton, Oregon

ABSTRACT The antebrachial organ of the ring-tailed lemur (*Lemur catta*) is a highly differentiated cutaneous appendage composed of atypical apocrine sweat glands and of clumps of large interstitial cells. These cells have many similarities to steroid-secreting cells, most notably an extensive agranular reticulum, which occurs in several forms. Commonly it consists of random tubules, but at times these are compacted into tight masses. The cisternae sometimes are distended with dense inclusions. Often the agranular reticulum differentiates into a rigidly patterned crystalloid composed of stacked layers of parallel, interconnected tubules. The three-dimensional structure of the crystalloid is identical in both sexes, but the crystalloid of the male is scaled down in all its dimensions by a factor of about 0.9 as compared to that of the female. The interstitial cells, like steroidogenic tissue, exhibit intense 3β-, 17β-, and 20α-hydroxysteroid dehydrogenase activity and contain abundant esterases; thiobutyric esterase activity is limited to the agranular reticulum.

For comparative purposes, examination has been made of several other tissues having agranular reticulum: testicular interstitial cells, corpus luteum, adrenal cortex, and sebaceous cells of *Lemur catta*, rat meibomian glands, and the Leydig cells of human testis. The Reinke crystalloid of human testicular interstitial cells is totally unlike the crystalloid of the interstitial cell of the antebrachial organ.

The antebrachial organ, a prominent cutaneous appendage found uniquely in the prosimian primates *Lemur catta* and *Hapalemur griseus* is a scentmarking gland located on the flexor surface of the forearm (fig. 1). Interstitial cells occurring in nests between the coils of unusual apocrine sweat glands (Kneeland, '66) were described first by Affolter ('38) who did not ascribe any function to them. Montagna ('62) in characterizing this organ in *L. catta* histochemically compared these cells to testicular Leydig cells on the basis of similar histochemical properties and the presence of large hexagonal crystalloids; he concluded that these cells comprise an endocrine organ of unknown function. Since the fine structural features of testicular interstitial cells (Fawcett and Burgos, '60; Christensen and Fawcett, '61; Crabo, '63; Christensen, '65; Christensen and Fawcett, '66) and of other steroid-secreting cells (Enders '62; Scharrer '64; Lennep and Madden, '65; Brenner '66) are well known — namely an abundant agranular reticulum, prominent mitochondria, and quantities of lipid — comparison of the interstitial cells of the antebrachial organ to such cells may be useful in elucidating any possible endocrine function. This study is an electron microscopic and histochemical analysis of these interstitial cells, observed in various stages of the reproductive cycle of the ring-tailed lemur.

MATERIAL AND METHODS

Tissue was obtained from the antebrachial organ, scalp, adrenal, testis and ovary of *Lemur catta*. Biopsy specimens of the antebrachial organ were obtained of females in several phases of the estrus cycle as determined by vaginal smears (Evans and Goy '68) both in estrus and out of season and of a female in mid-pregnancy and immediately postpartum. Specimens were obtained from males in season, as judged by fertile mating, and out of season, as indicated by an empty scrotum. Human testis was obtained from two patients aged 65 and 72 who were undergoing orchidectomy for prostatic cancer.

The tissue was fixed for 3–6 hours in one of the following: 1% OsO_4-collidine

[1] Publication no. 187 of the Oregon Regional Primate Center, supported in part by grants FR 00163 and AM 08445 from the National Institutes of Health. A part of this study was presented as a demonstration at the 79th Session of the American Association of Anatomists, April 1966 (Fahrenbach and Kneeland, '66).

——— 1960 Increase in the number of nuclei along with the enlargement of muscle fibers in the soleus of the growing rat. Proc. Canad. Fed. Biol. Soc., 3: 22.

——— 1961 Increase in the number of nuclei in various striated muscles of the growing rat. Anat. Rec., 139 225–226.

——— Unpublished material.

Enesco, M., and C C Altmann 1963 Size of cell population and number of cells extruded daily in the small intestine of the adult rat. Anat. Rec (Proc) 145: 226–227

Enesco M and C. P Leblond 1962 Increase in cell number as a factor in the growth of the organs and tissues of the young male rat. J Embryol exp Morph. 10: 530–562.

Enesco M., and D Puddy 1964 Increase in the number of nuclei and weight in skeletal muscle of rats in various ages. Am J Anat., 114 235–244

Eränkö O 1955 Quantitative Methods in Histology and Microscopic Histochemistry Little Brown and Co. Toronto.

Fry R. J M., S Lesher W E. Kisieleski and G Sacher 1963 Cell proliferation in the small intestine In: Cell Proliferation Lamerton and Fry eds. Blackwell Scientific Publications, Oxford pp. 213–236.

Fry R. J M., S Lesher and H. I. Kohn 1961 Age effect on cell-transit time in mouse jejunal epithelium. Amer J Physiol., 201: 213–216.

——— 1962 Influence of age on the transit time of cells of the mouse intestinal epithelium. III. Ileum Lab. Invest., 11: 289–253

Greulich R. C and C P Leblond 1953 Radioautographic visualization of radiocarbon in the organs and other tissues of newborn rats following administration of C^{14} labeled bicarbonate. Anat. Rec., 115: 559–585.

Leblond C. P 1959 Classical technics for study of the kinetics of cellular proliferation. In: The Kinetics of Cellular Proliferation, Stohlman, ed. Grune and Stratton New York, pp. 31–49.

——— 1965 The time dimension in histolog Amer J Anat., 116: 1 28.

Leblond, C. P., and C. E. Stevens 1948 The constant renewal of the intestinal epithelium in the albino rat. Anat. Rec., 100: 357–37

Leblond, C. P., C. E. Stevens and R. Bogoroch 1948 Histological localization of newly forme desoxyribonucleic acid. Science, 108, 531-533.

Leblond C. P and B E. Walker 1956 Renewal of cell populations. Physiol. Rev 36 255–276.

Lesher S., R. J M. Fry and H. I. Kohn 1961 Influence of age on transit time of cells of mouse intestinal epithelium. I. Duoden Lab. Invest. 10: 291–300.

——— 1961b Age and generation time of th mouse duodenal epithelial cell. Exp. Cell Re 24: 334–343.

——— 1961c Aging and the generation cycl of intestinal epithelial cells in the mous Gerontologia, 5: 176–181

Loran, M. R. and T T Crocker 1963 Popu lation dynamics of intestinal epithelia in th rat two months after partial resection of th ileum. J Cell Biol., 19: 285–292.

O'Connor T M. 1966 Cell dynamics in th intestine of the mouse from late fetal life maturity Am. J Anat., 118: 525–536.

Schneider W C. 1945 Phosphorus compou in animal tissues. I Extraction and estimatio of DNA and RNA. J biol. Chem., 161 29 303

Stevens Hooper C. E. 1961 Use of colchici for the measurement of mitotic rate in th intestinal epithelium. Am. J Anat., 10 231–244

Walker B. E. 1957 Sites of cellular renew visualized by radioautography after C^{14}-adeni injection. Anat. Rec., 127: 383 (Proc.)

Walker B E., and C. P Leblond 1958 Sit of nucleic acid synthesis in the mouse visua lized by radioautography after administrati of C^{14} labeled adenine and thymidine. Ex Cell Res., 14 510–531

ine Structure of Steroidogenic Cells of a rimate Cutaneous Organ [1]

JEAN KNEELAND SISSON AND WOLF H. FAHRENBACH

Department of Electron Microscopy Oregon Regional Primate Research Center Beaverton, Oregon

ABSTRACT The antebrachial organ of the ring-tailed lemur (*Lemur catta*) is a highly differentiated cutaneous appendage composed of atypical apocrine sweat glands and of clumps of large interstitial cells. These cells have many similarities to steroid-secreting cells, most notably an extensive agranular reticulum, which occurs in several forms. Commonly it consists of random tubules, but at times these are compacted into tight masses. The cisternae sometimes are distended with dense inclusions. Often the agranular reticulum differentiates into a rigidly patterned crystalloid composed of stacked layers of parallel, interconnected tubules. The three-dimensional structure of the crystalloid is identical in both sexes, but the crystalloid of the male is scaled down in all its dimensions by a factor of about 0.9 as compared to that of the female. The interstitial cells, like steroidogenic tissue, exhibit intense 3β- 17β-, and 20α-hydroxysteroid dehydrogenase activity and contain abundant esterases; thiobutyric esterase activity is limited to the agranular reticulum.

For comparative purposes, examination has been made of several other tissues having agranular reticulum testicular interstitial cells, corpus luteum, adrenal cortex, and sebaceous cells of *Lemur catta* rat meibomian glands, and the Leydig cells of human testis. The Reinke crystalloid of human testicular interstitial cells is totally unlike the crystalloid of the interstitial cell of the antebrachial organ.

The antebrachial organ, a prominent cutaneous appendage found uniquely in the prosimian primates *Lemur catta* and *Hapalemur griseus* is a scentmarking gland located on the flexor surface of the forearm (fig. 1) Interstitial cells, occurring in nests between the coils of unusual apocrine sweat glands (Kneeland, '66) were described first by Affolter ('38) who did not ascribe any function to them. Montagna ('62) in characterizing this organ in *L. catta* histochemically compared these cells to testicular Leydig cells on the basis of similar histochemical properties and the presence of large hexagonal crystalloids; he concluded that these cells comprise an endocrine organ of unknown function. Since the fine structural features of testicular interstitial cells (Fawcett and Burgos, '60; Christensen and Fawcett, '61; Crabo, '63; Christensen, '65 Christensen and Fawcett, '66) and of other steroid-secreting cells (Enders '62, Scharrer '64 Lennep and Madden, '65 Bremner '66) are well known — namely an abundant agranular reticulum, prominent mitochondria, and quantities of lipid — comparison of the interstitial cells of the antebrachial organ to such cells may be useful in elucidating any possible endocrine function. This study is an electron microscopic and histochemical analysis of these interstitial cells, observed in various stages of the reproductive cycle of the ring-tailed lemur

MATERIAL AND METHODS

Tissue was obtained from the antebrachial organ, scalp, adrenal, testis and ovary of *Lemur catta*. Biopsy specimens of the antebrachial organ were obtained of females in several phases of the estrus cycle as determined by vaginal smears (Evans and Goy '66) both in estrus and out of season, and of a female in mid-pregnancy and immediately postpartum. Specimens were obtained from males in season, as judged by fertile mating, and out of season, as indicated by an empty scrotum. Human testis was obtained from two patients aged 65 and 72 who were undergoing orchidectomy for prostatic cancer

The tissue was fixed for 3–6 hours in one of the following: 1% OsO_4-collidine

[1] Publication no. 197 of the Oregon Regional Primate Center, supported in part by grants FR 00163 and AM 08445 from the National Institutes of Health. A part of this study was presented as a demonstration at the 79th Session of the American Association of Anatomists, April 1966 (Fahrenbach and Kneeland, '66).

——— 1960 Increase in the number of nuclei along with the enlargement of muscle fibers in the soleus of the growing rat. Proc. Canad. Fed. Biol. Soc., *3*: 22.

——— 1961 Increase in the number of nuclei in various striated muscles of the growing rat. Anat. Rec., *139* 225–226.

——— Unpublished material.

Enesco, M., and G G Altmann 1963 Size of cell population and number of cells extruded daily in the small intestine of the adult rat. Anat. Rec (Proc.) *145*: 226–227

Enesco M., and C P Leblond 1962 *Increase* in cell number as a factor in the growth of the organs and tissues of the young male rat. J Embryol exp Morph., *10*: 530–562.

Enesco, M., and D Puddy 1964 Increase in the number of nuclei and weight in skeletal muscle of rats in various ages Am. J Anat., *114* 235–244

Eränkö O 1955 Quantitative Methods in Histology and Microscopic Histochemistry Little Brown and Co., Toronto

Fry R J M., S. Lesher W E. Kisieleski and G Sacher 1963 Cell proliferation in the small intestine. In: Cell Proliferation Lamerton and Fry eds. *Blackwell Scientific Publications*, Oxford, pp 213–236.

Fry R. J M., S. Lesher and H. I Kohn 1961 Age effect on cell-transit time in mouse jejunal epithelium. Amer J Physiol., *201*: 213–216.

——— 1962 Influence of age on the transit time of cells of the mouse intestinal epithelium. III Ileum. Lab Invest., *11*: 289–253

Greulich, R. C. and C. P Leblond 1953 Radioautographic visualization of radiocarbon in the organs and other tissues of newborn rats following administration of C^{14} labeled bicarbonate Anat. Rec., *115*: 559–585

Leblond, C. P 1959 Classical technics for study of the kinetics of cellular proliferation. In: The Kinetics of Cellular Proliferation, Stohlman, ed. Grune and Stratton New York, pp 31–49.

——— 1965 The time dimension in histology Amer J Anat., *116*: 1–28.

Leblond C. P., and C. E. Stevens 1948 The constant renewal of the intestinal epi in the albino rat. Anat. Rec., 100: 357–37

Leblond, C. P., C. E. Stevens and R. Bogoroch 1948 Histological localization of newly formed desoxyribonucleic acid. Science, 108. 531–533.

Leblond, C. P and B. E. Walker 1956 Renewal of cell populations. Physiol. Rev 36 255–276.

Lesher S., R. J M. Fry and H. I. Kohn 1961a Influence of age on transit time of cells of mouse intestinal epithelium. I. Duodenum. Lab. Invest. 10: 291–300.

——— 1961b Age and generation time of the mouse duodenal epithelial cell. Exp. Cell Res., 24: 334–343.

——— 1961c Aging and the generation cycle of intestinal epithelial cells in the mouse. Gerontologia, *5*: 176–181

Loran, M. R., and T T Crocker 1963 Population dynamics of intestinal epithelia in the rat two months after partial resection of the ileum. J Cell Biol., *19*: 285–292.

O'Connor T M. 1966 Cell dynamics in the intestine of the mouse from *late fetal* life to maturity Am. J Anat., *118*: 525–536.

Schneider W C. 1945 Phosphorus compound in animal tissues. I. Extraction and estimation of DNA and RNA. J biol. Chem., *161*: 293–303.

Stevens Hooper C. E. 1961 Use of colchicine for the measurement of mitotic rate in the intestinal epithelium. Am. J Anat., 108 231–244

Walker B E. 1957 Sites of cellular renewal visualized by radioautography after C^{14}-adenine injection. Anat. Rec., 127: 383 (Proc.).

Walker B. E., and C. P Leblond 1958 Sites of nucleic acid synthesis *in the* mouse visualized by radioautography after administration of C^{14} labeled adenine and thymidine. Exp. Cell Res., *14*: 510–531

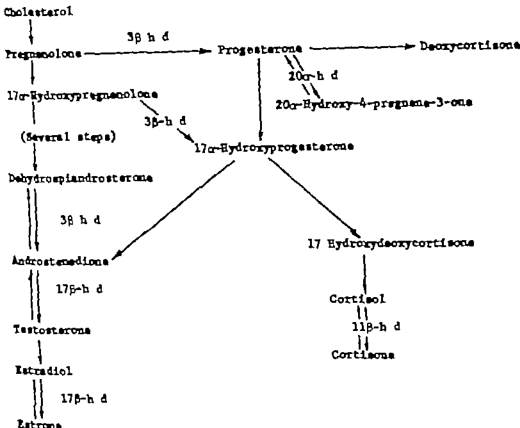


Fig. 2 Diagram showing some of the enzymes which mediate the interconversions of steroid hormones. Activities of 3β- 17β- and 20α-hydroxysteroid dehydrogenases have been demonstrated histochemically in this study with dehydroepiandrosterone, estradiol, and 20α-hydroxy-4-pregnene-3-one, respectively as substrates.

Lipid occurs also in the form of heterogeneous osmiophilic bodies, presumably lipopigment or residual bodies (figs. 6 10 18) The Golgi complex is not extensive and is difficult to distinguish from vesicular elements of the agranular reticulum. Only rarely are patches of granular endoplasmic reticulum seen, although numbers of free ribosomes occur The surface of the cell is relatively smooth, without interdigitations, microvilli, or pronounced marginal ruffling on occasion, inpocketings occur so that large areas of cell surface are invaginated into the cell mass (fig. 10) These may appear in section as isolated islands, containing layers of dense external-lamina material and a few collagen fibrils. At the cell surface and especially around these inpocketings small vesicles are seen in great numbers.

The agranular reticulum, which pervades all of the cytoplasm not occupied by other organelles, consists usually of randomly-disposed tubular and vesicular elements but at times it is arranged in whorls or tight masses of tubules. The latter (fig. 6) are so compact as to exclude mitochondria or other organelles; they are presumed to be "precrystalloid" formations. The intracisternal contents of the agranular reticulum are generally more opaque than the surrounding cytoplasm and sometimes the cisternae are dilated with very dense inclusions which assume a rounded shape up to 1 μ in diameter (figs. 6 7 8 11). These rounded cisternae which for

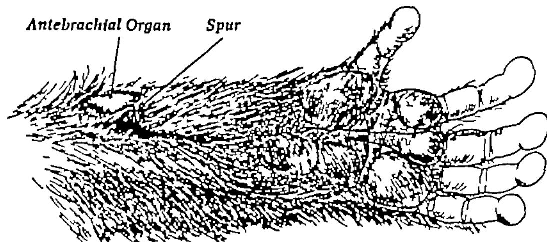


Fig 1 Drawing of *Lemur* forearm showing position of antebrachial organ. A horny spur accompanies the organ in the male. (Reproduced with permission from Evans and Goy '66).

(Bennett and Luft '59) 1% OsO4 buffered with 1% cacodylate with 4 5% sucrose added 1% glutaraldehyde-collidine-4 5% sucrose followed by 1% OsO4-collidine-sucrose or 3 1% glutaraldehyde-0 1 M cacodylate followed by 1% OsO4-cacodylate (Bell and Barrnett, 65) After fixation the tissues were dehydrated rapidly in cold ethanol and embedded in Araldite (Luft, '61) Thin sections stained with potassium permanganate or with aqueous uranyl acetate and lead citrate (Reynolds '63) were examined in a Philips 200 electron microscope Thick sections were stained with Toluidine Blue or with Sudan Black.

Histochemical analyses were performed on glutaraldehyde-fixed tissues for thiobutyric esterase (Bell and Barrnett, 65) and for acid phosphatase (Novikoff 61) The following enzymes (fig 2) were studied in frozen sections (20 μ) 3β-hydroxysteroid dehydrogenase (Wattenberg '58 Levy et al 59) with dehydroepiandrosterone as substrate 17β hydroxysteroid dehydrogenase (Pearson and Grose 59; Koide and Mitsudo 65 Baillie and Mack, '66) with estradiol as substrate and 20α-hydroxysteroid dehydrogenase (Balogh '64) with 20α-hydroxy-4-pregnene-3-one [1] as substrate. Control incubations with and without substrates were performed on a number of different tissues in addition to the antebrachial organ.

OBSERVATIONS

The interstitial cells of the antebrachial organ of *Lemur catta* are large polyhedral cells 10–25 μ in diameter Although occurring in clusters between apocrine sweat glands (figs. 3 4) each interstitial cell is isolated by an external lamina and by connective tissue fibrils (figs. 4 6) which also separate the interstitial cells from the sweat glands and from blood vessels and nonmyelinated nerve fibers. Thus, there is no intimate association of the interstitial cells with blood vessels nor any evident relationship between interstitial tissue and sweat glands.

These cells are characterized by large numbers of organelles including one or two vesicular nuclei, quantities of lipid, and an abundant agranular reticulum. The cytoplasmic matrix is fairly homogeneous and of moderate opacity with occasional clusters of glycogen granules within it. Mitochondria are plentiful they are ovoid or rodlike and 0 5–1 0 μ in diameter The mitochondrial matrix is dense, and the cristae are branched and tortuous (fig. 6) Sudanophilic lipid droplets of moderate electron opacity occur in variable amounts in all cells at times becoming so extensive as to fill the cell completely (fig 4) Since the agranular reticulum usually envelops the droplets it is not possible to discern whether the lipid is membrane bounded.

[1] Ikapharm, Ramat-Gan, Israel.

For comparative purposes, a survey has been made of several other tissues which are known to have or are suspected of having crystalloids. These include the testicular Leydig cells, corpus luteum, adrenal cortex, and sebaceous glands of *Lemur catta*, rat meibomian glands, and the Leydig cells of human testis. The testicular interstitial cells of *L. catta* contain an abundant agranular reticulum, much lipid, and mitochondria with villous cristae but no crystalloids have been seen. The corpus luteum of *L. catta* consists of a highly vascularized mass of lipid-rich luteal cells. The luteal cells (fig. 20) have a tubular agranular reticulum which is sometimes arranged in whorls or compact masses of tubules similar to the "precrystalloid" formation of the interstitial cells of the antebrachial organ, but no crystalloids have been encountered the mitochondria of these cells have lamelliform cristae. The cells of the adrenal cortex of *L. catta* have an agranular reticulum, mitochondria with villous cristae and abundant lipids they are quite similar to adrenal cortical cells of *Macaca mulatta* (Brenner '66) The sebaceous glands of *L. catta*, which have an agranular reticulum, do not contain crystalloids. The meibomian glands of the rat, however do have crystalloids (fig. 24) which are composed of agranular reticulum. Human testicular interstitial cells contain the so-called Reinke crystalloid. This organelle is not composed of agranular reticulum but is a latticework of minute filamentous or tubular structures about 50 A in diameter which produce a honeycomb pattern in one orientation (fig. 21) and a strictly rectangular pattern at right angles to this orientation (fig. 22) Crystalloids which are virtually identical to the Reinke crystalloid have been described (Yates '66a,b) in adrenal cortical and luteal cells of triparanol-treated hamsters.

DISCUSSION

The comparison by Montagna ('62) of the interstitial cells of the antebrachial organ to steroid-secreting cells is based on morphological and histochemical similarities, but there are also a few discrepancies. For example, the antebrachial organ has quantities of oxidative enzymes and abundant esterases (Montagna and Yun, '62) as do for instance testicular Leydig cells (Niemi and Ikonen, '62; Baillie '64 Bell and Barrnett, '65) but these enzymes are not by any means restricted to steroidogenic tissues. More specific histochemical methods for demonstrating enzyme activity in steroid-secreting tissues are those for the hydroxysteroid dehydrogenases (Wattenberg, '58; Levy et al. '59 Balogh '64); some of these enzymes (as discussed below) have shown activity in the interstitial cells of the antebrachial organ. On the other hand the mitochondria of these cells do not have villous cristae as do the mitochondria of testicular interstitial cells of rabbit (Crabo '63) rat (Schwarz and Merker '65) mouse (Baillie, '64; Christensen and Fawcett, '66) man (Fawcett and Burgos, '60 Gordon et al. '64) and lemur and of adrenal cortical cells of many species (Brenner '66; Lindner '66 Long and Jones '66) Neither however do the mitochondria of luteal cells in the ovary of man (Lennep and Madden, '65) mink and armadillo (Enders, '62) and lemur (fig. 20) or of the steroid secreting prothoracic glands of blattarian insects (Scharrer '64). The Reinke crystalloid of human testicular interstitial cells, to which the crystalloid of the antebrachial organ was first compared (Montagna, '62) is not composed of agranular reticulum, rather as seen in human Leydig cells (figs. 21 22; see also Fawcett and Burgos '60 and Yamada, '62) and in specialized circumstances in ovary and adrenal cortex (Yates, '66a,b) the Reinke crystalloid displays a latticework of minute filaments. There are no crystalloids in ovarian luteal cells testicular interstitial cells or adrenal cortical cells of *Lemur catta* nor have any been reported in the interstitial cells of the antebrachial organ of *Hapalemur griseus* (Affolter '38) The most obvious similarity of the interstitial cells of the antebrachial organ to steroidogenic tissue, at the electron microscopic level, is the abundance of agranular reticulum, the morphological feature particularly characteristic of steroid-secreting cells (Christensen, '65) Tightly compacted masses of tubules of agranular reticulum ("precrystalloid formations") are seen in testicular interstitial cells of the opossum (Christensen and Fawcett, '61) rabbit (Crabo '63) and rat (Murakami, '66) and

the sake of convenience will be referred to as "inclusion bodies" are sudanophobic and accumulate in masses which extend 5–7 µ (figs. 5 10)

The most highly organized configuration of the agranular reticulum is that of a crystalloid This organelle is often hexagonal reaches a size of 7–10 µ (fig 5) and is composed of layers of tubules of agranular reticulum (figs. 9 13) An occasional crystalloid is incomplete centrally enclosing parts of the cytoplasm or "inclusion bodies" (fig 11) Microfilaments of 50–70 Å diameter and of indeterminate length are associated intimately with the crystalloid and lie in the adjacent cytoplasm close to its periphery (fig 11) Although in most micrographs the crystalloid has an appearance of unintelligible complexity it has been possible to infer its three-dimensional structure from fortunately-oriented sections In one of these (fig. 13) the plane of section is virtually parallel to one set of tubules and slants through the crystalloid at a slight angle normal to this set The resultant moiré pattern is an indication of repetitive regular arrays of tubules and thus provides the observer with an index of the third dimension in other words, an image such as figure 13 contains the same information as serial sections through eight layers of the crystalloid

The crystalloid consists of a set of parallel tubules hexagonally packed in cross section (ABABABA packing) A second set of identical parallel tubules also disposed in an hexagonally packed array (A'B A'B A) interpenetrates between the layers of tubules of the first set at an angle of 120 (refer to figs 14 16) The tubules of set one and set two are continuous with each other by means of two types of interconnections Long interconnectors perpendicular to the axial direction of the set-one and set-two tubules connect any given tubule of set one to a tubule of set two removed by one layer (A to A B to B) For each long connector there are two short connectors both joining for example an A tubule to the adjacent A tubule (or B to B) Each short connector is offset by 120 from the long connector about the axis of the tubule of origin and rotated approximately 30 about an axis which coincides with that of the long connector so that long and short connectors describe a helix with respect to their tubule of origin. The predicted triradiate array of long and short connectors as seen along the axis of the tubule of origin is visible in figure 12. It follows from this description that the crystalloid is, in fact, composed of two interpenetrating crystalloids, since the arrays of A and A tubules and B and B tubules remain separate and without continuity with each other (i.e. there are no A to B or A to B junctions)

In certain respects the interstitial cell differs between male and female. Although all the main inclusions — crystalloids, masses of "inclusion bodies, and lipid droplets — may be found in the same cell, this is not usually the case. In general, the more extensive the amount of lipid, the fewer are other organelles. Some correlation has been possible between morphological variability (e.g number of crystalloids) and seasonal cyclicity since biopsies have been obtained both in males and in females in several phases of the reproductive cycle. The interstitial cell of the male almost always contains aggregations of "inclusion bodies" particularly when out of season while the cell of the female usually contains larger quantities of sudanophilic lipids out of season and more crystalloids in season. In the male about 10% of the interstitial cells contain crystalloids in the female perhaps 25–30% and sometimes up to 90% of the cells have them Although the three-dimensional structure of the crystalloid is identical in male and female, the diameter of the tubules is not being about 300 Å in the female and about 270 Å in the male

Histochemically several enzyme systems are demonstrable Three β 17β- and 20- hydroxysteroid dehydrogenases are abundant in the interstitial cells of both male and female (fig 19) Thiobutyric esterase activity is intense in both male and female and is limited to the agranular reticulum, it is especially prominent on the membranes of the crystalloid (fig 17) Acid phosphatase activity (fig 18) is limited to well-defined membrane-bounded bodies, presumably lysosomes and is absent from the "inclusion bodies."

hetic output of the system but also simple physical aspects of the membrane, such as preferred curvature of membranes disposed as tubules. The maintenance of this degree of order would require the expenditure of energy far beyond that required for the upkeep of randomly-distributed agranular reticulum. If the crystalloid is indeed maintained against an unfavorable dynamic gradient, it would indicate the higher biosynthetic efficiency of this membrane complex. The functional activity of the crystalloid in steroidogenesis is in opposition to that of the Reinke crystalloid, which is considered to represent a storage organelle for steroid precursors (Yates, '65b). In testicular interstitial cell tumors, there are rarely any Reinke crystalloids, whether the tumors are androgenic (Cook et al., '62 Bayer et al., '65) or estrogenic (Gordon et al., '64 Smith et al., '66) presumably because the tumor cells do not store significant amounts of steroids but release them as rapidly as they are synthesized (Cook et al. '62); Reinke crystalloids are found, however in arrhenoblastoma (a masculinizing adenoma of the ovary) along with minimal 3β-hydroxysteroid dehydrogenase activity (Goldberg et al. '63b). The "precrystalloid" formations of the agranular reticulum resemble strongly the masses of tubules seen in rabbit luteal cells during early pseudopregnancy when 3β-hydroxysteroid dehydrogenase activity is marked (Blanchette '66) and these formations exhibit strong thiobutyric esterase activity; for these reasons, they are considered "precrystalloid" formations rather than effete crystalloids.

The role of the "inclusion bodies" is more conjectural than that of the crystalloid. The "inclusion bodies" appear to be identical to the small granules" described by Christensen and Fawcett ('66) in testicular interstitial cells of mice although these authors did not demonstrate any connection of these granules with the agranular reticulum. The "inclusion body is not a lysosome, as shown by the absence of acid phosphatase activity (fig 18) furthermore, the absence of acid phosphatase activity indicates that these bodies are not an expression of degradative cellular metabolism. They are more likely storage organelles. This interpretation is supported by the intimate association of "inclusion bodies" with crystalloids (fig. 11) by their relative lack of thiobutyric esterase activity (fig. 17) and by the appearance of large masses of "inclusion bodies" in postseason males (figs. 7 10)

The variability of the cytology of the interstitial cell in relation to reproductive season is more pronounced in the female than in the male. This is to be expected, if gonadal hormones are involved, since the male has only a broad sexual season while the female has several estrus cycles within that season (Evans and Goy '66) The cell cycle as reconstructed from many biopsies, is believed to be as follows. During the nonbreeding season, lipid accumulates in the female cell (fig. 4) With the advent of the breeding season, the lipid disappears, and the number of crystalloids increases markedly being maximal (90%) during estrus when, presumably the cell is secreting most actively If the female becomes pregnant, the number of crystalloids decreases slowly (to 50–60%) while there is a gradual accumulation of masses of "inclusion bodies" (fig. 5) during the post partum period, lipid increases to the off season level and crystalloids and "inclusion bodies" decrease. If the female does not become pregnant, the number of crystalloids decreases precipitously and lipid increases rapidly In the male the masses of "inclusion bodies" wax and wane somewhat with season, but crystalloid and lipid levels remain low

The interstitial cell of the antebrachial organ exhibits many morphological and histochemical characteristics of steroidogenic cells but it is not possible to determine whether these cells are secreting gonadal or adrenal cortical steroids Although ectopic steroid-secreting cells have been described as adrenal rests (Seliger et al. '66) there are no precise morphological or histochemical criteria for differentiating adrenal cortical cells from those of the ovary or testis (Savard et al '60) The same complement of hydroxysteroid dehydrogenases is found histochemically in all three tissues (Deane and Rubin, '65; Davies et al. '66 Baillie and Mack, '66) The Reinke crystalloid, long considered characteristic of human testicular interstitial cells has been found also in hilar cells of

in luteal cells of the rabbit (Blanchette '66) man (Lennep and Madden 65) and lemur (fig 20) as well as in the interstitial cells of the antebrachial organ In the testicular interstitial cells of the guinea pig the agranular reticulum occurs as fenestrated cisternae and random tubules (Christensen '65)

Complex arrangements of smooth tubules have been reported in isolated instances in non steroidogenic tissues. The rat plasma cell (fig 23) may display a lattice-like array of tubules which are in continuity with the rough endoplasmic reticulum (J F Kent personal communication) The pigment-producing test cell of tunicate ovary contains a large Golgi complex whose membranes have a "honey comb" appearance (Kessel and Beams '65). In rat meibomian cells a "grid of intercommunicating tubules" has been described as Golgi apparatus (Palay '58); further observations indicate this structure to be a differentiation of the agranular reticulum (fig 24) Although an abundant agranular reticulum is found not only in steroid-secreting cells but also in such lipid metabolizing cells as sebaceous cells adipose cells (Williamson '64) or liver cells engaged in cholesterol biosynthesis (Jones and Armstrong '65) it is apparently unrelated to those smooth-surfaced membrane systems which have been implicated in ion transport, such as that found in chloride cells of the gastric mucosa (Ito and Winchester '63) and of fish gill (Philpott and Copeland 63; Philpott '66a,b) or in the sarcoplasmic reticulum of striated muscle (Franzini-Armstrong '64 Costantin et al. 65) The agranular reticulum of steroid-secreting cells has been implicated directly in the biosynthetic process (Jones and Armstrong '65 Christensen and Fawcett '66; Long and Jones, '66) and a number of enzymes which mediate the synthesis of steroid hormones from cholesterol have been found in the microsome fraction (Christensen '65; Deane and Rubin, '65; Blanchette 66)

Several hydroxysteroid dehydrogenases enzymes which control certain steps of steroidogenesis, have been demonstrated histochemically in a variety of tissues 3β Hydroxysteroid dehydrogenase for example has been demonstrated in primate adrenal, ovary and placenta (Goldberg et al. '63a; Deane and Rubin, '65 Koide and Mitsudo '65) and in progesterone-secreting tumors (Goldberg et al., '63b) Although early attempts to demonstrate this enzyme in primate testis were unsuccessful, (Goldberg et al '63a; Maeir '65) 3β-hydroxysteroid dehydrogenase activity has been demonstrated in normal human testis (Baillie and Mack, '66). Activity of 17β-hydroxysteroid dehydrogenase is present in adrenal ovary placenta, and testis (Pearson and Grose, '59 Deane and Rubin, '65; Koide and Mitsudo, '65 Davies et al., '66 Baillie and Mack, '66) 20α-Hydroxysteroid dehydrogenase an enzyme which indicates progesterone metabolism, occurs in rat ovaries (Balogh '64 Pupkin et al., '66). Although 20α-hydroxysteroid dehydrogenase might be considered to control a degradative step (Pupkin et al. '66) 3β- and 17β hydroxysteroid dehydrogenases mediate steps in the synthesis of several steroids (fig. 2) Activities of both 3β- and 17β-hydroxysteroid dehydrogenases, as well as that of 20α-hydroxysteroid dehydrogenase have been demonstrated in the interstitial cells of the antebrachial organ (fig. 19). Hence it is a justifiable assumption that the interstitial cells — more specifically the agranular reticulum and its crystalloids — are engaged in steroidogenesis.

The crystalloid is probably the chief organelle of steroid synthesis. The intense thiobutyric esterase activity of the membranes of the crystalloid indicates that this is an active rather than an inert organelle, even though esterase activity may not itself be indicative of steroidogenesis but may be active only in maintaining the membranes of the crystalloid The fact that the diameter of the tubules composing the crystalloid of the male is smaller than that of the female can be considered an expression of a subtle sexual dimorphism in the membrane properties of the agranular reticulum which is recognized only when the reticulum has differentiated into a rigid pattern such as a crystalloid. These differential membrane properties might be influenced by quantitative or qualitative differences in the enzyme complement of the membranes These enzymes probably form an integral part of the membrane structure and could influence not only the biosyn-

Franzini-Armstrong, C. 1964 Fine structure of sarcoplasmic reticulum and transverse tubular system in muscle fibers. Fed. Proc., 23 887–895.
Goldberg, B., G. E. S. Jones and D. A. Turner 1963a Steroid 3β-ol dehydrogenase activity in human endocrine tissues. Am. J Obstet. Gynec., 86 349–359
Goldberg, B., G. E. S. Jones and J D Woodruff 1963b A histochemical study of steroid 3β-ol dehydrogenase activity in some steroid-producing tumors. Am. J Obstet. Gynec., 86 1003–1014.
Gordon, G B L. R. Miller and K. C. Bensch 1964 Electron microscopic observations on the gonad in the testicular feminization syndrome. Lab. Invest., 13 152–160.
Hurley H. J and W B Shelley 1960 The Human Apocrine Sweat Gland in Health and Disease. Charles C Thomas, Springfield, Illinois. pp. 64–73.
Ito, S., and R. J Winchester 1963 The fine structure of the gastric mucosa in the bat. J Cell Biol., 16 541–577
Jones, A. L., and D T Armstrong 1965 Increased cholesterol biosynthesis following phenobarbital induced hypertrophy of agranular endoplasmic reticulum in liver Proc. Soc. Exper. Biol. Med., 119: 1136–1139.
Kessel, R. G., and H. W Beams 1963 An unusual configuration of the Golgi complex in pigment-producing "test" cells of the ovary of a tunicate Styela. J Cell Biol., 25 55–67
Ettinger, G 1966 Unpublished observations.
Knoeland, J E. 1966 Fine structure of the sweat glands of the antebrachial organ of Lemur catta. Z. Zellforsch., 73: 521–533.
Leide, S. S., and S. M. Mitrudo 1965 Histochemical study of 3β- and 17β-hydroxysteroid dehydrogenases in human term placenta. Endocrinology 76: 403–407
Lennep, E. W and L. M. Madden 1965 Electron microscopic observations on the involution of the human corpus luteum of menstruation. Z. Zellforsch., 66: 365–380.
Levy H., H. W Deane and B L. Rubin 1959 Visualization of steroid-3β-ol dehydrogenase activity in tissues of intact and hypophysectomized rats. Endocrinology 65 932–943.
Lindner, E. 1966 Die Sacculi mitochondriales der Diskochondrien und Sphaerochondrien in der Nebennierenrinde von Igel (Erinaceus europaeus L.) Z. Zellforsch., 72: 212–235.
Long, J. A., and A. L. Jones 1966 The fine structure of the zona glomerulosa and zona fasciculata of the adrenal cortex of the opossum. Anat. Rec., 154 376–379
Luft, J H. 1961 Improvements in epoxy resin embedding methods. J Biophys. Biochem. Cytol., 9 409–414
Macir D. M. 1965 Species variation in testicular Δ^5-3β-hydroxysteroid dehydrogenase activity absence of activity in primate Leydig cells. Endocrinology 76 463–469.
Montagna, W 1962 The skin of lemurs. Ann. N. Y Acad. Sci., 102: 190–209
Montagna, W and J S Yun 1962 The skin of primates. X. The skin of the ring-tailed lemur (Lemur catta) Am. J Phys. Anthrop., 20 95–118.
Murakami, M. 1966 Elektronenmikroskopische Untersuchungen am interstitiellen Gewebe des Rattenhodens, unter besonderer Berücksichtigung der Leydigschen Zwischenzellen. Z. Zellforsch., 72. 139–156.
Niemi, M., and M. Ikonen 1962 Cytochemistry of oxidative enzyme systems in the Leydig cells of the rat testis and their functional significance Endocrinology 70 167–174
Novikoff, A. B. 1961 Lysosomes and related particles. In The Cell, Vol. II ed. by J Brachet and A. E. Mirsky Academic Press, New York, pp. 423–488.
Palay S. L. 1958 The morphology of secretion. In Frontiers in Cytology S. L. Palay ed. Yale Univ Press, New Haven. pp. 305–342.
Pearson, B., and F Grose 1959 Histochemical demonstration of 17β-hydroxysteroid dehydrogenase by use of a tetrazolium salt. Proc. Soc. Exp Biol. Med., 100 636–638.
Philpott, C. W 1966a The ultrastructural localization of polyanion in the "chloride cell" of sea water adapted Fundulus. Anat. Rec., 154 402.
——— 1966b The use of horseradish peroxidase to demonstrate functional continuity between the plasmalemma and the unique tubular system of the chloride cell. J Cell Biol., 31 86A.
Philpott, C. W and D. E. Copeland 1963 Fine structure of chloride cells from three species of Fundulus J Cell Biol., 18 389–404
Pupkin, M., H. Bratt, J Weisz, C. W Lloyd and K. Balogh 1966 Dehydrogenases in the rat ovary I. A histochemical study of Δ 3β- and 20α-hydroxysteroid dehydrogenases and enzymes of carbohydrate oxidation during the estrous cycle. Endocrinology 79 316–327
Rennels, E. G. 1966 Observations on the ultrastructure of luteal cells from PMS and PMS-HCG treated immature rats. Endocrinology 79 373–386.
Reynolds, E. S. 1963 The use of lead citrate at high pH as an electron-opaque stain in electron microscopy J Cell Biol., 17 208–212.
Savard, J R. I. Dorfman, B. Baggett, L. L. Fielding, L. L. Engel, H. T McPherson, L. M. Lister D S Johnson, E. C. Hamblen and F L. Engel 1960 Clinical, morphological, and biochemical studies of virilizing tumor in the testis. J. Clin. Invest., 29 534–553.
Scharrer B. 1964 The fine structure of blattarian prothoracic glands. Z. Zellforsch., 64 301–326.
Schwarz, W., and H. J Merker 1965 Die Hodenzwischenzellen der Ratte nach Hypophysektomie und nach Behandlung mit Choriongonadotropin und Amphenon B. Z. Zellforsch., 65 272–284
Seliger W G., A. J Blair and H. W Mossman 1966 Differentiation of adrenal cortex-like tissue at the hilum of the gonads in response to adrenalectomy Am. J Anat., 118 615–630
Smith, B. D C. R. Lerner and W R. Anderson 1966 Microscopic appearance of the gonads in testicular feminization." Anat. Rec., 154 424.
Wattenberg, L. W 1958 Microscopic histochemical demonstration of steroid-3β-ol dehydrogen-

the ovary (Savard et al. 60) in ovarian luteal cells and in adrenal cortical cells (Yates 66a b) Testicular tumors, in which Reinke crystalloids are rarely seen are identified as originating from Leydig cells on the basis of hormone assays (Cook et al 52; Savard et al. 60 Bayer et al 65) Biochemical analysis of the antebrachial organ of a female *Lemur catta* by ultraviolet absorption spectroscopy and by gas chromatography (Kittinger 66) has been attempted but the amount of tissue available was insufficient to demonstrate unequivocal steroidogenic activity How ever the requisite membrane and enzyme systems for steroid biosynthesis appear to be present in the interstitial cells of the antebrachial organ The variability of their cytology as related to reproductive season suggests the involvement of gonadal steroids (possibly an estrogen) rather than adrenal cortical steroids Since fluctuations in the morphology of the interstitial cell with season are not accompanied by concomitant changes in the secretory activity of the sweat glands of the antebrachial organ, these can be discounted as a possible target organ especially since the influence of gonadal hormones on apocrine glands has been disclaimed (Hurley and Shelley '60) Thorough analysis of the interactions of the interstitial cells with the pituitary and with other endocrine organs would require a broad experimental approach involving gland extirpation and replacement therapy an impracticable approach in an animal as rare as *Lemur catta*.

ACKNOWLEDGMENTS

We thank Dr John F Kent, Connecticut College for permission to use his unpublished electron micrograph Dr Mary Bell for assistance with the electron histochemistry and Mrs. Audrey Griffin and Mr Nick Roman for excellent technical assistance

LITERATURE CITED

Affolter M. 1938 Les organes cutanés brachiaux d'*Hapalemur griseus* Bull. Acad. Malgache Tananarive *20*: 77–100.

Baillie, A. H 1964 Age changes in the mitochondria and succinoxidase system of the Leydig cell. Z. Zellforsch. *62*: 72–79

Baillie A. H., and W S. Mack 1966 Hydroxysteroid dehydrogenases in normal and abnormal human testes. J Endocrin., *35*: 239–248.

Balogh, K. 1964 A histochemical method for the demonstration of 20α-hydroxysteroid dehydrogenase activity in rat ovaries. J Histochem. Cytochem., *12*: 670–673.

Bayer J M., E. Tonutti, W Nocke, L. Nocke, H. Breuer H. Schriefers und E. R. Smith 1965 Klinische, morphologische und biochemische Untersuchungen bei einem androgenbildenden Hodentumor Klin. Wschr., *43*: 1023–1031.

Bell M., and R. J Barrnett 1965 The use of thiol-substituted carboxylic acids as histochemical substrates. J Histochem. Cytochem., *13*: 611–628.

Bennett, H. S., and J H. Luft 1959 S-collidine as a basis for buffering fixatives. J. Biophys. Biochem. Cytol., *6*: 113–114.

Blanchette E. J 1966 The fine structure of the endoplasmic reticulum of "luteinized" ovarian cells and isolated microsomes in relation to Δ5-3β-hydroxysteroid dehydrogenase activity Anat. Rec., *154*: 318

Brenner R. M. 1966 Fine structure of adrenal cortical cells in adult male rhesus monkeys. Am. J Anat., *119*: 429–454

Christensen, A. K. 1965 The fine structure of testicular interstitial cells in guinea pigs. J Cell Biol., *26*: 911–935.

Christensen, A. K., and D W Fawcett 1961 The normal fine structure of opossum testicular interstitial cells. J Biophys. Biochem. Cytol., *9*: 653–670.

——— 1966 The fine structure of testicular interstitial cells in mice. Am. J Anat., *118*: 551–572.

Cook, C. D., R. E. Gross, B J Landing and A. I. Zygmuntowicz 1952 Interstitial cell tumor of the testis. Study of a 5-year-old boy with pseudo-precocious puberty J Clin. Endocrin. and Metab., *12*: 725–734.

Costantin, L. L., C. Franzini-Armstrong and R. J. Podolsky 1965 Localization of calcium-accumulating structures in striated muscle fibers. Science *147*: 158–160.

Crabo B. 1963 Fine structure of the interstitial cells of the rabbit testes. Z. Zellforsch., *61*: 587–604

Davies, J., G R. Davenport, J L. Norris and P I. C. Rennie 1966 Histochemical studies of hydroxysteroid dehydrogenase activity in mammalian reproductive tissues. Endocrinology *78*: 667–671

Deane H. W., and B L. Rubin 1965 Identification and control of cells that synthesize steroid hormones in the adrenal glands, gonads and placentae of various mammalian species. Arch. Anat. Microsc. et Morph. Exper., *54*: 49–66.

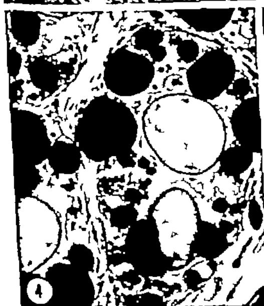
Enders, A. C. 1962 Observations on the fine structure of lutein cells. J Cell Biol., *12*: 101–113

Evans, C S., and R. W Goy 1966 Social behavior and reproductive cycles in captive ring-tailed lemurs (*Lemur catta* L.) In preparation.

Fahrenbach, W H., and J E. Kneeland 1966 Crystalloids of the agranular reticulum. Anat. Rec., *154* 501.

Fawcett, D W and M. H Burgos 1960 Studies on the fine structure of the mammalian testis. II. The human interstitial tissue. Am. J Anat., *107*: 245–269

3





ase in tissue sections. J Histochem Cytochem. 6 225–232.
Williamson J R. 1964 Adipose tissue Morphological changes associated with lipid mobilization J Cell Biol., 20 57–72.
Yamada E. 1962 Some observations on the fine structure of the interstitial cell in the human testis. In Fifth International Congress for Electron Microscopy Vol. 2, ed. by S. S. Breese, Academic Press, New York, pp. LL-1.
Yates R. D 1966a The effects of triparanol on luteal cells of pregnant female Syrian hamsters. Anat Rec., 154 445.
——— 1966b The effects of triparanol on the adrenocortical cells of the zona fasciculata of Syrian hamsters. Z. Zellforsch., 71 41 52.

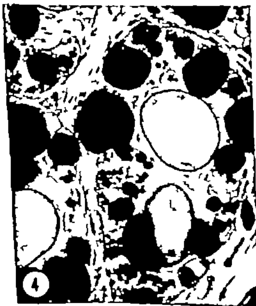
PLATE 1

EXPLANATION OF FIGURES

3 Light micrograph of the dermal part of the antebrachial organ. Clumps of interstitial cells nestle between large atypical apocrine sweat glands. Crystalloids are present in several cells (arrows) Glutaraldehyde Toluidine Blue 500 ×

4 Sudan Black-stained plastic section of the antebrachial organ demonstrating the large quantities of lipid in the interstitial cells of an out-of-season female The connective tissue is lightly counterstained with Toluidine Blue OsO_4 375 ×

5 Nest of interstitial cells of a pregnant female One cell has a large hexagonal crystalloid and two contain masses of "inclusion bodies" (arrows) Glutaraldehyde Toluidine Blue 1500 ×


4


5

PLATE 2

EXPLANATION OF FIGURE

6 Low power electron micrograph of portions of two interstitial cells from a *female in estrus*. Some of the agranular reticulum is dispersed randomly and some is disposed in tight masses of tubules ("*precrystalloid formations*") Other areas of agranular reticulum are dilated with "*inclusion bodies*" (*arrows*) The vesiculated area (G) is assumed to be a Golgi complex Several lipopigment bodies (*Lp*) are present in the cytoplasm A nonmyelinated nerve runs between the cells (*upper left*) Unless indicated otherwise all electron micrographs are of sections of osmium-fixed material stained with uranyl acetate and lead citrate. 17 000 × Inset Enlargement of a mitochondrion with especially tortuous cristae. 28 000 ×

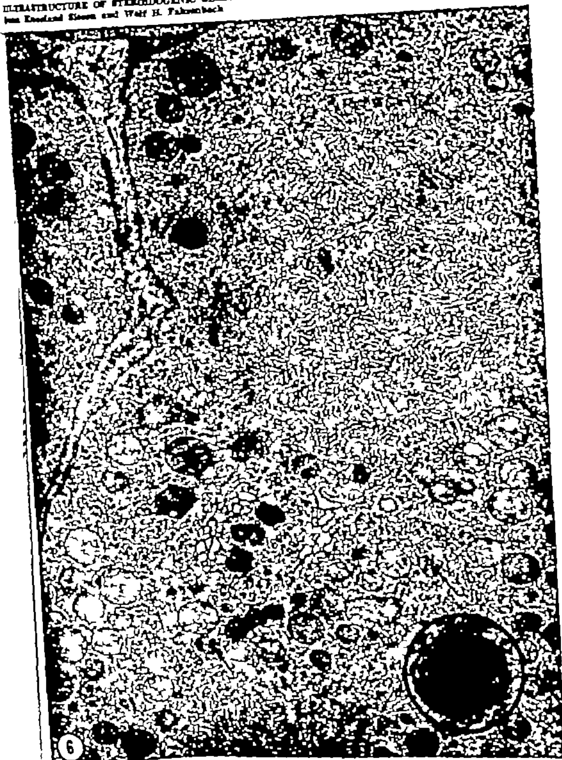

6

PLATE 3

EXPLANATION OF FIGURES

7 The agranular reticulum occurs in several forms in the interstitial cell Here "inclusion bodies" are formed from cisternae of the agranular reticulum which are dilated with dense granular contents. 31,000 ×

8 In this section a portion of the agranular reticulum forms a complex tubular ("precrystalloid") array while adjacent portions are dilated into "inclusion bodies" 30 000 ×

9 The continuity of the tubules of the agranular reticulum with those of the *crystalloid* is seen clearly along the periphery of the crystalloid (arrow) 43,000 ×



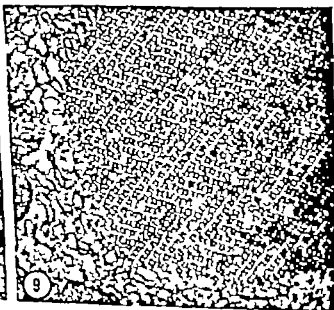


PLATE 4

EXPLANATION OF FIGURE

10 An interstitial cell from a postseason male in which a large part of the agranular reticulum is dilated with inclusion bodies which form a massive aggregate in the cytoplasm. Several lipopigment complexes (Lp) are present also The surfaces of the cell are infolded extensively forming several inpocketings containing dense external-lamina material (arrows) 10,500 ×


10

PLATE 5

EXPLANATION OF FIGURES

11 "Inclusion bodies" of varying density are enclosed in the tubules of this crystalloid of a male. Microfilaments are seen in cross section at the periphery of the crystalloid (lower left). Glutaraldehyde fixation has failed to preserve the tubular structure of the agranular reticulum in the cytoplasm surrounding the crystalloid. Permanganate stain. 25,000 ×

12 The triradiate array of interconnectors is seen in the plane of this section of a crystalloid (arrows) from the same animal as figure 11. Osmium fixation has yielded a "foamy" cytoplasm similar to that seen above with glutaraldehyde. Permanganate stain. 50,000 ×

11

12

PLATE 6

EXPLANATION OF FIGURE

13 Interstitial cell with well-developed hexagonal crystalloid The plane of section is virtually parallel to one set of tubules and slants through eight layers of tubules, creating a moiré pattern. It is from a section such as this that the three-dimensional morphology can be reconstructed The observer's eye should follow the darker tubules rather than concentrate on the lighter profiles, which represent lacunae in the crystalloidal lattice. 47,000 ×

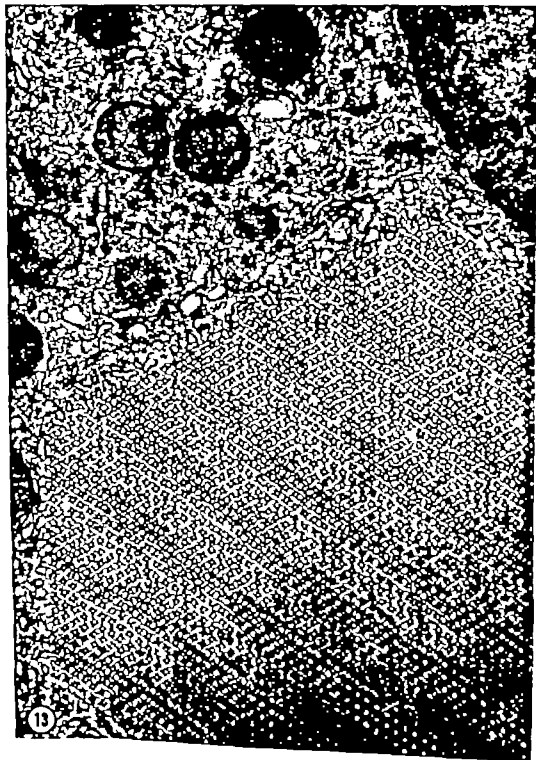

13

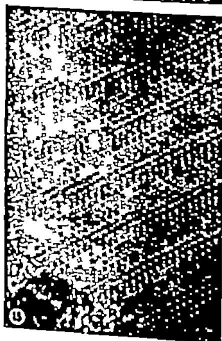
PLATE 7

EXPLANATION OF FIGURES

14 The orientation of this section through a crystalloid is such that one set of tubules lies almost parallel to the plane of section (A–B') As the section passes at an angle through the crystalloid, successive layers of this set are encountered (B A B) Similarly successive layers of A–B tubules appear for short distances. Long connectors appear in precise cross section and can be traced between their tubules of origin (long rows of arrows) In the tracing of connections, it is essential to distinguish between open continuity and contiguity of tubules. One pair of short connectors is shown by the set of arrows at the upper left (A–B) Light spaces at O indicate roughly rhombic lacunae in the crystalloid that is extratubular interstices. 95,000 ×

15 The two figures are a stereogram mounted at 62 mm interocular distance They may be viewed by the wide-eyed or more easily by the cross-eyed method although an adjustable stereoscope will yield much better relief The angle of section produces a shingled effect of successive partly overlapping tiers of the crystalloid a feature which appears at first viewing as a hill-and-dale effect. Long connectors, being viewed on end appear particularly clear in stereoscopy

PLATE 7



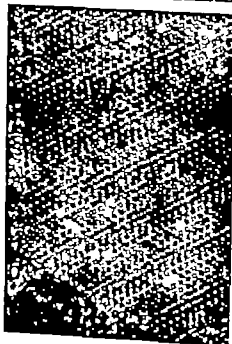


PLATE 7

EXPLANATION OF FIGURES

14 The orientation of this section through a crystalloid is such that one set of tubules lies almost parallel to the plane of section (A–B) As the section passes at an angle through the crystalloid, successive layers of this set are encountered (B' A B) Similarly successive layers of A–B tubules appear for short distances. Long connectors appear in precise cross section and can be traced between their tubules of origin (long rows of arrows) In the tracing of connections, it is essential to distinguish between open continuity and contiguity of tubules One pair of short connectors is shown by the set of arrows at the upper left (A–B) Light spaces at O indicate roughly rhombic lacunae in the crystalloid that is, extratubular interstices. 85,000 ×

15 The two figures are a stereogram mounted at 62 mm interocular distance They may be viewed by the wide-eyed or more easily by the cross-eyed method although an adjustable stereoscope will yield much better relief The angle of section produces a shingled effect of successive partly overlapping tiers of the crystalloid, a feature which appears at first viewing as a hill-and-dale effect. Long connectors, being viewed on end appear particularly clear in stereoscopy

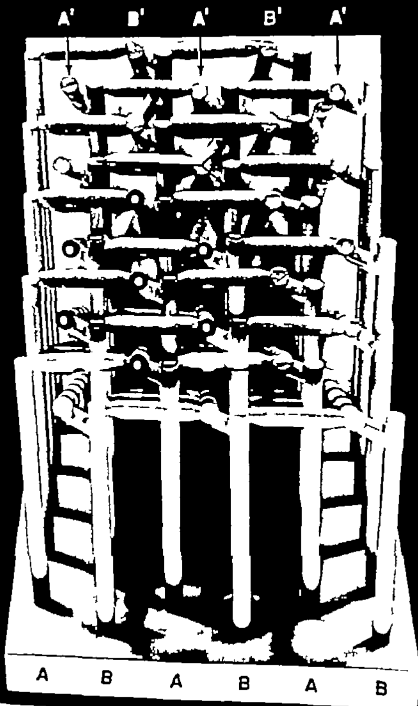

A'
B'
A'
B'
A'
16
A
B
A
B
A
B

PLATE 8

EXPLANATION OF FIGURE

16 Three-dimensional reconstruction of the crystalloid The model is expanded in contrast to the tight packing of the tubules *in vivo* The hexagonal array of the A–B and A–B tubules is shown by dashes and small circles, respectively The triradiate arrow indicates the disposition of long and short connectors about one tubule of origin (A); both lead into B tubules, just as connectors from A tubules are continuous only with B tubules. The long connectors form a double hexagonal pattern as seen from the side of the model.


A'
B'
A'
B'
A'
16
A
B
A
B
A
B

PLATE 9

EXPLANATION OF FIGURES

17 Electron micrograph of an interstitial cell from an estrus female reacted for thiobutyric esterase. The reaction product is found on the membranes of the agranular reticulum and is especially prominent on those of the crystalloid. Very little reaction product is seen on the parts of the agranular reticulum which are dilated into "inclusion bodies" (arrow). Mitochondria (M) and lipid (L) are unreactive. Glutaraldehyde 33 000 ×

18 Electron micrograph of an interstitial cell reacted for acid phosphatase The reaction product is limited to lysosomes (arrows) Nucleus, agranular reticulum and "inclusion bodies" are unreactive Glutaraldehyde 17,000 ×

19 Light micrograph of a 20 μ frozen section reacted for 17β-hydroxysteroid dehydrogenase Only the interstitial cells are reactive The granules in the sweat glands are brown pigment and are readily distinguished from the blue formazan deposits.

17





PLATE 10

EXPLANATION OF FIGURE

20 Luteal cell from the corpus luteum of *Lemur catta* containing mitochondria with lamelliform cristae and an abundant tubular agranular reticulum part of which occurs as whorls similar to the "precrystalloid" formations of the interstitial cells of the antebrachial organ No crystalloids have been seen in luteal cells Glutaraldehyde; permanganate stain. 28,000 ×


20

PLATE 11

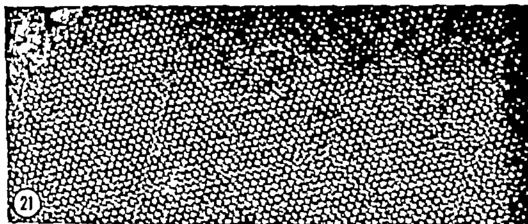
EXPLANATION OF FIGURES

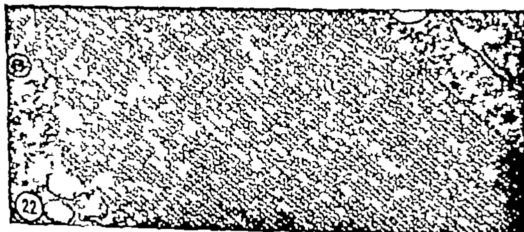
21 Reinke crystalloid from a Leydig cell of the human testis. The substructural pattern is much smaller than that seen in the crystalloid of the antebrachial organ. The crystalloid apparently is composed of a complex network of 50 Å filaments which constitute the boundaries of the roughly prismatic spaces Glutaraldehyde 110,000 ×

22 Reinke crystalloid from a human testicular interstitial cell sectioned at right angles to the plane of the crystalloid above The square pattern of the constituent filaments indicates that the hexagonally disposed spaces in figure 21 are not tubules but only interstices in an open latticework. Glutaraldehyde 63,000 ×

23 Rat plasma cell. The complex array of smooth tubules is in continuity with the endoplasmic reticulum. Glutaraldehyde 22,000 × (Micrograph courtesy of Dr John F Kent, Connecticut College)

24 Rat meibomian gland Crystalloidal configuration of the agranular reticulum 27 000 ×


21


22


23


24

PLATE 11

EXPLANATION OF FIGURES

21 Reinke crystalloid from a Leydig cell of the human testis. The substructural pattern is much smaller than that seen in the crystalloid of the antebrachial organ The crystalloid apparently is composed of a complex network of 50 Å filaments which constitute the boundaries of the roughly prismatic spaces Glutaraldehyde. 110,000 ×

22 Reinke crystalloid from a human testicular interstitial cell, sectioned at right angles to the plane of the crystalloid above The square pattern of the constituent filaments indicates that the hexagonally disposed spaces in figure 21 are not tubules but only interstices in an open latticework. Glutaraldehyde 63,000 ×

23 Rat plasma cell. The complex array of smooth tubules is in continuity with the endoplasmic reticulum. Glutaraldehyde 22,000 × (Micrograph courtesy of Dr John F Kent, Connecticut College)

24 Rat meibomian gland. Crystalloidal configuration of the agranular reticulum. 27,000 ×

Some Aspects of Spermiogenesis in a Lizard

ALLEN W. CLARK [1]

Department of Anatomy, University of Wisconsin, Madison, Wisconsin

ABSTRACT Spermatids of the American chameleon *Anolis carolinensis* have been examined with the electron microscope during the period from the first appearance of caudal sheath microtubules to the stage of differentiation just before the caudal sheath disappears. The caudal sheath microtubules are arranged initially in the form of a helix with a very low pitch. As the condensation of the chromatin and the elongation of the nucleus proceed, the caudal sheath helix unwinds. Shortly before the caudal sheath disappears, the sheath microtubules are oriented parallel to the longitudinal axis of the nucleus and the sheath resembles those found in other vertebrate spermatids. Assuming that the caudal sheath is functionally related in some way to the changes that occur in the nucleus, it is proposed that the unusual arrangement of the caudal sheath in *A. carolinensis* spermatids is a device to avoid a large excess of microtubules clustered around the nucleus at the end of nuclear elongation.

In the late nineteenth century several light microscopists, among them Kölliker (1899), Benson (1892) and Mèves (1899), observed a structure in the spermatids of a representative number of vertebrates which was referred to by Lenhossék (1898) as the *manchette*. Although there was some controversy over the formation and composition of this structure (see the review in the paper by Burgos and Fawcett, '55) it was generally agreed that the *manchette* or caudal sheath had the appearance of a cylinder which extended backward from the nucleus toward the tail. Mèves (1899) in describing spermiogenesis in the guinea pig, interpreted the wall of the cylinder to be composed of minute, parallel filaments each of which had an anterior insertion on the nuclear membrane and a posterior ending that was free in the cytoplasm. Mèves believed that these filaments arose in the cytoplasm and increased throughout spermiogenesis.

With the advent of the electron microscope, many of the speculations about the nature of the caudal sheath could be resolved. In 1955 Burgos and Fawcett described the fine structure of the spermatid of the cat, *Felis domestica*. According to their observations, the caudal sheath in the cat spermatid was composed of a large number of 250 Å microtubules which appeared to arise from both cusps of a C-shaped "nuclear ring" located at the caudal end of the acrosomal cap. The microtubules were long and straight, they were located near the outer nuclear envelope, and they were oriented parallel to the longitudinal axis of the spermatid. Burgos and Fawcett were unsure about the ultimate fate of the caudal sheath.

Shortly after this initial report, Rebhun ('57) observed a caudal sheath composed of microtubules in the spermatid of the pulmonate snail, *Otala lactea* and Roth ('58) made a similar observation on the spermatid of the snail, *Helix aspersa*. Sotelo and Trujillo-Cenóz ('58) found a caudal sheath composed of microtubules in the spermatid of the rat, *Mus norvegicus* much like that found in the cat spermatid. Gatenby and Dalton ('59) also reported a microtubular caudal sheath in the spermatid of the earthworm, *Lumbricus herculeus*.

In 1962, Nagano described the fine structure of the developing spermatid of the domestic chicken. The caudal sheath in this spermatid also was found to be composed of a large number of microtubules, the orientation and location of which corresponded closely with those found in the spermatid of the cat. However, the origin of the rooster caudal sheath appeared to be either several dense rings or else a spiral density close to the caudal end of the acrosomal cap. Nagano

[1] Present address: Department of Zoology, University of California, Berkeley 94720.

speculations about its significance will be discussed.

MATERIALS AND METHODS

Two species of lizards, the American chameleon, *Anolis carolinensis* and the horned toad, *Phrynosoma cornutum*, were used in this study. Several fixatives and buffer systems were tried and none were found to be satisfactory. The best approximation appeared to be 0.1M cocodylate buffered formaldehyde glutaraldehyde (Karnovsky '65). Testes were fixed at room temperature for 30 minutes and then rinsed for an equal time with five changes of buffer. The tissues were then post fixed with 1% OsO_4 for one hour. All the buffer solutions were adjusted to pH 7.6 and 10^{-3} M $CaCl_2$ was added to them. The tissues were dehydrated rapidly in a graded series of ethyl alcohols and embedded in Epon 812 (Luft, '61). Blocks were sectioned on a Porter-Blum ultramicrotome by means of glass knives. The sections were picked up on carbon reenforced parlodion coated grids, stained with lead citrate (Reynolds, '63) and examined with an RCA EMU 3E electron microscope.

OBSERVATIONS

Since the number and complexity of the structural changes during spermiogenesis in *Anolis carolinensis* are great and their significance is obscure, the description of the spermatid in this paper will be limited to the period beginning with the appearance in the cytoplasm of the microtubules which form the caudal sheath and ending with the stage of differentiation when the caudal sheath is about to disappear.

Caudal sheath microtubules are *first* seen in the intermediate spermatids of *A. carolinensis*. This intermediate stage is easily recognized in the electron microscope by the appearance of the acrosomal vesicle which is large and seems to be filled with a slightly flocculent, very electron-transparent material (fig. 1). At this stage, the posterior surface of the spherical acrosomal vesicle fits snugly into a cup-shaped indentation in the anterior surface of the spermatid nucleus. The acrosomal granule is well developed and is found at the deepest part of the indentation.

As differentiation proceeds, there occurs an almost total displacement of cytoplasm from the anterior pole of the spermatid so that the anterior surface of the acrosomal vesicle becomes directly apposed to the plasmalemma (fig. 5) which in turn is apposed to the plasmalemma of the Sertoli cell. The vesicle is flattened and its posterior surface appears to cover a greater area of the nucleus. The anterior pole of the nucleus, in turn, is flattened although there remains a central depression which appears to accommodate the acrosomal granule. As the nucleus becomes elongated, the central depression disappears and becomes the point of the bullet-shaped nucleus (fig. 6). The acrosomal vesicle becomes further spread out and acquires the shape of a cap over the anterior nuclear surface while spreading of the acrosomal granule is also evident.

As the cap grows down over the nucleus (fig. 8) its posterior margin is accompanied by a thin cylindrical projection of Sertoli cell cytoplasm. This projection of the Sertoli cell therefore fits into the spermatid like the tongue of a cylindrical tongue-and-groove joint. As shown in figures 8–12 and 16 the outer wall of the groove is formed by a cylindrical projection of spermatid cytoplasm. From this stage until late in spermiogenesis, no important changes can be discerned within the acrosome. The shape of the cap changes in concert with the change in shape of the anterior end of the nucleus, both becoming long and slender (figs. 11–16).

Between the membrane of the acrosomal vesicle and the outer nuclear membrane is a layer of granular material which may be seen clearly in figure 5 where it appears to be thin and without any structure. As differentiation progresses, the layer becomes thicker although in figure 8 it still lacks any structure. However, at the tip end of the nucleus of a late spermatid (fig. 11) the layer of material appears to have an altered granular substructure. In figure 16 the substructure has the appearance of bristles or rods about 100A thick and 500A long. Further away from the tip the substructure has the appearance of fibers also about 100A thick, which wind caudally around the nucleus in a helix of steep pitch. It is believed that the

observed late spermatids which lacked a caudal sheath and he suggested that the structure may be lost completely in the spermatazoon.

More recently microtubular caudal sheaths have been observed in the spermatid of the earthworm *Lumbricus terrestris* by Bradke ('63) and by Anderson et al ('66) in the spermatids of flatworms by Silvera and Porter ('64) in the spermatid of the cricket, *Gryllus domesticus* by Schin (65); in the spermatid of the mouse by Porter ('65) and in the spermatids of several Isopods by Fain Maurel ('66) In all of these instances the microtubules of the caudal sheath closely resemble those described in the cat by Burgos and Fawcett in that they are long and relatively straight, they are located close to the outer nuclear envelope and they are oriented parallel to the longitudinal axis of the spermatid

Microtubules arranged rather differently also have been reported in several papers on sperm cell fine structure Manton ('59) observed microtubules arranged in a U shaped sling about the nucleus of the spermatozoid of the bracken fern, *Pteridium aquilinum* According to Christensen ('61) a layer of microtubules lying just beneath the plasmalemma, spirals up the length of the spermatozoon of the flatworm *Plagiostomum* A similar arrangement of microtubules was reported to occur in the spermatozoon of the cestode *Hymenolopis diminuta*, by Lumsden ('65)

Several recent papers have described the fine structure of coccid spermatozoa These highly unusual spermatozoa appear to lack flagella, acrosomes mitochondria, centrioles and intracellular membranes Moses and Coleman ('64) and Robison ('66) have shown that concentric sheaths of microtubules surround a core of chromatin material. The microtubules run parallel to the longitudinal axis of the cell for some distance and in the species examined by Moses and Coleman, *Steatococcus tuberculatus* the microtubules appear to spiral around the chromatin core Moses ('66) recently investigated spermiogenesis in *S tuberculatus* and suggested that the sheaths of microtubules take the place of the nuclear envelope He reported that the two chromosomes in this spermatid migrate sequentially down the tube formed by the sheaths and in close association with them.

It is important to note that in the cited instances of spiral or helically wound microtubule sheaths in sperm cells this arrangement is a feature of the mature spermatozoon. An instance of a helical arrangement of microtubules in a spermatid has been reported by Tandler and Moriber ('66) to occur during spermiogenesis in the water-strider *Gerris remigis* The spermatid of this animal has a very large acrosomal vesicle which is filled with tubules. These acrosomic tubules are 130Å in diameter and they all become oriented parallel to the long axis of the acrosome as differentiation proceeds. Outside the acrosomal membrane, closely applied to it, and extending along the outer nuclear membrane to the vicinity of the basal corpuscle are 55–75 cytoplasmic microtubules which are 220Å in diameter and are usually oriented parallel to the long axis of the acrosome. Occasionally however these microtubules are arranged in a helix with a steep pitch Tandler and Moriber do not comment further on the arrangement or the fate of these cytoplasmic microtubules.

Among these reports on vertebrate and invertebrate spermiogenesis, there are none that are concerned with the fine structure of reptilian spermatids. Recently however Boisson and Mattei ('66) described spermiogenesis in the snake *Python sebae* The manchette or caudal sheath in the late spermatids of this snake appears much like the caudal sheaths of the vertebrates mentioned above. This arrangement is also true for the late spermatids of the American chameleon *Anolis carolinensis* discussed in the following paper The arrangement of the caudal sheath microtubules in the intermediate spermatids of these two species however appears to be quite different from those instances mentioned above although the interpretation of this difference given by Boisson and Mattei is not the same as the one given in this paper

The change in configuration of the caudal sheath microtubules in the spermatids of *A. carolinensis* will be described and

the flagellum emerges from the cell (figs. 3 6, 10 15) The basal corpuscle is composed of a proximal and a distal centriole. As shown in figures 3 6 10 and 15 the proximal centriole fits in a shallow invagination in the posterior surface of the nucleus and is separated from the outer nuclear membrane by a thin layer of granular material. Another mass of granular material has the shape of a flattened doughnut, in the center of which the distal centriole lies The double-headed arrow in figure 3 indicates a structure that appears to connect the ring of granular material to the distal centriole It is only at the stage shown in figure 15 that further differentiation of the centrioles is initiated. The nuclear surface and one end of the proximal centriole are progressively covered by a cap of dense material which ultimately extends posteriorly along one side of the distal centriole.

Transverse and longitudinal profiles of microtubules are often seen either in the substance of or around the periphery of the granular ring which surrounds the distal centriole (figs. 3, 6 10 15 18) The intermediate stage shown in figures 1 2 and 3 is the first point at which microtubules appear along the lateral nuclear envelope and begin the formation of the caudal sheath. The number of their cross-sections gradually increases until the stage shown by figure 8 is reached. Here the microtubule cross-sections are evenly distributed along the outer nuclear membrane, some very close to the membrane, others at the same level located as far away as 0.1μ or more. The microtubules intervene between the outer nuclear membrane and other membranous elements of the cytoplasm which at this stage contains many smooth vesicular profiles.

Although sections of spermatids like those in figures 7 and 8 might lead one to conclude that the caudal sheath is composed of microtubule hoops, it is evident from favorable sections of later stages that they are arranged in a helix. The pitch of this helix which initially is very low (fig. 8) gradually increases in steepness as nuclear elongation continues (figs. 11 17 19) Shortly before they disappear the caudal sheath microtubules are arranged exactly like those already described in the spermatids of other vertebrates. In figure 13 the microtubules are virtually parallel to the *longitudinal* axis of the spermatid nucleus.

The sheath appears to insert caudally in the ring of granular material which surrounds the distal centriole. This observation is most easily made on sections of late spermatids like that in figure 15 The anterior insertion of the sheath is not so obvious, at least in intermediate spermatids. Many sections of stages like that seen in figures 7 and 8 have been examined and no continuous insertion has been observed, although there may be an asymmetrical or discontinuous point of insertion which has escaped observation. In later spermatids however, a symmetrical structure associated with the sheath does develop at the caudal end of the acrosomal cap. The structure appears to be a ring of granular material and may correspond to the "nuclear ring" of other vertebrate spermatids. Although most of the caudal sheath microtubules insert at this ring, other microtubules extend on beyond the caudal end of the acrosomal cap. They lie very close to the plasmalemma and form the outer wall of the groove into which the tongue of Sertoli cell cytoplasm fits (figs. 12, 18) The way in which these latter microtubules terminate is unknown. Just before the microtubules disappear they begin to draw away from the outer nuclear membrane and become arranged in a circle (fig 23) The microtubules are connected to each other by means of short arms approximately 40Å thick. Throughout the period described in this paper the microtubules of the *A. carolinensis* caudal sheath have an outer diameter of approximately 240Å.

Although they have not been examined as extensively spermatids of the *P cornutum*, have also been studied with the electron microscope. There appear to be small differences in the details of fine structure between the spermatids of the two species however in exactly the same fashion as in *A. carolinensis* the caudal sheath in *P cornutum* begins as a helix with a very low pitch that gradually unwinds. The caudal sheath microtubules of both species are believed to disappear without a trace in the spermatozoon.

bristles and fibers represent different aspects of the same structure and that the substructure of the granular layer at this stage actually consists of a number of parallel fins or ribs about 100Å thick and 500Å high which wind down around the outer nuclear membrane for some distance.

The outer nuclear membrane appears to be modified where it is in contact with the acrosomal membrane While there is the suggestion of this modification in figure 1 it can be seen in figures 5 and 8 that the membrane is thicker and more osmiophilic At the stage shown in figure 5 the rest of the nuclear envelope appears to be unremarkable except in the region around the basal corpuscle where nuclear pores have become evident. The concentration of nuclear pores increases to a maximum at the stage shown in figures 8 9 and 10 when the pores are arranged around the indentation accommodating the proximal centriole As nuclear elongation and chromatin concentration reach a culmination the pores are no longer evident (fig 15) In figure 15 a profile of redundant nuclear envelope is seen to extend caudally from the right side of the nucleus.

The nucleoplasm of the intermediate spermatid shown in figure 1 is finely granular and evenly dispersed These characteristics change rapidly with the appearance of short, randomly oriented threads (fig 5) As differentiation proceeds the threads become thicker longer and more osmiophilic and are oriented parallel to the anterior posterior axis of the nucleus (fig 8) At the anterior end of the nucleus the threads of chromatin insert in to a thin layer of granular material covering the inner surface of that portion of the inner nuclear membrane which underlies the acrosome At the posterior end of the nucleus, the chromatin threads also insert into a layer of granular material however the way in which the layer is arranged differs from the anterior end of the nucleus. In the region of the nuclear pores the layer of granular material has been lifted away and a space has been left between it and the inner nuclear membrane (figs 8 9)

At this stage the appearance of the nucleus in transverse section is unexpected. In *A carolinensis* the threads of chromatin are actually an interconnected meshwork giving the nucleoplasm the appearance of a maze (figs. 20 22) This may imply the chromatin is organized in long parallel sheets which are interconnected. On the other hand the chromatin threads of a *P cornutatum* spermatid at a slightly later stage are thick, sharply defined, and arranged in an hexagonal array with slender fibrillar interconnections between threads (fig 21)

With continued differentiation the nucleus becomes long and slender as the chromatin mesh condenses. In figures 17 and 19 the mesh appears to have undergone a helical twisting as it condenses. Finally the chromatin becomes so dense that in figures 13 and 23 no internal structure can be resolved In figure 13 the nucleus is curved or scimitar-shaped This observation is corroborated by the similar appearance of late spermatids in the light microscope

The cytoplasm of the spermatid throughout the period of differentiation discussed here is characterized by many vesicular profiles although the number decreases near the end of spermiogenesis. Some of these profiles are studded with RNP granules but most are smooth-surfaced. Also there are many free ribosomes either single or in strands or rosettes and a prominent Golgi complex. In figure 1 the latter is close to the anterior surface of the acrosomal vesicle and to another body which may be part of the complex although it has a distinctive structure This body is composed of a number of membranous tubes, closely fitting and with a uniform outside diameter of 400Å It has the appearance of a very compact and freely anastomosing smooth endoplastic reticulum. Both this body and the Golgi complex migrate away from the acrosomal region and are seen in a more and more posterior location as differentiation proceeds (figs 11 22 23)

Structures which are well developed in the intermediate spermatid and undergo little further modification during the period under discussion are the "ring centriole" or annulus and the basal corpuscle. The first is a ring of very dense material closely applied to the plasmalemma where

speculate about the unusual initial arrangement of the sheath in the *A. carolinensis* spermatid. It is apparent from a comparison of figures 1 and 23 that, during nuclear elongation, the diameter of the nucleus is greatly and uniformly reduced. Measurements indicate the diameter of the fully condensed nucleus is one sixth to one seventh the diameter of the nucleus at the beginning of elongation. If the caudal sheath microtubules in the intermediate spermatid of *A. carolinensis* were arranged from the beginning of elongation as they are in the intermediate spermatids of the cat (Burgos and Fawcett, '55) the chicken (Nagano '62) and the mouse (Porter '65) that is if they were uniformly distributed around the periphery of the nucleus and were oriented like barrel staves, parallel to the longitudinal axis of the cell, then there would be a large (perhaps five-fold) excess of microtubules around the nucleus at the end of elongation.

This excess might be avoided in either of two ways. First, there might be a selective deletion of microtubules and a simultaneous addition to the ends of those remaining in the sheath. A second way would be to begin with a lesser number of caudal sheath microtubules close to their final length and wrap them around the intermediate nucleus in the form of a helix. The unwinding of the helix and the elongation of the nucleus then might be coordinated in such a way that the lateral surface of the nucleus is evenly covered by the sheath and the function of the sheath smoothly accomplished. I propose that the helical arrangement of the caudal sheath in *A. carolinensis* spermatids is a device to avoid a large excess of microtubules at the end of nuclear elongation as well as the effort required to delete and lengthen microtubules during elongation.

The foregoing proposal does not imply any specific function for microtubules. If microtubules are completely passive cytoskeletal elements the two ends of the caudal sheath helix in *A. carolinensis* spermatids may be pulled apart as the spermatid elongates, and lead to a reduction in the diameter of the helix and a constricting action of the caudal sheath upon the nucleus. The active role then might be given over to the nucleus which would use the caudal sheath like a corset. If, on the other hand, microtubules are contractile elements, a contraction of the caudal sheath microtubules would lead to an increase in the steepness of the helix pitch and a similar constriction of the nucleus. Of course, these two alternatives depend on both ends of the caudal sheath having firm attachments that are capable of rotating as the sheath unwinds.

A final conjecture about microtubule function in caudal sheaths arises from a similarity between their situation in spermatids and the close physical proximity between microtubules and the differentiating nematocyst in *Hydra* cnidoblasts, described by Slautterback ('63) It is interesting that in the former case microtubules have a close physical proximity to an intense concentration of chromatin, while in the latter they are physically close to a protein crystallization. In both cases the microtubules might be involved in the translocation of ions and the concomitant manipulation of local cytoplasmic gelation.

Definitive statements about microtubule function must await their isolation and biochemical analysis. Even then, care must be exercised in generalizing beyond the system from which they come.

ACKNOWLEDGMENTS

This work was supported by Public Health Service grant GM 723–04 of the National Institutes of Health. The author is greatly indebted to Dr David B. Slautterback whose advice and encouragement made this investigation possible and to Nora E. Barclay and Arthur D Loewy for their critical reading of the manuscript.

LITERATURE CITED

Anderson, W A., A. Weissman and R. A. Ellis 1966 A comparative study of microtubules in some vertebrate and invertebrate cells. Z. Zellforsch., 71 1–13.

Boisson, C., and X. Mattei 1966 La spermiogenèse de Python sebae Gmelin, observée au microscope électronique. Ann. Sci. Nat. Zool., 8 363–390.

Bradke, D. L. 1963 Special features of spermatogenesis in *Lumbricus terrestris*. Anat. Rec., 145 360.

Burgos, M. H., and D W Fawcett 1955 Studies on the fine structure of the mammalian testis. I. Differentiation of the spermatids in the cat

DISCUSSION

While it will never be the decisive method the comparison of small morphological variations among metamorphosing spermatids of different species may permit some conclusions to be drawn about the functional significance of the changes that occur Most of the structural changes in differentiating spermatids of *A carolinensis* are like those in the few vertebrate spermatids already examined with the electron microscope However, the change which takes place in the arrangement of the caudal sheath is unusual and may contribute to the elucidation of this cytoplasmic element.

A similar change may occur in the spermatids of the snake *Python sebae* examined by Boisson and Mattei (66) However these authors believe the microtubules seen near the nuclear membrane of the intermediate spermatid are short and perhaps derived from the nuclear membrane Furthermore they suggest that these tubules and precursors of the *manchette* which serves as a protective and nutritive perinuclear reticulum. While their proposal for the function of the caudal sheath may be correct, it is probable that the origin and configuration of the caudal sheath in the spermatids of *P sebae* is as described here for the spermatids of *A. carolinensis* Since an identical configurational change occurs in the caudal sheath of the horned toad *P corunatum* this change may be common among the spermatids of lizards and among reptiles in general.

It may be supposed that in *A. carolinensis* the ring of granular material surrounding the distal centriole is either a modified centriolar satellite or a satellite derivative which may participate in the formation of caudal sheath microtubules. Such an aggregation of granular high-density material has been suggested as the source of microtubules in the atypical spermatozoon of a rotifer (Koehler and Birky '66) According to Murray et al. ('65) a broad zone of amorphous material around the centrioles seems to be the source of mitotic spindle tubules in dividing rat thymic lymphocytes. Similarly a dense ground plasm around the centriole of the earthworm is interpreted as the source of mitotic spindle tubules by Anderson et al. (66)

Unlike the other vertebrate spermatids that have been described (Burgos and Fawcett 55 Nagano '62; Porter '65) no continuous, anteriorly located structure into which microtubules insert has been observed in the intermediate spermatids of *A. carolinensis* In latter spermatids, such a structure is found at the caudal end of the acrosomal cap and it resembles in location and shape the "nuclear ring described by Burgos and Fawcett in the cat spermatid. That an asymmetrical or discontinuous insertion point in the intermediate spermatid of *A carolinensis* escaped detection is a distinct possibility

Burgos and Fawcett ('55) and Nagano (62) did not speculate about the function of the caudal sheaths in the spermatids which they described. As already mentioned Boisson and Mattei ('66) suggested that the caudal sheath in the python spermatid serves as a protective and nutritive perinuclear reticulum. Porter ('65) on the other hand mentioned the remarkable straightness and rigid appearance of the caudal sheath microtubules in the mouse spermatid. Porter suggested further that the caudal sheath may serve a cytoskeletal function and act as a framework to guide the elongation of the nucleus. Anderson et al (66) have suggested the same function for the caudal sheath microtubules in the earthworm spermatid.

It should be recognized that these speculations and those to follow about the function of the caudal sheath are based on the assumption that this structure is involved with the elongations of the nucleus, an assumption that has no basis in experimental fact. The close physical proximity between the sheath and the nucleus while very suggestive may be purely coincidental and a consequence of stringent packing requirements in the spermatids Speculations about microtubule function based on the peculiarities of their arrangement in caudal sheaths are twice removed from experimental fact, or rather they form one segment of a circular argument that may not correspond to reality at any point.

If the assumption is made that the caudal sheath is functionally associated with the elongation of the nucleus we can then

speculate about the unusual initial arrangement of the sheath in the *A. carolinensis* spermatid. It is apparent from a comparison of figures 1 and 23 that, during nuclear elongation, the diameter of the nucleus is greatly and uniformly reduced. Measurements indicate the diameter of the fully condensed nucleus is one sixth to one seventh the diameter of the nucleus at the beginning of elongation. If the caudal sheath microtubules in the intermediate spermatid of *A. carolinensis* were arranged from the beginning of elongation as they are in the intermediate spermatids of the cat (Burgos and Fawcett, '55) the chicken (Nagano, '62) and the mouse (Porter '65) that is if they were uniformly distributed around the periphery of the nucleus and were oriented like barrel staves, parallel to the longitudinal axis of the cell, then there would be a large (perhaps five-fold) excess of microtubules around the nucleus at the end of elongation.

This excess might be avoided in either of two ways. First, there might be a selective deletion of microtubules and a simultaneous addition to the ends of those remaining in the sheath. A second way would be to begin with a lesser number of caudal sheath microtubules close to their final length and wrap them around the intermediate nucleus in the *form* of a helix. The unwinding of the helix and the elongation of the nucleus then *might be* coordinated in such a way that the lateral surface of the nucleus is evenly covered by the sheath and the function of the sheath smoothly accomplished. I propose that the helical arrangement of the caudal sheath in *A. carolinensis* spermatids is a device to avoid a large excess of microtubules at the end of nuclear elongation as well as the effort required to delete and lengthen microtubules during elongation.

The foregoing proposal does not imply any specific function for microtubules. If microtubules are completely passive cytoskeletal elements, the two ends of the caudal sheath helix in *A. carolinensis* spermatids may be pulled apart as the spermatid elongates, and lead to a reduction in the diameter of the helix and a constricting action of the caudal sheath upon the nucleus. The active role then might be given over to the nucleus which would use the caudal sheath like a corset. If on the other hand, microtubules are contractile elements a contraction of the caudal sheath microtubules would lead to an increase in the steepness of the helix pitch and a similar constriction of the nucleus. Of course, these two alternatives depend on both ends of the caudal sheath having firm attachments that are capable of rotating as the sheath unwinds.

A final conjecture about microtubule function in caudal sheaths arises from a similarity between their situation in spermatids and the close physical proximity between microtubules and the differentiating nematocyst in *Hydra* cnidoblasts, described by Slautterback ('63) It is interesting that in the former case microtubules have a close physical proximity to an intense concentration of chromatin, while in the latter they are physically close to a protein crystallization. In both cases the microtubules might be involved in the translocation of ions and the concomitant manipulation of local cytoplasmic gelation.

Definitive statements about microtubule function must await their isolation and biochemical analysis. Even then, care must be exercised in generalizing beyond the system from which they come.

ACKNOWLEDGMENTS

This work was supported by Public Health Service grant GM 723–04 of the National Institutes of Health. The author is greatly indebted to Dr. David B Slautterback whose advice and encouragement made this investigation possible and to Nora E. Barclay and Arthur D Loewy for their critical reading of the manuscript.

LITERATURE CITED

Anderson, W A., A. Weissman and R. A. Ellis 1966 A comparative study of microtubules in some vertebrate and invertebrate cells. Z. Zellforsch., 71 1–13.

Boisson, C., and X. Mattei 1966 La spermiogenèse de *Python sebae* Gmelin, observée au microscopie électronique. Ann. Sci. Nat. Zool., 8 363–390.

Bradke, D L. 1963 Special features of spermatogenesis in *Lumbricus terrestris*. Anat. Rec., 145 360.

Burgos, M. H., and D. W Fawcett 1955 Studies on the fine structure of the mammalian testis. I. Differentiation of the spermatids in the cat

DISCUSSION

While it will never be the decisive method the comparison of small morphological variations among metamorphosing spermatids of different species may permit some conclusions to be drawn about the *functional significance* of the changes that occur Most of the structural changes in differentiating spermatids of *A carolinensis* are like those in the few vertebrate spermatids already examined with the electron microscope However the change which takes place in the arrangement of the caudal sheath is unusual and may contribute to the elucidation of this cytoplasmic element

A similar change may occur in the spermatids of the snake *Python sebae* examined by Boisson and Mattei ('66) However these authors believe the microtubules seen near the nuclear membrane of the intermediate spermatid are short and perhaps derived from the nuclear membrane Furthermore, they suggest that these tubules and precursors of the *manchette* which serves as a protective and nutritive perinuclear reticulum. While their proposal for the function of the caudal sheath may be correct, it is probable that the origin and configuration of the caudal sheath in the spermatids of *P sebae* is as described here for the spermatids of *A carolinensis* Since an identical configurational change occurs in the caudal sheath of the horned toad *P cornutum*, this change may be common among the spermatids of lizards and among reptiles in general.

It may be supposed that in *A carolinensis* the ring of granular material surrounding the distal centriole is either a modified centriolar satellite or a satellite derivative which may participate in the formation of caudal sheath microtubules Such an aggregation of granular high-density material has been suggested as the source of microtubules in the atypical spermatozoon of a rotifer (Koehler and Birky '66) According to Murray et al. ('65) a broad zone of amorphous material around the centrioles seems to be the source of mitotic spindle tubules in dividing rat thymic lymphocytes. Similarly a dense ground plasm around the centriole of the earthworm is interpreted as the source of mitotic spindle tubules by Anderson et al. ('66)

Unlike the other vertebrate spermatids that have been described (Burgos and Fawcett, 55; Nagano '62 Porter '65) no continuous, anteriorly located structure into which microtubules insert has been observed in the intermediate spermatids of *A. carolinensis* In latter spermatids, such a structure is found at the caudal end of the acrosomal cap and it resembles, in location and shape the "nuclear ring" described by Burgos and Fawcett in the cat spermatid. That an asymmetrical or discontinuous insertion point in the intermediate spermatid of *A carolinensis* escaped detection is a distinct possibility

Burgos and Fawcett ('55) and Nagano ('62) did not speculate about the function of the caudal sheaths in the spermatids which they described. As already mentioned Boisson and Mattei ('66) suggested that the caudal sheath in the python spermatid serves as a protective and nutritive perinuclear reticulum Porter ('65) on the other hand mentioned the remarkable straightness and rigid appearance of the caudal sheath microtubules in the mouse spermatid. Porter suggested further that the caudal sheath may serve a cytoskeletal function and act as a framework to guide the elongation of the nucleus Anderson et al ('66) have suggested the same function for the caudal sheath microtubules in the earthworm spermatid

It should be recognized that these speculations and those to follow about the function of the caudal sheath are based on the assumption that this structure is involved with the elongations of the nucleus an assumption that has no basis in experimental fact The close physical proximity between the sheath and the nucleus while very suggestive may be purely coincidental and a consequence of stringent packing requirements in the spermatids Speculations about microtubule function based on the peculiarities of their arrangement in caudal sheaths are twice removed from experimental fact, or rather they form one segment of a circular argument that may not correspond to reality at any point.

If the assumption is made that the caudal sheath is functionally associated with the elongation of the nucleus we can then

GC
MB
AcVe
AcGr
Nu
1

Nu

(*Felis domesticus*) J Biophys. Biochem. Cytol., 1: 287–300.
Christensen, A. K. 1961 Fine structure in an unusual spermatozoan in the flatworm *Plagiostomum*. Biol. Bull. *121:* 416.
Fain-Maurel M. 1966 Contribution à l'histologie et à la caryologie de quelques Isopods. Spermiogenèse et infrastructure du spermatozoïde des *Oniscidés* et des *Cymothoïdés* Ann. Sci. Nat. Zool., *8:* 1–188.
Gantenby J B., and A. J Dalton 1959 Spermiogenesis in *Lumbricus herculeus*. An electron microscope study J Biophysic. Biochem. Cytol., *6:* 45–52.
Karnovsky M. J 1965 A formaldehyde-glutaraldehyde fixative of high osmolality for use in electron microscopy J Cell Biol. *27:* 137A–138A.
Koehler J K., and C W Birky 1966 An electron microscope study of the dimorphic spermatozoa of *Asplanchna* (Rotifera) Z. Zellforsch., *70* 303–321
Kölliker R. A. 1899 Handbuch der Gewebel ehre des Menschen. Wilhelm Engelmann, Leipzig pp 417–455
Lenhossek, M. v 1898 Untersuchungen über Spermatogenese. Arch. mikr Anat., *51* 215–316.
Luft, J H 1961 Improvements in epoxy resin embedding methods. J Biophys. Biochem. Cytol., *9: 409–414*
Lumsden R. D 1965 Microtubules in the peripheral cytoplasm of cestode spermatozoa. J Paras., 51: 929–931
Manton L 1959 Observations on the microanatomy of the spermatozoid of the bracken fern (*Pteridium aquilinum*) J Biophys. Biochem. Cytol., *6* 413–418.
Mèves, F 1899 Ueber Struktur und Histogenese der *Samenfäden des Meerschweinchens.* Arch Mikr Anat., *54:* 329–402.
Moses, M J 1966 Microtubules in the aflagellate sperm of a coccid (*Steatococcus tuberculatus*) Anat. Rec., *154:* 391
Moses, M. J., and J R. Coleman 1964 Structural patterns and the functional organizations of chromosomes, In: The Role of Chromosomes in Development. M. Locke, ed. Academic Press New York, pp. 11–49
Murray R. G., A. S. Murray and A. Pizzo 1965 The fine structure of mitosis in rat thymic lymphocytes. J *Cell Biol., 26 601–619*
Nagano T 1962 Observations on the fine structure of the developing spermatid in the domestic chicken. J Cell Biol. *14:* 193–205.
Porter K. R. 1965 Illustrations of cell fine structure In: Ideas in Modern Biology J A. Moore, ed. The Natural History Press, Garden City New York, pp. 95–124
Rebhun L. I. 1957 Nuclear changes during spermiogenesis in a pulmonate snail. J Biophys. Biochem. Cytol., *3:* 509–524.
Renson, G 1882 De la spermatogenèse chez les mammifères. Arch. biol., *3:* 291–332.
Reynolds, E. S. 1963 The use of lead citrate at high pH as an electron-opaque stain in electron microscopy J Cell *Biol. 17:* 208–212.
Robison W G 1966 Microtubules in relation to the motility of a sperm syncytium in an armored scale insect. J Cell Biol., 29 251–265.
Roth, L. E. 1958 A filamentous component of protozoan fibrillar systems. J Ultrastruct. Res., *1:* 223–234.
Schin, K. S 1965 Meiotische Prophase und Spermatidenreifung bei *Gryllus domesticus* mit besonderer Berücksichtigung der Chromosomenstruktur Z. Zellforch., *65:* 481–513.
Silvera M., and K. R. Porter 1964 The spermatozoids of flatworms and their microtubular systems. Protoplasma, *59:* 240–265.
Slautterback D. B 1963 Cytoplasmic microtubules. I. Hydra. J Cell Biol., *18:* 367–388.
Sotelo J R., and O Trujillo-Cenóz 1958 Electron microscope study of the kinetic apparatus in animal sperm cells. Z. Zellforsch., *48:* 565–601
Tandler B., and L. G. Moriber Microtubular structures associated with the acrosome during spermiogenesis in the water-strider *Gerris remigis* (Say) J Ultrastruct. Res., *14:* 391–404

PLATE 1

EXPLANATION OF FIGURES

1 An electron *micrograph showing a portion of an intermediate spermatid of Anolis carolinensis. A large acrosomal vesicle (AcVe) appears* to be filled with a slightly flocculent, electron transparent material. The acrosomal granule (AcGr) is found at the deepest part of the nuclear depression that accommodates the vesicle. The nucleoplasm at this stage is finely granular and evenly distributed. A prominent Golgi complex (GC) is found close to the acrosomal vesicle and a membranous body (MB) Nu, nucleus. × 21,000

2 A more highly magnified portion of the electron micrograph in figure 1 The membranous body is seen to be composed of a number of closely fitting membranous tubes with a uniform outside diameter of 400Å. Transverse sections of microtubules (arrows) are the forerunners of the caudal sheath. Nu, nucleus. × 50,000.

PLATE 2

EXPLANATION OF FIGURES

3 An electron micrograph showing the caudal region of an intermediate *A. carolinensis* spermatid at the same stage of differentiation as that shown in figure 1. A ring of very dense material, the annulus (AN) is applied to the plasmalemma at the place where the flagellum emerges from the cell. The proximal centriole (PCe) is found in a shallow depression in the posterior surface of the nucleus. Surrounding the distal centriole (DCe) is a ring of granular material (Gr). The double arrow indicates a structure which connects the granular ring and the distal centriole. Single arrows indicate microtubules associated with the granular ring. × 44 000

4 An enlargement of the electron micrograph in figure 5. The nucleoplasm in this more differentiated spermatid has taken the form of short, randomly oriented threads. The nuclear envelope adjacent to the flattened acrosomal vesicle is thick and osmiophilic. A layer of granular material (L) lies between the nuclear envelope and the acrosomal vesicle. The latter still is characterized by a central depression which accommodates the acrosomal granule (AcGr). Arrows indicate profiles of microtubules close to the outer nuclear membrane. × 41,000.

P.Ce
Gr
D.Cp
An

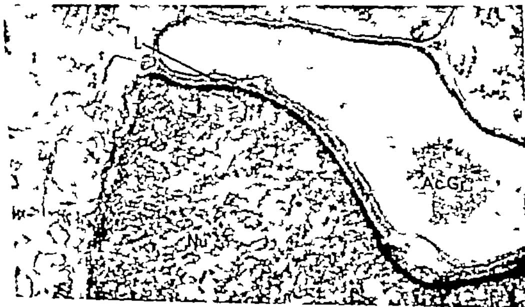


PLATE 2

EXPLANATION OF FIGURES

3 An electron micrograph showing the caudal region of an intermediate *A. carolinensis* spermatid at the same stage of differentiation as that shown in figure 1 A ring of very dense material, the annulus (AN) is applied to the plasmalemma at the place where the flagellum emerges from the cell. The proximal centriole (PCe) is found in a shallow depression in the posterior surface of the nucleus. Surrounding the distal centriole (DCe) is a ring of granular material (Gr) The double arrow indicates a structure which connects the granular ring and the distal centriole Single arrows indicate microtubules associated with the granular ring. × 44,000

4 An enlargement of the electron micrograph in figure 5 The nucleoplasm in this more differentiated spermatid has taken the form of short, randomly oriented threads The nuclear envelope adjacent to the flattened acrosomal vesicle is thick and osmiophilic. A layer of granular material (L) lies between the nuclear envelope and the acrosomal vesicle The latter still is characterized by a central depression which accommodates the acrosomal granule (AcGr) Arrows indicate profiles of microtubules close to the outer nuclear membrane × 41 000


SC
Ac Ve
Nu

PLATE 3

EXPLANATION OF FIGURE

5 An electron micrograph of an intermediate *A. carolinensis* spermatid at the stage where the cytoplasm has migrated away from the acrosomal region of the cell. The acrosomal vesicle (AcVe) has flattened in concert with the anterior surface of the nucleus (Nu). Arrows mark microtubule profiles in the developing caudal sheath. × 15 000

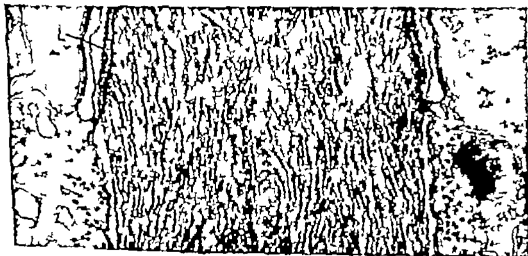


PLATE 4

EXPLANATION OF FIGURES

6 An enlargement of the electron micrograph in figure 5. Most of the structures pointed out in figure 3 have remained unchanged. The arrow indicates a transverse section of a microtubule in the substance of the granular ring. The cytoplasm is characterized by many membranous profiles most of which are smooth surfaced. NP nuclear pore. × 34,000

7 An enlargement of the electron micrograph in figure 8. Careful examination of this section and many others at this stage of differentiation reveals no continuous structure into which the caudal sheath microtubules (arrows) insert. The chromatin at this stage is in the form of long threads or perhaps long interconnecting sheets (see figure 20 for a cross-section of the nucleus at this stage) and is inserted into a thin layer of granular material covering the inner surface of the inner nuclear membrane. The layer of granular material (L) is closely applied to the outer nuclear membrane. × 43,000

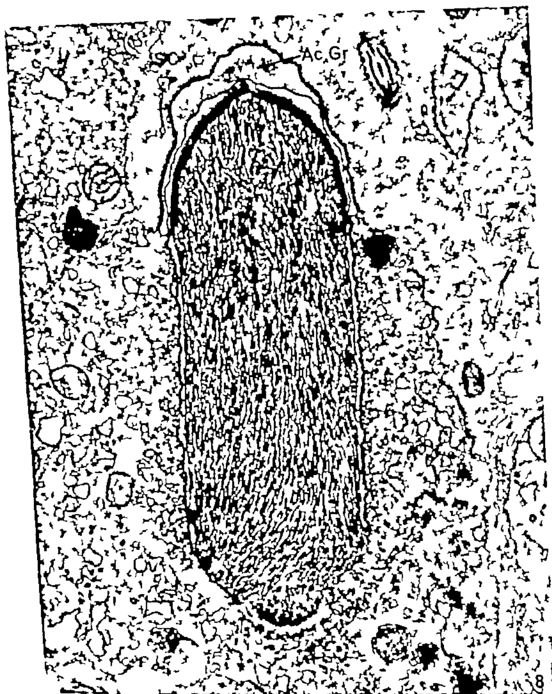

Ac.Gr
8

PLATE 5

EXPLANATION OF FIGURE

8 An electron micrograph of an *A. carolinensis* spermatid in which the nucleus has begun to undergo marked elongation. The acrosome has been flattened into a cap over the bullet-shaped anterior surface of the nucleus (Nu) while spreading of the acrosomal granule (AcGr) is evident. The cytoplasm is characterized by large numbers of *smooth membrane profiles*. SC, Sertoli cell. × 23,000.



NP
Ce
OG
An
10

PLATE 6

EXPLANATION OF FIGURES

9 An enlargement of the electron micrograph in figure 8 showing the posterior end of the spermatid nucleus The section is just outside the invagination in the nucleus which accommodates the proximal centriole, but instead passes through the band of nuclear pores (NP) in the nuclear envelope that surrounds the centriolar invagination. It is apparent that the chromatin threads do not insert on the portion of the nuclear envelope containing the pores. Arrows indicate caudal sheath microtubules. × 43,000

10 An electron micrograph of an intermediate *A carolinensis* spermatid at approximately the same stage of differentiation as that shown in figure 8 The complex of structures around the basal corpuscle are much as before with the exception of an increase in the number of pores (NP) in the nuclear membrane immediately adjacent to the invagination accommodating the proximal centriole (PCe) An annulus; D Ce, distal centriole × 50 000

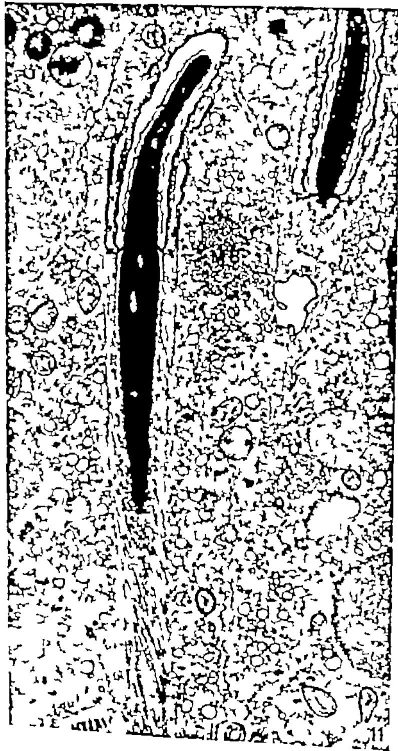

11

PLATE 7

EXPLANATION OF FIGURE

11 An electron micrograph of an *A. carolinensis* spermatid at a stage of differentiation where the caudal sheath helix has begun to unwind. In this oblique section the increased pitch of the helix is apparent. The membranous body (MB) referred to in the text is seen at the same level as the caudal end of the acrosomal cap. × 16,000

LIZARD SPERMIOGENESIS
Allen W. Clark

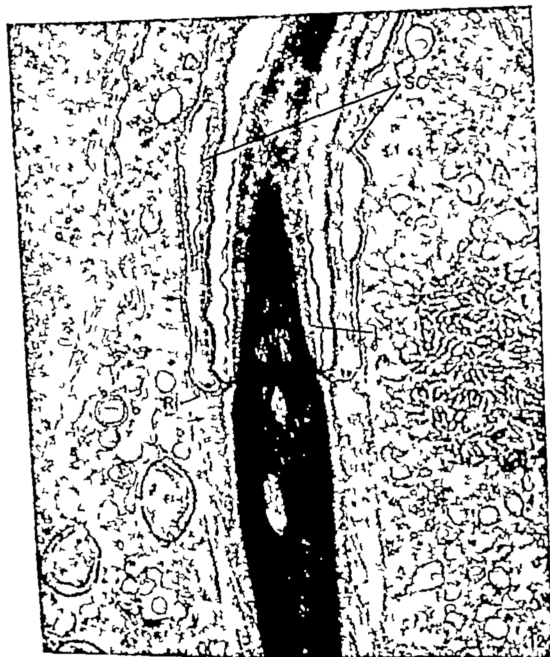


PLATE 8

EXPLANATION OF FIGURE

12 An enlargement of the electron micrograph in figure 11 At this stage of differentiation a continuous nuclear ring" (Ri) is apparent at the caudal end of the acrosomal cap Many of the caudal sheath microtubules insert into this ring (single arrows) however a few microtubules continue on beyond the caudal end of the acrosomal cap (double arrows) These microtubules lie very close to the plasmalemma forming the outer wall of the groove into which the tongue of Sertoli cell cytoplasm (SC) fits L layer of granular material. × 43,000


13

PLATE 9

EXPLANATION OF FIGURE

13 An electron micrograph of a late *A. carolinensis* spermatid at a stage of differentiation where the caudal sheath helix has almost completely unwound. The condensation of the chromatin has been completed. In its migration away from the acrosome the Golgi complex (GC) has reached the level of the basal corpuscle. × 23 000


18

PLATE 8

EXPLANATION OF FIGURE

13 An electron micrograph of a late *A. carolinensis* spermatid at a stage of differentiation where the caudal sheath helix has almost completely unwound. The condensation of the chromatin has been completed. In its migration away from the acrosome, the Golgi complex (GC) has reached the level of the basal corpuscle. × 23,000.

PLATE 10

EXPLANATION OF FIGURES

14 An electron micrograph of a late *A. carolinensis* spermatid showing an oblique longitudinal section through the caudal end of the acrosomal cap. The section reveals a portion of the caudal sheath helix, which by this stage is almost completely unwound. Almost all the microtubules in this plane of section insert into the "nuclear ring." × 39,000

15 An enlargement of the electron micrograph in figure 13 showing the region around the basal corpuscle. The ring of granular material (Gr) surrounding the distal centriole is seen to be the posterior place of insertion for the sheath microtubules (arrows). A profile of redundant nuclear envelope (RE) is seen to extend posteriorly from the right side of the nucleus. At this stage the basal corpuscle has been modified. The nuclear surface and one end of the proximal centriole are covered by a cap of dense material which also extends posteriorly along one side of the distal centriole. × 39 000


SC
SC
16




18



PLATE 11

EXPLANATION OF FIGURES

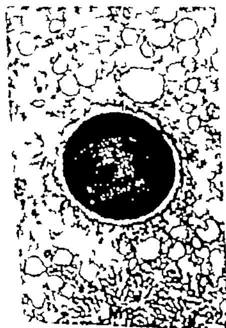
16 An electron micrograph showing the anterior cranial tip of an *A. carolinensis* spermatid nucleus at a stage comparable to that shown in figure 11. The double arrows indicate two areas where one may observe the substructure of the granular layer that is closely applied to the outer nuclear membrane. The granular layer appears to be organized into fins or ribs 100 Å thick and 500 Å high which wind caudally for some distance around the nucleus in a helix of steep pitch. Single arrows indicate microtubules which extend beyond the caudal end of the acrosomal cap and lie very close to the plasmalemma forming the outer wall of the groove into which the tongue of Sertoli cell cytoplasm (SC) fits. × 39,000

17 19 Electron micrographs of *Anolis* spermatids at a stage comparable to that shown in figure 11. These oblique sections clearly show the helical arrangement of the caudal sheath as well as the apparent twisting of the chromatin mesh. × 38,000

18 An electron micrograph of an *Anolis* spermatid at a stage comparable to that shown in figure 11. This longitudinal section of the posterior end of the nucleus is just outside the invagination that accommodates the proximal centriole. A large segment of the ring of granular material (Gr) surrounding the distal centriole may be seen. This ring is intimately associated with microtubules of the caudal sheath (arrows). × 38 000

20

21



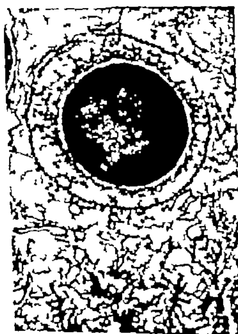


PLATE 12

EXPLANATION OF FIGURES

20 A transverse section through an intermediate *Anolis* spermatid comparable to the stage of differentiation shown in figure 8 The chromatin is arranged in the form of a loose meshwork. Around the outer nuclear membrane profiles of caudal sheath microtubules (arrows) are visible × 38,000

21 An electron micrograph of a transverse section through an intermediate spermatid of the horned toad, *Phrynosoma cornutum*. The stage of differentiation is somewhat later than that shown in figure 19 The chromatin is in the form of threads arranged in hexagonal lattice with slender fibrillar interconnections. Segments of caudal sheath microutbules (arrows) are visible around the periphery of the nucleus. × 38,000

22 An electron micrograph of a transverse section through a late *A carolinensis* spermatid comparable to the stage of differentiation shown in figure 11 The chromatin mesh has condensed although substructure is still visible. Caudal sheath microtubules are visible around the periphery of the nucleus. Some of these tubules are in perfect transverse section (double arrows) while others are cut more obliquely (single arrows) indicating the caudal sheath helix has a steep pitch at this stage of differentiation. MB membranous body × 38,000.

23 An electron micrograph of a transverse section through an *A carolinensis* spermatid just before the caudal sheath disappears At this stage the chromatin has become uniformly condensed. The caudal sheath microtubules around the periphery of the nucleus are almost all in transverse section (arrows) MB membranous body × 38,000

The Structure and Relationships of Horizontal Cells and Photoreceptor-bipolar Synaptic Complexes in Goldfish Retina [1]

WILLIAM K. STELL

Department of Anatomy and Section of Ophthalmology, Department of Surgery, The University of Chicago School of Medicine, Chicago, Illinois

ABSTRACT   After impregnation of goldfish retina by the rapid Golgi method, two classes each of photoreceptor bipolar and horizontal cells were observed by light microscopy. Interconnections between these elements in the outer plexiform (first synaptic) layer were investigated by electron microscopy of ultrathin sections, in which the processes of impregnated cells are easily distinguished. Dendrites of large bipolar cells (Cajal's "bipolaires destinés aux bâtonnets") appeared to contact the synaptic endings of both rods and cones, while those of small bipolars (Cajal's "bipolaires destinées aux cônes") appeared to contact only cones. Processes from horizontal cells of the vitread level (Cajal's "cellules horizontaux intermédiaires") appeared to contact only rods, while those from horizontal cells of the sclerad level (Cajal's "cellules horizontaux externes") appeared to contact only cones. The structures formerly called "synaptic vacuoles" are the terminals of horizontal cell processes in the goldfish, and by analogy they should be so identified in all vertebrates. Teleostean horizontal cells are not typical of neurons or glia cells, but are morphologically intermediate between them. Their most interesting properties are their unique relationship to photoreceptor synaptic endings and their segregation into rod and cone subsystems along with the corresponding photoreceptor and bipolar cells. Although their specific function is not clear, some role in information processing therefore appears likely.

The outer plexiform layer of the vertebrate retina contains the first synapses of the visual system. Light-microscopic investigations showed that photoreceptor and bipolar cells are coupled there, and suggested that processes of transverse elements, the horizontal cells, also are present (Ramón y Cajal, 1893; Polyak, '41). Until very recently electron microscopists have concentrated on the receptor-bipolar component of this complex region (Cohen, '63) and the classic reconstruction of guinea pig synaptic complexes from serial sections by Sjöstrand ('58) demonstrated only receptor-receptor and receptor-bipolar contacts. Several electron-microscopic studies of this region in teleostean retinas (Sjöstrand, '59, '60; Villegas, '60, '61; Takayama, '61; Engström, '63) have left open the question of cell interconnections in this layer.

Certain slow intraretinal responses recorded with microelectrodes have attracted considerable attention since their discovery in the teleostean retina by Svaetichin ('53). These responses, thought at first to be action potentials of individual cone cells, were shown later to arise from deeper layers (Svaetichin and MacNichol, '58) and are now designated "S-potentials." Since they do not resemble neuronal responses they have been thought by some investigators to arise in accessory or non-neuronal elements (Svaetichin, Negishi, and Fatehchand, '65), although certain properties are so curious that one may question whether the S-potentials are recorded intracellularly or extracellularly (Tomita, '65). Concurrent investigations of teleostean horizontal cells by light and electron microscopy demonstrated none of the characteristics of typical neurons

[1] Submitted in partial fulfillment of requirements for the degree of Doctor of Philosophy in Anatomy at the University of Chicago.

[2] Medical Scientist Fellow of the Life Insurance Medical Research Fund. This work was also supported in part by United States Public Health Service Training grants in Anatomy 5T1-GM-94 and 5T1-GM-136, and Ophthalmic Sciences Training grant B079 from the National Institute of Neurological Diseases and Blindness, National Institutes of Health, United States Public Health Service.

The author's current address is Laboratory of Neurophysiology, National Institute of Neurological Diseases and Blindness, National Institutes of Health, Bethesda, Maryland 20014.

Am. J. Anat., 121: 401–424.

The Structure and Relationships of Horizontal Cells and Photoreceptor-bipolar Synaptic Complexes in Goldfish Retina[1]

WILLIAM K. STELL

Department of Anatomy and Section of Ophthalmology, Department of Surgery, The University of Chicago School of Medicine, Chicago, Illinois[2]

ABSTRACT After impregnation of goldfish retina by the rapid Golgi method, two classes each of photoreceptor, bipolar, and horizontal cells were observed by light microscopy. Interconnections between these elements in the outer plexiform (first synaptic) layer were investigated by electron microscopy of ultrathin sections, in which the processes of impregnated cells are easily distinguished. Dendrites of large bipolar cells (Cajal's "bipolaires destinés aux bâtonnets") appeared to contact the synaptic endings of both rods and cones, while those of small bipolars (Cajal's "bipolaires destinées aux cônes") appeared to contact only cones. Processes from horizontal cells of the vitread level (Cajal's "cellules horizontaux intermédiaires") appeared to contact only rods, while those from horizontal cells of the sclerad level (Cajal's "cellules horizontaux externes") appeared to contact only cones. The structures formerly called "synaptic vacuoles" are the terminals of horizontal cell processes in the goldfish, and by analogy they should be so identified in all vertebrates. Teleostean horizontal cells are not typical of neurons or glia cells, but are morphologically intermediate between them. Their most interesting properties are their unique relationship to photoreceptor synaptic endings and their segregation into rod and cone subsystems along with the corresponding photoreceptor and bipolar cells. Although their specific function is not clear, some role in information processing therefore appears likely.

The outer plexiform layer of the vertebrate retina contains the first synapses of the visual system. Light microscopic investigations showed that photoreceptor and bipolar cells are coupled there and suggested that processes of transverse elements, the horizontal cells, also are present (Ramón y Cajal, 1893; Polyak, '41). Until very recently electron microscopists have concentrated on the receptor-bipolar component of this complex region (Cohen, '63) and the classic reconstruction of guinea pig synaptic complexes from serial sections by Sjöstrand ('58) demonstrated only receptor-receptor and receptor-bipolar contacts. Several electron-microscopic studies of this region in teleostean retinas (Sjöstrand, '59, '60; Villegas, '60, '61; Takayama, '61; Engström, '63) have left open the question of cell interconnections in this layer.

Certain slow intraretinal responses recorded with microelectrodes have attracted considerable attention since their discovery in the teleostean retina by Svaetichin ('53). These responses, thought at first to be action potentials of individual cone cells, were shown later to arise from deeper layers (Svaetichin and MacNichol, '58) and are now designated "S-potentials." Since they do not resemble neuronal responses, they have been thought by some investigators to arise in accessory or non-neuronal elements (Svaetichin, Negishi, and Fatehchand, '65), although certain properties are so curious that one may question whether the S-potentials are recorded intracellularly or extracellularly (Tomita, '65). Concurrent investigations of teleostean horizontal cells by light and electron microscopy demonstrated none of the characteristics of typical neurons

[1] Submitted in partial fulfillment of requirements for the degree of Doctor of Philosophy in Anatomy at the University of Chicago.

[2] Medical Scientist Fellow of the Life Insurance Medical Research Fund. This work was also supported in part by United States Public Health Service Training grants in Anatomy 5T1-GM-84 and 5T1-GM-136, and Ophthalmic Sciences Training grant 5079 from the National Institute of Neurological Diseases and Blindness, National Institutes of Health, United States Public Health Service.

The author's current address is Laboratory of Neurophysiology, National Institute of Neurological Diseases and Blindness, National Institutes of Health, Bethesda, Maryland 20014.

(Selvín de Testa, '66 Villegas 60 '61 Villegas and Villegas 63) and the site of recording of S-potentials of the "luminosity type" was localized to horizontal cell layers by dye-marking techniques (Svaetichin and MacNichol '58 Mitarai et al. 61) Some investigators therefore have considered the teleostean horizontal cells to be glial elements whose complementary interactions with neurons give rise to S-potentials (Svaetichin Negishi and Fatehchand '65)

The present studies were undertaken in 1964 to investigate the nature of teleostean horizontal cells their probable contacts in the first synaptic layer and their role in retinal function An application of the rapid Golgi method was developed which allows direct correlation of the architecture and ultrastructure of retinal cells without serial sectioning (Stell '64 65a) Our studies on the goldfish retina are presented here in greater detail and implications of the structure and relationships of horizontal cells and photoreceptor bipolar synaptic complexes are discussed.

MATERIALS AND METHODS

The retinas of over thirty common goldfish (*Carassius auratus*) were studied Three- to 4-inch-long fish obtained from the Auburndale Goldfish Company (Chicago) were kept in the laboratory in recirculating filtered aerated tap water at 18 –23°C Most of the retinas were taken at midday from animals kept in daylight and were considered fully light adapted. The eyes were enucleated the anterior half removed and the posterior half immersed in fixative After 15–60 minutes the sclera or sclera plus choroid was dissected away the retina was cut into pieces several millimeters on a side and fixation was resumed in fresh fluid No attempt was made to study specific retinal regions.

Primary fixation for conventional ultrastructural study was accomplished by 60–90 minutes in ice-cold 3 3% osmium tetroxide buffered to pH 7 4 with 0 1 M $K_2Cr_2O_7$-NaOH (Dalton '55) or 0 1 M $NaHCO_3$-HCl (Wood and Luft, '65) Veronal acetate (Palade, '52) veronal acetate with calcium (Palay et al. '62) s-collidine (Bennett and Luft '59) and 0 1 M sodium phosphate with or without added sucrose were also employed as buffers but none gave as consistent or uniform preservation as dichromate and bicarbonate The specimens were washed briefly in cold buffer dehydrated rapidly in ethanol series passed through propylene oxide and embedded in Shell Epon-812 epoxy resin (Luft, '61) Sections were cut on a Sorvall MT 1 or MT 2 ultramicrotome with glass or DuPont diamond knives, picked up on carbon-cast, formvar-coated copper grids and stained with basic lead (Millonig 61) or ethanolic uranyl acetate (Gibbons and Grimstone '60) They were examined in an RCA EMU-2A electron microscope with Canalco stigmator and external power supply or in an RCA EMU 3D electron microscope DuPont Kronar film and Kodak medium contrast plates were used Adjacent 1-μ sections were stained with alkaline azure II methylene blue (Richardson Jarett, and Finke 60) or a modified Bielschowsky ammoniacal silver reagent (Stell '66)

The rapid Golgi method was employed for correlative study by light and electron microscopy as described previously (Stell, 65a) and summarized in text figure 1 Retinas were prepared by the triple-impregnation procedure modified slightly after Ramón y Cajal (1893) dehydrated embedded in Epon and sectioned at 80 μ before the completion of polymerization. Sections were examined in the light microscope and selected regions containing well impregnated cells were remounted for further sectioning Ultrathin sections and 1-μ sections were prepared as described above and the progress of sectioning was followed by examining the transilluminated block. This procedure will be referred to hereafter as the "Golgi-EM" method

OBSERVATIONS

Light microscopy

In preparations stained with Richardson s method the retina of the goldfish appears very similar to that of the carp as described by Heinrich Müller (1857) It is duplex in that it has cones with large pyramidal "pedicles" and rods with small, round to ovoidal "spherules" for

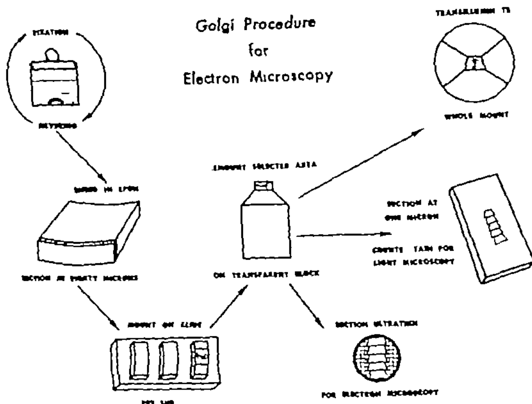


Fig. 1 Diagram illustrating method for direct correlation of retinal cytoarchitecture and ultrastructure in rapid Golgi preparations. See text for further explanation.

synaptic terminals. The vitread faces of the cone pedicles lie in a single plane against the thin plexus of cell processes forming the outer plexiform layer proper while the rod spherules occupy the spaces between the narrower portions of the pedicles. Most of the bipolar cells have small cell bodies with scant cytoplasm, which lie in the middle of the inner nuclear layer; while a few larger bipolars generally closer to the outer plexiform layer have spherical to flask-shaped cell bodies with more abundant cytoplasm.

Between the bipolar cell layer proper (inner nuclear layer) and the outer plexiform layer are found the horizontal cells. Two zones appear in this region in histologic sections. In the zone toward the outer plexiform layer are one to two layers of flattened, polygonal to stellate cells with horizontally elongated nuclei. These cells are in mutual contact except where the layer is penetrated by processes of bipolar or Müller cells In the zone toward the bipolar cell layer are long, pale-staining cylindrical processes about 5 μ in diameter most of which are oriented horizontally but some of which dip midway into the mass of bipolar cell bodies We have not definitely identified a nucleus or cell body of such elements. Cell bodies of the Müller fibers which stain intensely with the Bielschowsky reagent, are found among the bipolar cell bodies

The wealth of architectural detail seen in Golgi preparations adds significantly to the information derived from more conventional studies. Although we have observed only a few examples of each cell type all those observed agree well with those shown by Ramón y Cajal (1892, 1893) The pale cylindrical processes described above, which correspond to the "cellules horizontaux internes" of Cajal, appear to have neither axons nor fine, branching, dendrite-like processes. Thus

they do not appear to be true horizontal cells comparable to those in the goldfish and other animals and they will not be considered further in this paper

There are then two architectural types each of bipolar and horizontal cells (fig 11) The more numerous small bipolars have rounded cell bodies about 8 μ in diameter which emit a single fine primary dendrite and a more slender axon The dendrite forms an enlarged preterminal knob which gives off several short, horizontal secondary dendrites in the outer plexiform layer These dendrites are 1 μ or less in diameter taper rapidly and emit a few barely visible processes sclerad (toward the sclera) The dendritic field is roughly circular in the horizontal plane and about 20–25 μ in diameter The axon ends in fine free terminals at multiple levels in the inner plexiform layer The less numerous larger bipolars have spherical or flask-shaped cell bodies at least 8–10 μ in diameter which emit a stout primary dendrite and a small axon In the outer plexiform layer the primary dendrite divides into many secondary dendrites which spread over a circular field about 40–70 μ in diameter They taper gradually from a base which is about 2–3 μ thick and send finer terminal processes directly sclerad at irregular intervals The axon 1–2 μ in diameter traverses the inner plexiform layer and terminates in an irregularly-shaped mass measuring 4–8 μ across near the level of the ganglion cell bodies

The horizontal cell layer proper measures 5–10 μ vertically and comprises cells of two types[4] The more numerous horizontal cells of the sclerad row resemble the "cellules horizontaux externes" of Cajal except that we have been unable to demonstrate an axon In our few well impregnated examples of these cells the perikarya which measure about 5 μ vertically and 15–25 μ horizontally present smooth vitread and lateral contours and send about 6–10 processes sclerad. Since some cells of this type are displaced vitread by crowding the processes vary in length from about 5–15 μ depending upon the obliquity of their course and the displacement of the cell body Typically the first part of a process is nearly straight and about 0 5–1 0 μ in diameter tapering sclerad Terminally the process turns slightly and bears a 1–4 μ spherical or ovoidal end-bulb in the layer of the cone pedicles The horizontal cells of the vitread row resemble the "cellules horizontaux intermédiaires" of Cajal except for the absence of a demonstrable axon in our preparations These cells are more flattened and extend farther laterally than those of the sclerad type they are shaped to fill the spaces between the sclerad horizontal cells the vitread cylindrical processes and the interspersed bipolar and Müller cells They appear to be roughly stellate in form although precise determination of the form and size of individual elements has been rendered difficult by their tendency to be impregnated only partially or in thick clusters. Tapering processes 2–5 μ thick at the base extend from the cell body and horizontal processes to the outer plexiform layer where they divide candelabra-like into many fine branches. The branches at first run horizontally and then curve sclerad bearing at the tip an ovoidal swelling measuring about 1 μ by 2 μ usually with the long axis vertical The terminal swellings lie at the level of the rod spherules

Electron microscopy

The photoreceptor-bipolar cell synaptic complexes and horizontal cells in the goldfish resemble in ultrastructure those described in various vertebrates by other investigators (Cohen 63; Meller and Eschner '65 Missotten '65a b Sjöstrand, 65; Yamada and Ishikawa '65) Structures peculiar to teleosts also are found (Stell 64 and below)

The synaptic complexes of rods and cones are similar to one another in form and ultrastructure Characteristic presynaptic organelles are small vesicles and synaptic lamellae (synaptic ribbons) The

[4] If Cajal s "internal" horizontal cell are not truly horizontal cells, then his "intermediary" cells are not intermediary The present observations should be confirmed and extended in the retinas of other species, so that nomenclature based upon function can be established In the mean time we have dopted new purely descriptive names which we hope will eliminate ambiguity Cajal' "cellules horizontaux externes" will be called "sclerad (toward the sclera) horizontal cells." Cajal's "cellules horizonta x intermédiaires" will be called "vitread (to body) horizont l cells.

vesicles, which are round to ovoid and about 400–600Å in diameter are scattered throughout the synaptic terminals. They are especially associated with the synaptic lamella, as a layer which forms an apparent halo around the lamella where it is cross-sectioned. They are usually separated from the lamella by 300–500Å, and they are likewise separated from the plasma membranes. Granules 200–300Å in diameter which stain selectively with lead, are observed in cone pedicles but not in rod spherules they have no special relationship to either the plasma membranes or lamella.

The synaptic lamella is a flattened saccule, approximately rectangular in outline, measuring close to 1 μ on each side. In cross-sections, it appears trilaminar with strongly uranylophilic outer layers enclosing an electron-lucent inner layer Its broad surfaces are covered with an 100–200Å amorphous surface coat of moderate electron density which in turn is separated from the nearest vesicles by an electron-lucent zone of 100–200Å. Three edges of the lamella are closed by continuity of the outer layers and bear the same relationship to the surrounding cytoplasm as the broad surfaces of the lamella. The fine structure and relations of the fourth edge have been obscured by their complexity This edge is near the plasma membrane along its full length, although no continuity of lamella and membrane has been observed. Sometimes structures resembling the arciform density of Ladman ('58) are seen between them. The plasma membrane along this edge is out folded to form what we shall call the presynaptic ridge, which projects into and subdivides the postsynaptic compartment. Seen from within the photoreceptor terminal, the presynaptic ridge is a trough in which lies one edge of the synaptic lamella.

Postsynaptic processes are oriented similarly with respect to the presynaptic ridge in both rod and cone synaptic complexes In cross-sections through the lamella (figs 3 4) one finds profiles of postsynaptic processes of one type on either side of the ridge and of a different type opposite the summit of the ridge. Each rod synaptic complex consists of a single "unit" comprising the spherule with its presynaptic vesicles and lamella and the postsynaptic processes of two types Each cone synaptic complex consists of roughly a dozen such units ar ranged in a hemisphere at the vitread face of the pedicle; here, however adjacent units may overlap by sharing the same lateral postsynaptic process (fig. 11 top)

Although the rod and cone synaptic complexes thus share a common architectural pattern they show important dif ferences in the fine structure of the postsynaptic processes and their junctions with the photoreceptor terminals The lateral postsynaptic processes (immediately adjacent to the presynaptic ridge) in the rod synaptic complex are about 100–200 mμ in diameter (fig. 3) They contain occasional lead-stainable granules 300Å in diameter and vesicles 400Å in diameter in the light-adapted diurnal state. Elements similar in structure to the lateral processes are seen around the entire periphery of the ovoidal festoon of postsynaptic processes but farther from the presynaptic ridge (fig 3) Subsurface cisterns in the rod spherules are loosely associated with these processes Elements of a second type pass through the center of the cluster and ter minate at or near the summit of the presynaptic ridge These processes are about 50–150 mμ in diameter and show neither granules nor vesicles. Processes of the first type correspond to the "synaptic vacuoles" and those of the second type to the bipolar dendrites in Sjöstrand's ('58) description of the guinea pig alpha-receptor-bipolar synapse

The lateral elements in the cone synaptic complexes are irregular clublike 1 μ expansions of processes about 0.5 μ in diameter ("p" fig. 4) The cytoplasm contains scattered material of low electron density sometimes arranged in fibrils or tubules. Although some of these terminals are obviously branched the extent of branching is unknown. The endings bear numerous knobby projections ("k" fig. 4) except along the presynaptic ridge The knobs are about 100 mμ in diameter and project about 200–300 mμ beyond the clublike terminals 100Å beneath the membrane of the knobs is an electron-dense collar or plaque, 100Å thick, which

is stained intensely with uranyl or lead salts (fig 4 inset) Clusters of several processes of another type, only 50–150 mμ in diameter terminate instead opposite the summit of the presynaptic ridge They appear identical in structure to processes described above in the corresponding position in the rod synaptic complexes

Horizontal cells of the two classes can be differentiated not only by their size form, and location but also by their ultra structure. The sclerad cells have three different regions (fig 2) The vitread region contains the flattened nucleus. The intermediate region has a single supranu clear Golgi apparatus unlike that of typical neurons scattered ribosomes and smooth-surfaced cisternae 200–300Å lead-stainable granules and many mitochon dria, with a cross-sectional diameter of about 500 mμ The sclerad region is char acterized by a fringe of processes 0.5–1 0 μ in diameter which project into the outer plexiform layer The cytoplasm of these processes lacks the organelles found in the cell body and resembles instead that of the clublike endings in the cone syn aptic complexes (fig 4) The displaced sclerad horizontal cells are identical in structure to other cells of the sclerad type except that their processes are longer and the intermediate zone of cytoplasm is attenuated to fit between the undisplaced cells Since the vitread horizontal cells are more attenuated than any of the sclerad cells similar regional differentiation in their cell body is not readily observed Their nuclei and mitochondria appear simi lar to those of the sclerad cells except that in the vitread cells the mitochondria are slightly smaller and both the mitochon dria and the smooth-surfaced cisternae are less abundant.

Bipolar cells can be discriminated clearly from both horizontal and Müller cells toward the vitread border of the in ner nuclear layer their differentiation from amacrine cells is less certain Nuclei of the smaller bipolar cells measure about 4–7 μ and are surrounded by scant cytoplasm. At the poles of the perikaryon the cytoplasm is more abundant and contains mitochondria, sparsely and irregularly distributed cisternae of rough-surfaced endoplasmic reticulum free ribosomes, spheri cal membrane-bound granular bodies about 300 mμ in diameter and elements of the Golgi apparatus Elsewhere, the perikaryal cytoplasm contains few organelles and constitutes a very thin layer about 100 mμ thick, except where mitochondria are present The mitochondrial profiles, 500 mμ and more in diameter at the perikaryal poles are only 300 mμ in diameter later ally and usually indent the nuclear envelope. The large bipolar cells are similar to the small ones except that their perikaryon is particularly large at the sclerad pole and is everywhere at least 500 mμ thick. The various organelles, including vesicles of the Golgi apparatus, are distributed throughout the perikaryon and the mitochondria are not reduced in diameter laterally The primary dendrites of bipolars of both types contain longitudinal microtubules about 225–250Å in diameter large (up to 1 μ diameter) mitochondria of the type seen in the cell bodies and occasional 200–300Å lead-stainable granules The axons and teledendrons of the bipolar cells have been examined and are similar in structure to those described elsewhere (Dowling and Boycott, '65 '66)

The outer plexiform layer which is 1–2 μ thick comprises processes of two broad classes intertwined in a framework of Müller cell processes. Processes of one type in the outer plexiform layer range from 0 1–2.0 μ in diameter and contain microtubules a few lead-stainable granules and if large enough to accommodate them, mitochondria the ultrastructure of these elements is like that of the primary dendrites of bipolar cells. Processes of the other type under 1 μ in diameter contain amorphous or filamentous material and lead-staining granules but never microtubules or mitochondria the ultrastructure of these elements is like that of the proximal processes of the sclerad horizontal cells and the clublike endings in the cone synaptic complexes.

Finer architecture in Golgi preparations

The Golgi preparations of Ramón y Cajal (1893) suggested that photoreceptor cells contact both bipolar and horizontal cells in the outer plexiform layer and that there are subclasses

horizontal cells specific for rods and cones. Combining this information with our observations on the ultrastructure of the goldfish retina, we may predict that the central and lateral postsynaptic processes in rod and cone synaptic complexes represent elements of different types, the one a bipolar and the other a horizontal cell. The lateral elements in cone synaptic complexes appear to be processes from sclerad horizontal cells because of their size, form, and ultrastructure. By analogy the lateral elements in rod synaptic complexes should be processes from vitread horizontal cells, and by elimination the central processes should be dendrites of bipolar cells of the appropriate subclass.

These predictions were confirmed and extended with the Golgi-EM method. Two sclerad and two vitread horizontal cells and one small and two large bipolar cells were selected for apparent completeness of impregnation and separation from other impregnated structures. In the case of the vitread horizontal cells however it was necessary to examine not one but a cluster of cells, all apparently of the same type. After a cell was characterized by its appearance in the light microscope a small block containing it was remounted for thin-sectioning. Further optical study of the whole mount and 1-μ sections confirmed that the selected cell was the only impregnated element included in the ultrathin sections. Finally the ultrathin sections were examined to determine the location of impregnated processes in the outer plexiform layer The ultrastructure of organelles in the impregnated cell was compared to that of organelles in cells studied by conventional electron microscopy Thus we could ensure for example that an impregnated bipolar cell dendritic tree with unimpregnated cell body would not be mistaken for a horizontal cell. Distinctions between cells of different types were made easily by the size, shape, and location of the impregnated elements and by the characteristic ultrastructure of their membrane-bound organelles which were "spared" (not invaded) by the impregnating material. For cleaner preparations, the impregnating material was allowed to dissolve during sectioning, leaving spaces which were its equivalent for the identification of cell processes. This equivalence was confirmed by following the spaces in a few adjacent sections to show that they were not artifacts of sectioning Space-containing elements in the postsynaptic enclosure were identified as terminal processes of the impregnated cell. Space-containing elements between photoreceptor synaptic endings or free in the outer plexiform layer were identified as preterminal processes of the impregnated cell in the absence of contacts showing special features of synapses.

The results of applying this method are illustrated for the vitread horizontal cells (figs. 8 9; see also Stell, '65a) In sections through impregnated processes of these cells spaces appeared in the lateral and peripheral postsynaptic elements of the rod synaptic complexes as well as in preterminal processes throughout the outer plexiform layer The analogous elements in cone synaptic complexes and the central postsynaptic elements of both rod and cone complexes were never impregnated in these preparations. The same pattern was observed in all 30 rod synaptic complexes in which contacts were made with impregnated processes of vitread horizontal cells Therefore we can conclude that the processes of vitread horizontal cells pass between the sclerad horizontal cells, divide in candelabra fashion at the outer plexiform layer and pass through that layer to terminate as the lateral and peripheral process in numerous rod synaptic complexes. Each rod spherule contacts the process of but one vitread horizontal cell. Similarly about eight processes of impregnated sclerad horizontal cells were shown to terminate laterally in the cone synaptic complexes, on either one side or both sides of a given presynaptic ridge. Yet in each cone synaptic complex which received an impregnated process, about two-thirds of the clublike lateral processes were not impregnated, suggesting that impregnation of the horizontal cell was incomplete or that more than one horizontal cell may contact each pedicle. Thus we conclude that the stout, unbranched processes of sclerad horizontal cells terminate in complex club-like endings which ramify about several presynaptic ridges of

is stained intensely with uranyl or lead salts (fig 4 inset) Clusters of several processes of another type only 50–150 mμ in diameter terminate instead opposite the summit of the presynaptic ridge They appear identical in structure to processes described above in the corresponding position in the rod synaptic complexes

Horizontal cells of the two classes can be differentiated not only by their size form and location but also by their ultrastructure The sclerad cells have three different regions (fig 2) The vitread region contains the flattened nucleus. The intermediate region has a single supranuclear Golgi apparatus, unlike that of typical neurons; scattered ribosomes and smooth-surfaced cisternae; 200–300A lead stainable granules; and many mitochondria with a cross-sectional diameter of about 500 mμ The sclerad region is characterized by a fringe of processes 0 5–1 0 μ in diameter which project into the outer plexiform layer The cytoplasm of these processes lacks the organelles found in the cell body and resembles instead that of the clublike endings in the cone synaptic complexes (fig 4) The displaced sclerad horizontal cells are identical in structure to other cells of the sclerad type except that their processes are longer and the intermediate zone of cytoplasm is attenuated to fit between the undisplaced cells Since the vitread horizontal cells are more attenuated than any of the sclerad cells similar regional differentiation in their cell body is not readily observed Their nuclei and mitochondria appear similar to those of the sclerad cells except that in the vitread cells the mitochondria are slightly smaller and both the mitochondria and the smooth-surfaced cisternae are less abundant

Bipolar cells can be discriminated clearly from both horizontal and Müller cells; toward the vitread border of the inner nuclear layer their differentiation from amacrine cells is less certain Nuclei of the smaller bipolar cells measure about 4–7 μ and are surrounded by scant cytoplasm At the poles of the perikaryon the cytoplasm is more abundant and contains mitochondria sparsely and irregularly distributed cisternae of rough-surfaced endoplasmic reticulum free ribosomes spherical membrane-bound granular bodies about 300 mμ in diameter and elements of the Golgi apparatus. Elsewhere the perikaryal cytoplasm contains few organelles and constitutes a very thin layer about 100 mμ thick except where mitochondria are present. The mitochondrial profiles 500 mμ and more in diameter at the perikaryal poles are only 300 mμ in diameter laterally and usually indent the nuclear envelope. The large bipolar cells are similar to the small ones except that their perikaryon is particularly large at the sclerad pole and is everywhere at least 500 mμ thick The various organelles including vesicles of the Golgi apparatus are distributed throughout the perikaryon and the mitochondria are not reduced in diameter laterally The primary dendrites of bipolars of both types contain longitudinal microtubules about 225–250A in diameter large (up to 1 μ diameter) mitochondria of the type seen in the cell bodies and occasional 200–300A lead-stainable granules The axons and teledendrons of the bipolar cells have been examined and are similar in structure to those described elsewhere (Dowling and Boycott '65 66)

The outer plexiform layer which is 1–2 μ thick comprises processes of two broad classes intertwined in a framework of Müller cell processes Processes of one type in the outer plexiform layer range from 0 1–2 0 μ in diameter and contain microtubules a few lead-stainable granules and if large enough to accommodate them mitochondria the ultrastructure of these elements is like that of the primary dendrites of bipolar cells Processes of the other type under 1 μ in diameter contain amorphous or filamentous material and lead-staining granules but never microtubules or mitochondria the ultrastructure of these elements is like that of the proximal processes of the sclerad horizontal cells and the clublike endings in the cone synaptic complexes.

Finer architecture in Golgi preparations

The Golgi preparations of Ramón y Cajal (1893) suggested that photoreceptor cells contact both bipolar and horizontal cells in the outer plexiform layer and that there are subclasses of bipolar and

receptor bipolar and sclerad horizontal cells are easily identified. Since the finest terminals are nearly featureless different subclasses cannot be distinguished by ultrastructure alone. Occasionally entire processes can be followed from cell body to termination in a single ultrathin section. In this way Meller and Eschner ('65) and Yamada and Ishikawa ('65) have demonstrated contacts of horizontal cell processes with cone pedicles in the retina of fishes and higher vertebrates. Missotten ('65a b) and Stell ('65b) have confirmed the existence of similar contacts in primates.

Thus the evidence obtained by a wide variety of techniques, including the Golgi-EM method, is in good agreement. We prefer the Golgi-EM approach because of its directness in correlating cytoarchitecture with ultrastructure and its advantages in the rapid sampling of large numbers of cells of a selected type. There is no reason why it should not be combined with serial sectioning to even greater advantage. Variants of the Golgi method and other classical neurohistological techniques may be widely applicable in the study of fine structure (Blackstad, '65 Westrum and Lund, '66)

In general it may be said that the pattern of photoreceptor synaptic contacts we have observed in the goldfish holds for other vertebrates examined by appropriate methods Bipolar dendrites terminate between horizontal cell processes, usually opposite the presynaptic ridge and elements found opposite the summit of the presynaptic ridge bipolar cell dendrites. Horizontal cell processes terminate at the sides of the presynaptic ridges and elements found beside the presynaptic ridges are horizontal cell processes. To the exceptions already noted by Sjöstrand ('65) and Missotten (Missotten, Appelmans, and Michiels '63 Missotten DeHauwere and Guzik, '64) more perhaps will be added. For the present, however evidence on the identity of processes in the photoreceptor synaptic complexes of all vertebrates is remarkably consistent. Inappropriate terms such as distal vacuole" proximal vacuole, and synaptic vacuole" should be discarded. The terms "bipolar dendrite and "horizontal cell process should be used in their stead, except where shown to be inapplicable in a specific case.

Often synaptic junctions show a number of distinctive features including mitochondria and vesicles clustered in the presynaptic terminals and modifications in the thickness spacing and electron-density of the apposed synaptic membranes (DeRobertis '58 '64; Palay '58 Gray '59) In the case of the photoreceptor-bipolar cell junctions, these criteria are of little use the most convincing argument that they are synaptic is that the known functional pathway is from photoreceptor to bipolar cell. Mitochondria are often absent, as in the goldfish. Vesicles are present, but only DeRobertis has reported the clustering about presynaptic membranes usually seen in synapses. Although DeRobertis ('64) noted a subsynaptic web and junctional filaments in unspecified synapses in fish retinas, typical modification of membranes and specializations of the intercellular cleft are not observed often in most retinas (Cohen 65)

The most characteristic organelle in the retinal junctions is the synaptic lamella or ribbon, observed first by Sjöstrand ('53) in photoreceptor terminals in the guinea pig and found subsequently in the retinas of all vertebrates examined (Cohen '63) Morphologically similar structures have been observed in synaptic terminals of retinal bipolar cells (Kidd, '62 Dowling and Boycott, '65 '66) amphibian pineal photoreceptors (Kelly '64 Kelly and Smith, 64) arthropod photoreceptors (Trujillo-Cenoz, '65) and hair cells of the cochlea (Smith, '61; Smith and Sjöstrand, 61a,b Cordier '64) vestibular system (Flock, '64) and lateral line system (Trujillo-Cenoz, '61 Porte-Delaveuve '64; Flock, '65 Hama, '65) Similar structures are encountered in sensory cells which contact only one and therefore afferent, element (Barets and Szabo '62; Mullinger '64) Apparently when present in synaptic terminals they are responsible for presynaptic rather than postsynaptic functions, although under some circumstances they may be dissociated from synaptic functioning (Wolfe, '65) The close relationship of bipolar cell dendrites

a single cone pedicle. Each pedicle contacts one to several processes from sclerad horizontal cells

In the same way the central postsynaptic processes which terminate near the summit of the presynaptic ridge were identified as dendrites of bipolar cells (figs. 5–7) All of the ten observed terminals of the impregnated small bipolar cell were found in cone synaptic complexes between unimpregnated processes of sclerad horizontal cells. Some cone pedicles probably contact several dendrites of a single small bipolar (fig 10) Thus the dendrites of each small bipolar cell terminate centrally in one or more synaptic units of each cone pedicle Because a very large number of dendrites is observed in each cone synaptic complex, it appears that each pedicle contacts the dendrites of many bipolar cells Most of the thirty observed terminals of the impregnated large bipolars were found in rod synaptic complexes between unimpregnated processes of vitread horizontal cells A small proportion were found instead in cone synaptic complexes and were indistinguishable from the dendrites of small bipolars. From the predominance of small bipolar cells in the inner nuclear layer the multiplicity of their contacts with each cone pedicle and the minor contribution of dendrites from large bipolars to cone synaptic complexes, we estimate that most of the dendrites in these complexes are derived from small bipolar cells Thus the dendrites of each large bipolar cell terminate centrally in the synaptic complexes of many rods and a few cones Most rod spherules contact a single dendrite from a large bipolar cell while each cone pedicle contacts many dendrites of small bipolars and a few of large bipolars

Processes of Müller cells are not observed in photoreceptor synaptic complexes, and the cylindrical processes of Cajal's "cellules horizontaux internes" lack sclerad appendages Horizontal cell axons were not demonstrated in our preparations and interreceptor processes which are seen on cone pedicles in Golgi preparations (Ramón y Cajal 1893) were not investigated in this study With these exceptions all elements of the outer plexiform layer in the goldfish retina are accounted for by the above observations, and so the identity of components of the photoreceptor synaptic complexes and the contact relations of the several cell types can be summarized as in figure 11

DISCUSSION

Retinal synaptology and structure of the outer plexiform layer

The present Golgi-EM studies have confirmed the existence in the goldfish retina of two broad classes each of photoreceptor bipolar and horizontal cells. Subclasses of these cells are segregated into rod and cone systems which overlap to a limited degree only in the dendritic contacts of the large bipolar cells. Architectonic relationships of the three elements are similar in each system The bipolar cell dendrites terminate directly opposite the presynaptic ridge containing the synaptic lamella while the horizontal cell processes terminate beside it as the structures called "synaptic vacuoles" by Sjöstrand ('58)

All of these findings have been anticipated by observations with more conventional methods of light and electron microscopy Ramón y Cajal (1892–1893) argued that second-order retinal cells with narrow dendritic fields are related to the high-acuity cone system while cells with wide dendritic fields are related to the high-sensitivity rod system Cajal's illustrations showed that "dendrites" of the two true horizontal cell varieties in cyprinid fishes terminate at different synaptic levels Both Cajal and Polyak identified classes of rod- and cone-related bipolar cells in many vertebrates

Confirmation of these hypotheses awaited the higher resolution of the electron microscope which has made available several new approaches. One might assume that axons and dendrites of specific subclasses have characteristic ultrastructure and may therefore be identified along their entire length. Dowling and Boycott ('66) have validated this approach in the identification of processes in the inner plexiform layer of the human retina If similar reasoning is applied in the case of the goldfish outer plexiform layer only the larger processes of photo-

glial cells are not. Thus the structural interrelationships of cells in nervous tissue are of great importance in determining their functional classification. For this reason, the observations that horizontal cells have dendrite-like processes in elasmobranchs (Neumayer 1897) and axons as well as dendrites in teleosts (Ramón y Cajal, 1893) are of great relevance, although unfortunately other investigators have been unable to repeat the demonstration of axons in teleosts (Verrier '28; the present work) The assumed homology of horizontal cells throughout the vertebrate series, supported by the striking similarity of their photoreceptor contacts shown by electron microscopy suggests that they may all perform similar functions. The neuronal nature of horizontal cells in vertebrates above teleosts, supported by both light and electron-microscopic evidence (Ramón y Cajal, 1893 Polyak, 41 '57 Dowling, Brown, and Major '66) has yet to be confirmed electrophysiologically however While the morphology of the horizontal cell processes and their relationship to the photoreceptor complexes differ from the relations of astroglial cell processes to synaptic regions described by Peters and Palay ('65) neither is there convincing ultrastructural evidence that the photoreceptor-horizontal cell junction is functionally synaptic. The argument of Meller and Eschner ('65) that the horizontal cells are neurons because the photoreceptor-horizontal cell junction is synaptic therefore does not follow

The most impressive fact of teleostean horizontal cell morphology is that processes from each cell establish contacts of a specific type with photoreceptor cells of a specific class. That is, these cells are morphologically part of organized multicellular networks concerned with the processing of specific visual information (photopic-chromatic or scotopic-achromatic) In this respect, they are more like neurons than neuroglia, and so we do not agree with Svaetichin (Svaetichin, Negishi, and Fatehchand, '65) that the S-potentials are directly related to the activity of glial controller" cells. By virtue of the strategic location of their processes, the horizontal cells are in a position to influence and be influenced by conditions in either the photoreceptor synaptic endings the bipolar cell dendrites, or the intercellular clefts. The elaborate area of contact between the photoreceptor and the horizontal cell suggests that important transactions take place at this contact. No other zones of specialized contact between horizontal cells and other elements have been observed in the goldfish. Since there is no strong evidence for a polarity of interactions at the interface between them, we conclude for the present that visual information of some kind is transferred in *both* directions between photoreceptor and horizontal cells The kind of information transferred remains to be determined.

It is most significant that, by means of a suitable method, one can show easily not only that horizontal as well as bipolar cells make contact with photoreceptor cells, but also that specific subtypes of these cells are segregated into different multicellular assemblies. These structural assemblies are concerned with such easily recognized functions as rod vision and cone vision. It should not be difficult to find subassemblies concerned with even more refined functions such as cone-bipolar cell systems for primary colors. Investigations such as these are remarkable in confirming many of the earlier ideas of light microscopists, notably Cajal and Polyak. They hold promise of being particularly fruitful in investigations of the intermediate levels of the retina, which have not yet yielded to the strivings of electrophysiologists. They further encourage the search for morphologically distinguishable neural units which can be correlated with distinct functions

ACKNOWLEDGMENTS

I wish to thank Dr William L. Doyle for his unfailing assistance, advice, and support. I am indebted also especially to Dr Edward F MacNichol, Jr., for stimulating and encouraging these studies, and to Dr D Kent Morest for suggesting many beneficial changes in the manuscript.

LITERATURE CITED

Bairati, A., and S. Iurato 1962 Experimental data on the termination of the efferent fibers to the inner ear. Proc. Fifth Intern. Congr. Electron Microscopy 2 U-2.

to the presynaptic ridge is therefore to be expected

Most of the above mechanoreceptor cells establish also apparently synaptic contacts of a second type The receptor cells are contacted by additional terminals containing mitochondria and clustered vesicles and the synaptic membranes are especially electron-dense and are separated by a wide smooth cleft. A flattened saccule or double-membrane pair resembling the "subsurface cisterns" first described by Rosenbluth (62) is found in the receptor cells opposite these processes The structural similarity of these terminals to synaptic boutons suggested that they are presynaptic to the receptor cell, and sectioning of the efferent olivocochlear bundle confirmed that this is so by causing them to degenerate (Bairati and Iurato '62 Iurato 62 Kimura and Wersäll 62 Spoendlin and Gacek, '63 Smith and Rasmussen '65) Kelly and Smith (64) have observed similar terminals on frog pineal photoreceptor cells. One might think that the junctions of vitread horizontal cells with rod spherules in the goldfish retina are of this type and that the vitread horizontal cells are presynaptic to the rods The subsurface cisterns are unreliable postsynaptic markers however Although they do occur sometimes postsynaptically (Rosenbluth '62 Estable-Puig '64 Bodian '65) similar structures are found at other sites related primarily to neuroglia (DeRobertis and Gerschenfeld, 61 Kuwabara 65)

Thus the evidence from functional pathways and comparative ultrastructure is most consistent with a presynaptic role for the synaptic lamella in photoreceptor bipolar cell transmission The photoreceptor horizontal cell junctions however lack the distinctive morphological features of synapses The functional properties of these junctions can be known only from the functions and pathways subserved by the horizontal cells

Structure and function of teleostean horizontal cells

Heinrich Müller (1851 1857) in describing "die Zwischenkörnerschicht" was first to note two layers of horizontally oriented cells between the outer and inner nuclear layers of teleostean retinas. The large flattened polygonal cells of the sclerad layer were interconnected by short, stout processes to form a sheet penetrated by scattered small spaces for the passage of radially oriented structures The deeply incised much flattened stellate cells of the vitread layer with their fine, branching processes formed a more open "syncytium" perforated by large spaces. Similar cells were described under various names by others (Vintschgau 1853 W Müller 1874 Reich 1874 Schwalbe 1874 Hannover 1876 Retzius 1881 Ranvier 1882 Krause 1884 1886a b 1889a b Schiefferdecker 1886) Except for Reich and Krause the early investigators believed these cells to be supporting elements because of their form relationships, and cytoplasmic structure Unlike typical neurons they failed to stain selectively with methylene blue (Ramón y Cajal 1893) although it must be noted that the same behavior was shown by photoreceptor cells (Dogiel 1888) and the large bipolar cells of teleosts (Ramón y Cajal '33) More recent light microscope studies of horizontal cells in teleosts (Selvin de Testa, '66) and mammals (Lessell and Kuwabara, '63 Gallego '65) agree that these cells appear to be either glia or morphological intermediates between glia and neurons but not neurons Electron microscope studies of teleostean horizontal cells (Villegas '60 '61 Villegas and Villegas '63 Meller and Eschner '65 Yamada and Ishikawa, 65 and the present work) have demonstrated absence of Nissl substance and of the kind of Golgi apparatus typical of neurons (Palay and Palade '55); frequently they have shown instead such features as fragility to osmotic stress and cytoplasmic fibrillar contents (Villegas and Villegas '63) and lead-staining granules which are supposed to be common features of glial cells (DeRobertis and Gerschenfeld '61; Palay et al 62 Mugnaini and Walberg '64 Schultz, '64)

Cytological properties are only one kind of evidence however Despite some recent objections (e g Glees '58) the most distinctive property that sets neuroglia apart from neurons is that neurons are involved in the transfer and analysis of information along nervous pathways while

glial cells are not. Thus the structural interrelationships of cells in nervous tissue are of great importance in determining their functional classification. For this reason, the observations that horizontal cells have dendrite-like processes in elasmobranchs (Neumayer 1897) and axons as well as dendrites in teleosts (Ramón y Cajal, 1893) are of great relevance although unfortunately other investigators have been unable to repeat the demonstration of axons in teleosts (Verrier '28; the present work) The assumed homology of horizontal cells throughout the vertebrate series supported by the striking similarity of their photoreceptor contacts shown by electron microscopy suggests that they may all perform similar functions. The neuronal nature of horizontal cells in *vertebrates above teleosts* supported by both light and electron-microscopic evidence (Ramón y Cajal, 1893; Polyak, 41 '57; Dowling, Brown, and Major '66) has yet to be confirmed electrophysiologically however While the morphology of the horizontal cell processes and their relationship to the photoreceptor complexes differ from the relations of astroglial cell processes to synaptic regions described by Peters and Palay ('65) neither is there convincing ultrastructural evidence that the photoreceptor-horizontal cell junction is functionally synaptic. The argument of Meller and Eschner ('65) that the horizontal cells are neurons because the photoreceptor-horizontal cell junction is synaptic therefore does not follow

The most impressive fact of teleostean horizontal cell morphology is that processes from each cell establish contacts of a specific type with photoreceptor cells of a specific class. That is these cells are morphologically part of organized multicellular networks concerned with the processing of specific visual information (photopic-chromatic or scotopic-achromatic) In this respect, they are more like neurons than neuroglia, and so we do not agree with Svaetichin (Svaetichin, Negishi, and Fatehchand, '65) that the S-potentials are directly related to the activity of glial controller" cells. By virtue of the strategic location of their processes the horizontal cells are in a position to influence and be influenced by conditions in either the photoreceptor synaptic endings the bipolar cell dendrites or the intercellular clefts The elaborate area of contact between the photoreceptor and the horizontal cell suggests that important transactions take place at this contact. No other zones of specialized contact between horizontal cells and other elements have been observed in the goldfish. Since there is no strong evidence for a polarity of interactions at the interface between them, we conclude for the present that visual information of some kind is transferred in *both* directions between photoreceptor and horizontal cells. The kind of information transferred remains to be determined.

It is most significant that, by means of a suitable method, one can show easily not only that horizontal as well as bipolar cells make contact with photoreceptor cells, but also that specific subtypes of these cells are segregated into different multicellular assemblies. These structural assemblies are concerned with such easily recognized functions as rod vision and cone vision. It should not be difficult to find subassemblies concerned with even more refined functions, such as cone-bipolar cell systems for primary colors. Investigations such as these are remarkable in confirming many of the earlier ideas of light microscopists notably Cajal and Polyak. They hold promise of being particularly fruitful in investigations of the intermediate levels of the retina which have not yet yielded to the strivings of electrophysiologists. They further encourage the search for morphologically distinguishable neural units which can be correlated with distinct functions

ACKNOWLEDGMENTS

I wish to thank Dr William L. Doyle for his unfailing assistance, advice and support. I am indebted also especially to Dr Edward F MacNichol, Jr., for stimulating and encouraging these studies and to Dr D Kent Morest for suggesting many beneficial changes in the manuscript.

LITERATURE CITED

Bairati, A., and S. Iurato 1962 Experimental data on the termination of the efferent fibers to the inner ear Proc. Fifth Intern. Congr. Electron Microscopy 2: U-2.

to the presynaptic ridge is therefore to be expected

Most of the above mechanoreceptor cells establish *also apparently* synaptic contacts of a second type The receptor cells are *contacted by* additional terminals containing mitochondria and clustered *vesicles and* the synaptic membranes are especially electron-dense and are separated by a wide smooth cleft. A flattened saccule or double-membrane pair resembling the "subsurface cisterns" first described by Rosenbluth (62) is found in the receptor cells opposite these processes The structural similarity of these terminals to synaptic boutons suggested that they are presynaptic to the receptor cell and sectioning of the efferent olivocochlear bundle confirmed that this is so by causing them to degenerate (Bairati and Iurato 62; Iurato '62 Kimura and Wersäll 62 Spoendlin and Gacek, '63 Smith and Rasmussen '65) Kelly and Smith (64) have observed similar terminals on frog pineal photoreceptor cells One might think that the junctions of vitread horizontal cells with rod spherules in the goldfish retina are of this type and that the vitread horizontal cells are presynaptic to the rods The subsurface cisterns are unreliable postsynaptic markers however Although they do occur sometimes postsynaptically (Rosenbluth 62 Estable-Puig '64 Bodian '65) similar structures are found at other sites related primarily to neuroglia (DeRobertis and Gerschenfeld 61 Kuwabara '65)

Thus the evidence from functional pathways and comparative ultrastructure is most consistent with a presynaptic role for the synaptic lamella in photoreceptor-bipolar cell transmission The photoreceptor horizontal cell junctions however lack the distinctive morphological features of synapses The functional properties of these junctions can be known only from the functions and pathways subserved by the horizontal cells

Structure and function of teleostean horizontal cells

Heinrich Müller (1851 1857) in describing "die Zwischenkörnerschicht" was first to note two layers of horizontally oriented cells between the outer and inner nuclear layers of teleostean retinas. The large flattened polygonal cells of the sclerad layer were interconnected by short, stout processes to form a sheet penetrated by scattered small spaces for the passage of radially oriented structures. The deeply incised, much flattened stellate cells of the vitread layer with their fine branching processes formed a more open "syncytium" perforated by large spaces. Similar cells were described under various names by others (Vintschgau 1853 W Müller 1874 Reich 1874; Schwalbe 1874 Hannover 1876 Retzius 1881 Ranvier 1882 Krause 1884 1886a,b 1889a,b Schiefferdecker 1886) Except for Reich and Krause the early investigators believed these cells to be supporting elements because of their form relationships, and cytoplasmic structure. Unlike typical neurons they failed to stain selectively with methylene blue (Ramón y Cajal 1893) although it must be noted that the same behavior was shown by photoreceptor cells (Dogiel, 1888) and the large bipolar cells of teleosts (Ramón y Cajal '33) More recent light microscope studies of horizontal cells in teleosts (Selvín de Testa, 66) and mammals (Lessell and Kuwabara, '63 Gallego '65) agree that these cells appear to be either glia or morphological intermediates between glia and neurons but not neurons Electron microscope studies of teleostean horizontal cells (Villegas '60 '61 Villegas and Villegas '63 Meller and Eschner '65 Yamada and Ishikawa, '65 and the present work) have demonstrated absence of Nissl substance and of the kind of Golgi apparatus typical of neurons (Palay and Palade 55) frequently they have shown instead such features as fragility to osmotic stress and cytoplasmic fibrillar contents (Villegas and Villegas 63) and lead-staining granules which are supposed to be common features of glial cells (DeRobertis and Gerschenfeld 61 Palay et al. '62 Mugnaini and Walberg 64 Schultz, '64)

Cytological properties are only one kind of evidence however Despite some recent objections (e g Glees '58) the most distinctive property that sets neuroglia apart from neurons is that neurons are involved in the transfer and analysis of information along nervous pathways while

Missotten, L., M. Appelmans and J Michiels 1963 L'ultrastructure des synapses des cellules visuelles de la rétine humaine. Bull. Mém. Soc. Franç. Ophtalm., 76 59–82.
Missotten, L., E. DeHauwere and A. Guzik 1964 L'ultrastructure de la rétine humaine. A propos des cellules bipolaires et de leurs synapses. Bull. Soc. Belge Ophtalm., 137 277–293.
Mitarai, G., G. Svaetichin, E. Vallecalle, R. Fatehchand, J Villegas and M. Laufer 1961 Glia-neuron interactions and adaptational mechanisms of the retina. In: Neurophysiologie und Psychophysik des visuellen Systems, R. Jung and H. Kornhuber eds. Springer-Verlag, Göttingen, pp. 463–481.
Mugnaini, E., and F Walberg 1964 Ultrastructure of neuroglia. Ergeb. Anat. Entwick., 37: 194–236.
Müller, H. 1851 Zur Histologie der Netzhaut. Z. wiss. Zool., 3 234–237
——— 1857 Anatomisch-physiologische Untersuchungen über die Retina bei Menschen und Wirbelthieren. Z. wiss. Zool., 8 1–122.
Müller, W 1874 Ueber die Stammes-entwicklung des Sehorganes der Wirbelthiere. Beitr. Anat. Physiol. Festgabe C. Ludwig. Vogel, Leipzig.
Mullinger A. M. 1964 The fine structure of ampullary electric receptors in *Amiurus*. Proc. Roy Soc. Lond., B *160*: 345–359
Neumayer, L. 1897 Der feinere Bau der Selachier Retina. Arch. mikroskop. Anat., 48 83–111.
Palade, G. E. 1952 A study of fixation for electron microscopy J Exp Med., *95* 285–298.
Palay S. L. 1958 The morphology of synapses in the central nervous system. Exp. Cell Res., Suppl. *5* 275–293.
Palay, S. L., S. M. McGee-Russell, S. Gordon, Jr. and M A. Grillo 1962 Fixation of neural tissues for electron microscopy by perfusion with solutions of osmium tetroxide. J Cell Biol., *12*. 385–410.
Palay S. L., and G. E. Palade 1955 The fine structure of neurons. J Biophys. Biochem. Cyt., *1* 69–78.
Peters, A., and S. Palay 1965 An electron microscopic study of the distribution and patterns of astroglial processes in the central nervous system. J Anat., 99 419 (abstract)
Polyak, S. L. 1941 The Retina. University of Chicago Press, Chicago.
Polyak, S. L. 1957 The Vertebrate Visual System. University of Chicago Press, Chicago.
Ponde-Delaverre, B. 1964 Particularités morphologiques de la région synaptique des cellules sensorielles des neuromastes du Goujon, *Gobio fluviatilis* (Cuv Val.) C. R. Acad. Sci. Paris, 258 6222–6224.
Ramón y Cajal, S. 1892 La retina de los teleósteos y algunas observaciones sobre la de los vertebrados superiores. Anales Soc. espan. Hist. nat., Ser. II, 21 281–306
Ramón y Cajal, S. 1893 La rétine des vertébrés. La Cellule, 9 121–255.
Ramón y Cajal, S. 1933 Neuron Theory or Reticular Theory? Objective evidence of the anatomical unity of nerve cells. Transl. M. U Purkiss and C. A. Fox. Instituto Ramón y Cajal, Madrid, 1954.
Ranvier L. 1882 Traité technique d'histologie. F Savy Paris, pp. 733–759
Reich, M. 1874 Zur Histologie der Hechtretina. Arch. Ophthalmol., 20 1–14.
Retzius, G. 1881 Beiträge zur Kenntnis der inneren Schichten der Netzhaut des Auges. Biol. Untersuch., Ser. I, *1* 89–104.
Richardson, K. C., L. Jarett and E. H. Finke 1960 Embedding in epoxy resin for ultrathin sectioning in electron microscopy Stain Techn., 35 313–323.
Rosenbluth, J 1962 Subsurface cisterns and their relationship to the neuronal plasma membrane. J Cell Biol., *13* 405–421.
Schiefferdecker P 1886 Studien zur vergleichenden Histologie der Retina. Arch. mikroskop. Anat., 28 305–396.
Schultz, R. L. 1964 Macroglial identification in electron micrographs. J Comp. Neur., *122*: 281–295.
Schwalbe, G. 1874 Die retina. In: Handbuch der gesamten Augenheilkunde, von A. Graef und T Saemisch, eds. W Engelmann, Leipzig. Vol. 1 pp. 254–457
Selvín de Testa, A. 1966 Morphological studies on the horizontal and amacrine cells of the teleost retina. Vision Res., *6* 51–59.
Sjöstrand, F S. 1953 The ultrastructure of the retinal rod synapses of the guinea pig eye. J. Appl. Phys., 24 1422 (abstract)
——— 1958 Ultrastructure of retinal rod synapses of the guinea pig eye as revealed by three-dimensional reconstructions from serial sections. J Ultrastr. Res., *2*: 122–170.
——— 1959 The ultrastructure of the retinal receptors of the vertebrate eye. Ergeb. Biol., *21* 128–160
——— 1965 The synaptology of the retina. In Ciba Found. Symp Colour Vision. Little, Brown and Co., Boston, pp. 110–144.
Smith, C. A. 1961 Innervation patterns of the cochlea. The internal hair cell. Ann. Otol. Rhin. Laryng., 70: 504–527
Smith, C. A., and G. Rasmussen 1965 Degeneration in the efferent nerve endings in the cochlea after axonal section. J Cell Biol., 26 63–77
Smith, C. A., and F S. Sjöstrand 1961a A synaptic structure in the hair cells of the guinea pig cochlea. J Ultrastr. Res., *5* 184–192.
——— 1961b Structure of the nerve endings on the external hair cells of the guinea pig cochlea as studied by serial sections. J Ultrastr. Res., *5* 523–556.
Spoendlin, H., and R. Gacek 1963 Electronmicroscopic study of the efferent and afferent innervation of the organ of Corti in the cat. Ann. Otol. Rhin. Laryng., 72 660–686.
Stell, W K. 1964 Correlated light and electron microscope observations on Golgi preparations of goldfish retina. J Cell Biol., 23 89A (abstract)
——— 1965a Correlation of retinal cytoarchitecture and ultrastructure in Golgi preparations. Anat. Rec., *153* 389–398.

Barets A and T Szabo 1962 Appareil synaptique des cellules sensorielles de l'ampoule de Lorenzini chez la Torpelle *Torpedo marmorata*. J Microsc 1: 47–54
Bennett, H S. and J H Luft 1959 S-collidine as a basis for buffering fixatives. J Biophys. Biochem. Cyt., 6: 113–114
Blackstad T W 1965 Mapping of experimental axon degeneration by electron microscopy of Golgi preparations. Z. Zellforsch. mikroskop Anat., 67: 819–834
Bodian, D 1965 A suggestive relationship of neuronal RNA with specific synaptic sites Anat. Rec., 151 444 (abstract)
Cohen, A. I. 1963 Vertebrate retinal cells and their organization Biol. Rev 38: 427–459
——— 1965 Some electron microscopic observations on inter-receptor contacts in the human and macaque retinae J Anat., 99 595–610
Cordier R. 1964 Sur la double innervation des cellules sensorielles dans l'organe de Corti du Pigeon. C R. Acad. Sci. Paris, 258 6238–6240
Dalton, A. J 1955 A chrome-osmium fixative for electron microscopy Anat. Rec. 121 281
DeRobertis, E. 1958 Submicroscopic morphology and function of the synapse. Exp Cell Res., Suppl 5 347–369
——— 1964 Histophysiology of Synapses and Neurosecretion. Macmillan New York, pp 100–121
DeRobertis E. and H M Gerschenfeld 1961 Submicroscopic morphology and function of glial cells. Intern. Rev Neurobiol 3: 1–65.
Dogiel, A. S 1888 Ueber das Verhalten der nervösen Elemente in der Retina der Ganoiden Reptilien Vögel und Säugetiere. Anat. Anz., 3 133–143
Dowling, J E., and B B Boycott 1965 Neural connections in the retina: Fine structure of the inner plexiform layer Cold Spring Harbor Symp Quant Biol., 30 393–402.
——— 1966 Organization of the primate retina: electron microscopy Proc. Roy Soc. B 166: 80–111
Dowling J E. J E. Brown and D Major 1966 Synapses of horizontal cells in rabbit and cat retinas. Science, 153 1639–1641
Engström, K. 1963 Structure, organization and ultrastructure of the visual cells in the teleost family *Labridae* Acta Zool., 44: 1–41
Estable-Puig J F 1964 Interneuronal contacts in the central nervous system Program Electron Microscopy Soc. Amer., p 23 (abstract)
Flock, A. 1964 Structure of the macula utriculi with special reference to directional interplay of sensory responses as revealed by morphological polarization. J Cell Biol., 22: 413–431
——— 1965 Electron microscopic and electrophysiological studies on the lateral line canal organ. Acta Oto-Laryng., Suppl. 199: 1–90
Gallego A. 1965 Connexions transversales au niveau de couches plexiformes de la rétine Actualités Neurophysiol., 16: 5–27
Gibbons I. R., and A. V Grimstone 1960 On flagellar structure in certain flagellates. J Biophys. Biochem. Cyt., 7: 697–716.
Glees, P 1958 The biology of neuroglia: a summary In: The Biology of Neuroglia, W F Windle ed. Charles C Thomas, Springfield, Ill, pp 234–242.
Gray E. G. 1959 Axo-somatic and axodendritic synapses of the cerebral cortex: an electron microscope study J Anat., 93: 420–433.
Hama, K. 1965 Some observations on the fine structure of the lateral line organ of the Japanese sea eel *Lyncozymba nystromi*. J Cell Biol., 24: 193–210
Hannover A. 1876 La rétine de l'homme et des vertébrés A F Höst and Fils, Copenhagen.
Iurato S 1962 Efferent fibers to the sensory cells of Corti's organ. Exp Cell. Res., 27: 162–164
Kelly D E. 1964 An ultrastructural analysis of the paraphysis cerebri in newts. Z. Zellforsch. mikroskop Anat. 64: 778–803.
Kelly D E., and S W Smith 1964 Fine structure of the pineal organs of the adult frog, *Rana pipiens*. J Cell Biol., 22. 653–674
Kidd M 1962 Electron microscopy of the inner plexiform layer of the retina in the cat and the pigeon. J Anat., 96: 179–187
Kimura, R. and J Wersäll 1962 Termination of the olivocochlear bundle in relation to the outer hair cells of the organ of Corti in guinea pig Acta Oto-Laryng. 55 11–32.
Krause W 1884 Die Retina. I. Die Membrana fenestrata der Retina. II. Zur Entwicklungsgeschichte der Retina. Intern. Monatsschr Anat. Hist. 1 225–254
——— 1886a Die Retina II Die Retina der Fische (1) Intern. Monatsschr Anat. Hist., 3. 8–38.
——— 1886b Die Retina II. Die Retina der Fische (2) Intern. Monatsschr Anat. Hist., 3. 41–73
——— 1889a Die Retina. II Die Retina der Fische (3) Intern. Monatsschr Anat. Hist., 6. 206–223
——— 1889b Die Retina I. Die Retina der Fische (4) Intern Monatsschr Anat. Hist., 6: 250–269
Kuwabara, T 1965 Microtubules in the retina. In: The Structure of the Eye II Symposium, J W Rohen ed. Schattauer Verlag, Stuttgart, pp 69–84
Ladman A. J 1958 The fine structure of the rod-bipolar cell synapse in the retina of the albino rat. J Biophys. Biochem. Cyt. 4 459–466.
Lessell, S and T Kuwabara 1963 Retinal neuroglia. Arch. Ophthalm., 70 671–678
Luft, J H. 1961 Improvements in epoxy resin embedding methods. J Biophys. Biochem Cyt., 9 409–414
Meller K., and J Eschner 1965 Vergleichende Untersuchungen über die Feinstruktur der Bipolarzellschicht des Vertebratenretina Z. Zellforsch mikroskop. Anat., 68 550–567
Millonig G. 1961 A modified procedure for lead staining of thin sections. J Biophys Biochem Cyt. 11 736–739.
Missotten, L. 1965a The ultrastructure of the human retina. Arscia Uitgaven N V Brussels.
——— 1965b The synapses in the human retina. In: The Structure of the Eye II. Symposium. J W Rohen ed. Schattauer Verlag Stuttgart, pp. 17–28

——— 1965b Discussion of retinal synaptology In: The Structure of the Eye. II. Symposium, J W Rohen ed. Schattauer-Verlag, Stuttgart, pp. 27–28

——— 1966 *The structure of horizontal cells and synaptic relations in the outer plexiform layer of the goldfish retina, as revealed by the Golgi method and electron microscopy* Ph.D Dissertation, The University of Chicago.

Svaetichin, G 1953 The cone action potential. Acta Physiol. Scand. 29 (Suppl. 106): 565–600.

Svaetichin, G., and E. F MacNichol Jr 1958 Retinal mechanisms for chromatic and achromatic vision. Ann. N Y Acad Sci., *74:* 385–404

Svaetichin G., K. Negishi and R. Fatehchand 1965 Cellular mechanisms of a Young-Hering visual system. In: Ciba Found. Symp. Colour Vision Little Brown, Boston, pp. 178–205.

Takayama T 1961 Comparative anatomy of vertebrate visual cells by electron microscopy (II) Folia Ophthalm. Jap *12* 515–523.

Tomita T 1965 Electrophysiological study of the mechanisms subserving color coding in the fish retina. Cold Spring Harbor Symp. Quant. Biol., *30:* 559–568.

Trujillo-Cenoz, O 1961 Electron microscope observations on chemo- and mechano-receptor cells of fishes. Z. Zellforsch. mikroskop. Anat. *54:* 654–676.

——— 1965 Some aspects of the structural organization of the arthropod eye. Cold Spring Harbor Symp. Quant. Biol. *30:* 371–382.

Verrier M.-L. 1928 Les yeux et la vision des poissons. Bull. Biol. France. Belg., Suppl. XI.

Villegas, G M. 1960 Electron microscopic study of the vertebrate retina. J Gen. Physiol., *43* (6, Part 2): 15–43.

——— 1961 Comparative ultrastructure of the retina in fish monkey and man. In: Neurophysiologie und Psychophysik des visuellen Systems R. Jung and H. Kornhuber eds. Springer *Verlag, Göttingen, pp. 3–13,* 23–24

Villegas, G M., and R. Villegas 1963 Neuroglia relationship in the bipolar cell layer of the fish retina. J Ultrastr Res., *8* 89–106.

Vintschgau, M. 1853 Ricerche sulla struttura della retina dell'uomo, degli animali vertebrate e dei cefalopodi. Sitz. Kaiserl. Akad. Wiss. Wien math.-naturw Cl., *11:* 943–1056.

Westrum, L. E., and R. D. Lund 1966 Formalin perfusion for correlative light- and electron-microscopical studies of the nervous system. J Cell. Sci., *1:* 229–238.

Wolfe D E. 1965 The epiphyseal cell: an electron-microscopic study of its intercellular relationships and intracellular morphology in the pineal body of the albino rat. Progr. Brain *Res., 10:* 332–376.

Wood, R. L., and J H. Luft 1965 The influence of buffer systems on fixation with osmium tetroxide. J Ultrastr Res., *12:* 22–45.

Yamada, E., and T Ishikawa 1965 Some observations on the fine structure of vertebrate retina. Cold Spring Harbor Symp. Quant. Biol., *30:* 383–392.


3


4

Abbreviations

C,c cone pedicle
cl subsurface cistern
D,d bipolar cell dendrite
G Golgi apparatus
IN inner nuclear layer
IP inner plexiform layer
k knobby projection from process of sclerad horizontal cell
L, synaptic lamella (synaptic ribbon)
M, Müller cell process
N nucleus of sclerad horizontal cell
ON outer nuclear layer
OP outer plexiform layer
p p process of horizontal cell
R,r rod spherule
SH, sh, sclerad horizontal cell
VH vh, vitread horizontal cell

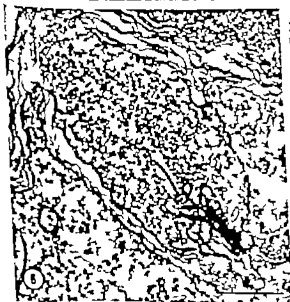
PLATE 1

EXPLANATION OF FIGURES

2 Survey electron micrograph of outer plexiform and horizontal cell layers in light adapted goldfish retina in near vertical section. Horizontal cells of the sclerad row sometimes displaced vitread (as cell to the left) send processes toward the photoreceptor synaptic terminals The more attenuated process of a horizontal cell of the vitread row is seen also, Osmium-dichromate fixation lead staining. Marker 5 μ × 5300

3 Electron micrograph of rod spherules in light-adapted goldfish retina, separated by a leaflet of Müller cell cytoplasm. Many cross-sectioned processes are clustered in an enclosure opposite the synaptic lamella, which lies in a ridge of rod cytoplasm projecting into the enclosure. The central dendrites, which lie directly opposite this presynaptic ridge appear featureless. The processes which lie opposite the subsurface cisterns of the spherule either lateral to the ridge (p) or elsewhere in the periphery of the mass of postsynaptic processes (p) contain granules or vesicles. Osmium-bicarbonate fixation, lead staining. Marker 1 μ × 24,800

4 Electron micrograph of portion of a cone pedicle and outer plexiform layer in light-adapted goldfish retina. Small featureless dendrites, similar to those in the rod synaptic complex (fig 3) terminate opposite the presynaptic ridge. A larger process from the outer plexiform layer reaches the side of the ridge This process ramifies and sends off knobby projection which bear electron-dense structures separated from the plasma membrane by a narrow electron-lucent space (arrow in inset) Osmium-dichromate fixation, lead staining. Main figure markers 1 μ × 26,500. Insert: marker 0 1 μ × 53,000


6


C
L
7

PLATE 2

EXPLANATION OF FIGURES

5 Electron micrograph of thin section through dendritic tree of a large bipolar cell in goldfish retina impregnated by the rapid Golgi method. The space left by dissolving of the impregnating material during sectioning and a "spared" mitochondrion are seen in a preterminal dendrite (d') Other smaller preterminal dendrites lacking mitochondria are impregnated also Of the five rod spherules indicated only the second from the left receives no dendrite from the impregnated cell In two of the others, termination of impregnated dendrites at the presynaptic ridge is shown (arrows) Lead-stained. Marker 1 μ × 13 700

6 Electron micrograph of another section from the same preparation as figure 5 An impregnated bipolar cell dendrite penetrates the rod spherule and terminates at the presynaptic ridge Adjacent lateral and peripheral postsynaptic processes are unimpregnated Lead-stained. Marker 1 μ. × 17,000

7 Electron micrograph of cone pedicle in dendritic field of same preparation as figure 5 and 6 An impregnated dendrite is seen at the presynaptic ridge (arrow) Adjacent processes lateral to the ridge are unimpregnated. Electron-density of the subsurface structures in the knobby projections is marked. Lead-stained Marker 1 μ. × 17,900


8


9

PLATE 3

EXPLANATION OF FIGURES

8–9 Electron micrographs of near-serial thin sections through a goldfish rod spherule penetrated by the process of a Golgi-impregnated vitread horizontal cell (cf *Stell*, '65a figures 6, 7) The plane of sectioning is parallel to the synaptic lamella (fig 8) The impregnated process winds itself around an unimpregnated bipolar cell dendrite (arrow) and a tongue of rod cytoplasm (*) to end near the presynaptic ridge. Lead-stained. Marker 1 μ. × 23,000

10 Electron micrograph of cone pedicle in dendritic field of a Golgi impregnated small bipolar cell in goldfish retina. Several impregnated dendrites are seen preterminally *en route* and one terminates at the summit of the presynaptic ridge (arrow) Nearby processes at the side of the ridge are unimpregnated. Lead-stained. Marker 1 μ. × 20 100


8


9

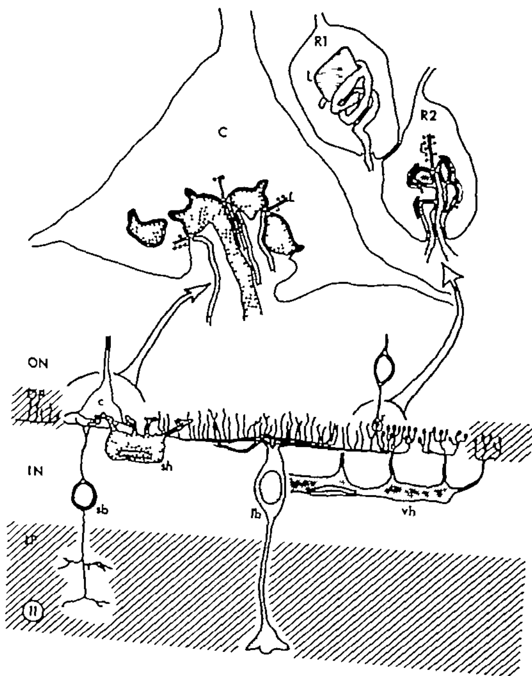
PLATE 4

EXPLANATION OF FIGURE

11 Diagrams summarizing the structure and relationships of cells in the distal part of the goldfish retina. Structures contributing to the cone synaptic complexes are shown on the left, while structures contributing to the rod synaptic complexes are shown on the right. The appearance of the cells by light microscopy of Golgi preparations is shown below while their appearance by electron microscopy of ultrathin sections is shown above. Cells of the same type are shaded to correspond in the upper and lower diagrams. Müller cells although present among the cells in this region are not shown.

Each cone pedicle (C c) contacts processes from horizontal cells of the sclerad row (sh) and from both small (sb) and large (lb) bipolar cells. Each rod spherule (R2, r) contacts processes from horizontal cells of the vitread row (vh) and from large bipolar cells (lb). In R1 the form and relationship of the vitread horizontal cell terminal to the synaptic lamella (L) are shown in three dimensions. In R2, the structure seen in ultrathin sections when the synaptic lamella is cross-sectioned is shown in two dimensions.

Not drawn strictly to scale


R1
L
R2
C
ON
c
IN
sh
sb
fb
vh
11

Local Uterine Regulation of the Corpus Luteum

THEODORE V FISCHER[1]
Department of Anatomy University of Wisconsin Medical School, Madison, Wisconsin

ABSTRACT In order to determine if the well known uterine inhibition of the guinea pig corpus luteum is a local affect, a series of partial hysterectomies were performed. Some groups were subjected to one-half or three-fourths hysterectomies alone, while in others one ovary was also removed on either the side retaining some or the side losing all uterine tissue. *In addition*, two groups in which all ovarian and uterine tissue was preserved were subjected to unilateral or bilateral complete surgical separation of all communicating structures between uterus and ovary Sham-operated, totally hysterectomized, and unilaterally ovariectomized groups were used as controls.

In all groups in which an ovary left in the animal was separated from direct contact with its uterine horn, the estrous cycles became long and erratic, or were arrested completely due to the persistance of active corpora lutea in those ovaries. However corpora lutea regressed normally in all ovaries left in their normal relationship to a uterine horn. These results indicate that the uterine regulatory factor does reach the ovary by some local route.

The mammalian uterus has, since ancient times been known as the organ in which the young undergo embryonic development, yet only within the last 45 years has it been suspected of playing a more subtle role in the physiology of reproduction. Experiments conducted by Loeb ('23, '27) upon the guinea pig demonstrated that, in at least this one form, the uterus is capable of contributing to the regular cyclic rhythmicity of the ovary by periodically curtailing the functional life of the corpus luteum. Loeb found that removal of the uterus a few days after estrus resulted in a sudden and complete cessation of all cyclic activity for a period much longer than the normal duration of pregnancy The corpora lutea in these anestrous animals were evidently in a state of high activity they were larger than those of pregnancy and were composed of large polygonal cells many of which were in mitosis.

Histological examination of the vagina and mammary glands gave additional evidence that the corpora lutea were actively secreting progesterone Since Loeb's work, this phenomenon in the guinea pig has been amply confirmed by many others and has been proven to exist in other mammals. In all cases where hysterectomy provokes a disruption of the sexual cycle the corpus luteum is maintained in an apparently functional state.

Loeb's experiments quickly stimulated interest in the field of utero-ovarian relationships. Studies were made of many different mammals to determine whether the effect of hysterectomy was of a more general occurrence. In recent years, it has also been found that distension of the uterus results in the opposite phenomenon, the early regression of corpora lutea and concomitant shortening of the estrous cycle (Moore and Nalbandov '53) The results of the various types of experiments performed during these years fall into three main groups.

1 *No apparent uterine influence on the ovary*

Marsupials Hartman ('25) could detect no change from the normal cyclic pattern in nine opossums hysterectomized for up to six weeks and so concluded that the operation was without effect. Hysterectomy in another marsupial, the Australian brush possum (*Trichosurus vulpecula*), has also been shown to be without effect (Clark and Sharman, '65)

Carnivores Deanesly and Parkes ('33) hysterectomized six ferrets, all of which subsequently demonstrated normal cyclic activity and a normal duration of pseudopregnancy Likewise hysterectomy in the dog (Cheval, '34; Unterberger '30) or cat

[1] Present address: Department of Anatomy, The University of Michigan, Ann Arbor, Michigan 48104.

'36). With this large amount of evidence against the theory of uterine influence, there seemed to be little point in further study. However none of the earlier workers had examined the life span of the corpus luteum in an animal hysterectomized during pregnancy or before or during pseudopregnancy, a period of luteal activity following copulation. In a study on just these particulars Asdell and Hammond ('33) achieved a breakthrough and reopened the whole subject. They completely hysterectomized prepuberal rabbit does and then after puberty mated them and compared them with pseudopregnant and pregnant controls. They found that the functional life of the corpora lutea was 16 days in an unoperated pseudopregnant control, but 25 days in the hysterectomized pseudopregnant animal, as evidenced by ovulation upon copulation at these times. This effect on pseudopregnancy was soon verified (Loeb and Smith '36; Gillard, '37 Chu, Lee and You, 46) and a similar luteal maintenance of 35 days was seen when the pregnant uterus was removed (Greep, 41). Recently it has been shown that the luteotrophic effect of hysterectomy may be cancelled by administration of luteinizing hormone (Mathis and Foote '65). Most of the experimental evidence to date agrees with Asdell and Hammond's ('33) work, but a few papers claim other effects such as ovarian degeneration (Seasums and Murphy '33) and increase in interstitial gland tissue (Mishell and Motyloff 41 Tenney Parker and Robbins, '55 '58; Robbins, '63). In a more carefully controlled experiment, Zacinai and Lapis ('61) contradict the claim of the latter group of workers, observing that the amount of interstitial tissue in the ovaries of control and totally hysterectomized animals alike increases with age. They maintain that the main long-term effect of hysterectomy in the nonpregnant or nonpseudopregnant rabbit is the inability of the ovary to produce ripe follicles.

Rat. In the rat, like the rabbit, early investigators were fairly united in denying any luteotrophic effect of hysterectomy. Hysterectomized rats continued to show normal estrous cycles (Long and Evans, '22; Durrant, '26 '31; Loeb, '27; Haupstein and Bühler '36; Ramsey Peckham and Greene, 47). Some claimed the operation to also be without any long-term effect on ovarian histology (Murphy '34; Shelesnyak and Schwarz, 44) while others argued that ovarian degeneration could be expected (Kross '22; Winter '32; Haupstein and Bühler '36). In contrast, Mandl and Zuckerman ('51) report satisfactory ovarian hypertrophy upon uterine extirpation. Mavromati ('32) states that persistent estrus resulted from hysterectomy but this may have been due instead to the accidental blocking of the oviduct, a condition which also causes this type of reaction (Fels, '54).

Bradbury ('37) discovered that, when pseudopregnancy was induced in a hysterectomized rat, the pseudopregnant cycle was prolonged from the control duration of 12 days to about 18 days. When the hysterectomy was performed up to day 16 of pregnancy estrus did not return until day 22, which would have been term for the pregnancy. These results have been confirmed by others (Bradbury Brown and Gray '50 Perry and Rowlands, '61). Perry and Rowlands ('61) also found that, when performed during pseudopregnancy hysterectomy always resulted in an increase in duration of that pseudopregnancy to about 19 days.

Pieces of estrus-rat uteri transplanted into the peritoneum of pseudopregnant hysterectomized rats shortened the pseudopregnancy to its normal duration (9–15 days) whereas control transplants of diestrus-rat uteri, frozen estrus-rat uteri, or estrus-rabbit uteri had no ability to shorten the period (Hechter Fraenkel, Lev and Soskin, 40). This would suggest that the rat uterus produces a hormone that curtails the functional life of the corpus luteum.

Other workers (Malven, '64 Malven and Hansel '65) using bovine endometrial extracts have been unable to shorten the long pseudopregnant cycle of hysterectomy but they found that vasopressin was capable of reducing the duration to that of normal pseudopregnancy. They feel that the uterus acts through the nervous system to release vasopressin from the posterior pituitary which then acts locally on the anterior pituitary to release an unknown luteolytic hormone. Silbiger and

(Baldin '39) brings about no ovarian or cyclic changes.

Primates The hysterectomized baboon continues to have normal cycles for several years (Gillman and Gilbert, 51) In the rhesus monkey the operation does not interrupt the normal cycle or interfere in any way with ovulation and the formation and regression of corpora lutea (Hartman '32 Burford and Diddle '36 Van Wagenen and Catchpole 41; Speert, 42)

In the human there has long been much controversy on the nature of the ovarian response to hysterectomy Since hysterectomy in the woman is common for various types of uterine pathology the subject has important practical aspects Two main lines of thought have developed: (1) hysterectomy in some way soon leads to typical menopausal symptoms caused by the degeneration of the ovaries; (2) hysterectomy is generally without effect. It is noteworthy that there has been little evidence for luteal preservation any apparent changes tend to be degenerative. Representative of the first group is Graves ('17) who at the time of hysterectomy either removed both ovaries, transplanted them or allowed them to remain *in situ*. He found that in all cases menopausal symptoms were produced and upon re-examination of some patients the ovaries proved to be atrophic or in stages of cystic degeneration. Other workers claimed ovarian cystic degeneration and menopausal symptoms in hysterectomized patients (Vineberg, '15 Kretzschmar and Gardiner '35) On the other hand it is argued that the menopausal symptoms are brought about by interference with the ovarian blood supply and, when care is taken to preserve the vessels the ovary remains unaffected by hysterectomy (Keitler '04) Supporting this view are Hawks ('21) and Tamis ('34) who have observed postoperative histories of many hysterectomy patients and find that, while menopausal symptoms are present in a large proportion of cases in which the ovaries have also been removed a reduction in both percentage of complaining patients and severity of menopausal symptoms occurs when an ovary is left in place and much more improvement is seen if both ovaries are retained. They claim also that both normal follicular growth and corpus luteum formation occur Still Doran ('05) and Tamis ('34) maintain that subtotal hysterectomy is more likely to prevent surgical menopause than is total that the presence of some endometrium is necessary for the normal function of the ovary In a recent study Zaczek ('63) followed the histories of 30 hysterectomy patients who retained both ovaries and oviducts. Upon laparotomy and re-examination within two years he found normal appearing follicles and corpora lutea.

Most of the work in the human has been concerned with detecting possible changes in the ability of the ovary to continue to ovulate normally Little had been done in a controlled effort to determine the effect on persistence of the corpora lutea until Andreoli ('65) hysterectomized women having normal 28-day cycles performing the operation on days 17 and 18 or 24 and 25 of the menstrual cycle Luteal function was determined by daily urinary pregnanediol analyses and vaginal smears. In the 17 and 18-day group, five out of six patients showed prolonged luteal function up to day 36 in one case whereas all women in the 24- and 25-day group soon ceased to show any signs of luteal function. Thus, in woman a slight prolongation of the life of the corpus luteum may be produced by hysterectomy soon after ovulation

Summary In none of these three groups, marsupials, carnivores or primates is there much evidence that the uterus plays any significant role in limiting the functional life of the corpus luteum. Normal ovarian function regularly occurs without it.

2. *Uterine influence on the ovary during pseudopregnancy*

Rabbit One of the earliest experiments on the effect of hysterectomy on the ovary was conducted on rabbits by Grammatikati (1889) He found no disruption of the normal ovarian histology; ovulation was uninhibited and corpora lutea formed normally He concluded that there is no uterine influence on the ovary in this species Many other early investigators corroborated his finding (Keitler '04 Mandl and Buerger '04 Bond '06; Burckhard, '06; Foges '06 Unterberger 30; Siegmund '34

'38) With this large amount of evidence against the theory of uterine influence there seemed to be little point in further study However, none of the earlier workers had examined the life span of the corpus luteum in an animal hysterectomized during pregnancy or before or during pseudopregnancy a period of luteal activity following copulation. In a study on just these particulars Asdell and Hammond ('33) achieved a breakthrough and reopened the whole subject. They completely hysterectomized prepuberal rabbit does and then, after puberty mated them and compared them with pseudopregnant and pregnant controls. They found that the functional life of the corpora lutea was 16 days in an unoperated pseudopregnant control, but 25 days in the hysterectomized pseudopregnant animal, as evidenced by ovulation upon copulation at these times. This effect on pseudopregnancy was soon verified (Loeb and Smith, '36 Gillard '37; Chu Lee and You, 46) and a similar luteal maintenance of 35 days was seen when the pregnant uterus was removed (Greep 41) Recently it has been shown that the luteotrophic effect of hysterectomy may be cancelled by administration of luteinizing hormone (Mathis and Foote '65) Most of the experimental evidence to date agrees with Asdell and Hammond's ('33) work, but a few papers claim other effects such as ovarian degeneration (Sessums and Murphy '33) and increase in interstitial gland tissue (Mishell and Motyloff 41; Tenney Parker and Robbins '55 '58 Robbins '63) In a more carefully controlled experiment, Zaolnai and Lapis ('61) contradict the claim of the latter group of workers, observing that the amount of interstitial tissue in the ovaries of control and totally hysterectomized animals alike increases with age. They maintain that the main long-term effect of hysterectomy in the nonpregnant or nonpseudopregnant rabbit is the inability of the ovary to produce ripe follicles.

Rat. In the rat, like the rabbit, early investigators were fairly united in denying any luteotrophic effect of hysterectomy Hysterectomized rats continued to show normal estrous cycles (Long and Evans, '22; Durrant, '26 '31; Loeb '27; Haupstein and Bühler, '36; Ramsey Peckham and Greene, 47) Some claimed the operation to also be without any long-term effect on ovarian histology (Murphy '34; Shelesnyak and Schwarz, 44) while others argued that ovarian degeneration could be expected (Kross '22 Winter '32; Haupstein and Bühler '36) In contrast, Mandl and Zuckerman ('51) report satisfactory ovarian hypertrophy upon uterine extirpation. Mavromati ('32) states that persistent estrus resulted from hysterectomy but this may have been due instead to the accidental blocking of the oviduct, a condition which also causes this type of reaction (Fels '54)

Bradbury ('37) discovered that, when pseudopregnancy was induced in a hysterectomized rat, the pseudopregnant cycle was prolonged from the control duration of 12 days to about 18 days. When the hysterectomy was performed up to day 16 of pregnancy estrus did not return until day 22, which would have been term for the pregnancy These results have been confirmed by others (Bradbury Brown and Gray '50; Perry and Rowlands '61) Perry and Rowlands ('61) also found that, when performed during pseudopregnancy hysterectomy always resulted in an increase in duration of that pseudopregnancy to about 19 days.

Pieces of estrus-rat uteri transplanted into the peritoneum of pseudopregnant hysterectomized rats shortened the pseudopregnancy to its normal duration (9–15 days) whereas control transplants of di estrus-rat uteri, frozen estrus-rat uteri, or estrus-rabbit uteri had no ability to shorten the period (Hechter Fraenkel, Lev and Soskin 40) This would suggest that the rat uterus produces a hormone that curtails the functional life of the corpus luteum.

Other workers (Malven, '64; Malven and Hansel, '65) using bovine endometrial extracts, have been unable to shorten the long pseudopregnant cycle of hysterectomy but they found that vasopressin was capable of reducing the duration to that of normal pseudopregnancy They feel that the uterus acts through the nervous system to release vasopressin from the posterior pituitary which then acts locally on the anterior pituitary to release an unknown luteolytic hormone. Silbiger and

(Baldin '39) brings about no ovarian or cyclic changes.

Primates The hysterectomized baboon continues to have normal cycles for several years (Gillman and Gilbert '51) In the rhesus monkey the operation does not interrupt the normal cycle or interfere in any way with ovulation and the formation and regression of corpora lutea (Hartman '32 Burford and Diddle '36 Van Wagenen and Catchpole 41 Speert 42)

In the human there has long been much controversy on the nature of the ovarian response to hysterectomy Since hysterectomy in the woman is common for various types of uterine pathology the subject has important practical aspects Two main lines of thought have developed: (1) hysterectomy in some way soon leads to typical menopausal symptoms caused by the degeneration of the ovaries (2) hysterectomy is generally without effect. It is noteworthy that there has been little evidence for luteal preservation; any apparent changes tend to be degenerative Representative of the first group is Graves (17) who at the time of hysterectomy either removed both ovaries transplanted them or allowed them to remain *in situ* He found that in all cases menopausal symptoms were produced and upon reexamination of some patients the ovaries proved to be atrophic or in stages of cystic degeneration Other workers claimed ovarian cystic degeneration and menopausal symptoms in hysterectomized patients (Vineberg 15 Kretzschmar and Gardiner '35) On the other hand it is argued that the menopausal symptoms are brought about by interference with the ovarian blood supply and when care is taken to preserve the vessels the ovary remains unaffected by hysterectomy (Keitler '04) Supporting this view are Hawks ('21) and Tamis ('34) who have observed postoperative histories of many hysterectomy patients and find that while menopausal symptoms are present in a large proportion of cases in which the ovaries have also been removed a reduction in both percentage of complaining patients and severity of menopausal symptoms occurs when an ovary is left in place and much more improvement is seen if both ovaries are retained. They claim also that both normal follicular growth and corpus luteum formation occur Still Doran ('05) and Tamis ('34) maintain that subtotal hysterectomy is more likely to prevent surgical menopause than is total that the presence of some endometrium is necessary for the normal function of the ovary In a recent study Zaczek (63) followed the histories of 30 hysterectomy patients who retained both ovaries and oviducts. Upon laparotomy and re-examination within two years, he found normal-appearing follicles and corpora lutea

Most of the work in the human has been concerned with detecting possible changes in the ability of the ovary to continue to ovulate normally Little had been done in a controlled effort to determine the effect on persistence of the corpora lutea until Andreoli (65) hysterectomized women having normal 28-day cycles performing the operation on days 17 and 18 or 24 and 25 of the menstrual cycle Luteal function was determined by daily urinary preganediol analyses and vaginal smears. In the 17 and 18-day group five out of six patients showed prolonged luteal function up to day 36 in one case whereas all women in the 24- and 25-day group soon ceased to show any signs of luteal function Thus in woman a slight prolongation of the life of the corpus luteum may be produced by hysterectomy soon after ovulation.

Summary In none of these three groups, marsupials carnivores or primates, is there much evidence that the uterus plays any significant role in limiting the functional life of the corpus luteum. Normal ovarian function regularly occurs without it

2 *Uterine influence on the ovary during pseudopregnancy*

Rabbit. One of the earliest experiments on the effect of hysterectomy on the ovary was conducted on rabbits by Grammatikati (1889) He found no disruption of the normal ovarian histology; ovulation was uninhibited and corpora lutea formed normally He concluded that there is no uterine influence on the ovary in this species. Many other early investigators corroborated his finding (Keitler '04; Mandl and Buerger '04; Bond, '06 Burckhard, '06; Foges, '08 Unterberger 30 Siegmund '34

Rothchild ('63) would agree with this hypothesis. In their work with hysterectomized rats they found no evidence that the uterus reduces the amount of luteotrophic hormone produced and argue indirectly that the hypophysial factor liberated is luteinizing hormone which in the rat is luteolytic.

Another phenomenon which results in prolonged pseudopregnancy in the rat is the production of massive deciduomata early in pseudopregnancy (Ershoff and Deuel 43; Velardo Dawson, Olsen and Hisaw 53) In this condition produced by trauma to the endometrium the endometrial stromal cells become large polyhedral glycogen rich decidual cells. In this case just as in the hysterectomized animal the corpora lutea are maintained until about day 20 or 21 when the next estrus ensues The conditions of hysterectomy and conversion to massive deciduomata are similar in that both entail loss of normal endometrium. Melampy Anderson and Kragt (64) found that unilateral hysterectomy or unilateral deciduomata lengthened pseudopregnancy but not to the same extent as total hysterectomy or bilateral deciduomata. Thus presence of even one nontraumatized uterine horn has a luteolytic effect on the ovaries However this could be overcome by injections of luteotrophic hormone They suggest that normal endometrium produces an active luteolytic substance a property lost by conversion to decidual tissue

Recently Anderson Melampy and Chen (66) have produced evidence indicating that this luteolytic endometrial action may be a local effect. In hemihysterectomized rats when the ovary adjacent to the excised uterine horn was also removed the duration of pseudopregnancy was less than that of the unoperated controls when the opposite ovary was removed, the cycle became significantly longer than the preoperative controls and comparable to animals subjected to hemihysterectomy alone When the ovaries were transplanted to the kidney capsule and the uterus left in place pseudopregnancy duration was increased Thus increase in pseudopregnancy length occurs whenever the ovaries are spatially separated from their respective uterine horns.

3 *Uterine influence on the ovary during the estrous cycle*

Guinea pig Unlike the workers studying the animals whose pseudopregnant cycle were affected by hysterectomy there has been general agreement among almost all authors that this operation results in greatly increased estrous cycle length in the guinea pig sheep, cattle and swine.

The classic studies of Loeb ('23 '27) referred to on page 425 gave impetus to further work on this species. The prolongation of luteal function following hysterectomy during the estrous cycle or pregnancy was soon amply confirmed (Desclin and Brouha '32 Herlant '33 Fellner '33) Rowlands ('61) in a careful study of the effects of hysterectomy at different times of the cycle has more recently corroborated the early studies finding that the longest luteal maintenance occurs when the hysterectomy is done on or before day 5 When done on day 15 the approaching ovulation may not be inhibited in which case however the corpora lutea of that ovulation are maintained.

To attempt to modify the prolonged luteal maintenance following hysterectomy various types of experimental procedure have been employed Loeb ('27) performed partial hysterectomies and uterine autotransplants. He reported that corpora lutea were maintained for a more limited duration following partial hysterectomy a finding which has since been well substantiated (Butcher and Chu 61 Butcher Chu and Melampy 62a Howe '65) Howe (65) observed long term cyclic behavior in partially hysterectomized guinea pigs and found that they return to the normal pattern after five cycles. Although Loeb ('27) was unable to induce the return of estrus by means of uterine autotransplants he believed that a technique which would allow better preservation of the grafted tissue might do this. Later workers (Butcher and Chu 61 Butcher Chu and Melampy 62b) were able to restore a very irregular cyclic pattern with uterine autoplants having viable endometrium These cycles were similar to the moderately lengthened irregular cycles obtained in partially hysterectomized animals.

Other experiments aimed at clarifying the exact role of the uterus in the regulation of the corpus luteum have been somewhat contradictory. Hill ('62) feels that uterine and ovarian innervation is important in the mechanism of luteal regression. He denervated the uterus and found that the corpus luteum was maintained as in the hysterectomized condition. His findings are difficult to reconcile with those of Butcher et al. ('62b) whose functional uterine transplants were unquestionably not innervated.

Several investigators have examined the effects of various hormones and hypophysectomy on the corpora lutea of hysterectomy. Spies, Gier and Wheat ('61) gave exogenous progesterone and estrogen, and found these hormones to be without any abbreviating effect on the prolonged corpora lutea, but did find them able to block ovulation in intact guinea pigs. The inability of estrogen to cause luteal regression was soon confirmed by Rowlands ('62) who also found that even hypophysectomy of the hysterectomized guinea pig was unable to cause luteal regression, although a marked atrophy of the follicular apparatus and interstitial gland occurred. In addition he reported prolactin to be without any luteotrophic effect in the intact guinea pig. It seems that the pituitary plays little or no role in the normal periodic luteal regression, a hypothesis strengthened by the recent studies of Perry and Rowlands ('62) and Heap, Perry and Rowlands ('65) who found that hypophysectomy before day 8 results in prolonged luteal maintenance, even permitting gestation, but that the operation done after day 10 leads to quite normal luteal regression. These facts would indicate that the cyclic luteal degeneration in intact guinea pigs may be due to a direct effect of the uterus upon the ovary, independent of hypophysial factors. Issue has been taken with this by Deanesly and Perry ('65) who found luteal regression in hysterectomized guinea pigs having tablets of progesterone implanted in the subcutaneous tissue. In guinea pigs treated similarly they found estrogen injections to cause fresh ovulations; however, no regression of the old corpora lutea was evident. These workers therefore, maintain that the uterus acts indirectly on the ovary by causing release of some hypophysial factor.

Nevertheless, further evidence favoring the hypothesis of direct uterine influence on the ovary has been gathered by experiments on uterine distension. By suturing inert beads into the uterine lumen, several investigators (Moore '61; Donovan '61; Donovan and Traczyk, '62) were able to bring about the premature degeneration of corpora lutea, causing reduction of estrous cycle length to 12–14 days. This reaction occurred most readily when two beads were placed in each horn, but a significant reduction in cyclic duration could also be obtained with four beads in one horn (Bland and Donovan, '65a,b). In those guinea pigs subjected to unilateral uterine distension, homolateral luteal regression occurred between days 10–14, the corpora on the operated side being significantly smaller than on the control side (Bland and Donovan, '65a).

Sheep. In the sheep Wiltbank and Casida ('56) discovered that hysterectomy resulted in exceptionally long luteal maintenance which extended the normal 16-day cycle length to at least 100 days, at which time the animals were slaughtered. Subsequent work has confirmed their findings (Kiracofe and Spies, '63; Denamur and Mauleon, '63). Partial hysterectomy is also somewhat effective: increasing the amount of uterine tissue removed increases the percentage of ewes showing lengthened cycles (Moor and Rowson, '64) but the duration of luteal maintenance was not determined. Endometrial extracts were found to be unable to cause luteal regression by Kiracofe, Spies and Gier ('63). The same workers found that ligation of some of the uterine vessels in the intact ewe prolonged luteal function to at least 25 days. As in the guinea pig, hypophysectomy of the hysterectomized ewe shortly after ovulation will permit luteal maintenance, but not when done as late as day 20 (Denamur and Mauleon, '63). Recently Collins, Inskeep, Howland, Pope and Casida ('66), in a study on artificially induced corpora lutea, found that both the spontaneous corpora and those induced by HCG (human chorionic gonadotropin) were maintained in the hysterectomized ewe. They found that luteal weight decreased as compared with

Rothchild (63) would agree with this hypothesis In their work with hysterectomized rats they found no evidence that the uterus reduces the amount of luteotrophic hormone produced, and argue indirectly that the hypophysial factor liberated is luteinizing hormone which in the rat is luteolytic.

Another phenomenon which results in prolonged pseudopregnancy in the rat is the production of massive deciduomata early in pseudopregnancy (Ershoff and Deuel 43 Velardo Dawson Olsen and Hisaw '53) In this condition produced by trauma to the endometrium the endometrial stromal cells become large polyhedral glycogen-rich decidual cells. In this case just as in the hysterectomized animal, the corpora lutea are maintained until about day 20 or 21 when the next estrus ensues. The conditions of hysterectomy and conversion to massive deciduomata are similar in that both entail loss of normal endometrium Melampy Anderson and Kragt ('64) found that unilateral hysterectomy or unilateral deciduomata lengthened pseudopregnancy but not to the same extent as total hysterectomy or bilateral deciduomata. Thus presence of even one nontraumatized uterine horn has a luteolytic effect on the ovaries However this could be overcome by injections of luteotrophic hormone They suggest that normal endometrium produces an active luteolytic substance a property lost by conversion to decidual tissue.

Recently Anderson, Melampy and Chen (66) have produced evidence indicating that this luteolytic endometrial action may be a local effect. In hemihysterectomized rats, when the ovary adjacent to the excised uterine horn was also removed, the duration of pseudopregnancy was less than that of the unoperated controls when the opposite ovary was removed the cycle became significantly longer than the preoperative controls and comparable to animals subjected to hemihysterectomy alone When the ovaries were transplanted to the kidney capsule and the uterus left in place pseudopregnancy duration was increased Thus increase in pseudopregnancy length occurs whenever the ovaries are spatially separated from their respective uterine horns.

3 *Uterine influence on the ovary during the estrous cycle*

Guinea pig Unlike the workers studying the animals whose pseudopregnant cycle were affected by hysterectomy there has been general agreement among almost all authors that this operation results in greatly increased estrous cycle length in the guinea pig sheep cattle and swine.

The classic studies of Loeb ('23 '27) referred to on page 425 gave impetus to further work on this species. The prolongation of luteal function following hysterectomy during the estrous cycle or pregnancy was soon amply confirmed (Desclin and Brouha, '32 Herlant, '33 Fellner '33) Rowlands ('61) in a careful study of the effects of hysterectomy at different times of the cycle has more recently corroborated the early studies finding that the longest luteal maintenance occurs when the hysterectomy is done on or before day 5 When done on day 15 the approaching ovulation may not be inhibited in which case however the corpora lutea of that ovulation are maintained.

To attempt to modify the prolonged luteal maintenance following hysterectomy various types of experimental procedure have been employed. Loeb ('27) performed partial hysterectomies and uterine autotransplants. He reported that corpora lutea were maintained for a more limited duration following partial hysterectomy a finding which has since been well substantiated (Butcher and Chu '61 Butcher Chu and Melampy 62a Howe '65) Howe (65) observed long term cyclic behavior in partially hysterectomized guinea pigs and found that they return to the normal pattern after five cycles. Although Loeb ('27) was unable to induce the return of estrus by means of uterine autotransplants, he believed that a technique which would allow better preservation of the grafted tissue might do this Later workers (Butcher and Chu '61 Butcher Chu and Melampy '62b) were able to restore a very irregular cyclic pattern with uterine autoplants having viable endometrium. These cycles were similar to the moderately lengthened irregular cycles obtained in partially hysterectomized animals.

son, Rathmacher and Melampy '66) and appears to indicate that, in the pig, a direct luteolytic factor from the nonpregnant uterus may be responsible for the normal cyclic regression of corpora lutea.

Summary The guinea pig, ewe, heifer and pig are alike in the extreme prolongation of the life of the corpus luteum following hysterectomy. Viable uterine autotransplants result in normal cyclic behavior and luteal regression. In all of these species, the hypophysis does not seem to play an important part in luteal regression, nor do ovarian steroid hormones. Uterine distension was found to cause shortened cycles in guinea pigs, sheep and cattle. Evidence of local uterine regulation of the ovary was seen in cases of uterine distension in the guinea pig and in partial hysterectomy and unilateral gestation in the pig.

A naturally occurring ovarian asymmetry during pregnancy which may be similar to the experimental work done on the pig except, of course, that gestation is not interrupted, has been noted in the Canadian porcupine by Mossman and Judas ('49). Here accessory corpora lutea which are formed in both ovaries from unruptured follicles soon disappear from the ovary of the nonpregnant side, indicating either a local luteotrophic or luteolytic action by the uterus, or both.

Because of the profound effect of hysterectomy on the ovary of the guinea pig, and since the guinea pig is taxonomically related to the porcupine (Order: Rodentia, Suborder: Hystricomorpha) it is of interest to determine whether or not the uterus in this form also exerts a direct local inhibition on the ovary and if so by what route the uterine factor reaches the ovary.

MATERIAL AND METHODS

Experiment I

Forty female guinea pigs were fed a balanced guinea pig chow diet and given water containing veterinary terramycin. No vaginal smears were taken, but the animals were checked daily for vaginal opening for at least two estrous cycles. The day of vaginal opening was designated day 0. Those showing cycles between 14 and 19 days were used. The animals were arbitrarily divided into six groups of five each, except for group C which contained 15, and were operated upon between days 3–5 (inclusive) of the estrous cycle. The type of surgical intervention was as follows: Group A — sham operation, nothing removed although the uterus was handled; Group B — totally hysterectomized; Group C — one uterine horn removed, Group D — unilaterally ovariectomized Group E — one uterine horn and the ovary of the same side removed; Group F — one uterine horn plus the opposite ovary removed.

Groups A, B and D none of which were subjected to unilateral hysterectomy were used as controls. All groups were closely observed postoperatively for about three cycles or 100 days in case of very long cycles or acyclic behavior after which time they were killed by an overdose of Nembutal, and autopsied. The ovaries were fixed in Zenker formol solution for histological examination, dehydrated with an ascending series of alcohols and cyclohexanone embedded in paraffin and sectioned at 10 μ. Every tenth section was mounted and stained with Groat's tetrachrome stain. The presence of corpora lutea in the ovaries was noted, and their appearance evaluated for estimation of functional activity.

RESULTS

The estrous cycle lengths of all groups are given in table 1 and shown diagrammatically in figure 1. These data were obtained from two pre-operative cycles, three postoperative cycles in animals from groups A, D and E, and one to three postoperative cycles in groups C and F. Estrous cycles of the sham-operated controls (A) and the unilaterally ovariectomized controls (D) remained unaffected. The totally hysterectomized controls (group B) showed acyclic behaviour as expected, with only one animal returning to estrus (97 days). Thus the figure given in the table is probably much less than a true average. It is given merely as an indication of the extreme cyclic interruption typical of hysterectomized guinea pigs. Groups C (hemihysterectomy alone) and F (hemihysterectomy plus contralateral ovariectomy) exhibited postoperative estrous cycles averaging nearly twice the normal

intact controls but that the progesterone *content was increased.*

The opposite reaction was discovered by Moore and Nalbandov ('53) who were able to produce premature regression of the corpus luteum of the ewe by distension of the uterus with an inert bead. They found that removal of the bead or denervation of the segment containing it returned cyclic activity to normal. These observations which have been confirmed (Inskeep Oloufa, Howland Pope and Casida '62) support the hypothesis that a neural stimulus from the uterus is capable of bringing about luteal regression.

Cattle As in sheep hysterectomy of cattle during the luteal phase of the estrous cycle results in a definite maintenance of the corpus luteum (Wiltbank and Casida '56 Anderson Neal and Melampy '62 Malven 64) In studies on reactions of hysterectomized heifers to hormone treatments it was found that while the progesterone content of the hysterectomized animal is greater than that of the cycling or pregnant one estrogen is capable of reducing it in all three groups (Kaltenbach Niswender Zimmerman and Wiltbank, '64) Hypophysial extracts were given to hysterectomized heifers by Malven and Hansel ('64) but failed to cause luteal regression. On the other hand a significant shortening of the estrous cycle in the intact heifer was noticed upon uterine distension or injection of oxytocin (Armstrong and Hansel '59 Hansel and Wagner '60) It was later found that, while oxytocin continues to bring about precocious luteal degeneration and subsequent ovulation in partially hysterectomized heifers it is *completely without effect in* those subjected to total hysterectomy (Anderson and Bowerman '63 Anderson, Bowerman and *Melampy* 65) This would suggest that the uterus may be a necessary intermediary in the reaction of the ovary to oxytocin *in this* species.

Swine Hysterectomy in the pig also results in a marked suspension of the estrous cycle *with luteal maintenance* for at least 120 days when the operation is done during pregnancy or before day 16 of the 21–23 day *cycle* (du Mesnil du Buisson and Dauzier '59 Spies Zimmerman, Self and Casida '60; Anderson Butcher and Melampy '63) If done after day 18 in the proestrous phase of the cycle, the imminent ovulation usually occurs after which that set of corpora lutea is maintained (Anderson et al. '63) It was found that both the spontaneously formed corpora and those induced during the estrous cycle would be equally maintained by hysterectomy (Neill and Day '64) In a study on the effects of hypophysectomy du Mesnil du Buisson and Leglise ('63) found that in hypophysectomized animals corpora lutea form normally and are maintained until the normal time of their regression but even hysterectomy cannot prolong their life in this condition. However they were maintained for about 20 days by hypophysial extracts HCG and LH (du Mesnil du Buisson Leglise and Anderson '64; Anderson Leglise du Mesnil du Buisson and Rombauts '65) Spies et al. ('60) were unable to cause recurrence of estrus by uterine autotransplants but others using a technique that ensures a more adequate blood supply have been able to bring about normal cyclic behavior (Anderson et al '63; du Mesnil du Buisson and Rombauts 63)

Investigating the effects of partial hysterectomy Anderson, Butcher and Melampy ('61) reported that normal cycles ensued upon retention of at least *half of* one uterine horn, a finding confirmed by du Mesnil du Buisson (61) who noted *also a striking asymmetry in the ovaries* of acyclic pigs retaining less than 26 cm of one horn. In these animals the ovary *on the side adjacent to the remaining* uterine fragment was devoid of corpora lutea, whereas corpora were well devel*oped in the opposite ovary* This uterine asymmetry can also be experimentally induced during pregnancy Upon merely severing one horn from the uterine body and mating the animal du Mesnil du Buisson (61) was unable to establish implantation although fertilization regularly occurred If the sterile horn was removed before day 14 gestation proceeded normally In cases where gestation occurs in the presence of some remaining sterile uterine tissue corpora lutea regress on the nonpregnant side. This unilateral luteal regression has recently been confirmed (Rathmacher and Anderson 63; Ander

pora lutea showed moderate degeneration. As expected, the control groups A (sham hysterectomy) and D (unilateral ovariectomy) as well as experimental group E (unilateral hysterectomy and ovariectomy on the same side) all demonstrated young corpora lutea. Due to the compensatory hypertrophy of the remaining ovary in unilaterally ovariectomized animals, twice as many corpora lutea were produced per ovary in groups D E and F as in that of a sham-operated control. Totally hysterectomized animals of group B exhibited corpora lutea that were maintained in a mature, seemingly functional, condition until the time of autopsy at 100 days (4 cases) and 20 days (1 case, following a 87-day cycle) This same ovarian histology was noted in the remaining ovary from animals of group F (unilateral hysterectomy and ovariectomy on the opposite side) which were autopsied at days 20 22, 35 50 and 79 In group C however which lost one uterine horn only a very striking ovarian asymmetry was evident. Most of these animals exhibited long irregular cycles and were autopsied on days 4 6 (animals with normal cycles) 20 (2 cases) 22, 24 (2 cases) 25 (5 cases) 26 44 and 46. Except for the two animals having normal cycles mature corpora lutea were present in the ovary on the operated side, many showing mitosis and indicating active secretion, however in the opposite ovary no trace of active luteal tissue could be found, although in some ovaries severely degenerated corpora lutea bore witness to the fact that ovulation had occurred. Plate 1 figures 3 and 4 demonstrates a typical pair of group C ovaries removed at 26 days. In one case, a group C animal was autopsied just as the vagina was beginning to open, 24 days after the preceding estrus both ovaries showed recently ruptured follicles but only the ovary on the operated side demonstrated corpora from the previous ovulation.

MATERIAL AND METHODS

Experiment II

Thirty-six female guinea pigs were utilized in a second experimental series. Animal care was the same as above The operative groups were as follows: I. Separation of all structures between one uterine horn and its ovary II. Separation of all structures between each uterine horn and its ovary III. Three-quarter hysterectomy: removal of one uterine horn and the caudal half of the other IV Three-quarter hysterectomy: removal of one uterine horn and the cephalic half of the other V Three-quarter hysterectomy: removal of one uterine horn and adjacent ovary plus the caudal half of the other horn. VI. Three-quarter hysterectomy: removal of one uterine horn and the opposite ovary plus the caudal half of the other horn.

Animals were autopsied at various times after an estrous period, after having undergone 0–5 estrous cycles. At autopsy the ovaries were removed and treated as before.

RESULTS

The estrous cycle length data are summarized in table 2 and shown graphically in figure 2. In addition to the six groups examined in this experiment, a control

TABLE 2

Effect of three-fourths hysterectomies and vascular separations on estrous cycle length

Group	Length of cycles (days)			
	Preoperative		Postoperative	
	Mean ± S.E.	Range	Mean ± S.E.	Range
I	15.9 ± 0.26	14–17	26.0 ± 2.39	12–62
II	16.2 ± 0.28	15–18	33.7 ± 6.36	12–70
III	16.6 ± 0.25	15–18	32.0 ± 6.19	14–42
IV	16.8 ± 0.44	15–19	30.2 ± 5.24	16–61
V	16.4 ± 0.47	13–19	20.2 ± 2.54	13–69
VI	16.2 ± 0.49	14–19	21.6 ± 1.66	12–31
Control	16.6 ± 0.41	15–19	17.0 ± 0.41	15–21

Significantly different, P = 0.05.
No significant difference.

TABLE 1

Effect of partial hysterectomies on the estrous cycle length

Group	Length of cycle (days)			
	Preoperative		Postoperative	
	Mean ± S.E.	Range	Mean ± S.E.	Range
A	16.5±0 41	15–19	17.0±0 41 [2]	15–21
B	16.2±0.20	15–17	> 99 4	97–> 100
C	16.4±0.20	15–20	26.6±2.86 [1]	12–56
D	16.4±0.49	14–19	16.8±0.40 [2]	14–20
E	16.6±0.20	15–17	16.6±0.30 [2]	14–18
F	16.2±0.26	15–17	34 1±2.02 [1]	17–78

[1] Significantly different, P = 0.05.
[2] No significant difference.

duration both being significantly greater than the preoperative values but both varied markedly ranging from a subnormal low of only 12 days (2 animals in group C) to a high of 78 days (1 group F animal) Thus these operations result in a complete loss of cyclic rhythmicity with a distinct tendency to increase the diestrous interval. But, in these two groups the exact averages are not very meaningful because of the great individual variation In group E however where the ovary on the same side was removed with the uterine horn no lengthening of the cycle from the control value was detected nor was cyclic irregularity of any kind observed.

Two main functional types of corpora lutea were noticed histologically depending on whether the ovaries were taken from normally cycling animals or animals with prolonged cycles In the former case, since the guinea pigs were autopsied from days 4 through 6 of the fourth postoperative cycle, the corpora lutea were young and in the process of becoming organized. In the latter case since the animals were autopsied many days past the time estrus should have normally recurred the corpora lutea were usually mature showing also mitotic and secretory activity (as evidenced by very granular or even frothy cytoplasm) In a few cases these older cor

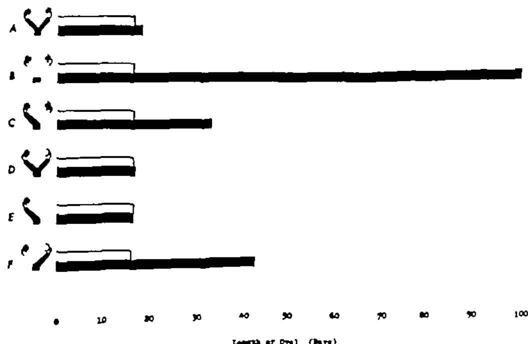


Fig. 1 Mean estrous cycle duration for groups of experiment I. Upper bar represents preoperative cycles, lower the postoperative.

half horn and one ovary) but having the ovary and uterine fragment on opposite sides, demonstrates a significant difference between pre- and postoperative estrous cycle means. In every case within this group, moderate cyclic prolongation is encountered.

Three natural divisions occur among the six experimental groups and their ovarian histology will be considered separately. The first consists of groups I and II, from which no uterine tissue was removed but merely unilateral (I) or bilateral (II) separations made. Ovaries from both groups had mature corpora lutea as should have been expected, since the guinea pigs of group II were autopsied on days 15, 19, 32, 35, 38 and 54, and those of group I on days 8, 15, 19, 22, 38 and 80. The difference between them is this: all animals of group II showed mature corpora lutea in both ovaries, whereas in group I mature corpora lutea occurred only in the ovary on the operated side while the ovary remaining adjacent to the uterine horn had only degenerating corpora lutea (days 15 and 19 autopsies) or a complete lack of them. The lone exception is GP 135 H, autopsied on day 8, much before luteal regression would be expected. Young corpora lutea occurred in both ovaries in this case.

The second comparison consists of groups III and IV, each of which was subjected to three-quarter hysterectomy. Animals of group III retained only the cephalic half of one horn and experienced no operative interference between this segment and its ovary, while group IV kept only the caudal half of one horn and was subjected to a considerable surgical disturbance between that segment and its ovary. Group III was autopsied on days 0 (estrus), 19, 77, 93 and 94 (2 cases); group IV on days 16, 17, 51, 77 (2 cases) and 84. With the exception of GP 154 H which was autopsied at estrus *following* a normal 18-day cycle, all group III animals demonstrated a marked ovarian asymmetry, having mature corpora lutea on the side lacking any uterine tissue while on the side where the uterine fragment kept its normal relationship to the ovary none were present. There seems to be no histological difference between the asymmetric ovaries of these three-quarter hysterectomized animals and those of group I in which a mere unilateral separation between uterus and ovary was made. Group IV did not react with such uniformity. In half (3) of the animals, the same type of ovarian asymmetry occurred as in group III, but in the other three guinea pigs autopsied on days 16, 51 and 84 no hint of luteal degeneration was present in either ovary. Thus combining groups III and IV (and excluding the aforementioned animal GP 154 H) 73% had unilateral luteal preservation and 27% bilateral, the latter all being confined to group IV.

The last comparison was made between the remaining ovary of animals of groups V and VI. Guinea pigs of group V, retaining the cephalic half of one horn and the adjacent ovary, were autopsied on days 0 (following a 13-day cycle), 0 (following an 18-day cycle), 13, 14, 33 and 83; those of group VI, which kept a cephalic uterine horn fragment and contralateral ovary, were autopsied on days 20, 31, 32, 60, 76 and 79. In none of the first four animals of group V was there any evidence of persistent corpora lutea, all showed signs of regression. The last two cases of that group however did indicate prolonged luteal preservation. On the other hand, when the ovary and uterine fragment are opposite (group VI) luteal maintenance seems to be the rule, five out of six showing this well. Only in the animal autopsied on day 20 (GP 123 H) was there considerable degeneration of the corpus luteum, but still no sign of a new ovulation.

DISCUSSION

Butcher et al. ('62a) by removal of one and three-quarter uterine horns and the ovary on the side that lost all uterine tissue observed a significant shortening of the postoperative estrous cycle as compared with guinea pigs which were simply partially hysterectomized. They asserted that the moderate prolongation of the estrous cycle brought about by partial hysterectomy may be negated by removing an ovary and reasoned that the amount of ovarian tissue remaining in the animal may be important in regulating cyclic duration: the more ovarian tissue, the longer the cycle in the partially hysterectomized

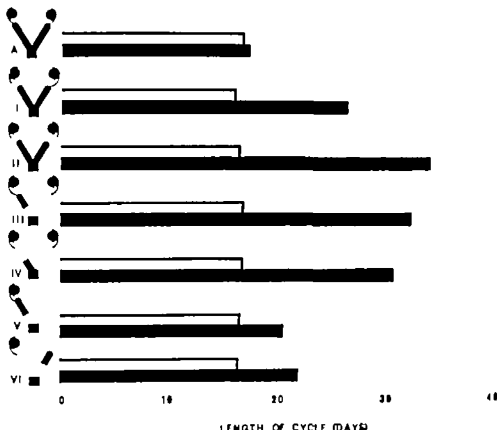


Fig. 2 Mean estrous cycle duration for groups of experiment II. Upper bar represents preoperative cycles lower the postoperative Group A is the sham operated control group from experiment I.

group is appended which is the sham hysterectomy group from experiment I, group A. These data are derived from two preoperative cycles in all groups and from a variable number (1–5) of postoperative cycles. The cycle of autopsy was disregarded in all cases in the calculations. In every group except group V and the sham controls the postoperative cycles average significantly larger than the preoperative means. In using the *t* test to make comparisons between groups it was found that the postoperative means of groups I and II (unilateral vs bilateral separations) do not differ significantly nor do those of groups III and IV (one horn plus caudal half removed vs one horn plus cephalic half removed) Groups I through IV were also compared with the hemihysterectomy group of experiment I (group C) and in no case was a significant difference detected which indicates that the same type of cyclic alteration occurs whether one removes one and one-half uterine horns one horn only or merely cuts between one or both horns and the ovaries. In group V a three-quarter hysterectomy plus unilateral ovariectomy where the retained uterine fragment was adjacent to the remaining ovary the mean postoperative cycle duration although larger was not significantly different from the preoperative. Upon examination of the individual animals records the reason becomes apparent at once. Four of the six in this group had almost completely normal cycles falling within the acceptable preoperative range (2 exceptions: 23 and 28 days from 15 observations on the 4 animals) One had long irregular cycles of 24 59 and 28 days and the last (which was not used in the calculations) was autopsied without coming into estrus after 83 days. Thus it seems that group V retains about the minimum amount of uterine tissue required for normal cyclic regularity Group VI on the other hand although retaining the same amount of uterine tissue as group V (one

mals an inhibitory factor could presumably pass locally to the ovary on the intact side but not to the operated side, since the intervening tissues are removed. It may well be that very limited amounts of the factor are produced or that it has a short period of activity and, when local access to an ovary is possible, it arrives in sufficient concentration to exert a strong effect but, when this local access is prevented, it becomes diluted or partially inactivated in the total blood volume of the animal, so that its action upon the contralateral ovary is weak, and hence luteal regression is slower Of course, when the entire uterus is removed there is no uterine factor at all to inhibit the corpus luteum and it then may be maintained to the limit of its intrinsic life span.

More evidence for the idea of local uterine inhibition is brought by the results of separations between uterus and ovary while conserving all parts of both organs. Both the characteristics of the postoperative estrous cycles and the ovarian histology are very reminiscent of that following partial hysterectomy Although the uterine factor may have been produced in both uterine horns exactly as in the intact animal, it is prevented from affecting the ovary because of the separation. In the one case, the unoperated side reacted by normal luteal regression, as would be expected, but the operated side showed well preserved corpora which testify to the inability of the factor to act across the surgical barrier in normally effective amounts. In the other case, bilateral separations resulted in bilateral luteal preservation. Here, just as in cases of partial hysterectomy the uterine factor could only exert its indirect systemic action, bring about the abnormally slow degeneration of the corpora lutea. These separation experiments suggest that anatomical structures lying in the interval between the uterine horn and the ovary are responsible for conveying the uterine factor to the ovary

Through these data, strong evidence has been gathered that the uterus does, in fact, directly exert a regulatory effect on the corpus luteum through some local route. Both the nature of the inhibitory factor and the precise anatomical route by which it arrives at the ovary are problems which need further investigation.

ACKNOWLEDGMENTS

The author wishes to thank Dr H. W Mossman for his helpful advice and encouragement. This work was supported by the N.I.H. Training grant 5 T1 GM 723-04 and by The Ford Foundation Fund 133-4297 in Reproductive Physiology

LITERATURE CITED

Anderson, L. L., and A. M. Bowerman 1963 Utero-ovarian function in oxytocin-treated heifers. J Animal Sci., 22: 1136.

Anderson, L. L., A. M. Bowerman and R. M. Melampy 1965 Oxytocin on ovarian function in cycling and hysterectomized heifers. J Animal Sci., 24 964–968.

Anderson, L. L., R. L. Butcher and R. M. Melampy 1961 Subtotal hysterectomy and ovarian function in gilts. Endocr 69 571–580.

——— 1963 Uterus and the occurrence of estrus in pigs. Nature, 198 311–312.

Anderson, L. L., P C. Leglise, F du Mesnil du Buisson and P Rombauts 1965 Interaction des hormones gonadotropes et de l'uterus dans le maintien du tissu lutéal ovarian chez la Truie. C. R. Acad. Sci., 261 3675–3678.

Anderson, L. L., R. M. Melampy and C. L. Chen 1966 The uterus and ovarian activity in the pseudopregnant rat. Anat. Rec., 154 308.

Anderson, L. L., F Neal and R. M. Melampy 1962 Hysterectomy and ovarian function in beef heifers. Am. J Vet. Res., 23: 794–802.

Anderson, L. L., R. P Rathmacher and R. M. Melampy 1966 The uterus and unilateral regression of corpora lutea in the pig. Am. J Physiol., 210: 611–614.

Andreoli, C. 1965 Corpus luteum activity after hysterectomy in women. Acta Endocr., 50: 65–69.

Armstrong, D. T., and W Hansel 1959 Alteration of the bovine estrous cycle with oxytocin. J Dairy Sci., 42: 533–542.

Asdell, S. A., and J Hammond 1933 Effects of prolonging the life of the corpus luteum in the rabbit by hysterectomy Am. J Physiol., 103 600–605.

Baldin, A. 1929 Über die Ovarialfunktion nach Uterusexstirpation. Arch. Gynäk., 168 191–208.

Bland, K. P., and B. T Donovan 1965a Local control of luteal function by the uterus of the guinea pig. Nature, 207 866–868.

——— 1965b A quantitative study of the effect of uterine distension on the estrous cycle of the guinea pig. J Physiol., 179 34P–35P

Bond, C. J 1906 Some points in uterine and ovarian physiology and pathology in rabbits. Brit. Med. J., 2: 121–127

Bradbury J T 1937 Prolongation of the life of the corpus luteum by hysterectomy in the rat. Anat. Rec., 70 suppl. p. 51.

guinea pig This *seems to be a* somewhat inadequate explanation for the present study clearly demonstrates that there is a marked difference in the *degree of luteal* preservation in the remaining ovary depending on whether it is on the operated or intact side. When the *remaining ovary* is on the intact side these data agree well with those of Butcher et al. (62a) but when it is on the side losing uterine tissue no difference is detected in degree of luteal maintenance and estrous cycle characteristics from that of a partially hysterectomized animal retaining both ovaries In short, partial hysterectomy with removal of the opposite ovary has no effect in retaining rhythmicity whereas removal of the homolateral ovary allows normal cyclic activity to continue The critical factor appears to be not the amount of ovarian tissue remaining but the location of the conserved ovary

That ovarian location is important is further demonstrated by the ovarian asymmetry which occurs after partial hysterectomy *with conservation of both ovaries.* Here also as earlier demonstrated by Butcher et al ('62a) partial hysterectomy *results* in *moderate* cyclic *prolongation* They make no mention of the histological appearance of the ovaries removed late in the lengthened cycle which the present study finds to be a most interesting condition. As expected in lengthened cycles produced by partial hysterectomy mature corpora lutea were always present in animals autopsied after day 15 but never in any ovary adjacent to a uterine horn. Those animals autopsied on days 0 4 6 and 8 all demonstrated that ovulation had indeed taken place normally in both ovaries Of the groups *exhibiting asymmetry* five animals were autopsied at about the normal time of estrus, on days 15 16 17 and 19 (2 *cases*) The ovaries of all except the one killed on day 16 showed mature corpora on one side and moderate to severe luteal regression on the other (figs 5 6) It would thus seem that the ovarian asymmetry develops rather early, usually at about the time normal bilateral luteal regression begins in the cycling animal.

In its effect upon the duration of the postoperative estrous cycle three-quarter hysterectomy in the guinea *pig seems to* be no more potent than removal of one horn only It appears that the cephalocaudal position of the conserved uterine fragment *does have* some effect upon ovarian asymmetry although not upon the estrous cycle duration Bilateral luteal maintenance *sometimes occurred when the uterine fragment* was retained in the caudal position.

The utero-ovarian separation groups form an *interesting part of this study* Although all uterine tissue was retained in all animals both groups exhibited behavior typical of partially hysterectomized animals All experienced postoperative cyclic interruption and the ovaries demonstrated the expected prolonged luteal maintenance However again reminiscent of the situation occurring in partially hysterectomized animals this extended life of the corpus luteum was seen only in those ovaries which had been separated from the uterine horn. Therefore whereas bilateral separations resulted in bilateral luteal preservation unilateral separations produced the familiar ovarian asymmetry It thus appears *that* mere *isolation from uterine* tissue is sufficient to prolong luteal life that it makes no difference whether the *horn is completely removed* from the animal or spatially separated from its ovary This situation is comparable to the uterine autotransplant experiments, and yields similar results.

By what mechanism does the uterus exert an influence on the ovary? This question was first considered by Loeb in 1927 He felt the most likely explanation to be that of a uterine hormonal factor which acts to bring about luteal regression. a hypothesis supported by investigations of uterine autotransplants (Hechter Fraenkel *Lev and Soskin* 40 *Chu*, Lee and You 46 Anderson Butcher and Melampy '63) and endometrial extracts (Bradbury Brown and Gray '50) The evidence of this study indicates that the inhibitory action of the guinea pig uterus may well be an essentially local effect. From work reviewed here it seems likely that the uterus produces an unknown luteolytic internal secretion Normally however the factor produced by each uterine *horn reaches the* homolateral ovary and primarily exerts its effects upon the corpora lutea in that ovary alone In partially hysterectomized ani

mals an inhibitory factor could presumably pass locally to the ovary on the intact side but not to the operated side, since the intervening tissues are removed. It may well be that very limited amounts of the factor are produced or that it has a short period of activity and when local access to an ovary is possible, it arrives in sufficient concentration to exert a strong effect but when this local access is prevented, it becomes diluted or partially inactivated in the total blood volume of the animal, so that its action upon the contralateral ovary is weak, and hence luteal regression is slower Of course, when the entire uterus is removed, there is no uterine factor at all to inhibit the corpus luteum and it then may be maintained to the limit of its intrinsic life span.

More evidence for the idea of local uterine inhibition is brought by the results of separations between uterus and ovary while conserving all parts of both organs. Both the characteristics of the postoperative estrous cycles and the ovarian histology are very reminiscent of that following partial hysterectomy Although the uterine factor may have been produced in both uterine horns exactly as in the intact animal, it is prevented from affecting the ovary because of the separation. In the one case, the unoperated side reacted by normal luteal regression, as would be expected, but the operated side showed well preserved corpora which testify to the inability of the factor to act across the surgical barrier in normally effective amounts. In the other case, bilateral separations resulted in bilateral luteal preservation. Here, just as in cases of partial hysterectomy the uterine factor could only exert its indirect systemic action, bring about the abnormally slow degeneration of the corpora lutea. These separation experiments suggest that anatomical structures lying in the interval between the uterine horn and the ovary are responsible for conveying the uterine factor to the ovary

Through these data, strong evidence has been gathered that the uterus does *in fact*, directly exert a regulatory effect on the corpus luteum through some local route. Both the nature of the inhibitory factor and the precise anatomical route by which it arrives at the ovary are problems which need further investigation

ACKNOWLEDGMENTS

The author wishes to thank Dr H. W Mossman for his helpful advice and encouragement. This work was supported by the N.I.H Training grant 5 T1 GM 723-04 and by The Ford Foundation Fund 133-4297 in Reproductive Physiology

LITERATURE CITED

Anderson, L. L., and A. M. Bowerman 1963 Utero-ovarian function in oxytocin-treated heifers. J Animal Sci., 22: 1136.

Anderson, L. L., A. M. Bowerman and R. M. Melampy 1965 Oxytocin on ovarian function in cycling and hysterectomized heifers. J Animal Sci., 24 964–968

Anderson, L. L., R. L. Butcher and R. M. Melampy 1961 Subtotal hysterectomy and ovarian function in gilts. Endocr 69 571–580.

——— 1963 Uterus and the occurrence of estrus in pigs. Nature, 198 311–312.

Anderson, L. L., P C. Léglise, F du Mesnil du Buisson and P Rombauts 1965 Interaction des hormones gonadotropes et de l'uterus dans le maintien du tissu lutéal ovarien chez la Truie. C. R. Acad. Sci., 261 3675–3678.

Anderson, L. L., R. M. Melampy and C. L. Chen 1966 The uterus and ovarian activity in the pseudopregnant rat. Anat. Rec., 154 308.

Anderson, L. L., F Neal and R. M. Melampy 1962 Hysterectomy and ovarian function in beef heifers. Am. J Vet. Res., 23 794–802.

Anderson, L. L., R. P Rathmacher and R. M. Melampy 1966 The uterus and unilateral regression of corpora lutea in the pig. Am. J Physiol., 210: 611–614.

Andreoli, C. 1965 Corpus luteum activity after hysterectomy in women. Acta Endocr 50: 65–69.

Armstrong, D. T and W Hansel 1959 Alteration of the bovine estrous cycle with oxytocin. J Dairy Sci., 42: 533–542.

Asdell, S. A., and J Hammond 1933 Effects of prolonging the life of the corpus luteum in the rabbit by hysterectomy Am. J. Physiol., 103 600–605.

Baldin, A. 1939 Über die Ovarialfunktion nach Uterusexstirpation. Arch. Gynäk., 169 191–206.

Bland, K. P and B. T Donovan 1965a Local control of luteal function by the uterus of the guinea pig. Nature, 207 866–868.

——— 1965b A quantitative study of the effect of uterine distension on the estrous cycle of the guinea pig. J Physiol., 179 349–359

Bond, C. J. 1906 Some points in uterine and ovarian physiology and pathology in rabbits. Brit. Med. J 2: 121–127

Bradbury J T 1937 Prolongation of the life of the corpus luteum by hysterectomy in the rat. Anat. Rec., 70 suppl. p. 51.

Bradbury J T., W E. Brown and L. A. Gray 1950 Maintenance of the corpus luteum and physiologic actions of progesterone. Rec. Prog. Hormone Res., *5:* 151–194.

Burckhard, G. 1906 Experimentelle Untersuchungen über die Verhaltung der Ovarien and Tuben, sowie des Uterusrestes nach vollständiger resp. teilweiser Entfernung des Uterus beim Kaninchen. Zeitschr. Geb. Gynäk., *58:* 63–77

Burford, T H., and A. W Diddle 1936 Effect of total hysterectomy upon the ovary of the *Macacus rhesus.* Surg. Gynec. Obst., *62:* 701–707

Butcher R. L. and K. Y Chu 1961 Relation of the uterus to the estrous cycle in the guinea pig. J Animal Sci., *20:* 967

Butcher R. L. K. Y Chu and R. M. Melampy 1962a Utero-ovarian relationships in the guinea pig. Endocr., *71:* 810–815.

——— 1962b Effect of uterine autotransplants on the estrous cycle in the guinea pig. Endocr., *70:* 442–443.

Cheval, M. 1934 Ovarian and uterine grafts. Proc. Royal Soc. Med., *27:* 1395–1406.

Chu, J P., C. C. Lee and S. S. You 1946 Functional relation between the uterus and the corpus luteum. J Endocr., *4:* 392–398.

Clark, M. J., and G B Sharman 1965 Failure of hysterectomy to affect the ovarian cycle of the marsupial *Trichosurus vulpecula.* J Reprod. Fertil., *10:* 459–462.

Collins, W E., E. K. Inskeep B E. Howland, A. L. Pope and L. E. Casida 1966 Effects of hysterectomy and corpus luteum induction on the pituitary-ovarian relationship in the ewe. J Animal Sci., *25:* 87–91

Deanesly R., and A. S. Parkes 1933 The effect of hysterectomy on the estrous cycle of the ferret. J Physiol., *78:* 80–84

Deanesly R., and J Perry 1965 Corpus luteum control in hysterectomized guinea pigs. J Endocr., *32:* 153–160

Denamur R., and P Mauleon 1963 Contrôle endocrinien de la persistance du corps jaune chez les Ovins. C. R. Acad. Sci., 257: 527–530.

Desclin, L., and L. Brouha 1932 Etude expérimentale des modifications gravidiques de l'hypophyse chez la cobaye Arch. Biol., Paris, *42:* 167–183

Donovan, B T 1961 The role of the uterus in the regulation of the *oestrous cycle. J Reprod.* Fertil., *2:* 508–510

Donovan, B T., and W Traczyk 1962 The effect of uterine distension on the oestrous cycle of the guinea pig. J Physiol., *161:* 227–236.

Doran A. H. G. 1905 Subtotal hysterectomy for fibroids: The after history of 60 cases: Preservation of the ovary and the Abel-Zweifel theory Lancet, *2:* 1310–1318.

Du Mesnil du Buisson, F 1961 Possibilité d'un fonctionnement dissemblable des ovaires pendant la gestation chez la Truie. C. R. Acad. Sci. 253: 727–729

Du Mesnil du Buisson, F., and L. Dauzier 1959 Contrôle mutuel de l'uterus et de l'ovaire chez la Truie. Ann de Zoötech., *8: Suppl.,* 147–159.

Du Mesnil du Buisson, F., and P C. Leglise 1963 Effet de l'hypophysectomie sur les corps jaunes de la Truie. Résultats préliminaires. C. R. Acad. Sci., 257: 261–263.

Du Mesnil du Buisson, F., P C. Leglise and L. L Anderson 1964 Hypophysectomy in pigs. J Animal Sci., *23:* 1226–1227

Du Mesnil du Buisson, F., and P Rombauts 1963 Effet d'autotransplants utérines sur le cycle oestrien de la Truie. C. R. Acad. Sci, *256:* 4984–4985.

Durrant, E. P 1926 Effect of hysterectomy on the estrous cycle in the white rat. Am. J Physiol. *78:* 234.

——— 1931 Relation of hysterectomy of long standing to vountary activity in the white rat. Am. J Physiol., *97:* 519

Ershoff, B. H., and H. J Deuel 1943 Prolongation of pseudopregnancy by induction of deciduomata in the rat. Proc. Soc. Exp. Biol. Med., *54:* 167–168.

Fellner O 1933 Der Uterus als innersekretorisches Organ. Pflügers Arch. ges. Physiol., *231:* 410–425.

Fels, E. 1954 Effet de la ligature tubaire sur la *fonction ovarienne chez le* rat. C. R. Soc Biol., *148:* 1668.

Gillard, J L. 1937 Effects of hysterectomy on mammary gland development in a rabbit. Am. J Physiol., *120:* 300–303.

Gillman, J., and C. Gilbert 1951 A case report of hysterectomy on ovarian activity in the female baboon. J Obst. Gynec. Brit. Emp., *51:* 495–498.

Grammatikati, J 1889 Experimentelle Untersuchungen über das weitere Schicksal der Ovarien und Tuben nach der Total-extirpation des Uterus bei Kaninchen. Zentralblt. Gynäk., *13:* 105–107

Graves, W P 1917 Transplantation and retention of ovarian tissue after hysterectomy *Surg. Gynec. Obst. 25: 315–323.*

Greep R. O 1941 Effects of hysterectomy and of estrogen treatment on volume changes in the corpora lutea of pregnant rabbits. Anat. Rec. *80: 465–477*

Hansel, W., and W C. Wagner 1960 Luteal inhibition in the bovine as a result of oxytocin injections uterine dilatation, and intrauterine infusions of seminal and preputial fluids. J. Dairy Sci., *43:* 796–805.

Hartman, C. G. 1925 Hysterectomy and the oestrous cycle in the opossum. Am. J Anat., *35* 25–29

——— 1932 Studies in the reproduction of the monkey (*Macacus Pithecus rhesus*) with special reference to menstruation and pregnancy Carnegie Inst. Contr to Embryology No. 23 1–161

Haupstein, P., and E. Bühler 1936 Experimentelle Untersuchungen über die Stellung des Uterus im sexualhormonalen System. Arch. Gynäk, *162:* 1–13

Hawks, E. M. 1921 The ovary after hysterectomy for fibroids. Am. J Obst. Gyn., *1:* 959–963.

Heap, R. B J S. Perry and I. W Rowlands 1965 The effect of hypophysectomy on the corpus luteum of the nonpregnant guinea pig. Acta Endocr., *50:* suppl. 100, 76.

Hechter, O., M. Fraenkel, M. Lev and S. Soskin 1940 Influence of the uterus on the corpus luteum. Endocr., 26: 680–683.

Heitz, M. 1933 Recherches préliminaire sur les modifications provoquées par l'hysterectomie chez la cobaye. C. R. Soc. Biol., 114: 273–275.

Hill, R. T 1962 Paradoxical effects of ovarian secretions. In The Ovary S. Zuckerman, ed. Academic Press, New York, vol. 2, pp. 231–261.

Howe, G. R. 1965 Influence of the uterus upon cyclic ovarian activity in the guinea pig. Endocr., 77 412–414

Inskeep, E. K., M. M. Oloufa, R. E. Howland, A. L. Pope and L. E. Casida 1962 Effect of experimental uterine distension on estrual cycle length in ewes. J Animal Sci., 21: 331–332.

Kaltenbach, C. C., G. D. Niswender D R. Zimmerman and J. N Wiltbank 1964 Alteration of ovarian activity in cycling, pregnant, and hysterectomized heifers with exogenous estrogens. J Animal Sci., 23: 995–1001.

Keller, H. 1904 Über das anatomische und funktionelle Verhalten der belassenen Ovarien nach Extirpation des Uterus. Monatschr. Geb. Gynäk., 20: 698–753.

Kiracofe, G., and H. Spies 1963 Length of corpus luteum maintenance in hysterectomized ewes. J. Animal Sci., 22: 862.

Kiracofe, G., H. Spies and H. Gier 1963 Effects of uterine extracts and ligatures in hysterectomized ewes. J Animal Sci., 22: 862.

Kretschmar, N. R., and S. Gardiner 1935 A consideration of the surgical menopause after hysterectomy and the occurrence of cancer in the stump following subtotal hysterectomy Am. J Obst. Gynec., 29 168–175.

Kross, I. 1922 Degeneration of conserved ovaries after hysterectomy in the rat. Am. J Obst. Gyn., 4: 408–412.

Loeb L. 1923 The effect of extirpation of the uterus on the life and function of the corpus luteum in the guinea pig. Proc. Soc. Exp. Biol. Med., 20: 441–443.

——— 1927 The effects of hysterectomy on the system of sex organs and periodicity of the sex cycle in the guinea pig. Am. J. Physiol., 83: 202–224.

Loeb, L., and M. G. Smith 1936 The effect of hysterectomy on the duration of life, retrogression of corpora lutea and secondary sex organs in the rabbit. Am. J. Anat., 58 1–25.

Long, J. A., and H. M. Evans 1922 The oestrous cycle in the rat and its associated phenomena. Mem. Univ Calif., 6: 1–126.

Malven, P 1964 Factors controlling luteal regression in rats and cattle. Diss. Abstracts, 25: no. 64–12, 836.

Malven, P., and W Hansel 1964 Ovarian function in dairy heifers following hysterectomy J. Dairy Sci., 47 1388–1393.

——— 1965 Effect of bovine endometrial extracts vasopressin, and oxytocin on duration of pseudopregnancy in hysterectomized and intact rats. J Reprod. Fertil., 9: 207–215.

Mandl, A., and S. Zuckerman 1951 Ovarian hypertrophy after unilateral hysterectomy Endocr., 7 339–343.

Mandl, L., and O Buerger 1904 Die biologische Bedeutung der Eierstöcke nach Entfernung der Gebärmutter F Deuticke, Leipzig.

Mathis, R. M., and W C. Foote 1965 Effects of estradiol, LH and hysterectomy on rabbit corpora lutea. J Animal Sci., 24: 925.

Mavromati, L. 1932 L'influence de l'utérus sur la sécrétion folliculaire de l'ovaire. C. R. Soc. Biol., 110: 651–653.

Melampy R. M., L. L. Anderson and C. L. Kragt 1964 Uterus and life span of rat corpora lutea. Endocr., 74 501–503.

Mitchell, D R., and L. Motyloff 1941 The effect of hysterectomy upon the ovary Endocr., 28: 426–440.

Moor R. M., and L. E. A. Rowson 1966 Local uterine mechanisms affecting luteal function in the sheep. J Reprod. Fertil., 11 307–311.

Moore, W W 1961 Effect of uterine distension on the estrous cycle of the guinea pig. Physiologist, 4: 76.

Moore, W W., and A. V Nalbandov 1953 Neurogenic effects of uterine distension on the estrous cycle of the ewe. Endocr., 53: 1–11.

Mossman, H. W., and I. Judas 1949 Accessory corpora lutea, lutein cell origin and the ovarian cycle in the Canadian porcupine. Am. J Anat., 85 1–39

Murphy D. P 1934 The weight of rat ovaries after hysterectomy Anat. Rec., 60: 77–81.

Neill, J D., and B. N Day 1964 Relationship of developmental stage to regression of the corpus luteum in swine. Endocr., 74: 355–360.

Perry J S., and I. W Rowlands 1961 Effect of hysterectomy on the ovarian cycle of the rat. J Reprod. Fertil., 2: 332–340.

——— 1962 The effect of hypophysectomy on the ovarian cycle of the guinea pig. J Endocr., 25 v–vi.

Ramsey B., B. M. Peckham and R. B. Greene 1947 Non-effect of hysterectomy on the ovary Federation Proc., 6 184.

Rathmacher, R. P., and L. L. Anderson 1963 Sterile uterine horn and embryonic survival in pigs. J Animal Sci., 22: 1139.

Robbins, S. 1963 Effect of hysterectomy on the rabbit ovary Am. J Obst. Gynec., 86: 367–373.

Rowlands, I. W 1961 Effect of hysterectomy at different stages of the life cycle of the corpus luteum in the guinea pig. J. Reprod. Fertil., 2: 341–350.

——— 1962 The effect of oestrogens, prolactin and hypophysectomy on the corpora lutea and vagina of hysterectomized guinea pigs. J Endocr., 24: 105–112.

Sessums, J V., and D. P Murphy 1933 The influence of the endometrium upon the rabbit ovary after hysterectomy Surg. Gyn. Obst., 56: 600–609.

Shelesnyak, M. C., and H. Schwartz 1944 Effect of hysterectomy in the infantile rat on the state of the adult ovary Endocr., 34 135–136.

Siegmund, H. 1934 Ovarialfunktion nach Uterusexstirpation. Arch. Gynäk., 157 223–226.

——— 1935 Vom Schonen der Ovarialfunktion nach Uterusexstirpation. Arch. Gynäk., 163 155–163.

Silbiger M. and I. Rothchild 1963 The influence of the uterus on the corpus luteum pituitary relationship in the rat. Acta Endocr., *43:* 521–538

Speert, H. 1942 Non-effect of hysterectomy upon the mammary gland of the monkey Endocr., *31:* 97–99

Spies, H., H. Gier and J Wheat 1961 Ovarian changes in hormone-treated hysterectomized and cycling guinea pigs. J Animal Sci., *20:* 979

Spies, H. G., D R. Zimmerman H. L. Self and L. E. Casida 1960 Effect of exogenous progesterone on the corpora lutea of hysterectomized gilts. J Animal Sci., *19:* 101–108.

Tamis, A. B 1934 Menopausal symptoms and ovarian *function following hysterectomy* Am. J Obst. Gyn. *28:* 48–60

Tenney B., F Parker Jr and S. Robbins 1955 The effect of hysterectomy in ovarian function in the rabbit. Am. J Obst. Gyn. *70:* 889–893.

——— 1958 Experimental evidence for the existence of a uterine hormone. Am. J Obst. Gyn., *75:* 858–862.

Unterberger F 1930 Experimentelle Untersuchungen über die Tätigkeit der Eierstöcke nach Uterusextirpation. Zentrblt. Gynäk., *54:* 655–656.

Van Wagenen G., and H. R. Catchpole 1941 Hysterectomy and ovarian function in the monkey (*M mulatta*) Proc. Soc. Exp Biol. Med., *46:* 580–582.

Velardo J T., A. B. Dawson, A. G Olsen and F L. Hisaw 1953 *Sequence of histological* changes in the uterus and vagina of the rat during prolongation of pseudopregnancy associated with the presence of deciduomata. Am. J Anat. 93 273–305.

Vineberg, H N 1915 What is the fate of the ovaries left *in situ* after hysterectomy? Surg. Gynec. Obst., 21: 559–567

Wiltbank, J N., and L. E. Casida 1956 Alteration of ovarian activity by hysterectomy J. Animal Sci., *15:* 134–140.

Winter E. W 1932 Über das anatomische und functionelle Verhalten der Eierstöcke nach Uterusextirpation. Arch. Gynäk., 150: 609–611.

Zaczek, T 1963 Ovarian function after hysterectomy Am. J Obst. Gyn., *85:* 102–103.

Zsolnai, B., and K. Lapis 1961 Über die morphologischen Veränderungen in der nach Extirpation des Uterus bzw Endometriums zurückgelassenen Eierstöcken. Acta Chir Acad. Sci. Hung., 2: 335–348.

PLATE 1

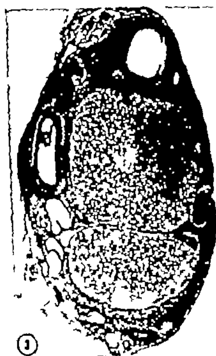
EXPLANATION OF FIGURES

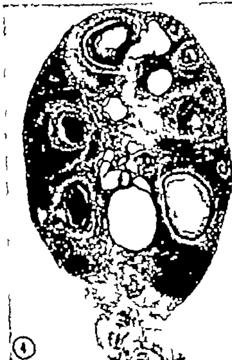
3 Left ovary from an animal of group C from which the left uterine horn was removed *showing persistent normal corpora lutea* after 28 days. This animal had not returned to estrus × 18.

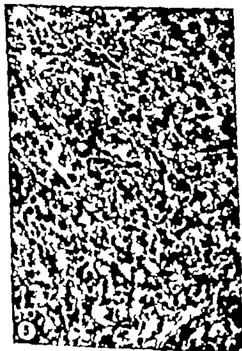
4 Right ovary from same animal as figure 3 *also removed at 28 days.* Note the complete absence of corpora lutea. × 18.

5 Left ovary of a group *IV animal autopsied 17 days after estrus.* The right horn and the cephalic half of the left horn was previously excised. Note the nuclear pyknosis and cytoplasmic vacuolization indicative of luteal regression. × 190

6 Right ovary from the same animal as figure 5 also removed at 17 days. The luteal cells show no signs of degeneration. × 190


3


4


5


6

Observations on the Fine Structure of Spermatozoa of the Bush Baby (*Galago senegalensis*), the African Green Monkey (*Cercopithecus aethiops*) and Man

J. M. BEDFORD

Department of Physiology, Royal Veterinary College, London, and The Worcester Foundation for Experimental Biology, Shrewsbury, Massachusetts

ABSTRACT A description is given of some fine structural features of mature spermatozoa from the bush baby (*Galago senegalensis*), the African green monkey (*Cercopithecus aethiops*) and man, with additional comments on sperm from the slow loris (*Nycticebus coucang*) and the crab-eating macaque (*Macaca irus*). The arrangement of the sperm organelles in these primates is similar to that demonstrated in the sperm of other mammals, but notable species differences do occur. The bush baby spermatozoon, for instance, displays a complex system of membranes which envelop the neck and anterior midpiece. The human spermatozoon, unlike that of many other mammals, has no subacrosomal space or "perforatorium." This structure is quite prominent, however, in lorisoid and macaque spermatozoa, and it is shown in the bush baby that its electron-dense material extends posteriorly from the apex of the head in the space between the inner acrosome and nuclear membranes. In electron microscope preparations of anthropoid spermatozoa, the cell membrane which overlies the acrosome cap only occasionally displays the swollen distorted form seen commonly here in the spermatozoa of prosimians, and previously in various other mammals.

In contrast to the uniform spermatozoa obtained from the lorisoid and macaque monkeys, a significant proportion of spermatozoa in the human samples examined showed many abnormal features including misshapen sperm nuclei, cystic formations in the rostral region of the acrosome cap, and irregular alignment of mitochondria in the neck and midpiece.

The advent of better methods of tissue preparation for electron microscopy in recent years has allowed critical examination of the fine structure of the sperm head in several species of eutheria (for reviews see Blom and Birch-Andersen, '65; Fawcett, '65; Hancock, '66). It has become apparent from such studies that although the form of the mammalian sperm may vary somewhat, the occurence and basic arrangement of its various organelles are similar in widely different species. Typically the sperm head consists of a highly condensed elongate nucleus, the rostral surface of which is covered by the acrosome cap, a membrane limited sack moulded to the nuclear surface and filled with a homogeneous material. It seems likely that this acrosomal material is enzymic in nature and may well be instrumental in allowing passage of the sperm through the zona pellucida (Srivastava, Hartree and Adams, '65). Posterior to the acrosome cap the nucleus is covered by a more diffuse material limited internally by the nuclear membrane, and externally by the plasma membrane of the sperm head. Although bound closely to this material in the posterior region of the head, the plasma membrane appears to be only loosely adherent to the underlying acrosome cap in mature sperm (Bedford, '65). Beneath the apical and antero-lateral surface of the acrosome cap in the rabbit (Hadek, '63; Bedford, '64), rat (Piko and Tyler, '64), bull, ram and dog (Nicander and Bane, '66) lies a clearly delineated space which almost certainly corresponds to the rod-like perforatorium seen in rodent sperm with the light microscope (Clermont, Einberg, Leblond and Wagner, '55; Austin and Bishop, '58). This subacrosomal space is much less prominent, however, in sperm from the cat and horse (Nicander and Bane, '66) and has not been detected in

Present address: Department of Anatomy, Columbia College of Physicians and Surgeons, New York, New York 10032.
See note added in proof.

human spermatozoa. The subacrosomal space has been shown in many species to be occupied by amorphous electron-dense material (Nicander and Bane, '66) but such material is apparently often absent from this cavity in preparations of guinea pig (Fawcett '65) and bat sperm (Fawcett and Ito '65)

Although we now have a general picture of the components of the mammalian sperm head little is known of the fine structure of mature primate spermatozoa The formation of the acrosome cap in the human spermatid has been clearly described (Fawcett and Burgos, 55 Anberg, '57) but electron microscopic studies of whole-mount preparatons of mature human spermatozoa have revealed little structural detail and even with thin-sectioning techniques (Anberg 57 Schultz Larsen 58 Chrzanowski, '65) difficulties of specimen preparation have prevented clear visualization of ultrastructure and have sometimes led to misinterpretation. In the present study the fine structure of the sperm head and neck has been examined in spermatozoa from several different species of primate This report is mainly concerned with spermatozoa from the bush baby (Galago senegalensis) from the African green monkey (Cercopithecus aethiops) and from man with brief reference to those of the slow loris (Nycticebus coucang) and the crab-eating macaque (Macaca irus)

MATERIALS AND METHODS

Samples of spermatozoa were obtained from a fertile bush baby (*Galago senegalensis*) and from a slow loris (*Nycticebus coucang*) an African green monkey (*Cercopithecus aethiops*) and a crab-eating macaque (*Macaca irus*) by removal and incision of the cauda epididymidis The spermatozoa released from the tubules of the cauda were suspended in Hank s solution at 37°C. Ejaculated human spermatozoa were obtained from regular donors by masturbation. In all cases the spermatozoa were concentrated by centrifugation at 3 000 rpm for 15 minutes and were fixed in buffered osmium tetroxide with 5% sucrose added, for a period of two hours. The sperm pellets were then dehydrated in ascending concentrations of ethanol from 30-100% during one hour followed by immersion in acetone for one hour and were embedded in araldite. Thin sections stained with uranyl acetate and lead citrate were viewed in an electron microscope (RCA EMU 3F or Phillips 200).

OBSERVATIONS

Prosimii

Viewed from its dorsal aspect, the sperm head of the bush baby and slow loris appears oval in its shape. From the lateral aspect however the head is flattened to some degree and appears asymmetrical because of an acrosomal flange or hook which projects from the rostral region of the head in the dorso-ventral plane (fig. 1) The anterior two-thirds of the nuclear surface is covered by the acrosome (fig. 2) The plasma membrane though remaining closely opposed in the postacrosomal region always appeared elevated away from the underlying acrosome when these sperm were fixed as free-swimming cells. It was particularly noticeable that sperm were sometimes adherent to cells or other sperm by the region of the plasma membrane which covers the acrosome cap likewise particulate surface debris was present on the sperm surface only over the supraacrosomal region of the plasma membrane (fig 2) Rostral to the apex of the nucleus in the bush baby and slow loris there lies a clearly defined subacrosomal space occupied by electron-dense material which extends caudally in the space between the inner border of the acrosome cap and the nuclear membrane (fig. 3) Although the subacrosomal space shown in figure 3 does not appear to be completely filled with this diffuse material this apical cavity was totally occupied in many sperm in the same preparation

In both the bush baby (fig 4) and slow loris the connecting piece and centriole of the neck region were commonly offset in a somewhat eccentric position with respect to the implantation fossa at the base of the nucleus A major difference in the fine structure of bush baby and slow loris sperm lies however in the neck region, which in the latter species often exhibits a modest scroll of evaginated nuclear membrane comparable with that in the bat

(Fawcett and Ito, '65). In bush baby sperm, on the other hand, there occurs an intricate system of membranes which extend caudally from the head-neck junction to surround the anterior part of the mitochondrial sheath (figs. 2, 4, 5, 8). This membrane complex is not merely a component of the cytoplasmic droplet, which migrates along the midpiece (fig. 2) leaving behind the membranes and tubules of the neck region. The examples shown in figures 4-8 suggest that the neck complex in the bush baby consists of membrane sheets interspersed by groups of tubules, which apparently are oriented at random. In figure 5 some tubular elements appear to pass into the cylinder of the centriole and also into the central region bounded by the columns of the connecting piece. Although the nuclear membrane can be seen to leave the surface of the nucleus at the points marked with arrows in figures 4 and 5 it seems unlikely that the whole complex shroud of membranes originates from extensions of the nuclear membrane. This point may be clarified by study of earlier stages in the development of these spermatozoa.

Anthropoidea

African green monkey (*Cercopithecus aethiops*). Electron microscope observations have been made also on the head of the spermatozoon from the crab-eating macaque (*Macaca irus*). The following description applies equally to the spermatozoon of this latter species, since it does not differ essentially in its fine structure from that of the African green monkey.

From its dorsal aspect, the symmetrical sperm head has an almost rounded appearance; the nucleus is flattened dorsoventrally and tapers throughout the region covered by the acrosome cap (fig. 8). The acrosome, which covers the anterior two-thirds of the nucleus, does not display the type of apical swelling seen commonly in rabbit and ungulate spermatozoa, but does exhibit the posterior equatorial constriction which is present in the sperm of several other mammals (Nicander and Bane '66). A well defined subacrosomal space filled with electron-dense material protrudes deeply into the thickness of the acrosome cap along its apical border (fig. 8). It has not proved possible to detect clearly any material in the narrow space between the inner acrosome and nuclear membranes. It should be noted, however, that this space is not interrupted by any definitive structure at the posterior border of the acrosome, and appears to be confluent with that occupied by diffuse material in the postacrosomal region of the sperm head (figs. 7, 8).

The plasma membrane appeared, typically, in close apposition to the material which lies in postacrosomal region of the sperm head (figs. 7, 8). Although in figure 8 the plasma membrane appears swollen away from the acrosome in the manner commonly observed in the spermatozoa of other eutheria, this type of membrane distortion was not typical of free macaque spermatozoa in which the plasma membrane generally remained moulded to the contour of the acrosome cap.

The neck region of the monkey sperm shows no unusual features. The connecting piece/centriole complex abuts against a thick basal plate set symmetrically in a relatively shallow implantation fossa (figs. 7, 8). Although a small membranous scroll formed by redundant nuclear envelope was sometimes present in the neck region, this was in no way comparable to the membrane complex in the neck region of bush baby spermatozoa.

In view of the comments on ejaculated human spermatozoa which follow it seems pertinent to mention that in phase and electron microscopic observations of the lorisoid and macaque sperm described above, no obviously abnormal sperm cells were noted.

Man

Contrary to some early descriptions of the anatomy of ejaculated human spermatozoa, the sperm nucleus can be seen to extend as far as the apex of the head (figs. 9–14). The nucleus is rather pear-shaped in lateral view but within the population of normal spermatozoa there occurs some variation in head shape which cannot be wholly accounted for by difference in the plane or angle of section (figs. 9-14.) In sections stained with uranyl acetate and lead, the nuclear material of most sperm heads appeared homogeneous and devoid

of any crystalline or granular organization on occasion however nuclei in the same sections presented a tesellated appearance (fig 14) faintly suggestive of incomplete chromatin condensation

As has been noted previously (see Fawcett '58) vacuoles occur commonly in the nucleus of mature human spermatozoa. In the present investigation these nuclear spaces appeared sometimes to be occupied by a sparse granular material of much lower density than that of the surrounding nucleus (fig 11)

The acrosome cap of the human spermatozoon covers rather more than two-thirds of the surface of the nucleus and with the exception of a definite posterior constriction apparent in figures 10 11 12 and 14 is remarkably uniform in its thickness There was no increase in the relative electron-density of the acrosomal material within the constricted posterior region of the cap as has been claimed by Nicander and Bane ('66) in the sperm of certain other species In contrast to the macaque and prosimian spermatozoa examined the human sperm cell does not possess a definitive subacrosomal space or "apical body" and neither is there any concentration of electron-dense material at the apex of the head between the inner acrosome and nuclear membranes (figs 9–14) In suitably preserved specimens however it is possible to detect some material lodged between the plasma and nuclear membranes in the postacrosomal region of the head (fig 10 inset 13 14) As in most macaque spermatozoa (see above) the plasma membrane of ejaculated human spermatozoa was usually apposed often closely to the underlying acrosome for this reason the swollen supra-acrosomal membrane seen in figure 14 should be considered as an exception to the normal disposition of this membrane in thin sections of human spermatozoa. Several types of gross abnormality of the sperm head have been well documented with the light microscope (Williams '64) and examples of some of these have been seen in the electron microscope in the present study With the exception of a few sperm which displayed cysts at the apex of the acrosome most of the more extreme variations in head shape were due to malformation of the nucleus rather than the acrosome cap

The anatomy of the neck region does not differ basically from that depicted by Anberg ('57) The head and neck regions of the human spermatozoon are apposed over an almost flat surface and there is no evidence of a true implantation fossa at the base of the nucleus such as occurs, for instance in the boar (Nicander and Bane, ('62) bull (Blom and Birch-Andersen '65) and bat (Fawcett and Ito '65) The nuclear envelope along the posterior border of the nucleus always appeared particularly dense and sharply outlined in a way suggestive of some modification of its nature in this junctional zone between head and neck (figs 14-18) On three occasions in sections through the center of the human sperm head a small knob-like projection apparently deriving from nuclear envelope, could be seen to intrude through the basal plate (fig 15) however this projection may possibly have been an artefact of preparation When viewed from the dorsoventral aspect the centriole of the human sperm appears to be set at right angles to the long axis of the sperm and not at 45° as in many other mammals this difference can probably be attributed to the absence in human sperm of an implantation fossa, and consequent horizontal apposition of the connecting piece/centriole complex with the posterior border of the head. Attention is drawn particularly to figure 17 in this sperm elements can be seen to emanate from the centriole which are reminiscent of the microtubules found in a variety of tissues and particularly in association with centrioles and their satellites (Porter '65)

The neck region of many ejaculated human sperm commonly displayed residual cytoplasmic elements which according to Williams ('64) should not necessarily be regarded as a pathological feature The elements of this remnant can be seen as small vesicles either rounded or flattened in figures 15 16 and 18 The most rostrally placed mitochondria lie in close apposition to the segmented columns of the connecting piece from which originate the outer longitudinal fibers of the midpiece In contrast to the orderly arrangement of the mitochondria in the sperm of other species

which have been studied with the electron microscope, displacement of mitochondria, either singly or in clusters was apparent in a significant proportion of the spermatozoa in the human ejaculates examined (figures 16 17 18)

DISCUSSION

The present observations indicate that, in general, the fine structure of spermatozoa from monkeys and man is similar to that of the spermatozoa of other mammals studied. There are, nevertheless, marked species differences in certain aspects of sperm structure, within the primate group. For example, in both the bush baby and the slow loris the acrosome cap displays a rostral flange or hook (figs. 1 2) which is not present in tupaioid spermatozoa or in sperm from any of six different species of anthropoid monkey observed by the author Rather surprisingly perhaps, the striking membrane complex which envelops the neck and upper midpiece of bush baby spermatozoa (figs. 2, 4 6) does not appear to be present in the related slow loris. It is not possible at present to offer any suggestion as to the likely function of this neck membrane complex in the spermatozoa of the bush baby

Unlike human spermatozoa, those of both lorisoid and macaque monkeys possess a distinct apical subacrosomal space comparable to that described in several other mammals (Nicander and Bane '66) Contrary to suggestions derived from studies of rodent sperm with the light microscope (Clermont et al., '55 Austin and Bishop '58) or as whole mounts in the electron microscope (Clermont et al., '55) figure 3 shows that the subacrosomal space, the homologue of the rodent perforatorium, is not a rostral extension of the nuclear membrane. The material of this apical structure lies within the space bounded by the inner membrane of the acrosome cap and the nuclear surface, and extends caudally between these structures. From the standpoint of current efforts to elucidate the functional significance of the various organelles of the mammalian sperm head, the most interesting feature of human sperm lies in the absence of any structure comparable to the subacrosomal space or perforatorium. The appearance and anatomical location of this feature in rodent sperm and to a lesser extent in the sperm of other mammals, is highly suggestive. Yet if one assumes that at fertilization there occurs a series or pattern of physiological events common to all mammals its absence in the sperm of man would seem to bring into question the functional importance of a localized accumulation of subacrosomal material at the apex of the nucleus.

Although the classical "post-nuclear cap" is relatively inconspicuous in the human sperm, there nevertheless appears to be diffuse material in this region which extends forward beneath the acrosome cap and external to the nuclear envelope (fig 10) Bearing in mind the absence of any definitive barrier at the junction of the acrosome cap with the postacrosomal region of the head (figs. 8 10) it is quite possible that the subacrosomal layer of amorphous material may be confluent with the material which lies between the nuclear envelope and plasma membrane in the postacrosomal region. If this is so the sperm nucleus may be thought of as being invested over most of its surface by a layer of material which tends to accumulate at the apex (except in man) and also over the postacrosomal region of the nucleus.

The existence of an acrosome cap in human spermatozoa has often been debated; quite probably it has been the relatively discrete proportions of this organelle which have contributed largely to the doubts as to its presence. The claim by Chrzanowski ('65) that the human acrosome cap fuses at its posterior border with the nuclear membrane is incorrect, and it is clear that the relationships of the acrosome cap in human sperm are similar to those in other mammals. Nicander and Bane ('66) have suggested that the type of posterior acrosomal constriction evident in figures 9 10 11 and 14, may well be responsible for the appearance of an "equatorial segment" in many mammalian sperm viewed in the light microscope. An equatorial segment does not appear clearly in human sperm in the light microscope, but this apparently conflicting point may possibly be explained by the reasoning of Nicander and Bane ('66) in the case of horse and cat sperm, that in these species

the relatively thick sperm nucleus may mask the visual effects of a relatively thinner acrosomal cap in the dense mid nuclear region. In contra-distinction to the claim of these latter authors no evidence has been obtained to indicate that in uniformly stained sections there is a relative concentration of the material in the constricted posterior zone of the acrosome cap in any of the primates or several other mammals examined in this laboratory

The well known morphological heterogeneity of spermatozoa in ejaculates from fertile men (Williams 64; MacLeod and Gold 51) stands in striking contrast to the relatively uniform morphology of sperm populations from the other primates examined in this study and in ejaculates from laboratory and domestic animals The question as to what constitutes a morphologically "normal" human spermatozoon has been raised on several occasions and has not yet been answered satisfactorily In this present context, it was of considerable interest to observe that apart from grossly abnormal sperm cells there occurred a subtle range of variation in shape of the nucleus in what might be considered as "normal" sperm heads The origin of the types of fine structural abnormality noticed most commonly in human spermatozoa, i e mitochondrial displacement, extreme variation in nuclear shape and occasional cyst formation at the apex of the acrosome, lie probably at the testicular rather than the epididymal level Less obvious imperfections which probably also arise at the testicular level are the intra nuclear vacuoles or cavities (fig 11) and occasionally the mottled texture of the nucleus somewhat suggestive of incomplete chromatin condensation (fig 14) The latter feature noted in previous studies of human spermatozoa (Anberg 57 Schultz Larsen '58) has not been noted in the sperm of other mammals Although vacuoles were occasionally present in the rostral half of the nucleus in some of the human sperm studied in no case was an open apical cavity of the type shown by Schultz Larsen ('58) observed. This acrosome-filled cavity is included in diagrammatic representations of the structure of the human sperm by Schultz Larsen ('58) and later by Williams ('64) From the present observations and those of other workers (Fawcett and Burgos '56; Anberg '57), it seems unlikely however that this apical acrosome-filled vacuole can be regarded as a normal feature of the sperm head in man

ACKNOWLEDGMENTS

My thanks are due to Professor E. C. Amoroso F.R.S for providing the monkeys used in this investigation I wish, also, to express my gratitude to Dr L. F Carazos Department of Anatomy Tufts Medical School for his generosity in making the facilities of his department available to me during part of this study This work has been supported in part by NIH grant HD-01476-06 and also by NIH grant HD-03472 awarded to Dr M. C. Chang

LITERATURE CITED

Anberg, A. 1957 The ultrastructure of the human spermatozoon. Acta Obst. Gyn. Scand. 36 Suppl. 2, 1

Austin C. R., and M. W H. Bishop 1958 Some features of the acrosome and perforatorium in mammalian spermatozoa. Proc. Roy Soc. (London) Ser B *148*: 234

Bedford J M. 1964 Fine structure of the sperm head in ejaculate and uterine spermatozoa of the rabbit. J Reprod. Fert., *7*: 221.

——— 1965 Changes in the fine structure of the rabbit sperm head during passage through the epididymis. J Anat., *99*: 891

Blom, E., and A. Birch Andersen 1965 The ultrastructure of the bull sperm. II. The sperm head. Nord Vet., *17*: 193.

Chrzanowski, S. 1965 The ultrastructure of human spermatozoa. Ginek. Polska, 36 517

Clermont, Y., E. Einberg, C. P Leblond and S. Wagner 1955 The perforatorium—an extension of the nuclear membrane of the rat spermatozoon. Anat. Rec., *121*: 1

Fawcett D W 1958 The structure of the mammalian spermatozoon. Intern. Rev Cytol., *7*: 195.

——— 1965 The anatomy of the mammalian spermatozoon with particular reference to the guinea pig Z. Zellforsch., *67*: 279.

Fawcett, D W., and M. H. Burgos 1956 Observations on the cytomorphosis of the germinal and interstitial cells of the human testis. Ciba Colloq on Aging, Churchill, Vol. 2, P 86.

Fawcett, D W., and S. Ito 1965 The fine structure of bat spermatozoa. Am J Anat. 116 567

Hadek, R. 1963 Study on the fine structure of the rabbit sperm head. J Ultrastruct. Res., *9* 110.

Hancock, J L. 1966 The ultrastructure of mammalian spermatozoa. In Advances in Reproductive Physiology Academic Press, P 125.

MacLeod, J., and R. Z. Gold 1951 The male factor in fertility and infertility IV Sperm

morphology in fertile and infertile marriage. Fertil. and Steril., 2: 394.

Nicander L., and A. Bane 1962 Fine structure of boar spermatozoa. Z. Zellforsch., 57: 390.

——— 1966 Fine structure of the sperm head in some mammals, with particular reference to the acrosome and the subacrosomal substance. Z. Zellforsch., 72: 496.

Piko, L., and A. Tyler 1964 Fine structural studies of sperm penetration in the rat. Proc. Fifth Intern. Congr. Animal Reprod., Trento, Vol. II, P 372.

Porter, K. R. 1966 Cytoplasmic microtubules and their functions. In: Principles of Biomolecular Organization. Ciba Found. Symp., Wolstenholme and O'Connor eds. Churchill, P 308.

Schultz-Larsen, J 1958 The morphology of the human sperm. Acta Path. Microbiol. Scand. Suppl., P 128.

Srivastava, P N., C. E. Adams and E. F Hartree 1965 Enzymic action of acrosomal preparations in the rabbit ovum, in vitro. J Reprod. Fertil., 10: 61.

Williams, W W 1964 Sterility Published by the author Springfield, Mass.

Note added in proof Recent unpublished electron microscope observations of fertilization in the rabbit, have shown that the outer membrane and content of the acrosome is lost before penetration of the zona substance begins. It is now assumed, therefore, that the zona lysin is associated with the persistent inner membrane of the acrosome cap.

Abbreviations

a acrosome cap
b basal plate
c, connecting piece
cc centriole
cv cytoplasmic vesicle
d cytoplasmic droplet
e constricted posterior region of acrosome cap
m, mitochondrion
n, nucleus
nm, nuclear envelope
p plasma membrane
s, electron-dense material of the subacrosomal space
t, possible microtubules
v vacuole in the sperm nucleus

PLATE 1

EXPLANATION OF FIGURES

All electron micrographs stained with uranyl acetate and lead citrate.

1 Sperm from vas deferens of the slow loris. Note the hooked apical extension of the acrosome cap Phase contrast × 1 710.

2 Central sagittal section of sperm from the vas deferens of the bush baby Note that only that region of the plasma membrane overlying the acrosome cap is attractive to particulate debris (arrowed) in the medium. The neck and anterior midpiece are enveloped by a complex system of membranes and tubules which remain after the cytoplasmic droplet (d) has migrated along the midpiece × 19,800.

3 Sagittal section of the apical region of the bush baby sperm head. The subacrosomal space(s) is almost filled by diffuse material which extends posteriorly (arrowed) in the space between the nucleus (n) and the inner limiting membrane of the acrosome cap (a) × 109,800.


2
3
S
d
1

Abbreviations

a acrosome cap
b, basal plate
c, connecting piece
cc centriole
cv cytoplasmic vesicle
d cytoplasmic droplet
e constricted posterior region of acrosome cap
m, mitochondrion
n nucleus
nm nuclear envelope
p plasma membrane
s, electron-dense material of the subacrosomal space
t, possible microtubules
v vacuole in the sperm nucleus

PLATE 1

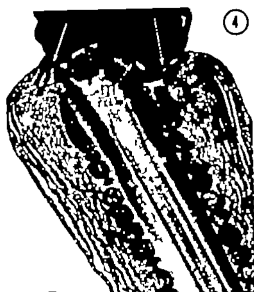
EXPLANATION OF FIGURES

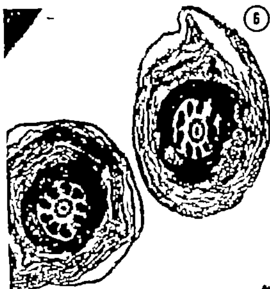
All electron micrographs stained with uranyl acetate and lead citrate.

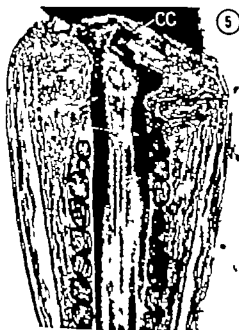
1 Sperm from vas deferens of the slow loris. Note the hooked apical ex tension of the acrosome cap. Phase contrast × 1 710.

2 Central sagittal section of sperm from the vas deferens of the bush baby Note that only that region of the plasma membrane overlying the acrosome cap is attractive to particulate debris (arrowed) in the medium. The neck and anterior midpiece are enveloped by a complex system of membranes and tubules which remain after the cytoplasmic droplet (d) has migrated along the midpiece × 19,800.

3 Sagittal section of the apical region of the bush baby sperm head. The subacrosomal space(s) is almost filled by diffuse material which extends posteriorly (arrowed) in the space between the nucleus (n) and the inner limiting membrane of the acrosome cap (a) × 109,800.


4


6


CC
5

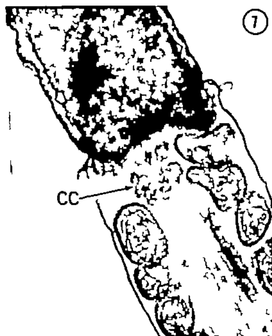

7
CC

PLATE 2

EXPLANATION OF FIGURES

4 Higher magnification of the neck region of the sperm in figure 2. The perimitochondrial complex consists of tubules and apparently of membrane sheets which intermingle in a random way; the nuclear envelope leaves the nucleus at its lateral borders (arrowed) but there is no clear evidence that this becomes continuous with the membrane complex. The base of the sperm head is set asymmetrically upon the connecting-piece/centriole complex; note that the initial mitochondrion (m) is interposed between the basal plate and the segmented column of the connecting piece × 29,640

5 Neck region of bush baby sperm. Elements of the tubulomembrane complex can be seen lying within the centriole cylinder (ce) and between the columns of the connecting piece (c) × 29,640

6 Transverse sections through the midpiece region of the bush baby sperm tail. The tubulomembrane complex is in close proximity to and entirely envelops the mitochondrial sheath. The tail fibers show the 9 + 9 + 2 arrangement seen typically in the midpiece region. × 25 740

7 Sagittal section of the neck of the sperm of the African green monkey The plasma membrane is clearly continuous at the junction between the head and tail. Mitochondria are positioned at the level of the centriole (c) which is seen in transverse section Hollow arrows indicate the diffuse material which occupies the space between plasma and nuclear membranes in the postacrosomal region × 39,780.

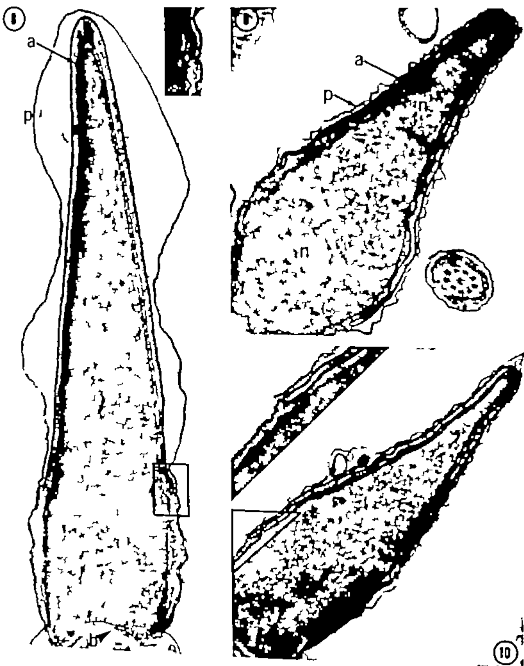

8
a
p
b
9
a
p
n
n
10

PLATE 3

EXPLANATION OF FIGURES

8 Central sagittal section of the head of the sperm of the African green monkey Note that the subacrosomal space at the apex of the nucleus is filled with electron-dense material. There is no definitive barrier at the posterior border of the acrosome between the subacrosomal and postacrosomal space (see inset) × 36,250

9–14 Central or paracentral sagittal sections of sperm heads in the human ejaculate.

9 The nucleus appears rather pear-shaped in lateral view Note the absence of an apical subacrosomal space × 24 750.

10 Diffuse material is present in the postacrosomal space beneath the acrosome cap Note the relatively slender appearance of this sperm head and the abrupt constriction of the acrosome cap towards its posterior border × 24 750.

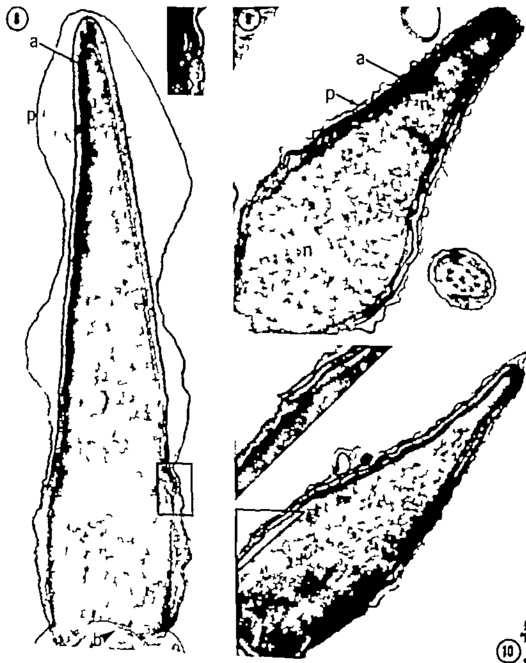

8
a
p
b
a
p
n
n
10

PLATE 3

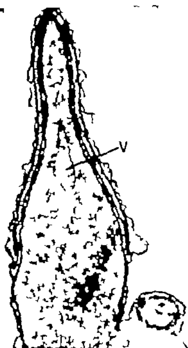
EXPLANATION OF FIGURES

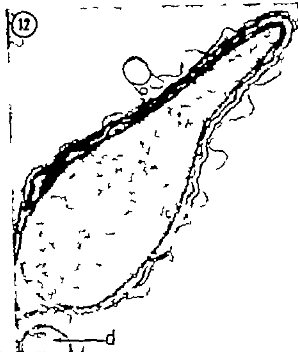
8 Central sagittal section of the head of the sperm of the African *green monkey* *Note that the subacrosomal space at the apex of the nucleus is filled with electron-dense material.* There is no definitive barrier at the posterior border of the acrosome between the subacrosomal and postacrosomal space (see inset) × 38,250

9–14 Central or paracentral sagittal sections of sperm heads in the human ejaculate

9 The nucleus appears rather pear-shaped in lateral view Note the absence of an apical subacrosomal space × 24 750

10 Diffuse material is present in the postacrosomal space beneath the acrosome cap *Note the relatively slender appearance of this sperm* head and the abrupt constriction of the acrosome cap towards its posterior border × 24 750


11
v


12
d


13

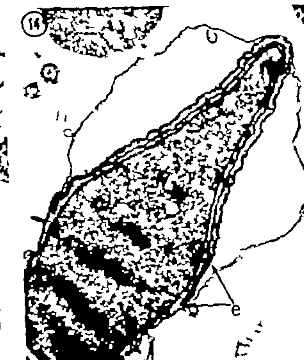

14
e

PLATE 4

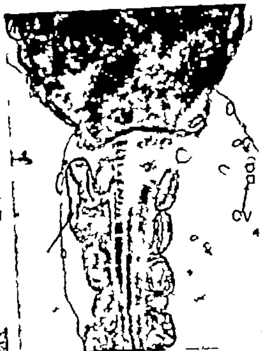
EXPLANATION OF FIGURES

11 Note the nuclear vacuole (v) which appears to be occupied by granular material of low density The acrosome cap becomes abruptly constricted in its posterior region × 24 000

12, 13 Sections of human sperm which give no indication of a defined apical subacrosomal space A nuclear vacuole is apparent in figure 13 × 24,000

14 The nucleus shows a tessellated or patchy appearance suggestive of incomplete condensation. The swollen disposition of the plasma membrane seen here occurs commonly in electron micrographs of the sperm of many mammals, but is not typical of mature human spermatozoa This sperm head clearly demonstrates the constricted posterior region (c) of the acrosome cap × 24 750.


15
nm
cv


cv


17
cc
c


18
cv

PLATE 5

EXPLANATION OF FIGURES

15–18 Neck region of the human spermatozoon.

15 The nuclear envelope appears densely stained over the base of the nucleus. The "knob" at its center may possibly be an artifact of preparation. × 78,260

16 Note the obvious cytoplasmic remnant in the neck region. One of the mitochondria (arrowed) is not aligned with the remainder. × 36,400

17 This sperm also shows one nonaligned mitochondrion (arrowed). Microtubules (t) appear to originate from the centriole (co). × 36 400

18 This sperm displays a cytoplasmic remnant which contains flattened and tubular vesicles (cv). Mitochondria of abnormal size (arrowed) have become bunched at one point along the midpiece. × 36 400

The Fine Structure of Neurons and Satellite Cells in the Trigeminal Ganglion of Cat and Monkey [1,2]

ANSELMO PINEDA, DAVID S. MAXWELL AND LAWRENCE KRUGER

Long Beach Veterans Administration Hospital and the Department of Anatomy and Brain Research Institute UCLA School of Medicine Los Angeles, California

ABSTRACT Neurons and satellite cells in the trigeminal ganglion of cats and monkeys fixed by aldehyde perfusion were examined in the electron microscope. The fixative employed and its tonicity appear to be critical factors in accounting for some of the differences noted in earlier descriptions. With satisfactory preservation, only one variety of neuron is seen on the basis of cytoplasmic and nuclear features, although there is a substantial size range. Interdigitating processes of neurons into the satellite cell capsule probably accounts for the axon terminals and intracapsular nerve nets reported in early metallic impregnation studies. Axonal glomeruli are encased in satellite cells and become myelinated by Schwann cells as the axon leaves the region of the neuron soma.

Satellite cells reveal layers of attenuated processes forming unusual membrane complexes around the axons. The external surfaces of the satellite cells are completely invested with prominent basal lamina, which is continuous with that surrounding the Schwann cell at the first "internode."

Sensory ganglion cells constitute one of the best understood models of neuronal structure and have been examined by innumerable investigators in the past century The characteristics of trigeminal ganglion cells and their surrounding cellular elements have been described primarily on the basis of methylene blue and chromate metallic impregnations (Ehrlich, 1886 Dogiel, 1896; Ramón y Cajal, '07 Castro, '32) The ganglion cells were shown to possess a single axon arranged in an intracapsular glomerulus. Essentially one type of capsular cell was originally described with silver impregnation techniques (Río-Hortega, Polak and Prado 42) but recent workers have extended the classification of satellite cells (Scharenberg, '52 Ortiz-Picón, '55)

The introduction of electron microscopy and gradual methodological improvement in preservation of nervous tissue suitable for fine structural analysis has provided means for reappraisal of some of the problems posed in classical microscopy Several studies have dealt with the fine structure of spinal ganglia in a variety of animals (Beams et al., '52; Hossack and Wyburn '54; Hess '55; Dawson, Hossack and Wyburn, '55; Wyburn, '58; Cervós-Navarro '59 '60; Rosenbluth '62a, Rosenbluth and Palay '60 Andres '61; Kotani and Kawashima, '61 Hiroaka and van Breeman, '63; Tennyson, '65) The trigeminal ganglion has also been recently described in several species (Dixon, '63a,b Moses, Beaver and Ganote '65; Beaver Moses and Ganote '65) The organelles of ganglion and satellite cells have largely been identified, and some experimental evidence has been adduced to distinguish lipofuscin and neuromelanin pigments (Moses, Beaver and Ganote '65 Beaver Moses and Ganote, '65)

The present study deals with the fine structure of the trigeminal ganglion observed in aldehyde-perfused material. The trigeminal was chosen because of the large size of ganglion cells and axons as well as the high proportion of myelinated fibers. The present description of the normal ganglion is presented in order to provide a baseline for studies in progress on neuron chromatolysis and Wallerian axonal degeneration after rhizotomy

Findings with the present method of tissue preservation indicate a reappraisal of the classification of ganglion cells neuron-satellite relations the question of an intracapsular axonal plexus, and the possibility of different types of satellite cells. A pre-

[1] Supported by U.S.P.H.S. grants NB [illegible] and NB [illegible].

[2] The technical assistance of Mrs. Olga [illegible] and Mrs. [illegible] is gratefully acknowledged.

branes, each cluster composed of several pairs of lamellae or chains of vesicles (fig. 3) with coated vesicles" often found near by The rough endoplasmic reticulum is not uniformly dispersed throughout the cytoplasm, but is principally clustered into Nissl bodies (figs. 3, 7 8, 10) along with rosettes of ribosomes (figs. 3, 4, 5 9 10) As in other neurons, microtubules of about 200 Å units diameter and fine neurofila ments, form small bundles which swirl through the cytoplasm between the Nissl bodies (figs. 3–5) A few glycogen-like granules can be identified in neuronal cytoplasm and in the axon (figs. 6 12) Some restricted areas of cytoplasm display ac cumulations of dense inclusions (figs. 1 3, 10) These probably correspond, for the most part, to lipofuscin or other pigment (melanin) granules of light microscopy Oil blue N and diamine silver oxide have recently been shown to respectively stain these organelles in trigeminal neurons (Moses, Beaver and Ganote '65) The most common form of these inclusions is an irregularly shaped electron-opaque structure, homogeneous in texture, except for a "bubble" or "blister" These electron transparent areas are presumed to have contained a lipid which was extracted dur ing preparation of the tissue. Associated with these inclusion bodies are other less electron-opaque organelles displaying internal structure (fig. 3) These may be granular or laminated in texture and occasionally display clear vacuoles similar to that seen in lipofuscin bodies. Our tentative interpretation is that the less electron-opaque organelles may be lysosomes at various stages in the formation of lipofuscin residual bodies (Gordon Miller and Bensch, '65)

The ganglion cells display a wide range of sizes but, in our material, after satisfactory preservation with aldehyde perfusion methods the matrix density of the cytoplasm is relatively uniform from cell to cell (fig. 1) We therefore find no basis for classifying ganglion cells into light and dark groups (Castro, '32; Blair Bacsich and Davies, '36 Bacsich and Wyburn, '33; Hossack and Wyburn, '54; Andres '61; Kotani and Kawashima '61) with the present methods of tissue preservation. Electron-microscopically we have similarly failed to find a basis for such classification.

The ganglion cell surface is commonly found to be thrown into folds or villous-like surface evaginations (figs. 2 4 5 6) These evaginations interdigitate with the processes of satellite cells. Such evaginations are more extensively developed in monkey than in cat ganglion, and it is our impression that, in the monkey the larger cells display a more extensively developed surface redundancy than the smaller The evaginations tend to be larger and more prominent near the origin of the axon (fig. 6) These processes" of the neuronal perikaryon are probably the structural basis for the descriptions in older light microscopic literature based on metallic impregnations of "*dendrites*" or of intracapsular nerve nets

A single axon arises from the soma, but there are no cytoplasmic features which *distinguish* axoplasm from somatoplasm at this point, although in agreement with some published figures of the axon origin (*Wyburn*, '38) we have not observed Nissl bodies in this region. The axon is invested with satellite cells and, near the soma, may display numerous evaginations similar to (although generally larger than) those found on the surface of the soma (fig. 6) Light microscopic study of metal-impregnated trigeminal ganglion cells reveals the frequent occurrence of axonal glomeruli (Ramón y Cajal, '07) especially in association with larger ganglion cells. The axon and its investing satellite cells *form* a tangled skein around the ganglion cell. Such an arrangement probably accounts for the presence of several axon profiles in different orientations around the ganglion cells (figs. 1 2, 7 8) This arrangement *probably* also is the basis for the rare occurrence of an appreciable length of longitudinally sectioned initial (unmyelinated) segment The axon contains only mitochondria longitudinally oriented neurofilaments and microtubules (figs. 6, 11 12, 13) and occasional dense bodies of about the same size as mitochondria. The dense bodies exhibit some internal structure and tend to accumulate at the first "node" and subsequently at nodes of Ranvier along the myelinated portion of the axon (fig. 13) On the basis of their internal structure

liminary account of some of these findings has been presented elsewhere (Pineda '66)

MATERIALS AND METHODS

Adult monkeys (3 *Macaca mulatta* and 1 *Macaca speciosa*) and two adult cats were used in the present study The animals were anesthetized with sodium pentobarbital and a tracheal cannula inserted The cannula was connected to bottled gas providing a mixture consisting of 10% carbon dioxide 20% oxygen and 70% nitrogen. In the cats the chest was opened widely and, in the monkeys the abdominal wall was opened along the costal margin and the thorax entered through the diaphragm. The pericardium was incised while the animal was artificially respired. The right atrium was opened widely and an incision was made in the left ventricle near the apex of the heart. A cannula approximately one-half the diameter of the aorta was inserted through the ventricular incision up to the base of the aorta. The cannula was connected to a supply of fixative at room temperature under pressure provided by a compressed air line. The pressure was maintained initially at a predetermined value (300 mm Hg for one monkey 200 to 250 mm Hg for the others and 180 mm Hg for the cats) The perfusion was begun as soon as the cannula was inserted into the heart. In all cases the animals were respired and the tissue color was pink at the time of beginning the perfusion The monkeys were perfused at a rate of approximately 1 5 liters per minute and the cats at a rate of 0 5–1 0 liter per minute for the first minute. The perfusion pressures were then gradually lowered and adjusted to maintain a flow of approximately 0 1–0 2 liter per minute for the monkeys and 0 1 liter per minute for the cats for from 5–7 minutes. The perfusion was then stopped and the tissue excised for immersion in buffered OsO

The fixative employed was maintained at pH 7.2–7 35 with cacodylate-HCl buffer (sodium cacodylate dimethyl sodium arsenate) One cat and one monkey were perfused with fixative in 0 15 M cacodylate (290 milliosmols); the rest of the animals were perfused with fixative in 0 1 M buffer (215 milliosmols) This variation of buffer concentration was employed as a means of varying the tonicity of the perfusate In all cases the buffer solution contained 1% formaldehyde (after Pease, '64) 2% glutaraldehyde (Fisher biological grade) and 0 01% $CaCl_2$. The final osmolarity equalled respectively about 1270 and 1350 milliosmols for the 0 1 M and 0 15 M buffers with fixative and $CaCl_2$ added. Two hours of post fixation was accomplished in 1% OsO_4 with the same buffer concentration as the perfusate and containing 0.01% $CaCl_2$. The tissue was then rapidly dehydrated in graded ethanol, and embedded in Araldite (Ciba) Thick sections (one half micron) were cut to locate the ganglion cells and then thin sections for electron microscopy were cut, stained with lead citrate (Venable and Coggeshall, '65) and then examined and photographed in either the RCA EMU 3-E or the Hitachi HU-11A electron microscopes.

RESULTS

Ganglion cells One-half micron sections of tissue prepared for electron microscopy but stained and studied with the light microscope have proven useful for studying the organization of the ganglion (figs 1 2) The ganglion cells are completely invested with a capsule of satellite cells, and commonly by an axonal glomerulus. The nuclear regions of the satellite cells may indent the profile of the ganglion cells, but in these preparations, the distinction is easily made between satellite cell and ganglion cell on the basis of cytoplasmic density

The nucleus of neurons in the trigeminal ganglion displays evenly dispersed chromatin following aldehyde perfusion fixation (fig 1) although chromatin clumping has been observed with other fixatives (Hess '55 Andres '61 Hiroaka and van Breeman '63) The nuclear envelope is conspicuous and interrupted occasionally by nuclear pores. The outer leaflet of the envelope is irregularly studded with ribonucleoprotein particles (ribosomes) and the cleft is often seen to be continuous with the channels of the rough endoplasmic reticulum as in other tissues Mitochondria are abundant tend to be elongated, and commonly contain a dense matrix (fig 3) The Golgi apparatus consists of numerous clusters of smooth mem-

membranes are adjacent to one another and form a faint line (fig. 11) In such regions (figs. 11 13) the membrane arrangement superficially resembles compact myelin. However the approximated membranes combine to form an intermediate line of less density than the external surfaces of the plasma membranes, and no intermediate lines appear between adjacent processes (fig. 11) The areas of "compact myelin on the ganglion cell or on the initial segment, are similar in appearance and formation to the more extensive areas found on the ganglion cells of the eighth nerve (Rosenbluth, '62b) and ciliary ganglion (Hess, '65) and presumably are formed in the same manner. The basal lamina of the satellite cell is continuous with that investing the myelin of the first "internode (fig. 13) In this respect the first node is similar to those elsewhere in peripheral nerve, except that on the neuronal side of this "node the axonal investment is a satellite cell, not a Schwann cell and myelin.

DISCUSSION

The classification of sensory ganglion cells into sub-types on the basis of cytoplasmic characteristics has been proposed by numerous authors (Hossack and Wyburn '54; Dawson et al. '55; Hess '55 Cervós-Navarro '59; Andres, '61; Kotani and Kawasima, '61; Rosenbluth, '62a; Dixon, '63; Tennyson, '65) These authors recognized large light cells with aggregated endoplasmic reticulum (Nissl bodies) separated by filaments, and small dark cells with diffuse endoplasmic reticulum and few filaments. A similar difference has long been known in light microscopy (Blair Bacsich and Davies, '36) and evidence has been adduced to show an extensive glomerular axon associated with the large "light cells (Ramón y Cajal, '09 Andres, '61) and a multiangular appearance in the small "dark cells suggestive of artifact (Bacsich and Wyburn, '53) The present study based upon aldehyde perfused material and discounting possible special differences, would appear to provide little support for the clear division of cell types observed with other methods of fixation, although it is possible that material less than optimally preserved might display more "dark" neurons. The distinction based on quantity of aggregated endoplasmic reticulum and filaments would appear unwarranted, since the observed distribution of organelles is what might be expected in cells of different sizes. It seems likely (although difficult to demonstrate) that the larger neurons possess a more extensive glomerular axon. The functional significance of the increased length of the "unipolar" axons commonly observed in the trigeminal ganglion remains remarkably obscure.

The relationship between the ganglion cell surface and its surrounding satellite cells has been studied extensively and there have been some discrepancies concerning the arrangement at the neuronal surface (Hossack and Wyburn, '54; Hess, '55; Wyburn, '58; Cervós-Navarro '60 Pannese, '60; Rosenbluth and Palay '60; Andres '61 Kotani and Kawashima, 61 Rosenbluth, '62a, Dixon, '63; Beaver Moses and Ganote '65 Moses Beaver and Ganote '65 Tennyson, '65) Although virtually all workers have observed some interdigitation between neuronal and satellite processes, some have reported smooth contours (Hossack and Wyburn, '54 Dixon, '63a) or that the neuronal surface does not display irregularities, but short neuronal processes frequently thrust into the inner zone of the capsule (Rosenbluth and Palay '60) The essential problem is concerned with the recognition of the intracapsular axonal plexus observed in light microscopy with methylene blue and reduced silver methods (Ehrlich, 1886 Dogiel, 1896; Ramón y Cajal, '07 Scharf '54) The consistent preservation of oriented filaments and microtubules in axons in aldehyde perfused material and the demonstration of neuronal processes which can often be traced as interdigitating villi or protuberances (figs. 5–8) and which lack the above axonal features provide a basis for serious doubt concerning the suggested intracapsular axonal network (Wyburn, '58 Rosenbluth and Palay '60) It may also be relevant to note that no one has yet reported vesicle-containing axon terminals or morphological signs of synaptic contacts in sensory ganglia, thus rendering it highly

and two limiting membranes they appear to be related to mitochondria and are similar in morphology (but do not occur in such concentration) to the altered mitochondria occurring in axons in the early stages of Wallerian degeneration (Webster 62) Small numbers of these are probably a normal occurrence in myelinated fibers. The initial segment resembles axoplasm elsewhere in peripheral nerve; it would seem inappropriate to attempt to draw any analogy between dendrites and these axons

Satellite cells The satellite cells invest the ganglion cell bodies and the unmyelinated segment of the axons (figs 1 2, 6 7) These cells display a moderate range of nuclear and cytoplasmic matrix density Although satellite cells do not appear to constitute a morphologically uniform class of cells we find no light or electron microscopic basis for subclassification. The nuclei are round or elongated and may display some variability in chromatin aggregation. More commonly the chromatin is uniformly dispersed with a thin dense band of uniform thickness adhering to the inner surface of the inner leaflet of the nuclear membrane (figs. 4 9) The nuclear envelope exhibits numerous pores and the outer leaflet is continuous with the rough endoplasmic reticulum This latter membrane system is scanty and is limited in its distribution to the perikaryon and proximal portions of the cytoplasmic processes of these cells (fig 9) The cells investing initial segments of the axon commonly display denser cytoplasm than those investing perikarya (fig 7) This cytoplasmic matrix density is exaggerated in material preserved with perfusates of higher tonicity (fig 10) Under these circumstances the satellite cells exhibit changes suggesting a pronounced osmotic sensitivity apparently in excess of that in neurons Cells appear shrunken and pulled away from the neurons leaving presumably artifactitious spaces between the satellite cells and their ganglion cells. In our experience in ganglia satisfying commonly accepted criteria for good fixation the satellite cell investment of the neuron is an intimate one and in such material we have not observed spaces or "cisterns" between satellite cells and ganglion cells. Neurons consistently fail to display matrix densities in excess of that of the investing satellite cells, regardless of fixative concentration employed.

The Golgi membranes mitochondria and occasional lysosome-like dense bodies in the satellite cells are not distinctive. Glycogen-like granules are sometimes observed in the cytoplasm (figs. 11 12) There are numerous fine filaments in the perinuclear cytoplasm (fig 8) and parallel to the long axis of the axon along the initial segment (fig 12) The satellite cells display surface redundancy in the form of folds or processes on the surface of the cell which faces the neuron (figs. 2, 4 5 6) These folds or processes may form several layers of investing cytoplasm and plasma membranes and interdigitate with the surface evaginations of the neuron. The outer (abneuronal) surface of the satellite cells is invested with a basal lamina (figs. 8, 10) which is continuous from one satellite cell to the next and may extend some distance in between adjacent satellite cells, or satellite cell processes but is never found between satellite cell and neuronal plasma membranes. The inner (adneuronal) surface redundancy of the satellite cell is more extensively developed in the monkey than in the cat corresponding to the greater degree of development of neuronal surface evaginations in these animals.

The initial segment of the axon is similarly invested and the most proximal region is covered by several overlapping satellite cells each contributing several layers of processes (figs. 6 8) In the more distal regions of the initial segment, however the satellite cells appear to more nearly approximate the Schwann cell relationship to unmyelinated axons in which a length of axon is embedded in an invagination of Schwann cell plasma membrane (figs. 12, 13) In the distal regions of the initial segment however the axon is much larger than the normal unmyelinated fiber of peripheral nerve and the satellite cell investment is commonly multi layered (figs 11 12) The individual members of the multi-layered processes around the initial segment can become extremely thin and in occasional areas lengths of processes can be found from which the cytoplasm has been entirely extruded so that the cytoplasmic leaflets of two plasma

Kotani, M., and K. Kawashima 1961 Observations of the spinal ganglion cells of senile mice with the electron microscope. Okajimas Fol. Anat. Jap., 37 451–467

Kruger, L., and D. S. Maxwell 1966 Electron microscopy of oligodendrocytes in normal rat cerebrum. Am. J. Anat., 118: 411–460.

Maxwell, D. S., and L. Kruger 1965 The fine structure of astrocytes in the cerebral cortex and their response to focal injury produced by heavy ionizing particles. J Cell Biol., 25 141–157

Moses, H. L., D. L. Beaver and C. E. Ganote 1965 Electron microscopy of the trigeminal ganglion. 1. Comparative ultrastructure. Arch. Path., 79 541–556.

Ortiz-Picón, J M. 1955 The neuroglia of the sensory ganglia. Anat. Rec., 121 513–529.

Pannese, E. 1960 Observations on the morphology submicroscopic structure and biological properties of satellite cells (s.c.) in sensory ganglia of mammals. Z. f. Zellforsch., 52: 567–597

Pease, D. C. 1964 Histological Techniques for Electron Microscopy Second Edition, Academic Press, New York.

Pineda, A. 1966 Electron microscopy of trigeminal ganglia relationship between nervous and other cellular elements. Anat. Rec., 154: 402.

Ramón y Cajal, S., 1907 Die Struktur der sensiblen Ganglien des Menschen und der Tiere. Ergeb. Anat., 16: 177–215.

——— 1909 Histologie du système nerveux de l'homme et des vertébrés, vol. 1. Maloine, Paris.

Rio-Hortega, P del, M. Polak and Y M. Prado 1942 Investigaciones sobre la neuroglia de los ganglios sensitivos. Arch. Histol. (B. Aires) 1: 233–275.

Rosenbluth, J 1962a The fine structure of neurons and satellite cells in spinal ganglia of the toad. Anat. Rec., 142: 344.

——— 1962b The fine structure of acoustic ganglia in the rat. J Cell Biol., 12: 329–359.

Rosenbluth, J., and S. L. Palay 1960 Electron microscopic observations on the interface between neurons and capsular cells in dorsal root ganglia of the rat. Anat. Rec., 136: 268.

Scharenberg, K. 1953 Glia and the elements of Schwann of the human Gasserian ganglion. Trab. Inst. Cajal Invest. Biol., 44 75–94.

Scharf, J H. 1958 Sensible Ganglien. In Handbuch der mikroskopischen Anatomie des Menschen, Bd. IV/1. Springer: Berlin-Gottingen-Heidelberg.

Tarlov I. M. 1937 Structure of the nerve root 1. Nature of the junction between the central and the peripheral nervous system. Arch. Neurol. Psych., 37 555–583.

Tennyson, V M. 1965 Electron Microscopic study of the developing neuroblast of the dorsal root ganglion of the rabbit embryo. J Comp. Neur., 124: 267–318.

Venable, J., and R. Coggeshall 1965 A simplified lead citrate stain for use in electron microscopy J Cell Biol., 25: 407–408.

Webster, H. deF 1962 Transient, focal accumulation of axonal mitochondria during early stages of Wallerian degeneration. J Cell Biol., 12: 361–377

Wyburn, G. M. 1958 The capsule of spinal ganglion cells. J Anat. (Lond.) 92: 528–533.

unlikely that intracapsular axons (if present) innervate ganglion cells It has also been suggested that the pericellular plexus is derived from fine branches of the initial segment of axon (Wyburn 58) but this would seem most unlikely in the present material. Axons other than the initial segment of the "unipolar" process and its extensive glomerulus enveloped in a layered satellite cell sheath cannot be identified and their presence might reasonably be questioned The extensive interdigitations of long neuronal protuberances from the large trigeminal ganglion cells might be a reflection of a functional (presumably metabolic) interaction with the multiple layers of satellite cell processes.

The nature of the capsule cells has been complicated by various claims that the satellite cells are of both neural crest and neuroglial origin (Scharenberg 52 Ortiz Picón '55) Although islands of neuroglia of central nervous system origin can be detected extending into cranial nerves (Tarlov '37; Horstmann 56 Maxwell Kruger and Pineda in prep) it is clear that the satellite cells surrounding the ganglion cell perikaryon and initial axon segment are of a single variety Despite silver affinity and morphology resembling glia in silver carbonate preparations the capsule cells can be distinguished readily from astrocytes and oligodendrocytes (Maxwell and Kruger '65 Kruger and Maxwell '66) in the electron microscope on the basis of arrangement of processes and cytoplasmic organelles The arrangement and number of layers of satellite cell processes appear to be more extensive in trigeminal than in spinal ganglia as might be expected on the basis of cell size (Pannese 60) and display a tendency to shrink away with employment of perfusates of higher tonicity (fig 10) possibly accounting for some of the variety of form observed in metallic impregnations which are not easily reconciled with electron microscopic observa ions It is noteworthy that the apparent osmotic sensitivity of satellite cells is less evident in ganglion cells although there is a tendency for the neuron to display smoother surface contours when the method of fixation results in shrinkage of satellite cells.

LITERATURE CITED

Andres, K. H. 1961 Untersuchungen über den Feinbau von Spinalganglien. Z. f. Zellforsch., 55 1–48.

Baecich P., and G M Wyburn 1953 Formalin-sensitive cells in spinal ganglia. Quart. J. micr. Sci. 94: 89–92.

Beams H. W V L. van Breeman, D. M. Newfang and T C. Evans 1952 A correlated study on spinal ganglion cells and associated nerve fibers with the light and electron microscopes. J Comp. Neur., 96: 249–281.

Beaver D. L. H. L. Moses and C. E. Ganote 1965 Electron microscopy of the trigeminal ganglion 11 Autopsy study of human ganglia. Arch Path., 79: 557–570

Blair D M., P Baecich and F Davies 1936 The nerve cells in the spinal ganglia. J. Anat (Lond.) 70: 1–9.

Castro F 1932 Sensory ganglia of cranial and spinal nerves: "Normal and Pathological. In: Cytology and Cellular Pathology of the Nervous System, vol. 1 W Penfield, ed. Paul B. Hoeber. New York, pp. 93–143.

Cervós-Navarro, J 1959 Elektronenmikroskopische Untersuchungen an Spinalganglien. I Nervenzellen. Arch. Psychiat. Nervenkr, 199 643–662.

——— 1960 Elektronenmikroskopische Untersuchungen an Spinalganglien. 11. Satellitenzellen. Arch. Psychiat. Nervenkr 200: 267–283.

Dawson, I. M. J Hossack and G. M. Wyburn 1955 Observations on the Nissl's substance, cytoplasmic filaments and the nuclear membrane of spinal ganglion cells. Proc. Roy Soc. Lond. B 144: 132–142.

Dixon, A. D 1963a Fine structure of nerve cell bodies and satellite cells in trigeminal ganglion. J Dent. Res., 42: 990.

——— 1963b Ultrastructure of nerve fibers in the trigeminal ganglion of the rat. J. Ultrastruct. Res. 8: 107–121

Dogiel, A. S. 1896 Der Bau der Spinalganglien bei den Saugertieren. Anat. Anz., 12: 140–152.

Ehrlich, P 1886 Über die Methylenblaureaction der lebenden Nervensubstanz. Dtsch. med. Wschr pp. 49–52.

Gordon, G B., L. R. Miller and K. G. Bensch 1965 Studies on the intracellular digestive process in mammalian tissue culture cells. J. Cell Biol., 25: 41–55.

Hess, A. 1955 The fine structure of young and old spinal ganglia. Anat. Rec., 123: 399–423.

——— 1965 Developmental changes in the structure of the synapse on the myelinated cell bodies of the chicken ciliary ganglion. J. Cell Biol., 25: 1–20.

Hiroaka, J., and V L. van Breeman 1963 Ultrastructure of the nucleolus and the nuclear envelope of spinal ganglion cell. J Comp. Neur. 121: 69–88

Horstmann E. 1956 Zur Frage der Struktur markhaltiger zentraler Nervenfasern. Z. f. Zellforsch, 45: 18–30.

Hossack, J., and G M. Wyburn 1954 Electron microscopic studies of spinal ganglion cells. Proc. Roy Soc. Edin., 65B 239–250.

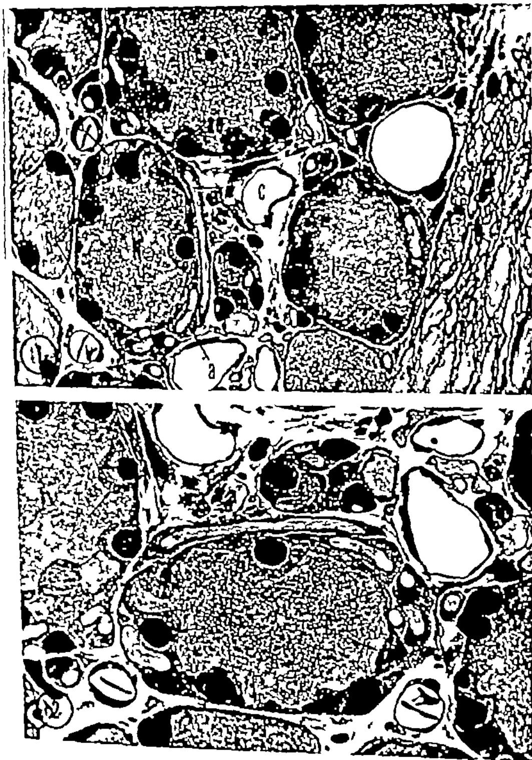

C
a

PLATE 1

EXPLANATION OF FIGURE

1 Light micrograph of trigeminal ganglion of monkey One-half micron thick section stained with basic fuchsin. Several neurons are to the left and center myelinated fibers to the right. One of several capillary profiles is indicated (c) A neuron (N) gives rise to an axon (ao) which surrounds the neuron in a glomerular arrangement, so that several profiles of the axon are seen (a) The neuron and initial segment are invested in a satellite cell capsule (s) Satellite cell cytoplasm is more dense than that of the neuron. Near the nucleus satellite cells indent the surface of the ganglion cell. In the neuron to the right, a patch of vesicular material (l) is presumed to correspond to lipofuscin. × 840.

2 Higher magnification light micrograph of the neuron indicated by N in figure 1 Light areas in the satellite cells adjacent to the neuron, (arrows) correspond to cytoplasmic evaginations of the neuron (see figs. 4 5) × 1450.

PLATE 1

EXPLANATION OF FIGURES

1 Light micrograph of trigeminal ganglion of monkey One-half micron thick section stained with basic fuchsin. Several neurons are to the left and center myelinated fibers to the right. One of several capillary profiles is indicated (c) A neuron (N) gives rise to an axon (ao) which surrounds the neuron in a glomerular arrangement, so that several profiles of the axon are seen (a) The neuron and initial segment are invested in a satellite cell capsule (s) Satellite cell cytoplasm is more dense than that of the neuron. Near the nucleus *satellite cells indent the surface of the ganglion cell.* In the neuron to the right a patch of vesicular material (l) is presumed to correspond to lipofuscin. × 840.

2 Higher magnification light micrograph of the neuron indicated by N in figure 1 Light areas in the satellite cells adjacent to the neuron (arrows) correspond to cytoplasmic evaginations of the neuron (*see* figs. 4 5) × 1450

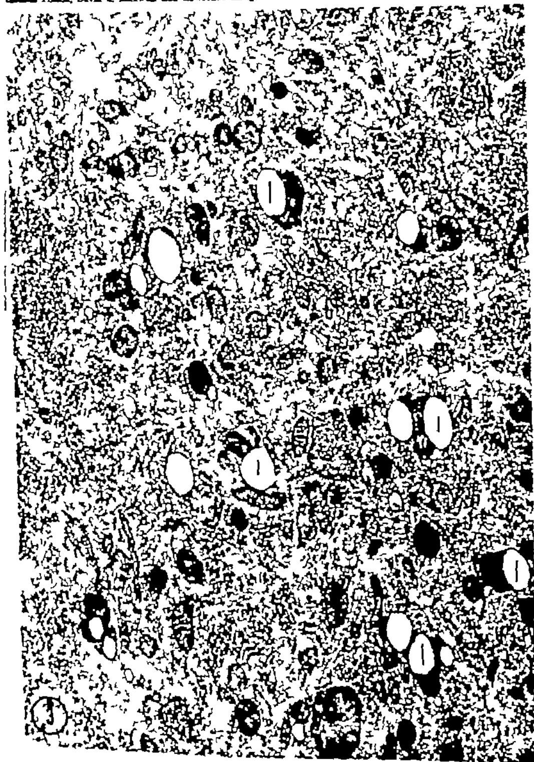


PLATE 2

EXPLANATION OF FIGURE

3 Neuron cytoplasm monkey ganglion. The features of the cytoplasm typical of these cells include Golgi apparatus (G) and prominent Nissl bodies (N) Between the Nissl bodies, the cytoplasm contains numerous filaments and microtubules. The mitochondria display a relatively dense matrix A spectrum of inclusions is evident in the cytoplasm of this cell. These range from dense lipofuscin granules (l) to similar vacuolated granules (l) displaying internal structure in their more dense regions × 20 000

4
5

PLATE 3

EXPLANATION OF FIGURES

4 5 Satellite cells and neurons, monkey ganglion. Cytoplasmic evaginations of the neuron (lower half of each figure) interdigitate with processes of the more dense satellite cells (upper half of each figure) In figure 4 the continuity of these evaginations with the cytoplasm of the neuron soma is indicated (single arrows) Two processes may abut (double arrows) accounting for the figures in early light microscopic literature of processes or "dendrites" forming loops in the capsule. The cytoplasmic continuity demonstrated in figure 4 is not evident in figure 5 (arrows) but the profiles are apparently of the same origin. Figure 4 × 26 000; figure 5, × 30,000


5

PLATE 4

EXPLANATION OF FIGURES

6 Neuron monkey ganglion The neuron soma is above the axon emerging sweeps down the left side of the figure and turns across the bottom. Processes of satellite cells (S) are more dense than the cytoplasm of the neuron and interdigitate with large evaginations of the axoplasm (a) Glycogen-like granules may be observed in the cytoplasm of both axon and satellite cells. × 30,000


1

PLATE 5

EXPLANATION OF FIGURE

7 Photomontage of three electron micrographs of monkey ganglion. Two ganglion cells are indicated (1 above right 1 below right, N) The complex ganglion cell interrelations with capsular cells (S) should be compared with the smooth investment of the glomerular portion of the axon (a) Two incomplete profiles of myelinated axons are seen to the left × 7,500

GEMINAL GANGLION FINE STRUCTURE
...tsue Pineda, David S. Maxwell and Lawrence Kruger



PLATE 8

EXPLANATION OF FIGURE

8 Trigeminal ganglion monkey A small blood vessel lumen occupies the upper left corner of the figure Neuron cytoplasm is seen in the lower right corner (N) The neuron is invested with satellite cell cytoplasm (S) The nucleus of the satellite cell has been cut tangentially (n) Cytoplasmic filaments and microtubules are prominent in the perinuclear cytoplasm The outer surface of the satellite cell is covered with a basal lamina (arrows) Axonal profiles (a) also closely invested with satellite cell processes, are probably part of an axonal glomerulus × 10,000



PLATE 7

EXPLANATION OF FIGURE

9 Satellite cell nucleus and cytoplasm, monkey trigeminal ganglion. The nucleus is cut tangentially revealing circular arrays at the nuclear surface (arrows) which may represent the site of nuclear "pores." The neuronal cytoplasm with which the cell is associated, is indented by the perinuclear region of the cell at the top of the figure and the lower left. The surface of the satellite cell facing the neuron above is thrown into folds and processes. × 29,000



PLATE 8

EXPLANATION OF FIGURE

10 Neuron and satellite cell preserved with glutaraldehyde-formaldehyde fixative buffered in 0.15 M cacodylate cat trigeminal ganglion. With this treatment satellite cells appear shrunken, with dense cytoplasm, attenuated processes and spaces or cisterns (c) appear between the processes and the neuron surface The production of such shrinkage artifact permits visualization of the limited extent to which the basal laminar material extends from the external surface of the satellite cell into the spaces between processes (arrows) The neuron above right, appears less severely affected by the "hypertonic" fixative × 16,500.


C
C
C
C
10

PLATE 9

EXPLANATION OF FIGURES

11 Axon and satellite cell investment monkey ganglion. An initial segment of axon (N) is invested with several layers of satellite cell cytoplasm External to this is a basal lamina (b) a process of a fibroblast (f) and above satellite cell cytoplasm (S) associated with a neuron (not illustrated) Two of the processes of the axonal investment (p and p) have become attenuated and the cytoplasm has been extruded (S and S) so that the cytoplasmic surfaces meet creating an intermediate line (i) The resulting membrane configuration superficially resembles myelin although in the case of myelin the lines indicated by (i) would be the major dense lines of myelin Note also that the outer surface of the plasma membranes of the two processes do not join to form an intermediate line but remain separated by a 150–200 A extracellular gap (e) × 57,500.

12 Axon monkey ganglion The initial segment (a) is invested by a single layer of satellite cell cytoplasm (S) containing longitudinally oriented filaments × 43,000


12

PLATE 10

EXPLANATION OF FIGURE

13 Axon in the region of the first "node" monkey ganglion. The initial segment of the axon (a) is invested (below) with several layers of satellite cell cytoplasm. At the first node several dense bodies (d) are present in the axoplasm Beyond this point (above) the axon is myelinated Note that the basal lamina of the satellite cell and the Schwann cell is continuous across the "node" (b) The circular myelin profile (top) is probably due to a fold or redundancy in the myelin sheath (common near nodes of Ranvier) and presumably contains Schwann cell cytoplasm. The cell at the lower left, probably a fibroblast exhibits a lobulated nucleus (n) × 20 000



Catagen in the Hairless House Mouse[1]

D. F. G. ORWIN,[2] H. B. CHASE AND A. F. SILVER
Division of Biological and Medical Sciences, Brown University, Providence, Rhode Island

ABSTRACT A morphological and histochemical study was made of some aspects of the catagen phase of the first hair cycle in hairless (*hr*) mice.

The histochemical tests used included those for sulphydryl and disulfide groups, collagen, and periodic acid-Schiff-reactive materials. Measurements were made of skin thickness, follicle length and for follicles in catagen VI and VII, epithelial column length, length of hair shaft in the skin, the width of glassy membrane and connective tissue sheath, and the width of collagen in the glassy membrane. The results showed that:

1. The mutant epithelial column shortens at a slower than normal rate so that at catagen VII, the total follicle length is greater than normal. The position of the mutant hair shaft in the skin is normal at this stage.

2. The keratinization sequence of the mutant club appears normal. The failure to form an anchoring brush is associated with morphological variation in the cell shapes and fibrils of the club.

3. The inner root sheath of the mutant follicle, although apparently keratinizing in the normal sequence, extends further up the follicle than normal and also further down, enclosing the club.

4. The glassy membrane and connective tissue sheath of the mutant are abnormally narrow due mainly to a marked reduction in collagen and to a narrower band of PAS-positive material.

Hereditary hairlessness (*hr*) in the house mouse can be attributed to a single recessive gene (Snell, '31; Chew et al., '31). The first macroscopic manifestation in homozygous hairless animals is hair loss around the eyes and front paws, occurring 10–14 days after birth (David, '31). The loss of hair progresses posteriorly from the head as a wave and is completed for most follicles by 21 days of age (Crew et al., '31; Mann, '61). During the second hair cycle only vibrissae and some tylotrichs produce hairs and these are usually abnormal (Mann, '61).

Hair loss and the failure of hair to regrow have been attributed to various events and malformations occurring during the catagen phase (Straile et al. '61) of the hair cycle. According to David ('31) the club ends of the mutant are abnormal and responsible for hair loss. Chase and Mann ('60) stated that hair loss is caused by failure of the anchoring club to keratinize. Both David ('31) and Chase ('54a) reported the presence of an abnormal extension of the inner root sheath around the club. Several authors (David, '31; Chase et al., '52; Montagna et al. '52) reported that the epithelial column of the catagen follicle of the mutant does not undergo shortening but attenuates and eventually breaks so that the continuity between the follicle and the dermal papilla is destroyed. Chase ('54a, b, c) found the glassy membrane around the epithelial columns to be unusually thin in the mutant, and attributed this to a deficiency in collagen formation leading to the ultimate failure of the column to shorten.

These varied results suggested the need for a more precise study of events in the late catagen stages of the mutant follicle.

MATERIALS AND METHODS

Inbred mice of the Hr/Hech strain of the genotype *ccAAbbDDpp Hr/hr* were used. The genotype can first be established at 10–14 days when hair loss commences on the front feet of homozygous recessive animals. Comparisons of different characteristics were made between mice of the genotype *Hr/hr* and mice of the genotype

[1] This work was supported by USPHS Research grant CA-00088 and a Training grant GM-00582. The senior author was also assisted by a New Zealand Wool Research Fellowship.

The aid of Miss H. Kendella in histochemical techniques and Dr. James F. Kidwell in statistical matters is gratefully acknowledged.

[2] Present address: Wool Research Organization of New Zealand, Private Bag, Christchurch, New Zealand.

hr/hr The paired animals were always littermates of the same sex, and were processed together Since mutant follicles in substages of catagen beyond catagen VI are abnormal, they were arbitrarily (but not unreasonably) classed in substage VII when the epithelial column was longer than normal for the same relative position of the club in the follicle as in normal catagen VII. In the next stage catagen VIII the *epithelial column is still longer* than normal and hair loss has usually occurred.

Biopsies were taken from the middorsal skin of 42 animals. Six pairs of tissue (animals ages 12–19 days) were treated by the method of Barrnett and Seligman ('52 '54) to demonstrate sulfhydryl and disulfide groups Five pairs, from animals 15–17 days old were treated according to the method of McManus (48) to demonstrate periodic acid-Schiff reactive (PAS) material. The glycogen test was made according to the procedure of Gomori (52) Five pairs of tissue were fixed in Bouins solution at pH 1.8 embedded in paraffin and stained with Van Gieson s stain and hematoxylin An additional five pairs of tissue were processed according to Green ('60) and treated with 2 ml of 0 1% solution of collagenase in 0 9% NaCl for 45 minutes at 37 C.

Sections were cut serially at 7 μ, with blocks oriented so as to obtain longitudinal sections of hair follicles

Measurements were made with an ocular micrometer and an oil immersion lens was used Measurements of general follicle dimension were made on tissue processed for the collagen test. For each animal follicles in catagen II, VI and VII which were entirely visible in longitudinal section from dermal papilla to the follicular orifice were used for measurements The measurements made were thickness of skin from the epidermis to the top of the panniculus carnosus muscle, the total length of the follicle the length of the epithelial column from the club to the end of the dermal papilla of catagen VI and VII follicles and the length of the hair shaft in the skin; i.e. from the club to the surface of the skin in catagen VI and VII follicles The same numbers of follicles were measured in both animals of a pair Thus 52 follicles in catagen II were measured 26 follicles per genotype. The breakdown of numbers of follicles measured for the five pairs was four in the *Hr/hr* animal and four in the *hr/hr* animal of the first pair and 5,5 5,5; 6,6 and 6 6 for the other four pairs, respectively Seventy four follicles in catagen VI were measured the numbers for the five pairs being 5 5 5,5 7 7 8,8 and 12,12 follicles *Of the follicles* in catagen VII, 70 were measured comprising 5 5 5,5 6,6, 9 9 and 10 10 follicles for the five pairs of animals The data were subjected to an analysis of variance developed for nested samples with unequal subsample numbers (Snedecor 56)

Measurements of epithelial column and related structures were made on PAS-stained material. Follicles used for measurements were those in catagen VI which had been sectioned so that the epithelial column between the club and dermal papilla was clearly definable. The total width of the glassy membrane and connective tissue sheath and the width of the epithelial column were measured at the same locus of the same section. Random selection of follicles was practiced, the serial sections enabling duplication of measurements to be avoided. Data were obtained from measurements on 20 follicles per animal. Three values were obtained for each follicle at approximately equal intervals along the epithelial column and the results averaged, in order to reduce errors resulting from the plane of sectioning Both sets of data were subjected to an analysis of variance developed for nested samples (Snedecor 56) The correlation coefficients for the relationship of width of epithelial column and width of glassy membrane and connective tissue sheath were also determined.

Measurements of the width of the Van Gieson-positive material in the glassy membrane were made in a similar way on the Van Gieson-stained material. The correlation coefficients for the relationship of this parameter to the width of the epithelial columns were also determined.

The formation of the hair club and the internal root sheath (IRS) during catagen were studied in the material demonstrating sulfhydryl and disulfide groups.

Measurements of the IRS were made along the ectal margin of follicles between the end of the IRS as defined by its form and concentration of sulfhydryl groups, and the dermo-epidermal junction. Data were obtained on 15 follicles per animal. In two pairs, all follicles were in late anagen VI while in the other three pairs the follicles were almost exclusively in catagens VI and VII. In all pairs, measurements on follicles at a particular substage of catagen were matched by measurements on an equal number of follicles at the same substage in the other animal. The values obtained were subjected to the analysis of variance developed for nested samples by Snedecor ('56)

OBSERVATIONS

I. *Spatial observations: Dimension of skin and follicle components in catagen*

The skin of the mutant is thinner than that of the nonmutant (table 1)

Follicles of both genotypes are approximately the same overall length at catagen II, and both types shorten as they progress into catagen VI and VII (table 2) However the nonmutant follicle becomes considerably shorter than the mutant by catagen VI, and even more so by catagen VII (table 5)

The entire follicle in late catagen may be considered in terms of its two main components, viz. the epithelial column and the hair shaft within the skin. Both components shorten between the substages of catagen VI and VII (tables 3 4) The length of the mutant hair shaft within the skin is deeper than normal in catagen VI (table 4) but at the same level as the nonmutant by catagen VII (table 5 figs 13 14) The epithelial column is the same length in catagen VI for both genotypes, but by catagen VII the normal epithelial column is considerably shorter than that of the mutant (table 5)

To sum up in catagen VI, the mutant follicle is longer than the nonmutant follicle. Although the epithelial column is normal in length, the hair shaft is deeper in the skin. By catagen VII, the follicles of both genotypes have shortened, and the hair shafts lie at similar levels

TABLE 1

Analysis of variance of hairless and normal skin thickness at catagen II VI and VII

Source	D.F	Mean square	F
Stage of hair cycle	2	7,081	0.16
Pairs within stages	12	43,123	1.23
Genotypes within pairs within stages	15	35,181	12.43($F_{.01}$ = 2.16)
Error	106	2,832	

D.F degrees of freedom.

TABLE 2

Analysis of variance of hairless and normal follicle lengths at catagen II, VI and VII

Source	D.F	Mean square	F
Stage of hair cycle	2	1,092,278	108.6($F_{.01}$ = 6.93)
Pairs within stages	12	14,867	0.3
Genotypes within pairs within stages	15	44,064	13.8($F_{.01}$ = 2.16)
Error	106	3,189	

TABLE 3

Analysis of variance of hairless and normal epithelial column lengths measured at catagen VI and VII

Source	D.F	Mean square	F
Stage of hair cycle	1	72,883	56.2($F_{.01}$ = 11.3)
Pairs within stages	8	1,284	0.06
Genotypes within pairs within stages	10	16,043	26.1($F_{.01}$ = 2.47)
Error	134	721	

TABLE 4

Analysis of variance of hair shaft lengths remaining in the skin in hairless and normal follicles undergoing catagen VI and catagen VII

Source	D.F	Mean square	F
Stage of hair cycle	1	884,008	97.3 ($P_{.01}$ = 11.3)
Pairs within stages	8	9,088	0.39
Genotypes within pairs within stages	10	23,628	5.41 ($P_{.01}$ = 2.47)
Error	124	4,370	

TABLE 5

The means and standard deviations of various follicle dimensions for three stages of catagen

Stage of catagen	Genotype		Thickness of skin	Length of follicle	Length of epithelial column	Length of hair shaft in skin
II	hr/hr	Mean (μ)	297	757		
		St. dev	51	48		
	Hr/hr	Mean (μ)	422	736		
		St. dev	121	70		
VI	hr/hr	Mean (μ)	307	585	123	472
		St. dev	40	74	29	88
	Hr/hr	Mean (μ)	381	468	96	374
		St. dev	93	78	23	75
VII	hr/hr	Mean (μ)	329	480	202	274
		St. dev	53	58	35	62
	Hr/hr	Mean (μ)	357	364	105	259
		St. dev	77	61	26	45

in the skin The mutant follicle, however shortens in overall length to a lesser extent than does the nonmutant due solely to the small degree of shortening of the epithelial column

II *The formation of the club*

The sequence of keratinization of the normal club is similar to the keratinization sequence of the terminal region of the hair shaft as indicated by the stain for sulfhydryl groups The hair formed during normal catagen consists of a nonmedullated nonpigmented region of cortex which terminates in the club The changes in cell shape and in concentration of sulfhydryl groups in this region occur in a characteristic time sequence which is similar to that described for the cortex of hair produced in anagen During catagen IV to VII as the cells of the terminal hair shaft move up the follicle they change from round cells containing weakly staining sulfhydryl (-SH) "fibrils" to elongated cells containing large amounts of intensely staining -SH positive fibrils which run parallel to the longitudinal axis of the hair shaft (figs. 1 2) I catagen VII, the cortical cells undergo abrupt transition from -SH positive -SH negative (fig 13) and in so doi became positive for disulfide groups.

The sequence of keratinization in m tant follicles is similar to the nonmuta but the fibrils and cells shapes are ab rant. In catagen IV and V the cells most presumptive clubs are round a weakly positive for sulfhydryl groups. catagen VI most mutant clubs like no mutants stain maximally for sulfhydr groups (fig 4) but the cells remain mo rounded than normal and the fibrils a more wavey (fig 3) In catagen VII mo mutant follicles have completed th sequence with clubs that are unreacti for sulfhydryl groups (fig 14) and po tive for disulfide groups.

In both mutant and nonmutant follicle the epithelial cells around the club and th epithelial column itself are weakly reacti for sulfhydryl groups The glassy mem brane around the epithelial column unreactive for sulfhydryl groups whi both the fibroblasts of the connective tiss

eath and the cells of the dermal papilla e weakly reactive.

PAS-stained sections of the same materi show differences in nuclear shapes parallel the differences in cell shapes scribed above for nonmutant and mu- nt clubs in catagen VI (figs. 5 8 10)

III. *The terminal development of the inner root sheath* (IRS)

There is a marked difference between e two genotypes in the terminal develop- ent of the IRS but the same sequence of ents occurs in the process of keratiniza on. The term *keratinization* is used here o mean the hardening process undergone y cells which form the IRS The final ard product of IRS cells is different in everal ways from the keratin of the hair ortex, and although IRS cells may con- ain sulfhydryl groups demonstrable by e Barrnett-Seligman staining method, ey do not give a positive disulfide reac- ion, since, unlike keratinized cortical cells, hey contain very little cystine (cf Mercer t al., '64)

Of the three layers of the IRS; viz. Henle s, Huxley's and the cuticle of the RS Henle's is definable in its final form, irst. It does not become strongly -SH ositive, whereas Huxley's and the cuticu- ar layers attain maximal sulfhydryl- taining at approximately the level of the ransition zone from -SH-positive to -SH egative in the terminal cortex.

The differences in the termination of RS production between mutant and non- mutant follicles includes both the upper and lower ends of the IRS. At the lower end of the IRS the normal course of events s as follows. Henle s layer appears in its final form as early as catagen V It rarely extends down past the greatest width of the club. As the club keratinizes, Huxley's layer becomes -SH-positive but only to a region just above the club. This region represents the usual lower terminal point of the IRS (fig. 2) A single and sometimes double line of cells which is apparently continuous with Huxley s and/or Henle s layer can usually be defined extending around the base of the club These cells represent the capsule and they show only a weak reaction for -SH similar to the reaction of the cells of the epithelial column.

In the mutant follicle the initial de- velopment of the IRS during its abnormal club formation is similar to that of the nonmutant IRS (fig. 3) However as this club undergoes keratinization the lower end of the IRS does not terminate above the club. Henle s layer extends lower down than does the normal (fig. 4) and Hux- ley s layer while increasing normally in sulfhydryl group concentration completely invests the base (fig 9) Thus, on com- pletion of keratinization the mutant club is completely encased in a hard extension of the IRS.

In both genotypes the upper terminal of the IRS moves to a more superficial position in the follicle between the stages of anagen VI and catagen VI VII (tables 6 7) However the final upper level of IRS attained or maintained, by the mu- tant is higher than in the normal (figs. 11 12, table 8)

It was also found, in both genotypes that the length of the region of the follicle between the top of the IRS and the dermo- epidermal junction decreases significantly between anagen VI and catagen VI, VII follicles (table 6 7) This suggests that part of the follicle shortening that takes place during catagen occurs in the region of the outer root sheath between the end of the IRS and the dermo-epidermal junction.

IV *The glassy membrane and connective tissue sheath of follicles in catagen VI and VII*

A. *Collagen.* In both genotypes the glassy membrane gives a positive reaction for Van Gieson s stain which is abolished by collagenase (figs. 15–18) In this way collagen may be demonstrated all along the length of the epithelial column from the base of the club down to the dermal papilla. However there is considerably less collagen in the glassy membrane of the mutant.

B *Periodic acid Schiff positive material.* In both genotypes the inner edge of the collagen-containing stratum of the thick- ened glassy membrane gives a positive PAS reaction which is not abolished by diastase and thus not indicative of glyco-

gen (figs 19, 20) This region is less well defined in the case of the mutant.

C *Width of glassy membrane and connective tissue sheath.* The total width of the glassy membrane and connective tissue sheath is significantly less in the mutant than in the non mutant follicle (table 8) Considerable variation also occurs in the total width of the glassy membrane and connective tissue sheath among mice of the same genotype

The total width of the glassy membrane plus connective tissue sheath is poorly correlated with the width of the epithelial column (r *Hr/hr* = 0.30 r *hr/hr* = 0.05), indicating that size of the follicles measured is not the reason for the difference observed between genotypes.

D *Width of the Van Gieson-positive material in the glassy membrane* The region containing Van Gieson-positive material is significantly narrower in the

TABLE 6

Analysis of variance of measurements of the distance from the end of the inner root sheath to the dermo-epidermal junction of follicles in anagen VI and catagen VI and VII. All measurements were made along the ectal margin of the follicles

Source	D.F	Mean square	F
Genotypes	1	164,030	6.68 ($P_{.05}$ = 5.32)
Mice of the same genotype	8	24,566	39.97 ($P_{.01}$ = 2.63)
Error	140	615	

The means and standard deviations of measurements between the end of the IRS and the dermo-epidermal junction of follicles in anagen VI and catagen VI and VII: *Hr/hr* 164.70 μ ± 41.5; *hr/hr* 97.50 μ ± 45.0.

TABLE 7

Tukey's test for the significant difference found among the means of mice of the same genotype in the analysis of variance presented in table 6

Animal	Stage of hair cycle	Means	$\bar{x}$ − 119 1	$\bar{x}$ − 143.8	$\bar{x}$ − 154.5	$\bar{x}$ − 202.7
		μ				
		Hr/hr				
1	Anagen VI	203.2	84.1	59 4	48.7	0.5
2	Anagen VI	202.7	83 6	58.9	48.2	
3	Catagen VI and VII	154.5	35.4	10.7		
4	Catagen VI and VII	143.8	24.7			
5	Catagen VI and VII	119.1				

Animal	Stage of hair cycle	Means	$\bar{x}$ − 62.0	$\bar{x}$ − 70.0	$\bar{x}$ − 71.7	$\bar{x}$ − 129.2
		μ				
		hr/hr				
1	Anagen VI	159.8	97.8	89.8	88.1	30.6
2	Anagen VI	129.2	67.2	59.2	57.5	
3	Catagen VI and VII	71.7	9 7	1 7		
4	Catagen VI and VII	70.0	8.0			
5	Catagen VI and VII	62.0				

D = 28.61.

TABLE 8

Analysis of variance of the total width of the glassy membrane and connective tissue sheath of follicles in catagen VI

Source	D.F	Mean square	F
Genotypes	1	86.13	10 19 ($P_{.05}$ = 5.32)
Mice of the same genotype	8	8.51	11.54 ($P_{.01}$ = 2.61)
Error	190	0 74	

Mean width and standard deviation of the glassy membrane and connective tissue sheath: *Hr/hr* 4.97 μ ± 1.07; *hr/hr* 3.65 μ ± 0.98.

TABLE 8

Analysis of variance of the width of the Van Gieson-positive material in the glassy membrane of mutant and normal follicles in catagen VI

Source	D.F	Mean square	F
Genotypes	1	122.38	150.8 ($P_{.01}$ = 11.26)
Mice of the same genotype	8	0.81	1.44
Error	190	0.56	

The means and standard deviations of the width of the Van Gieson positive material in the glassy membrane of mutant and non-mutant follicles in catagen VI. Hr/hr 4.40 μ ± 0.[illegible]; hr/hr 1.84 μ ± 0.[illegible].

mutant than in the nonmutant (table). Since there is a low correlation between the width of this region and the width of the epithelial column (r Hr/hr = 0.12 r hr/hr = 0.12) it is probable that the difference between genotypes is not due to the size of the follicles measured.

DISCUSSION

The study of catagen follicles has indicated that, in both genotypes studied, the cortex produced during catagen undergoes changes in concentration of sulfhydryl groups during keratinization similar to those described for the cortex of anagen follicles by Elsen et al. ('53) and Hardy ('52) Furthermore, the catagen cortex becomes positive for disulfide linkages when fully keratinized, which is another characteristic of keratinized anagen cortex (Giroud et al., '51; Montagna, '62)

The club of the normal catagen follicle appears to undergo the same developmental sequence during keratinization as the cortex, with the exception that the nuclei at the bottom of the club appear to elongate only partially Apart from this, the club appears to be an extension of the cortex.

The mutant club however deviates from the described sequence in two respects: (1) the failure of a comparatively high proportion of club cells to elongate, and (2) the failure of the *fibrillar* substructure of the keratin to be consistently oriented along the longitudinal axis of the hair shaft. The latter situation appears to be a rare phenomenon in animal hairs of this size (Earland, '62) Although the cause of these abnormalities is undetermined, it is probable that they are closely associated with each other The failure of the cells to elongate normally provides a basis for the abnormal club endings depicted by David ('31)

The evidence indicates that the statement by Chase and Mann ('60) to the effect that the mutant club fails to keratinize may need modification as, on the basis of the criteria used in this study the cells of the mutant club appear to keratinize

The extension of the hardened inner root sheath around the mutant club reported here is consistent with the finding of inner root sheath remains around the mutant club by David ('31) and Chase ('54a) Contact of the club with nonkeratinized cells seems to be necessary to prevent the hair from falling out. In the mutant during late catagen, the club is enclosed in the hardened IRS and has lost contact with nonkeratinized cells. Hair loss occurs at this time whereas the hair in the nonmutant is not lost until much later This concept of hair loss is in general agreement with David ('31) and Chase and Mann ('60) although these authors placed more importance on the abnormal club endings.

The finding that the inner root sheath of the mutant follicle extends to a higher region of the follicle than the inner root sheath of nonmutant follicles is important for two reasons. First, this difference was demonstrated in follicles undergoing anagen VI as well as those undergoing catagen VI and VII. Although the youngest animals in this study were only 12 days old their follicles were in the later stages of anagen VI, so it is probable that this difference is present in follicles at the start of anagen VI; i.e., two or three days after birth (Hardy '49) This difference represents, then, a probable means of identifying mutant animals at a considerably earlier age than has been possible to date. Second, the difference in the extension of the IRS in the higher regions

gen (figs 19 20) This region is less well defined in the case of the mutant.

C *Width of glassy membrane and connective tissue sheath.* The total width of the glassy membrane and connective tissue sheath is significantly less in the mutant than in the non mutant follicle (table 8) Considerable variation also occurs in the total width of the glassy membrane and connective tissue sheath among mice of the same genotype

The total width of the glassy membrane plus connective tissue sheath is poorly correlated with the width of the epithelial column (r *Hr/hr* = 0.30 r *hr/hr* = 0.05), indicating that size of the follicles measured is not the reason for the difference observed between genotypes.

D *Width of the Van Gieson-positive material in the glassy membrane* The region containing Van Gieson-positive material is significantly narrower in the

TABLE 6

Analysis of variance of measurements of the distance from the end of the inner root sheath to the dermo-epidermal junction of follicles in anagen VI and catagen VI and VII
All measurements were made along the ectal margin of the follicles

Source	D.F	Mean square	F
Genotypes	1	164,030	6.68($P_{.01}$ = 5.32)
Mice of the same genotype	8	24,566	39.97($P_{.01}$ = 2.63)
Error	140	615	

The means and standard deviations of measurements between the end of the IRS and the dermo-epidermal junction of follicles in anagen VI and catagen VI and VII: *Hr/hr* 164.70 μ ± 42.5, *hr/hr* 97.50 μ ± 45.0.

TABLE 7

Tukey's test for the significant difference found among the means of mice of the same genotype in the analysis of variance presented in table 6

Animal	Stage of hair cycle	Means	$\bar{x}$ – 119.1	$\bar{x}$ – 143.8	$\bar{x}$ – 154.5	$\bar{x}$ – 202.7
		μ				
		Hr/hr				
1	Anagen VI	203.2	84 1	59 4	48.7	0.5
2	Anagen VI	202.7	83.6	58.9	48.2	
3	Catagen VI and VII	154.5	35.4	10 7		
4	Catagen VI and VII	143.8	24 7			
5	Catagen VI and VII	119 1				

Animal	Stage of hair cycle	Means	$\bar{x}$ – 62.0	$\bar{x}$ – 70.0	$\bar{x}$ – 71.7	$\bar{x}$ – 129.2
		μ				
		hr/hr				
1	Anagen VI	159.8	97.8	89.8	88.1	30.6
2	Anagen VI	129.2	67.2	59.2	57.5	
3	Catagen VI and VII	71 7	9 7	1 7		
4	Catagen VI and VII	70 0	8.0			
5	Catagen VI and VII	62.0				

D = 28.61.

TABLE 8

Analysis of variance of the total width of the glassy membrane and connective tissue sheath of follicles in catagen VI

Source	D.F	Mean square	F
Genotypes	1	86.13	10.12($P_{.01}$ = 5.32)
Mice of the same genotype	8	8.51	11.54($P_{.01}$ = 2.61)
Error	190	0.74	

Mean width and standard deviation of the glassy membrane and connective tissue sheath. *Hr/hr* 4.97 μ ± 1.07; *hr/hr* 3.65 μ ± 0.86.

Green, J. A. 1960 Digestion of collagen and reticulin in paraffin sections by collagenase. Stain Technology 35: 273.

Hardy, M. H. 1949 The development of mouse hair in vitro with some observations on pigmentation. J. Anat., 83: 364.

——— 1952 The histochemistry of hair follicles in the mouse. Am. J. Anat., 90: 285.

Mann, S. J. 1961 The phenogenetics of hair mutants in the house mouse: hairless, rhino, ragged and opossum. Ph.D. Thesis, Brown University Providence, Rhode Island.

McManus, J. F. A. 1948 Histological and histochemical uses of periodic acid. Stain Technology 23: 99.

Mercer, E. H., R. L. Munger, G. E. Rogers and S. I. Roth 1964 A suggested nomenclature for fine-structural components of keratin and keratin-like products of cells. Nature, 201: 367.

Montagna, W., H. B. Chase and H. P. Melaragno 1952 The skin of hairless mice. I. The formation of cysts and the distribution of lipids. J. Inv. Derm., 19: 83.

Montagna, W. 1962 The structure and Function of Skin. 2nd Edition, Academic Press, New York.

Rogers, G. E. 1957 Electron microscope observations on the glassy of the hair follicle. Exp. Cell Res., 13: 521.

Snedecor, G. W. 1956 Statistical Methods. Iowa State College Press, Ames, Iowa.

Snell, G. D. 1931 Inheritance in the house mouse, the linkage relations of short-ear hairless and naked. Genetics, 16: 42.

Straile, W. E., H. B. Chase and C. Arsenault 1961 Growth and differentiation of hair follicles between periods of activity and quiescence. J. Exp. Zool., 148: 205.

——— 1962 Possible functions of the external root sheath during growth of the hair follicle. J. Exp. Zool., 150: 207.

Wolbach, S. B. 1951 Hair cycle of the mouse with its importance in the study of sequences of experimental carcinogenesis. Ann. N.Y. Acad. Sci., 53: 517.

of the follicle may be helpful in determining the mechanism by which the IRS is broken down. It has been postulated by Montagna ('62) and Straile ('62) that in the normal follicle the IRS is degraded by an enzyme (keratinase) Thus, in the mutant follicle the difference may be accounted for by alterations in the enzyme or proteins of the IRS sheath so that the IRS cannot be degraded at the normal level neither deep nor superficial

It is possible that in the mutant follicle the extension of the IRS up to the vicinity of the pilary canal could cause the widened hair canals noted by Fraser ('46) and believed by him to be due to hyperkeratosis of the outer root sheath surrounding the pilary canal.

The fact that the mutant follicle does not shorten normally (David '31 Chase et al '52 Montagna et al. '52) has been confirmed in this study Previous findings have drawn attention to the difference in length of the epithelial columns of mutant and nonmutant follicles at catagen VII (Chase et al '52 Montagna et al '52) This study presents evidence that the entire mutant follicle has a slower rate of shortening throughout catagen than does the nonmutant follicle It was also shown for both genotypes that the outer root sheath between the end of the inner root sheath and the dermo-epidermal junction shortens between anagen VI and catagen VI and VII This suggests that follicular shortening involves other follicle regions besides the epithelial column formed during catagen V and VI Hair movement is apparently largely unaffected by the different extents of follicular shortening since the mutant hair rises to about the same level in the skin as does the nonmutant hair by catagen VII

The demonstration of collagen in the thickened glassy membrane of catagen VI follicles by the collagenase test has confirmed Wolbach's interpretation ('51) of stained mouse follicles. The collagen of the thickened glassy membrane of catagen VI presumably represents an increase in thickness of the layer of collagen observed in an electron microscope study of the glassy membrane of developing mouse follicles (Rogers '57)

The failure of the glassy membrane to thicken in the mutant follicle has been suggested by Chase as a reason for the failure of the mutant epithelial column to shorten (Chase '54a Chase, '54b Chase '54c) This suggestion is based on the assumption that the glassy membrane is thickened by the laying down of collagen and that the mutant follicle cannot do this. We have shown that both collagen deposition and epithelial column shortening are present in the mutant but that both functions are less than normal This supports the idea that collagen is necessary for the shortening of the epithelial column.

LITERATURE CITED

Barrnett, R. J., and A. M. Seligman 1952 Histochemical demonstration of protein-bound sulfhydryl groups. Science, 116: 323.

——— 1954 Histochemical demonstration of sulfhydryl and disulfide groups of protein. J. Nat. Canc. Inst., 14: 769

Chase H B., and W Montagna 1952 The development and consequences of hairlessness in the mouse. Genetics, 37: 573

Chase, H. B. 1954a Growth of the hair Physiol. Rev., 34: 113.

——— 1954b The causative defect in the hairless mouse. Caryologia VI, suppl., 632.

——— 1954c Somes examples of gene-controlled functional disturbances in the mouse. J Nat. Canc. Inst. 15 (3): 655.

Chase, H B., and S J Mann 1960 Phenogenetic aspects of some hair and pigment mutants J Cell and Comp. Physiol., 56: 103.

Crew F A E., and L. Mirskaia 1931 The character "hairless" in the mouse. J Genet., 25: 17

David L. T 1931 The external expression and comparative dermal histology of hereditary hairlessness in mammals. Zeitschr f Zellforsch. u. mikro Anat., 14 616.

Earland, C., P R. Blakey and J G. P Stell 1962 Molecular orientation of some keratins. Nature 196: 1287

Eisen A. Z., W Montagna and H. B Chase 1953 Sulfhydryl groups in the skin of the mouse and guinea-pig. J Nat. Canc. Inst., 14: 341.

Fraser F C. 1946 The expression and interaction of hereditary factors producing hypotrichosis in the mouse: Histology and experimental results. Can. J Res., 24D: 10.

Giroud A. and C. P Leblond 1951 The keratinization of epidermis and its derivatives, especially the hair as shown by X ray diffraction and histochemical studies. Ann. New York Acad. Sci., 53 613.

Gomori G L. 1952 Microscopic Histochemistry University of Chicago Press, Chicago.


1
2
3
4

PLATE 1

EXPLANATION OF FIGURES

Figures 1 through 4 are longitudinal sections of follicles cut at 7 μ and stained for sulfhydryl groups × 680

1 Normal follicle in early catagen VI. The SH group-positive fibrils are apparent and their orientation can be seen to be generally parallel to the longitudinal axis of the hair shaft (middle arrow) The lighter staining nuclei (lower arrow) are elongated except around the bottom of the club Henle's layer (upper arrow) is apparent.

2 *Normal follicle in catagen VI The club is staining maximally* for sulfhydryl groups. The *partially elongated nuclei are visible* at the bottom of the club (lower arrow) The inner root sheath has completed its development and terminates well above the club (upper arrow)

3 Hairless follicle in early catagen VI. The fibrillar nature of the staining is apparent. The orientation of the fibrils in the club is, in general, not parallel to the longitudinal axis of the hair shaft. Several lighter staining round nuclei can be seen in the club (lower arrow) *Henle's layer is visible near the club* (upper arrow)

4 Hairless follicle in catagen VI. The nuclei of the maximally staining club have still not elongated (lower arrow) Henle's layer can be seen extending almost around the base of the club (upper arrow)

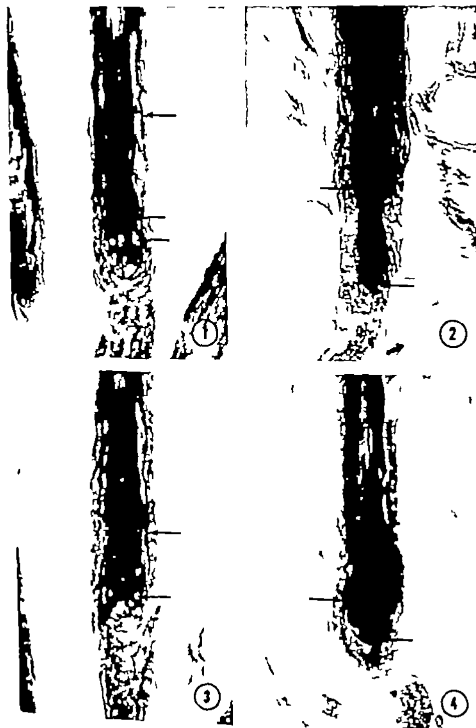

1
2
3
4

PLATE 2

EXPLANATION OF FIGURES

Figures 5 through 8 are longitudinal sections of follicles cut at 7 μ and stained for periodic acid-Schiff reactive material. × 680.

5 Normal follicle in catagen V The nuclei of the club are still round.

6 Normal follicle in catagen VI. The nuclei of the cells of the club are elongated except at the bottom of the keratinizing club (arrow) The transition between club and capsule is gradual

7 Hairless follicle in catagen V The round nuclei of the club are apparent (arrow)

8 Hairless follicle in catagen VI A high proportion of the cells in the club have not elongated (arrow) There is a clear demarcation between club (including Huxley's layer) and capsule


5


6


7


8

PLATE 3

EXPLANATION OF FIGURES

9 Hairless follicle in catagen VI Henle's layer extends past the club Huxley's layer can be seen enclosing the club (arrow) Stained for sulfhydryl groups. × 680

10 Hairless follicle in catagen VII. Nuclei are not visible in the fully keratinized club Note the concave end of the club (arrow) PAS stain. × 680

11 Normal follicle The upper arrow indicates the orifice of the sebaceous gland The upper end of the inner root sheath is indicated by the lower arrow Stained for sulfhydryl groups × 440.

12 Hairless follicle The upper arrow indicates the orifice of the sebaceous gland. The end of the inner root sheath (lower arrow) extends almost to the orifice of the sebaceous gland. Stained for sulfhydryl groups. × 440

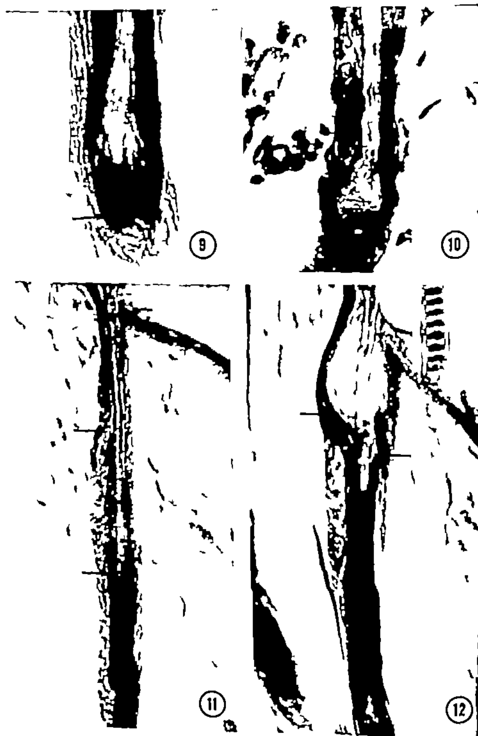

9
10
11
12

PLATE 4

EXPLANATION OF FIGURES

13 Longitudinal section of a normal (*Hr/hr*) follicle in catagen VII. The club (upper arrow) is situated in the follicle at the level of the junction of the dermis and hypodermis. The lower arrow points to the shortening epithelial column. Stained for sulfhydryl groups. × 210

14 Longitudinal section of a hairless (*hr/hr*) follicle in catagen VII. The club (upper arrow) is situated in the follicle at the level of the junction of the dermis and hypodermis. The longer than normal epithelial column (lower arrow) is apparent. Stained for sulfhydryl groups. × 210.

15 Longitudinal section of a normal follicle. The Van Gieson staining material of the thickened glassy membrane (arrow) is apparent on both sides of the epithelial column. Van Gieson's stain. × 680.

16 Longitudinal section of a normal follicle. The inability of the glassy membrane to take up Van Gieson's stain following treatment with collagenase is apparent (arrow). Van Gieson's stain. × 680


13


15


14


16

PLATE 4

EXPLANATION OF FIGURES

13 Longitudinal section of a normal (*Hr/hr*) follicle in catagen VII. The club (upper arrow) is situated in the follicle at the level of the junction of the dermis and hypodermis. The lower arrow points to the shortening epithelial column. Stained for sulfhydryl groups. × 210.

14 Longitudinal section of a hairless (*hr/hr*) follicle in catagen VII. The club (upper arrow) is situated in the follicle at the level of the junction of the dermis and hypodermis. The longer than normal epithelial column (lower arrow) is apparent. Stained for sulfhydryl groups. × 210.

15 Longitudinal section of a normal follicle. The Van Gieson staining material of the thickened glassy membrane (arrow) is apparent on both sides of the epithelial column. Van Gieson's stain. × 680.

16 Longitudinal section of a normal follicle. The inability of the glassy membrane to take up Van Gieson's stain following treatment with collagenase is apparent (arrow) Van Gieson's stain. × 680.


17


18


19

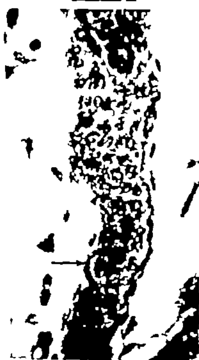


PLATE 5

EXPLANATION OF FIGURES

17 Longitudinal section of a hairless follicle. The less well defined Van Gieson-staining material in the thickened glassy membrane is indicated by the arrow Van Gieson's stain. × 680

18 Longitudinal section of a hairless follicle Van Gieson-positive material is no longer found in the thickened glassy membrane following treatment with collagenase (arrow) Van Gieson's stain × 680

19 Longitudinal section of a normal follicle. Periodic acid-Schiff-positive material is apparent along the inner margin of the thickened glassy membrane (arrow) PAS stain. × 680

20 Longitudinal section of a hairless follicle. Periodic acid-Schiff-positive material is present along the inner edge of the thickened glassy membrane (arrow) PAS stain × 680

Movement of Palatine Shelves in Untreated and Teratogen-treated Mouse Embryos [1]

LAWRENCE M. ROSS [2] AND BRUCE E. WALKER
Department of Anatomy, The University of Texas Medical Branch, Galveston, Texas

ABSTRACT Movement of palatine shelves in living mouse embryos after tongue displacement was evaluated by direct observation and by re-examination of the shelves after freezing or submersion in fixative. Effect on shelf function of suspending the embryos in saline or plasma was compared with manipulations in air. Measurements were made of head dimensions and residual space between the palatine shelves in embryos fixed in the cocoon or after experimental manipulation. All methods of evaluating palatine shelf behavior indicated movement toward the midline by the anterior portions of the shelves after tongue displacement. Experiments with complete detachment of the tongue demonstrated that the tongue contributes to the flattening of the shelves into a horizontal plane by exerting pressure from below.

The same techniques applied to embryos treated with cortisone, vitamin A and x-ray demonstrated reduced movement of palatine shelves toward the midline when compared with untreated embryos. The reduction was greatest with x-irradiation and least with hypervitaminosis A.

Movement of the palatine shelves from a vertical (sagittal) to a horizontal (transverse) plane has been recognized by many authors as a critical phase in development of the secondary palate (Peter '24; Lazzaro, '40; Walker and Fraser '56; Asling et al., '60; Zeller et al., '64; Coleman, '65). Operative displacement of the tongue in living embryos supported the hypothesis of an intrinsic shelf force since the shelves were observed to move into a horizontal position (Walker and Fraser, '56). Numerous investigations have subsequently been directed toward finding a physicochemical basis for shelf movement (Larsson, '60 '62; Walker '61 Jacobs '64 '66). However the concept of intrinsic force on the basis of *in vivo* observations has to be reconsidered in view of work by Anup ('63). He evaluated palatine shelf behavior in living embryos manipulated in saline as compared to air and concluded that "the elevation of the palatine shelves in nonsubmerged embryos following displacement of the tongue is due, primarily to surface tension rather than intrinsic shelf force. In a preliminary report, Ross ('64) confirmed a difference between air and fluid media, but still found evidence for shelf movement in fluid media after displacement of the tongue. Shelf movement has been implicated also in the action of teratogens which cause cleft palate (Walker and Fraser '57 Walker and Crain '60 '61; Callas and Walker '63 Chamberlain, '66). The brief observations on shelf movement in teratogen-treated, living embryos by Walker and Fraser ('57) have been considerably extended by Ross ('64 '65).

Since the question of whether an intrinsic shelf force exists is obviously critical to further analysis of normal and cleft palate development, an effort has been made in the experiments reported here to provide qualitative and quantitative evaluations of *in vivo* shelf movement in both normal and teratogen-treated mouse embryos.

MATERIALS AND METHODS

Pregnant A/J strain mice were used for observations on normal or teratogen-treated embryos the mating procedure and timing of embryos being carried out as described previously (Walker and Fraser '56). For observations on embryos developing cleft palate, pregnant mice were given four daily doses of 2.5 mg cortisone at eleven and one-third to fourteen and one-third days postconception, or 10,000 units vita-

[1] This investigation was supported by N.I.H. research grant HD 00312 from the National Institute of Child Health and Human Development. Computation service was supported by N.I.H. grant FR 00254.
[2] Trainee, supported by N.I.H. Anatomical Training grant GM 486.

mersion differed from manipulation in air ($x^2 = 4.03$, $p < 0.05$)

Effects of tongue displacement were evaluated further by comparing the results of transferring embryos from saline or plasma to Bouin's fixative with the results of freezing the fluid medium and contained embryo on dry ice. With the latter method, there was very good correlation between *in vivo* observations and observations on embryos subsequently frozen (table 1) The considerable number of vertical shelves seen following fixation in Bouin's fluid reflects the opportunity for shelves to move while the embryos were being transferred between fluids, with the return to vertical probably being facilitated by pressure from the tongue and lower jaw Since the results with the two techniques differed significantly ($x^2 = 11.52$, $p < 0.001$) embryos in subsequent experiments (tables 2–5) were immersed in Bouin's fixative along with the serum or saline in which they were bathed, to decrease the opportunities for further shelf movement after the initial observation *in vivo*.

Histological sections of the palate region of embryos in which the tongue was removed after displacement revealed a morphology quite different from any material obtained by fixation *in utero*. The palatine shelves were horizontally oriented and a gap was present between the shelves (fig. 12) However the shelves were a considerable distance from the nasal septum. For comparison, figures 10 and 11 illustrate sections through the palates of untreated embryos in which the tongue was left intact after displacement. Again the shelves are horizontal and a gap is present, but the shelves are closer to the nasal septum. These differences are less obvious with gross dissection, as illustrated in figure 3. However the advantage of dissected material is that it provides a 3-dimensional view whereas shelf morphology in sections varies considerably with different section levels. For example the embryo in figure 13 was found to have shelves almost as horizontal as those shown in figure 12, when sections at the level of the eyes were studied.

An intermediate condition of shelf movement was more commonly seen when the tongue was completely detached, or when the embryo had been exposed to a teratogen, than in control embryos with simple tongue displacement. This condition is difficult to recognize in photographs; it exists for both shelves in figure 7 The shelves have moved far enough to obscure the internal nares but have not flattened into the horizontal plane. When this condition is viewed in section both the medial and lateral walls of each shelf are seen to slant toward the midline (figs. 15 17) Shelf movement in teratogen-treated embryos included a full range of possible positions. In figure 6, the shelves of a cortisone-treated embryo have deviated only slightly from the initial vertical plane (compare with fig 1) In contrast, the anterior half of each shelf in figure 5 has flattened into the horizontal plane A similar contrast can be observed in the x-irradiated embryos shown in figures 8 and 9 although the flattening of the anterior portion of the shelves in figure 8 is minimal. Sections (figs. 14, 16) provide confirmation of the flattening of shelves anteriorly in two teratogen-treated embryos with only minimal extension toward the midline in the x-irradiated embryo.

Results of observations on control and teratogen-treated litters are reported in table 2. In nearly all control embryos the shelves appeared to move into a horizontal position after tongue displacement, whereas shelf movement frequently appeared incomplete in teratogen-treated embryos. When the tongue was displaced, but not cut away from the embryo a number of the shelves seen to have moved during *in vivo* observation were found to have returned to a vertical plane after fixation. In contrast, vertical shelves were rare after fixation, in embryos that had their tongue completely removed. The reverse situation pertained to the horizontal state which was maintained in most cases if the tongue was left in the mouth but was mostly lost to a near horizontal or intermediate state if the tongue was cut out. The interaction of these factors renders unsatisfactory an average gap area for comparison of the two *in vivo* control groups (table 4)

Statistical comparison of treatment groups in table 2 is more conveniently

min A by stomach tube at eleven and one-third and twelve and one-third days post conception or 300 r x irradiation at eleven and one-third days postconception (Walker and Fraser '57 Walker and Crain 60 Callas and Walker 63) At a range of time intervals from 14 days 15 hours to 15 days 14 hours the pregnant mice were anesthetized with amobarbital sodium and the embryos were exposed by cutting through the abdominal wall cornua and embryonic membranes. The umbilical cord was severed and the embryo was placed in a paraffin well to which 0 9% sodium chloride or mouse plasma was added unless observations were to be made in air With the aid of a dissecting microscope the tongue was displaced downwards with glass instruments or severed at the base and removed with forceps The position of the palatine shelves before and after tongue manipulation was estimated visually Immediately after manipulation the embryos were fixed by one of three methods (1) transfer of the embryo from saline or plasma to Bouin s fluid; (2) transfer of the paraffin well to a thermos with solid CO_2; (3) submersion of the paraffin well in Bouin s fluid The latter two methods had the advantage of maintaining the embryo in its original bath of saline or plasma while fixation was progressing Frozen heads were cut in half through a coronal plane at the midpalatine level or else allowed to thaw in absolute ethanol. The palate region of Bouin s fixed embryos was studied by dissecting away the lower jaw Measurements were made with an ocular scale or grid and involved total head length width of the head just posterior to the eyes maximum width of the palate width of each shelf the gap between the shelves at the level of maximum shelf width and the total area of the gap between the shelves. Selected embryos were embedded in paraffin, serially sectioned, and stained with hematoxylin and eosin

RESULTS

Displacement of the tongue in living embryos operatively exposed to air confirmed the observations of Walker and Fraser ('56). Embryos exposed ca 14 days, 22 hours postconception usually had one or both palatine shelves in a vertical (sagittal) position (figs. 1 2) When the tongue was pulled from between the shelves they moved to a horizontal (transverse) position and met in the midline. The same maneuver on embryos submerged in saline or mouse blood plasma produced an effect differing from the preceding primarily in the greater turgor of the shelves as deduced by pressing on the shelves with a glass probe and the persistance of a gap between the shelves after they had progressed toward the horizontal from an initial vertical plane (figs. 3, 4, 10 11) These differences between air and fluid media could be reproduced by transfer of the same embryo from air to fluid or vice versa. Shelf movement was usually confined to the anterior half of each shelf as can be seen by comparing figures 3 and 4 with figures 1 and 2. As a consequence sections through the nasal septum (figs. 10 11) showed good horizontal positioning of the shelves whereas sections taken further back in the head showed intermediate to ventrical shelf orientation Embryos in which the palatine shelves were observed to go from vertical to horizontal after tongue displacement in each of the three media are listed in table 1 The use of saline or plasma as the fluid medium gave essentially the same results with Bouin s fixation ($x^2 = 1\ 54$ $p > 0.20$ with fluid but the combined results with fluid

TABLE 1

Palatine shelf position after fixation in cont... embryos All embryos listed had vertical shel... that were observed to move into a horizontal p... tion after tongue displacement during the in v... observation period. The embryos were then fi... in Bouin s fluid or frozen to re-evaluate sh... position.

	Type of medium		
	Air	Saline	Flu...
No. embryos observed	20	24	[illegible]
Shelf position after Bouin s fixation:			
Horizontal	18	9	[illegible]
Vertical	2	3	
Shelf position after freezing: [1]			
Horizontal	—	10	[illegible]
Vertical	—	0	

[1] Six embryo heads lost due to shatter at the t... of sectioning.

TABLE 4

Developmental rating and head and palate measurements of control and teratogen-treated embryos (mean ± standard error)

	Fixed in utero (Embryo vertical)	Manipulated in vivo							
		Tongue displaced				Tongue completely removed			
	Control	Control	Cortisone	Vitamin A	X-ray	Control	Cortisone	Vitamin A	X-ray
No. embryos	31	38	32	53	68	51	89	48	55
Chron. age (days/hrs)	14/23.5 ±0/0	14/20 ±0/0.5	15/1.5 ±0/0.5	15/0 ±0/0.5	15/3 ±0/0.5	15/20.5 ±0/0.5	15/3 ±0/0.5	15/1 [*] ±0/0.5	15/3 ±0/0.5
Morphological rating	8.0 ±0.51	5.1 ±0.66	13.2 ±0.37	—	—	7.9 ±0.44	13.1 ±0.45	—	—
Weight (mg)	163.3 ±3.62	136.7 ±3.15	165.0 ±3.47	192.3 [*] ±4.31	108.4 [*] ±2.03	146.1 [*] ±3.10	164.8 [*] ±2.50	215.1 ±3.51	105.7 ±2.75
Palate width	36.3 ±0.59	34.1 ±0.31	36.1 [*] ±0.41	37.9 ±0.58	30.8 ±0.33	34.3 [*] ±0.91	34.9 ±0.16	39.0 [*] ±0.31	29.4 ±0.94
Shelf width	24.0 ±0.30	25.1 ±0.66	24.8 ±0.48	27.3 ±0.30	19.5 ±0.36	28.7 [*] ±0.25	27.1 [*] ±0.18	30.9 ±0.37	21.5 [*] ±0.28
Head width	76.7 ±0.52	72.4 [*] ±0.92	76.0 ±0.72	79.3 ±0.35	59.5 ±0.51	73.6 ±0.41	75.5 ±0.57	81.1 ±0.37	58.4 ±0.51
Head length	130.0 ±0.57	111.2 ±1.53	122.8 [*] ±1.49	133.8 ±1.06	100.1 [*] ±0.97	115.0 [*] ±0.88	121.5 ±0.80	135.8 ±0.97	97.8 ±1.17
Gap width	12.4 ±0.19	8.0 ±0.57	11.2 ±0.60	10.6 ±0.36	11.3 ±0.37	5.6 ±0.35	7.8 [*] ±0.17	8.1 ±0.19	7.9 [*] ±0.16
Gap width / Head width	0.16 ±0.007	0.11 [*] ±0.006	0.14 ±0.011	0.13 ±0.005	0.19 [*] ±0.001	0.07 [*] ±0.25	0.10 [*] ±0.002	0.10 ±0.002	0.13 [*] ±0.003
Gap area	44.2 ±0.92	31.0 ±1.06	44.3 [*] ±1.30	47.6 [*] ±0.93	36.1 [*] ±0.63	26.5 ±0.56	30.6 ±0.66	30.6 [*] ±0.93	25.8 ±0.84
Gap area / Head area	0.0047 ±0.00012	0.0038 ±0.00021	0.0045 ±0.00013	0.0049 ±0.000"0	0.0060 [*] ±0.00007	0.0033 ±0.00006	0.0043 [*] ±0.00006	0.0039 [*] ±0.00008	0.0050 [*] ±0.00006

[a] Indicates statistical significance from the control series fixed in utero ($p < 0.02$).
[b] Indicates statistical significance from the control series within that treatment group ($p < 0.01$).
[c] Indicates statistical significance from the control series fixed in utero ($p < 0.01$).

achieved by assigning numerical values of one to four to the four shelf positions recognized from vertical through horizontal and computing a mean position (table 3). *In vivo* observations on all teratogen treated groups differed from the controls but not all of these differences were confirmed after fixation (table 3). Statistical evaluation revealed that x-irradiated embryos consistently had less shelf

TABLE 2

Shelf movement estimated by in vivo observation and shelf position evaluated after fixation in embryos which had vertical shelves when first released from embryonic membranes. Stage 3 indicates one shelf was horizontal and the other shelf was vertical. Intermediate indicates both shelves were at a 45° angle

Treatment	No. of embryos	In vivo observations		Shelf position			Post fixation	
		Movement	Number	Vert.[1]	Stage 3	Interm.[1]	N. Horiz.[1]	Horiz.[1]
Tongue displaced								
Control	36	to horizontal	31	6	4	0	0	21
		to intermediate	5	2	2	0	0	1
Cortisone	32	to horizontal	6	0	1	0	0	5
		to near horizontal	5	3	0	0	0	2
		to intermediate	21	9	5	0	0	7
Vitamin A	53	to horizontal	14	0	3	0	0	11
		to near horizontal	27	2	7	0	0	18
		to intermediate	12	4	4	0	0	4
X irradiation	68	to horizontal	1	0	0	0	0	1
		to near horizontal	21	8	5	0	0	8
		to intermediate	29	18	5	0	0	6
		little or none	17	16	1	0	0	0
Tongue completely removed								
Control	51	to horizontal	49	0	0	25	20	4
		to near horizontal	2	0	0	0	2	0
Cortisone	88	to horizontal	12	0	0	7	4	1
		to near horizontal	34	0	0	17	14	3
		to intermediate	42	1	0	39	2	0
Vitamin A	48	to horizontal	22	0	0	2	20	0
		to near horizontal	15	0	0	3	11	1
		to intermediate	11	0	0	5	6	0
X irradiation	55	to horizontal	1	0	0	1	0	0
		to near horizontal	15	0	0	11	4	0
		to intermediate	31	0	0	29	2	0
		little or none	8	1	0	6	1	0

[1] Abbreviations: Vert., vertical; Interm., intermediate; N Horiz., near horizontal; Horiz., horizontal.

TABLE 3

Mean values for shelf position observed in vivo and after fixation in control and teratogen-treated embryos

	Control	Cortisone	Vitamin A	X-ray
Tongue displaced				
Mean position observed in vivo	3.72	2.53[1]	3.04[1]	2.09[1]
Mean position after fixation	3.00	2.43	3.13	1.81[1]
Tongue completely removed				
Mean position observed in vivo	3.94	2.68[1]	3.23[1]	2.16[1]
Mean position after fixation	2.76	2.38[1]	2.81	2.10[1]

[1] Indicates statistical significance from the control series within that treatment group ($p < 0.01$).

no such systematic reduction in gap width or area was present. Frequently the gap increased or else did not deviate significantly from zero correlation. One exception was the tendency for gap area to decrease with embryonic growth in cortisone-treated embryos (but only if the tongue was left in place)

DISCUSSION

Submersion of living mouse embryos in saline or plasma and manual displacement of the tongue rapidly led to movement of the palatine shelves from a sagittal to a horizontal plane in many of the embryos studied at an appropriate stage of development. Evidence for such movement came, not only from observations at the time of operation, but also from study of the embryos after they were fixed. Fixation of shelf position by freezing should have given the best representation of the *in vivo* state and in such embryos the palatine shelves were almost in contact with the nasal septum, to which they would have fused during normal development. Evidence of movement was derived also from comparison of the gap between the palatine shelves relative to the size of the head, which was less in operated embryos than in embryos fixed *in utero* despite the more advanced developmental age of the latter This movement is presumably caused by some intrinsic force. These results do not support Atnip's ('63) conclusion that the palatine shelves do not move when the embryo is submerged in fluid. His brief report does not provide an opportunity for close comparison of the two experiments to search for an explanation of the discrepancy However Atnip's observation that the shelves behaved differently in fluid than in air was confirmed. Specifically the shelves were more turgid, their movement to a transverse plane was less extreme and the shelves did not make contact with each other in the midline when submerged in fluid.

Experiments involving complete removal of the tongue demonstrated that the tongue induced greater flattening of palatine shelves in the transverse plane than was achieved with the tongue removed. Evidence for this effect was derived from observations on intact and sectioned palatine shelves. Movement of shelves from a vertical to a horizontal plane occurred with the tongue cut out, but the shelves were further from the nasal septum than when the tongue was left in place. Considering the conditions *in utero* the greater restriction of space might explain the closer approximation of the palatine shelves under such conditions. However even *in utero* a stage is seen in which the shelves are horizontal, but do not touch namely stage 4 (Walker and Fraser '56) If this stage occurs consistently during palate development, then some period of time is probably needed for complete flattening of the shelves possibly accomplished through pressure from the tongue and lower jaws. Thus, contact in the midline by the shelves would not be expected during the brief period of *in vivo* manipulation, since fixation was begun immediately following manipulation.

An opposite effect of the tongue was seen in the greater number of shelves returning to a vertical condition if the tongue was not cut out. This effect was obviously due to the net upward force on the shelves being directed more toward a spreading of the shelves, than to a flattening effect in shelves that had not moved far enough toward the midline. The condition of one shelf vertical and the other shelf horizontal (stage 3) seen when the tongue was displaced but not cut out, could similarly be explained by the tongue acting asymmetrically to flatten one shelf, while being sufficiently lateral to the other shelf to return it to a vertical position Since the intermediate shelf condition after complete tongue removal always consisted of both shelves being at a 45 angle there exists a qualitative difference between the two series that appears to be explainable only by the hypothesis that tongue pressure causes the stage 3 phenomenon

The effect of cleft palate-producing teratogens was to retard shelf movement. This was observed at the time of operation and was generally confirmed by estimation of shelf position in fixed embryos. Since both of the foregoing methods are quite subjective measurements were made on the fixed embryo heads. The cortisone and

movement than controls cortisone-treated embryos had less movement in three of the four categories and vitamin A treated embryos showed the least reduction in shelf movement.

Measurement of the palatine shelves and associated areas provided an alternative and presumably more accurate method of evaluating the results of tongue displacement. Furthermore possible disproportionate changes in growth of these structures due to the teratogens might be revealed by such measurements In table 4 comparison is made between control and treated groups for factors relating to stage of embryonic development and dimensions of structures in the head including width and area of the gap between the shelves Since the size of the head could be expected to influence the size of the gap appropriate ratios are provided to more accurately assess differences between treatment groups Probability values derived from *t* tests are indicated in table 4 and reveal significant differences between most treated groups when compared to controls Controls for *in vivo* experiments were at a slightly earlier development age than those fixed *in utero* This younger developmental stage is reflected in the smaller dimensions of the head The lesser palate gap relates to the selection of *in utero* embryos with vertical shelves and provides evidence that the shelves moved toward the midline in the *in vivo* group Cortisone- and vitamin A treated embryos were more advanced than *in vivo* controls and had greater head dimensions yet their relative gap width or area was also greater Embryos which had received x ray treatment did not differ in chronological age from controls but were smaller in all other dimensions except those pertaining to gap ratios The latter were significantly increased

Comparing measurements within a group the correlation of morphological rating or embryonic weight with gap width or area was negative for *in vivo* control embryos (table 5) which indicated a decrease in gap with progressive embryonic development. As a check on this method correlations with head dimensions were also calculated and found to be positive. However in the teratogen treated groups

TABLE 5

Correlation coefficients for correlation of morphological rating or weight with head and gap measurements from embryos of untreated and teratogen-treated mice

Factors correlated		Tongue displaced				Tongue completely removed			
x	y	Control	Cortisone	Vitamin A	X-ray	Control	Cortisone	Vitamin A	X-ray
Morphological rating	Gap width	−0.5057 [1]	+0.1807	—	—	−0.7896 [1]	+0.0679	—	—
	Gap area	−0.4704 [1]	−0.4135 [2]	—	—	−0.7090	−0.1661	—	—
	Head width	+0.7430 [1]	+0.8370 [1]	—	—	+0.8175 [1]	+0.7818 [1]	—	—
	Head length	+0.7844 [1]	+0.9294 [1]	—	—	+0.7456 [1]	+0.8734 [1]	—	—
Weight	Gap width	−0.4629 [1]	+0.0316	+0.3611 [1]	+0.1689	−0.5865	+0.0334	+0.3071	−0.1471
	Gap area	−0.4367 [1]	−0.4968 [1]	+0.0402	−0.1186	−0.5445	−0.2067	−0.2782	−0.1116
	Head width	+0.9389 [1]	+0.8565 [1]	+0.8948 [1]	+0.7913 [1]	+0.7093	+0.8027	+0.6700	+0.6316
	Head length	+0.9308	+0.9316	+0.8389	+0.7777	+0.6149	+0.8643	+0.7969	+0.8251

[1] Indicates statistical significance from zero ($p < 0.01$).
[2] Indicates statistical significance from zero ($p < 0.05$).

——— 1965 Amniotic fluid measurements in cortisone and x-irradiated mice. Proc. Soc. Exp. Biol. Med., 118 606–609.

Walker, B. E., and B Crain 1960 Effects of hypervitaminosis A on palate development in two strains of mice. Am. J Anat., 107 49–58.

——— 1961 Abnormal palate morphogenesis in mouse embryos induced by riboflavin deficiency Proc. Soc. Exp. Biol. Med., 107: 401–405.

Walker B E., and F C. Fraser 1956 Closure of the secondary palate in three strains of mice. J Embryol. Exp. Morph., 4 176–189.

——— 1957 The embryology of cortisone-induced cleft palate. J Embryol. Exp. Morph., 5 201–209.

Zeller K. B., S. Weinstein and R. D Gibson 1964 A study of the morphology and the time of closure of the palate in the albino rat. Arch. Oral Biol., 9 545–554.

vitamin A treated embryos were at a slightly later developmental stage than controls which should have favored greater shelf movement Nevertheless the gap between palatine shelves had a greater area relative to the surrounding head in teratogen-treated embryos than in controls after manual displacement of the tongue which thus demonstrated retardation in movement of the shelves toward the midline. Irradiated embryos were retarded relative to controls by all criteria except chronological age which is consistent with previous reports on the effects of this teratogen Gap area in such embryos was greater than controls despite a smaller head size the difference being more extreme than with the other two teratogens

Within a group of normal embryos gap width or area should decrease with advancing developmental age until obliterated by fusion of the palatine shelves Such a correlation was found in both of the *in vivo* control groups In teratogen treated groups there was either no correlation or else there was an increase in gap with age which indicated inhibition by the teratogens of a normal increased tendency of the shelves to move together with increased age

Thus a basic effect of the three teratogens studied is inhibition of an intrinsic tendency for the palatine shelves to move toward the midline However before considering this as the only or even primary cleft palate-inducing effect of these teratogens the role of the tongue in palate closure needs to be further evaluated The experiments presented here show that it probably plays a significant role in palate closure, but the question of whether teratogens affect this aspect of palate development has not yet received much attention Fujino et al. (64) listed defective tongue musculature as one result of vitamin A treatment. Trasler and Fraser (63) explained the cleft palate associated with cleft lip in strain A/J mice as being due to inhibition of tongue displacement by the large median process that develops in these embryos Inhibition of tongue displacement was also considered to be the basis for cleft palate in experiments with amniotic sac puncture (Walker and Fraser '57 Trasler et al. '56; Walker '59) However amniotic fluid deficiency was not found to correlate with development of cleft palate after cortisone or x ray treatment (Walker, '65)

LITERATURE CITED

Asling, C. W., M. M. Nelson, H. L. Dougherty, H. V Wright and H. M. Evans 1960 The development of cleft palate resulting from maternal pteroylglutamic (folic) acid deficiency during the latter half of gestation in rats. Surg. Gyn. Obst., *111*: 19–28.

Atnip, R. L. 1963 The role of surface tension in experimentally induced elevation of embryonic palatal shelves. Anat. Rec., *145* 306.

Callas G., and B. E. Walker 1963 Palate morphogenesis in mouse embryos after x-irradiation. Anat. Rec., *145*: 61–71

Chamberlain, J G. 1966 Development of cleft palate induced by 6-aminonicotinamide late in rat gestation. Anat. Rec., *156*: 31–40.

Coleman, R. D 1965 Development of the rat palate. Anat. Rec., *151*: 107–118.

Fujino H., S. Handa and T Katsuki 1964 An experimental study of cleft palate. Proc. Congenital Anomal. Res. Assoc., *4*: 25–26.

Jacobs, R. M. 1964 Histochemical study of morphogenesis and teratogenesis of the palate in mouse embryos. Anat. Rec., *148*: 691–697

——— 1966 Effects of cortisone acetate upon hydration of embryonic palate in two inbred strains of mice. Anat. Rec., *156*: 1–4.

Larsson, K. S. 1960 Studies on the closure of the secondary palate. II. Occurrence of sulpho mucopolysaccharides in the palatine processes of the normal house mouse. Exp. Cell Res. *21*: 498–503.

——— 1962 Studies on the closure of the secondary palate III. Autoradiographic and histochemical studies in the normal mouse embryo. Acta Morph. Neer Scand., 4 349–367

Lazzaro, C. 1940 Sul meccanismo di chiusura del palato secondairo. Monit. Zool. Ital., 51 249–273.

Peter K. 1924 Die entwicklung des säugetier gaumens. Ergebn. Anat. Entwicklungsgesch 25: 488–564

Ross, L. M. 1964 *In vivo* palatine shelf movement following cortisone treatment. Anat. Rec., *148*: 328–329

——— 1965 *In vivo* palatine shelf movement in mice after maternal treatment with several teratogens Anat. Rec., *151*: 406.

Trasler, D G., and F C. Fraser 1963 Role of tongue in producing cleft palate in mice with spontaneous cleft lip Devel. Biol., *6*: 45–60.

Trasler D G., B E. Walker and F C. Fraser 1956 Congenital malformations produced by amniotic-sac puncture. Science *124*: 439.

Walker B. E. 1959 Effects on palate development of mechanical interference with the fetal environment. Science *130*: 981.

——— 1961 The association of mucopolysaccharides with morphogenesis of the palate and other structures in the mouse embryo. J Embryol. Exp. Morph., *9*: 22–31

PALATINE SHELF MOVEMENT
Lawrence M. Ross and Bruce E. Walker



PLATE 1

EXPLANATION OF FIGURES

1 The head of an untreated embryo fixed *in utero* is shown with lower jaw and tongue removed. It has the vertical palatine shelf condition which constituted the starting point for most *in vivo* manipulation. All embryos illustrated in this article were at approximately the same stage of development, with chronological ages ranging from 14 days 18 hours to 15 days 3 hours postconception and with morphological ratings of 10–13 where applicable.

2 An untreated embryo fixed *in utero* with its left shelf in a horizontal (transverse) plane and its right shelf in a vertical (sagittal) plane. Although this condition rarely prevailed at the start of *in vivo* manipulations it was uniquely useful for comparison of shelf movement under natural and artificial conditions within the same embryo, as illustrated in the next figure.

3 *The left shelf of this* control embryo was *horizontal before its tongue was removed in vivo.* The right shelf has moved to an essentially horizontal plane but is not as close to the nasal septum as the left shelf.

4 The tongue of this control embryo was displaced, but not removed. The shelves have moved into a horizontal position anteriorly but have not flattened and extended toward the midline sufficiently to bridge the gap between nasal and mouth cavity.

5 The mother of this embryo was treated with cortisone. The embryo's tongue was displaced by *in vivo* manipulation and the shelves were observed to go horizontal, anteriorly.

6 This embryo also received cortisone but its tongue was completely removed instead of just displaced. The shelves are inclined toward the midline compared to the embryo in figure 1 *but they are not flattened into the horizontal plane.*

7 The palatine shelves of this vitamin A-treated embryo moved to an intermediate position after complete removal of the tongue. Compare the obscuring of internal nares and flattening of shelf contours with the condition of equivalent structures in figure 1.

8 An x-irradiated embryo after tongue displacement, showing flattening of the shelves anteriorly with a large residual gap.

9 An x-irradiated embryo after complete removal of the tongue showing incomplete flattening of the shelves *anteriorly.*




11


12




14



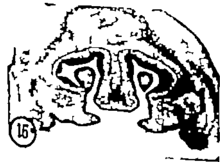

16



PLATE 2

EXPLANATION OF FIGURES

10 This section taken at the level of the nasal septum (i.e. anterior third of the palate) of a control embryo after tongue displacement shows the shelves to be horizontal but below the septum and separated from each other by a substantial gap.

11 The tongue was displaced in this control embryo and solid CO_2 was applied to embryo and surrounding fluid, with postfixation in chilled ethanol, then Bouin's fluid. This method confirmed the *in vivo* observation that the shelves moved to a horizontal position

12 The tongue was completely removed from this control embryo and the consequent horizontal positioning of the shelves, without movement toward the nasal septum, can be seen.

13 An embryo similar to the preceding with shelves close to an intermediate position at this level, but horizontal in sections taken more caudally

14 The shelves of this vitamin A-treated embryo moved to a horizontal plane at the level of the nasal septum after tongue displacement.

15 The shelves are at the intermediate position in this cortisone-treated embryo, after complete removal of the tongue.

16 Anteriorly the shelves became horizontal in this x irradiated embryo after tongue displacement.

17 After removal of the tongue the shelves retained an intermediate position in this x irradiated embryo

The Fine Structure and Development of the Peritubular Contractile Cell Component in the Seminiferous Tubules of the Mouse [1]

MICHAEL H. ROSS

Department of Anatomy New York University School of Medicine New York, New York

ABSTRACT Testes of sexually mature, as well as newborn and young mice of varying ages were studied by electron microscopy. The seminiferous tubules in the mature mouse possess a single cell layer of extremely flattened cells which form a sheath-like structure around the epithelium of the tubule. These peritubular cells are characterized by cytoplasmic filaments and other features which are typical of smooth muscle cells. A basement lamina is associated with the interstitial or peripheral surface of the cell. Peripherally there is an additional cellular layer consisting of connective tissue fibrocytes.

In newborn animals, the cells surrounding the tubule epithelium consist of a homogeneous population of fibroblasts, 3–4 layers in thickness. With growth and development of the testes the number of cell layers is reduced and the cells become more attenuated. At 13 days, those cells which are closest to the epithelium show localized aggregates of fine filaments, as well as what appears to be the elaboration of a basement lamina. By 17 days, the cytoplasmic filaments are more numerous and the basement lamina is well defined; by 19 days, the cells closely resemble the peritubular muscle cells of the adult.

The probable functional role of these cells is discussed with respect to both sperm transport and the production and maintenance of the surrounding connective tissue stroma.

Until recently the structure of the seminiferous tubules in the mammalian testis has been regarded as consisting of a complex stratified epithelium which is invested by a capsule or tunica propria of fibroelastic tissue and flattened fibroblasts. Since the sperm within the tubules are not motile, the manner in which they are transported to the efferent ducts has consequently been considered to involve either a continuous pushing effect, *a vis a tergo* which theoretically might be provided by the constant release of new sperm or by the secretion and flow of fluid from the tubules to the proximal region of the epididymal duct. Evidence for the fluid conveyance of the nonmotile sperm lies chiefly in the demonstration that ligation of the ductuli efferentes results in a striking increase in testicular fluid (van Wagenen '24 Oslund, '26 Young, '33). Also distal to the point of ligation the sperm become retarded in their movement (Toothill and Young, '31).

On the basis of several subsequent studies there is also evidence indicating that a contractile mechanism may play a role in conveying the nonmotile sperm along the length of the seminiferous tubules. Roosen-Runge ('51) by means of cinematographic recording, demonstrated contractile activity in the seminiferous tubules of the rat and dog. The contractions not only affected the shape and width of the lumen but were also noted to travel along the length of the tubule. Rhythmic contractile activity has also been described by Cross ('58) in the testis of the rabbit.

Because of the apparent absence of smooth muscle, Roosen-Runge ('51) suggested that the contractile activity seen in the rat and dog testes is caused by contraction and relaxation of the Sertoli cells. Although Cross ('58) did not define the site wherein the contractile activity originated in the rabbit testis, it was stated that they (the tubules) did not exhibit contractions of their own — a finding consistent with the absence of smooth muscle in their walls. The observed activity however was thought to facilitate the passage of sperm toward the efferent ducts.

---

[1] Supported in part by grant AM-05-[illegible] from the National Institutes of Health.

light microscope level indicates that these cells are typical connective tissue fibrocytes.

In the electron microscope, the dense band is revealed to consist of a single layer of extremely flattened cells which forms a sheath that completely surrounds the tubule (fig. 2). On the interstitial side of this cellular sheath, there is a second cellular layer. The cells which form this outer layer can be readily identified as fibrocytes (figs. 2, 3). Their thin cytoplasmic processes tend to follow the surface contours of the tubule, but there are gaps of variable dimensions between the processes of adjacent fibrocytes.

In contrast to this outer layer of fibrocytes, the cells of the inner layer which for descriptive purposes are designated here as peritubular cells, form a functionally continuous sheath. The opposing or contiguous membranes of neighboring peritubular cells are separated by a space of 160–200 Å. The cytoplasmic portion of these cells is thicker than the processes of the fibrocytes, and at low magnifications appears appreciably more electron-dense.

The morphology of the cytoplasmic organelles e.g. the Golgi apparatus, mitochondria, and the rough-surfaced endoplasmic reticulum, is essentially the same in both the fibroblasts and the peritubular cells. However there is a difference as regards the distribution of these organelles in the two cell types. Because of the very attenuated processes of the fibrocyte, there are few areas in the peripheral parts of the cell where such structures can be found. In the peritubular cells, both mitochondria and profiles of the endoplasmic reticulum tend to be centrally disposed along the breadth of the cell rather than being generally restricted to the nuclear region, as is the case with the fibrocytes (figs. 1, 3, 6). Furthermore the peritubular cells are noticeably richer in mitochondria.

In addition to the cytoplasmic components just mentioned, lipid droplets are frequently observed in both the fibrocyte processes and the cytoplasm of the peritubular cells (figs. 4, 5). These same inclusions are also occasionally observed in the endothelial cells of the intertubular capillaries (fig. 2). Often the lipid droplets are of such size that there is a conspicuous bleb or protrusion in the cell at the site where they are contained.

At higher magnifications, it becomes evident that the greater density of the cytoplasm of the peritubular cells is due to the presence of fine filaments (~ 40 Å in diameter) which are comparable in appearance to the myofilaments seen in smooth muscle cells (figs. 8, 11, 23, 25). The filaments are arranged in a parallel array and occupy the major portion of the cytoplasm. In addition, there are several other structures found in the peritubular cells which are also common to smooth muscle. Small interfilamentous dense areas which have been variously referred to as dense bodies (Caesar et al. '57) attachment devices (Pease and Molinari, '60) or fusiform densities (Bloom and Fawcett, '62) are also evident. These structures appear as small irregular areas whose density is greater than the surrounding region of cytoplasm. They are usually located in close apposition to the plasma membrane (figs. 6, 8, 11).

The cell membrane also contains small vesicular in-pocketings of the kind characteristically seen in smooth muscle cells (figs. 8, 11). These membranous invaginations, or pinocytotic vesicles occur along the outer and inner surfaces of the cell, but are absent at the junction of adjoining cells. Since this kind of structure is also commonly seen in endothelial cells and in fibrocytes it is not in itself a distinguishing criterion in terms of cell identification. However the combination of the pinocytotic vesicles along with the cytoplasmic filaments and dense areas, establishes a basic similarity between the peritubular cell component and smooth muscle cells in other organs.

Although the fine structure of the peritubular cell may also be regarded as being similar to myoepithelium (see Tandler and Ellis '65) the location of these cells is such that they are within a connective tissue compartment. In effect, the peritubular cells are separated or isolated from the seminiferous epithelium by a narrow space which contains the epithelial basement lamina and varying amounts of collagen fibrils (figs. 7, 8, 9). Fibrocytes, however are conspicuously absent in this connective tissue compartment. Peripheral

More recent studies utilizing the electron microscope have revealed that a contractile-type cell is present in the connective tissue framework of the seminiferous tubules Clermont ('58 '60) reported the presence of cells surrounding the seminiferous epithelium in the rat which resembled smooth muscle cells Similar findings have subsequently been reported by Lacy and Rotblat ('60) Brökelmann ('60) and Leeson and Leeson ('63) The presence of contractile-type cells in the human testis has also recently been reported (Ross and Long 66) While these studies point out that the contractile component bears a close resemblance to smooth muscle cells its exact nature is not entirely clear Clermont (58) regarded these cells as a new type of contractile epithelium Lacy and Rotblat (60) on the other hand considered these same contractile elements as "a type of smooth muscle cell but of a different level of organization than that found in smooth muscle of other organs" In the human testis the cytoplasm of the contractile cells is identical in most respects to smooth muscle although a possible relationship to connective tissue cells has been suggested by virtue of the relative prominence of its endoplasmic reticulum and the absence of typical fibrocytes in the supporting stroma (Ross and Long 66)

In view of the apparent significance of a contractile component associated with the seminiferous tubules it is desirable to clarify the nature of these cells with respect to their specific role and functional capacity The present report based on a study of the mouse testis is concerned with the structural organization of the peritubular contractile system in the adult animal as well as the developmental changes which give rise to this system

MATERIALS AND METHODS

The testes utilized in this study were obtained from mature male albino mice 3–5 months old as well as newborn and young mice of 7 13 17 19 21 and 25 days of age Specimens from a total of six animals in each of the above age groups were examined The tissues were prepared for electron microscopic study by fixing in a 3% phosphate-buffered glutaraldehyde solution pH 7 4 (Sabatini et al '63) followed by fixing in a 1% osmium tetroxide solution also phosphate-buffered Generally the entire testis was placed in the glutaraldehyde solution for a period of two hours and then thin slices, several millimeters in thickness were cut from the surface of the organ and placed in the osmium tetroxide solution for 1–1.5 hours (In order to reduce the problem of tubule separation the tissue slices were not cut into smaller pieces until they had a chance to harden in the alcohol solution) Following fixation the specimens were dehydrated in a graded series of ethanol solutions and embedded in Epon 812 (Luft 60)

Thin sections of the epon-embedded specimens were cut on a Huxley microtome and stained with either lead citrate (Reynolds 65) or lead hydroxide (Millonig '61) to enhance contrast In addition thick sections 1–2 μ thick, were cut for examination in a phase-contrast microscope An RCA EMU 2c electron microscope was used for observation and recording of the findings.

OBSERVATIONS

Adult animals

Phase-contrast examination of epon-embedded specimens from the testes of mature mice reveals a thin dense band which surrounds the epithelial component of the seminiferous tubules. The location of this band corresponds in part to what is generally regarded as the connective tissue investment or tunica propria of the tubules In well preserved specimens, the density and general nature of this band, however readily distinguishes it from a typical connective tissue component. Although there is no appreciable cytoplasmic detail evident at the level of resolution afforded by phase-contrast optics its cellular nature is apparent by virtue of the irregularly spaced elongated nuclei which it contains (fig 1)

Nuclei of similar size and shape are also noted in the stroma between adjacent tubules (fig 1) They are frequently closely applied to the dense band surrounding the epithelium of the seminiferous tubule The shape of these nuclei and the inability to discern the extent of their cytoplasm at the

the rough-surfaced endoplasmic reticulum. These features, in combination with a prominent Golgi region, are characteristic of connective tissue cells actively engaged in collagen synthesis (Porter '66). Indeed, the presence of "immature" collagen fibrils in the extracellular environment would tend to support the contention that, during this early period, collagen is being produced. For these reasons the cells described here are designated as fibroblasts.

By the seventh day after birth only minor changes are evident with regard to the appearance of the fibroblasts and the extracellular formed elements. The fibroblasts tend to be flatter or more elongate than those observed in the neonate and those lying closest to the tubule epithelium have formed an almost distinctive single cell layer (fig. 18). The cells forming this inner layer tend to be in close apposition to one another at their peripheral margins and, in this respect, more closely resemble the arrangement of the peritubular contractile cell component of the adult. The fibroblasts located outside of this layer seem to lack any specific orientation. The appearance of the cytoplasm, however, is the same in both the inner and outer cell layers.

At 13 days a significant change is noted with respect to the inner or peritubular layer of fibroblasts. The cytoplasm of these cells still possesses an abundance of ribosomes as well as an extensive granular endoplasmic reticulum (figs. 19, 20). Occasionally, however, localized aggregates of fine filaments are observed in the cytoplasm (fig. 20). In addition, an amorphous extracellular material is seen in relation to the outer surface of the cell. Although this substance is somewhat poorly defined and may be absent or discontinuous in certain regions, where present it is similar in appearance to the basement lamina of the peritubular contractile cells of the adult.

At 17 days this same extracellular component is well defined and may be clearly recognized as a basement lamina (figs. 21–23). The fine cytoplasmic filaments are also considerably more numerous at 17 days and occupy a substantial portion of the cytoplasm (fig. 23). The fibroblasts residing peripherally to the basement lamina, however, are unaltered in appearance.

By 19 days most of the cells adjacent to the tubule closely resemble the peritubular smooth muscle cells seen in the adult (figs. 24, 25). The cells are flat and form an uninterrupted cellular sheath. Myofilaments can be readily recognized at this stage and occupy a substantial portion of the cytoplasm. Along with this there is a reduction in the endoplasmic reticulum and the number of free ribosomes in the cytoplasm. The plasma membrane also exhibits pinocytotic vesicles although they are relatively scarce. The cytoplasmic densities along the plasma membrane are, however, not apparent at this stage of development.

While the peritubular cells at this later stage (17–19 days) are, for the most part, comparable to that seen in the adult, there are some cells which retain certain features that characterize the fibroblast. Despite the presence of numerous cytoplasmic filaments, these cells also contain dilated profiles of endoplasmic reticulum, a large Golgi region, and areas of cytoplasm which are still rich in ribosomes (figs. 22, 24). Their appearance suggests that they may still retain the capacity for the production of connective tissue proteins and polysaccharide substances. In the 23-day-old animal, cells of this type are considerably more difficult to find.

DISCUSSION

Recent electron microscopic studies of the testis in both rat and man have demonstrated the presence of a contractile-type cell in the boundary tissue of the seminiferous tubules. In the mouse testis a thin connective tissue layer forms the peripheral limits of the tubule but, significantly, there is also a well defined single layer of flattened cells, the peritubular cell component, that forms an uninterrupted cellular sheath within this surrounding connective tissue framework. Despite a similarity in the light microscope between the fibrocytes of the more peripheral connective tissue component and the cells which form the peritubular sheath, the fine structural characteristics of their cytoplasm are quite different. Unlike the fibrocytes, the peritubular cells possess the fine structural features of smooth muscle cells.

to the peritubular cell layer the connective tissue is more typical in that fibrocytes as well as other connective tissue cells such as macrophages are present (figs. 2 3)

On the interstitial or peripheral surface of the peritubular cell an amorphous material identical in appearance to the basement lamina of the seminiferous epithelium is present The opposite surface facing the epithelium is devoid of this material (figs 3–5 23 25)

Occasionally cells are observed in the peritubular cell sheath which lack the contractile features described above The cytoplasm is quite scant and appears relatively clear or electron-translucent. Furthermore few organelles are noted in their cytoplasm In the few instances where these "clear" cells were observed it was noted that the peritubular cell component still retained its sheath-like integrity by overlapping the interposed clear cell (fig. 9)

The arrangement of the tissues surrounding the seminiferous epithelium is the same throughout all but the terminal portion of the tubule In this region fibrocytes are found in place of the contractile peritubular cells The site of transition from the one cell type to the other has not been observed However adjacent tubules have been observed in the region of the mediastinum testis wherein one tubule still retains the typical peritubular cell component while in the other presumably the terminal part of the seminiferous tubule it is lacking (fig 10) The site normally occupied by the contractile cells contains instead typical fibrocytes The structural differences between these two parts of the tubule are readily apparent when observed at higher magnifications (figs 11 12)

Within this same area there is also some variation with respect to the appearance and location of basement lamina material In several specimens the epithelial basement lamina varied in thickness and in occasional sites appeared to consist of several distinct layers (figs. 10 11) Similar appearing material is sometimes encountered between various connective tissue cells in the interstitial spaces (fig 10) However there appears to be no definitive relationship between this basement lamina like material and any of the cells within the connective tissue stroma.

New-born and sexually immature animals

In the newborn the tubules appear as solid cords of epithelial cells which are surrounded by several layers of elongate cells. In the phase contrast microscope, there is no evidence of the distinctive dense band which defines the site of the peritubular cell component. Instead a homogeneous population of elongate connective tissue cells 2–3 layers in thickness, is observed surrounding each of the epithelial cords (fig 13) These cells appear to possess a relatively abundant cytoplasm much of which is in the form of long cytoplasmic processes. The nuclei are elongate and contain several nucleoli. Mitotic figures are occasionally observed at this stage Leydig cells are also observed in small groups or singly peripheral to the elongated cells surrounding the cord epithelium

When observed in the electron microscope the connective tissue cells can be identified readily as consisting of a homogeneous population with regard to cell type (fig 14) The cytoplasm is characterized by an abundance of free ribosomes and profiles of granular endoplasmic reticulum (figs 15–17) The cisternae of the endoplasmic reticulum are usually dilated and contain a moderately electron-dense, homogeneous substance (figs. 16 17) Mitochondria are also relatively numerous. Other than the Golgi region which often appears to be quite extensive there are no other particularly prominent features displayed by these cells The plasma membrane is relatively smooth and lacks the pinocytotic vesicles

The extracellular spaces contain varying amounts of collagen The diameter of the unit collagen fibrils is relatively uniform, but is smaller (~ 250 A) than those observed in the adult (figs. 15 16) The basement lamina of the tubule epithelium is also thinner than that seen in the adult (figs 15 16 17)

The connective tissue component described here differs from that of the adult testis in several significant respects. The cells are larger than the typical fibrocytes and contain a considerably greater quantity of free ribosomes as well as more numerous and often dilated profiles of

files of the rough-surfaced endoplasmic reticulum. This and other features enable us to identify these cells as fibroblasts. However during postnatal development, there is a clearly evident transformation of some of these cells into contractile or smooth muscle cells. This change or transformation is limited to the single layer of fibroblasts which are in closest proximity to the tubule epithelium. As early as 13 days, there is evidence of the production of a basement lamina along the outer or peripheral surface of the cell, as well as the production of cytoplasmic filaments within the cell. At 17 days, the basement lamina is well established and the cytoplasm is filled with numerous and presumably contractile filaments. The cells more removed from the tubule epithelium are essentially unchanged.

In a similar study of the rat testis, Leeson and Leeson ('63) described a layer of low cuboidal cells around the tubule epithelium in the neonate. External to this layer a second cellular layer or zone containing numerous fine processes of mesenchymal cells of the interstitium was described. Although the origin of the inner cell layer seemed obscure these investigators concluded that it probably arose from mesenchymal cells of the interstitium since they lie external to the basement membrane of the tubule. Because of the magnifications and limited areas of the cells depicted in their illustrations, it is difficult to compare the basis for their findings with those of the present study. However in at least one of their micrographs a well defined cytoplasmic process is seen extending from a "cuboidal" cell.

While it may simply be a question of semantics to classify or describe the connective tissue cells of the newborn and very young animal as mesenchymal cells versus fibroblasts, the latter term appears more appropriate in view of the fact that collagen as well as other proteins and polysaccharides are undoubtedly being synthetized during this period of rapid post natal growth. By 13 days the amount of collagen present around the tubule is not markedly different from that which is observed in the young adult. It thus appears that the cells which give rise to the peritubular smooth muscle layer initially participate in the formation of the interstitial supporting stroma along with the more peripheral population of connective tissue cells. While these findings do not confirm those of Baillie ('64) with respect to the developmental pattern of the peritubular cells they closely parallel the observations of Leeson and Leeson ('63) who noted that the peritubular component in the rat testis appears virtually adult in morphology by 22 days.

The possibility that the peritubular smooth muscle cells are a result, not of a cellular transformation from fibroblasts but rather from other cells which migrated into the area appears quite remote. Although no statistical counts of the number of cells within the interstitial spaces were made at the various time intervals studied, there was no apparent increase in the number of cells present after the first week. Furthermore some of the peritubular cells observed in the 17-day-old animals contained dilated profiles of the rough-surfaced endoplasmic reticulum and areas of cytoplasm still rich in ribosomes (fig. 22) thus resembling to some extent the fibroblasts seen in the earlier stages. At the same time these cells possess the fine cytoplasmic filaments characteristic of smooth muscle cells. The morphology of such cells thus suggests that they do indeed undergo a transformation from fibroblasts to smooth muscle cells. The observation would further suggest that for a short interval, at least, the peritubular cells may be actively synthesizing substances for extracellular deposition, while at the same time they may have acquired the ability to contract.

In terms of function, a variety of roles including physical support, regulation of the composition of fluids which enter the tubule and facilitation of sperm transport by maintenance of pressure have been postulated for the boundary tissue of the tubules. The production and maintenance of the connective tissue stroma by the interstitial cell elements clearly provide for the physical support and integrity of the individual tubules. The possible regulation of the composition of fluids entering the tubule was suggested by Regaud ('01) who noted that the peritubular cells in the rat testis, when examined in silver preparations exhibited a polygonal pattern similar

In the human testis contractile cells are also present around the tubule epithelium but in a multilayered arrangement instead of sheath like (Ross and Long 66) As might be anticipated the organization of the boundary tissue in the mouse testis is not unlike that of the rat. The observations reported here are essentially in agreement with the findings reported by Clermont ('58) and Lacy and Rotblat (60) in their studies of the boundary tissue in the rat testis Both Clermont and Lacy and Rotblat have indicated that the tissue surrounding the seminiferous epithelium is composed of four principle layers two of which are cellular and two of a noncellular nature i e basement lamina plus collagen It was also reported that the cytoplasm of the peri tubular cells or interlamellar cells as they are designated by Clermont, resembles smooth muscle cytoplasm in that it con tains fine filaments and characteristic pino-cytotic vesicles along the plasma mem brane The cells comprising the outer layer were identified as typical connective tissue cells

Certain differences between these two species however do appear to exist. In the rat testis an amorphous material re-sembling basement lamina is present along both the outer and inner surfaces of the peritubular cells (Clermont 58 Lacy and Rotblat '60) In the mouse only a single comparable layer is present, and this is found along the outer or peripheral sur face of the peritubular cells. Also in the rat testis a thickening of the plasma mem brane at the junction of adjacent cells bearing a resemblance to the intercalated discs of cardiac muscle was reported (Cler mont, '58) Similarly Leeson and Leeson (63) reported the presence of a small desmosome between adjacent cells In the mouse testis there is no evidence of any specialized attachment device along the cell surface However it is possible that these structure correspond to the cyto-plasmic densities associated with the myo-filaments rather than a desmosome or other type of attachment device

In regard to the nature of these cells Clermont ('58) has suggested that the inner cell layer should be considered as a new type of contractile epithelium While these cells do indeed possess an epithelial character by virtue of their contiguous ar rangement, on the basis of location in a connective tissue compartment as well as ultrastructural characteristics and develop-mental pattern they would more appropri-ately fit in the general category of smooth muscle This interpretation is more in agreement with the statement of Lacy and Rotblat ('60) who consider the peritubular cells in the rat testis to be a type of smooth muscle but of a different level of organiza-tion than is usually encountered in smooth muscle cells of other organs. This distinc tion was prompted primarily by the im pression that they contained fewer fila ments than are seen in typical smooth muscle cells The appearance of the peri tubular cells as observed in this study however does not support such a distinc tion On the basis of the fine structura features it seems quite justifiable to con sider the peritubular cell as a smooth mus cle cell. Indeed the numerous cytoplasmic filaments in these cells combined with the presence of charactristic cytoplasmic den sities are comparable in general appear ance to that of smooth muscle cells o other organs

In regard to the developmental pattern of the peritubular component, there is a marked similarity between the develop mental pattern of smooth muscle in the media of the chick aorta as described by Karrer (60) and the changes which are described in the present paper According to Karrer s findings in young embryos, the media or at least that portion of the aortic wall which topographically corresponds to the media in the fully developed aorta, consists entirely of cells which have the appearance of fibroblasts In older em-bryos however certain cells of the media were reported to resemble smooth muscle cells These cells showed evidence of fine cytoplasmic filaments and a reduction in the extent of the endoplasmic reticulum. Their overall appearance was clearly indic ative of smooth muscle Accordingly Kar rer hypothesized that, as development pro-ceeds the fibroblasts are transformed into smooth muscle cells

Similarly in the testis of the newborn mouse all of the cells surrounding the cord of tubule epithelium are characterized by an abundance of free ribosomes and

files of the rough-surfaced endoplasmic reticulum. This and other features enable one to identify these cells as fibroblasts. However during postnatal development, there is a clearly evident transformation of some of these cells into contractile or smooth muscle cells. This change or transformation is limited to the single layer of fibroblasts which are in closest proximity to the tubule epithelium. As early as 13 days, there is evidence of the production of a basement lamina along the outer or peripheral surface of the cell, as well as the production of cytoplasmic filaments within the cell. At 17 days, the basement lamina is well established and the cytoplasm is filled with numerous and presumably contractile filaments. The cells more removed from the tubule epithelium are essentially unchanged.

In a similar study of the rat testis Leeson and Leeson ('63) described a layer of low cuboidal cells around the tubule epithelium in the neonate. External to this layer a second cellular layer or zone containing numerous fine processes of mesenchymal cells of the interstitium was described. Although the origin of the inner cell layer seemed obscure, these investigators concluded that it probably arose from mesenchymal cells of the interstitium since they lie external to the basement membrane of the tubule. Because of the magnifications and limited areas of the cells depicted in their illustrations it is difficult to compare the basis for their findings with those of the present study. However in at least one of their micrographs a well defined cytoplasmic process is seen extending from a "cuboidal" cell.

While it may simply be a question of semantics to classify or describe the connective tissue cells of the newborn and very young animal as mesenchymal cells versus fibroblasts, the latter term appears more appropriate in view of the fact that collagen as well as other proteins and polysaccharides are undoubtedly being synthesized during this period of rapid postnatal growth. By 13 days the amount of collagen present around the tubule is not markedly different from that which is observed in the young adult. It thus appears that the cells which give rise to the peritubular smooth muscle layer initially participate in the formation of the interstitial supporting stroma along with the more peripheral population of connective tissue cells. While these findings do not confirm those of Baillie ('64) with respect to the developmental pattern of the peritubular cells, they closely parallel the observations of Leeson and Leeson ('63) who noted that the peritubular component in the rat testis appears virtually adult in morphology by 22 days.

The possibility that the peritubular smooth muscle cells are a result, not of a cellular transformation from fibroblasts, but rather from other cells which migrated into the area appears quite remote. Although no statistical counts of the number of cells within the interstitial spaces were made at the various time intervals studied, there was no apparent increase in the number of cells present after the first week. Furthermore some of the peritubular cells observed in the 17-day-old animals contained dilated profiles of the rough-surfaced endoplasmic reticulum and areas of cytoplasm still rich in ribosomes (fig. 22) thus resembling to some extent the fibroblasts seen in the earlier stages. At the same time these cells possess the fine cytoplasmic filaments characteristic of smooth muscle cells. The morphology of such cells thus suggests that they do indeed undergo a transformation from fibroblasts to smooth muscle cells. The observation would further suggest that for a short interval, at least, the peritubular cells may be actively synthesizing substances for extracellular deposition while at the same time they may have acquired the ability to contract.

In terms of function a variety of roles including physical support, regulation of the composition of fluids which enter the tubule and facilitation of sperm transport by maintenance of pressure have been postulated for the boundary tissue of the tubules. The production and maintenance of the connective tissue stroma by the interstitial cell elements clearly provide for the physical support and integrity of the individual tubules. The possible regulation of the composition of fluids entering the tubule was suggested by Regaud ('01) who noted that the peritubular cells in the rat testis when examined in silver preparations exhibited a polygonal pattern similar

to that of endothelial Regaud interpreted the cells forming this layer as modified connective tissue cells and suggested that this sort of cellular arrangement might serve as a protective device regulating the composition of the fluids which enter the tubule The electron microscopic studies offer no support for this hypothesis but confirm the epithelial-like arangement of the peritubular cells

In consideration of the structure of the tubule wall as determined from electron microscopic examination it is possible to arrive at a more elucidating concept as regards the function of the peritubular cells. Clermont (58) has suggested that these cells may play a role in the release of spermatozoa from the epithelium and in their transportation to the rete testis While there is no indication that spermatozoa require physical movement to effect their release from the Sertoli cell it does seem likely that the contractile waves as described by Clermont and others would facilitate the movement of sperm along the length of the tubule A small decrease in size of the outside diameter of the tubule as a result of contraction of the peritubular cells at any given point would be reflected in a decrease in the volume of the lumen at this same point Thus if the contraction moves as a wave the fluid contained within the lumen would be forced to take a directional flow or in effect be pumped along the length of the tubule Since the sperm come to be suspended within this same fluid medium after their release from the Sertoli cell they would presumably be carried along in a passive manner The movement of the spermatozoa would thus be dependent upon both the constant secretion of fluid into the tubule and the rhythmic contractions of the tubule wall In view of the relatively rapid movement of sperm contained within the tubule such a hypothesis may afford a more plausible explanation than a mechanism which is dependent only upon the secretion and flow of fluid

In addition to contractile activity it appears that the peritubular cell component may also play a role in connective tissue metabolism in the sexually mature animal. As a result of the transformation of the inner layer of fibroblasts into smooth muscle cells a space or compartment adjacent to the tubule epithelium is established in the maturing animal. Because of the epithelial like arrangement of the smooth muscle there is no communication or continuity between this space and the interstitium lying peripheral to the muscle cells. The interesting feature is that, within the compartment, collagen fibrils are observed but no cells are present. In older animals collagen is found in increased amounts but again no cells are observed in this space (unpublished observations).

Presumably in the young sexually mature animal most, if not all, of the collagen present within this space or compartment is produced prior to the transformation of fibroblast to smooth muscle cell. However, any further deposition of collagen or other components of the ground substance would seemingly have to arise as a product of either the epithelium or the peritubular smooth muscle cells Although it has been shown that epithelial cells can be stimulated to synthesize small amounts of collagen (Green and Goldberg '65) the one notable feature which suggests that in this situation it is the smooth muscle cells which are involved is the relatively frequent observation of profiles of the granular endoplasmic reticulum in their cytoplasm In smooth muscle cells observed in most other organs there is a relative paucity of cell organelles and the endoplasmic reticulum is constituted largely of smooth surfaced membranes (Rhodin, '62). Thus as compared to smooth muscle in most other sites, the extent of the rough-surfaced endoplasmic reticulum in the peritubular contractile cells is unusual and could be interpreted as being concerned with the synthesis of connective tissue proteins.

The contractile cell component observed in the human testis also exhibits a relatively prominent rough surfaced endoplasmic reticulum (Ross and Long '66) Interestingly the contractile cells are not arranged in a single epithelial-like layer but instead consist of overlapping cells, 3–4 layers in thickness which are separated from one another by variable amounts of collagen fibrils Furthermore unlike the mouse testis typical fibrocytes are not observed in the connective tissue stroma. This

finding thus also suggests that the contractile cells have the capacity to maintain the connective tissue of the interstitium.

While the inference that the peritubular cells perform a secretory function on the basis of morphology alone is somewhat speculative, other instances suggesting a relationship between the production of connective tissue fibers and smooth muscle cells have been reported. In early atherosclerotic and arteriolarsclerotic lesions (Parker '60; Parker et al. '64 Buck, '61 '62; Parker and Odland, '66) as well as in the pregnant and estrogen-stimulated uterus (Laguens and Lagrutta, '64 Ross and Klebanoff, '67) a marked increase in the rough-surfaced endoplasmic reticulum of smooth muscle cells is observed at a time when connective tissue fibers are being produced. Since both the fibroblast and smooth muscle cell are of mesodermal origin, the interconversion of the one cell type to the other as well as an inherent or latent capacity of smooth muscle cells to maintain a connective tissue environment, seems reasonable to anticipate.

LITERATURE CITED

Baillie, A. H. 1964 Ultrastructural differentiation of the basement membrane of the mouse seminiferous tubule. Quart. J. Micr. Sci., 105: 303–307

Brökelmann, J. 1960 Limiting layers of the seminiferous tubule in the albino rat. J Appl. Physiol., 31 1644 (abstract).

Buck, R. C. 1961 Intimal thickening after ligature of arteries. An electron microscopic study Circ. Res., 9 418–426.

——— 1962 Lesions in the rabbit aorta produced by feeding high cholesterol diet followed by a normal diet. An electron microscopic study Brit. J. Exp Path., 43 236–240.

Clermont, Y 1958 Contractile elements in the limiting membrane of the seminiferous tubules of the rat. Exp. Cell Res., 15 438–440.

——— 1960 The fine structure of the limiting membrane of the seminiferous tubule in the rat. Fourth Int. Conf. on Electron Micros., Berlin, 1958. Proc., 2: 429.

Cross, B A. 1958 Hypothalamic influences on sperm transport in the male and female genital tract. In Endocrinology of Reproduction. C. W Lloyd, ed. Academic Press, New York.

Ellis, Richard A. 1965 Fine structure of the myoepithelium of the eccrine sweat glands of man. J Cell Biol., 27 551–564

Green, H and B. Goldberg 1965 Synthesis of collagen by mammalian cell lines of fibroblastic and non fibroblastic origin. Proc. Nat. Acad. Sciences, 53 1360–1365

Karrer H. E. 1960 Electron microscope study of developing chick embryo aorta. J Ultrastruct. Res., 4: 420–454

Lacy D., and J Rotblat 1960 Study of normal and irradiated boundary tissue of the seminiferous tubules of the rat. Exp. Cell Res., 21 49–70.

Laguens, R., and J Lagrutta 1964 Fine structure of human uterine muscle in pregnancy Am. J. Obs. Gyn., 89: 1040–1048.

Leeson, C. R., and T S. Leeson 1963 The post natal development and differentiation of the boundary tissue of the seminiferous tubule of the rat. Anat. Rec., 147 243–259.

Luft, J. H. 1961 Improvements in epoxy resin embedding methods. J Biophys. Biochem. Cytol., 9 409–414.

Millonig, G. 1961 A modified procedure for lead staining of thin sections. J. Biophys. Biochem. Cytol., 11 736–739.

Oslund, R. M. 1926 Ligation of vasa efferentia in rats. Am. J. Physiol., 77 83–90.

Parker F 1960 Electron microscopic study of experimental atherosclerosis. Am. J Path., 36 19–53.

Parker, F and G. F Odland 1966 A correlative histochemical, biochemical and electron microscopic study of experimental atherosclerosis in the rabbit orta with special reference to the myo-intimal cell. Am. J Path., 48 197–239.

Parker F G. Odland, J W Ormsby and R. H. Williams 1964 In Evolution of the Atherosclerotic Plaque. R. J Jones, ed. U of Chicago Press, pp. 35–49.

Porter K. R. 1966 Mesenchyme and Connective Tissue in Histology R. O Greep, ed. McGraw-Hill, New York.

Regaud, C. 1901 Études sur la structure des tubes seminifères et sur la spermatogenèse chez les mammifères. Arch. D'Anatomie Microscopique, 4 101–155.

Reynolds, E. S. 1963 The use of lead citrate at high pH as an electron-opaque stain for electron microscopy J Cell Biol., 17 208–212.

Rhodin, J A. G. 1962 Fine structure of vascular walls in mammals with special reference to smooth muscle component. Physiol. Rev., suppl. 5, 42. 48–87

Roosen-Runge, E. C. 1951 Motions of the seminiferous tubules of the rat and dog. Anat. Rec., suppl. 153, 109 413 (abstract)

Ross, M. H., and I. R. Long 1966 Contractile cells in human seminiferous tubules. Science, 153 1271–1273.

Ross, R., and S J Klebanoff 1967 Fine structural changes in uterine smooth muscle and fibroblasts in response to estrogen. J Cell Biol., 32: 155–158.

Sabatini, D. D., K. Bensch and R. J Barrnett 1963 Cytochemistry and electron microscopy. The preservation of cellular ultrastructure and enzymatic activity by aldehyde fixation. J Cell Biol., 17 19–58.

to that of endothelial Regaud interpreted the cells forming this layer as modified connective tissue cells and suggested that this sort of cellular arrangement might serve as a protective device regulating the composition of the fluids which enter the tubule The electron microscopic studies offer no support for this hypothesis but confirm the epithelial like arangement of the peritubular cells

In consideration of the structure of the tubule wall as determined from electron microscopic examination it is possible to arrive at a more elucidating concept as re gards the function of the peritubular cells Clermont (58) has suggested that these cells may play a role in the release of spermatozoa from the epithelium and in their transportation to the rete testis While there is no indication that spermatozoa require physical movement to effect their release from the Sertoli cell it does seem likely that the contractile waves as described by Clermont and others would facilitate the movement of sperm along the length of the tubule A small decrease in size of the outside diameter of the tubule as a result of contraction of the peritubular cells at any given point would be reflected in a decrease in the volume of the lumen at this same point Thus if the contraction moves as a wave the fluid contained within the lumen would be forced to take a directional flow or in effect be pumped along the length of the tubule Since the sperm come to be suspended within this same fluid medium after their release from the Sertoli cell they would presumably be carried along in a passive manner The movement of the spermatozoa would thus be dependent upon both the constant secretion of fluid into the tubule and the rhythmic contractions of the tubule wall In view of the relatively rapid movement of sperm contained within the tubule such a hypothesis may afford a more plausible explanation than a mechanism which is dependent only upon the secretion and flow of fluid

In addition to contractile activity it appears that the peritubular cell component may also play a role in connective tissue metabolism in the sexually mature animal As a result of the transformation of the inner layer of fibroblasts into smooth muscle cells a space or compartment adjacent to the tubule epithelium is established in the maturing animal. Because of the epithelial-like arrangement of the smooth muscle there is no communication or continuity between this space and the interstitium lying peripheral to the muscle cells. The interesting feature is that within the compartment collagen fibrils are observed but no cells are present. In older animals collagen is found in increased amounts but again no cells are observed in this space (unpublished observations)

Presumably in the young sexually ma ture animal most if not all of the collagen present within this space or compartment is produced prior to the transformation of fibroblast to smooth muscle cell. However any further deposition of collagen or other components of the ground substance would seemingly have to arise as a product of either the epithelium or the peritubular smooth muscle cells Although it has been shown that epithelial cells can be stimu lated to synthesize small amounts of col lagen (Green and Goldberg '65) the one notable feature which suggests that in this situation it is the smooth muscle cell which are involved is the relatively fre quent observation of profiles of the gran ular endoplasmic reticulum in their cyto plasm In smooth muscle cells observe in most other organs there is a relativ paucity of cell organelles and the endo plasmic reticulum is constituted largely c smooth-surfaced membranes (Rhodin '62) Thus as compared to smooth muscle in most other sites, the extent of the rough-surfaced endoplasmic reticulum in the peritubular contractile cells is unusual and could be interpreted as being concerned with the synthesis of connective tissue proteins

The contractile cell component observed in the human testis also exhibits a rela tively prominent rough-surfaced endoplasmic reticulum (Ross and Long '66) Inter estingly the contractile cells are not ar ranged in a single epithelial like layer but instead consist of overlapping cells 3–4 layers in thickness which are separated from one another by variable amounts of collagen fibrils Furthermore unlike the mouse testis typical fibrocytes are not observed in the connective tissue stroma This


Ep
Flb
PC
Mac
Cap
Flb
PC
Mac
Ep
1
2

Tandler B 1965 Ultrastructure of the human submaxillary gland III. Myoepithelium. Z. Zellforsch, 68: 852–863

Toothill M. C., and W C. Young 1931 Time consumed by spermatozoa in passing through the ductus epididymis of the guinea pig as determined by means of India ink injections. Anat. Rec 50 95–107

van Wagenen, G. 1924 Changes in the testis of the rat following ligation of the ductuli efferentia. Anat. Rec., 29: 399 (abstract).

Young W C. 1933 Die resorption in den Ductuli Efferents der Maus und ihre Bedeutung für das Problem der Unterbindung im Hoden-Nebenhodensystem. Z. Zellforsch. u. mikroscop. Anat., 17: 729–759

PLATE 1

EXPLANATION OF FIGURES

1 Phase-contrast micrograph from the testis of a three-month-old mouse showing portions of two adjacent tubules with an intervening small blood vessel. Both tubules are bounded by a thin dense band. A single nucleus (arrow) can be seen within this band in the upper tubule Another nucleus (arrowhead) of similar size and shape can be seen in the interstitium. × 1800

2 Low-power electron micrograph showing the same tubules as in figure 1 but cut more distally in the specimen block. The interstitium contains portions of two macrophages (Mac) a capillary (Cap) and the processes of several fibrocytes (F) Immediately adjacent to the tubule epithelium (Ep) is the peritubular cell component (PC) which corresponds to the thin dense band seen in the phase-contrast microscope The cytoplasm of the peritubular cells also appears more electron-dense than that of the surrounding cells. × 7600

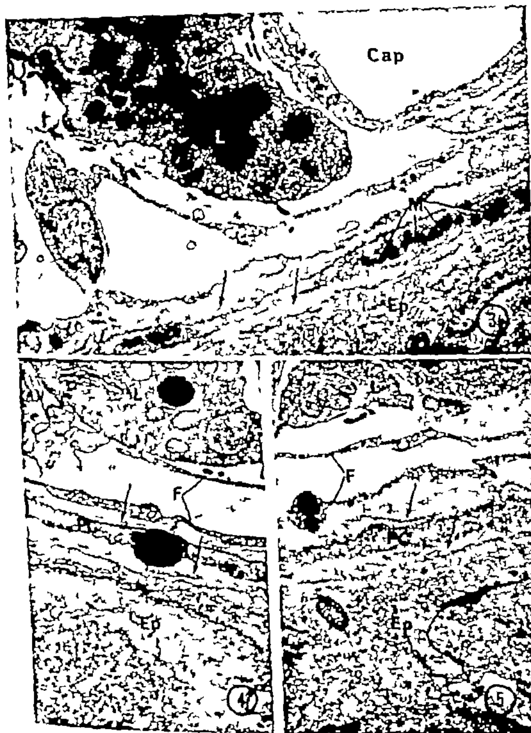

Cap
L
M
Ep
3
L
F
Ep
4
F
MC
Ep
5

PLATE 2

EXPLANATION OF FIGURES

3 A segment of a peritubular cell which reveals a number of mitochondria (M) The basement lamina (arrows) of both the epithelium (Ep) and the peritubular cell is just perceptible at this magnification. The two very thin less dense cytoplasmic strands lying above the peritubular cell are fibrocyte processes The lower process is an extension from the cell body of the fibrocyte (F) seen at the left The upper portion of the figure reveals part of a Leydig cell (L) and a capillary (Cap) × 11,500.

4 5 Portions of the tubule showing the epithelium (Ep) a peritubular cell (PC) and the more peripheral fibrocyte processes (F) A lipid droplet is seen in the peritubular cell in figure 4 and in the fibrocyte process in figure 5 Leydig cell cytoplasm (L) is present in the upper portion of both figures. Basement lamina of the epithelial and peritubular cells is indicated by arrows. × 11 400

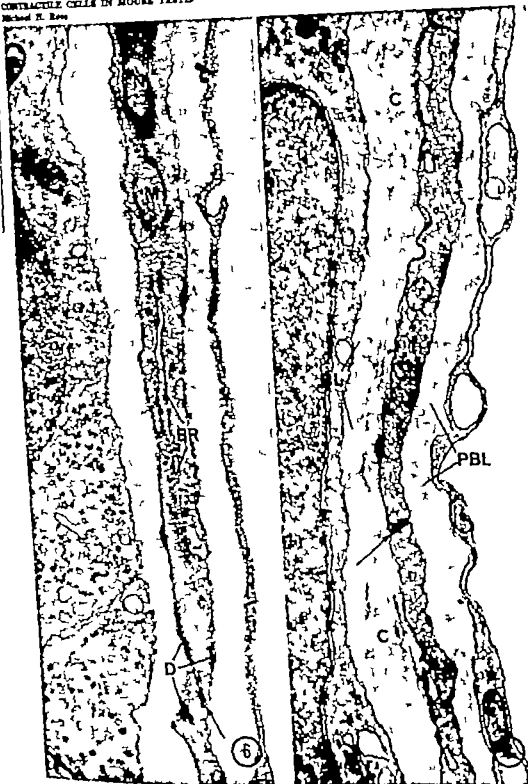

C
BR
PBL
C
D
6

PLATE 3

EXPLANATION OF FIGURES

6 A peritubular cell showing part of its nucleus (N) a mitochondrion (M) and an elongate profile of the granular endoplasmic reticulum (ER) The apposition of one cell with another is seen in the lower portion of the figure (arrow) In this same general area small cytoplasmic densities (D) of the type found in smooth muscle are seen. The thin cytoplasmic process on the right is a component of the outer fibrocyte layer × 29,000

7 An area similar to that of figure 6 again showing the close apposition of the peritubular cells (arrow) Several of the cytoplasmic densities are also evident. A number of collagen fibrils (C) cut in varying planes are seen between the epithelial basement lamina (BL) and the peritubular cell. The basement lamina of the peritubular cell (BL) is also clearly evident in this micrograph. × 29,000


C
BR
PBL
C
D
6

PLATE 4

EXPLANATION OF FIGURES

8 A higher power electron micrograph showing the epithelium (Ep) and its basement lamina (BL) in the lower part of the figure. The cytoplasm of the peritubular cell has a punctate appearance due to the numerous cross-sectional profiles of the fine filaments which it contains. Pinocytotic vesicles (PV) and dense areas (arrows) are seen adjacent to the cell surface. Mitochondria (M) are also evident. The basement lamina (PBL) of the peritubular cell is also indicated. Above and below the peritubular cell are cross-sectional profiles of collagen fibrils (C). × 59,000.

9 A "clear" cell is shown here bounded by the peritubular cell basement lamina (PBL) above and the cytoplasmic processes of the peritubular cells below. A small group of collagen fibrils (C) are seen in the space between the epithelial basement lamina (BL) and the peritubular cell. × 26,000

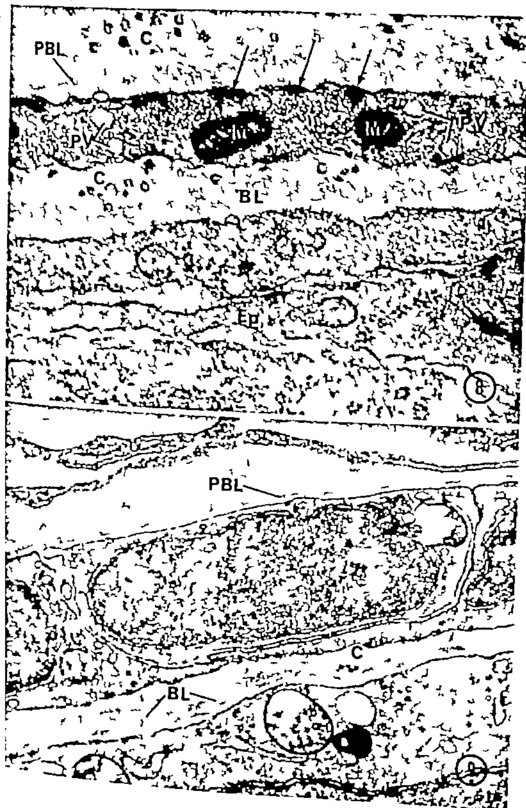

PBL
C
PV
PV
C
BL
Ep
8
PBL
C
BL
9

PLATE 5

EXPLANATION OF FIGURE

10 An electron micrograph showing an area in the vicinity of the terminal portion of the seminiferous tubules. The cells adjacent to the tubule epithelium (Ep) on the left side of the micrograph are typical of the peritubular contractile cells (PC) The cell processes immediately adjacent to the epithelium on the right side of the micrograph are typical of fibrocytes The areas included in the rectangles are shown at higher magnifications in figures 11 and 12. The micrograph also shows a marked alteration of the basement lamina on the left (arrows) where it appears multilayered. Near the center of the micrograph and also further to the right, there is additional basement lamina material (arrowheads) within the connective tissue matrix. The cell marked "X" which appears to be entirely surrounded by basement lamina material could not be identified with any certainty Portions of two Leydig cells (L) are seen between the two tubules × 11,500.


PC
L

PLATE 6

EXPLANATION OF FIGURES

11 A higher power electron micrograph of the area within the rectangle in the upper left of figure 10 In this micrograph the tubule epithelium (Ep) is at the top and immediately below is the thick multilayered basement lamina. The cytoplasm of the peritubular contractile cell has a dense and stippled appearance due to the fine filaments which it contains Among the mitochondria (M) are profiles of the endoplasmic reticulum (ER) A few cytoplasmic densities (D) and pinocytotic vesicles (arrow) are also evident. Collagen fibrils (C) are seen in cross-section above the peritubular cell and in longitudinal section below × 37,000

12 A high power electron micrograph of the area within the rectangle in the upper right of figure 10 A portion of an epithelial cell (Ep) and basement lamina of the tubule is seen at the lower right. A thin cytoplasmic process of a fibrocyte (F) is immediately above. The features which characterize the peritubular contractile cell are not evident in this cell despite its immediate location. × 37,000


Ep
C
ER
D
M
D
C
11
F
Ep
12

PLATE 7

EXPLANATION OF FIGURES

13 A phase contrast micrograph showing portions of two epithelial cords (tubules) from the testis of a newborn mouse. The epithelial component is surrounded by several layers of elongate connective tissue cells which constitute the bulk of the cellular portion of the interstitium. These cells exhibit cytoplasmic processes which are easily resolvable at this magnification. × 1800

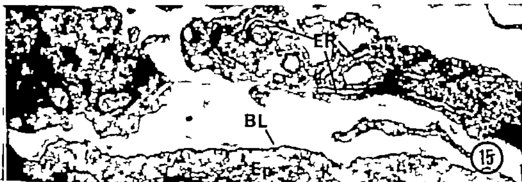
14 An electron micrograph of an area similar to that shown in figure 13 and from the same specimen. The flattened cells surrounding the epithelial cords represent a homogeneous population. A capillary (Cap) is located near the center of the figure. × 7200.


Cap
14

PLATE 8

EXPLANATION OF FIGURES

15, 16, 17 Representative areas showing the epithelium (Ep) and the surrounding connective tissue cells from three different newborn animals. A thin epithelial basement lamina (BL) is evident in each figure. The connective tissue cells are characterized by numerous profiles of endoplasmic reticulum (ER) many of which are markedly dilated and contain a moderately electron-dense material. The cytoplasmic matrix also contains an abundance of ribosomes. The conective tissue matrix contains a number of fine collagen fibrils (CF) (Fig. 15, × 16,500; Fig 16 × 19 000; Fig. 17 × 21,000.)



ER
BL
16

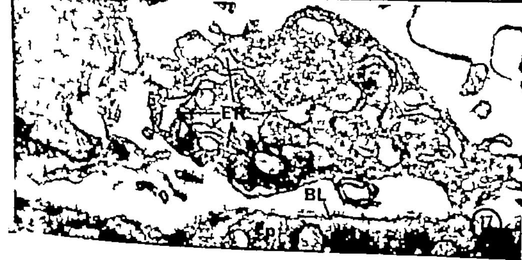


PLATE 9

EXPLANATION OF FIGURE

18 A low power electron micrograph which includes portions of two adjacent cords from the testis of a one-week-old animal. The fibroblasts adjacent to the epithelial cords (Ep) appear to form a distinctive layer as a result of their close apposition to one another. The fibroblasts located more peripherally appear to be less organized. At this stage there is no apparent change in the general nature of the cytoplasm of these cells. × 9250


EP
18

PLATE 10

EXPLANATION OF FIGURES

19 An electron micrograph showing the peritubular tissue components in the testis of a 13-day-old animal The cells (F) immediately adjacent to the epithelium (Ep) as well as the more peripherally located cells still retain the general characteristics of the fibroblast. The granular endoplasmic reticulum (ER) is prominent and numerous ribosomes are present. In this specimen an amorphous material (arrows) similar in appearance to the epithelial basement lamina (BL) is present along the peripheral surface of the connective tissue cells × 19 000

20 A higher power micrograph of an area similar to that shown in figure 19 The cell on the left in the micrograph contains a number of aggregated small particle-like bodies (arrowhead) which are interpreted as cross-sectional profiles of cytoplasmic filaments. A cisterna of the endoplasmic reticulum (ER) is also evident as well as a number of ribosomes A dense and almost flocculent material (arrow) which presumably represents an early stage in the formation of a basement lamina is seen along the cell surface in the upper portion of the micrograph. × 58 000

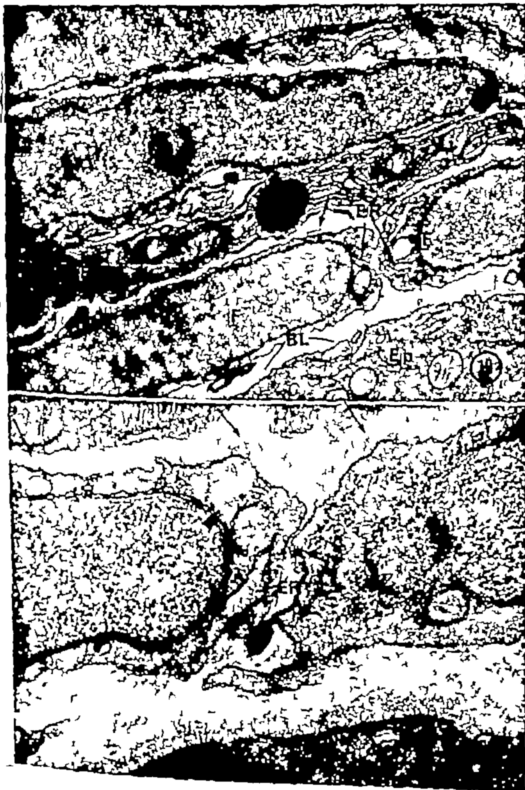

BL
Ep
10

PLATE 11

EXPLANATION OF FIGURES

21 A low power micrograph showing the periphery of two adjacent tubules and the organization of the peritubular tissue components in a 17-day-old animal The epithelial basement lamina (BL) is just perceptible at this magnification. The newly formed basement lamina of the peritubular cells is also recognizable in the region indicated by the arrows. × 7800

22 A portion of a peritubular cell from a 17-day-old animal which still contains dilated profiles of the endoplasmic reticulum and numerous ribosomes. The basement lamina of this cell is evident in the region indicated by the arrows. The epithelial (Ep) component is seen in the bottom of the micrograph. × 27,500

23 A portion of the epithelium (Ep) and peritubular cell from a tubule adjacent to the one shown in figure 22. The cytoplasm of the peritubular cell contains numerous cytoplasmic filaments which are just perceptible at this magnification Most of the cell surface seen in the micrograph is covered by a basement lamina (arrows) × 27,500


BL
21
22
Ep
23

PLATE 12

EXPLANATION OF FIGURE

24 A low power electron micrograph of a portion of two adjacent tubules from a 10-day-old animal. The degree of development of the peritubular cells (PC) at this time is not markedly different from the adult animal. In one cell however the appearance and extent of the endoplasmic reticulum (arrows) is similar to the adjacent fibroblasts, and in another cell a relatively extensive Golgi region (G) is seen. × 8600


PC
PC
PC
24

Transformation of Rat Small Lymphocytes with Allogeneic Lymphoid Cells [1]

M. ROY SCHWARZ
Department of Biological Structure University of Washington School of Medicine Seattle Washington

ABSTRACT Blastogenesis was observed in cultures containing lymphoid cells of the thymus glands, spleens, lymph nodes, thoracic duct lymph and blood of two genetically dissimilar rat strains. In thymus cultures, the large and medium cells in the culture inoculum gave rise by division to small lymphocytes. The majority of the blast cells originated from the small lymphocytes of both donors, although not all small cells underwent transformation. Subsequently some blasts divided, giving rise to more blast cells, while others served as precursors of small lymphocytes, thereby completing the cycle of small lymphocyte → blast → small lymphocyte. Similar blastogenesis was observed in mixed cultures containing newborn thymic cells but was not observed in mixed splenic cultures until the donors were three days of age

The *in vitro* exposure of mammalian lymphoid cells to a number of substances results in the appearance of large, apparently immature cells which subsequently undergo intense proliferation. Among these materials, are phytohemagglutinin (Nowell, '60), various "known antigens (Elves Roath, Taylor and Israels '63 Pearmain Lycette and Fitzgerald, '63) antilymphoid cell serum (Gräsbeck, Nordman and de la Chapelle '64) antisera against serum proteins of the donor animals from which the cultured lymphoid cells were obtained (Sell and Gell, '65) genetically foreign or allogeneic cells (Bain, Vas and Lowenstein '64) staphlococcal extract (Ling, Spicer James and Williamson, '65) and recently an extract of the pokeweed *Phytolacca americana* (Farnes Barker Brownhill and Fanger '64)

A mixture of genetically foreign cells may closely approximate an *in vitro* homograft reaction and therefore has received especial interest as a possible means of histocompatability typing. Brain et al. ('64) reported unequivocal transformation in cultures containing peripheral blood leucocytes from two unrelated human donors but little or no response was observed in mixtures of leucocytes from two identical twins. Similar results have been reported by Rieke ('66) from mixtures of thoracic duct lymphocytes from two nonrelated strains of rats and, by Chapman and Dutton ('63) and Dutton ('65) from cultures containing mixtures of splenic or lymph node cells from rabbits, mice or rats. While the latter authors were unable to demonstrate blastogenesis in mixtures of rabbit thymus cells Schwarz ('66) in a preliminary paper reported that rat thymic cells possessed this potential. The present paper will report further studies of mixed rat thymic cultures in which the cell type responding, the progeny of the transformed or blast cells and the age of animals whose cells respond has been explored In addition results of culturing rat cells from lymph node, spleen, blood and thoracic duct lymph will be presented

MATERIALS AND METHODS

General procedures Throughout this study the highly inbred but genetically foreign strains of Lewis and Brown Norway (Chocolate) rats were employed as cell donors. Routinely animals weighing 100–200 gm were utilized but in specific instances newborn or 12–18 month-old rats were used.

Thymic cells were obtained from donors sacrificed by an intracardiac lethal injection of diabutal (Diamond Laboratories Des Moines Iowa) The gland was then freed following a midsternal incision care being taken to avoid the mediastinal lymph nodes located lateral to the thymus. A sus-

The term blast refers only to the morphological appearance of these cells and does not relate to their proliferative potential.
See footnote 1.

Am. J. Anat., 121: 559-570.

Transformation of Rat Small Lymphocytes with Allogeneic Lymphoid Cells [1]

M. ROY SCHWARZ
Department of Biological Structure University of Washington School of Medicine Seattle Washington

ABSTRACT Blastogenesis was observed in cultures containing lymphoid cells of the thymus glands, spleens, lymph nodes, thoracic duct lymph and blood of two genetically dissimilar rat strains. In thymus cultures, the large and medium cells in the culture inoculum gave rise by division to small lymphocytes. The majority of the blast cells originated from the small lymphocytes of both donors, although not all small cells underwent transformation. Subsequently some blasts divided, giving rise to more blast cells, while others served as precursors of small lymphocytes, thereby completing the cycle of small lymphocyte → blast → small lymphocyte. Similar blastogenesis was observed in mixed cultures containing newborn thymic cells but was not observed in mixed splenic cultures until the donors were three days of age.

The *in vitro* exposure of mammalian lymphoid cells to a number of substances results in the appearance of large, apparently immature cells which subsequently undergo intense proliferation. Among these materials are phytohemagglutinin (Nowell, '60), various known antigens (Elves Roath, Taylor and Israels, '63 Pearman, Lycette and Fitzgerald, '63) antilymphoid cell serum (Gräsbeck, Nordman and de la Chapelle, '64) antisera against serum proteins of the donor animals from which the cultured lymphoid cells were obtained (Sell and Gell, '65) genetically foreign or allogeneic cells (Bain, Vas and Lowenstein, '64) staphlococcal extract (Ling, Spicer James and Williamson, '65) and recently an extract of the pokeweed *Phytolacca americana* (Farnes, Barker Brownhill and Fanger '64)

A mixture of genetically foreign cells may closely approximate an *in vitro* homograft reaction and, therefore has received special interest as a possible means of histocompatability typing Brain et al ('64) reported unequivocal transformation in cultures containing peripheral blood leucocytes from two unrelated human donors but little or no response was observed in mixtures of leucocytes from two identical twins. Similar results have been reported by Rieke ('66) from mixtures of thoracic duct lymphocytes from two nonrelated strains of rats and by Chapman and Dutton ('65) and Dutton ('65) from cultures containing mixtures of splenic or lymph node cells from rabbits mice or rats While the latter authors were unable to demonstrate blastogenesis in mixtures of rabbit thymus cells Schwarz ('66) in a preliminary paper reported that rat thymic cells possessed this potential. The present paper will report further studies of mixed rat thymic cultures in which the cell type responding, the progeny of the transformed or blast cells and the age of animals whose cells respond has been explored. In addition, results of culturing rat cells from lymph node spleen blood and thoracic duct lymph will be presented

MATERIALS AND METHODS

General procedures Throughout this study the highly inbred but genetically foreign strains of Lewis and Brown Norway (Chocolate) rats were employed as cell donors. Routinely animals weighing 100–200 gm were utilized but, in specific instances, newborn or 12–18 month-old rats were used.

Thymic cells were obtained from donors sacrificed by an intracardiac, lethal injection of diabutal (Diamond Laboratories Des Moines Iowa) The gland was then freed, following a midsternal incision care being taken to avoid the mediastinal lymph nodes located lateral to the thymus. A sus-

[1] The term blast refers only to the morphological appearance of these cells and does not relate to their proliferative potential.
See footnote 1.

Am. J. A... 121 839–870.

pension of thymic cells was made by mincing the gland with fine scissors and gently *stirring the fragments in Eagle s Minimum* Essential Medium (MEM) (Microbiological Associates Bethesda Maryland) Lymph node and splenic cell suspensions were prepared by employing identical methods to those used for thymus while thoracic duct lymphocytes were isolated by the methods of either Reinhardt and Li (45) or Bollman Cain and Grindlay (48) Blood leucocytes were obtained by collecting cardiac blood in heparinized syringes allowing the blood to stand at 4 C for 15–30 minutes and then centrifuging at low speeds in a desk centrifuge The leucocyte-rich plasma was then removed and the cells separated from the plasma by centrifugation To reduce the number of contained erythrocytes the cells of the blood and spleen were exposed to an 0 84% solution of NH Cl for 15 minutes following which they were washed three times in Hank s balanced salt solution (BSS) (Microbiological Associates) The cells of the respective organs were then placed in 5–30 cm of MEM supplemented with 5–35% fresh adult male Lewis rat serum and 500 units of procaine penicillin G per cm of culture The serum was routinely harvested immediately prior to culture initiation but in one series of experiments it stored at − 4 C for 4 7 9 12 16 and 21 days prior to use When one half of the cells were supplied by each donor the concentrations employed per cm^{3} of culture medium which gave the most reproducible maximal responses (and the range of concentrations employed) were as follows thymus 8×10^{6} (range 2–40) blood 4×10^{6} (range 2–4) thoracic duct lymph 4×10^{6} (range 2–8) lymph node 4×10^{6} (range 2–8) and spleen 4×10^{6} (range 2–18) Routinely cultures were sacrificed after three days at 37 C although in some cases (see specific experiments below) variable periods were employed Immediately prior to sacrifice or at intervals during incubation the cultures were pulsed for 30 minutes with H^{3} thymidine (TTH 4 μc/ml 1 9 or 6 7 c/mM) After washing three times in BSS smears and/or hypotonic preparations of the contained cells were processed radioautographically according to the method of Everett, Rieke Reinhardt and Yoffey (60). Routine exposure times of 3–10 days were employed except in specific instances indicated below

Cell counts were performed at varying times by use of routine laboratory hemocytometers The cells as viewed on smears were divided into a large and medium cell group (LMC) with nuclear diameters of greater than 7 μ and a small cell group with diameters of 7 μ or less. The LMC consisted of transformed cells phagocytic or nonphagocytic reticular elements, large and medium lymphocytes and plasmocytic cells The small cell category was composed of small lymphocytes, and mature plasma cells which were seen on extremely rare occasions

Progeny of LMC in the culture inoculum In this study five 10 cm^{3} mixed cultures were initiated in the routine manner except that 0 15 μc of H^{3}-thymidine (specific activity 1 9 c/mM) was added per cm of medium At both one and thirty hours after initiation cell samples were obtained and the per cent labeled small lymphocytes was determined from radioautographs of these samples. To determine if a radioactive DNA precursor was continuously available the supernatant fluids from the 30-hour cultures were exposed for one hour to nonlabeled three-day-old mixed thymic cultures which contained DNA synthesizing cells. After washing, smearing and radioautographic processing, the cells were evaluated for contained radioactivity

Cell type responding in mixed thymic cultures The first experiment consisted of mincing thymus cells from six Brown Norway (BN) and six Lewis donors in MEM. The cells were then washed in BSS counted, and the Lewis and BN elements incubated separately at 37 C in solutions of MEM, containing 30–33% serum 500 units of penicillin G and 20–30 × 10^{6} cells/cm^{3} of medium Twenty four hours later cell counts were performed the cell washed in BSS and mixed cultures were prepared from the preincubated cells in the usual fashion After 24 48 and 72 hours of incubation the per cent LMC and per cent small cells were determined from smears of the cultured cells.

In the second group of experiments, Lewis and BN cells were again preincubated for 24 hours (see above) during which time they were continuously exposed to (a) 50 μc/ml or (b) 0 1 μc/ml of TTH (6.7 c/mM) The cells were then washed, an aliquot of the cells was smeared and 5 cm^3 mixed cultures were prepared in the usual manner except that 25 μgm of nonradioactive thymidine was added to each of the incubations to dilute re-utilization of radioactive metabolites to a nondetectable level. After 24 hours of incubation, aliquots of the cultured cells were smeared and the culture fluid replaced with media identical to that used to initiate the cultures. Forty-eight hours after mixing, the cultures were terminated by smearing and the per cents labeled LMC and small lymphocytes were determined on radioautographs of the cells obtained immediately or 48 hours after TTH. Exposure times for (a) and (b) above were 1 and 3 days respectively

Transformation of cells from both donors. The first of two experiments consisted of preparing four groups of nine mixed thymic cultures in the usual manner except that the ratio of Lewis to BN cells in the culture inoculum was varied as follows 100 0 90:10 80 20 60 40 50 50 40 60 20 80 10:90 and 0 100 After three days, the cultures were pulsed for one-half hour with 4 μc/ml of H^3-thymidine (specific activity 6 7 c/mM) and smears of the contained cells were processed radioautographically

In a second experiment, the donor Lewis and BN rats received 3/4 μc of H^3-thymidine (specific activity 6.7 c/mM) per gram body weight, every six hours for five days so as to label all small lymphocytes formed during this period (Caffrey Everett and Rieke '66) Ten hours after the last H^3 thymidine injection, the animals were sacrificed, the spleens lymph nodes and thymus glands were minced and the suspended cells were washed three times with BSS Routinely 5 cm mixed thymic mixed splenic and mixed lymph node cultures, containing 20 μgm of cold carrier thymidine were then prepared, utilizing the radioactive cells from either the injected Lewis or the BN rats and nonradioactive elements of the reciprocal rat strain After 48 hours the cultured cells were washed three times with BSS smeared, and evaluated for the presence of labeled blasts after radioautographic processing with exposure times of 4–8 weeks.

Progeny of the blast cells The first experiment consisted of preparing ten 20 cm^3 mixed thymic cultures employing five different pairs of donor animals The first group of five cultures was pulsed with H^3 thymidine (6 7 c/mM ½ μc per ml of culture medium) from 32–34 hours after culture initiation, while the second group of five cultures was pulsed with H^3-thymidine for four hours (1 9 c/mM; ¼ μc/ml of culture fluid) beginning 44 hours after mixing the cells Subsequently the cells were washed three times in BSS and returned to 20 cm of routine medium supplemented with 95 μgm of cold carrier" thymidine At 0 4 14 27 and 38 hours after the pulse to the first group of cultures and at 0 3 7 10 13 16 24 44 72, 98 and 116 hours after the pulse to the second group aliquots of the contained cells were obtained and processed radioautographically

A second study consisted of preparing five 20 cm^3 mixed thymic cultures. At 3 6 10 and 14 days after initiation, the medium was exchanged and smears were prepared of the contained cells for evaluation of the cell types present.

Transformation of all small lymphocytes In this investigation routinely prepared 10 cm mixed thymic cultures were exposed to 0.2–0 4 μc/cm^3 of H^3-thymidine (1 9 c mM) during the entire 72-hour incubation period. Continuous availability of the isotope was assured by replacing the culture medium every 24 hours with a new isotope-containing solution. After two exchanges, of after 72 hours the cultured cells were washed and smeared Subsequently the exchanged media or supernatants of the cultures which had been stored at 4 C were incubated for one hour with unlabeled thymic cells some of which were synthesizing DNA. Smears of these latter cells together with smears of the cultured cells were then processed radioautographically

RESULTS

General culture results Beginning 30 hours after initiation large immature cells

pension of thymic cells was made by mincing the gland with fine scissors and gently stirring the fragments in Eagle s Minimum Essential Medium (MEM) (Microbiological Associates Bethesda Maryland) Lymph node and splenic cell suspensions were prepared by employing identical methods to those used for thymus while thoracic duct lymphocytes were isolated by the methods of either Reinhardt and Li (45) or Bollman Cain and Grindlay (48) Blood leucocytes were obtained by collecting cardiac blood in heparinized syringes allowing the blood to stand at 4 C for 15–30 minutes and then centrifuging at low speeds in a desk centrifuge The leucocyte-rich plasma was then removed and the cells separated from the plasma by centrifugation To reduce the number of contained erythrocytes the cells of the blood and spleen were exposed to an 0 84% solution of NH_4Cl for 15 minutes following which they were washed three times in Hank s balanced salt solution (BSS) (Microbiological Associates) The cells of the respective organs were then placed in 5–30 cm of MEM supplemented with 5–35% fresh adult male Lewis rat serum and 500 units of procaine penicillin G per cm³ of culture The serum was routinely harvested immediately prior to culture initiation but in one series of experiments it stored at − 4 C for 4 7 9 12 16 and 21 days prior to use When one-half of the cells were supplied by each donor the concentrations employed per cm³ of culture medium which gave the most reproducible maximal responses (and the range of concentrations employed) were as follows thymus 8×10^6 (range 2–40) blood 4×10^6 (range 2–4) thoracic duct lymph 4×10^6 (range 2–8) lymph node 4×10^6 (range 2–8) and spleen 4×10^6 (range 2–18) Routinely cultures were sacrificed after three days at 37 C although in some cases (see specific experiments below) variable periods were employed Immediately prior to sacrifice or at intervals during incubation the cultures were pulsed for 30 minutes with H^3-thymidine (TTH 4 μc/ml 1 9 or 6 7 c/mM) After washing three times in BSS smears and/or hypotonic preparations of the contained cells were processed radioautographically according to the method of Everett Rieke Reinhardt and Yoffey ('60) c Routine exposure times of 3–10 days were employed except in specific instances indicated below

Cell counts were performed at varying times by use of routine laboratory hemocytometers The cells as viewed on smears were divided into a large and medium cell group (LMC) with nuclear diameters of greater than 7 μ and a small cell group with diameters of 7 μ or less. The LMC consisted of transformed cells phagocytic or nonphagocytic reticular elements, large and medium lymphocytes and plasmocytic cells. The small cell category was composed of small lymphocytes, and mature plasma cells which were seen on extremely rare occasions

Progeny of LMC in the culture broth In this study five 10 cm³ mixed cultures were initiated in the routine manner except that 0 15 μc of H^3 thymidine (specific activity 1 9 x/mM) was added per cm³ of medium At both one and thirty hours after initiation cell samples were obtained and the per cent labeled small lymphocytes was determined from radioautographs of these samples. To determine if a radioactive DNA precursor was continuously available the supernatant fluids from the 30-hour cultures were exposed for one hour to nonlabeled three-day-old mixed thymic cultures which contained DNA-synthesizing cells After washing smearing and radioautographic processing the cells were evaluated for contained radioactivity

Cell type responding in mixed thymic cultures The first experiment consisted of mincing thymus cells from six Brown Norway (BN) and six Lewis donors in MEM The cells were then washed in BSS counted, and the Lewis and BN elements incubated separately at 37 C in solutions of MEM containing 30–33% serum 500 units of penicillin G and 20–30 × 10^6 cells/cm³ of medium Twenty four hours later cell counts were performed the cell washed in BSS and mixed cultures were prepared from the preincubated cells in the usual fashion After 24 48 and 72 hours of incubation the per cent LMC and per cent small cells were determined from smears of the cultured cells.

In the second group of experiments ewis and BN cells were again preincu- ated for 24 hours (see above) during hich time they were continuously ex sed to (a) 50 μc/ml or (b) 0 1 μc/ml f TTH (6.7 c/mM) The cells were then ashed, an aliquot of the cells was smeared nd 5 cm³ mixed cultures were prepared n the usual manner except that 25 μgm f nonradioactive thymidine was added to ach of the incubations to dilute re-utiliza on of radioactive metabolites to a non etectable level. After 24 hours of incu- ation, aliquots of the cultured cells were meared and the culture fluid replaced ith media identical to that used to initi- te the cultures. Forty-eight hours after iting, the cultures were terminated by mearing and the per cents labeled LMC nd small lymphocytes were determined n radioautographs of the cells obtained mmediately or 48 hours after TTH Ex osure times for (a) and (b) above were and 3 days, respectively

Transformation of cells from both do- ors. The first of two experiments con- sisted of preparing four groups of nine ixed thymic cultures in the usual man- er except that the ratio of Lewis to BN ells in the culture inoculum was varied s follows 100 0 90 10 80:20 60:40 0 50 40 60 20 80 10 90 and 0 100 fter three days, the cultures were pulsed or one-half hour with 4 μc/ml of H^3-thy midine (specific activity 6.7 c/mM) and mears of the contained cells were proc ssed radioautographically

In a second experiment, the donor Lewis nd BN rats received 3/4 μc of H^3-thymi- line (specific activity 6 7 c/mM) per gram ody weight, every six hours for five days, o as to label all small lymphocytes formed luring this period (Caffrey Everett and Rieke '66) Ten hours after the last H^3 thymidine injection the animals were sacrificed, the spleens lymph nodes and thymus glands were minced and the sus- pended cells were washed three times with BSS. Routinely 5 cm³ mixed thymic mixed splenic and mixed lymph node cul- tures, containing 20 μgm of cold carrier" thymidine were then prepared, utilizing the radioactive cells from either the in- jected Lewis or the BN rats and nonradio- active elements of the reciprocal rat strain.

After 48 hours the cultured cells were washed three times with BSS smeared, and evaluated for the presence of labeled blasts after radioautographic processing with exposure times of 4–8 weeks.

Progeny of the blast cells The first ex periment consisted of preparing ten 20 cm mixed thymic cultures employing five different pairs of donor animals. The first group of five cultures was pulsed with H thymidine (6.7 c/mM; ½ μc per ml of culture medium) from 32–34 hours after culture initiation, while the second group of five cultures was pulsed with H -thymi- dine for four hours (1.9 c/mM ½ μc/ml of culture fluid) beginning 44 hours after mix ing the cells Subsequently the cells were washed three times in BSS and returned to 20 cm³ of routine medium supplemented with 95 μgm of cold carrier thymidine At 0 4 14 27 and 38 hours after the pulse to the first group of cultures, and at 0 3 7 10 13 16 24 44 72, 98 and 116 hours after the pulse to the second group ali- quots of the contained cells were obtained and processed radioautographically

A second study consisted of preparing five 20 cm³ mixed thymic cultures. At 3 6 10 and 14 days after initiation the me- dium was exchanged and smears were pre- pared of the contained cells for evaluation of the cell types present.

Transformation of all small lymphocytes In this investigation routinely prepared 10 cm³ mixed thymic cultures were exposed to 0.2–0 4 μc/cm³ of H^3-thymidine (1.9 c/mM) during the entire 72-hour incuba tion period Continuous availability of the isotope was assured by replacing the cul ture medium every 24 hours with a new isotope-containing solution. After two ex changes of after 72 hours, the cultured cells were washed and smeared Subse- quently the exchanged media or superna tants of the cultures which had been stored at 4 C were incubated for one hour with unlabeled thymic cells, some of which were synthesizing DNA. Smears of these latter cells together with smears of the cultured cells were then processed radio- autographically

RESULTS

General culture results Beginning 30 hours after initiation large immature cells

pension of thymic cells was made by mincing the gland with fine scissors and gently stirring the fragments in Eagle s Minimum Essential Medium (MEM) (Microbiological Associates Bethesda Maryland) Lymph node and splenic cell suspensions were prepared by employing identical methods to those used for thymus while thoracic duct lymphocytes were isolated by the methods of either Reinhardt and Li (45) or Bollman Cain and Grindlay (48) Blood leucocytes were obtained by collecting cardiac blood in heparinized syringes allowing the blood to stand at 4 C for 15–30 minutes and then centrifuging at low speeds in a desk centrifuge The leucocyte-rich plasma was then removed and the cells separated from the plasma by centrifugation To reduce the number of contained erythrocytes the cells of the blood and spleen were exposed to an 0 84% solution of NH Cl for 15 minutes following which they were washed three times in Hank s balanced salt solution (BSS) (Microbiological Associates) The cells of the respective organs were then placed in 5–30 cm of MEM supplemented with 5–35% fresh adult male Lewis rat serum and 500 units of procaine penicillin G per cm^3 of culture The serum was routinely harvested immediately prior to culture initiation but in one series of experiments it stored at − 4 C for 4 7 9 12 16 and 21 days prior to use When one half of the cells were supplied by each donor the concentrations employed per cm^3 of culture medium which gave the most reproducible maximal responses (and the range of concentrations employed) were as follows thymus 8×10^6 (range 2–40) blood 4×10^6 (range 2–4) thoracic duct lymph 4×10^6 (range 2–8) lymph node 4×10^6 (range 2–8) and spleen 4×10^6 (range 2–18) Routinely cultures were sacrificed after three days at 37 C although in some cases (see specific experiments below) variable periods were employed Immediately prior to sacrifice or at intervals during incubation the cultures were pulsed for 30 minutes with H^3 thymidine (TTH 4 μc/ml 1 9 or 6 7 c mM) After washing three times in BSS smears and/or hypotonic preparations of the contained cells were processed radioautographically according to the method of Everett Rieke Reinhardt and Yoffey (60) Routine exposure times of 3–10 days were employed except in specific instances indicated below

Cell counts were performed at varying times by use of routine laboratory hemocytometers. The cells as viewed on smears were divided into a large and medium cell group (LMC) with nuclear diameters of greater than 7 μ and a small cell group with diameters of 7 μ or less. The LMC consisted of transformed cells, phagocytic or nonphagocytic reticular elements, large and medium lymphocytes and plasmocytic cells. The small cell category was composed of small lymphocytes, and mature plasma cells which were seen on extremely rare occasions

Progeny of LMC in the culture inoculum In this study five 10 cm mixed cultures were initiated in the routine manner except that 0 15 μc of H^3 thymidine (specific activity 1 9 c/mM) was added per cm^3 of medium. At both one and thirty hours after initiation cell samples were obtained and the per cent labeled small lymphocytes was determined from radioautographs of these samples. To determine if a radioactive DNA precursor was continuously available the supernatant fluids from the 30-hour cultures were exposed for one hour to nonlabeled three-day-old mixed thymic cultures which contained DNA-synthesizing cells. After washing, smearing and radioautographic processing, the cells were evaluated for contained radioactivity

Cell type responding in mixed thymic cultures The first experiment consisted of mincing thymus cells from six Brown Norway (BN) and six Lewis donors in MEM The cells were then washed in BSS counted and the Lewis and BN elements incubated separately at 37 C in solutions of MEM containing 30–33% serum 500 units of penicillin G and 20–30 × 10^6 cells/cm^3 of medium Twenty four hours later cell counts were performed the cell washed in BSS and mixed cultures were prepared from the preincubated cells in the usual fashion After 24 48 and 72 hours of incubation the per cent LMC and per cent small cells were determined from smears of the cultured cells

ditions described above routinely supported growth for 70–98 hours without changing the medium, although longer culture periods resulted in a progressively greater amount of cell degeneration which was initially represented by cytoplasmic vacuolation. Clusters of cells as seen in figure 4 were observed more frequently in experimental than in control cultures. These islets consisted of a variable number of small lymphocytes and blast cells which surrounded and indented the slightly basophilic cytoplasm of a centrally located reticular cell. The nucleus of the central cell was composed of fairly dispersed, homogeneous chromatin and one or more nucleoli. Occasionally the cytoplasm was vacuolated.

A similar transformation of cells to that observed in thymus cultures was detected in mixtures of lymph node (fig 5) spleen, thoracic duct lymph and blood cells. Blasts were also observed when any of the aforementioned lymphoid populations from the Lewis rats were mixed with any lymphoid population from BN donors *i.e.* thymus × spleen thymus × lymph node spleen × lymph node etc (fig 6) In splenic and blood cultures, optimal responses were obtained when the red blood cell content of the culture inoculum was reduced by 15-minute exposures to ammonium chloride Longer contact with this hypotonic solution resulted in diminished numbers of enlarged cells. In contrast to mixtures of newborn thymus cells which showed

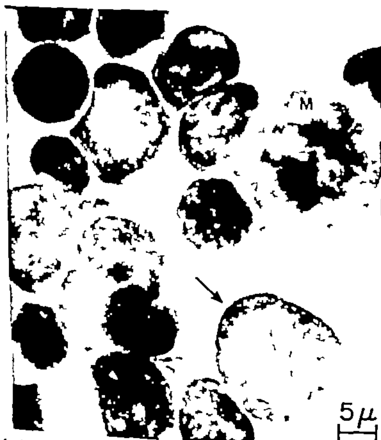


Fig. 4 A cluster or islet of cells observed in thymus cultures as described in figure 1. Note the mitotic figure (M) and the cytoplasmic border of phagocytic reticular cell (R) which appears to be indented by the lymphoid elements (arrow)

(fig 1) were observed in mixed thymic cultures but were not observed as frequently in nonmixed or isologously mixed incubation (Schwarz, '66) The typical cell which varied in diameter from 10–20 μ had a basophilic cytoplasm a large oval nucleus with dispersed chromatin threads and occasionally one or more demonstrable nucleoli. From 30–72 hours of culture there was a steady increase in the frequency of cells with nuclear diameters of greater than 7 μ (fig 2) This increase of LMC consisted mainly of transformed cells (95% at 72 hours) and was paralleled by an increased number of H^3 thymidine-incorporating cells (fig 3)

In the incubations involving thymus cells the use of freshly prepared serum or serum frozen for up to 22 days was equally proficient in supporting transformation Although apparently immature cells were seen in cultures containing 5–10% serum maximal responses occurred when serum concentrations of 15–35% were employed Marginally detectable responses were observed with 2–4 or from $10–40 \times 10^6$ thymic cells/cm³ of culture fluid but most satisfactory results were obtained with 8×10^6 cells (4×10^6/cm³ from each donor) Penicillin G was routinely incorporated into the culture medium albeit no change in the blastogenic response and no contamination was noted when this bacteriocidal agent was deleted While maximum transformation occurred when young adult rats served as thymus donors a reduced but detectable response was observed in mixed cultures containing cells from animals as young as five hou[rs] and as old as 18 months The culture co[...]

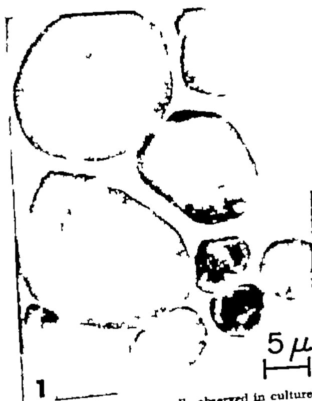


Fig. 1 Typical blast cells observed in cultures 72 hours after initiation with equal numbers of thymus cells from newborn to 18-month-old Lewis and Brown Norway (BN) rats.

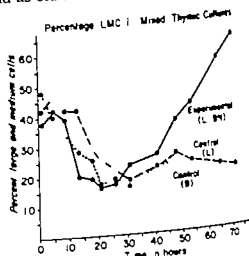


Fig 2 The per cent large and medium cel[ls] (LMC) (nuclear diameters of greater than 7 [μ]) with time in mixed or nonmixed cultures [initi]ated with equal numbers of thymus cells fr[om] young adult Lewis and/or BN rats.

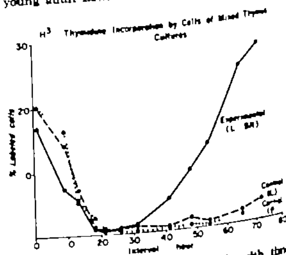


Fig 3 The per cent labeled cells with thy[midine] in mixed or nonmixed cultures initiated with equal numbers of thymus cells from young adult Lewi and or BN rats

lines described above routinely supported growth for 70–96 hours without changing the medium, although longer culture periods resulted in a progressively greater amount of cell degeneration which was initially represented by cytoplasmic vacuolation. Clusters of cells as seen in figure 4 were observed more frequently in experimental than in control cultures. These islets consisted of a variable number of small lymphocytes and blast cells which surrounded and indented the slightly basophilic cytoplasm of a centrally located reticular cell. The nucleus of the central cell was composed of fairly dispersed, homogeneous chromatin and one or more nucleoli. Occasionally the cytoplasm was vacuolated.

A similar transformation of cells to that observed in thymus cultures was detected in mixtures of lymph node (fig 5) spleen thoracic duct lymph and blood cells. Blasts were also observed when any of the aforementioned lymphoid populations from the Lewis rats were mixed with any lymphoid population from BN donors, i.e., thymus × spleen, thymus × lymph node spleen × lymph node etc (fig 6) In splenic and blood cultures optimal responses were obtained when the red blood cell content of the culture inoculum was reduced by 15-minute exposures to ammonium chloride Longer contact with this hypotonic solution resulted in diminished numbers of enlarged cells. In contrast to mixtures of newborn thymus cells which showed



Fig. 4 A cluster or islet of cells observed in thymus cultures as described in figure 1. Note the mitotic figure (M) and the cytoplasmic border of a phagocytic reticular cell (R) which appears to be indented by the lymphoid elements (arrow)



Fig. 5 Blast cells, one in late telophase from a 72 hour culture initiated with lymph node cells from Lewis and BN rats

marked blastogenesis (fig 1) mixed cultures initiated with spleen cells from new born rats did not evidence blastogenesis However by three days of age or after small lymphocytes had appeared in the developing spleen (Holyoke Latta and McLean 66) transformed elements in greater numbers than controls were observed in mixed cultures This interpretation was rendered more difficult than in cultures of adult cells because of the hemopoietic blasts present in the spleens at this age When thymic cells from either new born or adult rats of different sexes (but of the same strain) were cultured together no blastogenesis resulted

Progeny LMC in culture inoculum One hour after the beginning of exposure to H thymidine except for an extremely rare instance no small lymphocytes were labeled Thus it would appear that small lymphocytes did not synthesize DNA and it follows that they did not as small cells undergo mitosis In contrast after 30 hours of continuous H^3 thymidine exposure when 30% (range 21–39%) of all cells were LMC 25% (range 22–26%) of the small lymphocytes were labeled This latter result indicated that small lymphocytes had derived from LMC which labeled during the 30-hour pulse of H^3 thymidine. That the H^3 thymidine and/or its radioactive metabolite(s) was available for incorporation throughout the culture period was supported by the fact that the supernatant from the 30-hour incubations labeled DNA-synthesizing cells of control cultures

Cell type responding In the first experiment, after 24 hours the percentage of all cells which were small lymphocytes had increased from the 65–75% found in the inoculum to 90–95% in both Lewis and BN incubations In this same interval, the mean loss of Lewis and BN cells was 29% and 27% respectively with greater attrition occurring at higher initial cell concentrations When these preparations, containing mainly small lymphocytes, were incubated together for one two or three days a typical blastogenic response was observed Blast cells appeared earlier in these studies than in parallel cultures which were not preincubated While these results suggested that small lymphocytes were precursors of blasts it did not exclude the proliferation or direct modulation of LMC in the culture inoculum into blast cells

To investigate the possibility of proliferation and/or direct modulation, both Lewis and BN cells were exposed to high concentrations of H^3 thymidine during the preincubation period so as to destroy by radiation the proliferating cells Alternately identical cells were incubated for 24 hours with low concentrations of H^3 thymidine so as to label proliferating LMC and their division products without destroying either In the former study 50–60% of the LMC (which constituted less than 10% of the total cells present) manifested extremely heavy labeling at the end of the preincubation period. Twenty four and 48 hours after mixing only rarely was a labeled cell including blasts and small lymphocytes observed This suggested that the heavily labeled cells were destroyed by the large doses of radiation and were not necessary for the formation of blast cells In the second experiment 50–60% of the LMC and 10–12% of the small lymphocytes were la-



Fig. 8 Blast cells and a mitotic figure in cultures, 72 hours after initiation with lymph node and thymus cells from Lewis and BN rats, respectively

beled by the low concentrations of H³-thymidine. One and two days after mixing, 3–5% (average, 4.1%) of the blasts were labeled. This result indicated that if the labeled LMC served as precursors of the blasts, only a small percentage possessed this possibility. A more likely explanation is that small lymphocytes served as precursor cells and that the labeled blasts represented labeled small lymphocytes which had derived from labeled LMC (see *Progeny of LMC in the culture inoculum*) and had subsequently enlarged.

Transformation of cells from both donors. The first of two general types of experiments in this study consisted of varying the percentage of cells contributed by both donors, to determine if blast cells arose from both donors cells or from predominantly one donor's cells. As can be seen by figure 7, only minor differences were noted in the per cent LMC and the per cent labeled cells when the culture inoculum consisted of 10–90% BN cells and a reciprocal number of Lewis cells. A slight but reproducible increase in the frequency of LMC and labeled cells was noted in mixed thymic cultures when 50% or more of the cells were contributed by Lewis donors. A similar response was observed by Dutton in mixed splenic cultures of the rat ('65).

In the second experiment, labeled thymic cells were obtained from either BN or Lewis donors and cultured with unlabeled cells from the reciprocal donor. Radioautographs revealed 25–30% of the blasts were labeled, irrespective of which of the two donors was exposed to H³-thymidine. That not all blasts were labeled after 48 hours was interpreted as indicating that no significant detectable re-utilization of radioactive metabolites had occurred.



Fig 5 Blast cells, one in late telophase from a 72 hour culture initiated with lymph node cells from Lewis and BN rats.

marked blastogenesis (fig 1) mixed cultures initiated with spleen cells from newborn rats did not evidence blastogenesis However by three days of age or after small lymphocytes had appeared in the developing spleen (Holyoke Latta and McLean 66) transformed elements in greater numbers than controls were observed in mixed cultures This interpretation was rendered more difficult than in cultures of adult cells because of the hemopoietic blasts present in the spleens at this age When thymic cells from either newborn or adult rats of different sexes (but of the same strain) were cultured together no blastogenesis resulted

Progeny LMC in culture inoculum One hour after the beginning of exposure to H^3 thymidine except for an extremely rare instance no small lymphocytes were labeled Thus it would appear that small lymphocytes did not synthesize DNA and it follows that they did not as small cells undergo mitosis In contrast after 30 hours of continuous H^3-thymidine exposure when 30% (range 21–39%) of all cells were LMC 25% (range 22–26%) of the small lymphocytes were labeled. This latter result indicated that small lymphocytes had derived from LMC which labeled during the 30-hour pulse of H^3 thymidine That the H^3-thymidine and/or its radioactive metabolite(s) was available for incorporation throughout the culture period was supported by the fact that the supernatant from the 30-hour incubations labeled DNA-synthesizing cells of control cultures

Cell type responding In the first experiment after 24 hours the percentage of all cells which were small lymphocytes had increased from the 65–75% found in the inoculum to 90–95% in both Lewis and BN incubations In this same interval, the mean loss of Lewis and BN cells was 29% and 27% respectively with greater attrition occurring at higher initial cell concentrations. When these preparations, containing mainly small lymphocytes, were incubated together for one two or three days a typical blastogenic response was observed. Blast cells appeared earlier in these studies than in parallel cultures which were not preincubated While these results suggested that small lymphocytes were precursors of blasts, it did not exclude the proliferation or direct modulation of LMC in the culture inoculum into blast cells

To investigate the possibility of proliferation and/or direct modulation both Lewis and BN cells were exposed to high concentrations of H -thymidine during the preincubation period so as to destroy by radiation the proliferating cells Alternately identical cells were incubated for 24 hours with low concentrations of H thymidine so as to label proliferating LMC and their division products without destroying either In the former study 50–60% of the LMC (which constituted less than 10% of the total cells present) manifested extremely heavy labeling at the end of the preincubation period Twenty four and 48 hours after mixing only rarely was a labeled cell including blasts and small lymphocytes observed This suggested that the heavily labeled cells were destroyed by the large doses of radiation and were not necessary for the formation of blast cells. In the second experiment 50–60% of the LMC and 10–12% of the small lymphocytes were la-

with a half-time of 13–15 hours although the labeling intensity immediately and 38 hours after thymidine was so heavy and light, respectively that accurate quantitation was precluded. This result was interpreted as indicating that at least some of the initially labeled blast cells gave rise by division to more blast cells, which in turn served as precursors for more blasts, etc.

As the above experiment did not eliminate the possibility that an equal number of labeled and unlabeled blasts served as precursors of cell types other than blasts (the per cent labeled blasts remained constant) cultures were pulsed with H³-thymidine after a significant number of blasts had appeared. Immediately after the pulse the only labeled cells detected were LMC, of which 92–98% were typical blast cells. As early as three hours thereafter definitively labeled small lymphocytes were observed in mixed thymic cultures but not in cultures containing either Lewis or BN thymus cells alone (fig. 9). After 24 hours a few labeled small lymphocytes were observed in control, nonmixed cultures but the frequency never approached the maximum of 4% observed in mixed incubations. While no definitive trends in the per cent labeled small lymphocytes were noted in mixed or nonmixed cultures between 3 and 98 hours such cells were always present. By 116 hours the contained cells had become vacuolated and were undergoing degeneration. Because all cells initially labeled were LMC and because 92–98% of these were blasts, these results were interpreted as indicating that some blast cells gave rise to small lymphocytes thereby completing the cycle

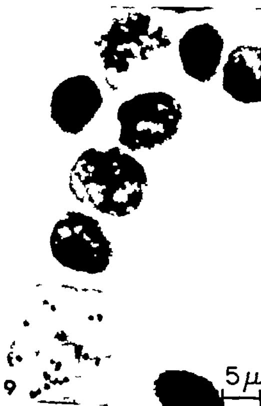


Fig. 9 Labeled small lymphocytes and a labeled blast cell observed in mixed cultures which were pulsed for four hours with H³-thymidine, beginning 44 hours after initiation. The pictured cells were taken three hours after the pulse, which labeled only LMC, of which 92–98% were typical blasts.

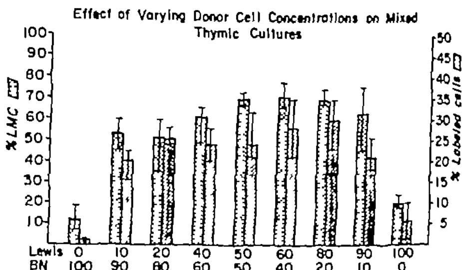


Fig. 7 The effect, as measured by per cent labeled cells and per cent LMC, of varying the percentage of thymic cells contributed to mixed cultures by Lewis and BN donor rats. The range of values observed are indicated by the narrow line bars.

Similar results were observed in mixed lymph node or spleen cultures in which either one of the donors had been exposed to H thymidine In addition when labeled or unlabeled thymus cells from either a BN or Lewis donor were cultured with labeled or unlabeled spleen or lymph node cells from the reciprocal strain of rats respectively labeled blasts were observed When radioautographic exposure times of five weeks were employed in these experiments a reduced labeling intensity of thymus cells as compared to spleen or lymph node cells was noted Correspondingly in experiments involving thymus cells radioautographs were exposed for eight weeks Results of this series of experiments suggested that when lymphoid elements from the thymus spleen and lymph node of Lewis rats are cultured with cells from either the thymus spleen or lymph node of the BN rat blast cells originate from small lymphocytes contributed by both donors

Progeny of blasts The first group of experiments consisted of following the per cent labeled blasts in cultures which had been pulse-labeled with H -thymidine at the time typical blasts were first detected Figure 8 indicated that 50–54% of the blasts were labeled immediately after this exposure to H^3-thymidine as well as throughout the following 27 hours of culture The slight decrease observed at 38 hours was interpreted as reflecting the division of blasts with concomitant reduction of radioactivity to a level below that detectable by the method and exposure times employed The grain density decreased progressively during this interval

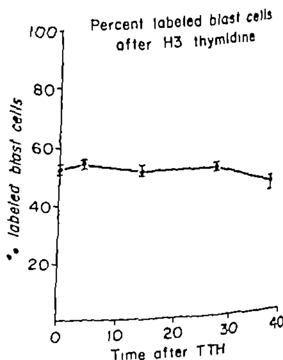


Fig. 8 The per cent labeled blasts with time in mixed thymic cultures which were pulsed with H thymidine from 32–34 hours after initiation. The bars indicate the range of values observed

From the short-term studies reported here blasts of mixed thymic cultures appear to give rise to more blasts as well as to small lymphocytes. Whether the daughter blasts will eventually form small lymphocytes and/or plasma cells remains to be studied. The evidence suggesting a small lymphocyte → blast → small lymphocyte cycle was, however identical to that observed in cultures containing rat thymus cells and phytohemagglutinin (Schwarz and Rieke, '66) or pokeweed mitogen (Schwarz, '67a) as well as in graft-versus-host reaction *in vivo* (Gowans, '62)

The inability to perpetuate mixed cultures beyond 7–9 days supported the findings of others and may reflect an *in vitro* homograft rejection phenomenon, with both donor cells reacting against those elements of the opposite animal (MacLennan, '65) The report by David-Farkdy MacLean and Gordon ('66) that skin grafts were rejected in an accelerated fashion after transfusion of cells from mixed splenic or blood cultures would support this hypothesis. Ginsberg and Sachs ('65) findings that rat lymphoid cells destroyed allogenic or xenogenic fibroblasts and the reports of enhanced transformation during and after skin homograft rejection (Oppenheim, Wang and Frei, '65 Moynihan, Jackson and Hardy '65) would also suggest a similar reaction. The latter authors, however did not determine the absolute number of cells or the total H^3 C^{14}-thymidine incorporation of the blastogenic response and as such, the percentage comparisons may not reflect an absolute difference.

While the results of the thymic studies reported are consistent with the transformation of small lymphocytes they did not exclude the possibility that the small numbers of nonlabeled LMC which persisted after preincubation with H^3-thymidine had served as precursors of the blast elements. This suggestion seems remote in view of the report of blastogenesis in cultures initiated with virtually pure preparations of rat thoracic duct small lymphocytes (Rieke, '66) In addition, the problem of whether the small lymphocytes which responded were of thymic origin or whether they represented blood-borne elements present in the thymus remains to be solved. Studies bearing on this problem revealed that in routine, 3 cm^3 cultures less than 540 of the lymphoid cells initially present were of blood origin (Schwarz, '67b) If all such cells had responded only 3.0×10^{-4}% of the elements in the culture inoculum would be enlarging. This suggestion seems unlikely in that, early in the response when DNA synthesis is initially observed, the number of cells proliferating would have been below the level of detection with the present methods

ACKNOWLEDGMENTS

This work was supported in part by USPHS grant AI-06150 and in part by USPHS grant GM-06309

The excellent technical assistance of Miss Nancy Edson and Mrs. Janice Kolloen as well as the advice and encouragment of Drs. N B Everett and W O Rieke is gratefully acknowledged.

LITERATURE CITED

Bain, B., M. R. Vas and L. Lowenstein 1964 The development of large immature mononuclear cells in mixed leucocyte cultures. Blood, 23 108–116.

Bollman, L. J J C. Cain and J H. Grindlay 1948 Techniques for the collection of lymph from the liver small intestine or thoracic duct of the rat. J Lab. Clin. Med., 33 1349–1352.

Caffrey R. W N. B. Everett and W O Rieke 1966 Radioautographic studies of reticular and blast cells in the hemopoietic tissues of the rat. Anat. Rec., 155 41–58.

Chapman, N D., and R. W Dutton 1965 The stimulation of DNA synthesis in cultures of rabbit lymph node and spleen cell suspensions by homologous cells. J Exp. Med., 121 85–100

Claman, H. N 1966 Human thymus cell cultures — evidence of two functional populations. Proc. Soc. Exp. Biol. and Med., 121 236–240.

Coons, A. H., E. H. Leduc and J. M. Connolly 1955 Studies on antibody production. I. A method for the histochemical demonstration of specific antibody and its application to a study of the hyperimmune rabbit. J Exp. Med., 102: 49–60.

David-Farkdy M. R., L. D MacLean and J Gordon 1966 Transfer of transplantation immunity by leukocytes sensitized *in vitro*. Leukocyte Culture Conference, Montreal, Canada, October 14–15, 1966.

Dutton R. W 1965 Further studies of the stimulation of DNA synthesis in cultures of spleen cell suspensions by homologous cells in inbred strains of mice and rats. J Exp. Med., 122: 759–770.

of small lymphocyte → blast → small lymphocyte

In an attempt to reveal the ultimate progeny of the continuously proliferating blast cells long term cultures were prepared Smears of the contained cells revealed intact blasts for up to six days but of the few persisting cells at 10 and 14 days virtually all revealed degenerative changes

Transformation of all small lymphocytes In this study cultures were exposed continuously to H^3 thymidine for three days so as to label any cells which were synthesiz ing DNA during this period As only an extremely rare small lymphocyte incor porated H^3 thymidine any of these cells which contained radioactivity must have originated from DNA-synthesizing blasts which labeled and gave rise to small lymphocytes After 72 hours of culture 2 8–5 3% of the small lymphocytes were la beled That a DNA precursor(s) was continuously available was demonstrated by the presence of labeled cells which had been exposed to the exchanged supernatant from the culture This result suggests that many of the small lymphocytes remain in the culture without undergoing transforma tion

DISCUSSION

The results of these studies indicate that some of the small lymphocytes from the thymus gland spleen lymph node thoracic duct lymph and blood of the rat will transform into blast cells when exposed to allogeneic lymphoid cells The discrepancy between the thymus response in this study and the lack of a transforma tion in Chapman and Dutton s (65) rabbit investigations remains unexplained It was not however due to the percentage of fresh versus preserved serum employed or to the number of cells per cm of cul ture medium as initially suggested (Schwarz, 66) Alternate explanations may include a difference in the histocompatability barrier between the two strains of rabbits and rats employed or an intrinsic difference in the blastogenic potential of the thymic lymphocytes from these two animals It must be added that the thymus lymphocytes of guinea pigs have not been demonstrated to undergo blastogenesis in the presence of foreign lymphoid cells at concentrations routinely employed in transforming blood cultures (Oppenheim, '67). In contrast, human thymus cells will respond to phytohemagglutinin and pokeweed mitogen (Claman, '66 Schwarz, 67) and swine thymus transforms under the influence of the former substance (Weber '66)

The appearance of islets in mixed cultures has led some authors to suggest that this is the active unit in the blastogenic response and possibly in the immune response and possibly in the immune reaction in general (McFarland and Heilman 65 Coons Leduc and Connolly '55) Support for this concept is found in the following observations (a) lymphocytic foot processes indent the cytoplasm of macrophages in mixed cultures (b) when mixed cells are forced into more intimate, *in vitro* contact a larger amount of H^3 thymidine was incorporated by the contained cells (Moorhead Connolly and McFarland 66) and (c) *in vitro* cytoplasmic bridges have been demonstrated between splenic macrophages and lymphocytes across which an RNA-protein complex may pass to stimulate transformation of lymphocytes during the immune response (Schoenberg Munaw Moore and Weisberger '64 Fishman Hammerstrom and Bond 63) Less harmonious observations are (a) the presence of these cell clusters in control cultures where little if any blastogenesis was noted (general results above) and (b) the induction of blastogenesis in cultures containing homologous peripheral blood cells and the cell free supernatant from cultures of un mixed or mixed leucocyte incubations (Hashem and Rosen 64 Kasakura and Lowenstein 65)

It has been suggested that the blast cells observed in tissue cultures are the *in vitro* equivalent of the large pyroninophilic cell seen in lymph nodes and spleens of animals undergoing immune responses While both cell types are known to arise from small lymphocytes (Gowans McGregor Cowans and Ford '62 Schwarz and Rieke 66) their exact progeny remains subject to debate Lymphocytes (Gowans et al '63 62) and plasma cells (Langevoort '63 Fudenberg and Hirschhorn '64) have been suggested as the most likely possibilities

The Effects of Hypophysectomy on the Digestive Glands of the Mouse [1]

RICHARD MORTSON KOERKER
Department of Anatomy, The University of Michigan Medical School, Ann Arbor, Michigan

ABSTRACT The objective was to observe the influence of hypophysectomy on the secretory cells of digestive glands in the mouse and to compare these findings with those reported for other mammalian species. Hypophysectomy of the mouse induced involutional changes in glandular cells concerned with secretion of proteins and mucins, and in those involved in ion transport or release. Gastric chief cells, pancreatic acinar cells, and serous cells of submandibular tubules were markedly involuted; acinar cells of the parotid gland were changed less significantly. Gastric mucous neck cells and mucous acinar cells of the submandibular and sublingual glands contained less secretory material. A colloidal iron-positive variety of mucous neck cell became dominant. These changes were less profound than those which occurred in most types of zymogenic cells. Parietal cells became atrophic and contained a greatly contracted intracellular canalicular system. Salivary ducts of the parotid and sublingual glands showed partial involution. It was concluded that, as in the rat and man, protein-secreting cells of the digestive tract of the mouse depend on the support of pituitary hormones. Those cells which secrete mucopolysaccharides or are involved in ion transport also require pituitary hormones for complete maintenance of their structure and function.

Schooley, Riddle and Bates (41) first demonstrated that the pituitary gland influences the digestive system, by observing a loss in weight of the gastrointestinal tract in the pigeon after hypophysectomy. More recently others have shown that the hypophysis exerts significant control over the structure and function of digestive glands in the rat. Thus, all zymogenic cells which have been studied are dependent on the support of pituitary and other hormones for maintenance of normal structure and full secretory activity. These include the gastric chief cell (Baker and Abrams, '54) acinar cells of the pancreas (Haist, '55) and parotid gland (Baker and Abrams, '55) zymogenic cells of the submandibular serous ducts (Lacassagne and Chamorro, 40) and cells of Paneth in the intestine (Baker et al. '58). In addition mild structural involution (Baker and Abrams, '54; Baker and Clark, '61) and functional depression (Crafts and Walker, 47) take place in the gastric parietal cells after pituitary ablation.

In contrast to the rather detailed information available concerning the action of hormones on the digestive glands of the rat, relatively little is known about their effects in other mammals. Investigations carried out on the stomach indicate that regressive changes occur during pituitary deficiency in the cat (Cutting et al., '37; Haeger et al. '53) and man (Laumonier et al., '63; Dotevall and Westling '63). In this report, the influence of hypophysectomy on the histology and histochemistry of the gastric mucosa, pancreas and parotid, submandibular and sublingual glands of the mouse will be described. Such information will help to indicate the extent to which digestive glands of mammals in general are dependent on hormonal stimulation.

MATERIALS AND METHODS

The experiments were carried out on young adult male ICR Swiss mice. Hypophysectomy was performed by the transauricular method of Falconi and Rossi ('64). Completeness of hypophysectomy was verified by histological observation of serial sections of the pituitary region. Incompletely hypophysectomized mice were discarded. A nonhypophysectomized mouse

[1] Supported in part by research grant AM 00131 14 from the United States Public Health Service.
From a dissertation submitted in partial fulfillment of the requirements for the Doctor of Philosophy degree.

Elves M. W S Roath, G Taylor and M. C. G Israels 1963 The *in vitro* production of anti body lymphocytes. Lancet, *I:* 1292–1293.

Everett, N B., W O Rieke W O Reinhardt and J M Yoffey 1960 Radioisotopes in the study of blood cell formation with special reference to lymphocytopoiesis In: Ciba Foundation Symposium on Haemopoiesis. J & A. Churchill, London, pp. 43–66.

Farnes P B. E. Barker L. E. Brownhill and H. Fanger 1964 Mitogenic activity in Phytolacca americana (pokeweed) Lancet, II: 1100–*1101*

Fishman M. R. A. Hammerstrom and V P Bond 1963 *In vitro* transfer of macrophage RNA to lymph node cells. *Nature 198* 549–551

Fudenberg, H H. and K. Hirschhorn 1964 Agammaglobulinemia: the fundamental defect. Science *145:* 611–612.

Ginsberg, H., and L. Sachs 1965 Destruction of mouse and rat embryo cells in tissue culture by lymph node cells from unsensitized rats. J Cell and Comp Physiol., *66:* 199–220

Gowans, J R. 1962 The fate of parenteral strain small lymphocytes in F_1 hybrid rats. Ann. N Y Acad. Sci., *99:* 432–455.

Gowans, J L., D D McGregor D M. Cowen and C. E. Ford 1962 Initiation of immune responses by small lymphocytes Nature, *196:* 651–655

Gräsbeck, R., C. T Nordman and A. de la Chapelle 1964 The leucocyte-mitogenic effect of serum from rabbits immunized with human leucocytes. Acta Medica Scand., Suppl. *412:* 39–47

Hashem, N., and F S. Rosen 1964 Mitogenic fractions in human peripheral lymphocyte ex tracts Lancet, *I:* 201–202.

Holyoke, E. A., J S. Latta and J V McLean 1968 A study of the ultrastructure of the developing spleen in the albino rat. J Ultra struct. Res., *15:* 87–99

Kasakura, S., and L. Lowenstein 1965 A factor stimulating DNA synthesis derived from the medium of leucocyte cultures. Nature, *208:* 794–795

Langevoort, H L. 1963 The histophysiology of the antibody response I. Histogenesis of the plasma cell reaction in rabbit spleens. Lab Invest. *12:* 106–118

Ling N R. E. Spicer K. James and N Williamson 1965 The activation of human peripheral lymphocytes by products of staphylococci. Brit. J Haematol., II: 421–431

MacLaurin, B. P 1965 Homograft interaction in the test tube. Lancet, *II:* 816–821.

McFarland, W., and D H. Heilman 1965 Lymphocyte foot appendages: its role in lymphocyte function and in immunological reactions. Nature 205 887–888.

Moorhead, J F., J J Connolly and W McFarland 1966 Cell interaction: its importance in immunological reactions in vitro. Leukocyte Culture Conference Montreal, Canada, October 14–15 1966.

Moynihan P., J F Jackson and J D. Hardy 1965 Lymphocyte transformation as an in *vitro* histocompatability test. *Lancet, I* 453-455.

Nowell, P C. 1960 Phytohemagglutinin: an initiator of mitosis in cultures of normal human leucocytes. Cancer Res., 20 462–466

Oppenheim, J J 1967 Personal communication.

Oppenheim, J J., J Wang and E. Frei 1965 *The effect of* skin homograft rejection on recipients and donor mixed leukocyte cultures. J Exp. Med., *122:* 651–664

Pearman, G., R. R. Lycette and P H. Fitzgerald 1963 Tuberculin-induced mitosis in peripheral blood leucocytes. Lancet, I: 637–638.

Reinhardt, W O., and C. H. Li 1945 Cell count, rate of flow and protein content of cervical lymph in the rat. Proc. Soc. Exp. Biol., 58 321–323.

Rieke, W O 1966 Lymphocytes *from* thymectomized rats: immunologic proliferative and metabolic properties. Science, *152:* 535-538.

Sell, S. and P G. H Gell 1965 *Studies on* rabbit lymphocytes *in vitro*. I. Stimulation of blast transformation with an antiallotype serum. J Exp. Med., *122:* 423–440.

Schoenberg, M. D., V R. Mumaw R. O. Moore and A. S. Weisberger 1964 Cytoplasmic interactions between macrophages and lymphocytic cells in antibody synthesis. Science, *143:* 964–965

Schwarz, M. R. 1966 Blastogenesis in cultures containing genetically-dissimilar thymic cells. Immunology *10:* 281–283

——— 1967a Personal observations.

——— 1967b Paper in preparation.

Schwarz, M. R., and W O Rieke 1966 The effect of phytohemagglutinin on rat thymus cells *in vitro*. Anat. Rec., *155:* 493–501

Weber W T 1966 The *in vitro* response of thymic lymphocytes of the pig to phytohemagglutinin. J Cell Physiol., *67:* 285–299.

TABLE 1

Summary of distribution of animals and technical methods used

Number of mice				Technical methods	
Experiment I		Experiment II		Fixation	Stain
Hyp.	Control	Hyp.	Control		
				Stomach	
11	18	12	12	FAA	PAS [1]-azure II, colloidal iron-PAS
7	9	12	12	FAA	Colloidal iron
4	8	12	12	FAA	α-Amylase digestion; PAS
7	14	12	8	Regaud's fluid	Altmann-Masson
				Pancreas	
10	18	12	12	Bouin's	Hematoxylin-Masson; azure II-eosin
7	14	10	12	Zenker-formol	Azure II-phloxine; Altmann-Masson
4	7	6	6	Champy's fluid	Altmann-Masson
3	4	5	3	Champy's fluid	Post-osmication
				Salivary glands	
11	17	12	19	FAA	PAS-azure II; colloidal iron; colloidal iron-PAS
3	6	5	3	FAA	α-Amylase digestion; PAS
7	14	10	11	Zenker formol	Altmann-Masson

Hyp. = hypophysectomized.
FAA = formalin-alcohol-acetic acid.
PAS = periodic acid-Schiff.

TABLE 2

The effect of hypophysectomy on weights of the body and stomach

Treatment	No. of mice	Body weight (g)			Stomach	
		Initial	Final		Weight (mg)	Organ wt. (mg) / Body wt. (g) × 10,000
		Experiment I Ad libitum-fed				
Control	18	23.9 ± 0.9	23.1 ± 0.5		230.2 ± 17.7 [a]	69.1 ± 5.0
Hyp.	11	23.1 ± 0.4	18.8 ± 0.5		138.5 ± 9.9	75.5 ± 5.5
		P	< 0.01		< 0.01	NS
		Experiment II Pair-fed				
Control	12	25.9 ± 1.4	24.7 ± 1.2		275.7 ± 15.0	112.6 ± 5.1
Hyp.	12	23.7 ± 1.1	19.4 ± 0.6		164.9 ± 7.1	80.2 ± 3.5
		P	< 0.01		< 0.01	< 0.01
Control Exp. I vs. Control Exp. II				P	NS	< 0.01

Hyp. = hypophysectomized P = probability of error; NS = not significantly different at P < 0.05.
[a] Standard error of the mean.
[illegible] mice.
[illegible] mice.

control mice did not differ from that of the ad libitum-fed controls except for the pancreas and submandibular gland. Pancreatic acini were smaller and the serous tubules of the submandibular gland were reduced in diameter as a result of pair feeding. Generally no other histological effects were noted which could be attributed to food restriction. Therefore, the effects of hypophysectomy as described in the following account apply to both experiments unless stated to the contrary.

With respect to the normal structure of the stomach, pancreas and salivary glands in the mouse, this presentation will be concerned only with those observations which have not been previously reported. The histology of these glands has been de-

was retained as a control for each hypophy sectomized animal.

The mice were fed a diet consisting of Purina mouse breeder chow supplemented with lettuce bread and cod liver oil. In or der to evaluate the influence of food intake on the results obtained the animals were arranged in two experiments In Experi ment I 11 hypophysectomized mice and 18 controls were allowed to eat *ad libi- tum*. In Experiment II each of 12 non- hypophysectomized control mice was pair fed against a hypophysectomized animal so that the control received the amount of food eaten by its operated mate on the previous day During the first seven days of this experiment the mice were not paired but the operated animals were fed daily the average amount of food consumed by hypophysectomized mice as determined by previous observations Each hypophysec tomized mouse was kept in the same cage as its pair fed control the two mice being separated by a screen. Since ingestion of food elicits structural changes in the di gestive glands the animals were starved for 8–12 hours before being killed. This was shown to be the optimal starvation time by preliminary experiments. Practi cally complete degranulation occurred in both the parotid gland and pancreas of some control mice if more than a 12 hour starvation time was employed.

When 8–10 weeks had elapsed after hy- pophysectomy the stomach pancreas and salivary glands were removed while the animals were under sodium amytal anes- thesia. The organs were dissected free of contiguous tissue and weighed The fol lowing procedure was developed to make possible a clean excision of the parotid gland so that reproducible weights could be obtained. The cervical skin with parotid gland attached was stretched by grasping it between the thumb and index finger and then pulling it over the index finger The outline of the parotid gland was clearly visible and the gland could be freed from the connective tissue. Histological sections showed that minimal fat and connective tissue were retained.

The following fixatives were used for the purposes and times indicated: formalin- alcohol acetic acid (FAA) (48 hours at 4 C) for the demonstration of ribonucleo- protein mucoprotein and glycogen, Cham- py s fluid (24 hours) and post-osmication for three days at 37 C for the Golgi appa ratus; Regaud's fluid (96 hours) for mito- chondria; Zenker formol (5 hours) for ribonucleic acid (RNA) and mitochondria, and Bouin s fluid (24 hours) for general tissue structure. The extent to which each fixative was used is summarized in table 1. Some stomachs were injected with fixative to effect uniform distension of the organ and thus, permit accurate observation of change in mucosal thickness. Areas of mu- cosa along the greater curvature were used for study Tissues fixed in Regaud's fluid or Zenker formol were post-chromated in 3% potassium dichromate for three days. After embedding in either paraffin or cel- loidin and paraffin sections were cut at 3–5 µ.

A variety of staining procedures (table 1) were employed for the following pur poses Hematoxylin-Masson was used to reveal general tissue structure azure II for cytoplasmic and nuclear basophilia, peri- odic acid-Schiff (PAS) (Hotchkiss, '48) for neutral mucopolysaccharides, colloidal iron (Rinehart and Abul Haj '51) for acid mucopolysaccharides and PAS-col- loidal iron (Mowry 58) to differentiate acid from neutral mucopolysaccharides. Certain slides were digested with a buff ered α-amylase or in buffer alone before staining with PAS as a control for the demonstration of glycogen. For study of mitochondria tissues fixed in Regaud's Champy s or Zenker formol fixatives were stained with the Altmann-Masson proc dure (Severinghaus and Thompson, '39

The significance of the differences be tween quantitative data for control and hy pophysectomized groups was determined by the Wilcoxon two sample test (Ste and Torrie '60) Significance was attri uted to differences with less than a 5 probability of error

OBSERVATIONS

Hypophysectomized mice lost weight after the operation (table 2) The body weight of pair fed control mice showed little change (Experiment II, table 2) The control mice (Experiment I) which ate *ad libitum* continued to gain in weight. The histology of digestive glands in the pair-fed

contained less secretory material (fig. 4) In 21 of 23 animals the colloidal iron-positive variety of mucous neck cell was dominant, and only rarely were the other varieties seen. Transitional cells containing both PAS-positive and colloidal iron-positive material were dominant in the one exceptional case. The nucleus and mitochondria were unchanged.

After hypophysectomy the number of parietal cells per fundic gland appeared to be unchanged, but they were strikingly atrophic (figs. 4 6 8) The cytoplasm maintained a pink mottled appearance with *PAS* staining. The perinuclear halo which in controls marked the location of intracellular canaliculi, was no longer present. Rather, the PAS-positive material was arranged as a dense clump on the luminal side of the nucleus which indicated that a profound alteration had occurred in the structure of the intracellular canaliculi. This conclusion was confirmed by observation of stomachs fixed in Regaud's fluid and stained with the Altmann-Masson procedure (fig. 8) In them the canaliculi also seemed to be restricted to the luminal side of the nucleus. Thus, the intracellular canaliculi, which in controls cupped around the nucleus from its luminal side and extended into the basal region of the parietal cell, were reduced to a small area between the nucleus and the glandular lumen. Consequently instead of forming two distinctly separate perinuclear rings mitochondria filled the entire cytoplasmic area basal and lateral to the nucleus (fig. 8) In parietal cells of hypophysectomized mice. The total number of mitochondria was reduced. Atrophy of the parietal cells appeared to be partly responsible for the increased caliber of the glandular lumen. Nuclear size was slightly decreased and chromatin usually appeared more compact.

Chief cells appeared to be reduced in number per fundic gland and were remarkably involuted (fig. 2) being changed from the high columnar form characteristic of the controls (fig. 11) to a low cuboidal shape (fig. 12) Fewer secretory granules were present per cell and the extensive, granule-filled apical area seen in control animals had disappeared. In some hypophysectomized mice chief cells had no visible granules at all. The total amount of basophilic material and the intensity of staining with azure II were reduced. Mitochondria were shorter wider and fewer in number (figs 9 10) Chromatin was more compact. In 17 of 22 operated mice, nucleoli were smaller than in the controls

The pancreas

Control mice The diameter of pancreatic acini of pair fed controls was somewhat less than that of *ad libitum* fed control mice although glandular weights and gland weight/body weight ratios were not different in the two groups (table 3)

For study of the size number and distribution of organelles employment of several procedures was necessary Secretory granules were not preserved consistently by Bouin's fluid but, after fixation in Champy's fluid or Zenker formol followed by Altmann-Masson staining they appeared intensely and uniformly stained (fig. 15) Cells in acini adjacent to pancreatic islets were usually filled with granules, while in other areas of the gland the storage of granules varied from acinus to acinus. Evaluation of the amount of cytoplasmic basophilia in pancreatic acinar cells was difficult since the distribution of basophilic material was affected by the number of secretory granules. It was concentrated basally in granule-filled cells and arranged more diffusely in granule-poor cells. A fine network of basophilic material consistently surrounded the secretory granules (fig. 13). Mitochondria appeared as darkly stained threads of varied thickness and length (fig. 15) They were most numerous beneath the nucleus and were arranged with their long axes parallel to the base of the cell; laterally they were oriented perpendicular to the base of the cell. The Golgi apparatus (fig. 17) consisted of a reticular network located above the nucleus and dispersed among the supranuclear secretory granules Large nuclei with chromatin clumped along the nuclear membrane and with large, irregularly shaped nucleoli were seen in *ad libitum*-fed controls In contrast, nucleoli of pair-fed controls (fig. 13) were somewhat smaller and rounder

Hypophysectomized mice Hypophysectomy caused involution of the pancreas as shown by its lower absolute weight in hypophysectomized mice of both experiments

scribed by Fekete (41) Additional information on the submandibular gland was presented by Lacassagne (40) Junqueira ('64) Junqueira et al (49) Raynaud (60) and Schätzle (62) The histochemistry of mucins in the submandibular and sublingual glands and stomach was analyzed by Spicer (60) and Spicer and Jarrels ('61) Parks (61) reported on the histology and ultrastructure of the parotid gland.

The stomach

Control mice The difference between the mean stomach weights of the *ad libitum* and pair fed controls was not significant (table 2) but between the mean organ weight/body weight ratios the difference was significant (P < 0 01) Thus absolute weight of the stomach appears to be unaffected by reduced food intake

Mucous neck cells were interposed among the parietal cells in the area of the mucosa just above the chief cells (fig 1) In FAA fixed material three histochemically different varieties of mucous neck cells were observed in stomachs stained with colloidal iron-PAS (fig 3) To one group of mucous neck cells colloidal iron imparted an aquamarine color The stained material was in the form of tightly packed granules The cytoplasm of a second group of mucous neck cells stained red with PAS The third group contained both PAS-positive cytoplasm and colloidal iron positive granules In an individual stomach the colloidal iron positive cells were usually smaller than the PAS-positive cells Cells containing both PAS- and colloidal iron positive material varied in size. All three varieties were present in a single animal usually within a single fundic gland and one variety was numerically dominant No single varety was consistently dominant in all control animals.

When PAS staining was used after FAA fixation the cytoplasm of parietal cells stained pink and had a mottled appearance Mucoprotein which appeared to be associated with the microvilli of intracellular canaliculi, stained more intensely creating a perinuclear halo of PAS-positive material (fig 5) The PAS-positive material was not glycogen as indicated by its resistance to digestion with α amylase nor was it an acid mucopolysaccharide, since it did not stain with colloidal iron. Large rounded mitochondria were found everywhere in the cytoplasm except in that area occupied by intracellular canaliculi (fig. 7) Thus mitochondria were arranged in two rings one surrounding the nuclear membrane and the other being situated inside the plasmalemma. The zone between these rings of mitochondria coincided with the position of intracellular canaliculi as indicated by the PAS-positive halo.

In addition to the basally located cytoplasmic basophilia of chief cells, a fine network of basophilic material outlined the secretory granules (fig 11) The long thread like mitochondria of chief cells (fig 9) were oriented randomly in the subnuclear region and vertically in the area lateral to the nucleus Chief cell nuclei contained large nucleoli and fine chromatin material.

Hypophysectomized mice In both experiments the weight of the stomach was less in hypophysectomized than in control mice (table 2) These differences, when considered as absolute values or in relation to body weight (except in Experiment I) were significant at less than the 1% level of confidence which indicated that the stomach may be more sensitive to hormonal withdrawal than the body as a whole The results in Experiment II also demonstrate that the reduction in stomach weight after pituitary excision is not due to reduced food intake.

The fundic mucosa in hypophysectomized mice was thinner than in the controls (fig 2) The lumina of the fundic glands were often enlarged as compared with control mice in which they were seldom visible in microscopic sections. Dilation of the fundic lumina appeared more pronounced after fixation in Regaud's fluid than in FAA. It was most prominent in the middle one-third of the mucosa (parietal cell area) (figs. 6 8) and less so in the base of the fundic gland.

Although no changes were observed in surface and nondifferentiated cells mucous neck cells were altered by pituitary excision The number of mucous neck cells per fundic gland appeared to be increased in hypophysectomized mice. The cells were usually smaller than those of controls and

basally in 13 of 22 hypophysectomized mice (fig. 25) However the decrease in basophilia was less pronounced than in the other glands studied. Mitochondria were thinner and appeared to be more concentrated due to the loss of intervening secretory granules (fig 21) Nuclei and nucleoli were unchanged.

The duct system of the parotid gland was also affected by hypophysectomy The diameter of salivary ducts and size of their lining cells were reduced (fig. 21) Basal striations were no longer visible (fig. 25) Mitochondria in the subnuclear region were shorter, randomly oriented and more densely packed than in controls. Cells lining the intercalated ducts were less basophilic but their PAS-positive granules were unaffected.

The submandibular gland

Control mice The submandibular glands of pair-fed control mice weighed less than those of *ad libitum*-fed controls (P < 0.01) but the means of the gland weight/body weight ratios for the two control groups did not differ significantly (table 4) Thus, with respect to weights, the submandibular gland and body responded to restricted food intake in parallel fashion.

The diameter of the submandibular serous tubules in paired-fed control mice was less than that of the *ad libitum*-fed controls. The large granules in the apical half of the serous tubular cells stained with the Altmann-Masson procedure (fig 30) A diffuse cytoplasmic basophilia was present in the basal area (fig. 28) where the mitochondria seemed to be compressed by the accumulated serous granules (fig. 30) In partly degranulated cells some mitochondria were visible in the supranuclear zone. Mitochondria were randomly oriented and, when cut longitudinally appeared as short rods.

Acinar cells of the submandibular gland were filled with mucous secretory material. Cytoplasmic basophilia was most dense in the basal area (fig 28 inset) but occurred elsewhere in the cytoplasm also. When stained with colloidal iron-PAS the mucous secretion appeared dark blue (fig. 26)

Hypophysectomized mice The mean weight of the submandibular gland in hypophysectomized mice and the mean gland weight/body weight ratios were reduced (P < 0 01) (table 4) The effect of hypophysectomy on the histology of the submandibular gland of the mouse has been described by Lacassagne and Chamorro (40) and Shafer and Muhler ('60)

As noted by these workers the marked atrophy of the serous tubules, with a loss of serous granules (figs. 27 31) and cytoplasmic basophilia and a decrease in nuclear size (fig. 29) were observed. The following new observations were made. A chronic sialitis was often present after hypophysectomy Glycogen granules became more prevalent in the apical region of serous tubular cells. Mitochondria were more fre-

TABLE 4

The effect of hypophysectomy on weights of the submandibular and sublingual glands

Treatment	No. of mice		Submandibular gland: Weight (mg)	Submandibular gland: Gland wt. (mg) / Body wt. (g) x 10,000	Sublingual gland: Weight (mg)	Sublingual gland: Gland wt. (mg) / Body wt. (g) 10,000
			Experiment I	Ad libitum-fed		
Control	18		33.5 ± 2.1	25.0 ± 0.8	10.7 ± 0.5	3.2 ± 0.2
Hyp.	11		17.4 ± 0.7	9.2 ± 0.4	5.9 ± 0.2	3.1 ± 0.2
		P	< 0.01	< 0.01	< 0.01	NS
			Experiment II	Pair-fed		
Control	12		57.2 ± 4.7	22.8 ± 1.1	12.1 ± 0.7	4.9 ± 0.2
Hyp.	12		19.6 ± 1.1	10.1 ± 0.5	8.4 ± 0.5	4.3 ± 0.3
		P	< 0.01	< 0.01	< 0.01	NS
Control Exp. I vs. Control Exp. II		P	< 0.01	NS	NS	< 0.01

Hyp. = hypophysectomized; P = probability of error; NS = not significantly different at P < 0.05. Standard error of the mean.

TABLE 3

The effect of hypophysectomy on weights of the pancreas and parotid gland

Treatment	No. of mice		Pancreas Weight (mg)	Pancreas Gland wt. (mg) / Body wt. (g) × 10,000	Parotid gland Weight (mg)	Parotid gland Gland wt. (mg) / Body wt. (g) × 10,000
			Experiment I	Ad libitum-fed		
Control	18		291.3 ± 30.2 [1]	87.9 ± 9.0	26.8 ± 1.5 [2]	8.1 ± 0.6
Hyp.	11		115.0 ± 13.7	60.5 ± 6.7	16.1 ± 1.4 [3]	8.0 ± 0.5
		P	< 0.01	< 0.05	< 0.01	NS
			Experiment II	Pair-fed		
Control	12		231.7 ± 16.4	92.8 ± 4.5	28.0 ± 1.7 [4]	10.9 ± 1.1
Hyp	12		167.3 ± 19.6	85.3 ± 9.0	16.9 ± 0.9 [4]	9.2 ± 0.6
		P	< 0.01	NS	< 0.01	NS
Control I vs. Control II		P	NS	NS	NS	< 0.05

Hyp. = hypophysectomized; P = probability of error; NS = not significantly different at $P < 0.05$.

[1] Standard error of the mean.
[2] Eight mice.
[3] Four mice.
[4] Six mice.

(table 3) as compared with the controls. In only Experiment I, was the mean gland weight/body weight ratio reduced

Loss of weight of the pancreas was reflected in its histology Acinar diameter and cell size were less in hypophysectomized mice when compared with both *ad libitum* fed and pair fed controls (figs 14 16) Although much less numerous the number of secretory granules was more uniform among the acinar cells of hypophysectomized mice than of controls The peri islet acinar cells showed less degranulation than other acinar cells Cytoplasmic basophilic material was reduced in amount and less intensely stained both basally and between the secretory granules Mitochondria were thinner and shorter (fig 16) The Golgi apparatus was condensed into a compact supranuclear body (fig 18) Nuclei and nucleoli were often smaller and the chromatin was more compactly arranged.

The parotid gland

Control mice The absolute weight of the parotid gland was not affected by pair feeding but the difference between the mean gland weight/body weight ratios of pair-fed and *ad libitum* fed controls was significant (table 3)

Acinar cells of the parotid gland were pyramidal and contained basal cytoplasmic basophilic material (fig. 24) which extended as a fine network among the apical secretory granules. Mitochondria were short rods and were randomly oriented in the basal half of the acinar cell (fig. 19). Epithelial cells lining salivary ducts were columnar lightly PAS-positive and possessed basal striations (figs. 22, 24) Most mitochondria were located in the basal area of the cell and arranged parallel to the basal striations a few were scattered in the apical cytoplasm. They were long and thin (fig 20) The cells lining the intercalated ducts were low cuboidal and possessed a small area of cytoplasmic basophilia on either side of the nucleus. The background cytoplasm stained rose with PAS and sometimes contained PAS-positive granules. These granules were not glycogen since digestion with α-amylase did not remove them

Hypophysectomized mice The mean weight of the parotid gland was reduced after hypophysectomy (table 3) However the mean gland weight/body weight ratio remained unchanged.

Histological changes induced in the parotid gland by hypophysectomy were similar to but not as great as, those elicited in the pancreas. Parotid acini were smaller (fig 23) the epithelial cells being reduced in size and containing fewer secretory granules (fig. 25) than those of controls. Basophilia was absent from the apical granulated region and was reduced

nose they are located in the deeper one-third of the mucosa. Since Helander ('64) could not differentiate mucous neck cells from surface cells in the fundic mucosa of the mouse with the electron microscope, the blue color imparted to mucous neck cells by colloidal iron, as contrasted with the purple color of the surface mucous cells, indicates that they are a unique cell type. The three histochemically different varieties of normal mucous neck cells have not been observed previously. Whether they represent different functional types, different stages in a secretory process, or indicate transformation of one distinct type into a second is not now clear. Spicer ('60) was unable to demonstrate acid radicals in the mucopolysaccharide in mucous neck cells of the mouse without prior chemical treatment, but the intense stain imparted to their intracellular granules by colloidal iron indicates clearly that acid mucopolysaccharides are present.

The perinuclear halo of PAS-positive material in the parietal cell of the normal mouse stomach, which reveals the position of the intracellular canaliculus, probably results from the presence of mucopolysaccharide on the surface of the canalicular wall. A filamentous coat containing mucopolysaccharide has not been seen with the electron microscope covering the intracanalicular microvilli of parietal cells in several mammalian species (Ito, '61 and Ito and Winchester '63) but Sedar ('65) observed it in the frog.

Comparison of the effects of hypophysectomy in the mouse with other mammals

In most respects, the digestive glands of the mouse resemble those of the rat and other animals in their response to hypophysectomy. However some endpoints are affected differently in the mouse.

Stomach. Involution of the gastric mucosa appears to be a general characteristic of pituitary deficiency in mammals having been reported in the cat (Haeger et al., '53) rat (Baker and Abrams, '54; Crean, '63a) and man (Dotevall and Westling, '63). These changes appear also in association with panhypopituitarism in man (Laumonier et al., '63). Similarly the absence of histological change in the surface mucous cells and nondifferentiated cells after hypophysectomy of the mouse is characteristic of the rat (Baker and Abrams, '54; Corpron, '66). However some functional depression in mucus production is indicated by its reduced content in the stomach (Robert et al., '66).

Mucous neck cells of the mouse are altered significantly by hypophysectomy in contrast to the minor changes reported in other animals. The irregular reduction in the amount of mucoid material in individual mucous neck cells is seen with the light microscope in both mouse and rat (Baker and Abrams, '54) although no alteration in ultrastructure was observed by Corpron ('66). Unique to the mouse are the apparent increase in the number of mucous neck cells and the predominance of the colloidal iron-positive variety of mucous neck cell which result from pituitary ablation.

In agreement with Crean's ('63a, b) observations in the rat, the number of parietal cells per fundic gland does not seem to be reduced by hypophysectomy in the mouse. However their size and structure are altered greatly in the mouse in contrast to the minor structural changes reported for parietal cells of the rat. Of special significance is the change in canalicular structure, as revealed by two staining procedures. This was not apparent in earlier light microscopic studies of rat gastric mucosa and only slight change in the canalicular microvilli was seen by Corpron ('66) with the electron microscope. It is probable that cytological alteration of comparable degree has not been induced previously in the parietal cells of any animal by experimental manipulation. Although some workers (Vial and Orrego '60; Sedar and Friedman, '61) have reported ultrastructural change in parietal cells after stimulation Ito ('61) claimed that the form of intracellular canaliculi cannot be used as an index of physiological state because of its extreme normal variation.

The decreases in size of chief cells and their nuclei, in the number of pepsinogen granules and mitochondria, and in cytoplasmic basophilia after pituitary ablation of the mouse are identical with the changes observed in the hypophysectomized rat

quently arranged perpendicular to the base of the serous tubular cells (fig 31) The smaller diameter of the involuted serous ducts and their more numerous intracellular PAS-positive granules (fig 29) were the only features which enabled one to differentiate them from the non serous portions of the intralobular duct system

In addition to the reported atrophy of serous tubules mucous acini (figs 27 29) were reduced in diameter and their epithelial cells were smaller in hypophysec tomized mice than in controls. PAS-positive material was decreased in total amount less intensely stained and had a foamy appearance in contrast to the granular form characteristic of the mucin in most acini of controls The colloidal iron PAS procedure revealed the secretory material to be aqua green (fig 27) in contrast to its blue color in acinar cells of control mice Cytoplasmic basophilia was somewhat re- ruced in total amount and staining inten sity (fig 29) Nuclei of mucous cells appeared slightly smaller but nucleoli were unchanged Intercalated ducts were unal tered even though they appeared more prominent because of the acinar involution

The sublingual gland

Control mice As compared with *ad libitum* feeding restriction of food intake by pair feeding did not affect the weight of the sublingual glands but increased the mean gland weight/body weight ratio ($P < 0\ 01$) (table 4) The change in the latter value reflects considerable loss in body weight without a comparable reduction in weight of the gland

The secretory material of mucous acinar cells (fig 32) had a foamy appearance when stained with PAS With combined colloidal iron and PAS material staining with PAS was found in the apical part of the cell while other regions reacted in- tensely to colloidal iron The nucleus was displaced basally by the accumulated intra cellular secretion and basophilic material was scattered in the cytoplasm around it

Epithelial cells of the salivary ducts in control animals had prominent basal striations (fig 34) which stained with colloidal iron (fig 36) In 6 of 21 animals scattered cells of the salivary ducts were filled with granules (Spicer and Jarrels, 61) which did not react with either PAS or colloidal iron but stained intensely with the Altmann-Masson procedure (fig. 34). These granules were of the same size and staining properties as those of the serous tubules found in the submandibular gland Mitochondria (fig 34) were dis- tributed along the basal striations and scattered throughout the cytoplasm of the duct cells.

Hypophysectomized mice The mean absolute weight of the sublingual gland was reduced in hypophysectomized mice ($P < 0\ 01$) (table 4) but the mean gland weight/body weight ratios were unaffected. Thus the sublingual gland was no more sensitive to withdrawal of pituitary hor- mones than was the body as a whole Histologically the acinar diameter (figs. 33 35) was reduced and acinar cells con- tained less secretory material. The staining properties of the intracellular mucin cyto- plasmic RNA, nuclei, nucleoli and mito- chondria were not changed Salivary ducts were narrower (fig 35) and the granulated cells had disappeared. Epithelial cells of salivary ducts were lower and their basal regions contained a few vacuoles (fig. 37) and less distinct basal striations. Mitochon- dria were shorter smaller (fig 35) and no longer arranged between basal striations as in the controls. Nuclei contained clumped chromatin and nucleoli were less distinct. Intercalated ducts became rela- tively more prominent after hypophysec- tomy due to involution of the acini.

DISCUSSION

Normal histology of the mouse digestive system

The digestive glands of the normal mouse differ histologically from those of other mammals in several ways. Although mucous neck cells have been demonstrated in several mammalian species Lillibridge (64) and Helander ('62, '64) were un- able to identify them in man and mouse respectively by means of electron micros- copy In agreement with Fekete (41) my observations reveal the presence of mucous neck cells in the mouse. As com- pared with their superficial position in the gastric mucosa of most mammals in the

rotease (Halst, '55; Baker Reid and Doom, '58) amylase (Barrett et al. '55) and lipase (Bicknell and Baker '62); submandibular amylase and protease (Srebny et al., '57); and amylase in the parotid gland (Baker, Klegman, Logan and Garner '56)

The structural and histochemical alterations elicited in zymogenic cells by hypophysectomy when interpreted on the basis of available biochemical data, suggest that protein synthesis is deficient in protein-secreting cells. Thus, the decrease in nucleolar size, amount of cytoplasmic basophilia, size of the Golgi apparatus, and in the number of secretory granules, all may be taken as indicators of interference at several points in the pathway of protein synthesis. Since RNA of the nucleolus is representative of rRNA (De Robertis et al., '65) reduction in size of the nucleolus after hypophysectomy may suggest that a block occurs in the formation of rRNA. The reduction in cytoplasmic basophilia after pituitary ablation reflects a reduction in RNA, although the RNA fraction that accounts for this basophilia has not been finally identified. Nevertheless, the profound loss of basophilia in chief cells and pancreatic acinar cells indicates that ribosomes are depleted from the cytoplasm, a reduction in number having been demonstrated by Corpron ('66) in chief cells of the rat. The involvement of rough-surfaced endoplasmic reticulum and ribosomes in protein synthesis has been revealed by both biochemical procedures (Korner '59; Hultin, '64 and many others) and electron microscopy combined with radioautography (Kurosumi, '61; Caro and Palade, '64) Furthermore, a deficiency in the capacity of ribosomes to form polypeptides after hypophysectomy has been demonstrated for the liver by Korner ('59) and for the prostate gland after castration by Liao and Williams-Ashman ('62). It is probable that the ribosomes of zymogenic cells are also deficient in their protein-synthesizing capacity in the absence of pituitary hormones.

It is currently held that polypeptides pass from ribosomes into the cisternae through which they move to the Golgi apparatus. Here, the secretory product is enclosed by a smooth-surfaced membrane and becomes microscopically visible. A direct relationship between size of the Golgi apparatus and secretory activity has long been recognized in many types of secretory cells (Kirkman and Severinghaus, '38; Dalton '61) Thus, contraction of the Golgi apparatus in pancreatic acinar cells of both mouse and rat after pituitary ablation indicates further that the production of protein is retarded. The depletion of secretory granules from zymogenic cells also reflects decreased production of secretion, since there is no evidence that release of secretion from the cell is accentuated by hypophysectomy

The effect of hypophysectomy on acid production and ion transport

Production of acid by the stomach is influenced by pituitary hormones A reduction in acid secretion and/or an elevation of pH occurs in the stomach of the rat (Crafts and Walker 47 Baker and Abrams, '55) cat (Cutting et al., '37) and man (Dotevall and Westling, '63) after hypophysectomy This effect correlates well with the decrease in size (Baker and Abrams '54) and in total number of parietal cells (Friedman '53; Crean, '63a,b) present after pituitary ablation of the rat and with the profound involution of parietal cells observed in the mouse.

Ion transport also occurs in the ducts of salivary glands, where cell morphology may be correlated with function. Junqueira ('64) demonstrated a relationship between the histology of the salivary ducts and ion composition of the saliva. The involution of salivary ducts which occurs in the mouse parotid and sublingual glands after pituitary removal suggests that ion transport across their epithelium is altered. On the other hand, in the submandibular gland Taurog et al. ('59) did not detect any change in the iodine-concentrating capacity of the submandibular gland of the mouse after hypophysectomy In accord with this observation, basal striations do not disappear from the nongranulated cells in salivary ducts of the submandibular gland in the mouse.

(Baker and Abrams 54) and similar to those occurring in human panhypopituitarism (Laumonier et al. 63) Corpron (66) verified these results in the rat with the electron microscope.

Pancreas The pancreas of the mouse undergoes the same changes after hypophysectomy as seen in other animals These include loss in weight as observed in the dog (Koster '30) pigeon (Schooley et al. 41) and rat (Haist, '55) and decreases in acinar diameter acinar cell size number of secretory granules amount of cytoplasmic RNA number and size of mitochondria, and in nuclear size as observed in the rat (Baker and Abrams '55 Sesso et al. 55) Condensation of the Golgi apparatus in pancreatic acinar cells occurs also in the rat (Baker personal communication)

Parotid gland. Changes in the parotid gland of the mouse after hypophysectomy are generally similar to those occurring in the rat although the loss in weight appears to be somewhat greater in the rat (Baker and Abrams 55) Alteration in morphology of acinar mitochondria in the mouse contrasts with Dewey s ('58) negative findings in the rat. In both mouse and rat (Baker and Abrams '55) depletion of cytoplasmic basophilia is not as great as in the gastric chief cells and pancreas. Atrophy of the salivary ducts in the hypophysectomized mouse appears more pronounced than that seen by Baker and Abrams (55) and Dewey ('58) in the rat, but is of approximately the same magnitude as that reported by Yoshimura (56)

Submandibular gland. The loss in weight of the submandibular gland after hypophysectomy agrees with reports for the mouse (Lacassagne and Chamorro 40) dog (Argonz, '61) cat (Kahlson and Renvall '56) and rat (Baker and Abrams 55) Atrophy of the serous tubules with depletion of their zymogenic granules also seems to be a general phenomenon since it has now been observed in the mouse (Lacassagne and Chamorro 40) rat (Sreebny et al. '57) cat (Kahlson and Renvall, '56) and dog (Argonz, '61)

Earlier workers (Lacassagne and Chamorro 40 Gabe '50 Taurog et al '59) observed no acinar changes in the mouse after hypophysectomy However in this study a decrease in submandibular acinar size with a loss of cytoplasmic basophilia and secretory material was observed. Somewhat similar changes were found in the rat by Baker et al. ('64) Yoshimura ('56) and in the dog by Argonz ('61) Binder et al. (57) reported a fall in RNA content of the acinar cells in the rat and Kronman (63) and Baker et al. ('64) described a decrease in the PAS-staining intensity of the mucous acini of the rat. Only Sreebny et al. (57) found pituitary removal to be without effect on submandibular acinar cells in the rat. Therefore complete agreement does not exist but most evidence indicates that the hypophysis exerts a regulatory influence over the production of submandibular mucus.

Sublingual gland. Of all major digestive glands the sublingual glands are affected the least by removal of the pituitary gland Nevertheless, as in the rat (Baker and Abrams '55) the mean absolute weight, the mean gland weight body weight ratio and the amount of mucin in acinar cells are decreased in the mouse In contrast, Kronman ('63) saw no histological changes in the rat. The involution of striated ducts accompanied by increased mitochondrial concentration and the degranulation of some ductal epithelial cells after hypophysectomy appear to be unique to the mouse.

The effect of hypophysectomy on protein synthesis

The considerable evidence now available for the rat and mouse indicates that in general protein-producing cells of the digestive system undergo greater atrophy after hypophysectomy than do other epithelial cell types For the mouse this conclusion is made evident by the structural responses of gastric chief cells acinar cells of the pancreas and parotid glands and serous cells in the submandibular and sublingual ducts. Biochemical data are available from study of other species to prove that this histological involution represents a true functional depression Thus, in the rat, storage or secretion of the following enzymes is decreased after hypophysectomy: pepsin (Baker and Abrams '54) pancreat

Hotchkiss, R. D. 1948 A microchemical reaction resulting in the staining of polysaccharide structures in fixed tissue preparations. Arch. Biochem., 16: 131–141.

Hendler, T 1964 Ribosomal functions related to protein synthesis. In: International Review of Cytology vol. 16. G. H. Bourne and J F Danielli, eds. Academic Press, New York, pp. 1–30.

Ito, S. 1961 The endoplasmic reticulum of gastric parietal cells. J Biophys. Biochem. Cytol., 11: 333–347

Ito, S., and R. J. Winchester 1963 The fine structure of the gastric mucosa in the bat. J Cell Biol., 16: 541–577

Junqueira, L. C. U. 1964 Studies on the physiology of rat and mouse submaxillary glands. III. On the function of the striated ducts of the mammalian salivary glands. In: Salivary Glands and Their Secretions. L. M. Sreebny and J. Meyer, eds. Macmillan, New York, pp. 123–132.

Junqueira, L. C., A. Fajer, M. Rabinovitch and L. Frankenthal 1949 Biochemical and histochemical observations on the sexual dimorphism of mice submaxillary glands. J Cell. Comp. Physiol., 34: 129–158.

Kahlson, G., and S. Rosvall 1958 Atrophy of salivary gland following adrenalectomy or hypophysectomy and the effect of DOCA in cats. Acta Physiol. Scand., 37 150–158

Kirkman, H., and A. E. Severinghaus 1938 A review of the Golgi apparatus. Part III. Anat. Rec., 71 79–104.

Korner, A. 1959 The effect of hypophysectomy of the rat and of treatment with growth hormone on the incorporation of amino acids into liver proteins in a cell-free system. Biochem. J., 73: 61–71.

Koster, S. 1930 Experimentelle Untersuchung der Hypophysenfunktion beim Hunde. Pflüg. Arch. f. Physiol., 224: 212–216.

Kronman, J. H. 1963 A histochemical study of hypophysectomy-induced changes in rat submandibular and sublingual glands. Am. J Anat., 113: 327–345.

Kurosumi, K. 1961 Electron microscopic analysis of the secretion mechanism. In: International Review of Cytology vol. 11. G. H. Bourne and J. F Danielli, eds. Academic Press, New York, pp. 1–124.

Lacassagne, A. 1940 Dimorphisme sexuel de la glande sous-maxillaire chez la Souris. C. R. Soc. Biol., 133 180–181.

Lacassagne, A., and A. Chamorro 1940 Réactions à la testostérone de la glande sous-maxillaire atrophiée consécutivement à l'hypophysectomie chez la Souris. C. R. Soc. Biol., 134 223–224.

Lemonnier R., C. Faye, E. Martin, J P Hardouin and Ch. Debray 1963 La muqueuse gastrique au cours des maladies endocriniennes. Étude anatomo-biopsique et expérimentale. Arch. Anat. Pathol., 11 53–68.

Liao, S. and H. G. Williams-Ashman 1962 An effect of testosterone on amino acid incorporation by prostatic ribonucleoprotein particles. Proc. Nat. Acad. Sci., U S., 48 1956–1964.

Lillibridge C. B. 1964 The fine structure of normal human gastric mucosa. Gastroenterology 47: 269–290.

Mowry R. W. 1958 Improved procedure for the staining of acidic polysaccharides by Müller's colloidal (hydrous) ferric oxide and its combination with the Feulgen and periodic acid-Schiff reactions. Lab. Invest., 7 566–576.

Parks, H. F. 1961 On the fine structure of the parotid gland of mouse and rat. Am. J Anat., 108 303–329

Raynaud, J. 1960 *Contrôle hormonal de la glande sous-maxillaire de la Souris.* Bull. Biol. de France et Belgique, 94 400–524.

Rinehart, J. F., and S. K. Abul-Haj 1951 Improved method of histological demonstration of acid mucopolysaccharides in tissues. Arch. Path., 52: 189–194.

Robert, A., J P Phillips and J E. Nezamis 1966 Gastric secretion and ulcer formation after hypophysectomy and administration of somatotrophic hormone. Am. J Dig. Dis., 11 546–552.

Schätzle, W 1962 Histochemie der Speicheldrüsen. Acta Histochem., 13: 68–112.

Schooley J. P., O. Riddle and R. W Bates 1941 Replacement therapy in hypophysectomized juvenile pigeons. Am. J Anat., 69 123–158.

Sedar A. W 1965 Fine structure of the stimulated oxyntic cell. Fed. Proc., 24 1360–1367.

Sedar A. W., and M. H. F Friedman 1961 Correlation of the fine structure of gastric parietal cell (dog) with functional activity of the stomach. J Biophys. Biochem. Cytol., 11 349–364

Sesso, A., J. H. Tramezzani, V Valeri and R. H. Migliorini 1955 Action de l'hypophysectomie sur les acides nucléiques et l'activité sécrétoire du pancréas du Rat, d'après des études biochimiques et cytologiques. C. R. Acad. Sci., 241 775–777

Severinghaus, A. E., and K. W Thompson 1939 Cytological changes induced in the hypophysis by prolonged administration of pituitary extract. Am. J Path., 15 391–412.

Shafer, W. G., and J. C. Muhler 1960 Endocrine influences upon the salivary glands. Ann. N Y Acad. Sci., 96 215–227

Spicer S. S. 1960 A correlative study of the histochemical properties of rodent acid mucopolysaccharides. J Histochem. Cytochem., 8 18–35.

Spicer S. S., and M. H. Jarrels 1961 Histochemical reaction of an aromatic diamine with acid groups and periodate engendered aldehydes in mucopolysaccharides. J Histochem. Cytochem., 9 368–379

Sreebny L. M., J Meyer E. Bachem and J P Weinmann 1957 Restoration of enzymatic activity in the submaxillary gland of the hypophysectomized albino rat. Endocrinology 60: 200–204.

Steel, R. G. D and J. H. Torrie 1960 Principles and Procedures of Statistics. McGraw-Hill, New York.

Taurog, A., G. D Potter and I. L. Chaikoff 1959 The effect of hypophysectomy and of TSH on the mouse submaxillary iodide pump. Endocrinology 64 1038–1051

CONCLUSIONS

It was concluded that, as in the rat, the protein-secreting cells of the digestive tract of the mouse depend on the support of pituitary hormones This principle appears to be applicable to other mammals as well Also the cells of the mouse digestive glands which secrete mucopolysaccharides or are involved in ion transport require the action of pituitary hormones for maintenance of their structure and function The degree of dependence on pituitary stimulation varies with the type of cell and species of animal

ACKNOWLEDGMENT

I wish to thank Professor Burton L. Baker for his direction of this research

LITERATURE CITED

Argonz, J J 1961 Glandes salivaires des Chiens hypophysectomisés. C. R. Soc. Biol., *155*: 165–168.

Baker B L., and G D Abrams 1954 Effect of hypophysectomy on the cytology of the fundic glands of the stomach and on the secretion of pepsin. Am. J Physiol., *177*: 409–412.

——— 1955 Growth hormone (somatotropin) and the glands of the digestive system. In: The Hypophyseal Growth Hormone Nature and Actions. R. W Smith, O H. Gaebler and C N H Long, eds. McGraw Hill, New York, pp 107–123.

Baker B. L., H. W Clapp and J A. Light 1964 Hormonal influences on the cytology and physiology of salivary glands. In: Salivary Glands and Their Secretions. L. M. Sreebny and J Meyer eds. Macmillan, New York, pp 63–80.

Baker B L., and R. H. Clark 1961 Influence of hypophysectomy on oxidative enzymes and size of parietal cells in gastric mucosa. Proc. Soc. Exp Biol. Med., *106*: 65–67

Baker B L., J F Kent and E. C. Pliske 1958 Histological response of duodenum to X irradiation in hypophysectomized rats Rad. Res., *9* 48–58.

Baker B L., J H. Klegman, R. G Logan and R. L. Garner 1956 Reduction in parotid amylase after hypophysectomy Endocrinology *59*: 254–255.

Baker B L., N L. Reid and N Thoms 1956 Reduction in pancreatic proteinase after hypophysectomy Am. J Physiol., *186*: 57–59

Barrett, J L., M. T *Nishikawara* and R. E. Haist 1955 Effects of hypophysectomy and of under nutrition on amylolytic activity of the pancreas of the rat. Am. J *Physiol.*, *182* 35–38

Bicknell, J M., and B L. Baker 1962 Influence of hypophysectomy on the lipolytic activity of the rat pancreas. Endocrinology *71* 853–856.

Bixler D., J C. Muhler R. C. Webster and W G Shafer 1957 *Changes* in submaxillary gland ribonucleic acid following hypophysectomy thyroidectomy and various hormone treatment. Proc. Soc. Exp. Biol. Med., *94*: 531–534.

Caro, L. G and G. E. Palade 1964 Protein synthesis, storage, and discharge in the pancreatic exocrine cell. J Cell Biol., *20*: 473–495.

Corpron R. E. 1966 The ultrastructure of the gastric mucosa in normal and hypophysectomized rats. Am. J Anat., *118* 53–89.

Crafts, R. C. and B. S. Walker 1947 The effects of hypophysectomy on gastric acidity of adult female rats. Endocrinology *40*: 395–402.

Crean G P 1963a The effect of hypophysectomy on the gastric mucosa of the rat. Second World Congress of Gastroenterology Munich, *2*: 87–91

——— 1963b The endocrine system and the stomach. In: Vitamins and Hormones. Academic Press, New York, vol. 21, pp. 215–280.

Cutting W C., E. C. Dodds R. L. Noble and P C. Williams 1937 Pituitary control of alimentary blood flow and secretion. Gastric secretion and blood flow in hypophysectomized animals. Proc. Royal Soc., London, ser B, *123* 49–59.

Dalton A. J 1961 Golgi apparatus and secretion granules. In: The Cell, vol. II. J Brachet and A. E. Mirsky eds. Academic Press, New York, pp 603–620

De Robertis, E. D P W W Nowinski and F A Saez 1965 Cell Biology W B. Saunders, Philadelphia, p. 315.

Dewey M M. 1958 A histochemical and biochemical study of the parotid gland in normal and hypophysectomized rats. Am. J. Anat., *102*: 243–271

Dotevall, G., and H. Westling 1963 *Gastric acid* secretion before and after hypophysectomy in man. Acta Med. Scand., *174*: 777–780.

Falconi, G., and G I. Rossi 1964 Transauricular hypophysectomy in rats and mice. Endocrinology *74*: 301–303

Fekete, Elizabeth 1941 Histology In: Biology of the Laboratory Mouse. G D. Snell, ed Blakiston Philadelphia, pp. 89–167

Friedman, M. H. F 1953 *The response of different regions of the gastrointestinal tract to normal and abnormal stimuli (influence of* feeding inert bulk material and of hypophysectomy) J Nat. *Cancer Inst.*, *13* 1035–1038.

Gabe M. 1950 Action de la thyroxine sur la glande sous-maxillaire du Rat hypophysectomisé. *C. R. Acad* Sci., 230 1317–1318.

Haeger K., *D Jacobsohn* and *G* Kahlson 1953 Atrophy *of the* gastrointestinal mucosa following hypophysectomy or adrenalectomy Acta Physiol. Scand., *30* (suppl. 111): 161–169.

Haist, R. E. *1955* The influence *of growth* hormone and other factors on the islets of Langerhans and the pancreas. In: The *Hypophyseal* Growth Hormone Nature and Actions. R. W Smith O H Gaebler and C. N *H* Long, eds. McGraw-Hill, New York, pp. 437–447

Helander H. F 1962 Ultrastructure *of fundus* glands of the mouse gastric mucosa. J Ultrastructure Res., suppl. 4 1–123

——— 1964 Ultrastructure of gastric glands of refed mice J Ultrastructure Res., *10*: 160–175.


P
P
C
1
P
C
2
a
b
P
3
P
4

Vial, J D., and H. Orrego 1960 Electron microscope observations on the fine structure of parietal cells. J Biophys Biochem. Cytol., 7: 367–372.

Yoshimura, F 1958 Cytological changes in rat salivary glands following hypophysectomy and somatotrophic hormone administration. Okajimas Folia Anat. Jap., 28: 195–205.

PLATE 1

EXPLANATION OF FIGURES

Figures 1 and 2: fixed in FAA, stained with PAS-azure II, 4 μ, × 100 Figures 3 and 4: fixed in FAA stained with colloidal iron-PAS, 4 μ, × 1000.

1 Gastric mucosa of a pair-fed control mouse. Chief cells (C) are columnar and have basally located cytoplasmic basophilia and a granule-filled apex. *They are* found in the lower one-third of the mucosa. Parietal cells (P) are primarily located in the middle one-third of the mucosa as well as being scattered in the neck and base of the fundic glands. *Mucous* neck cells (arrow) are interposed among parietal cells in the area just superficial to the chief cells. Mucous surface cells extend from the gastric pits (GP) onto the surface.

2 Gastric mucosa of a mouse, 70 days after hypophysectomy As compared with figure 1 the mucosa *is* thinner *Chief* cells (C) appear to be *decreased in* number and size and have fewer granules and less cytoplasmic basophilia. Parietal cells (P) are smaller Mucous neck cells (arrow) appear more numerous. Mucous surface cells are unchanged The lumina of the fundic glands are dilated.

3 Gastric mucosa *of an ad libitum*-fed control mouse. *Three histochemically* different varieties of mucous neck cells are shown. Colloidal iron-positive mucous neck cells (a) stain darkly with colloidal iron (black) PAS-positive mucous neck cells (b) are lightly stained with PAS (grey) A transition phase is shown in which PAS-positive mucous neck cells contain colloidal iron-positive granules (arrow) Parietal cells (P) are large

4 Gastric mucosa of a mouse 70 days after hypophysectomy As compared with figure 3, the total number of mucous neck cells appears to be increased per fundic gland. Only the colloidal iron positive mucous neck cells (black) are present. The lumina of the fundic glands are dilated (arrow) *Parietal cells* (P) are reduced in size.


GP
P
1
C
P
2
C
a
b
P
3
P
4

PLATE 2

EXPLANATION OF FIGURES

Figures 5 and 6: fixed in FAA stained with PAS-azure II 4 μ, × 1000. Figures 7, 8, 9 and 10: fixed in Regaud's fluid stained with Altmann Masson 3 μ, × 1550.

5 Gastric mucosa of an *ad libitum* fed control mouse The parietal cells are large and have large nuclei with prominent nucleoli and sparse chromatin. A perinuclear halo of PAS-positive material (arrow) indicates the position of the intracellular canaliculi which cup around the nucleus from the luminal side

6 Gastric mucosa of a mouse, 68 days after hypophysectomy The parietal cells (P) are smaller and have smaller nuclei and nucleoli and coarsely clumped chromatin. No halos of PAS-positive material are present but clumps of PAS-positive material are found on the luminal side of the nucleus (arrow) The fundic lumina are dilated as compared with the control (fig 5)

7 Gastric mucosa of an *ad libitum* fed control mouse. The parietal cells (P) are large and have large rounded mitochondria (M) located along the cell and nuclear membranes. The area (arrow) between the two rows of mitochondria indicates the location of the cup-shaped intracellular canaliculi and corresponds with the PAS-positive perinuclear halo (fig. 5)

8 Gastric mucosa of a mouse 68 days after hypophysectomy The parietal cells (P) are smaller The intracellular canaliculi do not cup around the nucleus, being limited to the luminal area of the cell. The luminal openings of the canaliculi are dilated (arrow) Mitochondria (M) are reduced in number and tend to be arranged around the basal aspect of the nucleus in a cup-like formation The glandular lumen (L) is dilated as compared with that of the control (fig. 7)

9 Gastric mucosa of a pair fed control mouse Chief cells are illustrated. Their apical portions are filled with large secretory granules (G) The mitochondria (arrow) are long and thread-like and are located predominantly basal and lateral to the nucleus (N)

10 Gastric mucosa of a mouse, 68 days after hypophysectomy Chief cells are illustrated. Their secretory granules are sparse Mitochondria (arrow) are shorter and wider than in the control (fig 9) Their arrangement follows the contour of the nucleus (N)


P
5
6
M
P
L
7
8
N
G
9
10

PLATE 3

EXPLANATION OF FIGURES

Figures 11 and 12: fixed in FAA stained with PAS-azure II, 4 μ, × 1000. Figures 13 and 14: fixed in Zenker formol stained with azure II phloxine 3 μ × 600

11 Gastric mucosa of a pair fed control mouse The chief cells (C) are columnar The cytoplasmic basophilia (E) is dense basally and basophilic material is sparsely distributed among the secretory granules. Secretory granules (G) are not fixed but the distribution of vacuoles shows that they filled the apex of the cell. The nuclei have prominent nucleoli (arrow) and fine chromatin.

12 Gastric mucosa of a mouse 68 days after hypophysectomy The chief cells are low cuboidal. The cytoplasmic basophilia (E) is reduced to smaller areas around the nucleus Almost no secretory granules are present The nuclei are smaller the chromatin coarser and the nucleoli (arrow) smaller as compared with the control (fig 11)

13 Pancreatic acinar cells from a pair-fed control mouse The pancreatic cells are large and filled with granules (G) The cytoplasmic basophilia (E) is abundant basally and distributed as a fine network among the apical secretory granules. The nuclei have prominent nucleoli (arrow)

14 Pancreatic acinar cells from a mouse 57 days after hypophysectomy The acini and acinar cells are reduced in size and have fewer secretory granules (G) as compared with the control (fig 13) The cytoplasmic basophilia (E) is reduced in total amount and staining intensity The nuclei have more compact chromatin and smaller nucleoli (arrow)


C
E
G
11


E
12


E
G
13


E
G
14

PLATE 3

EXPLANATION OF FIGURES

Figures 11 and 12: fixed in FAA stained with PAS-azure II, 4 μ × 1000. Figures 13 and 14: fixed in Zenker formol, stained with azure II-phloxine 3 μ × 600.

11 Gastric mucosa of a pair fed control mouse. The chief cells (C) are columnar. The cytoplasmic basophilia (E) is dense basally and basophilic material is sparsely distributed among the secretory granules. Secretory granules (G) are not fixed but the distribution of vacuoles shows that they filled the apex of the cell. The nuclei have prominent nucleoli (arrow) and fine chromatin.

12 Gastric mucosa of a mouse 68 days after hypophysectomy. The chief cells are low cuboidal. The cytoplasmic basophilia (E) is reduced to smaller areas around the nucleus. Almost no secretory granules are present. The nuclei are smaller, the chromatin coarser and the nucleoli (arrow) smaller as compared with the control (fig. 11)

13 Pancreatic acinar cells from a pair fed control mouse. The pancreatic cells are large and filled with granules (G). The cytoplasmic basophilia (E) is abundant basally and distributed as a fine network among the apical secretory granules. The nuclei have prominent nucleoli (arrow)

14 Pancreatic acinar cells from a mouse 57 days after hypophysectomy. The acini and acinar cells are reduced in size and have fewer secretory granules (G) as compared with the control (fig. 13). The cytoplasmic basophilia (E) is reduced in total amount and staining intensity. The nuclei have more compact chromatin and smaller nucleoli (arrow)

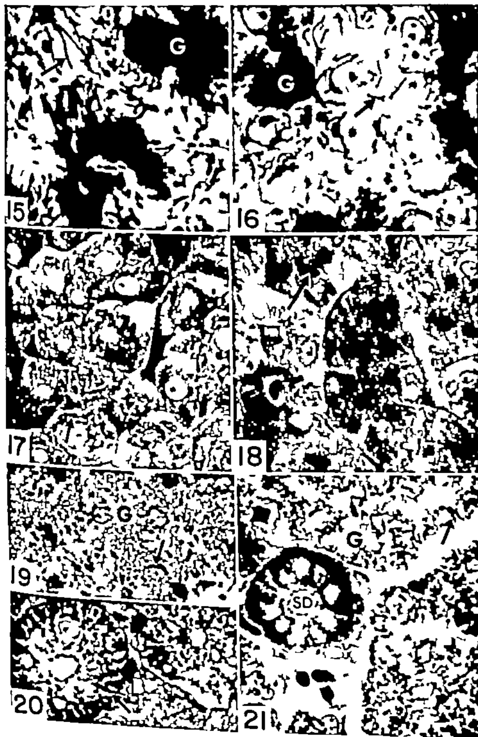

G
15
G
16
17
18
G
19
G
SD
20
21

PLATE 4

EXPLANATION OF FIGURES

Figures 15 and 16: fixed with Zenker-formol stained with Altmann-Masson, 3 μ, × 1700. Figures 17 and 18: fixed with Champy's fluid post-osmicated 3 μ, × 1000. Figures 19, 20 and 21: fixed with Zenker-formol stained with Altmann-Masson, 3 μ × 1000.

15 Pancreatic acinar cells from a pair-fed control mouse. The mitochondria (arrow) are long string-like structures in the basal area and extend to the secretory granules (G) in the apex of the cells.

16 Pancreatic acinar cells from a mouse 73 days after hypophysectomy. The mitochondria (arrow) are shorter and finer than those of the control (fig. 15). They often follow the curvature of the nucleus and are located basal, lateral and apical to it. Fewer secretory granules (G) are present.

17 Pancreatic acinar cells from an *ad libitum* fed control mouse. The Golgi apparatus (arrow) is distributed throughout most of the supranuclear region of the cell among the secretory granules.

18 Pancreatic acinar cells from a mouse 86 days after hypophysectomy. The Golgi apparatus (arrow) is smaller and more compact than that in the control (fig. 17).

19 Parotid acinar cells from a pair-fed control mouse. The acinar cells are filled with granules (G). Mitochondria (arrow) are rod-like and randomly oriented.

20 Parotid salivary ducts from a pair-fed control mouse. Mitochondria (arrow) are primarily located basal to the nucleus paralleling the basal striations (B). A few mitochondria are present apical to the nucleus.

21 Parotid gland from a mouse 71 days after hypophysectomy. The acini are smaller with fewer granules (G). The acinar mitochondria (arrow) appear more numerous than those in the control (fig. 19) due to the loss of granules. They are located around the nucleus and are thinner. The salivary ducts (SD) are smaller in diameter and their cells are lower and narrower as compared with those of the control (fig. 20). Basal striations are absent. Nuclei are smaller. Mitochondria of the salivary duct (SD) are more concentrated, smaller and randomly oriented. They are found around the nucleus as well as basal to it.

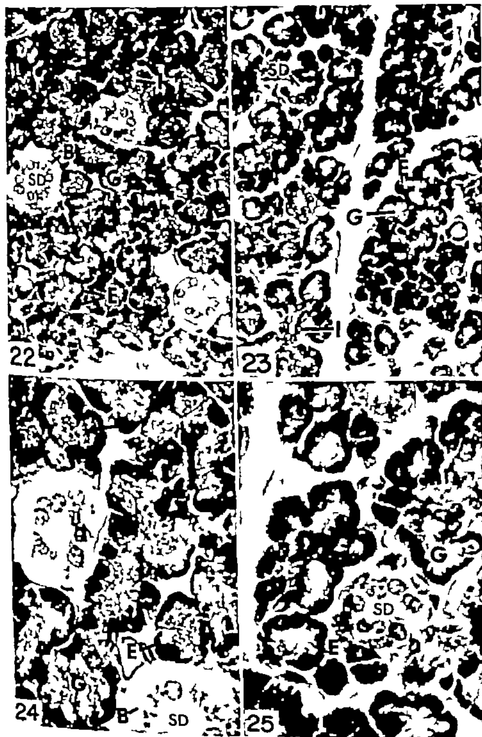

SD
B
SD
G
E
22
SD
E
G
I
23
E
G
B
SD
24
G
SD
E
25

PLATE 5

EXPLANATION OF FIGURES

Figures 22 and 23: fixed in FAA stained with PAS-azure II 5 µ, × 400.
Figures 24 and 25 fixed in FAA, stained with PAS-azure II, 5 µ, × 925.

22 Parotid gland of a pair fed control mouse The acinar cells have dense basal cytoplasmic basophilia (E) and are filled with secretory granules (G) Intercalated ducts (I) are seen. The salivary ducts (SD) are lined by columnar cells with prominent basal striations (B)

23 Parotid gland of a mouse 71 days after hypophysectomy The acinar diameters are smaller than those of the control (fig. 22) Intercalated ducts (I) are not greatly changed. They appear prominent because of the acinar involution.

24 Parotid gland of a pair fed control mouse The acinar cells have basally located cytoplasmic basophilia (E) which extends as a fine network (arrow) among the granules (G) The salivary ducts (SD) have basal striations (B)

25 Parotid gland of a mouse 71 days after hypophysectomy The acinar cells have fewer secretory granules (G) and less cytoplasmic basophilia (E) The salivary ducts (SD) are smaller and lined by low cuboidal cells Cells of the salivary ducts have lost their basal striations and have smaller nuclei.


S
G
26


S
27


G
E
E
S
28

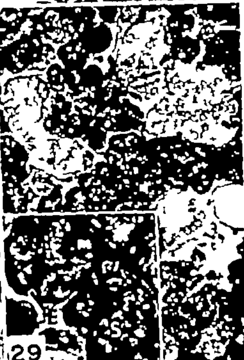

E
S
29

PLATE 6

EXPLANATION OF FIGURES

Figures 26 and 27 fixed in FAA, stained with colloidal iron PAS $5\ \mu$, $\times 400$. Figures 28 and 29: fixed in FAA stained with PAS-azure II $5\ \mu$, $\times 400$.

26 Submandibular gland of a pair fed control mouse Mucous acini are filled with secretory material (S) which stains intensely with colloidal iron. Epithelial cells of serous tubules are charged with secretory granules (G)

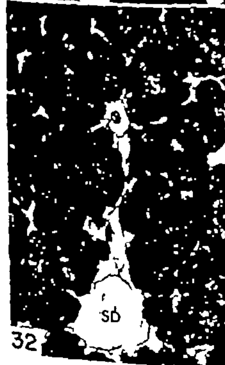
27 Submandibular gland of a mouse 71 days after hypophysectomy The mucous acini are smaller and contain less secretory material. The secretory material (S) stains less intensely with colloidal iron as compared with that of the control (fig 26) Serous tubules are profoundly atrophied (arrow)

28 Submandibular gland from a pair fed control mouse The serous tubular cells are filled with granules (G) and possess minimal basal cytoplasmic basophilia (E) (inset) Mucous acinar cells are filled with secretory material (S) (inset) and have dense basal cytoplasmic basophilia (E) (inset)

29 Submandibular gland of a mouse 57 days after hypophysectomy The serous tubules are atrophied with loss of granules and cytoplasmic basophilia. The mucous acini are smaller and possess less secretory material (S) (inset) and somewhat less cytoplasmic basophilia (E) (inset) as compared with the control (fig. 28 inset) Cells of the serous tubules appear to contain more PAS-positive granules (arrow) than those in the control (fig 28)


G
30


S
31


S
SD
32

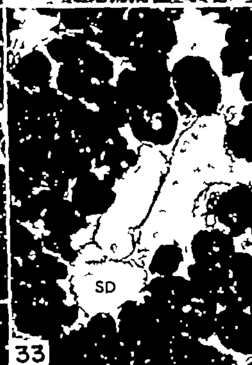

S
SD
33

PLATE 7

EXPLANATION OF FIGURES

Figures 30 and 31: fixed in Zenker-formol stained with Altmann-Masson 3 μ, × 1000 Figures 32 and 33: fixed in FAA stained with colloidal iron-PAS 5 μ, × 400.

30 Submandibular gland from an *ad libitum* fed control mouse. Mitochondria of the serous tubular cells (arrow) are small randomly oriented and located chiefly in the basal half of the cells Serous tubular cells are filled with granules (G)

31 Submandibular gland from a mouse 68 days after hypophysectomy The serous tubules (ST) are atrophied and depleted of granules Nuclei of the serous tubular cells are smaller as compared with those of the control (fig. 30) Mitochondria (arrow) tend to be wider as compared with those of the control (fig. 30) Some mitochondria are oriented perpendicularly to the base of the cell

32 Sublingual gland from a pair fed control mouse The mucous acini are filled with secretory material (S) The salivary duct (SD) is lined with high columnar epithelium. An intercalated duct (arrow) is shown

33 Sublingual gland from a mouse 68 days after hypophysectomy The mucous acini are smaller and have less secretory material (S) Cells of the salivary duct (SD) are involuted as compared with the control (fig 32) Intercalated ducts are not involuted (arrow)


A
G
SD
34
SD
A
35
36
V
37

PLATE 8

EXPLANATION OF FIGURES

Figures 34 and 35 fixed in Zenker formol, stained with colloidal iron PAS, 3 μ × 1000 Figures 36 and 37; fixed in FAA stained with colloidal iron-PAS 5 μ × 2062.

34 Sublingual gland of an *ad libitum* fed control mouse Mitochondria (arrow) of salivary duct (SD) cells are concentrated basally paralleling the basal striations. Scattered granulated cells (G) are present in the ducts Mucous acini (A) are illustrated.

35 Sublingual gland of a mouse 87 days after hypophysectomy Cells of salivary ducts (SD) are smaller with less prominent basal striations and smaller nuclei. The mitochondria (arrow) are more concentrated randomly arranged in the basal area and smaller than the control (fig 34) No granulated cells are present. Mucous acini (A) are smaller

36 Salivary duct in the sublingual gland of a pair-fed control mouse The duct cells have large nuclei and considerable material in the infranuclear region which stains with colloidal iron (arrow)

37 Salivary duct of a sublingual gland of a mouse 68 days after hypophysectomy The duct cells are lower have smaller nuclei and less infranuclear cytoplasmic material which stains with colloidal iron Some vacuoles (V) are present in the basal area.

Ultrastructural and Histochemical Analysis of Cytoplasmic Laminar Bodies in Lateral Geniculate Neurons of Adult Cat [1]

PAUL F DOOLIN KEVIN D. BARRON AND SHARON KWAK
Neuropathology Research Section, Veterans Administration Hospital, Hines, Illinois; Department of Pathology Loyola University Stritch School of Medicine Chicago Illinois; and Department of Neurology and Psychiatry Northwestern University Medical School, Chicago, Illinois

ABSTRACT The structure of highly organized, cytoplasmic laminar bodies (CLB) of cat lateral geniculate body neurons is described. CLB are derived from endoplasmic reticulum (ER). The occurrence of other cytoplasmic bodies also derived from ER and mesh-like in composition is noted. Stacks of dense membranous elements, restricted to one pole of each type of cytoplasmic body were encountered. Mention is made of the relative persistence of CLB in atrophic neurons that show marked changes including loss of cytoplasmic granular ER.

The tubules of CLB are normally coextensive with the granular ER. The topographic relationships of CLB with other cellular organelles such as mitochondria, Golgi complex and the nucleus are discussed.

Routine staining techniques clearly demonstrate the CLB in 2 μ paraffin sections of tissue fixed by perfusion with buffered formalin. Histochemical tests show that CLB are chemically complex structures containing protein lipid and polysaccharide components.

In 1964 Morales et al. described the ultrastructural features of a distinctive laminated cytoplasmic structure found in neurons of the adult feline lateral geniculate body (LGB) Subsequently the electron microscopic observations of Morales and associates ('64) were confirmed by Smith et al. ('64) In a light microscope study reported more than a decade prior to the publications cited above acidophilic cytoplasmic inclusions, apparently identical to the bodies described by Morales and co-workers ('64) were recognized by Szlachta and Habel ('53) in LGB neurons of the adult cat.

Incidental to an investigation of retrograde degeneration of adult, feline LGB neurons (Barron et al., '67) we have recorded ultrastructural and histochemical observations on the cytoplasmic laminated bodies (CLB) distinctive of these nerve cells. The results have been reported in preliminary fashion (Doolin and Barron, '66) Subsequently we undertook and completed a more extensive study of CLB and have determined additional information which may prove pertinent to an understanding of the ultrastructural and histochemical nature of these organelles. The new data on the composition of CLB form the basis of this report.

MATERIALS AND METHODS

Fine structure study

Eleven cats were used in the ultrastructural part of the study The left lateral and posterolateral gyri were removed by suction from nine animals that were subsequently sacrificed at periods of five (2 animals) 14 (2 animals) 28 32, 42, 70 and 112 days postoperatively Some observations on this material were reported elsewhere (Barron et al., '67) in a description of the neuronal alterations which accompany retrograde degeneration.

Primary fixation was accomplished by intra-aortic perfusion with phosphate-buffered formalin (1688 milliosmol, 37 C, pH 7.6) while the animals were anaesthetized with sodium pentobarbital (Karlsson and Schultz, '65) The period of time that lapsed from opening the thoracic cavity to onset of perfusion was 20–30 seconds. Four to five liters of perfusate were ad-

[1] Supported in part by grant NB 04788 of the National Institutes of Health.

[2] The work of Szlachta and Habel was brought to our attention by Dr. Donald Duncan.

Carbohydrates

(1) Periodic acid-Schiff (PAS) (after McManus in Pearse, '61 p. 832)

(2) PAS after malt diastase digestion (Barka and Anderson, '63) p. 94)

(3) PAS after α-amylase digestion (Takeuchi, '58)

(4) PAS after β-amylase digestion (Takeuchi, '58)

(5) PAS after acetylation and deacetylation (after Lillie in Pearse, '61 p. 832)

(6) Performic acid-Schiff (Lillie '65 p 183).

(7) PAS after bromination (Lillie '65 p. 500).

(8) Alcian blue for acidic mucopolysaccharides (Barka and Anderson, '63 p 77)

(9) Sulfation-toluidine blue reaction for neutral mucopolysaccharides (after Mowry in Lillie, '65 p. 189)

Miscellaneous

(1) Weil stain for myelin.

(2) Toluidine blue for metachromasy pH 7 1 (Swift, '55)

(3) Safranine O

(4) Nuclear-fast red.

OBSERVATIONS

Histological and ultrastructural findings

As previously reported by others (Morales et al., '64 Smith et al., '64) the CLB a highly organized discrete laminar structure, is usually found in neuronal perikarya (figs. 1 7–9) Occasionally it appears in dendrites (fig. 6) In the cells where the laminar body is present, one per neuron is the norm. Very rarely however two bodies per cell are noted. The organelle is commonly detected in medium-sized neurons (maximum diameter ca. 20–25 μ) Relatively seldom is one located in the very small or very large cells. Its position in the cytoplasm is not fixed. It has been observed in a juxtanuclear location (figs. 7 8) in midregion residence between the nucleus and cell boundary and in a peripheral disposition adjacent to the plasmalemma (fig. 18)

Phase-contrast and light microscopic scanning of 2 μ Epoxy and paraffin sections (stained and unstained) reveals that CLB generally occur in clusters of nerve cells. If a body is observed, usually several more are easily spotted in the same field (fig 18) There are large areas, however where dozens of neurons can be scrutinized without locating any CLB except for an exceptional isolated one.

An attempt was made to estimate the frequency of CLB occurrence by making counts in hematoxylin and eosin-stained tissue sections Counting all neurons in 2 μ paraffin sections, serially spaced at 6 μ intervals 151 CLB were observed in a population of 1 613 neurons from the A and A layers of the dorsal geniculate nucleus. CLB counts restricted to those cells with nuclei in the plane of section likewise yielded approximately a 9% return. When counts were made only on cells with nucleoli in the field, 4% of a total of 1,822 neurons contained the laminar body More CLB appeared to reside in the A than in the A layer

In figures 1–3 some recognized fine structural details (Morales et al., '64; Smith et al., '64 Doolin and Barron, '66) are evident. The oval CLB approximately 3×2 μ in diameter are characterized by curved, parallel sheets of dense-walled agranular tubules that range from 120–200 Å in diameter and repeat at 600–750 Å intervals (figs 1–3) An irregular amorphous region of moderate density lies between the tubular arrays. The rows of tubules appear to consist of intertwining rope-like strands (fig. 3) The tubules often are coextensive with granular endoplasmic reticulum (ER) external to the body proper (fig. 2) "Unravelling" of the individual component strands (fig. 3) reveals that each daughter" strand is narrower in diameter than the parental" bundle from which it issues. Continuity with the outer member of the bilaminar nuclear envelope is occasionally in evidence (fig. 7) No membrane delimits the CLB periphery Numerous cytoplasmic islands containing mitochondria, lysosomes, granular and agranular ER, and free rosette ribosomes often are dispersed throughout the laminated body and have been illustrated by others (Morales et al. '64 Smith et al., '64)

Occasionally lipofuscin bodies in the surrounding cytoplasm are in close apposition to the laminar complex. Sometimes the CLB partially envelope a dense struc-

ministered for 12–15 minutes One milliliter respectively of sodium heparin and sodium nitrite was given intravenously a few minutes before sacrifice

At the termination of perfusion, the brain was excised and the dorsal nuclei of the left and right lateral geniculate bodies (LGB) were dissected free. A part of each geniculate nucleus was immediately immerse-fixed for three hours in cold 1% osmium tetroxide (0 01 M phosphate buffer pH 7 6 443 milliosomol) (Karlsson and Schultz, '65) The remaining geniculate tissue was left in cold perfusate for 3–6 hours then transferred to cold buffered sucrose (0.3 M, 607 milliosomol) overnight and finally post fixed in cold OsO_4 for three hours

Subsequent to cold ethanol dehydration and Epon 812 embedment (Luft, 61) the tissue was thin-sectioned with glass knives employing the Sorvall MT 2 and Cambridge ultramicrotomes Double staining of gray and silver sections with uranyl acetate and lead hydroxide (Karnovsky '61) was performed on ribbons mounted on substrate-free grids The RCA EMU 3F electron microscope operated at 50 KV and equipped with a 35 μ objective aperture was used in this investigation.

Histochemical study

After sodium pentobarbital anaesthesia, nine normal adult cats were perfused through the left ventricle and aorta with one of two fixatives:

(1) One liter of 1% calcium-formalin (Baker 46) containing 5% sucrose and employed at 2–4°C

(2) Two to three liters of 4% paraformaldehyde at 37 C (Karlsson and Schultz, 65)

One hour following the termination of perfusion, the brain was excised and 2–3 mm coronal brain slices including the LGB were immersed in their respective perfusates (2–4 C) for 12–18 hours. In some instances 5 μ frozen sections were taken from one part of this material. The remaining tissue was ethanol-dehydrated and paraffin-embedded Paraffin sections 2 μ and 5 μ thick were prepared for slide histochemistry Each reaction was repeated from 2–6 times.

A summary of the histochemical tests carried out on the CLB and the results are given in tables 1 to 5. Appropriate controls were employed to check the specificity of all reactions. The methods used for the detection of nucleic acids, lipids, polysaccharides and proteins are as follows

Nucleic acids

(1) Toluidine blue (0.05–0 1%) pH 4 for detection of RNA (Herman, Nicholas and Boricious, '50) and in additional variations of pH at one unit increments from pH 5–9; toluidine blue in combination with ribonuclease extraction (Brachet, '57)

(2) Thionin (0 05–0 1%) pH 3.65 (Windle Rhines and Rankin, 43) and in additional variations of pH at one unit intervals from pH 3–9

(3) Gallocyanin-chromalum (after Einarson in Pearse '61 p. 826)

(4) Feulgen reaction (Pearse '61 p. 822)

Lipids

(1) Sudan Black B in 70% alcohol (after McManus in Pearse '61 p. 850)

(2) Sudan Black B for masked lipids (after Ackerman in Pearse, '61 p. 850)

(3) Acetone-Sudan Black for bound lipids (after Berenbaum in Pearse, '61, p. 851)

(4) Sudan Black B in propylene glycol (after Chifelle and Putt in Pearse '61 p. 855)

(5) Oil Red O in isopropyl alcohol for neutral fats (after Lillie 65 p 854)

(6) Acid hematin (after Baker in Pearse, 61 p 848)

Proteins

(1) Bromphenol blue (after Maria in Barka and Anderson '63 p 64)

(2) Bromsulfalein (Silverman and Glick, 66)

(3) Millon (after Bensley and Gersh in Pearse '61 p 791)

(4) DDD reaction (after Barrnett and Seligman in Pearse '61 p 807)

(5) Eosin before and after acetylation blockade (Pearse 61 p 796)

(6) Eosin after cold sulfation (Lillie 65 p 255)

(7) Eosin after sulfation and methylation (Lillie '65 p 255)

Carbohydrates

(1) Periodic acid-Schiff (PAS) (after McManus in Pearse, '61 p. 832)

(2) PAS after malt diastase digestion (Barka and Anderson, '63) p. 94)

(3) PAS after α-amylase digestion (Takeuchi, '58)

(4) PAS after β-amylase digestion (Takeuchi, '58)

(5) PAS after acetylation and deacetylation (after Lillie in Pearse, '61 p. 832)

(6) Performic acid-Schiff (Lillie, '65 p 183)

(7) PAS after bromination (Lillie, '65 p. 600)

(8) Alcian blue for acidic mucopolysaccharides (Barka and Anderson, '63 p 77)

(9) Sulfation-toluidine blue reaction for neutral mucopolysaccharides (after Mowry in Lillie, '65 p. 189)

Miscellaneous

(1) Weil stain for myelin.

(2) Toluidine blue for metachromasy pH 7.1 (Swift, '55)

(3) Safranine O

(4) Nuclear-fast red.

OBSERVATIONS

Histological and ultrastructural findings

As previously reported by others (Morales et al., '64; Smith et al., '64) the CLB a highly organized discrete laminar structure, is usually found in neuronal perikarya (figs. 1 7–9) Occasionally it appears in dendrites (fig. 6) In the cells where the laminar body is present, one per neuron is the norm. Very rarely however two bodies per cell are noted. The organelle is commonly detected in medium-sized neurons (maximum diameter ca. 20–25 μ) Relatively seldom is one located in the very small or very large cells. Its position in the cytoplasm is not fixed. It has been observed in a juxtanuclear location (figs. 7 8) in midregion residence between the nucleus and cell boundary and in a peripheral disposition adjacent to the plasmalemma (fig. 18)

Phase-contrast and light microscopic scanning of 2 μ Epoxy and paraffin sections (stained and unstained) reveals that CLB generally occur in clusters of nerve cells. If a body is observed, usually several more are easily spotted in the same field (fig 18) There are large areas however where dozens of neurons can be scrutinized without locating any CLB except for an exceptional isolated one.

An attempt was made to estimate the frequency of CLB occurrence by making counts in hematoxylin and eosin-stained tissue sections. Counting all neurons in 2 μ paraffin sections, serially spaced at 6 μ intervals 151 CLB were observed in a population of 1 613 neurons from the A and A_1 layers of the dorsal geniculate nucleus. CLB counts restricted to those cells with nuclei in the plane of section likewise yielded approximately a 9% return. When counts were made only on cells with nucleoli in the field, 4% of a total of 1,822 neurons contained the laminar body More CLB appeared to reside in the A than in the A_1 layer

In figures 1–3 some recognized fine structural details (Morales et al., '64; Smith et al., '64 Doolin and Barron, '66) are evident. The oval CLB approximately 3×2 μ in diameter are characterized by curved, parallel sheets of dense-walled agranular tubules that range from 120–200 Å in diameter and repeat at 600–750 Å intervals (figs. 1–3) An irregular amorphous region of moderate density lies between the tubular arrays. The rows of tubules appear to consist of intertwining rope-like strands (fig 3) The tubules often are coextensive with granular endoplasmic reticulum (ER) external to the body proper (fig 2) "Unravelling" of the individual component strands (fig. 3) reveals that each "daughter strand is narrower in diameter than the "parental" bundle from which it issues. Continuity with the outer member of the bilaminar nuclear envelope is occasionally in evidence (fig. 7) No membrane delimits the CLB periphery Numerous cytoplasmic islands, containing mitochondria, lysosomes, granular and agranular ER, and free rosette ribosomes often are dispersed throughout the laminated body and have been illustrated by others (Morales et al., '64 Smith et al., '64)

Occasionally lipofuscin bodies in the surrounding cytoplasm are in close apposition to the laminar complex. Sometimes the CLB partially envelope a dense struc

ture (fig 15) identity unknown with complex internal morphology The Golgi system (figs 4 5 8) often can be found in the vicinity of the laminated body Infrequently large sweeps of agranular membranes that appear to be part of the Golgi system are apposed to the CLB (fig 1)

At one pole of the highly organized lamellar CLB there often lies a restricted stack of dense membranes (figs. 4 5) embedded in but obviously standing out sharply from the surounding array of less dense tubular sheets. These polarized elements of a dimension similar to the CLB tubules proper are separated by relatively structureless regions ranging from 150–400 A in width (figs 4 5) A minute fuzz like density however is noted on the external surface of some of the profiles of this polarized stack of dense membranes (figs 4 5) which may be seen to be in direct continuity with the granular ER (fig 5) Whether these stacked dense elements (figs 4 5) are tubular in nature or represent profile views of flattened cisterns cannot be determined without sections normal to the plane depicted in figures 4 5 Thus far cross or tangential views have not been encountered and that the stacks are cisternal in nature is strongly suspected

On rare occasions the cytoplasm of LGB neurons displays a complex system of smooth membranes that forms a compact, oval, 3-dimensional structure 3–5 μ in diameter (figs 10–12) Whether this system represents the CLB in another functional state or is a different organelle remains undetermined[3] Like the highly organized CLB however the tangled tubules in this irregular lattice of tubular elements are in continuity with peripheral granular ER (fig 10) No limiting membrane separates this body from the cytoplasm. Trapped cytoplasmic elements (figs 10 12) such as mitochondria and ribosomes are to be found deep within the tangled mesh of tubules Cisterns of particle studded ER peripheral to one pole of the tubular skein are extensively dilated (figs 10 11) with their limiting membranes partially denuded of RNP particles A stack of parallel dense membranes (figs 11 12) noted at one pole of the irregular lattice structure is very similar to that described above for the regularly structured CLB (figs. 4 5) Also a fuzz-like substance on the exterior of some of the membranes of the dense stack (fig. 11) may be in evidence The narrow lumens bounded by closely apposed parallel dense membranes are coextensive with the agranular tubules of the body proper (fig. 11) They abruptly enlarge at points of transition between the dense membrane set and the mesh-like lattice of the body proper

A presumptive stage in the genesis of a CLB is shown in figure 13. A cistern of granular ER narrows to a very small channel with the membranous walls of the single tubular element becoming denser In the region of tight membrane apposition, ribonucleoprotein (RNP) particles are lacking the adjacent areas (340 A in width) between neighboring parallel cisterns have become moderately dense and each contains a fine parallel intermediate filament with linearly arranged dot-like densities and fine threads interconnecting with adjacent cisternal membranes. The neighboring ER cisterns are unreduced in diameter and lack ribosomes on the side exposed to the parallel dense membranes. This description parallels in part, that given by Rosenbluth ('62) for subsurface and deeply buried cisternal stacks of rat cortical neurons and acoustic ganglion cells

The configuration in figure 14 is included here as a possible early stage in the formation of a CLB Granular ER is continuous with the agranular tubules. An alternate possibility however that would permit the interpretation of this array as a grazing section through the tip of a CLB cannot be excluded

Frequently small granular bodies (fig 16) spherical to oval in contour and approximately 1 μ in cross-section are noted in the neuronal cytoplasm. Often no internal structure is present but occasionally scattered linear profiles and a presumptive cytoplasmic island with ribosomes, smooth membranes and dense spherical

[3] Unequivocal evidence is now in hand clearly showing that the highly organized CLB (fig. 1) and the lattice-like structure (fig. 10) are integral components of the same body The reticular lattice of tubular elements is also present in dendrites.

structures are found (fig. 16). A membrane between this type of body and the cytoplasm does not exist.

In neurons undergoing retrograde atrophy CLB are more resistant than the granular tubular ER to the structural changes which accompany the phenomenon. Five days after visual cortex extirpation, there is a marked reduction in rough-surfaced ER (Barron et al., '67). At 14 days, this loss is advanced and is accompanied by the appearance of many single free RNP particles in the cytoplasm (fig. 8). The organized CLB appears to be *relatively* resistant to the conditions leading to dissolution of particle-studded tubular ER. Intact bodies have been detected in atrophic neurons as long as 112 days post operatively (Barron et al., '67). Instances of a probable partial disintegration of CLB however, are not lacking. In the body depicted in figure 8 which derives from an obviously degenerate neuron the middle region appears disorganized and has acquired a lattice appearance that recalls the structure in figures 10–12. Lattice-like bodies have been detected in atrophic nerve cells. The occurrence in degenerating neurons of a structure, such as depicted in figure 8, where ultrastructural features of both types of body are evident in the same cytoplasmic inclusion, might suggest that CLB are related to the lattice-like bodies and that the latter may represent a stage in the degradation of organized CLB. Ultrastructural observations on normal neurons which suggest a link between the two types of body have been mentioned in the preceding.

The atrophic neuron in figure 9 contains mitochondria which are draped about and tightly apposed to a CLB; one of these organelles may have fused with the dense matrix of the body. This condition has not been observed in normal neurons.

On but one occasion was a laminated body noted in a glia cell. The identity of this cell (fig. 17) which derives from an atrophic LGB is unknown. Parallel rows of presumptive intertwining dense tubules spaced apart by an average distance of 450 Å, are coextensive with agranular endoplasmic reticular profiles in the surrounding cytoplasm.

Histochemical findings

In tissues fixed in paraformaldehyde or calcium formalin CLB were unstained by toluidine blue and thionin (table 1). The Gallocyanin-chromalum method also did not stain the laminar body. The Feulgen reaction was negative.

Four procedures for the Sudan Black B method gave positive results (table 2). Acetone extracted the color from bodies that were subsequently restainable by Sudan Black B. A deep positive coloration was produced by acid hematin. Pyridine extraction did not block the reaction but actually permitted a deeper coloration by acid hematin. A negative reaction was noted by the Oil red O technique.

Bromphenol blue and bromsulfalein yielded markedly positive bodies (table 3). The Millon reaction was faintly positive. The DDD reaction produced stained laminar organelles with frozen sections permitting a more pronounced coloration.

A deep pink structure with red dots was produced by the PAS test (table 4). Malt diastase and α- and β- amylase digestions

TABLE 1
Nucleic acids

Reaction	Fixation	Section	CLB results
Toluidine blue, 0.05–0.1% pH 4.0–9.0	Paraformaldehyde Ca formalin	Paraffin, 2 μ Paraffin, 2 μ	Negative
Thionin, 0.1% pH 3.0–9.0	Paraformaldehyde Ca formalin	Paraffin, 2 μ	Negative
Chrome-alum gallocyanin	Paraformaldehyde	Paraffin, 2 μ	Negative
Feulgen	Paraformaldehyde Ca formalin	Paraffin, 2 μ	Negative

TABLE 2
Lipids

Reaction	Fixation	Section	CLB results
Sudan Black B	Paraformaldehyde Ca formalin	Paraffin, 2 μ Paraffin 2 μ	Gray Blue-gray (deep)
Acetone extracted	Ca formalin	Paraffin, 2 μ	Sudan staining abolished; restainable with Sudan Black B
Pyridine extracted	Ca formalin	Paraffin, 2 μ	Sudan staining abolished
Sudan Black B for masked lipids	Ca formalin	Paraffin, 2 μ	Dark gray
Acetone-Sudan Black for bound lipids	Ca formalin	Paraffin 2 μ	Gray-brown
Propylene-Glycol-Sudan Black B method for lipids	Paraformaldehyde Ca formalin	Paraffin 2 μ Paraffin, 2 μ	Pale blue Deeper blue
Acid hematin	Ca formalin	Frozen section, 5 μ	Dark gray-brown
Pyridine extraction followed by acid hematin	Ca formalin	Frozen section, 5 μ	Deep dark-gray
Oil red O	Ca formalin	Paraffin 2 μ	Negative

TABLE 3
Proteins

Reaction	Fixation	Section	CLB results
Bromphenol blue	Ca formalin	Frozen section 5 μ	Blue
Bromsulfalein	Ca formalin	Paraffin 2 μ	Blue-purple
Millon	Paraformaldehyde	Paraffin 2 μ	Very faintly orange
Eosin after amino group acetylation	Ca formalin	Paraffin, 2 μ	Eosinophilia abolished
DDD	Ca formalin	Frozen section, 5 μ	Red-pink
Hematoxylin and eosin	Paraformaldehyde Ca formalin	Paraffin, 2 μ Paraffin 2 μ	Pink with clear dots Pink with clear dots
Eosin after cold sulfation	Ca formalin	Paraffin 2 μ	Eosinophilia reduced
Eosin after sulfation followed by methylation	Ca formalin	Paraffin, 2 μ	Bright eosinophilia restored

did not abolish the PAS reaction Calcium formol fixed tissue yielded deeper PAS staining than specimens fixed in paraformaldehyde Acetylation blocked the PAS reaction and deacetylation renewed it. Positive PAS staining was apparent after bromination but no coloration was produced by the performic acid Schiff (PFAS) procedure Alcian blue staining was negative Sulfation, followed by toluidine blue produced a deep blue CLB with no apparent metachromasy

Routine hematoxylin and eosin preparations (table 3) resulted in deep pink

TABLE 4

Carbohydrates

Reaction	Fixation	Section	CLB results
PAS	Paraformaldehyde Ca formalin	Paraffin, 2 μ Paraffin, 2 μ	Deep pink Deep pink
Unoxidized control	Ca formalin	Paraffin, 2 μ	Negative
PAS after malt diastase	Ca formalin	Paraffin, 2 μ	Deep pink
PAS after α-amylase	Ca formalin	Paraffin, 2 μ	Deep pink
PAS after β-amylase	Ca formalin	Paraffin, 2 μ	Deep pink
PAS after acetylation	Ca formalin	Paraffin 2 μ	Negative
PAS after deacetylation	Ca formalin	Paraffin, 2 μ	Deep pink
PAS after performic acid	Ca formalin	Paraffin, 2 μ	Negative
PAS after bromination	Ca formalin	Paraffin, 2 μ	Deep pink
Alcian blue	Paraformaldehyde Ca formalin	Paraffin, 2 μ	Negative
Toluidine blue after sulfation	Paraformaldehyde Ca formalin	Paraffin, 2 μ	Deep blue

TABLE 5

Miscellaneous

Reaction	Fixation	Section	CLB results
Weil	Ca formalin	Paraffin, 2 μ	Black
Safranin O	Ca formalin	Paraffin, 2 μ	Deep pink
Nuclear-fast red	Ca formalin	Paraffin, 2 μ	Deep pink

staining of the CLB. *Amino blockade by* acetylation completely inhibited the staining reaction of eosin while sulfation greatly diminished it (table 3).

The Weil procedure, usually employed as a myelin stain, gave intensely stained black bodies (table 5). Safranin O and Neutral Red demonstrated the CLB also.

DISCUSSION

Histological and ultrastructural characteristics

In the last few years a number of instances of the occurrence of "layered" bodies in various tissues has been recorded. Uchizono ('62) reported them in the sixth abdominal ganglion of the crayfish. Miller ('58) linked structured bodies to photoreceptors in invertebrates. Friedmann et al. ('65) found them in degenerating sensory epithelium of the human macula in Ménière's disease and Hilding and House ('64) did likewise in the macula of non-Ménière's patients. Campiche ('60) located organized bodies in alveolar lung cells of young rats. Naumann and Wolfe ('63) detected them under the subcommissural organ of the rat brain, whereas Wetzstein et al. ('63) noted them in the subcommissural organ. Frithiof and Wersäll ('66) saw very small lamellar objects in oral epithelium. Frog and turtle pigment epithelial cells revealed prominent lamellar bodies (Porter and Yamada, '60). Morales and Duncan ('66) have recently reviewed some of these reports and point out several features that appear to delineate the geniculate CLB from lamellar structures located in other tissues. We are in agreement that the geniculate laminar complex does differ in many respects from lamellar bodies found elsewhere with the exception of the complex shown by Morales and Duncan ('66) in the cat cerebellar cortex.

The statement that CLB are stained blue by hematoxylin and are not stained by the PAS, Millon and DDD procedures (Dustin and Barron, '60) is an error.

Although they state that the laminar structure in stellate neurons is less complexly folded than its LGB counterpart, their text figures 1 and 2 of a stellate laminar body are very similar to our text figure 7 which portrays a geniculate neuronal CLB

The occurrence of a segregated stack of dense parallel membranes at one pole of the CLB (fig 4 5) coextensive with external granular ER and resembling the plates of a condenser is a new observation The significance of this restricted configuration is enigmatic. The similarity however between these membranes and and a similar "condenser type"[8] stack in the tubular lattice-like structure in figures 11 and 12 may represent a link between these two apparently dissimilar bodies. The segregated stacks of dense membranes illustrated by us are unlike the "lamellar bodies" described by Herndon ('64) in rat Purkinje neurons perfuse-fixed by buffered cold osmium tetroxide. "Lamellar bodies" which derive from ER, were observed also by Morales and Duncan ('66) in formaldehyde-perfused cat cerebellum In contrast to the "condenser-type" stacks we described the cisterns of "lamellar bodies" are dilated (Herndon '64) rather than narrowed. Further lamellar bodies occur in the cytoplasm (Herndon '64 Morales and Duncan '66) a location where we have never encountered them in geniculate neurons Indeed, in an extensive ultrastructural survey of nerve cells of feline LGB and cervical cord conducted over more than two years we have yet to observe "lamellar bodies" in material rapidly perfused with warm formaldehyde according to the directions of Karlsson and Schultz ('65)

The mesh-like smooth tubular profiles of the lattice-like bodies (figs 10–12) somewhat resemble the agranular elements described in pigment epithelial cells of the frog and rat retina (Porter and Yamada '60) and the hypertrophied smooth tubules of the hamster liver ER (Jones and Fawcett, '66) The lattice-like body of cat geniculate nerve cells bears a resemblance also to the structure described by Karlsson ('66) in rat LGB neurons and termed by him "complex convolutions." Ordered arrays of parallel tubules derived from ER were noted by Karlsson to be associated with the complex convolutions of rat LGB but the tubules were wider and their walls less electronopaque than the stacks (figs. 11 12) of dense membrane-lined channels seen in cat material. Karlsson did not describe structures resembling the highly organized cytoplasmic bodies (CLB) of the cat geniculate neuron.

CLB sometimes bear a close topographic relationship to other cellular organelles. The Golgi complex is often in close juxtaposition (figs 1 4 5 8) Sometimes, a large quantity of agranular tubules that appear to be Golgi components partially envelop a laminar body (fig 1) A link with the nucleus is suggested by the continuity of the CLB with the external nuclear membrane (fig 7) Lipofuscin is sometimes very near the laminar structure. The significance of the dark structure partially enveloped by a laminar body in figure 15 is unknown.

Resolving the origin of the CLB awaits studies supplemental to static micrographs. The frequent continuity of the highly organized lamellar body with tubular granular ER plus a similar connection between the agranular lattice-like edifice and particle-studded ER does suggest that modified ergastoplasm is involved in the formation of these structures The relative persistence of the ordered organelle in atrophic neurons when tubular rough-surfaced E R has disappeared may reflect a possible significant functional difference between the two continuous membrane systems The meaning of a link with the nucleus via granular ER could only be speculated on at this point. Indeed, the functional significance of CLB is unknown. Their detection by Morales and Duncan ('66) in stellate neurons of the cerebellum eliminates the possibility that they might be confined to the visual pathway

The frequency of occurrence of the laminar structure must be viewed with caution at the present time. Our estimate that 9% of geniculate neurons contain a CLB might not hold if the sample were extended to the entire LGB Although our counts were taken from several 2 μ sections

[8] The likening of the polarized stack of dense membranes to a condenser-set is meant in a morphological sense and does not imply that the membranes have specialized electrical properties.

parated by 6 μ intervals the starting slot was an area where CLB's were present. As pointed out previously there are places where scores of neurons in the A and A₁ layer do not contain the structure. The laminated structure occurring in an identified dark glial cell was detected on only one occasion. The repeating dense layers appear to be composed of interlocking tubules in a fashion similar to that described for the neuronal CLB. The repeating unit, however is smaller in the glial cell.

Histochemical Findings

The histochemical data support the conclusion that the CLB is chemically complex and contains a considerable amount of protein some lipid and, perhaps, polysaccharide, but no nucleic acid. On the basis that lipids, surviving paraffin embedment, should permit decolorization by extraction procedures with subsequent restaining (Lillie '65) a lipid component, identity unknown, has been demonstrated for CLB by the Sudan Black B procedure. The presence of phosphatides may be suggested in view of the nondemonstrability of neutral lipid with Oil Red O (Pearse, '61). For more informative data however, tests should be performed on fresh material. Results from the phospholipid staining method (acid hematin) are inconclusive. Extraction with hot pyridine did not prevent staining by acid hematin. As noted by Pearse ('61) fixed tissue is unsuitable for identification of contained lipids on the basis of solubility in organic solvents. Use of unfixed tissue would be required for more definitive information, but the preparation of stained, thin, raw frozen sections containing neurons in a satisfactory state of structural integrity would be a formidable technical problem.

A relatively high concentration of protein is indicated by the marked reactions with bromphenol blue and bromsulfalein. Intense eosinophilia, that is abolished when amino groups are acetylated prior to eosin staining, reflects a relatively high concentration of amino groups that are probably associated with protein and are available for dye binding. The Millon reaction, although rather faintly positive supports the presence of protein. The red-pink color after DDD indicates a sparse distribution of sulphydryl groups.

A complete lack of nucleic acid at a histochemical level of detection, is revealed by the negative Feulgen reaction for DNA and the nonstaining for RNA by toluidine blue and thionin. These results are supported by the inability to demonstrate histochemically any DNA or RNA by the gallocyanin-chromalum method. RNA basophilia in Nissl substance was abolished completely by RNAase digestion the unstained CLB remained undisturbed and were easily detectable by phase-contrast microscopy. That the bodies are stainable by toluidine blue after combined formaldehyde and osmium fixation followed by epon embedment (Morales et al. '64 Doolin and Barron, '66) cannot be considered evidence for the presence of nucleic acids. Many tissue components are stainable under these conditions including myelin, mitochondria and/or dense bodies etc.

A positive PAS reaction in paraffin sections that is blocked by acetylation and renewed by deacetylation is considered as presumptive evidence for the presence of a polysaccharide with free 1,2-glycol groups (Pearse '61). Leblond et al. ('57) are in agreement especially if glycogen is not the reacting agent and periodic-acid oxidation is employed. A positive PAS test in the CLB after the malt diastase digestion procedure eliminates glycogen as a source of the reacting polysaccharide. It would appear that the PAS reaction is not due to unsaturated lipids and sphingomyelins because the reaction with these substances cannot be prevented by prolonged acetylation (Pearse, '61). Also further support for the nonparticipation of lipid in the PAS reaction comes from the negative results that follow the PFAS procedure and the positive staining by PAS subsequent to bromination. A negative Alcian blue reaction indicates the absence of an acid mucopolysaccharide. Lack of a neutral polysaccharide is shown by the inability to demonstrate metachromasy with toluidine blue after sulfation.

The significance of the marked staining of the CLB with the Weil procedure, Safranin and Neutral Red is undetermined. These histologic technics are mentioned since they permit demonstration of the

laminar bodies in formalin fixed and paraffin-embedded LGB

It is concluded that CLB are not only architecturally complex at the ultrastructural level but also are histochemically complex structures containing protein lipid and polysaccharide components

LITERATURE CITED

Baker J R. 1946 The histochemical recognition of lipine Quart. J Micr Sc., 87: 441–470

Barka, T and P J Anderson 1963 Histochemistry Theory Practice and Bibliography Harper and Row New York.

Barron K. D P F Doolin and J Oldershaw 1967 Ultrastructural observations on retrograde atrophy of lateral geniculate body 1 Neuronal Alterations. J Neuropath. and Exp Neurol. XXVI, 2 300–326

Brachet J 1957 Biochemical Cytology Academic Press, New York.

Campiche M 1960 Lamellar inclusions in the alveolar lung cells of the young rat J Ultrastruc. Res. 3: 302–312.

Doolin P F., and K. D Barron 1966 Ultrastructure and histochemistry of cytoplasmic laminar bodies (CLB) in lateral geniculate neurons of the cat. Sixth International Congress for Electron Microscopy Kyoto II, pp 453–454

Friedmann, I. T Cawthorne and E. S. Bird 1965 The laminated cytoplasmic inclusions in the sensory epithelium of the human macula J Ultrastruc. Res. 12: 92–103.

Frithiof L., and J Wersäll 1966 Phospholipid-like granules in keratinizing oral epithelium. The Swedish Cancer Society Yearbook 4 I. Pathology pp 88–91

Herman, H., J S Nicholas and J K. Boricious 1950 Toluidine blue binding by developing muscle tissue: Assay and data on the mechanism involved. J Biol. Chem., 184: 321–332.

Herndon R. M. 1964 Lamellar bodies, an unusual arrangement of the granular endoplasmic reticulum. J Cell Biol. 20 338–342.

Hilding D A. and W F House 1964 An evaluation of the ultrastructural findings in the utricle in Ménierè's disease Laryngoscope, 74: 1135–1148.

Jones, A. L., and D W Fawcett 1966 Hypertrophy of the agranular endoplasmic reticulum in hamster liver induced by phenobarbital. J Histochem. and Cytochem., 14 215–232.

Karlsson U., and R. L. Schultz 1965 Fixation of the central nervous system for electron microscopy by aldehyde perfusion J Ultrastruc Res., 12: 160–186.

Karlsson, U., 1966 Three-dimensional studies of neurons in the lateral geniculate nucleus of the rat. I. Organelle organization in the perikaryon and its proximal branches. J Ultrastruc. Res., 16 429–481

Karnovsky M. J 1961 Simple methods for "staining with lead" at high pH in electron microscopy J Biophys Biochem Cytol. 11: 729–732.

Leblond C P., R. E. Glegg and D Eiding
1957 Presence of carbohydrate with fre
2-glycol groups in site stained by the period
acid-Schiff technique. J Histochem. a
Cytochem., 5 445–458.

Lillie R. D 1965 Histopathologic Techn
and Practical Histochemistry McGraw Hi
New York.

Luft, J H. 1961 Improvements in epoxy e
bedding methods. J Biophys. and Biochem
Cytol. 9 409–414

Miller W H 1958 Fine structures of so
invertebrate photoreceptors. Ann. N Y Aca
Sci. 74: 204–209

Morales, R. and D Duncan 1966 Multilamin
ated bodies and other unusual configurations o
endoplasmic reticulum in the cerebellum o
the cat. An electron microscopic study J
Ultrastruc. Res., 15: 480–489

Morales R., D Duncan and R. Rehmet 196
A distinctive laminated cytoplasmic body i
the lateral geniculate neurons of the ca
J Ultrastruc. Res., 10 116–123.

Naumann R. A., and D E. Wolfe 1963 A
striated intercellular material in rat brai
Nature 4481 701–703

Pearse A. G. E. 1961 Histochemistry Theo
retical and applied. Little Brown, Boston.

Porter K. R., and E. Yamada 1960 Studie
on the endoplasmic reticulum. V Its form an
differentiation in pigment epithelial cells o
the frog retina. J Biophys. and Biochem
Cytol. 8 181–205.

Rosenbluth, J 1962 Subsurface cisterns and
their relationship to the neuronal plasma mem
brane J Cell Biol., 13 405–421

Silverman, L., and D Glick 1966 Studies in
histochemistry LXXXV Histochemical demon
stration of protein with bromsulfalein. J
Histochem. and Cytochem., 14 425–426.

Smith J M., J L. O'Leary A. B Harris and
J Gay 1964 Ultrastructural features of the
lateral geniculate nucleus of the cat. J Comp.
Neur 123 357–376.

Swift, H 1955 Cytochemical technique for
nucleic acids In The Nucleic Acids, II E.
Chargoff and J N Davidson, eds., Academic
Press New York, pp 51–92.

Szlachta H. L. and R. E. Habel 1953 In-
clusions resembling Negri bodies in the brains
of nonrabid cats Cornell Veterinarian, 43
207–212.

Takeuchi T 1958 Histochemical demonstra-
tion of branching enzyme (amylo-1 4 → 1
6-transglucosidase) in animal tissues. J Histo-
chem. and Cytochem., 6 208–216.

Uchizono, K. 1962 The structure of possible
photoreceptive elements in the sixth abdominal
ganglion of the cray fish. J Cell Biol., 15: 151
154

Wetzstein, R. A. Schwink and P Stanka 1963
Die periodisch structurierten körper im subcom-
missuralorgan der ratte. Z. Zellforsch. Mikro-
skop. Anat., 61 493–523.

Windle W F R. Rhines and R. Rankin 1943
A Nissl method using buffered solutions of
thionin Stain Tech 18: 77–85.

PLATE 1

EXPLANATION OF FIGURES

1 A CLB partially surrounded by an enormous sweep of agranular membranes (asterisks) that are probably Golgi derivatives. Note the proximity of smooth membranes (apparently Golgi) to the CLB The arrow denotes a link between laminar tubules and cytoplasmic granular ER. Note the partially unravelled, less dense and narrower "daughter" strands (midregion of the CLB) which contrast with the denser "parental" bundles in the outer peripheral regions. The CLB lacks a peripheral limiting membrane. × 34,000

2, 3 An agranular tubule is coextensive with external granular ER (arrow fig 2) (× 68 000) The rope-like arrangement of intertwining tubules that forms the dense parallel sheets is more clearly evident when the component strands are partially "unravelled" (arrows fig 3) (× 51,000)

4 5 Adjacent sections showing a restricted stack of dense membranes localized at one pole of a CLB Note the continuity of the dense elements with the external granular ER (arrow in fig. 5) G. C., Golgi complex. × 68 000

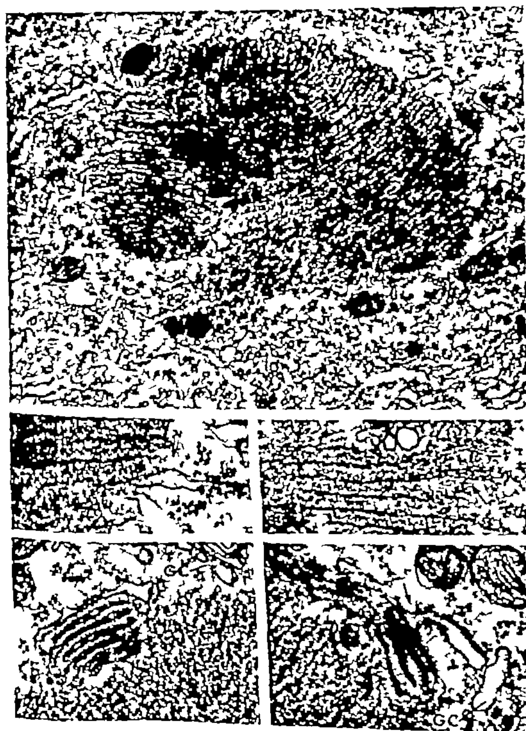

GC
GC

PLATE 2

EXPLANATION OF FIGURES

6 A laminar body in presumptive dendrite × 38,000

7 A CLB linked to the nucleus (N) via granular ER (arrow) that is coextensive with the outer member of the bilaminar envelope × 68 000

8 An atrophic geniculate neuron (14 days postoperatively) clearly showing the marked loss of cytoplasmic granular tubular ER and the appearance of single RNP particles. The CLB appears to be in partial disarray (see text) Golgi complexes (arrows) *N* nucleus × 30,000

9 An atrophic neuron (70 days postoperatively) The fusion of a mitochondrion with a CLB (arrow) has not been detected in normal cells Ly lysosome; Cc, centriole × 42,500




N




Ly
C

PLATE 3

EXPLANATION OF FIGURES

10 A view of a lattice-like arrangement of agranular tubules, coextensive with external granular ER of normal dimensions (small arrows) and also with highly dilated ER that shows partial denudation of membrane-bound RNP particles (asterisk) The upper large arrow denotes a cytoplasmic island with ribosomal elements a mitochondrion and a smooth membranous profile The lower large arrow points to a trapped mitochondrion. × 30 000

11 A "condenser-set of dense membranes (similar to those in fig. 12) polarized at one end of an oval body composed of smooth tubules in lattice-like arrangement. Note the abrupt dilatation of the narrow cisterns at the transition points of the "condenser membranes with the tubular lattice (arrows) An irregular fuzz like substance may be present on the external surface of the dense profiles, especially the third member from the left. Continuity of agranular membranes in the mesh-like body with the dilated external rough ER partially denuded of RNP particles is evident. × 68,000

12 A low power micrograph of an oval 3-dimensional reticular structure composed of a complex system of smooth membranous tubules Note the "condenser-set" of polarized membranes whose individual members are sometimes in continuity with each other via dilated extension at the edge (arrow) A trapped mitochondrion is visible × 17 000

LAMELLAR BODIES IN GENICULATE NEURONS

Paul F Doolin, Kevin D. Barron and Sharon Kwak



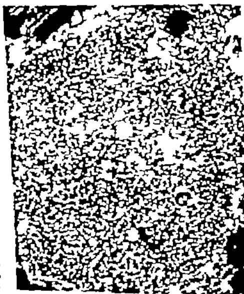


PLATE 4

EXPLANATION OF FIGURES

13 A presumptive early stage in the genesis of a CLB. Note the extreme reduction of the lumen of a granular ER profile with the concomitant loss of RNP particles and increase in membrane density where the tubular wall is compressed. A moderately dense region with a faint intermediate dot-studded line (arrows) lies between the dense element and the subadjacent ER profiles. The sides of the latter facing the altered membranes of the dense segment are devoid of ribosomes a condition not prevailing on the walls exposed to the surrounding cytoplasm. × 68,000

14 Another presumptive early stage in the formation of a CLB. Granular ER (arrows) that is coextensive with ribosome-denuded ER is in continuity with smooth tubules in the "incipient laminar body × 48,000

15 A dense structure unbounded by an external membrane and containing varying granular patterns, is partially enveloped by a CLB × 68,000

16 A small granular body that is frequently seen in neuronal cytoplasm. Note the absence of a limiting membrane and the suggestion of a cytoplasmic island (asterisk) containing ribosomes dense bodies and a smooth membranous element. Linear profiles (arrows) reminiscent of tubules in the CLB are evident in the granular matrix. × 59,500









PLATE 4

EXPLANATION OF FIGURES

13 A presumptive early stage in the genesis of a CLB Note the extreme reduction of the lumen of a granular ER profile with the concomitant loss of RNP particles and increase in membrane density where the tubular wall is compressed. A moderately dense region with a faint intermediate dot-studded line (arrows) lies between the dense element and the subadjacent ER profiles. The sides of the latter facing the altered membranes of the dense segment, are devoid of ribosomes a condition not prevailing on the walls exposed to the surrounding cytoplasm × 68,000

14 Another presumptive early stage in the formation of a CLB Granular ER (arrows) that is coextensive with ribosome-denuded ER is in continuity with smooth tubules in the "incipient laminar body × 48,000

15 A dense structure unbounded by an external membrane and containing varying granular patterns, is partially enveloped by a CLB × 68 000

16 A small granular body that is frequently seen in neuronal cytoplasm. Note the absence of a limiting membrane and the suggestion of a cytoplasmic island (asterisk) containing ribosomes dense bodies and a smooth membranous element. Linear profiles (arrows) reminiscent of tubules in the CLB are evident in the granular matrix × 59,500

LAMINAR BODIES IN GENICULATE NEURONS
Paul F. Doolin, Kevin D. Barron and Sharon Kwak

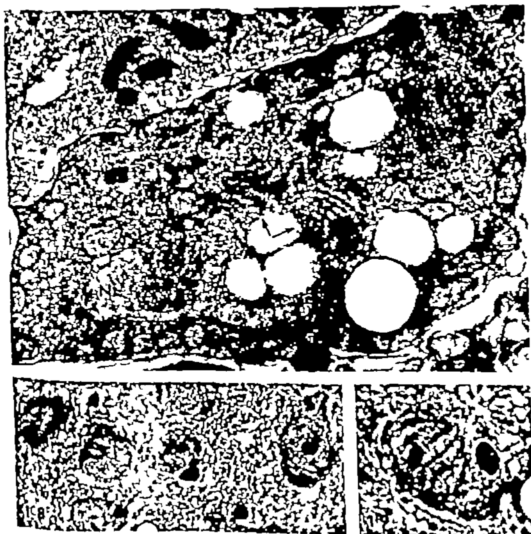
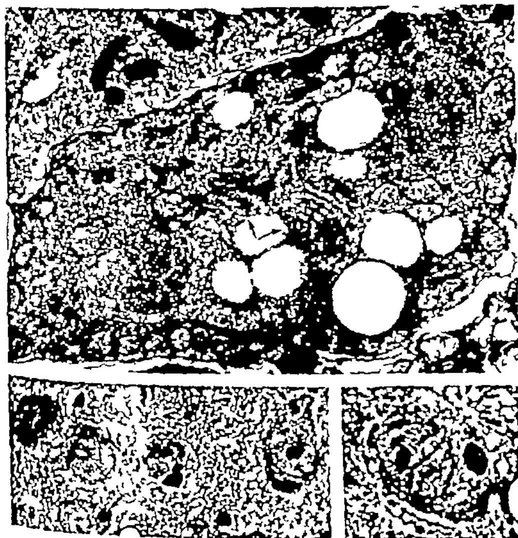


PLATE 5

EXPLANATION OF FIGURES

17 A dense glial cell identity undetermined containing a cytoplasmic laminar body (arrows) Continuity of the laminar tubules with external smooth cytoplasmic ER profiles can be detected. × 30 000

18 19 Light photomicrographs of a 2 μ paraffin section stained with hematoxylin and eosin Arrows denote three neurons, in a single microscopic field each containing a CLB (fig. 18) (× 1,024) In figure 19 (× 2,000) a laminar body (arrow) is clearly delineated. Note the light dots that represent cytoplasmic islands N nucleus.



Striated Muscle Cells in the Thymus of Reptiles and Birds: An electron microscopic study [1]

ELIO RAVIOLA AND GIUSEPPINA RAVIOLA

Department of Anatomy, Harvard Medical School, Boston, Massachusetts

ABSTRACT Striated muscle cells, the "myoid cells" of light microscopic literature, are consistently found in the thymus of reptiles and birds. Round or elongated myoid cells resemble adult skeletal or cardiac muscle fibers; however the location of the nucleus, the course of the myofibrils, the arrangement and proportion of the thick and thin filaments, and the morphology and topography of the membranous components of the sarcoplasm are variable. Other myoid cells which contain either primitive myofibrils, irregular bundles of myofilaments associated with primitive Z plaques, or thick and thin filaments alone scattered throughout the cytoplasm, recall the various stages of the development of skeletal and cardiac muscle fibers. In these cells the ribosomes are often, but not always abundant and appear in places arranged in helices and rosettes. It is suggested that a postnatal myogenesis takes place in the thymus. Anomalous muscle cells contain thin filaments almost exclusively. In some of these cells, thin filaments are arranged in I-segments that appear either independent of each other or interdigitated in pseudosarcomeres. Finally some myoid cells appear to have degenerated. Desmosomes join myoid cells to reticular cells, to other myoid cells, and to epithelial cells in the walls of intraparenchymal cysts. The origin of the myoid cells from reticular cells is suggested.

In 1888, Mayer described in the thymus of the frog large concentrically striated bodies, displaying a pattern of cross-banding identical with the striation of the skeletal muscle fibers. He interpreted these bodies as sarcolytes, that is products of the degeneration of exogenous muscle fibers (Mayer 1888). Sarcolytes were also reported by Schaffer (1893) in the thymus of a teleost. Subsequent, accurate studies by Pensa ('02, '04, '05) demonstrated that muscle cells either elongated and transversely striated or round and radially striated, are commonly present in the thymus of birds, reptiles and anuran amphibians. Pensa's observations were repeatedly confirmed (Hammar '05a,b '09; Weissenberg, '07; Dustin '09) and extended to the teleostean thymus (Hammar '08; Hagen '36). Striated muscle cells were also occasionally found in the thymus of mammals, especially in fetuses and young individuals (Hammar '05b; Pappenheimer '10; Dustin and Baillez, '14; Salkind, '15; Wassjutotschkin, '18; Henry '66).

In order to stress the imperfect resemblance of the thymic muscle elements to striated muscle fibers, Hammar ('05a,b) introduced the name "myoid cells," which has since been generally employed.

Myoid cells were thought to be devoid of any function and incapable of contraction (Hammar '05b, '09). According to Hammar ('05b) they are not innervated, whereas according to Terni ('29) they are.

In this paper we confirm with the electron microscope that striated muscle cells commonly occur in the thymus of reptiles and birds and we describe their fine structure.

A preliminary account of this study has been published elsewhere (Raviola and Raviola, '66); other reports on the fine structure of the striated muscle cells in the thymus have recently appeared in abstract (Van de Velde and Friedman, '66; Strauss, Kemp and Douglas, '66).

MATERIALS AND METHODS

The investigation was carried out on the thymuses of eight turtles (*Pseudemys scripta elegans*), twelve snakes (*Natrix rhombifera*), seven pigeons and one chicken; males and females were used. All reptiles and one pigeon were less than one year old, six pigeons were 1–3 years old, and the chicken was four days old. Both turtles

[1] Supported by grant [illegible] from the Institute of General Medical Sciences, National Institutes of Health, United States Public Health Service.
Both authors are on leave of absence from the Institute of Human Anatomy of the University of Pavia, Pavia, Italy.

and snakes had been kept in captivity and were killed during the fall and the winter

The thymus was fixed either in phosphate-buffered, 2% osmium tetroxide at pH 7 0 or in the formaldehyde-glutaraldehyde mixture of Karnovsky (65) followed by osmium tetroxide postfixation The specimens were dehydrated in methanol and embedded either in Epon or Araldite For light microscopy 0 5–1 μ thick sections were stained with toluidine blue (Richardson Jarett and Finke 60) For electron microscopy thin sections were stained with uranyl acetate followed by lead citrate (Venable and Coggeshall 65) Micrographs were taken with the electron microscopes RCA 3F and Siemens Elmiskop 1

OBSERVATIONS

In the thymuses of all the animals investigated cells were present which have in common with both skeletal and cardiac muscle fibers the presence of cytoplasmic cross-striated fibrils and thus correspond to the myoid cells of the light microscopic literature

Myoid cells were numerous in the thymuses of the turtles the snakes and the 1 to 3-year-old pigeons Only a few myoid cells were found in the thymuses of the pigeon less than one year old and of the 4-day-old chick therefore these two subjects were not studied with the electron microscope

In the thymus of the turtle myoid cells are scattered everywhere in the lobule in the thymus of the snake they are mainly concentrated in the central region of the lobule and decrease in number towards the periphery in the thymus of the pigeon they are located both in the medulla and at the boundary region between cortex and medulla. In places they occur in clusters

Myoid cells are extremely varied in fine structure. One variety approximates the morphology of adult muscle fibers a second variety the morphology of embryonal muscle fibers and a third variety finally is represented by anomalous muscle cells displaying a large deficiency of thick myofilaments These three categories are not, however intended to be a rigid classification. In fact, all myoid cells are in varying degree atypical muscle elements

Myoid cells that most closely resemble adult muscle fibers are rounded, pear shaped or elongated (figs 1 3, 4) Round or oval myoid cells (figs. 1 4) are preponderant in the thymus of all the animals investigated They are up to 30 μ in diameter and generally possess a single nucleus either centrally or eccentrically located cells with up to four nuclei were also observed Elongated (fig 3) or pear shaped cells appear to be more frequent in the thymus of turtles they may reach 70 μ in length and 15 μ in thickness with the nucleus commonly located at one pole.

In round or oval myoid cells myofibrils run extremely variable courses (fig. 1) at the cell periphery they are often oriented in concentric bundles or sheaths, while in the central region of the cell they are intertwined or arranged in vortices. Sometimes all the myofibrils are snarled in a confused tangle and are seen longitudinally obliquely and transversely cut in a single section from the same cell. When myofibrils are concentrically arranged and corresponding bands of adjacent myofibrils are roughly in register the myoid cell acquires the peculiar radial striation that attracted the attention of light microscopists.

In most elongated or pear-shaped cells, the myofibrils roughly parallel in direction the main axis of the cell (fig 3) Corresponding bands of adjacent myofibrils are seldom in register and bundles of myofilaments continuously pass from one to the next myofibril In cross-section the myofibrils have an irregular outline and often fuse with each other they are not however as largely confluent as in cardiac muscle fibers (Porter and Palade '57 Fawcett and Selby '58)

In both round and elongated cells, the myofibrils are independent of the sarcolemma[1] an insertion of myofilaments upon the cell membrane similar to that reported at the myotendinous junction (Muir 61) or at the intercalated discs (Poche and Lindner '55) is lacking

In longitudinally cut myofibrils (figs 1 3 10a) a regular succession of Z lines

[1] According to Fawcett and Selby ('58) and Fawcett ('68) we take the sarcolemma to be the plasma membrane of the muscle fibers and the external lamina to be the adjacent extracellular boundary layer homologous to the basement lamina of epithelia.

divides sarcomeres 1.4–2 μ in length. Commonly the sarcomeres display over most of their extent the pattern of interdigitated thick and thin filaments which is typical of the A band. I bands are narrow and an H zone is generally lacking. Thus, the myofibrils are contracted. An M band is present, but is sometimes ill defined. On both sides of the M band, a thin light strip is often present which corresponds to the pseudo H-zone of Huxley ('65). Thin filaments become thicker and denser where they merge with the Z band.

In cross-sectioned myofibrils (fig. 2) thick filaments are 100–160A and thin filaments 40–65A in diameter. Thick filaments are often but not always, arranged in a hexagonal pattern. Each thick filament is surrounded by a variable number of thin filaments, sometimes fewer but generally more than six; in some myoid cells of the pigeon there are more than twelve. When six thin filaments surround each thick one, the arrangement of the thin filaments approximates the geometrical relationship that is typical of vertebrate skeletal muscle where each thin filament is shared by three adjacent thick filaments. In cross-sections through Z lines, the square lattice characteristic of striated muscle fibers (Knappeis and Carlsen, '62; Franzini-Armstrong and Porter '64; Reedy '64) is seen.

The interfibrillar sarcoplasm is permeated by cisternae, tubules, and vesicles that probably belong to the sarcoplasmic reticulum and the T system. However a complete reconstruction of both the morphology and topographical relationships of the membranous components of the sarcoplasm is prevented by the disorderly course of the myofibrils. In turtles, branching and anastomosing tubules of the sarcoplasmic reticulum are often arranged in a regular network with circular meshes (fig. 3) but it is unclear which region of the sarcomere is ensheathed. Elongated profiles, sandwiched between two cisternae of the sarcoplasmic reticulum, are commonly found, the complex resembles a triad, except that its long axis is often parallel to the myofibrils. Only occasionally in elongated myoid cells in which corresponding bands of adjacent myofibrils are in register do triads appear regularly distanced at the level of the Z lines. In the myoid cells of the snake triads were occasionally seen at the junction between A and I bands, but more commonly they occur scattered throughout the interfibrillar sarcoplasm. The distribution of the triads is consistently irregular in the myoid cells of the pigeon.

Mitochondria in moderate numbers are irregularly dispersed among the myofibrils (fig. 1) or concentrated near the nucleus. In the myoid cells of the turtles and snakes as well as in other thymic parenchymal cells, the mitochondrial matrix contains prominent dense granules up to 650A in diameter. A small number of glycogen granules is scattered throughout the inter and intrafibrillar sarcoplasm. Free ribosomes are scarce. Stacks of Golgi cisternae surrounded by vesicles are commonly found in a juxtanuclear situation, but occasionally they occur in the interstices among the myofibrils or near the sarcolemma.

The nucleus of the myoid cells is irregular in shape and has a prominent nucleolus. Chromatin clumps adhere to the nuclear membrane (fig. 4) and the nucleolus.

Round or elongated myoid cells resembling embryonal striated muscle fibers were commonly found in the thymuses of turtles and snakes, and less frequently in that of pigeons.

Some of these cells (fig. 4) recall the latest stages of myogenesis, as described by Hay ('63) Allen and Pepe ('65) and Heuson-Stiennon ('65). Long myofibrils lie parallel to the main axis of the cell or encircle the nucleus, and are divided by Z lines into sarcomeres of uniform length; thin and thick filaments are interdigitated over the whole sarcomere but the myofibrils are ill defined and M bands are only occasionally seen; free ribosomes in helices or rosettes are often abundant in the plentiful interfibrillar sarcoplasm.

In other immature myoid cells (fig. 5) the cytoplasm is permeated by irregular bundles of thick and thin filaments running in all directions in a disorderly array. The bundles are either attached to or crossed by irregular plaques of variable density which reveal in suitable sections the tetragonal lattice of the Z lines. A

similar picture in immature muscle fibers was described by Hay (63) as "clumps of filaments" associated with "primitive Z band material" The plentiful sarcoplasm contains a variable number of branching and anastomosing tubules, triads mitochondria and glycogen granules The ribosomes are abundant in some cells scarce in others and often appear arranged in helices and rosettes (fig 5 insert)

In turtles only a few myoid cells with a pale homogeneous nucleus resemble myoblasts as described by Hay ('63) Allen and Pepe (65) and Heuson-Stiennon (65) Some of them contain a few bundles of thin and thick filaments either free or associated with Z-band material while others (fig 6) contain only filaments of a different diameter singly dispersed throughout the cytoplasm which is fairly rich in polyribosomes

Anomalous myoid cells of the pigeon almost recall smooth muscle cells because of the preponderant number of thin filaments the disorderly course of the myofibrils and the irregular shape of the Z bands These latter however display the square lattice typical of skeletal muscle fibers and appear in places regularly spaced along the myofibrils

In the thymuses of the turtles different kinds of anomalous muscle cells are found Some of them contain a cluster of large and irregular plaques of Z-band material affording attachment to a few mostly thin filaments (fig 7) In other cells many thick filaments are concentrated in a limited area of the cytoplasm but are very scarce in the surrounding regions where thin filaments are preponderant. In a third kind of cell, thick filaments are either exceedingly rare or lacking at least in the plane of section (figs 8 9) and thin filaments are arranged in bundles attached to both sides of Z lines (fig 9 insert) similar bundles or "I-segments" were obtained by Huxley (63) from the homogenization of skeletal muscle fibers in a relaxing medium

In a few myoid cells of the turtle (fig 9) the cytoplasm contains besides I-segments large bundles of thin filaments which are crossed by Z lines at regular intervals of 1–1 1 μ. The portion of bundle that intervenes between two consecutive Z
lines displays over its whole extent the
appearance of the I band of relaxed mus-
cle fibers (fig 10b) In places, a thin,
lighter band is found adjacent to the Z
line At both extremities the bundle is
provided with a regular fringe of thin
filaments, which are 0.9-1 μ in length and
terminate freely in the sarcoplasm with
all their ends in register "Pseudosarco
mere" appears to be an appropriat
designation for the repeat unit in thes
bundles of thin filaments. The simultane
ous occurrence of both I-segments an
pseudosarcomeres in the cytoplasm of th
same cell suggests that the pseudosarc
meres result from the interdigitation
two sets of thin filaments belonging
two facing I-segments The length of th
pseudosarcomeres is in fact, slight
higher than that of the terminal fringe
thin filaments This being so the lig
band close to the Z line of some pseu
sarcomeres would reflect an incompl
interdigitation of the two sets of th
filaments and might contain a single
of them

In the thymuses of all the anim
studied, myoid cells are found which w
the light microscope have pycnotic nu
and intensely stained cytoplasm. With
electron microscope these cells are
regularly oval or rounded and exhib
uniformly high density of cytopla
Organelles are closely packed and
cross-banding of the myofibrils is diffi
to discern. These cells are probably de
erate Their fate however remains
scure because they are only occasio
contained in the lumen of cysts and n
were found engulfed in phagocy
vacuoles

The myoid cells indiscriminately co
any component of the thymic lobule
places they appear completely surrou
by reticular lymphoid and other n
cells (figs. 4 8) while in other pl
they are adjacent to or even compl
embedded in the intralobular conne
tissue bundles. In places they contac
adventitia of the vessels (fig 1) In
ties only are they found at the peri
of the lobule, contiguous with the pe
ular connective tissue capsule (fig
In the thymus of snakes myoid cell
found intercalated between the epithelial

cells of the wall of intraparenchymal cysts or contained in the lumen of these latter. Flattened reticular cells are occasionally seen partially encircling myoid cells.

An external lamina consistently intervenes between the sarcolemma of the myoid cells and the connective tissue (fig. 1), but where the myoid cells are contiguous to other cells of the lobule, the external lamina is discontinuous or lacking (figs. 4, 8 11 12) This finding corroborates the light microscopic observations that myoid cells lack a "sarcolemma (Terni, '29; Teichmann, 42)

In all the animals in this study a small number of desmosomes were found connecting the myoid cells with neighboring reticular (figs. 8 11) and myoid cells. In the myoid cell, the bundle of filaments which originates from the desmosome runs a short path in the sarcoplasm without merging with neighboring myofibrils. In the thymus of snakes desmosomes connect myoid cells with the epithelial cells of the wall of the cysts (fig. 12); the latter cells are provided with a brush border or with cilia.

No obvious relationships exist between the level of organization of the filamentous component in the cytoplasm of the myoid cells and either their location in the thymic lobule, the presence of an external lamina, or the presence of desmosomal connections.

No nerve process was clearly identified contacting the sarcolemma or the external lamina of the myoid cells.

DISCUSSION

The observation of Pensa ('02, '04) that the thymus of reptiles and birds contains striated muscle cells is confirmed by the present electron microscopic investigation. Myoid cells were found in the thymuses of all the animals investigated; therefore, they do not represent an exceptional finding such as the striated muscle fibers sporadically reported in the tonsil (Töpfer '02; Glas, '05) thyroid (Wölfler 1883; Müller 1896 Crispino '02 Bargmann, '39), pineal (Nicolas '00 Dimitrova, '01 Wolfe '65) and bone marrow (Piazza, '09) Moreover the myoid cells are neither embedded in the wall of the vessels nor joined by intercalated discs thus as already pointed out (Pensa, '02) they are different from the cardiac muscle fibers of the wall of thoracic veins of some mammals (Stieda 1877 Karrer '60)

The myoid cells in which the myofilaments are highly organized in sarcomeres and fibrils differ from both skeletal and cardiac muscle fibers in several features the cell shape is variable; the nuclei are not constantly peripheral or central the myofibrils have an extremely irregular course the ratio of thin to thick filaments is inconstant the geometrical arrangement of the filaments is approximate the frequency and topography of the triads is variable the external lamina is incomplete or lacking where the myoid cells contact other thymic parenchymal cells.

Myoid cells that contain primitive myofibrils or irregular clumps of filaments associated with plaques of Z-band material resemble embryonal muscle fibers but this resemblance too, is approximate. Both the cell shape and the course of the myofibrils are variable a myotube stage (Boyd, '60) *sensu stricto* does not exist, although cells are found with a comparable myofibrillar pattern the quantity of free ribosomes irregularly fluctuates from one cell to another and the extent of the membranous components of the sarcoplasm seems to vary independently of the degree of organization of the filamentous component. Finally a correlation seems to exist in skeletal muscle fibers between cellular differentiation and the presence of an external lamina, which appears at a certain stage of development (Allen and Pepe '65) and disappears during dedifferentiation (Hay '59) Such a correlation seems to be lacking in myoid cells which may be provided with a complete or incomplete external lamina regardless of the level of organization of their filaments into sarcomeres and fibrils.

Light microscopists reported that in birds and reptiles myoid cells increase in number with increasing age (Dustin, '09; Terni, '27 '29; Pirocchi, '36); it was therefore suggested that striated muscle cells are also formed in the thymus during postnatal life (Dustin, '09) This hypothesis is verified by the finding of myoid cells resembling embryonal muscle fibers in the thymus of the animals investigated. Th

it appears unlikely either that myoid cells resembling embryonal muscle fibers represent intermediate stages of the dedifferentiation of adult muscle elements or that the whole population of immature myoid cells is "frozen" at an embryonal stage since the time of the development of the thymus

We do not know however whether the myogenesis in the thymus is restricted to the youth of the animal or lasts for the entire life of the organ In Dustin s opinion ('09) new myoid cells are formed in the reptilian thymus every spring and degenerate during the fall the renewal becoming slower with the involution of the organ.

The presence of both embryonal and degenerated myoid cells is clear evidence that the muscle elements of the thymus do not represent a stable population at least in the species and for the ages we have studied Our data, however do not seem to substantiate Weissenberg s ('07) and Dustin s ('09) belief that myoid cells are originally elongated but later become rounded and finally degenerate No regressive features were in fact found in most of the round cells examined in this study furthermore immature myoid cells appear either round or elongated

Morphological differences between myoid cells and adult or embryonal muscle fibers possibly result from a disturbed myogenesis under anomalous environmental influences The multifarious organization of the cytoplasm of the mature myoid cells would thus reflect the fact that myogenesis is unequally disturbed in different places. Furthermore the developmental process may be intermittent, for ribosomes are scarce in several immature myoid cells

Cells containing almost exclusively thin filaments and Z-band material certainly result from a primitive derangement of the developmental process Any other process leading to the disappearance of the thick filaments alone appears in fact hardly conceivable. If thick filaments alone can be defective in anomalous muscle cells the synthesis of the thick filaments and that of the thin ones might not be so strictly correlated as suggested by their simultaneous appearance during the development of the skeletal and cardiac muscle (Lindner '60 Bergman 62 Hay 63 Firket, '63 Fischman 65 Dessouky and Hibbs, '65)

It should be noted, by the way that muscle cells which contain I-segments alone, either isolated or interdigitated in pseudosarcomeres constitute a further confirmation of the theory (Huxley and Hanson, 54) that myofibrils are built up by the overlapping array of two independent types of filaments

If a postnatal myogenesis takes place in the thymus it appears unlikely that myoid cells originate from myoblasts of the musculature of the branchial arches, which have been trapped in the thymus during development (Pensa, '04) Alternative opinions to the inclusion hypothesis are either the continuous neoformation of the myoid cells from the thymic reticular cells (Hammar '05b '09 Pappenheimer 10 Teichmann 42 Bargmann, 43) or their intermittent origin from perivascular and interstitial connective tissue cells (Dustin, 09) The observations that substantiate Dustin s idea are disproved by the electron microscope. Immature myoid cells are not necessarily located near the adventitia of the vessels and the connective tissue cells from which the myoid cells would derive actually are the flattened reticular cells that separate the thymic parenchyma from both the wall of the vessels and the intra- and interlobular connective tissue septa.

The electron microscopic finding that myoid cells are inserted by means of desmosomes into the network of the thymic reticular cells may represent circumstantial evidence that myoid cells originate from reticular cells Obviously the presence of desmosomes does not imply *per se* that joined cells arise from a common precursor There is no reason to suppose that desmosomes have another significance beyond that of intercellular attachment devices. However the contention that connective tissue cells or myoblasts are trapped in the thymic parenchyma and establish secondary desmosomal connections with the reticular cells appears rather unlikely

The function of the myoid cells remains obscure In our material, their myofibrils are generally contracted. However a con-

traction during fixation does not necessarily imply that the myoid cells spontaneously contract in the living organ. In any case their contraction would probably be ineffective in facilitating an ordered traffic of lymphocytes through the thymus: myoid cells do not seem strategically located in the lobule they lack a tendon and possess too few desmosomes to pull successfully the reticular cells. Finally we have not seen any nerve fibers in contact with the myoid cells, although Terni ('29) saw many of them in specimens impregnated with the Cajal technique. We therefore believe that a function of the myoid cells should not be sought among possible mechanical effects of their contraction.

The presence in the thymus of striated muscle cells devoid of any obvious function seems at first sight a curiosity of no importance in the economy of the organ. Myoid cells, however are not the only seemingly extraneous component of the thymus. In all the animals investigated, we consistently found cysts surrounded by epithelial cells provided with a brush border or with cilia, mucus-secreting cells and reticular cells containing a large vacuole bounded by microvilli (figs. 13 14). Similar findings were sporadically reported also in mammalian thymuses (cfr Bargmann, 43 Hoshino, '62, 63 Clark, '63 '66 Kohnen and Weiss, '64 Ito and Hoshino, '66) and variously regarded as remnants of the original epithelial primordia of the organ (Kohnen and Weiss, '64) or presumptive sites of production of a thymic hormone (Clark, '66)

The heterogeneous but consistent population of muscle and epithelial cells might be an indication of an intrinsic property of the thymic environment, rather than the result of a fortuitous developmental anomaly Furthermore, both myoid and epithelial cells are joined by desmosomes to the reticular cells and might arise from them. Cells in the thymus, perhaps reticular cells, at least in restricted regions of the lobule or in limited periods of the life of the organ, might not be irreversibly differentiated and might acquire a very large prospective capacity The subsequent evolution of these cells seems to be completely shut off from the mechanisms that guarantee in fully developed organs, an homogeneous cell population as a paradoxical result, cells appear side by side that are usually found in organs other than the thymus.

It has been speculated (Burnet, '62) that in the thymus "self" reactive lymphocytes might be eliminated or inhibited by the contact with the corresponding antigenic determinants. We cannot exclude the possibility that the heterogeneous population of muscle and epithelial cells of the thymus might provide the collection of "self" components which is required by Burnet's theory However, the cell varieties we have found are limited in number and do not allow construction of a miniaturized test organism.

It has been shown that sera of myasthenic patients, especially if bearing a thymoma, and sera of patients with a thymoma unassociated with myasthenia contain antibodies which react *in vitro* with both the A bands of the striated muscle fibers and the cytoplasm of epithelial cells in the thymus of calves and human fetuses. Also cells of thymomas in myasthenic patients seem to react with the corresponding sera. On this basis, the hypothesis was advanced that the appearance in thymic epithelial cells of antigenic determinants common with the skeletal muscle may promote an autoimmune reaction either responsible of or concomitant with the *myasthenia gravis* (van der Geld Feltkamp and Oosterhuis '64 Strauss, van der Geld, Kemp, Exum and Goodman, '65; van der Geld and Strauss '66- Strauss and van der Geld, '68)

Recently however myoid cells of the thymus of turtles were seen to bind antimuscle globulins of myasthenic patients (Strauss, Kemp and Douglas, '66) and epithelial cells in the thymus of calves were seen to bind an antibody to muscle I bands, which is also present in the serum of normal subjects (Vetters, '66) Consequently it has been suggested that the epithelial cells which in mammalian thymuses bind antimuscle globulins, actually are the myoid cells of the light microscopic literature

As myoid cells are so widely distributed in vertebrate thymus and antimuscle se-

rum globulins are not exclusively found in myasthenic subjects at the present time no convincing evidence exists that striated muscle cells in the human thymus might be involved in the pathogenesis of *myasthenia gravis*

ACKNOWLEDGMENTS

The authors wish to thank Dr Don W Fawcett for the revision of the manuscript and Dr Jean Paul Revel for many helpful discussions during the course of the work.

LITERATURE CITED

Allen E. R. and F A. Pepe 1965 Ultrastructure of developing muscle cells in the chick embryo. Am. J Anat., *116:* 115–148

Bargmann, W 1939 Die Schilddrüse. In: Möllendorff's Handbuch der mikroskopischen Anatomie des Menschen. Vol. VI, Part 2 Springer Berlin.

——— 1943 Der Thymus. In: Möllendorff's Handbuch der mikroskopischen Anatomie des Menschen. Vol. VI, Part 4 Springer Berlin.

Bergman R. A. 1962 Observations on the morphogenesis of rat skeletal muscle Bull. Johns Hopkins Hosp., *110* 187–201

Boyd J D 1960 Development of striated muscle. In: The structure and function of muscle. Vol. I, G H. Bourne ed., Academic Press New York.

Burnet, F M. 1962 Role of the thymus and related organs in immunity Brit. Med. J *ii:* 807–811

Clark, S. L. 1963 The thymus in mice of strain 129/J studied with the electron microscope. Am. J Anat., *112:* 1–34.

——— 1966 Cytological evidences of secretion in the thymus. In: The thymus: experimental and clinical studies. G E. W Wolstenholme and R. Porter eds., Churchill, London pp. 3–30

Crispino, M. 1902 Contributo alla istologia delle formazioni annesse alla glandola tiroide. Il Policlinico Sez. medica, *9* 294–316.

Dessouky D A., and R. G Hibbs 1965 An electron microscope study of the development of the somatic muscle of the chick embryo Am. *J Anat. 116:* 523–586.

Dimitrova, Z. 1901 Recherches sur la structure de la glande pinéale chez quelques mammifères. Nevraxe, *2:* 259–321

Dustin, A. P 1909 Contribution à l'étude du thymus des reptiles. Cellules épithélioïdes, cellules myoïdes et corps de Hassal. Arch. Zool. exp. gen. *5e Série T II:* 43–227

Dustin, A. P., et G Baillez 1914 Sur l'existence de cellules myoïdes dans le thymus des mammifères. Ann. Boll. Soc. roy Sci. med. nat. Bruxelles *72:* 123–125

Fawcett, D W 1966 An atlas of fine structure. The cell, Saunders, Philadelphia.

Fawcett, D W., and C. C. Selby 1958 Observations on the fine structure of the turtle atrium. J Biophys. Biochem. Cytol., *4* 63–72.

Firket, H. 1963 Etude de l'ultrastructure de burgeons musculaires en régénération pendant la myogénèse. J Microscopie, *2:* 639–641

Fischman, D A. 1965 The fine structure of embryonic chick skeletal muscle. Anat. Rec. (abs.) *151:* 350.

Franzini-Armstrong, C., and K. R. Porter 1964 The Z disc of skeletal muscle fibrils. Z. Zellforsch. *61:* 661–672.

Glas, E. 1905 Zur Frage der Sarkolyse. Anat. Anz., *26:* 155–171

Hagen, F v 1936 Die wichtigsten Endokrinen des Flussaals. Zool. Jahrbücher *61:* 467–538.

Hammar J A. 1905a Zur Histogenese und Involution der Thymusdrüse. Anat. Anz., *27* 23–*30*

——— 1905b Zur Histogenese und Involution der Thymusdrüse. Anat. Anz., *27:* 41–89.

——— 1908 Zur Kenntnis der Teleostierthymus. Arch. mikr Anat., *73* 1–68.

——— 1909 Fünfzig Jahre Thymusforschung. Kritische Übersicht der normalen Morphologie. Erg. Anat. Entwickl., *19:* 1–274.

Hay E. D 1959 Electron microscopic observations of muscle dedifferentiation in regenerating Amblystoma limbs. Develop. Biol., *1:* 555–585.

——— 1963 The fine structure of differentiating muscle in the salamander tail. Z. Zellforsch., *59:* 6–34

Henry K. 1966 Mucin secretion and striated muscle in the human thymus. Lancet, I: 183–185.

Heuson-Stiennon, J A. 1965 Morphogenèse de la cellule musculaire striée, étudiée au microscope électronique. I.-Formation des structures fibrillaires. J Microscopie, *4:* 657–678.

Hoshino, T 1962 The fine structure of ciliated vesicle-containing reticular cells in the mouse thymus. Exp. Cell Res., *27:* 615–617

——— 1963 Electron microscopic studies of the epithelial reticular cells of the mouse thymus. Z. Zellforsch., *59* 513–529.

Huxley H. E. 1963 Electron microscope studies on the structure of natural and synthetic protein filaments from striated muscle. J. Mol Biol. *7* 281–308.

——— 1965 Structural evidence concerning the mechanism of contraction in striated muscle. In: Muscle. W M. Paul, E. E. Daniel, C M. Kay and G Monckton eds., Pergamon Press, Oxford, pp. 3–28.

Huxley H., and J Hanson *1954* Changes in the cross-striations of muscle during contraction and stretch and their structural interpretation. Nature *173* 973–976.

Ito T and T Hoshino *1966* Fine structure of the epithelial reticular cells of the medulla *of* the thymus in the golden hamster Z. Zellforsch., *69* 311–318.

Karnovsky M. J 1965 A formaldehyde-glutaraldehyde fixative of high osmolality for use in electron microscopy J Cell Biol., *27:* 137–138 A.

Karrer H. E. 1960 The striated musculature of blood vessels. II — Cell interconnections and cell surface J Biophys. Biochem. Cytol., *8* 135–150

Knappeis, G. G., and F. Carlsen 1962 The ultrastructure of the Z disc in skeletal muscle. J. Cell Biol., 13: 323–335.

Kohnen, P., and L. Weiss 1964 An electron microscopic study of thymic corpuscles in the guinea pig and the mouse. Anat. Rec., 148: 29–42.

Lindner, E. 1960 Myofibrils in the early development of chick embryo hearts as observed with the electron microscope. Anat. Rec. (abs.) 136: 234–235.

Mayer, S. 1886 Die sogenannten Sarkoplasten. Anat. Anz., 1: 231–235.

——— 1888 Zur Lehre von der Schilddrüse und Thymus bei den Amphibien. Anat. Anz., 3: 97–103.

Muir, A. R. 1961 Observations on the attachment of myofibrils to the sarcolemma at the muscle-tendon junction. In: Electron Microscopy in Anatomy. Arnold, London, pp. 267–277.

Müller, L. R. 1896 Beiträge zur Histologie der normalen und erkrankten Schilddrüse. Beitr. path. Anat., 19: 127–180.

Nicolas, M. A. 1900 Note sur la présence de fibres musculaires striées dans la glande pinéale de quelques mammifères. C. R. Soc. Biol., 52: 876–877.

Pappenheimer, A. M. 1910 A contribution to the normal and pathological histology of the thymus gland. J. Med. Res., 22: 1–75.

Pensa, A. 1902 Osservazioni a proposito di una particolarità di struttura del timo. Boll. Soc. med.-chir. Pavia: 198–202.

——— 1904 Ancora a proposito di una particolarità di struttura del timo ed osservazioni sullo sviluppo del timo negli anfibi anuri. Boll. Soc. med.-chir. Pavia: 65–79.

——— 1905 Osservazioni sulla struttura del timo. Anat. Anz., 27: 529–541.

Piazza, C. 1909 Un caso di inclusioni muscolari nel midollo osseo femorale di un cane. Anat. Anz., 34: 250–254.

Pirocchi, L. 1936 Contributo alla conoscenza del timo degli uccelli. Arch. zool. It., 23: 409–431.

Poche, R., and E. Lindner 1955 Untersuchungen zur Frage der Glanzstreifen des Herzmuskelgewebes beim Warmblüter und beim Kaltblüter. Z. Zellforsch., 43: 104–120.

Porter, K. R., and G. E. Palade 1957 Studies on the endoplasmic reticulum. III — Its form and distribution in striated muscle cells. J. Biophys. Biochem. Cytol., 3: 269–300.

Raviola, E., and G. Raviola 1966 Fine structure of the myoid cells in reptilian and avian thymus. Anat. Rec. (abs.) 154: 403.

Reedy M. K. C. 1964 Discussion. Proc. Roy Soc. London, Series B, 160: 458–460.

Richardson, K. C., L. Jarett and E. H. Finke 1960 Embedding in epoxy resins for ultrathin sectioning in electron microscopy. Stain Technol., 35: 313–323.

Salkind, J. 1915 Contributions histologiques à la biologie comparée du thymus. Arch. Zool. exp. gen., 55: 81–322.

Schaffer, J. 1893 Über den feineren Bau der Thymus und deren Beziehungen zur Blutbildung. Sitzungsber. Akad. Wiss. Wien, Math. Naturwiss. Kl., 102: 336–341.

Stieda, L. 1877 Ueber quergestreifte Muskelfasern in der Wand der Lungenvenen. Arch. mikr. Anat., 14: 243–248.

Strauss, A. J. L., P. G. Kemp, Jr. and S. D. Douglas 1966 Myasthenia gravis. Lancet, 1: 772–773.

Strauss, A. J. L., and H. W. R. van der Geld 1966 The thymus and human diseases with auto-immune concomitants, with special reference to myasthenia gravis. In: The thymus: experimental and clinical studies. G. E. W. Wolstenholme and R. Porter eds., Churchill, London, pp. 416–439.

Strauss, A. J. L., H. W. R. van der Geld, P. G. Kemp, Jr. E. Dubois Exum and H. C. Goodman 1965 Immunological concomitants of myasthenia gravis. Ann. N. Y. Acad. Sci., 124: 744–766.

Teichmann, W. 1942 Über die myoiden Zellen des Thymus (Untersuchungen am Thymus von Schlangen). Z. Zellforsch., 32: 194–206.

Terni, T. 1927 Sulle modificazioni istologiche prodotte nel timo dalla castrazione e dall'età. Monit. zool. It., 38: 300–308.

——— 1929 Ricerche istologiche sull'innervazione del timo dei sauropsidi. Z. Zellforsch., 9: 377–434.

Töpfer H. 1908 cited by J. A. Hammar, 1909.

van der Geld, H., T. E. W. Feltkamp and H. J. G. H. Oosterhuis 1964 Reactivity of myasthenia gravis serum γ-globulin with skeletal muscle and thymus demonstrated by immunofluorescence. Proc. Soc. Exp. Biol. Med., 115: 782–785.

van der Geld, H. W. R., and A. J. L. Strauss 1966 Myasthenia gravis. Immunological relationship between striated muscle and thymus. Lancet, 1: 57–60.

Van de Velde, R. L., and N. B. Friedman 1966 Muscular elements of the thymus. Fed. Proc., 25: 661.

Venable, J. H., and R. Coggeshall 1965 A simplified lead citrate stain for use in electron microscopy. J. Cell Biol., 25: 407–408.

Vetters, J. M. 1966 Myasthenia gravis. Lancet, 1: 314.

Wassjutotschkin, A. M. 1913 Untersuchungen über die Histogenese des Thymus. III. Über die myoiden Elemente des Thymus beim Menschen. Anat. Anz., 50: 547–551.

Weissenberg, R. 1907 Über die quergestreiften Zellen der Thymus. Arch. mikr. Anat., 70: 193–226.

Wolfe, D. E. 1965 The epiphyseal cell: an electron microscopic study of its intercellular relationships and intracellular morphology in the pineal body of the albino rat. Progress in Brain Research, J. Ariëns Kappers and J. P. Schadé eds., Elsevier, Amsterdam, 10: 332–386.

Wölfler, A. 1880 Ueber die Entwickelung und den Bau des Kropfes. Arch. klin. Chir., 25: 1–97.

PLATE 1

EXPLANATION OF FIGURE

1 Turtle thymus. An elongated myoid cell is contiguous to the adventitia of a vessel (Adv). Cross-banded myofibrils are irregularly arranged throughout the sarcoplasm and appear to be cut either longitudinally or obliquely. The sarcomeres display over most of their extent, the pattern of interdigitated thick and thin filaments typical of the A band. The I bands (I) are narrow and an H zone is lacking; the myofibrils are thus contracted. Z lines (Z) and a M band (M) are indicated. The sarcoplasm contains mitochondria, glycogen granules, ribosomes, and smooth surfaced tubules of the sarcoplasmic reticulum (SR). On the upper right, an external lamina (EL) follows the outer surface of the sarcolemma. On the lower left, a similar but less distinct, lamina intervenes between the myoid cell and a connective tissue bundle. × 24 400


EL
Adv
El
1

PLATE 2

EXPLANATION OF FIGURES

2 Snake thymus. In a cross-sectioned myofibril, thick filaments appear arranged in orderly hexagonal pattern. In the encircled area thin filaments also conform to a regular hexagonal pattern and each thin filament is shared by three thick filaments. Elsewhere thin filaments are less regularly distributed. × 122,500.

3 Turtle thymus. In an elongated myoid cell the sarcoplasmic reticulum is represented by a fairly regular network of branching and anastomosing tubules. Three elongated profiles closely adhere to each other (double arrow); the complex resembles a triad but the central element runs parallel to the myofibrils. At the center and upper left, round or elongated profiles (single arrows) probably represent sections of a T tubule interwoven with cisternae or tubules of the sarcoplasmic reticulum. × 28,000

4 Turtle thymus. On the lower right, a round myoid cell contains a few myofibrils, which surround the nucleus. Only at the arrows, a faint external lamina intervenes between the myoid cell and neighboring lymphocytes. In the myoid cell at the upper left myofibrils are ill defined and the interfibrillar sarcoplasm is abundant. M bands are indistinct. This cell closely resembles skeletal muscle fibers in the last stages of development. × 18,200


2
3
4
MYOID CELL
MYOID CELL

PLATE 3

EXPLANATION OF FIGURES

5 Snake thymus In this myoid cell irregular bundles of myofilaments are scattered throughout the cytoplasm and appear in places associated with plaques of Z-band material (Z) The nucleus contains an evenly dispersed nucleoplasm. Smooth-surfaced profiles and glycogen granules are also present. In places, the ribosomes (insert) are plentiful and arranged in helices or rosettes. The degree of cell organization is comparable with early stages in the development of the skeletal muscle. × 30 400; insert × 60,000

6 Turtle thymus. Isolated filaments of variable diameter are dispersed throughout the cytoplasm of a myoid cell. The arrows point to thicker filaments. Ribosomes are fairly abundant; the nucleoplasm is evenly dispersed. The cell resembles an early myoblast. × 28,000

7 Turtle thymus. Myoid cell containing a cluster of irregular plaques of Z-band material upon which thin filaments are inserted. Only a few thick filaments are seen (arrows) × 30,400


5
7
6

PLATE 4

EXPLANATION OF FIGURE

8 Turtle thymus. A round myoid cell at the periphery of the lobule contains many bundles of thin filaments entangled in a confused mass, and exceedingly scarce thick filaments. Thin filaments are associated with faint Z lines. On the upper left, a myoid cell is seen, displaying the usual myofibrillar pattern. Notice how prominent the Z lines are in comparison with those contained in the previous cell. The arrow at the upper left corner points to a desmosome joining a process of a myoid cell to another process, possibly belonging to a reticular cell. × 13,300


1

PLATE 5

EXPLANATION OF FIGURE

9 Turtle thymus. A myoid cell lacking thick filaments, at least in the plane of section The cytoplasm contains besides I-segments (square bracket) a large bundle of thin filaments (double headed arrow) crossed by Z lines in regular sequence A lighter band is occasionally seen near the Z line (single headed arrow) In I-segments (insert) the two sets of thin filaments attached to both sides of the Z line have approximately the same length. × 18,300; insert × 32,700


9

PLATE 6

EXPLANATION OF FIGURES

10a b Turtle thymus. A portion of the cross-banded bundle of thin filaments of figure 9 is seen at higher magnification (10b) Segments of the bundle which intervene between successive Z lines display over their whole extent the organization of the I bands of relaxed skeletal muscle fibers. At the left, the bundle ends as a fringe of thin filaments of uniform length. The repeat unit (arrow) is much shorter than the highly contracted sarcomeres of another myoid cell of the same specimen containing both kinds of myofilaments (fig. 10a) It is suggested that the pseudosarcomeres of figure 10b arise from the interdigitation of two sets of thin filaments belonging to facing I-segments. Magnification of both figures × 34,200

11 Turtle thymus. Desmosome (arrow) joining a myoid cell (right) to a reticular cell (left) Both cells are located at the periphery of the lobule and are separated from the connective tissue by the perilobular external lamina (EL) A Z line in the myoid cell is indicated (Z) × 30 400

12 Snake thymus A myoid cell (below) is joined by a desmosome (arrow) to an epithelial cell in the wall of a cyst in the thymic parenchyma. The epithelial cell is provided with an irregular brush border In the myoid cell, cross-sections of Z bands are indicated (Z) × 33,000





E

11

12

PLATE 6

EXPLANATION OF FIGURES

10a, b Turtle thymus. A portion of the cross-banded bundle of thin filaments of figure 9 is seen at higher magnification (10b) Segments of the bundle which intervene between successive Z lines display over their whole extent the organization of the I bands of relaxed skeletal muscle fibers. At the left, the bundle ends as a fringe of thin filaments of uniform length. The repeat unit (arrow) is much shorter than the highly contracted sarcomeres of another myoid cell of the same specimen containing both kinds of myofilaments (fig. 10a) It is suggested that the pseudosarcomeres of figure 10b arise from the interdigitation of two sets of thin filaments belonging to facing I-segments. Magnification of both figures, × 34,200

11 Turtle thymus. Desmosome (arrow) joining a myoid cell (right) to a reticular cell (left) Both cells are located at the periphery of the lobule and are separated from the connective tissue by the perilobular external lamina (EL) A Z line in the myoid cell is indicated (Z) × 30 400.

12 Snake thymus. A myoid cell (below) is joined by a desmosome (arrow) to an epithelial cell in the wall of a cyst in the thymic parenchyma. The epithelial cell is provided with an irregular brush border. In the myoid cell, cross-sections of Z bands are indicated (Z) × 33,000.

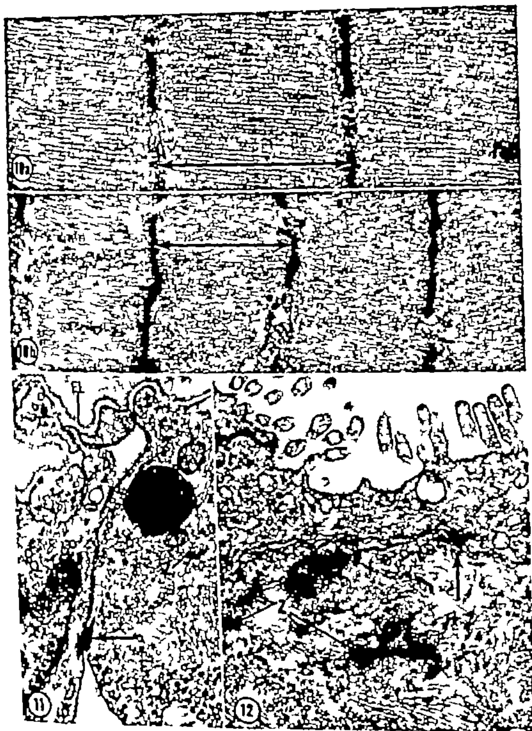

10a
10b
11
12

PLATE 7

EXPLANATION OF FIGURES

13 Snake thymus A cyst in the thymic parenchyma is bounded by epithelial cells provided with an irregular brush border × 14 700

14 Snake thymus Reticular cell containing a cytoplasmic vacuole whose wall is provided with many long microvilli. The cell also contains bundles of tonofilaments (arrows) and is joined by desmosomes (D) to neighboring reticular cells. × 19,000

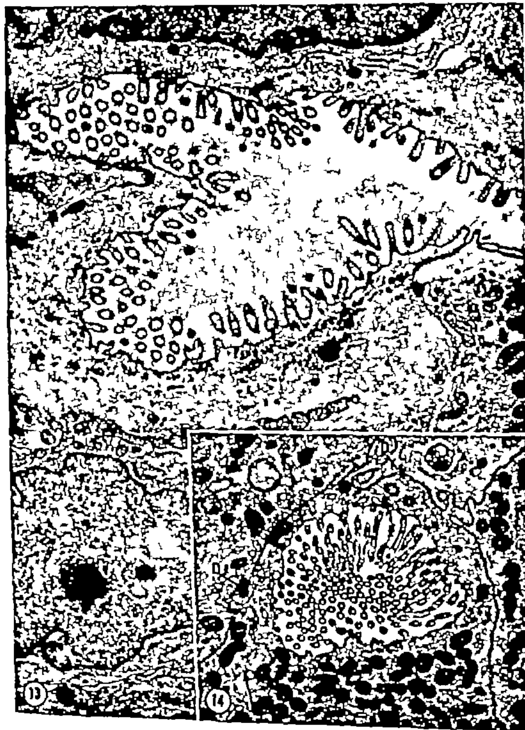

13
14

PLATE 7

EXPLANATION OF FIGURES

13 Snake thymus. A cyst in the thymic parenchyma is bounded by epithelial cells provided with an irregular brush border × 14 700

14 Snake thymus. Reticular cell containing a cytoplasmic vacuole, whose wall is provided with many long microvilli. The cell also contains bundles of tonofilaments (arrows) and is joined by desmosomes (D) to neighboring reticular cells. × 19,000

Fine Structure of Nerves in the Regenerating Limb of the Newt *Triturus* [1]

THOMAS L. LENTZ
Department of Anatomy, Yale University School of Medicine
New Haven, Connecticut

ABSTRACT The structural integrity of some tissues and the regeneration of extremities in some vertebrates depends upon the nervous system. To investigate the structure of nerves exhibiting trophic function, nerves in regenerating forelimbs of adult newts, *Triturus viridescens* were studied with the electron microscope. Nerve fibers sprout from the transected axons, 2–3 days after amputation of the limb and invade all portions of the blastema and epidermis in large numbers. Regenerating nerve fibers contain greatly increased amount of smooth-surfaced channels of endoplasmic reticulum containing moderately dense material, an increased number of microtubules, and large (1000 Å) membrane-bounded dense granules. The latter were not observed normally and could be distinguished from synaptic vesicles and dense-core vesicles thought to contain catechol amines. In larger nerves, the organelles are distributed in the peripheral axoplasm around a central zone containing neurofilaments.

The relationship of the fine structural changes occurring during regeneration to the trophic action of nerves and the regeneration of nerve fibers is discussed. The tortuous membranous tubules of endoplasmic reticulum could serve as channels for the transport of substances, either trophic material or materials necessary for growth of the nerve, down the axon. Microtubules may play role in the regulation of form of the growing axon and also be related to axoplasmic flow or migration of particles (e.g., granules) along their length. The large membrane-bounded dense granules appearing during regeneration resemble neurosecretory granules, which have been associated with regeneration in some invertebrates. These structures could, therefore contain a trophic substance or hormone that is transported down the axon, released into the intercellular spaces, and controls subsequent regeneration of the limb.

The nervous system is necessary for the regeneration of body parts of many invertebrate and vertebrate animals Among invertebrates nerves are essential for the regeneration of portions of hydra (Lentz and Barnett '63) planaria (Child, 10) annelids (Morgan '02) and arthropods (Needham, '52) In vertebrates the regeneration of limbs and tails of larval and adult newts and salamanders, of barbels and fins of fish, and of tails of lizards depends upon the nervous system (see reviews by Singer '52, '60) Although extremities in higher vertebrates including man do not regenerate nerves exert a trophic function as evidenced by the dependence of the structural integrity of structures such as taste buds (Guth, '57) muscle (Tower '39) and other neurons (Bodian, 42) on innervation The trophic effect of nerves arises in the nerve cell body and does not depend upon the functional type of nerve (sensory motor or sympathetic) but instead requires a threshold number of nerve fibers (Singer '52)

Nerves appear to be most important early in regeneration, being necessary for the accumulation of mesenchymatous cells to form a blastema and for the transformation of the blastema into a regenerate with morphogenetic determination (Schotté and Butler 44) Several suggestions have been offered to explain the manner in which nerves exert a trophic influence during regeneration the most widely accepted theory being that the trophic effect is due to release of a chemical substance or neurohumor necessary for regeneration and growth (Singer '52, '60) Little is known, however about the mechanism by which this process might occur or the nature of the postulated chemical or hormone. For example the relationship of basic neuronal processes such as protein synthesis, axoplasmic flow and neurosecretion to trophic activity has not been determined. These or similar processes could be related to the

[1] This work was supported by grant from the National Cancer Institute (TICA-5005), National Institutes of Health, United States Public Health Service.

Fine Structure of Nerves in the Regenerating Limb of the Newt *Triturus* [1]

THOMAS L. LENTZ
Department of Anatomy Yale University School of Medicine
New Haven, Connecticut

ABSTRACT The structural integrity of some tissues and the regeneration of extremities in some vertebrates depends upon the nervous system. To investigate the structure of nerves exhibiting trophic function, nerves in regenerating forelimbs of adult newts, *Triturus viridescens*, were studied with the electron microscope. Nerve fibers sprout from the transected axons, 2–3 days after amputation of the limb, and invade all portions of the blastema and epidermis in large numbers. Regenerating nerve fibers contain a greatly increased amount of smooth-surfaced channels of endoplasmic reticulum containing moderately dense material, an increased number of microtubules, and large (1000 A) membrane-bounded dense granules. The latter were not observed normally and could be distinguished from synaptic vesicles and dense-core vesicles thought to contain catechol amines. In larger nerves, the organelles are distributed in the peripheral axoplasm around a central zone containing neurofilaments.

The relationship of the fine structural changes occurring during regeneration to the trophic action of nerves and the regeneration of nerve fibers is discussed. The tortuous membranous tubules of endoplasmic reticulum could serve as channels for the transport of substances, either trophic material or materials necessary for growth of the nerve, down the axon. Microtubules may play a role in the regulation of form of the growing axon and also be related to axoplasmic flow or migration of particles (e.g., granules) along their length. The large membrane-bounded dense granules appearing during regeneration resemble neurosecretory granules, which have been associated with regeneration in some invertebrates. These structures could, therefore, contain a trophic substance or hormone that is transported down the axon, released into the intercellular space, and controls subsequent regeneration of the limb.

The nervous system is necessary for the regeneration of body parts of many invertebrate and vertebrate animals. Among invertebrates nerves are essential for the regeneration of portions of hydra (Lentz and Barrnett, '63) planaria (Child, '10) annelids (Morgan, '02) and arthropods (Needham, '52). In vertebrates the regeneration of limbs and tails of larval and adult newts and salamanders, of barbels and fins of fish, and of tails of lizards depends upon the nervous system (see reviews by Singer '52, '60). Although extremities in higher vertebrates including man do not regenerate, nerves exert a trophic function as evidenced by the dependence of the structural integrity of structures such as taste buds (Guth, '57) muscle (Tower '39) and other neurons (Bodian, 42) on innervation. The trophic effect of nerves arises in the nerve cell body and does not depend upon the functional type of nerve (sensory motor, or sympathetic) but instead requires a threshold number of nerve fibers (Singer '52)

Nerves appear to be most important early in regeneration being necessary for the accumulation of mesenchymatous cells to form a blastema and for the transformation of the blastema into a regenerate with morphogenetic determination (Schotté and Butler 44). Several suggestions have been offered to explain the manner in which nerves exert a trophic influence during regeneration, the most widely accepted theory being that the trophic effect is due to release of a chemical substance or neurohumor necessary for regeneration and growth (Singer '52 60) Little is known, however about the mechanism by which this process might occur or the nature of the postulated chemical or hormone. For example the relationship of basic neuronal processes such as protein synthesis, axoplasmic flow and neurosecretion to trophic activity has not been determined. These or similar processes could be related to the

[1] This work was supported by grant from the National Cancer Institute (TICA-5085), National Institutes of Health, United States Public Health Service.

production transportation and release of the hypothesized trophic substance The present experiments were undertaken to investigate the trophic activities of the nervous system at the fine structural level

MATERIALS AND METHODS

Adult newts *Triturus viridescens viridescens* and *Triturus viridescens dorsalis* were used with both subspecies yielding identical results Operations were performed on newts anesthetized in MS-222 (tricaine methanesulfonate Sandoz Pharmaceuticals Hanover N J) Limbs were amputated through the lower third of the upper forelimb The protruding end of the humerus was trimmed off following retraction of the muscles The animals were placed on damp paper in covered finger bowls fed chopped beef liver once a week and the limbs allowed to regenerate for 1 3 7 14 21 or 35 days At the end of each period the distal tip of the regenerating limb (epidermis and blastema) was excised for fixation. For study of normal tissues the epidermis and underlying dermis were removed from the limbs of normal newts at the same level at which amputations were performed (upper forelimb)

The excised tissues were immediately placed in cold 5% glutaraldehyde in 0 05 M cacodylate buffer (pH 7 2) for one hour The fixed tissues were rinsed over night in cold buffer and refixed for one hour in cold 1% osmium tetroxide buffered with veronal acetate (pH 7 2) and containing 0 2 M sucrose The tissues were dehydrated in cold ethanol and embedded in Maraglas (Freeman and Spurlock, 62) Sections were cut on a Porter Blum microtome stained with lead hydroxide (Feldman 62) and examined with an RCA EMU 3F electron microscope For light microscopy 1–2 μ plastic sections were cut and stained with 0 1% toluidine blue

OBSERVATIONS

Light microscopic observations

The structure of the epidermis of the newt is similar to that of the frog (Farquhar and Palade 65) The epidermis of the normal limb is 5–6 cell layers thick (fig 2) Nerves are not numerous in the epidermis of the forelimb there are only one or two intraepidermal fibers in each 10 μ cross-section through the upper arm (Singer 49) These nerves usually do not extend beyond the bottom two layers of cells A basement membrane separates the epidermis from the underlying dermis. Nerve fibers in the *stratum spongiosum* of the dermis are unmyelinated and form a plexus which sends branches into the epidermis The *stratum compactum* or deeper layer of the dermis contains larger nerves composed of unmyelinated and myelinated fibers (fig 2) Small nerves leave the larger bundles to enter the superficial dermal plexus

Within 12 hours of amputation of the limb epidermal cells migrate from the edge of the wound to cover the stump. The epidermis increases in thickness so that by ten days after amputation it is 10–12 cell layers thick (fig 3) Nerve fibers in the epidermis increase during regeneration entering singly or in fascicles of 5–10 fibers and extending beyond the basal layers (Singer 49) A basement membrane does not separate the epidermis from the underlying tissues until regeneration is nearly complete In the first 2–3 days following amputation phagocytic cells enter the wound and remove debris. Subsequently connective tissue cells and fibers and capillaries become numerous beneath the epidermis By about eight days these cells are replaced by mesenchymal cells which accumulate to form a blastema (fig 3) These cells are undifferentiated, stellate and widely separated by intercellular material These mesenchymal cells are derived by dedifferentiation from connective tissue cells muscle and cartilage, proximal to the wound (Hay 62) The mesenchymal cells divide rapidly causing the blastema to enlarge Redifferentiation of cartilage and muscle begins at this time and morphogenesis begins during the fourth week. Digits appear during the fifth week and a normal limb forms subsequently

Nerve fibers grow out from the transected nerve stumps at two days (Weiss and Walker '34 Litwiller '38 Singer 49). Unmyelinated fibers branch and invade all portions of the regenerate reaching their highest numbers between 10 and 20 days during the period of most rapid growth of

the regenerate (Singer 49) Later in development, nerve fibers decrease in number, some become myelinated, form functional connections (e.g., with muscle) and reorganize into normal nerve patterns.

Electron microscopic observations

Normal epidermal nerves. Few nerve fibers occur in the epidermis of the normal upper limb. Most of these are situated in the basal strata of the epidermis and are located in intercellular spaces (fig. 4) A few nerves are completely enveloped by the cytoplasm of an epithelial cell (fig. 5) These nerves are intercellular and not truly intraepithelial because the plasma membranes of the nerve and epithelial cell and an intervening intercellular space separate the cytoplasm of the nerve and epithelial cell. The neurites are small and usually less than 1 µ in diameter All are unmyelinated and not enveloped by Schwann cells. The axoplasm is of low density and contains few organelles. Sometimes a small round mitochondrion with two or three cristae is present (fig 4) Some fibers contain small vesicles, 500 Å in diameter with relatively clear contents. Larger vesicles (800 Å) also occur and these have moderately dense contents (dense-core or granular vesicles) (fig. 5) Most nerve fibers contain small irregular granules, 300 Å in diameter presumably particulate glycogen (fig. 5) Microtubules were not observed in the epidermal nerves of normal limbs.

Epidermal nerves of regenerating limbs During regeneration, especially from 3–21 days, neurites are much more abundant in the epidermis adjacent to and extending over the wound surface. They occur in the dilated intercellular spaces which contain amorphous material of low density (figs. 6, 7). Many extend beyond the basal layer into the intermediate layers. These nerves differ in several respects from those of the normal epidermis. The nerves of the regenerating epidermis often occur in small groups of two or three (fig. 6) and may be larger with bulbous enlargements along their length (fig. 7) The most noticeable feature of these nerves is the presence of a large number of smooth-surfaced, membranous channels These structures (described in greater detail in a following section) are ~ 250 Å in diameter contain material of moderate density and pursue a wavy course in the longitudinal axis of the fiber (fig. 7) Microtubules, not seen in normal epidermal fibers, also occur in the regenerating fibers (fig 6). These structures are 200–220 Å in diameter with a core of low density Mitochondria are more elongated, being oval or filamentous (figs. 6 7) Particulate glycogen was not observed during the first 21 days of regeneration. Clear vesicles and dense-core vesicles occur but it could not be determined if these structures are more numerous during regeneration.

Normal dermal nerves Nerve fibers in the superficial dermal plexus occur singly or in small bundles The nerves near the epidermis are unmyelinated and enveloped by a thin layer of Schwann cell cytoplasm (fig. 8) The axoplasm contains a few round or oval mitochondria and neurofilaments but vesicles and microtubules are sparse. A few isolated smooth tubular cisternae with contents of low density occur Other dermal nerves, not nearly as numerous, contain more vesicles (fig 9) The vesicles are either 500 Å in diameter with clear contents or 800 Å in diameter with moderately dense material occupying a central core. These nerves closely resemble adrenergic nerves (Grillo and Palay '62 Richardson, '62; Pellegrino de Iraldi et al., '63)

More deeply situated dermal nerves are larger and composed of several myelinated axons and many unmyelinated axons (fig 10) The axoplasm of the large myelinated nerves is moderately dense and contains mitochondria, neurofilaments large membrane-bounded clear spaces, a few microtubules, and occasionally vesicles. The microtubules are distributed in clusters of 3–5 throughout the axoplasm. The axoplasm of the unmyelinated nerves is less dense than that of the myelinated nerves and contains fewer neurofilaments and microtubules. Mitochondria and glycogen granules are present. A few 800 Å dense-core vesicles and 500 Å clear vesicles occur in the axons (fig. 10)

Nerves within blastema of regenerating limb Nerves were observed in the blastema beneath the epidermis throughout regeneration. Early in regeneration, they

occur singly or in small bundles of two or three fibers and are not enveloped, or only partially covered by Schwann cells The nerves occur in the intercellular spaces and show no consistent relationships to other cell types. Nerves are most numerous in the blastema 21 days after transection (21 days) At this time they occur in large bundles of 5–50 fibers (fig 11) The smaller nerves are contiguous but larger nerve fibers and the entire nerve bundle is loosely enveloped by cytoplasmic proc esses of Schwann cells (fig 12) Nerves are less numerous by 35 days but occur as well defined bundles more completely enclosed by Schwann cells and outer connec tive tissue elements (fig 13)

The nerves of the regenerate differ strik ingly especially at 14–21 days from nor mal dermal nerves Smooth-surfaced cisternae of endoplasmic reticulum (Palay 56) become much more abundant (figs. 11 12) These tubular channels pursue a wavy course but are generally situated in the longitudinal axis of the axon. In small axons they are evenly distributed (fig. 12) but, in large axons they occur in the peripheral regions of the axoplasm (fig 12) The central region of the large axons is occupied by neurofilaments but is other wise nearly devoid of organelles (figs. 12, 13) The smooth-surfaced channels have an irregular diameter (225–300 A) and contain material of medium density (figs. 11 12) Enlargements up to 1000 A in di ameter and with less dense contents sometimes occur along the channels.

Microtubules are also more numerous in regenerating fibers than normal (fig 13) They are distributed evenly in small fibers but in large axons are situated peripherally as is the case with the smooth surfaced channels (figs 12 13) Microtubules could be distinguished from the latter by their smaller diameter (200–220 A) straight course in the axon, thinner walls and centers of low density (fig 12) Neurofilaments are ~ 85 A in diameter (fig 12) Mitochondria, membranous profiles vesicles, and large membrane-bounded granules are situated at the periphery of the axon. These nerves contain many vesicles that are 500 A in diameter with clear or moderately dense contents (fig 11) A few small dense-core vesicles (800 A) are present. By 35 days glycogen particles occur in some nerves (fig. 13)

A membrane-bounded structure, not observed in the normal limb nerves and different from the small clear vesicles and dense-core vesicles, appears during regeneration. These structures are membrane-bounded granules with a diameter of 900–1300 A usually 1000–1100 A (figs. 11 12, 14) The moderately dense material sometimes occupies the entire space within the membrane or more commonly is separated from the membrane by a halo of low density The density of these granules is similar to that of the contents of the membranous channels. The granules occur in the peripheral axoplasm and may be situated adjacent to the plasma membrane of the neurite Some of the large vesicles appear empty Granules or vesicles were not observed in the intercellular spaces The large granules were first observed at three days, are most abundant at 21 days and are less common by 35 days.

Some nerve fibers have terminal swellings or enlargements (fig 14) These swellings are thought to represent growth cones or growing end bulbs. Membranous channels large dense granules, vesicles, neurofilaments and microtubules occur in these enlargements A few mitochondria and dilated apparently empty membranous sacs are also present The channels of smooth endoplasmic reticulum have a more variable diameter in this region, with local distensions and swellings. The channels sometimes appear continuous with the larger membranous sacs large vesicles, or the membrane enclosing dense granules (fig 14) Dense granules are very abundant in the growing end bulbs and are often situated in close apposition to the plasma membrane (fig. 14)

All of the nerves observed in the blastema were unmyelinated and remyelinization did not occur in the time course of this experiment. The large myelinated nerves immediately adjacent to the blastema undergo retrograde degeneration that, in this region does not differ morphologically from Wallerian degeneration. Nerves containing dense-core vesicles and thought to be sympathetic occur in the blastema in small numbers but do not appear to differ from normal.

DISCUSSION

A large number of small unmyelinated nerve fibers grow out from the transected nerves following amputation of the limb and invade the epidermis and blastema of the regenerate. These nerves differ from normal, and the structural changes may be associated with regrowth of the fibers and the trophic action of nerves during regeneration. There are three conspicuous changes in these axons during regeneration. These are an increase in the number of membranous channels of endoplasmic reticulum, increase in number of microtubules and the appearance of large membrane-bounded dense granules. The differences between normal dermal nerves and regenerating blastemal nerves are summarized diagrammatically in figure 1

Abbreviations

BM, basement membrane	NF neurofilaments
C, collagen	Ph, phagocytic cell
Ch, channels (smooth endoplasmic reticulum)	PC, pigment cell
DG, dense granules	S, space
DV dense vesicles	SC Schwann cell
F fibroblast	SCm, stratum compactum
Gly glycogen	SCr, stratum corneum
IS intercellular space	SG, stratum germinativum
M, mitochondria	SGr, stratum granulosum
MA, macula adherens	SS, stratum spinosum
MC, mesenchymal cell	SSp, stratum spongiosum
MN myelinated nerve	SV synaptic vesicles
MT microtubules	V vesicles

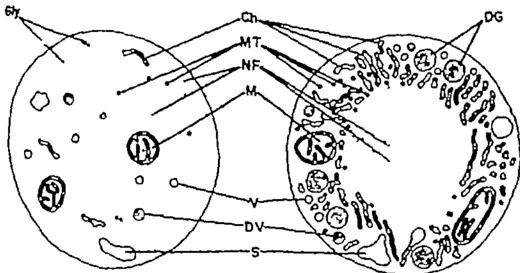


Fig. 1 Diagram comparing a nerve fiber from the dermis of a normal limb and a fiber from the blastema of regenerating limb. The normal nerve contains glycogen (Gly) a few scattered microtubules (MT) and evenly distributed neurofilaments (NF) A few isolated small smooth-surfaced channels (Ch) with clear contents are present. In the nerve fiber from the regenerating limb, the organelles are situated peripherally around a central zone containing neurofilaments (NF) The channels (Ch) are very numerous and contain moderately dense material. Microtubules (MT) are also more numerous than normal. Large (~ 1000 Å) membrane-bounded dense granules (DG) not observed normally are present. Mitochondria (M) membrane-bounded spaces (S) small (500 Å) clear vesicles (V) and larger (800 Å) dense core vesicles (DV) occur in both nerves.

occur singly or in small bundles of two or three fibers and are not enveloped or only partially covered by Schwann cells. The nerves occur in the intercellular spaces and show no consistent relationships to other cell types. Nerves are most numerous in the blastema 21 days after transection (21 days) At this time they occur in large bundles of 5–50 fibers (fig 11) The smaller nerves are contiguous but larger nerve fibers and the entire nerve bundle is loosely enveloped by cytoplasmic processes of Schwann cells (fig 12) Nerves are less numerous by 35 days but occur as well defined bundles more completely en closed by Schwann cells and outer connective tissue elements (fig 13)

The nerves of the regenerate differ strik ingly especially at 14–21 days from nor mal dermal nerves Smooth-surfaced cisternae of endoplasmic reticulum (Palay '56) become much more abundant (figs 11 12) These tubular channels pursue a wavy course but are generally situated in the longitudinal axis of the axon In small axons they are evenly distributed (fig 12) but in large axons they occur in the peripheral regions of the axoplasm (fig 12) The central region of the large axons is occupied by neurofilaments but is other wise nearly devoid of organelles (figs 12 13) The smooth-surfaced channels have an irregular diameter (225–300 Å) and contain material of medium density (figs. 11 12) Enlargements up to 1000 Å in diameter and with less dense contents sometimes occur along the channels.

Microtubules are also more numerous in regenerating fibers than normal (fig 13) They are distributed evenly in small fibers but, in large axons are situated periph erally as is the case with the smooth-surfaced channels (figs 12, 13) Microtubules could be distinguished from the latter by their smaller diameter (200–220 Å) straight course in the axon thinner walls and centers of low density (fig 12) Neurofilaments are ~ 85 Å in diameter (fig 12) *Mitochondria*, membranous profiles vesicles and large membrane-bounded granules are situated at the periphery of the axon These nerves contain many ves icles that are 500 Å in diameter with clear or moderately dense contents (fig 11) A few small dense-core vesicles (800 Å) are present. By 35 days, glycogen particles occur in some nerves (fig. 13)

A membrane-bounded structure not observed in the normal limb nerves and different from the small clear vesicles and dense-core vesicles appears during regeneration These structures are membrane-bounded granules with a diameter of 900–1300 Å usually 1000–1100 Å (figs. 11 12, 14) The moderately dense material sometimes occupies the entire space within the membrane or more commonly is separated from the membrane by a halo of low density The density of these granules is similar to that of the contents of the membranous channels. The granules occur in the peripheral axoplasm and may be situated adjacent to the plasma membrane of the neurite. Some of the large vesicles appear empty Granules or vesicles were not observed in the intercellular spaces The large granules were first observed at three days, are most abundant at 21 days and are less common by 35 days.

Some nerve fibers have terminal swellings or enlargements (fig 14) These swellings are thought to represent growth cones or growing end bulbs. Membranous channels large dense granules vesicles neurofilaments and microtubules occur in these enlargements A few mitochondria and dilated apparently empty membranous sacs are also present The channels of smooth endoplasmic reticulum have a more variable diameter in this region with local distensions and swellings The channels sometimes appear continuous with the larger membranous sacs large vesicles, or the membrane enclosing dense granules (fig 14) Dense granules are very abundant in the growing end bulbs and are often situated in close apposition to the plasma membrane (fig 14)

All of the nerves observed in the blastema were unmyelinated and remyelinization did not occur in the time course of this experiment. The large myelinated nerves immediately adjacent to the blastema undergo retrograde degeneration that, in this region does not differ morphologically from Wallerian degeneration Nerves containing dense-core vesicles and thought to be sympathetic occur in the blastema in small numbers but do not appear to differ from normal.

tubules seemed to terminate as vesicular distensions or in the membrane enclosing the dense granules.

Growing end bulbs have been described during regeneration of the sciatic nerve of rabbits (Blümcke and Niedorf '65; Blümcke et al., '68). Vesicles and tubules of endoplasmic reticulum were described. The latter were considered to develop from neurofilaments which were thought to swell into thicker tubules and develop spindle-shaped distensions and vesicular expansions. The vesicular expansions then broke apart to form solitary vesicles. In the present study distensions were also observed along the channels of smooth endoplasmic reticulum and it appears that these could give rise to free vesicles. However the origin of the channels from neurofilaments could not be confirmed.

Microtubules also are abundant in regenerating axons. Although several functions have been suggested for these structures, there appears to be a consistent relationship between microtubules and a supportive role that confers form (Tilney and Porter '65; Gibbins et al. '66) on the one hand, and cytoplasmic streaming (Ledbetter and Porter, '63; Tilney and Porter, '65) or migration of particles (Bickle et al., '66; Lentz, '67) on the other. The increase in microtubules during regeneration, therefore, could be associated with both the outgrowth of the axons providing support or regulating form, and the flow of axoplasm or vesicles down the growing fiber. In the larger nerves the microtubules are located peripheral to a central zone of axoplasm containing primarily neurofilaments. Vesicles, granules and other organelles are distributed in the outer cortex. It seems reasonable to suppose that the microtubules delineate a relatively rigid central area of the axon, providing support for the outgrowing fiber, from an outer area in which there is more rapid streaming or migration of axoplasm and organelles. Microtubules as well as membranous channels could be associated with either regeneration or trophic function. If microtubules play a role in streaming, however, it seems likely they are related to both processes, because, in either case newly synthesized material flows down the axon.

It is difficult to separate those changes associated with trophic activity from those related to regeneration because, in most situations where there is regeneration of nerve fibers there will also be a trophic effect on the previously denervated structures that are being reinnervated. One means of distinguishing these processes might be study of growing nerves during normal development, before the tissues become dependent on innervation. In this regard, immature axons contain a large number of microtubules (Gonatas and Robbins, '64; Peters and Vaughn '67) which supports the notion that these structures confer form on the outgrowing axons.

Regeneration of the limb in newts is dependent upon the nervous system (Singer '52). The present studies indicate that, if a trophic substance is produced by neurons it could be transported down the axon either within greatly proliferated smooth membranous channels or as large membrane-bounded granules. The latter seem *more significant in relation to trophic* activity because packaging in granules is the mechanism usually employed by cells exporting a product. Furthermore these granules resemble neurosecretory granules, which have been associated with regeneration in other forms. This material may be the morphological counterpart of the trophic substance or hormone that is necessary for regeneration.

LITERATURE CITED

Bickle, D., L. G. Tilney and K. R. Porter 1966 Microtubules and pigment migration in the melanophores of *Fundulus heteroclitus* L. Protoplasma, *61*: 322–345.

Blümcke, S., and H. R. Niedorf 1965 Elektronenoptische Untersuchungen an Wachstumsendkolben regenerierender peripherer Nervenfasern. Virchows Arch. Path. Anat., *340*: 93–104.

Blümcke, S., H. R. Niedorf and J. Rode 1966 Axoplasmic alterations in the proximal and distal stumps of transected nerves. Acta Neuropath., *7*: 44–61.

Bodian, D. 1942 Cytological aspects of synaptic function. Physiol. Rev., *22*: 146–169.

Bunge, R. P., M. P. Bunge and E. R. Peterson 1965 An electron microscope study of cultured rat spinal cord. J. Cell Biol., *24*: 163–191.

Child, C. M. 1910 The central nervous system as a factor in the regeneration of polyclad Turbellaria. Biol. Bull., *19*: 333–338.

The functional type of nerve fiber observed in the regenerate was generally not known Presumably most are sensory because the ratio of sympathetic to motor to sensory fibers in the upper limb is approximately 1:6:22 (Singer 46) Some of the fibers growing into the epidermis must be sensory because the regenerate is sensitive (to a greater degree than the normal limb) to mechanical stimulation (Singer 49) Fibers containing 800 A dense-core vesicles are presumed to be sympathetic and do not appear to change in number or appearance during regeneration

Large membrane-bounded granules with a diameter of 900–1300 A occur during regeneration but were not observed in normal fibers These granules which are larger than synaptic vesicles and dense-core vesicles closely resemble neurosecretory granules in size and density Neurosecretion has been associated with regeneration in several invertebrates including hydra (Lentz, 65a 65b) planaria (Lender and Klein '61) and annelids (Clark et al 62) In transected hydra neurosecretory granules are released by nerves at the site where a head will appear (Lentz '65a) and exogenous administration of isolated granules induces supernumerary head formation (Lentz, 65b) It was suggested that, in hydra, neurosecretory granules contain a growth-stimulating or form-regulating substance Similarly it is possible that the membrane-bounded granules appearing during limb regeneration of the newt contain a trophic substance or hormone that is released into the intercellular spaces and controls subsequent regeneration of the limb

Vesicles are present in regenerating axons but do not appear to increase in number significantly Glimstedt and Wohlfart (60) Hay ('60) Blümcke and Niedorf (65) and Blümcke et al. (66) also noted the presence of vesicles in regenerating nerve fibers The small vesicles (500 A) with clear contents are probably synaptic vesicles containing acetylcholine (DeRobertis et al 63 Whittaker et al. '64) and the slightly larger vesicles (800 A) with dense contents may contain adrenergic transmitters (Pellegrino de Iraldi and DeRobertis '63 VanOrden et al '66) It has been suggested that acetylcholine exerts a trophic effect (Welsh 46) Evidence for a role of acetylcholine in regeneration includes the observations that regeneration is inhibited by blocking agents (e.g., atropine) of acetylcholine substances that protect or mimic the action of acetylcholine (e g physostigmine) do not interfere with regeneration acetylcholine is present in greater than normal amounts during the time nerves are playing their most significant role (first 21 days) and decreases thereafter; and the concentration of acetylcholinesterase bears an inverse relationship to that of acetylcholine (Singer '60) On the other hand regeneration of denervated limbs cannot be sustained by infusion of acetylcholine acetylcholine is present in denervated limbs; and sensory fibers which contain little acetylcholine in comparison to motor fibers, can sustain regeneration in the absence of other fibers (Singer '60) On these bases Singer ('60) concluded that acetylcholine is not responsible for regeneration. Little attention has been paid to adrenergic substances because destruction of sympathetic fibers does not influence regenerative capacity (Singer 42) Although the evidence suggests that regeneration is not controlled by cholinergic and adrenergic transmitters these substances should not be completely ruled out and perhaps deserve additional study in view of their well known effects on membrane potential and permeability

Membranous tubules of the smooth endoplasmic reticulum become extremely abundant in the regenerating axons and contain moderately dense material. It seems possible that they could serve as channels for the transport of substances down the axon as suggested by Hay ('60) and Bunge et al (65) especially since dense material occurs within the cisternae If this system of tubular channels is associated with synthesis or transport of substances during regeneration these materials may be associated with either growth of the axon or trophic activity The density and texture of the dense material within these channels closely resembles that of the large membrane-bounded granules. It is not known whether this similarity is coincidental or whether there is any relationship between the two structures but, in a few cases membranous

Webb, J. E. 1946 Evidence of a trophic action of acetylcholine in a planarian. Anat. Rec., 94: 421.

Whittaker, V. P., I. A. Michaelson and R. J. A. Kirkland 1964 The separation of synaptic vesicles from nerve ending particles ("Synaptosomes") Biochem. J., 90: 293–303.

Clark, R. B., M. E. Clark and R. J G Ruston 1962 The endocrinology of regeneration in some errant Polychaetes. In: Neurosecretion. H. Heller and R. B Clark, eds. Academic Press New York, pp 275–286.

DeRobertis E., A. R. de Lores Arnaiz, L. Salganicoff A. Pellegrino de Iraldi and L. M. Zieher 1963 Isolation of synaptic vesicles and structural organization of the acetylcholine system within brain nerve endings J Neurochem., 10: 225–235

Farquhar M. G., and G E. Palade 1965 Cell junctions in amphibian skin. J Cell Biol., 26 263–291

Feldman D G 1962 A method of staining thin sections with lead hydroxide for precipitate-free sections J Cell Biol. 15: 592–595

Freeman J A., and B O Spurlock 1962 A new epoxy embedment for electron microscopy J Cell Biol. 13: 437–443

Gibbins, J R. L. G. Tilney and K. R. Porter 1966 Microtubules in primary mesenchyme cells of sea urchin embryos. Anat. Rec. 154: 347

Glimstedt, G and G Wohlfart 1960 Electron microscopic studies on peripheral nerve regeneration. Lunds Univ Arsskr., N.F., Avd. 2, Bd. 56 Nr 16: 1–22.

Gonatas N K. and E. Robbins 1964 The homology of spindle tubules and neuro-tubules in the chick embryo retina. Protoplasma, 59: 377–391

Grillo M. A., and S. L. Palay 1962 Granule containing vesicles in the autonomic nervous system. Fifth Intern. Cong. Electron Microscopy Academic Press, New York, Vol. 2, U–1

Guth, L. 1957 The effects of glossopharyngeal nerve transection on the circumvallate papilla of the rat. Anat. Rec., 128: 715–732.

Hay E. D 1960 The fine structure of nerves in the epidermis of regenerating salamander limbs. Exp Cell Res., 19: 299–317

——— 1962 Cytological studies of dedifferentiation and differentiation in regenerating amphibian limbs. In: Regeneration. D Rudnick, ed. Ronald Press New York, pp 177–210.

Ledbetter M. C., and K. R. Porter 1963 A "microtubule" in plant cell fine structure. J Cell Biol. 19: 239–250.

Lender T., and N Klein 1961 Mise en évidence de cellules sécrétrices dans le cerveau de la Planaire *Polycelis nigra*. Variation de leur nombre au cours de la régénération posterieure. C. R. Acad. Sci., Paris, 253: 331–333

Lentz, T L. 1965a Fine structural changes in the nervous system of the regenerating hydra. J Exp. Zool., 159: 181–194

——— 1965b Hydra: Induction of supernumerary heads by isolated neurosecretory granules. Science 150: 633–635.

——— 1967 Rhabdite formation in planaria: The role of microtubules. J Ultrastruct. Res., 17: 114–126.

Lentz, T L., and R. J Barrnett 1963 The role of the nervous system in regenerating hydra: The effect of neuropharmacological agents. J Exp. Zool., 154: 305–328.

Litwiller R. 1938 Quantitative studies on nerve regeneration in amphibia. II. Factors controlling nerve regeneration in regenerating limbs. J Exp. Zool. 79: 377–397

Morgan, T H. 1902 Experimental studies of the internal factors of regeneration in the earthworm. Roux Arch. Entwicklungsmech. Org., 14 563–591

Needham, A. E. 1952 Regeneration and Wound Healing. Methuen, London.

Palay S L. 1956 Synapses in the central nervous system. J Biophys. Biochem. Cytol., 2, Suppl., pp. 193–202.

Pellegrino de Iraldi, A., and E. DeRobertis 1963 Action of reserpine, iproniazid and pyrogallol on nerve endings of the pineal gland. Int. J Neuropharm., 2: 231–239

Pellegrino de Iraldi, A., H. F Duggan and E. DeRobertis 1963 Adrenergic synaptic vesicles in the anterior hypothalamus of the rat Anat. Rec., 145 521–531

Peters, A., and J E. Vaughn 1967 Microtubules and filaments in the axons and astrocytes of early postnatal rat optic nerves. J Cell Biol., 32: 113–119

Richardson, K. C. 1962 The fine structure of autonomic nerve endings in smooth muscle of the rat vas deferens. J Anat., Lond., 96: 427–442.

Schotté O E., and E. G. Butler 1944 Phases in regeneration of the urodele limb and their dependence upon the nervous system. J Exp. Zool., 97: 95–121.

Singer M. 1943 The nervous system and regeneration of the forelimb of adult *Triturus*. I. The role of the sympathetics. J Exp. Zool., 90: 377–400.

——— 1946 The nervous system and regeneration of the forelimb of adult *Triturus* V The influence of number of nerve fibers, including a quantitative study of limb innervation. *J Exp* Zool., 101: 299–338

——— 1949 The invasion of the epidermis of the regenerating forelimb of the urodele *Triturus* by nerve fibers. J Exp. Zool., *111*: 189–210

——— 1952 The influence of the nerve in regeneration of the amphibian extremity *Quart.* Rev Biol., 27: 169–200

——— 1960 Nervous mechanisms in the regeneration of body parts in vertebrates. In: Developing Cell Systems and their Control. D. Rudnick, ed. Ronald Press, New York, 115–133.

Tilney L. G and K. R. Porter 1965 Studies on microtubules in Heliozoa. I. The fine structure of *Actinosphaerium nucleofilum* (Barrett) with particular reference to the axial rod structure Protoplasma 60 317–344

Tower S S 1939 The reaction of muscle to denervation Physiol. Rev 19 1–48.

VanOrden, L. S., F E. Bloom R. J Barrnett and N J Giarman 1966 Histochemical and functional relationships of catecholamines in adrenergic nerve endings. I. Participation of granular vesicles. J Pharm. Exp. Ther., *154*: 185–199

Weiss P., and R. Walker 1934 Nerve patterns in regenerated urodele limbs. Proc. Soc. Exp Biol. Med. 31 810–812.


SS
SGr
SG
BM
SCr
PC

PLATE 1

EXPLANATION OF FIGURE

2 Epidermis and dermis from the upper arm of a normal newt. The epidermis is 5–8 cell layers thick and consists of an outer *stratum corneum* (SCr) of flattened cornified cells, *stratum granulosum* (SGr) *stratum spinosum* (SS) and a basal *stratum germinativum* (SG) A basement membrane (BM) separates the epidermis from the dermis. Pigment cells (PC) or melanophores occur below the basement membrane. The superficial layer of the dermis or *stratum spongiosum* (SSp) is composed of loosely arranged connective tissue fibers and cells and contains small blood vessels, pigment cells, and fat cells. Large glands occur in the *stratum spongiosum* The deeper *stratum compactum* (SCm) contains more densely packed connective tissue fibers. A large nerve with myelinated fibers (MN) is situated in the *stratum compactum* SC, Schwann cell. × 1 130

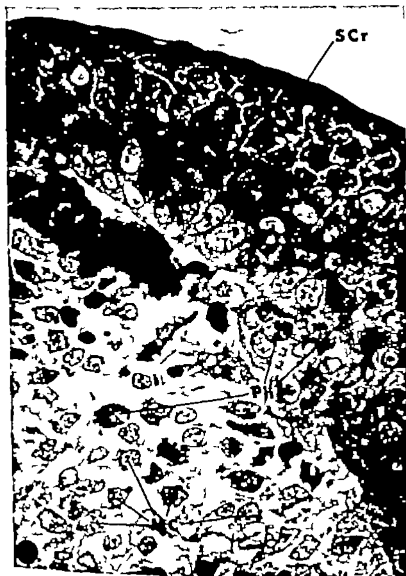

SCr
P

PLATE 2

EXPLANATION OF FIGURE

3 Epidermis and underlying blastema 21 days after amputation of the limb The epidermis is considerably thicker than normal The cells of the basal layer (SG) are large and densely packed. A basement membrane is lacking between the epidermis and blastema The blastema is composed of irregularly shaped mesenchymal cells (MC) with fine cytoplasmic processes The cells are separated by large *amounts of* intercellular ground substance A few phagocytic cells (Ph) occur in the epidermis and blastema A cluster of densely staining erythrocytes is situated beneath the epidermis. SCr *stratum corneum* × 790.


SCr
P

PLATE 2

EXPLANATION OF FIGURE

3 Epidermis and underlying blastema 21 days after amputation of the limb The epidermis is considerably thicker than normal The cells of the basal layer (SG) are large and densely packed. A basement membrane is lacking between the epidermis and blastema The blastema is composed of irregularly shaped mesenchymal cells (MC) with fine cytoplasmic processes The cells are separated by large amounts of intercellular ground substance A few phagocytic cells (Ph) occur in the epidermis and blastema A cluster of densely staining erythrocytes is situated beneath the epidermis SCr *stratum corneum* × 790







7

PLATE 3

EXPLANATION OF FIGURES

4 Epidermal nerve of normal limb. The nerve is situated in the intercellular space. The axoplasm is of low density and contains a small mitochondrion (M) MA *macula adhaerens* × 41,500.

5 Epidermal nerve of normal limb. The nerve appears to be completely enveloped by an epithelial cell A narrow intercellular space (IS) separates the plasma membrane of the axon from that of the epithelial cell. A "mesaxon" appears to be lacking which indicates that the nerve passes through a tunnel in the epithelial cell. The axoplasm is of low density and contains glycogen particles (Gly) Small (500 Å) vesicles with clear contents (V) and larger (800 Å) vesicles with a dense core (DV) are present × 46,000

6 Group of three nerves in the epidermis of a 35-day regenerate The nerves occur in the intercellular space and contain mitochondria small vesicles (V) with moderately dense contents, microtubules (MT) and smooth-surfaced channels (Ch) × 52,000.

7 Epidermal nerve of a 21-day regenerate. One region (bottom) of the fiber is enlarged. The axoplasm is denser than normal and contains many smooth-surfaced channels pursuing a wavy course roughly in the longitudinal axis of the nerve. Moderately dense material occurs within the cisternae of these structures. Mitochondria are abundant and are oval or elongated in shape. A few small vesicles and larger dense-core vesicles (arrows) are present. × 30 000

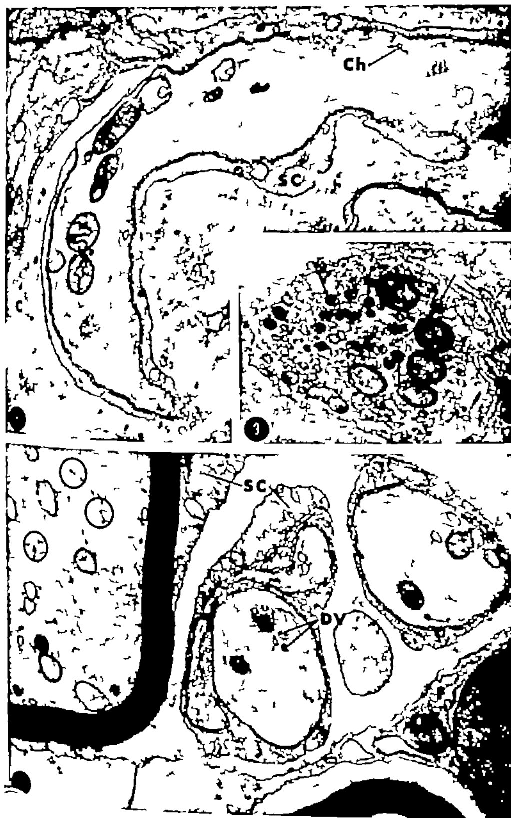

Ch
SC
C
SC
DV

PLATE 4

EXPLANATION OF FIGURES

8 Unmyelinated nerve in the *stratum spongiosum* of the normal dermis. The fiber is enveloped by Schwann cell (SC) cytoplasm and contains neurofilaments, mitochondria and large membrane-bounded spaces. A few small smooth membranous channels (Ch) are present. C, collagen. × 28,500.

9 Small unmyelinated nerve in the dermis of a normal limb. The axon contains small (500 Å) vesicles with relatively clear contents and larger (800 Å) vesicles with dense contents (arrows) Mitochondria and glycogen granules are present. × 45,500

10 Myelinated and unmyelinated fibers from a large deeply situated nerve bundle of a normal limb The myelinated axon contains mitochondria membrane-bounded spaces, and microtubules occurring in small clusters (circles) Neurofilaments are evenly distributed in the axoplasm. The small unmyelinated fibers contain mitochondria membrane-bounded spaces a few neurofilaments, glycogen and dense-core vesicles (DV) Microtubules are sparse SC Schwann cell F fibroblast of the endoneurium × 31 000.

SC
M
M
Ch
S
NF
S
Ch
MT
SC

PLATE 5

EXPLANATION OF FIGURES

11 Nerves within the blastema of a 21-day regenerate. A large number of individual fibers, most of them not completely enveloped by Schwann cells, comprise the nerve bundle The axons contain irregular tubular profiles with moderately dense contents mitochondria clear spaces and small vesicles A number of membrane-bounded dense granules, (900–1300 A in diameter) are present (arrows) Compare with figure 7 × 45,500

12 Unmyelinated nerves in the blastema of a 21-day regenerate. The smaller fibers (left) are not completely enveloped by Schwann cell (SC) cytoplasm while the large axon (right) is completely surrounded The axons contain mitochondria (M) membrane-bounded spaces (S) microtubules (MT) neurofilaments (NF) membranous tubular channels (Ch) and large dense granules (arrows) The membranous channels contain material of medium density The channels have a greater diameter thicker walls and denser contents than microtubules Note that, in the large axon the organelles are located in the periphery of the axoplasm external to a central core of filaments. In all fibers, some of the dense granules are situated near the plasma membrane. Compare with figure 7 × 45,000


SC
NF
MT
MT
Gh
Gly
MT

PLATE 6

EXPLANATION OF FIGURE

13 Nerve bundle in the blastema of a 35-day regenerate. These unmyelinated nerves contain mitochondria microtubules (MT) membranous channels (Ch) and a few dense granules (arrows) One axon contains glycogen particles (Gly) Note that, in the larger fiber (top) neurofilaments (NF) occupy a central region of the axoplasm that is of low density and is nearly devoid of organelles. Microtubules, mitochondria, channels and granules are situated in an outer cortex where the axoplasm is denser Schwann cell (SC) cytoplasm partially encloses the nerve bundle × 48 000


S
S
11

PLATE 7

EXPLANATION OF FIGURE

14 Growth cone or growing end bulb. The nerve fiber enters the field from the left (between lines) and terminates as a large swelling. A few mitochondria, large membrane-bounded spaces (S) neurofilaments, and microtubules are present. The smooth channels of endoplasmic reticulum contain moderately dense material and have an irregular diameter. The channels appear to form connections with vesicles, large dilatations, or the membrane enclosing dense granules (small arrows). Dense granules are numerous in the end bulb and some occur in very close proximity to the plasma membrane (large arrows). × 36,500

The Relationship of Nucleotidase Activity to Catecholamine Storage Sites in Adrenomedullary Tissue [1]

JOE C. WOOD

Department of Anatomy The University of Arkansas Medical Center Little Rock, Arkansas

ABSTRACT Tissues were either fixed in 3% glutaraldehyde and treated histochemically to demonstrate nucleotidephosphatase activity and catecholamines or in 2.5% potassium dichromate (pH 4.1) for demonstration of catecholamines. Frozen sections (10 μ) were examined with the light microscope or following the histochemical procedures 1 mm cubes of tissue were treated with 1% OsO_4 and prepared for electron microscopy

Light microscopy demonstrates groups of norepinephrine cells in adrenal medullary tissue of cats and rats. Nucleotidetriphosphatase activity is found along nerve fibers, between epinephrine cells and concentrated in norepinephrine cell areas. The same is true for diphosphatase localization but with less intense activity Nucleotidemonophosphatase activity is located primarily at the site of norepinephrine cells.

Electron microscopy shows triphosphatase activity along membranes of chromaffin cells and nerve fibers, at canaliculi and nerve terminals, and in sinusoidal cells. Diphosphatase activity is present at similar sites and shows some intracellular activity Monophosphatase activity is present at cell membranes and intracellularly appears closely related to catecholamine storage granules. It is postulated that since nucleotides are apparently instrumental in the binding of catecholamines, nucleotidephosphatase action effects a mechanism of catecholamine release from the storage sites and permits passage through the cell membranes.

Electron microscopic studies of the adrenal medulla have been performed by a number of workers. Some of these investigations have been carried out using osmium tetroxide (de Robertis and Ferreira '57; Eränkö and Hanninen, '60 Yates et al., '62 Yates, '64a Benedeczky et al. '65) some using glutaraldehyde followed by osmium tetroxide (Coupland and Hopwood '66) and others using more specific methods for the localization of norepinephrine-containing cells (Tramezzani et al. '64 Wood and Barrnett, '63 '64) In one instance one of the methods (Wood and Barrnett, '63, '64) was modified and used for the electron microscopic localization of catecholamines (CAMs) in the central nervous system, and the stoichiometric nature of the identifying reaction was established (Wood, '66a) Investigations of this nature should lead to a functional appraisal of the adrenomedullary cells and their two main CAMs, epinephrine (E) and norepinephrine (NE) Functional studies using stimulation of the nerve supply to the adrenal (de Robertis and Ferreira, '57) and drug studies using reserpine (Yates, '64b) have been conducted however due to the different methods of approach and the types of animals used, correlation of the findings is difficult. Also to date no functional studies have been done utilizing the more specific methods of CAM localization.

The relationship of the adenine nucleotides especially adenosinetriphosphate (ATP) to CAMs in the storage granules of the adrenal medulla (Hillarp et al. '59; Blaschko and Helle '63) and in nerve terminals (von Euler et al '63) has been the foundation for the recent hypothesis advanced about CAM storage sites (Colburn and Maas '65) This apparently workable scheme provides the hypothesis whereby a phosphate-splitting enzyme is instrumental in the release of the CAM from the storage granule and/or the cell. Chemical work has been done on the phosphatases of the

[1] This investigation was supported by USPHS grant [illegible] and National Science Foundation grant [illegible].

[2] Present address Department of Anatomy The University of Texas Medical School at San Antonio, 7[illegible] [illegible] Drive, San Antonio, Texas 78[illegible].

intermediate type of reaction between TPase and MPase with the activity being located at the cellular level as well as along nerve fibers, canaliculi and intercellular areas.

All histochemical reactions run on unfixed tissue sections produced similar results to those seen in fixed tissues however the degree of reactivity was much greater with the former but the preservation of the tissue was not adequate. Additional controls run in the lead nitrate incubation medium without substrate and treated with ammonium sulfide produced no demonstrable reactions. All confirming reactions were performed for light microscopy only

CAM localization is shown in figure 1 which is a frozen section from cat adrenal medulla fixed in the potassium dichromate mixture for four hours. The phase contrast micrograph shows dark NE cells with large granules and the more homogeneous and lighter appearing E cells. Rat medullary tissue presented similar results. Glutaraldehyde-dichromate-treated tissue presents a similar picture; however the E cells do not have a granular appearance as those in figure 1 This has been reported previously (Wood and Barrnett, '63 '64) Figures 2 and 3 show TPase and MPase activity respectively in rat adrenomedullary tissue, with the NPase activity being confined to the areas previously described. It is to be pointed out in figure 2 that there is a considerable degree of concentrated TPase activity in the NE cell areas. This is also true for DPase activity while the MPase activity (fig. 3) is confined primarily to the NE cells alone. Electron microscopic studies of the detailed localization of CAMs are shown in figures 4 and 5 Figure 4 shows the effect of the potassium dichromate (pH 4 1) incubation following glutaraldehyde in the rat. The NE granules are extremely dark and are more dense than those of the E cells. There is a greater degree of artifact at the NE loci as compared to the E stores which is often the case. NE localization is in agreement with other works (Tramezzani et al., '64; Wood and Barrnett, '63, '64; Coupland and Hopwood, '66) however figure 5 demonstrates a mixed type of cell which appears to be an E cell that contains a number of NE granules. This type of reaction was seen in both rat and cat material. Figure 6 represents a photograph taken from tissue treated for MPase activity but which showed no direct enzymatic activity This tissue was treated with OsO following incubation and defines the E and NE cells with the osmium-glutaraldehyde reaction as described by Coupland and Hopwood ('66) It is to be observed in this micrograph and in figure 4 that, not only are the NE granules darker but that they are of a myriad of sizes, the smallest of which are of a size that is not seen in E cells. This is another method by which NE cells may be differentiated from E cells when the specific dichromate method is not employed. The minute-sized granules were found in both cat and rat material. Even smaller NE-positive granules were found in E cells (fig. 4)

No effort was made to separate E and NE cells on the basis of light and dark cells with the methods employed. Generally it was observed that E cells appear as both "light" and dark" types; however no "dark NE cells were seen. There appears to be little difference between light and dark cells except for electron opacity in the cytoplasmic area between the granules and the other cell organelles. This area is extremely compact and appears to contain more free ribosomal material.

Electron microscopic studies of NPases present a close correlation with what is seen in the light microscope. With the light microscope (fig. 2) TPase activity is concentrated around the NE cells and at the borders of the E cells. Electron microscopically TPase activity is not as easily demonstrated as other NPase reactions. Figure 7 shows TPase activity on the surface of an endothelial cell while figure 8 demonstrates the same activity along an unmyelinated nerve fiber and an adjacent chromaffin cell. Neither preparation was stained on the grid thus, there is a lack of contrast and organelle definition. Figure 9 depicts TPase reactivity at the border of a chromaffin cell and within a canaliculus. The small granules within the cell identify this as an NE cell and there is an indication that there is some degree of TPase activity at the granule membrane level. DPase activity follows the same pattern of distribution as that of TPase with

adrenal medulla (Banks 65 Hagen and D'Iorio '65) however only two abstracts (Wood 65–66b) relate this enzyme to specific adrenomedullary cells The need for this study of adrenomedullary tissue which relates CAM sites to nucleotidephosphatase (NPase) enzymes is apparent especially as a prelude to forthcoming functional studies

MATERIALS AND METHODS

Adult male rats were sacrificed by decapitation and adult cats were sacrificed by intrathoracic injections of nembutal. Adrenal glands were removed sliced and fixed for four hours in cold 3% glutaralde hyde in 0 2 M sodium cacodylate buffer (pH 7 2) Portions of fixed adrenomedul lary tissues were dissected into 1 mm cubes Half the cubes were rinsed for four hours in the cacodylate buffer before being transferred to a cold (4 C) potassium dichromate incubation medium which consisted of 2 5% potassium dichromate and 2% sodium sulfate in a 0 2 M acetate buffer at pH 4 1 for 6–24 hours. The remaining cubes were rinsed overnight in cold 0 2 M tris-maleate buffer (pH 7 2) Following the rinse these cubes were incubated in a cold (4 C) Wachstein Meisel (57) medium for 30 minutes After the two kinds of incubations alternate cubes were rinsed in the respective cold buffers and one-half the cubes from each incuba tion were treated with osmium tetroxide (OsO_4) (Luft 61) for two hours All cubes were dehydrated in ethanol at room tem perature and embedded in Epon Sections were made on an LKB Ultratome and selected grids were stained first with uranyl acetate and then lead citrate (Kim 66) Examinations and micrographs were made with a Siemens IA electron microscope

Control sections from each adrenal gland were prepared in order to test the validity of each reaction These controls consisted of fresh unfixed tissue which was treated with the potassium dichromate medium for six hours sectioned on a freezing mi crotome at 10 μ mounted on glass slides and covered with glycerine jelly and cover slips Fresh unfixed tissue sections were incubated with the complete NPase media treated with ammonium sulfide mounted with glycerine jelly and covered with glass coverslips. Glutaraldehyde-fixed tissues were sectioned incubated in the NPase media minus the substrate for 30 minutes treated with ammonium sulfide, mounted and covered as above Glutar aldehyde-fixed tissues were also sectioned, treated with the potassium dichromate incubation medium and mounted as the preceding sections Light microscopy and photomicrography were done with a Zeiss Universal Photomicroscope

RESULTS

The histochemical localization of CAMs in all animals agrees wth previous findings (Hillarp 55 Eränkö 55 Wood '63) NPase activity is dependent on the substrate employed. When adenosine triphosphate (ATP) is used as a substrate to demonstrate adenosinetriphosphatase ac tivity the reaction is largely confined to the intercellular areas, i e cell membranes, canaliculi and to the nerve fibers As a confirmation of the triphosphatase (TPase) activity inosinetriphosphate cytosinetriphosphate and guanosinetriphosphate were also used as substrates All three triphosphate substrates lead to reactions in the same areas as those seen when ATP is employed Cytosinetriphosphate produces a strong reaction with the same localization as ATP and the reaction is at the maximum within a 20-minute incubation time Inosinetriphosphate produces an adequate reaction within 30 minutes however guanosinetriphosphate produces reactions that are poor The reactions that did occur showed the same reactive areas as those found with ATP

Adenosinemonophosphate (AMP) was used as a substrate to show monophosphatase (MPase) enzymatic activity which was confirmed by the use of inosinemonophosphate MPase reactions are either confined to the intracellular areas of the norepinephrine (NE) cells or to the membranes of the NE cells Light microscopy in this instance could not be used to localize MPase activity with respect to cell structures. Diphosphatase (DPase) was demonstrated by both adenosinediphosphate (ADP) and inosinediphosphate with the ADP being the substrate of choice due to the fact that it gave a more rapid reaction DPase activity demonstrated an in-

ates a reduction of chromate however, the possibility of a chelate complex of a heavy metal with the Schiff base as discussed by Smith ('63) still exists. It is evident that the final reaction product needs to be analyzed and defined. The mechanism of the dichromate reaction (Wood, '63) and the glutaraldehyde dichromate reactions (Wood and Barrnett, '63 '64) are apparently different as indicated (Wood, '64a) however, both have their use in experimental work, and either or both may eventually have use as *quantitative* procedures. The simple dichromate procedure presented here is easily usable and has been used in the past on a number of different animals (Bell, '65) at the light microscopic level. The electron microscopic method can be used at both the light and electron microscopic levels. NE localization in figure 4 shows the characteristic NE granules as demonstrated by Tramezzani ('64) and Wood and Barrnett ('63 '64). It is to be noted that the NE granules are not consistently larger than the E granules, since some of the NE-positive stores measure as small as 120 A. It is possible that these microgranules may be responsible for the second pool or presumably nongranular pool of CAMs as presented by workers in the chemical areas (Bertler et al., '60) These microgranules" were seen in both the cat and the rat and even smaller similar reacting granules are visualized in the E cells as well (fig. 4) The other type of granules seen in the E cells of figure 5 indicates that NE may occur in E cells in more than one form, i.e., microgranules (fig. 4) and the regular-sized granules (fig. 5) of the E cells. Figure 6 shows, as did Coupland and his co-workers ('58) that a specific cytochemical reaction is not necessary for the determination of NE cells. This micrograph demonstrates that the microgranules are different in size than those of the E cells; therefore an NE cell may be differentiated in more than one way and these cells are definitely different in their granular components. Further study of the microgranules could be done by determining the effect of stress or very small doses of CAM-depleting drugs, such as reserpine on these microgranules. In this way one might determine whether the microgranule stores are more labile than those of the regular or "classical" granules Such experiments are currently being initiated and may produce results which will clarify discussions of the past concerning granule size and the type of CAM present (Benedeczky et al. '66)

As mentioned this investigation does not attempt to determine the significance of "light" and "dark" cells of the adrenal medulla. However it is worth noting that light and dark cells are seen with the methods used in this study From the observations made in this study it was not possible to separate dark and light cells as to E and NE categories although most dark cells encountered seemed to be of the E or the mixed type. Previous work, using the light microscope (Wood, '62–'64) did not specifically describe light and dark cells for the reason that dark cells were found to occur more often in the sections taken from the area immediately adjacent to where the fresh tissue was sliced prior to fixation. It was then believed that the dark cells were the result of trauma to the cells and thus were an artifact. Since the tissues used in the current study were also sliced prior to fixation this possibility also exists here It seems that the means by which the light and dark cell controversy could be resolved would be by comparing perfused preparations with those fixed by immersion following slicing of the fresh tissue. Such a work would require little extra effort and can be combined with any future study of adrenomedullary tissue. Such a study is of extreme importance before true evaluation of drug and stress studies of adrenomedullary tissue can be made.

Nucleotidephosphatase (NPase) reactions indicate a certain degree of specificity, depending on substrate as stated in Results. This has been previously reported for adrenomedullary tissue of various animals by Bell ('65) with the use of the light microscope. The endothelial reaction shown in figure 7 correlates with other work (Marchesi and Barrnett, '63) on endothelial cells; however at the current state of evaluation the role if any cannot be determined for such a site of enzymatic activity and the relationship to CAM stores and release of these stores. The results shown in figure 8 of the NPase activity

the exception that the reaction was easier to produce and that there is a higher incidence of intracellular reactivity however the DPase reaction must be clarified before further comment can be made.

Of the NPases studied, MPase was the easiest to localize with the electron microscope and seemed to give the largest amount of information MPase activity was localized in the areas similar to those for TP and DPase but with greater consistency and in larger amounts MPase results are summarized in figures 10 and 11 Figure 10 presents cat adrenomedullary tissue treated for MPase activity and viewed unstained The central unidentifiable cell in the micrograph shows some degree of positive activity within the Golgi region. This cell is surrounded by chromaffin cells (C) with all possessing a high degree of membrane MPase activity There is a high degree of intracellular nonspecific activity in the cell of the upper right corner of the micrograph This nonspecific activity is considered to be due to artifact and tissue damage resulting from the handling and processing of the tissue. Figure 11 shows a cross-section of nerve fibers in cat adrenal tissue. There is marked activity along the chromaffin cell membrane in the canaliculi, around the unmyelinated nerve fibers at nerve terminals and in the large intercellular space. More detailed studies of MPase activity are seen in figure 12. Figure 12 shows a longitudinal section through an unmyelinated fiber demonstrating MPase activity Microtubules within the chromaffin cells and the nerve fiber show no enzymatic activity The nerve terminal in figure 13 demonstrates a high degree of activity and shows a protoplasmic process abutting on the nerve-ending surface Figure 14 shows an interconnecting cilium with demonstrable MPase activity located within the Golgi zone of a chromaffin cell. Figure 15 shows MPase activity along the intercellular system and into the subendothelial space Such activity is also localized in vesicles within the chromaffin cells and in pinocytotic vesicles within the endothelial cells

The chromaffin cell orientation in both the cat and the rat at times follows that described by Bennett (41) The cells in figure 16 appear to be oriented toward the venous spaces The nuclei of these cells are located away from the venous spaces and toward the larger canaliculi and nerve terminals however these findings are not consistent enough to indicate a definite polarity The intercellular spaces are continuous with the subendothelial spaces and contain one or more dilations along the lateral border of the chromaffin cells. Figure 17 shows a high-power view of an area in which a number of intercellular spaces approach the subendothelial space and appear in some instances to form a large common canaliculus. The cell membranes in many places are characterized by having connecting dense areas. This is especially true in the areas of the large canaliculi (fig 18) which are toward the nuclear pole of the chromaffin cells.

Detailed studies of the nerve endings on the chromaffin cells showed that these endings possessed both granular and agranular vesicles with the latter predominating (figs 13 19 20) The granular vesicles were compared on a density basis with E and NE-containing cells. From figure 20 it can be seen that the granular vesicles of the nerve terminals do not have the density of the positively reacting NE granules within the chromaffin cells however, there definitely are positive NE loci along nerve fiber bundles (fig 21) Also such reactive areas were seen at a Schmidt-Lanterman cleft (fig 22) and these were seen to possess the artifact characteristic of that at the NE granules within the NE-containing chromaffin cells

DISCUSSION

The CAM localizations in these investigations correlate well with former results (Hillarp and Hökfelt '55 Eränkö '55 Wood '63; Tramezzani et al. '64; Wood and Barrnett '63 64 Coupland et al 66) The reaction of the aldehyde group of glutaraldehyde with the unsubstituted amino group of norepinephrine to form water and the Schiff monobase as presented by Tramezzani and co-workers ('64) is quite workable and the stoichiometry of the reaction has been established (Wood, 66a) Tramezzani and co-workers ('64) developed the concept of the reduction of silver salts by the Schiff monobase and the final reaction product (Wood, '66a) indi-

number of micrographs however it is most appreciated in figure 17 where a number of small canaliculi appear to be opening into the subendothelial space while others connect with a larger canaliculus which seems to possess its own basement membrane. In many areas dilations of the canaliculi were seen and many of these contained NPase-reactive areas. From this information it would seem that NPase activity would provide for the gradual release of CAMs from the adrenal medullary cells. It is conceivable that all cells would eventually communicate with the subendothelial space via the intercellular and canalicular systems. As postulated by Bennett ('41) the cat shows some degree of orientation of the chromaffin cells toward the venous spaces of the adrenal medulla. It is to be pointed out that this is in a limited number of cells and only those around the veins show this polarity (Bell, '65). The nerve terminals are located away from the venous areas as are larger canaliculi, while connecting intercellular spaces communicate with the subendothelial space. The dense connecting areas mentioned in Results often interrupt the canalicular spaces and are of various lengths, presumably due to the plane of section. It is evident that the connecting areas are predominant at the large canalicular areas which lie alongside or at the apical region of the chromaffin cells; i.e., this is the area of the nerve terminals.

Detailed observations were made on nerve endings in order to gain some insight as to the reactivity of the granular vesicles. As has been mentioned, enzymatic activity was not within the nerve terminal, but rather outside the terminal membrane. Catecholamine (CAM) reactions were negative in both the granular and agranular vesicles of nerve terminals. All granular vesicles observed were either of the density of the E granules or less and, when compared on the same micrograph with the density of NE granules it is evident that they do not give the unsubstituted amine reactions. These granules do not produce the artifact of the reaction which is also characteristic of CAM storage sites. On the other hand, loci found along nerve fiber bundles did exhibit the characteristic NE reaction. Possibly these were portions of NE cells often seen in the adrenal cortex or maybe another type of extramedullary chromaffin tissue. The nerve terminals along myelinated nerve fibers which did react positively were found to possess the positive CAM artifact and are the same types of endings as described by Bodian and Taylor ('63).

It can generally be said that the NE reaction depending on the heavy metals, as presented by Tramezzani and co-workers ('64) and Wood and Barrnett ('63, '64) and confirmed chemically by Wood ('66a) is a valid one. It is significant that the *in vitro* reaction can be arrested by the addition of a chelating compound (Versene) since this relates to the necessity for a metal ion to complete the reaction.

The NPases studied in this work follow a pattern of distribution similar to that presented by other workers in other tissues. There is the general opinion that such enzymatic activity may not be significant in the release of CAMs from their storage sites. On the other hand, there is a degree of specificity depending on the substrate used, and Bell ('65) has shown other enzymatic specificities for adrenomedullary cells. It should also be pointed out that recent preliminary work shows that (Wood, '66b) reserpine-induced CAM losses are accompanied by increased TPase activity in rat adrenomedullary tissue. These functional studies are currently being followed now that an evaluation of the tissue and its reaction products have been accomplished.

It has been noted in the descriptions of the micrographs that cells with a decreased number of granules possess an increased number of microvesicles and microtubules. Also it is evident that the diameter of the microvesicles and the microtubules are approximately the same and the former may represent cross-sections of the latter. These structures may also represent extensions of the Golgi zone or granule forming structure of the chromaffin cells and thus may be more prevalent in the absence of CAM granules. Again, further information on this type of projection may be gained from new functional studies, for Yates ('63) has shown an increase in the number of such vesicles following depletion of CAM granules by reserpine injection.

along the nerve fiber and along the cell membranes correlate with those of the light microscope (fig 2) This may also have no real relationship to CAM action; however it is highly possible that this enzyme plays a role in membrane permeability to sodium and potassium and the propagation of the nerve impulse along the fiber Hagen and D'Iorio ('65) have stated that adrenomedullary ATPase is not sodium- or potassium activated however these studies were made on medullary homogenates and it seems that further electron microscopic studies are indicated to confirm the chemical studies or possibly to further question the differences indicated by the present work. The evidence in figure 9 indicates a high degree of activity in the canalicular spaces and in the areas of the granule membranes It is evident from the microgranules present that this is an NE cell and the granular membrane activity shown lends credence to the concepts of Hillarp ('58)

The MPase reaction (fig 3) is not due to the reduction of the lead salts of the incubation medium by the glutaraldehyde-CAM reaction product for with treatment of control tissues at the light microscope reaction level it was determined that the tris-maleate buffer inhibits the reaction of the metal salt with the Schiff base and the electron microscopic examination of MPase-positive areas reveals no specific densities in the granules of NE cells, but primarily at the cell membrane level When the structure of tris-maleate is examined one is aware of the amino group in the moiety which in all probability competes with the unsubstituted amino group of the CAM for the Schiff base either for reduction or for the formation of the chelate product. Also when glutaraldehyde is added to the tris-maleate buffer a precipitate is formed It is therefore believed that the NPase reaction product is truly of enzymatic formation until proven otherwise It is to be pointed out that the results here are derived from normal tissue and do not report the result of drug administration or nerve stimulation.

MPase activity was generally intense with the electron microscopic localization when the area being investigated was within NE cells or around ganglion cells. The reactions of ganglion cells have been reported elsewhere (Bell '66) The results shown in figures 10–15 indicate a similarity to the sites of activity as produced by the two other NPase reactions. The central cell in figure 10 shows localized specific activity in the Golgi zone as compared to the nonspecific activity seen in the upper right portion of the micrographs. Localized specific activity such as in the Golgi region and along an intrusion of the cell membranes into the chromaffin cells is considered significant as is the reactivity along the nerve fibers and in the canalicular spaces The reactive sites in the canalicular spaces were seen to be of rosette appearance and this may be true along the membranes of the individual cells however due to the limited spaces between cells, such a configuration is not visible or it may be true that the reactive areas in the canalicular spaces are a result of diffusion of the reaction product from the border of the canaliculus Microtubules and collagen did not react to the NPase activities however an occasional interconnecting cilium was seen to have a positive reaction at its periphery (fig 14) These cilia were generally seen within the Golgi region of the chromaffin cells and may well represent a functional connection to the metabolic centers of these cells The reaction product along nerve fibers was quite striking as long as the fibers were of the nonmyelinated type Myelinated fibers showed none of the reaction product for enzymatic activity On the contrary nerve endings were found to be rich in NPase activity and this appears logical since this is an area of rapid exchange of ions. The NPase activity can be demonstrated along the canalicular system into the subendothelial space and in the pinocytotic vesicles of the endothelial cells Often specific activity could be seen within the small cisternae of the chromaffin cells which may or may not be continuous with the canalicular system. It seems logical that such a system would provide for the passage of amines from the adrenomedullary cells into the canalicular system and on into the subendothelial space and hence into the blood stream via the vesicles of the endothelial cells or by another mechanism. The extensiveness of the canalicular system is appreciated in a

number of micrographs however it is most appreciated in figure 17 where a number of small canaliculi appear to be opening into the subendothelial space while others connect with a larger canaliculus which seems to possess its own basement membrane. In many areas, dilations of the canaliculi were seen and many of these contained NPase-reactive areas. From this information it would seem that NPase activity would provide for the gradual release of CAMs from the adrenal medullary cells. It is conceivable that all cells would eventually communicate with the subendothelial space via the intercellular and canalicular systems. As postulated by Bennett ('41), the cat shows some degree of orientation of the chromaffin cells toward the venous spaces of the adrenal medulla. It is to be pointed out that this is in a limited number of cells and only those around the veins show this polarity (Bell, '65). The nerve terminals are located away from the venous areas as are larger canaliculi, while connecting intercellular spaces communicate with the subendothelial space. The dense connecting areas mentioned in Results often interrupt the canalicular spaces and are of various lengths presumably due to the plane of section. It is evident that the connecting areas are predominant at the large canalicular areas which lie alongside or at the apical region of the chromaffin cells; i.e. this is the area of the nerve terminals.

Detailed observations were made on nerve endings in order to gain some insight as to the reactivity of the granular vesicles. As has been mentioned, enzymatic activity was not within the nerve terminal, but rather outside the terminal membrane. Catecholamine (CAM) reactions were negative in both the granular and agranular vesicles of nerve terminals. All granular vesicles observed were either of the density of the E granules or less and when compared on the same micrograph with the density of NE granules, it is evident that they do not give the unsubstituted amine reactions. These granules do not produce the artifact of the reaction which is also characteristic of CAM storage sites. On the other hand, loci found along nerve fiber bundles did exhibit the characteristic NE reaction. Possibly these were portions of NE cells often seen in the adrenal cortex or maybe another type of extramedullary chromaffin tissue. The nerve terminals along myelinated nerve fibers which did react positively were found to possess the positive CAM artifact and are the same types of endings as described by Bodian and Taylor ('63).

It can generally be said that the NE reaction depending on the heavy metals, as presented by Tramezzani and co-workers ('64) and Wood and Barrnett ('63, '64) and confirmed chemically by Wood ('66a) is a valid one. It is significant that the *in vitro* reaction can be arrested by the addition of a chelating compound (Versene) since this relates to the necessity for a metal ion to complete the reaction.

The NPases studied in this work follow a pattern of distribution similar to that presented by other workers in other tissues. There is the general opinion that such enzymatic activity may not be significant in the release of CAMs from their storage sites. On the other hand, there is a degree of specificity depending on the substrate used and Bell ('65) has shown other enzymatic specificities for adrenomedullary cells. It should also be pointed out that recent preliminary work shows that (Wood, '66b) reserpine induced CAM losses are accompanied by increased TPase activity in rat adrenomedullary tissue. These functional studies are currently being followed now that an evaluation of the tissue and its reaction products have been accomplished.

It has been noted in the descriptions of the micrographs that cells with a decreased number of granules possess an increased number of microvesicles and microtubules. Also it is evident that the diameter of the microvesicles and the microtubules are approximately the same and the former may represent cross-sections of the latter. These structures may also represent extensions of the Golgi zone or granule-forming structure of the chromaffin cells and thus may be more prevalent in the absence of CAM granules. Again, further information on this type of projection may be gained from new functional studies, for Yates ('63) has shown an increase in the number of such vesicles following depletion of CAM granules by reserpine injection.

It seems probable that the chromaffin cell membrane possesses an inherent amount of NPase activity which may indeed be a type of NPase activity common to many other types of cells Although granular membranes and granules appear to contain little if any enzymatic activity the possibility exists that this activity is quite specific and not in a state to be visualized in the present study It seems highly probable that the granule-membrane enzymatic system may be activated as the granule and its membrane approach the cell membrane At this time the CAM and the nucleotide are split from each other with both being released from the granule core The granule membrane then would remain within the cell and would recombine or reform into the empty vesicles and microvesicles seen within the cells which were relatively devoid of dense granules. Such a hypothesis would correlate well with the information gained from the present work and from that of other workers summarized in the two preceding paragraphs. The functional work will be fully reported in the near future and it is hoped that further information regarding the relation of NPase enzymes to CAM release may be gained

ACKNOWLEDGMENT

The author wishes to acknowledge the very able technical assistance of Mrs Brenda Ryker and Mrs Ann B Spikes

LITERATURE CITED

Banks P 1965 The adenosine-triphosphatase activity of adrenal chromaffin granules. Biochem. J., 95: 490–496.

Bell, N L 1965 Comparative histochemistry of mammalian adrenomedullary tissue. Anat. Rec., 151: 485–486.

Benedeczky L, A. Puppi, A. Tigyi and K. Lissak 1965 Electron microscopic study of adrenaline and noradrenaline secretion of the adrenal medulla. Acta Biol. Hung., 15: 285–298

——— 1966 Various cell types in the adrenal medulla. Nature 209: 592–594

Bertler A. N A. Hillarp and E. Rosengren 1960 Some observations on the synthesis of catechol amines in the adrenaline-containing cells of the suprarenal medulla. In: Adrenergic Mechanisms. J R. Vane ed. Little Brown Boston. pp. 100–102.

Blaschko, H., and K. B Helle 1963 Interaction of soluble protein fractions from bovine adrenal medullary granules with adrenaline and adenosinetriphosphate. J Physiol., 169: 120P

Bodian, D., and N Taylor 1963 Synapse arising at central node of ranvier and note ation of the central nervous system. 139 330–332.

Colburn, R. W., and J W Maas 1965 Adenosine triphosphate-metal-norepinephrine ternary complexes and catecholamine binding. Nature, 208: 37–41

Coupland R. E., and D Hopwood 1966 The mechanism of the differential staining reaction for adrenaline- and noradrenaline-storing granules in tissues fixed in glutaraldehyde. J Anat., 100: 227–243

de Robertis, E., and A. V Ferreira 1957 A multivesicular catechol-containing body of the adrenal medulla of the rabbit. Exper Cell Res., 12: 575–581

Eränkö, O 1955 Fluorescing islets, adrenaline and noradrenaline in the adrenal medulla of some common laboratory animals. Ann. Med. Exp. Biol. Fenn., 33: 278–290.

Eränkö O., and L. Hänninen 1960 Electron microscopic observations on the adrenal medulla of the rat. Acta Path. et Microbiol. Scand., 50: 126–132.

Euler U S. v., F Lishajko and L. Stjärne 1963 Catecholamines and adenosine triphosphate in isolated adrenergic nerve granules. Acta Physiol. Scand. 59: 495–496.

Hagen P., and A. D'Iorio 1965 Studies with the ATPase of adrenal medulla. Can. J Biochem., 43: 1633–1642.

Hillarp N A. 1958 Enzymic systems involving adenosine phosphates in the adrenaline and noradrenaline containing granules of the adrenal medulla. Acta Physiol. Scand., 42: 144–165.

Hillarp N A., and B Hökfelt 1955 Histochemical demonstration of noradrenaline and adrenaline in the adrenal medulla. J Histochem. Cytochem., 3: 1–5.

Hillarp N A., B Jönsson and G Thieme 1959 Adenosinephosphates in the rat adrenal medulla. 1 Adrenal medulla in minimal secretory activity Acta Physiol. Scand., 47 310–319.

Kim, K S. 1966 Personal communication. Department of Anatomy University of Arkansas Medical School.

Luft, J H 1961 Improvements in epoxy resin embedding methods. J Biophys. Biochem. Cytol., 9: 409–414

Marchesi, V T., and R. J Barrnett 1963 The demonstration of enzymatic activity in pinocytotic vesicles of blood capillaries with the electron microscope. J Cell Biol., 17: 547–556.

Smith W F 1963 Schiff bases. Organic Chem. Bull., 35: 1–5.

Tramezzani, J H. S. Chiocchio and G. F Wassermann 1964 A technique for light and electron microscopic identification of adrenalin- and noradrenalin-storing cells. J Histochem. Cytochem., 12: 890–899

Wachstein M. and E. Meisel 1957 Histochemistry of hepatic phosphatases at a physiologic pH Am. J Clin. Path., 27: 13–23.

Wood, J G 1962 Identification of and observations on noradrenalin and adrenalin containing cells in the adrenal medulla. Anat. Rec., 142: 292.

——— 1963 Identification of and observations on epinephrine and norepinephrine-containing cells in the adrenal medulla. Am. J Anat., 112: 285-304.

——— 1965 The fine structural relationship of catecholamine storage sites to the presence of adenosinetriphosphatase in adrenomedullary tissue. Eighth International Congress of Anatomists — Wiesbaden, pp. 128–129

——— 1966a Electron microscopic localization of amines in central nervous tissue. Nature, 209: 1131 1133.

——— 1966b Light and electron microscopic studies of the relationship of nucleotide phosphatase activity to catecholamine storage sites in adrenomedullary tissue. Anat. Rec., 154 443.

Wood, J. G., and R. J Barrnett 1963 Histochemical differentiation of epinephrine and norepinephrine granules in the adrenal medulla with the electron microscope. Anat. Rec., 145 301–302.

——— 1964 Histochemical demonstration of norepinephrine at a fine structural level. J Histochem. Cytochem., 12: 197–209

Yates, R. D. 1963 An electron microscopic study of the effects of reserpine on adrenomedullary cells of the Syrian hamster Anat. Rec., 146 29–45.

——— 1964a A light and electron microscopic study correlating the chromaffin reaction and granule ultrastructure in the adrenal medulla of the Syrian hamster. Anat. Rec., 149 237–250.

——— 1964b Fine structural alterations of adreno-medullary cells of the Syrian hamster following intraperitoneal injections of insulin. Tex. Rep. Biol. Med., 22: 756–763.

Yates, R. D J G. Wood and D Duncan 1962 Phase and electron microscopic observations on two cell types in the adrenal medulla of the Syrian hamster. Tex. Rep. Biol. Med., 20: 494–502.

PLATE 1

EXPLANATION OF FIGURES

1 Cat adrenomedullary tissue treated with potassium dichromate (pH 4.1) for four hours and sectioned at 10 μ on a freezing microtome. Groups of norepinephrine (NE) cells with large granules are indicated by arrows and show sharp contrast to the epinephrine (E) cells which with this method, appear almost homogeneous. Phase contrast micrograph. × 435.

2 Rat adrenomedullary tissue treated for adenosine triphosphatase (TPase) activity and photographed with ordinary light. TPase activity is shown as black dense areas between epinephrine (E) cells. Norepinephrine (NE) cell groups are conspicuous by the large degree of TPase activity at the sites of cell islands. × 145

3 Rat adrenal tissue treated histochemically to demonstrate monophosphatase (MPase) activity shows positively reacting cell groups which are norepinephrine (NE) cells in the adrenal medulla, while epinephrine (E) cells are not reactive. Adrenal cortical (C) tissue demonstrated in the lower right-hand corner of the photograph is essentially nonreactive. × 145.


E
NE


E
NE.
C
3

PLATE 1

EXPLANATION OF FIGURES

1 Cat adrenomedullary tissue treated with potassium dichromate (pH 4.1) for four hours and sectioned at 10 µ on a freezing microtome. Groups of norepinephrine (NE) cells with large granules are indicated by arrows and show sharp contrast to the epinephrine (E) cells which with this method, appear almost homogeneous. Phase contrast micrograph. × 435.

2 Rat adrenomedullary tissue treated for adenosine triphosphatase (TPase) activity and photographed with ordinary light. TPase activity is shown as black dense areas between epinephrine (E) cells. Nor epinephrine (NE) cell groups are conspicuous by the large degree of TPase activity at the sites of cell islands. × 145.

3 Rat adrenal tissue treated histochemically to demonstrate monophosphatase (MPase) activity shows positively reacting cell groups which are norepinephrine (NE) cells in the adrenal medulla, while epinephrine (E) cells are not reactive. Adrenal cortical (C) tissue demonstrated in the lower right-hand corner of the photograph is essentially nonreactive. × 145.

NUCLEOTIDASE AND CATECHOLAMINE SITES
Joe G. Wood

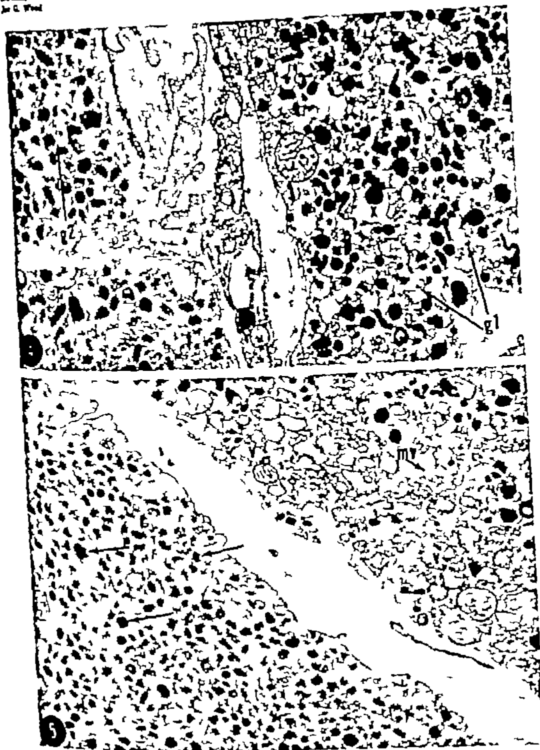


PLATE 2

EXPLANATION OF FIGURES

4 Rat adrenomedullary tissue glutaraldehyde fixation potassium dichromate incubation and subsequent treatment with 1% osmium tetroxide (OsO) Norepinephrine cells toward the right of the picture clearly show large dense chromium-positive NE granules which in many instances are surrounded by a rather large artifact (x) which is characteristic of NE reaction sites. Very small positively reacting micrograunules in NE cells are indicated by arrows (g1) These granules measure in the range of 100 Å and are also surrounded in many cases by the artifact resulting from treatment of NE-reactive sites. Portions of two E cells at the left of the picture show the nonreactive E granules with this method Epinephrine cells (indicated by E) demonstrate granules which are not exceedingly different in size than those in the NE cell group Micrograunules are present (left of E) in these epinephrine cells and are indicated by arrows g2. These microgranules are different in size than those found in the NE cells. × 30,000.

5 A portion of an NE cell appears in upper right corner of the electron micrograph and shows large dense chromium positively reacting granules surrounded by a certain degree of artifact. Cell in the lower left portion of the picture appears to be an E cell with occasional NE granules. These granules are indicated by arrows. Other structures present in the photograph are canaliculus (c) multivesicular body (mv) empty NE vesicles (v) × 12,000

g2
g1
4
m
5

PLATE 3

EXPLANATION OF FIGURES

6 Cat adrenomedullary tissue treated for DPase activity but nonreactive Shows the darker NE cell granules due to treatment with OsO_4. This NE cell also contains microgranules described in figure 4. Epinephrine (E) cells show nonreactive granules. × 12,000.

7 Cat adrenomedullary tissue treated for TPase activity demonstrates surface membrane of endothelial cell to be positively reactive for TPase activity (*arrows*) Other structures present are chromaffin cells (C) lumen of blood vessel (L) × 21,000

5

L

PLATE 3

EXPLANATION OF FIGURES

6 Cat adrenomedullary tissue treated for DPase activity but nonreactive. Shows the darker NE cell granules due to treatment with OsO. This NE cell also contains microgranules described in figure 4. Epinephrine (E) cells show nonreactive granules. × 12,000.

7 Cat adrenomedullary tissue treated for TPase activity demonstrates surface membrane of endothelial cell to be positively reactive for TPase activity (arrows). Other structures present are chromaffin cells (C) lumen of blood vessel (L). × 21,000.

PLATE 4

EXPLANATION OF FIGURES

8 Cat adrenomedullary tissue treated for TPase activity Unstained specimen shows low contrast chromaffin cells as (C) on either side of unmyelinated nerve fiber (N) reactive TPase sites along nerve-fiber membrane are indicated by arrows as are the reactive sites along the membrane of the chromaffin cells. × 12,000

9 TPase activity of cat adrenomedullary tissue shows sites of TPase activity (arrows) at the chromaffin cell membrane and in a subendothelial space (SE) At some points, granular membranes (m) indicate some degree of positive reactivity Classification of this cell as an NE cell is indicated by the presence of the small microgranules indicated at the arrows gl × 30,000

N
C
8

SE
9

PLATE 5

EXPLANATION OF FIGURE

10 Cat adrenomedullary tissue treated for MPase activity and viewed unstained. The central cell demonstrates a high degree of enzymatic activity at its cell border and there is some degree of MPase activity within the area of the Golgi region of the cell (arrow G). Other cells demonstrate MPase activity at their cell borders and there is a rosette-appearing enzymatic localization in the canaliculus (C). Other cells and cell borders show enzymatic activity and dilations of the intercellular space or canaliculi. There is a large degree of nonspecific activity in the upper right-hand corner of the photograph indicated by the small arrows. This presumably is due to artifact. × 12,000.


G
C
10

PLATE 6

EXPLANATION OF FIGURE

11 A summary electron micrograph of cat adrenomedullary tissue tre
for MPase activity and with OsO_4 This tissue shows canalicular
tem in the upper left hand corner with some degree of MPase acti
There is MPase activity at the cell border of the large chromaffin
The large intercellular space (IS) shows a high degree of ros
appearing enzymatic activity There is also activity present arc
the border of the nerve fiber (NF) and around the portion of a n
ending (NE) Other areas of activity are also obvious in this appa
nerve bundle area Other structures of note visible in the picture
rough endoplasmic reticulum (ER) mitochondria and microtub
(mt) × 24,000

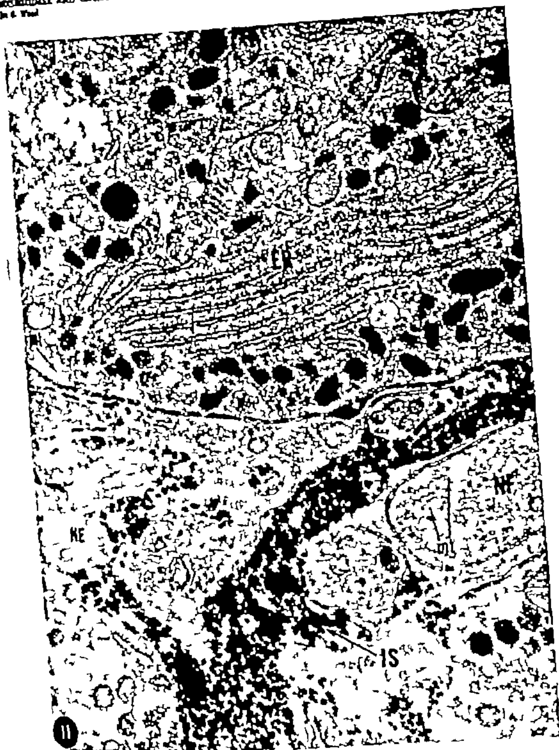

NF
NE
IS
11

PLATE 7

EXPLANATION OF FIGURES

Transverse section through a nerve fiber taken from cat adrenomedullary tissue treated for MPase activity. The areas between the membrane of the nerve fiber and the adjacent chromaffin cells on either side show a considerable degree of MPase activity. Microtubules (mt) and neurofibrillae (nf) present within the nerve fiber are nonreactive, as are the microtubules (mt) and microvesicles (mv). The chromaffin cells within this picture demonstrate a paucity of granules but a high degree of development of the microtubular system. × 24,000.

Nerve ending taken from cat adrenomedullary tissue treated for MPase activity demonstrates nerve terminal adjacent to two chromaffin cells with a protoplasmic extension (arrows) making contact with the nerve terminal membrane. The nerve terminal primarily contains agranular vesicles, and there is evidence of no enzymatic activity within the nerve terminal itself. The enzymatic activity is present at the periphery and the distal end of this nerve terminal. Canaliculus (C) with enzymatic activity. × 18,000.

Electron micrograph of cat adrenomedullary tissue treated for MPase activity. Photograph taken from the Golgi zone of a chromaffin cell, demonstrating interconnecting cilium with MPase activity at the border of the cilium. Other structures evident in this region are the microvesicles and mitochondria, plus occasional granules present in the Golgi area. × 69,000





PLATE 7

EXPLANATION OF FIGURES

12 Transverse section through a nerve fiber taken from cat adrenomedullary tissue treated for MPase activity. The areas between the membrane of the nerve fiber and the adjacent chromaffin cells on either side show a considerable degree of MPase activity. Microtubules (mt) and neurofibrillae (nf) present within the nerve fiber are nonreactive, as are the microtubules (mt) and microvesicles (mv). The chromaffin cells within this picture demonstrate a paucity of granules but a high degree of development of the microtubular system. × 24,000.

13 Nerve ending taken from cat adrenomedullary tissue treated for MPase activity demonstrates nerve terminal adjacent to two chromaffin cells with a protoplasmic extension (arrows) making contact with the nerve terminal membrane. The nerve terminal primarily contains agranular vesicles, and there is evidence of no enzymatic activity within the nerve terminal itself. The enzymatic activity is present at the periphery and the distal end of this nerve terminal. Canaliculus (C) with enzymatic activity. × 18 000

14 Electron micrograph of cat adrenomedullary tissue treated for MPase activity. Photograph taken from the Golgi zone of a chromaffin cell, demonstrating interconnecting cilium with MPase activity at the border of the cilium. Other structures evident in this region are the microvesicles and mitochondria, plus occasional granules present in the Golgi area. × 69,000

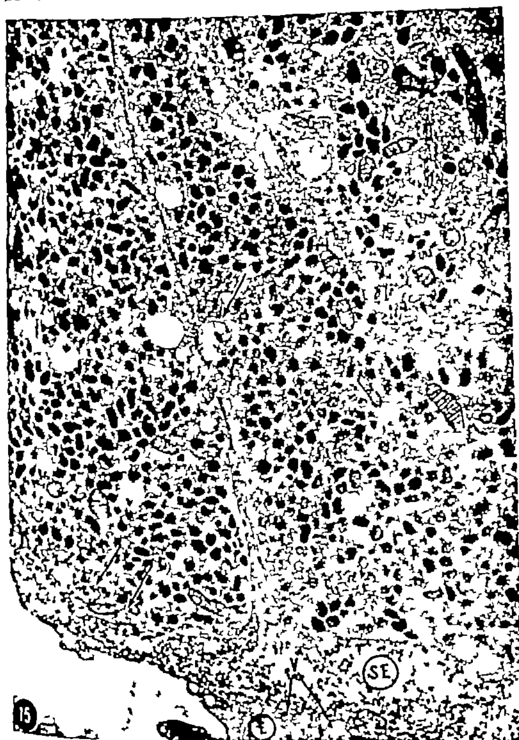

15
SE

PLATE 8

EXPLANATION OF FIGURE

15 Cat adrenomedullary tissue treated for MPase activity demonstrates enzymatic activity in the intercellular space extending between the chromaffin cells. Each chromaffin cell contains a number of dilations which may or may not be canaliculi. The intercellular space extends from between the chromaffin cells on to the subendothelial space (SE) There is a considerable degree of enzymatic activity along the intercellular space and on into the subendothelial space Also at the periphery of the chromaffin cell, there is a high degree of enzymatic activity located within vesicles of the chromaffin cells (arrows) There is also some degree of activity within small vesicles (v) of the endothelial cells (E) It should also be pointed out, in this micrograph that the chromaffin cell in the upper right corner of the picture demonstrates a paucity of granules and a high degree of development of the intercellular tubular system × 12,000.


C
C
C
C
E
16

PLATE 9

EXPLANATION OF FIGURE

16 Rat adrenomedullary tissue treated for TPase activity. However reactive sites are not present. Subsequently treated with 1% OsO_4 and stained with uranyl acetate and lead citrate. This low-power micrograph demonstrates the polarity of the cells immediately surrounding the veins (V) of the adrenal medulla. Endothelial (E) cell. The intercellular spaces are seen approaching the subendothelial space. Along the intercellular spaces numerous small canaliculi (c) are visible. Toward the apical end of the cell large interconnecting canaliculi (C) are present with many protoplasmic projections of the chromaffin cells into the canalicular space. Also at this area can be seen nerve terminals (NT) predominantly composed of agranular vesicles. Lysosomes (L). × 6000.


C
C
NJ
C
E
V
16

PLATE 10

EXPLANATION OF FIGURES

17 Electron micrograph of cat adrenomedullary tissue illustrating an area immediately adjacent to a vein (V) The complexity of the canalicular system is illustrated in this micrograph in that numerous canaliculi are present and can be seen connecting with the subendothelial (SE) space. Dilations within the chromaffin cells are indicated by D There appears to be one large common canaliculus (C) which receives two or more small intercellular spaces or connecting canaliculi. Other structures visible in the micrograph are microvesicles (mv) pinocytotic vesicles (pv) and an erythrocyte (E) × 14 000.

18 Rat adrenomedullary tissue treated for TPase activity but showing nonreactive areas This micrograph depicts an area of junction of a number of chromaffin cells at a common canalicular space which would be comparable to the spaces indicated in figure 16. In this area can be seen the dense cell border junctions (arrows); also, a nerve ending (NE) is present. Other structure indicated in the photograph is lysosome (L) × 12 000


SE
V
C
D
PV
17

PLATE 11

EXPLANATION OF FIGURES

19 Cat adrenomedullary tissue treated for DPase activity and with 1% OsO_4 and stained with uranyl acetate and lead citrate. Central structure in the photograph is a nerve terminal of primarily the agranular vesicle type. The two granular vesicles present (arrows) do not approach the density of the granules in the adjacent chromaffin cells. This nerve terminal appears to be at the border of three and possibly four chromaffin cells and at a large canalicular space. Other structures present in the micrograph are microtubules (mt) and microvesicles, the latter being located in the cell with a fewer number of granules. × 18,000.

20 Cat adrenomedullary tissue treated for DPase activity and stained in the usual manner. The OsO_4 reaction product of the glutaraldehyde NE complex is shown in the chromaffin cells in the left portion of the photograph. This cell is also identified as an NE cell by the presence of the small dense microgranules (mg). Other structures present in the photograph in the interconnecting areas and cells are microtubules (mt). Canaliculi are also present. The granular vesicles (arrows) in the nerve fiber structure at the right portion of the photograph do not approach the density of the NE granules in the chromaffin cell. This is indirect evidence that norepinephrine is not localized to the granules in the nerve terminals. × 15,000

mt
mv
19

mt
mp
20

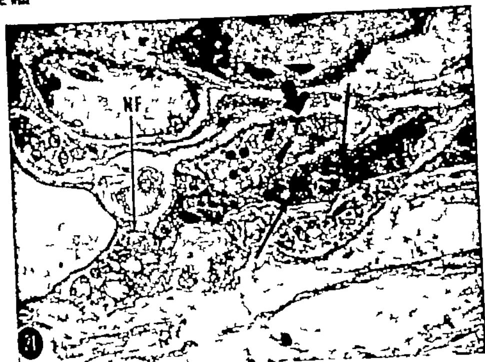
PLATE 11

EXPLANATION OF FIGURES

19 Cat adrenomedullary tissue treated for DPase activity and with 1% OsO_4 and stained with uranyl acetate and lead citrate. Central structure in the photograph is a nerve terminal of primarily the agranular vesicle type. The two granular vesicles present (arrows) do not approach the density of the granules in the adjacent chromaffin cells. This nerve terminal appears to be at the border of three and possibly four chromaffin cells and at a large canalicular space. Other structures present in the micrograph are microtubules (mt) and microvesicles, the latter being located in the cell with a fewer number of granules. × 18 000

20 Cat adrenomedullary tissue treated for DPase activity and stained in the usual manner. The OsO_4 reaction product of the glutaraldehyde NE complex is shown in the chromaffin cells in the left portion of the photograph. This cell is also identified as an NE cell by the presence of the small dense microgranules (mg). Other structures present in the photograph in the interconnecting areas and cells are microtubules (mt). Canaliculi are also present. The granular vesicles (arrows) in the nerve fiber structure at the right portion of the photograph do not approach the denstiy of the NE granules in the chromaffin cell. This is indirect evidence that norepinephrine is not localized to the granules in the nerve terminals. × 15,000.

NUCLEOTIDASE AND CATECHOLAMINE SITES
Joe G. Wood



BM

22

PLATE 12

EXPLANATION OF FIGURES

21 Cat adrenomedullary tissue treated for CAMs represents a section through a bundle of nerve fibers entering the adrenal medulla The unmyelinated fibers (NF) show no dichromate-positive tissue while there is considerable degree of reaction along the cell process indicated by arrows. This is presumed to be an extension of the norepinephrine cell into this area. Granular vesicles located in what appears to be a nerve fiber (NF arrows) do not show the density associated with the granules in the cell process. The granular vesicles in the structure immediately adjacent to this cell process are also less dense thus indicating that again granular vesicles of certain types do not possess NE reaction. × 12,000

22 Cat adrenomedullary tissue treated for CAMs reaction demonstrates a nerve terminal near a Schmidt Lanterman cleft. This structure demonstrates electron-dense granular vesicles in what appears to be a nerve terminal which also contains some microtubules. This nerve terminal appears to be separated at this point from the cleft by two basement membranes (BM) There is a considerable degree of artifact and the deneness of the granular vesicles indicates the presence of a reacting catecholamine in this area This type of reaction for granular vesicles is quite different from that described in the preceding photographs × 40,000

An Ultrastructural Study of Opaque Cytoplasmic Inclusions Induced by Triparanol Treatment [1]

I-LI CHEN [2] AND ROBERT D YATES [3]

Department of Anatomy The University of Texas Medical Branch, Galveston, Texas

ABSTRACT The administration of triparanol caused an hypertrophy of smooth membranes and the occurrence of numerous cytoplasmic bodies in smooth muscle fibers and parasympathetic ganglion cells in the myenteric plexus of the hamster ileum. The hypertrophied membranes were more evident in the early stages of treatment when the cytoplasmic bodies were relatively few in number. The cytoplasmic bodies were tentatively divided into four types as follows whorls of membranes (type I), labyrinthine aggregates of smooth membranes (type II) dense bodies with a reticular internal structure (type III) and crystalline bodies showing a regular lattice pattern (type IV) There were also many intermediate types of cytoplasmic bodies which exhibited more than one characteristic of the types mentioned above. The relative numbers of the cytoplasmic bodies seemed to be increased in the order of type I (or type II) type III, and type IV in proportion to the period of treatment. It is suggested that type IV cytoplasmic bodies are formed through the stages of type I (or type II) and type III, and that types I, II, and III in turn, form from hypertrophied smooth membranes. The formation of crystalline bodies from hypertrophied membranes may represent the inclusion of cytoplasmic organelles into autophagic vacuoles (lysis). After certain degrees of lysis, more resistant components of the hypertrophied membranes remain as residues. These residues, rich in phospholipids, are probably represented as crystalline bodies.

Triparanol is known to be an inhibitor of cholesterol biosynthesis. One of the sites of inhibitory action of the drug is in the conversion of desmosterol to cholesterol (Avigan et al. '60) Numerous clinical and biochemical reports have shown that the administration of triparanol is followed by a reduction in the cholesterol content of the plasma (Steinberg et al. '61) Various morphological effects of triparanol on tissues or organs also have been reported. In a light microscopic study King ('60) observed a consistent partial depletion of lipids in the zona fasciculata of the rat, dog and monkey adrenal gland. Similar results were obtained in the rat by Elsalo and Talanti ('62) Severe hepatic lesions were reported in turkey poults (Ball et al., '63) and dogs (Scamu et al. '62) subjected to triparanol treatment. In electron microscopic studies, Hruban et al. ('63 '65) and Swift and Hruban ('64) noted a marked increase in the amount of smooth-surfaced endoplasmic reticulum, a new formation of myeloid bodies as well as crystalline structures in hepatic and pancreatic acinar cells of triparanol-treated rats. In the adrenal cortical cells of the rat (Volk and Scarpelli, '64) and in various types of steroid-producing cells of Syrian hamsters (Yates '66a,b,c) treated with triparanol, similar hypertrophied smooth-surfaced endoplasmic reticulum and numerous dense bodies were observed. Yates demonstrated distinct, regularly arranged crystalline patterns in many of these dense bodies.

Another structure related to cholesterol metabolism the small intestine (Dietschy and Siperstein '65) was selected for the present study Our preliminary observations revealed that a large number of dense bodies were present in the smooth muscle fibers and parasympathetic ganglion cells of the treated animals. These bodies appeared to be in various stages of formation and, consequently the present research was concerned with their origin, development and detailed structure.

[1] Research supported by USPHS grants NB [illegible], NB [illegible] and AM [illegible].

[2] Sponsored by National Council on Science Development, Republic of China.

[3] Recipient of Career Research Development Award [illegible].

of ciliary basal bodies were seen to project from one end of the centriole. Smooth- and rough-surfaced endoplasmic reticulum were not well developed in these fibers but the smooth reticulum was more frequently found than was the rough variety both in the axial and peripheral sarcoplasm. Numerous pinocytotic vesicles were seen along the plasma membrane and communications between these vesicles and the smooth endoplasmic reticulum were sometimes encountered. Free ribosomes were scattered throughout the cytoplasm where organelles other than myofilaments occurred. The fine structure of the smooth muscle fibers in this work was, for the most part, consistent with the observations of Caesar et al. ('57) Bernard et al. ('64) and Smith ('64).

In the muscle fibers of triparanol-treated animals, the smooth-surfaced endoplasmic reticulum, pinocytotic vesicles, and Golgi elements seemed to have increased in amount, and large numbers of opaque bodies were present in the cytoplasm (fig. 1). These changes were first noted in animals treated for less than two days. The increase in smooth membranes was mostly recognizable at the periphery of the muscle fiber where the components of the Golgi complex do not occur The various types of smooth membranes included vacuoles, vesicles, anastomosing tubules, whorls and labyrinthine aggregates of closely packed membranes, as well as flattened sacs which usually showed a close association with the plasma membrane (figs. 3 4) The flattened sacs tended to be arranged in a whorl-like manner. Profiles suggesting a continuity between these sacs and the plasma membrane were sometimes encountered (fig. 3) Therefore it was suspected that the flattened sacs at the periphery of the muscle fiber could be derived from an invagination of the plasma membrane The occurrence of certain organelles namely free ribosomes vesicles or vacuoles, folded membranes, and mitochondria, sequestered by hypertrophied smooth membranes were not uncommon (figs. 5 7) In some cases the bounding membranes consisted of more than one layer (Hruban et al. '63; Steiner et al. '64 Novikoff and Shin, '64; Locke and Collins '65) and therefore were somewhat different from typical lysosomes in early stages of development. Occasionally a reticular structure was seen in the expanded portion of the bounding membrane (insert to fig. 7) In some favorable sections, portions of the labyrinthine aggregates of membranes appeared to be continuous with the smooth-surfaced endoplasmic reticulum or the dilated cisternae of the ergastoplasm (fig 6) The most striking feature of the smooth muscle fibers in the animals treated for more than three days was the appearance of numerous cytoplasmic bodies which were usually bounded by a unit membrane and showed either a reticular or crystalline internal structure The detailed structure of these cytoplasmic bodies will be described in a section to follow The morphological characteristics of the nucleus and the myofilaments did not seem to be affected by the triparanol treatment.

Fine structure of parasympathetic ganglion cells in the myenteric plexus

The perikarya of the postganglionic cells in the myenteric plexus were oval, pear shaped or irregular in their contours. The nucleus was eccentrically located and exhibited distinct nucleoli. The Nissl substance was not as well developed as in spinal ganglion cells, but there was still an appreciable amount of the rough-surfaced endoplasmic reticulum mainly composed of flattened cisternae and ribosomes (fig. 10) The rough-surfaced endoplasmic reticulum was rather diffusely distributed in the cytoplasm except within the Golgi region. Profiles of transformation of the rough-surfaced endoplasmic reticulum to Golgi vesicles were observed. Paired centrioles were found occasionally within the Golgi region. Mitochondria were scattered throughout the cytoplasm and showed ordinary internal structure Other types of organelles and inclusion bodies were found in the perikaryon of the postganglionic cell, but the opaque cytoplasmic bodies which will be described with the experimental animals were found infrequently in the controls.

The morphological changes of the organelles in the perikaryon of the postganglionic cell in triparanol-treated animals were essentially the same as those observed in smooth muscle fibers of the same animals.

MATERIALS AND METHODS

Twenty four adult male hamsters weighing from 70–100 gm were used in this study Hamsters were maintained on a diet of Purina laboratory chow and water ad libitum They were divided into experimental (20 animals) and control (4 animals) groups The animals of the experimental groups were given triparanol suspended in olive oil (240 mg/kg daily) by stomach tube for 1–8 days Two animals were given triparanol 12 hours prior to sacrifice All animals were sacrificed by decapitation at the end of the period of treatment.

Small pieces of the distal part of the ileum from both control and experimental animals were excised with scissors placed immediately into ice-cold fixative and sliced into small blocks about 1 mm in thickness The fixatives used were of the following composition (1) 1 33% osmic acid in 0 67 M s-collidine buffer (2) 1% osmic acid in 0 1 M Sörensen s phosphate buffer (3) 6 25% glutaraldehyde in 0 1 M Sörensen s phosphate buffer or (4) 6.25% glutaraldehyde in 0 1 M cacodylate buffer The preliminary work showed s-collidine-buffered osmium tetroxide was the best fixative for the preservation of the crystalline bodies and therefore it was used in most instances. After osmic acid fixation tissue slices were rapidly dehydrated with cold 50% 70% 95% and absolute ethanol, and embedded in Epon 812. Silver to gold sections were cut on a Porter Blum microtome and stained for approximately one minute with alcoholic uranyl acetate and one minute with lead citrate (Reynolds '63) The sections were examined in either an RCA EMU 3D or an RCA EMU-3G microscope using 50 or 100 KV accelerating voltages Electron micrographs were taken at original magnifications of 2,600–36 000 diameters and subsequently enlarged photographically to the desired size

Pieces of ileum from experimental and control animals were fixed in either cold glutaraldehyde cold formol-calcium-cadmium formol-calcium, or weak Bouin s fluid for histochemical studies on paraffin or frozen sections

Tests for phospholipids (1) Acid hematein test Formol-calcium-fixed paraffin sections were stained with acid hematein according to the method described by Baker (46) (2) Acid hematein-pyridine extraction technique Weak Bouin s fluid-fixed paraffin sections were first treated with pyridine then stained with acid hematein (Baker 46)

Test for proteins Formol-calcium-fixed paraffin sections were subjected to the following treatments (1) mercuric bromphenol blue (Pearse 60) (2) improved Sakaguchi reaction (Deitch '61)

Test for cholesterol. The technique employed by Weber et al. ('56) was applied on cold calcium-cadmium-formalin-fixed frozen sections (25 μ in thickness) For the purpose of controlling the staining some sections of adrenal glands and ileum of normal white Holtzman strain rats were stained simultaneously with those from the treated hamsters

Test for acid phosphatase Cold glutaraldehyde-fixed frozen sections (10 μ in thickness) were incubated in Gomori's medium for 30 minutes to one hour (Pearse 60)

Some histochemical tests were performed on thick osmic acid-fixed Epon-embedded sections These tests were (1) Sudan black B (McGee-Russell and Smale, 63) (2) Nile blue sulphate (McGee-Russell and Smale '63) (3) acid hematein test (Baker 46) and (4) *Nile blue* sulphate for phospholipids (Menschik, '53). The former two represent tests for lipids and the latter two for phospholipids.

RESULTS

Smooth muscle fibers in the tunica muscularis externa

In normal smooth muscle fibers of the tunica muscularis externa of control animals most of the organelles other than myofilaments were concentrated in the axial cytoplasm associated with both extremities of the elongated nucleus or to a lesser extent in the peripheral cytoplasm where few myofilaments occurred (fig 1) Mitochondria were the most abundant organelles of smooth muscle fibers and they showed the usual internal structure Paired centrioles were occasionally observed in the Golgi region. In several cases, structures very similar to pericentriolar filamentous bodies (Sakaguchi '65) or rootlets

predominated in the latter groups and were only occasionally seen in the 12-hour and 1-day-treated animals. The type I bodies were much more frequent than those of type II in all the experimental animals. The type III cytoplasmic bodies were the most common type in the animals treated for two, three and four days.

Histochemical analyses of the cytoplasmic bodies

All of the histochemical techniques were done at the light microscopic level. The results were consistent with those of adrenal cortical cells of triparanol-treated hamsters (Yates, '68a) and are summarized in table 1.

The histochemical data in table 1 suggest that the cytoplasmic bodies which occur in smooth muscle fibers and parasympathetic ganglion cells of triparanol-treated animals contain large amounts of phospholipids (A, 3 4 B 1 2) The results from tests used for the detection of proteins (B 3, 4) were negative.

DISCUSSION

Crystalline inclusions have been demonstrated in several types of cells in animals treated with triparanol. These include pancreatic acinar and hepatic cells (Hruban et al., '65) as well as steroid hormone-producing cells (Yates, '68a, b c) In the present study the crystalline bodies were found in all types of cells in the wall of the small intestine. These included surface epithelial, goblet crypt and connective tissue cells postganglionic cells of the myenteric plexus and smooth muscle fibers. However the crystalline bodies were much more abundant in the latter two cell types.

It is difficult to determine what types of cells are most susceptible to triparanol treatment. Factors such as steroid hormone production, the extent of development of the membrane system or the cholesterol content of the cell seem not to be related to the cells susceptability to triparanol. Considering each of these factors separately first, among the cells which have been shown to be affected by triparanol administration, only the adrenal cortical, testicular interstitial, and corpora luteal cells are known to produce large quantities of steroids. Second both rough and smooth endoplasmic reticulum are poorly developed in smooth muscle fibers. Third, the histochemical findings in this study showed that cholesterol was present in the surface epithelium and crypt cells but was absent in the smooth muscle fibers. Using autoradiographic techniques, Dietschy and Siperstein ('65) have established that cholesterol synthesis in the ileum occurs almost exclusively in the intestinal epithelial crypts. A decrease in the cholesterol content of the cell does not seem to be a unique factor in the formation of the peculiar cytoplasmic bodies. According to Blohm and Laughlin ('59) and Blohm et al. ('59) the cholesterol content in the erythrocytes of triparanol-treated

TABLE 1

Histochemical analyses of cytoplasmic bodies

	Staining of cytoplasmic bodies
A. Osmic acid-fixed Epon sections (about 1 μ in thickness)	
1. Sudan black B	Black
2. Nile blue sulphate	Blue-black
3. Acid hematein test	Dark blue
B. 10% formalin-fixed paraffin sections (5 μ in thickness)	
1. Acid hematein test	Dark bluish brown
2. Acid hematein-pyridine extraction technique	Negative
3. Mercuric bromphenol blue	Negative
4. Sakaguchi reaction	Negative
C. Frozen sections (fixed in glutaraldehyde or 10% formalin)	
1. Acid phosphatase activity	Negative
2. Cholesterol test	Negative

Only very weak acid phosphatase activity was revealed at the sites where the crystalline bodies were expected to be found.

Opaque bodies were commonly observed in the cytoplasm (fig. 11) However changes in the rough-surfaced endoplasmic reticulum were obvious The Nissl substance was more dispersed than in the control animals and most of the cisternae of rough surfaced endoplasmic reticulum were mod erately to widely expanded. The expanded cisternae of the endoplasmic reticulum either lacked ribosomes or exhibited very few on the membranes(figs 12 13) The details of the opaque cytoplasmic bodies in treated animals will be described in the following section.

Opaque cytoplasmic bodies in smooth muscle fibers and parasympathetic ganglion cells of triparanol treated animals

As previously mentioned numerous cytoplasmic bodies appeared in the smooth muscle fibers and the parasympathetic ganglion cells of triparanol-treated ani mals These cytoplasmic bodies were found in small numbers as early as 12 hours after initial treatment and they increased in number up to four days after treatment. Thereafter no appreciable increase in number of the cytoplasmic bodies was noticed at the light microscopic level In the smooth muscle fibers they occurred predominantly in the axial and to a lesser extent in the peripheral cytoplasm. In ganglion cells they were usually located in the vicinity or at the periphery of the Golgi region The cytoplasmic bodies showed noticeable structural differences and were therefore classified arbitrarily into the following four types type I whorls of smooth membranes type II, labyrinthine aggregates of closely packed smooth membranes type III dense bodies with retic ular internal structure; and type IV crystalline bodies which showed a regular lattice pattern Many of the structures exhibited intermediate features or possessed more than one characteristic of the types mentioned above.

The type I cytoplasmic bodies showed variations in their profiles (figs. 7 8) The most common type consisted of concentri cally arranged smooth membranes forming a whorl and it was not uncommon for a single cytoplasmic body to exhibit two or more such whorls. In others a portion of the cytoplasmic body formed parallel-arrayed folds of membranes The size and number of layers of membranes also dif fered from one cytoplasmic body to another No regular periodicity like that seen in the myelin sheath was observed in these whorl-like or lamellar structures. The type II cytoplasmic bodies were usually located freely in the cytoplasm, that is without any limiting membrane separating them from the surrounding cytoplasm (figs. 6 13) In some favorable sections, portions of the labyrinthine membranes appeared to be continuous with the endoplasmic reticulum Most of the cytoplasmic bodies belonging to type III (figs. 12, 13) were bounded by a single membrane The mesh size of the reticular network varied from one body to another ranging from the smallest mesh of type II to the largest subunits of type IV cytoplasmic bodies. The crystalline structures (type IV) were all bounded by a single membrane (figs. 9 14 15 16) There was usually a clear space of around 100 Å which separated the limit ing membrane from the crystalline body proper Several profiles of the lattice-work were revealed in the structures of type IV They were composed of hexagonally rhomboidally or rectangularly arranged electron translucent dots or subunits, 60–70 Å in diameter separated from each other by an electron-opaque substance 40–60 Å wide Occasionally banded patterns result ing from alternations of electron-translucent and opaque bands were encountered (fig 16) When the specimen was tilted 5–10 with respect to the path of the electron beam in the microscope the crystalline lattice changed from one pattern to another that is from hexagonal to rhomboidal or from rhomboidal to rectangular By tilting the specimen through 10 it was possible to enhance the contrast of the linear arrangement of the subunits in one direction or the other

All types of cytoplasmic bodies were found in the treated animals However there seemed to be a relationship between the period of treatment and the frequency of occurrence of certain types of cytoplasmic bodies. The relative numbers of types I and II were greater in the animals treated for three days than in those treated for four or more days while type IV bodies

predominated in the latter groups and were only occasionally seen in the 12-hour and 1-day-treated animals. The type I bodies were much more frequent than those of type II in all the experimental animals. The type III cytoplasmic bodies were the most common type in the animals treated for two, three and four days

Histochemical analyses of the cytoplasmic bodies

All of the histochemical techniques were done at the light microscopic level. The results were consistent with those of adrenal cortical cells of triparanol-treated hamsters (Yates, '66a) and are summarized in table 1.

The histochemical data in table 1 suggest that the cytoplasmic bodies which occur in smooth muscle fibers and parasympathetic ganglion cells of triparanol-treated animals contain large amounts of phospholipids (A, 3, 4 B, 1 2) The results from tests used for the detection of proteins (B, 3, 4) were negative.

DISCUSSION

Crystalline inclusions have been demonstrated in several types of cells in animals treated with triparanol. These include pancreatic acinar and hepatic cells (Hruban et al., '65) as well as steroid hormone producing cells (Yates '66a, b c) In the present study the crystalline bodies were found in all types of cells in the wall of the small intestine. These included surface epithelial, goblet, crypt and connective tissue cells, postganglionic cells of the myenteric plexus, and smooth muscle fibers. However the crystalline bodies were much more abundant in the latter two cell types.

It is difficult to determine what types of cells are most susceptible to triparanol treatment. Factors such as steroid hormone production, the extent of development of the membrane system or the cholesterol content of the cell seem not to be related to the cells susceptability to triparanol. Considering each of these factors separately first, among the cells which have been shown to be affected by triparanol administration only the adrenal cortical, testicular interstitial, and corpora luteal cells are known to produce large quantities of steroids. Second, both rough and smooth endoplasmic reticulum are poorly developed in smooth muscle fibers. Third, the histochemical findings in this study showed that cholesterol was present in the surface epithelium and crypt cells but was absent in the smooth muscle fibers. Using autoradiographic techniques, Dietschy and Siperstein ('65) have established that cholesterol synthesis in the ileum occurs almost exclusively in the intestinal epithelial crypts. A decrease in the cholesterol content of the cell does not seem to be a unique factor in the formation of the peculiar cytoplasmic bodies. According to Blohm and Laughlin ('59) and Blohm et al. ('59) the cholesterol content *in the erythrocytes of triparanol-treated*

TABLE 1
Histochemical analyses of cytoplasmic bodies

	Staining of cytoplasmic bodies
A. Osmic acid-fixed Epon sections (about 1 μ in thickness)	
1. Sudan black B	Black
2. Nile blue sulphate	Blue-black
3. Acid hematein test	Dark blue
B. 10% formalin-fixed paraffin sections (5 μ in thickness)	
1. Acid hematein test	Dark bluish brown
2. Acid hematein-pyridine extraction technique	Negative
3. Mercuric bromphenol blue	Negative
4. Sakaguchi reaction	Negative
C. Frozen sections (fixed in glutaraldehyde or 10% formalin)	
1. Acid phosphatase activity	Negative [1]
2. Cholesterol test	Negative

[1] Only very weak acid phosphatase activity was revealed at the sites where the crystalline bodies were expected to be found.

animals is decreased by one-half but no change in the cholesterol content in the nervous tissue of treated rats was noted. However in the present study no cytoplasmic bodies were seen in the erythrocytes while numerous crystalline structures were found in the neurons of the treated animals.

An interesting finding was the relationship between the initial appearance and later occurrence of cytoplasmic bodies during the periods of treatment. The relative numbers of cytoplasmic bodies seemed to increase in the order type I (or type II) type III and type IV in proportion to the length of treatment. Furthermore there were many intermediate types of cytoplasmic bodies in various stages of development Thus it is conceivable that the crystalline bodies of type IV are formed by progressive changes through the stages type I (or type II) and type III It has been proposed by Luzzati and Husson ('62) and Stoekenius ('62a b) that changes in temperature and in the content of water alter the phospholipids from the lamellar to the hexagonal phase or vice versa However in the present study the tissues were always prepared in ice-cold fixative and the temperature during dehydration was kept rather constant. Moreover not only did variable appearances of opaque bodies occur in the cytoplasm of a single cell, but also different patterns were observed within a single cytoplasmic body (fig 12) In figure 12 one cytoplasmic body shows a lamellar structure both along the margin and in the interior and a reticular pattern in other parts From such observations it is believed that the different appearance of the cytoplasmic bodies is not caused by fixation or handling However this could represent a dehydration process of the cytoplasmic body and it is quite possible that the crystalline structures which appear compact and show a regular pattern are formed from the other types of opaque bodies through a dehydration process. It is not unreasonable to assume that the water content of various types of the cytoplasmic bodies might be different at the time of fixation and consequently appear as different phases.

The histochemical data indicate that the opaque granules are rich in phospholipids, and possibly may represent hypertrophied membranes in autophagic vacuoles since such membranes sequestered by vacuoles were observed in this study It is not unreasonable to assume that, following a certain degree of lysis more resistant components of the membranes remain and represent the opaque granules. It has been demonstrated in hepatic and pancreatic acinar cells of triparanol-treated rats (Hruban et al. '65) that, where myeloid membranes are sequestered with cytoplasmic material a portion of the inclusion which contains cytoplasm shows a positive acid phosphatase reaction.

The exact 3-dimensional structure of the crystalline bodies has not been established but it can be postulated from the observations of various profiles that they are composed of closely packed small electron-translucent rods or tubules of undetermined length and are believed to be arranged in a hexagonal or rectangular pattern Each rod or tubule is surrounded by an electron-opaque material. Thus, in a section perpendicular to the length of the rods the profiles of hexagonally or rectangularly arrayed nets are revealed. The different patterns of the profiles of the crystalline bodies are probably due to different planes of section at various angles to the length of the rods or subunits of the crystalline bodies, and to the thickness of the sections. When the plane of section of a crystalline body is properly tilted with respect to the pathway of the electron beam the lattice-work changes from one pattern to another or it enhances the linear arrangement of the subunits in one direction and consequently both patterns are seen in some crystalline bodies A similar explanation has been given by Miller ('61), Karasaki ('63) and Maunsback ('66) In addition they have recognized another possible structure of the subunits in yolk platelets consisting of spherical particles such as revealed in the patterns of certain closely packed viral particles in ultra-thin sections (Dales and Franklin '62 Sjöstrand and Polson '58) The subunits in these amphibian yolk platelets which cause crystalline patterns are electron-opaque structures and superimposition of the spherical units to form linear electron-opaque bands due to the plane of section is readily pos-

tals. However, in the crystalline bodies of this study the subunits are electron-translucent and, if they are spherical, then no matter what the section angles may be, superimposition of these subunits to form electron-translucent bands cannot be expected. The appearance of the translucent bands alternating with the opaque bands in some crystalline bodies or in parts of the same crystalline body signifies that the subunits of the crystalline structure are rods or tubules rather than spheres or vesicles.

The appearance of more than one pattern of lattice work in a single crystalline structure is probably due to the fusion of more than one precursor cytoplasmic body during crystal formation, or the subunit tubules are slightly curved in such a way that in a given plane different patterns are seen within a single crystal. The profiles of two or more whorls of membranes which are sequestered by a limiting membrane are frequently encountered. This might imply that a single crystal can originate from the coalescence of more than one precursor cytoplasmic body. The similar mode of formation of protogranules through the coalescence of several smaller granules has been observed in juxtaglomerular cells (Barajas, '66).

The histochemical data of this study indicating that the cytoplasmic bodies are rich in phospholipids suggest that the structures seen in smooth muscle fibers and parasympathetic ganglion cells of treated animals are identical to those found in adrenal cortical cells of triparanol-treated hamsters (Yates '66a, Yates and Rappoport, '66). However it is possible that other substances such as desmosterol, triparanol, and certain enzymes related to cholesterol biosynthesis which are in amounts too small to be detected histochemically are entrapped in the phospholipid micelles of the dense bodies (Yates et al. '67).

At the present time more refined techniques for the isolation of these dense bodies are being undertaken and, consequently, definitive conclusions on their chemical nature awaits the results of these experiments.

LITERATURE CITED

Avigan, J., D. Steinberg, M. J. Thompson and E. Mosettig 1960 Inhibition of conversion of 24-dehydrocholesterol to cholesterol by MER-29. Fed. Proc., 19: 239.

Baker J. R. 1946 The histochemical recognition of lipine. Quart. J. Micr. Sci., 87: 441–470.

Ball, R. A., J. H. Sautter and R. E. Burger 1963 Toxicity of triparanol for the turkey poult. Arch. Path., 76: 633–639.

Barajas, L. 1966 The development and ultrastructure of the juxtaglomerular cell granule. J. Ultrastruct. Res., 15: 400–413.

Bernard, P. L., and J. H. G. Rhodin 1964 Fine structure of laminae muscularis mucosae. J. Ultrastruct. Res., 10: 489–497.

Blohm, T. R., T. Kariya, M. E. Laughlin and F. P. Palopoli 1959 Reduction of blood and tissue cholesterol by MER-29, a cholesterol inhibitor. Fed. Proc., 18: 369.

Blohm, T. R., and M. W. Laughlin 1959 Effects of MER-29, a cholesterol inhibitor on mammalian tissue lipides. Arch. Biochem. Biophy., 85: 250–263.

Caesar, R., G. A. Edwards and H. Ruska 1957 Architecture and nerve supply of mammalian smooth muscle tissue. J. Biophys. Biochem. Cytol., 3: 867–878.

Dales, S., and R. M. Franklin 1962 A comparison of the changes in fine structure of L cells during single cycles of viral multiplication, following their infection with viruses of Mengo and encephalomyocarditis. J. Cell Biol., 14: 281–302.

Deitch, A. D. 1961 An improved Sakaguchi reaction for microspectrophotometric use. J. Histochem. Cytochem., 9: 477–483.

Dietschy, J. M., and M. D. Siperstein 1965 Cholesterol synthesis by gastrointestinal tract: Localization and mechanisms of control. J. Clin. Invest., 44: 1311–1327.

Eisalo, A., and S. Talanti 1962 Effects of triparanol, dexamethasone and corticotropic hormone on the adrenal cortex of the rat. Ann. Med. Exp. Fenn., 40: 448–458.

Hruban, Z., B. Spargo, H. Swift, R. W. Wissler and R. G. Kleinfeld 1963 Focal cytoplasmic degradation. Amer. J. Path., 42: 675–683.

Hruban, Z., H. Swift and A. Slesers 1965 Effect of triparanol and diethanolamine on the fine structure of hepatocytes and pancreatic acinar cells. Lab. Invest., 14: 1652–1672.

Karasaki, S. 1963 Studies on amphibian yolk. I. The ultrastructure of the yolk platelet. J. Cell Biol., 18: 135–166.

King, W. M. 1960 The toxicology of MER-29. Progr. Cardiovasc. Dis., 2: 504–508.

Locke, M., and J. V. Collins 1965 The structure and formation of protein granules in the fat body of an insect. J. Cell Biol., 26: 857–884.

Luzzati, V., and F. Husson 1962 The structure of the liquid-crystalline phases of lipid-water systems. J. Cell Biol., 12: 207–219.

Mannsback, A. B. 1966 Electron microscopic observation of cytoplasmic bodies with crystal-

animals is decreased by one-half but no change in the cholesterol content in the nervous tissue of treated rats was noted However in the present study no cytoplasmic bodies were seen in the erythrocytes, while numerous crystalline structures were found in the neurons of the treated animals.

An interesting finding was the relationship between the initial appearance and later occurrence of cytoplasmic bodies during the periods of treatment. The relative numbers of cytoplasmic bodies seemed to increase in the order type I (or type II) type III and type IV in proportion to the length of treatment. Furthermore there were many intermediate types of cytoplasmic bodies in various stages of development. Thus it is conceivable that the crystalline bodies of type IV are formed, by progressive changes through the stages type I (or type II) and type III. It has been proposed by Luzzati and Husson ('62) and Stoekenius ('62a b) that changes in temperature and in the content of water alter the phospholipids from the lamellar to the hexagonal phase or vice versa. However in the present study the tissues were always prepared in ice-cold fixative and the temperature during dehydration was kept rather constant. Moreover not only did variable appearances of opaque bodies occur in the cytoplasm of a single cell but also different patterns were observed within a single cytoplasmic body (fig 12) In figure 12 one cytoplasmic body shows a lamellar structure both along the margin and in the interior and a reticular pattern in other parts From such observations it is believed that the different appearance of the cytoplasmic bodies is not caused by fixation or handling However this could represent a dehydration process of the cytoplasmic body and it is quite possible that the crystalline structures which appear compact and show a regular pattern are formed from the other types of opaque bodies through a dehydration process It is not unreasonable to assume that the water content of various types of the cytoplasmic bodies might be different at the time of fixation and consequently appear as different phases

The histochemical data indicate that the opaque granules are rich in phospholipids and possibly may represent hypertrophied membranes in autophagic vacuoles since such membranes sequestered by vacuoles were observed in this study It is not unreasonable to assume that, following a certain degree of lysis more resistant components of the membranes remain and represent the opaque granules. It has been demonstrated in hepatic and pancreatic acinar cells of triparanol-treated rats (Hruban et al. 65) that where myeloid membranes are sequestered with cytoplasmic material a portion of the inclusion which contains cytoplasm shows a positive acid phosphatase reaction

The exact 3-dimensional structure of the crystalline bodies has not been established but it can be postulated from the observations of various profiles that they are composed of closely packed small electron-translucent rods or tubules of undetermined length and are believed to be arranged in a hexagonal or rectangular pattern Each rod or tubule is surrounded by an electron-opaque material. Thus, in a section perpendicular to the length of the rods the profiles of hexagonally or rectangularly arrayed nets are revealed. The different patterns of the profiles of the crystalline bodies are probably due to different planes of section at various angles to the length of the rods or subunits of the crystalline bodies and to the thickness of the sections When the plane of section of a crystalline body is properly tilted with respect to the pathway of the electron beam the lattice-work changes from one pattern to another or it enhances the linear arrangement of the subunits in one direction and consequently both patterns are seen in some crystalline bodies A similar explanation has been given by Miller ('61) Karasaki ('63) and Maunsback (66) In addition, they have recognized another possible structure of the subunits in yolk platelets consisting of spherical particles such as revealed in the patterns of certain closely packed viral particles in ultra-thin sections (Dales and Franklin 62 Sjöstrand and Polson '58) The subunits in these amphibian yolk platelets which cause crystalline patterns are electron-opaque structures and superimposition of the spherical units to form linear electron-opaque bands due to the plane of section is readily pos-

line patterns in rat kidney proximal tubule cells. J Ultrastruct. Res. 14: 167–189
McGee-Russell, S. M., and N B Smale 1963 On colouring Epon-embedded tissue sections with Sudan black B or Nile blue A for light microscopy Quart. J Mic. Sci., 104: 109–115.
Menschik, Z. 1953 Nile blue histochemical method for phospholipids. Stain Technol., 28: 13–18
Miller F 1961 Lipoprotein granules in the cortical collecting tubules of mouse kidney J Biophys Biochem. Cytol., 9: 157–170
Novikoff A. B and W Y Shin 1964 The endoplasmic reticulum in the Golgi zone and its relations to microbodies, Golgi apparatus and autophagic vacuoles in rat liver cells. J Microscopie, 3: 187–206.
Pearse A. G E. 1960 In: Histochemistry Theoretical and Applied. Little Brown Boston, pp 792, 881.
Reynolds E. S. 1963 The use of lead citrate at high pH as an electron opaque stain in electron microscopy J Cell Biol., 17: 208–213
Sakaguchi, H. 1965 Pericentriolar filamentous bodies J Ultrastruct. Res., 12: 13–21
Scanu, A. W A. Hawk and I. H. Page 1962 Lethal effect on dogs of prolonged triparanol oral administration. Arch Path., 73: 445–450
Sjöstrand F S., and A. Polson 1958 Macrocrystalline patterns of closely packed polio-virus particles in ultrathin sections J Ultrastruct. Res., 1 365–374
Smith, D S. 1964 Structure of smooth muscle. In: Electron Microscopic Anatomy S. M. Kurtz, ed Academic Press New York and London, p 287
Steinberg, D., J Avigan and E. B. Feigelson 1961 Effects of triparanol (MER 29) on cholesterol biosynthesis and on blood sterol levels in man J Clin. Invest., 40: 884–893
Steiner J W., K. Miyai and M J Phillips 1964 Electron microscopy of membrane-particle arrays in liver cells of ethionine-intoxicated rats Amer J Path., 44: 169–213.
Stoeckenius, W 1962a Some electron microscopical observations on liquid-crystalline phases in lipid-water systems. J Cell Biol. 12: 221–229.
——— 1962b The molecular structure of lipid water systems and cell membrane models studied with the electron microscope. In: The Interpretation of Ultrastructure, R. J C. Harris ed., Academic Press, New York, p. 349.
Swift, H. and Z. Hruban 1964 Focal degradation as a biological process. Fed. Proc., 23: 1026–1037
Volk, T L., and D G Scarpelli 1964 Alteration of fine structure of the rat adrenal cortex after the administration of triparanol. Lab. Invest., 13: 1205–1214
Weber A. F., M. G. Phillips and J T Bell, Jr. 1956 An improved method for the Schultz cholesterol test. J Histochem. Cytochem., 4: 308–309
Yates R. D 1966a The effects of triparanol on adrenocortical cells of the zona fasciculata of Syrian hamsters. Z. Zellforsch., 71: 41–62.
——— 1966b The effects of triparanol on luteal cells of pregnant female Syrian hamsters. Anat. Rec., 154: 445.
——— 1966c Observations on crystalline cytoplasmic structures in steroid producing cells of Syrian hamsters treated with triparanol. Arch. Mex. Anat. 7: 78.
Yates R. D., and D. A. Rappoport 1966 An electron microscopic study of crystalline cytoplasmic bodies of triparanol treated Syrian hamsters. Sixth International Congress for Electron Microscopy (Kyoto) Vol. 2, p. 633.
Yates R. D., K. Arai and D. A. Rappoport 1967 Fine structure and chemical composition of crystalline cytoplasmic bodies of triparanol treated Syrian hamsters. Exp. Cell Res., 47: 459–478

Abbreviations

Cb Cytoplasmic body
Db Dense body
Der Dilated endoplasmic reticulum
G Golgi complex
M Mitochondria
I, Type I cytoplasmic body
II Type II cytoplasmic body
III Type III cytoplasmic body
IV Type IV cytoplasmic body
N Nucleus
Nl, Nucleolus
Pv Pinocytotic vesicle
Rer Rough-surfaced endoplasmic reticulum

PLATE 1

EXPLANATION OF FIGURES

1 Portions of several smooth muscle fibers from a control animal. Most cytoplasmic organelles other than myofilaments are concentrated in the axial cytoplasm at the poles of the elongated nuclei. Mitochondria are the most abundant organelles Both rough- and smooth-surfaced endoplasmic reticulum are poorly developed. A dense body is seen in one of the muscle fibers. Numerous pinocytotic vesicles are found in the cytoplasm near the plasma membrane. × 9 100

2 Portion of the tunica muscularis externa from an animal treated with triparanol for five days Note the numerous dense cytoplasmic bodies Such bodies are present either in the axial or peripheral cytoplasm in a few muscle cells. × 9 100

INTRANUCLEAR AND CYTOPLASMIC OPAQUE BODIES

Il Chen and Robert D. Yates

1

2

PLATE 2

EXPLANATION OF FIGURES

3 Transversely cut smooth muscle from a 1-day-treated animal showing smooth-surfaced membranes at the periphery of the fibers. These membranes presumably are formed by invaginations of the plasma membrane and tend to arrange in a whorl-like manner The arrow indicates a point of apparent continuation of the plasma membrane with the smooth membrane. Insert shows an almost complete whorl of smooth membranes. × 32 700

4 Portions of two adjacent muscle cells from a 12 hour-treated animal illustrating hypertrophied smooth membranes at the periphery of the fiber Such membranes include pinocytotic vesicles vacuoles of various sizes and anastomosing tubules. In several places the pinocytotic vesicles appear to open into larger vesicles or vacuoles. × 32 700

5 Portion of the Golgi region in the axial cytoplasm from a 1-day-treated animal. Note that some of the Golgi vesicles are sequestered by smooth membranes in two places. In one the bounding membrane is double instead of being characteristically single. × 32 700

6 Axial cytoplasm of a smooth muscle fiber from a 2-day-treated animal Two labyrinthine aggregates of smooth membranes belonging to type II and type IV cytoplasmic bodies are seen in this field. Arrows indicate the sites where membranous components of the type II bodies appear to be continuous with smooth-surfaced membranes × 32 700

7 The peripheral cytoplasm of the smooth muscle cell from a 2-day-treated animal. Several cytoplasmic bodies are shown one of which (I III) illustrates the characteristics of types I and III Note the profile in which free ribosomes and vesicles are trapped by spirally wound smooth membranes (the center of the picture) × 32,700

Insert illustrates a mitochondrion separated from the cytoplasm by two smooth membranes Note the portion of the membranes showing a reticular structure similar to that seen in type III cytoplasmic bodies. × 32,700


3
4
5
6
IV
II
I
I
I-I
7

PLATE 2

EXPLANATION OF FIGURES

3 Transversely cut smooth muscle from a 1-day-treated animal showing smooth-surfaced membranes at the periphery of the fibers These membranes presumably are formed by invaginations of the plasma membrane and tend to arrange in a whorl-like manner The arrow indicates a point of apparent continuation of the plasma membrane with the smooth membrane Insert shows an almost complete whorl of smooth membranes. × 32,700

4 Portions of two adjacent muscle cells from a 12 hour-treated animal illustrating hypertrophied smooth membranes at the periphery of the fiber Such membranes include pinocytotic vesicles, vacuoles of various sizes and anastomosing tubules. In several places, the pinocytotic vesicles appear to open into larger vesicles or vacuoles. × 32,700

5 Portion of the Golgi region in the axial cytoplasm from a 1-day-treated animal. Note that some of the Golgi vesicles are sequestered by smooth membranes in two places In one the bounding membrane is double instead of being characteristically single × 32 700

6 Axial cytoplasm of a smooth muscle fiber from a 2-day-treated animal. Two labyrinthine aggregates of smooth membranes belonging to type II and type IV cytoplasmic bodies are seen in this field. Arrows indicate the sites where membranous components of the type II bodies appear to be continuous with smooth-surfaced membranes. × 32,700

7 The *peripheral cytoplasm of the* smooth muscle cell from a 2-day-treated animal. Several cytoplasmic bodies are shown, one of which (I III) illustrates the characteristics of types I and III. Note the profile in which free ribosomes and vesicles are trapped by spirally wound smooth membranes (the center of the picture) × 32,700

Insert illustrates a mitochondrion separated from the cytoplasm by two smooth membranes. Note the portion of the membranes showing a reticular structure similar to that seen in type III cytoplasmic bodies. × 32 700.

[illegible] and Robert D. [illegible]

8

9

PLATE 3

EXPLANATION OF FIGURES

8 Portions of three adjacent smooth muscle fibers from an animal treated for three days Note the numerous cytoplasmic bodies concentrated in the axial cytoplasm of the muscle fiber Most of the bodies are of type I and show a considerable variation in size and appearance In two places profiles of vesicles and smooth membranes which are sequestered by limiting membranes are seen × 21 400

9 The axial cytoplasm of a smooth muscle fiber from a 4-day-treated animal. A few cytoplasmic bodies are seen in this field. Aside from the two cytoplasmic bodies which are labeled III and III IV all the others belong to type IV × 35,000

PLATE 4

EXPLANATION OF FIGURES

10 Portions of perikarya of three postganglionic cells in the myenteric plexus of a control animal Rough-surfaced endoplasmic reticulum, composed of flattened sacs studded with ribosomes is rather sparsely distributed in the cytoplasm. The Golgi complexes consist predominantly of lamellae. Free ribosomes are also seen in the cytoplasm. In the central neuron several dense bodies are present. These bodies are probably lysosomes or lipofuscin granules. × 13,000

11 Portion of the perikaryon of a postganglionic cell from a 5-day-treated animal Note the numerous dense bodies within the cytoplasm of the neuron and moderate dilation of the cisternae of the ergastoplasm in comparison with the neuron in figure 10 The cytoplasmic bodies tend to occur in the vicinity or at the periphery of the Golgi complex but are rarely found within the Golgi region. × 13,000.

M

Der

III

IV

13

PLATE 5

EXPLANATION OF FIGURES

12 Portion of the perikaryon of a postganglionic cell in the myenteric plexus from a 3-day-treated animal. Several cytoplasmic bodies of intermediate type are seen. Note one such cytoplasmic structure (arrow) consisting of a type I pattern in the interior and at the periphery and a type III pattern in the remainder of the body. × 35,000

13 Portion of a perikaryon of a postganglionic cell from a 5-day-treated animal. Aside from type III and type IV there are a few type I and type II bodies. Arrows indicate the sites where the membranous components of the cytoplasmic bodies seem to be continuous with the dilated endoplasmic reticulum. × 35,000




15



PLATE 6

EXPLANATION OF FIGURES

14–16 High power micrographs of crystalline bodies (type IV) showing different patterns of lattice work namely hexagonal (fig 14) rectangular (fig. 15) and banded (fig 16) × 104,000.

An Autoradiographic Study of Satellite Cells in Autonomic Ganglia

ROBERT CONRAD SCHWYN

Department of Anatomy, School of Medicine — School of Dentistry, Georgetown University, Washington, D. C.

ABSTRACT This investigation was undertaken to observe and to correlate the responses of satellite cells in autonomic ganglia to increased neuronal and synaptic activity. By electrically stimulating preganglionic nerve fibers terminating in the superior cervical sympathetic ganglion in 19 adult cats and concurrently injecting thymidine-H_3 into the stimulated animal, it was possible to alter the neuronal and synaptic activity within the superior cervical ganglion and subsequently observe from autoradiograms the cellular absorption of thymidine-H_3. The specific reaction encountered was incorporation of thymidine-H_3 into the nuclei of satellite cells. Absorption of thymidine by satellite cells and incorporation of this compound into their nuclear structure could be accelerated or inhibited by exposing the organism to specific drugs (viz. neostigmine and atropine sulfate) during the stimulatory period.

The results of this investigation combined with information gathered from studies in many other scientific areas implicate satellite cell participation in response to increased neuronal metabolism and possibly to increased synaptic activity. Satellite cells apparently proliferate to cope with the demands of increased ganglionic activity elicited by the experimental procedures employed in this study. Although specific reactions of satellite cells other than cellular proliferation were not identified in this study, their probability may provide a basis for further investigation.

HISTORICAL REVIEW

The neuron doctrine, formulated by Waldeyer in 1891 and championed by Ramon y Cajal during the years to follow (Rasmussen, '47) described the neuron as the anatomical, functional, embryological, and trophic unit of the nervous system. Under the guidance of these fundamental aspects of neurology our knowledge of neuron structure and function surged forward very rapidly, gathering momentum as it progressed. In comparison, information related to the functional significance of the non-nervous cellular components of the nervous system remained relatively stagnant. The original descriptive term applied to this mass of supporting cells was translated into the English language as "nerve glue" and was appropriate at that time. This trend of thought persisted during the great boom of neurological investigation.

The supporting cellular elements located in peripheral ganglia were also designated as neuroglia because they demonstrated anatomical structure and relationships similar to oligodendrocytes identified within the central nervous system. The functional capacities of these cells are even more obscure than those in the central nervous system. Although the term neuroglia appears in many textbooks and periodicals, many prominent neuroanatomists today hesitate to identify them as neuroglia, perhaps avoiding terminology that may not correctly reflect their functional or anatomical significance. For want of better descriptive terminology, the supporting cellular elements located in the superior cervical sympathetic ganglion will be referred to as interstitial or perineuronal satellite cells because of their anatomical location in relation to the neurons. Furthermore, perineuronal satellite cells will be classified as either primary or secondary satellite cells. The terminology referring to satellite cells does not include Schwann cells, endothelial cells, fibroblasts, or other connective tissue cells that may be present in the superior cervical ganglion.

Satellite cells within the ganglion were considered to be homologous to oligodendrocytes of the CNS, and were classified according to their position as capsular and

A portion of this work was completed at The Ohio State University, Columbus, Ohio, in partial fulfillment for the Degree of Doctor of Philosophy.

Present address: Department of Anatomy, School of Medicine, Wayne State University, 1400 Chrysler Freeway, Detroit, Michigan 48207.

METHODS

The superior cervical sympathetic ganglia of 19 healthy adult cats (*Felis domestica*) were utilized in the experimental procedures. Each animal was anesthetized intraperitoneally with Diabutal, 30 mg per kilogram of body weight. The cervical sympathetic trunk, lying within the carotid sheath, was then surgically exposed and isolated from the vagus nerve and carotid artery. The contralateral trunk was maintained as a control. Paired electrodes were applied to the very lightly myelinated preganglionic fibers of the exposed sympathetic trunk approximately one and one-half inches caudal to the superior cervical ganglion. A sine wave electric current of 0.01 volts at a frequency of ten pulses per second for a duration of 10 msec was administered continuously for a period not exceeding three hours. Adequate stimulation was indicated by complete retraction of the nictitating membrane and dilation of the pupil on the stimulated side of the animal.

The control animals were subjected to all the traumatic conditions of exposing the sympathetic trunk and applying electrodes in identically the same manner as all other animals. The stimulation period however was merely simulated for three hours with each of the four control animals referred to in table 1.

In addition to afferent stimulation of the superior cervical ganglion, some of the animals were injected intramuscularly with either neostigmine or atropine sulfate. Neostigmine was administered to three of the experimental animals at the onset of stimulation and every 45 minutes thereafter. The dosage per injection was 1 ml of a 1% aqueous solution. Four other animals received injections of atropine sulfate. One milliliter of a 1:1000 solution was administered at the onset of electrical stimulation and at 45 minute intervals. The remaining experimental animals received only electrical stimulation (see table 1).

TABLE 1

Operated animals injected with 0.5 mCi Thymidine-H_3	Quantity	Stimulation period	Drug administered
Control animals	4	none (simulated for 180 minutes)	none
Stimulated animals		minutes	
	2	30	none
	1	105	none
	2	120	none
	1	150	none
	2	180	none
	1	105	neostigmine
	1	120	neostigmine
	1	180	neostigmine
	4	180	atropine sulfate

Since the focus of study is deoxyribose nucleic acid (DNA) synthesis by satellite cells in the superior cervical ganglion thymidine-H_3 was injected into each animal as a precursor substance of nuclear DNA. Tritium (H_3) coupled to the number six position of the thymidine molecule is one of the most commonly used isotopes in autoradiography. It emits a low energy β particle (18 KEV maximum energy) lowest of any known isotope. The specific activity of thymidine-H_3 is greater than 10 000 mCi per millimole. Considering that the microscopic resolution of autoradiograms is inversely proportional to the energy of the β particle emission tritium therefore is capable of producing excellent resolution and sensitivity. Tritiated thymidine was obtained in 2 mCi quantities, 1 mCi being equal to 1 ml of solution. Each animal, including the four control animals, was injected intravenously with 0.5 mCi of thymidine-H_3 stock solution diluted to 2 ml with double distilled water as soon as the electrical stimulation was considered to be maximally effective. This interval varied with each animal, but it never exceeded three minutes. Stimulation times for each animal after thymidine-H_3 injection are recorded in table 1.

Bilateral superior cervical ganglia from each animal were removed immediately after the simulated or actual stimulation period and placed in 10% formalin preservative for 24 hours. Animals were sacrificed subsequent to the removal of

Thymidine (nominally 6-T) sterile aqueous solution TRK-61 was obtained from Nuclear-Chicago Corporation, 333 East Howard Avenue, Des Plaines, Illinois. Kodak nuclear track emulsion NTB-2 was obtained from Eastman Kodak Company 343 State Street, Rochester, New York.

interstitial by Kuntz and Sulkin (47a b) Cravioto and Merker (63) observed with the electron microscope a space of approximately 150–200 A between cell membranes Their description of satellite cells in the ganglion was not morphologically the same as those in the CNS They suggest however that they be compared to oligodendrocytes of the CNS in view of their abundance of endoplasmic reticulum. A further suggestion is implied that the connective tissue cells of autonomic ganglia take over the function of water metabolism performed in the CNS by astrocytes

Although there were early suggestions that neuroglia cells were involved in processes other than their own maintenance and neuron suspension there were insufficient experimental data to lend much support to the concept Within the last 20 years our understanding of neuroglia elements has increased but it has remained in the shadow of investigations conducted on neuronal function

More recently a vast amount of effort has been expounded upon the functional activities of neuroglia in the CNS by Niessing (59) Galambos (61) Hyden (61) De Robertis and Gerschenfeld (61) Hamberger and Hyden ('63) and Dan (64) However relatively few studies have been carried out on functional activities of supporting cells existing in autonomic ganglia and particularly the superior cervical ganglion In view of the relative sparseness of scientific data related to the functional significance of supporting cells in autonomic ganglia it has become necessary to pursue tangential material and attempt to correlate it with our knowledge of autonomic ganglia.

Autoradiographic studies of satellite cells in autonomic ganglia pertinent to this investigation have not been reported in the literature Therefore it became necessary to pursue autoradiographic investigations concerned with neuroglia in the CNS and apply some of the principles to studies of satellite cells in autonomic ganglia Autoradiographic techniques although relatively new and in early stages of application have been utilized very successfully during the past decade in determining the dynamics of cellular activity Almost any biochemical compound can be labeled with various radioisotopes. Autoradiographic identification of a cell component however depends largely upon the availability of the labeled compound and the time involved for its cellular abs

By injecting thymidine-H_3 into mice Smart and Leblond ('61) were able to tag some of the neuroglia cells In addition the labeling of neuroglia the nuclear configuration of these cells led to the suggestion of amitosis as a mode of cell division. Altman ('62) also using thymidine-H_3 reported degenerative and regenerative proliferation of neuroglia cells in response to lesions of the lateral geniculate body Altman (63) also demonstrated uptake of thymidine-H_3 by glia cells in a normal cat brain Most of the labeled cells however were ependymal cells or those cells located bilaterally along the midline. After crushing the hypoglossal nerve Sjöstrand ('65) observed a metabolic synthesis of DNA in astrocytes in the hypoglossal nucleus during regeneration of the nerve The labeling substance was also tritiated thymidine.

From the foregoing discussion, it is apparent that neuroglia cells play a considerably more dynamic functional role in the nervous system than was originally perceived by early investigators Although the physical supporting theory of neuroglia function has not been discarded it is looked upon presently by many as a passive or secondary activity of glia cells The present state of scientific investigation represents neuroglia as individual cellular elements related directly or indirectly to the metabolic activity of neurons

It is hoped that the results of this investigation will shed additional light upon the possibility of satellite cell involvement in neuronal metabolism and synaptic activity in autonomic ganglia The following information may be of value to those interested in the functional relationship existing between neurons and their supporting cellular elements in autonomic ganglia. Since facets of various disciplines are encountered during this study it is presumed that individuals involved in anatomical physiological biochemical and pathological research may find some aspect of this paper applicable to their own work.

METHODS

The superior cervical sympathetic ganglia of 19 healthy adult cats (*Felis domesticus*) were utilized in the experimental procedures. Each animal was anesthetized intraperitoneally with Diabutal, 30 mg per kilogram of body weight. The cervical sympathetic trunk, lying within the carotid sheath, was then surgically exposed and isolated from the vagus nerve and carotid artery. The contralateral trunk was maintained as a control. Paired electrodes were applied to the very lightly myelinated preganglionic fibers of the exposed sympathetic trunk approximately one and one-half inches caudal to the superior cervical ganglion. A sine wave electric current of 0.01 volts at a frequency of ten pulses per second for a duration of 10 msec was administered continuously for a period not exceeding three hours. Adequate stimulation was indicated by complete retraction of the nictitating membrane and dilation of the pupil on the stimulated side of the animal.

The control animals were subjected to all the traumatic conditions of exposing the sympathetic trunk and applying electrodes in identically the same manner as all other animals. The stimulation period however was merely simulated for three hours with each of the four control animals referred to in table 1.

In addition to afferent stimulation of the superior cervical ganglion, some of the animals were injected intramuscularly with either neostigmine or atropine sulfate. Neostigmine was administered to three of the experimental animals at the onset of stimulation and every 45 minutes thereafter. The dosage per injection was 1 ml of a 1% aqueous solution. Four other animals received injections of atropine sulfate. One milliliter of a 1:1000 solution was administered at the onset of electrical stimulation and at 45 minute intervals. The remaining experimental animals received only electrical stimulation (see table 1).

TABLE 1

Operated animals injected with 0.5 mCi Thymidine-H_3	Quantity	Stimulation period	Drug administered
Control animals	4	none (simulated for 180 minutes)	none
Stimulated animals		minutes	
	2	30	none
	1	105	none
	2	120	none
	1	150	none
	2	180	none
	1	105	neostigmine
	1	120	neostigmine
	1	180	neostigmine
	4	180	atropine sulfate

Since the focus of study is deoxyribose nucleic acid (DNA) synthesis by satellite cells in the superior cervical ganglion, thymidine-H_3 was injected into each animal as a precursor substance of nuclear DNA. Tritium (H_3) coupled to the number six position of the thymidine molecule is one of the most commonly used isotopes in autoradiography. It emits a low energy β particle (18 KEV maximum energy), lowest of any known isotope. The specific activity of thymidine-H_3 is greater than 10,000 mCi per millimole. Considering that the microscopic resolution of autoradiograms is inversely proportional to the energy of the β particle emission tritium therefore is capable of producing excellent resolution and sensitivity. Tritiated thymidine was obtained in 2 mCi quantities 1 mCi being equal to 1 ml of solution. Each animal, including the four control animals, was injected intravenously with 0.5 mCi of thymidine-H_3 stock solution diluted to 2 ml with double distilled water as soon as the electrical stimulation was considered to be maximally effective. This interval varied with each animal, but it never exceeded three minutes. Stimulation times for each animal after thymidine-H_3 injection are recorded in table 1.

Bilateral superior cervical ganglia from each animal were removed immediately after the simulated or actual stimulation period and placed in 10% formalin preservative for 24 hours. Animals were sacrificed subsequent to the removal of

---

Thymidine (nominally 6-T) sterile aqueous solution TRK-61 was obtained from Nuclear-Chicago Corporation, 333 East Howard Avenue, Des Plaines, Illinois. Kodak nuclear track emulsion NTB-2 was obtained from Eastman Kodak Company 343 State Street,

both ganglia Tissues were sectioned in paraffin at 7 μ according to the usual techniques and mounted on glass slides

Autoradiograms were prepared according to the dipping technique outlined by Joftes (63) Tissue sections were exposed to Kodak nuclear track emulsion NTB-2[a] for a ten day period After the autoradiograms were completed the underlying tissue sections were counterstained with Toluidine blue in order to identify exact cellular sites of radioactivity

A few ganglion sections from the unstimulated control animals were prepared in accordance with the procedures outlined by Lapham et al. (64) They were utilized to illustrate the basic cellular components within the superior cervical ganglion and to identify their shape and anatomical relationships prior to electrical stimulation and drug administration

OBSERVATIONS

Autoradiograms from this investigation are examined and described in three separate groups Superior cervical ganglia of control animals are presented initially to establish the general pattern of radioisotope activity in a normal ganglion The second group examined are ganglia removed from animals receiving only unilateral preganglionic stimulation The third group consists of ganglia removed from animals that were administered drugs viz. neostigmine and atropine sulfate in addition to receiving preganglionic stimulation.

Autoradiograms and underlying tissue sections were examined under the light microscope at a magnification of 500 × and under oil immersion at 1300 × Background fog typical in most autoradiograms was taken into consideration during identification of labeled nuclei. Background can be attributed to many unavoidable factors and is discussed very thoroughly by Danielli ('58) *General Cytochemical Methods* and by Caro and Tubergen (62)

A Observations of superior cervical ganglia removed from control animals

Most ganglion sections prepared from control animals revealed no evidence of nuclear labeling (fig. 2) However a few labeled nuclei of satellite cells could be identified widely dispersed throughout some of the control ganglia. This phenomenon is comparable to atropine-exposed ganglia described subsequently

Neurons within the superior cervical ganglion displayed an abundance of Nissl substance which was homogeneously dispersed throughout the cytoplasm. Nuclei of neurons were located near the center of the cell body Supporting satellite cells within the ganglia exhibited round or slightly oval nuclei and were identified by their location as either perineuronal or interstitial Some of the perineuronal satellite cells could be observed as primary capsular cells forming an incomplete layer of cells adjacent to the neurons. Other secondary satellite cells were positioned slightly outside the layer of primary cells. Interstitial satellite cells were arranged in a relatively even and randomly distributed pattern Ganglion sections represented by figure 1 were prepared specifically to illustrate the above description of cellular morphology and anatomical relationships in the superior cervical ganglion.

The nuclei of Schwann cells forming a sheath for preganglionic sympathetic nerve processes joining the ganglion were confined to neuron processes. In contrast to satellite cells the nuclei of Schwann cells appear more dense more oblong and were arranged in uniform parallel patterns along the neuron processes. Nuclei of Schwann cells do not contain the dense centrally located chromatin granule that is usually prominent in the nuclei of satellite cells. Fibroblasts and endothelial cells may also be distinguished from satellite cells on the basis of their nuclear configuration. Mast cells were present throughout the ganglia and along the nerves joining the ganglia. The cytoplasm of some mast cells displayed evidence of disintegration

B Observations of stimulated superior cervical ganglia

The examination of autoradiograms from the ganglia stimulated for 30 minutes revealed a few labeled nuclei of satellite cells per 7 μ section The labeled cells

tained at least three, but rarely more than three, black granules over their nuclei. The shape and arrangement of nuclei of satellite cells were similar to that of control ganglia previously described. Most neurons revealed no morphological indications of increased metabolic activity. Nuclei and cytoplasmic arrangement of the neurons appeared normal. The contralateral unstimulated ganglia were similar in appearance to control ganglia previously described in section A.

The greatest degree of radioactivity was observed in autoradiograms prepared from ganglia stimulated for a period longer than 90 minutes, (105–180 minutes). Many nuclei of satellite cells were heavily labeled (fig. 3). Some of the labeled cells were so densely covered with black granules that it was difficult to determine specific details of the nucleus or its outline. Densely labeled nuclei appear singly or in clusters of two or three. Each ganglion demonstrated a high degree of selectivity. Many heavily labeled nuclei or groups of labeled nuclei were identified adjacent to or surrounded by satellite cells completely void of radioisotope.

Most labeled cells were either primary or secondary perineuronal satellite cells (figs. 3, 4, 5). The remaining labeled cells were interstitial satellite cells (fig. 6). A great majority of neurons appear to be in a high degree of metabolic activity as determined by chromatolysis, a peripheral ring of Nissl substance and peripheral nucleus. The nuclei of some neurons appeared to touch the plasma membrane. Labeled perineuronal satellite cells were usually associated with neurons having the characteristics of increased metabolic activity (figs. 4, 5). The interstitial satellite cells that were labeled appeared randomly and no pattern of cellular distribution could be identified. Many cells did not display the round or slightly oval nuclear configuration presented by the nuclei of ganglia processed from control animals. The nuclei of these cells were distorted in such a fashion as to appear oblong, fusiform, and occasionally dumbbell-shaped. A thin strand of nuclear material, varying in length and width, joined the two nodular ends of dumbbell-shaped nuclei. Atypical nuclei were not considered to be technique artifacts since many normal nuclei were intermingled among them.

An occasional labeled satellite cell or group of satellite cells appeared in the unstimulated ganglia of these animals. Mast cells were prominent and displayed less evidence of cytoplasmic disintegration than those in the stimulated ganglia. Morphological characteristics of neuronal activity were similar to the characteristics displayed by neurons observed in unstimulated ganglia taken from control animals. The shape and distribution of satellite cells were similar to those observed in sections of control ganglia.

C. *Observations of ganglia removed from drug-injected animals*

1. *Neostigmine exposed animals.* The stimulated ganglia from neostigmine-injected animals are compared to the contralateral unstimulated ganglia. In addition, both stimulated and unstimulated ganglia are compared to ganglia described in sections A and B.

Many labeled nuclei of satellite cells were observed in the stimulated ganglia. The labeled nuclei could be identified singly or in clusters ranging from three to ten labeled nuclei per cluster. The quantity of labeled cells in these ganglia was approximately two to four times greater than the number observed in stimulated ganglia not exposed to drugs; compare figure 7 with figures 5 and 6. Nuclei varied extensively in the degree of labeling and quite often were not the typical round or oval shape. On the contrary they displayed many different shapes and sizes indicative of cell movement, as reported by Berg and Kallen ('59).

Labeled satellite cells were randomly dispersed and readily identifiable throughout the unstimulated ganglia of these animals. The shape and distribution of satellite cells, however, were similar in appearance to control ganglia described in section A.

Neuronal activity in the ganglia of the three operations of this section did not exhibit the high degree of metabolic stress that was prevalent in ganglion cells not exposed to drugs and stimulated for an identical period of time.

2. *Atropine sulfate exposed animals* The stimulated and contralateral unstimulated ganglia of those animals injected with atropine sulfate (fig 8) were very similar in appearance to each other and to the control ganglia described in section A. Small quantities of radioactive tracer were evident within the ganglia. Very rarely were any labeled nuclei observed. When a labeled satellite cell did appear it was usually a perineuronal satellite cell within a stimulated ganglion The neurons in all ganglia appeared to be in a normal functional state demonstrating nearly centrally positioned nuclei and evenly distributed Nissl substance. Satellite cells were randomly and evenly distributed, and most nuclei were round or slightly oval shaped

DISCUSSION

In order to develop a working hypothesis in an attempt to explain the significance of labeled satellite cells in the superior cervical ganglion it is necessary to consider the works of previous investigators in conjunction with results obtained from this study By means of autoradiograms it has been demonstrated that satellite cells increase their DNA component in response to highly increased neuronal activity and/or greatly increased synaptic activity Involvement of satellite cells in both activities simultaneously is very probable The absorption of thymidine-H, by satellite cells was further modified and controlled by the injection of certain drugs which are known to affect chemical transmission of an impulse from presynaptic to postsynaptic structures The degree of satellite cell activity also could be controlled by varying the duration of faradic stimulation.

Schwyn and Hall ('65) have reported quantitative increase of satellite cells from 50–100% in the superior cervical ganglion of cats after three hours of faradic stimulation of the cervical sympathetic trunk It seems reasonable to presume that labeled satellite cells observed from autoradiograms are the same cells responsible for the increased number when quantitative calculations were performed

It has been well established physiologically and biochemically that ionic and chemical changes occurring during the transmission, integration, and recovery thereafter of a nervous impulse requires an immediate and sufficient level of nutrients oxygen, and energy as well as metabolic pathways for removal of waste products. An attempt to calculate the the metabolic turnover in the ganglion during a continuous three hour stimulation period is beyond the scope of this study However the greatly accelerated metabolic and synaptic activities created during stimulation procedures are considered to be the most significant factors initially responsible for altered satellite cell activity within the stimulated ganglia.

The orientation of the nuclei of neurons and the concentration of Nissl substance in the stimulated ganglia were identical to the characteristics of metabolically altered neurons described by Richins and Hall ('58) Since postganglionic neurons exhibiting characteristics of metabolic stress were not directly stimulated it must be assumed that their altered metabolic activity is due to preganglionic stimulation. Even though neurons were observed in varying degrees of metabolic stress gross observation of ocular structures innervated by neurons located in the superior cervical ganglion indicated no deviation from normal functional efficiency under the stimulatory conditions In view of the stress conditions exhibited by ganglionic neurons from preganglionic electrical stimulation, it can be assumed that the metabolic activity and nutritional requirements are greatly increased

Most labeled satellite cells were related to neurons exhibiting characteristics of metabolic stress Since metabolites entering and leaving the ganglion cells are thought to pass through satellite cell cytoplasm the activity of satellite cells would be expected to increase if they were directly involved in relaying metabolites from capillaries to neurons Satellite cells may proliferate in an attempt to fulfill the great demands of neurons during such stressful conditions as elicited during this investigation

The satellite cell reaction to the environmental conditions within the stimulated ganglia was thymidine uptake from the blood and incorporation of this compound into nuclear substance. Since thymidine is a specific precursor of DNA it is gen

erally considered that synthesis of thymidine reflects some process of DNA turnover. When thymidine is readily available in vascular channels, a condition artifically produced by injection in this investigation its uptake and incorporation into nuclear structure would equally represent a process of DNA turnover Except during chromosomal replication nuclear DNA is considered to be metabolically inert. Therefore, autoradiographic demonstration of thymidine-H_3 uptake by cell nuclei indicates that labeled cells either were preparing for cell division while the thymidine was available or they are products of previously labeled cells (Taylor et al., '57 Hughes et al. '58 Leblond et al., '59 Altman, '63)

Experimental data compiled from this investigation and information from the works of other investigators also lend support to the idea, advocated by DeCastro ('51) that satellite cells could be directly related to synaptic activity Electron microscopic studies of Elfvin ('63) Cravioto and Merker ('63) and others have provided us with specific information regarding the exact anatomical relationship of satellite cells to neurons and their processes. From these studies it has been established that every neuron and its processes are covered by a sheath or capsule of satellite cells except at the synaptic site between cell membranes. The extracellular space, ranging from 150–200 A is bound laterally by satellite cells which have a very irregular boundary A few synaptic contacts have been found to exist between preganglionic fibers and ganglion cell bodies. The most abundant type of contact in autonomic ganglia, however is between preganglionic fibers and ganglion cell dendrites which extend only a short distance from the cell body This type of contact is characterized by preganglionic fibers running parallel to or winding around the dendrite to establish contacts at several different points. Both types (axosomatic and axodendritic) are primarily ensheathed by primary or secondary perineuronal satellite cells Most labeled satellite cells in comparison to this study were either primary or secondary perineuronal satellite cells and could be identified in typical relationship to highly active neurons.

The possibility of satellite cell involvement in synaptic activity was strengthened by controlling transmission of impulses at synaptic sites with drugs having antagonistic effects at sites of impulse transmission The effects of neostigmine are considered first.

Acetylcholine is the only known chemical transmitter in autonomic ganglia and it is very rapidly deactivated by cholinesterase immediately after it has performed its function of depolarizing postsynaptic membranes. It is the speed of this inactivation process which allows for rapid restoration of postsynaptic membranes and enables neurons to respond to the next stimulus in approximately 1 msec. Neostigmine breaks down cholinesterase and renders it ineffective. Consequently concentrations of acetylcholine are allowed to accumulate and act unopposed at synaptic areas when neostigmine is present at the time of neuronal stimulation. Continuous depolarization of postsynaptic membranes and increased metabolic activity of neurons involved seems very likely under these conditions Neostigmine does not inhibit the synthesis of cholinesterase therefore the presence of acetylcholine and continuous depolarization of postsynaptic membranes would theoretically stimulate production and release of cholinesterase from anatomical sites not yet specifically identified. Satellite cell participation in the production or release of cholinesterase most certainly must be considered since many authors (Koelle '50 Fredricsson and Sjoqvist, '62) have found, histochemically that satellite cells contain varying concentrations of specific and non-specific cholinesterase

Pappano and Volle ('62) have suggested that acetylcholine may cause depolarization of both presynaptic and postsynaptic elements. According to their proposal, the depolarization by acetylcholine of nerve terminals would result in a decrease in the amount of transmitter liberated by induced electrical stimulation, reduce the number of cells capable of responding to a preganglionic volley and decrease the amplitude of postganglionic action potential. Incomplete pupillary dilation and less obvious

2 *Atropine sulfate exposed animals* The stimulated and contralateral unstimulated ganglia of those animals injected with atropine sulfate (fig 8) were very similar in appearance to each other and to the control ganglia described in section A Small quantities of radioactive tracer were evident within the ganglia. Very rarely were any labeled nuclei observed When a labeled satellite cell did appear it was usually a perineuronal satellite cell within a stimulated ganglion The neurons in all ganglia appeared to be in a normal functional state, demonstrating nearly centrally positioned nuclei and evenly distributed Nissl substance Satellite cells were randomly and evenly distributed and most nuclei were round or slightly oval shaped

DISCUSSION

In order to develop a working hypothesis in an attempt to explain the significance of labeled satellite cells in the superior cervical ganglion it is necessary to consider the works of previous investigators in conjunction with results obtained from this study By means of autoradiograms it has been demonstrated that satellite cells increase their DNA component in response to highly increased neuronal activity and/or greatly increased synaptic activity Involvement of satellite cells in both activities simultaneously is very probable The absorption of thymidine-H_3 by satellite cells was further modified and controlled by the injection of certain drugs which are known to affect chemical transmission of an impulse from presynaptic to postsynaptic structures The degree of satellite cell activity also could be controlled by varying the duration of faradic stimulation

Schwyn and Hall ('65) have reported quantitative increase of satellite cells from 50–100% in the superior cervical ganglion of cats after three hours of faradic stimulation of the cervical sympathetic trunk. It seems reasonable to presume that labeled satellite cells observed from autoradiograms are the same cells responsible for the increased number when quantitative calculations were performed

It has been well established physiologically and biochemically that ionic and chemical changes occurring during the transmission, integration and recovery thereafter of a nervous impulse require an immediate and sufficient level of nutrients oxygen, and energy as well as metabolic pathways for removal of waste products An attempt to calculate the the metabolic turnover in the ganglion during a continuous three hour stimulation period is beyond the scope of this study However the greatly accelerated metabolic and synaptic activities created during stimulation procedures are considered to be the most significant factors initially responsible for altered satellite cell activity within the stimulated ganglia.

The orientation of the nuclei of neurons and the concentration of Nissl substance in the stimulated ganglia were identical to the characteristics of metabolically altered neurons described by Richins and Hall ('58) Since postganglionic neurons exhibiting characteristics of metabolic stress were not directly stimulated it must be assumed that their altered metabolic activity is due to preganglionic stimulation. Even though neurons were observed in varying degrees of metabolic stress, gross observation of ocular structures innervated by neurons located in the superior cervical ganglion indicated no deviation from normal functional efficiency under the stimulatory conditions In view of the stress conditions exhibited by ganglionic neurons from preganglionic electrical stimulation it can be assumed that the metabolic activity and nutritional requirements are greatly increased

Most labeled satellite cells were related to neurons exhibiting characteristics of metabolic stress Since metabolites entering and leaving the ganglion cells are thought to pass through satellite cell cytoplasm the activity of satellite cells would be expected to increase if they were directly involved in relaying metabolites from capillaries to neurons Satellite cells may proliferate in an attempt to fulfill the great demands of neurons during such stressful conditions as elicited during this investigation

The satellite cell reaction to the environmental conditions within the stimulated ganglia was thymidine uptake from the blood and incorporation of this compound into nuclear substance Since thymidine is a specific precursor of DNA it is gen-

tally identified and is in need of further exploration.

Although the preceding suggestions are in need of further investigation and may be disproved or modified in the future they present at this time a working hypothesis compiled from pertinent available knowledge of satellite cells in the superior cervical ganglion of the cat. There is evidence to suggest that satellite cells respond to increased metabolic and/or increased synaptic activity by proliferating. The mode of cellular division may be something other than normal mitosis. Satellite cell activity can be controlled further by the use of specific drugs known to influence nervous transmission at synaptic sites. This study has been performed on the cat superior cervical ganglion, however there is no reason to believe that the principles deducted from these data can not be applied to other autonomic ganglia in which the environmental conditions, cellular elements and chemical transmitter are similar As far as the evolution of biological systems is concerned, the autonomic nervous system is one of the oldest. Perhaps the knowledge compiled from the supporting cells within the autonomic nervous system can be applied with or without modifications to more newly developed and more complex portions of the nervous system whose biochemical properties are still in their infancy of exploration.

LITERATURE CITED

Altman, J. 1962 Autoradiographic studies of degenerative and regenerative proliferation of neuroglia cells with tritiated thymidine. Exp. Neurol., 5 302–318.

——— 1963 Autoradiographic investigation of cell proliferation in the brain of rats and cats. Anat. Rec., 145 573–591.

Berg, O and B. Kallen 1958 Studies of rat neuroglia cells in tissue culture. J. Neuropath. Exp Neurol., 18 438–467

Caro, L. G., and R. Tubergen 1962 High resolution autoradiography I. J. Cell Biol., 15: 173–188.

Cervós, H., and H. Merker 1962 Elektronenmikroskopische Untersuchungen an Satellitenzellen der Sympathischen Ganglien des Menschen. Archiv f Psychiatrie u. Nervenkrankheiten ges. Neurologie, 204 1–10.

Das, E. 1954 Interrelationship between the neurons and neuroglia. Neurologia, 3 360–378.

Danielli, J (ed.) 1963 General Cytochemical Methods. Academic Press Inc., New York.

De Robertis, E., and H. Gerschenfeld 1961 Submicroscopic morphology and function of glia cells. Intern. Rev Neurobiol., 3 1–63.

DeCastro, F 1931 Anatomical aspects of the ganglionic sympathetic transmission in mammals. Translated from Arch. Intern. de Physiol., 59 479

Elfvin, L. 1963 The ultrastructure of the superior cervical sympathetic ganglion of the cat, I. J Ultrastr. Res., 8 403–440.

——— 1963 Ultrastructure of the superior cervical ganglion, II. J Ultrastr Res., 8 441–476.

Fredricsson, B and F Sjoqvist 1962 A cytomorphological study of cholinesterase in sympathetic ganglia of the cat. Acta Morph. Neerlando-Scand., 5 140–166.

Galambos, R. 1961 A glia-neural theory of brain function. Natl. Acad. Sci. Proc., 47 129–136.

Hamberger A., and H. Hydén 1963 Inverse enzymatic changes in neurons and glia during increased function and hypoxia. J Cell Biol., 16: 521–525.

Hughes, W V Bond, G. Brecher E. Cronkite, R. Painter H. Quastler and F Sherman 1958 Cellular proliferation in the mouse as revealed by autoradiography with tritiated thymidine. Proc. Natl. Acad. Sci., 44: 476–483.

Hydén, H. 1961 Satellite cells in the nervous system. Sci. Am., 205 62–70.

Jaffee, D. 1963 Radioautography principles and procedures. J. Nuclear Med., 4: 143–154.

Koelle, G. 1950 The histochemical differentiation of types of cholinesterases and their localization in tissues of the cat. J Pharmacol. Exp. Ther., 100 158–179.

——— 1958 A new general concept of the neurohumoral function of acetylcholine and acetylcholinesterase. J Pharmacol. Exp. Ther 134. 146–153.

Kuntz, A., and N. Sulkin 1947 The neuroglia in the autonomic ganglia: cytologic structure and reaction to stimulation. J. Comp. Neur., 86 466–477

——— 1947 Hyperplasia of peripheral neuroglia, a factor in pathological changes in the autonomic ganglion cells. J Neuropath. Exp. Neurol., 6 323–331.

Lapham, L. 1961 A cytochemical study of the mechanism of division of astrocytes with reference to amitosis and its possible significance. Histochemie und Biochemie. Intern. Congr. Neuropath., 1 161.

Lapham, L., M. Johnstone and K. Brundjar 1964 A new paraffin method for the combined staining of myelin and glial fibers. J. Neuropath. Exp. Neurol., 23 156–160.

Leblond, C., B. Messier and B. Kopriwa 1959 Thymidine-H[3] as a tool for the investigation of the renewal of cell populations. Lab. Invest., 8 296–308.

Mason, D. 1962 A ganglionic stimulating action of neostigmine. Brit. J Pharmacol., 18 76–86.

——— 1962 Depolarizing action of neostigmine at an autonomic ganglion. Brit. J Pharmacol., 18 572–587

neuronal chromatolysis observed from neostigmine administered animals in this investigation lends support to this hypothesis Conversely the hypothesis may be utilized in an attempt to explain the effects of neostigmine. Mason (62a, b) has presented evidence that neostigmine is capable of exerting a direct stimulating action on the ganglion cells as well as acting in an anticholinesterase capacity This may partially account for the labeled satellite cell nuclei in unstimulated neostigmine-exposed ganglia

Koelle ('62) advanced the possibility that acetylcholine is continuously liberated in small quantities from nerve terminals in a resting state If cholinesterase were inhibited from immediately hydrolyzing the acetylcholine liberated in synaptic areas it seems probable that sufficient quantities of acetylcholine would build up over a period of time that would be capable of depolarizing postsynaptic membranes Thus, the same conditions would exist in an unstimulated ganglion with administration of neostigmine varying only in the degree of intensity Under these conditions if satellite cells were responding in some way to acetylcholine they would be expected to respond in the same capacity as they would in a stimulated ganglion but delayed considerably in their response The existence of many labeled nuclei of satellite cells in the unstimulated neostigmine-exposed ganglia is consistent with the apparent physiological conditions. It appears that the presence of neostigmine is either directly or indirectly responsible for the satellite cell reactions in unstimulated neostigmine-exposed ganglia since this is the only variable factor involved

Attempts to explain the normal appearance of neurons and satellite cells in atropine-exposed ganglia are considerably less complicated Atropine sulfate in autonomic ganglia is thought to compete with acetylcholine for postganglionic receptor sites With atropine blocking sites of impulse transmission mediated by acetylcholine there will be no postsynaptic depolarization no impulse transmission, no increased metabolic activity of ganglion cells and no effect of preganglionic stimulation relayed to pupillary structures of the eye The activity of satellite cells would be expected to remain unchanged after preganglionic stimulation if their response was to either increased synaptic transmission or to increased neuronal activity or both. With the exception of a few labeled satellite cells in the stimulated ganglia, the morphology and activity of satellite cells in atropine-exposed ganglia appeared to exhibit characteristics identical to normal satellite cells in the control ganglia. Perhaps the existance of a few labeled cells in stimulated ganglia can be explained on the basis of atropine immune receptor sites. Roszkowski ('61) reported the existence of pharmacological distinct cholinoceptive sites on postsynaptic membranes. He also observed that one of these sites could be blocked by atropine the other was not effected Takeshige et al. ('63) further supported the existence of two cholinoceptive sites and suggested the possibility of a third distinct site. The appearance of labeled satellite cells in some of the control ganglia and also in atropine-exposed ganglia may be attributed to specific labeling characteristics of individual satellite cells.

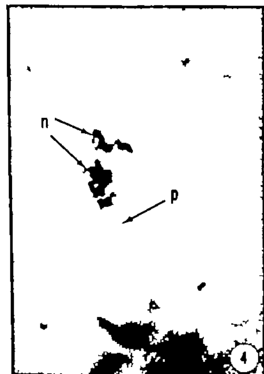
Nuclear configurations suggesting mitotic division have not been observed under the conditions of this or similar previous investigations performed in our laboratory If cellular proliferation is by mitotic mechanisms one would expect to observe mitotic figures in various phases of division Prophases and telophases should at least be fairly prominent since this type of cell division requires a considerable amount of time for completion This pattern was not observed in any histological section The probability of inconspicuous or unidentifiable mitotic figures is very unlikely therefore it becomes necessary to consider the likelihood of other proliferative mechanisms

Although very little is known about amitosis it apparently does not involve the cytoplasm of the cell to any large extent. Lapham ('61) suggested amitosis as an evolutionary method of increasing nuclear surface for transfer of chemical substances rather than cell replication to form new tissue Whatever the mode of cellular division may be under the conditions of this investigation it could not be specif


a
d
b
1


n
m
n
2


p
n
3


n
p
4

Niessing, K. 1959 The present state of investigation of neuroglia. Inst. Anat. Marburg (ref in Excerpta Medica, Sec. 8, V 13 p. 714 1960)

Pappano, A., and R. Volle 1962 The reversal by atropine of ganglionic blockade produced by acetylcholine. Life Sci., 1: 677–682.

Rasmussen, A. 1947 Some Trends in Neuroanatomy W C. Brown Company Dubuque, Iowa.

Richins, C., and J Hall 1958 Toluidine blue staining reactions in superior cervical and nodosal ganglion following stimulation and drug administration. J Neuropath. Exp. Neurol., 17: 333–337

Roszkowski, A. 1961 An unusual type of sympathetic ganglionic stimulant. J Pharmacol. Exp Ther., 132: 156–170

Schwyn, R., and J Hall 1965 Studies of neuroglial activity in autonomic ganglia during electrical stimulation and drug administration. Anat. Rec., 151: 414

Sjöstrand, J 1965 DNA synthesis in glia cells during nerve regeneration. Experimentia, 21: 142–145.

Smart, I., and C. Leblond 1961 Evidence for division and transformations of neuroglia cells in the mouse brain as derived from radioautography after injection of thymidine-H3. J Comp. Neur., 116: 349–367

Takeshige C., A. Pappano, W DeGroat and R. Volle 1963 Ganglionic blockade produced in sympathetic ganglia by cholinomimetic drugs. J Pharmacol. Exp. Ther., 141: 333–342.

Taylor J., P Woods and W Hughes 1957 The organization and duplication of chromosomes as revealed by autoradiographic studies using tritium labeled thymidine. Proc. Natl. Acad. Sci., 43: 122–128.

PLATE 1

EXPLANATION OF FIGURES

1 A normal superior cervical ganglion showing typical shape and location of (a) primary perineuronal satellite cell, (b) secondary perineuronal satellite cells, (c) interstitial satellite cell, and (d) normal appearing neuron. Fast green FCF and gallocyanin. × 500.

2 Photomicrograph of a control superior cervical ganglion. Showing normal morphological appearance of the neuron with slightly eccentric nucleus and homogeneously distributed Nissl substance. Capsular satellite cells (n) surround the nerve cell body Mast cells (m) are also present in this section. Toluidine blue. × 1300

3 Photomicrograph of an autoradiogram counterstained with toluidine blue. This section is a representative of a ganglion stimulated for 150 minutes. The relationship of labeled satellite cells (n) to metabolically active neuron (p) is readily identifiable. × 1300.

4 Photomicrograph of an autoradiogram counterstained with toluidine blue. This section is a representative of a ganglion stimulated for 150 minutes and demonstrates the relationship of labeled satellite cells (n) to metabolically active neuron (p) × 1300.


d
1


n
m
n
2


p
n
3


n
p
4

PLATE 2

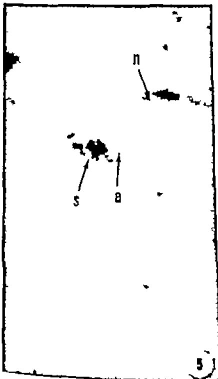
EXPLANATION OF FIGURES

5 Labeled secondary perineuronal satellite cells (s) related to assumed synaptic area (a) and to the stimulated neuron (n) Tissues were counterstained with toluidine blue. × 1300.

6 Labeled interstitial satellite cells (arrow) from a ganglion stimulated for 150 minutes. × 1300

7 Labeled satellite cells (arrow) from a stimulated neostigmine-exposed ganglion counterstained with *toluidine blue. Compare with* figures 5 and 6. × 1300.

8 Section from a stimulated atropine-exposed superior cervical ganglion showing normal appearing neurons and satellite cells. Compare with figures 5 6 and 7 × 1300.


n
s
a
5


6


7

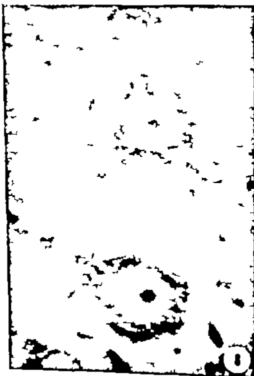

8

PLATE 2

EXPLANATION OF FIGURES

5 Labeled secondary perineuronal satellite cells (s) related to assumed synaptic area (a) and to the stimulated neuron (n). Tissues were counterstained with toluidine blue. × 1300

6 Labeled interstitial satellite cells (arrow) from a ganglion stimulated for 150 minutes. × 1300.

7 Labeled satellite cells (arrow) from a stimulated neostigmine-exposed ganglion counterstained with toluidine blue. Compare with figures 5 and 6. × 1300.

8 Section from a stimulated atropine-exposed superior cervical ganglion showing normal appearing neurons and satellite cells. Compare with figures 5, 6 and 7. × 1300

A Histochemical Study of Epithelial Mucin in the Chick Chorioallantois [1]

JAMES L. CONKLIN
Department of Anatomy, The University of Michigan, Ann Arbor, Michigan

ABSTRACT Histochemical methods demonstrate the accumulation of two types of mucous inclusion in the allantoic epithelial cells of the chick embryo.

One type of inclusion contains a sialomucin that is PAS-reactive, unstained by Alcian blue and other anionophilic dyes and is susceptible to digestion by Vibrio cholerae neuraminidase.

The second inclusion contains an apparent sulfomucin which is Alcianophilic at pH 1.0, unstained by anionophilic dyes after a methylation-demethylation sequence and resistant to testicular hyaluronidase. This sulfomucin exhibits PAS reactivity after desulfation procedures.

Both types of mucus occur in individual cells and are normal components of the chorioallantois. Accumulation of the inclusions is enhanced by lowering the pH of the allantoic fluid or as a result of organ transplantation.

Microscopic examination of chick chorioallantoic membrane (CAM) revealed the presence of abundant mucus-like material within and on the surface of the allantoic epithelial cells. It was also observed that transplantation of certain organs to the CAM apparently enhanced the accumulation of this mucus. An interest in the morphology and function of the intact and transplant-recipient CAM prompted a more extensive histochemical investigation of the allantoic mucus. The objective was to obtain additional information about the normal CAM as well as to be able to interpret the results of subsequent studies of organ transplantation.

MATERIALS AND METHODS

The material employed in this study consisted of samples of CAM from white leghorn chick embryos ranging in age from 7–18 days (Hamburger and Hamilton, '51), although 17–18 day CAM was most extensively used.

Samples of CAM were fixed in either 10% neutral-buffered formalin (pH 7.0), Bouin's fluid or 10% formalin containing 0.5% cetylpyridinium chloride. Following fixation, the samples were washed, dehydrated in graded ethanol and embedded in paraffin.

Sectioned samples were stained in the following:

(1) periodic acid Schiff (PAS) and colloidal iron-PAS (Mowry, '58); (2) aldehyde fuchsin (Gomori, '50) (prepared with basic fuchsin, C.I. 42500) with and without oxidation in Lugol's solution; (3) aldehyde fuchsin and Masson trichrome (Masson, '29) (acid fuchsin, C.I. 4285, Ponceau R, C.I. 16150, light green SF, C.I. 42095); (4) 0.01% aqueous azure A, cert. no. NAz 17, adjusted to pH 2.0 and 4.2 with hydrochloric acid; (5) 0.1% Alcian blue 8 GX (C.I. 74240) in 3% acetic acid (pH 2.5) or 0.5% Alcian blue in 0.1 N hydrochloric acid (pH 1.0).

Tissues stained with azure A were either rinsed in water and examined both before and after mounting in glycerogel or dehydrated in tertiary butyl alcohol and mounted in HSR. Routinely all other stained tissues were dehydrated in graded ethanol, cleared in xylene and mounted in HSR. The only exception to the preceding routine was to blot rather than dehydrate some sections after staining in Alcian blue (Lev and Spicer, '64).

Prior to the use of certain methods tissue sections were treated by incubation in acidified methanol (0.3 cm³ concentrated HCl in 40 cm³ methanol) for four hours at 37 C (mild methylation) or 60 C (strong methylation). After methylation some sections were subjected to a saponification step involving immersion in 1%

---

[1] Research supported by grant HD 00357 from the National Institute of Child Health and Development, National Institutes of Health.

Both types of mucous inclusions are present in most epithelial cells. The presence of both PAS-reactive and colloidal iron-positive inclusions in individual cells as well as the occurrence of mixed reactive material in the lumen of the allantois suggests that the allantoic cells contain at least two kinds of mucus and that this same material is secreted into the allantoic lumen.

To obtain additional information about the nature of the reactive groups in the mucous inclusions, control procedures were employed prior to the application of certain staining reactions.

While the use of alcohol-dehydrated, paraffin-embedded sections indicated that the PAS-reactive material was not lipid in character, some sections were further treated with hot chloroform-methanol before staining with PAS. Chloroform-methanol extraction did not alter the PAS staining of the inclusions. Also predigestion with amylase did not alter the the PAS staining of inclusions. In contrast, incubation of the sections in neuraminidase abolished all PAS staining of the inclusions. As anticipated, methylation of the tissue sections did not alter PAS staining. However after a methylation-demethylation sequence PAS staining of inclusions was greater than in untreated sections.

After either methylation or a methylation-demethylation sequence the inclusions were not stained by colloidal iron, Alcian blue, aldehyde fuchsin or azure A (fig. 4). Colloidal iron or Alcian blue staining of the inclusions was unaffected by either hyaluronidase or neuraminidase digestion (fig. 5).

The preceding results were nearly the same following fixation in either of the three fixatives. In general, staining was less intense following fixation in neutral buffered formalin. Results after fixation in CPF or Bouin's fixative were comparable.

DISCUSSION

The methods employed in this study fall into two categories. The first, the PAS reaction, is generally considered specific for reactive vicinal hydroxyl groups although certain lipids are also capable of reacting (Lillie '65). The remaining stains are those which exhibit an affinity for tissue anions such as sulfate, phosphate or carboxyl groups (Pearse '60). The specificity of these *anionophilic* stains is dependent, to some extent, on the pH at which they are employed.

The mucous inclusions of the allantoic epithelial cells are also of two types. There are inclusions which are only PAS-reactive and inclusions which are colloidal iron-positive, PAS-negative, when stained by a sequential stain. The appearance of similar material in the allantoic lumen suggest that at least two types of mucus produced by the allantoic epithelial cells is subsequently secreted into the allantoic fluid which does contain copious quantities of mucus (Needham, '50).

The identification of specific carbohydrates in tissue sections is difficult if not impossible with the methods employed. It is possible, however, to describe the nature of the reactive material in the mucous inclusions. The contents of one type of inclusion are PAS-reactive, unstained by anionophilic methods, resistant to hyaluronidase and amylase and susceptible to neuraminidase digestion. Avoiding the current dispute over the histochemical nomenclature of carbohydrates (Spicer et al. '65; Meyer '68; Saunders and Rosan, '66) it seems reasonable to consider the contents of this inclusion as a neuraminic acid-containing sialomucin. While the significance of its occurrence remains obscure, its presence is not unexpected. Neuraminidase occurs in the CAM in large quantities (Ada and Lind, '61; Cook and Ada, '63). Bogach et al. ('62) have isolated a sialic acid-containing material, sialoresponsin, from allantoic fluid following virus innoculation of the CAM. Although the localization of the CAM neuraminidase has not been demonstrated, it seems probable that it would occur in the allantoic epithelium where the sialomucin is found.

The second, most numerous type of mucous inclusion is intensely stained by procedures which have an affinity for negative groups. While colloidal iron and Alcian blue stain both sulfate and carboxyl groups, they are more specific if the pH of the staining solution is maintained well below the pK of carboxyl groups, (Lev and

KOH in 80% ethanol at 25 C for 20 minutes (Conklin 62)

To confirm the absence of reactive lipids sections were additionally extracted with chloroform methanol (1 1) at 60 C for 24 hours

Before staining for enzymatic digestion sections were incubated in solutions of either 0 5% α amylase (Nutritional Biochemicals) in 0 004 M acetate buffer (pH 5 5) at 37 C for three hours 0 5% testicular hyaluronidase in 0 1 M phosphate buffer (pH 5 5) at 37 C for four hours or 100 units of *Vibrio cholearae* neuraminidase (Behringe Chemical Works) in 0 05 M acetate buffer (pH 5 5) at 37 C for four hours As a control procedure other sections were incubated in "buffer only" solutions for a similar length of time

Since digestion with hyaluronidase did not alter the staining reactions sections of umbilical cord were incubated in the hyaluronidase solutions (controlled as above) to confirm the activity of this enzyme Such sections exhibited a marked reduction in staining after enzymatic digestion As the control procedure confirmed the specificity of the enzymatic digestions the results to be described include only the effects of digestion upon the staining reaction (table 1)

TABLE 1

Staining response of allantoic epithelial mucin

Procedure	Response
PAS	+
Colloidal iron	+
Alcian blue	+
Aldehyde fuchsin	+
Azure A, pH 4.2	+
Azure A pH 2.0	+
Colloidal iron PAS	+ +[1]
Methylation PAS	+
Methylation, colloidal iron	−
Methylation, azure A pH 4.2	−
Methylation azure A, pH 2.0	−
Methylation aldehyde fuchsin	−
Methylation, demethylation PAS	+[2]
Methylation demethylation colloidal iron	−
Methylation demethylation aldehyde fuchsin	−
Methylation demethylation azure A pH 4.2	−
Methylation demethylation, azure A pH 2.0	−
Amylase PAS	+
Neuraminidase PAS	−
Neuraminidase colloidal iron	+
Neuraminidase alcian blue	+
Hyaluronidase PAS	+
Hyaluronidase colloidal iron	+
Hyaluronidase alcian blue	+

− indicates that no staining occurred; + indicates an affinity for the stain.

[1] After thi sequence some inclusions are PAS-positive while some are stained by colloidal iron.

[2] After this sequence inclusions that were formerly PAS-negative are now PAS-reactive

RESULTS

The allantoic epithelium is a single layer of approximately cuboidal cells which line the inner surface of the chorioallantoic membrane (CAM)

The nuclei of the cells are located basally while the cytoplasm is most abundant at the apical end bordering on the allantoic lumen The apical surface of the cells exhibits short microvilli (Leeson and Leeson 63) which are indistinct when viewed with the light microscope

On about the ninth day of development inclusions appear in the supranuclear cytoplasm of the allantoic epithelial cells These inclusions increase until by the eighteenth day they appear to fill most of the apical cytoplasm (fig 1–3) Concomitantly similar material accumulates on the surface of the cells within the allantoic lumen

The inclusions because of their affinity for certain stains are subsequently termed *mucous inclusions* It seems probable that these mucous inclusions correspond to the weakly osmiophilic vacuoles observed by Leeson and Leeson (63) in an electron microscopic study of the chorioallantois

As indicated in table 1 the mucous inclusions of the allantoic epithelium are stained by many of the methods commonly employed in carbohydrate histochemistry They are colored a deep red by the PAS reaction and also stained by colloidal iron Alcian blue aldehyde fuchsin and azure A However when the inclusions are stained with a colloidal iron PAS sequence it is apparent that while most inclusions are stained by colloidal iron some inclusions are unstained by colloidal iron yet are PAS-reactive This duality in the staining of the inclusions is most evident in 10–12 day CAM when fewer inclusions are present The same duality in staining is exhibited by the mucus covering the surface of the epithelium

Spicer 64) which indicates that staining is due to sulfate (Phosphate groups are also weakly stained but can probably be discounted since they have not been reported in mucus) Staining with azure A at pH 2.0 and with aldehyde fuchsin while not specific is also indicative of sulfate groups That the anions in the mucous inclusions are sulfate rather than carboxyl groups is further indicated by the lack of staining which is observed after methylation-demethylation treatment of the tissue sections It is assumed (Lillie 65) that after a methylation-demethylation sequence only carboxyl groups are available for staining

Neuraminidase digestion did not alter the staining with colloidal iron and this reaction was also unaffected by hyaluronidase digestion Since hyaluronic acid and chondroitin sulfates A and C are digested by testicular hyaluronidase (Pearse 60 Lillie 65) the sulfated mucus (sulfomucin) is probably other than one of these three carbohydrates The enhancement of PAS reactivity of the mucous inclusions by methylation-demethylation suggests the presence of vicinal hydroxyl groups in the sulfomucin and the occurrence of sulfate in a position which prevents PAS reactivity (Lillie 65) Desulfation removes the hindrance effect of the sulfate and the molecule becomes PAS-reactive For the present the contents of the second type of mucous inclusion can only be identified as a sulfated mucin which also contains vicinal PAS-reactive groups and is lacking in demonstrable carboxyl groups Protein is present in both types of epithelial mucus as evidenced by bromphenol blue staining of the components following electrophoretic separation (unpublished observation)

Presently the significance of the allantoic mucus remains obscure It has been suggested that it is secreted in response to the accumulation of noxious materials in the allantoic fluid (Needham 50) This view is supported by the observation that artificial lowering of the pH of the allantoic fluid enhances mucus accumulation Other factors are also involved however since transplantation of certain tissues to the CAM also accelerates mucus accumulation In any event, the allantoic epithelium should provide an interesting tissue for the study of mucus synthesis and secretion since the cells are apparently capable of synthesizing two quite different types of mucous material.

ACKNOWLEDGEMENTS

I am grateful for the technical assistance of Mrs Lana Brock and Mrs Dorothy Kangas

LITERATURE CITED

Ada, G L. and P E. Lind 1961 Neuraminidase in the chorioallantois of the chick embryo. Nature 190 1169–1171

Bogoch S., R. F Gilfillan and P Evans 1962 Sialoresponsin: neuraminic acid-containing substance which accumulates in the chorioallantoid fluid during the first few minutes of virus infection Nature 196 649–651

Conklin J L. 1962 Staining properties of hyaline cartilage Am. J Anat 112. 259–267

Cook, B., and G L. Ada 1963 Neuraminase in tissues of the chick embryo and chick. Biochim. Biophys. Acta 73 454–461

Gomori, G 1950 Aldehyde fuchsin a new stain for elastic tissue Am. J Clin. Path., 20: 665–666.

Hamburger V and H. L. Hamilton 1951 A series of normal stages in the development of the chick embryo. J Morph 88 49–92.

Leeson T S., and C. R. Leeson 1963 The chorioallantois of the chick. Light and electron microscopic observations at various times of incubation. J Anat., 97 585–595

Lillie R. D 1965 Histopathologic Technic and Practical Histochemistry McGraw-Hill, New York.

Lev R. and S. S Spicer 1964 Specific staining of sulphate groups with alcian blue at low pH J Histochem., 12 309

Masson P 1929 Some histological methods: Trichrome staining and their preliminary technique J Techn. Methods, 12 75–90.

Meyer K. 1966 Problems of histochemical identification of carbohydrate-rich tissue components. J Histochem 14 605–606.

Mowry R. W 1958 Improved procedures for the staining of acidic polysaccharides by Muller's colloidal (hydrous) ferric oxide and its combination with the Feulgen and the periodic acid-Schiff reactions. Lab. Invest. 7 566–576

Needham, J 1950 Biochemistry and Morphogenesis. University Press, Cambridge.

Pearse A. G E. 1960 Histochemistry Theoretical and Applied. Little Brown Boston.

Saunders, A M., and R. C Rosan 1966 Histochemical nomenclature of carbohydrate-rich components J Histochem., 14 869.

Spicer S. S T J Leppi and P J Stoward 1965 Suggestions for a histochemical terminology of carbohydrate-rich tissue components J Histochem. 13 599–603


1
2
3
4
5

PLATE 1

EXPLANATION OF FIGURES

1 A section through the chorioallantoic membrane (CAM) From top to bottom are the ectodermal, mesodermal and entodermal components. The allantoic epithelial cells (arrow) contain copious amounts of mucus. Colloidal iron and PAS × 600

2 The mucus (arrow) of the allantoic epithelium as it appears after staining with aldehyde fuchsin. × 600

3 The allantoic epithelium and mucous components. The distinction between the two types of mucous inclusions is not apparent. Note the presence of mucus in the allantoic lumen (arrow) × 1600.

4 A section of CAM after a methylation-demethylation sequence and staining with colloidal iron Note the absence of stained material in the allantoic epithelium (arrow) × 400

5 The CAM after treatment with neuraminidase Only the mucous inclusions that are stained by colloidal iron (arrow) are visible (contrast with fig 1) Colloidal iron and PAS × 400

Notes on the Development of the Lung in Infancy and Early Childhood [1]

EDWARD A. BOYDEN
Department of Biological Struct re U iversity of Washi gton, Seattle Washington

ABSTRACT This account is based upon graphic reconstructions and wax models of the lungs of an infant five and one-half months of age and of a child 3.7 years old; also upon plastic injections of a 10-month lung and upon modelled serial sections of the bronchioles in a child six and two-thirds years of age.

In passing from the second postnatal month to the sixth month, the general pattern of a terminal bronchiole and its branches seems not to have changed. However, angulation of the crowded alveolar ducts becomes visible in the tenth month and may have produced small accessory saccules at such angles.

Sometime before the fourth year numerous alveoli of a new type have appeared, designated here as *ductular lveoli*, since they arise as invaginations of bronchiolar diverticula lined originally by columnar epithelium. These become the "spherical alveoli" of the adult and transform terminal bronchioles at this late stage into respiratory bronchioles. By the seventh year narrow *ductular processes* radiating from preterminal or terminal bronchioles, are beginning to penetrate adjacent alveoli, initiating the Lambert type of *collateral ventilation*. Thus, the centripetal advance of differentiation continues.

The present study is an attempt to follow the developing pattern of the lung from its configuration in neonatal and early postnatal periods to that of later infancy and early childhood. In the neonate as reconstructed by Boyden and Tompsett ('65) each *terminal* bronchiole gives rise to several generations of *smooth respiratory* bronchioles the last of which terminates in a pair of short *transitional ducts* lined only by flat epithelium. Each of these in turn gives rise to a cluster of some four generations of *alveolar saccules* Because the only alveoli are small and shallow indentations on the walls of saccules the saccules are considered to be the prime physiological units at birth. During the next two months larger alveoli develop in a centripetal direction, first converting smooth respiratory bronchioles into alveolar ducts and then terminal bronchioles into respiratory ones. So far no evidence has been found of a budding process that might result in the formation of new acini.

The lung of the five and one-half month infant

Figure 1B is a dissection of the fissural surface of the left lower lobe showing the distribution of the antero-medial basal bronchi, *B* and *B* (cf Boyden '55 Plate 6 and Chap. 8) The dash lines mark the serially sectioned block of tissue Figure 1A is a graphic reconstruction of the bronchioles within the sectioned block. The terminal spray of Ramus 8 on viewer's right (see asterisk) supplies a lobule on the costal surface Ramus *18a* is a terminal bronchiole of this spray which will be followed to the pleura through the fourth respiratory bronchiole *22a*.

Figure 17 presenting a higher magnification of this spray is a drawing of a wax model (reconstructed at × 50) showing the proximal bronchioles with associated arteries (red) and veins (blue) Stippled surfaces indicate the presence of cuboidal or pseudostratified columnar epithelium. This model identifies the position of the terminal bronchiole (*18a*) Since ramus *22a* — which we wish to follow — comes off the deeper side that surface also is drawn (fig 18) Ramus *22a* should be identified here.

The third degree of magnification is shown in figure 4 This is a drawing and photograph of a model (reconstructed at × 100) which carries bronchiole *22a*

[1] Supported by Research grant HD 00000, National Institutes of Health, U S. Public Health Service.

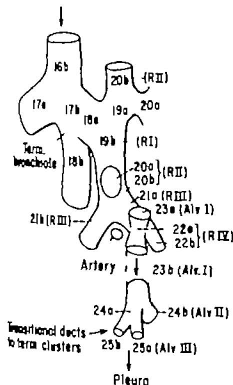


Fig. 8 Diagram analyzing the spray indicated by an asterisk in figure 1A (this is to be used in interpreting figs. 3, 4 5 17 18)

ject with wide branches shooting off at close intervals and at an acute angle.

The injected lung of a 10-month infant

When received as an injected gross specimen, the right lung of this infant measured 125 mm in length After it had been left overnight in concentrated HCl and then cleaned of all organic debris it was noted that the methacrylite had filled some of the alveolar ducts. Minute selected branches were then photographed stereoscopically for study

Higher power drawings of selected branches (fig. 7) suggest that a new factor in development is appearing. This is the angulation of the alveolar ducts. Although many of the ducts are broken or are incompletely injected, enough remains to show that at the angulations a small saccule is enlarging It is suggested that growth under compression may result in herniations of alveoli or groups of alveoli from which new saccules and increased ventilation may develop Even in the infant of five and one-half months (fig 5) such a zig zag pattern is becoming evident. Other information that makes this seem plausible is K. K. Pump's beautiful injections of adult acini ('64) If one looks at his diagrams, it is obvious that in an adult acinus there are numerous sessile saccules arising directly from respiratory bronchioles as well as from alveolar ducts In figure 7B the branches at the top may represent a small terminal cluster of alveolar ducts or fragments of such.

The lung of a child of 3 7 years

This child had been born prematurely at 36 weeks with myelomeningocele and hydrocephalus, but the lungs were normal. The zone chosen for study is the upper of the two anterior branches of the superior lingular segment (B⁴b1) In the graphic reconstruction (fig 8) the branches have been numbered with the upper lobe bronchus counted as no. 1 The most peripherally located cartilage lies at the bifurcation of the sixteenth branch. In the five and one-half month infant (fig. 1A) the lowest cartilage was located at the tenth branch of the antero-medial bronchus (i.e at the twelfth branch, if the lower lobe bronchus is counted as no 1) This is not unexpected as usually the advancing formation of cartilages keeps pace with growth but there is great variation both in embryonic stages (Bucher and Reid, '61) and in infancy (Boyden and Tompsett, '65)

Grossly (fig 8) there are other significant differences. In the peripheral branches the zone of flat epithelium (dash lines) in the walls of bronchioles extends inward from the pleura some three and one-fourth millimeters. In figure 1 the distance was one to one and one-half millimeters. It may be recalled that in the first 10.5 days after birth in the faster growing puppy lung, the cuboidal epithelium had retreated from a distance of 0 43 mm to that

For this beautiful preparation the writer is indebted to Dr David Tompsett of the Royal College of Surgeons, England, whose generous and skilled cooperation has long been source of inspiration.

For permanent record of these, the writer is indebted to Mr. Donne La Violette of the Department of Surgery

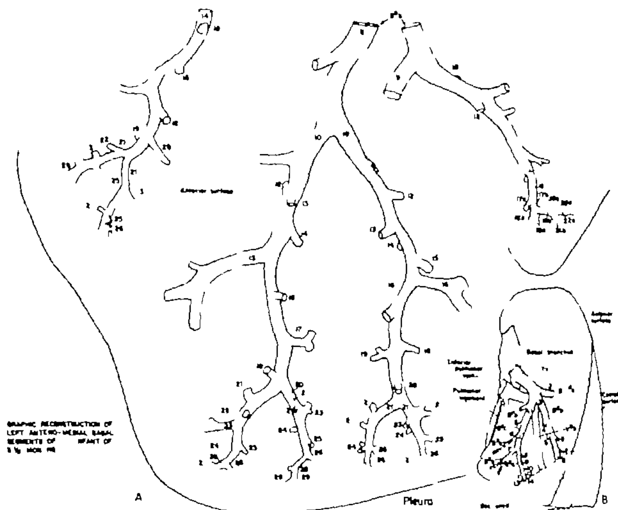


Fig. 1A A graphic reconstruction (× 6) of the distal portion of the left antero-medial basal bronchus of a male infant (Hu 8) five and one-half months old. The asterisk indicates the terminal spray from which wax models were reconstructed (figs 3 4 17 18)

Fig. 1B The dissected left lower lobe and the serially sectioned block of tissue (dashlines) from which reconstructions were made For photomicrograph of Section 413, see figure 5

through to the pleura. The reverse side of the model is shown in figure 3

To further orient the reader the pattern of branching has been diagrammed in figure 2 The terminal bronchiole of the spray (*18a*) is succeeded by four main line respiratory bronchioles (*19b 20b 21a 22a*) then by two alveolar ducts (*23b 24a*) the last of which bifurcates into short "transitional alveolar ducts (*25a, 25b*) each of which gives rise to a cluster of alveolar saccules These clusters are so closely packed that it is almost impossible to identify their branches beyond the main division of each (*26a b 26 a b*) But in general they seem like the clusters of earlier stages

Lastly the reader is supplied with a photomicrograph of Section 413 which passes horizontally through the terminal spray (fig 5) By turning this figure around one can study the models in figures 3 and 4 first from one side and then from the other The limits of the two clusters on the pleura are indicated by arrows.

In comparing these models and stages with those of the 37-day and 2-month infants no essential changes in pattern have been observed With increase in size and number of alveoli and increased inflation there is a greater compression of the interalveolar tissue and a crowding of branches so that the terminal spray while somewhat larger than earlier is more com-

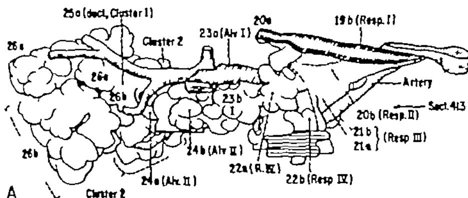


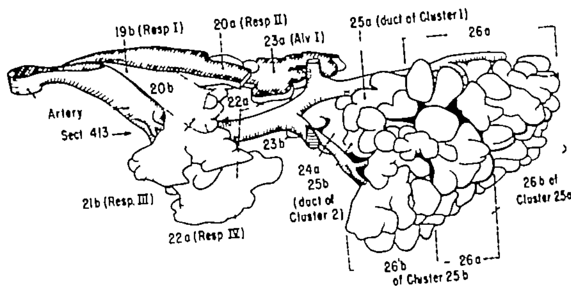


Fig. 4 The reverse side of the model shown in figure 3 (× 65) It is viewed, therefore, from the deep or costal side of the lower lobe and is continuation of structures drawn in figure 18. Cf photomicrograph in figure 5.

lar communications pictured by Lambert in 1955 However there is this important distinction: at this stage there is no communication with adjacent alveoli. Nor could such communications be found in the middle lobe of a child three years older

In this older child of six years and eight months such alveoli of ductular origin have grown larger and somewhat flask-shaped. Their form is illustrated in figure 15. This is a drawing of a wax model of two diverging bronchioles with their accompanying arterioles In this slice 0.25 mm thick, the left bronchiole shows three such ductular alveoli the right hand bronchiole a fourth.

A somewhat different pattern is presented in longitudinal setcions of the junction between a terminal and first respiratory bronchiole (fig 13) Here one may see five stages in the formation of ductular alveoli Number 3 is a diverticulum like that which was shown in figure 9 (nos. 2 and 1 are earlier stages) Number 4 is a cup-shaped one like that in figure 10 Then at five a complete alveolus has developed measuring 90 × 86 × 60 μ with its ductular orifice partly intact. These suggest Hayek's figure of "spherical alveoli" in the first respiratory bronchiole of an adult lung ('60) At the very end (no. 6) comes respiratory epithelium of the type found in the young infant the type in which alveoli arise from flat epithelium by the cutting in of septa. A point to be emphasized here is that this new mode of origin can be considered an extension of that centripetal process (although locally in the reverse direction) by which terminal bronchioles are converted into respiratory bronchioles.



A

Fig 3 Wax model (× 55) and explanatory drawing on the terminal branches of the spray (*) in figure 1A. This larger sized model (originally ×100) completes the branches of the smaller model shown in figure 17 It is viewed from the anterior surface of the lobe The stippled areas represent columnar epithelium Note that the two terminal clusters occupy almost half the distance from the terminal bronchiole to the pleura Cf photomicrograph in figure 5

of 3 16 mm from the pleura (Boyden and Tompsett 61)

Still further inward in the lung at 3 7 years is a zone in which a new method of forming alveoli is being developed in the walls of preterminal and terminal bronchioles Indeed the distal branches in figure 8 seem to be "peppered with these new structures They begin as much as 6 5 mm from the pleura The first phase (cf *arrow 417* fig 8) is an invagination of the columnar epithelium of the bronchiole to form a diminutive diverticulum (fig 9) For this reason they are here designated as *ductular alveoli*. After perforating the surrounding muscle layer each impinges on an adjacent but otherwise unrelated alveolus Then it expands into a cup-shaped sac the distal cells of which flatten out against the adjacent alveolus and appear almost pycnotic (fig 10) This cup is always filled with "dust cells, so that one wonders if they play any role in the differentiation of tissues Curiously enough several such "pocket alveoli may arise in the circumference of a bronchiole (fig 11) This section closely resembles the figures of "accessory bronchiole-alveo-

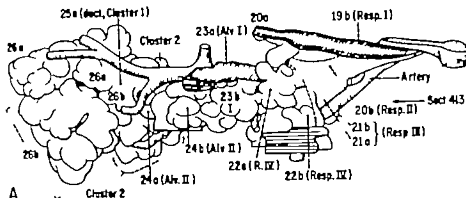




Fig. 4 The reverse side of the model shown in figure 3 (× 55) It is viewed, therefore, from the deep or costal side of the lower lobe and is a continuation of structures drawn in figure 18. Cf photomicrograph in figure 5.

lar communications pictured by Lambert in 1955 However there is this important distinction at this stage there is no communication with adjacent alveoli. Nor could such communications be found in the middle lobe of a child three years older.

In this older child of six years and eight months, such alveoli of ductular origin have grown larger and somewhat flask shaped. Their form is illustrated in figure 15. This is a drawing of a wax model of two diverging bronchioles with their accompanying arterioles. In this slice, 0.25 mm thick, the left bronchiole shows three such ductular alveoli, the right hand bronchiole a fourth.

A somewhat different pattern is presented in longitudinal setcions of the junction between a terminal and first respiratory bronchiole (fig. 13) Here one may see five stages in the formation of ductular alveoli. Number 3 is a diverticulum like that which was shown in figure 9 (nos 2 and 1 are earlier stages) Number 4 is a cup-shaped one like that in figure 10 Then at five a complete alveolus has developed, measuring 90 × 88 × 50 μ, with its ductular orifice partly intact. These suggest Hayek's figure of spherical alveoli in the first respiratory bronchiole of an adult lung ('60) At the very end (no 6) comes respiratory epithelium of the type found in the young infant, the type in which alveoli arise from flat epithelium by the cutting in of septa. A point to be emphasized here is that this new mode of origin can be considered an extension of that centripetal process (although locally in the reverse direction) by which terminal bronchioles are converted into respiratory bronchioles.

Fig. 5 Photomicrograph (× 60) of the 20 μ section (no. 413) passing through the lobule of the lung of the five and one-half month infant (Hu 8) For level of this section in the corresponding model see arrows in figures 3 and 4 For comparison with the models, the figure should be looked at first from one side and then from the other The arrows on the costal pleura indicate the limits of the two terminal clusters on the apex of the lobule The numbers within th cavities identify corresponding parts on the model

Fig. 6 Photomicrograph (27) of the 20 μ section (no 333) of the lung of the 3 7 year old infant (Hu 13) For level of this section in the orresponding wax model see arrow in figure 16 The bronchiole numbered 17a was once a terminal bronchiole but it now contains a pat h of flat epithelium (See fig 12 and "R, fig. 16)

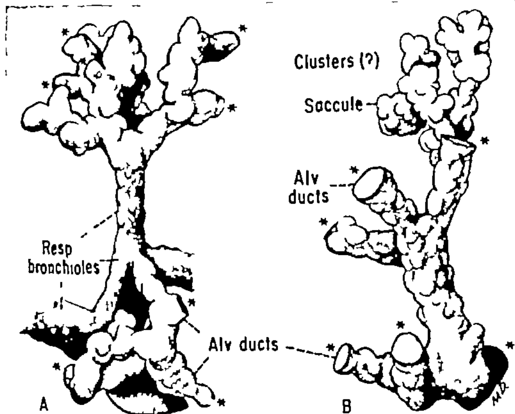


Fig. 7 Two tiny sprays from an injected lung of a 10-month infant drawn under a binocular microscope. The asterisks indicate broken or incomplete ends. A (× 30) sprays of alveolar ducts there and below Note angulation of ducts. B (× 60) Illustrating portions of a single cluster of alveolar saccules or portions of a pair of clusters. (Prepared by the writer but originally injected by Dr David Tompsett, Department of Anatomy Royal College of Surgeons, England.)

Another manifestation of bronchiolar activity at this level is the type found in the child six and two-third years and here designated "*ductular processes*" (fig 14) These are not the ordinary branches of a bronchiole — which are nearly the same diameter as the parent stem — but long narrow tubular outgrowths which often radiate in any direction from a terminal or preterminal bronchiole, and usually end blindly against an alveolus. Such is shown at the left, in figure 14 But on the right there is one that opens directly into an alveolus which in turn connects with many air spaces. Presumably this is an early stage — appearing first in the seventh year — of Lambert's system of *accessory bronchiole-alveolar communications* Certainly it closely resembles Krahl's figure 13C ('59) of a bronchiolar-alveolar communication in the lung of a sheep.

If further confirmation is needed attention is called to the "labyrinth of ducts" which is reconstructed in the wax mode of figure 15 Near the top of the model i the bronchiolar duct or ductular proces illustrated in figure 14 Just under this and to the left (fig 15) is a labyrinth o ducts originating from two sides of th bronchiole These ramify in the lymphoi tissue (fig 14) and then connect with ad

Unfortunately Dr Lambert's significant artic omits the age of individuals which her figures illu trate. All she says about age is that these communic tions occur in "normal human lungs of all a groups. However the writer could not find the either in the lungs of infants or the child 3.7 yea of age.

Fig. 5 Photomicrograph (× 60) of the 20 μ section (no. 413) passing through the lobule of the lung of the five and one-half month infant (Hu 8) For level of this section in the corresponding model see arrows in figures 3 and 4 For comparison with the models the figure should be looked at first from one side and then from the other The arrows on the costal pleura indicate the limits of the two terminal clusters on the apex of the lobule The numbers within the cavities identify corresponding parts on the model

Fig 6 Photomicrograph (27) of the 20 section (no 333) of the lung of the 3 7 year old infant (Hu 13) For level of this section in the corresponding wax model see arrow in figure 1(The bron hi le numbered 17a was once a t r minal bronchiole but it now contains a p t h f flat epithelium (See fig 12 and "R fig 16)



Figs. 9–11 Three 20 μ sections illustrating stages in the development of "ductular alveoli" in the 3.7-month infant. For location, see numbers 417, 463 and 830 in figure 8. *Figure 9* (× 370) diverticulum of a preterminal bronchiole penetrating its own muscle layer. *Figure 10* (× 370) later expansion of such a diverticulum into hollow sac, 72 μ wide ("ductular alveolus"). Its flattened cells press upon an earlier formed alveolus of the usual type. *Figure 11* (× 230) three such alveoli in one section. In these examples the thick epithelium of the bronchiole passes abruptly into flat epithelium, hence, the name, ductular alveoli.

Fig. 12 20 μ section (× 120) of the wall of a terminal bronchiole (*17a*) in child 3.7 years old. This is the area in figure 16 labelled "R" (for respiratory epithelium)

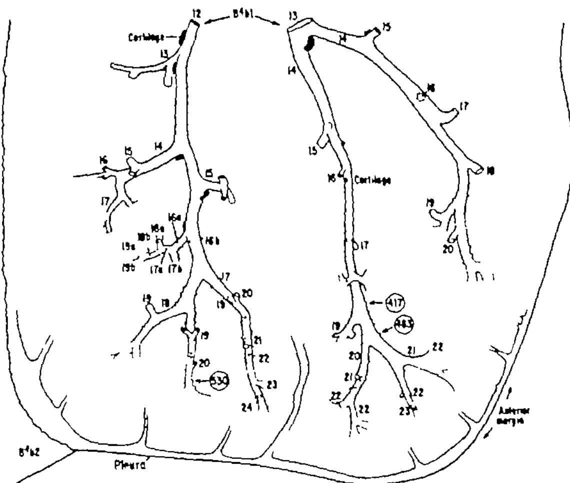
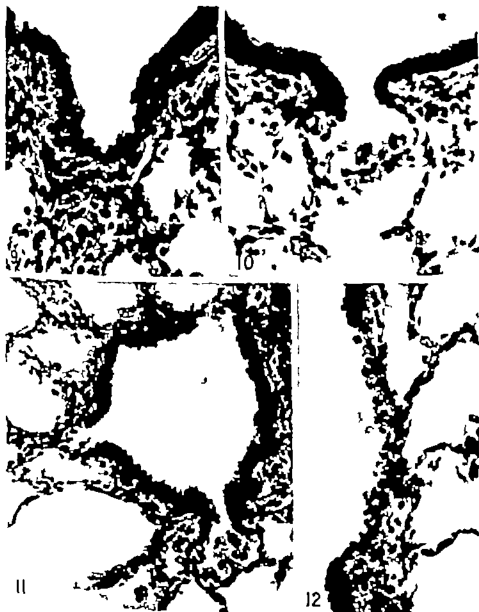


Fig 8 Graphic reconstruction (× 7.3) of peripheral bronchioles of a branch of the superior lingular segment of a male child 3 7 years of age (B⁴b1 cf Boyden 55 Chap 6) In numbering branches the count begins with the upper lobe bronchus. *Dashlines* on bronchioles indicate flat epithelium *Asterisk* indicates spray modelled in figure 16. *Numbers encircled* (417 463 530) indicate tiny di verticula shown at higher magnification in figures 9 10 11 respectively

jacent alevoli These closely resemble Krahl s figure 13D of the sheep lung where there are *two* such communicating ductu lar processes in the same section

The pattern of branching at 3 7 years Returning now to the lung of 3 7 years let us examine the wax model, constructed at × 50 which is shown in figure 16 A photomicrograph of Section 333 which passes through the center of the model is shown in figure 6 If one compares the models of the five and one-half month and 3 7 year lungs (figs 17 16) the bronchio- lar patterns seem at first to be similar But there is one important difference. The supposedly terminal bronchiole in the older spectrum — the one carrying the spray of respiratory bronchioles and alveolar ducts (*17a* fig 16) — has an area of respiratory epithelium in its wall (labelled "R in fig 16 and shown histologically in fig 6) Close study of serial sections shows that it arose from two flattened ductular alveoli Here the new process described above is transforming a terminal into a first respira tory bronchiole A glance at figure 8 to the right of the asterisk shows that di verticula like those shown in figures 9 and 10 have reached as far centrally as ramus *16*

A second point of interest is the arterial pattern In the older specimen (fig 16) the main arteries follow the branches of the bronchiole as far as the second respira tory but in the younger specimen (fig. 17) there is a striking variation Instead of



Figs. 9–11 Three 20 μ sections illustrating stages in the development of "ductular alveoli" in the 3.7-month infant. For location see numbers 417 463 and 530 in figure 8. *Figure 9* (× 370) a diverticulum of a preterminal bronchiole penetrating its own muscle layer. *Figure 10* (× 370) later expansion of such a diverticulum into a hollow sac, 72 μ wide ("ductular alveolus") Its flattened cells press upon an earlier formed alveolus of the usual type. *Figure 11* (× 230) three such alveoli in one section. In these examples the thick epithelium of the bronchiole passes abruptly into flat epithelium, hence, the name "ductular alveoli."

Fig. 12 20 μ section (× 120) of the wall of a terminal bronchiole (*17s*) in a child 3.7 years old. This is the area in figure 16 labelled "R" (for respiratory epithelium)





14

Fig 13 10 μ section (no. 906—slide 106) of a terminal bronchiole in a child six years and eight months old (× 120) Note five stages (1–5) in the formation of "ductular alveoli" (See text.)

Fig. 14 10 μ section (no. 1011-slide 115) through two preterminal bronchioles and accompanying arterioles in a child of six years and eight months (× 120) At the left, note a blind ductular process " At the right a corresponding process which is continuous with a series of alveolar spaces. (See text.)

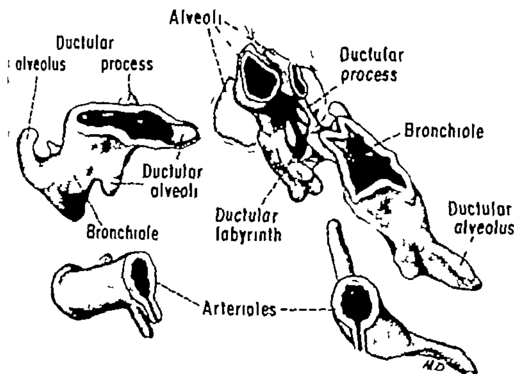


Fig. 15 A wax model (× 143) of the two diverging bronchioles shown in figure 14 (Sections 1004-1028 inclusive). On the left, note three "ductular alveoli"; on the right, the ductular process and the deeper ductular labyrinth both of which connect distally with alveoli. (See text.)

following bronchiole *19a* up from its base it gives off an earlier branch which descends from above to supply *19a* and all its subdivisions. *This* obliquely running arteriole should *not* be confused with the right-angled supernumerary arteries described by Elliott and Reid ('65). For discussion of supernumerary arteries in the 37-day infant lung, see Boyden ('65).

In conclusion, one may ask where this incomplete study of patterns in newborns infants and younger children leaves us. To summarize, it appears that a rapid qualitative change occurs within the first month or two after birth. *It is* then that alveoli in the terminal clusters enlarge, that alveoli develop *in* a centripetal direction, transforming *smooth* respiratory bronchioles into alveolar ducts and terminal bronchioles into respiratory ones. Quantitative analysis (*Dunnill*, '62) has also demonstrated a sharp rise in air tissue interface between birth and the third month. In the next few months the change is largely one of slow growth. Thus the pattern at five and one-half months (figs. 3 4) seems not to differ much from that at the end of the second month.

Sometime before the fourth year a new method of forming alveoli appears which gives rise to the zone of ductular alveoli shown in figure 8. This has transformed what at first seemed to be terminal bronchioles into first respiratory bronchioles. Toward the end of the sixth year collateral ventilation is introduced by the appearance on the then terminal or preterminal bronchioles, of radiating ductular processes which invade adjacent alveoli.

One of the chief remaining problems is to determine exactly what contribution to the acinus is made by the terminal clusters of alveolar saccules. As K. K. Pump's remarkable moulage injection of adult lungs have taught us the acinus is much more complicated than a simple spray made up

Fig. 13 10 μ section (no. 908—slide 108) of a terminal bronchiole in a child six years and eight months old (× 120) Note five stages (1–5) in the formation of "ductular alveoli (See text.)

Fig. 14 10 μ section (no. 1011–slide 115) through two preterminal bronchioles and accompanying arterioles in a child of six years and eight months (× 120) At the left, note a blind ductular process. At the right a corresponding process which is continuous with a series of alveolar paces. (See text)

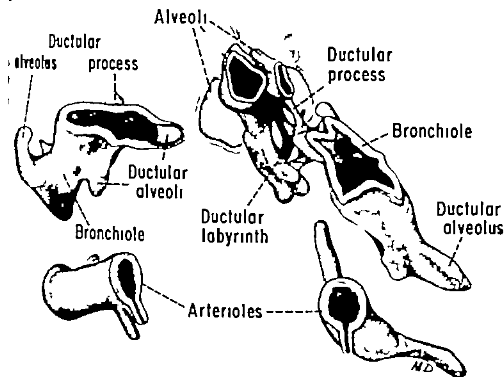


Fig. 15 A wax model (× 142) of the two diverging bronchioles shown in figure 14 (Sections 1004-[illegible] inclusive). On the left, note three "ductular alveoli"; on the right, the "ductular process" and the deeper ductular labyrinth both of which connect distally with alveoli. (See text.)

following bronchiole *19a* up from its base it gives off an earlier branch which descends from above to supply *19a* and all its subdivisions. This obliquely running arteriole should not be confused with the right-angled supernumerary arteries described by Elliott and Reid ('65). For discussion of supernumerary arteries in the 17-day infant lung, see Boyden ('65).

In conclusion, one may ask where this incomplete study of patterns in newborns, infants and younger children leaves us. To summarize, it appears that a rapid qualitative change occurs within the first month or two after birth. It is then that alveoli in the terminal clusters enlarge, that alveoli develop in a centripetal direction, transforming smooth respiratory bronchioles into alveolar ducts and terminal bronchioles into respiratory ones. Quantitative analysis (Dunnill, '62) has also demonstrated a sharp rise in air-tissue interface between birth and the third month. In the next few months the change is largely one of slow growth. Thus the pattern at five and one-half months (figs. 3, 4) seems not to differ much from that at the end of the second month.

Sometime before the fourth year a new method of forming alveoli appears which gives rise to the zone of ductular alveoli shown in figure 8. This has transformed what at first seemed to be terminal bronchioles into first respiratory bronchioles. Toward the end of the sixth year collateral ventilation is introduced by the appearance on the then terminal or preterminal bronchioles of radiating ductular processes which invade adjacent alveoli.

One of the chief remaining problems is to determine exactly what contribution to the acinus is made by the terminal clusters of alveolar saccules. As K. K. Pump's remarkable moulage injection of adult lungs have taught us the acinus is much more complicated than a simple spray made up

Fig. 16 Drawing (× 31.5) of a wax model of that spray of bronchioles in a child 3.7 years, which is indicated by an asterisk in figure 8. The model (originally × 50) is viewed from the costal side and, therefore, the reverse of that shown in figure 8. The arrows indicate the level of the photomicrograph presented in figure 6. Model and photomicrograph should be studied together. *Arteries* in red follow bronchioles; *veins* in blue are peripheral. *Stippled areas* indicate non-respiratory (i.e. cuboidal or columnar) epithelium; *clear areas* flat epithelium.

Figures 17 and 18 Drawings (× 31.5) of anterior and posterior aspects of a model (originally × 50) of the terminal spray of the five and one-half-month infant lung indicated by an asterisk in figure 1A. *Figure 17* shows the side drawn in figure 1A; *figure 18* the reverse side. The model in figure 4 carries bronchiole 22a out to the pleura. The pattern of arterioles in these two figures represents a not uncommon variation in which bronchus 19a (ascending from 18a) is not accompanied by an ascending artery but supplied prematurely from above. For normal pattern see figure 16.

successively of a terminal bronchiole several orders of respiratory bronchioles and an as yet undetermined number of alveolar ducts with sessile outgrowth scattered along the way

LITERATURE CITED

Boyden, E. A. 1955 Segmental Anatomy of the Lungs. A Study of the Patterns of the Segmental Bronchi and Related Blood Vessels. Blakiston Division, McGraw-Hill Book Co., New York, Toronto, London.

—— 1965 The terminal air sacs and their blood supply in 37-day infant lung. Am. J Anat., 116: 413–427

Boyden, E. A., ad D. H. Tompsett 1961 The postnatal growth of the lung in the dog. Acta Anat., 47 185–215.

—— 1965 The changing patterns in the developing lungs of infants. Acta Anat., 61 164–192.

Bucher U and L. Reid 1961 Development of the intrasegmental bronchial tree: the pattern of branching and development of cartilage at various stages of intrauterine life. Thorax, 16 207–218.

Dunnill, M. S. 1962 Postnatal growth of the lung. Thorax, 17 329–333

Elliott, F M., and L. Reid 1965 Some new facts about the pulmonary artery and its branching pattern. Clinical Radiology 16 193–198.

Hayek, H. von 1960 The Human Lung (revised and augmented by Vernon E. Krahl) Hafner Publ. Co., Inc., New York.

Krahl, V E. 1959 Microscopic anatomy of the lungs. Am. Rev Resp. Dis., 80 24–44.

Lambert, M. W 1955 Accessory bronchiole-alveolar communications. J Path. and Bact., 70 311–314

Pump K. K. 1964 The morphology of the finer branches of the bronchial tree of the human lung. Dis. Chest, 46 379–398.

Electron and Light Microscopic Observations on Relationships between Lymphocytes and Intestinal Epithelium [1]

ROLAND D MEADER AND DENNIS F LANDERS
Department of Anatomy University of Nebraska College of Medicine Omaha, Nebraska

ABSTRACT Correlated electron and light microscopic studies of the distribution, position, appearance migration and fate of lymphocytes with relation to the intestinal epithelium of the young adult rat, mouse hamster and man have been made. Under the conditions of this investigation, the lymphocytes which are normally present in the intestinal epithelium are intercellular in position, irrespective of their level within the epithelium. The great majority of these cells are located in the basal region of the epithelium, below the level of the epithelial cell nuclei. There was no evidence of lymphocytic degeneration. Lymphocytes migrated from the lamina propria into the epithelium and back again into the lamina propria, with no evidence of movement toward the free surface of the intestinal epithelium and extrusion into the lumen.

The distribution, position, morphology migration and fate of lymphocytes with relation to the intestinal epithelium of various laboratory animals and man have been the objects of numerous investigations which, unfortunately have resulted in many conflicting interpretations. In a series of studies concerning these phenomena in the duodenal epithelium of the mouse and man, Andrew et al. (45 46 47 '65) claimed that the lymphocytes are intracellular in position as evidenced by the vacuoles which surround them within the cytoplasm of the epithelial cells. They further observed that these intracellular lymphocytes undergo a series of degenerative changes characterized by pycnosis fragmentation and sometimes vacuolation. They have also stated that these lymphocytes migrate toward the free surface of the intestinal epithelium and are extruded into the lumen, which supports their claim that the lymphocytes are being eliminated from the body in this fashion.

Correlated electron and light microscopic studies of the intestinal epithelium of the rat, mouse hamster and man have led us to question the above proposed concepts of the relation and appearance of lymphocytes to the intestinal epithelial cells and therefore have indicated to us the necessity for re-evaluation of these proposals. In the present communication, evidence will be presented to show that lymphocytes normally present in the intestinal epithelium are definitely intercellular in position irrespective of their level within the epithelium. They exhibit no degenerative changes in this epithelial relationship and their migration occurs from the lamina propria into the epithelium and back again into the lamina propria, with no evidence of any movement toward the free surface of the intestinal epithelium and extrusion into the lumen.

MATERIALS AND METHODS

The observations which follow are based in part upon examination of portions of duodenum and ileum from 30 normal young adult female laboratory animals consisting of ten mice of a Swiss Albino stock each weighing 80–90 gm ten rats of the Sprague-Dawley strain, each weighing 120–130 gm; ten Syrian hamsters each weighing 115–120 gm. In addition human autopsy and biopsy specimens of grossly normal duodenum and ileum were obtained. The autopsy material consisted of specimens from two white males, 41 and 47 years of age and three white females 37 40 and 45 years of age. The cause of death in each case was accidental

[1] This study was supported by research grant from the National Institutes of Health (AM-[illegible]).
Department of Anatomy University of Nebraska College of Medicine, Omaha, Nebraska.

injury No more than three hours elapsed from the time of death to autopsy The biopsy specimens of duodenum and ileum were obtained from two white adult male patients ages 21 and 42 during abdominal surgery Less than 20 seconds elapsed between removal of the tissue and its immersion in fixing fluids

While the animals were under light ether anesthesia, the abdominal cavity was opened by a midline ventral incision The duodenum and ileum were quickly located with minimal handling and isolated Representative segments of tissue were removed from the above regions of the small intestine and placed immediately in their respective fixatives for electron and light microscopy

For electron microscopy the tissue was immersed immediately in a few drops of sucrose 2% buffered osmium tetroxide (Caulfield 57) and cut into 1 mm cubes which were further fixed for one hour at 3–5 C Only the pieces from the central part of the segment were retained as it was thought that possible trauma produced at the cut ends might disturb the normal relationships of the lymphocytes and epithelium. After fixation the tissues were dehydrated at room temperature in a graded series of ethyl alcohols for a total of one and one-half hours passed through propylene oxide and embedded in araldite epoxy resin Ultrathin sections (0 02–0 05 μ) were cut with glass knives in a Porter Blum microtome and selected for examination by using interference colors to judge their thickness After mounting on uncoated specimen grids sections stained with aqueous lead hydroxide (Venable and Coggeshall '65) subsequent to prestaining with uranyl acetate were examined in the RCA EMU 3G and Philips EM 100B electron microscopes Electron micrographs were taken at original magnifications of 1,300–15 000 and enlarged photographically to the desired size. To assist in orientation thicker companion sections (0 5–1 5 μ) were stained with 1% toluidine blue for light microscopy

For light microscopy representative segments of the same duodenum and ileum were fixed in 10% neutral formalin or sublimate alcohol For each animal and human 50 alternate or nonconsecutive 4–8 μ paraffin sections cut transversely to the longitudinal axis of the intestine were mounted and stained with Harris hematoxylin and eosin Heidenhain s iron hematoxylin or by the Feulgen method described by Stowell (45)

Sections of formalin fixed tissue were selected for counting in which the villi and crypts were cut approximately throughout their entire length Areas of the sections in which lymphocytes were counted included only the epithelium of the villi since it was not always possible to distinguish lymphocytes from mitotic stages of other cells in the epithelium of the crypts Alternate or nonconsecutive sections were used in making the cell counts to avoid duplication in the counting of the same cell All lymphocytes were counted except when less than half of the nucleus was included in the section This meant in practice, that nuclear fragments that were too small to be identified with certainty were left out of the counts The primary purpose of such cell counts was to determine the approximate number or abundance of lymphocytes in the epithelium of the villi as well as their level of distribution in relation to the nucleus of the columnar cells. Lymphocyte counts were taken from the epithelium of five villi for each of 50 sections for a total of 250 villi for each animal and human specimen or from a total of 2500 villi for each group of 10 animals and humans

OBSERVATIONS

Distribution of lymphocytes One of the features equally discernible with electron and light microscopy is the distribution and abundance of lymphocytes within the epithelial layer In man as in animal the great majority of the small lymphocytes normally present in the epithelial layer are located in the basal region below the level of the epithelial cell nuclei in close approximation to the basal lamina (fig 1) with few occurring at or above the level of the epithelial nuclei (fig 2) Approximately 97 6% of the total 54 700 lymphocytes considered for all three groups of animals were distributed below the level of the epithelial cell nuclei with 98 7% of a total 15 875 lymphocytes assuming

TABLE 1
Distribution and number of intercellular lymphocytes within the intestinal epithelium of the mouse rat, hamster and man

Number of animals	Total number of lymphocytes counted for each animal group	Below level of nucleus		Above level of nucleus	
		No.	%	*No.*	%
10 Mice	19,150	18,921	98.8	229	1.2
10 Rats	18,600	18,191	97.8	409	2.2
10 Hamsters	16,950	16,323	96.3	627	3.7
Totals	54 700	53,435	97.6	1265	2.4
7 Humans	15,875	15,669	98 7	206	1.3

this same distribution in the intestinal epithelium of man (table 1)

Position of lymphocytes. No doubt exists, as a result of our electron microscopic studies, that the lymphocytes at all levels in the intestinal epithelium of the duodenum and ileum, of both man and animal, are intercellular in position. This conclusion is based upon several facts which seem irrefutable In the first place it was common to observe the pushing apart of epithelial cells by the lymphocytes situated between them (fig. 3) Numerous cytoplasmic pseudopodia extended into the spaces between the epithelial cells or between the epithelial cells and the basal lamina. This was especially noticeable in the intercellular spaces below the level of the epithelial cell nuclei. In the second place, additional support for the intercellular position of the lymphocytes is seen in the presence of an apparent clear ring around each of them in light micrographs (figs. 1 2) This clear ring" was observed by electron microscopy to be composed of the unstained, nongranular cytoplasm of the lymphocyte and the surrounding intercellular space (fig. 3) as was suspected by light microscopy The identification of distinct intact cell membranes not ordinarily resolved with the light microscope not only of the lymphocytes but of the adjacent epithelial cell or cells surrounding them corroborates the concept of the intercellular position of the lymphocytes (fig. 3).

Appearance of lymphocytes A third feature rapidly discernible with electron microscopy but infrequently so with light microscopy is the appearance of the lymphocytes which will be described relative to their location in the lamina propria, their migration through the basal lamina and their position within the epithelial layer of the intestinal villi, with special reference to the latter

Lymphocytes in the lamina propria appeared to be morphologically similar to circulating lymphocytes. In light micrographs the nuclei were usually round or slightly oval. There was the usual characteristic clumping of the nuclear chromatin which frequently showed signs of peripheral condensation as evidenced by its intense peripheral staining Electron microscopy revealed the nucleus to be surrounded by the characteristic double membrane The nucleoplasm approached various densities characteristic of the pattern of densities corresponding to the nuclear chromatin of light microscopy The cytoplasm presents a somewhat heterogenous appearance with its denser organelles and inclusions sharply outlined against a less dense rather undifferentiated background which has a granular appearance. Sparse profiles of rough-surfaced endoplasmic reticulum were scattered throughout the cytoplasm. The mitochondria were few to moderate in number and dispersed at random in the cytoplasm. Relatively uniform, membrane-bound electron dense bodies, thought to be lysosomes on the basis of morphological criteria, were distributed throughout the cytoplasm.

Other than alterations produced in the general configuration of the lymphocyte during its actual passage through the basal lamina, the cell appeared to be normal (fig. 4) In some of these lymphocytes many of the cytoplasmic organelles were contained in the tail of the cytoplasmic body or ectoplasm trailing the nucleus

while in contrast that portion of the cytoplasmic body or endoplasm immediately preceding the nucleus either as a pseudopodial formation or thinned-out cytoplasmic cap was usually devoid of organelles.

The lymphocytes occurring above the basal lamina i.e in the intercellular spaces between the epithelial cells of the villi appeared normal (fig 3) Their shape was occasionally altered by surrounding structures and the number of dense osmophilic lysosome like bodies was increased

There were no mitoses in the villous epithelium This process seemed to be confined strictly to the epithelium of the crypts where mitotic figures were abundant.

Migration of lymphocytes The direction of movement of migrating lymphocytes through the basal lamina was indicated by two criteria The most obvious indication was the direction in which the basal lamina and associated collagenous fibrils were ruptured Those lymphocytes *which were moving out of the epithelium* into the lamina propria pushed the basal lamina and collagenous fibrils ahead of them so that the ruptured edges projected *into the* lamina propria The converse was true with those lymphocytes moving from the lamina propria into the epithelium The second criterion as set forth by Lewis ('31) was that the nucleus of the lymphocytes precedes the cytoplasm which streams behind similar to the handle of a mirror

Fate of lymphocytes Although this investigation does not attempt to establish the fate of the lymphocyte several phenomena were observed which would tend to refute the concept that these cells degenerate and are extruded into the intestinal lumen or transform into other types of cells.

The finding of greater numbers of lymphocytes in the intercellular spaces near the basal lamina (fig 1) suggests that they are not being eliminated into the intestinal lumen and that they are in this location possibly *because their* function occurs in this part of the epithelial layer There were no degenerative changes in the lymphocytes (figs. 3 4) nor were any of these cells "caught in the actual process of extrusion *from the villous epithelium into* the intestinal lumen. All migratory movement of the lymphocytes was between the epithelium and lamina propria.

DISCUSSION

The primary purpose of this study in addition to giving due consideration to other phenomena such as the distribution, appearance and migration of lymphocytes in relation to the cells of the intestinal epithelium was to see if electron microscopy would reveal the lymphocyte in this epithelial relationship clearly enough to clarify the issue left in doubt by the limited resolving power of the light microscope as to whether these cells (lymphocytes) are actually intracellular or intercellular in position

Distribution of lymphocytes There appears to be some controversy concerning the distribution of lymphocytes within the epithelial layer of the small intestine. The presence of a greater number of lymphocytes in the basal region of the epithelial layer i e *below the level of the epithelial cell nuclei*, while not in accord with the *observations* of Andrew et al ('45 '46 '47 '65) resembles the condition in the *intestinal epithelium of* the hamster (Kelsall '46)

A possible explanation for this basal distribution of lymphocytes is that they are not being eliminated into the intestinal lumen a concept which is not in agreement with the findings of Andrew et al. ('45 '46 '47 '65) *If* these lymphocytes were being extruded into the lumen one would find a more even distribution within the epithelial layer rather than the high concentration in the basal region

Another explanation is that their function occurs in this part of the epithelial layer Their function in this site however has not been established experimentally and the numerous theories are as diversified *as those regarding* the general function of lymphocytes.

Position of lymphocytes The electron microscopic demonstration of the true nature of the "clear rings" which encompass the lymphocytes and the identification *of* distinct cell membranes of both the lymphocytes and the adjacent epithelial cells has definitely confirmed the intercellular

position of the lymphocytes in the intestinal epithelium of both man and animal. Schaffer ('36) described lymphocytes in the intestinal epithelium of man as lying in deep niches in adjacent epithelial cells which is in complete accord with our observations. Further evidence in support of this concept is supplied by Wolfe-Heldegger ('39) who in describing the migration of lymphocytes in the intestines of the dog, cat, mouse guinea pig and rabbit, speaks of this process as occurring between the epithelial cells. Bloom and Fawcett ('64) also describe active migration of lymphocytes in the intestinal epithelium as occurring between the epithelial cells.

Our identification of the intercellular position of the lymphocytes is not in agreement with that of Andrew et al. (45 46 47 '65) Kelsall ('46) and Trowell ('58) who claim an intracellular position for these cells normally present in the intestinal epithelium. With respect to mouse and man, Andrew et al. (45 46 47 '65) have taken as evidence in support of this concept the presence of vacuoles enclosing the lymphocytes and the nuclear changes in the epithelial cells produced by the lymphocytes which they contain. We explain the presence of these vacuoles or "clear rings" around the lymphocytes on the basis of an intercellular position. Trowell's ('58) observations of this phenomenon in the intestinal epithelium of the rat, cat, dog and frog led him to support the claims of Andrew et al. ('45 46, 47 '65) Kelsall (46) speaks of lymphocytes within the intestinal epithelial cells of the hamster

Appearance of lymphocytes. Our description of the normal appearance of the lymphocytes irrespective of their level within the epithelial layer is not in agreement with *Andrew et al. (45 47)* According to these authors lymphocytes in the intestinal epithelium are either in mitosis or in a majority of instances undergoing marked morphological changes characterized by pycnosis, fragmentation and vacuolation, and these degenerative changes are directly correlated with the level within *the epithelial* cell.

Migration of lymphocytes The presence of lymphocytes in the lamina propria of the villi and their subsequent migration into the villous epithelium has been studied by many

One of the earliest reports was that of Von Arnstein (1867) who described migration of lymphocytes in the intestinal epithelium of the dog, cat rabbit and guinea pig The concept of actual ameboid movement accounting for the penetration of and subsequent intercellular migration of lymphocytes in the intestinal epithelium of the dog, cat, rabbit, mouse and guinea pig as described by Wolfe-Heldegger ('39) agrees with our own observations but not with those of Andrew and Andrew (45) who think of this phenomenon as being passive in nature and occurring only within the epithelial cells. Kelsall (46) speaks of ameboid movement in relation to migration of lymphocytes in the intestinal epithelium of the hamster Palay and Karlin ('59) in an electron microscopic study of fat absorption, found lymphocytes and eosinophils in the process of entering the epithelium from the lamina propria apparently between the cells.

Fate of lymphocytes Although no degenerative changes in lymphocytes nor extrusion of them into the intestinal lumen were observed, it has been claimed to be a conspicuous feature in the intestinal epithelium of the mouse (Andrew and Sosa, 47) and man (Andrew and Collings, 46) According to these investigators lymphocytes in the process of movement through the epithelial cells, undergo a series of degenerative changes and are extruded into the intestinal lumen as unrecognizable forms. According to Andrew and Sosa (47) "pictures of extrusion of lymphocytes both into the lumen of the crypts of Lieberkuhn or from the villus into the lumen of the intestine are common." We were never able to observe this phenomenon as *described by these* authors. The observations of Erf (40) that a marked and persistent lymphopenia occurs immediately following gastro-enterectomy in rabbits, does not support the hypothesis that lymphocytes are being eliminated into the intestinal lumen. Guieysse-Pellissier (12) stated that lymphocytes probably do not pass through the epithelium into the lumen of the normal intestines. Hellman ('34) suggested that the lymphocytes may remain in the intestinal epithelium as a

while in contrast that portion of the cytoplasmic body or endoplasm immediately preceding the nucleus either as a pseudopodial formation or thinned-out cytoplasmic cap was usually devoid of organelles

The lymphocytes occurring above the basal lamina i e in the intercellular spaces between the epithelial cells of the villi appeared normal (fig 3) Their shape was occasionally altered by surrounding structures and the number of dense osmophilic lysosome-like bodies was increased

There were no mitoses in the villous epithelium This process seemed to be confined strictly to the epithelium of the crypts where mitotic figures were abundant.

Migration of lymphocytes The direction of movement of migrating lymphocytes through the basal lamina was indicated by two criteria The most obvious indication was the direction in which the basal lamina and associated collagenous fibrils were ruptured Those lymphocytes which were moving out of the epithelium into the lamina propria pushed the basal lamina and collagenous fibrils ahead of them so that the ruptured edges projected into the lamina propria The converse was true with those lymphocytes moving from the lamina propria into the epithelium The second criterion as set forth by Lewis ('31) was that the nucleus of the lymphocytes precedes the cytoplasm which streams behind similar to the handle of a mirror

Fate of lymphocytes Although this investigation does not attempt to establish the fate of the lymphocyte several phenomena were observed which would tend to refute the concept that these cells degenerate and are extruded into the intestinal lumen or transform into other types of cells

The finding of greater numbers of lymphocytes in the intercellular spaces near the basal lamina (fig. 1) suggests that they are not being eliminated into the intestinal lumen and that they are in this location possibly because their function occurs in this part of the epithelial layer There were no degenerative changes in the lymphocytes (figs. 3 4) nor were any of these cells "caught" in the actual process of extrusion from the villous epithelium into the intestinal lumen. All migratory movement of the lymphocytes was between the epithelium and lamina propria.

DISCUSSION

The primary purpose of this study in addition to giving due consideration to other phenomena such as the distribution, appearance and migration of lymphocytes in relation to the cells of the intestinal epithelium was to see if electron microscopy would reveal the lymphocyte in this epithelial relationship clearly enough to clarify the issue left in doubt by the limited resolving power of the light microscope as to whether these cells (lymphocytes) are actually intracellular or intercellular in position

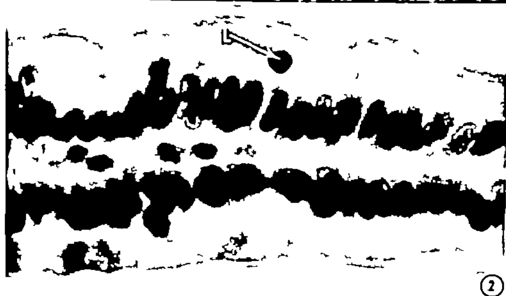
Distribution of lymphocytes There appears to be some controversy concerning the distribution of lymphocytes within the epithelial layer of the small intestine. The presence of a greater number of lymphocytes in the basal region of the epithelial layer i e below the level of the epithelial cell nuclei while not in accord with the observations of Andrew et al ('45 '46 '47 '65) resembles the condition in the intestinal epithelium of the hamster (Kelsall '46)

A possible explanation for this basal distribution of lymphocytes is that they are not being eliminated into the intestinal lumen a concept which is not in agreement with the findings of Andrew et al. ('45 '46 '47 '65) If these lymphocytes were being extruded into the lumen one would find a more even distribution within the epithelial layer rather than the high concentration in the basal region

Another explanation is that their function occurs in this part of the epithelial layer Their function in this site, however has not been established experimentally and the numerous theories are as diversified as those regarding the general function of lymphocytes

Position of lymphocytes The electron microscopic demonstration of the true nature of the "clear rings" which encompass the lymphocytes and the identification of distinct cell membranes of both the lymphocytes and the adjacent epithelial cells has definitely confirmed the intercellular


L
1


L
2

defensive barrier Kingsbury (44) never observed lymphocytes traversing the striated border of the intestinal epithelium. Kelsall (46) finding the majority of lymphocytes in the basal region of the intestinal epithelium of the hamster concluded that they were not being eliminated by way of the intestinal lumen

Another concept proposed by Andrew et al. (45 46 47 65) for the fate of the lymphocyte in addition to extrusion is that of "transformation" into other cell types Contrary to this opinion we never saw evidence of "transformation" of lymphocytes whereby these cells were providing nuclear material to the epithelial cells of the villi

The present investigation does not support any of these concepts as proposed by Andrew et al (45 46 47 65) for the fate of the lymphocyte in the intestinal epithelium

Because of the conspicuous migration of lymphocytes between the villous epithelium and the underlying lamina propria we believe that these cells have a definite function in this location and are not being eliminated into the intestinal lumen

LITERATURE CITED

Andrew W 1965 Lymphocyte transformation in epithelium. J Nat. Cancer Inst. 35 113–137

Andrew W and N V Andrew 1945 Mitotic division and degeneration of lymphocytes within the cells of intestinal epithelium in the mouse Anat Rec., 93: 251–277

Andrew W and C K. Collings 1946 Lymphocytes within the cells of the intestinal epithelium in man. Anat. Rec., 96 445–458

Andrew W and J M. Sosa 1947 Mitotic division and degeneration of lymphocytes within cells of intestinal epithelium in young and in adult white mice Anat. Rec. 97: 63–97

Bloom W., and D W Fawcett 1964 A textbook of histology W B. Saunders, Philadelphia. pp. 443–482.

Caulfield J B. 1957 Effects of varying the vehicle for OsO_4 in tissue fixation. J Biophys. Biochem Cytol. 3 827–830.

Erf L. A. 1940 Disappearance of intravenously injected lymphocytes in absence of gastro-intestinal tract. Am. J M. Sci., 200 1–11

Guieysse-Pellissier A 1912 Caryanabiose et greffe nucleaire Arch. Anat. Microsc., 13: 1–54

Hellman T 1934 Die Einlagerung von Zellen in Schleimhauten und Epithel. Antwort an J Sobotta in, Anat. Anz., 78 65–68.

Kelsall, M A. 1946 Lymphocytes in the intestinal epithelium and Peyer's patches of normal and tumor-bearing hamsters Anat. Rec., 96 391–410

Kingsbury B F 1944 Tonsillar epithelium and the lymphocyte: an examination of the palatine tonsil of the cat. Am. J Anat., 75: 233–261

Lewis, W H. 1931 Locomotion of lymphocytes. Bull, Johns Hopkins Hosp 49: 29–36.

Palay S L., and L J Karlin 1959 An electron microscopic study of the intestinal villus. II. The pathway of fat absorption J Biophys. Biochem. Cytol. 5: 373–384

Schaffer J 1936 Leukocyten in Epithel. von Mollendorff Handb. d mikr Anat des Menschen. Berlin Springer 2: (Part I) 92–96.

Stowell, R. E. 1945 Feulgen reaction for thymonucleic acid Stain Tech., 20: 45–58

Trowell O A 1958 The lymphocyte Int. Rev Cytol 7 236–293

Venable J H. and R. Coggeshall 1965 A simplified lead citrate stain for use in electron microscopy J Cell Biol 25: 407–408

Von Arnstein C 1867 Uber Becherzellen und ihre Beziehung zur Fettresorption und Sekretion. Arch. Mikr Anat., 39 527–547

Wolfs-Heidegger G 1939 Zur Frage der Lymphocytenwanderung durch das Darmepithel. Ztschr f mikr anat. Forsch., 45: 90–103

PLATE 1

EXPLANATION OF FIGURES

1 Intestinal villus from the duodenum of a young adult mouse showing the distribution of numerous lymphocytes (L) in the basal region of the epithelium. Observe that each lymphocyte is encompassed by "an apparent clear ring" which is comparable to the cytoplasm and surrounding intercellular space of the lymphocyte shown in figure 3. Hematoxylin and eosin × 495.

2 Autopsy specimen of intestinal villus from the duodenum of an adult human showing a normal lymphocyte (L) near the luminal border The lymphocyte can be observed pushing the cell membranes of the adjacent epithelial cells apart. Gallocyanin and eosin. × 903

Roland D. Meader and Dennis F. Landers



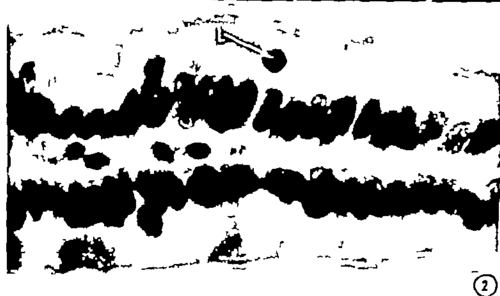


PLATE 2

EXPLANATION OF FIGURE

3 Normal lymphocyte (L) above the basal lamina (BL) in the intercellular space (ICS) between the basal portions of two adjacent epithelial cells (EC) from the duodenum of an adult male 47 years of age Observe the distinct, intact cell membranes (CM) of the lymphocyte and surrounding epithelial cells which completely separate these two cellular elements Observe the filamentous pseudopodia (PS) projecting from the surface of the lymphocyte indicating ameboid movement of this cell. Note that the visible cytoplasm of this lymphocyte and surrounding intercellular space are comparable to the "apparent clear rings" about the lymphocytes in figures 1 and 2. × 15,050


EC
ICS
EC
L
CM
BL
3

PLATE 3

EXPLANATION OF FIGURE

4 Normal lymphocyte (L) in process of passing through the basal lamina (BL) and associated collagenous fibrils from the lamina propria (LP) into the epithelium (E) in the ileum of a young adult hamster. Note the thinned-out cytoplasmic cap (CC) covering the leading edge of the nucleus with the majority of the cytoplasm trailing behind the nucleus. × 18,060


LP
LP
4

The Structure of the Proximal Tubule A morphological study of basement membrane cristae and their relationships in the renal tubule of the rat [1]

DOUGLAS WAUGH, ROBERT S. A. PRENTICE [2] AND D. YADAV
Departments of Pathology, Dalhousie University, Halifax, Canada and Queen's University, Kingston, Canada

ABSTRACT The basement membrane of the proximal tubule of the rat has a smooth outer surface and a series of closely spaced, transversely arranged inner ridges or cristae. By determining the specific plane of section in light and electron micrographs, the basal architecture of the tubule cells and its relationship to cristae can be elucidated. Toward the base of the cell, there are well defined linear cytoplasmic compartments parallel to the basement membrane cristae. From these, emanate terminal cytoplasmic villi which make final contact with the inner surface of the basement membrane. The arrangement appears well suited to the dual functions of adhesion between cell and basement membrane and large volume fluid transport.

Rhodin ('58a) and other modern histologists have depicted the renal tubule basement membrane as a simple tube with walls of uniform thickness and with smooth inner and outer surfaces (fig. 1). Earlier histologists (von Möllendorff '30; Zimmermann, 1898; Wedl, 1850) described a series of transverse rings on the inner aspect of the tubule basement membrane and these are well illustrated in the *camera lucida* drawings of von Möllendorff.

The present study was undertaken with a view to defining more precisely the 3-dimensional architecture of the proximal tubule basement membrane and of the immediately adjacent structures. Such structural definition is an essential first step in functional interpretation and in the recognition of abnormalities.

MATERIALS AND METHODS

Observations were made on young adult and weanling female Wistar rats that had been in the laboratory for periods varying from a few days to several weeks. A total of 63 animals was examined. Twenty four of these were untreated. The remaining animals were from a separate study of acute salt-loading. Thin sections of kidney from each animal were studied by light microscopy. Tissues from 49 of the 63 rats were examined with the electron microscope. There was no important difference in the structures to be described in untreated and in salt-loaded animals. Neither was there structural difference between weanlings and adult rats. Animals were allowed standard chow diet and water *ad libitum*, and only those that remained healthy and gained weight were studied.

Kidney tissue was obtained with the animal under light ether anaesthesia. The kidney was exposed through a midline abdominal incision and chilled buffered osmium tetroxide solution with sucrose (Caulfield and Trump '62) was dripped directly onto the surface of the exposed kidney for 20 minutes. This *in vivo* fixed tissue was excised with a razor blade, diced into small cubes and further fixed in the osmium tetroxide solution for one and one-half to two hours. The orientation of tissue blocks was carefully controlled so that observations could be made on adequately fixed tissue. The tissue was then passed through graded alcohols, propylene oxide and embedded in Epon 812 (Luft, '61).

Sections for electron microscopy were cut on a Porter Blum ultramicrotome, stained with uranyl acetate and/or lead citrate (Reynolds, '63) and examined in a Philips 75B or Philips EM 200 electron microscope.

For light microscopy sections from the epon-embedded blocks were cut at about one-half micron, transferred with a plati-

[1] Supported by grant MA 1462, Medical Research Council of Canada.
[2] Fellow, Medical Research Council of Canada. Present address: Department of Anatomy, Queen's University, Kingston, Canada.

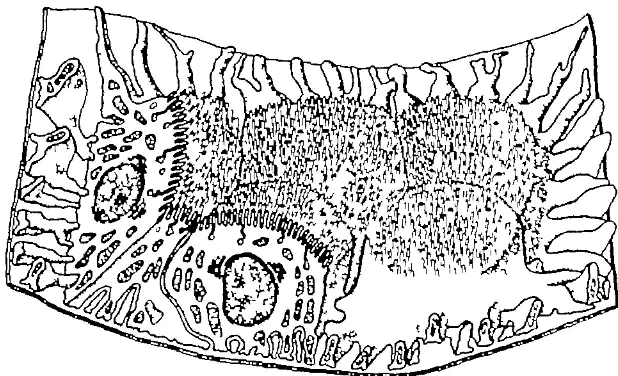


Fig. 1 Rhodin s concept of proximal tubule structure Note the smooth basement membrane of uniform thickness the basal interdigitating processes radiating laterally in all directions and the noninterlocking luminal cell borders Compare these features with those illustrated in figure 2. (Redrawn after Rhodin)

num loop to glass slides and stained by a modified silver methenamine procedure Paraffin sections of formalin fixed tissue were stained by periodic acid silver methenamine technique (Jones 57)

OBSERVATIONS

To form a concept of the anatomical structure of the complex region to be described it was necessary to maintain a 3-dimensional frame of mind while looking at 2-dimensional micrographs. Since it was apparent that the basement membrane as well as the adjacent cytoplasmic structure could be cut in an almost infinite variety of planes a careful estimate of the proper orientation of each section was essential in the development of an architectural concept. Orientation was achieved by careful observation of planes of section of such structures as microvilli vascular endothelium and the tubule as a whole

In thin light microscopy sections stained with silver methenamine the basement membrane was stained dark brown or black and stood out clearly Sections in the longitudinal plane of the proximal tubule (fig 4) showed the smooth outer surface of the basement membrane and a regular pattern of ridges cut in cross-section on the inner surface next to the base of tubule cells. In the remainder of this report these ridges are referred to as cristae The cristae were best seen in tangential rather than midline sections through the long axis of the tubule In nearly flat tangential sections (fig 5) the cristae were orientated transversely to the long axis of the tubule The transverse orientation of the cristae was confirmed by the fact that they could not be demonstrated in true cross-sections of tubules (fig 6) Although they were most prominent in the proximal tubules indistinct cristae could sometimes be seen

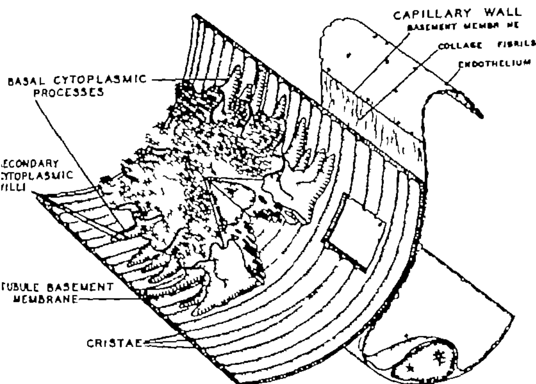
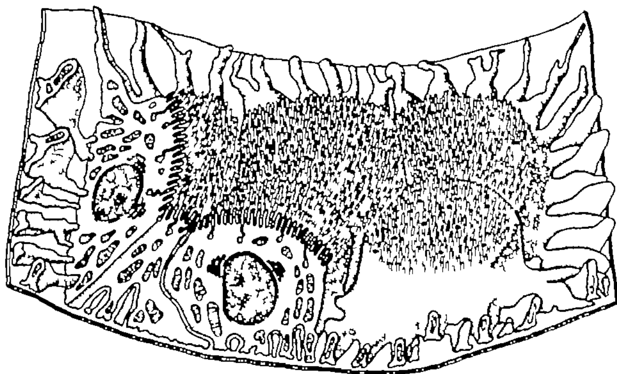


Fig. 2 A diagrammatic architectural representation of proximal tubule structure. Note: corrugated basement membrane with cristae on luminal side only; basal interdigitating cytoplasmic processes extending in transverse direction only parallel to cristae; complex radial apical cell processes which interlock with adjacent cells; the complex terminal cytoplasmic "villi" shown in simplified form (see fig. 3). Note the relationship of tubule to capillary wall, with collagen fibrils intervening between tubule and capillary basement membranes.

by light microscopy in the remainder of the tubule system in silver methenamine preparations.

Electron microscopy elaborated the features seen by light microscopy The cristae were found to be part of the basement membrane itself and the relationship of adjacent structures such as the base of the tubule cell and peritubular capillaries was well defined (figs. 6 7) As with light microscopy only sections in the plane of the longitudinal axis of the tubule showed the cristae clearly Longitudinal sections through the center of the tubule were necessary to demonstrate the cross-sectional profile of the cristae In such sections, the cristae appeared as rather subtle elevations amounting to one-third to one fourth of the total thickness of the basement membrane At some distance from the center of the long axis of the tubule the section plane became tangential and the height of the cristae was accentuated (figs 7 8) Such sections illustrated the regularity of the cristae and their interdigitation with cytoplasmic processes of the tubule cells. In extremely tangential sections (figs. 9 10) cristae could be shown to span the arc of the section and gave the appearance of bridging the edges of the portion of tubule. Between the cristae in such sections cytoplasmic compartments were seen as long cytomembrane-limited strips parallel to cristae (fig 9) These compartments lost their linear relationship with the cristae as they were traced into the more luminal portions of the cell (fig. 9) At the extreme basal region where the cytomem-



Proximal Convoluted Tubule (after Rhodin)

Fig. 1 Rhodin's concept of proximal tubule structure Note the smooth basement membrane of uniform thickness the basal interdigitating processes radiating laterally in all directions and the noninterlocking luminal cell borders. Compare these features with those illustrated in figure 2. (Redrawn after Rhodin)

num loop to glass slides and stained by a modified silver methenamine procedure Paraffin sections of formalin-fixed tissue were stained by periodic acid silver methenamine technique (Jones '57)

OBSERVATIONS

To form a concept of the anatomical structure of the complex region to be described it was necessary to maintain a 3-dimensional frame of mind while looking at 2-dimensional micrographs. Since it was apparent that the basement membrane as well as the adjacent cytoplasmic structure could be cut in an almost infinite variety of planes a careful estimate of the proper orientation of each section was essential in the development of an architectural concept. Orientation was achieved by careful observation of planes of section of such structures as microvilli vascular endothelium and the tubule as a whole

In thin light microscopy sections stained with silver methenamine the basement membrane was stained dark brown or black and stood out clearly Sections in the longitudinal plane of the proximal tubule (fig 4) showed the smooth outer surface of the basement membrane and a regular pattern of ridges cut in cross-section on the inner surface next to the base of tubule cells In the remainder of this report these ridges are referred to as cristae The cristae were best seen in tangential rather than midline sections through the long axis of the tubule In nearly flat tangential sections (fig 5) the cristae were orientated transversely to the long axis of the tubule The transverse orientation of the cristae was confirmed by the fact that they could not be demonstrated in true cross-sections of tubules (fig. 6) Although they were most prominent in the proximal tubules indistinct cristae could sometimes be seen



Fig. 4 Thin epon-embedded section of proximal tubule stained with silver methenamine. The plane of section is shown in the inset. The basement membrane (BM) is black and the regular projections of basement membrane material on the tubule cell side of the membrane are cristae (C) cut in cross-section. The height of the cristae is accentuated by the tangentiality of the section (see also fig. 3). × 975. (From *The Kidney* Int. Acad. of Path. Monograph Series, F. K. Mostofi, ed., D. E. Smith, series ed., Williams and Wilkins 1966.)

Fig. 5 Thin epon-embedded section of proximal tubules stained with silver methenamine. The approximate plane of section of tubule (A) is shown in the inset (i.e. tangential and oblique along the long axis of the tubule) The height of the cristae is accentuated to an extreme degree and in four areas they are continuous across the tubules (1, 2, 3, 4) × 675.

his and Bizzozero in 1901 referred to transverse striations in man protruding into the tubule basal membrane They appear in both cases to have been referring to the cristae. Heidenhain illustrated them in mouse kidney and von Möllendorff confirmed their presence in man.

All of these observers believed that the cristae were transversely orientated and von Möllendorff suggested that they formed a continuous spiral. Tasic ('18) on the other hand found them to be parallel only within the limits of individual cells, an observation so strikingly at variance with those of others (including the present authors) that it seems unlikely he could have been referring to the same structure.

Von Möllendorff concluded that "the basal membrane consists of an apparently homogeneous transparent skin which outwardly is connected to the interstitium and strengthened by a fibrous envelope and is inwardly connected with the epithelium in cement structures" From the present observations it would appear that von Möllendorff's fibrous envelope is in fact the layer of collagen fibrils which were seen invariably between capillary basement membrane and tubule basement membrane and occasionally between adjacent tubules with no intervening capillary Our findings indicate that the collagen is present in close relationship to capillaries since in sections where the tubule did not abut directly on a capillary collagen was frequently absent.

While the 3-dimensional architecture of the basement membrane structure can be relatively easily visualized (fig 2)

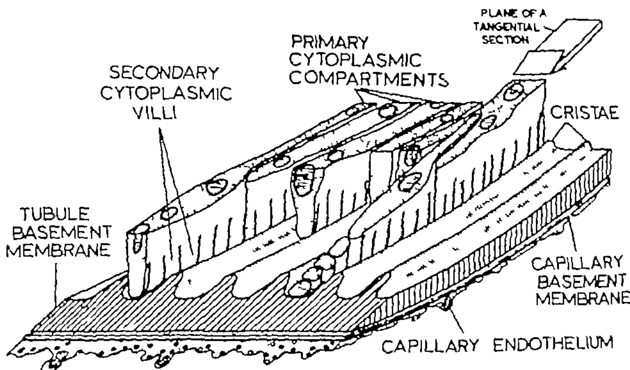


Fig 3 A diagrammatic representation of the 3-dimensional architecture of the basal region of the proximal tubule. The cellular structure consists of parallel cytoplasmic compartments (primary cytoplasmic compartments) from which emanate terminal secondary cytoplasmic "villi These "villi" are usually not as orderly and regular as the diagram suggests. As shown, the primary folds have a specific parallel orientation with the cristae of the basement membrane in the basal region of the cell. Capillary endothelial cell cytoplasmic structure is seen cut tangentially at the bottom and in cross-section along the right border

brane made contact with the basement membrane short cytoplasmic processes ("villi) emanated from the compartments (figs. 6 7 9) Mitochondria were not seen in the cytoplasm of the "villi," the latter being much smaller in cross-section than most mitochondria (fig 6)

The close proximity of capillary endothelium to tubule basement membrane lead to the conclusion that a section tangential to basement membrane would also be tangential to capillary endothelium This in fact was the case and was best demonstrated in rather thick sections (fig 7) The capillary fenestrations which on cross-section appeared as thin lines with central thickenings were seen in tangential sections as round or oval fenestrations with central electron-dense "knobs" (Rhodin 62) This appearance was interpreted as confirmation of the tangentiality of a given area of the section

Collagen fibrils were almost invariably seen separating basement membrane of the tubule from that of an adjacent capillary (fig 7) The fibrils tended to be rather widely separated without the formation of parallel bundles Collagen was much less frequently seen between abutting tubule basement membranes except in instances where a capillary was very close by In such areas a few fibrils sometimes extended from the capillary to lie between adjacent tubules (fig 8)

DISCUSSION

It is not always easy to relate the cristae observed in this study to structures described by earlier microscopists. The cristae do appear however to correspond to the "basal rings" described by C. Wedl in 1850 and to those illustrated by K. von Frisch in 1915 K W Zimmermann in 1898 described "basal striations" in rab-

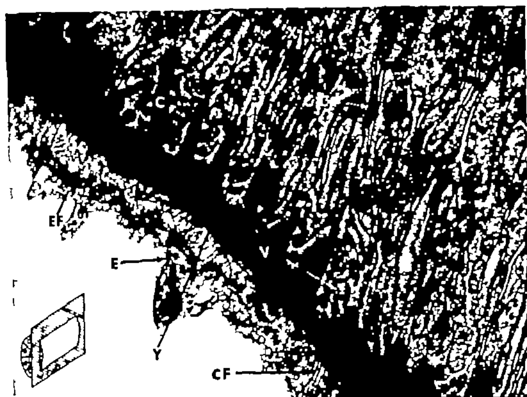


Fig. 7 Thick tangential section of basal area of proximal tubule. The plane of section is shown in the inset. The line XY is comparable to "plane of a tangential section" in figure 3. Note the round or oval cytoplasmic structures (V) between basement membrane cristae (C) which merge into long cytoplasmic compartments (CC) toward the top of the picture. These are shown diagrammatically in figure 3. Also note the collagen fibrils (CF) between the basement membrane of the tubule and the capillary endothelial cell cytoplasm (E). The endothelial fenestrations (EF) with their central electron-dense masses indicate the tangentiality of the section. Uranium and lead stain; × 22,500

mitochondria lying in the primary compartments and the secondary "villi." Many of these "villi" are cut in cross-section which indicates their rather irregular pattern. In this section (fig. 6) cristae are not seen. This is due to the plane of section which was confirmed by low power observation i.e. it is a true cross-section at right angles to the long axis of the tubule and parallel to the cristae.

The primary cytoplasmic compartments (called lamellae by Rhodin '58b) have a specific orientation at the base of the cell. They are parallel to each other and to the basement membrane cristae. This is seen in figures 7 and 9 and is depicted diagrammatically in figure 3. This orderly arrangement of compartments is soon lost as one moves up from the basement membrane into the body of the cell. This is illustrated in the upper left corner of figure 9 where cytoplasmic compartments enclosing mitochondria show an interlocking random arrangement as opposed to the linear pattern to the right where the section is very close to the basement membrane.

The transverse linear orientation of the basal cytoplasmic compartments deserves further comment. In 1958 Rhodin ('58a) published his diagrammatic representation of proximal tubule structure (fig. 1) in which the basement membrane is shown as having a uniform thickness and the tubule cells have basal processes radiating in all horizontal directions.

The present findings indicate that, while these processes exist, they do not have a radial arrangement but interlock with ad-



Fig. 6 Base of proximal tubule from a true cross-section of the tubule as indicated by the *inset*. Basement membrane cristae are not seen since the section is parallel to the cristae. The section is from a rat injected intraperitoneally with hypertonic sodium and as a result the cytoplasm is mod erately dehydrated with the formation of extracellular spaces (S) The latter enhances the demon stration of the terminal "villi (V) at the base of the cell many of which are cut in cross-section It should be noted that mitochondria do not occupy these "villi The capillary endothelial cell cytoplasm shows fenestrations (F) cut in cross-section. Lead stain; × 27,500

the structure of the immediately adjacent basal portion of the tubule epithelial cell is more complex and warrants further elaboration The interpretation arrived at here is shown in a 3-dimensional diagram matic representation (fig 3) in which the features seen in the electron micrographs (figs 6 7 9 10) are shown in simplified form In figure 3 the "plane of a tangential section" is approximately the plane of sec tion of figure 7 Figures 9 and 10 are even more tangential and the vertical cut through basement membrane on the right of figure 3 represents the plane of section of figure 6

The deep cristae and endothelial fenes trations seen in figure 7 are illustrated dia grammatically in figure 3 by the tangential cut through basement membrane and en dothelium Between individual cristae in figure 7 rows of round or oval membrane limited structures are seen When these are traced into the body of the cell they be come parallel linear plasma membrane-limited compartments We interpret the round or oval bodies seen in figure 7 as "villi" cut in an oblique plane and the strips as "primary cytoplasmic compart ments The secondary cytoplasmic villi" of figure 3 are not as uniform and orderly as the diagram suggests but are shown this way for simplicity Frequently they bend in different directions and vary in depth They are usually narrower than the pri mary cytoplasmic folds and do not con tain mitochondria the latter usually being larger than the "villi" Figure 6 illustrates the rather abrupt demarcation between

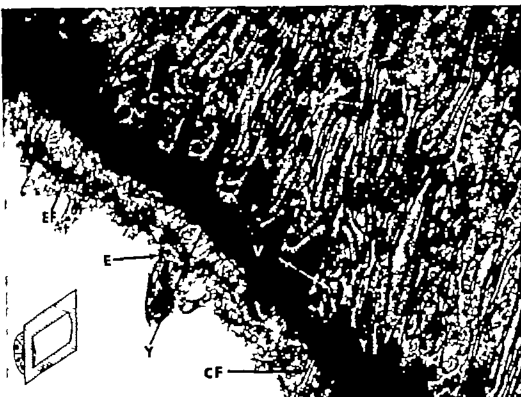


Fig. 7 Thick tangential section of basal area of proximal tubule. The plane of section is shown in the inset. The line XY is comparable to plane of a tangential section in figure 3. Note the round or oval cytoplasmic structures (V) between basement membrane cristae (C) which merge into long cytoplasmic compartments (CC) toward the top of the picture. These are shown diagrammatically in figure 3. Also note the collagen fibrils (CF) between the basement membrane of the tubule and the capillary endothelial cell cytoplasm (E) The endothelial fenestrations (EF) with their central electron-dense masses indicate the tangentiality of the section. Uranium and lead stain; × 22,500.

mitochondria lying in the primary compartments and the secondary villi. Many of these villi are cut in cross-section which indicates their rather irregular pattern. In this section (fig. 6) cristae are not seen. This is due to the plane of section which was confirmed by low power observation; i.e. it is a true cross-section at right angles to the long axis of the tubule and parallel to the cristae.

The primary cytoplasmic compartments (called lamellae by Rhodin '58b) have a specific orientation at the base of the cell. They are parallel to each other and to the basement membrane cristae. This is seen in figures 7 and 9 and is depicted diagrammatically in figure 3 This orderly arrangement of compartments is soon lost as one moves up from the basement membrane into the body of the cell. This is illustrated in the upper left corner of figure 9 where cytoplasmic compartments enclosing mitochondria show an interlocking random arrangement as opposed to the linear pattern to the right where the section is very close to the basement membrane.

The transverse linear orientation of the basal cytoplasmic compartments deserves further comment. In 1958 Rhodin ('58a) published his diagrammatic representation of proximal tubule structure (fig. 1) in which the basement membrane is shown as having a uniform thickness and the tubule cells have basal processes radiating in all horizontal directions.

The present findings indicate that, while these processes exist, they do not have a radial arrangement but interlock with ad-



Fig 6 Base of proximal tubule from a true cross-section of the tubule as indicated by the inset. Basement membrane cristae are not seen since the section is parallel to the cristae. The section is from a rat injected intraperitoneally with hypertonic sodium and as a result the cytoplasm is moderately dehydrated with the formation of extracellular spaces (S) The latter enhances the demonstration of the terminal villi" (V) at the base of the cell many of which are cut in cross-section. It should be noted that mitochondria do not occupy these "villi." The capillary endothelial cell cytoplasm shows fenestrations (F) cut in cross-section. Lead stain; × 27,500

the structure of the immediately adjacent basal portion of the tubule epithelial cell is more complex and warrants further elaboration The interpretation arrived at here is shown in a 3-dimensional diagrammatic representation (fig 3) in which the features seen in the electron micrographs (figs. 6 7 9 10) are shown in simplified form In figure 3 the "plane of a tangential section" is approximately the plane of section of figure 7 Figures 9 and 10 are even more tangential and the vertical cut through basement membrane on the right of figure 3 represents the plane of section of figure 6

The deep cristae and endothelial fenestrations seen in figure 7 are illustrated diagrammatically in figure 3 by the tangential cut through basement membrane and endothelium Between individual cristae in figure 7 rows of round or oval membrane-limited structures are seen When these are traced into the body of the cell they become parallel linear plasma membrane-limited compartments. We interpret the round or oval bodies seen in figure 7 as "villi" cut in an oblique plane and the strips as "primary cytoplasmic compartments" The secondary cytoplasmic villi" of figure 3 are not as uniform and orderly as the diagram suggests but are shown this way for simplicity Frequently they bend in different directions and vary in depth They are usually narrower than the primary cytoplasmic folds and do not contain mitochondria the latter usually being larger than the villi" Figure 6 illustrates the rather abrupt demarcation between



Fig. 7 Thick tangential section of basal area of proximal tubule. The plane of section is shown in the inset. The line XY is comparable to "plane of a tangential section" in figure 3. Note the round or oval cytoplasmic structures (V) between basement membrane cristae (C) which merge into long cytoplasmic compartments (CC) toward the top of the picture. These are shown diagrammatically in figure 3. Also note the collagen fibrils (CF) between the basement membrane of the tubule and the capillary endothelial cell cytoplasm (E). The endothelial fenestrations (EF) with their central electron-dense masses indicate the tangentiality of the section. Uranium and lead stain; × 22,500.

mitochondria lying in the primary compartments and the secondary villi. Many of these "villi" are cut in cross-section which indicates their rather irregular pattern. In this section (fig. 6) cristae are not seen. This is due to the plane of section which was confirmed by low power observation i.e. it is a true cross-section at right angles to the long axis of the tubule and parallel to the cristae.

The primary cytoplasmic compartments (called lamellae by Rhodin '58b) have a specific orientation at the base of the cell. They are parallel to each other and to the basement membrane cristae. This is seen in figures 7 and 9 and is depicted diagrammatically in figure 3. This orderly arrangement of compartments is soon lost as one moves up from the basement membrane into the body of the cell. This is illustrated in the upper left corner of figure 9 where cytoplasmic compartments enclosing mitochondria show an interlocking random arrangement as opposed to the linear pattern to the right where the section is very close to the basement membrane.

The transverse linear orientation of the basal cytoplasmic compartments deserves further comment. In 1958 Rhodin ('58a) published his diagrammatic representation of proximal tubule structure (fig. 1) in which the basement membrane is shown as having a uniform thickness and the tubule cells have basal processes, radiating in all horizontal directions.

The present findings indicate that, while these processes exist, they do not have a radial arrangement but interlock with ad-



Fig. 6 Base of proximal tubule from a true cross-section of the tubule as indicated by the inset Basement membrane cristae are not seen since the section is parallel to the cristae. The section is from a rat injected intraperitoneally with hypertonic sodium and as a result the cytoplasm is moderately dehydrated with the formation of extracellular spaces (S) The latter enhances the demonstration of the terminal "villi" (V) at the base of the cell many of which are cut in cross-section. It should be noted that mitochondria do not occupy these "villi. The capillary endothelial cell cytoplasm shows fenestrations (F) cut in cross-section Lead stain; × 27,500

the structure of the immediately adjacent basal portion of the tubule epithelial cell is more complex and warrants further elaboration The interpretation arrived at here is shown in a 3-dimensional diagrammatic representation (fig 3) in which the features seen in the electron micrographs (figs 6 7 9 10) are shown in simplified form In figure 3 the "plane of a tangential section" is approximately the plane of sec tion of figure 7 Figures 9 and 10 are even more tangential and the vertical cut through basement membrane on the right of figure 3 represents the plane of section of figure 6

The deep cristae and endothelial fenestrations seen in figure 7 are illustrated dia grammatically in figure 3 by the tangential cut through basement membrane and endothelium Between individual cristae in figure 7 rows of round or oval membrane-limited structures are seen When these are traced into the body of the cell they become parallel linear plasma membrane-limited compartments. We interpret the round or oval bodies seen in figure 7 as "villi cut in an oblique plane and the strips as primary cytoplasmic compart ments " The secondary cytoplasmic villi" of figure 3 are not as uniform and orderly as the diagram suggests but are shown this way for simplicity Frequently they bend in different directions and vary in depth They are usually narrower than the pri mary cytoplasmic folds and do not contain mitochondria the latter usually being larger than the "villi " Figure 6 illustrates the rather abrupt demarcation between

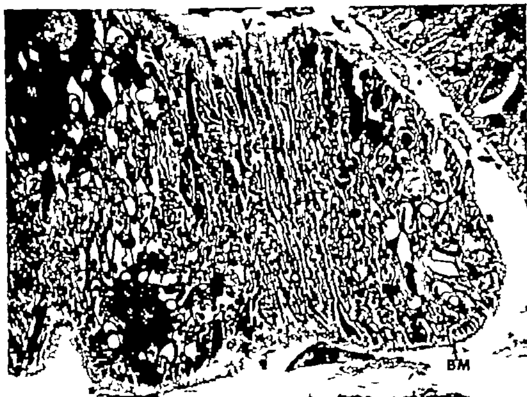


Fig. 9 Electron micrograph from a section cut in a plane similar to figure 5, i.e. very tangential to the wall of the proximal tubule. This, like figure 6, is from sodium-treated animal, and the resultant cellular dehydration makes more graphic the cytoplasmic compartmentalization. The cristae (C) of the basement membrane (BM) are seen extending across the arc of the tubule. One of these is branched (B). Between the cristae, cytoplasmic compartments (CC) are essentially linear and parallel to cristae. Cross-sections of terminal "villi" (V) are seen in some areas. In the upper left, where compartments contain mitochondria, the section extends to the interior of the cell and the linear orientation of compartments is lost. Uranium and lead stain; × 6,500.

structures. The close association of cristae and cell membranes does indeed suggest adhesion and their transverse orientation could well have the effect of resisting the traction resulting from the flow of urine through the tubule. The facts that cristae were imperfect or absent in the portions of the nephron distal to the proximal tubule and that these more distal portions had scant, poorly developed microvilli projecting into the lumen of the tubule are consistent with the theory of an adhesive function for the cristae. According to this interpretation distal cells lacking the maze of microvilli present in the proximal tubule would not be subject to as much traction by the flow of glomerular filtrate and thus would have less need of a strong anchoring mechanism. Traction should also be lessened in the distal system by the decreased volume and rate of flow of urine, although this might be partly or completely offset by changes in viscosity. In our experiments on acute sodium-loading in rats and in studies by Biava, Dyrda, Genest and Bencosme ('63) on kaliopenic renal lesions large extracellular spaces were demonstrated in which the cell membrane folds became widely separated from each other. The close approximation of the cell membrane to the basement membrane however remained intact which indicated that separation at this point is not easily achieved.

The second point of functional significance of the basal structure has to do with fluid and solute movement. The proximal renal tubule cell probably transports as great a flow of fluid and solutes across its



Fig. 8 Basal regions of a proximal tubule (PT) and a distal tubule (DT) The proximal tubule has been sectioned in a plane similar to that of figure 4 with resultant accentuation of the height of the cristae (C) Collagen fibrils (CF) are seen between the basement membranes of the two tubules. The distal tubule basement membrane is much thinner and does not show cristae. (This section is from a rat injected intraperitoneally with hypertonic saline) Lead stain; × 30,600

jacent cells only in the transverse plane of the tubule parallel to the basement membrane cristae This is illustrated diagrammatically in figure 2 If in addition to their transverse orientation basal projections extended in all other directions (i e radially) they would have to cross the cristae Figures 7 and 9 indicate that such crossing does not occur and that the basal compartments have a specific parallel orientation with the cristae

Scott ('64) interprets basement membrane cristae in male rats as a change attributable to age He concludes that with advancing age there is progressive thickening of the basement membrane and partial penetration of it by cytoplasmic processes of the overlying epithelial cells. Although no reference is made to the tangentiality of his sections the micrographs showing the deepest cristae appear to be tangential as indicated by the circular fenestrations in the endothelium of the adjacent capillary Scott states that the change was not seen in young adult rats. The fact that in the present study cristae were seen in weanling female Wistar rats is not in agreement with Scott's interpretation of them as a phenomenon of aging Indeed cristae were found to be no less prominent in weanlings than in young adult rats

The intimate and complex relationship of the basal portion of the cell to the corrugated basement membrane leads logically to speculation on the functional significance of such an arrangement Early observers (Frisch '15 Heidenhain '07; von Möllendorff '30 Zimmermann 1898) were unanimous in attributing an adhesive function to the cristae they are in fact referred to by von Möllendorff as "cement

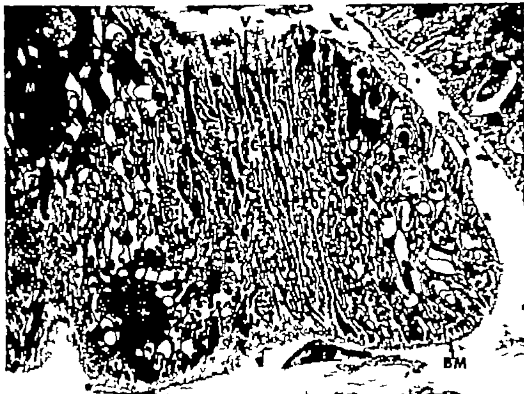


Fig. 8 Electron micrograph from a section cut in a plane similar to figure 6, i.e. very tangential to the wall of the proximal tubule. This, like figure 6, is from a sodium-treated animal, and the resultant cellular dehydration makes more graphic the cytoplasmic compartmentalization. The cristae (C) of the basement membrane (BM) are seen extending across the arc of the tubule. One of these is branched (B). Between the cristae, cytoplasmic compartments (CC) are essentially linear and parallel to cristae. Cross-sections of terminal "villi" (V) are seen in some areas. In the upper left, where compartments contain mitochondria, the section extends to the interior of the cell and the linear orientation of compartments is lost. Uranium and lead stain; × 6,800.

structures. The close association of cristae and cell membranes does indeed suggest adhesion and their transverse orientation could well have the effect of resisting the traction resulting from the flow of urine through the tubule. The facts that cristae were imperfect or absent in the portions of the nephron distal to the proximal tubule and that these more distal portions had scant, poorly developed microvilli projecting into the lumen of the tubule are consistent with the theory of an adhesive function for the cristae. According to this interpretation, distal cells lacking the maze of microvilli present in the proximal tubule would not be subject to as much traction by the flow of glomerular filtrate and thus would have less need of a strong anchoring mechanism. Traction should also be lessened in the distal system by the decreased volume and rate of flow of urine, although this might be partly or completely offset by changes in viscosity. In our experiments on acute sodium-loading in rats and in studies by Biava, Dyrda, Genest and Bencosme ('63) on kaliopenic renal lesions large extracellular spaces were demonstrated in which the cell membrane folds became widely separated from each other. The close approximation of the cell membrane to the basement membrane however remained intact which indicated that separation at this point is not easily achieved.

The second point of functional significance of the basal structure has to do with fluid and solute movement. The proximal renal tubule cell probably transports as great a flow of fluid and solutes across its



Fig 10 A tangential section of proximal tubule similar to figures 8 and 9 Although the preservation of cytoplasm of tubule and capillary cells is poor the basement membrane cristae (C) are well demonstrated. Moving toward the left of the micrograph, the cristae become more prominent and, just before the section passes through the basement membrane at the lower left, a crista spans the arc (CA) The tangentiality of the section is indicated by the capillary endothelial fenestrations (F inset) Lead stain; × 8,500

plasma membrane as any cell in the mammalian body The complex basal structure of proximal cells and of basement membrane appears ideally suited for high volume fluid transport. The surface area of the basal cytomembrane is increased in three ways (fig 3) (1) deep primary infoldings of plasma membrane are present (primary cytoplasmic compartments) (2) secondary cytoplasmic "villi" projecting from the compartments formed by the primary infoldings extend down to the basement membrane (3) the basement membrane cristae increase the overall area of virtually direct contact with cell membrane

Out of context but worthy of note is the shape of the luminal portion of the proximal tubule cell. Graffin and Foote ('39) and Bulger (65) described a pattern of complex interdigitation in the apical regions of tubule cells We have noted this consistently and have illustrated it in figure 2 This is not in agreement with the concept of Rhodin (fig 1) where the luminal cell borders are depicted as being relatively straight

Figure 2 summarizes the other features that have been discussed the orientation of basement membrane cristae the specific transverse orientation of interdigitating basal cell processes parallel to the cristae and the relationship of the cell to adjacent capillaries

LITERATURE CITED

Biava C I Dyrda J Genest and S A. Bencosme 1963 Kaliopenic nephropathy A correlated light and electron microscopic study Lab. Invest., 12 443

Bizzozero, E. 1901 Sulla membrana propria dei canalicoli uriniferi del rene umano. Arch. Sci. Med., 25, (cited by von Möllendorff)

Bulger, R. E. 1965 The shape of rat kidney tubule cells. Amer. J Anat., 116: 237

Caulfield, J. B., and B. F Trump 1962 Correlation of ultrastructure with function in the rat kidney Amer. J Path., 40: 199.

Frisch, Br. v 1915 Zum feineren Bau der Membrana propria der Harnkanälchen. Anat. Anz., 48: 294, (cited by von Möllendorff)

Graffin, A. L., and J. J. Foote 1939 Epithelial cell shapes in the first segment of the proximal tubule of the cat nephron. Amer. J. Anat., 65 173.

Heidenhain, M. 1907–1911 Plasma und Zelle. Bardelebens Handbuch der Anatomie, (cited by von Möllendorff).

Jones, D. B. 1957 Nephrotic glomerulonephritis. Amer. J. Path., 33: 313.

Luft, J. H. 1961 Improvements in epoxy resin embedding methods. J. Biophys. Biochem. Cytol., 9: 409

Möllendorff, W v 1930 Die Basalmembran. In: Handbuch der Mikroskopischen Anatomie des Menschen. VII/1. Harn und Geschlechtsapparat. Julius Springer, Berlin, pp. 55–61.

Reynolds, E. S. 1963 The use of lead citrate at high pH as an electron-opaque stain in electron microscopy J Cell Biol., 17: 208.

Rhodin, J 1958 Electron microscopy of the kidney Amer. J Med., 24: 661.

——— 1958 Anatomy of kidney tubules. Int. Rev Cytol., 7: 485.

——— 1962 The diaphragm of capillary endothelial fenestrations. J Ultrastruct. Res., 6: 171.

Scott, E. B. 1964 Modification of the basal architecture of renal tubule cells in aged rats. Proc. Soc. Exp. Biol. Med., 117 586.

Tanić, J 1918 Über die Beziehungen des Epithels der Harnkanälchen zur Basalmembran. Med. Diss. Bern, (cited by von Möllendorff)

Wedl, D. 1850 Über die Membrana propria der Harnkanälchen. Sitzgber Akad. Wiss. Wien, Math.-naturwiss. Kl. pp. 487–488, (cited by von Möllendorff)

Zimmermann, K. W 1898 Beiträge zur Kenntnis einiger Drüsen und Epithelien. Arch. mikrosk. Anat., 52: 659 (cited by von Möllendorff)

Index

A

B

C

D

E

F

G

H

I

K

L

M

N

O

P

R

T

U

V

W

Y